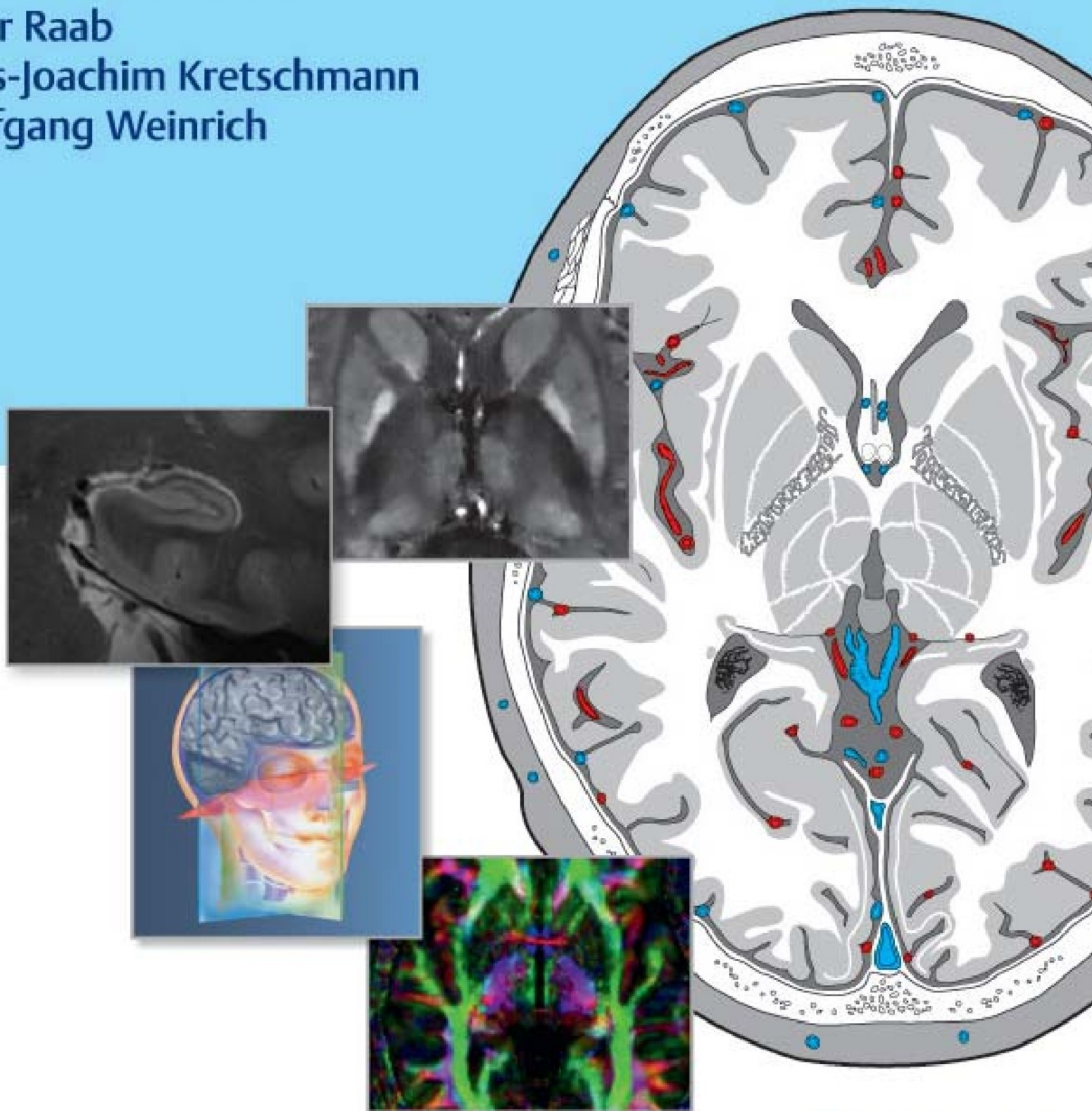


Cranial Neuroimaging and Clinical Neuroanatomy

Atlas of MR Imaging and Computed Tomography

Fourth Edition

Heinrich Lanfermann
Peter Raab
Hans-Joachim Kretschmann
Wolfgang Weinrich



Cranial Neuroimaging and Clinical Neuroanatomy

Atlas of MR Imaging and Computed Tomography

Fourth Edition

Heinrich Lanfermann, MD

Professor and Director

Department of Diagnostic and Interventional Neuroradiology

Hannover Medical School

Hannover, Germany

Peter Raab, MD

Senior Staff, Head of Neuroradiological Oncologic Imaging

Institute of Diagnostic and Interventional Neuroradiology

Hannover Medical School

Hannover, Germany

Hans-Joachim Kretschmann, MD

Professor and former Director

Department of Neuroanatomy

Hannover Medical School

Hannover, Germany

Wolfgang Weinrich, MD

Professor and former Head

Neurological Clinic

Nordstadt Hospital

Hannover, Germany

930 illustrations

Thieme

Stuttgart • New York • Delhi • Rio de Janeiro

Library of Congress Cataloging-in-Publication Data

Names: Lanfermann, Heinrich, author. | Raab, Peter, author. | Kretschmann, Hans-Joachim, author. | Weinrich, Wolfgang, author. | Preceded by (work): Kretschmann, Hans-Joachim. Cranial neuroimaging and clinical neuroanatomy.

Title: Cranial neuroimaging and clinical neuroanatomy: atlas of MR imaging and computed tomography / Heinrich Lanfermann, Peter Raab, Hans-Joachim Kretschmann, Wolfgang Weinrich.

Other titles: Klinische Neuroanatomie, kraniale MRT und CT. English | Atlas of MR imaging and computed tomography

Description: Fourth edition. | Stuttgart ; New York : Thieme, [2019] | Preceded by Cranial neuroimaging and clinical neuroanatomy / Hans-Joachim Kretschmann, Wolfgang Weinrich. 3rd ed., rev. and expanded. c2004. | Includes bibliographical references and index. |

Identifiers: LCCN 2018054037 (print) | LCCN 2018055899 (ebook) | ISBN 9783132418172 () | ISBN 9783136726044 (alk. paper)

Subjects: | MESH: Brain Diseases—diagnostic imaging | Brain—diagnostic imaging | Magnetic Resonance Imaging | Radiography | Tomography, X-Ray Computed | Neuroimaging | Atlases

Classification: LCC QM455 (ebook) | LCC QM455 (print) | NLM WL 17 | DDC 611/.810222—dc23

LC record available at <https://lcn.loc.gov/2018054037>

This book is an authorized translation of the 4th German edition published and copyrighted 2015 by Georg Thieme Verlag, Stuttgart. Title of the German edition: Klinische Neuroanatomie – kraniale MRT und CT

Translator: Renee Kulkarni, New Delhi, India.

Illustrators: Ingeborg Heike, Isernhagen, Germany.

Dr. Rudolf Mutschall, Hatten, Germany.

Barbara Gay, Bremen, Germany.

Dr. Peter Raab, Hannover, Germany

1st Italian edition 1989

3rd Japanese edition 2008

1st Portuguese edition 2007 (Brazil)

1st Spanish edition 1988

© 2019 Georg Thieme Verlag KG

Thieme Publishers Stuttgart
Rüdigerstrasse 14, 70469 Stuttgart, Germany
+49 [0]711 8931 421, customerservice@thieme.de

Thieme Publishers New York
333 Seventh Avenue, New York, NY 10001, USA
+1-800-782-3488, customerservice@thieme.com

Thieme Publishers Delhi
A-12, Second Floor, Sector-2, Noida-201301
Uttar Pradesh, India
+91 120 45 566 00, customerservice@thieme.in

Thieme Publishers Rio, Thieme Publicações Ltda.
Edifício Rodolpho de Paoli, 25º andar
Av. Nilo Peçanha, 50 – Sala 2508
Rio de Janeiro 20020-906 Brasil
+55 21 3172 2297 / +55 21 3172 1896

Cover design: Thieme Publishing Group

Typesetting by DiTech Process Solutions, India

Printed in Germany by CPI Books GmbH

ISBN 978-3-13-672604-4

Also available as an e-book:
eISBN 978-3-13-241817-2

Important note: Medicine is an ever-changing science undergoing continual development. Research and clinical experience are continually expanding our knowledge, in particular our knowledge of proper treatment and drug therapy. Insofar as this book mentions any dosage or application, readers may rest assured that the authors, editors, and publishers have made every effort to ensure that such references are in accordance with **the state of knowledge at the time of production of the book**.

Nevertheless, this does not involve, imply, or express any guarantee or responsibility on the part of the publishers in respect to any dosage instructions and forms of applications stated in the book. **Every user is requested to examine carefully** the manufacturers' leaflets accompanying each drug and to check, if necessary in consultation with a physician or specialist, whether the dosage schedules mentioned therein or the contraindications stated by the manufacturers differ from the statements made in the present book. Such examination is particularly important with drugs that are either rarely used or have been newly released in the market. Every dosage schedule or every form of application used is entirely at the user's own risk and responsibility. The authors and publishers request every user to report to the publishers any discrepancies or inaccuracies noticed. If errors in this work are found after publication, errata will be posted at www.thieme.com on the product description page.

Some of the product names, patents, and registered designs referred to in this book are in fact registered trademarks or proprietary names even though specific reference to this fact is not always made in the text. Therefore, the appearance of a name without designation as proprietary is not to be construed as a representation by the publisher that it is in the public domain.



This book, including all parts thereof, is legally protected by copyright. Any use, exploitation, or commercialization outside the narrow limits set by copyright legislation, without the publisher's consent, is illegal and liable to prosecution. This applies in particular to photostat reproduction, copying, mimeographing, preparation of microfilms, and electronic data processing and storage.

Contents

Preface	vii
Preface to the Third edition	viii
Acknowledgments to the Third edition	ix
Contributors	x
Abbreviations	xi
 Part I Introduction	 1
1 Introduction	3
1.1 Aims and Objectives	3
1.2 3D Coordinate Systems for Localization of Brain Structures	6
1.3 Intravital and Postmortem Neuroanatomy	8
1.4 Terminology	9
1.5 Information for Users	9
2 Tomography and Landmarks	11
2.1 Computed Tomography	11
2.2 Magnetic Resonance Imaging	11
2.3 Landmarks of Cross-sectional Imaging	12
2.4 Clinical Significance of Computer and Magnetic Resonance Tomography	15
 Part II Atlas	 17
3 Coronal Sections	19
4 Sagittal Sections	91
5 Transverse Sections	127
6 Brainstem	199
 Part III Topography of the Head and Neck	 223
7 Topography of the Cranium, Intracranial Spaces, and Contained Structures	224
7.1 Cranial Vault	224
7.2 Cranial Cavity	236
7.3 Intracerebral CSF Spaces.....	237
7.4 Cerebral Arteries and their Vascular Territories	257
7.5 Cerebral Veins.....	289
7.6 Cranial Nerves	296
7.7 Subdivisions of the Brain	303
7.8 Brain Maturation.....	346

8	Facial Topography	357
8.1	Facial Bones	351
8.2	Nasal Cavity and Paranasal Sinuses	358
8.3	Orbit	360
8.4	Oral Cavity	364
8.5	Masticatory Apparatus	366
8.6	Lateral Facial Region	366
9	Topography of the Head–Neck Region	369
9.1	Pharynx and Parapharyngeal Space	369
9.2	Craniocervical Junction	370
9.3	Vessels of the Head–Neck Region	373
Part IV Nervous System—Neurofunctional Systems and Neuroactive Substances		
10	Neurofunctional Systems	379
10.1	Sensory Systems	380
10.2	Gustatory System	400
10.3	Ascending Reticular System	400
10.4	Vestibular System	403
10.5	Auditory System	409
10.6	Visual System	416
10.7	Olfactory System	427
10.8	Motor Systems	430
10.9	Cerebellar Systems	450
10.10	Speech Areas	458
10.11	Limbic System	462
10.12	Autonomic Nervous System	470
10.13	Neuronal Networks	472
11	Neurotransmitters and Neuromodulators	483
11.1	Catecholaminergic Neurons	483
11.2	Serotonergic Neurons	485
11.3	Histaminergic Neurons	485
11.4	Cholinergic Neurons	486
11.5	GABAergic Neurons	486
11.6	Glutamatergic and Aspartatergic Neurons	487
11.7	Peptidergic Neurons	487
Part V Appendix		
12	Specimens and Technique	491
13	Bibliography	495
	Index	509

Preface

Is it possible to reinvent a “classic”? This is the question we asked ourselves when Prof. Kretschmann and Prof. Weinrich asked us to produce a new edition of this book.

This is our answer: Judicious advancements and meaningful additions have been made, new chapters on brain maturation and the petrous part of the temporal bone have been included, while existing sections on cranial vessels and “neurofunctional systems” have been elaborated on. It was also essential to adapt axial sections to conventional CT angulation sparing the orbits. The numbering of anatomical structures in the new illustrations was standardized for each double-sided page to allow rapid orientation. Descriptions of the development of cross-sectional imaging have been trimmed, since extremely diverse products are currently made by manufacturers of large equipment, the comprehensive evaluation of which is beyond the scope of this book. It is up to the reader to imagine the huge effort that went into this new edition: The detailed illustrations created by Prof. Kretschmann and Prof. Weinrich are based on the analogous transfer of anatomical cranial sections to high-resolution graphics.

This new edition with Thieme Publishers paves the way for a digital future. This was complex, but ultimately indispensable for access via the Internet. In addition, this required a change in the manner in which illustrations were referenced.

We would like to thank our colleagues of the Institute of Diagnostic and Interventional Neuroradiology, Hannover Medical School, who motivated and assisted us, especially Dr. Paulo Roberto Dellani for the computation and creation of fractional anisotropy graphics. The computation of quantitative susceptibility mapping was possible thanks to the generous cooperation of T. Liu, PhD, Cornell University, New York.

We would also like to thank all those involved at Thieme Publishers, especially Dr. Christian Urbanowicz, Susanne Huiss, MA, Ms. Martina Dörsam, and Ms. Anja Jahn, as well as the editor Dr. Doris Kliem and the graphic designer Ms. Barbara Gay for their exceptional contributions.

The fourth English edition was greatly supported by Mr. Stephan Konnry, Mrs. Gabriele Kuhn-Giovannini, Ms. Joanne Stead, Ms. Sarah Winters, Mr. Rohit Dev Bharadwaj, and Ms. Apoorva Goel (all at Thieme Publishers), as well as by Dr. Renee Kulkami, MD, who was responsible for the translation.

We would like to express our sincere gratitude to all of those who contributed to this fourth English edition.

Heinrich Lanfermann, MD

Peter Raab, MD

Hans-Joachim Kretschmann, MD

Wolfgang Weinrich, MD

Preface to the Third Edition

Our book *Neuroanatomy and Cranial Computed Tomography* first appeared in 1984. At that time computed tomography revolutionized the field of medicine, particularly neurology and neurosurgery. The purpose of the illustrations and text of our book was to provide necessary neuroanatomic information using images of anatomic slices. Our aim was to enable the reader to identify the complex structure of the brain on the monitor for diagnostic purposes to correlate the loss of function with the localization of the cerebral lesion.

The technique of magnetic resonance imaging permitted multiplanar presentations in all desired planes. The second edition, published in 1992 under a new title *Cranial Neuroimaging and Clinical Neuroanatomy*, presented graphic illustrations of anatomic slices in three standard planes.

For the third edition, the old MR and CT images of the atlas have been completely replaced with large-sized illustrations, and the number of images has almost doubled. Therefore, the amount of cerebral structures described has increased considerably. In addition, friends of the former editions encouraged us to introduce the arterial territories of the infratentorial space. Nevertheless, this book is intended as a tool for everyday practice. It aids the physician to correlate the patient's symptoms with the neuroimaging findings. This information considerably facilitates diagnosis and can be of great importance for the choice of therapy. The target readership includes neurologists, neurosurgeons, neuropsychiatrists, neurophysiologists, anatomists, physicians, traumatologists, oncologists, as well as students interested in the neuro-oriented specialties and especially physicians undergoing further training in clinical neurology.

Acknowledgments to the Third Edition

We would like to thank all colleagues engaged in the closely associated departments at the Hannover Medical School. Our grateful thanks especially to Prof. H. Becker, Department of Neuroradiology; Dr. G. Berding, Department of Nuclear Medicine; Prof. K. Gartner, Central Laboratory for Animal Experimentation; Prof. Claudia Grothe, Department of Neuroanatomy; Prof. H. Lippert; Prof. R. Pabst; and Dr. U. Thorns, Department of Functional and Applied Anatomy.

Prof. M. Samii gave us the opportunity to work in the recently opened International Neuroscience Institute (INI) in Hannover. The MR and CT images appearing in the third edition would not have been possible without the help of Prof. U. Piepgras, Dr. T. Liebig, Dr. C. Dalle Feste (INI), Mrs. B. Gehrmann, Mrs. M. Houbolt, and Mrs. A. Hohensee.

Prof. A. Schwartz and P. Brunotte of the Neurological Clinic, Nordstadt Krankenhaus, Klinikum Hannover were kind enough to give critical proposals and valuable clinical suggestions for improvements to the text. Prof. Jean A. Buettner-Ennever from the Institute of Anatomy, Ludwig-Maximilian University of Munich, Munich was most helpful in her comments relating to the vestibular and oculomotor systems.

We would also like to express our thanks to the former coworkers of the Department of Neuroanatomy, Hannover Medical School, who presented excellent dissertations on three-dimensional reconstructions of the functional systems and cerebral arteries: Dr. C. Buhmann, Dr. Andrea Gloger, Dr. S. Gloger, Dr. Anja Schmidt, Dr. Britta Vogt, Dr. H. Vogt, and Dr. D. Weirich. The results of these papers have been mentioned in the text. The technical aspects of our work were supported by Mrs. Nicola van Dornick, Mrs. Ingeborg Heike, and Mr. K. Rust. Dr. Anja Schmidt and Dr. C. Schrader provided invaluable help in correcting the drafts of the manuscripts. Mrs. Claudia Looock, Mrs. Riem Hawi, and Mrs. Zuleyha Demir dedicated many hours to reading through the completed manuscripts for final corrections.

Expertise and clinical advice were imparted by Prof. B. Terwey, Institute for Magnetic Resonance Diagnostics, Zentralklinikum Bremen; Dr. W. Ruempler, Radiological, Oncological and Nuclear Practice, Stade; and by Dr. A. Majewski and R.-H. Prawitz, MRT-Practice, Nordstadt Hannover.

We appreciate the constructive ideas and advice regarding fMRI given by Prof. J. Frahm, Max Planck Institute, Göttingen. J. Graessner, Siemens Hamburg

introduced to us newly specialized technical concepts in the presentation of MR atlas images and was of tremendous support in our work. We dedicate our thanks as well to H. Mahramzadeh, Regionales Rechenzentrum Niedersachsen, Hannover University for his practical assistance in the computergraphic processing of printed copies.

Dr. Gabriele Engelcke, Department of Radiology, Kinderkrankenhaus auf der Bult, Hannover and Dr. G. Glinzer together with Dr. R. Metz, Department of Neurology, Agnes-Karll-Krankenhaus, Laatzen/Hannover were kind enough to assist us with recommended omissions and additions to the texts.

Translation of new chapters and amendments to the third edition were undertaken by Mrs. Nicola van Dornick. Dr. Angela Krönauer kindly checked the complete text for any further changes required. For additional improvements we dedicate thanks to Mrs. Susanne Kretschmann and Dr. Anja Schmidt. The responsibility for the translation rests with the author (Dr. Kretschmann) only.

Following completion of the English manuscript we were grateful for the improvements recommended by M.J. T. FitzGerald, MD, Professor Emeritus of Anatomy, University of Galway, Ireland (author of the informative and awarded book *Clinical Neuroanatomy and Related Neuroscience*, Saunders 2002). For further improvements we thank Dr. V. Beckmann, Röttenbach; Dr. Louise McKenna, Siemens AG, Erlangen; Prof. Ruth G. Ramsey, MD, Medical Director Premier Health Services, Chicago; Dr. H. Requardt, Siemens AG; Erlangen; and Prof. G. Vossius, Institute of Biomedical Technics, University of Karlsruhe.

A big thank you is directed to our respective families for all their patience and understanding during the compilation of the book, especially to Dr. Britta Kretschmann and Mrs. Frauke Weinrich.

Mr. G. Krüger, Production Director of Thieme Publishers has been a supervisory figure behind our book since 1984 and is responsible for the excellent didactic compilation and the make-up of our work. Last but not least, we would like to express our thanks to Dr. C. Bergman, Dr. T. Pilgrim, and Dr. O. Schneider at Thieme Publishers for their loyal cooperation in the presentation of the text and illustrations of our book.

*Hans-Joachim Kretschmann
Wolfgang Weinrich*

Contributors

Eva Bültmann, MD

Senior Staff, Head of Neuroradiological
Pediatric Imaging
Department of Diagnostic and
Interventional Neuroradiology
Medical University Hannover (MHH)
Hannover, Germany

Anja Gieseemann, MD

Department of Diagnostic and
Interventional Neuroradiology
Medical University Hannover (MHH)
Hannover, Germany

Dina Wittfoth, MSc, PhD

Department of Diagnostic and
Interventional Neuroradiology
Medical University Hannover (MHH)
Hannover, Germany

Abbreviations

2D/3D	2-/3-dimensional	MEG	Magnetoencephalography
A	Anterior	MIP	Maximum-intensity projection
ACC	Anterior cingulate cortex	MPFC	Medial prefrontal cortex
ACTH	Adrenocorticotrophic hormone	MR	Magnetic resonance
AEP	Auditory evoked potential	MRA	Magnetic resonance angiography
AICA	Anterior inferior cerebellar artery	MRI	Magnetic resonance imaging
BA	Brodman's area	MRS	Magnetic resonance spectroscopy
BERA	Brainstem evoked response audiometry	MST	Medial superior temporal
BOLD	Blood oxygenation level dependent	MT	Middle temporal
CD-ROM	Compact disc read-only memory	MTG	Middle temporal gyrus
CHARGE-syndrom	Coloboma, heart defects, atresia choanae (also known as choanal atresia), growth retardation, genital abnormalities, and ear abnormalities	OCT	Optical coherence tomography
CNS	Central nervous system	OFA	Occipital face area
CSF	Cerebrospinal fluid	OFC	Orbitofrontal cortex
CT	Computed tomography	P	Posterior
CTA	Computed tomographic angiography	pACC	Paracingulate cortex
DAB	Diaminobenzidine	PC	Personal computer
DH	German horizontal	PCC	Posterior cingulate cortex
DLPFC	Dorsolateral prefrontal cortex	PET	Positron emission tomography
DMPFC	Dorsomedial prefrontal cortex	pgACC	Perigenual anterior cingulate cortex
DSA	Digital subtraction angiography	PICA	Posterior inferior cerebellar artery
DTI	Diffusion tensor imaging	PMA	Premotor area
DTPA	Diethylenetriaminepentaacetic acid	PPA	Parahippocampal place area
EEG	Electroencephalography	PPRF	Paramedian pontine reticular formation
FCAT	Federative Committee on Anatomical Terminology	PRL	Prolactin
FEF	Frontal eye field	QSM	Quantitative susceptibility mapping
FFA	Fusiform face area	R	Right
FISP	Fast imaging with steady preces	rs-fMRI	Resting-state functional magnetic resonance imaging
FLAIR	Fluid attenuated inversion recovery	S	Superior
FLASH	Fast low-angle shot	sACC	Subgenual anterior cingulate cortex
fMRI	Functional magnetic resonance imaging	SEP	Somatosensory evoked potential
FSH	Follicular stimulating hormone	SMA	Supplementary motor area
GABA	Gamma-aminobutyric acid	SOM	Supraorbital-meatal
GH	Growth hormone	SOSO	Supraorbital-suboccipital
I	Inferior	SPACE	Sampling perfection with application optimized contrasts using different flip angle evolutions
IFG	Inferior frontal gyrus	SPECT	Single-photon emission computed tomography
IOG	Inferior occipital gyrus	SPL	Superior parietal lobule
IPC	Inferoparietal cortex	STG	Superior temporal gyrus
IPL	Inferior parietal lobule	STH	Somatotropin hormone
IPS	Intraparietal sulcus	STS	Superior temporal sulcus
IV	Intravenous	SWI	Susceptibility-weighted imaging
L	Left	T1w	T1-weighted
LH	Luteinizing hormone	TOF	Time of flight
LO	Lateral occipital complex	TSE	Turbo-spin echo
M	Median plane	TSH	Thyrotropic hormone
MA	Meynert axis	VEP	Visual evoked potential
MCC	Middle cingulate cortex	VIP	Vasoactive intestinal polypeptide
MEDI	Morphology-enabled dipole inversion	VLPFC	Ventrolateral prefrontal cortex
MEDIC	Multiple-echo data image combination	VMPFC	Ventromedial prefrontal cortex
		VRT	Volume rendering technique

Part I

Introduction

1	Introduction	03
2	Tomography and Landmarks	11



1 Introduction

1.1 Aims and Objectives

Computed Tomography and MRI allow rapid and detailed diagnosis of circulatory disturbances, intracranial bleeding, other space occupying lesions as well as disorders of CSF circulation. These imaging methods are therefore of prime importance in the diagnostic armamentarium.

Modern **neuroimaging** is moreover employed for objective **follow-up**, for example, in documenting spontaneous regression of subdural hematomas and hygromas or the need for surgery thereof. MRI is an invaluable clinical tool in the diagnosis and **treatment follow-up** of multiple sclerosis and has furthered the development of new therapeutic concepts and monitoring of their efficiency. MRI being highly sensitive allows detection of small, millimeter-sized tumors (e.g., pituitary microadenomas, intracanalicular vestibular schwannomas) so that these may be successfully removed by microsurgery without loss of function.

Alongside diagnostic radiology, **interventional neuroradiology** has also gained in importance. This allows generally safer treatment of acute circulatory disorders in strokes and vascular malformations like aneurysms and arteriovenous fistulae, as compared to open surgery.

Widespread availability of the fascinating diagnostic capabilities of modern imaging methods may actually prove **disadvantageous** and even harmful for patients. It is not always possible to diagnose or exclude all intracranial, cerebral, or meningeal diseases with CT or MR. Unilateral symptoms do not always have a cerebral origin. Pathological findings evident on imaging at first sight are not always responsible for the patient's symptoms. Correlation between pathological findings seen on imaging and the patient's symptoms requires functional and topical knowledge of anatomy, which the present form of this book aims to facilitate.

The acquisition of knowledge in neuroradiology, neurology, neurosurgery, psychology, psychiatry, and neuroscience is an on-going process. Pathological findings have neither been described nor depicted in our illustrations, for which one would need to refer to relevant neuroradiological textbooks.^{22,87,258,272,441,511,557,653,654,655} Every referring physician and radiologist should be familiar both with merits and with limitations of neuroradiological techniques. This would prevent wrong investigations being performed at the wrong time and at the wrong site. Both the examiner and the referring physician should be aware of concrete facts pertaining to pathogenesis of disease (age of hemorrhage or an infarct, also inflammation, etc.).

The neurosciences continue to have high expectations of neuroradiology and further advancements therein; this applies especially to MRS, further developments in spiral CT and particularly to MRI. We therefore placed **MR and CT images of nearly the same size** as large-format anatomical atlas illustrations side-by-side. Some

atlas images required correction of details in instances where new or more precise information was available in literature or fresh insight was obtained through our own studies.

Tomographic images of the human body are obtained using modern **digital imaging methods**. Depicted slices are usually 1 to 10 mm in thickness. These slices are composed of small cuboids (so-called voxels; the term **voxel** is a contraction of two words, "volume" and "element"). Its height corresponds to slice thickness and the length of its edge to the image matrix. X-ray absorption and signal intensity are determined for every voxel in CT and MRI, respectively (see Sections 2.1 and 2.2). The calculated measurement from a voxel is assigned a gray value or a color as pixel on a monitor or film base (the term **pixel** is a contraction of two words, "picture" and "element").

Transverse (axial) sections (perpendicular to the body's long axis) are normally examined in **CT** due to the requisite rotational movement of the scanner. Frontal (coronal) sections are obtained by reformation. One of the advantages of **MRI** is that the sectional plane may be freely selected. Modern, spiral (**helical**) CT scanners do not obtain data by scanning objects slice after slice and then processing it. Instead a powerful X-ray tube rotates constantly around the patient's body while the patient continuously moves through the scanning field. A data set is thus obtained from a large measuring volume (volume scan) and is then secondarily processed to acquire an image. Thus, any slice position and slice thickness may be computed and selected from the volume data set. Scan times of multislice spiral CT lie well under a minute. 3D reconstruction of interesting structures may be obtained using sophisticated software and a powerful workstation. Multiplanar and 3D reconstruction thus allows high resolution visualization of cranial blood vessels (CTA) after IV bolus injection of contrast medium.

Digital cross-sectional imaging methods required **reorientation of the depiction of brain anatomy** with development of a modified topographical orientation for clinical applications. Traditional **neuroanatomy** is based on the development of the mammalian brain. The human forebrain developed an obtuse angle with the brainstem from an originally stretched out horizontal position as a result of pronounced brain development during evolution and the upright posture. Neuroanatomy of the human brain is depicted in at least two series of slices in many textbooks: One series of images (so-called frontal series) is aligned perpendicular to the long axis of the forebrain (**Forel axis**), while the other is perpendicular to the long axis of the brainstem (**Meynert axis**). This approach is especially practical for comparative neuroanatomy, allowing for a better comparison of neuroanatomical findings in animals with those in humans. The axes of the forebrain and the brainstem in most mammals approach a nearly straight line. In contrast

however the two long axes in the human brain form an obtuse angle of about 110 to 120° with each other. There exists, therefore, no ideal reference plane for transverse sections in humans, such that images obtained simultaneously for the forebrain and the brainstem conform to conventional neuroanatomical images.

Transverse sections parallel to the bicommissural line are obtained in MRI; this line runs through the midpoint of the anterior and posterior commissures. CT sections are conventionally obtained in a plane tangential to the roof of orbit (supraorbital-meatal line) due to its good

reproducibility while allowing protection of the radio-sensitive lens of the eye. In everyday work however the supraorbital-suboccipital line (see ► Fig. 1.1) is identified more quickly on the scout image (scout, localizer, topogram). This does not differ significantly from the supraorbital-meatal line and helps avoid planning delays resulting from poorly delineated contours of the internal auditory canal due to well pneumatized mastoids.

Ambrose¹³ preferred the bicommissural plane as the reference plane for CT, which connects the lateral angle of the eyelid (canthus) with the external auditory canal. This

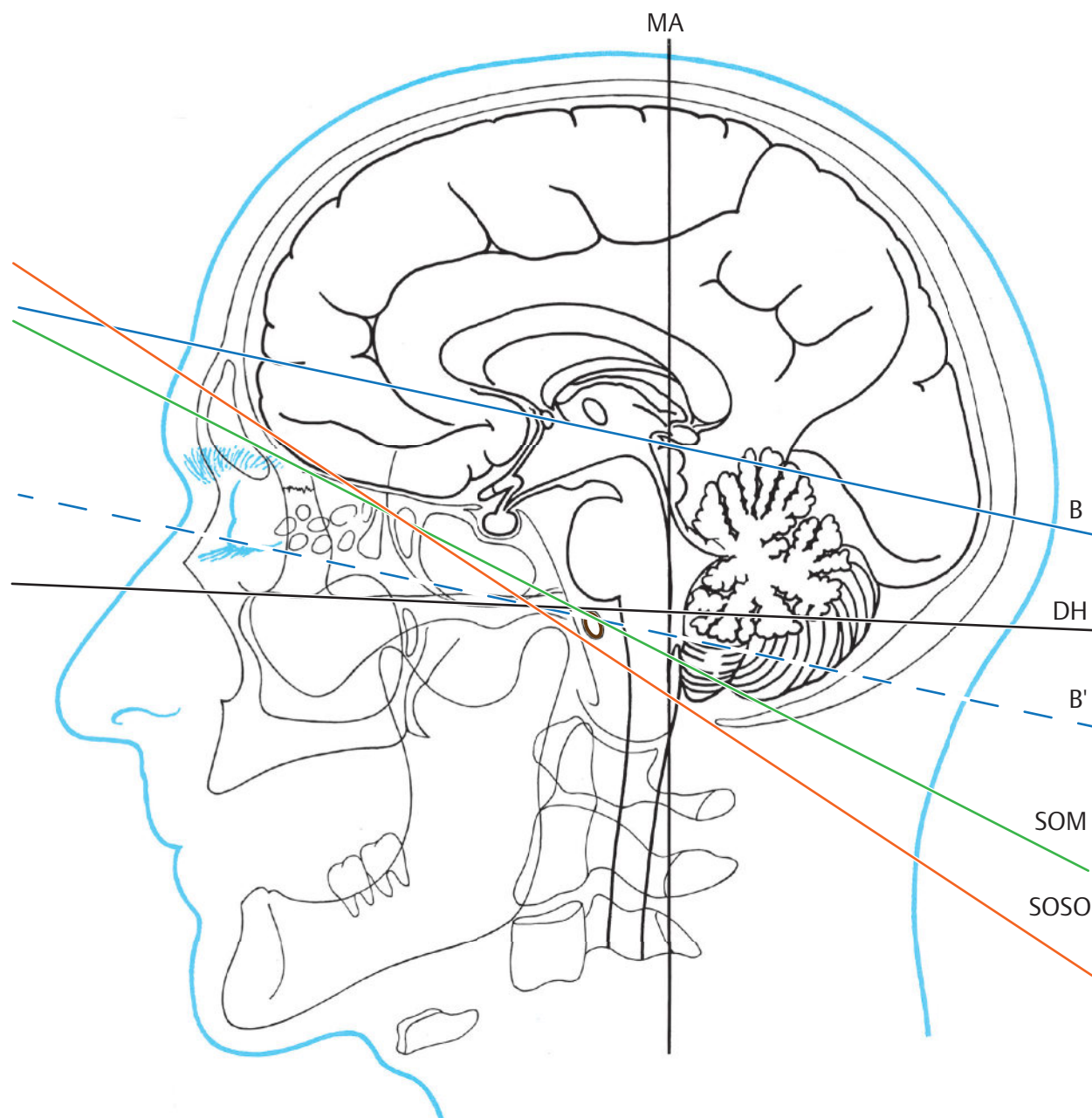


Fig. 1.1 Position of present and historical transverse (axial) slice angulations.

B = Bicommissural line (blue)
 B' = Copy of the bicommissural line (dotted blue)
 DH = Reid's base line (black)
 MA = Meynert axis (black)
 SOM = Supraorbital-meatal plane (green)
 SOSO = Supraorbital-suboccipital plane (red)
 External acoustic canal (brown)

historical sectioning plane has not been taken into account in the present new edition. The characteristics of these transverse imaging planes are described in Section 1.2.2.

Obtained intravital images oriented along sections running parallel to the frontal, bicommissural (MRI), and supraorbital-suboccipital planes differ from conventional neuroanatomical images acquired postmortem (see Section 1.3). The benefits of new cross-sectional imaging methods can however be fully exploited only when sufficient knowledge of 3D structures is available. A series of works were thus published in the last three decades, which reproduced macroscopic anatomy in transverse and multiplanar planes.^{60,208,219,333,442,532,572} Neurofunctional systems cannot however be depicted solely macroscopically since they are composed of macroscopic and microscopic findings and are especially developed from hodological outcomes. Hodology is the study of neuronal interconnections in the central nervous system. Thus, even the most refined techniques of macro- and microphotography of brain sections preclude the imaging of synaptic circuitry of individual neurofunctional systems.

This book therefore aims at the following:

1. **Depiction of brain anatomy in the atlas section of the book in the three conventional planes used in cross-sectional imaging:** Anatomical sections were employed to achieve this end. A drawing technique was developed for quick yet precise orientation, whereby anatomic structures were adapted to gray-scale CT and MR images. Gray scale T1-weighted MR images (see Section 2.2) correspond only partially to graphic illustrations. The illustrations however do not make an allowance for the wide spectrum of MR signal intensities of biological structures, which in turn depend on the selected examination sequence. Corresponding large-format CT and MR images in the atlas section (colored stripes at the edges) should enable readers to draw comparisons. All illustrations in the atlas section were derived from original preparations, see Chapter 12 (coronal and sagittal series, brainstem series), from test subjects (axial MRI series) or patient images (axial CT series). Macrophotography can only reproduce the surface of the slice. In contrast, CT and MRI display the contents of a slice since they transform voxels into pixels, as described. Illustrations are advantageous since important neuroanatomic structures like tracts and nuclei, not visible at the surface since they lie within the slice, may be graphically represented by interrupted lines or hatched areas. Microscopically recognizable structures, such as certain cortical areas, which could not have been depicted in isolation using macrophotography, have also been incorporated in our illustrations. The atlas images of this book (see ► Fig. 3.2 to ► Fig. 3.15, ► Fig. 4.2 to ► Fig. 4.7, and ► Fig. 5.2 to ► Fig. 5.30) were reproduced true to scale **in definite coordinate systems** in accordance with similar principles such as those in stereotactic atlases^{6,16,63,514,573,574} so that anatomical and neuroanatomical structures of the “model brain” could be rendered over a patient’s brain using a definite coordinate system. A detailed explanation for the above is outlined in Section 1.2.
2. **Graphic rendition of principal arterial territories in the supra- and infratentorial regions:** Blood vessels and their vascular territories have been depicted in detail in the coronal, sagittal, and transverse planes and compared with angiographic images. This should simplify the interpretation of CTA and MRA images and correlation of CT and MR findings with angiographic images (DSA) for clinicians. A depiction of the variability of vascular territories, which may be enabled by in vivo MRI methods of arterial spin labeling, have deliberately not been touched upon.
3. **Description and imaging of principal neurofunctional systems in multiplanar parallel slices:** The main tracts of the neurofunctional systems have been graphically represented in transverse sections, the most important of these additionally in coronal and/or sagittal sections. Equidistant slices were employed for this purpose in a right-angled coordinate system. The distance between two planes of the coronal, sagittal, and bicommissural series was 1 cm and 5 mm in the brainstem series, respectively. True-to-scale illustrations of slices have been positioned in a gray environment in such a manner that they are viewed vertically from below on the bicommissural (MRI) and supraorbital-suboccipital (CT) oriented parallel sections as well as from the front on the coronal and from the left on sagittal parallel sections. The observer can thus imagine a 3D reconstruction of individual structures through true-to-scale reproductions and optimal positioning of individual slices in a 3D coordinate system, as in the drawings in Chapters 6 to 9, or neurofunctional systems, as in the drawings in Chapter 10. A computerized graphic rendition of neurofunctional systems and the large arteries of the brain over and above the selected tomographic images (pertains to the third edition) has been published as a book and as CD ROM^{312,313} where these systems have been rendered in pseudo-3D and 3D. Real 3D reconstructions in different projections and combinations may be acquired on a PC using red–blue glasses.
4. **Elucidation of the relationship of the topography of neurofunctional systems with the site of a lesion and its clinical symptoms:** Individual neurofunctional systems and their cardinal symptoms have been described. This spatial knowledge will define investigations more precisely. Consensus between the clinical syndrome and the lesion detected on tomography confirms the topical diagnosis. Discrepancy between clinical symptoms and CT or MR findings requires a reevaluation of clinical findings and further diagnostic procedures. Moreover, the spatial relationship of the site of the lesion to neurofunctional systems may be indicative of prognostic outcome.
5. **Magnified rendition of the brain stem supplemented by T1w and T2w MEDIC–MR images:** Nuclei and

tracts lie closely packed together in the brain stem and therefore require magnification for their graphic representation. Thus, a brain stem series in 5 mm slices was appended to the bicommissural oriented axial series in a coordinate system defined by the Meynert plane. Bony artifacts in CT preclude satisfactory imaging of these fine structures. Only with MRI is low-noise imaging of the brain stem possible; signal loss induced by the clivus or the sphenoid sinus may occur in the MEDIC sequence.

Anatomical structures and their variants, relevant for everyday practice, have been depicted in the text of this book. We restricted ourselves to presently available and reliable findings pertaining to neurofunctional systems. Speculative information and not generally accepted research findings have not been taken into account.

The atlas, text, and supplemental illustrations focus on the depiction and description of neuroanatomy of the brain and its neurofunctional systems. The normal topography of the head and the craniocervical junction has also been discussed and depicted in illustrations, as diseases of these regions may spread to the brain and vice versa. Of prime importance is **normal cross-sectional anatomy** with presently feasible CT and MR representation of intravital anatomical relationships, while keeping functional aspects in mind. Special settings, magnified images or contrast medium administration for optimal imaging of individual regions, or structures (pituitary, blood vessels, etc.) have been dispensed with. Graphic representation and rendition of MR and CT images of pathological changes have been intentionally omitted. The text provides some information pertaining to pathological changes with clinical correlation. The physician thereby receives suggestions for optimal investigations in order to improve the meaningfulness of the chosen diagnostic study. A suitable imaging procedure may be selected while taking into account examination findings and neurophysiological data, simplifying investigations with a targeted approach and thereby optimizing treatment.

Interdisciplinary knowledge is an important prerequisite for optimal use of and comprehensive assessment by modern cross-sectional imaging methods. While the neuroradiologist requires a functional knowledge of anatomy to be able to deal with clinical problems in a competent fashion, the neurologist, neurosurgeon, radiation therapist, physician, pediatrician, etc. need to be familiar with both capabilities and diagnostic strengths of modern cross-sectional imaging methods. The objective of this book is to bridge the gap between the two in a simplified, universally understood manner.

1.2 3D Coordinate Systems for Localization of Brain Structures

The philosopher and mathematician Descartes (Latin: Cartesius) described analytical geometric fundamentals of 3D coordinate systems in 1637. Coordinate systems

are intermediaries between points and numbers. Every point in space may be specified by a right-angled or a Cartesian coordinate system. Numbers represent the distance from the respective x-, y- or z-axis, which intersect at their origin or zero point.

In 1906, Clarke and Horsley introduced the Cartesian coordinate system for the localization of brain structures during brain research on experimental animals. An apparatus was constructed using brass in accordance with Clarke's concept, whose coordinate system was aligned along the median plane of the head, the plane passing through the external auditory canal and the superior orbital margin. This orientation served as a platform to localize and examine individual brain structures for experimental research.⁶³ This stereotactic technique was used in humans only 40 years later. Spiegel and Wycis performed the first stereotactic operation on a patient's brain in 1947. Extra- or intracerebral coordinate systems have been in use since then.

1.2.1 Sagittal Planes

An important plane of orientation for coordinate systems of the human head is the median plane, which divides the "bilaterally symmetrical" head into two nearly equal halves. Clarke and Horsley deduced that asymmetry of the human head was more pronounced than that of cats and rhesus monkeys. The median plane is frequently defined as the yz- plane of coordinate systems. This plane is easy to set up as compared to the others since bilaterality aids orientation. Planes parallel to the median plane are the sagittal planes.

1.2.2 Transverse Planes

Various sloping transverse planes are employed in the neurosciences. The **German horizontal** (= Frankfurt horizontal) connects the inferior orbital margin with the superior margin of the external acoustic aperture (see ► Fig. 1.1; see also ► Fig. 5.1, label "DH"). Reference points of Reid's plane (baseline) are the inferior orbital margin and the midpoint of the external acoustic aperture.

The bicommissural plane connects the lateral angle of the eyelid (canthus) with the center of the external acoustic aperture. Ambrose¹³ described this plane as the "orbitomeatal plane." This term is however also used for the German horizontal plane. To avoid any confusion however the term "bicommissural plane" should be used in preference to "orbitomeatal plane."

Digital X-ray scout images (scout view, topogram) in **CT examinations** allow a highly reproducible angulation of the sectional plane tangential to the roof of orbit and to the inferior wall of the posterior edge of the foramen magnum (**supraorbito-suboccipital line**).

Due to the widespread clinical use of this sectional plane, appropriately angulated CT sections have been added in the new edition (see ► Fig. 5.16). Advantages are rapid alignment of the plane along the roof of orbit by tilting the gantry, high intraindividual constancy

and exclusion of the lens of the eye from the radiation field in most examinations, which also make it feasible for examinations of the posterior fossa. The central sulcus together with the adjoining precentral gyrus is seen lying more anteriorly in supraventricular sections as compared to images parallel to the bicommissural plane.

Magnetic Resonance Imaging Examinations

The patient is positioned as comfortably as possible for MR examinations of the brain to prevent movement artifacts. A median slice is obtained for anatomical orientation. Transverse sections are usually obtained next. Supplemental coronal and/or sagittal images are then obtained depending on the problem to be addressed.

A uniform reference plane is desirable for standard examinations in order to avoid additional topographic variability due to diverse tomographic angles. MR images have been obtained parallel to the **bicommissural plane** (see ►Fig. 5.2 to ►Fig. 5.15) for atlas illustrations in the transverse plane, while those for the brain stem have been obtained perpendicular to the Meynert axis (see ►Fig. 6.3 to ►Fig. 6.13, brainstem series); MR images of the brainstem series conform to this angulation.

The **bicommissural line** as defined by Talairach^{573,574} is a line passing through the superior edge of the anterior commissure and the inferior edge of the posterior commissure. Sampling of 50 brains showed an average angulation difference of less than 2° between the bicommissural plane and the bicommissural line. Extreme deviations lay at +9° and -5° (standard deviations = 1.4).

Coronal Planes

The sectional planes selected for the coronal series of atlas drawings in this book lie perpendicular to the German horizontal (see ►Fig. 3.2 to ►Fig. 3.15). The German horizontal was determined on the cephalogram (see ►Table 12.1) and transposed to the scalp. Precise coronal sections were obtained with the aid of a right angle and a special adjustment, as described in Chapter 12. MR and CT images conform to this angulation. The frontal plane was also named the "coronal plane." A coronal plane constructed through the center of the zig-zag coronal suture intersects the German horizontal at an angle of about 65°, unlike the frontal plane which intersects at 90°. Coronal and transverse sections allow a comparison of sides as a result of bilateral symmetry, thereby enabling easy identification of space-occupying lesions, circumscribed atrophy and abnormalities in density and signal intensity. Isolated, unhalved brains lack reference planes. Thus, illustrations of coronal sections of the brain in conventional atlases often differ significantly due to varying reference angles.^{115,132,238,446,472} Topography of brain structures when so modified may thereby simulate a variation.

Intracerebral Coordinates

Examination of the Supratentorial Region

Experience with stereotactic intervention has shown that bony and extracerebral reference planes for brain structures exhibit greater variation as compared to intracerebral reference systems.⁶³ Neurosurgeons most commonly use an intracerebral orientation plane for the supratentorial region which originates from the bicommissural plane. As mentioned earlier, the **bicommissural line**, as defined by Talairach, passes through the superior edge of the anterior commissure and the inferior edge of the posterior commissure since these structures were easily identifiable during ventriculography. Modern MR techniques allow precise determination of both commissures in the median plane. The diameter of the anterior commissure varies between 2 and more than 5 mm. A comparison between the bicommissural line in accordance with Talairach and a bicommissural line passing through the midpoints of both commissures can result in deviations of 7°. This may lead to deviations of more than 1 cm at the outer aspect of the brain with an average length of 17 cm between the frontal and occipital poles of the brain. Potential mistakes in the localization of brain structures may therefore be avoided if the **bicommissural line** is used, defined as a line running between the midpoints of the anterior and posterior commissures. In addition, the midpoints of both commissures may be more precisely determined than their margins as a consequence of the partial volume effect. The definition of the bicommissural line, running through the midpoints of both commissures, should be internationally accepted. The midpoint of the line between the anterior and posterior commissures may be used as the origin of this bicommissural coordinate system.

A direct comparison of sides is not feasible on **sagittal sections**. The only reference plane for parallel sagittal sections is the median plane, the special advantage of which is the feasibility of identifying and assessing midline structures of the brain, especially the brainstem. The gyri and sulci on the surface of the brain are also well visualized. The paramedian parieto-occipital sulcus and the calcarine sulcus are thus well seen, while the central sulcus and the lateral sulcus are identified over the convexity with their accompanying gyri. Reference planes essential for intracerebral coordinate systems (bicommissural and Meynert planes) are easily discernable in the median plane. The bicommissural line and the German horizontal have been used in sagittal images in the atlas section of this book. The selected **bicommissural line** passes through the midpoint of the anterior and posterior commissures and runs in the bicommissural plane, which lies perpendicular to the median plane (see ►Fig. 4.2). The bicommissural plane enables a comparison with stereotactic atlases^{16,514,573,574} while allowing 3D orientation with reference to extracerebral structures like cranial nerves, blood vessels, bones, and soft tissue structures, which have not been listed in the

aforementioned atlases. According to Steinmetz et al⁵⁵⁹ the great variability of the cortical gyri and sulci of the cerebrum limits the use of standardized localization systems, such as the Talairach stereotactic system.^{573,574} Neuroradiological landmarks have therefore been developed for clinical practice such that clinically important and significant gyri and sulci may be identified (see ► Fig. 7.52).^{231,642}

Examination of the Infratentorial Region

A Cartesian coordinate system is used for the infratentorial region, the main planes of which are the median plane, the plane through the floor of the IVth ventricle (Meynert plane) and the fastigial plane.⁶ The **fastigial plane** lies perpendicular to the median plane and to the floor of the IVth ventricle and runs through the fastigium (see ► Fig. 6.3). The straight line which runs in the median plane tangential to the floor of the IVth ventricle is called the “Meynert axis.” It determines the Meynert plane, which lies perpendicular to the median plane. The origin or zero point of this coordinate system is the intersection of the three aforementioned planes. The brainstem series of the atlas section (see ► Fig. 6.4 to ► Fig. 6.13) has been drawn up in this coordinate system. Magnified depiction of the brainstem (see ► Fig. 6.4b to ► Fig. 6.13b) takes into account the spatial density of nuclei and tracts as well as the clinical significance of these structures.

Coordinate Systems

These geometrical–analytical considerations for the localization of anatomical structures have been implemented by the manufacturers of the CT, MR, and PET equipment such that their images are depicted in a coordinate system. A depicted scale or the letters L (left) and R (right) aid orientation in this coordinate system.

Coordinate crosses or frames are used in stereotactic atlases.^{16,63,514,573,574} Their advantage over conventional atlases lies in enabling a better mental reconstruction of complicated brain structures such as the caudate nucleus, subthalamic nucleus, the internal capsule, or the central sulcus with the help of orientation planes aligned in the coordinate system or in the coordinate frame, in order to trace their course in multislice scans and thereby enable lesional correlation both anatomically as well as neurofunctionally. For these reasons, the four slice series of this book have been divided and illustrated in defined coordinate systems.

The idea of using **coordinate systems** for the localization of bony structures may also be applied to the mental reconstruction of complicated bony regions, such as the facial canal or the inner ear in the petrous part of the temporal bone. Bony reference planes, such as the German horizontal, the infra- or the supraorbital planes, retain their localizing significance for the surgeon, who must orient himself with the skull prior to operative interventions in order to spare venous sinuses and arteries during surgical procedures.

Inconsistencies of the positional relationship of the cranial bones and the brain may be demonstrated with the help of the German horizontal and the meatoververtical line. The meatoververtical line lies perpendicular to the German horizontal and runs through the midpoint of the external acoustic aperture. A study of 25 heads showed that the larger group (14 heads) was of a frontopetal type and the smaller group (11 heads) of an occipitopetal type.¹⁷⁹

- The cerebrum appears to be anteriorly displaced on a lateral view of the **frontopetal** type skull. The central sulcus runs more steeply upwards than in the occipitopetal type. The occipital lobe of the cerebrum lies far above the German horizontal. The occipital bone is shorter than that in the occipitopetal type on the lateral view.

The cerebrum is displaced more posteriorly on a lateral view of the **occipitopetal** type skull. The central sulcus does not extend so steeply upward but extends further backward as in the frontopetal type. The base of the occipital lobe lies just above the German horizontal or touches it.

1.3 Intravital and Postmortem Neuroanatomy

The differences between intravital and postmortem brain morphology became conspicuous with the introduction of CT and MRI. Air collects in the subarachnoid space after death. Gray–white matter differentiation becomes indistinct postmortem, especially in CT images. Blood flow signals and flow-related signal losses are not visualized on MR images after death.

Postmortem MR images of intracranially fixed brains show so many artifacts that in vivo MR images are considered more suitable for comparison with anatomical atlas images rather than postmortem MR tomograms. We therefore preferred using comparable intravital MR images of other individuals instead of MR images obtained from the same biological specimens used for atlas illustrations.

Changes occurring postmortem and those induced by histological techniques must be borne in mind when the findings observed in anatomical specimens are transposed to the living. Precise determination of volumes of the intracranial compartment, blood, **cerebrospinal fluid**, and brain tissue is difficult both in intravital and postmortem states. There are reasons to believe, however, that cerebrospinal fluid partially permeates into the brain tissue postmortem. This is indicated by the measurements of cerebrospinal fluid volumes.⁵³⁴ The volume of CSF spaces decreases after death. In 159 examined cases, cerebrospinal fluid volume was on an average 100 mL 3 hours postmortem and only 49 mL approximately 21 hours later.⁵³⁴ The difference between the volumes of the cranial cavity and the brain is smaller postmortem.⁴⁴⁴ Brain volume increases after death due to CSF absorption, which is influenced by the time interval between death and sectioning. Given

median volumes of 100 to 150 mL for CSF and 1200 to 1400 mL for the brain in the adult, errors of about 5% are expected with consistent postmortem diffusion of half the CSF into the brain. With probable nonlinear diffusion, volume increase postmortem will be correspondingly greater for the involved areas in the brain. The postmortem size of the cisterns can only be approximately transposed to in vivo conditions.

The proportion between the brainstem and the forebrain usually changes during extracranial fixation of brains. The brain is usually suspended from the basilar artery during fixation. Due to its slightly higher specific gravity as compared to the formalin fixation mixture, the end brain suspended in the container sinks downwards, particularly the occipital lobe, thereby changing its position and dimensions relative to the brainstem. Sections of extracranially fixed brains may therefore differ markedly from their in vivo counterparts. Intracranially fixed brains are preferred over those which have been extracranially fixed as far as the comparison of tomographic images with anatomical sections is concerned. All atlas drawings of the coronal and sagittal series as well as the brainstem series in this book are based on **intracranially fixed brains**, as elucidated in Chapter 12.

The brain loses 40 to 50% of its volume during paraffin or celloidin embedding processes in the production of **histological sections**.^{233,310} The brain does not shrink evenly when embedded in paraffin: The gray substance with its higher water content than white matter loses more volume. The frontal cortex containing about 84% of water shrinks on average by 51%, while white matter containing about 71% water shrivels by 42%.³¹¹ The size and shape of the brain structures can only be transposed with constraints from histologic specimens to in vivo conditions.

1.4 Terminology

International anatomical nomenclature enables better international communication. A new committee on anatomical terminology (Federative Committee on Anatomical Terminology) of the parent body of the National Associations of Anatomists (International Federation of Associations of Anatomists) includes representatives of national anatomical societies. All anatomists were allowed access to their suggested nomenclature for purposes of discussion. The final version was decided upon in 1997 and published in 1998 as **Terminologia Anatomica**.¹⁶² The equivalent English term was placed against each Latin anatomical name for the first time, thus permitting scientists and doctors worldwide to use the identical names for anatomical structures, an essential prerequisite for international medical communication. We have therefore used the *Terminologia Anatomica*.

The directional terms “cranialis” and “caudalis” have been replaced by “superior”/“inferior” and “ventralis”/“dorsalis” by “anterior”/“posterior” when referring to anatomical directions of the head in the *Terminologia Anatomica*. Topographical relationships of the head

are therefore termed “superior” or “inferior” and “anterior” or “posterior”. Eponyms have been specified in non-Latinized forms without declensions.

The *Terminologia Anatomica* distinguishes between “arteria” and “ramus” with respect to individual arteries. The diameter of these so-called rami is often larger than that of arteries (e.g., parietooccipital ramus and anterolateral central arteries). The term “ramus” is also common to branches of veins, nerves, bones, and bronchi. The unambiguous term “artery” has therefore been used for all arterial branches^{307,601} in accordance with clinical parlance.

1.5 Information for Users

The **atlas and serial images** of this book have been described in the following order: Coronal sections (see ► Fig. 3.2 to ► Fig. 3.15) have been arranged from anterior to posterior (anteroposterior), the sagittal sections of the right half of the head (see ► Fig. 4.2 to ► Fig. 4.7) from medial to lateral, and transverse sections (see ► Fig. 5.2 to ► Fig. 5.15 and ► Fig. 6.4 to ► Fig. 6.13) from inferior to superior. With the introduction of whole-body CT, transverse images were reproduced as being viewed from inferior. The left side of the body thus appears on the right in the image. This display has established itself almost universally in MRI and the CT of the head. For CT interpretation of a slice, conversion of voxels to pixels makes viewing from above equivalent to viewing from below—the designation of sides as “left” and “right” must however be kept in mind. MRI and CT correspond to volume analysis of slices rather than their superficial evaluation. What is important for the visual representation of an anatomical slice, however, is whether the image originates from the upper or lower aspect of the slice.

Slice numbers important for **spatial localization** of individual parallel slices have been specified in the following illustrations:

- For the 14 coronal sections in ► Fig. 3.1
- For the 6 sagittal sections in ► Fig. 4.1
- For the 14 sections of the transverse MR series in ► Fig. 5.1
- For the 14 sections of the transverse CT series in ► Fig. 5.16
- For the 10 sections of the brainstem series in ► Fig. 6.3

Slice numbers in the corresponding serial images have been highlighted by a special symbol (**encircled number**). The encircled slice number can be looked up in the aforementioned illustrations of the respective series for easy orientation.

The **atlas section** of the book has been provided with yellow **tabs** at the outer edge, to facilitate locating the individual series. **Anatomical structures** have been indicated by **numbers** in the illustrations. Where possible, these numbers form the main visual focus of the structure. A reference line helps where this is not graphically feasible. Numbers in the illustrations have

been listed consecutively from left to right and from top to bottom, which conforms to our reading habits. Exceptions are regions with dense numbering, where topographically adjacent structures have been consecutively labeled. Symmetrical paired structures have been numbered once. Paired structures lying in different positions (e.g. in the right and the left hemispheres) have been identified twice with the same number. A structure repeatedly encountered in a section, for example, the superior sagittal sinus (see ►Fig. 5.14b and ►Fig. 5.29a), retains its index number (e.g., “2”). The same structure in serial images has been given two different identification numbers if it has been differently sectioned, for example, head of caudate nucleus not sectioned (located at the posterior aspect of the slice, see ►Fig. 10.28), and the head of the caudate nucleus sectioned by the slice (see ►Fig. 10.28). **Each double page in the atlas has separate numbering, whereby the allocation of numbers on related facing pages is identical for easier retrieval.** A missing number with its label on the MR image on a double page implies that the corresponding anatomical structure can only be delineated in the schematic drawing and not in the corresponding MR image. Anatomical structures in MR legends have been assigned a differently colored numeral if they can be seen on the MR image but not on the schematic drawing. The numbering sequence follows the same rule as for the corresponding anatomical structures from left to right and from top to bottom; these numbers have been highlighted in blue font. Technical information has been listed in Chapter 12. Numbering of blood vessels, displayed in Sections 7.4 and 7.5, also takes into account

vascular territories and the direction of flow. Individual structures of neurofunctional systems have been identified sequentially in the slice.

While the description of topography has been deliberately kept to a minimum, several **illustrative cues** have been included. These may interfere with the reading flow, but simplify locating corresponding images. The reader can thus link verbal and graphical–visual information. A selection was necessary where more than nine illustrative cues were available for an anatomical structure. In several cases, text regarding the T1w and T2w MR images only referred to one image. Nevertheless, a comparison of the second illustration is recommended. All illustrative cues have been listed in the appended index.

The anatomical illustrations in the **atlas section** originated from **five individuals**. The coronal, sagittal, and brainstem series (first to third individuals from the third edition) were supplemented by T1- and T2-weighted MR images from the **fourth individual**. The T2-weighted MR images of the bicommissural series also originated from the fourth individual.

In addition to the MR images, a new transversal CT series of a **fifth individual** has been added, see Chapter 12 for details.

References to other chapters have been made using headings with decimal numbering (see Table of Contents). The decimal classification can also be found in the column headings on the right-hand page.

References to bibliography have been quoted in superscript. These figures can be found in the bibliography in the appendix.

2 Tomography and Landmarks

CT and MRI are widely used cross-sectional imaging modalities offering excellent imaging capabilities for the head and spine.

2.1 Computed Tomography

The **spiral** (helical) or volume **technique** is employed by modern CT devices. Secondary slices in a required 3D orientation and of desired thickness can be reconstructed from data obtained from transverse scanning of the examined measuring volume.^{258,272,282,344,350}

The image is displayed following the measurement of the X-ray absorption of voxels in the examined volume. The X-ray density of tissue of interest is specified in **HU**. This is assigned in accordance with certain default values.

The so-called partial volume effects may be minimized by a high-resolution matrix and minimal slice thickness. Partial volume effects, image artifacts, and prevailing examination conditions (contrast medium administration, restlessness, positioning) result in distinctive features that must be kept in mind during image evaluation.^{258,272,396,410,476,583} Artifacts may be reduced by setting the imaging plane while avoiding beam hardening, as well as by the addition of several thin slices to a slice in the desired thickness.²⁵⁸

Intravenous (IV) administration of **iodinated contrast medium** improves the informative value of the examination by opacifying both physiological (blood vessels) and pathological structures (many tumors, inflammation, etc.).^{250,476} A **CTA** may be performed using IV contrast medium administration as bolus with faster CT devices (short sampling times, continuous helical or volume measurement) and a shorter examination time. Smaller vessels of the brain may thus be depicted by data acquisition in spiral technique either as so-called 3D surface reconstruction, by MIP or by volume rendering processes.^{258,272,275,499,583}

2.2 Magnetic Resonance Imaging

The magnetically effective angular momentum (spin) of atomic nuclei with an odd number of nucleons (protons and neutrons) is used to generate MR images. The hydrogen nucleus possesses a large magnetic moment and is frequently present in organisms. Thus water-containing tissues as well as lipids and proteins with their high hydrogen atom content are particularly well visualized on MRI.^{134,272,350,364,441,557,583,657}

For a given magnetic field strength, the **MR signal** is determined by proton density, T1 relaxation time (spin lattice or longitudinal relaxation time), T2 relaxation time (spin-spin or transverse relaxation time), and by proton movements in the measuring volume. Signal intensity of each measuring volume (voxel) determines the gray-scale value of a pixel on the monitor.

Various **sequences** may be employed to induce excitation of hydrogen nuclei. These have an effect on image contrast and thus significantly influence the diagnostic value. The **SE technique** found wide acceptance within the first years since its inception. T1-weighted images and sequences enable exceptional depiction of anatomical details due to a favorable signal-to-noise ratio. CSF has a low T1 signal and is therefore dark, while it exhibits a high signal on T2 images and is consequently bright. Many pathological changes are well seen on T2-weighted images. T1 and T2 sequences are part of the basic configuration of MRI equipment. These have been selected as reference sequences in this book due to their wide availability and good contrast between gray and white matter.

Gradient echo sequences (Flash, FISP, etc.) enable shortening of examination times and reduction of movement artifacts while enabling depiction of flow and tissue perfusion with high temporal resolution and mapping of vessels (**MRA**).

The diagnostic problem to be addressed determines the selection of measurement criteria of an MRI examination. These include the volume to be examined, slice position, and measurement parameters, for example, slice thickness and interval, matrix, and the sequence to be employed. Critical picture elements must be well delineated and free of artifacts (so-called quality criteria). The cranium should be examined using **T1- and T2-weighted sequences**, thereby gaining high-contrast imaging of gray and white matter. Additional T2*-weighted sequences or those with greater susceptibility weighting (e.g., SWI) are indicated in certain situations, for example, in cerebrovascular disorders.²⁸⁷ The possibility of **potential errors** due to artifacts and inadequate performance of the examination is significantly greater than with other imaging techniques due to the large number of modifiable and interdependent measuring parameters. It is therefore not only technical quality assurance, but also one's medical knowledge which plays a vital role in deciding indication, implementation, evaluation, and assessment of MRI examinations.^{273,563}

Several parameters (proton density, relaxation times, etc.) of examined tissue are used in MRI for image acquisition.^{156,516,557,657} Image processing and reconstruction takes place in MRI in a similar fashion to CT, with the examiner selecting the window center (center) and window width (window). This determines the informative value of the examination, either contributing to image interpretation or taking away from it.

Paramagnetic substances (e.g., gadolinium-DTPA, gadolinium-diamide, manganese, and others) when used as **contrast medium** improve clinical information in certain cases. They shorten the T1 relaxation time in their areas of distribution, which in turn results in an increase in lesional signal intensity on T1 images as compared to their surroundings.^{265,439,557,655} A noncontrast T1 examination should be carried out prior

to the contrast injection using the same settings.²⁴⁰ Contrast medium administration in general provides the following information:¹³⁴

- Presence or absence of **contrast enhancement** of a lesion
- Extent of the area exhibiting contrast enhancement
- Enhancement pattern of this region
- Increase or decrease in lesional perfusion using dynamic examination

Structures of the skull base and the infratentorial region as well as the spinal canal are better appreciated on MRI than on CT due to higher soft tissue contrast and lack of interference by bony artifacts. That MRI has been rapidly accepted is justified by its high sensitivity for pathological cerebral and spinal processes due to its exceptionally good contrast resolution.⁵⁵⁷ MRI is well suited for the depiction of myelination of the central nervous system in young children and may therefore be used in the evaluation of disorders of myelination, myelogenesis as well as diffuse or focal demyelination.^{30,31,211,272,296,441,558,590} MRI in combination with its morphological and functional data is almost equal to CT and CTA in the differential diagnosis of acute stroke and evidence of hemorrhage, but superior to these modalities in excluding tumors. An infarcted area may be demonstrated as early as a few minutes after vascular occlusion using a diffusion-weighted sequence.

In vivo **MRS** is not yet in common use due to the complex technology involved,^{475,644,658} even though several promising observations have been made.^{126,330,364} In vivo MRS has a high specificity for the tissue in the measuring volume due to detection of the so-called chemical shift of molecules in the magnetic field. Not only is it suited for the identification of abnormal tissue (tumors, inflammation, necrosis, etc.) in the central nervous system, but also contributes to tumor grading.^{230,232,330,331,419,420}

fMRI has played an important role in the neurosciences for years.^{78,129,214,294,398,425} It helps mapping local changes in cerebral perfusion due to vasoneuronal coupling following targeted motor, visual, or sensory stimulation and may be used to localize short-term changes in **brain function** under defined paradigms.^{272,563} The technique is time consuming and the signal yield is low, so clinical use so far has been restricted to some very stable paradigms (motor, visual, auditory, and tactile paradigms; speech comprehension and production). Increasingly higher cognitive functions may be understood using higher field strengths and other methods including resting-state fMRI (see ► Section 10.13).^{25,58,118,207} fMRI can, for instance, guide a decision for or against cochlear implantation, and also aid in selecting the side for this procedure.⁵²⁸

2.3 Landmarks of Cross-sectional Imaging

Landmarks are those anatomical structures which are well seen and constantly visualized on cross-sectional imaging and best suited for topical orientation.

Topographic relationships of bony structures to blood vessels and CSF spaces were the predominant landmarks for **conventional neuroradiological procedures**, angiography, and myelography. Pathological processes in the intracranial and intraspinal regions were identified by deformation of contrast enhanced CSF spaces as well as by displacement of, or changes in, blood vessels. Contrast-enhanced CSF or the vascular system were used for special imaging procedures. Air-containing spaces (e.g., the nose, paranasal sinuses, pharynx, and trachea) enabled topical orientation outside of intracranial regions. Landmarks are therefore vital for spatial orientation. They are also useful in maintaining proper alignment on the image display.

Simultaneous display of several different anatomical structures in the region examined is an advantage of both **CT** and **MRI**, and is possible due to high soft tissue resolution which in turn is based on various physical, and to some extent, chemical parameters. This allows for **better identification of structural anatomical details** and significantly improves the detection of pathological findings. Image interpretation is simplified by constant imaging characteristics of anatomical structures and regions, while topical classification of findings on cross-sectional imaging is trickier. A prerequisite for a correct interpretation and topographic mapping is synoptic viewing of all sections and, insofar possible, multiplanar imaging using several sectional planes. Digital sagittal and coronal views (scout view, pilot, topogram, etc.) are essential and customary for spatial orientation during cross-sectional imaging (CT and MRI), especially of the spine. **Mapping of the tomographic image** in its spatial orientation is thus possible using measurement parameters. This common practice in the examination process prompted us to add a sketch of the section to each anatomical drawing and original illustration of imaging techniques, which enables topographic mapping of each individual slice.

2D gray-scale mapping of pixels in CT is determined by **attenuation of radiation** in the corresponding volume element (voxel). The range of absorption values is based on biologically relevant structures. These have therefore been predefined as air -1000 HU, water 0 HU, and dense bones +1000 HU and above.^{250,258,476} According to Hosten and Liebig as well as Nadjmi et al, various values^{258,410} may be determined on the cranial scan:

- **Air:** -1000 HU
- **Fat:** -100 to -30 HU
- **CSF spaces:** +5 to +10 HU
- **Brain tissue:** +20 to +40 HU
- **Contrast enhanced sinuses:** +50 to +200 HU
- **Calcification:** +30 to +1000 HU
- **Cranial bones:** up to +1000 HU and above

Bony structures of the head and spine as well as CSF spaces and air-containing regions (nose, sinuses, pharynx, and trachea) aid anatomical orientation on **CT**.

Imaging in **MRI** is determined by several complex physical and chemical processes. A large number of different excitation sequences of the object to be measured and various image filtration processes result in variable gray values of anatomic structures. The clinical problem

to be addressed and body parts or organs to be examined determine the choice of scan sequences (e.g., T1-, T2-weighting, and proton density). Please refer to special literature for detailed information.^{272,363,441,590}

2.3.1 Facial Bones

Bony structures and **air-filled regions** (nasal cavity, sinuses [see ▶Fig. 3.16 to ▶Fig. 3.20, ▶Fig. 5.31 to ▶Fig. 5.36, and ▶Fig. 4.8 to ▶Fig. 4.13], and mouth) enable anatomical orientation in coronal and transverse CT sections. This is simplified by bilateral symmetry of several structures in this region. Correct axial alignment of the head in the scan field may thereby be monitored. An angle of 10° to the canthomeatal plane is preferred for examination of the **orbit** in the transverse plane,^{254,258} which approximates the infraorbitomeatal line. The optic nerve and the rectus muscles can thereby be seen more clearly. The optic nerve seen running a tortuous course in normal forward gaze will be straightened by means of a slightly upward gaze.^{258,410} Orbital fat provides good contrast for the rest of the contents of the bony orbit. Additional coronal slices supplement the examination.^{250,258,263,272}

Bony orientation is largely dispensed within MR images. Advantages of this method in the evaluation of the facial region include multiplanar image display with free selection of sectional planes and higher soft tissue contrast. Artifacts from teeth usually remain localized and do not interfere with the image. Also, lacking in the region of the base of skull are bony beam hardening artifacts which interfere with CT image interpretation. The **bicommissural line** (connecting the anterior with the posterior commissure) is used for anatomical orientation in MRI. Intraorbital retrobulbar fat gives rise to a high MR signal on T1-weighted images. The recti and oblique eye muscles are thus well delineated. Examination in paraxial (sagittal-oblique)^{263,364} and coronal sections with fat suppression is best suited for optimal delineation of the **optic nerve** (see ▶Fig. 3.4b, ▶Fig. 3.5b, and ▶Fig. 4.5d) up to the optic chiasma (see ▶Fig. 4.2b and ▶Fig. 4.2d), while coronal and transverse sections are preferred for imaging of paranasal sinuses and the retromaxillary region. Nasal turbinates (see ▶Fig. 3.2b, ▶Fig. 3.3b, ▶Fig. 3.4b, and ▶Fig. 4.3d) and the musculature provide good anatomical orientation. Transverse sections through the nasopharynx frequently allow demarcation of a superficial mucosal compartment distinct from deeper sections; this may be significant in clinical practice.^{22,557}

2.3.2 Head–Neck Region

The width of the bony vertebral canal can be best assessed using CT. Scout films (scout view, topogram) are necessary for slice orientation and positioning. Air-filled regions (pharynx [see ▶Fig. 4.8] and larynx [see ▶Fig. 3.19]) are well seen. Equally well delineated are the dens of axis (see ▶Fig. 4.8), the atlas (see ▶Fig. 4.8), and the occipital bone (see ▶Fig. 5.18b and ▶Fig. 5.20b) with the spinal cord (see ▶Fig. 5.17b). Bony parts of the skull base and their foramina are important for

orientation. Special section orientations are required for the imaging of fine structures, with coronal sections where needed (see ▶Fig. 3.16 to ▶Fig. 3.25 and ▶Fig. 5.31 to ▶Fig. 5.36).^{254,258} The internal auditory canal and its aperture are usually well visualized with supraorbito-suboccipital alignment and are therefore important landmarks. Various authors have described special settings for imaging fine structures of the skull base.^{178,254,258,306,395,568}

Besides the cervical spine, the spinal cord, the medulla oblongata (see ▶Fig. 4.2b, ▶Fig. 5.3b, and ▶Fig. 6.4c), the spinal subarachnoid space, and basal cisterns serve as landmarks in MRI. Large neck vessels (internal and external carotid arteries and the internal jugular vein) are well delineated. Air-filled regions (oral cavity and pharynx [see ▶Fig. 3.6d, ▶Fig. 4.2b, ▶Fig. 5.2b, and ▶Fig. 5.3b]) are identifiable with all examination sequences. Anatomical relationships of the soft tissues of the neck and pathological structures therein are best seen on nonenhanced and fat-suppressed, contrast enhanced T1-weighted images as well as on fat-suppressed T2-weighted images. Technical details are to be found in subject literature.^{21,441}

2.3.3 Cranial Vault

Bony parts of the base and bony foramina are reference structures in CT, providing information about the selected section and its position. Rough guides to orientation are provided by the following structures:

- Occipital bone (see ▶Fig. 5.18b and ▶Fig. 5.20b)
- Petrous bone (see ▶Fig. 5.19b and ▶Fig. 5.20b)
- Mastoid cells (see ▶Fig. 5.18b and ▶Fig. 5.21b)
- Sphenoid sinus (see ▶Fig. 3.19 and ▶Fig. 4.8)
- Sella turcica/hypophyseal fossa (see ▶Fig. 5.35)
- Ethmoid cells (see ▶Fig. 3.17 and ▶Fig. 5.17b)
- Zygomatic arch (see ▶Fig. 3.17)
- Orbital margin (see ▶Fig. 3.17)

The hypoglossal canal (see ▶Fig. 5.31), jugular foramen (see ▶Fig. 6.5a), external auditory canal and its pore (see ▶Fig. 5.18b and ▶Fig. 5.19b), tympanic cavity, foramen lacerum, carotid canal (see ▶Fig. 5.32), foramen spinosum, and foramen ovale (see ▶Fig. 5.32) are inconstantly visualizable fine structures of the skull base. They can however serve as anatomical landmarks for intracranial structures when visualized. Thin slice thickness and supplemental coronal sections are necessary for targeted imaging of individual structures of the skull base. **HRCT** should be employed for the examination of bony structures.²⁷²

2.3.4 Cisterns and Ventricular System

CSF spaces are vital **landmarks** for CT (see ▶Fig. 7.3).^{185,250,545} Fine subarachnoid spaces may be obscured due to the partial volume effect or by radiodense structures. The unpaired posterior cerebellomedullary cistern (magna, see ▶Fig. 5.18b) and pontine cistern as well as the paired pontocerebellar cisterns

(see ►Fig. 5.20b) are identified at the level of the petrous bone approximately in a reference plane parallel to the supraorbito-suboccipital line. The anterior basal cisterns, the interpeduncular cistern (see ►Fig. 5.22b), and the superior cerebellar cistern are imaged immediately above this. The so-called pentagon is the median anterior basal cistern including the interpeduncular cistern. The pentagon usually appears five-sided on CT images, surrounding the pituitary stalk, optic nerves, and the optic chiasma. Anteriorly, the pentagon abuts the straight gyrus and is related at its lateral aspect to the uncus and the parahippocampal gyrus and posteriorly to the pons. The ambient cistern and quadrigeminal cistern (cisterna venae magnae cerebri, see ►Fig. 5.23b) are other important landmarks. Cisterns of the interhemispheric fissure and the sylvian fissures are very narrow in young patients, and appear distinctly wider especially in older patients and in atrophic brains. In certain situations, the cisterns may be better depicted with **contrast enhancement** of extra-cerebral CSF spaces, particularly the cisterns, by lumbar instillation of a suitable water soluble contrast medium. No standardized images of individual ventricular sections are available due to the great physiological variability of the width of the ventricular system and its easy deformation by space-occupying lesions. A bilaterally wide appearance is suggestive of hydrocephalus. The volume of the ventricular system may be calculated by measurement of the ventricular area on several CT images^{72,389,502,646} or by segmentation of 3D MR datasets.

CSF spaces also serve as an aid to orientation in **MRI**. These are imaged without hindrance by bony artifacts, this being of special importance in the region of the skull base and in the transition zone from the intracranial to the spinal subarachnoid space.⁵⁵⁷ The following cisterns appear hypointense on T1-weighted images and hyperintense on T2-weighted images:

- Posterior cerebellomedullary cistern (cisterna magna, see ►Fig. 3.11b, ►Fig. 3.11d, ►Fig. 4.2b, ►Fig. 4.2d, ►Fig. 5.3b, and ►Fig. 6.4c)
- Cerebellopontine cistern (see ►Fig. 6.8b and ►Fig. 6.10b)
- Pontine cistern (see ►Fig. 7.12a)
- Interpeduncular cistern (see ►Fig. 3.9b, ►Fig. 3.9d, ►Fig. 5.7b, and ►Fig. 6.12c)
- Ambient cistern (see ►Fig. 5.7b and ►Fig. 6.13c)
- Quadrigeminal cistern (cisterna venae magnae cerebri, see ►Fig. 5.7b, ►Fig. 5.8b, and ►Fig. 7.12b)
- Cistern of the cerebral valliculae (see ►Fig. 7.12a and ►Fig. 7.12b)

The cistern of the lateral cerebral fossa (see ►Fig. 4.6b, ►Fig. 5.9b, and ►Fig. 5.23b) is useful for the localization of the frontal and parietal opercula as opposed to the temporal operculum.

2.3.5 Blood Vessels

Sections of large arteries are identifiable on **CT**, the basilar artery (see ►Fig. 5.20b and ►Fig. 5.21b), and the internal carotid artery (see ►Fig. 5.19b and ►Fig. 5.21b). The arteries are particularly well visualized following IV

administration of contrast medium. The middle cerebral artery in the lateral sulcus and parts of the **Circle of Willis** are constantly visualized. Venous sinuses that serve as **landmarks** include the great cerebral vein (Galen), the inferior sagittal sinus, the straight sinus (see ►Fig. 5.25b) as well as the superior sagittal sinus (see ►Fig. 5.25b and ►Fig. 5.27b), and, less constantly, the transverse sinus.

Large **blood vessels** are well seen on **MRI**. Selected examination sequences determine the signal intensity. Blood vessels are therefore an important aid to orientation in the assessment of MR images. Cerebral vascular malformations are significantly better appreciated on MR images than on CT.²² **MRA** performed without contrast medium administration (see ►Fig. 7.15 and ►Fig. 7.27) has been increasingly replacing DSA in the diagnostic arena. MRA using a field strength of 3T is superior to one performed at lower field strengths. DSA is however still required as a supplemental examination for the demonstration of small arteries and veins as well as for assessment of hemodynamics and small vascular anomalies,^{134,441,557} although hemodynamics may also be demonstrated on MRI by time-resolved MRA.

Transcranial Doppler sonography facilitates the noninvasive assessment of arterial blood flow through the brain, diagnosis of vasospasm, and often provides evidence of arterial stenosis.^{139,421,618}

2.3.6 Dural Structures

Visualization of **cranial dura** on CT is the exception rather than the rule. **Dural duplications** are usually clearly identifiable. The falx cerebri is constantly visualized (see ►Fig. 5.23b, ►Fig. 5.24b, ►Fig. 5.25b, ►Fig. 5.26b, ►Fig. 5.27b, ►Fig. 5.28b, and ►Fig. 5.29b) with an increase in density following administration of contrast medium which opacifies the superior and inferior sagittal sinuses, the straight sinus, and the bridging veins, thereby delineating the boundaries of the falx cerebri. The tentorium of cerebellum with its inferior and lateral boundaries as defined by the confluence of sinuses, transverse and superior petrosal sinuses, its free edge extending toward the anterior clinoid processes, and parts of the straight sinus are well seen and are often delineated following administration of contrast medium only.^{439,441} The topographical position of the **incisura of the tentorium** varies considerably relating to the midbrain. Images of sections through the tentorium and the falx cerebri may exhibit a “Y” shape (see ►Fig. 5.25), while sections through the tentorium may appear V or M shaped. The **incisura of the tentorium** is identified on contrast CT by the anteromedial aspect of diverging bands.⁴¹⁸ The diverging bands enable depiction of the tentorium bilaterally using a guiding line if this structure is not demonstrated on the transverse unenhanced scan. This runs posteriorly from the lateral aspect of the ambient cistern (not from the medial part of the quadrigeminal cistern) lateral to the cranial vault, making an angle of 45° with the sagittal plane. Structures lateral to this guiding line lie in a supratentorial location, those which are medial are infratentorial.⁴¹⁸ In

contrast, the tentorium of cerebellum is usually clearly visualized on coronal sections.

The dura is also barely visible on **MRI**, or is demonstrable only after administration of contrast medium. In contrast however spaces bounded by the dura, the interhemispheric cistern (see ►Fig. 3.2d, ►Fig. 3.14d, and ►Fig. 3.15d) and the region between the occipital lobe and cerebellum, the transverse cerebral fissure, are clearly identified and therefore serve as important landmarks. No MR signal is usually seen with dural calcification while ossification may rise to a low or high signal.

2.4 Clinical Significance of Computer and Magnetic Resonance Tomography

CT and MRI have redefined the practice of medicine. This is especially true for diagnostic investigations involving intracranial and intraspinal regions. Classical

myelography has a high indicational threshold due to its invasive nature, being employed only when all other diagnostic measures have been exhausted. Modern cross-sectional imaging methods are virtually noninvasive, may be performed on an out-patient basis and are affordable as compared to in-patient examinations, advantages which also allow their use in **follow-up**. Myelography and DSA are however still necessary in special situations (see ►Section 2.3).

Various cross-sectional imaging procedures are now firmly entrenched in the diagnostic armamentarium. The focus of the examination depends on the respective specialty, the clinical problem to be addressed and the organ to be examined. Selection and implementation of the diagnostic procedure requires clinical experience and expertise with the concerned cross-sectional imaging modality. A knowledge of functional neuroanatomy is necessary for deciding on indications for CT or MRI, as also for interpretation and description of findings. This book aims to impart this knowledge to the user both through images and text.

3 Coronal Sections

Fourteen coronal sections have been described in this part of the book from anterior to posterior. ▶Fig. 3.1 describes the position of coronal sections; ▶Fig. 3.2, ▶Fig. 3.3, ▶Fig. 3.4, ▶Fig. 3.5, ▶Fig. 3.6, ▶Fig. 3.7, ▶Fig. 3.8, ▶Fig. 3.9, ▶Fig. 3.10, ▶Fig. 3.11, ▶Fig. 3.12, ▶Fig. 3.13, ▶Fig. 3.14, ▶Fig. 3.15, ▶Fig. 3.16, ▶Fig. 3.17, ▶Fig. 3.18, ▶Fig. 3.19, ▶Fig. 3.20, ▶Fig. 3.21, ▶Fig. 3.22, ▶Fig. 3.23, ▶Fig. 3.24, and ▶Fig. 3.25 reproduce anterior views of coronal sections.

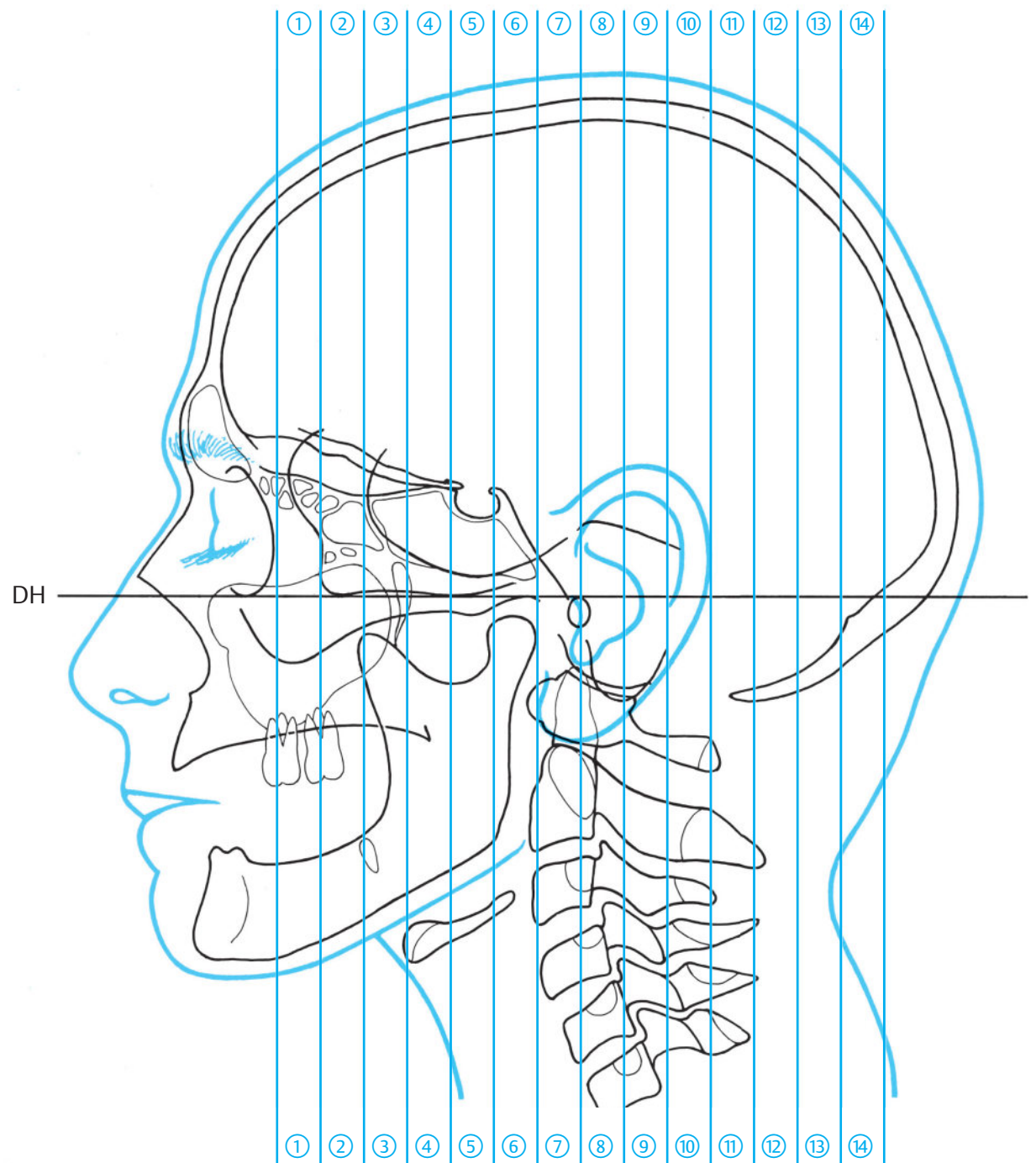


Fig. 3.1 Coronal sections. Encircled digits indicate the number of 1-cm-thick sections as viewed from the front. For details see ► Chapter 12. Roman numbers in the legends refer to the numerical identifiers of parts of the cerebellum (see ► Table 7.1). DH = German horizontal.

Fig. 3.1a Position of coronal sections in lateral view. The portrayed cross-section always corresponds to the line lying anterior (in the image on the left) to the encircled number of the slice concerned.

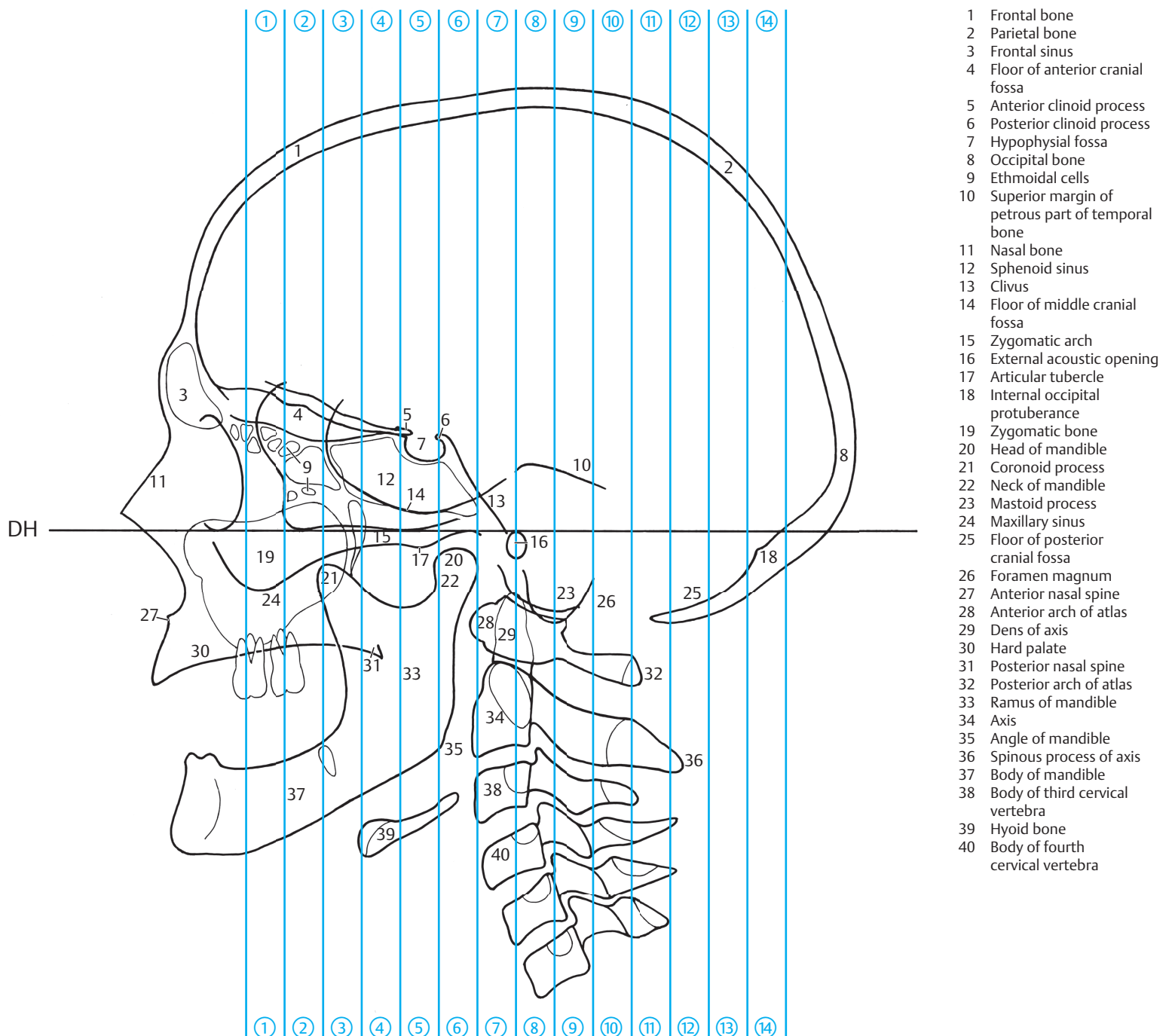


Fig. 3.1b Drawing based on a cephalogram from a. Cross-sections of 14 coronal sections were optimally transposed on to an X-ray image and numbered consecutively from anterior to posterior.

- 1 Paracentral lobule
- 2 Cingulate sulcus
- 3 Cingulate gyrus
- 4 Precuneus
- 5 Trunk (body) of corpus callosum
- 6 Parieto-occipital sulcus
- 7 Septum pellucidum
- 8 Frontal pole
- 9 Genu of corpus callosum
- 10 Fornix
- 11 Interventricular foramen (of Monro)
- 12 Splenium of corpus callosum
- 13 Interthalamic adhesion
- 14 Anterior commissure
- 15 Third ventricle
- 16 Cuneus
- 17 Lamina terminalis
- 18 Posterior commissure
- 19 Pineal gland
- 20 Optic chiasm
- 21 Superior colliculus
- 22 Mammillary body
- 23 Calcarine sulcus
- 24 Olfactory bulb
- 25 Olfactory tract
- 26 Optic nerve
- 27 Pituitary gland
- 28 Infundibulum
- 29 Oculomotor nerve
- 30 Aqueduct of midbrain
- 31 Inferior colliculus
- 32 Culmen (IV, V)
- 33 Primary fissure of cerebellum
- 34 Occipital pole
- 35 Declive (VI)
- 36 Temporal lobe
- 37 Pons
- 38 Fourth ventricle
- 39 Nodule of vermis (X)
- 40 Folium of vermis (VII A)
- 41 Uvula of vermis (IX)
- 42 Tuber of vermis (VII B)
- 43 Pyramid of vermis (VIII)
- 44 Medulla oblongata
- 45 Tonsil of cerebellum (H IX)
- 46 Spinal cord

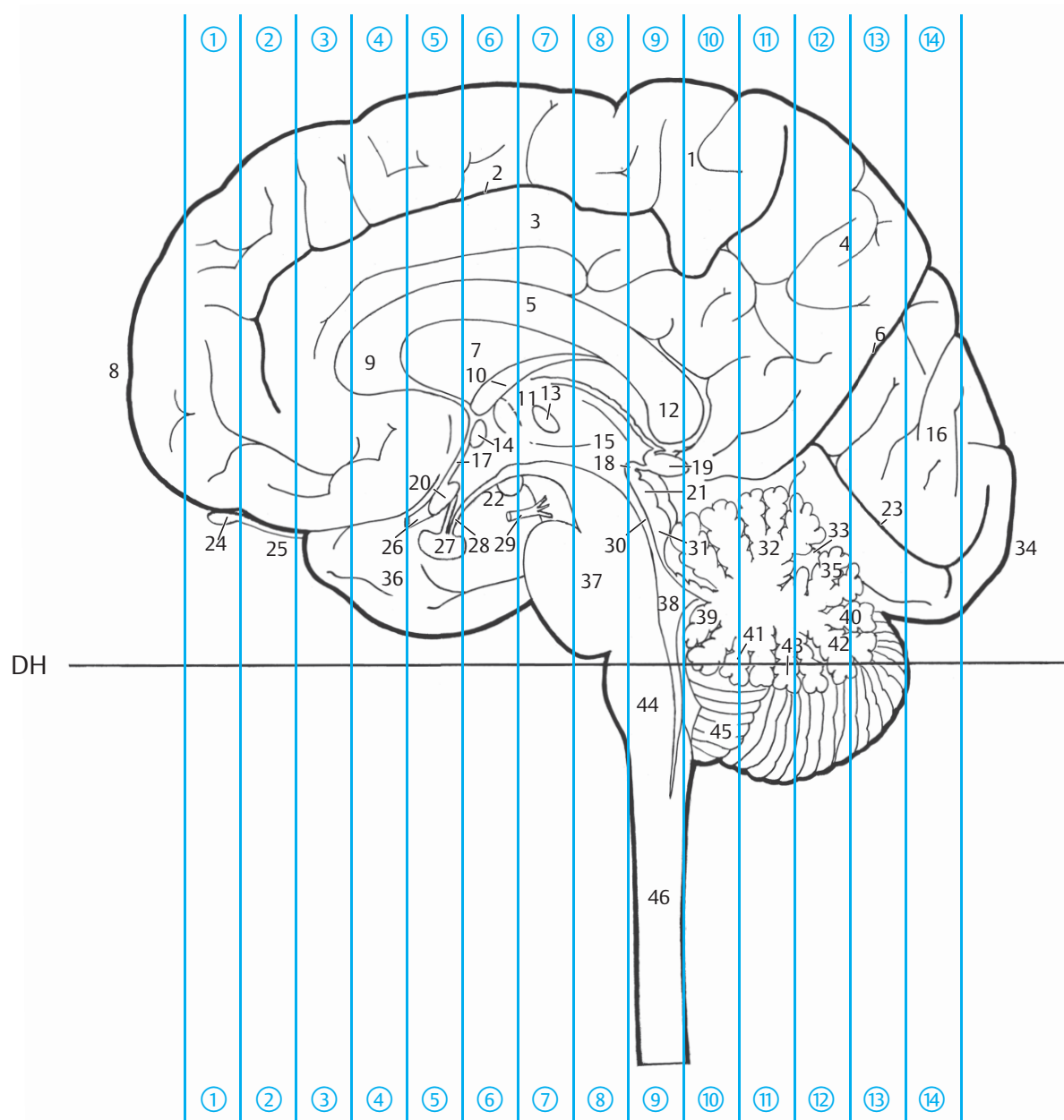


Fig. 3.1c Median view of the brain and upper spinal cord of the same head as in a and b. Coronal sections were assembled and numbered as in a.

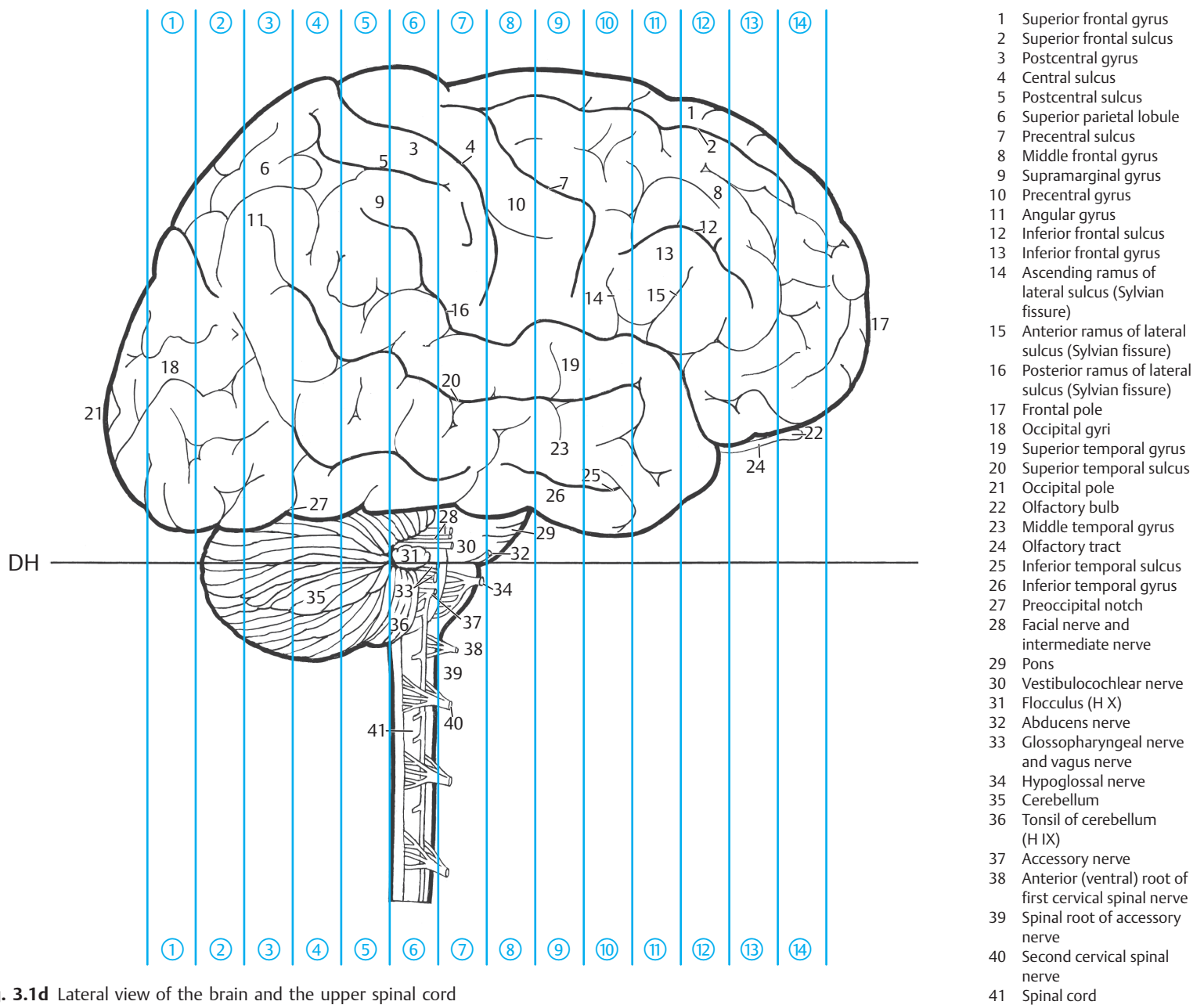
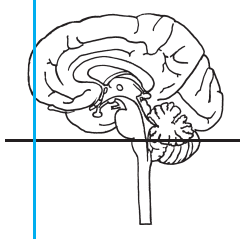


Fig. 3.1d Lateral view of the brain and the upper spinal cord of the same head as in a to c. Coronal sections were assembled and numbered as in a.



- 1 Longitudinal cerebral (interhemispheric) fissure
- 2 Superior frontal gyrus
- 3 Falx cerebri
- 4 Middle frontal gyrus
- 5 Dura mater
- 6 Supraorbital nerve
- 7 Ethmoidal cells
- 8 Optic disc
- 9 Fovea centralis of retina
- 10 Ethmoidal bulla
- 11 Eyeball
- 12 Semilunar hiatus
- 13 Middle nasal canal
- 14 Middle nasal concha
- 15 Infraorbital nerve
- 16 Nasal cavity
- 17 Nasal septum
- 18 Inferior nasal canal
- 19 Maxillary sinus
- 20 Inferior nasal concha
- 21 Oral cavity
- 22 Tongue
- 23 Hypoglossal nerve
- 24 Inferior alveolar nerve

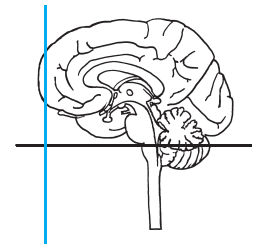
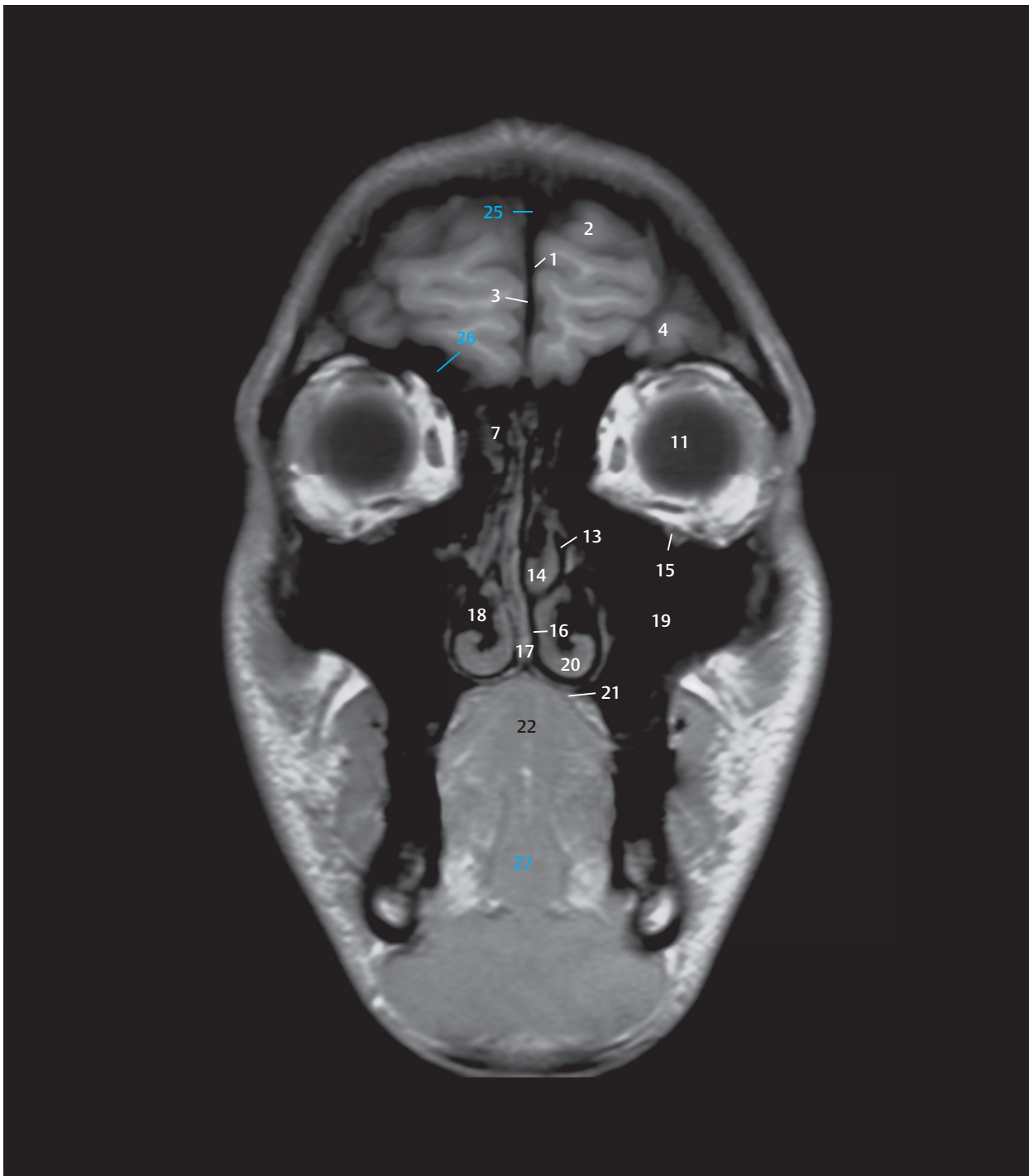


Fig. 3.2 1st coronal section.

DH = German horizontal

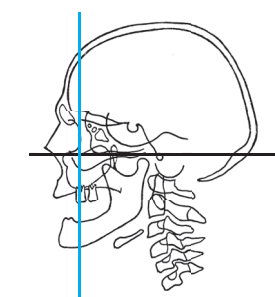
M = median plane

Fig. 3.2a Anterior view of first coronal section. The blue line on the top left shows the course of the sectional plane through the anterior part of the frontal lobe (see ► Fig. 3.1c). Nasal cavity, paranasal sinuses, oral cavity, brain structures, retina, and cranial nerves.



- 1 Longitudinal cerebral (interhemispheric) fissure
- 2 Superior frontal gyrus
- 3 Falx cerebri
- 4 Middle frontal gyrus
- 7 Ethmoidal air cells
- 11 Eyeball
- 13 Middle nasal canal
- 14 Middle nasal concha
- 15 Infraorbital canal with infraorbital nerve
- 16 Nasal cavity
- 17 Nasal septum
- 18 Inferior nasal canal
- 19 Maxillary sinus
- 20 Inferior nasal concha
- 21 Oral cavity
- 22 Tongue
- 25 Superior sagittal sinus
- 26 Frontal sinus
- 27 Genioglossus

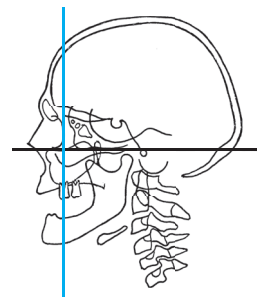
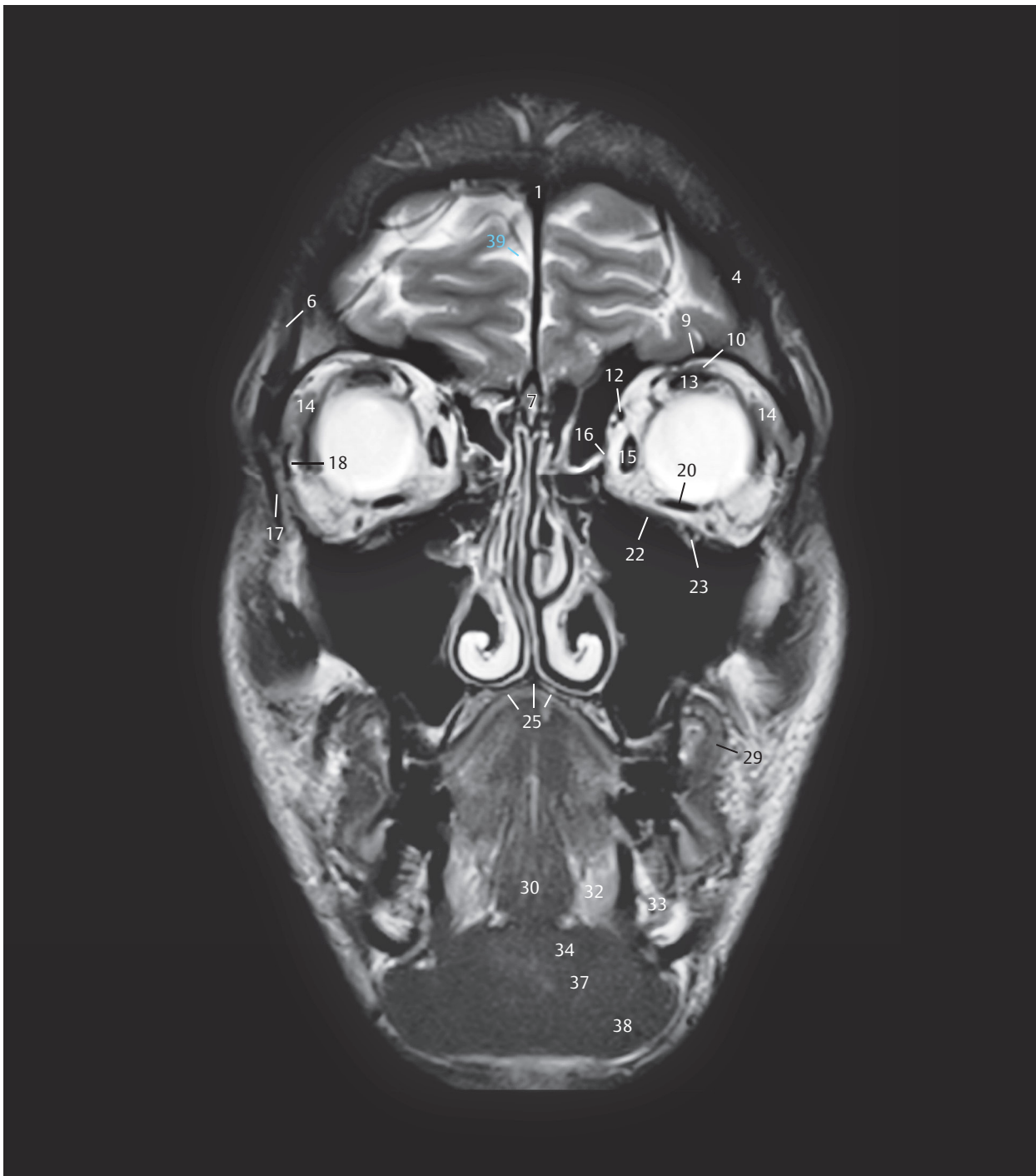
Fig. 3.2b Coronal T1w MR image (T1w FLASH sequence), corresponding approximately to the sectional plane in a and c. Brain structures are accentuated on the selected sequence with a field strength (magnetic flux density) of 3T. The two coronal MR series (see ►Fig. 3.2b, ►Fig. 3.3b, ►Fig. 3.4b, ►Fig. 3.5b, ►Fig. 3.6b, ►Fig. 3.7b, ►Fig. 3.8b, ►Fig. 3.9b, ►Fig. 3.10b, ►Fig. 3.11b, ►Fig. 3.12b, ►Fig. 3.13b, ►Fig. 3.14b, ►Fig. 3.15b, ►Fig. 3.2d, ►Fig. 3.3d, ►Fig. 3.4d, ►Fig. 3.5d, ►Fig. 3.6d, ►Fig. 3.7d, ►Fig. 3.8d, ►Fig. 3.9d, ►Fig. 3.10d, ►Fig. 3.11d, ►Fig. 3.12d, ►Fig. 3.13d, ►Fig. 3.14d, and ►Fig. 3.15d) were obtained from a 33-year-old man.



- 1 Superior sagittal sinus
- 2 Intermediomedial frontal artery
- 3 Anteromedial frontal artery
- 4 Frontal bone
- 5 Polar frontal artery
- 6 Temporalis
- 7 Crista galli
- 8 Medial frontobasal artery
- 9 Roof of orbit
- 10 Levator palpebrae superioris
- 11 Superior ophthalmic vein
- 12 Superior oblique
- 13 Superior rectus
- 14 Lacrimal gland
- 15 Medial rectus
- 16 Orbital plate
- 17 Zygomatic bone
- 18 Tendon of lateral rectus
- 19 Orbicularis oculi
- 20 Inferior rectus
- 21 Inferior oblique
- 22 Floor of orbit
- 23 Infraorbital artery and vein
- 24 Maxilla
- 25 Hard palate
- 26 Second molar tooth
- 27 First molar tooth (cut)
- 28 Submandibular duct
- 29 Buccinator
- 30 Genioglossus
- 31 Sublingual artery and vein
- 32 Sublingual gland
- 33 Body of mandible
- 34 Geniohyoid
- 35 Inferior alveolar artery and vein
- 36 Submental artery and vein
- 37 Mylohyoid
- 38 Anterior belly of digastric

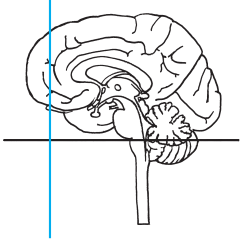


Fig. 3.2c Anterior view of the first coronal section. The blue line on the top left marks the position of the sectional plane at the level of the crista galli and the orbit (see ► Fig. 3.1b). Bony structures, muscles, and blood vessels.



- 1 Superior sagittal sinus
- 4 Frontal bone
- 6 Temporalis
- 7 Crista galli
- 9 Roof of orbit
- 10 Levator palpebrae superioris
- 12 Superior oblique
- 13 Superior rectus
- 14 Lacrimal gland
- 15 Medial rectus
- 16 Orbital plate
- 17 Zygomatic bone
- 18 Lateral rectus, tendon
- 20 Inferior rectus
- 22 Floor of orbit
- 23 Infraorbital canal with infraorbital artery, vein, and nerve
- 25 Hard palate
- 29 Buccinator
- 30 Genioglossus
- 32 Sublingual gland
- 33 Body of the mandible
- 34 Geniohyoid
- 37 Mylohyoid
- 38 Digastric, anterior belly
- 39 Interhemispheric cistern

Fig. 3.2d Coronal T2w MR image, corresponding approximately to the sectional plane in a and c.



- 1 Superior frontal gyrus
- 2 Falx cerebri
- 3 Middle frontal gyrus
- 4 Dura mater
- 5 Orbital gyri
- 6 Inferior frontal gyrus
- 7 Straight gyrus
- 8 Supraorbital nerve
- 9 Nasociliary nerve
- 10 Olfactory bulb
- 11 Optic nerve
- 12 Ethmoidal cells
- 13 Semilunar hiatus
- 14 Infraorbital nerve
- 15 Middle nasal canal
- 16 Middle nasal concha
- 17 Nasal septum
- 18 Nasal cavity
- 19 Maxillary sinus
- 20 Inferior nasal concha
- 21 Inferior nasal canal
- 22 Greater palatine nerve
- 23 Oral cavity
- 24 Tongue
- 25 Lingual nerve
- 26 Hypoglossal nerve
- 27 Inferior alveolar nerve

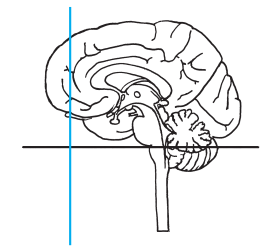
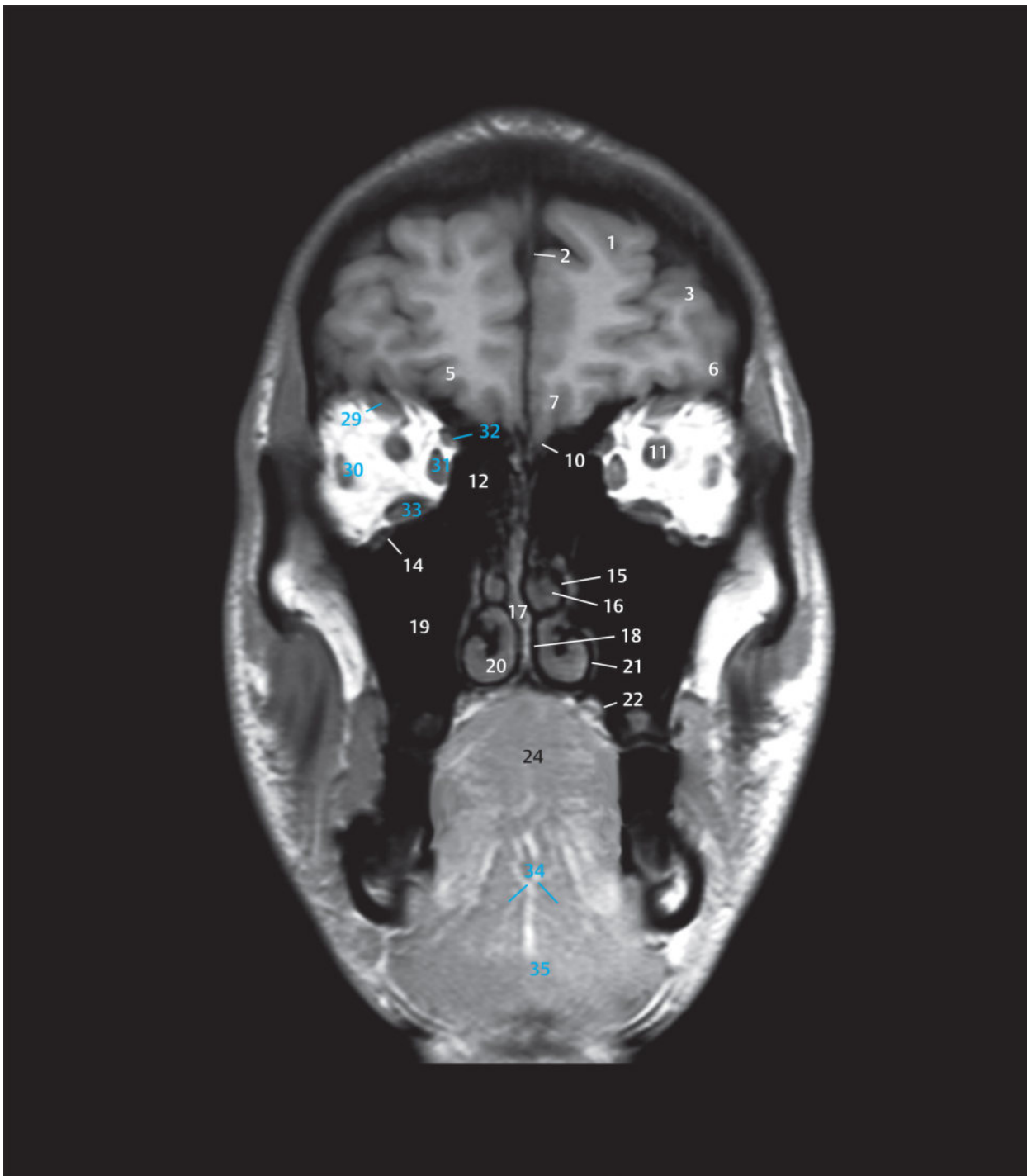


Fig. 3.3 2nd coronal section.

DH = German horizontal

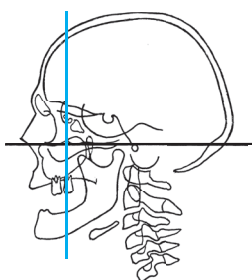
M = median plane

Fig. 3.3a Anterior view of the 2nd coronal section. The frontal lobe has been sectioned at the level of the olfactory bulb. Nasal cavity, paranasal sinuses, and cranial nerves.



- 1 Superior frontal gyrus
- 2 Falx cerebri
- 3 Middle frontal gyrus
- 5 Orbital gyri
- 6 Inferior frontal gyrus
- 7 Straight gyrus
- 10 Olfactory bulb
- 11 Optic nerve
- 12 Ethmoidal air cells
- 14 Infraorbital canal with infraorbital nerve
- 15 Middle nasal canal
- 16 Middle nasal concha
- 17 Nasal septum
- 18 Nasal cavity
- 19 Maxillary sinus
- 20 Inferior nasal concha
- 21 Inferior nasal canal
- 22 Greater palatine nerve
- 24 Tongue
- 29 Superior rectus
- 30 Lateral rectus
- 31 Medial rectus
- 32 Superior oblique
- 33 Inferior rectus
- 34 Genioglossus
- 35 Geniohyoid

Fig. 3.3b Coronal T1w MR image, corresponding approximately to the sectional plane in a and c.



- 1 Superior sagittal sinus
- 2 Anteromedial frontal artery
- 3 Frontal bone
- 4 Intermediomedial frontal artery
- 5 Polar frontal artery
- 6 Roof of orbit
- 7 Medial frontobasal artery
- 8 Levator palpebrae superioris
- 9 Superior oblique
- 10 Superior rectus
- 11 Superior ophthalmic vein
- 12 Ophthalmic artery
- 13 Ethmoid, cribriform plate
- 14 Medial rectus
- 15 Middle nasal canal
- 16 Temporalis
- 17 Orbital plate
- 18 Inferior rectus
- 19 Infraorbital artery and vein
- 20 Floor of orbit
- 21 Inferior nasal canal
- 22 Buccal fat pad (of Bichat)
- 23 Alveolar process of maxilla
- 24 Hard palate
- 25 Masseter
- 26 Greater palatine artery and vein
- 27 Second molar tooth (cut)
- 28 Buccinator
- 29 Sublingual gland
- 30 Submandibular duct
- 31 Body of mandible
- 32 Genioglossus
- 33 Sublingual artery
- 34 Inferior alveolar artery and vein
- 35 Submental artery and vein
- 36 Platysma
- 37 Geniohyoid
- 38 Mylohyoid
- 39 Anterior belly of digastric

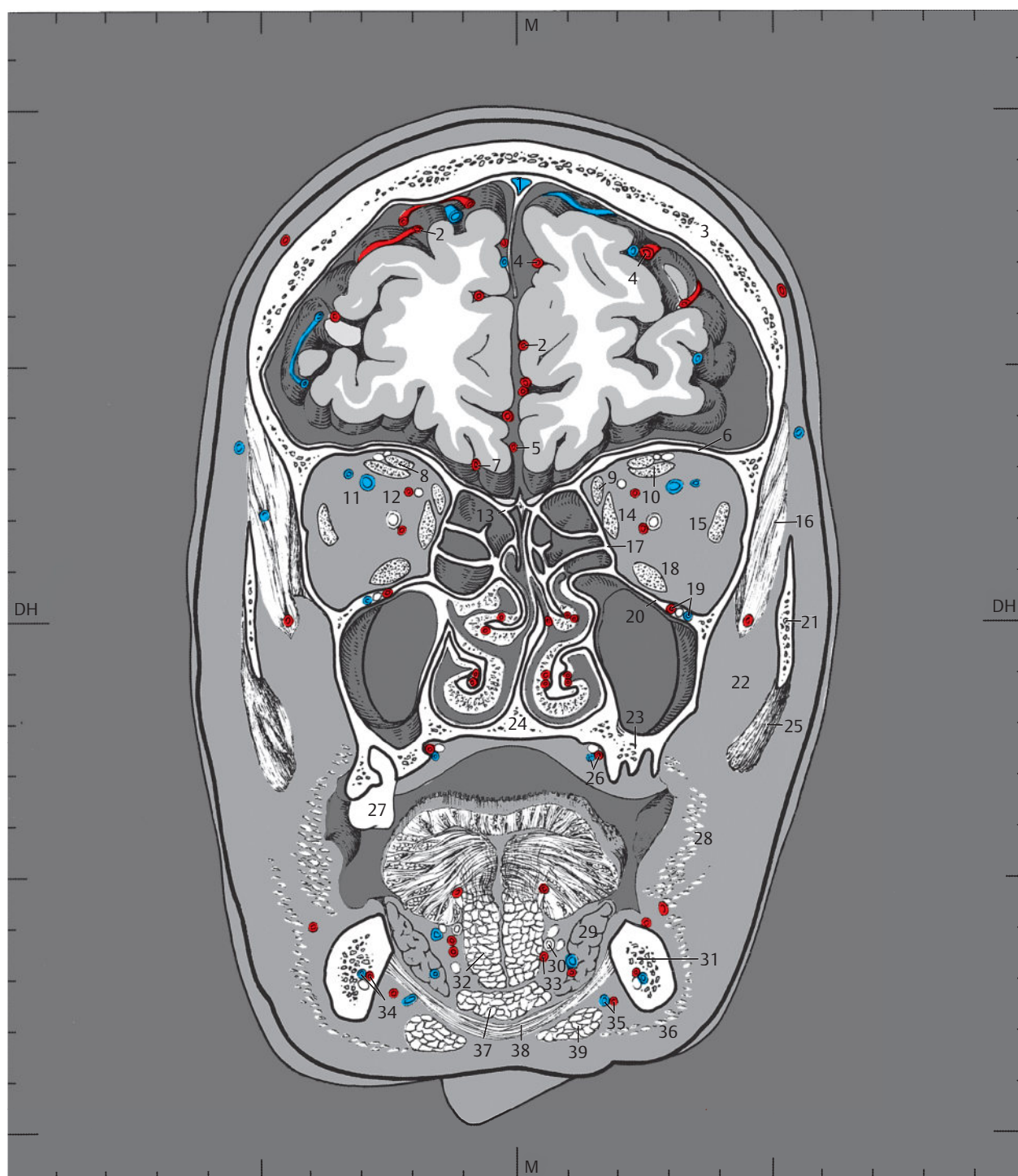
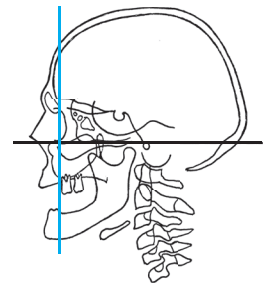
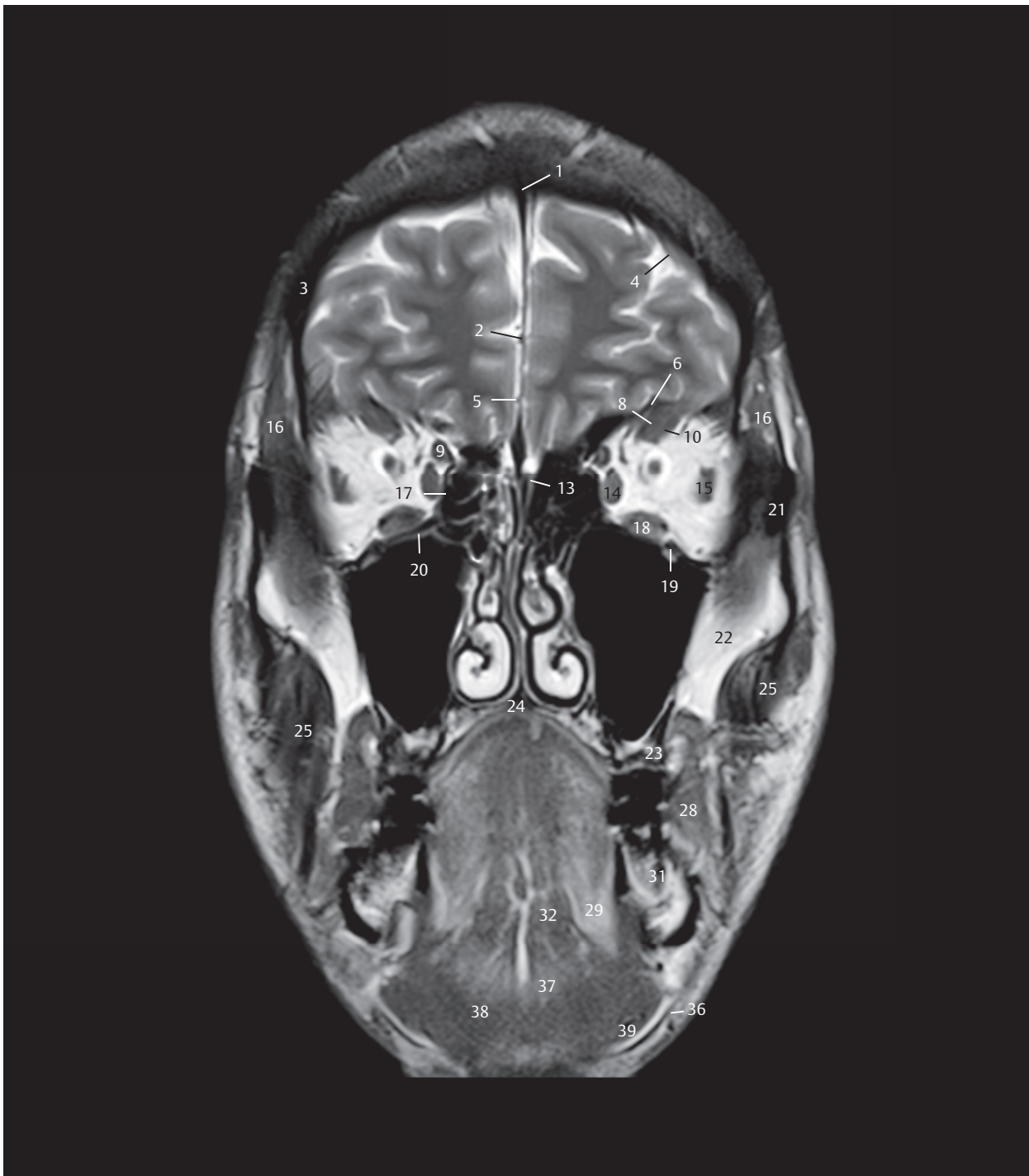
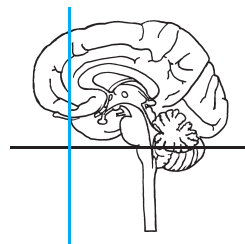


Fig. 3.3c Anterior view of the 2nd coronal section. The section lies approximately 6 mm behind the eyeball and roughly in the center of the body of the mandible. Bony structures, muscles, and blood vessels.



- 1 Superior sagittal sinus
- 2 Anteromedial frontal artery
- 3 Frontal bone
- 4 Intermediomedial frontal artery
- 5 Polar frontal artery
- 6 Roof of orbit
- 8 Levator palpebrae superioris
- 9 Superior oblique
- 10 Superior rectus
- 13 Ethmoid bone, Lamina cribrosa
- 14 Medial rectus
- 15 Lateral rectus
- 16 Temporalis
- 17 Orbital plate
- 18 Inferior rectus
- 19 Infraorbital canal with infraorbital artery, vein
- 20 Floor of orbit
- 21 Zygomatic bone
- 22 Buccal pad of fat
- 23 Maxilla, alveolar process
- 24 Hard palate
- 25 Masseter
- 28 Buccinator
- 29 Sublingual gland
- 31 Body of the mandible
- 32 Genioglossus
- 36 Platysma
- 37 Geniohyoid
- 38 Mylohyoid
- 39 Digastric, anterior belly

Fig. 3.3d Coronal T2w MR image, corresponding approximately to the sectional plane in a and c.



- 1 Falx cerebri
- 2 Superior frontal gyrus
- 3 Middle frontal gyrus
- 4 Cingulate sulcus
- 5 Cingulate gyrus
- 6 Dura mater
- 7 Inferior frontal gyrus
- 8 Orbital gyri
- 9 Straight gyrus
- 10 Trochlear nerve
- 11 Olfactory tract
- 12 Frontal nerve
- 13 Nasociliary nerve
- 14 Ethmoidal cells
- 15 Abducens nerve
- 16 Optic nerve
- 17 Inferior branch of oculomotor nerve
- 18 Middle nasal concha
- 19 Middle nasal canal
- 20 Infraorbital nerve
- 21 Nasal septum
- 22 Maxillary sinus
- 23 Inferior nasal concha
- 24 Nasal cavity
- 25 Inferior nasal canal
- 26 Palatine nerves
- 27 Oral cavity
- 28 Tongue
- 29 Lingual nerve
- 30 Inferior alveolar nerve
- 31 Hypoglossal nerve

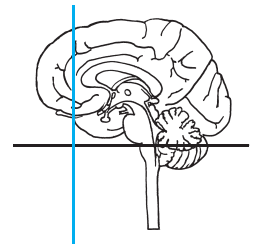
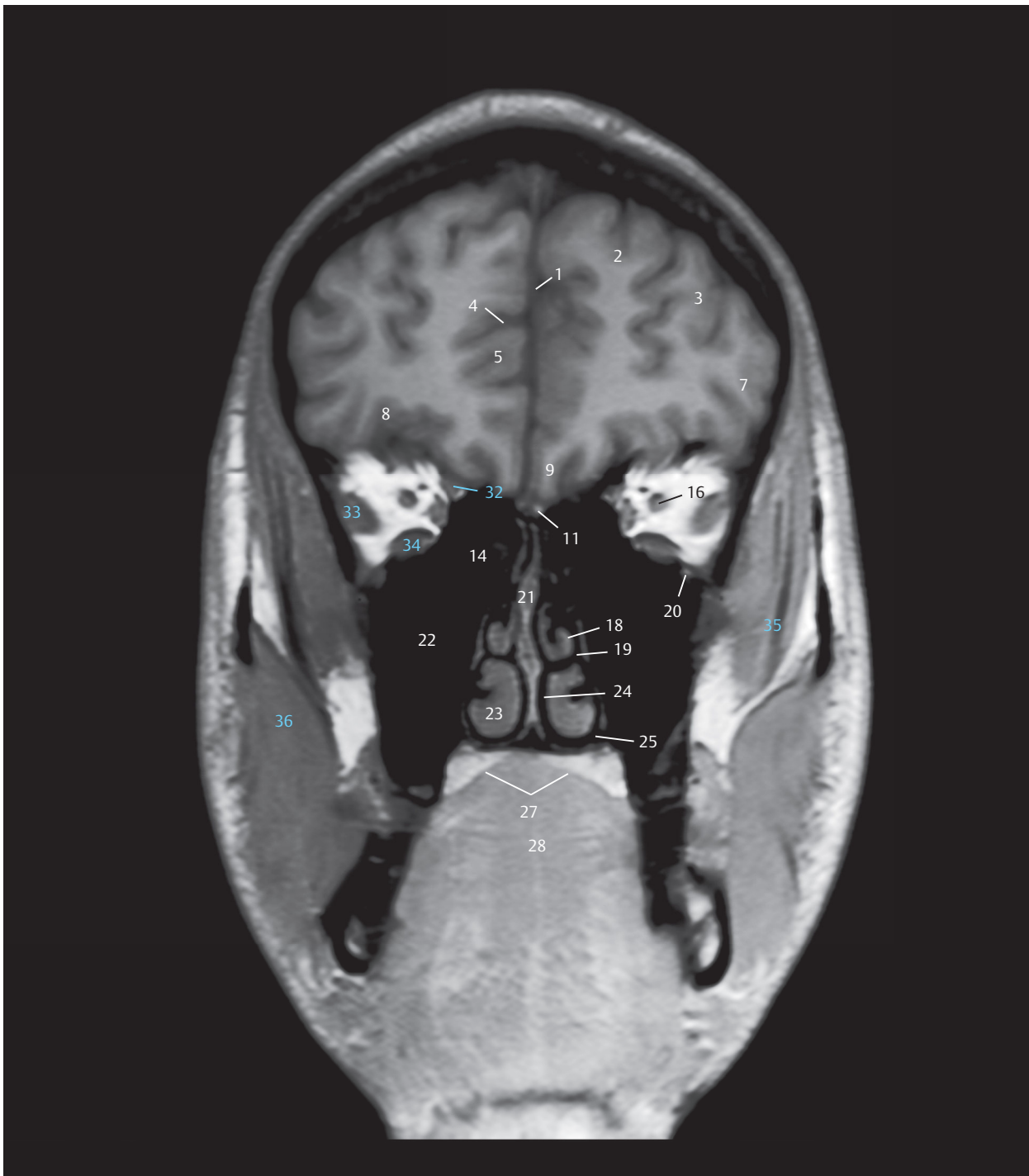


Fig. 3.4 3rd coronal section.

DH = German horizontal

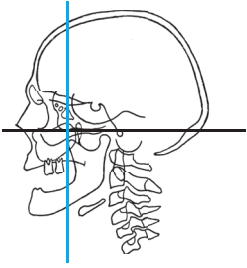
M = median plane

Fig. 3.4a Anterior view of the 3rd coronal section. The sectional plane lies in the frontal lobe approximately 8 mm anterior to the genu of corpus callosum (see ►Fig. 3.1c). The optic nerve, branches of the trigeminal nerve, and the hypoglossal nerve have been sectioned in the region of the facial skeleton. Nasal cavity, paranasal sinuses, oral cavity, brain structures, and cranial nerves.



- 1 Falx cerebri
- 2 Superior frontal gyrus
- 3 Middle frontal gyrus
- 4 Cingulate sulcus
- 5 Cingulate gyrus
- 7 Inferior frontal gyrus
- 8 Orbital gyri
- 9 Straight gyrus
- 11 Olfactory tract
- 14 Ethmoidal air cells
- 16 Optic nerve
- 18 Middle nasal concha
- 19 Middle nasal canal
- 20 Infraorbital canal with infraorbital nerve
- 21 Nasal septum
- 22 Maxillary sinus
- 23 Inferior nasal concha
- 24 Nasal cavity
- 25 Inferior nasal canal
- 27 Oral cavity
- 28 Tongue
- 32 Superior oblique
- 33 Lateral rectus
- 34 Inferior rectus
- 35 Temporalis
- 36 Masseter

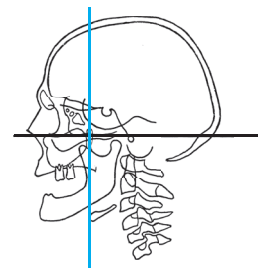
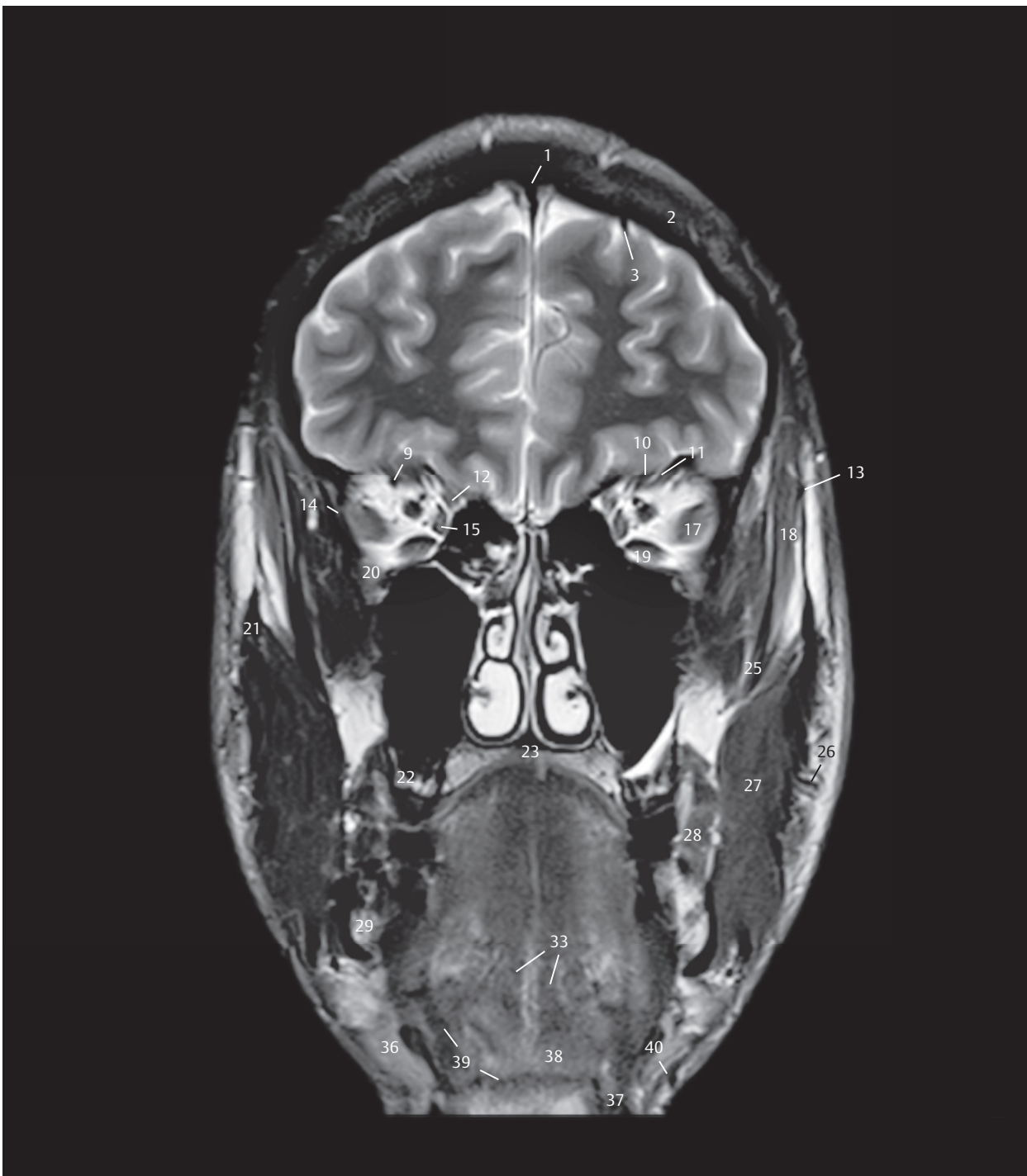
Fig. 3.4b Coronal T1w MR image, corresponding approximately to the sectional plane in a and c.



- 1 Superior sagittal sinus
- 2 Frontal bone
- 3 Intermediomedial frontal artery
- 4 Prefrontal artery
- 5 Anteromedial frontal artery
- 6 Lateral frontobasal artery
- 7 Polar frontal artery
- 8 Medial frontobasal artery
- 9 Superior ophthalmic vein
- 10 Levator palpebrae superioris
- 11 Superior rectus
- 12 Superior oblique
- 13 Superficial temporal artery, frontal branch
- 14 Greater wing of sphenoid
- 15 Medial rectus
- 16 Ophthalmic artery
- 17 Lateral rectus
- 18 Temporalis
- 19 Inferior rectus
- 20 Orbitalis
- 21 Zygomatic arch
- 22 Maxilla
- 23 Hard palate
- 24 Descending palatine artery and vein
- 25 Coronoid process
- 26 Parotid duct
- 27 Masseter
- 28 Buccinator
- 29 Body of mandible
- 30 Facial artery and vein
- 31 Inferior alveolar artery and vein
- 32 Submandibular duct
- 33 Genioglossus
- 34 Sublingual artery
- 35 Submental artery and vein
- 36 Submandibular gland
- 37 Anterior belly of digastric
- 38 Geniohyoid
- 39 Mylohyoid
- 40 Platysma

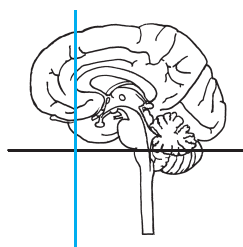


Fig. 3.4c Anterior view of the 3rd coronal section. The sectional plane runs close behind the center of the anterior cranial fossa, through the posterior third of the orbit and the coronoid process of the mandible. Bony structures, muscles, and blood vessels.



- 1 Superior sagittal sinus
- 2 Frontal bone
- 3 Intermediomedial frontal artery
- 9 Superior ophthalmic vein
- 10 Levator palpebrae superioris
- 11 Superior rectus
- 12 Superior oblique
- 13 Superficial temporal artery, frontal branch
- 14 Greater wing of sphenoid
- 15 Medial rectus
- 17 Lateral rectus
- 18 Temporalis
- 19 Inferior rectus
- 20 Orbitalis
- 21 Zygomatic arch
- 22 Maxilla
- 23 Hard palate
- 25 Coronoid process
- 26 Parotid duct
- 27 Masseter
- 28 Buccinator
- 29 Body of the mandible
- 33 Genioglossus
- 36 Submandibular gland
- 37 Digastric, anterior belly
- 38 Geniohyoid
- 39 Mylohyoid
- 40 Platysma

Fig. 3.4d Coronal T2w MR image, corresponding approximately to the sectional plane in a and c.



- 1 Falx cerebri
- 2 Superior frontal gyrus
- 3 Cingulate sulcus
- 4 Middle frontal gyrus
- 5 Cingulate gyrus
- 6 Genu of corpus callosum
- 7 Inferior frontal gyrus
- 8 Dura mater
- 9 Longitudinal cerebral (interhemispheric) fissure
- 10 Straight gyrus
- 11 Orbital gyrus
- 12 Olfactory tract
- 13 Optic nerve
- 14 Trochlear nerve
- 15 Oculomotor nerve
- 16 Pole of temporal lobe
- 17 Ophthalmic nerve
- 18 Abducens nerve
- 19 Sphenoid sinus
- 20 Maxillary nerve
- 21 Nasal septum
- 22 Middle nasal concha
- 23 Nasal cavity
- 24 Inferior nasal concha
- 25 Oral cavity
- 26 Tongue
- 27 Lingual nerve
- 28 Inferior alveolar nerve
- 29 Hypoglossal nerve

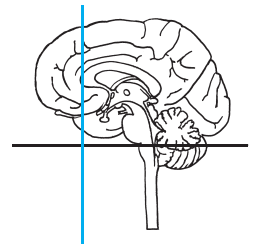
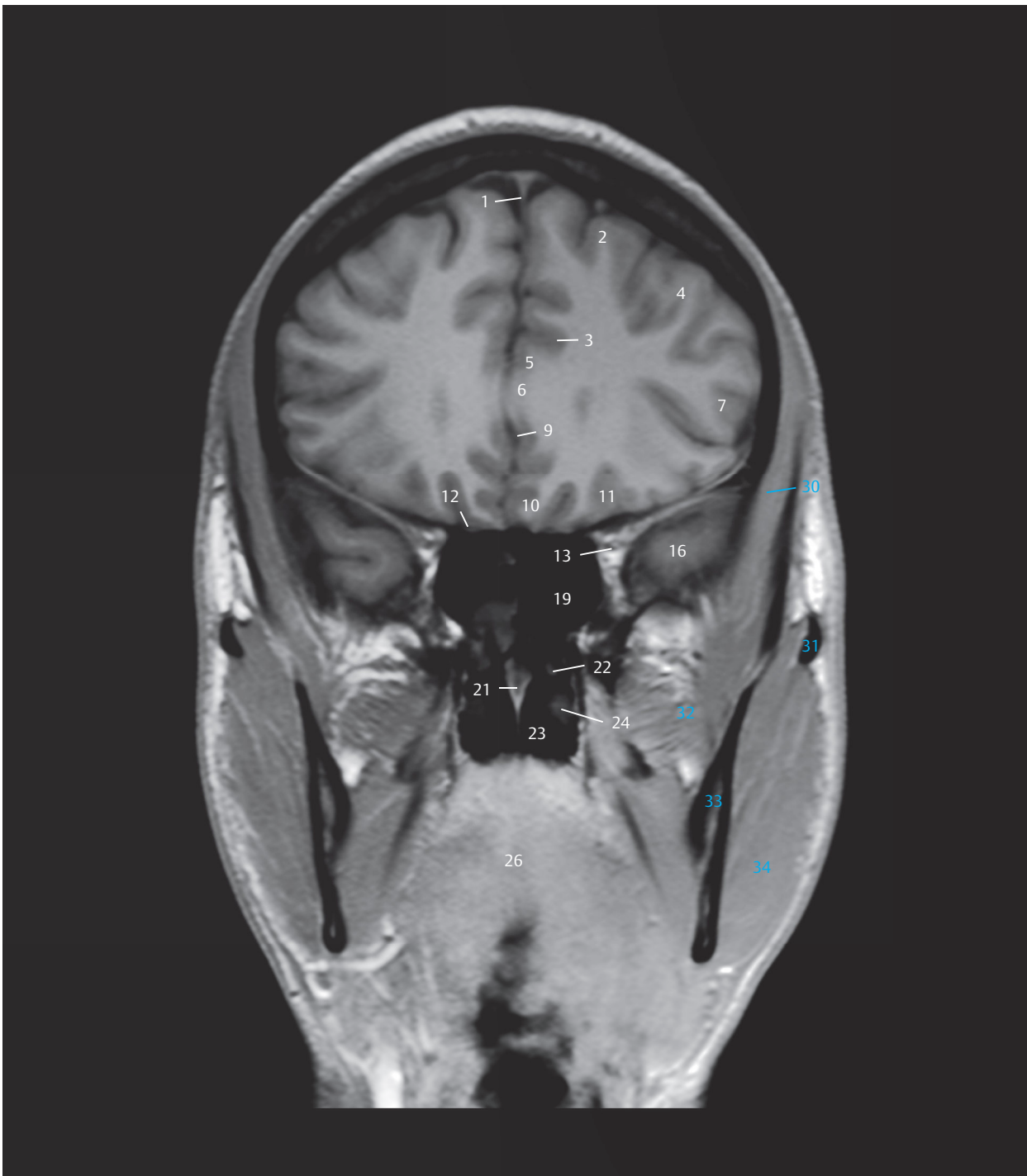


Fig. 3.5 4th coronal section.

DH = German horizontal

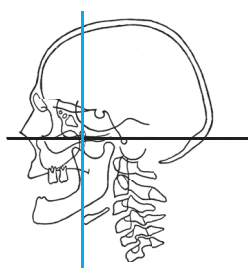
M = median plane

Fig. 3.5a Anterior view of the 4th coronal section. The frontal lobe has been sectioned at the level of the genu of corpus callosum. The abducent, oculomotor, and trochlear nerves, and the optic nerve lie close to each other at the orbital apex. The hypoglossal nerve and branches of the mandibular nerve lie in the region of the floor of the mouth. Nasal cavity and paranasal sinuses, brain structures, and cranial nerves.



- 1 Falx cerebri
- 2 Superior frontal gyrus
- 3 Cingulate sulcus
- 4 Middle frontal gyrus
- 5 Cingulate gyrus
- 6 Corpus callosum, genu (partially in the slice)
- 7 Inferior frontal gyrus
- 9 Longitudinal cerebral (interhemispheric) fissure
- 10 Straight gyrus
- 11 Orbital gyrus
- 12 Olfactory tract
- 13 Optic nerve
- 16 Temporal lobe, pole
- 19 Sphenoid sinus
- 21 Nasal septum
- 22 Middle nasal concha
- 23 Nasal cavity
- 24 Inferior nasal concha
- 26 Tongue
- 30 Temporalis
- 31 Zygomatic bone
- 32 Lateral pterygoid
- 33 Mandible
- 34 Masseter

Fig. 3.5b Coronal T1w MR image.



- 1 Superior sagittal sinus
- 2 Intermediomedial frontal artery
- 3 Prefrontal artery
- 4 Pericallosal artery
- 5 Anterior cerebral artery
- 6 Lateral frontobasal artery
- 7 Polar temporal artery of middle cerebral artery
- 8 Lesser wing of sphenoid
- 9 Ophthalmic artery
- 10 Superior ophthalmic vein
- 11 Inferior orbital fissure
- 12 Superficial temporal artery, frontal branch
- 13 Pterygopalatine fossa
- 14 Zygomatic arch
- 15 Temporalis
- 16 Maxillary artery
- 17 Lateral pterygoid plate
- 18 Lateral pterygoid
- 19 Medial pterygoid
- 20 Medial pterygoid plate
- 21 Soft palate
- 22 Tensor veli palatini
- 23 Coronoid process
- 24 Parotid duct
- 25 Pterygoid hamulus
- 26 Masseter
- 27 Ramus of mandible
- 28 Inferior alveolar artery and vein in mandibular canal
- 29 Sublingual artery
- 30 Mylohyoid
- 31 Submental artery and vein
- 32 Submandibular gland
- 33 Platysma
- 34 Digastric tendon
- 35 Hyoid bone
- 36 Thyroid cartilage

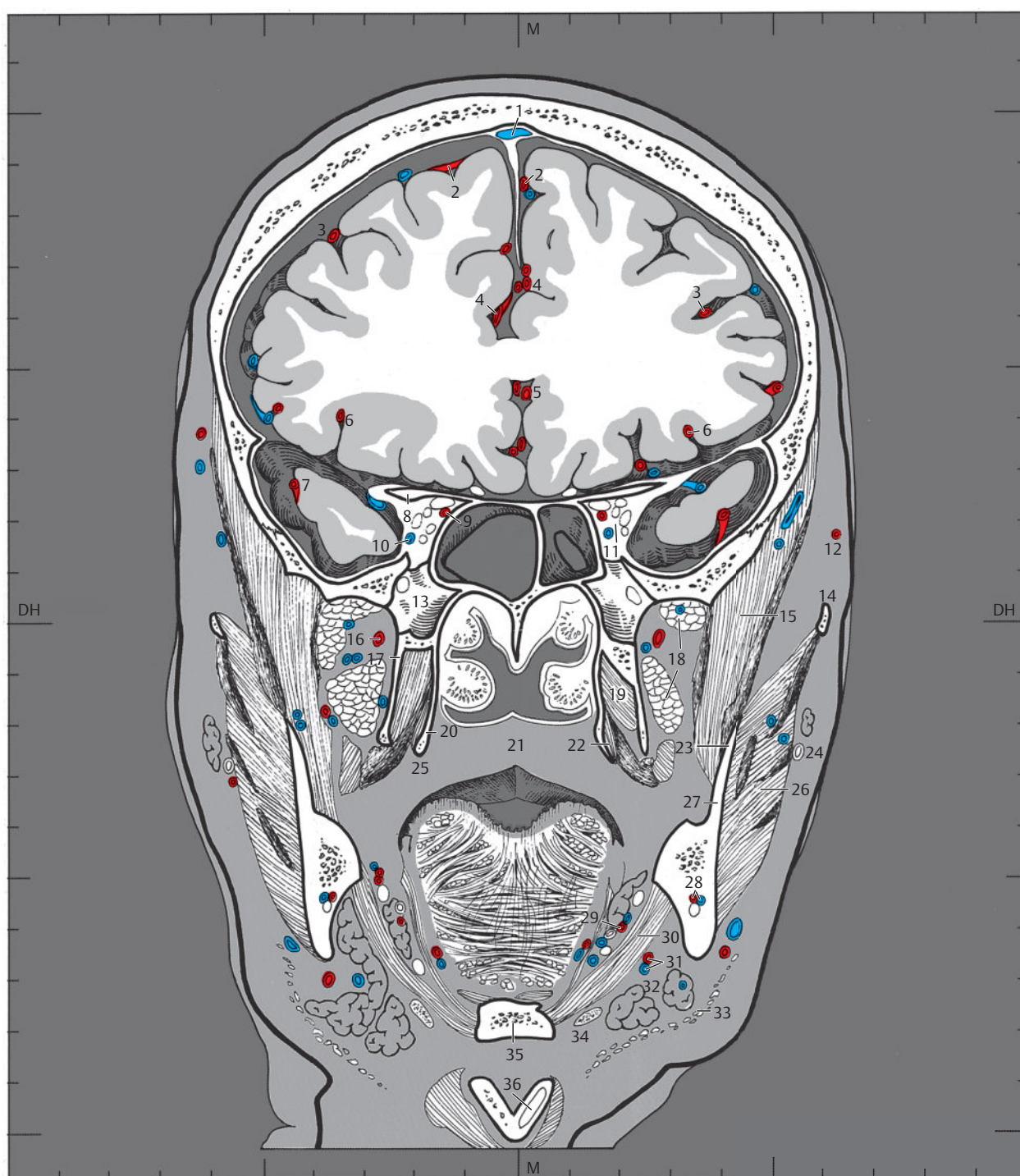
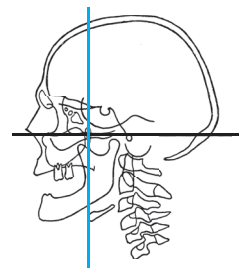
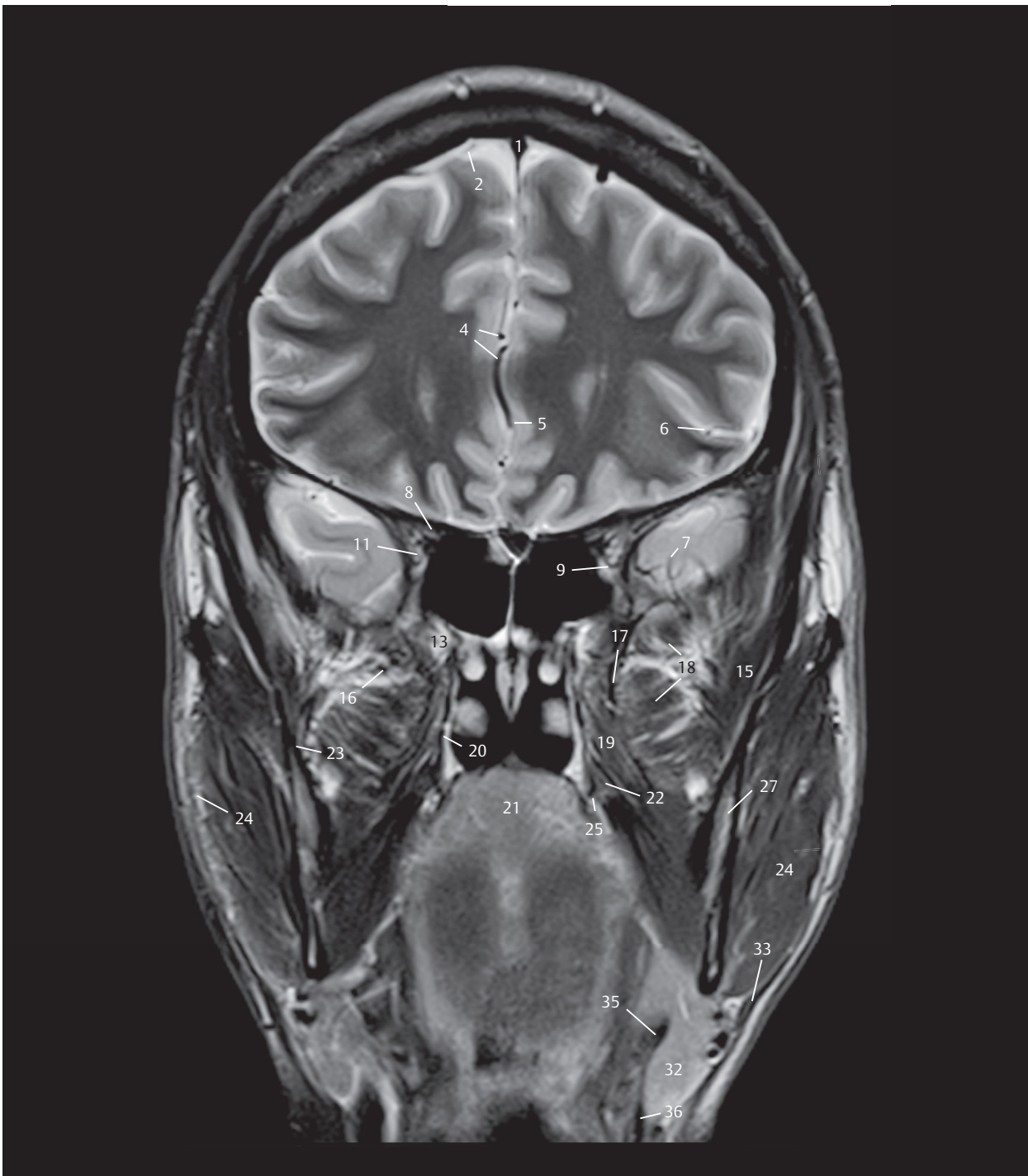
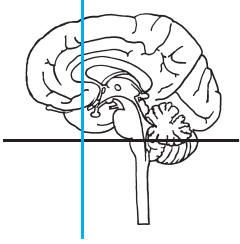


Fig. 3.5c Anterior view of the 4th coronal section. The anterior poles of the middle cranial fossa have been sectioned and lie under the lesser wings of the sphenoid. The optic canal and the superior orbital fissure can be identified in the sectional plane. The tongue has been sectioned at the level of the hyoid bone. Bony structures, muscles, and blood vessels.



- 1 Superior sagittal sinus
- 2 Intermediomedial frontal artery
- 4 Pericallosal artery
- 5 Anterior cerebral artery
- 6 Lateral frontobasal artery
- 7 Polar temporal artery
- 8 Sphenoid, lesser wing
- 9 Ophthalmic artery
- 11 Superior orbital fissure
- 12 Superficial temporal artery, frontal branch
- 13 Pterygopalatine fossa
- 14 Zygomatic arch
- 15 Temporalis
- 16 Maxillary artery
- 17 Pterygoid process, lateral plate
- 18 Lateral pterygoid
- 19 Medial pterygoid
- 20 Pterygoid process, medial plate
- 21 Soft palate
- 22 Tensor veli palatini
- 23 Coronoid process
- 24 Parotid duct
- 25 Pterygoid hamulus
- 26 Masseter
- 27 Ramus of mandible
- 32 Submandibular gland
- 33 Platysma
- 35 Hyoid bone
- 36 Thyroid cartilage

Fig. 3.5d Coronal T2w MR image.



- 1 Superior frontal gyrus
- 2 Falx cerebri
- 3 Middle frontal gyrus
- 4 Cingulate sulcus
- 5 Cingulate gyrus
- 6 Inferior frontal gyrus
- 7 Genu of corpus callosum
- 8 Frontal (anterior) horn of lateral ventricle
- 9 Head of caudate nucleus
- 10 Insula
- 11 Lateral sulcus (Sylvian fissure)
- 12 Putamen
- 13 Superior temporal gyrus
- 14 Straight gyrus
- 15 Olfactory tract
- 16 Optic chiasm
- 17 Optic nerve
- 18 Oculomotor nerve
- 19 Trochlear nerve
- 20 Middle temporal gyrus
- 21 Ophthalmic nerve
- 22 Abducens nerve
- 23 Sphenoid sinus
- 24 Maxillary nerve
- 25 Nasopharynx
- 26 Uvula
- 27 Inferior alveolar nerve
- 28 Palatine tonsil
- 29 Lingual nerve
- 30 Isthmus of fauces
- 31 Hypoglossal nerve

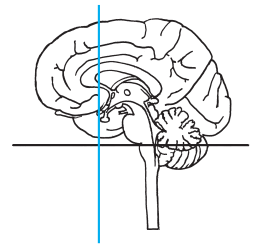
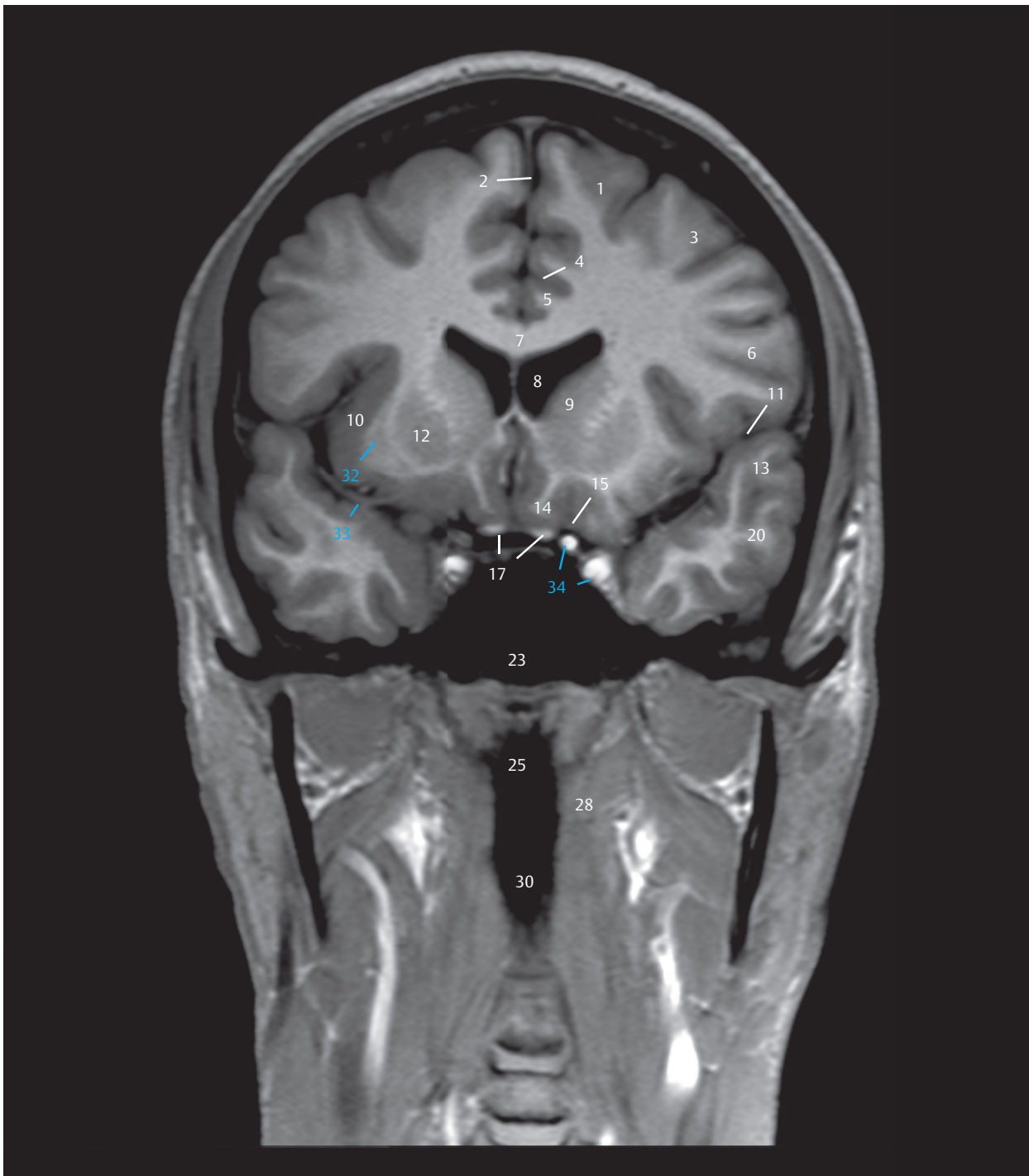


Fig. 3.6 5th coronal section.

DH = German horizontal

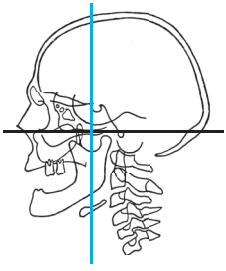
M = median plane

Fig. 3.6a Anterior view of the 5th coronal section. The frontal horns of the lateral ventricles have been sectioned in this plane. The optic chiasma lies in this slice. The lingual and hypoglossal nerves are identified lateral to the pharyngeal isthmus. Brain structures and cranial nerves.



- 1 Superior frontal gyrus
- 2 Falx cerebri
- 3 Middle frontal gyrus
- 4 Cingulate sulcus
- 5 Cingulate gyrus
- 6 Inferior frontal gyrus
- 7 Corpus callosum
- 8 Lateral ventricle, frontal horn
- 9 Head of caudate nucleus
- 10 Insula
- 11 Lateral sulcus
- 12 Putamen
- 13 Superior temporal gyrus
- 14 Straight gyrus
- 15 Olfactory tract
- 17 Optic nerve
- 20 Middle temporal gyrus
- 23 Sphenoid sinus
- 25 Pharynx, nasopharynx
- 28 Palatine tonsils
- 30 Isthmus of fauces
- 32 Claustrum
- 33 Middle cerebral artery
- 34 Internal carotid artery

Fig. 3.6b Coronal T1w MR image, corresponding to the sectional plane in a and c.



- 1 Superior sagittal sinus
- 2 Parietal bone
- 3 Posteromedial frontal artery
- 4 Bridging vein
- 5 Intermediomedial frontal artery
- 6 Prefrontal artery
- 7 Paracentral artery
- 8 Pericallosal artery
- 9 Insular arteries
- 10 Anterior cerebral artery
- 11 Basal vein (of Rosenthal)
- 12 Anterior clinoid process
- 13 Internal carotid artery
- 14 Temporal artery of middle cerebral artery
- 15 Cavernous sinus
- 16 Temporal bone
- 17 Superficial temporal artery, frontal branch
- 18 Temporalis
- 19 Sphenoid
- 20 Zygomatic arch
- 21 Maxillary artery
- 22 Lateral pterygoid
- 23 Nasopharynx
- 24 Parotid gland
- 25 Soft palate
- 26 Medial pterygoid
- 27 Inferior alveolar artery and vein
- 28 Masseter
- 29 Uvula
- 30 Styloglossus
- 31 Ramus of mandible
- 32 Submandibular gland
- 33 Facial artery
- 34 Epiglottis
- 35 Stylohyoid ligament
- 36 Lingual artery
- 37 Digastric tendon and stylohyoid
- 38 Greater cornu of hyoid bone
- 39 Platysma
- 40 Vestibular fold
- 41 Thyroid cartilage
- 42 Vocal fold

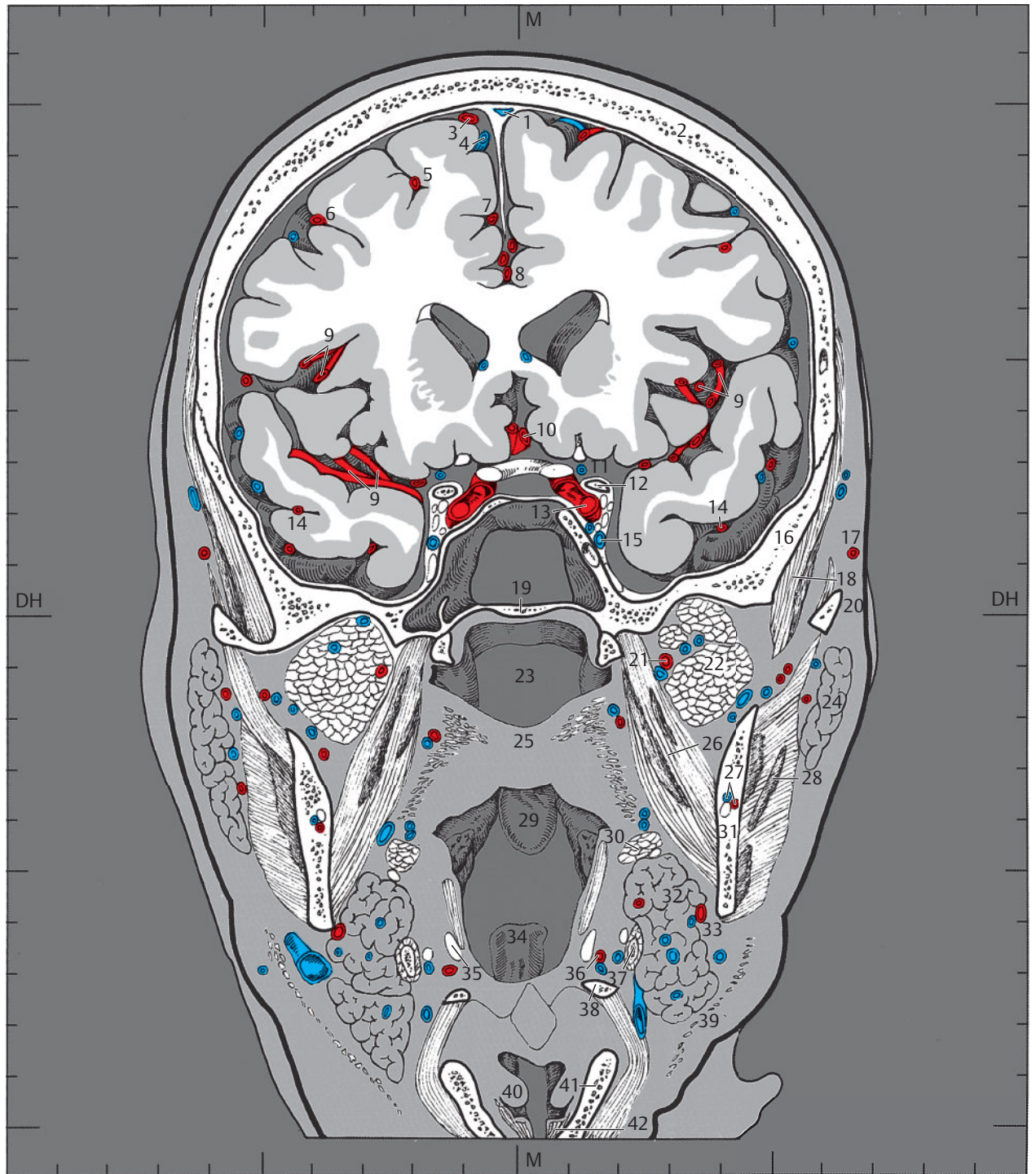
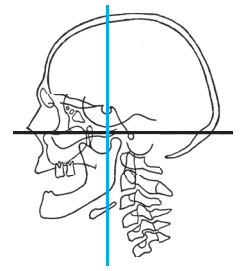
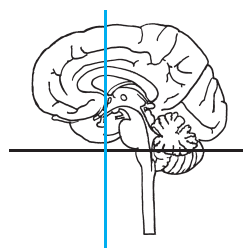


Fig. 3.6c Anterior view of the 5th coronal section. The sectional plane lies approximately in the center of the sphenoid bone at the level of the anterior clinoid process and in the center of the zygomatic arch. The nasopharynx, soft palate, and the uvula are visualized in this section. Bony structures, muscles, and blood vessels.



- 1 Superior sagittal sinus
- 2 Parietal bone
- 4 Bridging veins
- 7 Paracentral artery
- 8 Pericallosal artery
- 9 Insular arteries
- 10 Anterior cerebral artery
- 12 Anterior clinoid process
- 13 Internal carotid artery
- 15 Cavernous sinus
- 16 Temporal bone
- 18 Temporalis
- 19 Sphenoid
- 20 Zygomatic arch
- 21 Maxillary artery
- 22 Lateral pterygoid
- 23 Pharynx, nasopharynx
- 24 Parotid gland
- 26 Medial pterygoid
- 28 Masseter
- 30 Styloglossus
- 31 Ramus of mandible
- 32 Submandibular gland
- 34 Epiglottis
- 43 Internal capsule, anterior limb
- 44 Middle cerebral artery
- 45 Nucleus accumbens
- 46 Optic nerve

Fig. 3.6d Coronal T2w MR image, corresponding to the sectional plane in a and c.



- 1 Superior frontal gyrus
- 2 Falx cerebri
- 3 Middle frontal gyrus
- 4 Cingulate sulcus
- 5 Cingulate gyrus
- 6 Stratum subependymale
- 7 Trunk (body) of corpus callosum
- 8 Inferior frontal gyrus
- 9 Frontal (anterior) horn of lateral ventricle
- 10 Head of caudate nucleus
- 11 Septum pellucidum
- 12 Anterior limb of internal capsule
- 13 Lateral sulcus (Sylvian fissure)
- 14 Putamen
- 15 External capsule
- 16 Claustrum
- 17 Extreme capsule
- 18 Insula
- 19 Superior temporal gyrus
- 20 Anterior commissure (within the slice)
- 21 Anterior commissure
- 22 Superior temporal sulcus
- 23 Third ventricle
- 24 Optic tract
- 25 Middle temporal gyrus
- 26 Infundibular recess
- 27 Oculomotor nerve
- 28 Trochlear nerve
- 29 Parahippocampal gyrus
- 30 Abducens nerve
- 31 Trigeminal ganglion
- 32 Inferior temporal gyrus
- 33 Inferior temporal sulcus
- 34 Sphenoid sinus
- 35 Lateral occipitotemporal gyrus
- 36 Mandibular nerve
- 37 Glossopharyngeal nerve
- 38 Hypoglossal nerve
- 39 Nucleus accumbens

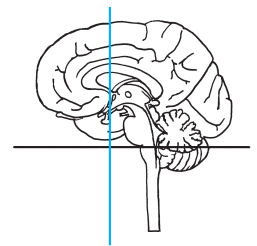
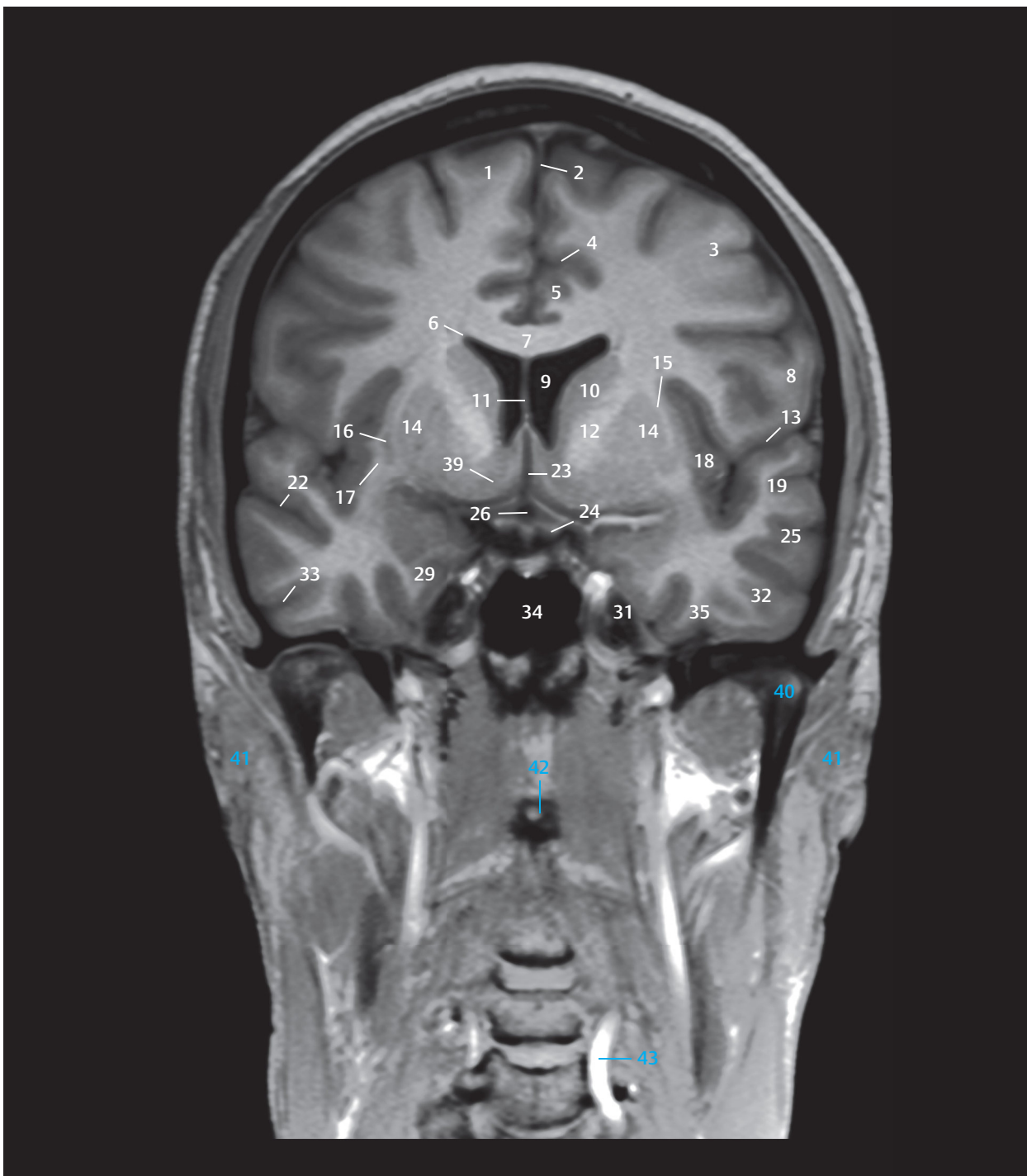


Fig. 3.7 6th coronal section.

DH = German horizontal

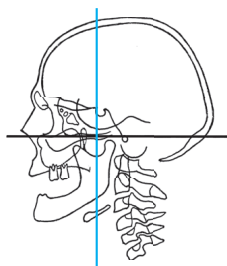
M = median plane

Fig. 3.7a Anterior view of the 6th coronal section. The sectional plane lies in the median region 2 mm anterior to the anterior commissure (interrupted lines within the slice). Its anterior extensions section the basal ganglia laterally. The abducens, oculomotor, and trochlear nerves lie lateral to the hypophysis. Brain structures and cranial nerves.



- 1 Superior frontal gyrus
- 2 Falx cerebri
- 3 Middle frontal gyrus
- 4 Cingulate sulcus
- 5 Cingulate gyrus
- 6 Stratum subependymale
- 7 Corpus callosum, body
- 8 Inferior frontal gyrus
- 9 Lateral ventricle, frontal horn
- 10 Head of caudate nucleus
- 11 Septum pellucidum
- 12 Internal capsule, anterior limb
- 13 Lateral sulcus
- 14 Putamen
- 15 External capsule
- 16 Claustrum
- 17 Extreme capsule
- 18 Insula
- 19 Superior temporal gyrus
- 22 Superior temporal sulcus
- 23 Third ventricle
- 24 Optic tract
- 25 Middle temporal gyrus
- 26 Infundibular recess
- 29 Parahippocampal gyrus
- 31 Trigeminal ganglion
- 32 Inferior temporal gyrus
- 33 Inferior temporal sulcus
- 34 Sphenoid sinus
- 35 Lateral occipitotemporal gyrus
- 39 Nucleus accumbens
- 40 Head of mandible
- 41 Parotid
- 42 Anterior arch of atlas
- 43 Vertebral artery

Fig. 3.7b Coronal T1w MR image, which corresponds to the plane in a and c.



- 1 Superior sagittal sinus
- 2 Posteromedial frontal artery
- 3 Parietal bone
- 4 Paracentral artery
- 5 Pericallosal artery
- 6 Artery of precentral sulcus
- 7 Superior thalamostriate (terminal) vein
- 8 Insular arteries
- 9 Middle cerebral artery
- 10 Anterior choroidal artery
- 11 Basal vein (of Rosenthal)
- 12 Posterior clinoid process
- 13 Cavernous sinus
- 14 Pituitary gland
- 15 Temporalis
- 16 Temporal artery of middle cerebral artery
- 17 Internal carotid artery
- 18 Sphenoid
- 19 Temporal bone
- 20 Superficial temporal artery
- 21 Mandibular fossa
- 22 Articular disc of temporomandibular joint
- 23 Head of mandible
- 24 Cartilage of pharyngotympanic tube
- 25 Pterygoid venous plexus
- 26 Levator veli palatini
- 27 Lateral pterygoid
- 28 Maxillary artery
- 29 Posterior pharyngeal wall of nasopharynx
- 30 Ramus of mandible
- 31 Medial pterygoid
- 32 Styloglossus
- 33 Constrictor of pharynx
- 34 Parotid gland
- 35 Posterior pharyngeal wall of oropharynx
- 36 Facial artery
- 37 Masseter
- 38 Stylohyoid ligament (ossified)
- 39 Posterior belly of digastric
- 40 Stylopharyngeus
- 41 Lingual artery
- 42 Greater cornu of hyoid bone
- 43 Platysma
- 44 Superior thyroid artery
- 45 Sternocleidomastoid
- 46 Thyroid cartilage

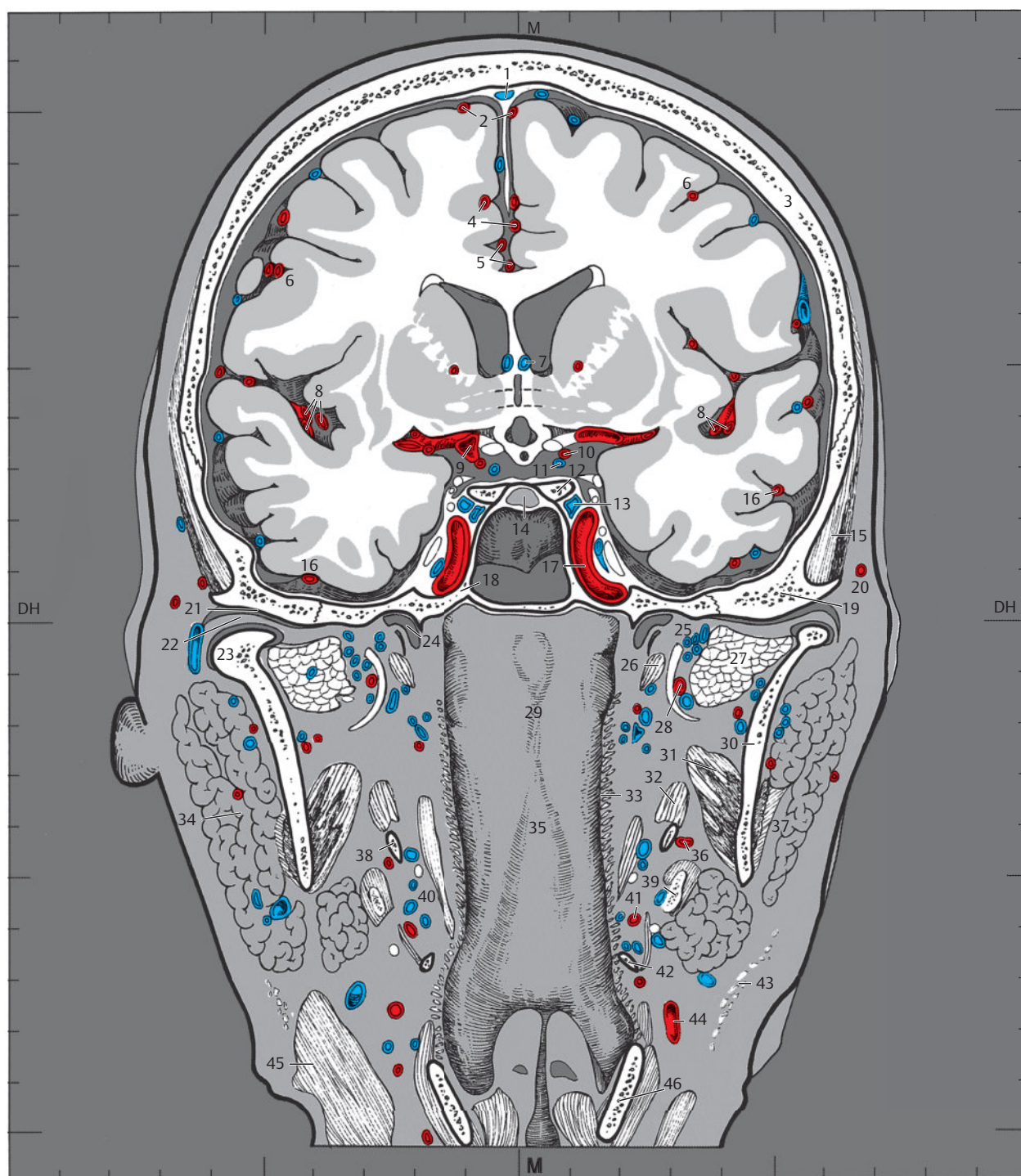
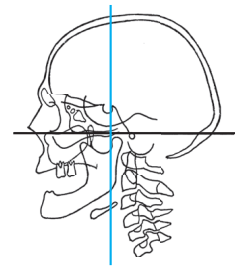
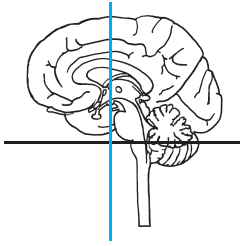


Fig. 3.7c Anterior view of the 6th coronal section. The sectional plane runs through the pituitary fossa at the level of the posterior clinoid processes and through both temporomandibular joints. The posterior wall of the pharynx lies in the anterior half of the 1-cm-thick slice. Bony structures, muscles, and blood vessels.



- 1 Superior sagittal sinus
- 3 Parietal bone
- 4 Paracentral artery
- 5 Pericallosal artery
- 7 Superior thalamostriate vein
- 8 Insular arteries
- 9 Middle cerebral artery
- 12 Posterior clinoid process
- 13 Cavernous sinus
- 14 Pituitary gland
- 15 Temporalis
- 17 Internal carotid artery
- 18 Sphenoid
- 19 Temporal bone
- 20 Superficial temporal artery
- 21 Mandibular fossa
- 23 Head of mandible
- 24 Auditory tube, cartilage
- 26 Levator veli palatini
- 27 Lateral pterygoid
- 28 Maxillary artery
- 29 Posterior pharyngeal wall, nasopharynx
- 30 Ramus of mandible
- 32 Styloglossus
- 34 Parotid gland
- 39 Digastric, posterior belly
- 45 Sternocleidomastoid
- 47 Bridging vein (superior cerebral vein)
- 48 Anterior cerebral artery
- 49 Meckel's cave
- 50 Vertebral artery

Fig. 3.7d Coronal T2w MR image, corresponding to the section in a and c.



- 1 Superior frontal gyrus
- 2 Middle frontal gyrus
- 3 Falx cerebri
- 4 Cingulate gyrus
- 5 Precentral gyrus
- 6 Trunk (body) of corpus callosum
- 7 Septum pellucidum
- 8 Frontal (anterior) horn of lateral ventricle
- 9 Body of caudate nucleus
- 10 Fornix
- 11 Choroid plexus
- 12 Genu of internal capsule
- 13 Interventricular foramen (of Monro)
- 14 Anterior nuclei of thalamus
- 15 Globus pallidus
- 16 Putamen
- 17 Insula
- 18 Lateral sulcus (Sylvian fissure)
- 19 Superior temporal gyrus
- 20 External capsule
- 21 Extreme capsule
- 22 Claustrum
- 23 Basal nucleus (of Meynert)
- 24 Third ventricle
- 25 Mammillary body with fornix
- 26 Optic tract
- 27 Amygdaloid body
- 28 Middle temporal gyrus
- 29 Temporal (inferior) horn of lateral ventricle
- 30 Hippocampus
- 31 Oculomotor nerve
- 32 Trochlear nerve
- 33 Anterior petroclinoid fold
- 34 Abducens nerve
- 35 Pons
- 36 Parahippocampal gyrus
- 37 Trigeminal nerve
- 38 Lateral occipitotemporal gyrus
- 39 Inferior temporal gyrus
- 40 Sphenoid sinus, posterior wall
- 41 Superior cervical ganglion
- 42 Vagus nerve (within the slice)
- 43 Sympathetic trunk (within the slice)
- 44 Hypoglossal nerve
- 45 Superior laryngeal nerve

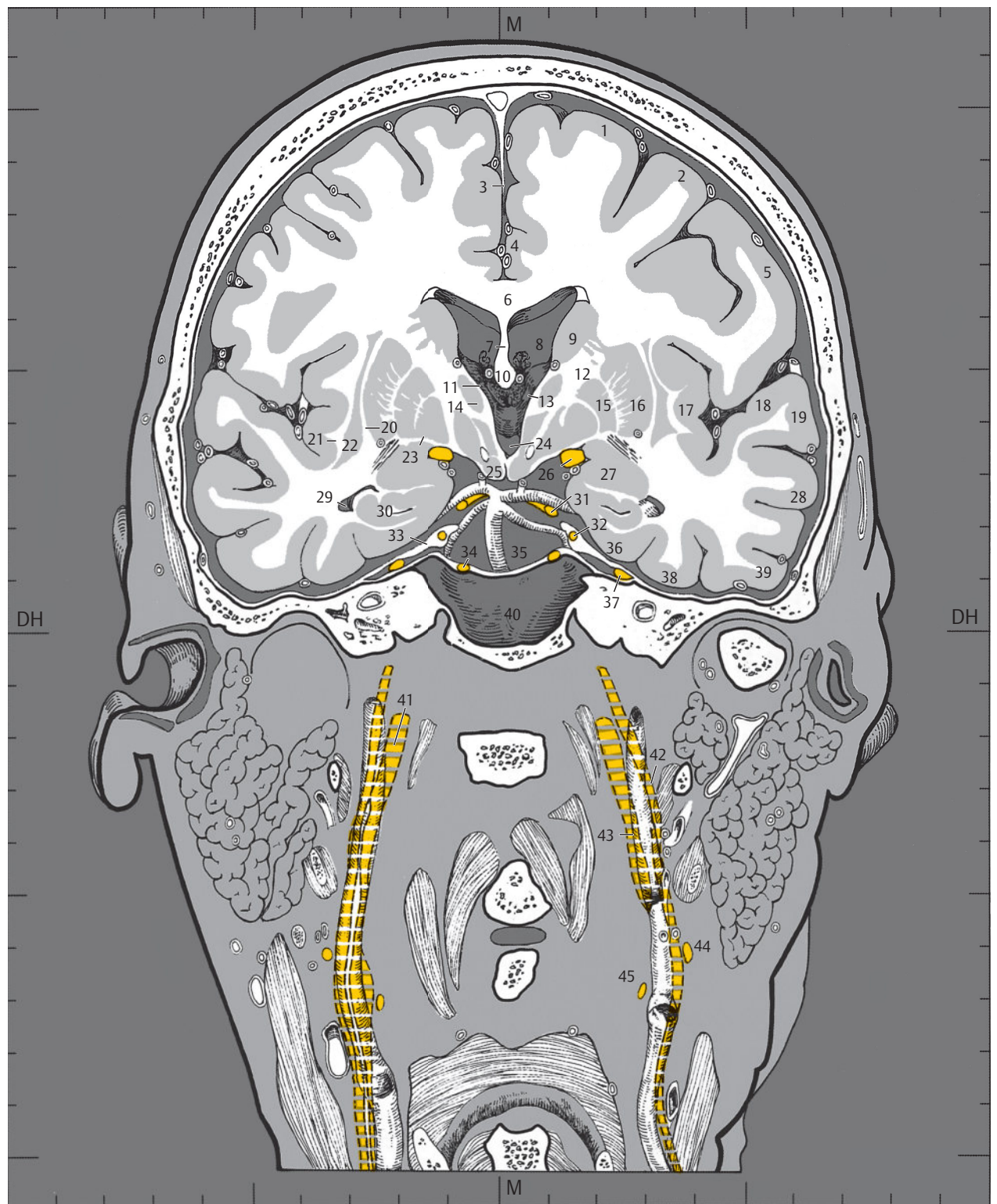
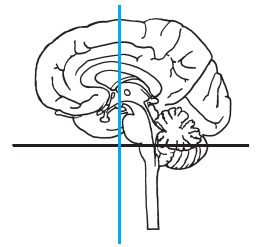
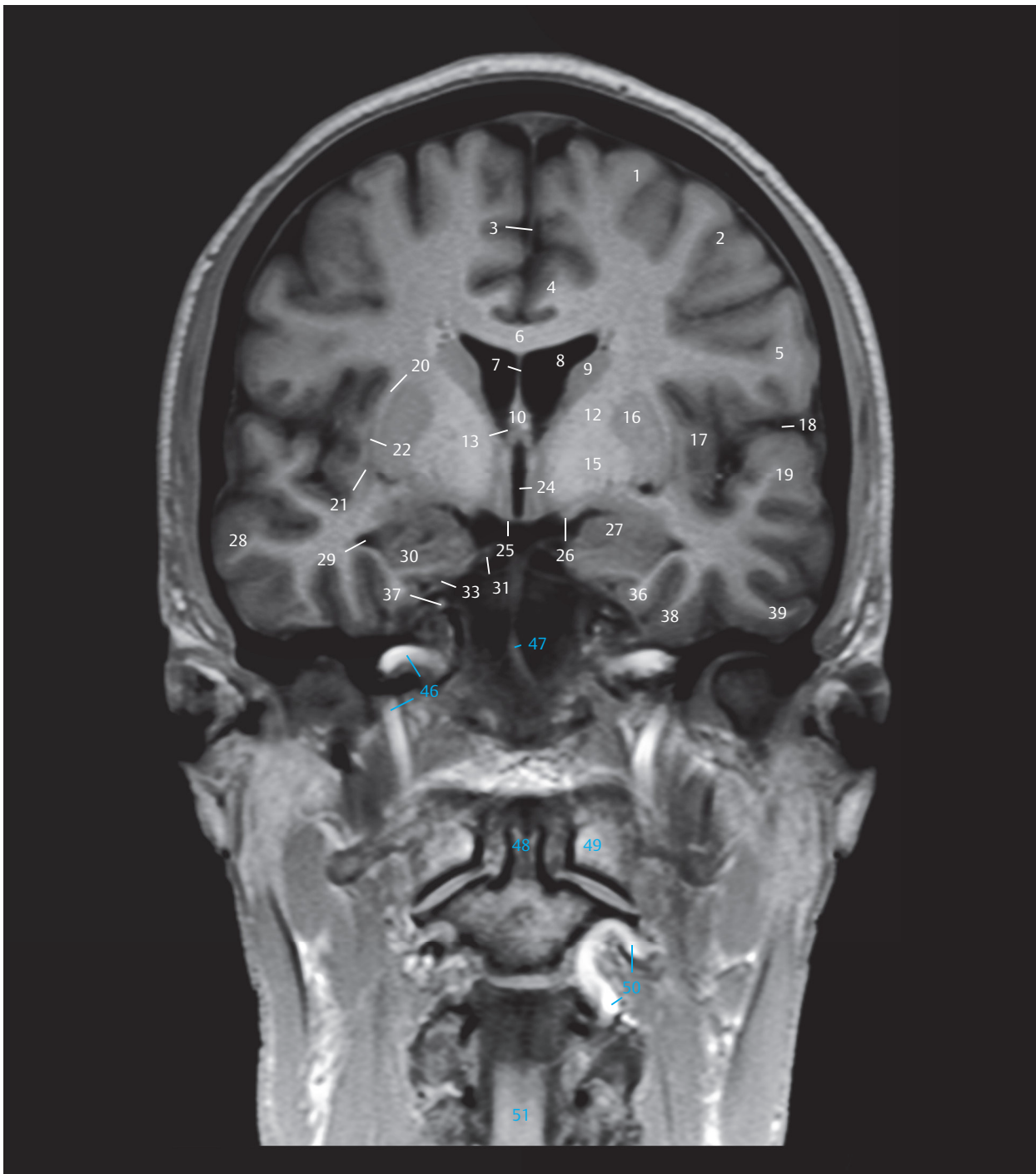


Fig. 3.8 7th coronal section.

DH = German horizontal

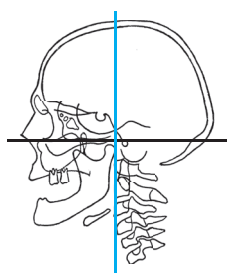
M = median plane

Fig. 3.8a Anterior view of the 7th coronal section. The interventricular foramina, the mammillary bodies and the anterior part of the inferior horn of the lateral ventricle lie in this plane. Brain structures and cranial nerves.



- 1 Superior frontal gyrus
- 2 Middle frontal gyrus
- 3 Falx cerebri
- 4 Cingulate gyrus
- 5 Precentral gyrus
- 6 Corpus callosum, body
- 7 Septum pellucidum
- 8 Lateral ventricle, frontal horn
- 9 Body of caudate nucleus
- 10 Fornix
- 12 Internal capsule, genu
- 13 Interventricular foramen (Monro)
- 15 Globus pallidus
- 16 Putamen
- 17 Insula
- 18 Lateral sulcus
- 19 Superior temporal gyrus
- 20 External capsule
- 21 Extreme capsule
- 22 Claustrum
- 24 Third ventricle
- 25 Mammillary body with fornix
- 26 Optic tract
- 27 Amygdaloid body
- 28 Middle temporal gyrus
- 29 Lateral ventricle, temporal horn
- 30 Hippocampus
- 31 Oculomotor nerve
- 33 Anterior petroclinoid fold
- 36 Parahippocampal gyrus
- 37 Trigeminal nerve
- 38 Lateral occipitotemporal gyrus
- 39 Inferior temporal gyrus
- 46 Internal carotid artery
- 47 Basilar artery
- 48 Dens
- 49 First cervical vertebra, lateral mass
- 50 Vertebral artery
- 51 Spinal cord

Fig. 3.8b Coronal T1w MR image, corresponding to the section in a and c.

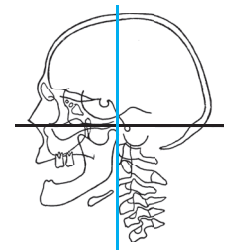
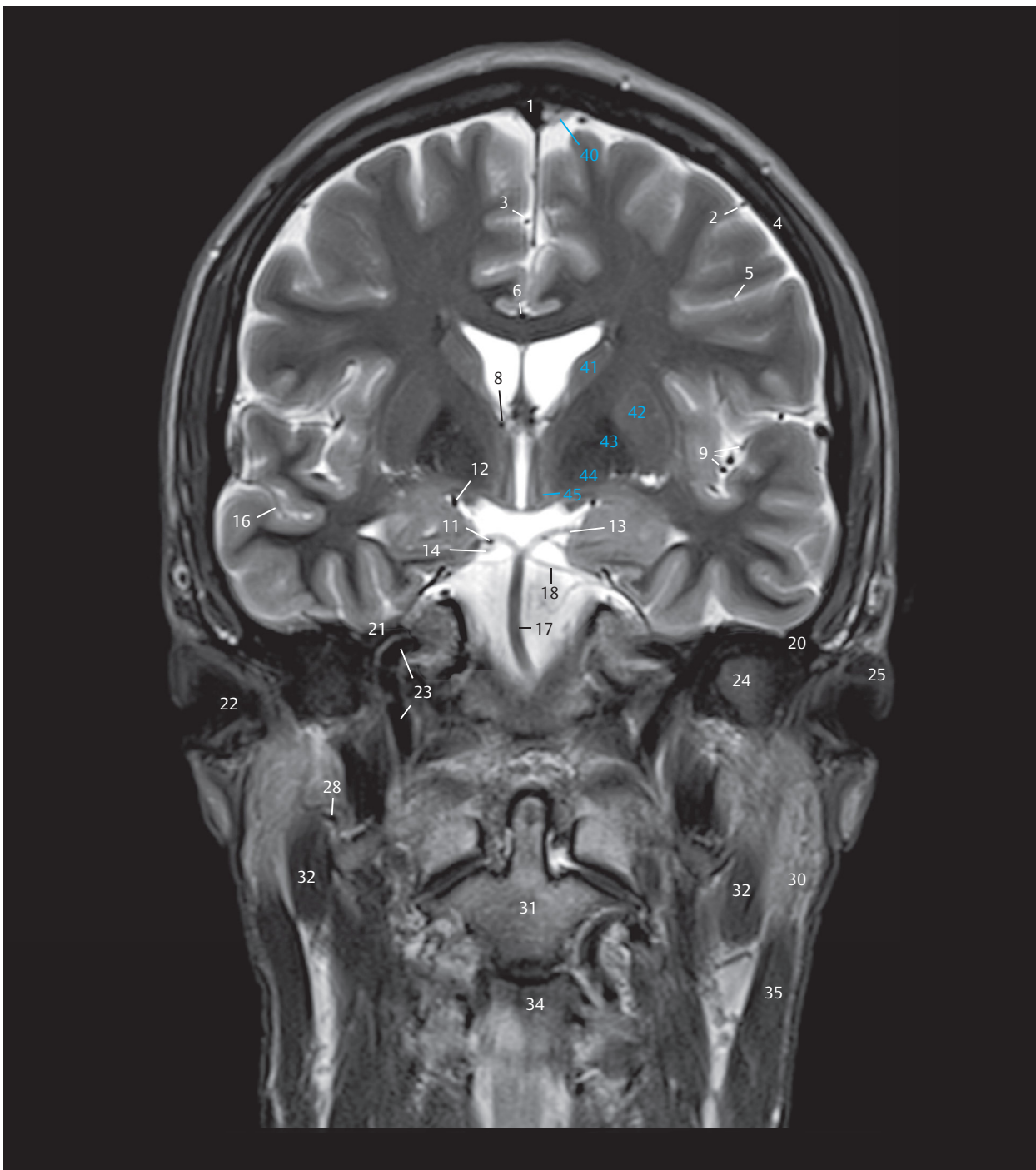


- 1 Superior sagittal sinus
- 2 Posteromedial frontal artery
- 3 Paracentral artery
- 4 Parietal bone
- 5 Artery of precentral sulcus
- 6 Pericallosal artery
- 7 Artery of central sulcus
- 8 Superior thalamostriate (terminal) vein
- 9 Insular arteries
- 10 Anterior choroidal artery
- 11 Posterior communicating artery
- 12 Basal vein (of Rosenthal)
- 13 Posterior cerebral artery
- 14 Oculomotor nerve
- 15 Temporalis
- 16 Temporal artery of middle cerebral artery
- 17 Basilar artery
- 18 Superior cerebellar artery
- 19 Middle meningeal artery
- 20 Temporal bone
- 21 Sphenoid
- 22 External acoustic canal
- 23 Internal carotid artery
- 24 Head of mandible (cut)
- 25 Auricle (pinna)
- 26 Anterior arch of atlas
- 27 External carotid artery
- 28 Occipital artery
- 29 Stylohyoid ligament (ossified)
- 30 Parotid gland
- 31 Axis
- 32 Posterior belly of digastric
- 33 External carotid artery (cut)
- 34 Third cervical vertebra
- 35 Sternocleidomastoid
- 36 Constrictor of pharynx
- 37 Cricoid cartilage
- 38 Common carotid artery
- 39 Thyroid cartilage



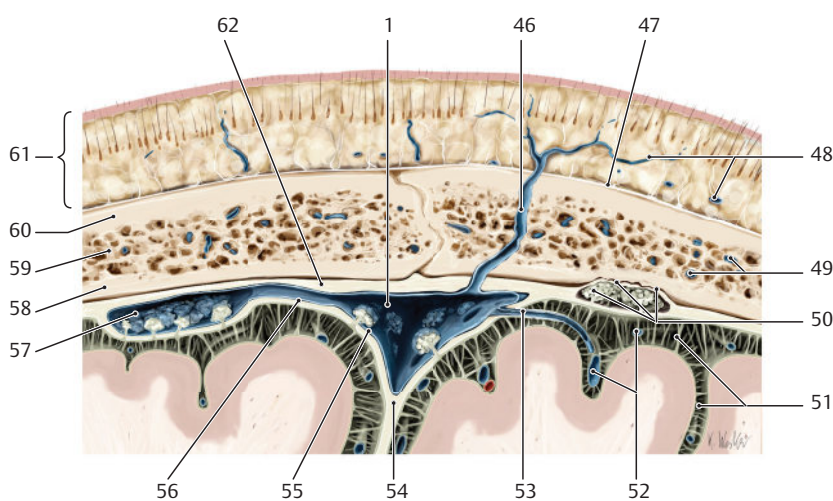
Fig. 3.8c Anterior view of the 7th coronal section. The sectional plane lies at the level of the anterior wall of the cartilaginous external auditory canal. Vertebral bodies have been evenly sectioned. The internal carotid arteries are seen ascending within this slice. Bony structures, muscles, and blood vessels.

Fig. 3.8e Coronal schematic drawing of the superior sagittal sinus, displaying its structure with arachnoid granulations. (Reproduced from Schuenke, Schulte, and Schumacher, *Atlas of Anatomy*, 2nd edition, ©2014, Thieme Publishers, New York. Illustration by Karl Wesker/Markus Voll.) ▶

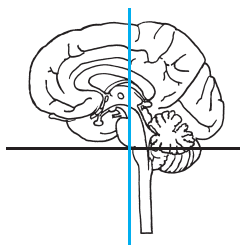


- 1 Superior sagittal sinus
- 2 Posteromedial frontal artery
- 3 Paracentral artery
- 4 Parietal bone
- 5 Artery of precentral sulcus
- 6 Pericallosal artery
- 8 Superior thalamostriate vein
- 9 Insular arteries
- 11 Posterior communicating artery
- 12 Basal vein (of Rosenthal)
- 13 Posterior cerebral artery
- 14 Oculomotor nerve
- 16 Middle cerebral artery, temporal branch
- 17 Basilar artery
- 18 Superior cerebellar artery
- 20 Temporal bone
- 21 Sphenoid
- 22 External acoustic canal
- 23 Internal carotid artery
- 24 Head of mandible
- 25 External ear
- 28 Occipital artery
- 30 Parotid gland
- 31 Axis
- 32 Digastric, posterior belly
- 34 Third cervical vertebra
- 35 Sternocleidomastoid
- 40 Arachnoid granulations
- 41 Caudate nucleus
- 42 Putamen
- 43 Globus pallidus lateral segment
- 44 Globus pallidus medial segment
- 45 Column of fornix

Fig. 3.8d Coronal T2w MR image, corresponding to the section in a and c.



- 1 Superior sagittal sinus
- 46 Emissary vein
- 47 Epicranial aponeurosis
- 48 Extracranial veins of the scalp
- 49 Diploic veins
- 50 Granular foveolae
- 51 Arachnoid septae
- 52 Superior cerebral veins
- 53 Bridging veins
- 54 Falx cerebri
- 55 Sinus endothelium
- 56 Cranial dura mater, meningeal layer
- 57 Lacuna lateralis with arachnoid villi (arachnoid granulations)
- 58 Internal table
- 59 Diploe
- 60 External table
- 61 Scalp
- 62 Cranial dura mater, periosteal layer



- 1 Superior frontal gyrus
- 2 Falx cerebri
- 3 Precentral gyrus
- 4 Central sulcus
- 5 Cingulate gyrus
- 6 Trunk (body) of corpus callosum
- 7 Postcentral gyrus
- 8 Central part (body) of lateral ventricle
- 9 Caudate nucleus
- 10 Choroid plexus of lateral ventricle
- 11 Lateral dorsal nuclei of thalamus
- 12 Fornix
- 13 Medial nuclei of thalamus
- 14 Ventral lateral nuclei of thalamus
- 15 Posterior limb of internal capsule
- 16 Putamen
- 17 Insula
- 18 Transverse temporal gyrus (of Heschl)
- 19 Lateral sulcus (Sylvian fissure)
- 20 Superior temporal gyrus
- 21 Third ventricle
- 22 Subthalamic nucleus
- 23 Globus pallidus
- 24 Temporal (inferior) horn of lateral ventricle
- 25 Red nucleus
- 26 Optic tract
- 27 Middle temporal gyrus
- 28 Substantia nigra
- 29 Tail of caudate nucleus
- 30 Interpeduncular cistern
- 31 Hippocampus
- 32 Parahippocampal gyrus
- 33 Trochlear nerve
- 34 Lateral occipitotemporal gyrus
- 35 Inferior temporal gyrus
- 36 Tentorium of cerebellum
- 37 Pons
- 38 Trigeminal nerve
- 39 Facial nerve and intermediate nerve
- 40 Vestibulocochlear nerve
- 41 Abducens nerve
- 42 Vagus nerve and glossopharyngeal nerve
- 43 Hypoglossal nerve
- 44 Facial nerve
- 45 Accessory nerve
- 46 Sympathetic trunk

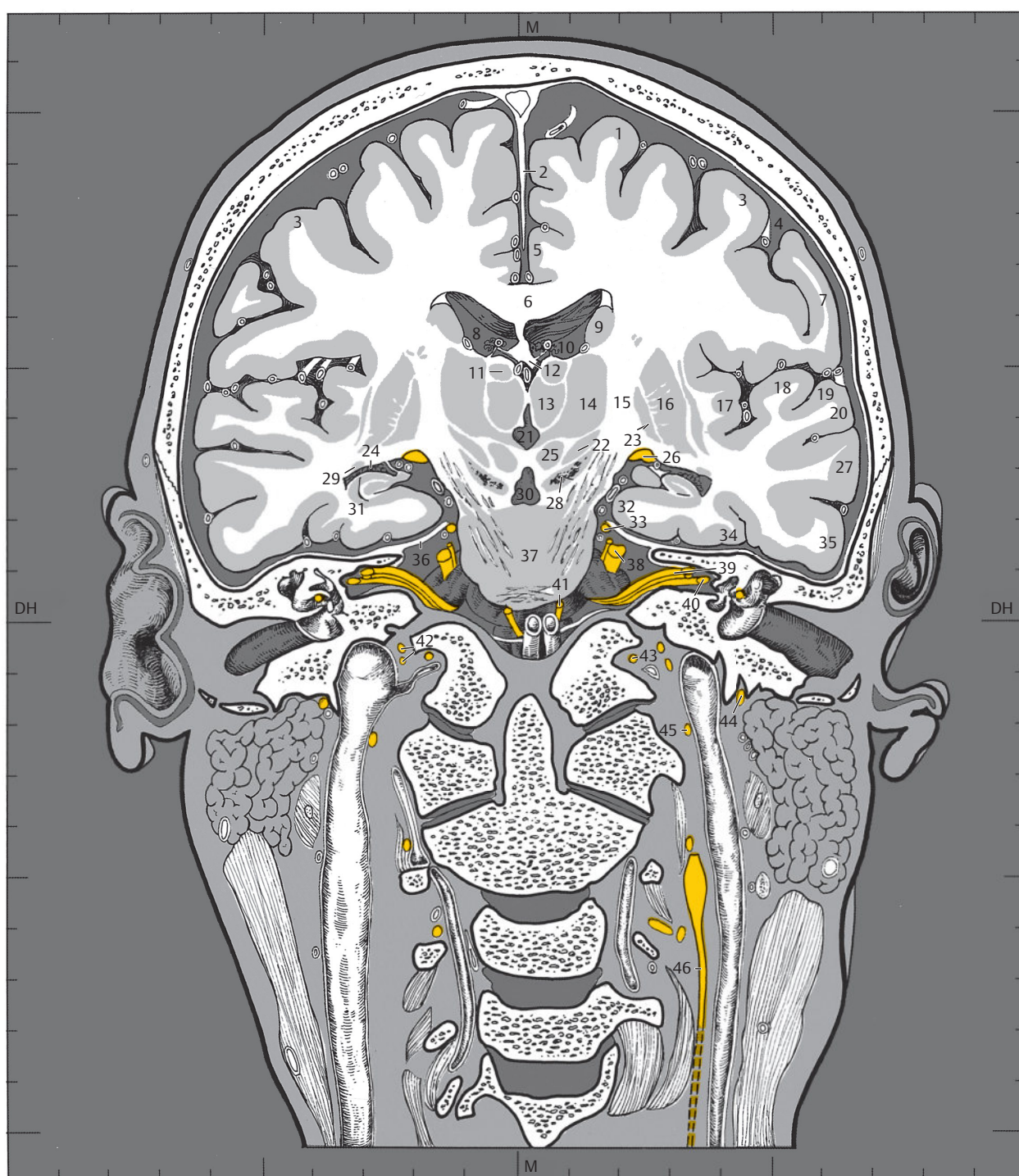
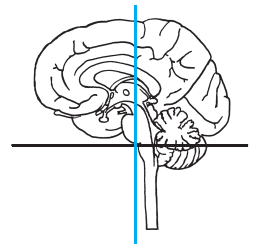
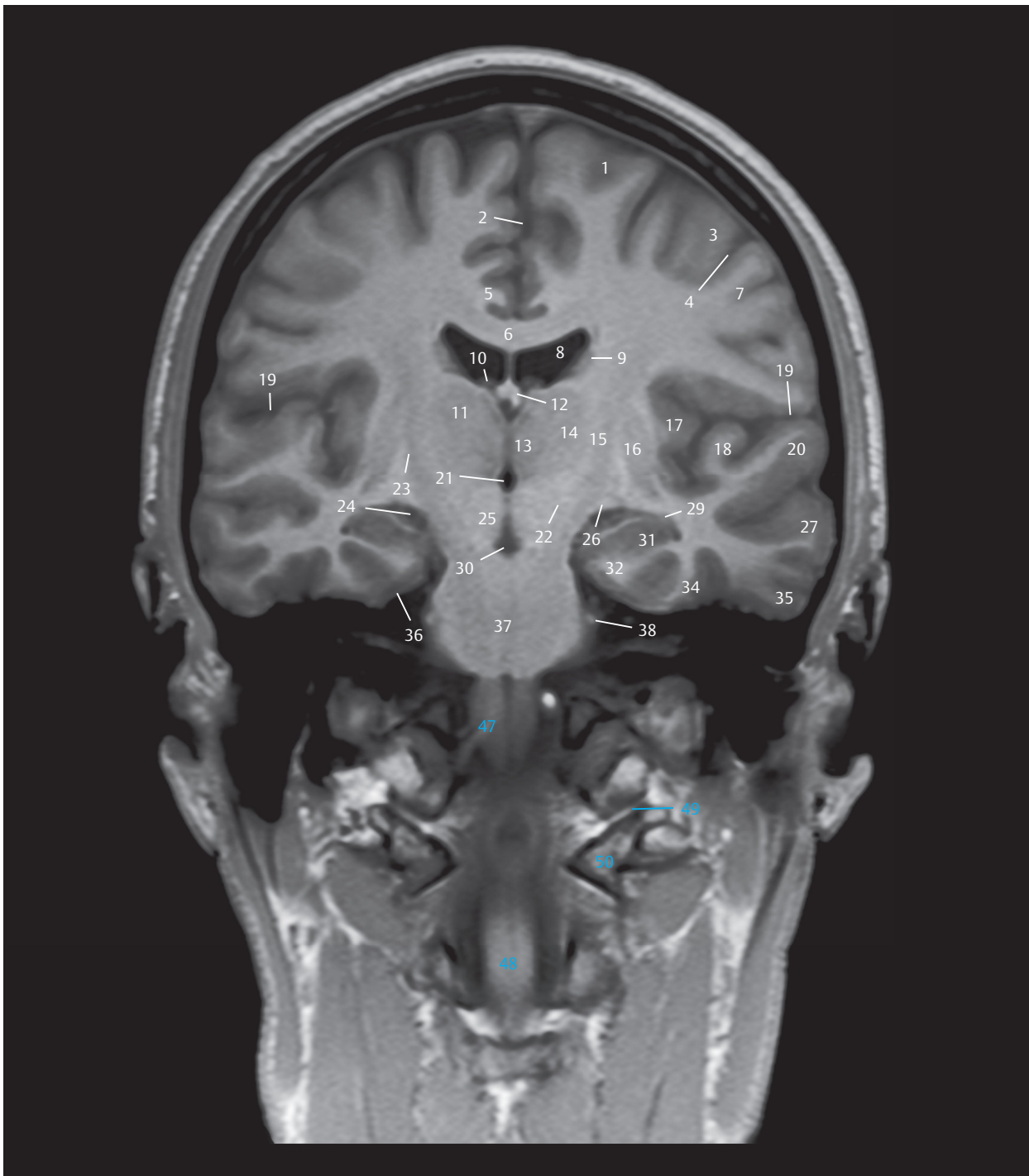


Fig. 3.9 8th coronal section.

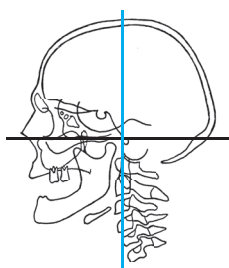
DH = German horizontal
M = median plane

Fig. 3.9a Anterior view of the 8th coronal section. The sectional plane runs through the endbrain, interbrain, midbrain and pons at the level of the interpeduncular fossa. The IVth, Vth, VIth, VIIth, and VIIIth cranial nerves are visualized within the cranial cavity while the VIIth, IXth, Xth, and XIIth nerves are seen outside of it. Brain structures and cranial nerves.



- 1 Superior frontal gyrus
- 2 Falx cerebri
- 3 Precentral gyrus
- 4 Central sulcus
- 5 Cingulate gyrus
- 6 Corpus callosum, body
- 7 Postcentral gyrus
- 8 Lateral ventricle, body
- 9 Caudate nucleus
- 10 Choroid plexus of lateral ventricle
- 11 Lateral dorsal nuclei of thalamus
- 12 Fornix
- 13 Medial nuclei of thalamus
- 14 Ventral lateral nuclei of thalamus
- 15 Internal capsule, posterior limb
- 16 Putamen
- 17 Insula
- 18 Transverse temporal gyrus (Heschl)
- 19 Lateral sulcus
- 20 Superior temporal gyrus
- 21 Third ventricle
- 22 Subthalamic nucleus
- 23 Globus pallidus
- 24 Lateral ventricle, temporal horn
- 25 Red nucleus
- 26 Optic tract
- 27 Middle temporal gyrus
- 29 Tail of caudate nucleus
- 30 Interpeduncular cistern
- 31 Hippocampus
- 32 Parahippocampal gyrus
- 34 Lateral occipitotemporal gyrus
- 35 Inferior temporal gyrus
- 36 Tentorium of cerebellum
- 37 Pons
- 38 Trigeminal nerve
- 47 Olive
- 48 Spinal cord
- 49 Atlanto-occipital joint
- 50 First cervical vertebra, lateral mass

Fig. 3.9b Coronal T1w MR image, approximately corresponding to the sectional plane in a and c.



- 1 Superior sagittal sinus
- 2 Bridging vein
- 3 Paracentral artery
- 4 Artery of precentral sulcus
- 5 Parietal bone
- 6 Precuneal artery
- 7 Artery of central sulcus
- 8 Pericallosal artery
- 9 Superior thalamostriate (terminal) vein
- 10 Internal cerebral vein
- 11 Insular arteries
- 12 Temporal artery of middle cerebral artery
- 13 Posterior choroidal artery
- 14 Basal vein (of Rosenthal)
- 15 Posterior cerebral artery
- 16 Temporal artery of posterior cerebral artery
- 17 Superior cerebellar artery
- 18 Temporal bone
- 19 Auricle (pinna)
- 20 Internal acoustic canal
- 21 Posterior inferior cerebellar artery (PICA)
- 22 Tympanic cavity
- 23 Tympanic membrane
- 24 External acoustic canal
- 25 Vertebral artery
- 26 Occipital condyle
- 27 Styloid process
- 28 Stylomastoid foramen
- 29 Atlanto-occipital joint
- 30 Dens of axis
- 31 Lateral mass of atlas
- 32 Posterior belly of digastric
- 33 Axis
- 34 Lateral atlantoaxial joint
- 35 Occipital artery
- 36 Intervertebral disc
- 37 Internal jugular vein
- 38 Body of third cervical vertebra
- 39 Sternocleidomastoid
- 40 Fourth cervical vertebra
- 41 Fifth cervical vertebra

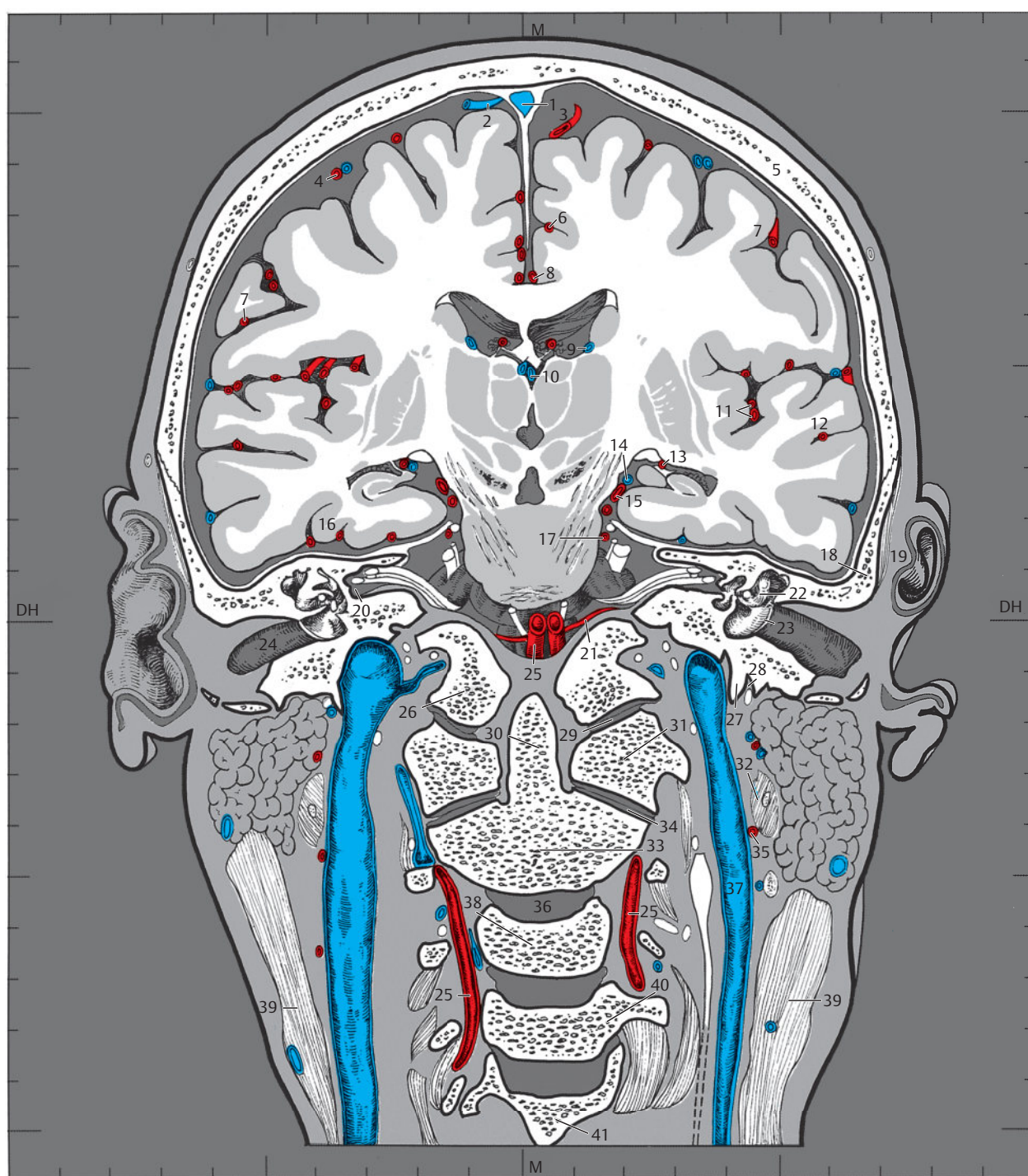


Fig. 3.9c Anterior view of the 8th coronal section. The bony external auditory canal, tympanic cavity and the internal auditory canal lie in this slice. The internal jugular veins course through the slice lateral to the dens and the cervical vertebral bodies. Bony structures, muscles, and blood vessels.

- 51-54 Different sectors of the hippocampus proper (Cornu ammonis, CA1-4)
- 55 Alveus
- 56 Fimbria of hippocampus
- 57 Fascia dentata
- 58 Subiculum
- 59 Presubiculum
- 60 Parasubiculum
- 61 Entorhinal cortex
- 62 Isocortex
- 63 Collateral sulcus

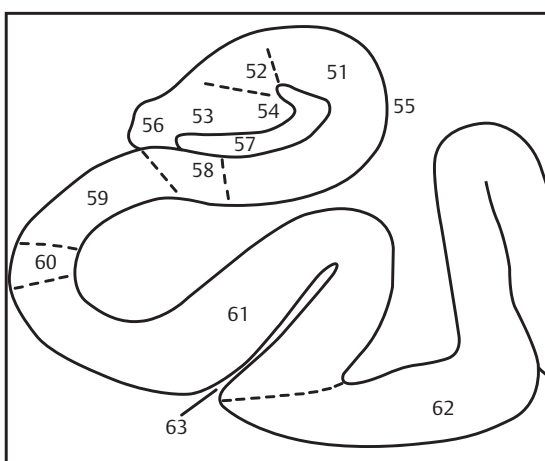
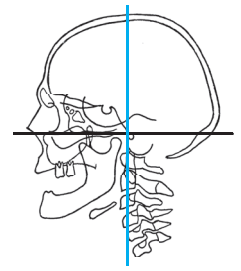
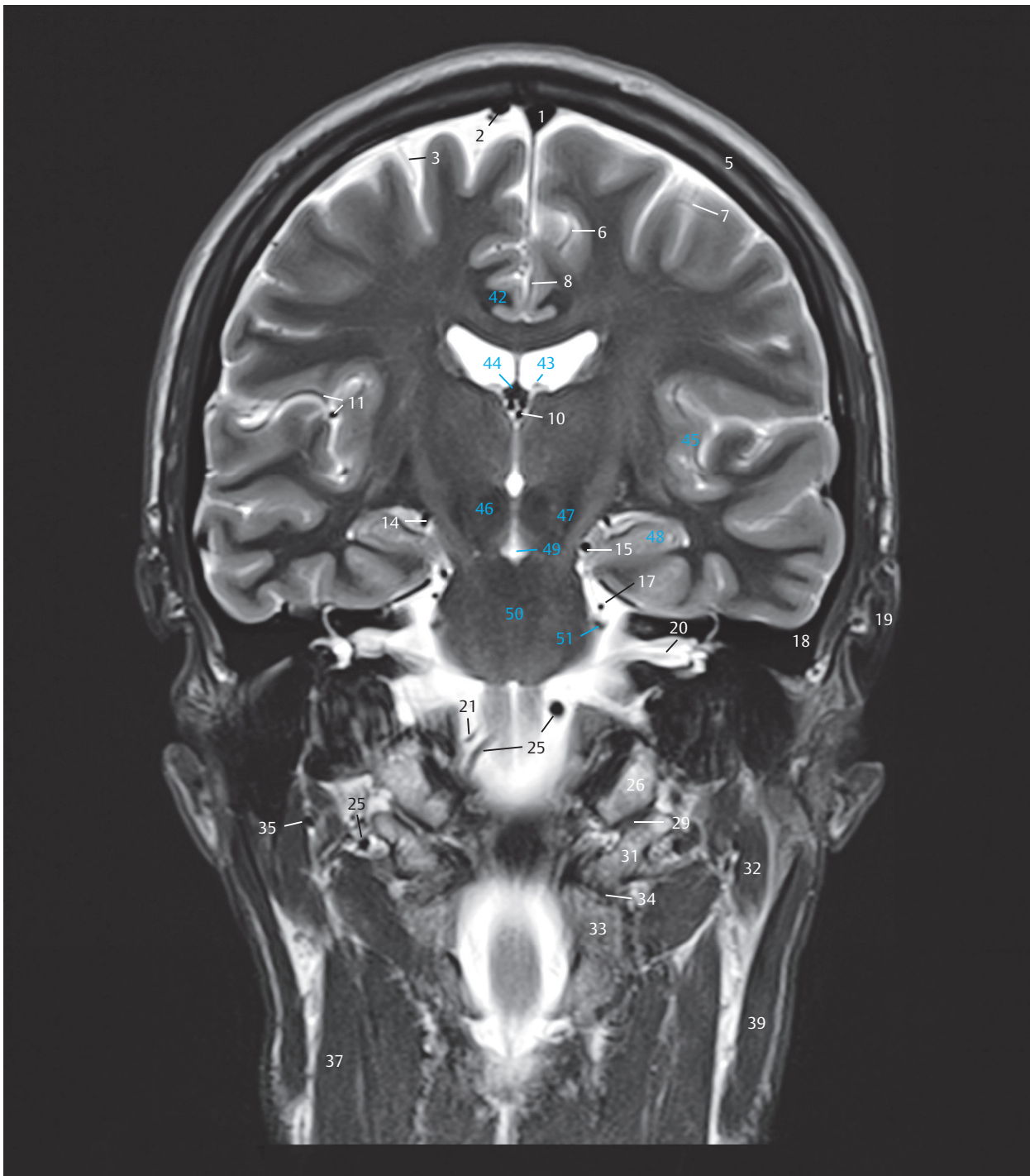
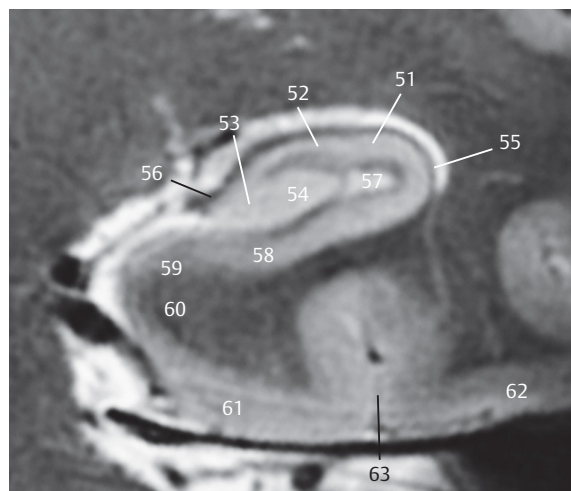


Fig. 3.9e Depiction of the anatomical structure of the hippocampus. (Source: [480])



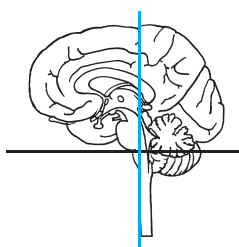
- 1 Superior sagittal sinus
- 2 Bridging veins
- 3 Paracentral artery
- 5 Parietal bone
- 6 Precuneal artery
- 7 Artery of central sulcus
- 8 Pericallosal artery
- 10 Internal cerebral vein
- 11 Insular arteries
- 14 Basal vein (of Rosenthal)
- 15 Posterior cerebral artery
- 17 Superior cerebellar artery
- 18 Temporal bone
- 19 External ear
- 20 Internal acoustic canal with facial nerve (lies apicoanteriorly) and vestibulocochlear nerve (lies posteriorly and inferiorly)
- 21 Posterior inferior cerebellar artery
- 25 Vertebral artery
- 26 Occipital condyle
- 29 Atlanto-occipital joint
- 31 Lateral mass of atlas
- 32 Digastric, posterior belly
- 33 Axis
- 34 Lateral atlantoaxial joint
- 35 Occipital artery
- 37 Internal jugular vein
- 39 Sternocleidomastoid
- 42 Cingulate gyrus
- 43 Choroid plexus
- 44 Fornix
- 45 Insula
- 46 Red nucleus
- 47 Substantia nigra
- 48 Hippocampus
- 49 Interpeduncular cistern
- 50 Pons
- 51 Trigeminal nerve

Fig. 3.9d Coronal T2w MR image, approximately corresponding to the sectional plane in a and c.



- 51-54 Different sectors of the hippocampus proper (CA1-4)
- 55 Alveus
- 56 Fimbria of hippocampus
- 57 Fascia dentata
- 58 Subiculum
- 59 Presubiculum
- 60 Parasubiculum
- 61 Entorhinal cortex
- 62 Isocortex
- 63 Collateral sulcus

Fig. 3.9f High resolution T2w MR image of the hippocampal formation with a field strength of 7T. (Source: With kind permission of Dr. J. Theysohn, University Hospital Essen.)



- 1 Superior frontal gyrus
- 2 Precentral gyrus
- 3 Postcentral gyrus
- 4 Central sulcus
- 5 Cingulate gyrus
- 6 Supramarginal gyrus
- 7 Central part (body) of lateral ventricle
- 8 Trunk (body) of corpus callosum
- 9 Caudate nucleus
- 10 Posterior transverse temporal gyrus
- 11 Anterior transverse temporal gyrus (of Heschl)
- 12 Fornix
- 13 Pulvinar of thalamus
- 14 Transverse temporal gyrus (of Heschl)
- 15 Superior temporal gyrus
- 16 Centromedian nucleus of thalamus
- 17 Posterior commissure
- 18 Medial geniculate body
- 19 Lateral geniculate body
- 20 Tail of caudate nucleus
- 21 Temporal (inferior) horn of lateral ventricle
- 22 Middle temporal gyrus
- 23 Aqueduct of midbrain
- 24 Periaqueductal gray substance
- 25 Trochlear nerve
- 26 Parahippocampal gyrus
- 27 Lateral occipitotemporal gyrus
- 28 Inferior temporal gyrus
- 29 Tentorium of cerebellum
- 30 Pons
- 31 Anterior lobe of cerebellum
- 32 Middle cerebellar peduncle
- 33 Primary fissure of cerebellum
- 34 Facial nerve and intermediate nerve
- 35 Vestibulocochlear nerve
- 36 Glossopharyngeal nerve and vagus nerve
- 37 Flocculus (H X)
- 38 Inferior olivary nucleus
- 39 Accessory nerve
- 40 Hypoglossal nerve
- 41 Pyramidal decussation
- 42 Anterior (ventral) root of first cervical spinal nerve
- 43 Spinal cord
- 44 Anterior (ventral) root of second spinal nerve
- 45 Second cervical spinal ganglion
- 46 Anterior median fissure
- 47 Anterior (ventral) root of fifth cervical spinal

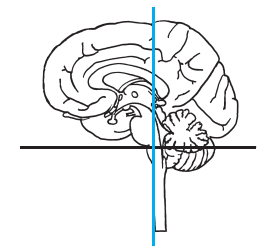
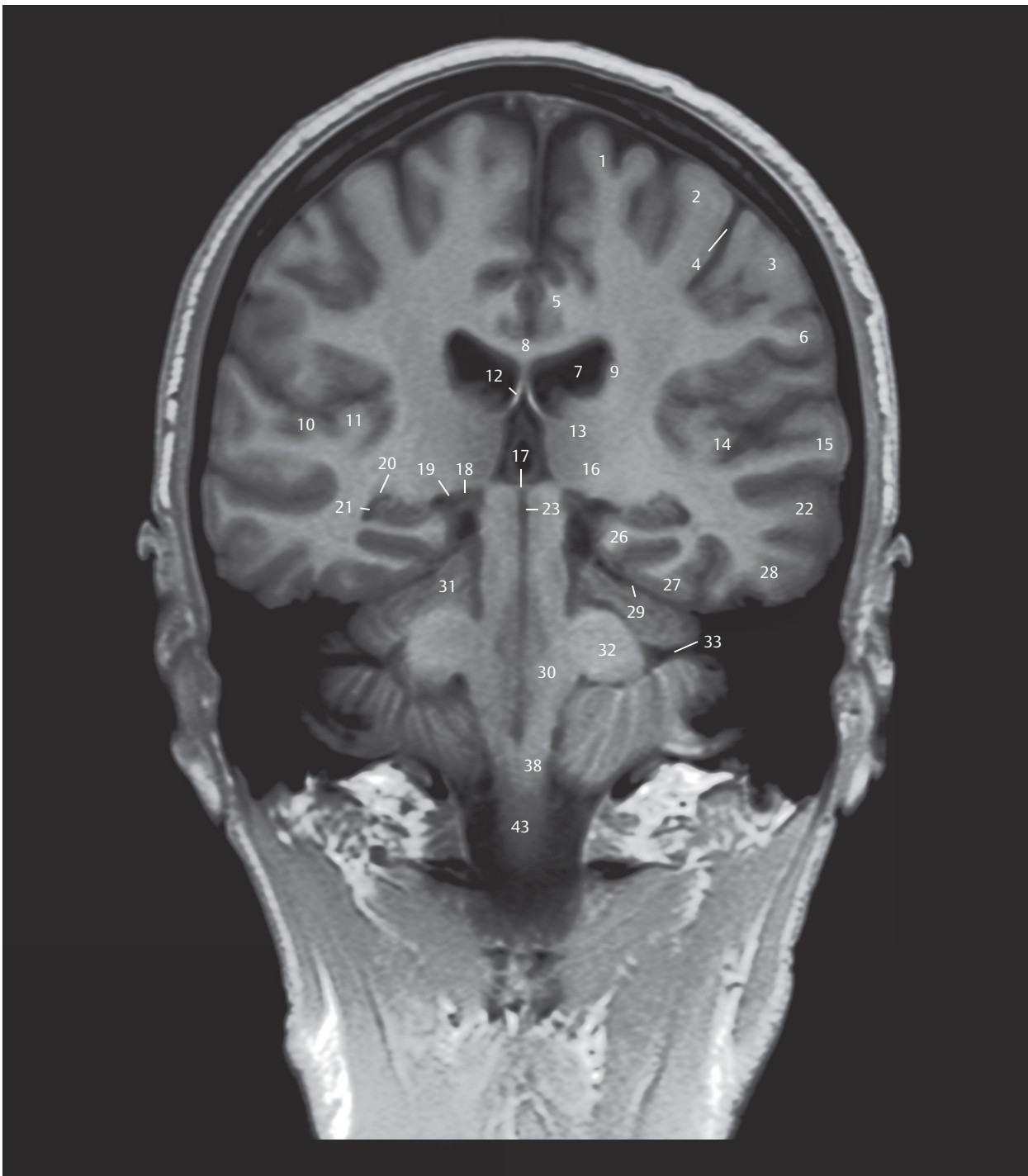


Fig. 3.10 9th coronal section.

DH = German horizontal

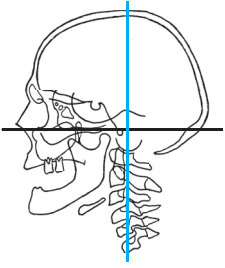
M = median plane

Fig. 3.10a Anterior view of the 9th coronal section. The posterior commissure has been sectioned in this slice. The lateral ventricle with cella media and inferior horn as well as the first part of the cerebral aqueduct can be seen. The VIIth, VIIIth, IXth, Xth, XIth, and XIIth cranial nerves arise from the brainstem. The quadrigeminal plate lies within the slice and is therefore not visible (see ► Fig. 3.1c).



- 1 Superior frontal gyrus
- 2 Precentral gyrus
- 3 Postcentral gyrus
- 4 Central sulcus
- 5 Cingulate gyrus
- 6 Supramarginal gyrus
- 7 Lateral ventricle, body
- 8 Corpus callosum, body
- 9 Caudate nucleus
- 10 Posterior transverse temporal gyrus (posterior Heschl's gyrus)
- 11 Anterior transverse temporal gyrus (anterior Heschl's gyrus)
- 12 Fornix
- 13 Pulvinar nuclei of thalamus
- 14 Transverse temporal gyrus
- 15 Superior temporal gyrus
- 16 Centromedian nuclei of thalamus
- 17 Posterior commissure
- 18 Medial geniculate body
- 19 Lateral geniculate body
- 20 Tail of caudate nucleus
- 21 Lateral ventricle, temporal horn
- 22 Middle temporal gyrus
- 23 Cerebral aqueduct (of Sylvius)
- 26 Parahippocampal gyrus
- 27 Lateral occipitotemporal gyrus
- 28 Inferior temporal gyrus
- 29 Tentorium of cerebellum
- 30 Pons
- 31 Anterior lobe of cerebellum
- 32 Middle cerebellar peduncle
- 33 Primary fissure
- 38 Inferior olivary nucleus
- 43 Spinal cord

Fig. 3.10b Coronal T1w MR image, approximately corresponding to the sectional plane in a and c.



- 1 Superior sagittal sinus
- 2 Paracentral artery
- 3 Artery of central sulcus
- 4 Precuneal artery
- 5 Anterior parietal artery
- 6 Parietal bone
- 7 Pericallosal artery
- 8 Superior thalamostriate (terminal) vein
- 9 Angular artery
- 10 Internal cerebral vein
- 11 Temporal branch of middle cerebral artery
- 12 Posterior choroidal artery
- 13 Medial occipital artery
- 14 Basal vein (of Rosenthal)
- 15 Lateral occipital artery
- 16 Superior cerebellar artery
- 17 Auricle (pinna)
- 18 Temporal bone
- 19 Sigmoid sinus
- 20 Posterior inferior cerebellar artery (PICA)
- 21 Vertebral artery
- 22 Occipital bone
- 23 Mastoid process
- 24 Atlanto-occipital joint
- 25 Occipital artery
- 26 Posterior belly of digastric
- 27 Vertebral vein
- 28 Lateral mass of atlas
- 29 Articular process and arch of axis
- 30 Articular process and arch of third cervical vertebra
- 31 Articular process and arch of fourth cervical vertebra
- 32 Sternocleidomastoid
- 33 Fifth cervical vertebra

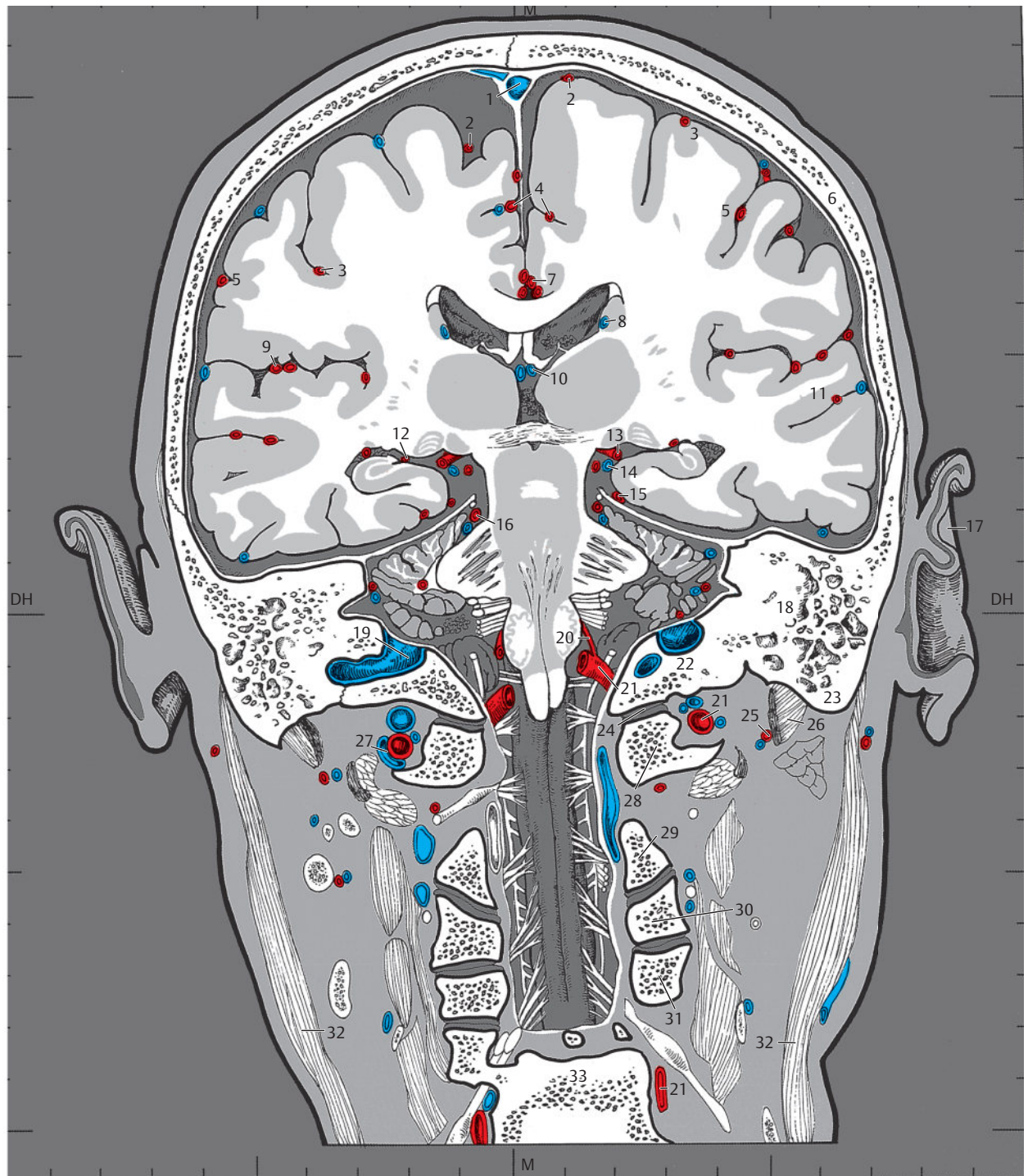
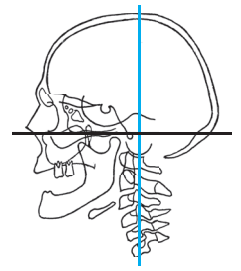
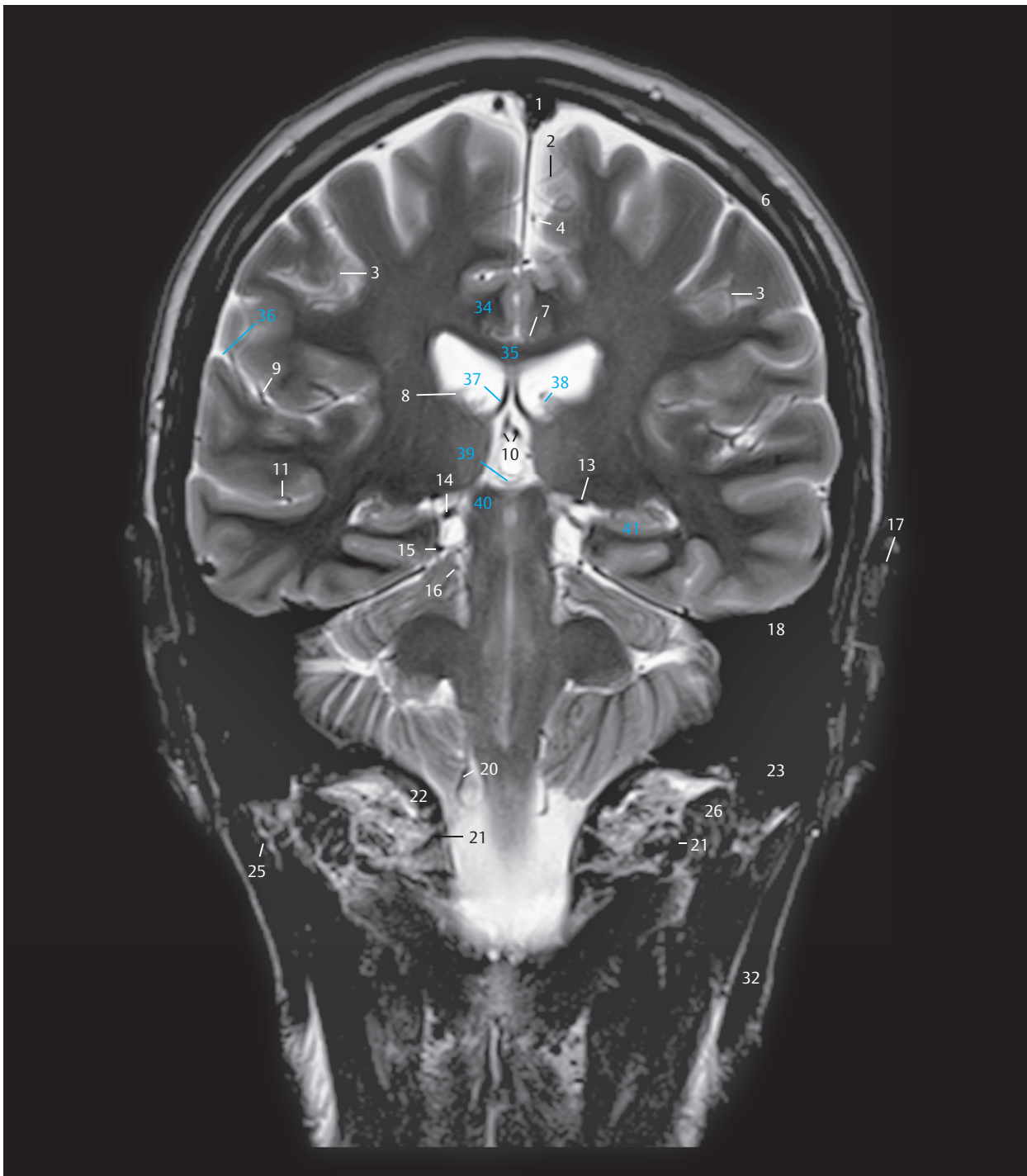
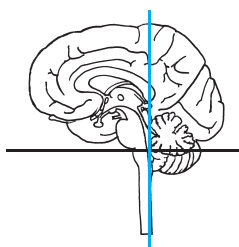


Fig. 3.10c Anterior view of the 9th coronal section. The slice lies approximately in the center of the mastoid process, opening up the posterior cranial fossa and the upper spinal canal in the region of the first four cervical vertebrae. Bony structures, muscles, and blood vessels.



- 1 Superior sagittal sinus
- 2 Paracentral artery
- 3 Artery of central sulcus
- 4 Precuneal artery
- 6 Parietal bone
- 7 Pericallosal artery
- 8 Superior thalamostriate vein
- 9 Angular artery
- 10 Internal cerebral vein
- 11 Middle cerebral artery, temporal branch
- 13 Medial occipital artery
- 14 Basal vein (of Rosenthal)
- 15 Lateral occipital artery
- 16 Superior cerebellar artery
- 17 External ear
- 18 Temporal bone
- 20 Posterior inferior cerebellar artery
- 21 Vertebral artery
- 22 Occipital bone
- 23 Mastoid process
- 25 Occipital artery
- 26 Digastric, posterior belly
- 32 Sternocleidomastoid
- 34 Cingulate gyrus
- 35 Corpus callosum, body
- 36 Lateral sulcus
- 37 Fornix
- 38 Choroid plexus
- 39 Pineal gland
- 40 Superior colliculus
- 41 Hippocampus

Fig. 3.10d Coronal T2w MR image, approximately corresponding to the sectional plane in a and c.



- 1 Precentral gyrus
- 2 Falx cerebri
- 3 Central sulcus
- 4 Paracentral lobule
- 5 Postcentral gyrus
- 6 Cingulate gyrus
- 7 Supramarginal gyrus
- 8 Lateral sulcus (Sylvian fissure)
- 9 Atrium of lateral ventricle
- 10 Splenium of corpus callosum
- 11 Tail of caudate nucleus
- 12 Superior temporal gyrus
- 13 Fornix
- 14 Pineal gland
- 15 Hippocampus
- 16 Middle temporal gyrus
- 17 Tentorium of cerebellum
- 18 Medial occipitotemporal gyrus
- 19 Lateral occipitotemporal gyrus
- 20 Inferior temporal gyrus
- 21 Anterior lobe of cerebellum
- 22 Primary fissure of cerebellum
- 23 Roof of fourth ventricle
- 24 Choroid plexus of fourth ventricle
- 25 Posterior lobe of cerebellum
- 26 Floor of rhomboid fossa (cut)
- 27 Cisterna magna (posterior cerebellomedullary cistern)
- 28 Suboccipital nerve
- 29 Greater occipital nerve
- 30 Third occipital nerve
- 31 Spinal cord

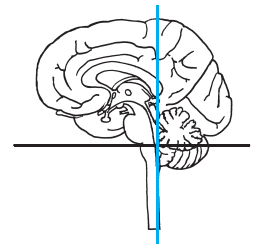
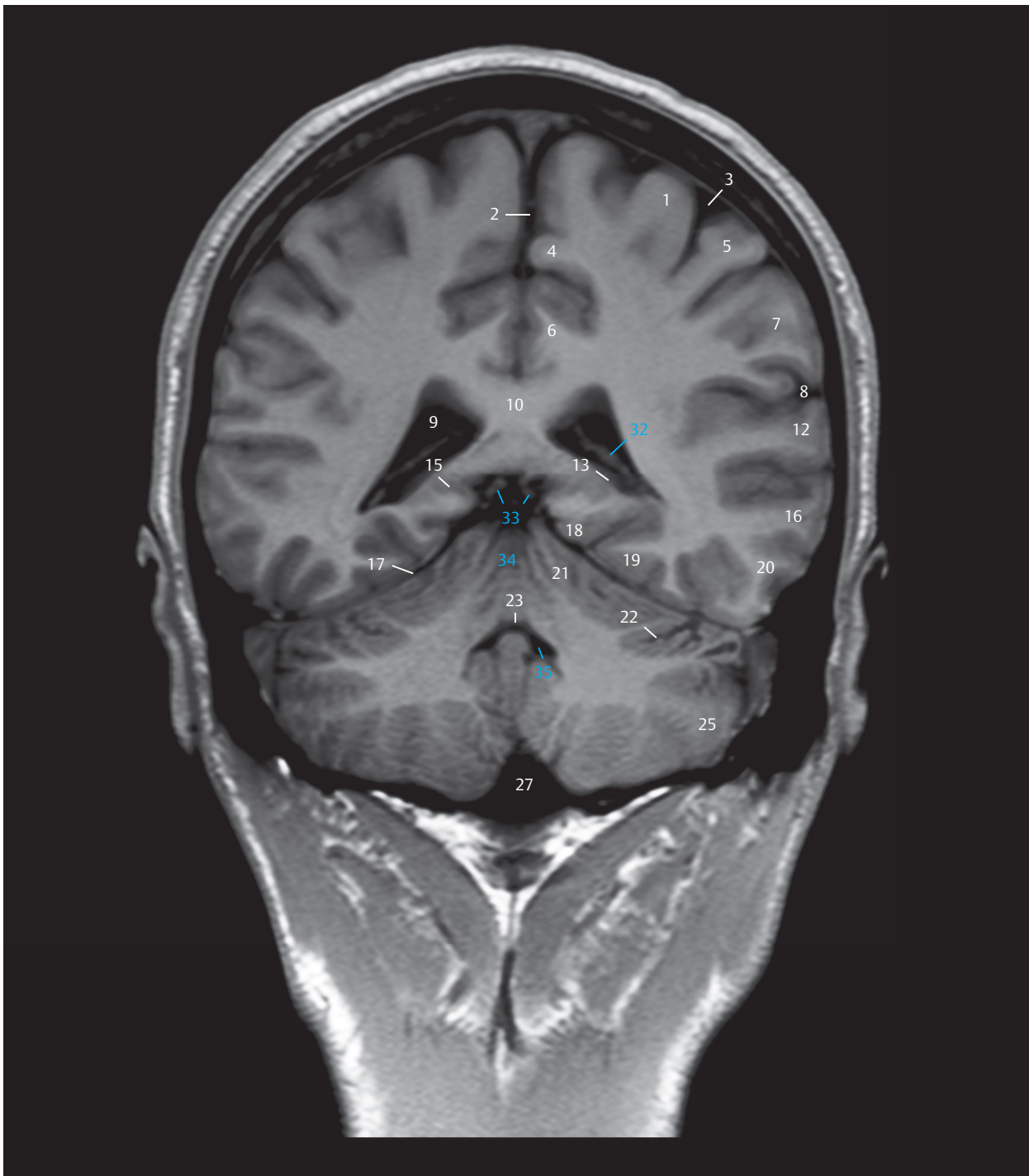


Fig. 3.11 10th coronal section.

DH = German horizontal

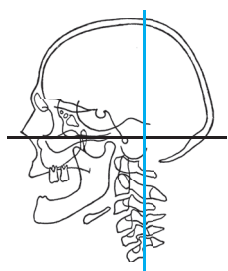
M = median plane

Fig. 3.11a Anterior view of the 10th coronal section. The splenium of the corpus callosum, collateral trigone of the lateral ventricle, the pineal gland, the floor of the rhomboid fossa, and the cerebellum as the floor of the IVth ventricle have been sectioned in the slice. Brain structures and branches of spinal nerves.



- 1 Precentral gyrus
- 2 Falx cerebri
- 3 Central sulcus
- 4 Paracentral lobule
- 5 Postcentral gyrus
- 6 Cingulate gyrus
- 7 Supramarginal gyrus
- 8 Lateral sulcus
- 9 Lateral ventricle, collateral trigone
- 10 Corpus callosum, splenium
- 12 Superior temporal gyrus
- 13 Fornix
- 15 Hippocampus
- 16 Middle temporal gyrus
- 17 Tentorium of cerebellum
- 18 Medial occipitotemporal gyrus
- 19 Lateral occipitotemporal gyrus
- 20 Inferior temporal gyrus
- 21 Anterior lobe of cerebellum
- 22 Primary fissure
- 23 Fourth ventricle, roof
- 25 Posterior lobe of cerebellum
- 27 Posterior cerebellomedullary cistern (magna)
- 32 Choroid plexus of lateral ventricle
- 33 Internal cerebral vein
- 34 Anterior lobe of cerebellum, vermis
- 35 Fourth ventricle

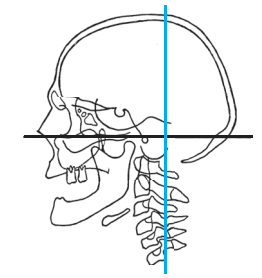
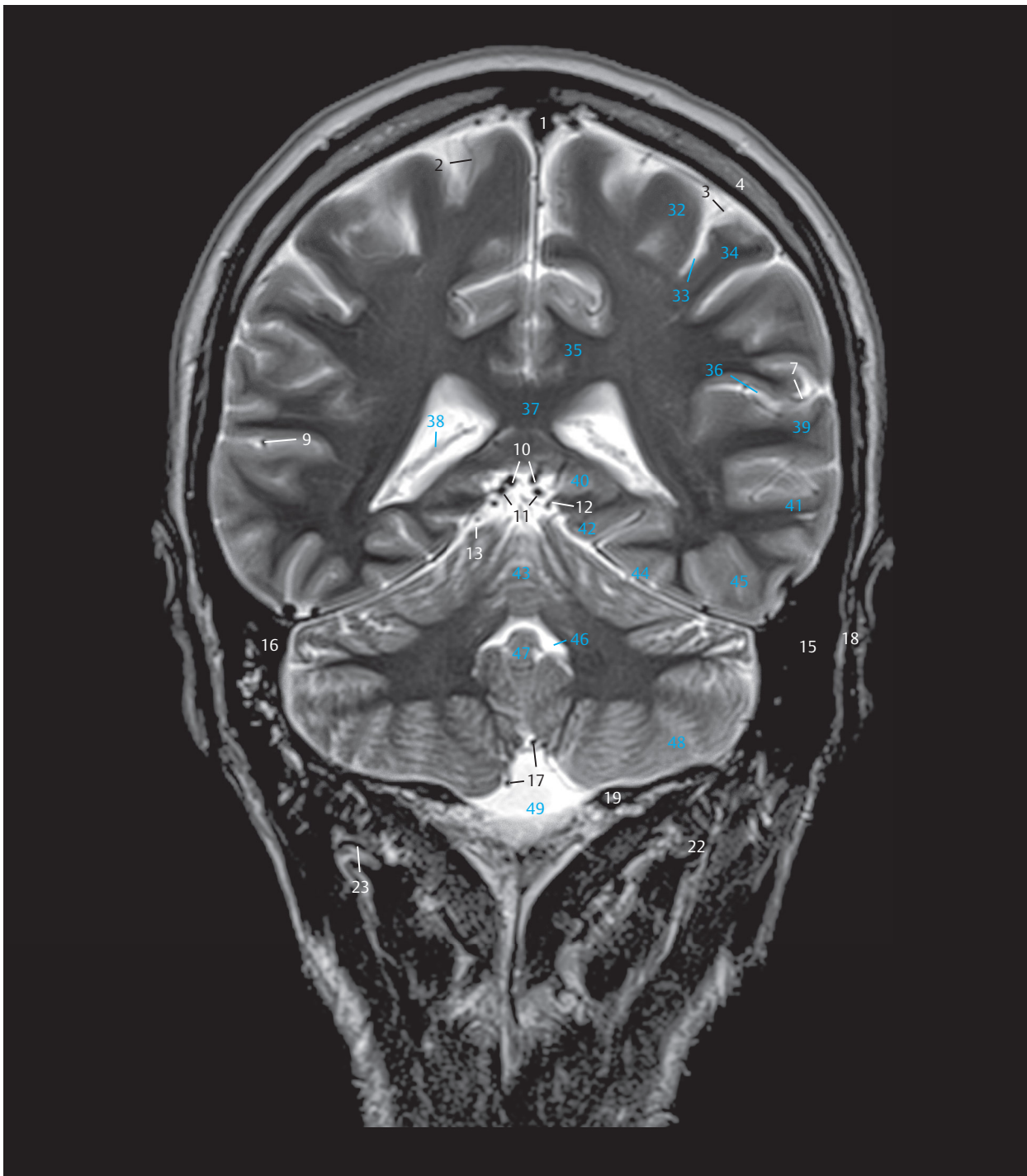
Fig. 3.11b Coronal T1w MR image, approximately corresponding to the sectional plane in a and c.



- 1 Superior sagittal sinus
- 2 Paracentral artery
- 3 Artery of central sulcus
- 4 Parietal bone
- 5 Precuneal artery
- 6 Anterior parietal artery
- 7 Angular artery
- 8 Superior thalamostriate (terminal) vein
- 9 Temporal artery of middle cerebral artery
- 10 Internal cerebral vein
- 11 Basal vein (of Rosenthal)
- 12 Medial occipital artery
- 13 Superior cerebellar artery
- 14 Lateral occipital artery
- 15 Temporal bone
- 16 Sigmoid sinus
- 17 Posterior inferior cerebellar artery (PICA)
- 18 Auricle (pinna)
- 19 Occipital bone
- 20 Vertebral vein (cut)
- 21 Vertebral artery (cut)
- 22 Obliquus capitis superior
- 23 Suboccipital venous plexus
- 24 Posterior arch of atlas
- 25 Occipital artery
- 26 Obliquus capitis inferior
- 27 Sternocleidomastoid
- 28 Arch of axis
- 29 Arch of third cervical vertebra
- 30 Arch of fourth cervical vertebra
- 31 Arch of fifth cervical vertebra

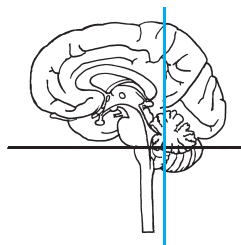


Fig. 3.11c Anterior view of the 10th coronal section. The section lies just behind the petrous part of the temporal bone and runs directly behind the center of the foramen magnum (see ► Fig. 3.1a). The upper cervical vertebrae have been sectioned at the level of the vertebral arch. Bony structures, muscles, and blood vessels.



- 1 Superior sagittal sinus
- 2 Paracentral artery
- 3 Artery of central sulcus
- 4 Parietal bone
- 7 Artery of angular gyrus
- 9 Middle cerebral artery, temporal branch
- 10 Internal cerebral vein
- 11 Basal vein (of Rosenthal)
- 12 Medial occipital artery
- 13 Superior cerebellar artery
- 15 Temporal bone
- 16 Sigmoid sinus
- 17 Posterior inferior cerebellar artery
- 18 External ear
- 19 Occipital bone
- 22 Obliquus capitis superior
- 23 Suboccipital venous plexus, vein
- 32 Precentral gyrus
- 33 Central sulcus
- 34 Postcentral gyrus
- 35 Cingulate gyrus
- 36 Lateral sulcus
- 37 Corpus callosum, splenium
- 38 Choroid plexus in lateral ventricle
- 39 Superior temporal gyrus
- 40 Hippocampus
- 41 Middle temporal gyrus
- 42 Medial occipitotemporal gyrus
- 43 Anterior lobe of cerebellum, vermis
- 44 Lateral occipitotemporal gyrus
- 45 Inferior temporal gyrus
- 46 Fourth ventricle
- 47 Nodule of vermis (X)
- 48 Posterior lobe of cerebellum
- 49 Posterior cerebellomedullary cistern (magna)

Fig. 3.11d Coronal T2w MR image, approximately corresponding to the sectional plane in a and c.



- 1 Precentral gyrus
- 2 Postcentral gyrus
- 3 Paracentral lobule
- 4 Falx cerebri
- 5 Supramarginal gyrus
- 6 Occipital (posterior) horn of lateral ventricle
- 7 Superior temporal sulcus
- 8 Superior temporal gyrus
- 9 Middle temporal gyrus
- 10 Anterior lobe of cerebellum
- 11 Medial occipitotemporal gyrus
- 12 Tentorium of cerebellum
- 13 Lateral occipitotemporal gyrus
- 14 Inferior temporal gyrus
- 15 Primary fissure of cerebellum
- 16 Uvula of vermis (IX)
- 17 Dentate nucleus
- 18 Posterior lobe of cerebellum
- 19 Cisterna magna (posterior cerebellomedullary cistern)
- 20 Greater occipital nerve
- 21 Third occipital nerve

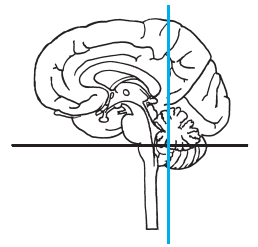
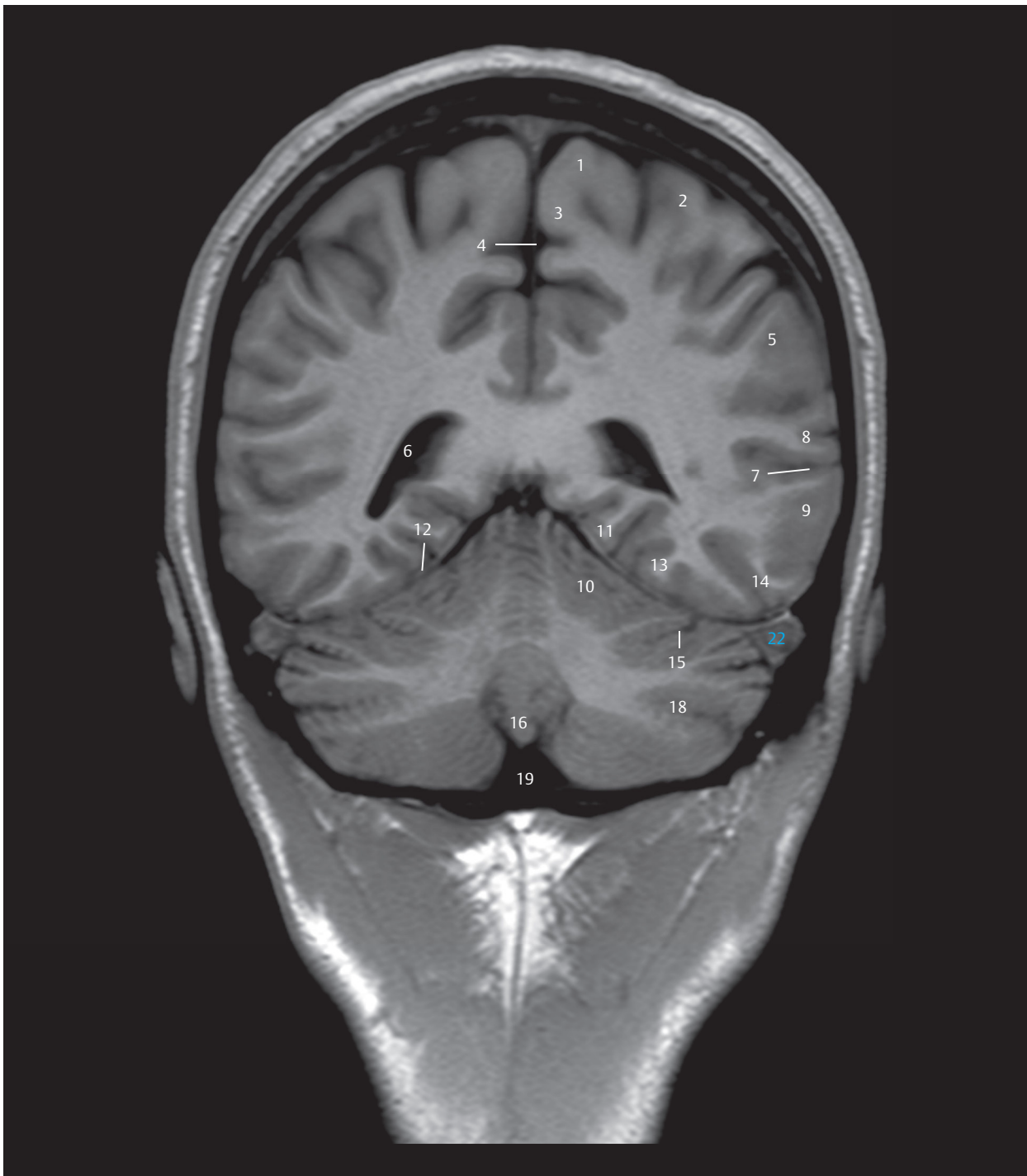


Fig. 3.12 11th coronal section.

DH = German horizontal

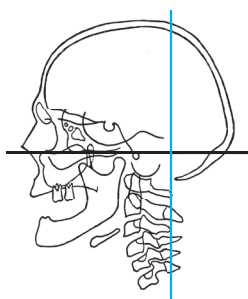
M = median plane

Fig. 3.12a Anterior view of the 11th coronal section. The posterior horn of the lateral ventricle forms a landmark in the supratentorial region. The cerebellum with the dentate nucleus is located in the infratentorial region. Brain structures and branches of spinal nerves.



- 1 Precentral gyrus
- 2 Postcentral gyrus
- 3 Paracentral lobule
- 4 Falx cerebri
- 5 Supramarginal gyrus
- 6 Lateral ventricle, occipital horn
- 7 Superior temporal sulcus
- 8 Superior temporal gyrus
- 9 Middle temporal gyrus
- 10 Anterior lobe of cerebellum
- 11 Medial occipitotemporal gyrus
- 12 Tentorium of cerebellum
- 13 Lateral occipitotemporal gyrus
- 14 Inferior temporal gyrus
- 15 Primary fissure of cerebellum
- 16 Uvula of vermis (IX)
- 18 Posterior lobe of cerebellum
- 19 Posterior cerebellomedullary cistern (magna)
- 22 Transverse sinus

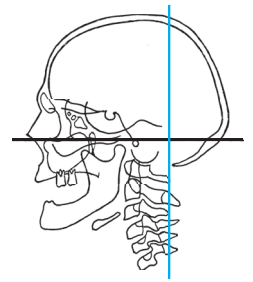
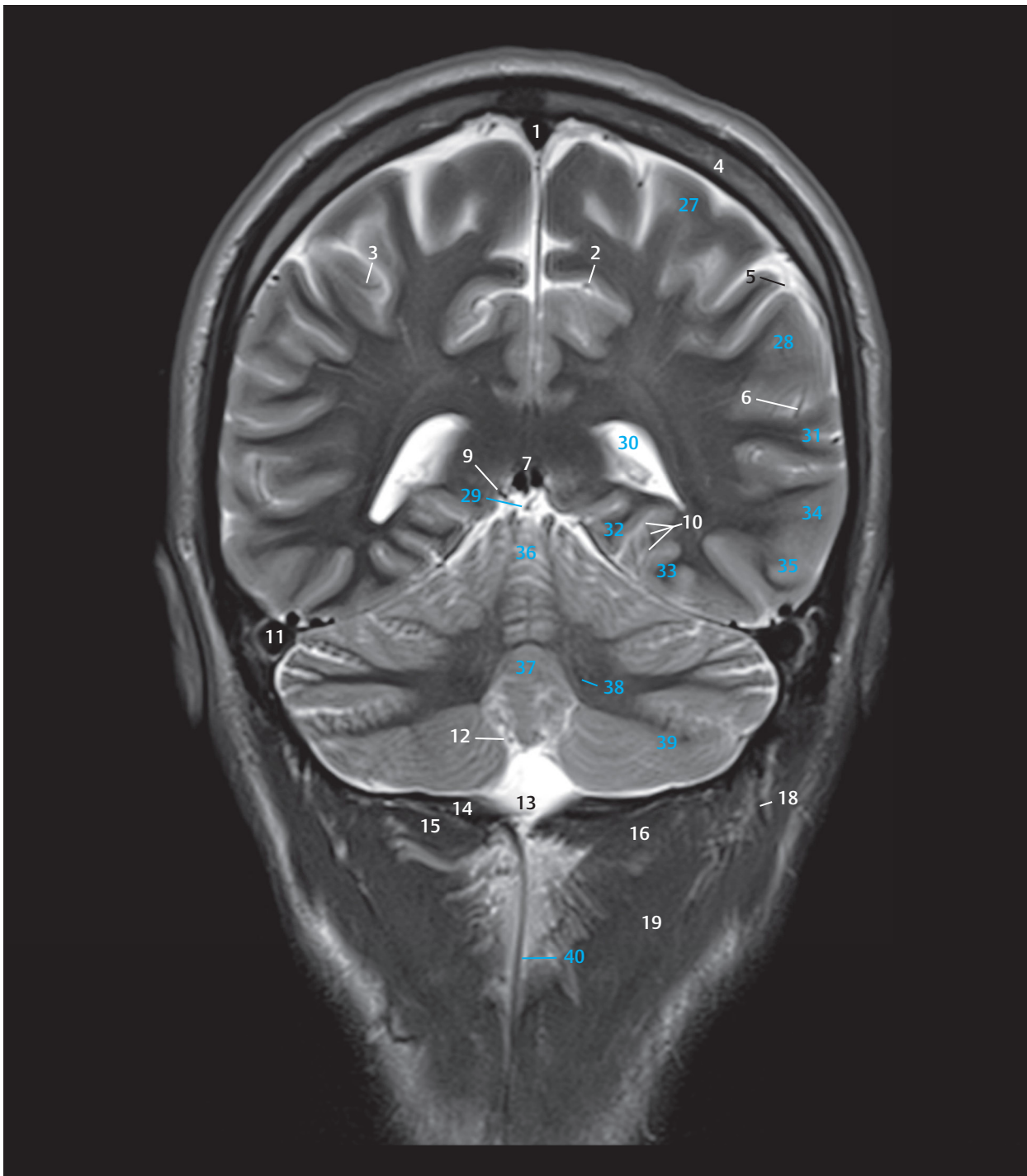
Fig. 3.12b Coronal T1w MR image, approximately corresponding to the sectional plane in a and c.



- 1 Superior sagittal sinus
- 2 Precuneal artery
- 3 Anterior parietal artery
- 4 Parietal bone
- 5 Posterior parietal artery
- 6 Angular artery
- 7 Straight sinus
- 8 Superior cerebellar artery
- 9 Medial occipital artery
- 10 Lateral occipital artery
- 11 Transverse sinus
- 12 Posterior inferior cerebellar artery (PICA)
- 13 Foramen magnum
- 14 Occipital bone
- 15 Rectus capitis posterior minor
- 16 Obliquus capitis superior
- 17 Posterior arch of atlas
- 18 Occipital artery
- 19 Splenius capitis
- 20 Obliquus capitis inferior
- 21 Spinous process of axis
- 22 Suboccipital venous plexus
- 23 Spinous process of third cervical vertebra
- 24 Spinous process of fourth cervical vertebra
- 25 Arch of fifth cervical vertebra
- 26 Arch of sixth cervical vertebra

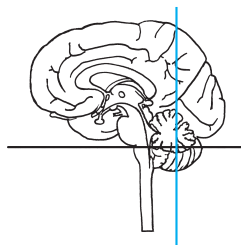


Fig. 3.12c Anterior view of the 11th coronal section. The posterior part of the foramen magnum lies in the slice. Bony structures, neck muscles, and blood vessels.



- 1 Superior sagittal sinus
- 2 Precuneal artery
- 3 Anterior parietal artery
- 4 Parietal bone
- 5 Posterior parietal artery
- 6 Artery of angular gyrus
- 7 Straight sinus
- 9 Medial occipital artery
- 10 Lateral occipital artery
- 11 Transverse sinus
- 12 Posterior inferior cerebellar artery
- 13 Foramen magnum
- 14 Occipital bone
- 15 Rectus capitis posterior minor
- 16 Obliquus capitis superior
- 18 Occipital artery
- 19 Splenius capitis
- 27 Superior parietal lobule
- 28 Supramarginal gyrus
- 29 Superior cerebellar cistern
- 30 Lateral ventricle, occipital horn
- 31 Superior temporal gyrus
- 32 Medial occipitotemporal gyrus
- 33 Lateral occipitotemporal gyrus
- 34 Middle temporal gyrus
- 35 Inferior temporal gyrus
- 36 Anterior lobe of cerebellum, vermis
- 37 Vermis of cerebellum
- 38 Dentate nucleus
- 39 Posterior lobe of cerebellum
- 40 Nuchal ligament

Fig. 3.12d Coronal T2w MR image, approximately corresponding to the sectional plane in a and c.



- 1 Superior parietal lobule
- 2 Longitudinal cerebral (interhemispheric) fissure
- 3 Falx cerebri
- 4 Precuneus
- 5 Angular gyrus
- 6 Parieto-occipital sulcus
- 7 Dura mater
- 8 Primary visual cortex
- 9 Cuneus
- 10 Occipital (posterior) horn of lateral ventricle
- 11 Middle temporal gyrus
- 12 Calcarine sulcus
- 13 Anterior lobe of cerebellum
- 14 Medial occipitotemporal gyrus
- 15 Lateral occipitotemporal gyrus
- 16 Inferior temporal gyrus
- 17 Tentorium of cerebellum
- 18 Primary fissure of cerebellum
- 19 Posterior lobe of cerebellum
- 20 Pyramid of vermis (VIII)
- 21 Cisterna magna (posterior cerebellomedullary cistern)
- 22 Greater occipital nerve
- 23 Third occipital nerve

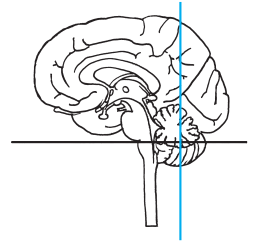
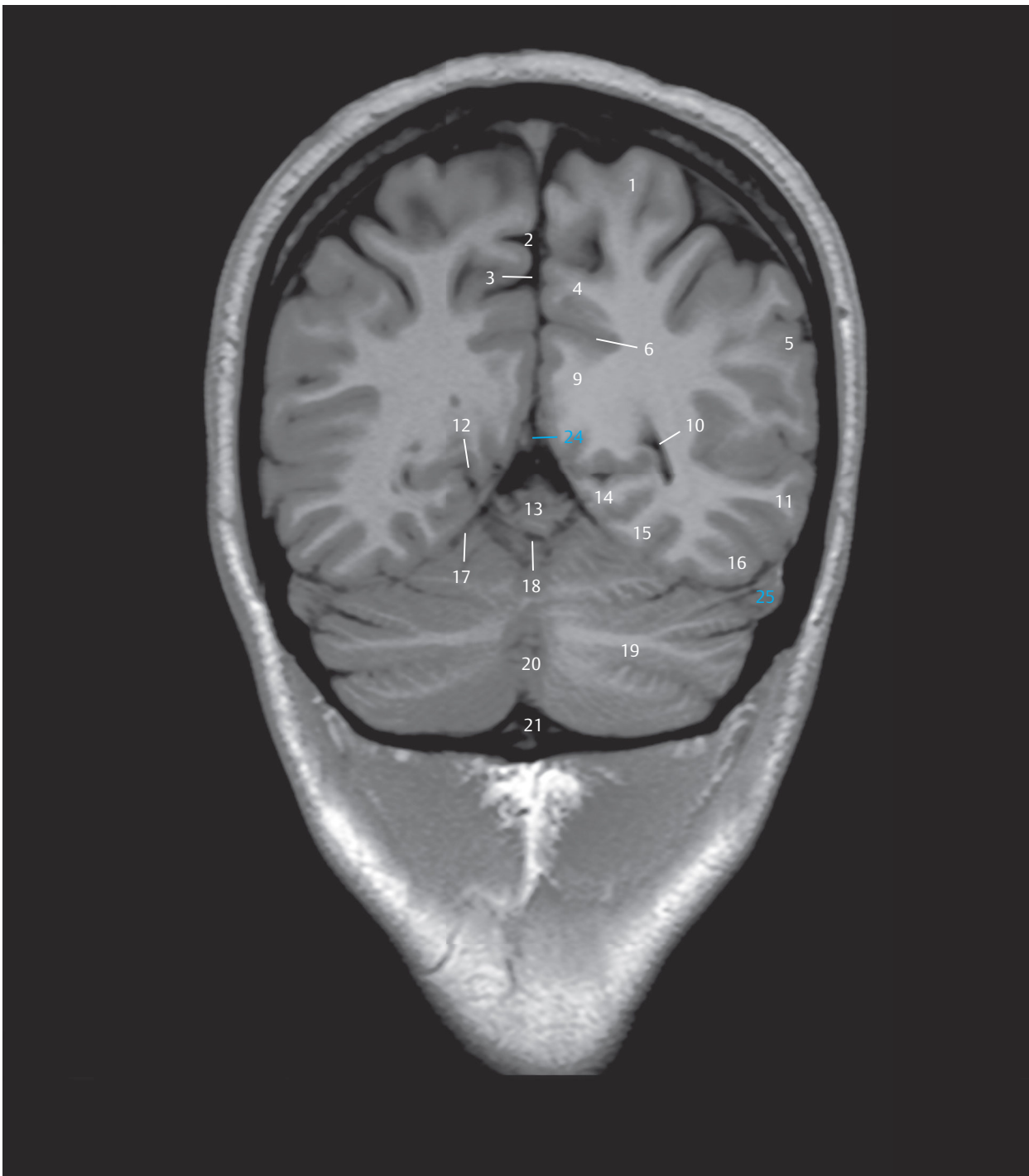


Fig. 3.13 12th coronal section.

DH = German horizontal

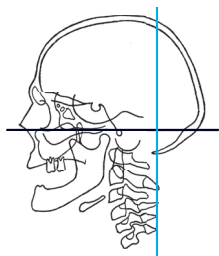
M = median plane

Fig. 3.13a Anterior view of the 12th coronal section. The posterior horn of the lateral ventricle has only been sectioned in the left cerebral hemisphere. The tentorium of cerebellum completely separates the supratentorial and infratentorial regions. Brain structures and branches of spinal nerves.



- 1 Superior parietal lobule
- 2 Longitudinal cerebral (interhemispheric) fissure
- 3 Falx cerebri
- 4 Precuneus
- 5 Angular gyrus
- 6 Parieto-occipital sulcus
- 9 Cuneus
- 10 Lateral ventricle, occipital horn
- 11 Middle temporal gyrus
- 12 Calcarine sulcus
- 13 Anterior lobe of cerebellum
- 14 Medial occipitotemporal gyrus
- 15 Lateral occipitotemporal gyrus
- 16 Inferior temporal gyrus
- 17 Tentorium of cerebellum
- 18 Primary fissure
- 19 Posterior lobe of cerebellum
- 20 Pyramid of vermis (VIII)
- 21 Posterior cerebellomedullary cistern (magna)
- 24 Straight sinus
- 25 Transverse sinus

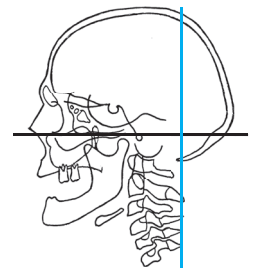
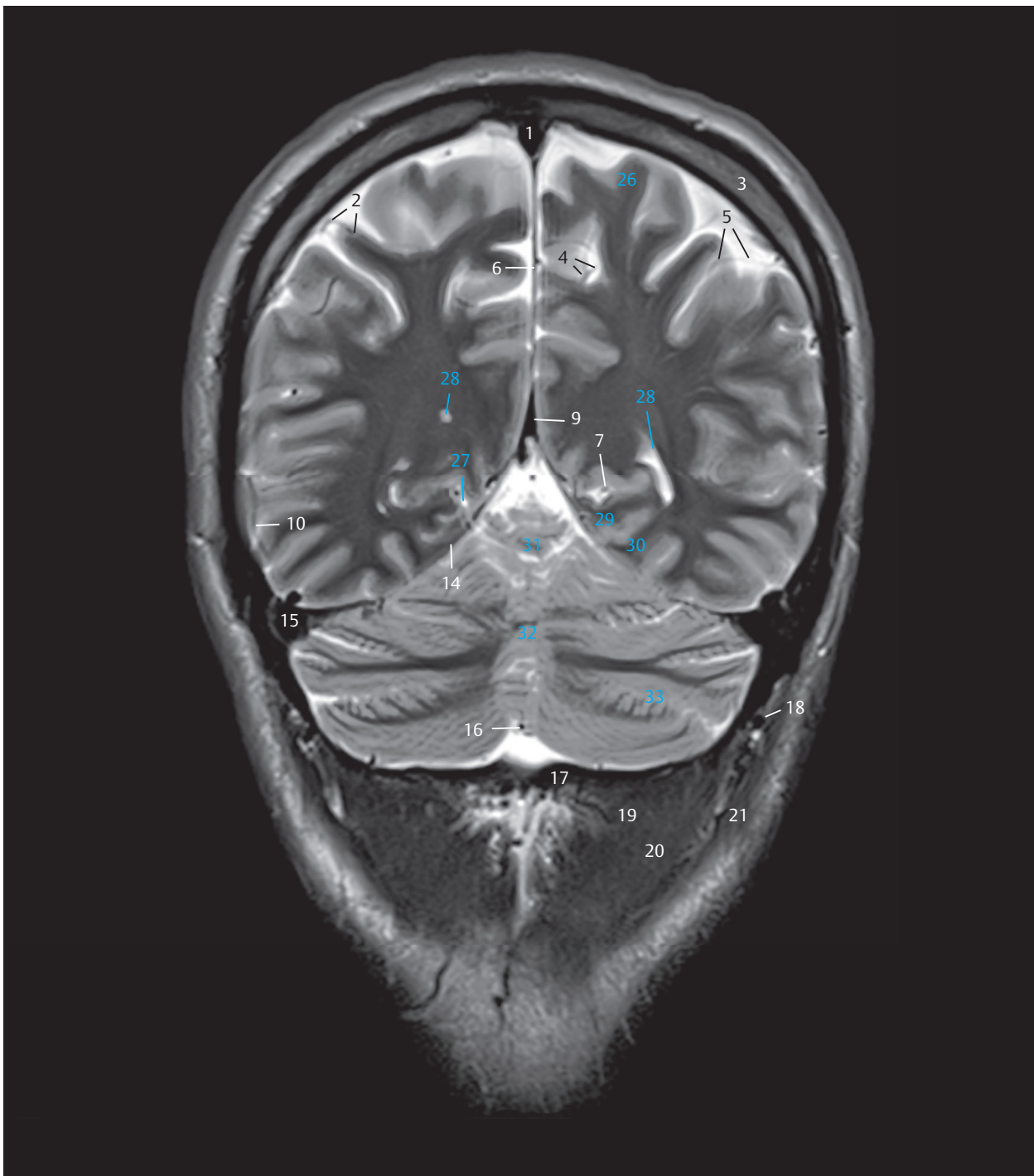
Fig. 3.13b Coronal T1w MR image, approximately corresponding to the sectional plane in a and c.



- 1 Superior sagittal sinus
- 2 Anterior parietal artery
- 3 Parietal bone
- 4 Precuneal artery
- 5 Posterior parietal artery
- 6 Falx cerebri
- 7 Parieto-occipital artery
- 8 Angular artery
- 9 Straight sinus
- 10 Temporo-occipital artery
- 11 Calcarine artery
- 12 Superior cerebellar artery
- 13 Lateral occipital artery
- 14 Tentorium of cerebellum
- 15 Transverse sinus
- 16 Posterior inferior cerebellar artery (PICA)
- 17 Occipital bone
- 18 Occipital artery
- 19 Rectus capitis posterior minor
- 20 Rectus capitis posterior major
- 21 Splenius capitis
- 22 Spinous process of axis
- 23 Suboccipital venous plexus
- 24 Spinous process of fourth cervical vertebra
- 25 Spinous process of fifth cervical vertebra

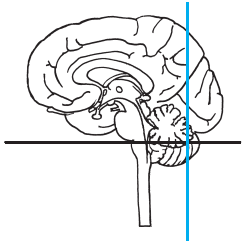


Fig. 3.13c Anterior view of the 12th coronal section. The slice lies behind the foramen magnum. Only three spinous processes of cervical vertebrae have been sectioned. Bony structures, neck muscles, and blood vessels.



- 1 Superior sagittal sinus
- 2 Anterior parietal artery
- 3 Parietal bone
- 4 Precuneal artery
- 5 Posterior parietal artery
- 6 Falx cerebri
- 7 Parieto-occipital artery
- 9 Straight sinus
- 10 Temporo-occipital artery
- 14 Tentorium of cerebellum
- 15 Transverse sinus
- 16 Posterior inferior cerebellar artery
- 17 Occipital bone
- 18 Occipital artery
- 19 Rectus capitis posterior minor
- 20 Rectus capitis posterior major
- 21 Splenius capitis
- 26 Superior parietal lobule
- 27 Parieto-occipital sulcus
- 28 Lateral ventricle, occipital horn
- 29 Medial occipitotemporal gyrus
- 30 Lateral occipitotemporal gyrus
- 31 Anterior lobe of cerebellum, vermis
- 32 Vermis of cerebellum
- 33 Posterior lobe of cerebellum

Fig. 3.13d Coronal T2w MR image, approximately corresponding to the sectional plane in a and c.



- 1 Superior parietal lobule
- 2 Longitudinal cerebral (interhemispheric) fissure
- 3 Precuneus
- 4 Angular gyrus
- 5 Falx cerebri
- 6 Parieto-occipital sulcus
- 7 Cuneus
- 8 Occipital gyri
- 9 Calcarine sulcus
- 10 Primary visual cortex
- 11 Dura mater
- 12 Medial occipitotemporal gyrus
- 13 Lateral occipitotemporal gyrus
- 14 Tentorium of cerebellum
- 15 Folium of vermis (VII A)
- 16 Posterior lobe of cerebellum
- 17 Greater occipital nerve
- 18 Third occipital nerve

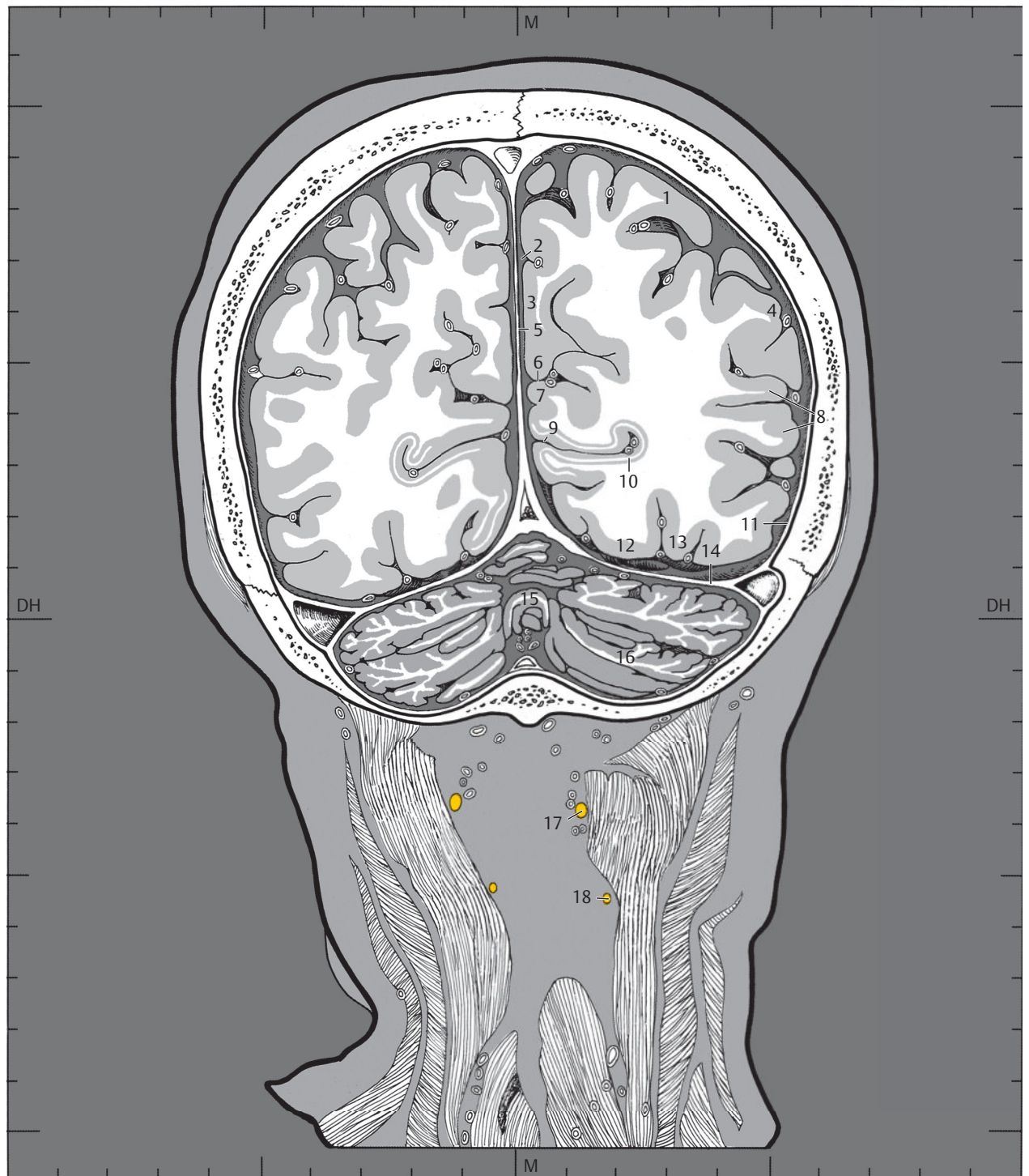
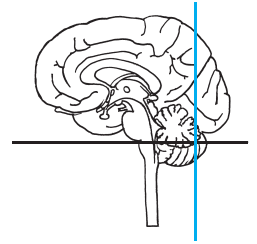
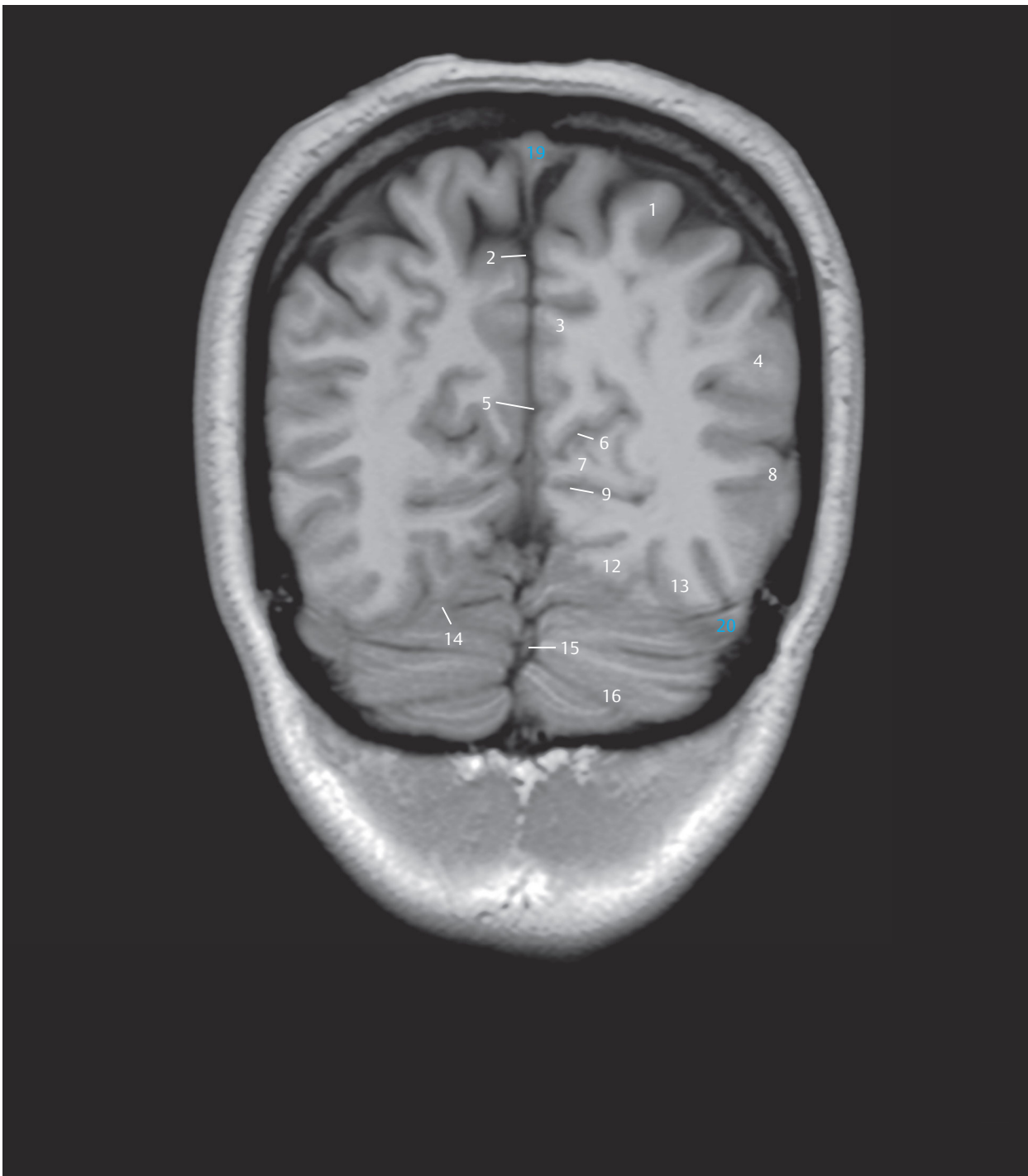


Fig. 3.14 13th coronal section.

DH = German horizontal

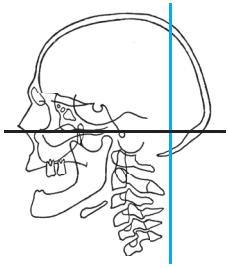
M = median plane

Fig. 3.14a Anterior view of the 13th coronal section. Only parts of the parietal and occipital lobes have been sectioned in the endbrain. Tangential section through the cerebellum. Brain structures and branches of spinal nerves.



- 1 Superior parietal lobule
- 2 Longitudinal cerebral (interhemispheric) fissure
- 3 Precuneus
- 4 Angular gyrus
- 5 Falx cerebri
- 6 Parieto-occipital sulcus
- 7 Cuneus
- 8 Occipital gyri
- 9 Calcarine sulcus
- 12 Medial occipitotemporal gyrus
- 13 Lateral occipitotemporal gyrus
- 14 Tentorium of cerebellum
- 15 Folium of vermis (VII A)
- 16 Posterior lobe of cerebellum
- 19 Superior sagittal sinus
- 20 Transverse sinus

Fig. 3.14b Coronal T1w MR image, approximately corresponding to the sectional plane in a and c.



- 1 Superior sagittal sinus
- 2 Precuneal artery
- 3 Posterior parietal artery
- 4 Parietal bone
- 5 Falx cerebri
- 6 Parieto-occipital artery
- 7 Angular artery
- 8 Calcarine artery
- 9 Temporo-occipital artery
- 10 Straight sinus
- 11 Tentorium of cerebellum
- 12 Lateral occipital artery
- 13 Transverse sinus
- 14 Posterior inferior cerebellar artery (PICA)
- 15 Occipital bone
- 16 Occipital artery
- 17 Semispinalis capitis
- 18 Splenius capitis
- 19 Ligamentum nuchae
- 20 Trapezius

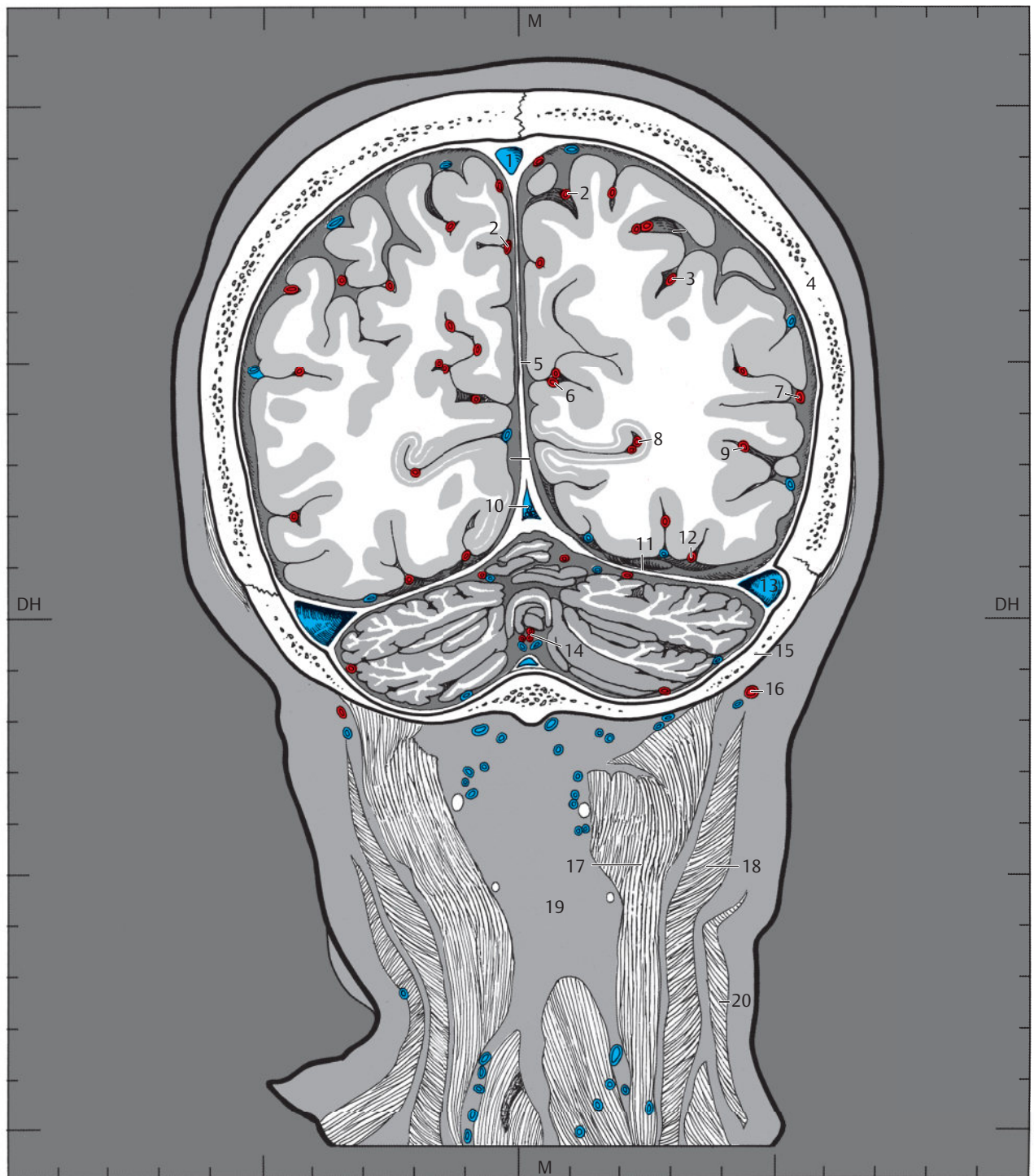
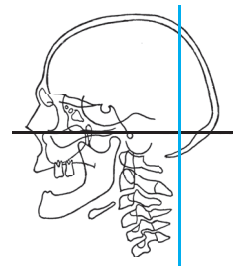
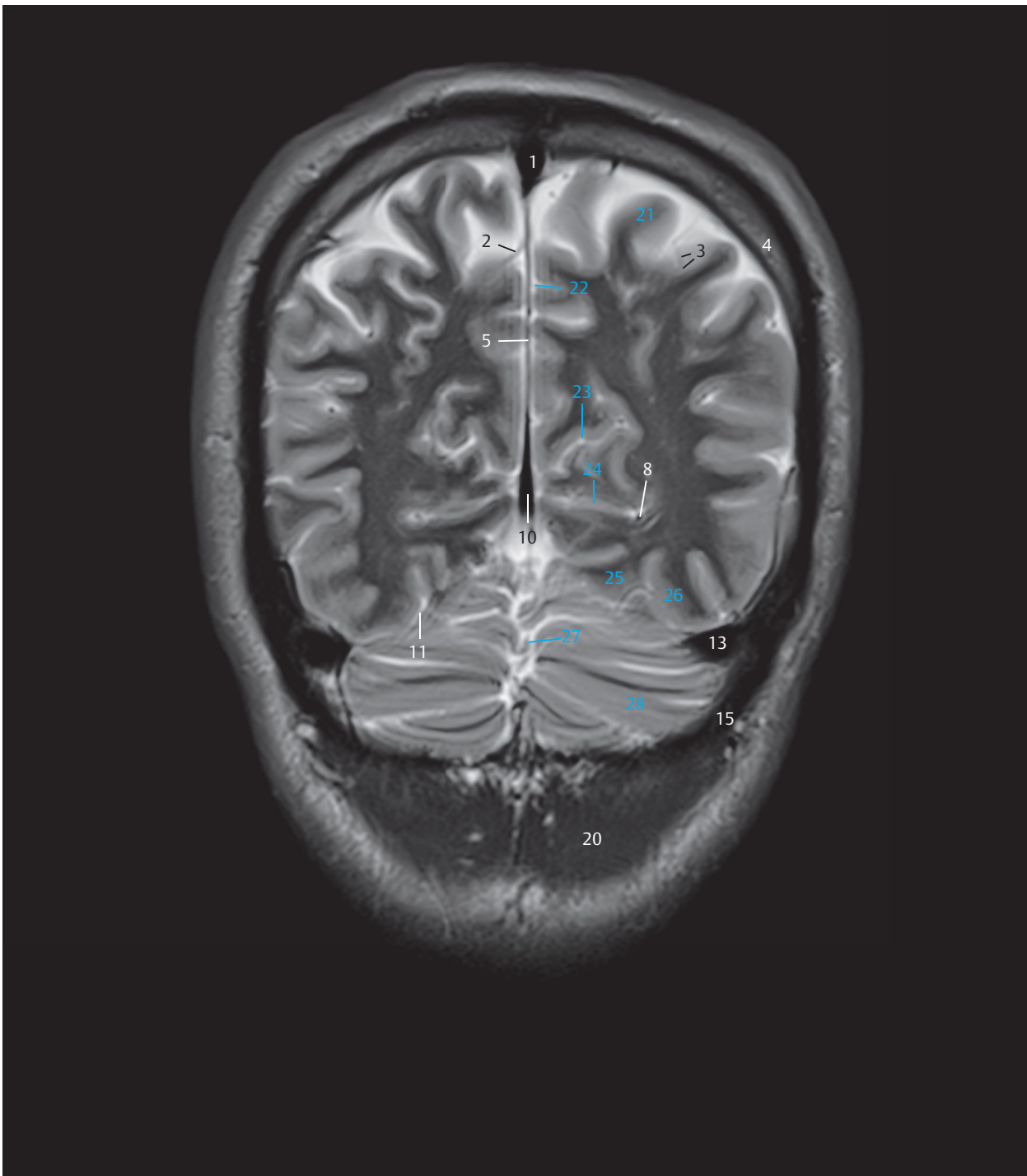
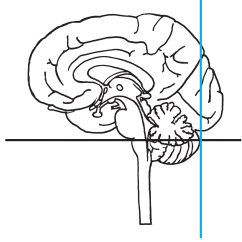


Fig. 3.14c Anterior view of the 13th coronal section. The parietal and occipital bones form a rounded bony ring. Bony structures, neck muscles, and blood vessels.



- 1 Superior sagittal sinus
- 2 Precuneal artery
- 3 Posterior parietal artery
- 4 Parietal bone
- 5 Falx cerebri
- 8 Calcarine artery
- 10 Straight sinus
- 11 Tentorium of cerebellum
- 13 Transverse sinus
- 15 Occipital bone
- 20 Trapezius
- 21 Superior parietal lobule
- 22 Interhemispheric cistern
- 23 Parieto-occipital sulcus
- 24 Calcarine sulcus
- 25 Medial occipitotemporal gyrus
- 26 Lateral occipitotemporal gyrus
- 27 Posterior lobe of cerebellum, vermis
- 28 Posterior lobe of cerebellum, hemisphere

Fig. 3.14d Coronal T2w MR image, approximately corresponding to the sectional plane in a and c.



- 1 Precuneus
- 2 Longitudinal cerebral (interhemispheric) fissure
- 3 Parieto-occipital sulcus
- 4 Falx cerebri
- 5 Occipital gyri
- 6 Cuneus
- 7 Primary visual cortex
- 8 Calcarine sulcus
- 9 Dura mater
- 10 Medial occipitotemporal gyrus
- 11 Lateral occipitotemporal gyrus
- 12 Greater occipital nerve

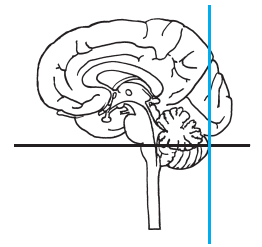
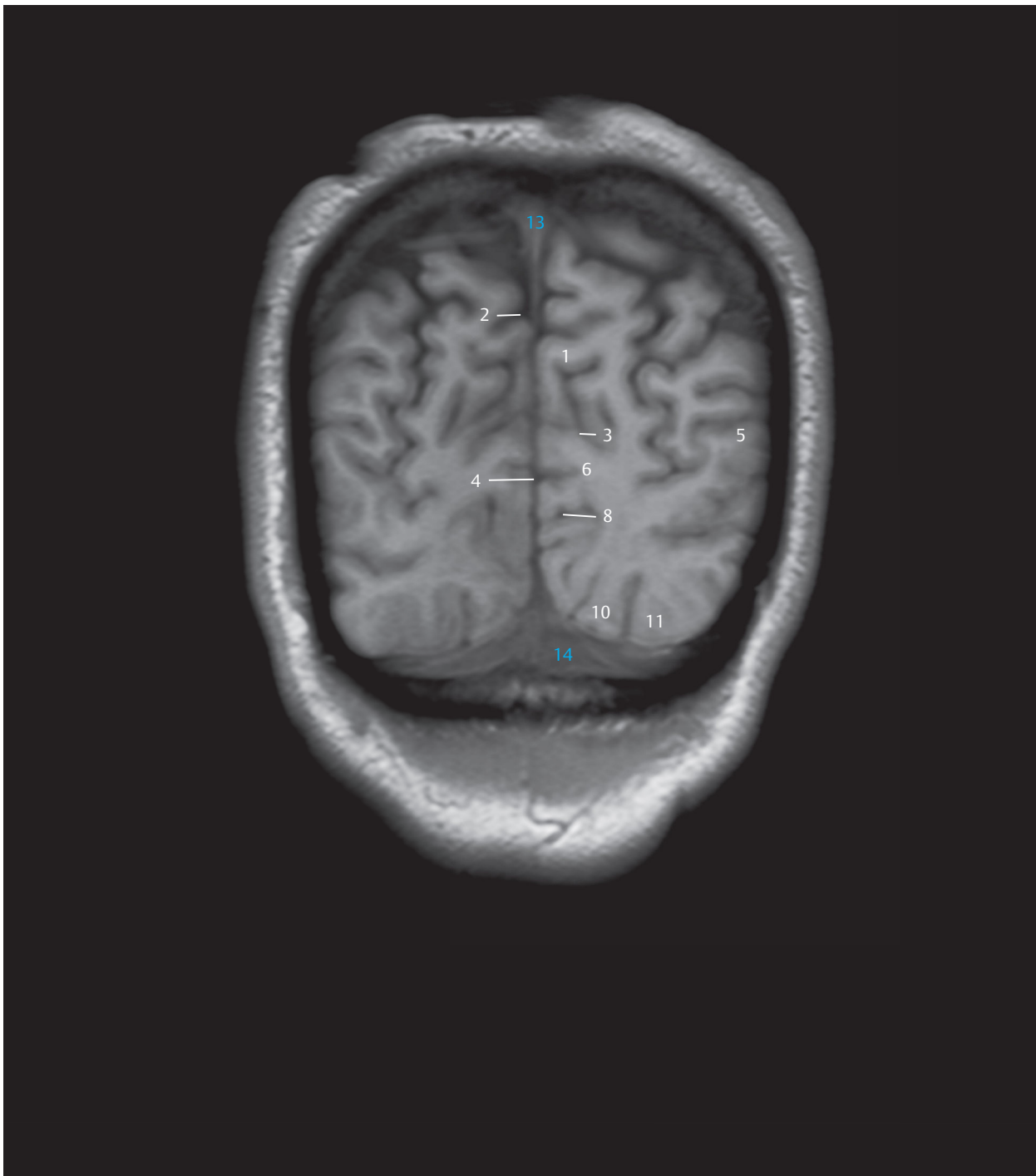


Fig. 3.15 14th coronal section.

DH = German horizontal

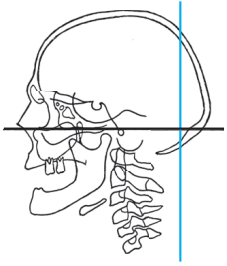
M = median plane

Fig. 3.15a Anterior view of the 14th coronal section. The posterior part of both cerebral hemispheres is composed almost entirely of the occipital lobes. Brain structures and branch of the second spinal nerve.



- 1 Precuneus
- 2 Longitudinal cerebral (interhemispheric) fissure
- 3 Parieto-occipital sulcus
- 4 Falx cerebri
- 5 Occipital gyri
- 6 Cuneus
- 8 Calcarine sulcus
- 10 Medial occipitotemporal gyrus
- 11 Lateral occipitotemporal gyrus
- 13 Superior sagittal sinus
- 14 Transverse sinus

Fig. 3.15b Coronal T1w MR image, approximately corresponding to the sectional plane in a and c.



- 1 Superior sagittal sinus
- 2 Parieto-occipital artery
- 3 Parietal bone
- 4 Angular artery
- 5 Calcarine artery
- 6 Temporo-occipital artery
- 7 Lateral occipital artery
- 8 Confluence of sinuses
- 9 Transverse sinus
- 10 Occipital bone
- 11 Occipital artery
- 12 Semispinalis capitis
- 13 Splenius capitis
- 14 Ligamentum nuchae
- 15 Trapezius

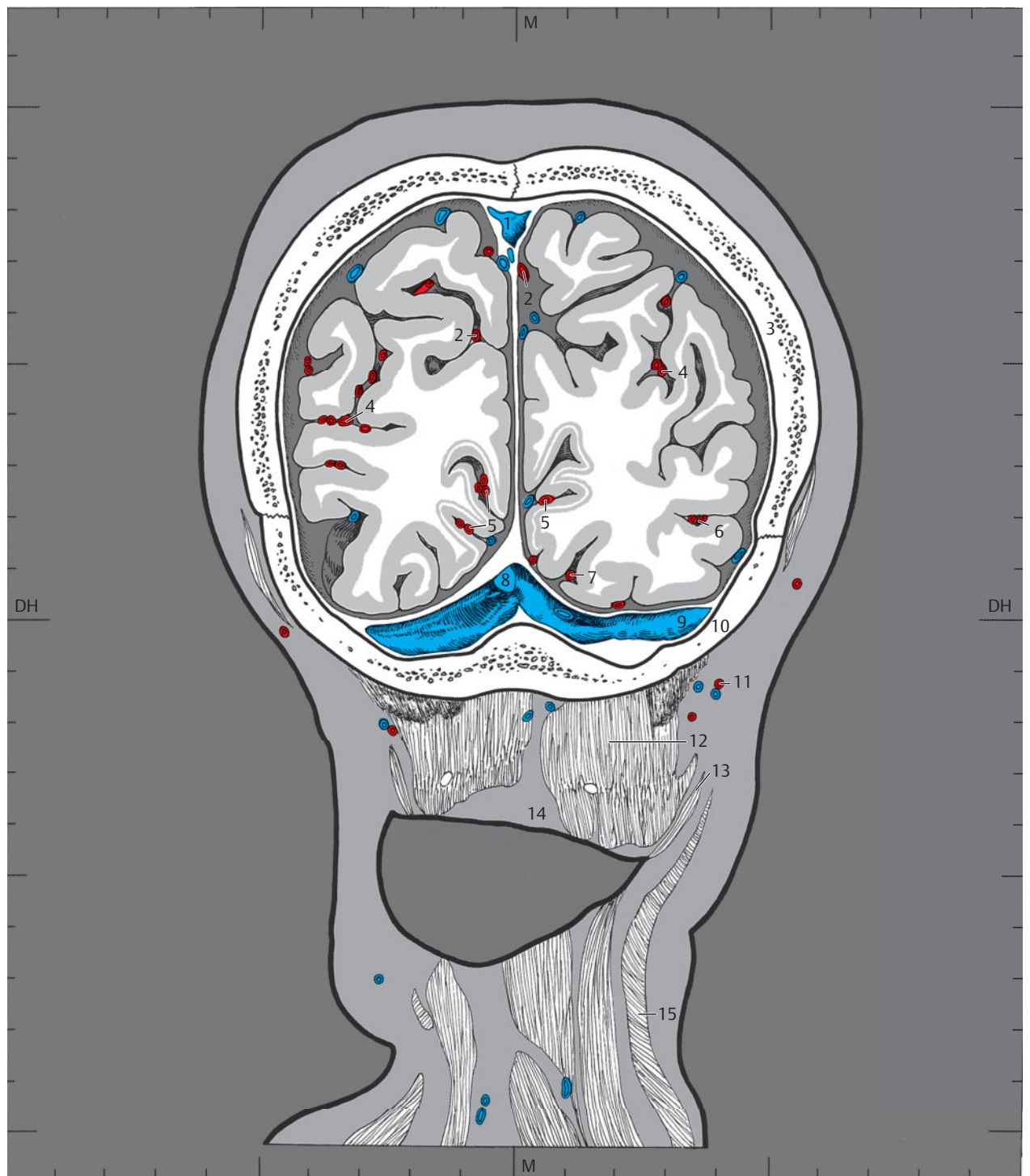
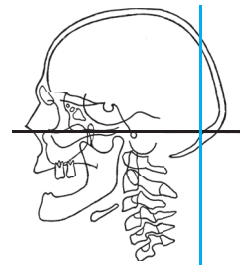
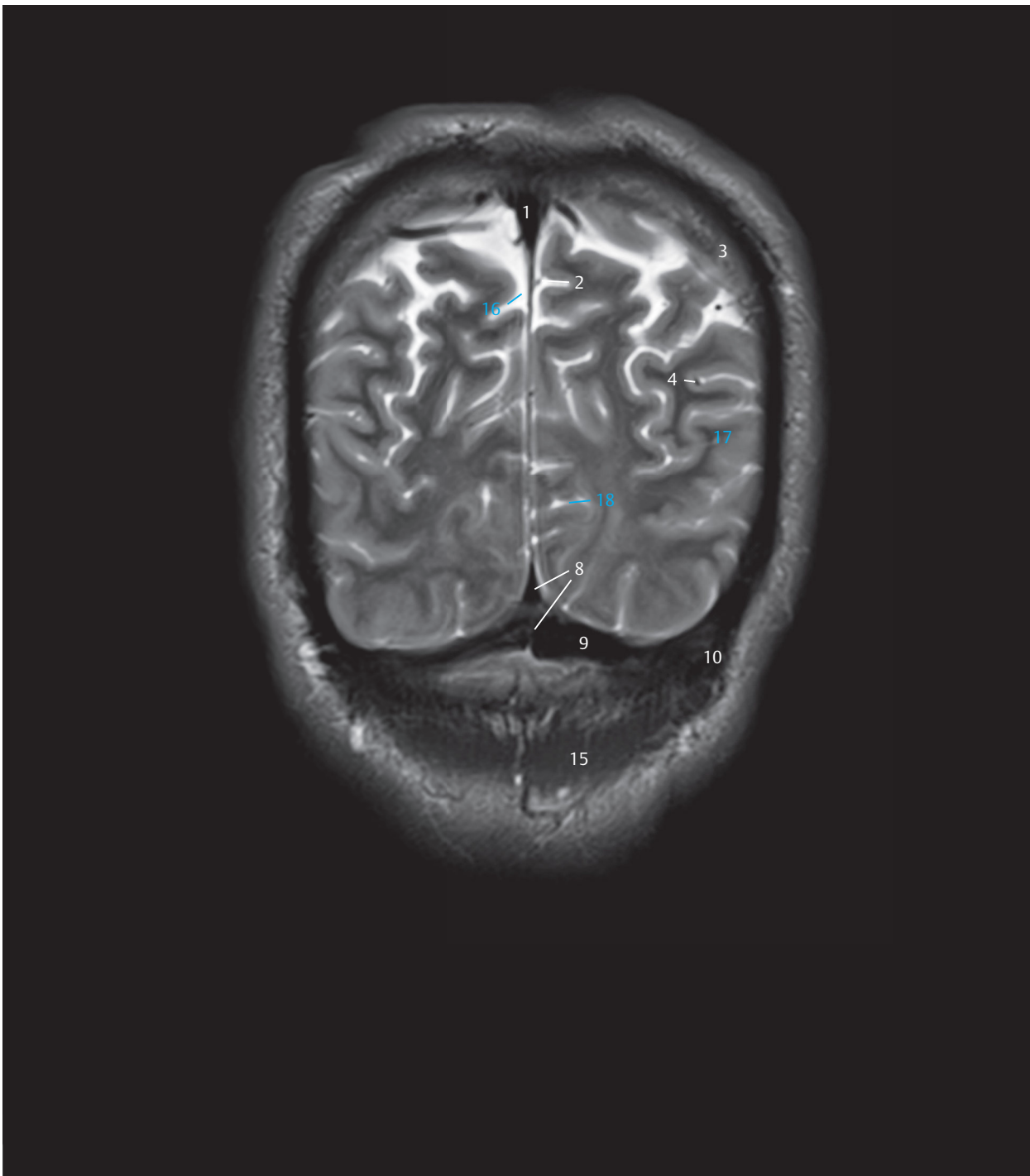
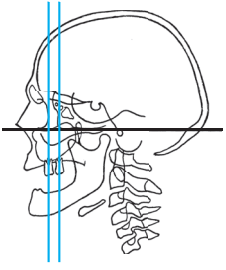


Fig. 3.15c Anterior view of the 14th coronal section, which contains the confluence of sinuses. The curvature of the neck created a gap while sectioning. Bony structures, neck muscles, and blood vessels.



- 1 Superior sagittal sinus
- 2 Parieto-occipital artery
- 3 Parietal bone
- 4 Angular artery
- 8 Confluence of sinuses
- 9 Transverse sinus
- 10 Occipital bone
- 15 Trapezium
- 16 Interhemispheric cistern
- 17 Occipital gyrus
- 18 Calcarine sulcus

Fig. 3.15d Coronal T2w MR image, approximately corresponding to the sectional plane in a and c.



- 1 Frontal bone
- 2 Anterior cranial fossa
- 3 Roof of orbit
- 4 Crista galli
- 5 Frontozygomatic suture
- 6 Orbital plate (papyracea)
- 7 Ethmoidal air cells
- 8 Orbit with eyeball
- 9 Middle nasal concha
- 10 Floor of orbit
- 11 Infra-orbital canal
- 12 Zygomatic bone
- 13 Nasal septum
- 14 Inferior nasal concha
- 15 Maxillary sinus
- 16 Hard palate
- 17 Maxilla
- 18 Second molar
- 19 First molar (sectioned)
- 20 Body of the mandible
- 21 Mandibular canal

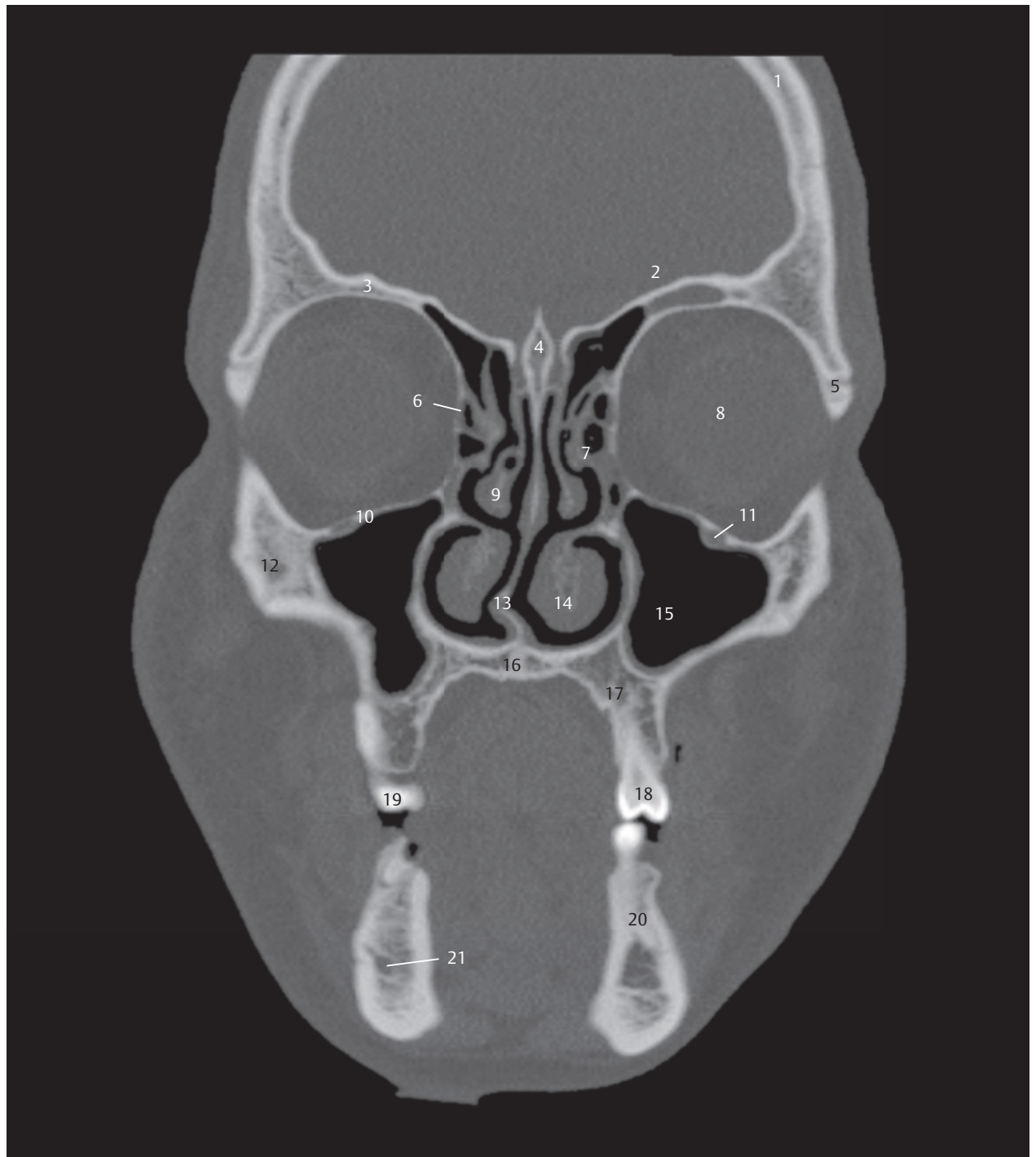
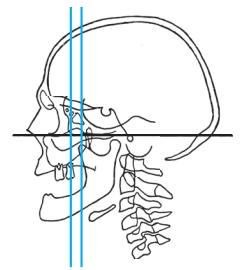
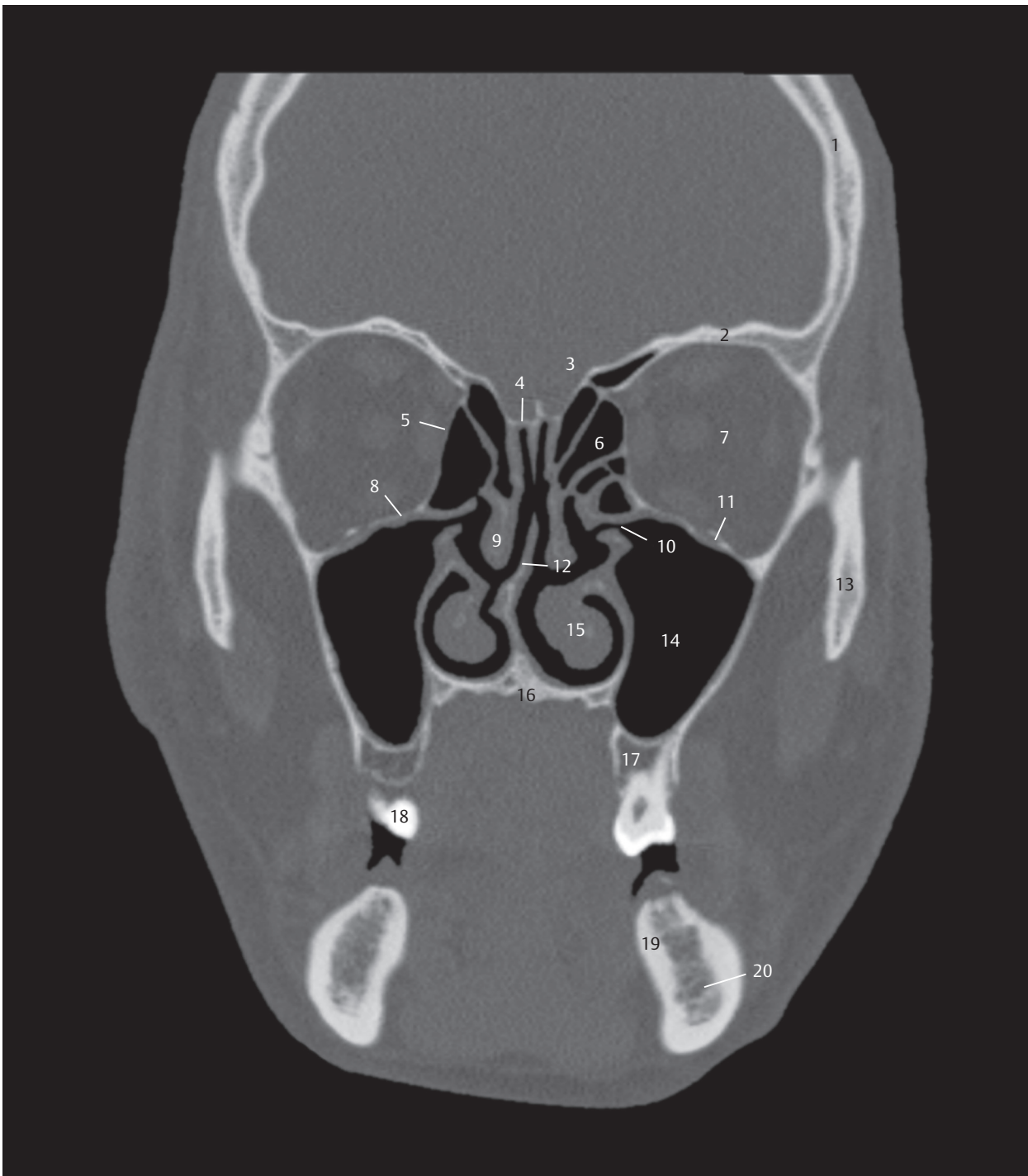
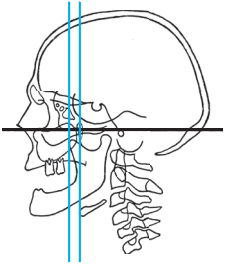


Fig. 3.16 1st coronal section. CT image, the position of which approximately corresponds to that of the first coronal section. This and the following CT images were obtained during a diagnostic examination; the calvarium is therefore incompletely depicted. Secondary coronal reconstruction from a thin, reconstruction-enabling transverse data set. Landmarks are the anterior cranial fossa with crista galli, the orbits, ethmoid cells, nasal turbinates, maxillary sinuses, and the mandible.



- 1 Frontal bone
- 2 Roof of orbit
- 3 Anterior cranial fossa
- 4 Lamina cribrosa
- 5 Orbital plate (papyracea)
- 6 Ethmoidal air cells
- 7 Orbit
- 8 Floor of orbit
- 9 Middle nasal concha
- 10 Ostiomeatal complex
- 11 Infra-orbital canal
- 12 Nasal septum
- 13 Zygomatic bone
- 14 Maxillary sinus
- 15 Inferior nasal concha
- 16 Hard palate
- 17 Maxilla
- 18 Second molar
- 19 Body of the mandible
- 20 Mandibular canal

Fig. 3.17 2nd coronal section. CT image, the position of which approximately corresponds to that of the second coronal section. Bony landmarks are the roof and floor of the orbit, nasal turbinates, maxillary sinuses, and the mandible.



- 1 Frontal bone
- 2 Anterior cranial fossa
- 3 Optic canal
- 4 Anterior clinoid process
- 5 Middle cranial fossa
- 6 Superior orbital fissure
- 7 Sphenoid
- 8 Sphenoid sinus
- 9 Pterygopalatine fossa
- 10 Zygomatic arch
- 11 Inferior nasal concha
- 12 Nasal septum
- 13 Pterygoid process
- 14 Soft palate
- 15 Ramus of mandible
- 16 Mandibular canal

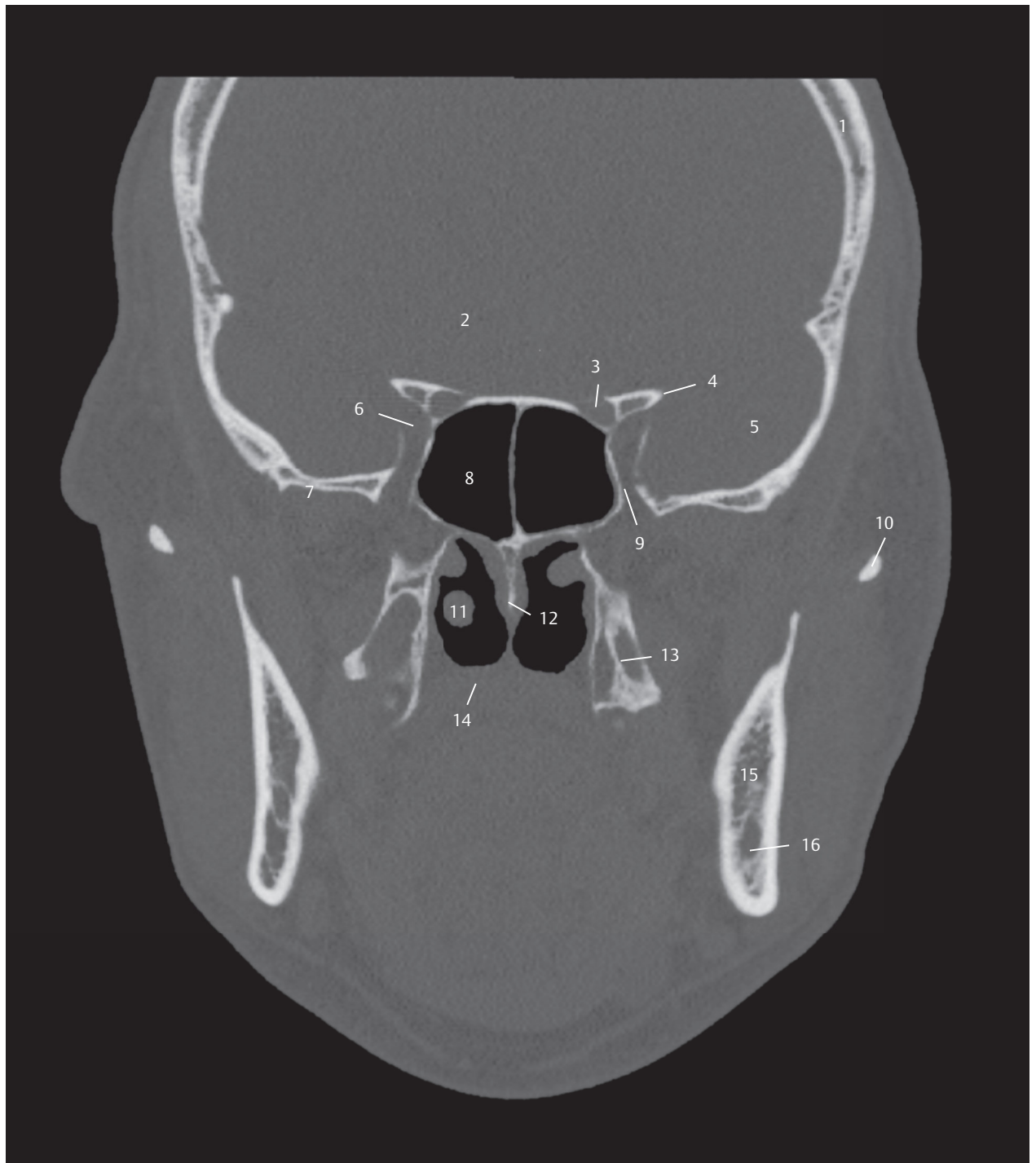
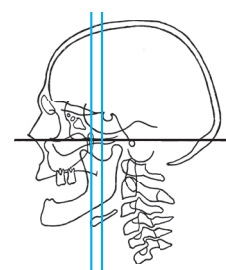
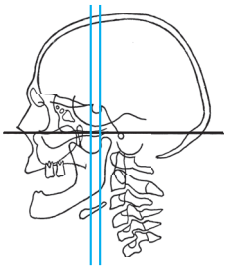


Fig. 3.18 3rd coronal section. CT image, the position of which approximately corresponds to that of the 4th coronal section. The illustration depicts the sphenoid bone, pterygopalatine fossa, and the optic canal.



- 1 Parietal bone
- 2 Squamosal suture
- 3 Sphenoid, lesser wing
- 4 Sphenoid sinus
- 5 Middle cranial fossa
- 6 Temporal bone
- 7 Sphenosquamosal suture
- 8 Foramen rotundum
- 9 Sphenoid
- 10 Pterygoid canal
- 11 Zygomatic arch
- 12 Pterygoid process, lateral plate
- 13 Pterygoid process, medial plate
- 14 Pterygoid fossa
- 15 Ramus of mandible
- 16 Mandibular canal
- 17 Hyoid bone, body

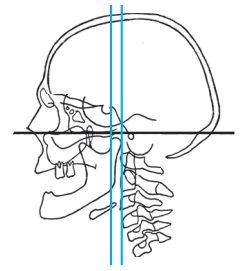
Fig. 3.19 4th coronal section. CT image, the position of which approximately corresponds to that of the 5th coronal section and includes the foramen rotundum and the pterygoid process of the sphenoid bone. The central part of the hyoid bone is also visible.



- 1 Parietal bone
- 2 Posterior clinoid process
- 3 Hypophysial fossa, sellar floor
- 4 Carotid sulcus
- 5 Middle cranial fossa
- 6 Temporal bone
- 7 Sphenoid sinus
- 8 Sphenoid
- 9 Foramen ovale
- 10 Carotid canal
- 11 Ramus of mandible
- 12 Hyoid bone, greater cornu
- 13 Thyroid cartilage (ossified)

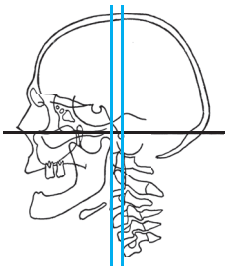


Fig. 3.20 5th coronal section. CT image, the position of which approximately corresponds to that of the 6th coronal section. The middle cranial fossa has been sectioned at the level of the posterior clinoid processes, sphenoid sinus, ramus of the mandible, and the lateral parts of the hyoid bone.



- 1 Parietal bone
- 2 Squamosal suture
- 3 Middle cranial fossa
- 4 Temporal bone
- 5 Sphenosquamosal suture
- 6 Mandibular fossa
- 7 Temporomandibular joint
- 8 Carotid canal
- 9 Sphenoid
- 10 Head of mandible
- 11 Pharyngeal tubercle
- 12 Neck of mandible
- 13 Anterior arch of atlas
- 14 Stylohyoid ligament (ossified)
- 15 Hyoid bone, greater cornu
- 16 Thyroid cartilage

Fig. 3.21 6th coronal section. CT image, the position of which approximately corresponds to that of the 7th coronal section. The middle cranial fossa has been sectioned at the level of the temporomandibular joints, the lateral parts of the hyoid bone, and the anterior arch of the first cervical vertebra.



- 1 Parietal bone
- 2 Squamosal suture
- 3 Upper edge of petrous bone
- 4 Temporal bone
- 5 Cochlea
- 6 Tympanic cavity with ossicles
- 7 External acoustic canal
- 8 Styloid process
- 9 Occipital bone
- 10 Atlanto-occipital joint
- 11 Lateral mass of atlas
- 12 Dens
- 13 Lateral atlantoaxial joint
- 14 Axis
- 15 Hyoid bone
- 16 Superior horn of thyroid cartilage

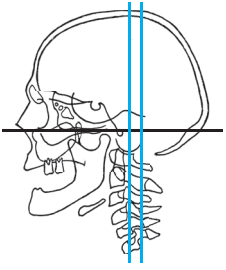


Fig. 3.22 7th coronal section. CT image, the position of which approximately corresponds to that of the 8th coronal section. It includes the petrous part of the temporal bone with the cochlea and the styloid process as well as the anterior part of the upper cervical spine.



- 1 Parietal bone
- 2 Squamosal suture
- 3 Arcuate eminence
- 4 Internal acoustic canal
- 5 Posterior cranial fossa
- 6 Jugular foramen
- 7 Hypoglossal canal
- 8 Facial canal
- 9 Mastoid cells
- 10 Temporal bone
- 11 Foramen magnum
- 12 Occipital condyle
- 13 Atlanto-occipital joint
- 14 Lateral mass of atlas
- 15 Transverse process of atlas
- 16 Lateral atlantoaxial joint
- 17 Axis
- 18 Third cervical vertebra
- 19 Thyroid cartilage (ossified)

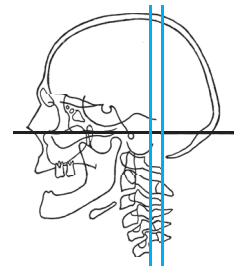
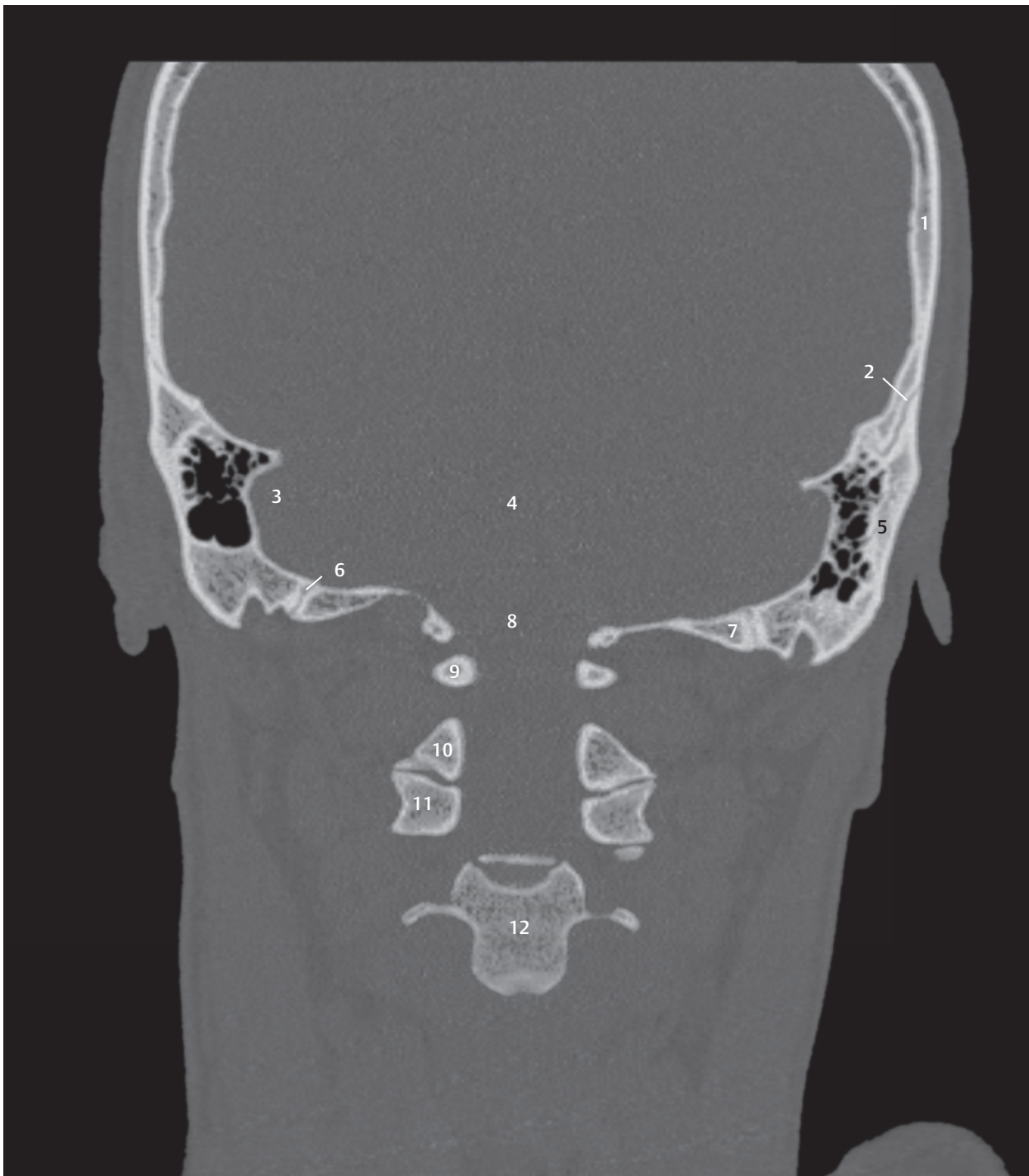
Fig. 3.23 8th coronal section. CT image, mildly posteriorly positioned than the 8th coronal section. The internal auditory canal, facial canal, and mastoid air cells are visible in the petrous part of the temporal bone. The first three cervical vertebrae are well seen.



- 1 Parietal bone
- 2 Squamosal suture
- 3 Superior semicircular canal
- 4 Vestibular labyrinth
- 5 Posterior cranial fossa
- 6 Temporal bone
- 7 Facial canal
- 8 Jugular foramen
- 9 Occipital bone
- 10 Foramen magnum
- 11 Occipitomastoid suture
- 12 Mastoid process
- 13 Atlanto-occipital joint
- 14 Lateral mass of atlas
- 15 Vertebral canal
- 16 Axis
- 17 Third cervical vertebra
- 18 Thyroid cartilage (calcified)
- 19 Cricoid cartilage (calcified)



Fig. 3.24 9th coronal section. CT image, the position of which approximately corresponds to that of the 9th coronal section. The posterior cranial fossa, which transitions to the spinal canal at the foramen magnum, lies medial to the petrous parts of the temporal bones.



- 1 Parietal bone
- 2 Squamosal suture
- 3 Sigmoid sinus, sulcus
- 4 Posterior cranial fossa
- 5 Temporal bone
- 6 Occipitomastoid suture
- 7 Occipital bone
- 8 Foramen magnum
- 9 Posterior arch of atlas
- 10 Arch of axis
- 11 Third cervical vertebra, articular process and arch
- 12 Fourth cervical vertebra

Fig. 3.25 10th coronal section. CT image, the position of which approximately corresponds to that of the 10th coronal section. The calvarium forms a bony ring (incompletely seen here) with a caudal opening at the foramen magnum.

4 Sagittal Sections

Sagittal MR images offer the advantage of the simultaneous depiction of facial bones and the cranial vault. The following structures are clearly seen in the median plane of the brain:

- Brainstem (medulla oblongata, pons, mesencephalon)
- Cerebellum
- Forebrain (diencephalon, telencephalon)

The craniocervical junction continues into the spinal cord. The typical shape of the corpus callosum and its lesions, as well as aplasia or atrophy thereof, are visualized in the median plane. The hypophysis and its pathological changes are also well delineated in the median plane and in a few paramedian sections. The bicommissural line is also well delineated in the median plane (see ►Fig. 1.1), thereby enabling a transposition of brain anatomy in stereotactic-oriented atlases onto corresponding MR images using a coordinate system

oriented in the bicommissural plane. Gyri and sulci of the endbrain are well defined in medial and lateral sagittal slices. Sulci run nearly perpendicular to the sectioned plane and are more distinctly visualized than the obliquely and tangentially coursing gyri due to the partial volume effect.

The ability to obtain sagittal sections counts as one of the merits of MRI, although sagittal reconstructions may also be obtained from CT volume data. Anomalies of midline structures of the brain are easily discernable on sagittal images; narrowing of the spinal canal by extradural space-occupying lesions or trauma sequelae may also be diagnosed (Section 9.2).

►Fig. 4.1 demonstrates the position of the six sagittal sections which have been depicted in the medial view in the next part of the atlas (►Fig. 4.2, ►Fig. 4.3, ►Fig. 4.4, ►Fig. 4.5, ►Fig. 4.6, ►Fig. 4.7, ►Fig. 4.8, ►Fig. 4.9, ►Fig. 4.10, ►Fig. 4.11, ►Fig. 4.12, and ►Fig. 4.13).

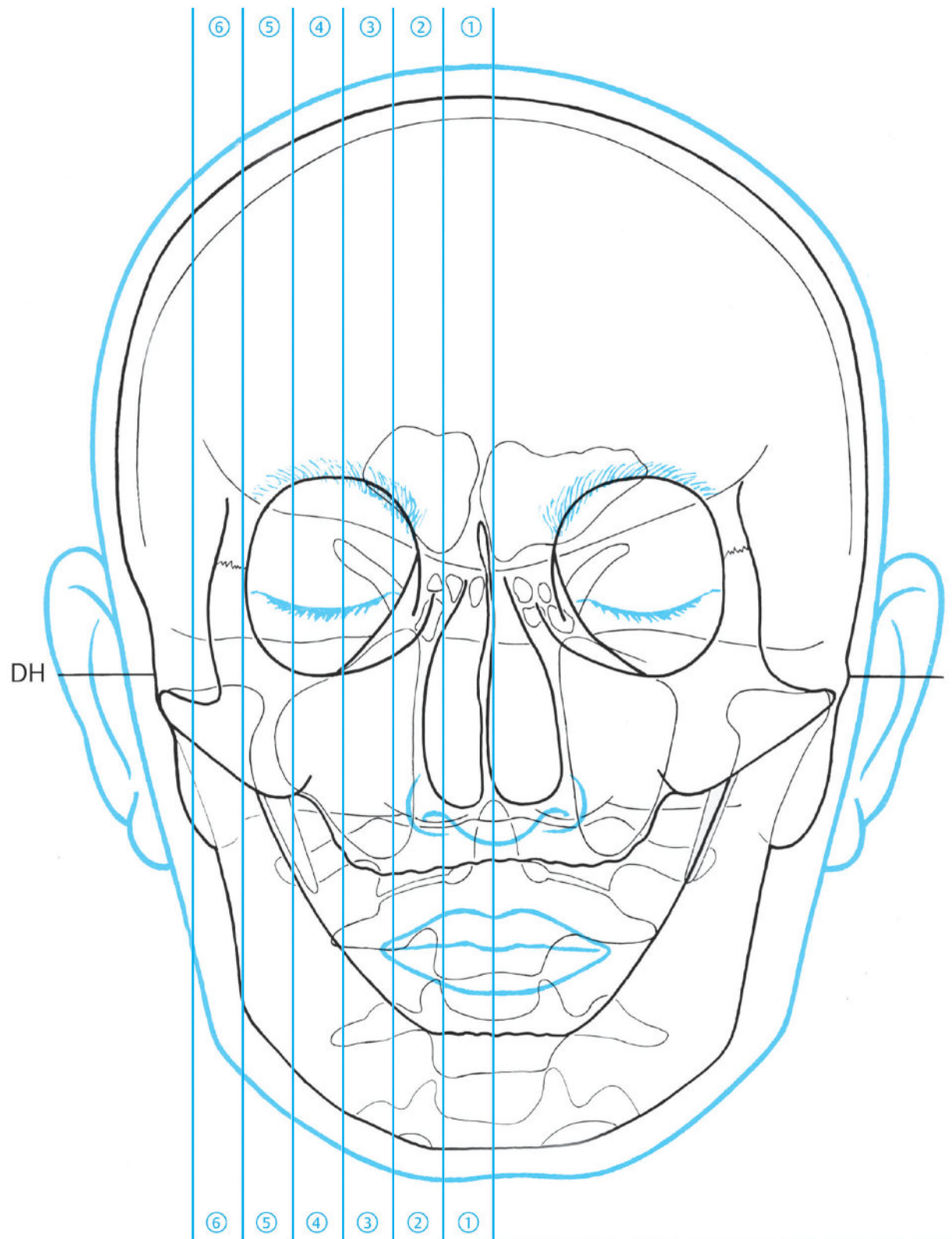


Fig. 4.1 Sagittal sections. The encircled digits indicate the number of 1-cm-thick sections. For details see ► Chapter 12. DH = German horizontal.

Fig. 4.1a Anterior view of the six sagittal sections. The illustrated cross-section always corresponds to the line lying medial to the encircled number of the slice concerned.

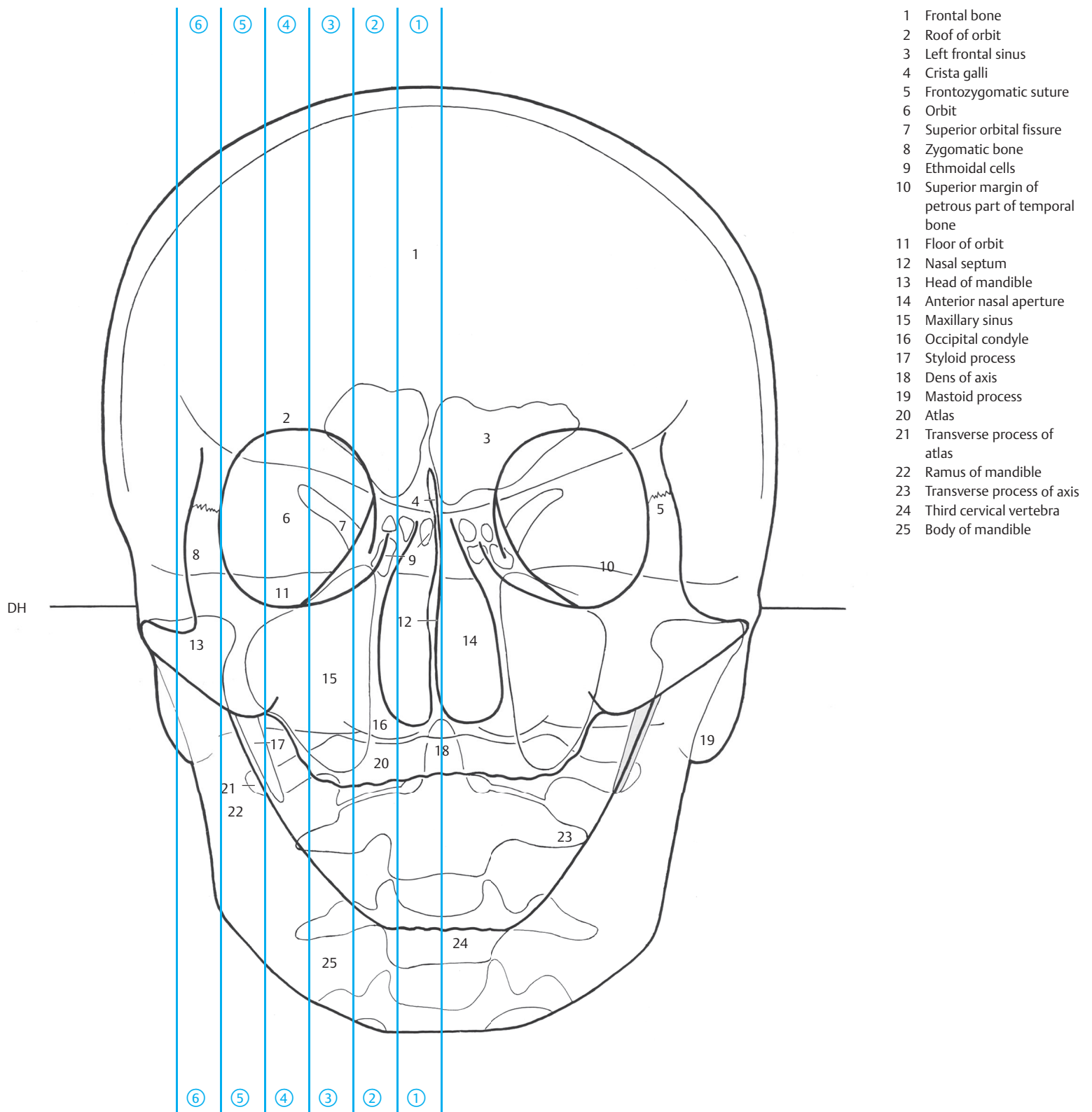


Fig. 4.1 b Illustration based on a cephalogram in an anteroposterior projection of the head from a. The six sagittal sections were drawn precisely and consecutively numbered from medial to lateral.

- 1 Longitudinal cerebral (interhemispheric) fissure
- 2 Superior frontal sulcus
- 3 Middle frontal gyrus
- 4 Superior frontal gyrus
- 5 Inferior frontal sulcus
- 6 Inferior frontal gyrus
- 7 Lateral sulcus (Sylvian fissure)
- 8 Superior temporal gyrus
- 9 Superior temporal sulcus
- 10 Middle temporal gyrus
- 11 Olfactory bulb
- 12 Interpeduncular fossa
- 13 Oculomotor nerve
- 14 Pole of temporal lobe
- 15 Pons
- 16 Trigeminal nerve
- 17 Facial nerve and intermediate nerve
- 18 Abducens nerve
- 19 Inferior olive
- 20 Vestibulocochlear nerve
- 21 Flocculus (H X)
- 22 Glossopharyngeal nerve
- 23 Vagus nerve
- 24 Pyramid of medulla oblongata
- 25 Tonsil of cerebellum (H IX)
- 26 Accessory nerve
- 27 Hypoglossal nerve
- 28 Anterior (ventral) root of first cervical spinal nerve
- 29 Second cervical spinal nerve
- 30 Spinal cord

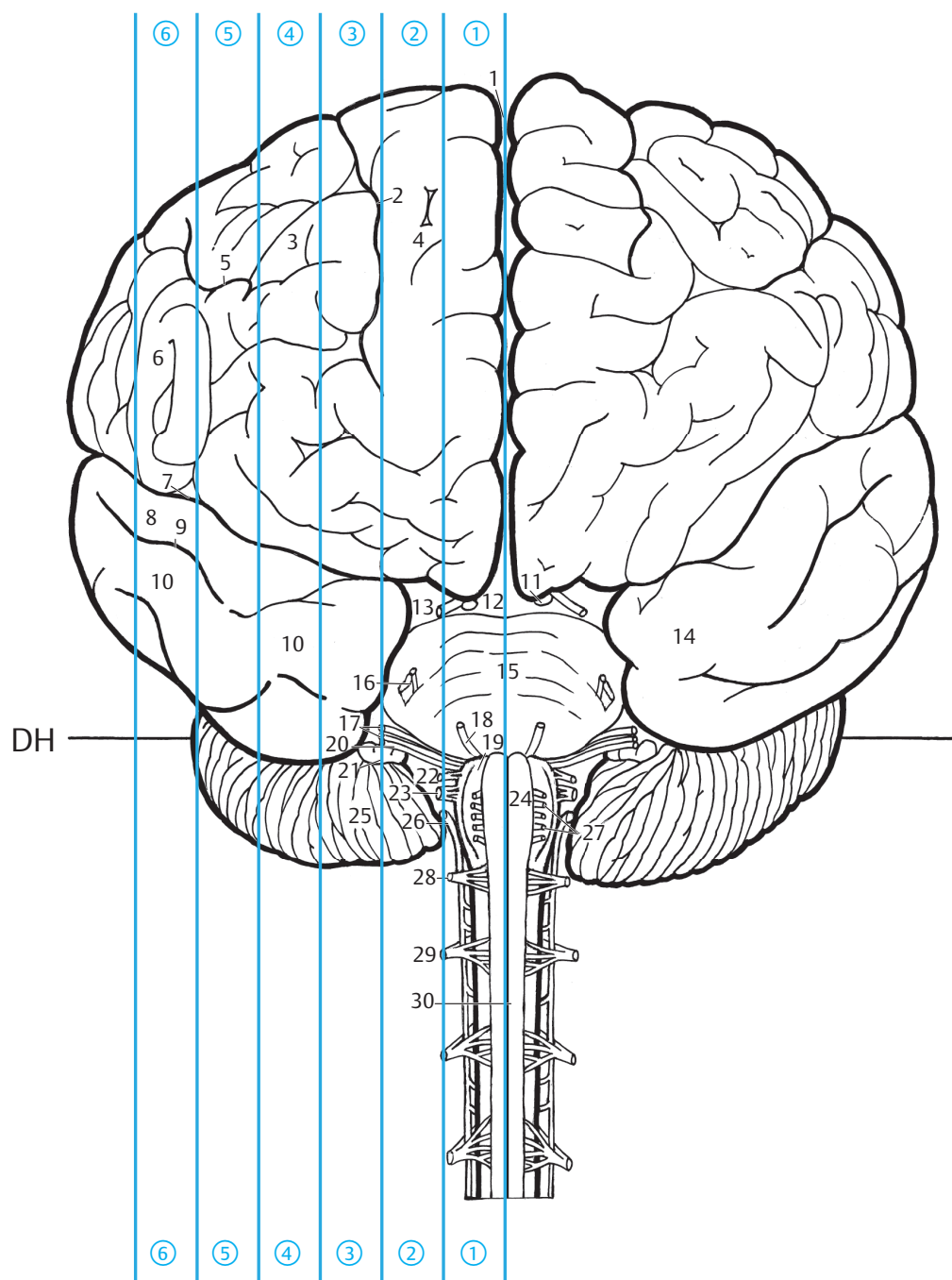


Fig. 4.1c Anterior view of the brain in a and b. The coronal plane runs perpendicular to the German horizontal. Sagittal sections were assembled and numbered as in a.

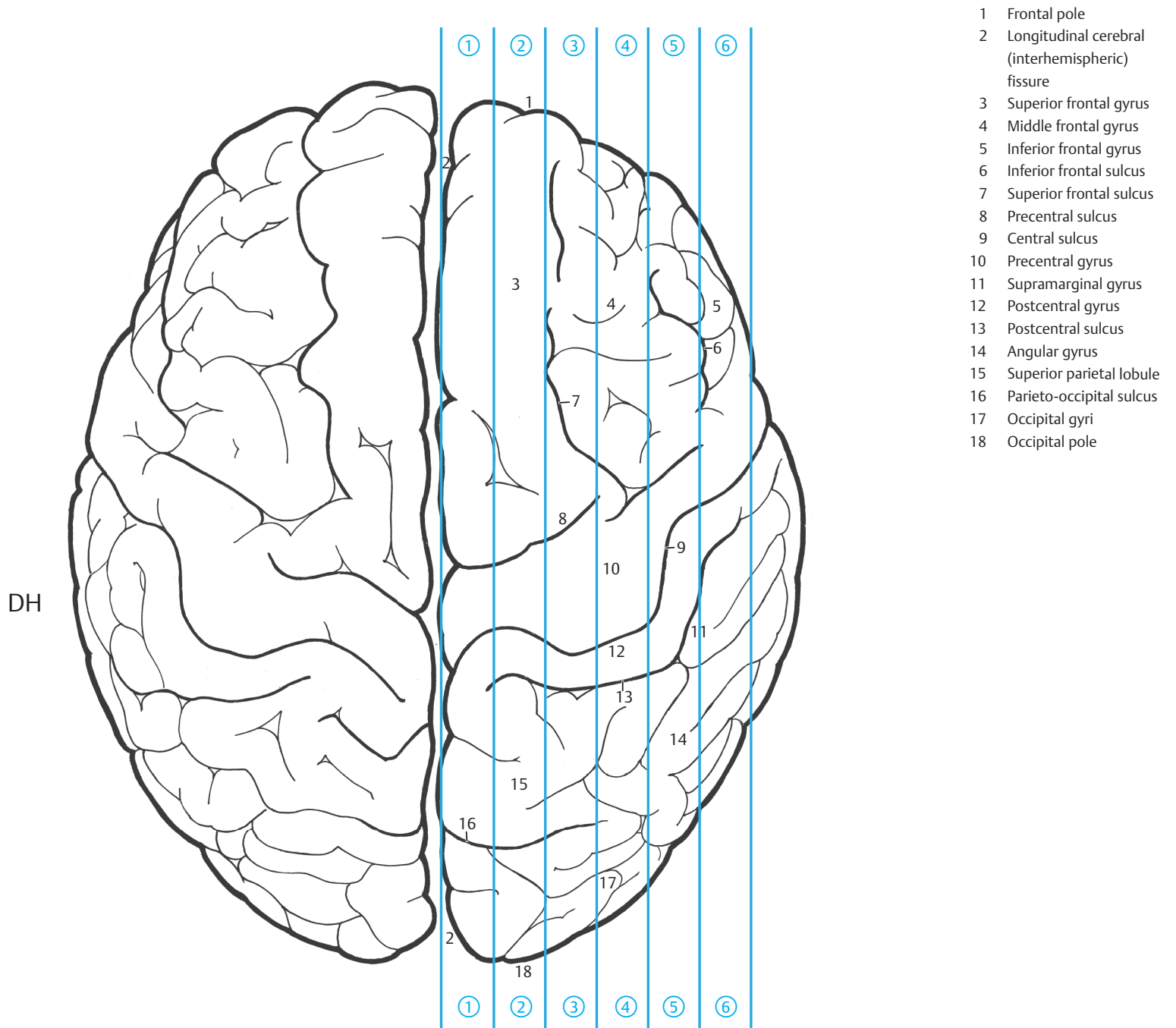
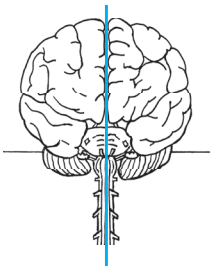


Fig. 4.1d View of the brain from a to c. Sagittal sections were assembled and numbered as in a.



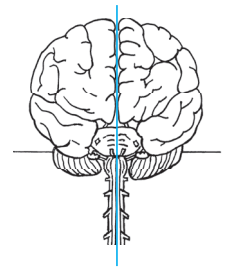
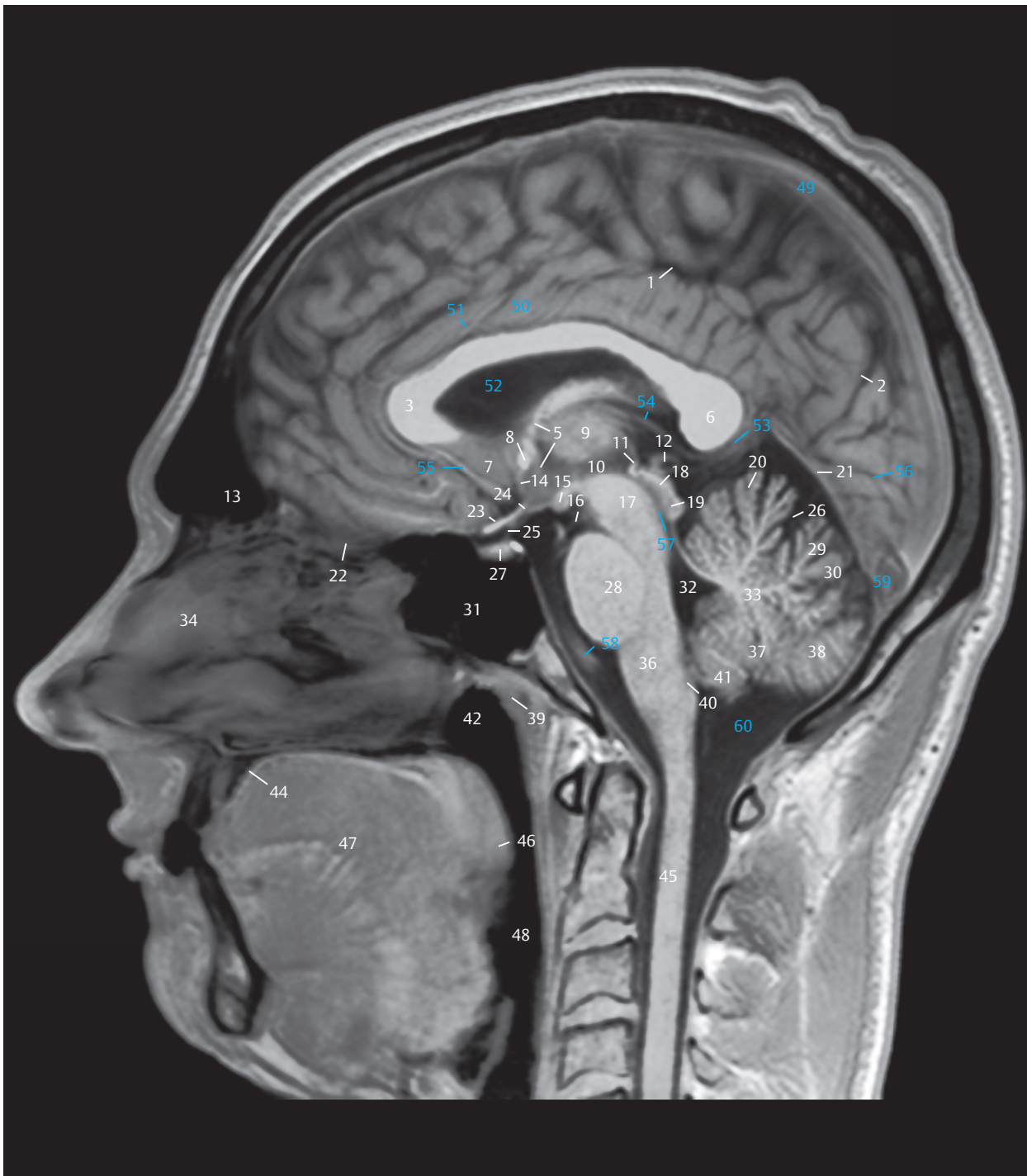
- 1 Cingulate sulcus
- 2 Parieto-occipital sulcus
- 3 Genu of corpus callosum
- 4 Septum pellucidum
- 5 Fornix
- 6 Splenium of corpus callosum
- 7 Paraterminal gyrus
- 8 Anterior commissure
- 9 Interthalamic adhesion
- 10 Third ventricle
- 11 Posterior commissure
- 12 Pineal gland
- 13 Left frontal sinus
- 14 Lamina terminalis
- 15 Mammillary body
- 16 Oculomotor nerve
- 17 Tegmentum of midbrain
- 18 Superior colliculus
- 19 Inferior colliculus
- 20 Culmen (IV, V)
- 21 Tentorium of cerebellum
- 22 Olfactory bulb and tract (within the slice)
- 23 Optic nerve
- 24 Optic chiasm
- 25 Infundibulum
- 26 Primary fissure of cerebellum
- 27 Pituitary gland
- 28 Pons
- 29 Declive (VI)
- 30 Folium of vermis (VII A)
- 31 Sphenoid sinus
- 32 Fourth ventricle
- 33 Nodule of vermis (X)
- 34 Nasal septum
- 35 Abducens nerve (within the slice)
- 36 Medulla oblongata
- 37 Uvula of vermis (IX)
- 38 Pyramis of vermis (VIII)
- 39 Pharyngeal tonsil
- 40 Obex of medulla oblongata
- 41 Tonsil of cerebellum (H IX)
- 42 Nasopharynx
- 43 Central canal
- 44 Oral cavity
- 45 Spinal cord
- 46 Uvula of palate
- 47 Tongue
- 48 Oropharynx



Fig. 4.2 Sagittal section.

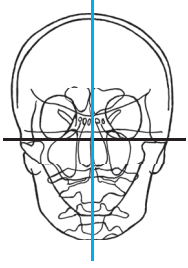
B = Bicommissural line
DH = German horizontal
MV = Meatoververtical line

Fig. 4.2a Medial view of the first sagittal section. The falx cerebri has been removed, so that the medial surface of the endbrain is visible. The IIIrd ventricle, aqueduct and the IVth ventricle are recognizable as landmarks for the diencephalon and the brainstem. Nasal septum and paranasal sinuses together with the oral cavity, brain, and structures of the spinal cord. The Isth, IIsth, IIIrd, and VIth cranial nerves have been graphically depicted, although they partly run within the slice.



- 1 Cingulate sulcus
- 2 Parieto-occipital sulcus
- 3 Corpus callosum, genu
- 5 Fornix
- 6 Corpus callosum, splenium
- 7 Paraterminal gyrus
- 8 Anterior commissure
- 9 Interthalamic adhesion
- 10 Third ventricle
- 11 Posterior commissure
- 12 Pineal gland
- 13 Frontal sinus
- 14 Lamina terminalis
- 15 Mammillary body
- 16 Oculomotor nerve
- 17 Tegmentum of midbrain
- 18 Superior colliculus
- 19 Inferior colliculus
- 20 Culmen (IV and V)
- 21 Tentorium of cerebellum
- 22 Olfactory bulb
- 23 Optic nerve
- 24 Optic chiasma
- 25 Infundibulum
- 26 Primary fissure of cerebellum
- 27 Pituitary gland
- 28 Pons
- 29 Declive (VI)
- 30 Folium of vermis (VII A)
- 31 Sphenoid sinus
- 32 Fourth ventricle
- 33 Nodule of vermis (X)
- 34 Nasal septum
- 36 Medulla oblongata
- 37 Uvula of vermis (IX)
- 38 Pyramid of vermis (VIII)
- 39 Pharyngeal tonsils
- 40 Medulla oblongata, obex
- 41 Tonsils of cerebellum (IX)
- 42 Pharynx, nasopharynx
- 44 Oral cavity
- 45 Spinal cord
- 46 Uvula
- 47 Tongue
- 48 Pharynx, oropharynx
- 49 Superior sagittal sinus
- 50 Cingulate gyrus
- 51 Pericallosal artery
- 52 Lateral ventricle
- 53 Great cerebral vein (Galen)
- 54 Internal cerebral vein
- 55 Anterior cerebral artery
- 56 Calcarine sulcus
- 57 Cerebral aqueduct (of Sylvius)
- 58 Basilar artery
- 59 Confluence of sinuses
- 60 Posterior cerebellomedullary cistern (magna)

Fig. 4.2b Sagittal T1w MR image (T1w FLASH sequence), approximately corresponding to a. Both sagittal MR series (see ►Fig. 4.2b, ►Fig. 4.3b, ►Fig. 4.4b, ►Fig. 4.5b, ►Fig. 4.6b, and ►Fig. 4.7b, and ►Fig. 4.2d, ►Fig. 4.3d, ►Fig. 4.4d, ►Fig. 4.5d, ►Fig. 4.6d, and ►Fig. 4.7d) were obtained from a 33-year-old man (volunteer). For technical data, see ►Chapter 12.



- 1 Coronal suture
- 2 Superior sagittal sinus
- 3 Parietal bone
- 4 Frontal bone
- 5 Posteromedial frontal artery
- 6 Paracentral artery
- 7 Precuneal artery
- 8 Intermediomedial frontal artery
- 9 Pericallosal artery
- 10 Lambdoid suture
- 11 Anteromedial frontal artery
- 12 Internal cerebral vein
- 13 Great cerebral vein (of Galen)
- 14 Parieto-occipital artery
- 15 Calcarine artery
- 16 Crista galli
- 17 Polar frontal artery
- 18 Origin of anterior communicating artery
- 19 Medial frontobasal artery
- 20 Anterior cerebral artery
- 21 Posterior cerebral artery
- 22 Superior cerebellar artery
- 23 Straight sinus
- 24 Nasal bone
- 25 Basilar artery
- 26 Confluence of sinuses
- 27 Internal occipital protuberance
- 28 Clivus
- 29 Anterior inferior cerebellar artery (AICA)
- 30 External occipital protuberance (inion)
- 31 Vertebral artery
- 32 Pharyngeal tubercle
- 33 Posterior inferior cerebellar artery (PICA)
- 34 Incisive canal of maxilla
- 35 Anterior arch of atlas
- 36 Dens of axis
- 37 Transverse ligament of atlas
- 38 Posterior arch of atlas
- 39 Spinous process of axis
- 40 Intervertebral disc
- 41 Genioglossus
- 42 Epiglottis
- 43 Third cervical vertebra
- 44 Body of mandible
- 45 Geniohyoid
- 46 Mylohyoid
- 47 Hyoid bone

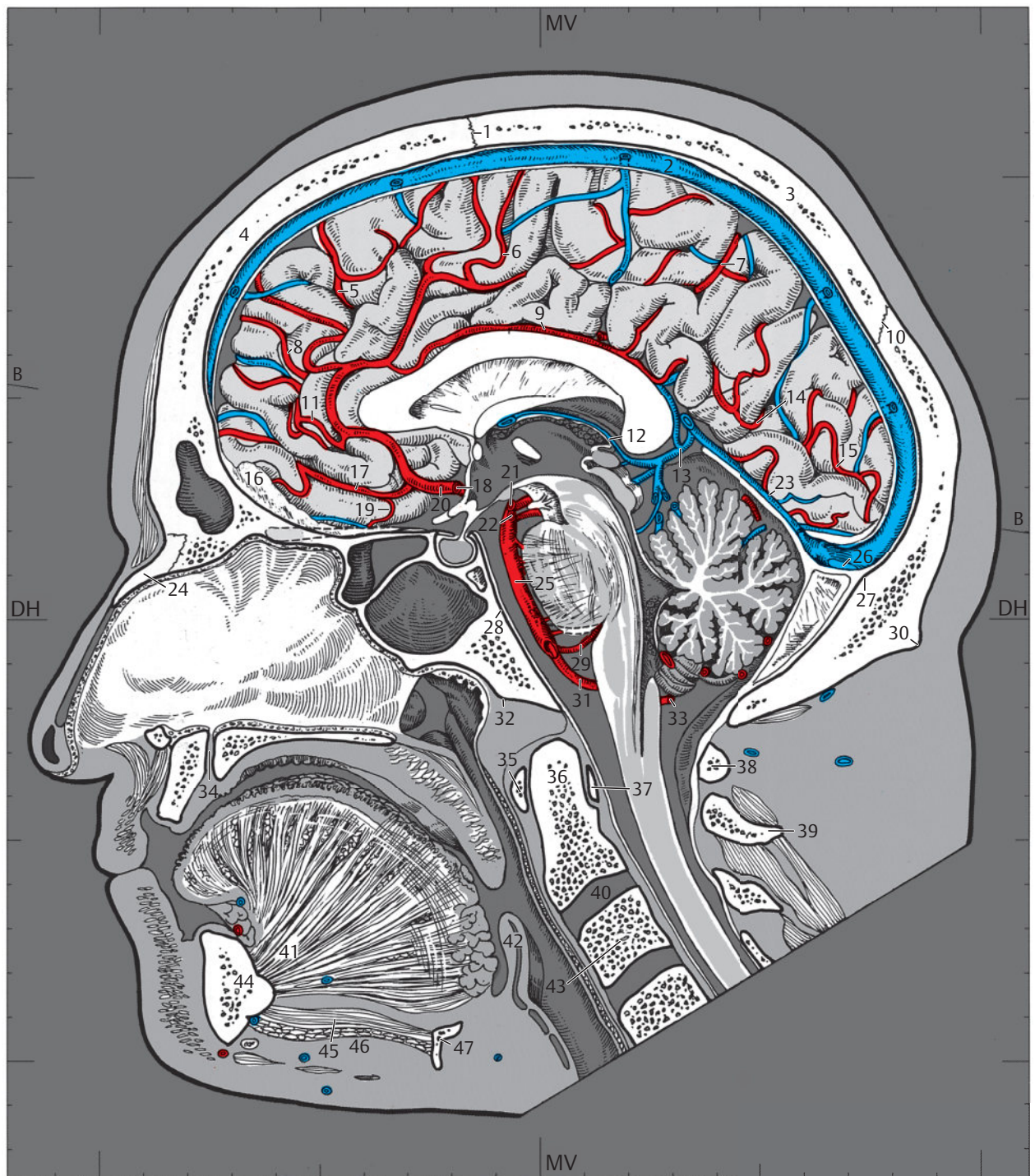
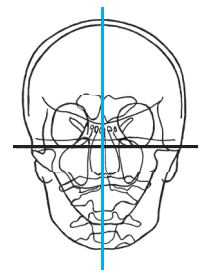
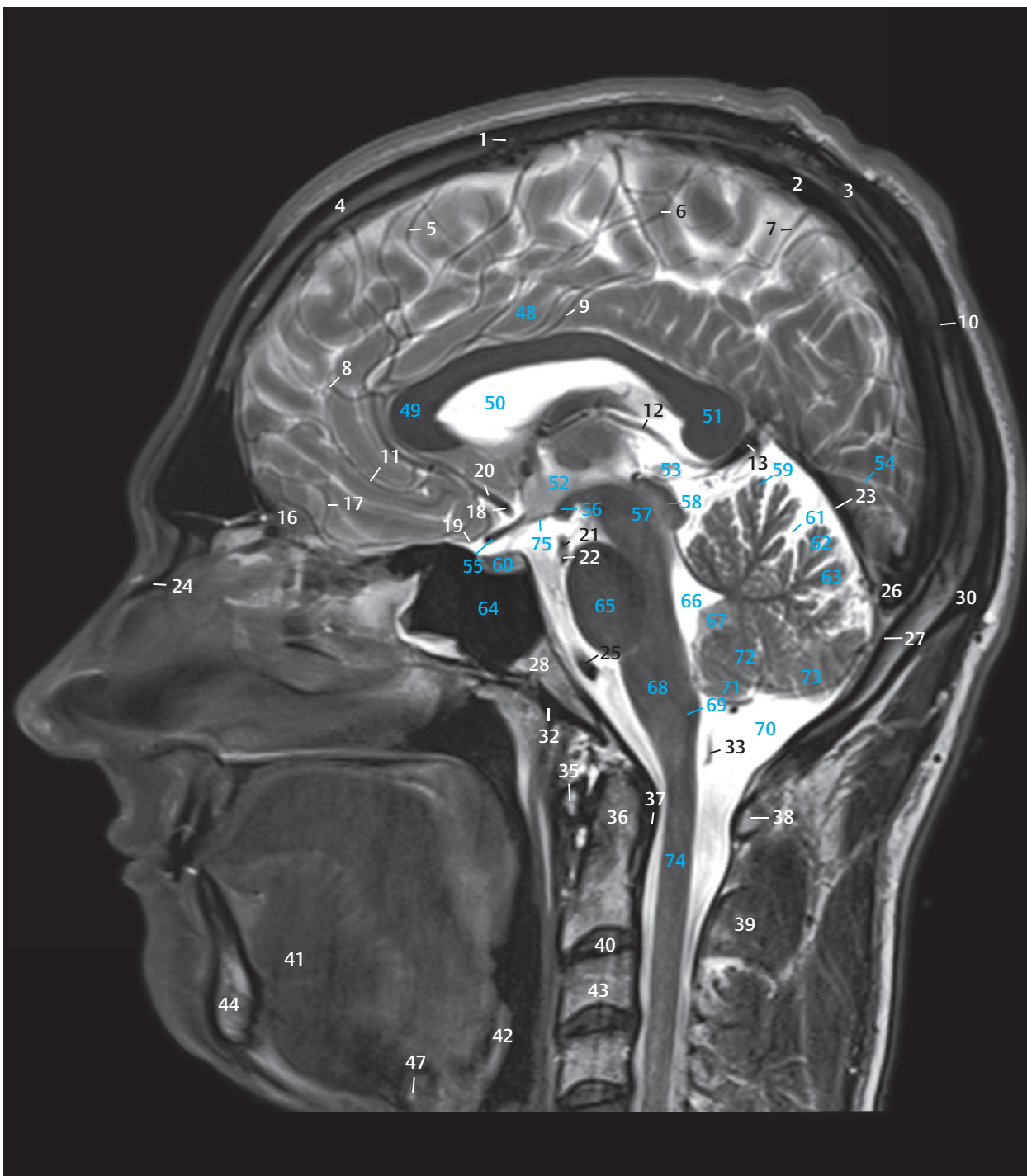


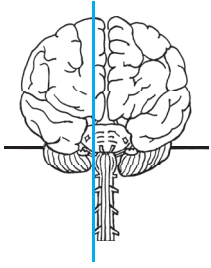
Fig. 4.2c Medial view of the first sagittal section of the right half of the head. The cranial cavity was opened in the plane of the crista galli and the internal occipital protuberance. The spinal canal has been halved in the midline at the level of the upper cervical vertebrae. Bony structures, muscles, and blood vessels.



- 1 Coronal suture
- 2 Superior sagittal sinus
- 3 Parietal bone
- 4 Frontal bone
- 5 Posteromedial frontal artery
- 6 Paracentral artery
- 7 Precuneal artery
- 8 Intermediomedial frontal artery
- 9 Pericallosal artery
- 10 Lambdoid suture
- 11 Anteromedial frontal artery
- 12 Internal cerebral vein
- 13 Great cerebral vein (Galen)
- 16 Crista galli
- 17 Polar frontal artery
- 18 Anterior communicating artery, origin
- 19 Medial frontobasal artery
- 20 Anterior cerebral artery
- 21 Posterior cerebral artery, origin
- 22 Superior cerebellar artery
- 23 Straight sinus
- 24 Nasal bone
- 25 Basilar artery
- 26 Confluence of sinuses
- 27 Internal occipital protuberance
- 28 Clivus
- 30 External occipital protuberance (inion)
- 32 Pharyngeal tubercle
- 33 Posterior inferior cerebellar artery
- 35 Anterior arch of atlas
- 36 Dens
- 37 Transverse ligament of atlas
- 38 Posterior arch of atlas
- 39 Spinous process of axis
- 40 Intervertebral disk
- 41 Genioglossus
- 42 Epiglottis
- 43 Third cervical vertebra
- 44 Body of the mandible
- 47 Hyoid bone
- 48 Cingulate gyrus
- 49 Corpus callosum, genu
- 50 Lateral ventricle
- 51 Corpus callosum, splenium
- 52 Third ventricle
- 53 Pineal gland
- 54 Calcarine sulcus
- 55 Optic chiasma
- 56 Mammillary body
- 57 Tegmentum of midbrain
- 58 Tectum of midbrain

Fig. 4.2d Sagittal T2w MR image, approximately corresponding to c.

- 59 Culmen (IV and V)
- 60 Pituitary gland
- 61 Primary fissure of cerebellum
- 62 Declive (VI)
- 63 Folium of vermis (VII A)
- 64 Sphenoid sinus
- 65 Pons
- 66 Fourth ventricle
- 67 Nodule of vermis (X)
- 68 Medulla oblongata
- 69 Medulla oblongata, obex
- 70 Posterior cerebellomedullary cistern (magna)
- 71 Cerebellar tonsils (IX)
- 72 Uvula of vermis (IX)
- 73 Pyramid of vermis (VIII)
- 74 Spinal cord
- 75 Tuber cinereum



- 1 Precentral gyrus
- 2 Postcentral gyrus
- 3 Superior frontal gyrus
- 4 Precuneus
- 5 Cingulate gyrus
- 6 Parieto-occipital sulcus
- 7 Caudate nucleus
- 8 Medial nuclei of thalamus
- 9 Choroid plexus of lateral ventricle
- 10 Pulvinar nuclei of thalamus
- 11 Primary visual cortex
- 12 Occipital gyri
- 13 Frontal sinus
- 14 Anterior commissure
- 15 Subthalamic nucleus
- 16 Calcarine sulcus
- 17 Olfactory tract
- 18 Optic nerve
- 19 Optic tract
- 20 Substantia nigra
- 21 Tentorium of cerebellum
- 22 Ethmoidal cells
- 23 Oculomotor nerve
- 24 Pons
- 25 Sphenoid sinus
- 26 Trigeminal nerve
- 27 Dentate nucleus
- 28 Semilunar hiatus
- 29 Facial nerve and intermediate nerve (within the slice)
- 30 Vestibulocochlear nerve (within the slice)
- 31 Abducens nerve
- 32 Middle nasal concha
- 33 Tonsil of cerebellum (H IX)
- 34 Glossopharyngeal nerve and vagus nerve
- 35 Inferior nasal concha
- 36 Hypoglossal nerve and hypoglossal canal
- 37 Nasal vestibule
- 38 Spinal root of accessory nerve
- 39 Anterior (ventral) root of first cervical spinal nerve
- 40 Posterior (dorsal) and anterior (ventral) roots of second cervical spinal nerve
- 41 Oral cavity
- 42 Palatine tonsil
- 43 Tongue
- 44 Lingual nerve
- 45 Oropharynx
- 46 Inferior alveolar nerve
- 47 Hypoglossal nerve

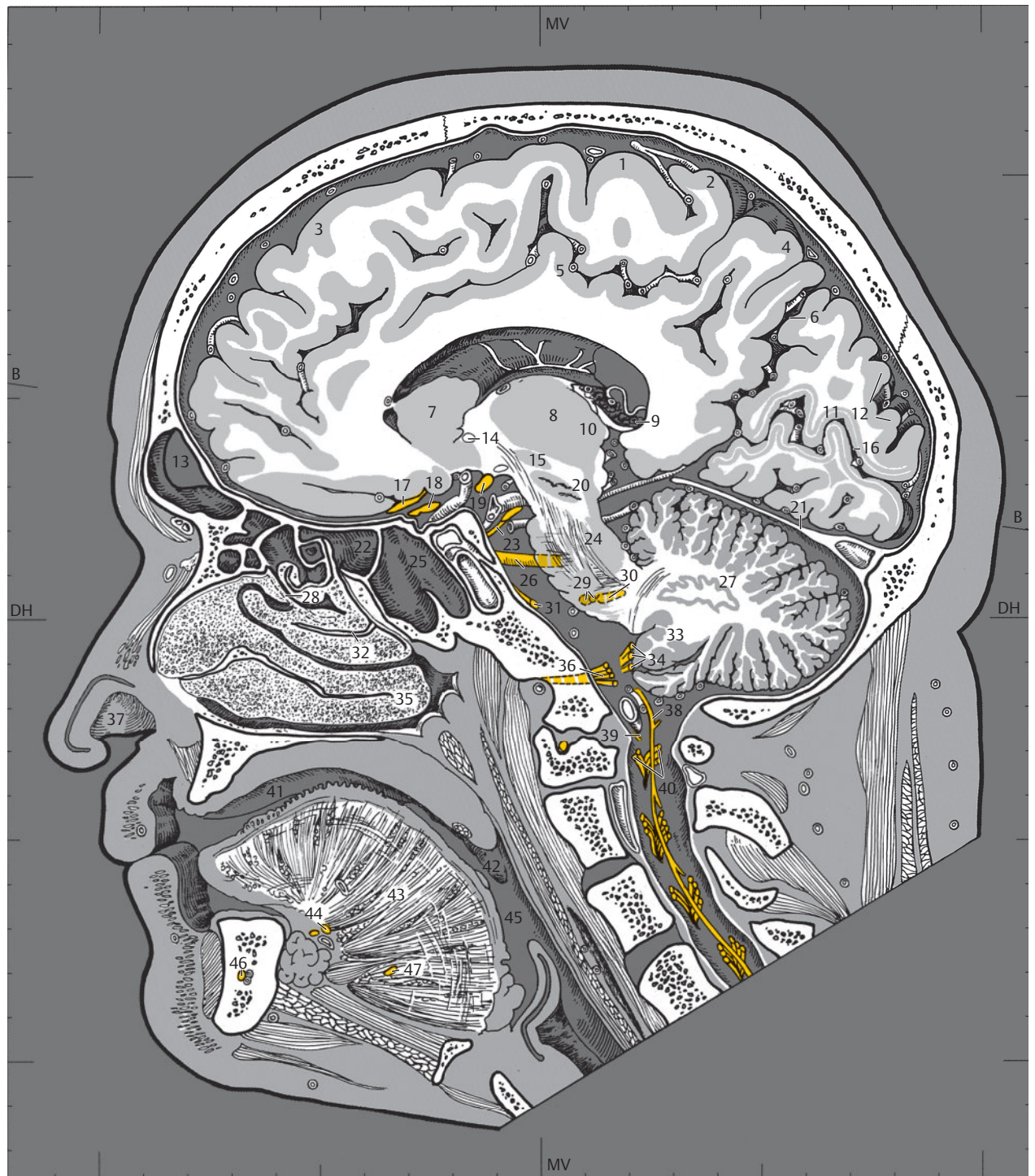
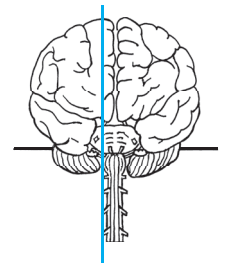
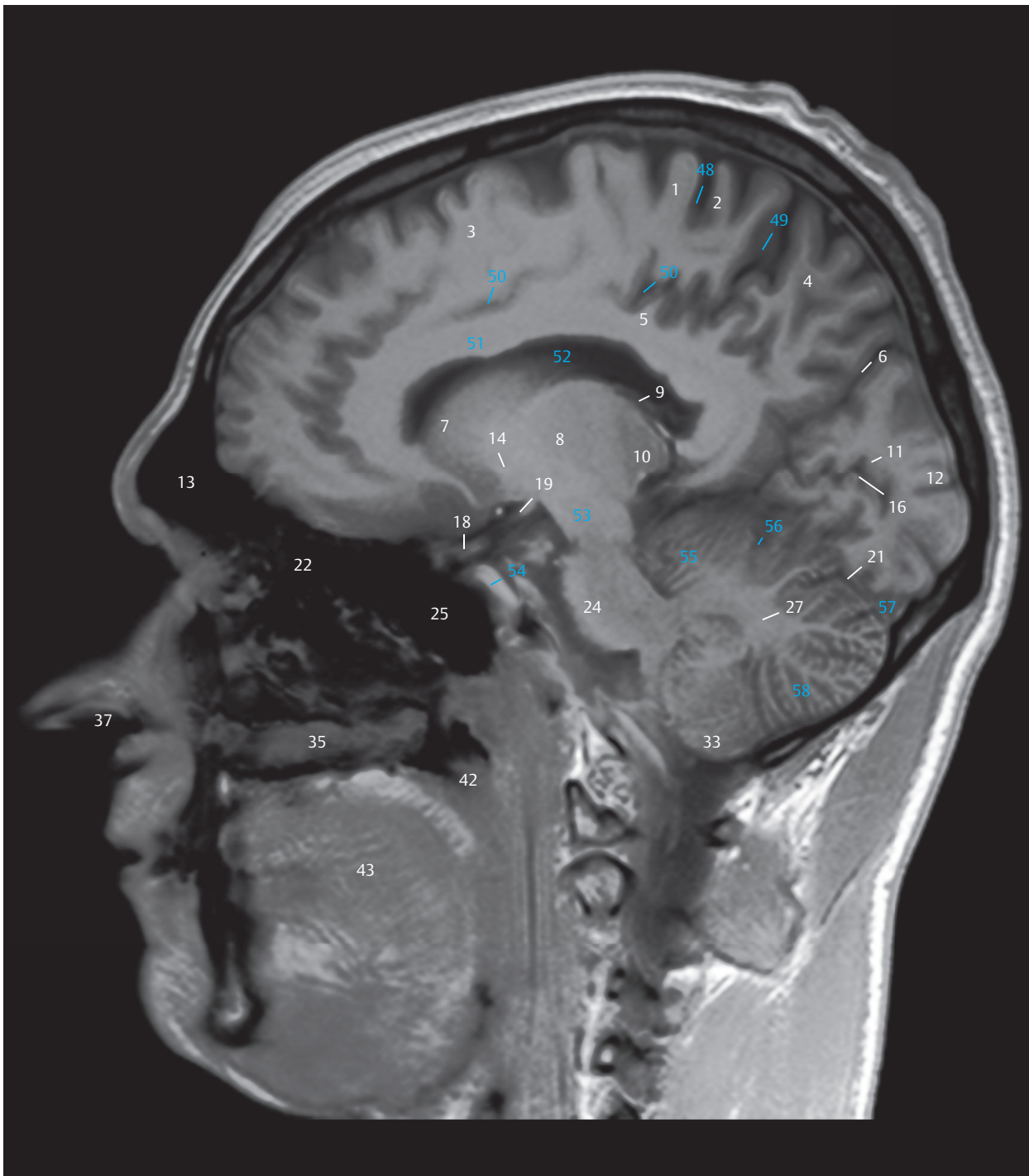


Fig. 4.3 Sagittal section.

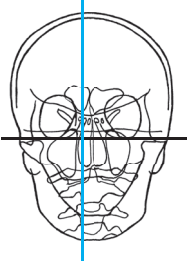
B = Bicommissural line
DH = German horizontal
MV = Meatoververtical line

Fig. 4.3a Medial view of the second sagittal section. The anterior and central parts of the right lateral ventricle are visible. The lateral aspects of the midbrain and the pons are the only parts of the brainstem that have been sectioned in this slice. The spinal roots of the XIth cranial nerve and I st spinal nerve can be identified in the vertebral canal. The enlarged turbinates have been tangentially sectioned in the nasal cavity. Paranasal sinuses, oral cavity, brain structures, as well as cranial and spinal nerves.



- 1 Precentral gyrus
- 2 Postcentral gyrus
- 3 Superior frontal gyrus
- 4 Precuneus
- 5 Cingulate gyrus
- 6 Parieto-occipital sulcus
- 7 Caudate nucleus
- 8 Medial nuclei of thalamus
- 9 Choroid plexus of lateral ventricle
- 10 Pulvinar nuclei of thalamus
- 11 Area striata
- 12 Occipital gyri
- 13 Frontal sinus
- 14 Anterior commissure
- 16 Calcarine sulcus
- 18 Optic nerve
- 19 Optic tract
- 21 Tentorium of cerebellum
- 22 Ethmoidal cells
- 24 Pons
- 25 Sphenoid sinus
- 27 Dentate nucleus
- 33 Tonsils of cerebellum (H IX)
- 35 Inferior nasal concha
- 37 Nasal vestibule
- 42 Palatine tonsil
- 43 Tongue
- 48 Central sulcus
- 49 Cingulate sulcus, marginal branch
- 50 Cingulate sulcus
- 51 Corpus callosum, body
- 52 Lateral ventricle
- 53 Midbrain
- 54 Internal carotid artery
- 55 Anterior lobe of cerebellum
- 56 Primary fissure of cerebellum
- 57 Transverse sinus
- 58 Posterior lobe of cerebellum

Fig. 4.3b Sagittal T1w MR image, approximately corresponding to the sectional plane in a and c. For technical data see ► Chapter 12.



- 1 Coronal suture
- 2 Posteromedial frontal artery
- 3 Paracentral artery
- 4 Parietal bone
- 5 Frontal bone
- 6 Precuneal artery
- 7 Anteromedial frontal artery
- 8 Lambdoid suture
- 9 Intermediomedial frontal artery
- 10 Parieto-occipital artery
- 11 Polar frontal artery
- 12 Calcarine artery
- 13 Medial frontobasal artery
- 14 Anterior cerebral artery
- 15 Anterior choroidal artery
- 16 Medial occipital artery
- 17 Internal carotid artery
- 18 Posterior clinoid process
- 19 Posterior cerebral artery
- 20 Superior cerebellar artery
- 21 Cavernous sinus
- 22 Transverse sinus
- 23 Occipital bone
- 24 Pharyngeal opening of pharyngotympanic tube
- 25 Posterior inferior cerebellar artery (PICA)
- 26 Vertebral artery
- 27 Maxilla
- 28 Hard palate
- 29 Levator veli palatini
- 30 Longus capitis
- 31 Atlas
- 32 Semispinalis capitis
- 33 Trapezius
- 34 Orbicularis oris
- 35 Constrictor of pharynx
- 36 Palatoglossus
- 37 Axis
- 38 Splenius capitis
- 39 Body of mandible
- 40 Sublingual gland
- 41 Epiglottis
- 42 Geniohyoid
- 43 Mylohyoid
- 44 Anterior belly of digastric
- 45 Platysma
- 46 Hyoid bone

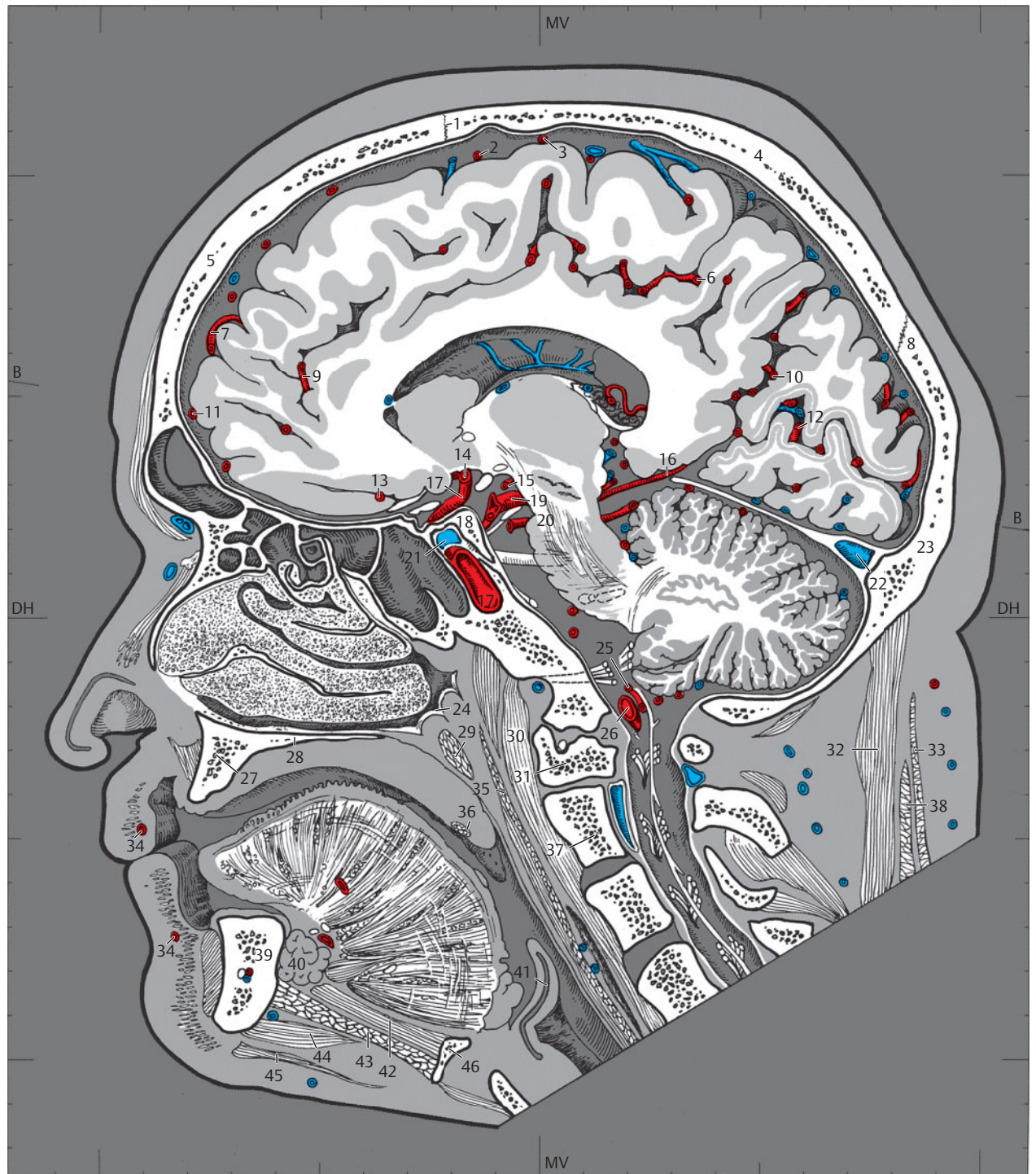
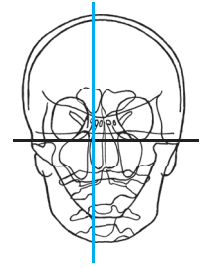
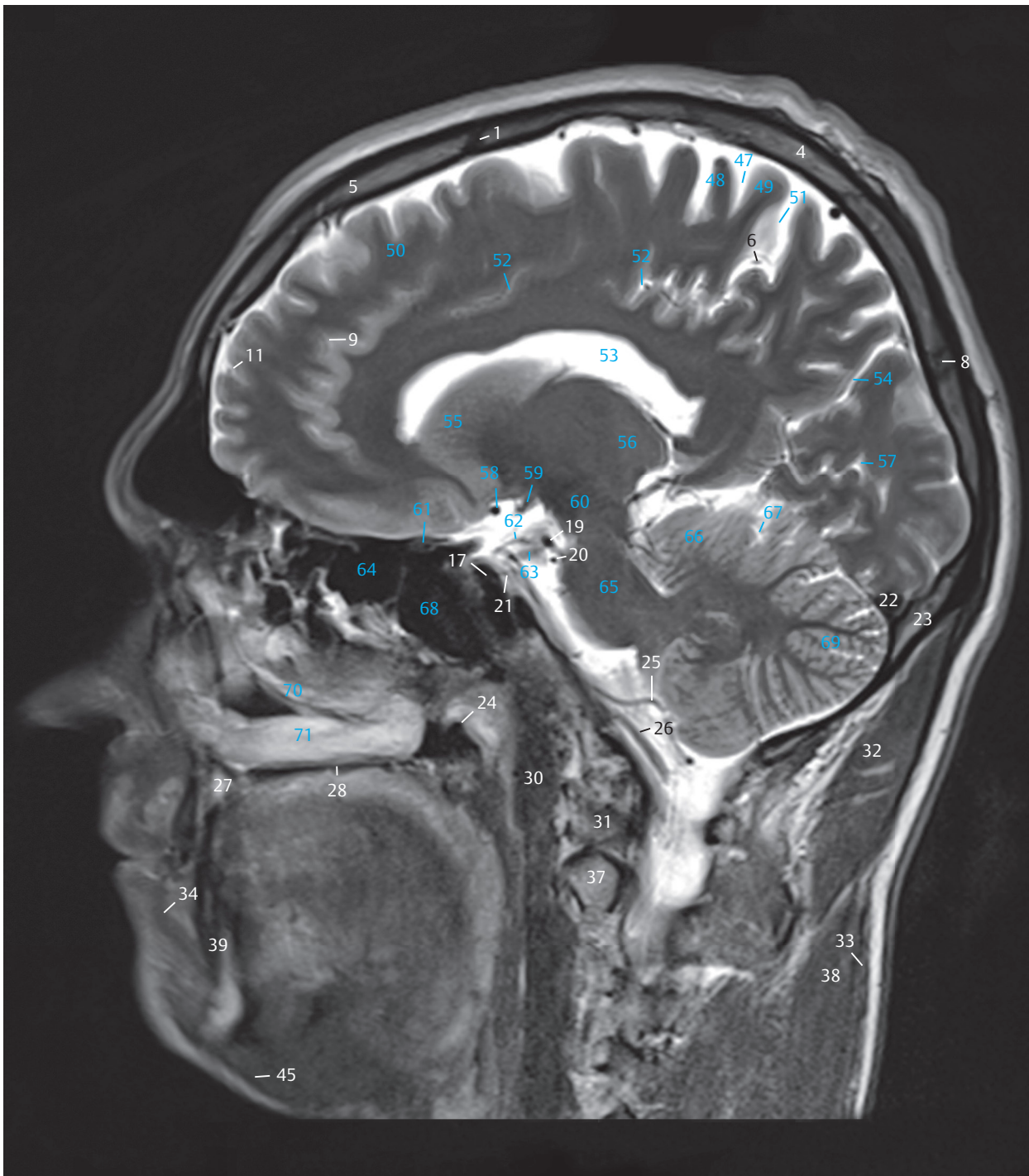
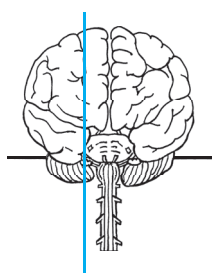


Fig. 4.3c Medial view of the second sagittal section. The section lying at a distance of 1 cm from the median plane lies lateral to the pituitary fossa and runs through the cavernous sinus and the foramen magnum. The orbit lies lateral to the section and has therefore not been opened. Bony structures, muscles, and blood vessels.



- 1 Coronal suture
- 4 Parietal bone
- 5 Frontal bone
- 6 Precuneal artery
- 8 Lambdoid suture
- 9 Intermediomedial frontal artery
- 11 Polar frontal artery
- 17 Internal carotid artery
- 19 Posterior cerebral artery
- 20 Superior cerebellar artery
- 21 Cavernous sinus
- 22 Transverse sinus
- 23 Occipital bone
- 24 Pharyngeal opening of pharyngotympanic tube
- 25 Posterior inferior cerebellar artery (PICA)
- 26 Vertebral artery
- 27 Maxilla
- 28 Hard palate
- 30 Longus capitis
- 31 Atlas
- 32 Semispinalis capitis
- 33 Trapezius
- 34 Orbicularis oris
- 37 Axis
- 38 Splenius capitis
- 39 Body of the mandible
- 45 Platysma
- 47 Central sulcus
- 48 Precentral gyrus
- 49 Postcentral gyrus
- 50 Superior frontal gyrus
- 51 Cingulate sulcus, marginal branch
- 52 Cingulate sulcus
- 53 Lateral ventricle
- 54 Parieto-occipital sulcus
- 55 Head of caudate nucleus
- 56 Thalamus
- 57 Calcarine sulcus
- 58 Middle cerebral artery
- 59 Optic tract
- 60 Midbrain
- 61 Optic nerve
- 62 Posterior communicating artery
- 63 Oculomotor nerve
- 64 Ethmoidal cells
- 65 Pons
- 66 Anterior lobe of cerebellum
- 67 Primary fissure of cerebellum
- 68 Sphenoid sinus
- 69 Posterior lobe of cerebellum
- 70 Middle nasal concha
- 71 Inferior nasal concha

Fig. 4.3d Sagittal T2w MR image, approximately corresponding to the sectional plane in a and c. For technical data see ► Chapter 12.



- 1 Superior frontal gyrus
- 2 Precentral gyrus
- 3 Postcentral gyrus
- 4 Parieto-occipital sulcus
- 5 Body of caudate nucleus
- 6 Occipital gyri
- 7 Putamen
- 8 Globus pallidus
- 9 Ventral posterolateral nuclei of thalamus
- 10 Pulvinar nuclei of thalamus
- 11 Frontal sinus
- 12 Anterior commissure
- 13 Optic tract
- 14 Posterior limb of internal capsule
- 15 Medial geniculate body
- 16 Fornix
- 17 Uncus of parahippocampal gyrus
- 18 Primary visual cortex
- 19 Medial occipitotemporal gyrus
- 20 Optic nerve
- 21 Oculomotor nerve
- 22 Trochlear nerve
- 23 Ophthalmic nerve
- 24 Abducens nerve
- 25 Trigeminal nerve
- 26 Palatine nerves
- 27 Maxillary nerve
- 28 Trigeminal ganglion
- 29 Facial nerve and intermediate nerve
- 30 Vestibulocochlear nerve
- 31 Glossopharyngeal nerve, vagus nerve, accessory nerve
- 32 Maxillary sinus
- 33 Hypoglossal nerve
- 34 Anterior (ventral) root of first cervical spinal nerve
- 35 Oral cavity
- 36 Superior cervical ganglion (in the lateral part of the slice)
- 37 Tongue
- 38 Posterior (dorsal) and anterior (ventral) roots of third cervical spinal nerve and ganglion
- 39 Inferior alveolar nerve
- 40 Lingual nerve

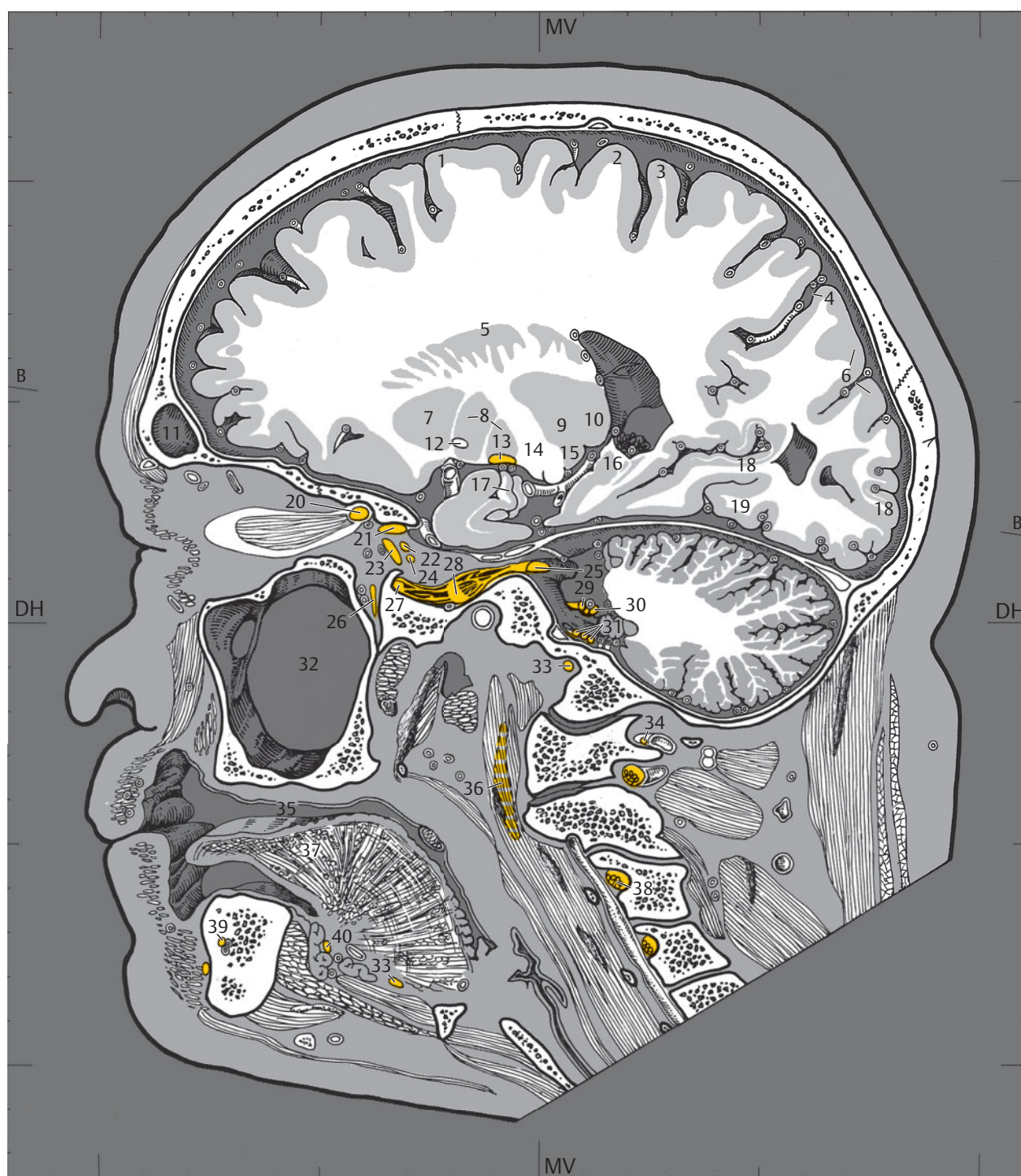
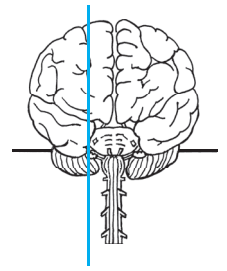
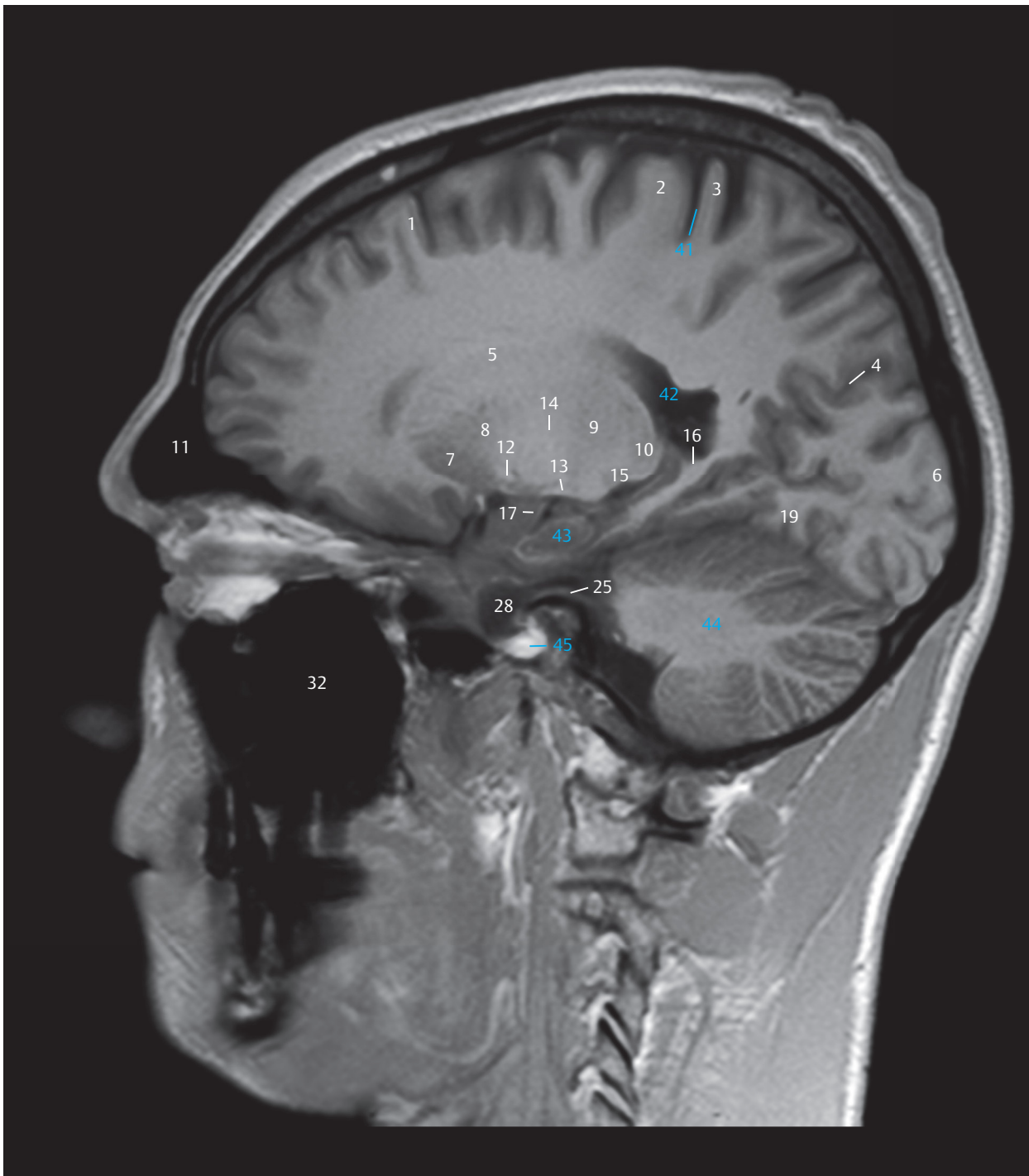


Fig. 4.4 Sagittal section.

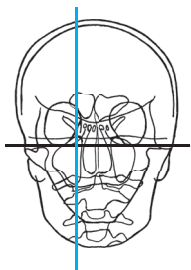
B = Bicommissural line
DH = German horizontal
MV = Meatovertical line

Fig. 4.4a Medial view of the third sagittal section. The section lies lateral to the brainstem at the level of the medial geniculate body. The temporal lobe has been sectioned tangentially. Paranasal sinuses, oral cavity, brain structures, cranial nerves, and the first spinal nerves.



- 1 Superior frontal gyrus
- 2 Precentral gyrus
- 3 Postcentral gyrus
- 4 Parieto-occipital sulcus
- 5 Body of caudate nucleus
- 6 Occipital gyri
- 7 Putamen
- 8 Globus pallidus
- 9 Ventral posterolateral nuclei of thalamus
- 10 Pulvinar nuclei of thalamus
- 11 Frontal sinus
- 12 Anterior commissure
- 13 Optic tract
- 14 Internal capsule, posterior limb
- 15 Medial geniculate body
- 16 Fornix
- 17 Uncus of parahippocampal gyrus
- 19 Medial occipitotemporal gyrus
- 25 Trigeminal nerve
- 28 Trigeminal ganglion (Meckel's cave)
- 32 Maxillary sinus
- 41 Central sulcus
- 42 Lateral ventricle
- 43 Hippocampus
- 44 Cerebellum
- 45 Internal carotid artery

Fig. 4.4b Sagittal T1w MR image, approximately corresponding to the sectional plane in a and c.



- 1 Coronal suture
- 2 Paracentral artery
- 3 Posteromedial frontal artery
- 4 Intermediomedial frontal artery
- 5 Anteromedial frontal artery
- 6 Parieto-occipital artery
- 7 Lambdoid suture
- 8 Occipitofrontalis, frontal belly
- 9 Polar frontal artery
- 10 Medial occipital artery
- 11 Calcarine artery
- 12 Roof of orbit
- 13 Middle cerebral artery
- 14 Posterior cerebral artery
- 15 Lateral occipital artery
- 16 Medial rectus
- 17 Superior orbital fissure
- 18 Superior cerebellar artery
- 19 Transverse sinus
- 20 Floor of orbit
- 21 Pterygopalatine fossa
- 22 Temporal bone
- 23 Internal carotid artery
- 24 Anterior inferior cerebellar artery (AICA)
- 25 Inferior petrosal sinus
- 26 Pharyngotympanic tube
- 27 Occipital condyle
- 28 Posterior inferior cerebellar artery (PICA)
- 29 Levator veli palatini
- 30 Atlanto-occipital joint
- 31 Tensor veli palatini
- 32 Orbicularis oris
- 33 Maxilla
- 34 Pterygoid hamulus
- 35 Lateral mass of atlas
- 36 Vertebral artery
- 37 Semispinalis capitis
- 38 Splenius capitis
- 39 Trapezius
- 40 Lateral atlantoaxial joint
- 41 Axis
- 42 Obliquus capitis inferior
- 43 Palatoglossus
- 44 Body of mandible
- 45 Anterior belly of digastric
- 46 Mylohyoid
- 47 Geniohyoid

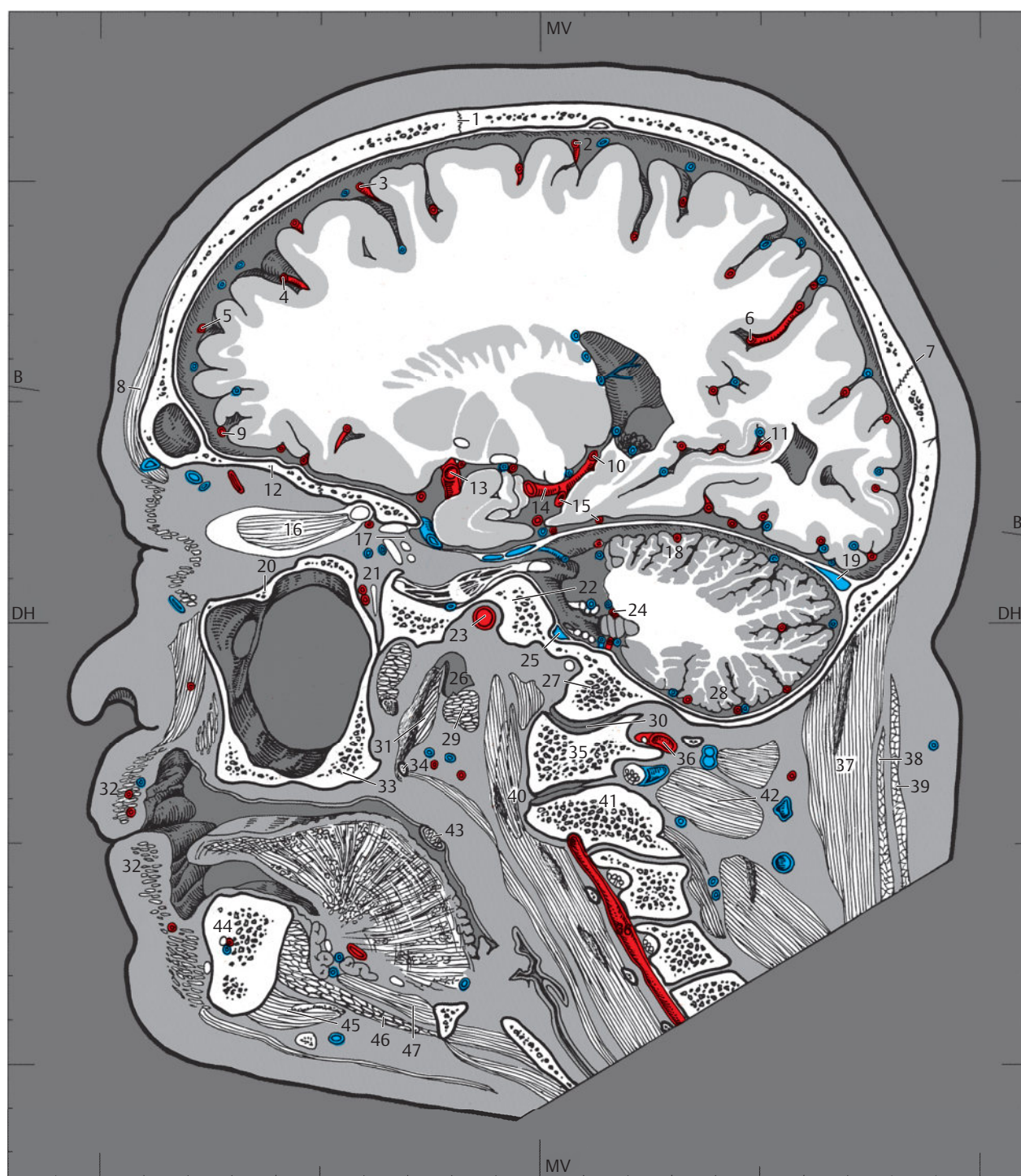
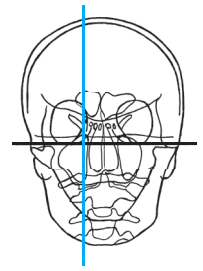
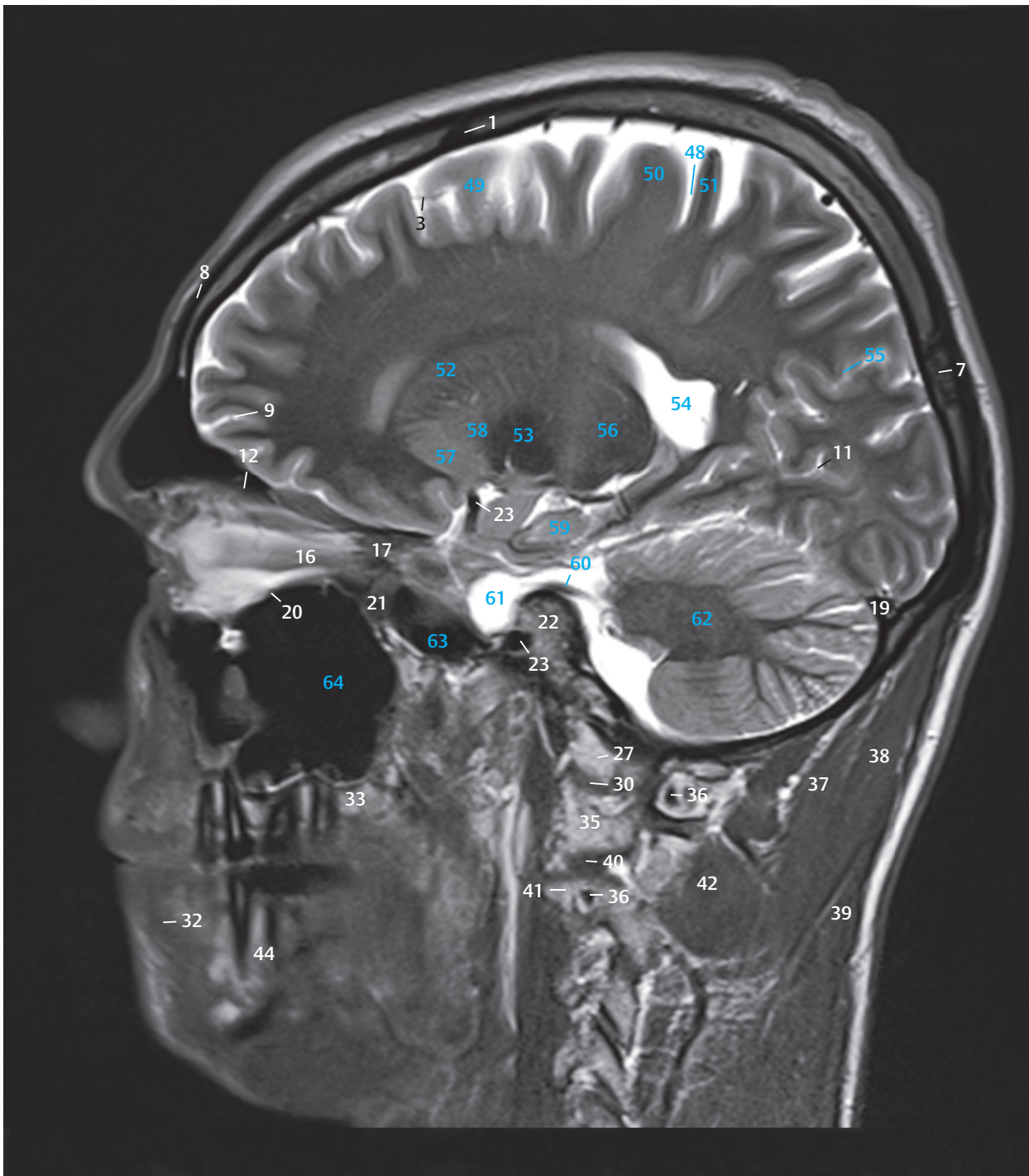
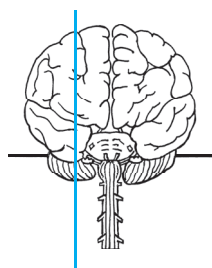


Fig. 4.4c Medial view of the third sagittal section. The section runs through the orbital apex, medial aspect of the superior orbital fissure, middle cranial fossa, and the parapharyngeal space. Bony structures, muscles, and blood vessels.



- 1 Coronal suture
- 3 Posteromedial frontal artery
- 7 Lambdoid suture
- 8 Occipitofrontalis, frontal belly
- 9 Polar frontal artery
- 11 Calcarine artery
- 12 Roof of orbit
- 16 Medial rectus
- 17 Superior orbital fissure
- 19 Transverse sinus
- 20 Orbital Floor
- 21 Pterygopalatine fossa
- 22 Temporal bone
- 23 Internal carotid artery
- 27 Occipital condyle
- 30 Atlanto-occipital joint
- 32 Orbicularis oris
- 33 Maxilla
- 35 Lateral mass of atlas
- 36 Vertebral artery
- 37 Semispinalis capitis
- 38 Splenius capitis
- 39 Trapezius
- 40 Lateral atlantoaxial joint
- 41 Axis
- 42 Obliquus capitis inferior
- 44 Body of the mandible
- 48 Central sulcus
- 49 Superior frontal gyrus
- 50 Precentral gyrus
- 51 Postcentral gyrus
- 52 Caudate nucleus
- 53 Internal capsule
- 54 Lateral ventricle
- 55 Parieto-occipital sulcus
- 56 Thalamus
- 57 Putamen
- 58 Globus pallidus
- 59 Hippocampus
- 60 Trigeminal nerve
- 61 Trigeminal ganglion
- 62 Cerebellum
- 63 Sphenoid sinus
- 64 Maxillary sinus

Fig. 4.4d Sagittal T2w MR image, approximately corresponding to the sectional plane in a and c.



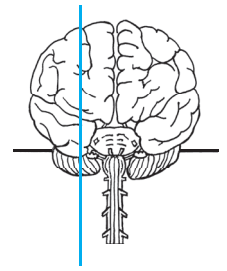
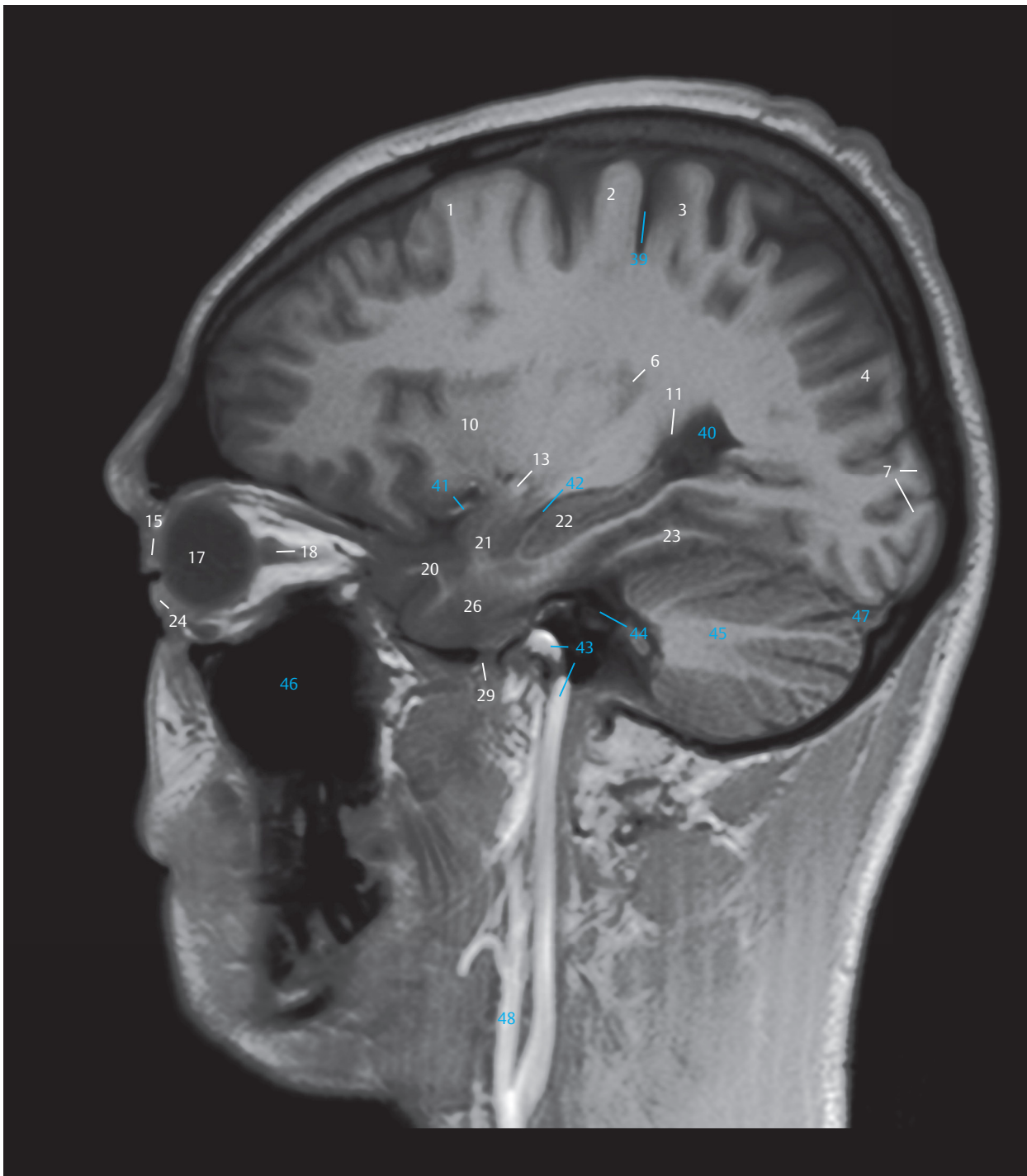
- 1 Middle frontal gyrus
- 2 Precentral gyrus
- 3 Postcentral gyrus
- 4 Angular gyrus
- 5 Extreme capsule
- 6 Cortex of insula
- 7 Occipital gyri
- 8 External capsule
- 9 Claustrum
- 10 Putamen
- 11 Tail of caudate nucleus
- 12 Frontal nerve
- 13 Anterior commissure
- 14 Choroid plexus of temporal (inferior) horn
- 15 Upper eyelid
- 16 Lens
- 17 Eyeball
- 18 Optic nerve
- 19 Abducens nerve
- 20 Middle temporal gyrus
- 21 Amygdaloid body
- 22 Hippocampus
- 23 Medial occipitotemporal gyrus
- 24 Lower eyelid
- 25 Infraorbital nerve
- 26 Inferior temporal gyrus
- 27 Facial nerve and intermediate nerve
- 28 Vestibulocochlear nerve
- 29 Mandibular nerve and otic ganglion
- 30 Vagus nerve
- 31 Glossopharyngeal nerve
- 32 Accessory nerve
- 33 Hypoglossal nerve
- 34 Superior cervical ganglion
- 35 Oral cavity
- 36 Sympathetic trunk (within the slice)
- 37 Inferior alveolar nerve
- 38 Lingual nerve



Fig. 4.5 Sagittal section.

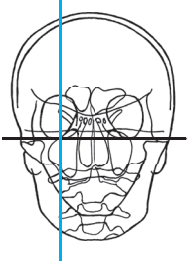
B = Bicommissural line
DH = German horizontal
MV = Meatovertical line

Fig. 4.5a Medial view of the fourth sagittal section. Parts of the endbrain lying lateral to the anterior horn and cella media of the lateral ventricle are visible in the supratentorial region, as also those which abut the inferior horn, like the hippocampus and the amygdala. The section runs through the cerebellar hemispheres in the infratentorial region. Brain structures and cranial nerves.



- 1 Middle frontal gyrus
- 2 Precentral gyrus
- 3 Postcentral gyrus
- 4 Angular gyrus
- 6 Insular cortex
- 7 Occipital gyri
- 10 Putamen
- 11 Tail of caudate nucleus
- 13 Anterior commissure
- 15 Upper eyelid
- 17 Eyeball
- 18 Optic nerve
- 20 Middle temporal gyrus
- 21 Amygdaloid body
- 22 Hippocampus
- 23 Medial occipitotemporal gyrus
- 24 Lower eyelid
- 26 Inferior temporal gyrus
- 29 Mandibular nerve and otic ganglion
- 39 Central sulcus
- 40 Lateral ventricle
- 41 Middle cerebral artery
- 42 Lateral ventricle, temporal horn
- 43 Internal carotid artery
- 44 Internal acoustic canal with facial nerve and vestibulocochlear nerve
- 45 Cerebellum
- 46 Maxillary sinus
- 47 Transverse sinus
- 48 External carotid artery

Fig. 4.5b Sagittal T1w MR image, approximately corresponding to the sectional plane in a and c.



- 1 Coronal suture
- 2 Artery of precentral sulcus
- 3 Frontal bone
- 4 Prefrontal artery
- 5 Parietal bone
- 6 Artery of central sulcus
- 7 Parietal artery
- 8 Angular artery
- 9 Insular artery
- 10 Lateral frontobasal artery
- 11 Lambdoid suture
- 12 Roof of orbit
- 13 Levator palpebrae superioris
- 14 Middle cerebral artery
- 15 Temporo-occipital artery
- 16 Lens
- 17 Superior rectus
- 18 Lateral rectus
- 19 Posterior cerebral artery, temporal branch
- 20 Inferior oblique
- 21 Inferior rectus
- 22 Orbitalis
- 23 Internal acoustic canal
- 24 Superior cerebellar artery
- 25 Transverse sinus
- 26 Occipital bone
- 27 Floor of orbit
- 28 Temporal bone
- 29 Cartilage of pharyngotympanic tube
- 30 Internal jugular vein near jugular foramen
- 31 Sigmoid sinus
- 32 Lateral pterygoid
- 33 Lateral pterygoid plate
- 34 Medial pterygoid
- 35 Internal carotid artery
- 36 Transverse process of atlas
- 37 Vertebral artery
- 38 Posterior inferior cerebellar artery (PICA)
- 39 Semispinalis capitis
- 40 Maxilla
- 41 Obliquus capitis inferior
- 42 Styloglossus
- 43 Axis
- 44 Splenius capitis
- 45 Trapezius

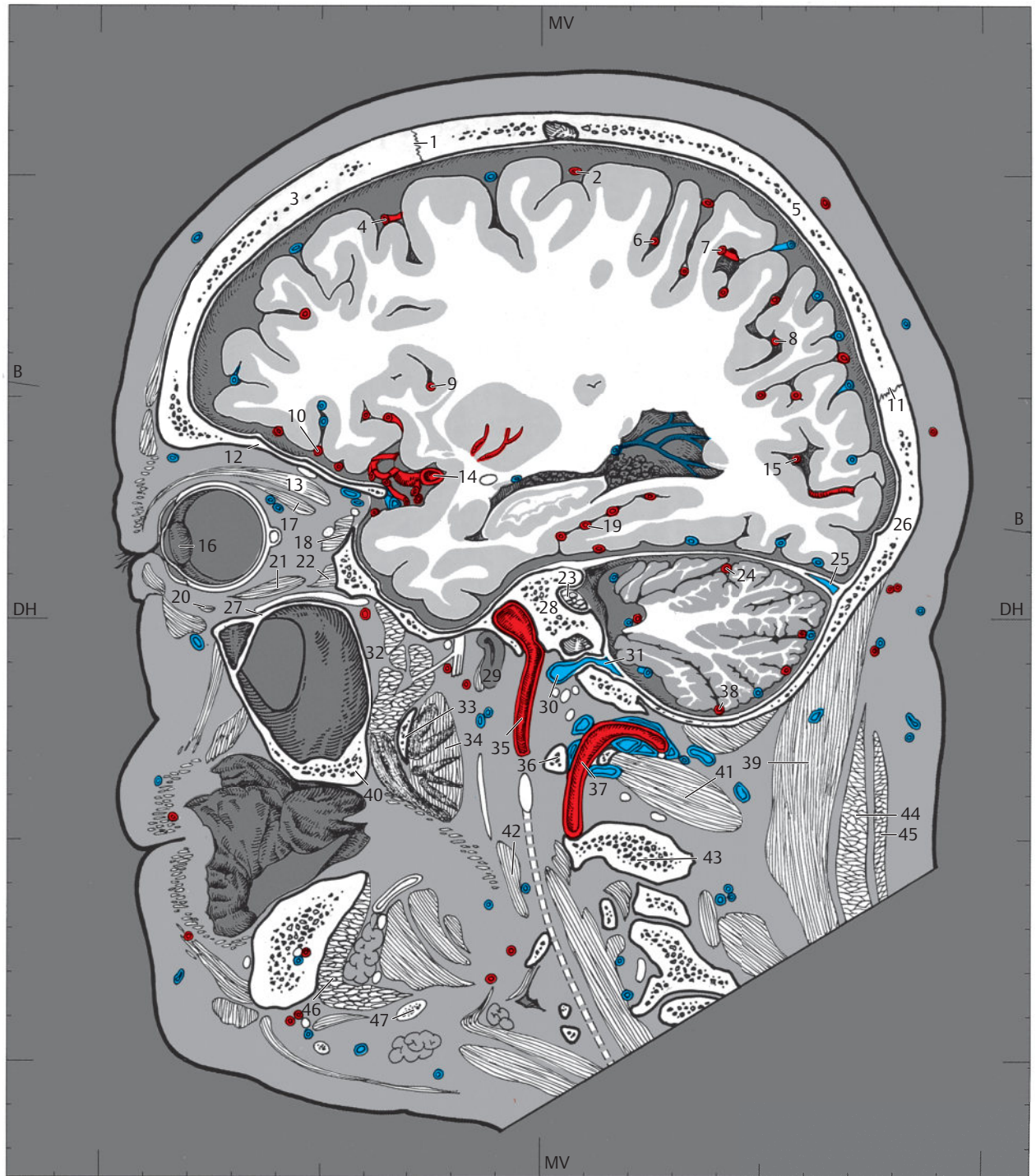
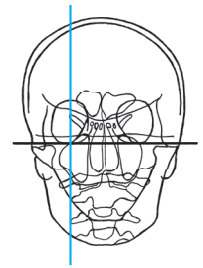
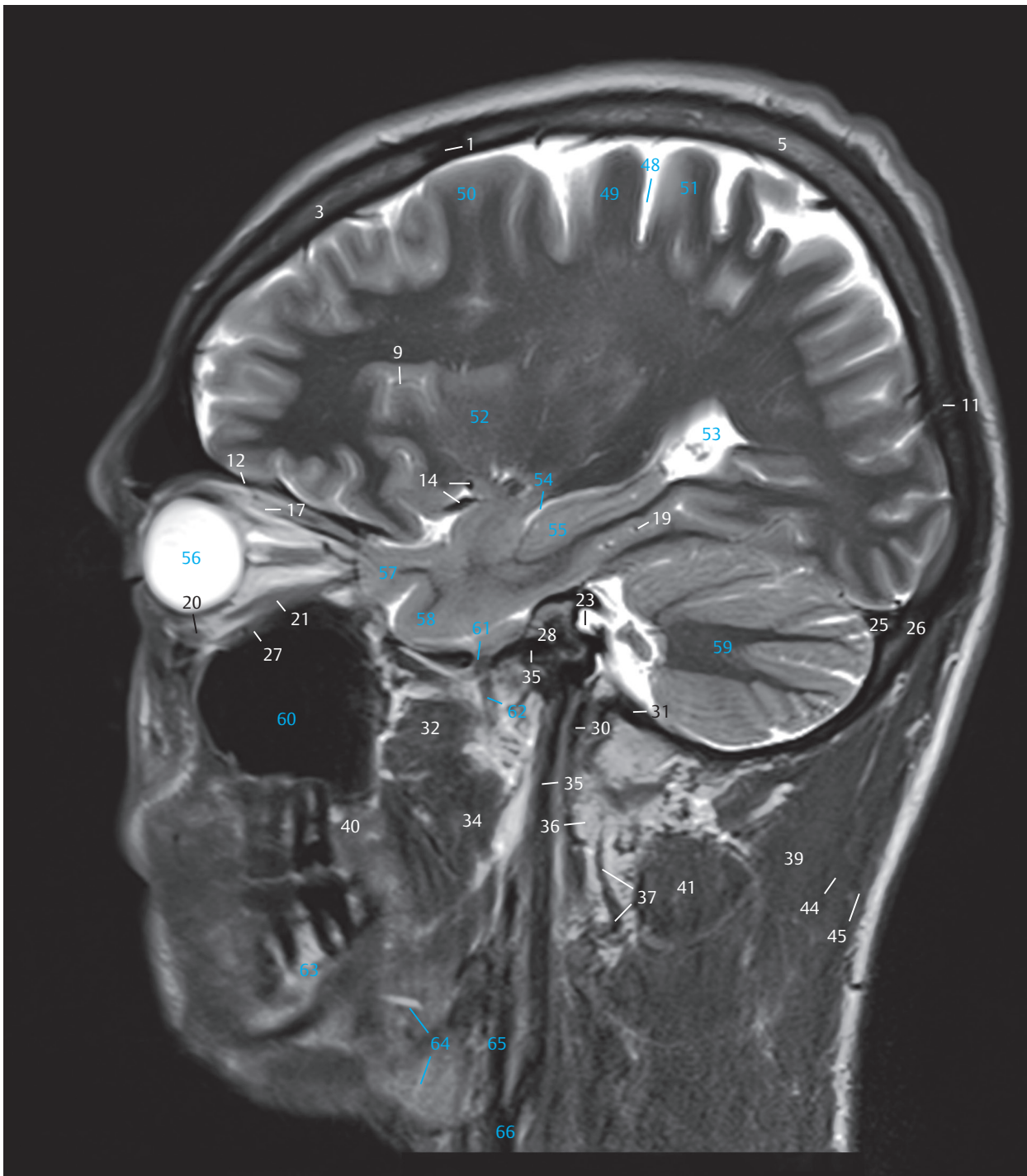
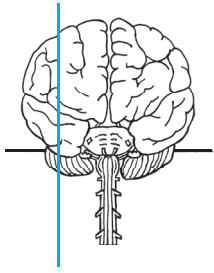


Fig. 4.5c Medial view of the fourth sagittal section. The section is closely apposed medially to the midplane of the eyeball, thereby sectioning the lens of the eye and the superior and inferior recti. The internal auditory canal, jugular foramen, and the parapharyngeal space are identifiable in this section. Bony structures, muscles, and blood vessels.



- 1 Coronal suture
- 3 Frontal bone
- 5 Parietal bone
- 9 Insular artery
- 11 Lambdoid suture
- 12 Roof of orbit
- 14 Middle cerebral artery
- 17 Superior rectus
- 19 Posterior cerebral artery, temporal branch
- 20 Inferior oblique
- 21 Inferior rectus
- 23 Internal acoustic canal, ostium
- 25 Transverse sinus
- 26 Occipital bone
- 27 Floor of orbit
- 28 Temporal bone
- 30 Internal jugular vein near jugular foramen
- 31 Sigmoid sinus
- 32 Lateral pterygoid
- 34 Medial pterygoid
- 35 Internal carotid artery
- 36 Transverse process of atlas
- 37 Vertebral artery
- 39 Semispinalis capitis
- 40 Maxilla
- 41 Obliquus capitis inferior
- 44 Splenius capitis
- 45 Trapezius
- 48 Central sulcus
- 49 Precentral gyrus
- 50 Middle frontal gyrus
- 51 Postcentral gyrus
- 52 Putamen
- 53 Lateral ventricle
- 54 Lateral ventricle, temporal horn
- 55 Hippocampus
- 56 Eyeball
- 57 Middle temporal gyrus
- 58 Inferior temporal gyrus
- 59 Cerebellum
- 60 Maxillary sinus
- 61 Foramen ovale
- 62 Mandibular nerve
- 63 Mandible
- 64 Submandibular gland
- 65 External carotid artery
- 66 Common carotid artery

Fig. 4.5d Sagittal T2w MR image, approximately corresponding to the sectional plane in a and c.



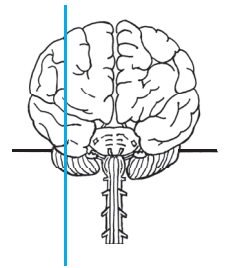
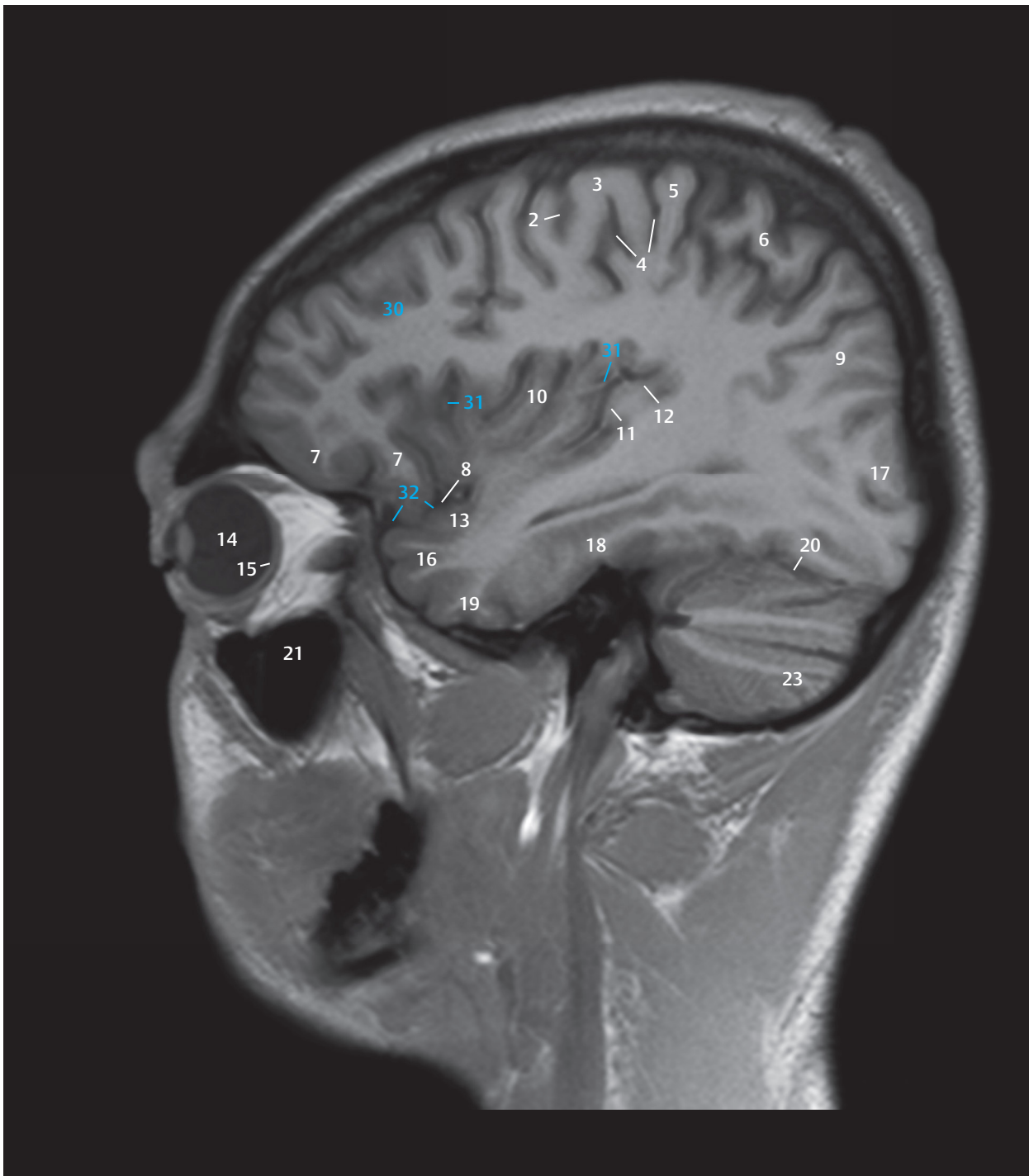
- 1 Dura mater
- 2 Precentral sulcus
- 3 Precentral gyrus
- 4 Central sulcus
- 5 Postcentral gyrus
- 6 Supramarginal gyrus
- 7 Inferior frontal gyrus
- 8 Lateral sulcus (Sylvian fissure)
- 9 Angular gyrus
- 10 Insular cortex
- 11 Anterior transverse temporal gyrus (anterior Heschl's gyrus)
- 12 Posterior transverse temporal gyrus (posterior Heschl's gyrus)
- 13 Superior temporal gyrus
- 14 Eyeball
- 15 Retina
- 16 Middle temporal gyrus
- 17 Occipital gyri
- 18 Lateral occipitotemporal gyrus
- 19 Inferior temporal gyrus
- 20 Tentorium of cerebellum
- 21 Maxillary sinus
- 22 Facial nerve and facial canal (within the slice)
- 23 Posterior lobe of cerebellum
- 24 Inferior alveolar nerve
- 25 Accessory nerve
- 26 Lingual nerve
- 27 Vagus nerve
- 28 Oral vestibule
- 29 Hypoglossal nerve



Fig. 4.6 Sagittal section.

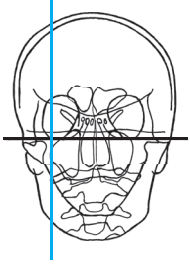
B = Bicommissural line
DH = German horizontal
MV = Meatoververtical line

Fig. 4.6a Medial view of the fifth sagittal section. The insula has been tangentially sectioned and lies in the lateral sulcus, surrounded by the insular arteries. Branches of the Vth, VIIth, Xth, XIth, and XIIth cranial nerves are visible. Brain structures and cranial nerves.



- 2 Precentral sulcus
- 3 Precentral gyrus
- 4 Central sulcus
- 5 Postcentral gyrus
- 6 Supramarginal gyrus
- 7 Inferior frontal gyrus
- 8 Lateral sulcus (Sylvian fissure)
- 9 Angular gyrus
- 10 Insular cortex
- 11 Anterior transverse temporal gyrus (anterior Heschl's gyrus)
- 12 Posterior transverse temporal gyrus (posterior Heschl's gyrus)
- 13 Superior temporal gyrus
- 14 Eyeball
- 15 Retina
- 16 Middle temporal gyrus
- 17 Occipital gyri
- 18 Lateral occipitotemporal gyrus
- 19 Inferior temporal gyrus
- 20 Cerebellar tentorium
- 21 Maxillary sinus
- 23 Posterior lobe of cerebellum
- 30 Middle frontal gyrus
- 31 Insular arteries
- 32 Cistern of lateral cerebral fossa

Fig. 4.6b Sagittal T1w MR image, approximately corresponding to the sectional plane in a and c.



- 1 Coronal suture
- 2 Frontal bone
- 3 Artery of precentral sulcus
- 4 Artery of central sulcus
- 5 Parietal bone
- 6 Prefrontal artery
- 7 Parietal artery
- 8 Angular artery
- 9 Insular arteries
- 10 Lateral frontobasal artery
- 11 Lambdoid suture
- 12 Lacrimal gland
- 13 Levator palpebrae superioris
- 14 Temporo-occipital artery
- 15 Lateral rectus
- 16 Middle cerebral artery, temporal branch
- 17 Occipital bone
- 18 Inferior oblique
- 19 Cochlea
- 20 Transverse sinus
- 21 Superior cerebellar artery (PICA)
- 22 Maxilla
- 23 Temporalis
- 24 Maxillary artery
- 25 Lateral pterygoid
- 26 Middle meningeal artery
- 27 Tympanic cavity
- 28 Facial canal (within the slice)
- 29 Temporal bone
- 30 Sigmoid sinus
- 31 Posterior inferior cerebellar artery (PICA)
- 32 Internal jugular vein
- 33 Styloid process
- 34 Transverse process of atlas
- 35 Obliquus capitis inferior
- 36 Medial pterygoid
- 37 Stylohyoid
- 38 Internal carotid artery
- 39 Semispinalis capitis
- 40 Splenius capitis
- 41 Trapezius
- 42 Mandible
- 43 Inferior alveolar artery and vein
- 44 Facial artery
- 45 Lingual artery
- 46 Posterior belly of digastric
- 47 Submandibular gland

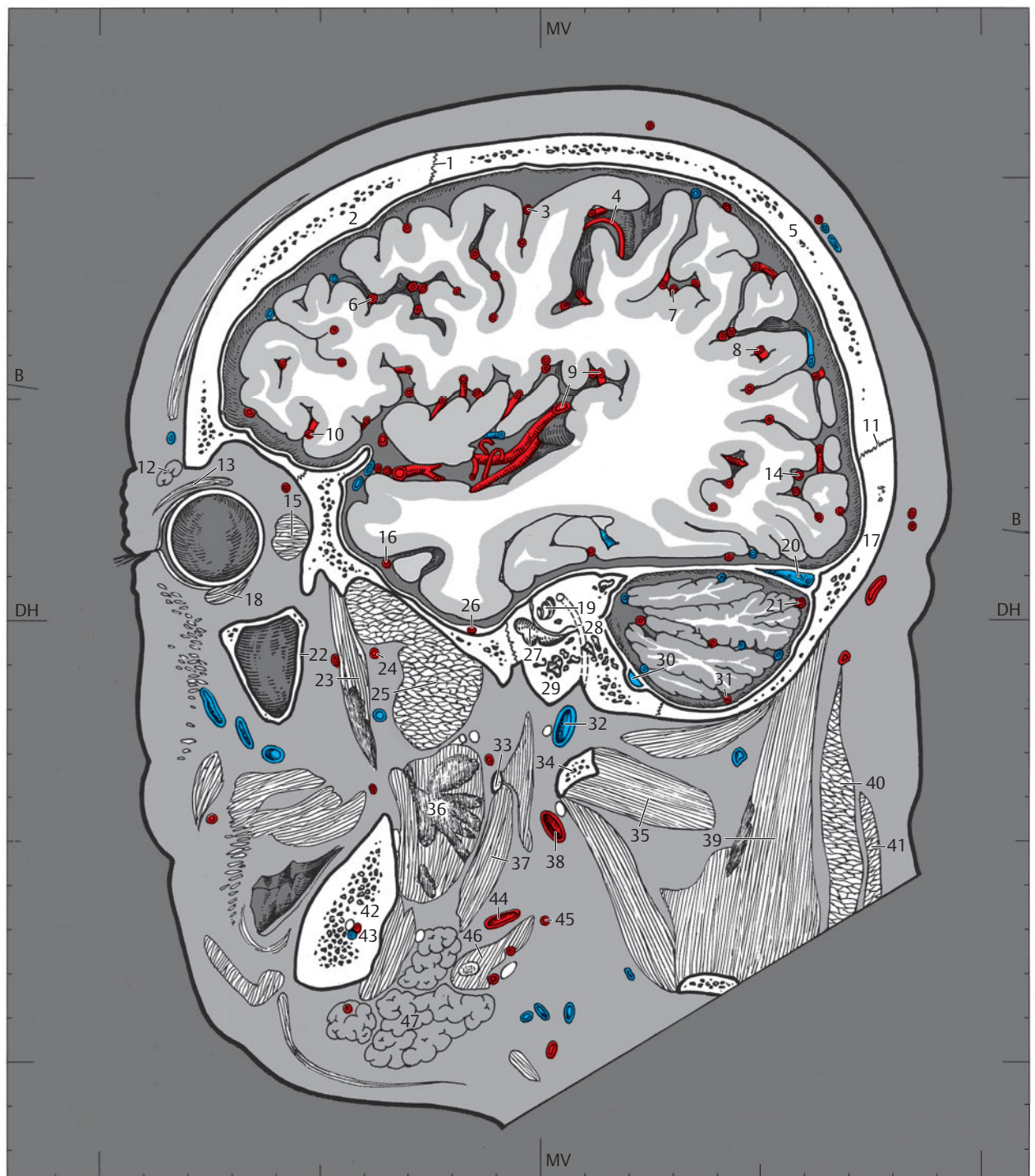
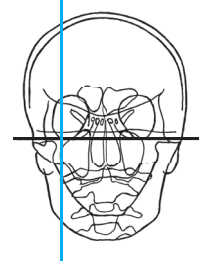
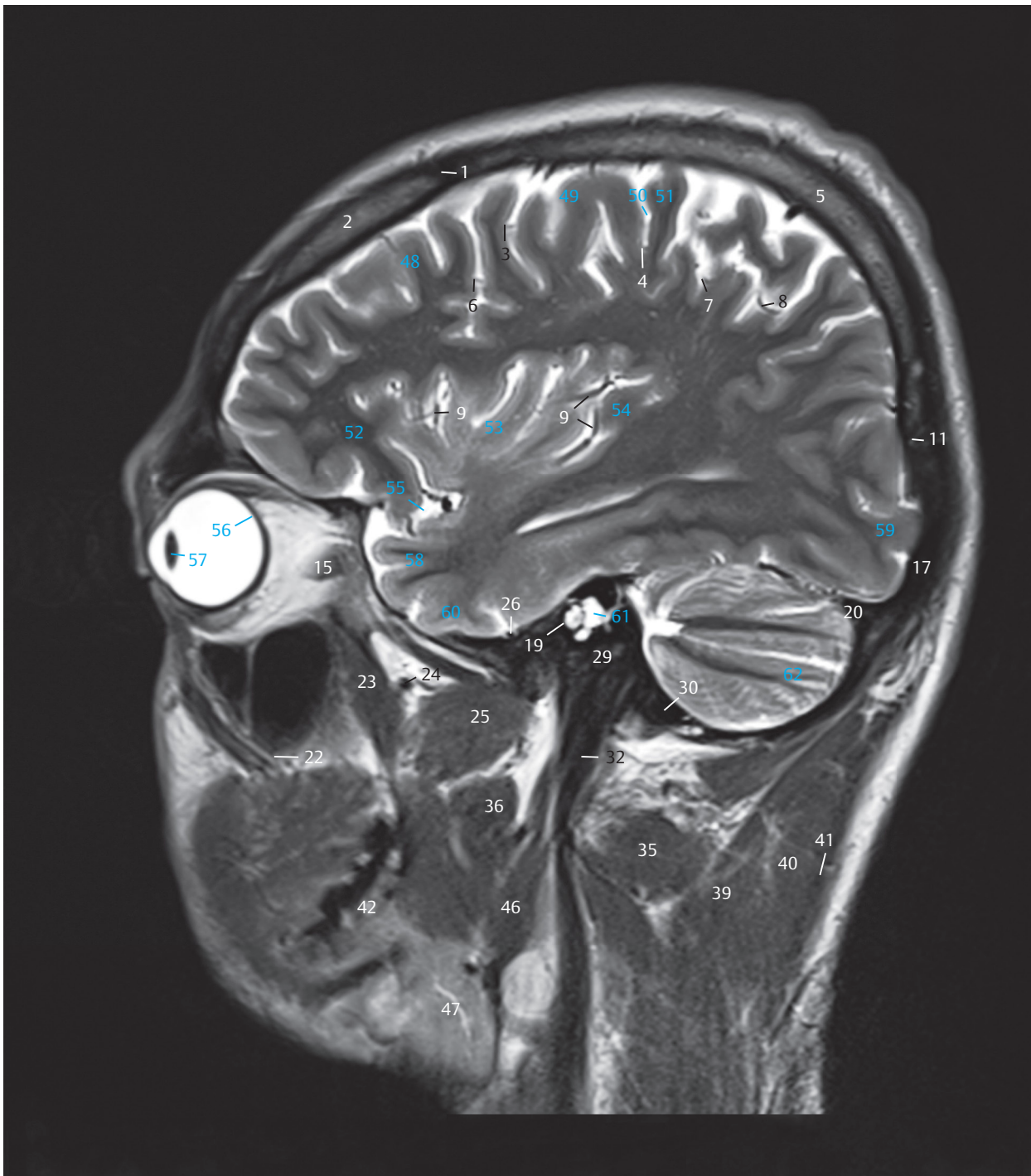
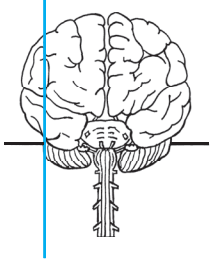


Fig. 4.6c Medial view of the fifth sagittal section. The lateral part of the eyeball has been sectioned. The skull base has been sectioned at the level of the cochlea. Bony structures, muscles, and blood vessels.



- 1 Coronal suture
- 2 Frontal bone
- 3 Artery of precentral sulcus
- 4 Artery of central sulcus
- 5 Parietal bone
- 6 Prefrontal artery
- 7 Parietal artery
- 8 Angular artery
- 9 Insular arteries
- 11 Lambdoid suture
- 15 Lateral rectus
- 17 Occipital bone
- 19 Cochlea
- 20 Transverse sinus
- 22 Maxilla
- 23 Temporalis
- 24 Maxillary artery
- 25 Lateral pterygoid
- 26 Middle meningeal artery
- 29 Temporal bone
- 30 Sigmoid sinus
- 32 Internal jugular vein
- 35 Obliquus capitis inferior
- 36 Medial pterygoid
- 39 Semispinalis capitis
- 40 Splenius capitis
- 41 Trapezius
- 42 Mandible
- 46 Digastric, posterior belly
- 47 Submandibular gland
- 48 Middle frontal gyrus
- 49 Precentral gyrus
- 50 Central sulcus
- 51 Postcentral gyrus
- 52 Inferior frontal gyrus
- 53 Insula
- 54 Transverse temporal gyrus
- 55 Cistern of lateral cerebral fossa
- 56 Eyeball
- 57 Lens
- 58 Middle temporal gyrus
- 59 Occipital gyri
- 60 Inferior temporal gyrus
- 61 Internal acoustic canal
- 62 Posterior lobe of cerebellum

Fig. 4.6d Sagittal T2w MR image, approximately corresponding to the sectional plane in a and c.



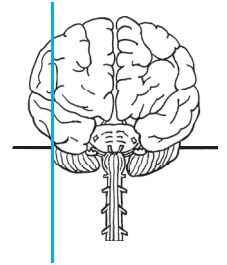
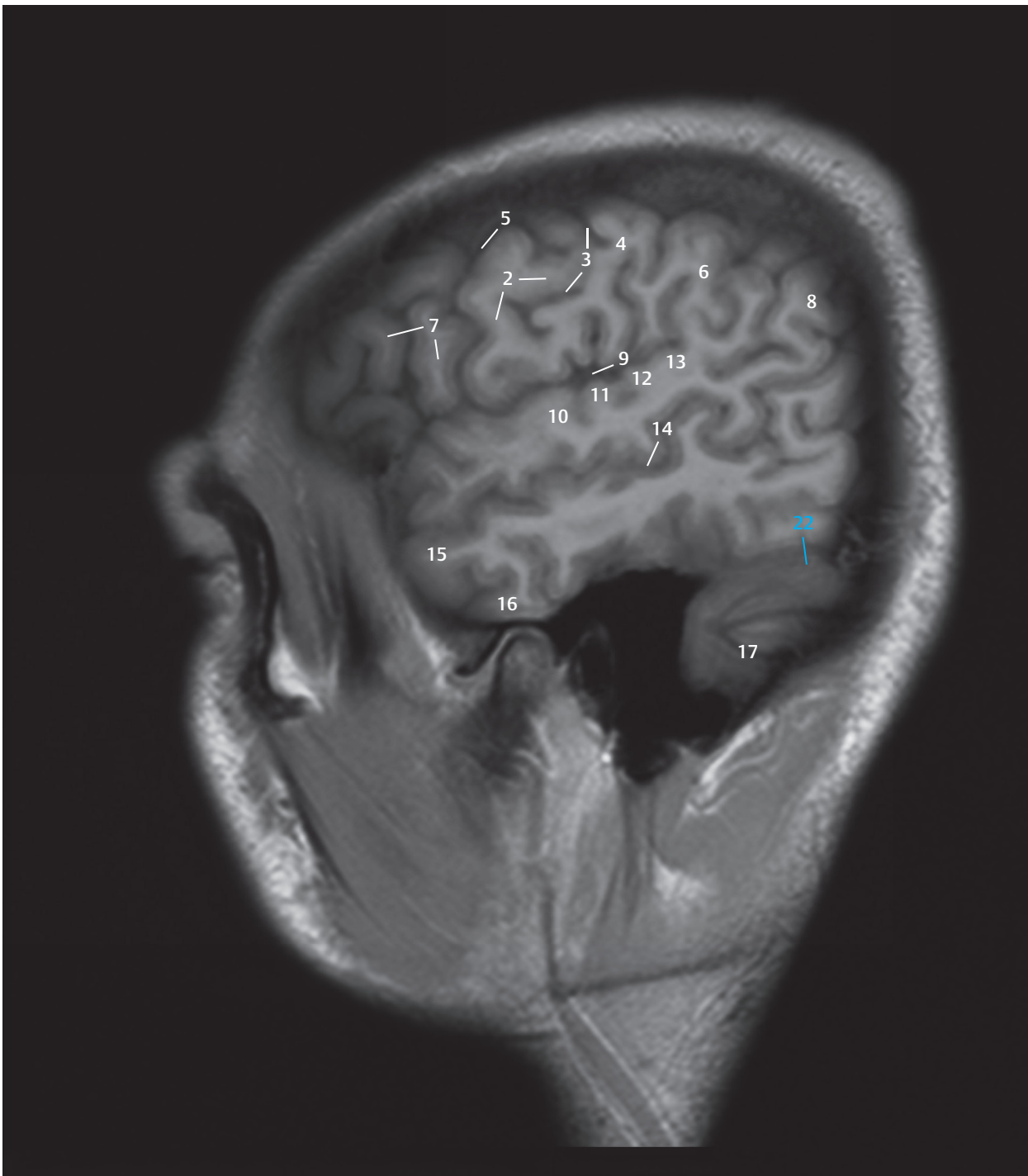
- 1 Dura mater
- 2 Precentral gyrus
- 3 Central sulcus
- 4 Postcentral gyrus
- 5 Precentral sulcus
- 6 Supramarginal gyrus
- 7 Inferior frontal gyrus
- 8 Angular gyrus
- 9 Lateral sulcus (Sylvian fissure)
- 10 Superior temporal gyrus
- 11 Anterior transverse temporal gyrus (anterior Heschl's gyrus)
- 12 Posterior transverse temporal gyrus (posterior Heschl's gyrus)
- 13 Temporal plane
- 14 Superior temporal sulcus
- 15 Middle temporal gyrus
- 16 Inferior temporal gyrus
- 17 Posterior lobe of cerebellum (tangentially cut)
- 18 Facial nerve
- 19 Inferior alveolar nerve
- 20 Accessory nerve
- 21 Vagus nerve



Fig. 4.7 Sagittal section.

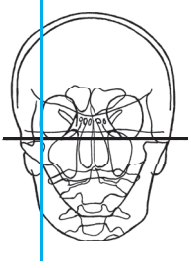
B = Bicommissural line
DH = German horizontal
MV = Meatovertical line

Fig. 4.7a Medial view of the sixth sagittal section. Parts of the cortex of the endbrain have been evenly sectioned, especially those which surround the lateral sulcus as operculum. Brain structures and cranial nerves.



- 2 Precentral gyrus
- 3 Central sulcus
- 4 Postcentral gyrus
- 5 Precentral sulcus
- 6 Supramarginal gyrus
- 7 Inferior frontal gyrus
- 8 Angular gyrus
- 9 Lateral sulcus
- 10 Superior temporal gyrus
- 11 Anterior transverse temporal gyrus (anterior Heschl's gyrus)
- 12 Posterior transverse temporal gyrus (posterior Heschl's gyrus)
- 13 Temporal plane
- 14 Superior temporal sulcus
- 15 Middle temporal gyrus
- 16 Inferior temporal gyrus
- 17 Posterior lobe of cerebellum
- 22 Transverse sinus

Fig. 4.7b Sagittal T1w MR image, approximately corresponding to the sectional plane in a and c.



- 1 Coronal suture
- 2 Frontal bone
- 3 Parietal bone
- 4 Artery of central sulcus
- 5 Artery of precentral sulcus
- 6 Parietal artery
- 7 Prefrontal artery
- 8 Angular artery
- 9 Temporo-occipital artery
- 10 Temporalis
- 11 Middle cerebral artery, temporal branch
- 12 Lambdoid suture
- 13 Zygomatic bone
- 14 Transverse sinus
- 15 Occipital bone
- 16 Articular tubercle
- 17 Mandibular fossa
- 18 Articular disc of temporomandibular joint
- 19 Head of mandible
- 20 External acoustic meatus
- 21 Sigmoid sinus
- 22 Coronoid process
- 23 Lateral pterygoid
- 24 Mastoid process
- 25 Emissary vein
- 26 Maxillary artery
- 27 Pterygoid venous plexus
- 28 Parotid gland
- 29 Masseter
- 30 Ramus of mandible
- 31 Inferior alveolar artery and vein in mandibular foramen
- 32 Medial pterygoid
- 33 External carotid artery
- 34 Longissimus capitis
- 35 Splenius capitis
- 36 Trapezius
- 37 Posterior belly of digastric
- 38 Internal jugular vein
- 39 Levator scapulae
- 40 Facial artery
- 41 Internal carotid artery
- 42 Platysma
- 43 Submandibular gland
- 44 Common carotid artery

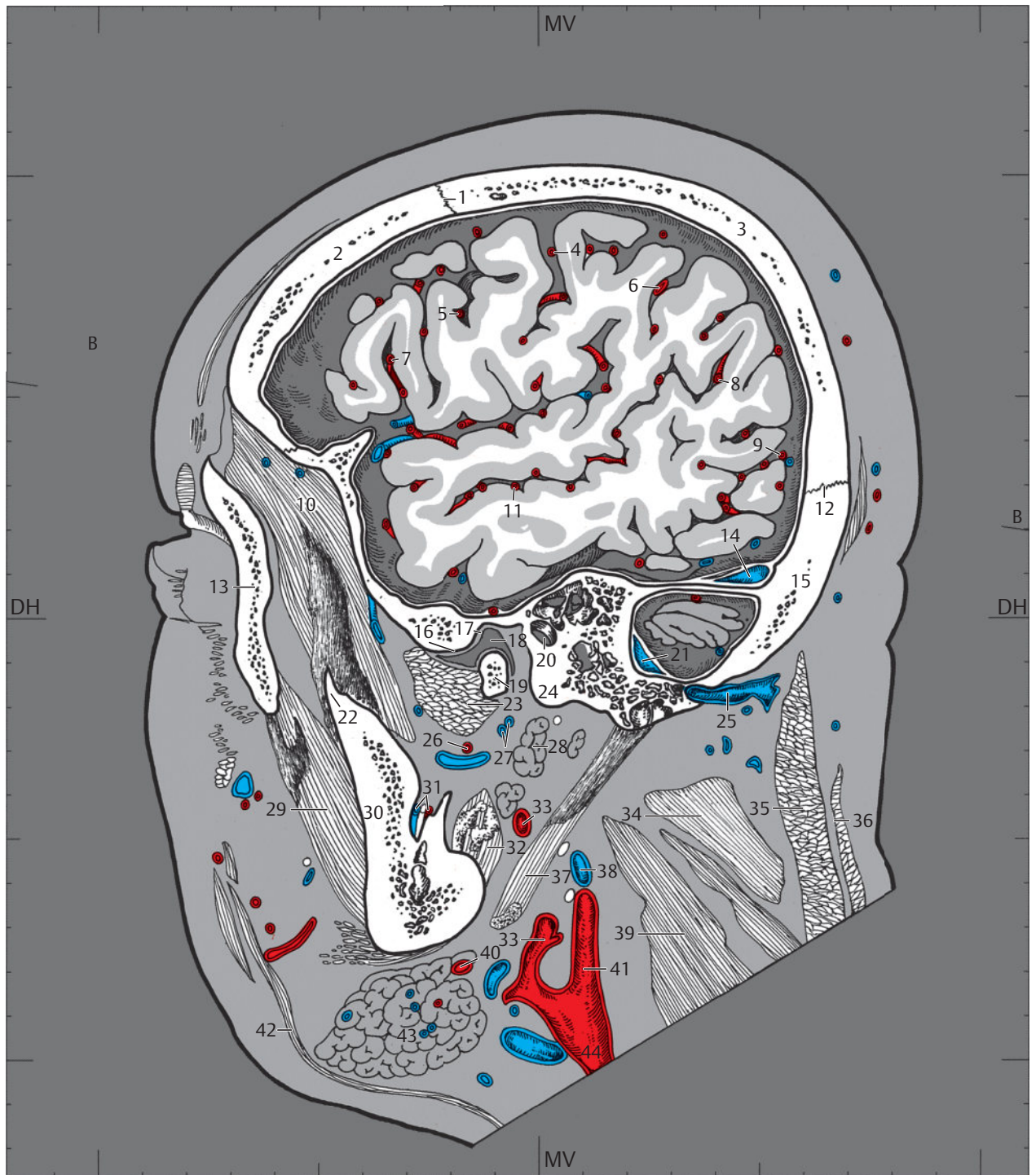
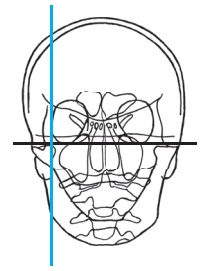
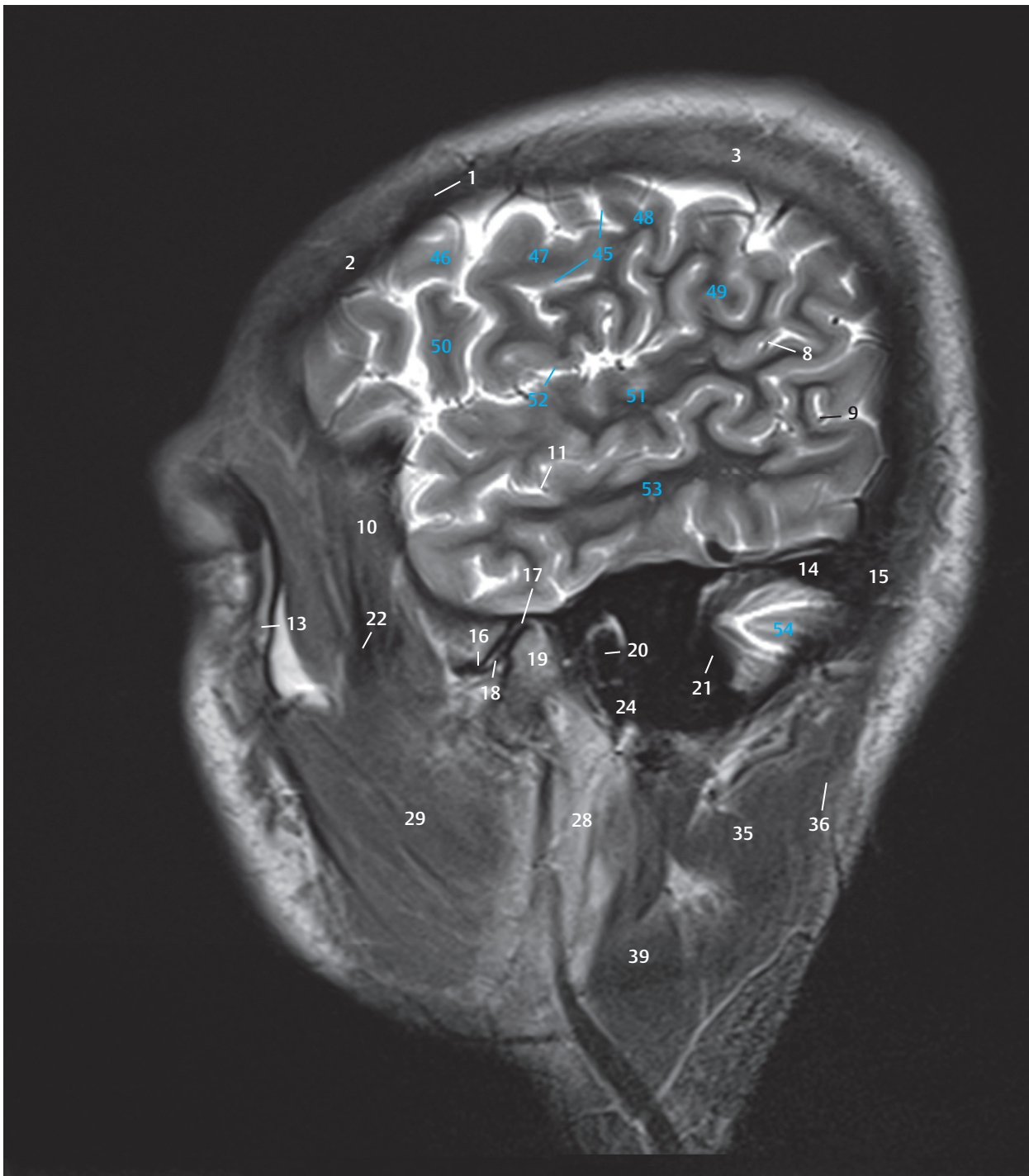
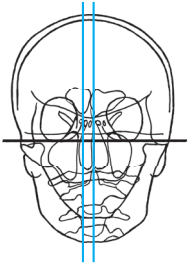


Fig. 4.7c Medial view of the sixth sagittal section. This section lies close to the orbit at its lateral aspect and contains the bony part of the auditory canal and the carotid bifurcation. Bony structures, muscles, and blood vessels.



- 1 Coronal suture
- 2 Frontal bone
- 3 Parietal bone
- 8 Artery of angular gyrus
- 9 Temporo-occipital artery
- 10 Temporalis
- 11 Middle cerebral artery, temporal branch
- 13 Zygomatic bone
- 14 Transverse sinus
- 15 Occipital bone
- 16 Articular tubercle
- 17 Mandibular fossa
- 18 Articular disk of temporomandibular joint
- 19 Head of mandible
- 20 External acoustic canal
- 21 Sigmoid sinus
- 22 Coronoid process
- 24 Mastoid process
- 28 Parotid gland
- 29 Masseter
- 35 Splenius capitis
- 36 Trapezius
- 39 Levator scapulae
- 45 Central sulcus
- 46 Middle frontal gyrus
- 47 Precentral gyrus
- 48 Postcentral gyrus
- 49 Supramarginal gyrus
- 50 Inferior frontal gyrus
- 51 Superior temporal gyrus
- 52 Lateral sulcus
- 53 Middle temporal gyrus
- 54 Posterior lobe of cerebellum

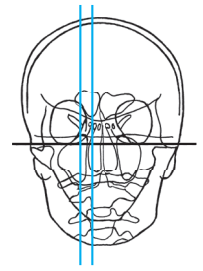
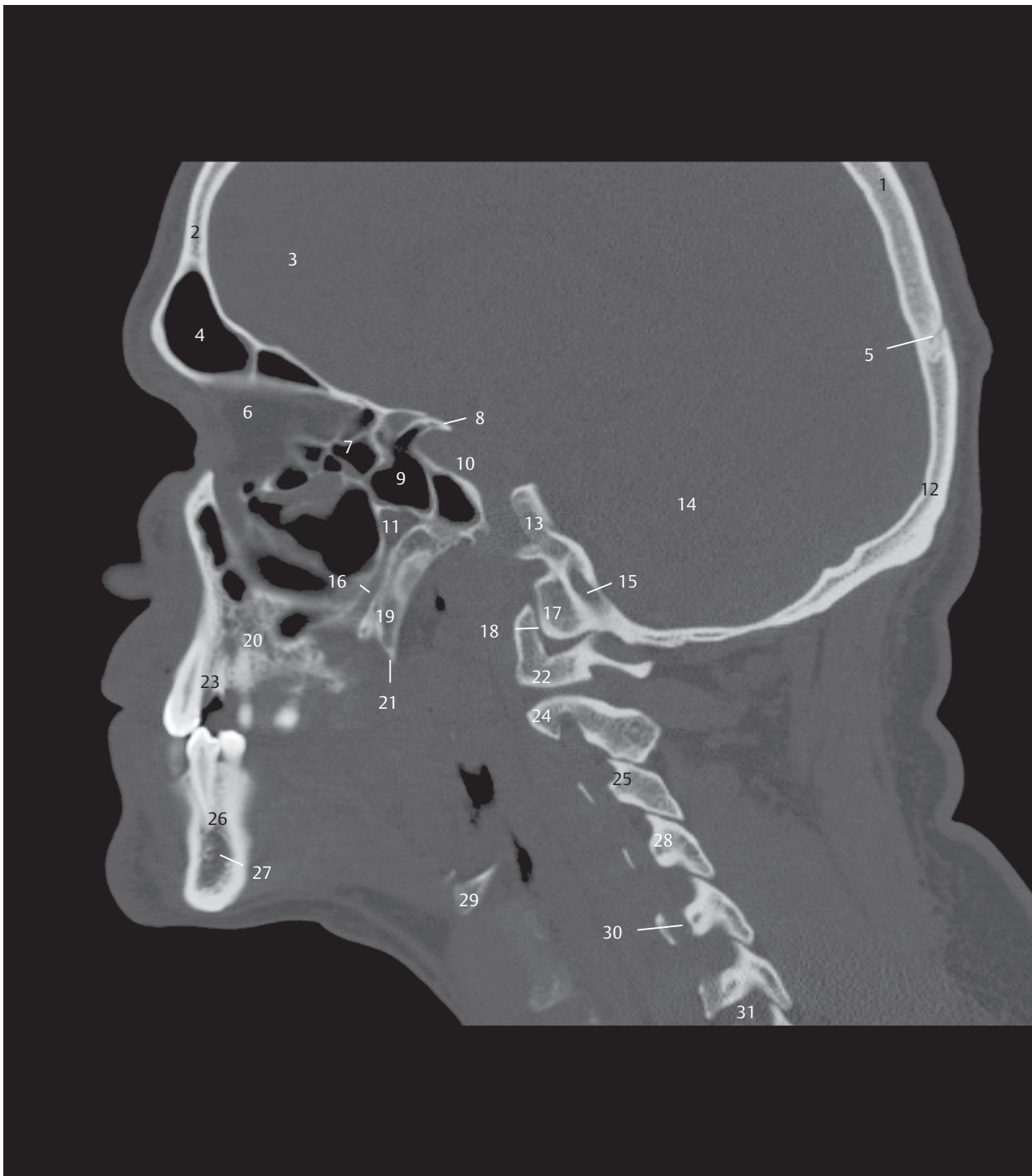
Fig. 4.7d Sagittal T2w MR image, approximately corresponding to the sectional plane in a and c.



- 1 Frontal bone
- 2 Parietal bone
- 3 Frontal sinus
- 4 Lambdoid suture
- 5 Crista galli
- 6 Anterior cranial fossa
- 7 Lamina cribrosa
- 8 Occipital bone
- 9 Tuberculum sellae
- 10 Dorsum sellae
- 11 Nasal bone
- 12 Hypophysial fossa
- 13 Nasal septum
- 14 Sphenoid sinus
- 15 Sphenoid bone
- 16 Clivus
- 17 Internal occipital protuberance
- 18 Posterior cranial fossa
- 19 External occipital protuberance (inion)
- 20 Pharyngeal tubercle
- 21 Anterior nasal spine
- 22 Posterior nasal spine
- 23 Pharynx, nasopharynx
- 24 Foramen magnum
- 25 Hard palate
- 26 Vertebral canal
- 27 Median atlantoaxial joint
- 28 Anterior arch of atlas
- 29 Alveolar process of maxilla
- 30 Posterior arch of atlas
- 31 Dens
- 32 Incisive canal
- 33 Spinous process of axis
- 34 Third cervical vertebra, spinous process
- 35 Third cervical vertebra
- 36 Body of the mandible
- 37 Hyoid bone
- 38 Fourth cervical vertebra
- 39 Thyroid cartilage
- 40 Trachea

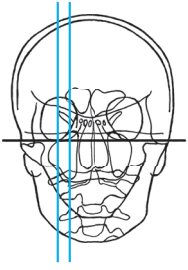


Fig. 4.8 Sagittal section. Sagittal CT image, the position of which approximately corresponds to that of the first sagittal section. This and the following sagittal CT images were obtained during a diagnostic examination; the cranial vault is therefore incompletely visualized. Secondary sagittal reconstruction from a thin, reconstruction-enabling transverse data set. Landmarks are the pituitary fossa, frontal and sphenoid sinuses, atlas, and dens.



- 1 Parietal bone
- 2 Frontal bone
- 3 Anterior cranial fossa
- 4 Frontal sinus
- 5 Lambdoid suture
- 6 Orbit
- 7 Ethmoidal cells
- 8 Anterior clinoid process
- 9 Sphenoid sinus
- 10 Carotid canal
- 11 Pterygopalatine fossa
- 12 Occipital bone
- 13 Sphenoid bone
- 14 Posterior cranial fossa
- 15 Hypoglossal canal
- 16 Greater palatine canal
- 17 Occipital condyle
- 18 Atlanto-occipital joint
- 19 Pterygoid process, medial plate
- 20 Maxilla
- 21 Pterygoid hamulus
- 22 Lateral mass of atlas
- 23 Alveolar process of maxilla
- 24 Axis
- 25 Third cervical vertebra, articular process
- 26 Body of the mandible
- 27 Mandibular canal
- 28 Fourth cervical vertebra, articular process
- 29 Hyoid bone
- 30 Foramen transversarium
- 31 Intervertebral foramen

Fig. 4.9 Sagittal section. CT image, the position of which approximately corresponds to that of the second sagittal section. The floor of the anterior and posterior cranial fossae has been sectioned in the cranial cavity. Landmarks are the ethmoidal cells, hard palate, mandible, and the contours of cervical vertebrae.



- 1 Frontal bone
- 2 Parietal bone
- 3 Frontal sinus
- 4 Anterior cranial fossa
- 5 Roof of orbit
- 6 Lambdoid suture
- 7 Sphenofrontal suture
- 8 Sphenoid bone
- 9 Anterior clinoid process
- 10 Orbit
- 11 Floor of orbit
- 12 Middle cranial fossa
- 13 Foramen rotundum
- 14 Pterygopalatine fossa
- 15 Carotid canal
- 16 Temporal bone
- 17 Occipital bone
- 18 Maxillary sinus
- 19 Hypoglossal canal
- 20 Posterior cranial fossa
- 21 Occipital condyle
- 22 Atlanto-occipital joint
- 23 Pterygoid hamulus
- 24 Maxilla
- 25 Lateral mass of atlas
- 26 Lateral atlantoaxial joint
- 27 Axis
- 28 Third cervical vertebra
- 29 Body of the mandible
- 30 Mandibular canal
- 31 Hyoid bone
- 32 Fourth cervical vertebra

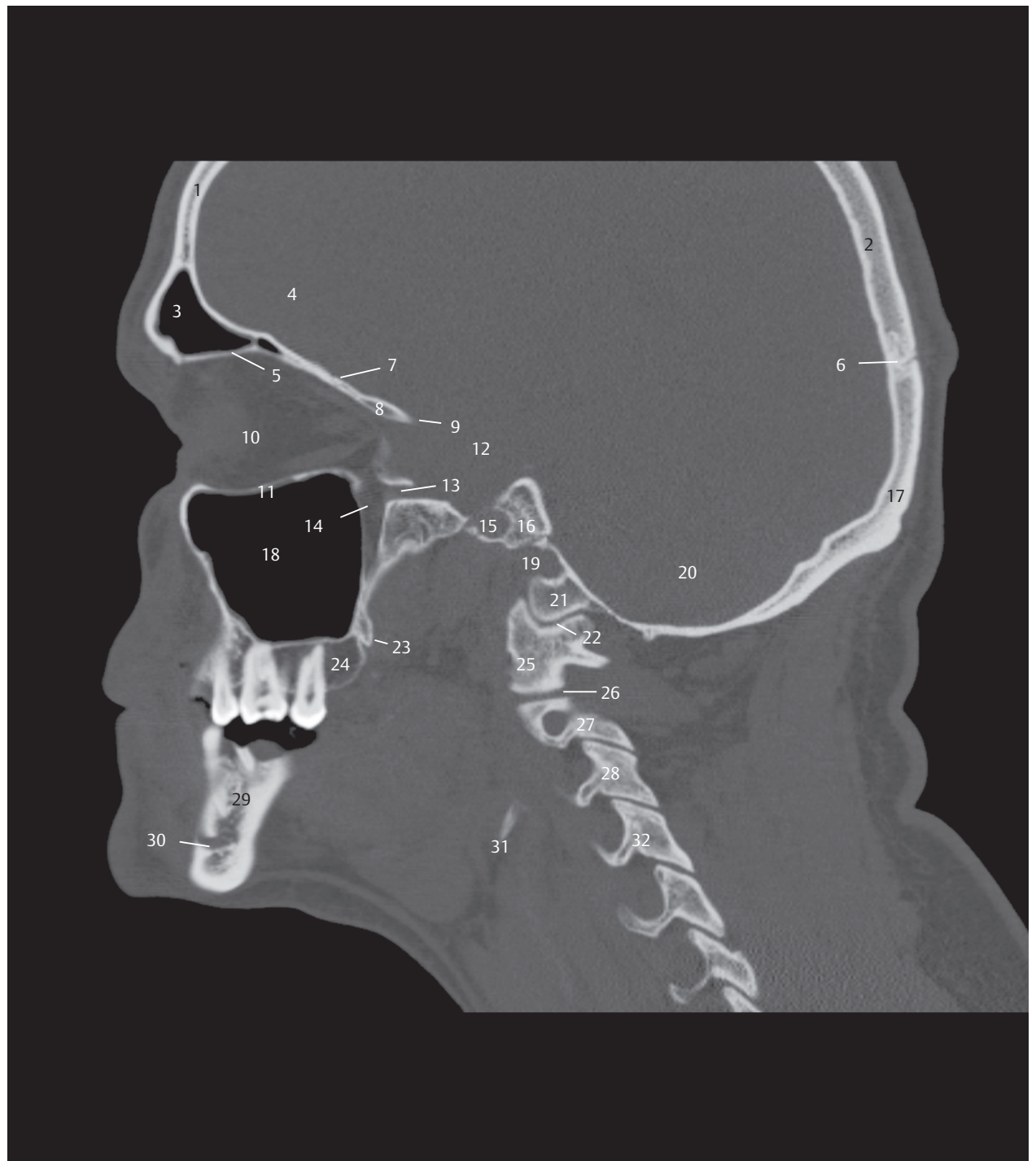
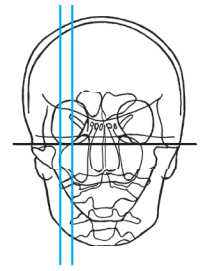
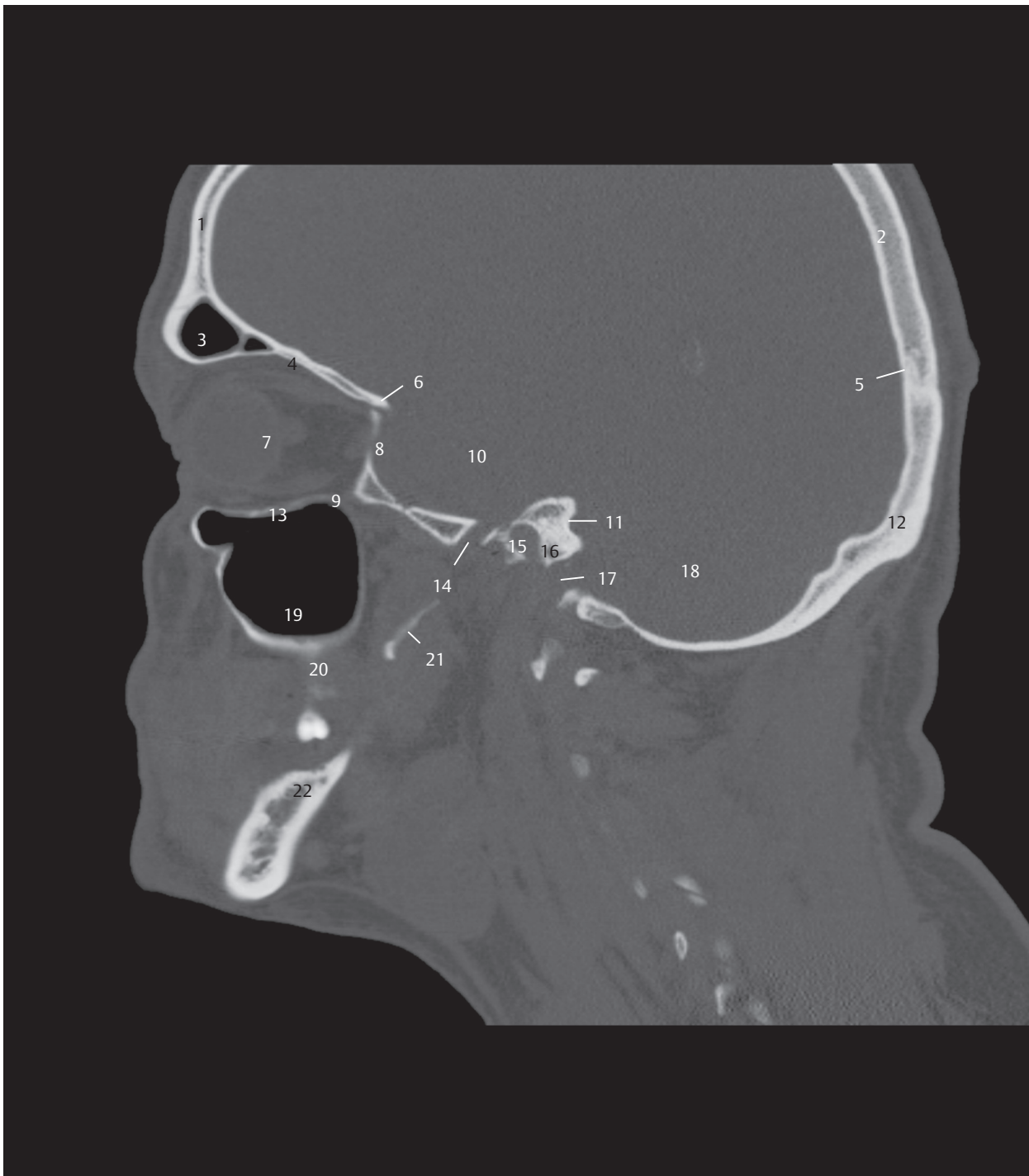
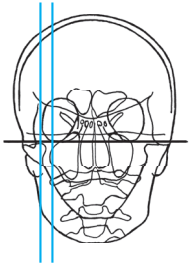


Fig. 4.10 Sagittal section. CT image, the position of which approximately corresponds to that of the third sagittal section. The roof and floor of orbit, maxillary sinus, mandible, and the contours of the cervical vertebrae are landmarks for the facial skeleton and the craniocervical junction.



- 1 Frontal bone
- 2 Parietal bone
- 3 Sphenoid sinus
- 4 Roof of orbit, floor of anterior cranial fossa
- 5 Lambdoid suture
- 6 Sphenoid bone, lesser wing
- 7 Orbit
- 8 Superior orbital fissure
- 9 Inferior orbital fissure
- 10 Middle cranial fossa
- 11 Opening of the internal acoustic canal
- 12 Occipital bone
- 13 Floor of orbit
- 14 Foramen ovale
- 15 Carotid canal
- 16 Temporal bone
- 17 Jugular foramen
- 18 Posterior cranial fossa
- 19 Maxillary sinus
- 20 Maxilla
- 21 Pterygoid process, lateral plate
- 22 Mandible

Fig. 4.11 Sagittal section. Sagittal CT image, corresponding to the fourth sagittal section. The terraces of the anterior, middle, and posterior cranial fossae are clearly delineated.



- 1 Frontal bone
- 2 Parietal bone
- 3 Lambdoid suture
- 4 Occipital bone
- 5 Arcuate eminence
- 6 Middle cranial fossa
- 7 Tympanic cavity
- 8 Posterior cranial fossa
- 9 Zygomatic bone
- 10 Facial canal
- 11 Temporal bone
- 12 Stylomastoid foramen
- 13 Styloid process
- 14 Mandibular canal
- 15 Ramus of mandible

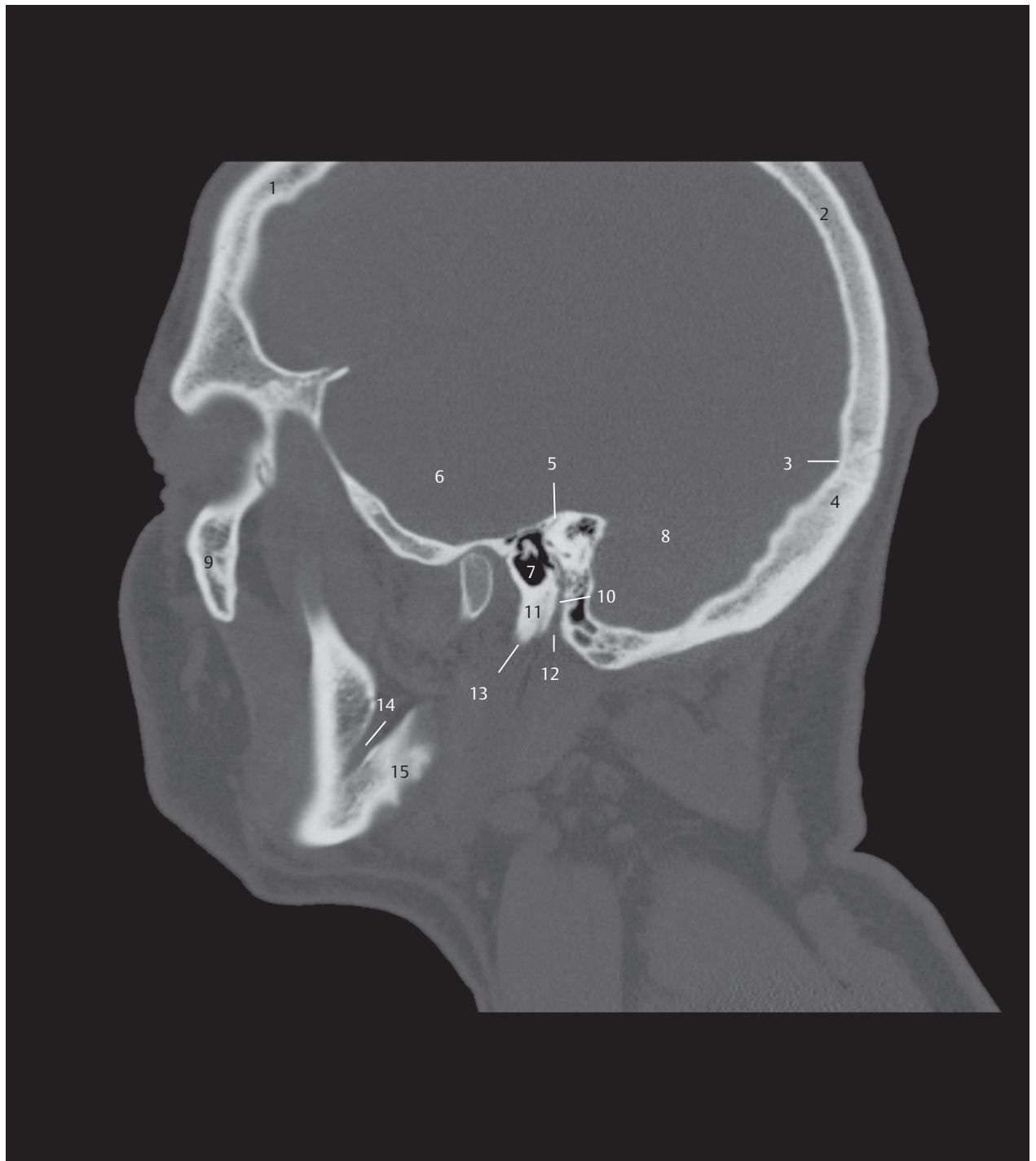
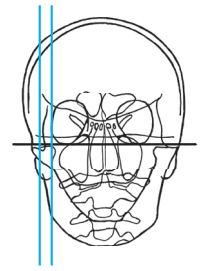
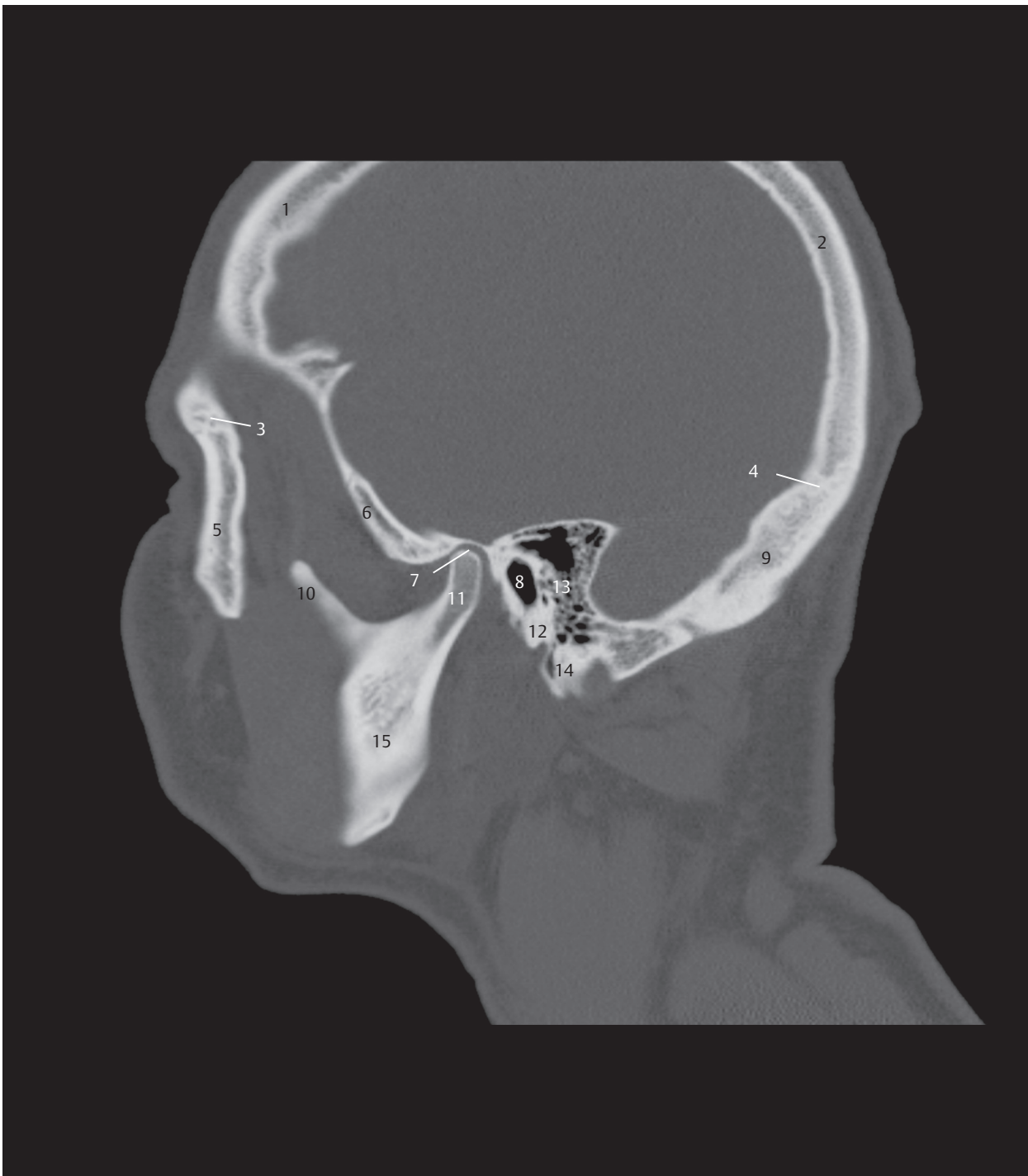


Fig. 4.12 Sagittal section. CT image, corresponding to the fifth sagittal section. The skull base has been sectioned at the level of the superior semicircular canal, the facial canal, the tympanic cavity, and the styloid process.



- 1 Frontal bone
- 2 Parietal bone
- 3 Frontozygomatic suture
- 4 Lambdoid suture
- 5 Zygomatic bone
- 6 Greater wing of sphenoid
- 7 Mandibular fossa
- 8 External acoustic canal
- 9 Occipital bone
- 10 Coronoid process
- 11 Condylar process
- 12 Temporal bone
- 13 Mastoid cells
- 14 Mastoid process
- 15 Ramus of mandible

Fig. 4.13 Sagittal section. CT image, corresponding to the sixth sagittal section. The section lies at the level of the temporomandibular joint and contains the mastoid process.

5 Transverse Sections

Fourteen transverse sections have been described in the following part of the book from inferior to superior. Fig. 5.1 illustrates the position of 14 MRI sections with angulation along the bicommissural line, depicted from ▶Fig. 5.2, ▶Fig. 5.3, ▶Fig. 5.4, ▶Fig. 5.5, ▶Fig. 5.6, ▶Fig. 5.7, ▶Fig. 5.8, ▶Fig. 5.9, ▶Fig. 5.10, ▶Fig. 5.11, ▶Fig. 5.12, ▶Fig. 5.13, ▶Fig. 5.14, and ▶Fig. 5.15. Transverse CT sections, reproduced from ▶Fig. 5.17, ▶Fig. 5.18, ▶Fig. 5.19, ▶Fig. 5.20, ▶Fig. 5.21, ▶Fig. 5.22, ▶Fig. 5.23, ▶Fig. 5.24, ▶Fig. 5.25, ▶Fig. 5.26, ▶Fig. 5.27, ▶Fig. 5.28, ▶Fig. 5.29, and ▶Fig. 5.30, were obtained

with angulation along the supraorbito-suboccipital plane (▶Fig. 5.16). Please consider that the following MR images in the bicommissural plane and CT images in the supraorbito-suboccipital plane (see ▶Fig. 5.2, ▶Fig. 5.3, ▶Fig. 5.4, ▶Fig. 5.5, ▶Fig. 5.6, ▶Fig. 5.7, ▶Fig. 5.8, ▶Fig. 5.9, ▶Fig. 5.10, ▶Fig. 5.11, ▶Fig. 5.12, ▶Fig. 5.13, ▶Fig. 5.14, ▶Fig. 5.15, and ▶Fig. 5.17, ▶Fig. 5.18, ▶Fig. 5.19, ▶Fig. 5.20, ▶Fig. 5.21, ▶Fig. 5.22, ▶Fig. 5.23, ▶Fig. 5.24, ▶Fig. 5.25, ▶Fig. 5.26, ▶Fig. 5.27, ▶Fig. 5.28, ▶Fig. 5.29, and ▶Fig. 5.30) were obtained from two individuals.

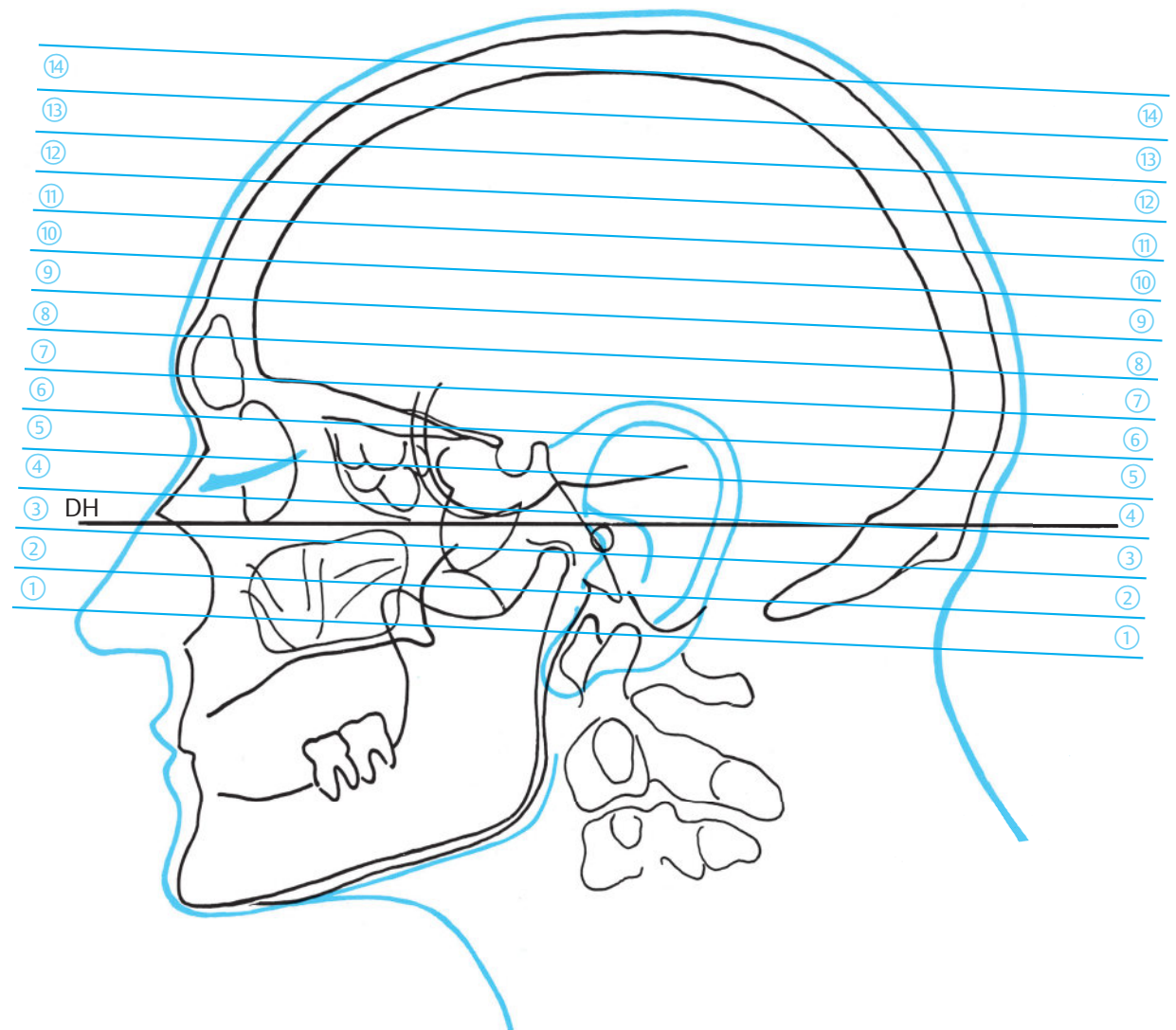


Fig. 5.1 Bicommissural sections. For specimen details see Chapter 12.

DH = German horizontal

Fig. 5.1a Position of the bicommissural planes in lateral view.

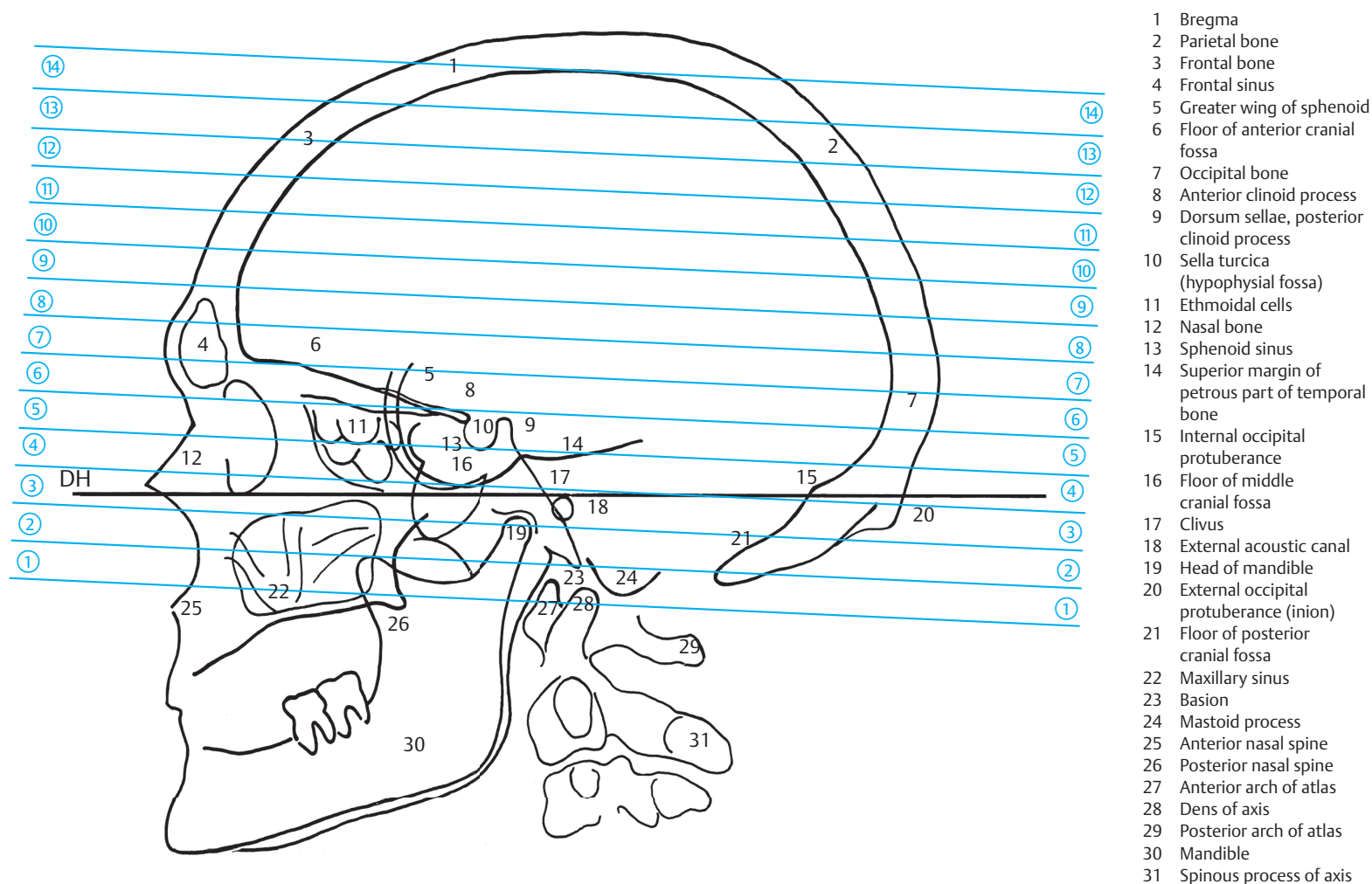


Fig. 5.1b Schematic representation based on an x-ray image of the same head as in a. The 14 sections of the bicommissural series have been contiguously numbered with encircled digits from inferior to superior and specify the approximate position.

- 1 Paracentral lobule
- 2 Precuneus
- 3 Cingulate sulcus
- 4 Cingulate gyrus
- 5 Trunk (body) of corpus callosum
- 6 Parieto-occipital sulcus
- 7 Frontal pole
- 8 Genu of corpus callosum
- 9 Septum pellucidum
- 10 Fornix
- 11 Splenium of corpus callosum
- 12 Cuneus
- 13 Interventricular foramen (of Monro)
- 14 Anterior commissure
- 15 Interthalamic adhesion
- 16 Third ventricle
- 17 Pineal gland
- 18 Posterior commissure
- 19 Superior colliculus
- 20 Calcarine sulcus
- 21 Lamina terminalis
- 22 Mammillary body
- 23 Midbrain
- 24 Aqueduct of midbrain
- 25 Inferior colliculus
- 26 Occipital pole
- 27 Olfactory bulb
- 28 Olfactory tract
- 29 Optic chiasm
- 30 Infundibulum and pituitary gland
- 31 Pons
- 32 Fourth ventricle
- 33 Cerebellum
- 34 Nodule of vermis (X)
- 35 Temporal lobe
- 36 Uvula of vermis (IX)
- 37 Pyramid of vermis (VIII)
- 38 Foramen cecum
- 39 Medulla oblongata
- 40 Tonsil of cerebellum (H IX)
- 41 Spinal cord

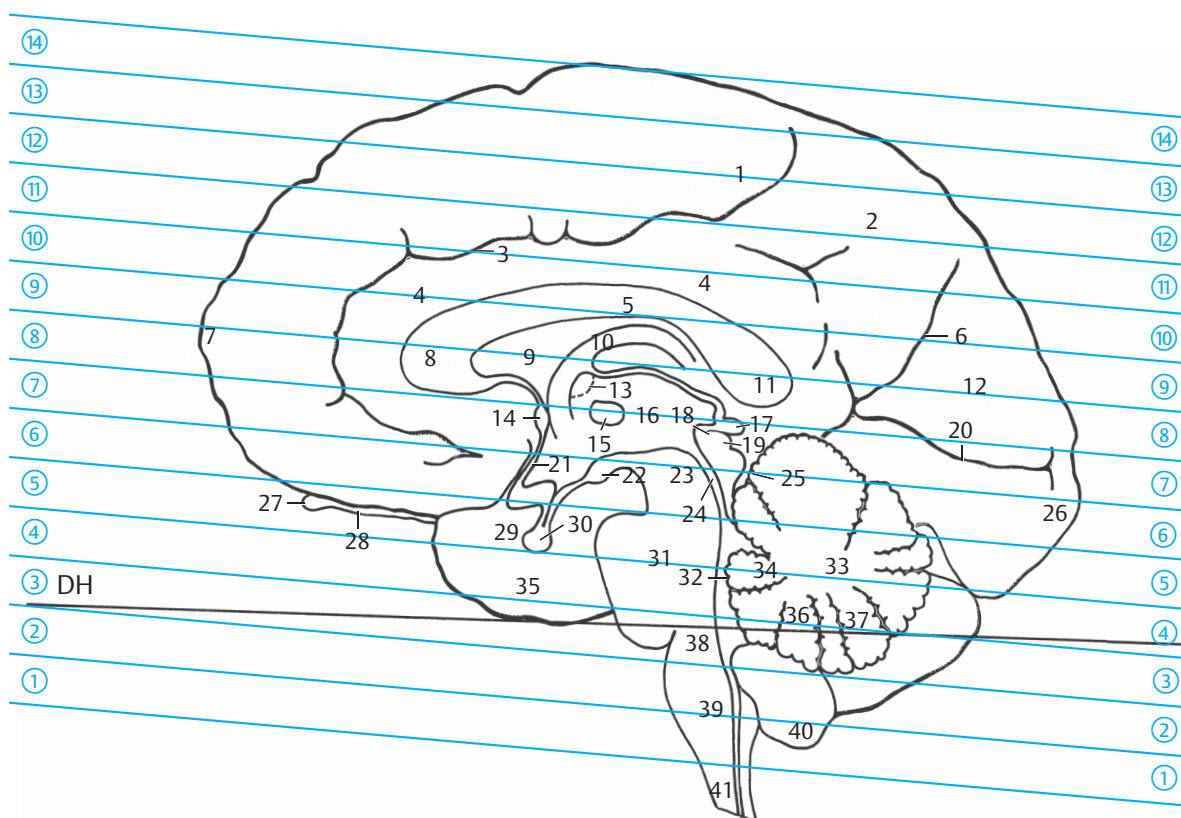


Fig. 5.1c Median view of the brain of the same head as in a. The sections of the bicommissural series have been numbered as in a.

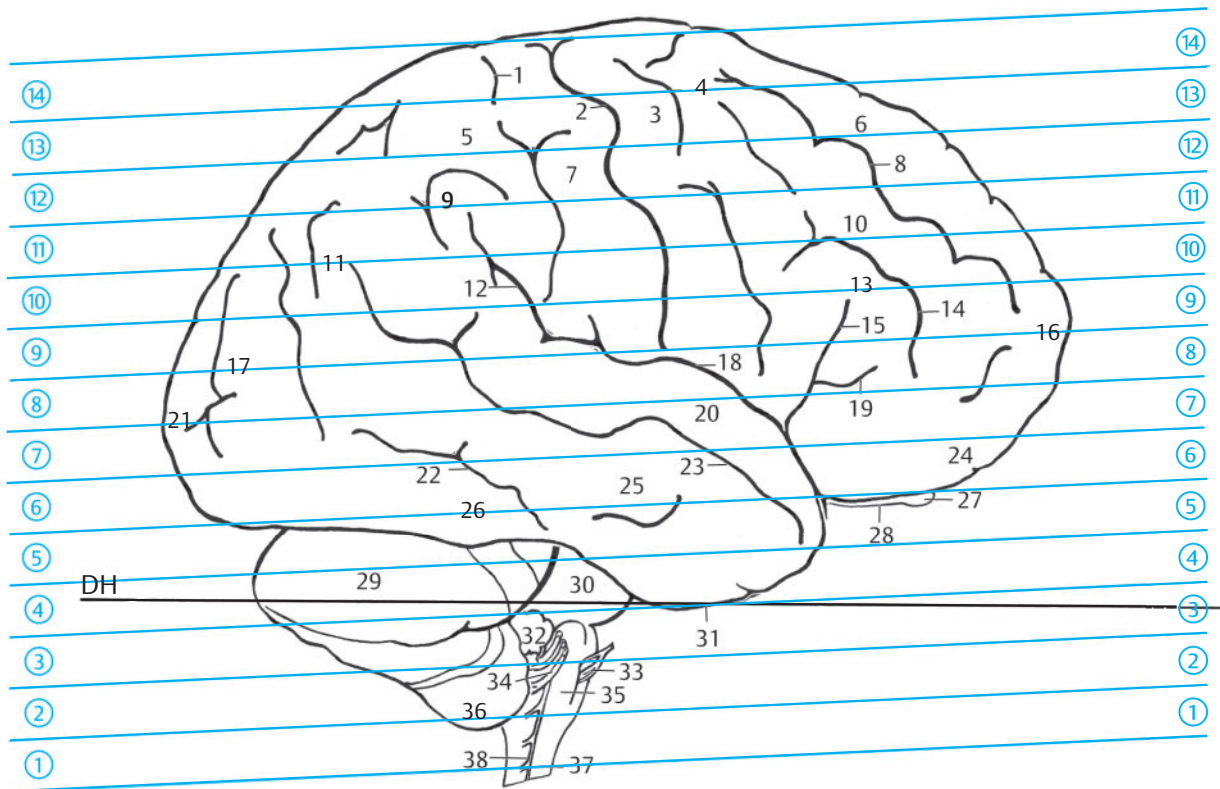
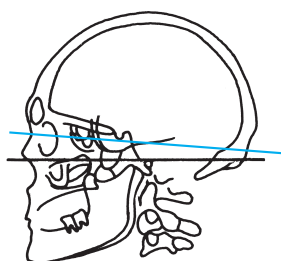


Fig. 5.1d Lateral view of the brain of the same head as in a and b. The sections of the bicommissural series have been numbered as in a.

- 1 Postcentral sulcus
- 2 Central sulcus
- 3 Precentral gyrus
- 4 Precentral sulcus
- 5 Superior parietal lobule
- 6 Superior frontal gyrus
- 7 Postcentral gyrus
- 8 Superior frontal sulcus
- 9 Supramarginal gyrus
- 10 Middle frontal gyrus
- 11 Angular gyrus
- 12 Posterior ramus of lateral sulcus (Sylvian fissure)
- 13 Inferior frontal gyrus
- 14 Inferior frontal sulcus
- 15 Ascending ramus of lateral sulcus (Sylvian fissure)
- 16 Frontal pole
- 17 Occipital gyri
- 18 Lateral sulcus (Sylvian fissure)
- 19 Anterior ramus of lateral sulcus (Sylvian fissure)
- 20 Superior temporal gyrus
- 21 Occipital pole
- 22 Inferior temporal sulcus
- 23 Superior temporal sulcus
- 24 Orbital gyri
- 25 Middle temporal gyrus
- 26 Inferior temporal gyrus
- 27 Olfactory bulb
- 28 Olfactory tract
- 29 Cerebellum
- 30 Pons
- 31 Base of temporal lobe
- 32 Flocculus (H X)
- 33 Hypoglossal nerve
- 34 Glossopharyngeal nerve, vagus nerve, accessory nerve
- 35 Medulla oblongata
- 36 Tonsil of cerebellum (H IX)
- 37 Spinal cord
- 38 Spinal root of accessory nerve



- 1 Maxilla, alveolar process
- 2 Tongue
- 3 Buccinator
- 4 Masseter
- 5 Lateral pterygoid
- 6 Pterygoid process, lateral plate
- 7 Medial pterygoid
- 8 Mandible
- 9 Pharynx, oropharynx
- 10 Mandibular canal
- 11 Retromandibular vein
- 12 Pterygoid venous plexus
- 13 Maxillary artery
- 14 Parotid
- 15 Internal jugular vein
- 16 Anterior arch of atlas
- 17 Internal carotid artery
- 18 Dens
- 19 Lateral mass of atlas
- 20 External ear
- 21 Anterior median fissure
- 22 Vertebral artery, V3-segment
- 23 Vertebral vein
- 24 Spinal cord
- 25 Posterior root C1 spinal nerve
- 26 Spinal cord, posterior funiculus
- 27 Posterior arch of atlas
- 28 Spinal dura mater
- 29 Obliquus capitis superior
- 30 Occipital artery
- 31 Rectus capitis posterior major
- 32 Rectus capitis posterior minor
- 33 Nuchal ligament
- 34 Splenius capitis
- 35 Semispinalis capitis
- 36 Trapezius

- I BS – Buccal space
- II MS – Masticator space
- III PMS – Parapharyngeal mucosal space
- IV RPS – Retropharyngeal space
- V PPS – Parapharyngeal space
- VI PS – Parotid space
- VII CS – Carotid space
- VIII PVS – Paravertebral space

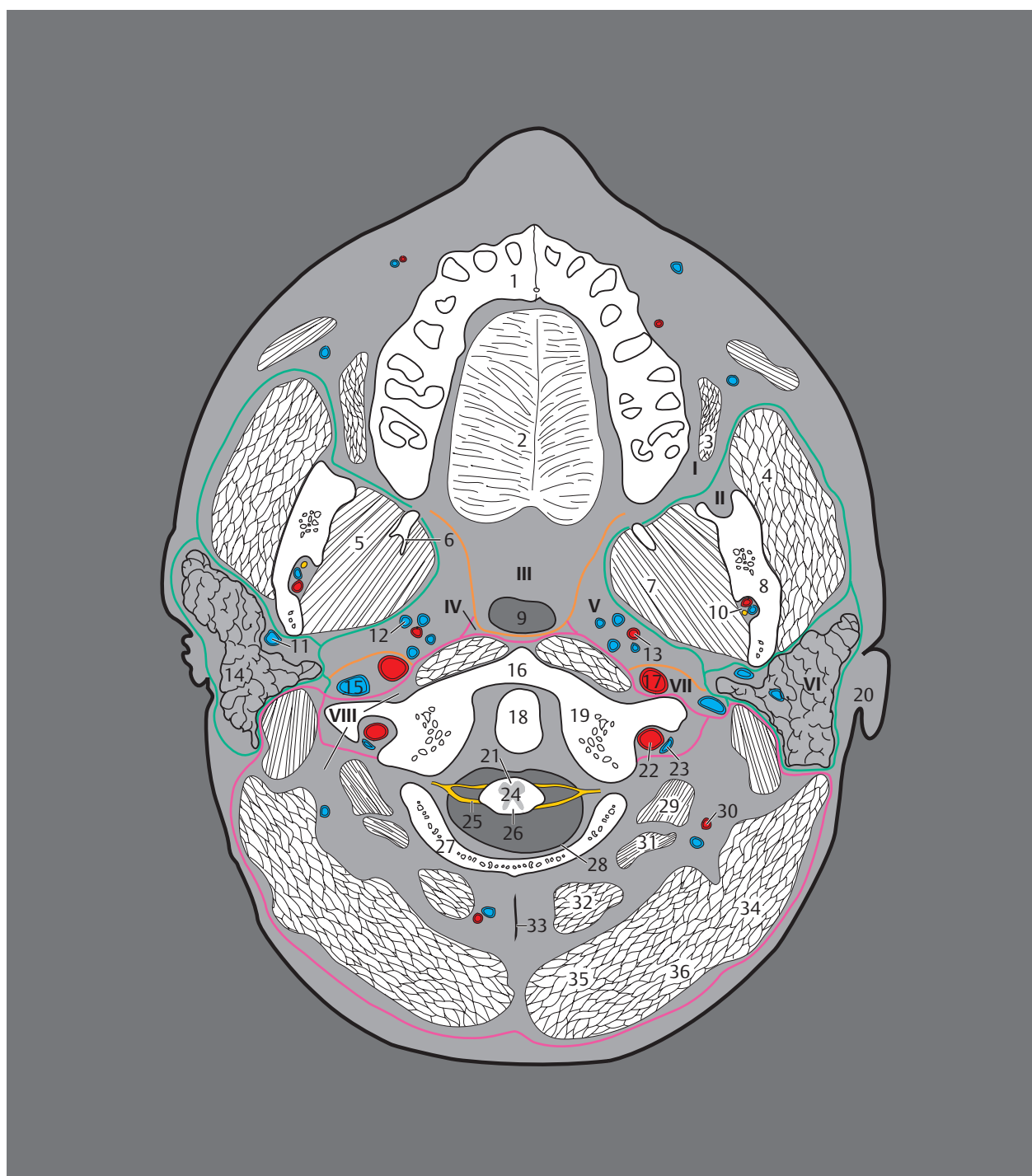
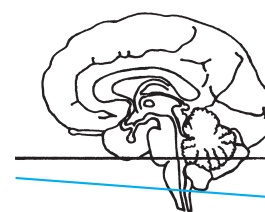
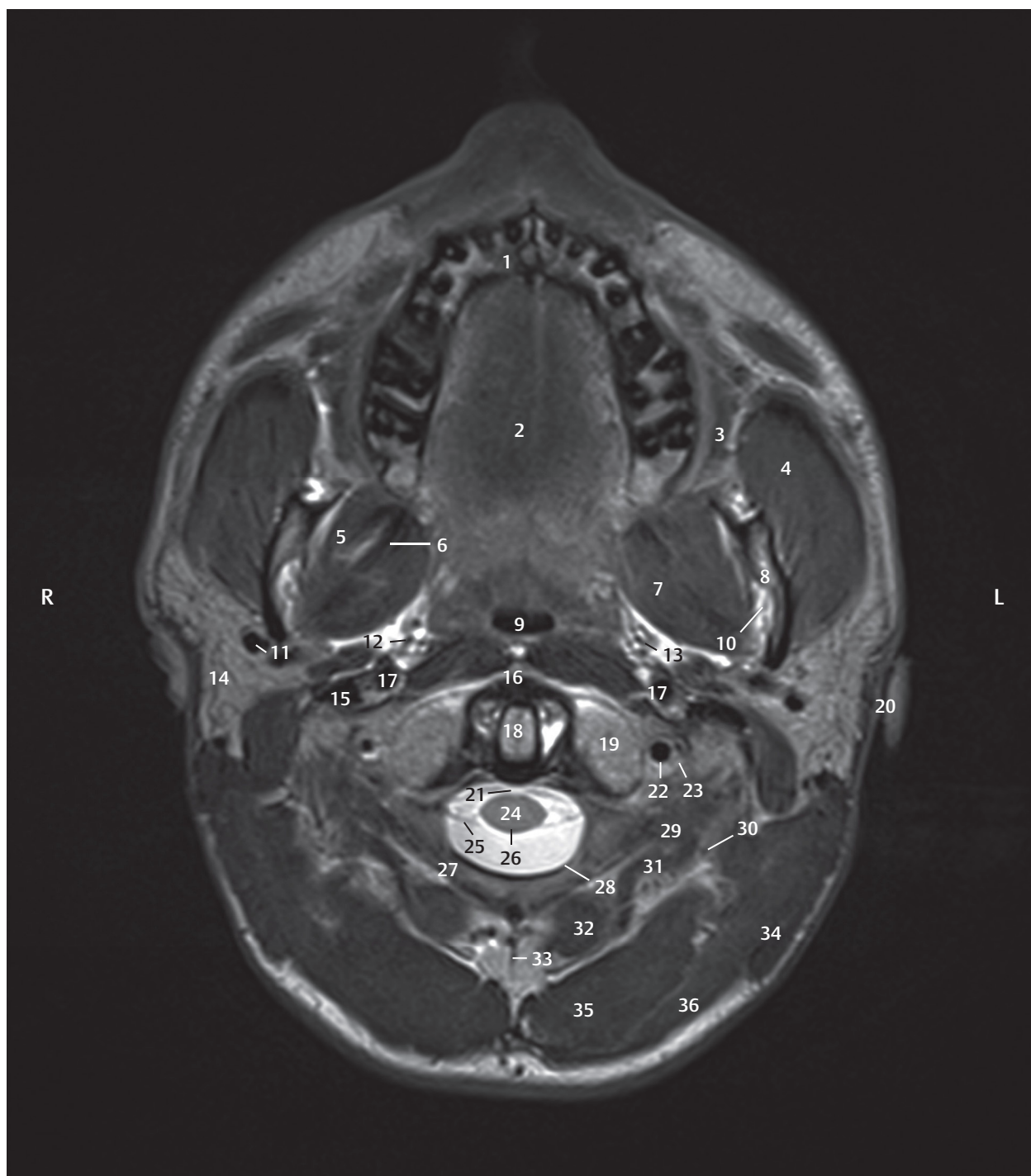


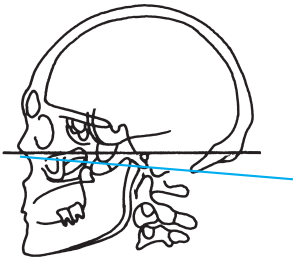
Fig. 5.2 1st bicommissural section.

Fig. 5.2a Inferior view of the first section of the bicommissural MRI series. The blue line in the signet marks the position of the sectional plane at the craniocervical junction at the level of the condyle and the atlas (see ► Fig. 5.1b). The three layers of the cervical fascia within the soft tissues of the head–neck junction have been color coded (*green* – superficial layer; *orange* – middle layer; *pink* – deep layer). Abbreviations listed in the legends correspond to names of fascial spaces (e.g., BS = buccal space; reproduced from Engelke C. Ganzkörper-Computertomographie. Spiral- und Multislice-CT. Stuttgart: Thieme; 2007). Spinal structures and spinal dura. Cervical fasciae and resulting spaces. Brain structures, blood vessels, and meninges.



- 1 Maxilla, alveolar process
- 2 Tongue
- 3 Buccinator
- 4 Masseter
- 5 Lateral pterygoid
- 6 Pterygoid process, lateral plate
- 7 Medial pterygoid
- 8 Mandible
- 9 Pharynx, oropharynx
- 10 Mandibular canal
- 11 Retromandibular vein
- 12 Pterygoid venous plexus
- 13 Maxillary artery
- 14 Parotid
- 15 Internal jugular vein
- 16 Anterior arch of atlas
- 17 Internal carotid artery
- 18 Dens
- 19 Lateral mass of atlas
- 20 External ear
- 21 Anterior median fissure
- 22 Vertebral artery, V3 segment
- 23 Vertebral vein
- 24 Spinal cord
- 25 Posterior root
- 26 Spinal cord, posterior funiculus
- 27 Posterior arch of atlas
- 28 Spinal dura mater
- 29 Obliquus capitis superior
- 30 Occipital artery
- 31 Rectus capitis posterior major
- 32 Rectus capitis posterior minor
- 33 Nuchal ligament
- 34 Splenius capitis
- 35 Semispinalis capitis
- 36 Trapezius

Fig. 5.2b T2w MR image (TSE sequence) oriented in the bicommissural plane, identical to the sectional plane in a (since it is the corresponding basis of the schematic representation in a). Structures of the brain are accentuated by the selected sequence. The bicommissural MR series was obtained from a 33-year-old man. The blue line in the signet shows the course of the sectional plane through the spinal cord in the midline (►Fig. 5.1c).

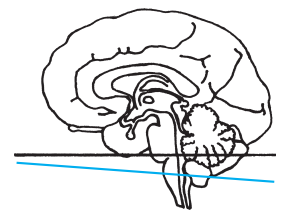
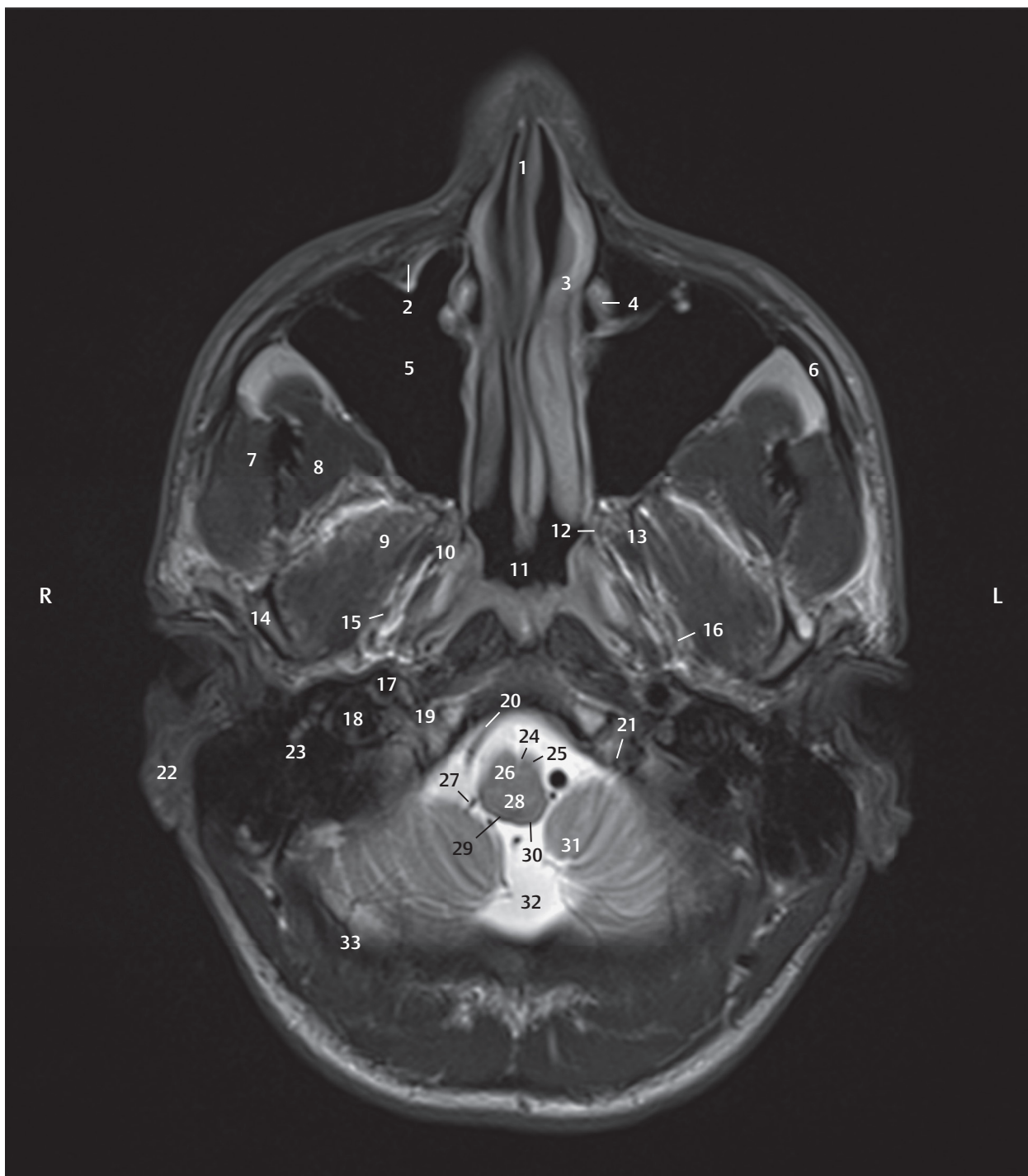


- 1 Nasal septum
- 2 Infraorbital canal with infraorbital nerve
- 3 Inferior nasal concha
- 4 Lacrimal duct
- 5 Maxillary sinus
- 6 Zygomatic bone
- 7 Masseter
- 8 Temporalis
- 9 Lateral pterygoid
- 10 Medial pterygoid
- 11 Nasopharynx
- 12 Medial part of pterygoid process
- 13 Lateral part of pterygoid process
- 14 Mandible
- 15 Mandibular nerve
- 16 Pterygoid venous plexus
- 17 Internal carotid artery
- 18 Internal jugular vein
- 19 Hypoglossal canal
- 20 Vertebral artery
- 21 Hypoglossal nerve
- 22 External ear
- 23 Mastoid process
- 24 Anterior median fissure
- 25 Pyramid
- 26 Inferior olivary nucleus
- 27 Posterior inferior cerebellar artery (PICA)
- 28 Medulla oblongata
- 29 Gracile tubercle
- 30 Cuneate tubercle
- 31 Tonsils of cerebellum (H IX)
- 32 Posterior cerebellomedullary cistern (magna)
- 33 Occipital bone



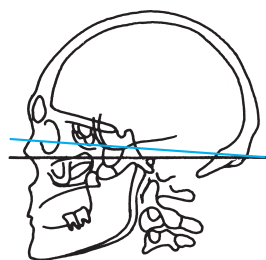
Fig. 5.3 2nd bicommissural section.

Fig. 5.3a Inferior view of the second section of the bicommissural series. The posterior cranial fossa has been sectioned just above the foramen magnum. The medulla oblongata and tonsils of cerebellum are seen in cut-section. Brain structures, blood vessels, and meninges.



- 1 Nasal septum
- 2 Infraorbital canal with infraorbital nerve
- 3 Inferior nasal concha
- 4 Lacrimal duct
- 5 Maxillary sinus
- 6 Zygomatic bone
- 7 Masseter
- 8 Temporalis
- 9 Lateral pterygoid
- 10 Medial pterygoid
- 11 Pharynx, nasopharynx
- 12 Medial part of pterygoid process
- 13 Lateral part of pterygoid process
- 14 Mandible
- 15 Mandibular nerve
- 16 Pterygoid venous plexus
- 17 Internal carotid artery
- 18 Internal jugular vein
- 19 Hypoglossal canal
- 20 Vertebral artery
- 21 Hypoglossal nerve
- 22 External ear
- 23 Mastoid process
- 24 Anterior median fissure
- 25 Pyramid
- 26 Inferior olivary nucleus
- 27 Posterior inferior cerebellar artery (PICA)
- 28 Medulla oblongata
- 29 Gracile tubercle
- 30 Cuneate tubercle
- 31 Tonsils of cerebellum (H IX)
- 32 Posterior cerebellomedullary cistern (magna)
- 33 Occipital bone

Fig. 5.3b T2w MR image oriented in the bicommissural plane, identical to the sectional plane in a.



- 1 Nasal septum
- 2 Eyeball
- 3 Zygomatic bone
- 4 Maxillary sinus
- 5 Ethmoidal air cells
- 6 Temporalis
- 7 Pterygopalatine fossa
- 8 Sphenoid sinus
- 9 Mandibular nerve
- 10 Foramen spinosum
- 11 Clivus
- 12 Head of mandible
- 13 Internal carotid artery
- 14 Bulb of jugular vein
- 15 Glossopharyngeal nerve/vagus nerve
- 16 Olive
- 17 Vertebral artery
- 18 External acoustic canal
- 19 Medulla oblongata
- 20 Mastoid
- 21 Fourth ventricle
- 22 Sigmoid sinus
- 23 External ear
- 24 Vermis
- 25 Emissary vein
- 26 Occipital artery
- 27 Posterior lobe of cerebellum, hemisphere

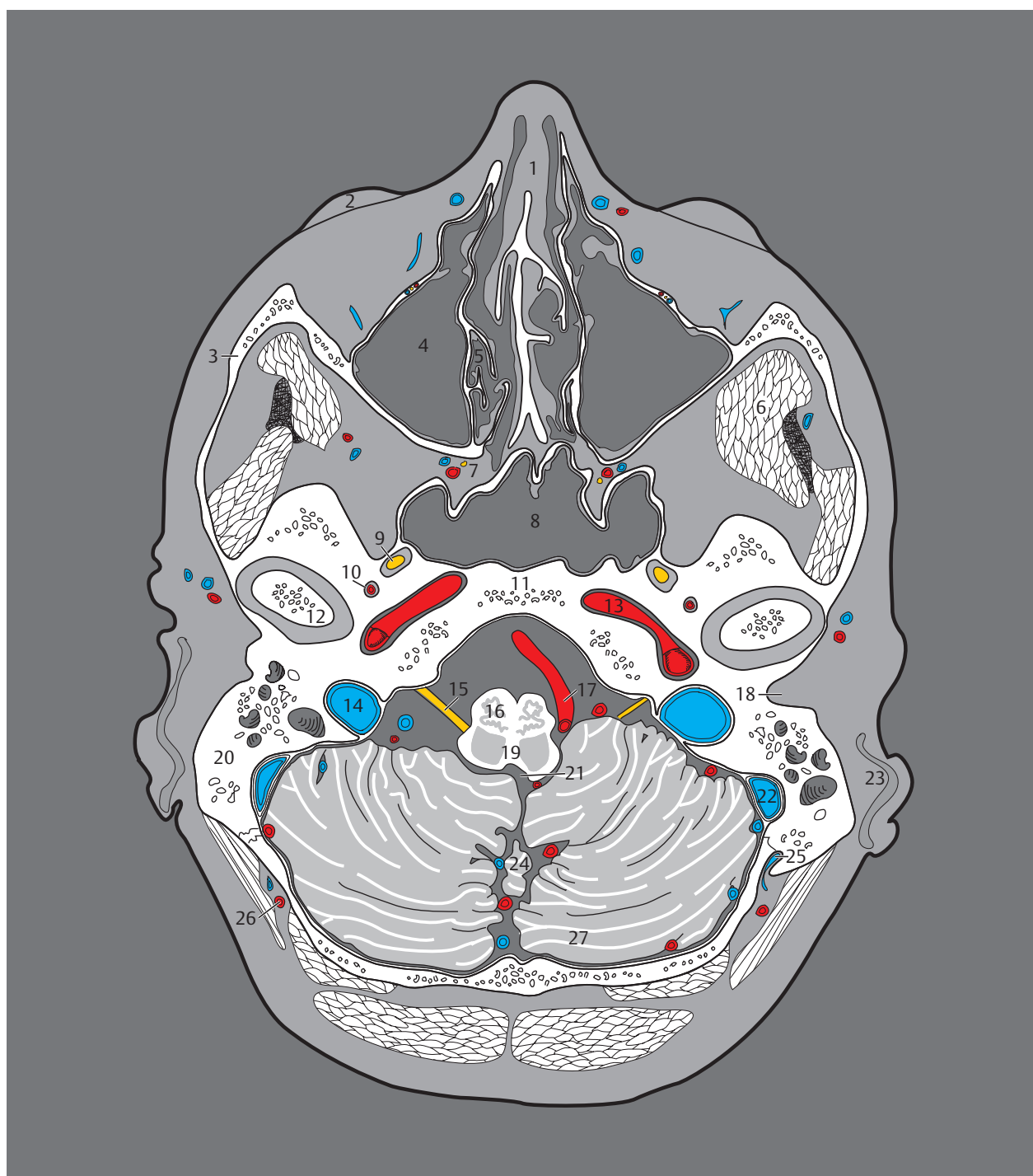
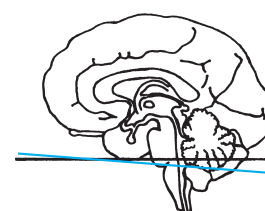
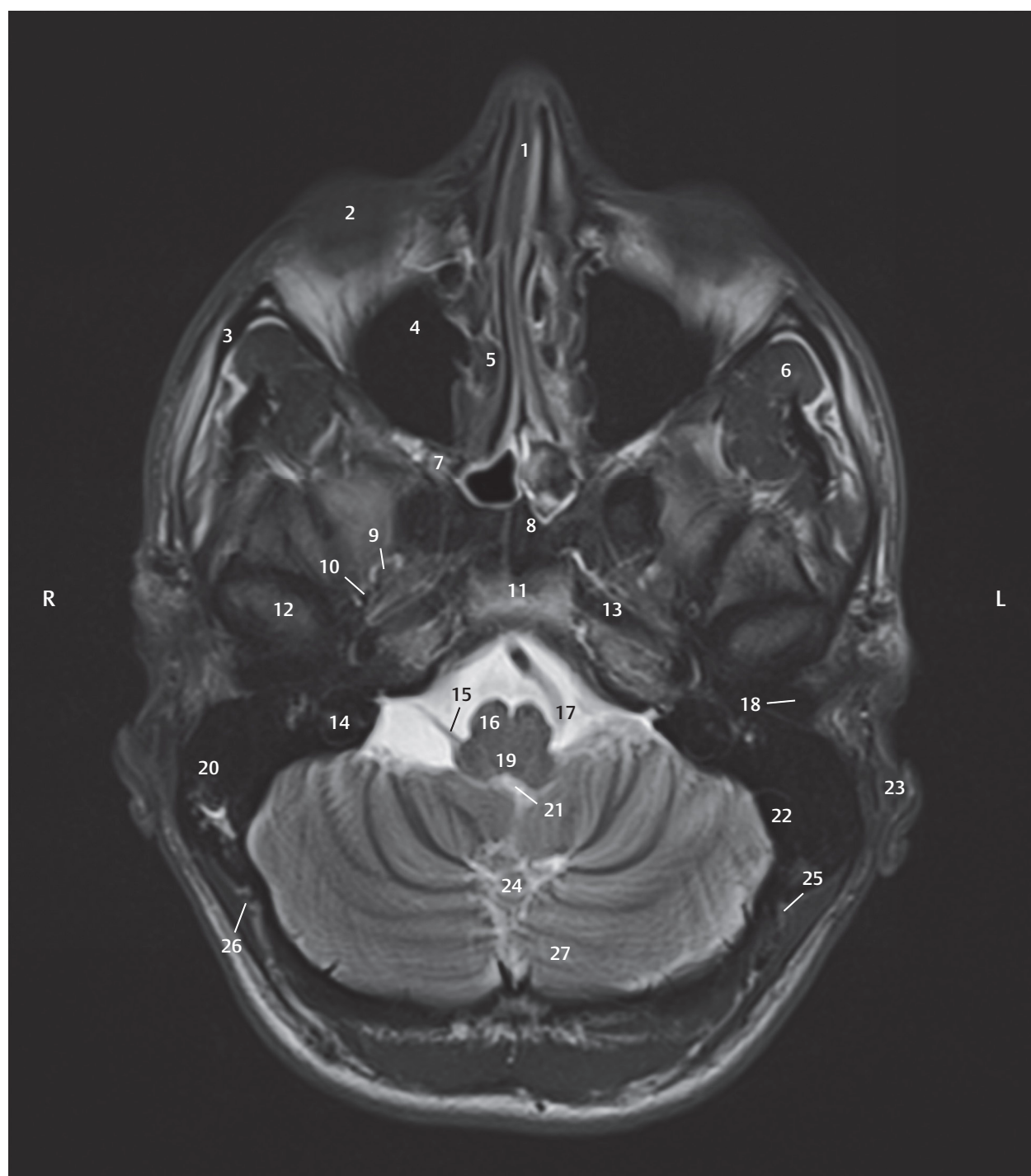


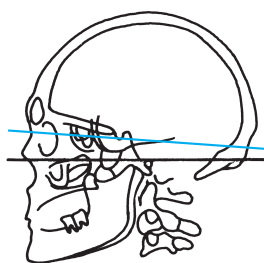
Fig. 5.4 3rd bicommissural section.

Fig. 5.4a View of the third section of the bicommissural MRI series. The sectional plane passes through the center of the lower margin of the eyeball, temporomandibular joints, and obliquely through the junction of the pons and medulla oblongata. Brain structures, blood vessels, and meninges.



- 1 Nasal septum
- 2 Eyeball
- 3 Zygomatic bone
- 4 Maxillary sinus
- 5 Ethmoidal air cells
- 6 Temporalis
- 7 Pterygopalatine fossa
- 8 Sphenoid sinus
- 9 Mandibular nerve
- 10 Foramen spinosum
- 11 Clivus
- 12 Head of mandible
- 13 Internal carotid artery
- 14 Bulb of jugular vein
- 15 Glossopharyngeal nerve/vagus nerve
- 16 Olive
- 17 Vertebral artery
- 18 External acoustic canal
- 19 Medulla oblongata
- 20 Mastoid
- 21 Fourth ventricle
- 22 Sigmoid sinus
- 23 External ear
- 24 Vermis
- 25 Emissary vein
- 26 Occipital artery
- 27 Posterior lobe of cerebellum, hemisphere

Fig. 5.4b T2w MR image oriented in the bicommissural plane, identical to the sectional plane in a.



- 1 Eyeball (with lens)
- 2 Zygomatic bone
- 3 Ophthalmic vein
- 4 Inferior rectus
- 5 Temporalis
- 6 Ethmoidal air cells
- 7 Pterygopalatine fossa
- 8 Sphenoid bone
- 9 Sphenoid sinus
- 10 Temporal lobe
- 11 Middle meningeal artery, frontal branch
- 12 Inferior temporal gyrus
- 13 Internal carotid artery
- 14 Cavernous sinus
- 15 Trigeminal nerve, Gasserian ganglion
- 16 Abducens nerve at the dural aperture
- 17 Basilar artery
- 18 Basilar sulcus
- 19 Cochlea
- 20 Anterior inferior cerebellar artery (AICA)
- 21 Pons
- 22 Internal acoustic canal
- 23 Facial nerve with intermediate nerve
- 24 Vestibulocochlear nerve
- 25 Temporal bone, petrous part
- 26 Posterior semicircular canal
- 27 Fourth ventricle
- 28 Middle cerebellar peduncle
- 29 Sigmoid sinus
- 30 Uvula of vermis (IX)
- 31 Vermis of cerebellum
- 32 Emissary vein
- 33 Posterior lobe of cerebellum, hemisphere
- 34 Occipital artery
- 35 Occipital bone

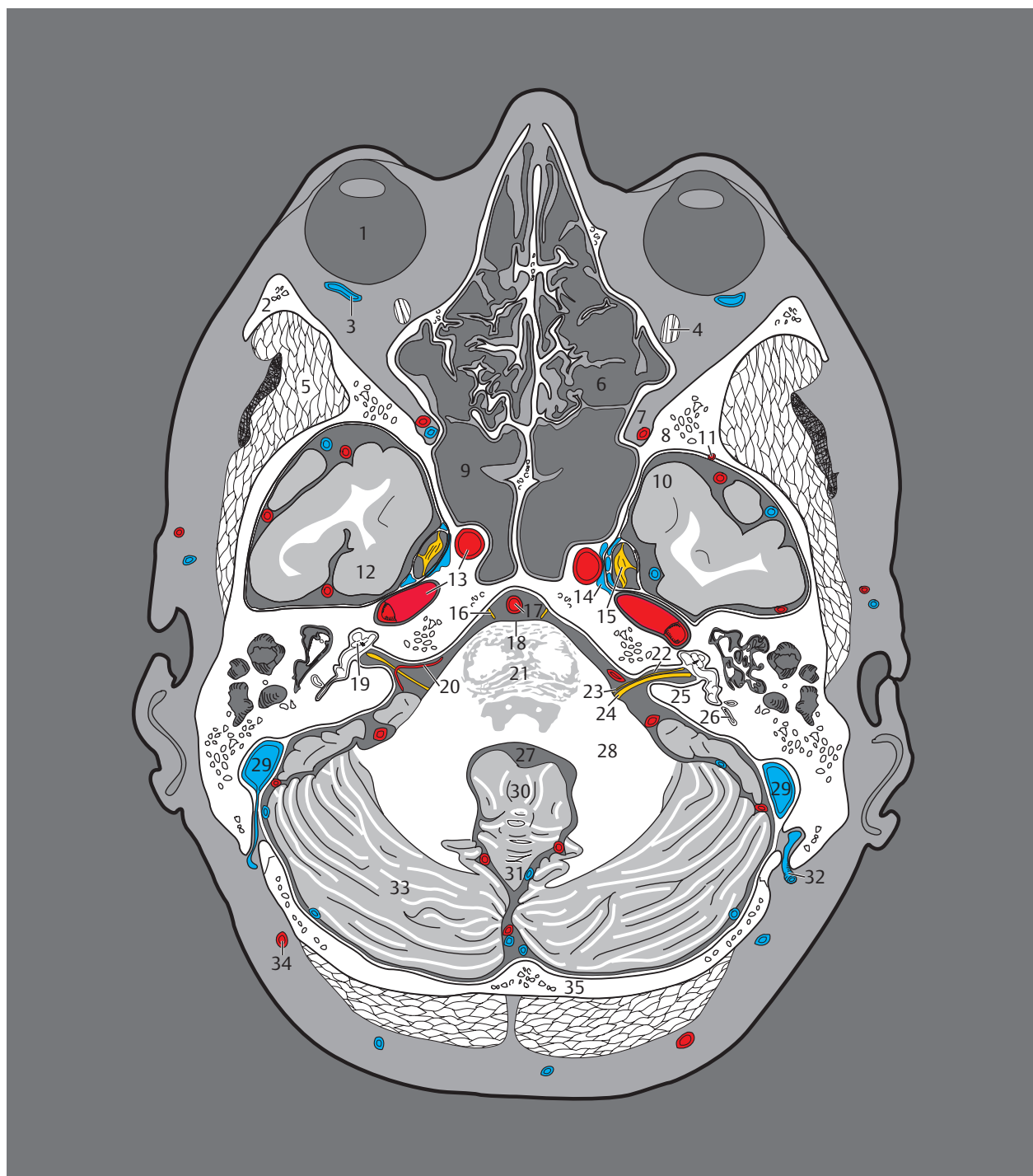
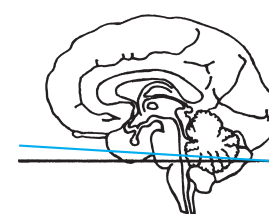


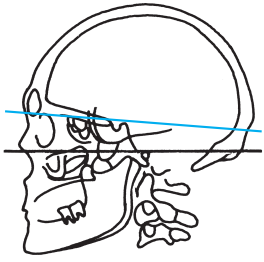
Fig. 5.5 4th bicommissural section.

Fig. 5.5a View of the fourth section of the bicommissural series. The temporal lobe has been sectioned in the middle cranial fossa while the pons and cerebellum have been sliced in the posterior cranial fossa. Brain structures, blood vessels, and meninges.



- 1 Eyeball (with lens)
- 2 Zygomatic bone
- 3 Ophthalmic vein
- 4 Inferior rectus
- 5 Temporalis
- 6 Ethmoidal air cells
- 7 Pterygopalatine fossa
- 8 Sphenoid bone
- 9 Sphenoid sinus
- 10 Temporal lobe
- 11 Middle meningeal artery, frontal branch
- 12 Inferior temporal gyrus
- 13 Internal carotid artery
- 14 Cavernous sinus
- 15 Trigeminal nerve, Gasserian ganglion
- 16 Abducens nerve at the dural aperture
- 17 Basilar artery
- 18 Basilar sulcus
- 19 Cochlea
- 20 Anterior inferior cerebellar artery (AICA)
- 21 Pons
- 22 Internal acoustic canal
- 23 Facial nerve with intermediate nerve
- 24 Vestibulocochlear nerve
- 25 Temporal bone, petrous part
- 26 Posterior semicircular canal
- 27 Fourth ventricle
- 28 Middle cerebellar peduncle
- 29 Sigmoid sinus
- 30 Uvula of vermis (IX)
- 31 Vermis of cerebellum
- 32 Emissary vein
- 33 Posterior lobe of cerebellum, hemisphere
- 34 Occipital artery
- 35 Occipital bone

Fig. 5.5b T2w MR image oriented in the bicommissural plane, identical to the sectional plane in a.



- 1 Frontal sinus
- 2 Ethmoidal air cells
- 3 Eyeball
- 4 Crista galli
- 5 Superior ophthalmic vein
- 6 Ophthalmic artery
- 7 Medial rectus
- 8 Medial frontobasal artery
- 9 Superior rectus
- 10 Temporalis
- 11 Straight gyrus
- 12 Olfactory bulb
(at the inferior edge
of the slice)
- 13 Sphenoid bone
- 14 Middle meningeal
artery, frontal branch
- 15 Temporal artery
- 16 Middle cerebral artery
- 17 Inferior temporal gyrus
- 18 Anterior clinoid process
- 19 Internal carotid artery
- 20 Optic chiasma
- 21 Infundibulum
- 22 Amygdaloid body
- 23 Hippocampus
- 24 Posterior communicating
artery
- 25 Basilar artery
- 26 Middle temporal gyrus
- 27 Posterior cerebral artery
- 28 Pons
- 29 Basal vein (of Rosenthal)
- 30 Parahippocampal gyrus
- 31 Tentorium of cerebellum
- 32 Locus caeruleus
- 33 Superior cerebellar artery
- 34 Fourth ventricle
- 35 Superior cerebellar
peduncle
- 36 Anterior lobe of cerebellum
- 37 Sigmoid sinus
- 38 External ear
- 39 Vermis of cerebellum
- 40 Lambdoid suture
- 41 Confluence of sinuses
- 42 Occipital bone
- 43 External occipital
protuberance (Inion)

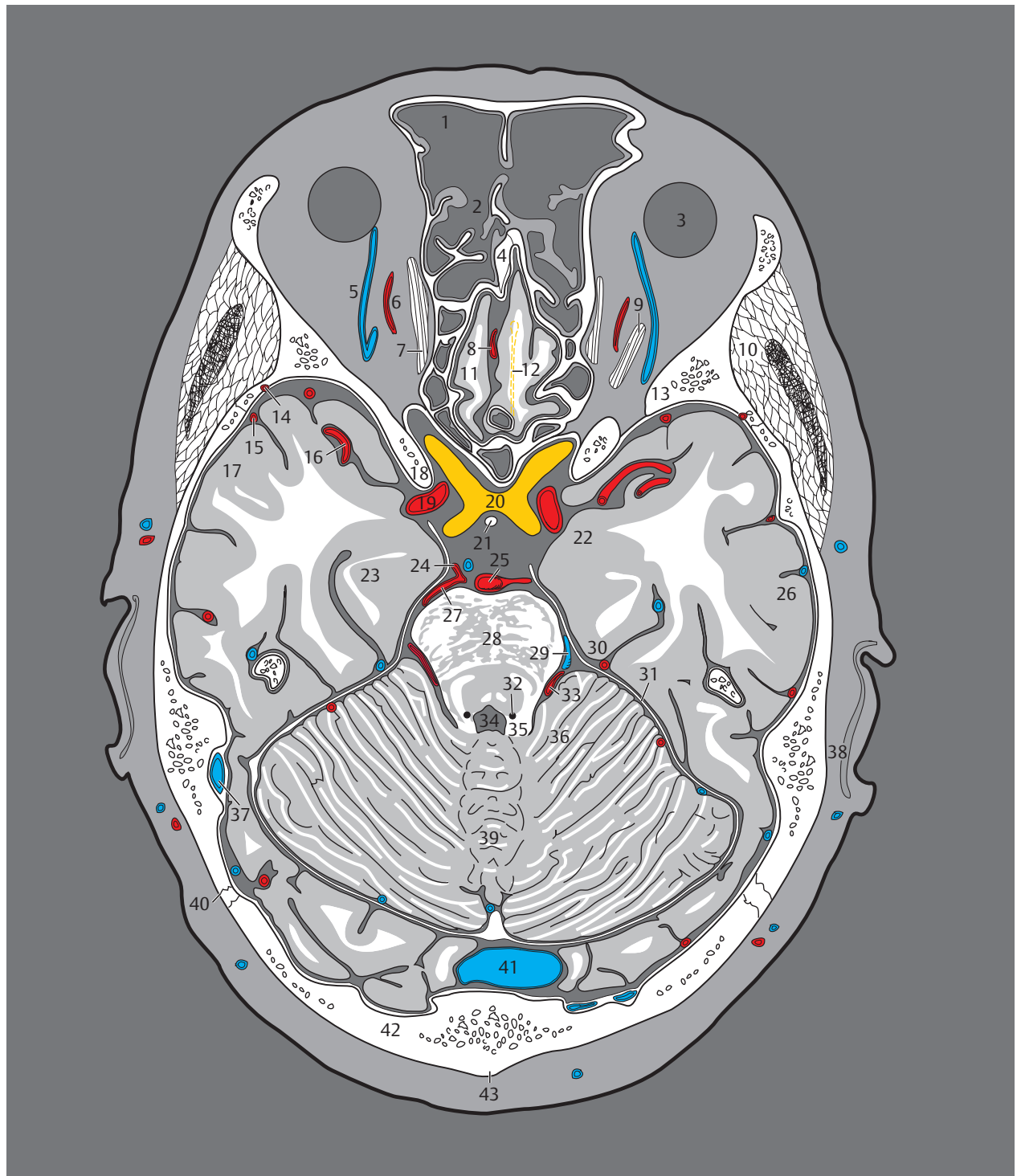
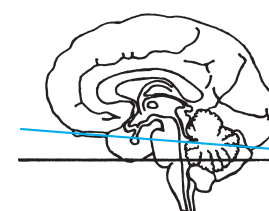
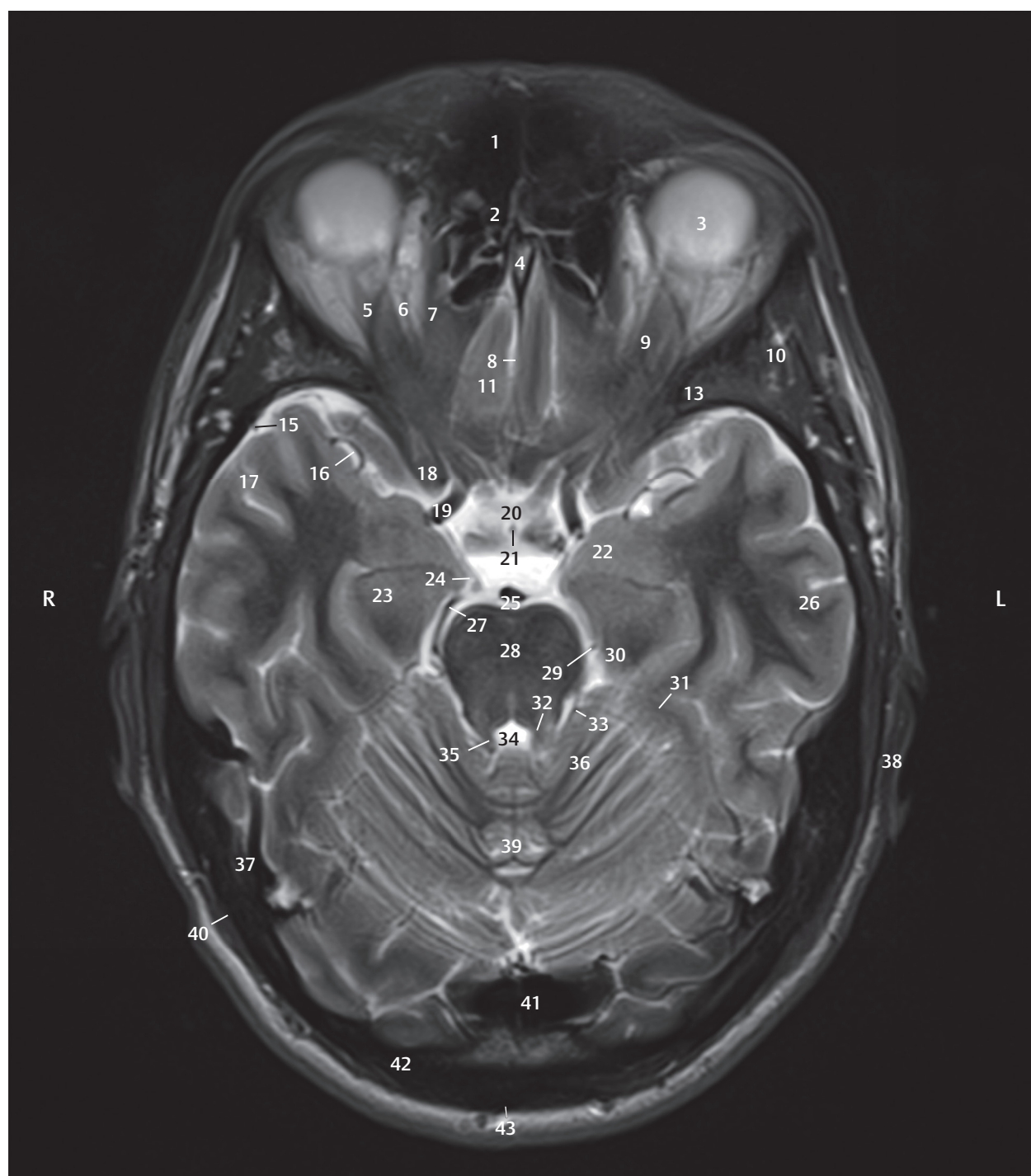


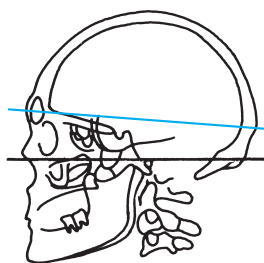
Fig. 5.6 5th bicommissural section.

Fig. 5.6a View of the fifth section of the bicommissural series. The sectional plane lies at the level of the entrance to the sella. On the left of the anterior cranial fossa, the olfactory bulb and tract have been indicated by a dotted line as located in the slice. These parts of the olfactory system lie in the olfactory groove. The frontal lobe, temporal lobe, infundibulum, mesencephalon, and cerebellum have been sectioned. Brain structures, blood vessels, and meninges.



- 1 Frontal sinus
- 2 Ethmoidal air cells
- 3 Eyeball
- 4 Crista galli
- 5 Superior ophthalmic vein
- 6 Ophthalmic artery
- 7 Medial rectus
- 8 Medial frontobasal artery
- 9 Superior rectus
- 10 Temporalis
- 11 Straight gyrus
- 13 Sphenoid bone
- 15 Temporal artery
- 16 Middle cerebral artery
- 17 Inferior temporal gyrus
- 18 Anterior clinoid process
- 19 Internal carotid artery
- 20 Optic chiasma
- 21 Infundibulum
- 22 Amygdaloid body
- 23 Hippocampus
- 24 Posterior communicating artery
- 25 Basilar artery
- 26 Middle temporal gyrus
- 27 Posterior cerebral artery
- 28 Pons
- 29 Basal vein (of Rosenthal)
- 30 Parahippocampal gyrus
- 31 Tentorium of cerebellum
- 32 Locus caeruleus
- 33 Superior cerebellar artery
- 34 Fourth ventricle
- 35 Superior cerebellar peduncle
- 36 Anterior lobe of cerebellum
- 37 Sigmoid sinus
- 38 External ear
- 39 Vermis of cerebellum
- 40 Lambdoid suture
- 41 Confluence of sinuses
- 42 Occipital bone
- 43 External occipital protuberance (Inion)

Fig. 5.6b T2w MR image oriented in the bicommissural plane, identical to the sectional plane in a.



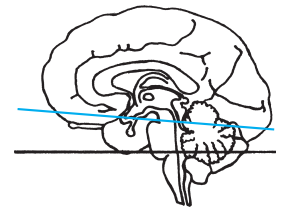
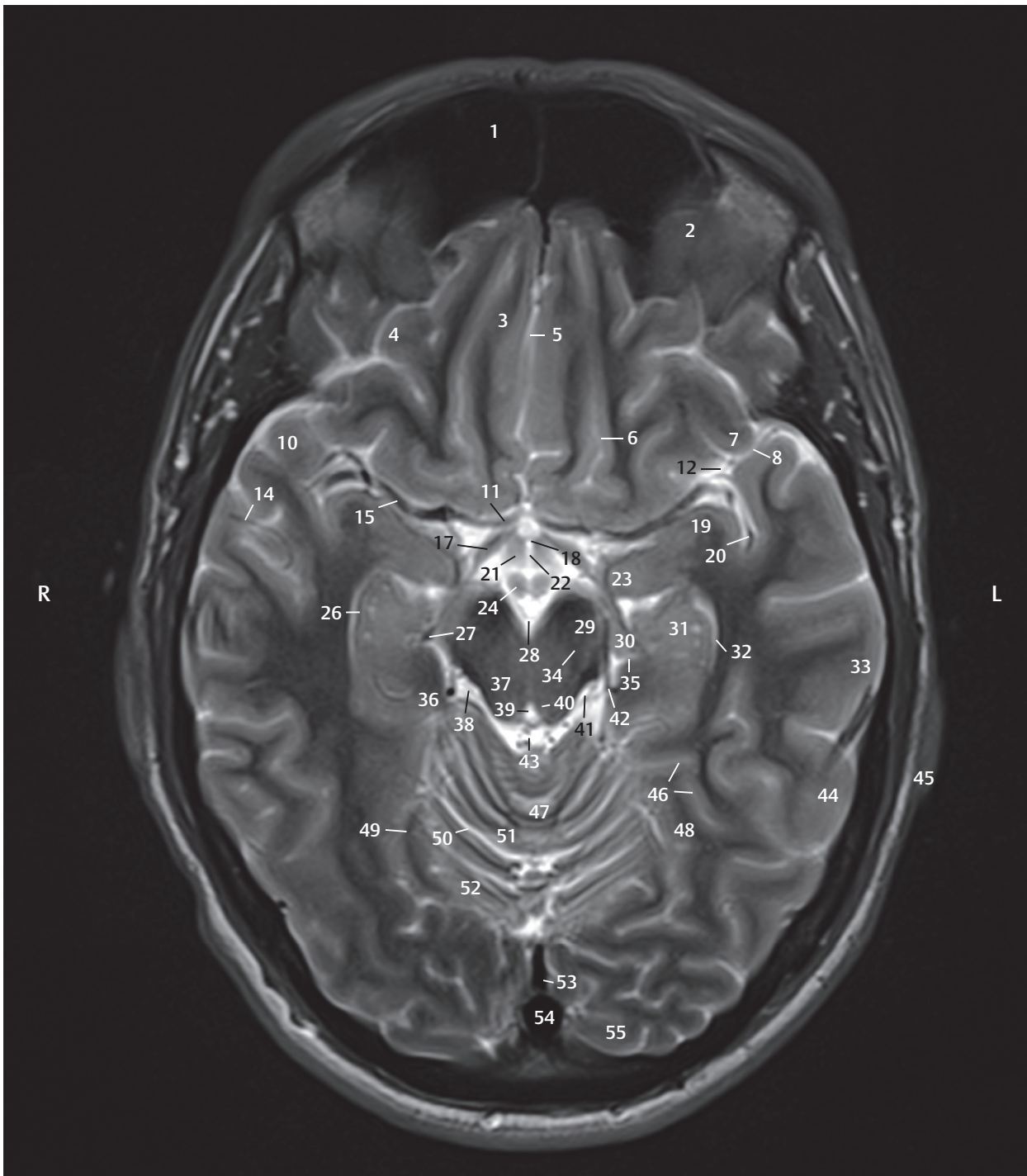
- 1 Frontal sinus
- 2 Frontal bone
- 3 Straight gyrus
- 4 Orbital gyri
- 5 Polar frontal artery
- 6 Olfactory sulcus
- 7 Inferior frontal gyrus
- 8 Lateral sulcus
- 9 Middle meningeal artery, branch
- 10 Superior temporal gyrus
- 11 Anterior cerebral artery
- 12 Cistern of lateral cerebral fossa
- 13 Superficial middle cerebral vein
- 14 Temporal artery
- 15 Middle cerebral artery
- 16 Anterolateral central arteries (lateral lenticulostriate arteries)
- 17 Optic tract
- 18 Lamina terminalis
- 19 Semilunar gyrus
- 20 Insular arteries
- 21 Hypothalamus
- 22 Third ventricle
- 23 Amygdaloid body
- 24 Mammillary body
- 25 Basilar artery
- 26 Alveus of hippocampus
- 27 Posterior cerebral artery
- 28 Interpeduncular cistern
- 29 Cerebral crus
- 30 Parahippocampal gyrus, uncus
- 31 Hippocampus
- 32 Lateral ventricle, temporal horn
- 33 Middle temporal gyrus
- 34 Substantia nigra
- 35 Hippocampal sulcus
- 36 Parahippocampal gyrus
- 37 Tegmentum of midbrain
- 38 Ambient cistern
- 39 Opening of the aqueduct of the midbrain in the fourth ventricle
- 40 Locus caeruleus
- 41 Medial occipital artery
- 42 Basal vein (of Rosenthal)
- 43 Quadrigeminal cistern
- 44 Inferior temporal gyrus
- 45 External ear
- 46 Collateral sulcus
- 47 Anterior lobe of cerebellum, vermis of cerebellum



- 48 Lateral occipitotemporal gyrus
- 49 Tentorium of cerebellum
- 50 Primary fissure
- 51 Anterior lobe of cerebellum, hemisphere
- 52 Posterior lobe of cerebellum, hemisphere
- 53 Straight sinus
- 54 Confluence of sinuses
- 55 Occipital gyri

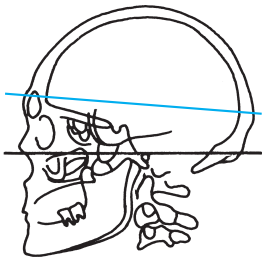
Fig. 5.7 6th bicommissural section.

Fig. 5.7a View of the sixth section of the bicommissural series. The frontal lobe, temporal lobe, hypothalamus, midbrain, cerebellum, and occipital lobe are seen in cut-section in this plane. Brain structures, blood vessels, and meninges.

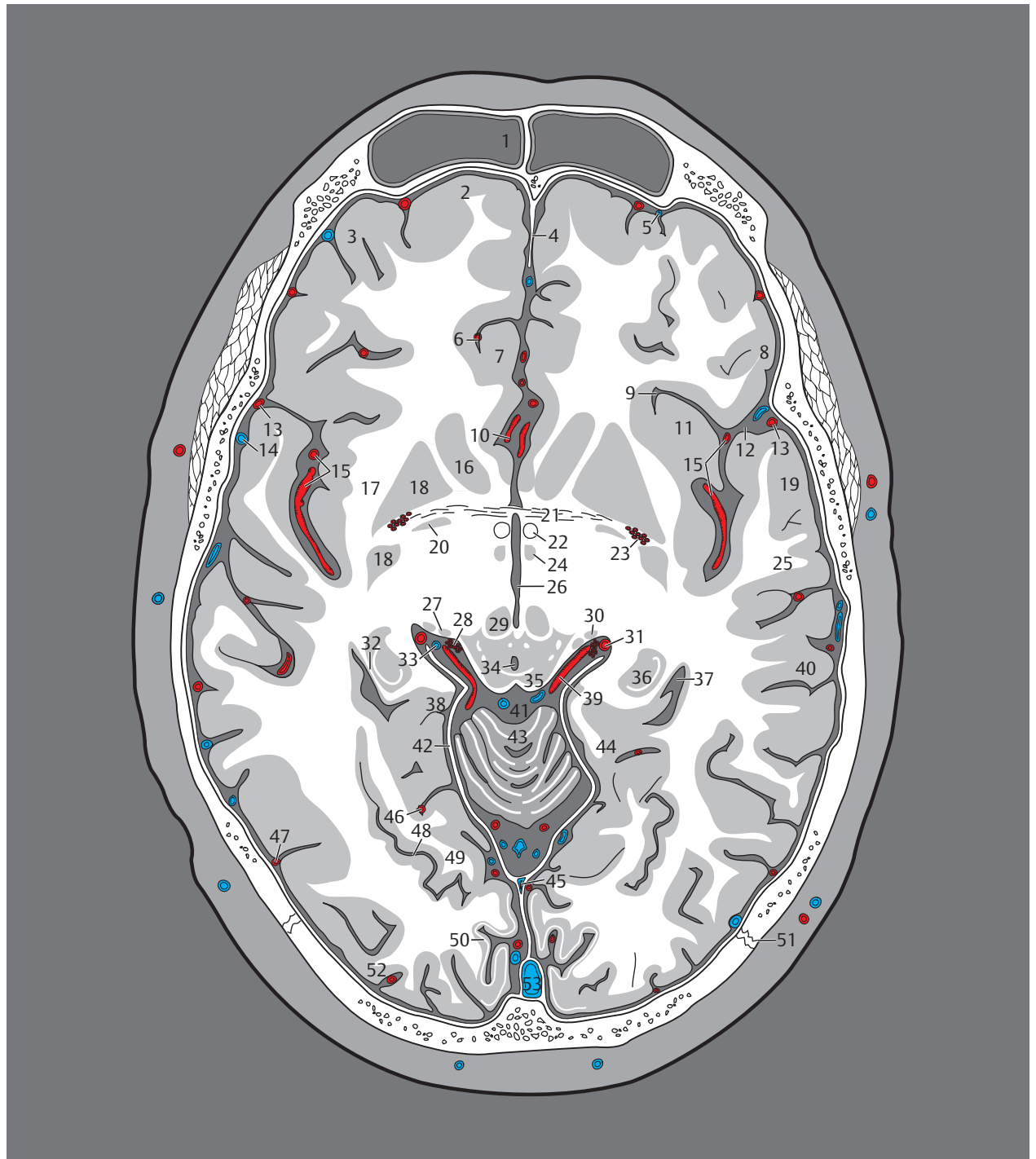


- 1 Frontal sinus
- 2 Frontal bone
- 3 Straight gyrus
- 4 Orbital gyri
- 5 Polar frontal artery
- 6 Olfactory sulcus
- 7 Inferior frontal gyrus
- 8 Lateral sulcus
- 10 Superior temporal gyrus
- 11 Anterior cerebral artery
- 12 Cistern of lateral cerebral fossa
- 14 Temporal artery
- 15 Middle cerebral artery
- 17 Optic tract
- 18 Lamina terminalis
- 19 Semilunar gyrus
- 20 Insular arteries
- 21 Hypothalamus
- 22 Third ventricle
- 23 Amygdaloid body
- 24 Mammillary body
- 26 Alveus of hippocampus
- 27 Posterior cerebral artery
- 28 Interpeduncular cistern
- 29 Cerebral crus
- 30 Parahippocampal gyrus, uncus
- 31 Hippocampus
- 32 Lateral ventricle, temporal horn
- 33 Middle temporal gyrus
- 34 Substantia nigra
- 35 Hippocampal sulcus
- 36 Parahippocampal gyrus
- 37 Tegmentum of midbrain
- 38 Ambient cistern
- 39 Opening of the aqueduct of the midbrain in the fourth ventricle
- 40 Locus caeruleus
- 41 Medial occipital artery
- 42 Basal vein (of Rosenthal)
- 43 Quadrigeminal cistern
- 44 Inferior temporal gyrus
- 45 External ear
- 46 Collateral sulcus
- 47 Anterior lobe of cerebellum, vermis of cerebellum
- 48 Lateral occipitotemporal gyrus
- 49 Tentorium of cerebellum
- 50 Primary fissure
- 51 Anterior lobe of cerebellum, hemisphere
- 52 Posterior lobe of cerebellum, hemisphere
- 53 Straight sinus
- 54 Confluence of sinuses
- 55 Occipital gyri

Fig. 5.7b T2w MR image oriented in the bicommissural plane, with a sectional plane identical to that in a.



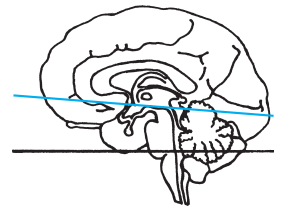
- 1 Frontal sinus
- 2 Superior frontal gyrus at the frontal pole
- 3 Middle frontal gyrus
- 4 Falx cerebri
- 5 Bridging veins
- 6 Anteromedial frontal artery
- 7 Cingulate gyrus
- 8 Inferior frontal gyrus
- 9 Circular sulcus of insula
- 10 Anterior cerebral artery
- 11 Insula
- 12 Lateral sulcus
- 13 Temporal artery
- 14 Superficial middle cerebral vein
- 15 Insular arteries
- 16 Head of caudate nucleus
- 17 External capsule
- 18 Putamen
- 19 Temporal lobe
- 20 Globus pallidus
- 21 Anterior commissure
- 22 Column of fornix
- 23 Anterolateral and anteromedial central arteries
- 24 Hypothalamus
- 25 Superior temporal gyrus
- 26 Third ventricle
- 27 Medial geniculate body
- 28 Medial and lateral posterior choroidal arteries
- 29 Red nucleus
- 30 Lateral geniculate body
- 31 Medial occipital artery
- 32 Alveus of hippocampus
- 33 Basal vein (of Rosenthal)
- 34 Aqueduct of midbrain
- 35 Superior colliculus
- 36 Hippocampus
- 37 Lateral ventricle, temporal horn
- 38 Parahippocampal gyrus
- 39 Posterior cerebral artery
- 40 Middle temporal gyrus
- 41 Quadrigeminal cistern
- 42 Tentorium of cerebellum
- 43 Anterior lobe, vermis of cerebellum



- 44 Lateral occipitotemporal gyrus
- 45 Straight sinus
- 46 Lateral occipital artery
- 47 Lateral occipital artery, branch
- 48 Collateral sulcus
- 49 Medial occipitotemporal gyrus
- 50 Area striata
- 51 Lambdoid suture
- 52 Occipital gyri
- 53 Superior sagittal sinus

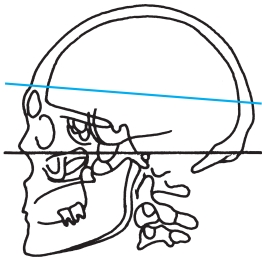
Fig. 5.8 7th bicommissural section.

Fig. 5.8a View of the seventh section of the bicommissural series. The striatum (putamen and caudate nucleus), hypothalamus, and inferior thalamus have been depicted. Only a small part of the infratentorial region is still included in this section. Brain structures, blood vessels, and meninges.

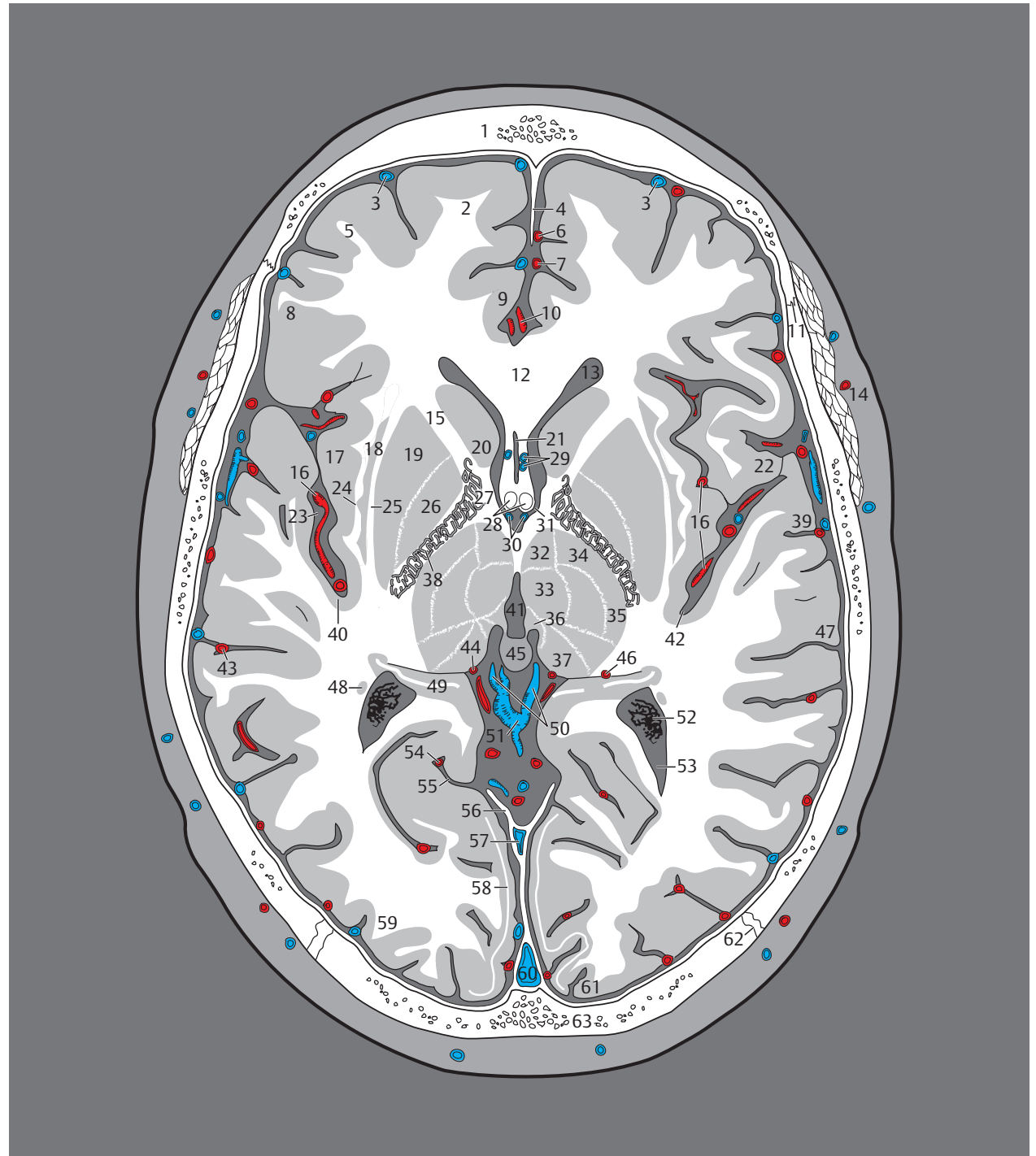


- 1 Frontal sinus
- 2 Superior frontal gyrus at the frontal pole
- 3 Middle frontal gyrus
- 4 Falx cerebri
- 5 Bridging veins
- 7 Cingulate gyrus
- 8 Inferior frontal gyrus
- 9 Circular sulcus of insula
- 10 Anterior cerebral artery
- 11 Insula
- 12 Lateral sulcus
- 13 Temporal artery
- 14 Superficial middle cerebral vein
- 15 Insular arteries
- 16 Head of caudate nucleus
- 17 External capsule
- 18 Putamen
- 19 Temporal lobe
- 20 Globus pallidus (section)
- 21 Anterior commissure
- 22 Column of fornix
- 23 Anterolateral and anteromedial central arteries with prominent perivascular spaces (Virchow-Robin spaces)
- 24 Hypothalamus
- 25 Superior temporal gyrus
- 26 Third ventricle
- 27 Medial geniculate body
- 28 Medial and lateral posterior choroidal arteries
- 29 Red nucleus
- 30 Lateral geniculate body
- 31 Medial occipital artery
- 32 Alveus of hippocampus
- 33 Basal vein (of Rosenthal)
- 34 Aqueduct of midbrain
- 35 Superior colliculus
- 36 Hippocampus
- 37 Lateral ventricle, temporal horn
- 38 Parahippocampal gyrus
- 39 Posterior cerebral artery
- 40 Middle temporal gyrus
- 41 Quadrigeminal cistern
- 42 Cerebellar tentorium
- 43 Anterior lobe, vermis of cerebellum
- 44 Lateral occipitotemporal gyrus
- 45 Straight sinus
- 47 Lateral occipital artery, branch
- 48 Collateral sulcus
- 49 Medial occipitotemporal gyrus
- 51 Lambdoid suture
- 52 Occipital gyri
- 53 Superior sagittal sinus

Fig. 5.8b T2w MR image oriented in the bicommissural plane, identical to the sectional plane in a.



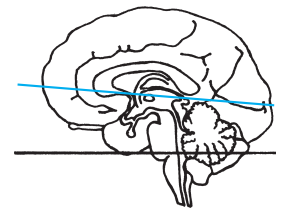
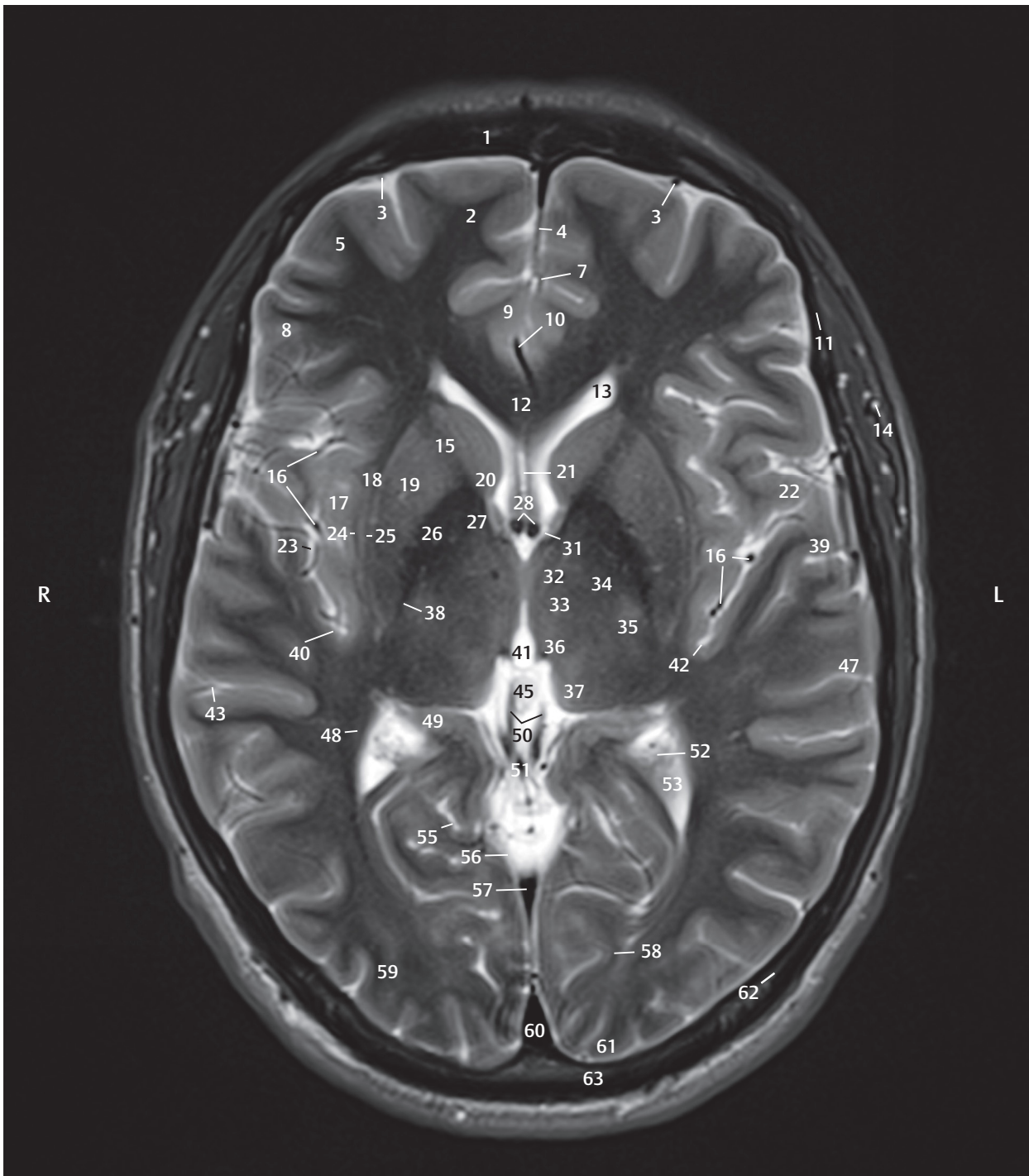
- 1 Frontal bone
- 2 Superior frontal gyrus
- 3 Superior cerebral vein
- 4 Falx cerebri
- 5 Middle frontal gyrus
- 6 Anteromedial frontal artery
- 7 Callosomarginal artery
- 8 Inferior frontal gyrus
- 9 Cingulate gyrus
- 10 Anterior cerebral artery
- 11 Coronal suture
- 12 Corpus callosum, genu
- 13 Lateral ventricle, frontal horn
- 14 Superficial temporal artery
- 15 Internal capsule, anterior limb
- 16 Insular arteries
- 17 Insula
- 18 Claustrum
- 19 Putamen
- 20 Head of caudate nucleus
- 21 Cavity of septum pellucidum
- 22 Precentral gyrus
- 23 Cistern of lateral cerebral fossa
- 24 Extreme capsule
- 25 External capsule
- 26 Globus pallidus
- 27 Internal capsule, genu
- 28 Column of fornix
- 29 Anterior vein of septum pellucidum
- 30 Internal cerebral vein
- 31 Interventricular foramen (Monro)
- 32 Anterior nuclei of thalamus
- 33 Medial nuclei of thalamus
- 34 Ventral lateral nuclei of thalamus
- 35 Lateral posterior nuclei of thalamus
- 36 Habenular nuclei
- 37 Pulvinar nuclei of thalamus
- 38 Internal capsule, posterior limb
- 39 Superior temporal gyrus
- 40 Transverse temporal gyri (Heschl's gyri)
- 41 Third ventricle



- 42 Circular sulcus of insula
- 43 Temporo-occipital artery
- 44 Posteromedial choroid artery
- 45 Pineal gland
- 46 Posterolateral choroid artery
- 47 Middle temporal gyrus
- 48 Tail of caudate nucleus
- 49 Hippocampus
- 50 Internal cerebral veins
- 51 Great cerebral vein (Galen)
- 52 Choroid plexus of lateral ventricle
- 53 Lateral ventricle, collateral trigone
- 54 Medial occipital artery
- 55 Parieto-occipital sulcus
- 56 Tentorium of cerebellum
- 57 Straight sinus
- 58 Area striata
- 59 Occipital gyri
- 60 Superior sagittal sinus
- 61 Occipital pole
- 62 Lambdoid suture
- 63 Occipital bone

Fig. 5.9 9th bicommissural section.

Fig. 5.9a View of the ninth section of the bicommissural series. The insula reaches its largest expanse in this section. The sectional plane also passes through the striatum (putamen and caudate nucleus), internal capsule, and thalamus. Brain structures, blood vessels, and meninges.



- 1 Frontal bone
- 2 Superior frontal gyrus
- 3 Superior cerebral vein
- 4 Falx cerebri
- 5 Middle frontal gyrus
- 7 Callosomarginal artery
- 8 Inferior frontal gyrus
- 9 Cingulate gyrus
- 10 Anterior cerebral artery
- 11 Coronal suture
- 12 Corpus callosum, genu
- 13 Lateral ventricle, frontal horn
- 14 Superficial temporal artery
- 15 Internal capsule, anterior limb
- 16 Insular arteries
- 17 Insula
- 18 Claustrum
- 19 Putamen
- 20 Head of caudate nucleus
- 21 Cavity of septum pellucidum
- 22 Precentral gyrus
- 23 Cistern of lateral cerebral fossa
- 24 Extreme capsule
- 25 External capsule
- 26 Globus pallidus
- 27 Internal capsule, genu
- 28 Column of fornix
- 31 Interventricular foramen (Monro)
- 32 Anterior nuclei of thalamus
- 33 Medial nuclei of thalamus
- 34 Ventral lateral nuclei of thalamus
- 35 Lateral posterior nuclei of thalamus
- 36 Habenular nuclei
- 37 Pulvinar nuclei of thalamus
- 38 Internal capsule, posterior limb
- 39 Superior temporal gyrus
- 40 Transverse temporal gyri (Heschl's gyri)
- 41 Third ventricle
- 42 Circular sulcus of insula
- 43 Temporo-occipital artery
- 45 Pineal gland
- 47 Middle temporal gyrus
- 48 Tail of caudate nucleus
- 49 Hippocampus
- 50 Internal cerebral veins
- 51 Great cerebral vein (Galen)

Fig. 5.9b T2w MR image oriented in the bicommissural plane, corresponding exactly to the selected sectional plane in a.

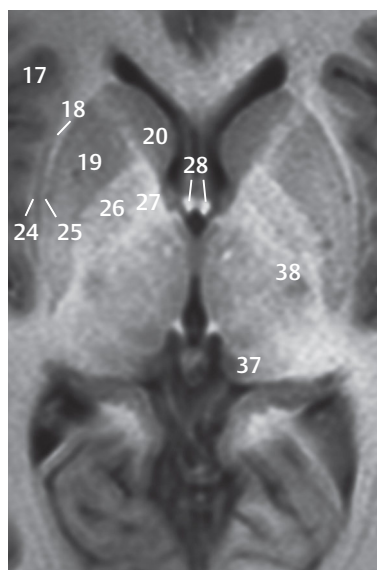
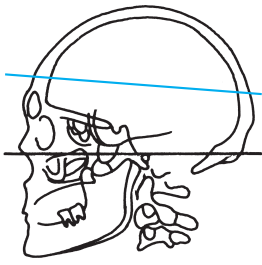


Fig. 5.9c T1w view detail of the eighth section of the bicommissural series. The basal ganglia regions are well demarcated from each other on the T1w sequence.



- 1 Frontal bone
- 2 Superior frontal gyrus
- 3 Superior cerebral vein
- 4 Prefrontal artery
- 5 Middle frontal gyrus
- 6 Falx cerebri
- 7 Callosomarginal artery
- 8 Cingulate sulcus
- 9 Cingulate gyrus
- 10 Minor forceps (frontal)
- 11 Inferior frontal gyrus
- 12 Coronal suture
- 13 Pericallosal artery
- 14 Corpus callosum, genu
- 15 Lateral ventricle, frontal horn
- 16 Artery of precentral sulcus
- 17 Precentral gyrus
- 18 Head of caudate nucleus
- 19 Superior choroid vein
- 20 Insula
- 21 Insular arteries
- 22 Putamen
- 23 Internal capsule, anterior limb
- 24 Superior thalamostriate vein
- 25 Lateral ventricle, body
- 26 Artery of central sulcus
- 27 Central sulcus
- 28 Cistern of lateral cerebral fossa
- 29 Internal capsule, posterior limb
- 30 Fornix
- 31 Thalamus
- 32 Postcentral gyrus
- 33 Superior temporal gyrus
- 34 Artery of angular gyrus
- 35 Posterolateral choroid artery
- 36 Tail of caudate nucleus
- 37 Lateral sulcus, posterior ramus
- 38 Lateral ventricle, occipital horn
- 39 Choroid plexus
- 40 Corpus callosum, splenium
- 41 Parietal artery
- 42 Major forceps (occipital)
- 43 Straight sinus
- 44 Parieto-occipital sulcus
- 45 Parietal bone
- 46 Parieto-occipital artery
- 47 Cuneus
- 48 Area striata
- 49 Calcarine artery
- 50 Occipital gyri
- 51 Superior sagittal sinus
- 52 Lambdoid suture
- 53 Occipital bone

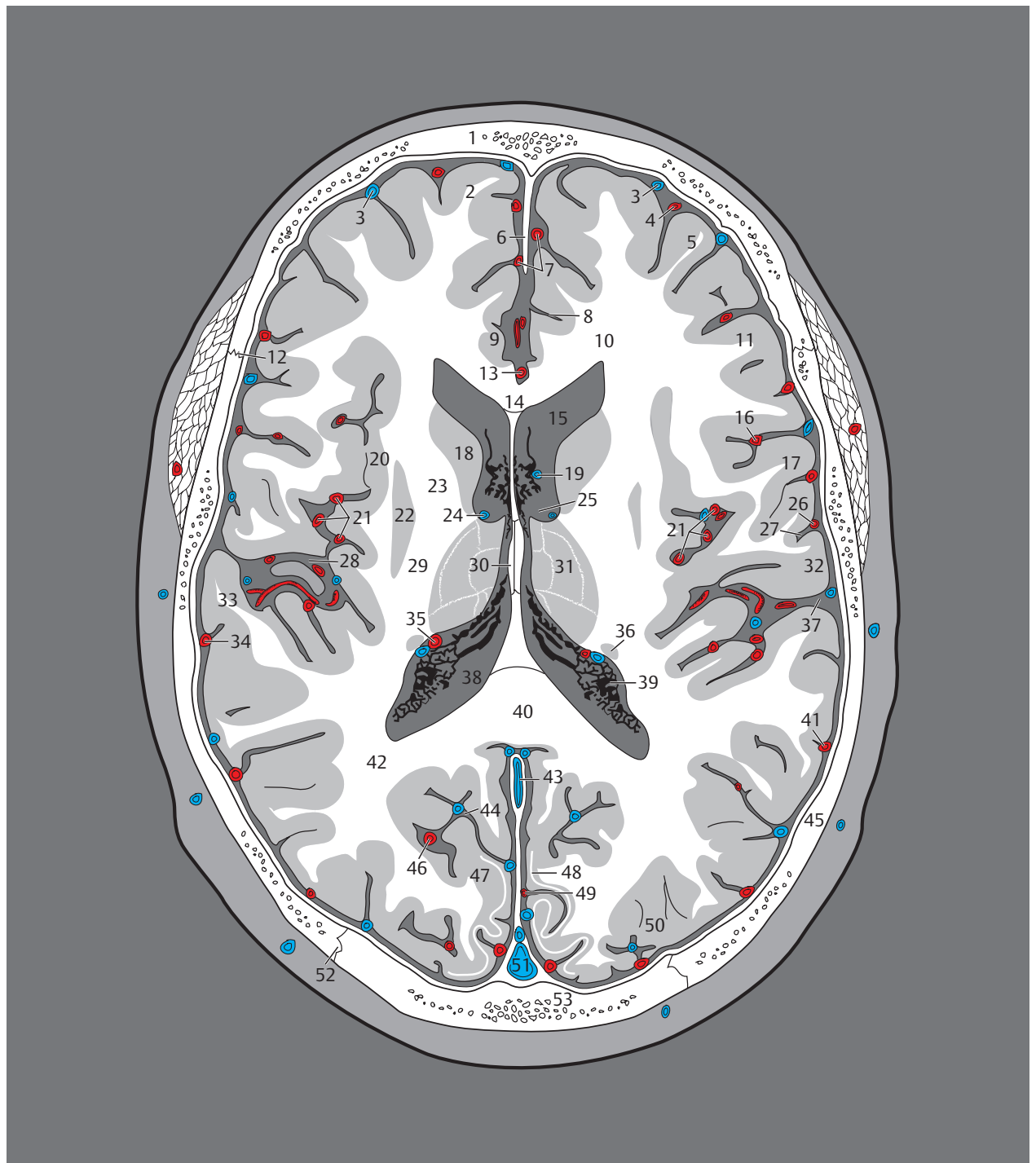
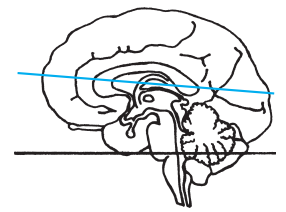
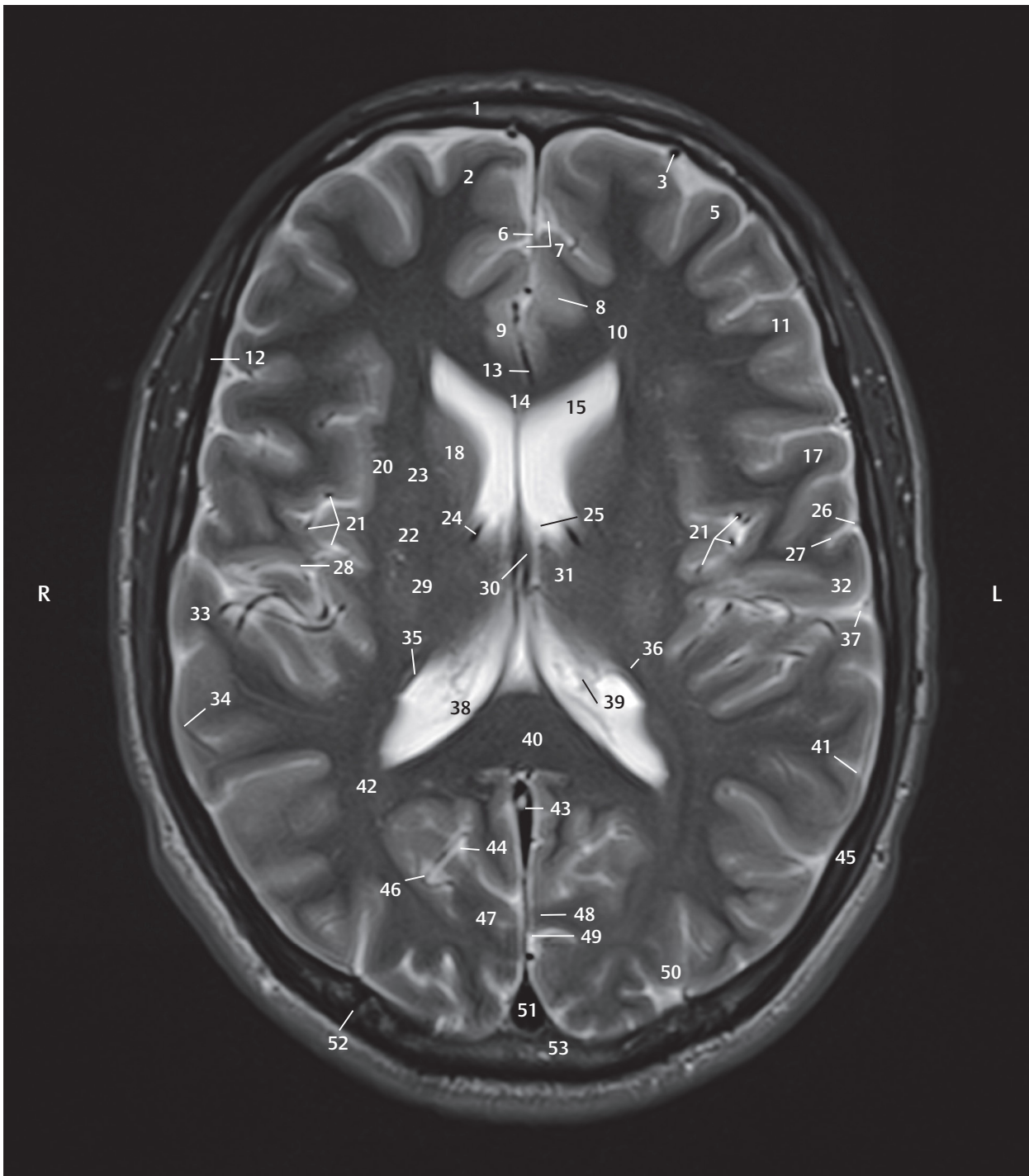


Fig. 5.10 9th bicommissural section.

Fig. 5.10a View of the ninth section of the bicommissural series. The sectional plane separates the falx cerebri into anterior and posterior parts. The superior part of the insula has been sectioned. The splenium of the corpus callosum is located between the collateral trigone of the right and left ventricles. Brain structures, blood vessels, and meninges.



- 1 Frontal bone
- 2 Superior frontal gyrus
- 3 Superior cerebral vein
- 5 Middle frontal gyrus
- 6 Falx cerebri
- 7 Callosomarginal artery
- 8 Cingulate sulcus
- 9 Cingulate gyrus
- 10 Minor forceps (frontal)
- 11 Inferior frontal gyrus
- 12 Coronal suture
- 13 Pericallosal artery
- 14 Corpus callosum, genu
- 15 Lateral ventricle, frontal horn
- 17 Precentral gyrus
- 18 Head of caudate nucleus
- 20 Insula
- 21 Insular arteries
- 22 Putamen
- 23 Internal capsule, anterior limb
- 24 Superior thalamostriate vein
- 25 Lateral ventricle, body
- 26 Artery of central sulcus
- 27 Central sulcus
- 28 Cistern of lateral cerebral fossa
- 29 Internal capsule, posterior limb
- 30 Fornix
- 31 Thalamus
- 32 Postcentral gyrus
- 33 Superior temporal gyrus
- 34 Artery of angular gyrus
- 35 Posterolateral choroid artery
- 36 Tail of caudate nucleus
- 37 Lateral sulcus, posterior ramus
- 38 Lateral ventricle, occipital horn
- 39 Choroid plexus
- 40 Corpus callosum, splenium
- 41 Parietal artery
- 42 Major forceps (occipital)
- 43 Straight sinus
- 44 Parieto-occipital sulcus
- 45 Parietal bone
- 46 Parieto-occipital artery
- 47 Cuneus
- 48 Area striata
- 49 Calcarine artery
- 50 Occipital gyri
- 51 Superior sagittal sinus
- 52 Lambdoid suture
- 53 Occipital bone

Fig. 5.10b T2w MR image oriented in the bicommissural plane, corresponding exactly to the selected sectional plane in a.

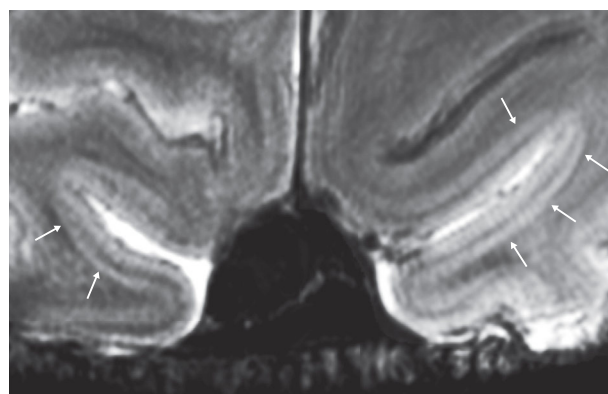
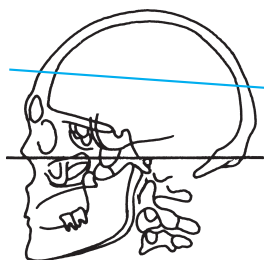


Fig. 5.10c Detail section of a transverse 7T-T2w MR image. The area striata is well delineated (the so-called Gennari stripe; arrows) and is as hyperintense as the cortex. (With kind permission of Prof. Forsting, University Hospital, Essen, Germany.)



- 1 Frontal bone
- 2 Superior sagittal sinus
- 3 Superior frontal gyrus
- 4 Superior cerebral vein
- 5 Middle frontal gyrus
- 6 Intermediomedial frontal artery
- 7 Falx cerebri
- 8 Prefrontal artery
- 9 Cingulate sulcus
- 10 Coronal suture
- 11 Callosomarginal artery
- 12 Pericallosal artery
- 13 Cingulate gyrus
- 14 Cingulum
- 15 Precentral sulcus
- 16 Artery of precentral sulcus
- 17 Precentral gyrus
- 18 Artery of central sulcus
- 19 Central sulcus
- 20 Lateral ventricle, body
- 21 Centrum semiovale
- 22 Postcentral gyrus
- 23 Postcentral sulcus
- 24 Parietal bone
- 25 Parietal artery
- 26 Inferior sagittal sinus
- 27 Supramarginal gyrus
- 28 Angular gyrus
- 29 Artery of angular gyrus
- 30 Precuneus
- 31 Parieto-occipital artery
- 32 Parieto-occipital sulcus
- 33 Occipital gyri
- 34 Cuneus
- 35 Superior sagittal sinus
- 36 Lambdoid suture
- 37 Occipital bone

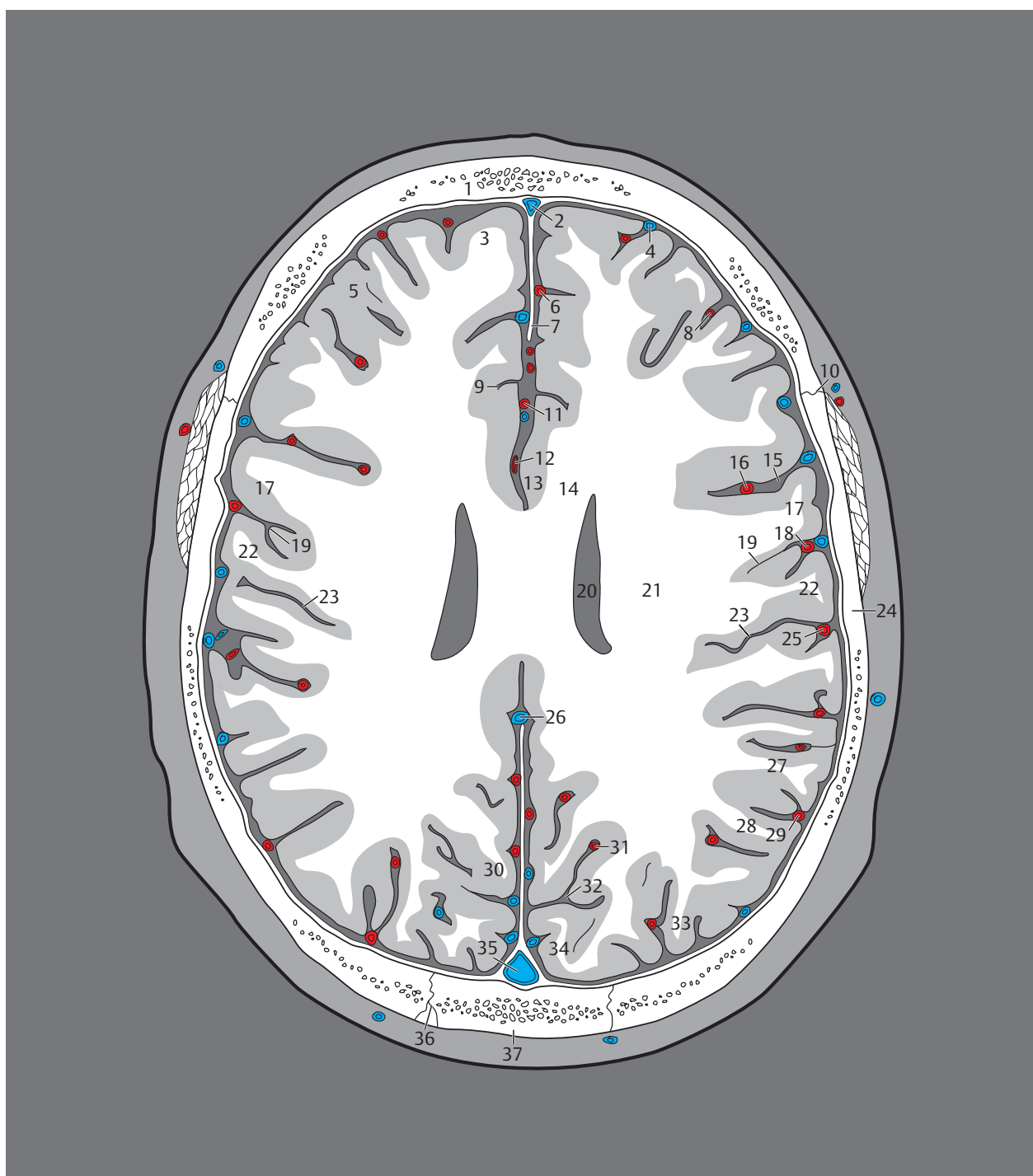
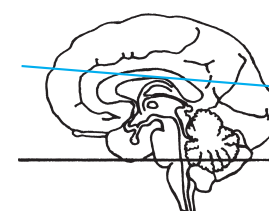
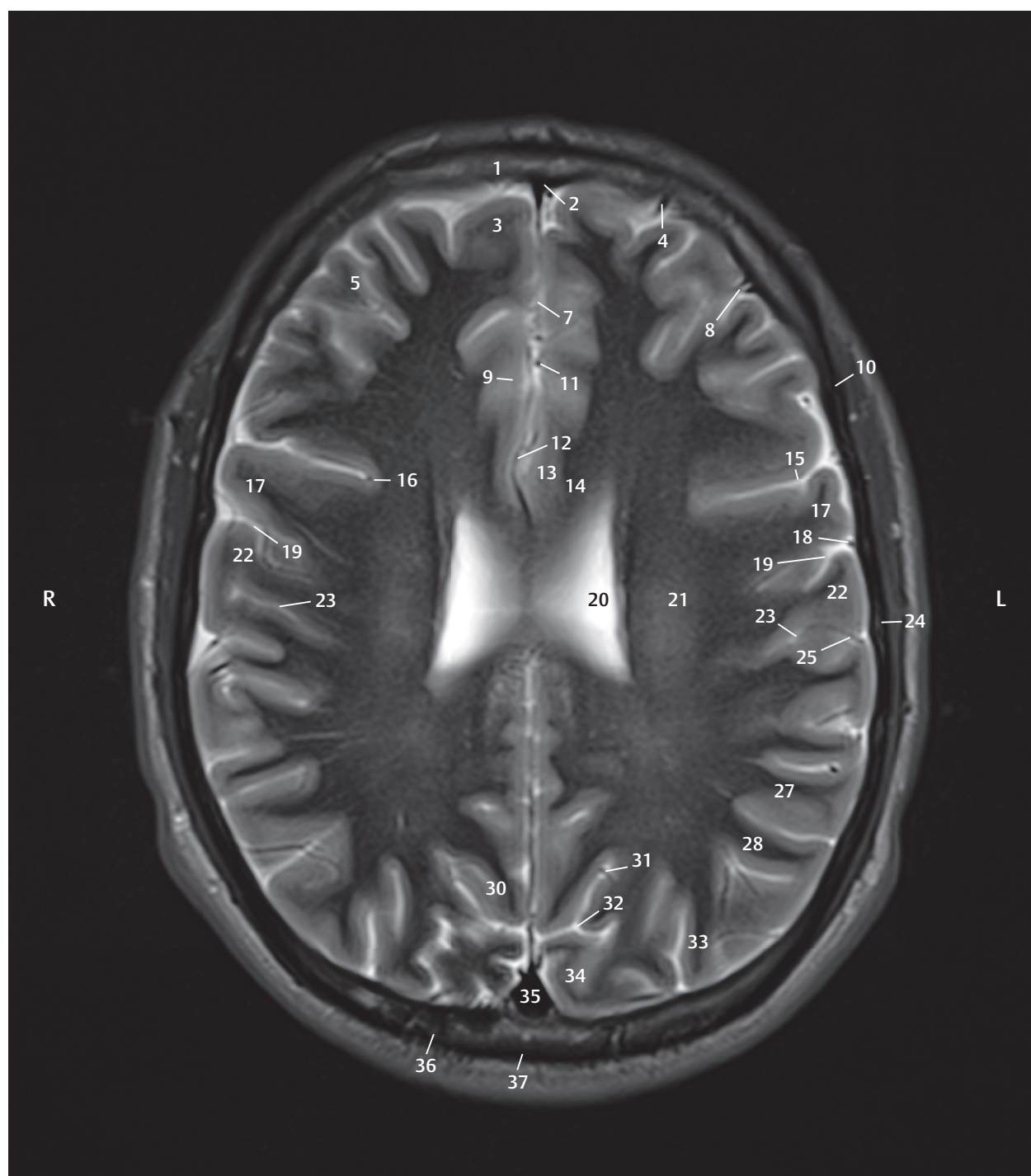


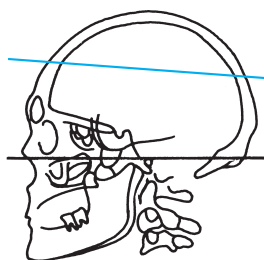
Fig. 5.11 10th bicommissural section.

Fig. 5.11a View of the 10th section of the bicommissural series. The sectional plane divides the falx cerebri into anterior and posterior parts, with the supracommissural part of the cingulate gyrus lying in between, partially obscuring the corpus callosum. Brain structures, blood vessels, and meninges.



- 1 Frontal bone
- 2 Superior sagittal sinus
- 3 Superior frontal gyrus
- 4 Superior cerebral vein
- 5 Middle frontal gyrus
- 7 Falx cerebri
- 8 Prefrontal artery
- 9 Cingulate sulcus
- 10 Coronal suture
- 11 Callosomarginal artery
- 12 Pericallosal artery
- 13 Cingulate gyrus
- 14 Cingulum
- 15 Precentral sulcus
- 16 Artery of precentral sulcus
- 17 Precentral gyrus
- 18 Artery of central sulcus
- 19 Central sulcus
- 20 Lateral ventricle, body
- 21 Centrum semiovale
- 22 Postcentral gyrus
- 23 Postcentral sulcus
- 24 Parietal bone
- 25 Parietal artery
- 27 Supramarginal gyrus
- 28 Angular gyrus
- 30 Precuneus
- 31 Parieto-occipital artery
- 32 Parieto-occipital sulcus
- 33 Occipital gyri
- 34 Cuneus
- 35 Superior sagittal sinus
- 36 Lambdoid suture
- 37 Occipital bone

Fig. 5.11b T2w MR image oriented in the bicommissural plane, corresponding exactly to the selected sectional plane in a.



- 1 Frontal bone
- 2 Superior sagittal sinus
- 3 Superior frontal gyrus
- 4 Superior cerebral vein
- 5 Middle frontal gyrus
- 6 Intermediomedial frontal artery
- 7 Falx cerebri
- 8 Prefrontal artery
- 9 Coronal suture
- 10 Callosomarginal artery
- 11 Cingulate sulcus
- 12 Cingulate gyrus
- 13 Precentral sulcus
- 14 Artery of precentral sulcus
- 15 Precentral gyrus
- 16 Centrum semiovale
- 17 Artery of central sulcus
- 18 Central sulcus
- 19 Postcentral gyrus
- 20 Paracentral artery
- 21 Parietal bone
- 22 Parietal artery
- 23 Precuneal artery
- 24 Supramarginal gyrus
- 25 Artery of angular gyrus
- 26 Angular gyrus
- 27 Precuneus
- 28 Falx cerebri
- 29 Parieto-occipital sulcus
- 30 Cuneus
- 31 Lambdoid suture
- 32 Occipital bone

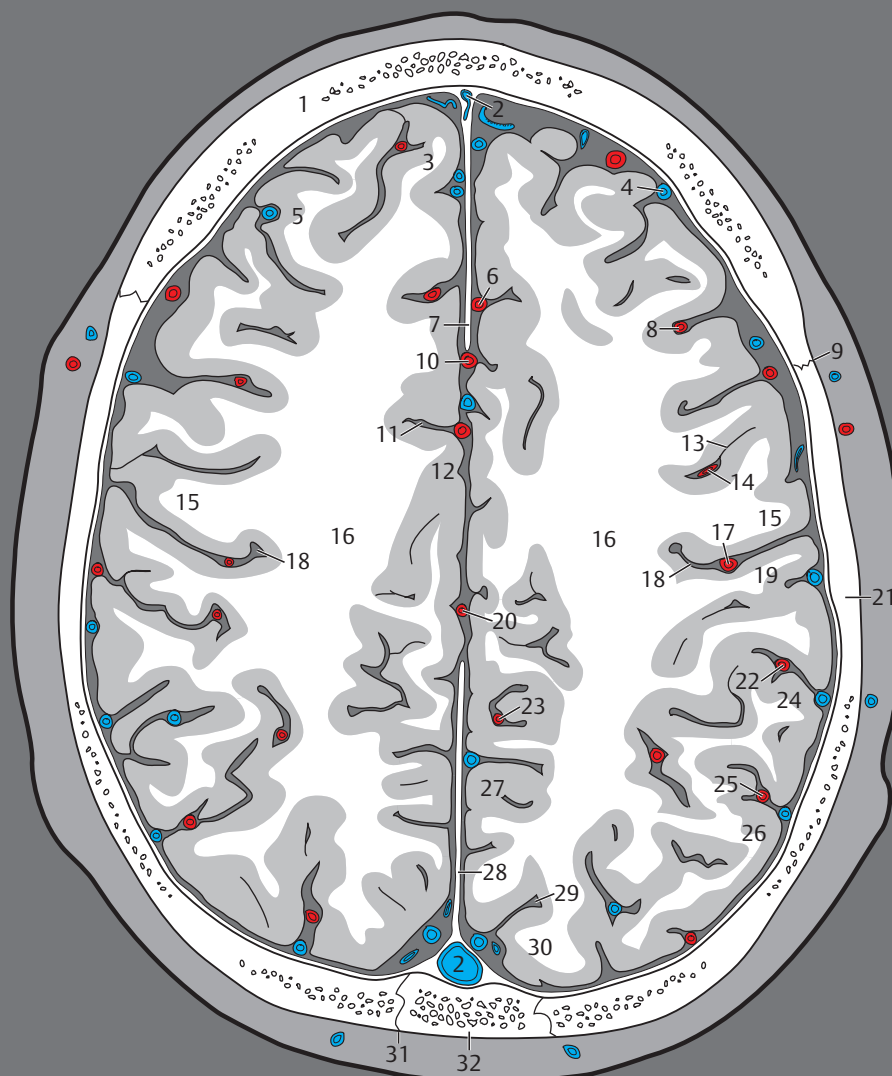
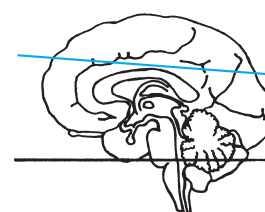
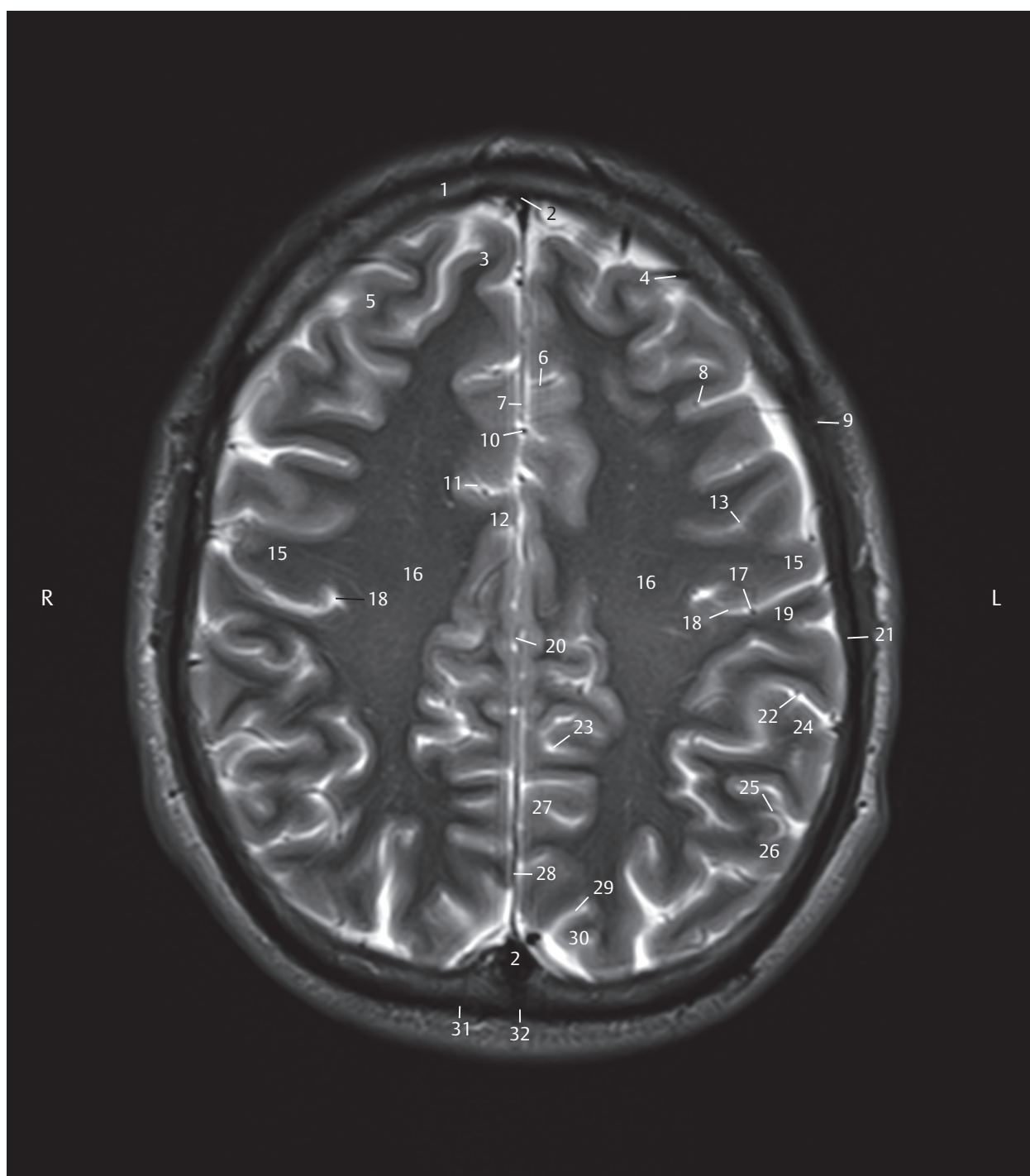


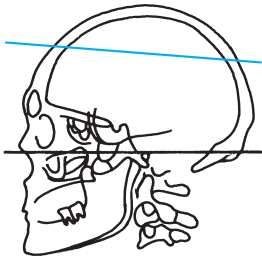
Fig. 5.12 11th bicommissural section.

Fig. 5.12a View of the 11th section of the bicommissural series. The cingulate sulcus has been sliced tangentially in the sectional plane. The falx cerebri separates the left and right hemispheres. The inferior edge of the falx cerebri runs through the middle of the slice and is not seen in the illustration. Brain structures, blood vessels, and meninges.



- 1 Frontal bone
- 2 Superior sagittal sinus
- 3 Superior frontal gyrus
- 4 Superior cerebral vein
- 5 Middle frontal gyrus
- 6 Intermediomedial frontal artery
- 7 Falx cerebri
- 8 Prefrontal artery
- 9 Coronal suture
- 10 Callosomarginal artery
- 11 Cingulate sulcus
- 12 Cingulate gyrus
- 13 Precentral sulcus
- 15 Precentral gyrus
- 16 Centrum semiovale
- 17 Artery of central sulcus
- 18 Central sulcus
- 19 Postcentral gyrus
- 20 Paracentral artery
- 21 Parietal bone
- 22 Parietal artery
- 24 Supramarginal gyrus
- 25 Artery of angular gyrus
- 26 Angular gyrus
- 27 Precuneus
- 28 Falx cerebri
- 29 Parieto-occipital sulcus
- 30 Cuneus
- 31 Lambdoid suture
- 32 Occipital bone

Fig. 5.12b T2w MR image oriented in the bicommissural plane, corresponding exactly to the selected sectional plane in a.



- 1 Frontal bone
- 2 Superior sagittal sinus
- 3 Superior frontal gyrus
- 4 Superior cerebral vein
- 5 Posteromedial frontal artery
- 6 Coronal suture
- 7 Middle frontal gyrus
- 8 Superior frontal sulcus
- 9 Parietal bone
- 10 Precentral sulcus
- 11 Precentral gyrus
- 12 Centrum semiovale
- 13 Central sulcus
- 14 Postcentral gyrus
- 15 Postcentral sulcus
- 16 Paracentral lobule
- 17 Paracentral artery
- 18 Cingulate sulcus, marginal branch
- 19 Falx cerebri
- 20 Superior parietal lobule
- 21 Precuneal artery
- 22 Precuneus
- 23 Sagittal suture

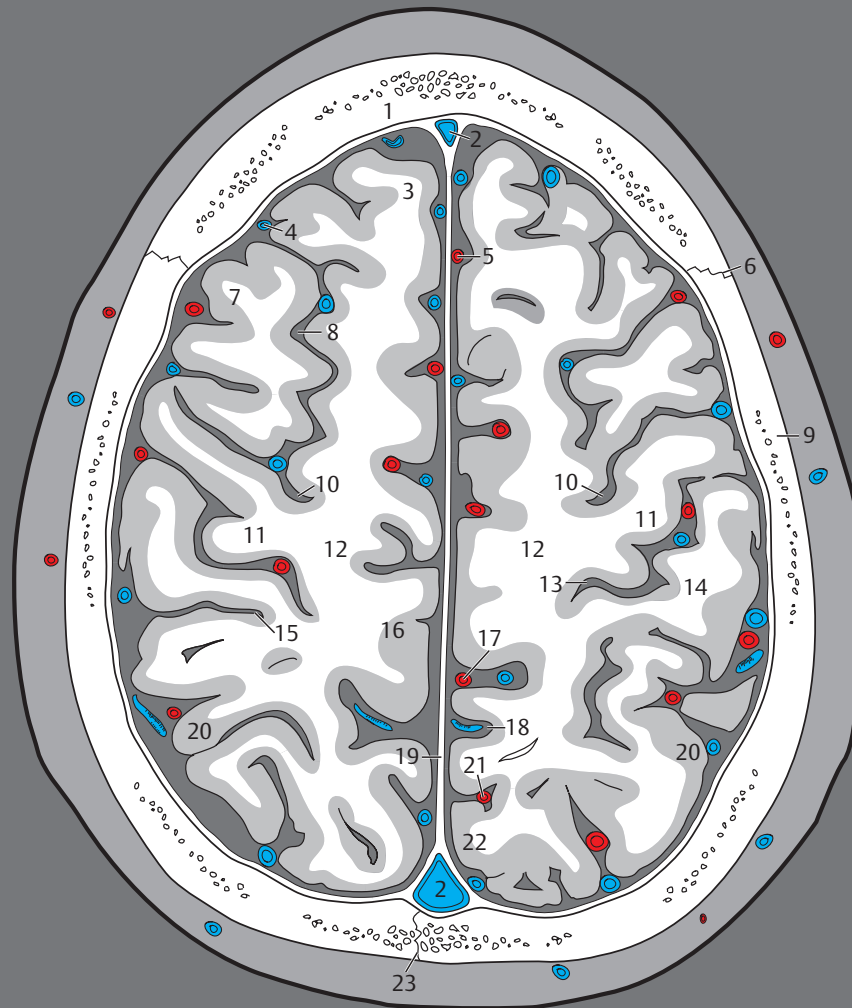
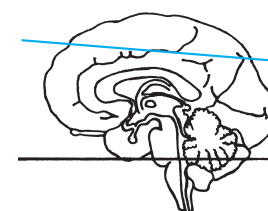
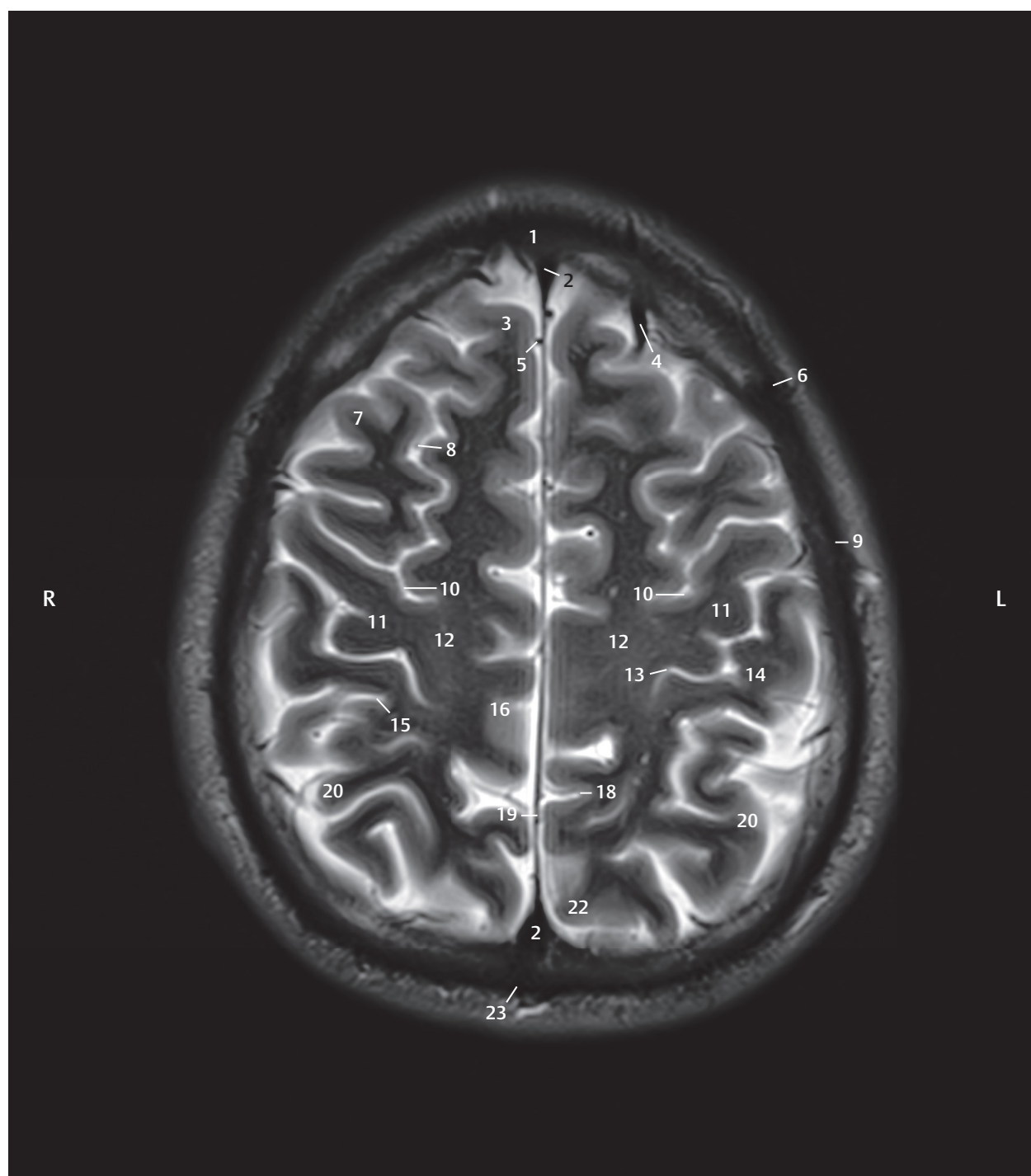


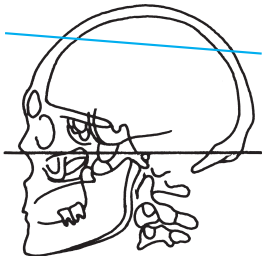
Fig. 5.13 12th bicommissural section.

Fig. 5.13a View of the 12th section of the bicommissural series. The falx cerebri separates the left hemisphere from the right completely in this slice and lies above the cingulate gyrus. Brain structures, blood vessels, and meninges.



- 1 Frontal bone
- 2 Superior sagittal sinus
- 3 Superior frontal gyrus
- 4 Superior cerebral vein
- 5 Posteromedial frontal artery
- 6 Coronal suture
- 7 Middle frontal gyrus
- 8 Superior frontal sulcus
- 9 Parietal bone
- 10 Precentral sulcus
- 11 Precentral gyrus
- 12 Centrum semiovale
- 13 Central sulcus
- 14 Postcentral gyrus
- 15 Postcentral sulcus
- 16 Paracentral lobule
- 18 Cingulate sulcus, marginal branch
- 19 Falx cerebri
- 20 Superior parietal lobule
- 22 Precuneus
- 23 Sagittal suture

Fig. 5.13b T2w MR image oriented in the bicommissural plane, corresponding exactly to the selected sectional plane in a.



- 1 Frontal bone
- 2 Superior sagittal sinus
- 3 Superior frontal gyrus
- 4 Superior cerebral vein
- 5 Posteromedial frontal artery
- 6 Coronal suture
- 7 Superior frontal sulcus
- 8 Precentral sulcus
- 9 Precentral gyrus
- 10 So-called knob on the precentral gyrus
- 11 Paracentral lobule
- 12 Central sulcus
- 13 Parietal bone
- 14 Paracentral artery
- 15 Postcentral gyrus
- 16 Postcentral sulcus
- 17 Superior parietal lobule
- 18 Precuneal artery
- 19 Precuneus
- 20 Sagittal suture

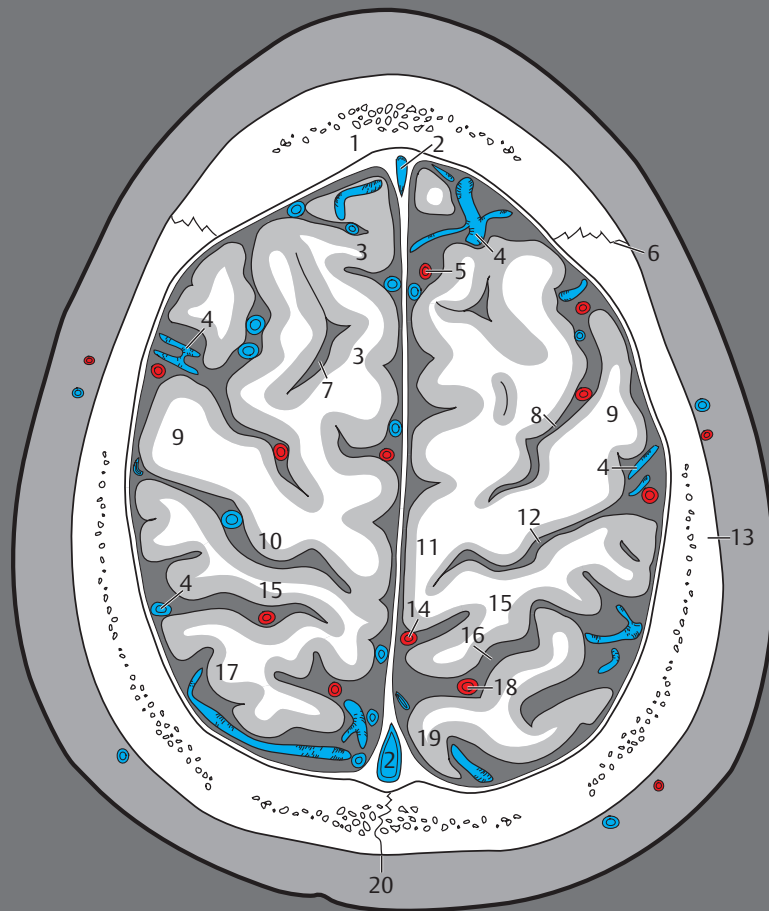
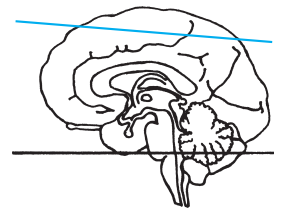
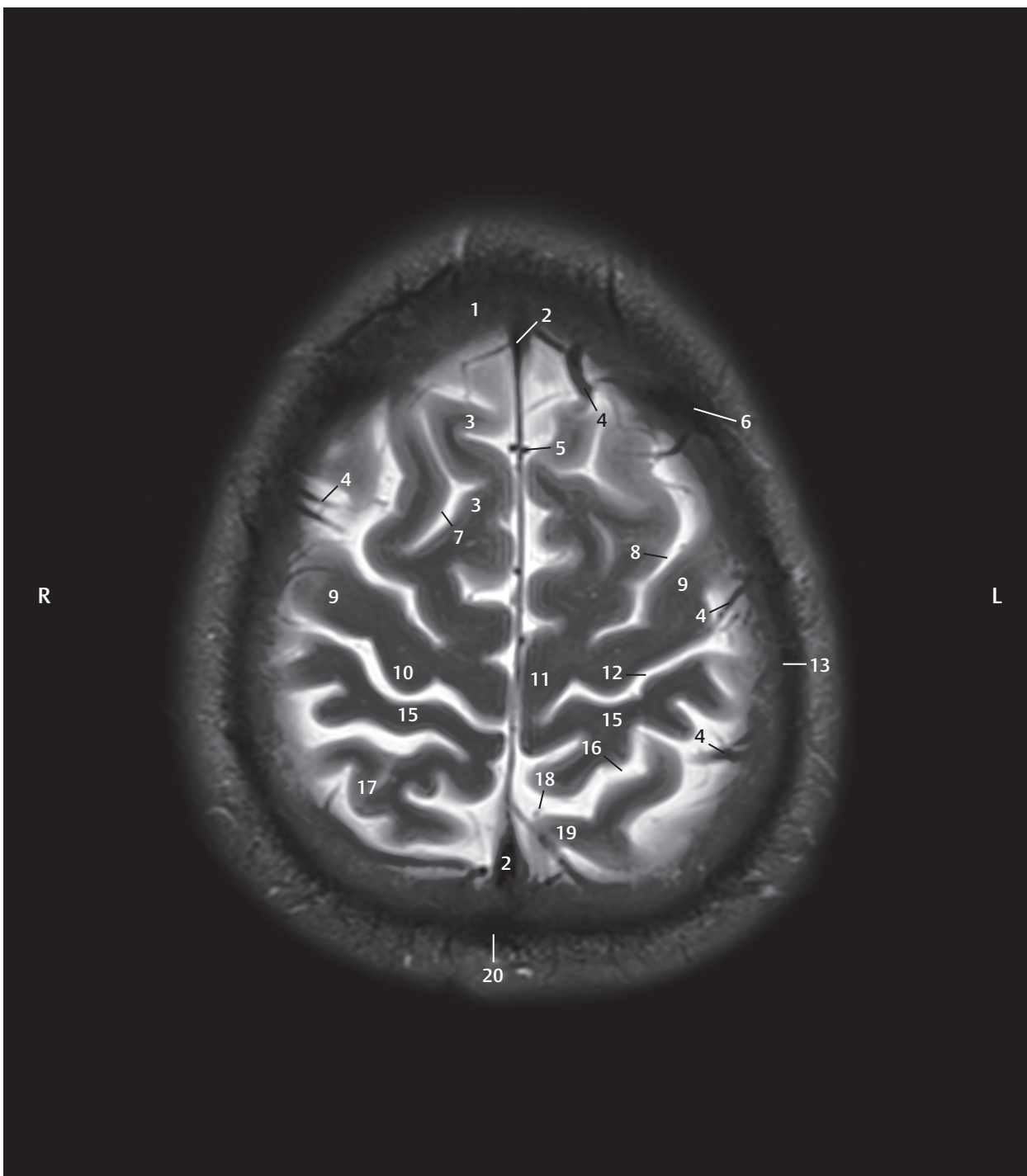


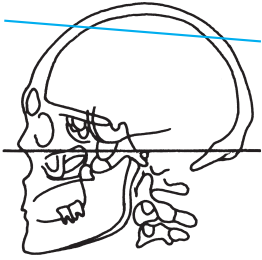
Fig. 5.14 13th bicommissural section.

Fig. 5.14a View of the 13th section of the bicommissural series. The central sulcus separates the frontal lobe from the parietal lobe. Brain structures, blood vessels, and meninges.



- 1 Frontal bone
- 2 Superior sagittal sinus
- 3 Superior frontal gyrus
- 4 Superior cerebral vein
- 5 Posteromedial frontal artery
- 6 Coronal suture
- 7 Superior frontal sulcus
- 8 Precentral sulcus
- 9 Precentral gyrus
- 10 So-called knob on the precentral gyrus
- 11 Paracentral lobule
- 12 Central sulcus
- 13 Parietal bone
- 15 Postcentral gyrus
- 16 Postcentral sulcus
- 17 Superior parietal lobule
- 18 Precuneal artery
- 19 Precuneus
- 20 Sagittal suture

Fig. 5.14b T2w MR image oriented in the bicommissural plane, corresponding exactly to the selected sectional plane in a.



- 1 Parietal bone
- 2 Superior sagittal sinus
- 3 Superior cerebral vein
- 4 Central sulcus
- 5 Sagittal suture

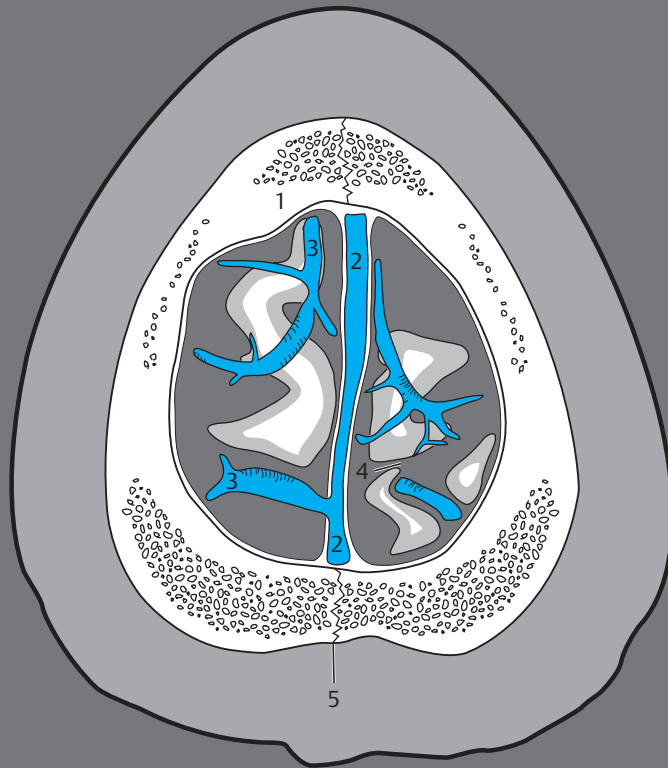
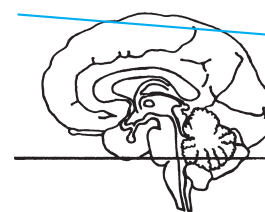
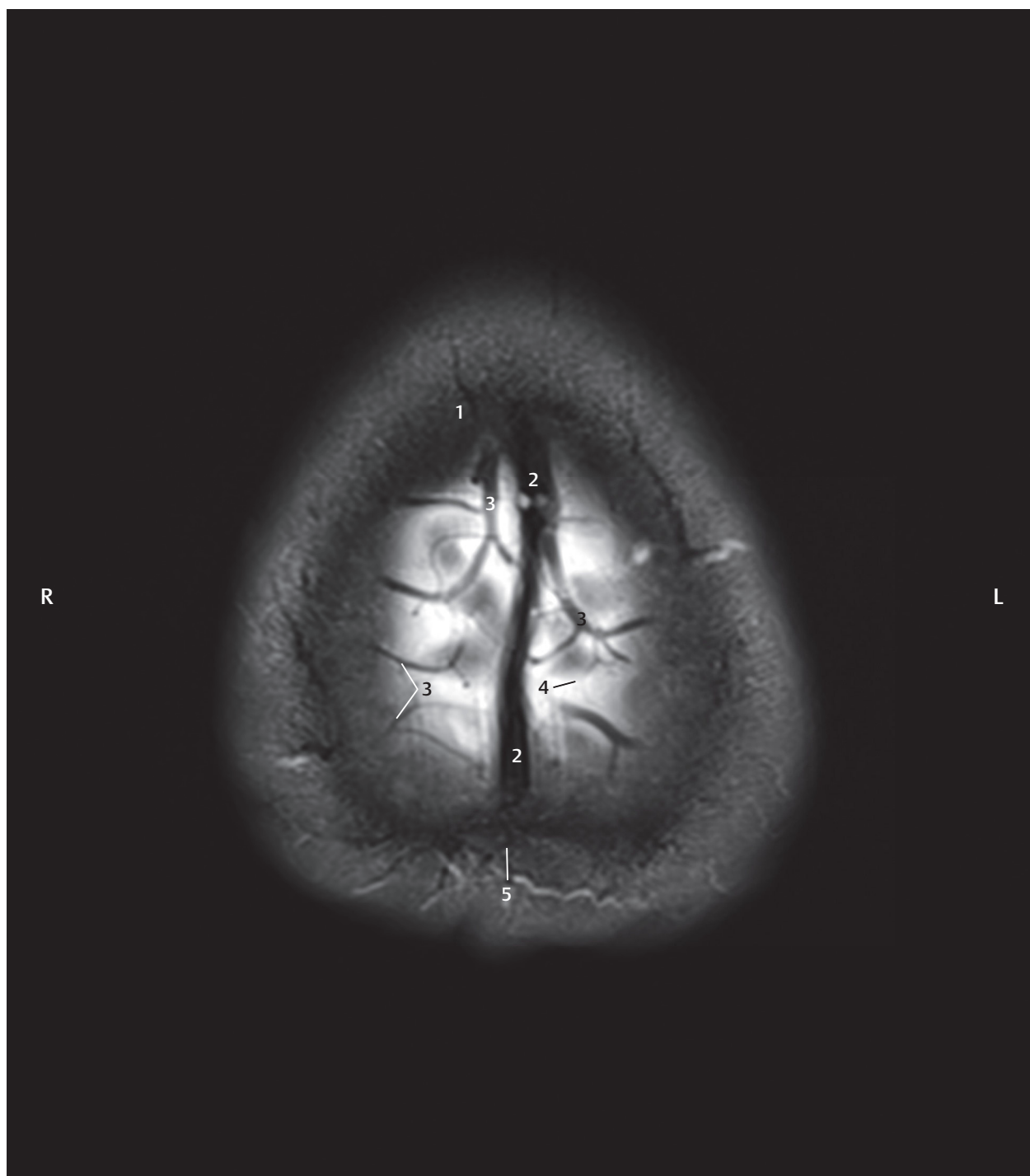


Fig. 5.15 14th bicommissural section.

Fig. 5.15a View of the 14th section of the bicommissural series. The central sulcus lies about 5 cm posterior to the bregma. Brain structures, blood vessels, and meninges.



- 1 Parietal bone
- 2 Superior sagittal sinus
- 3 Superior cerebral vein
- 4 Central sulcus
- 5 Sagittal suture

Fig. 5.15b T2w MR image oriented in the bicommissural plane, lying in the selected sectional plane as in a.

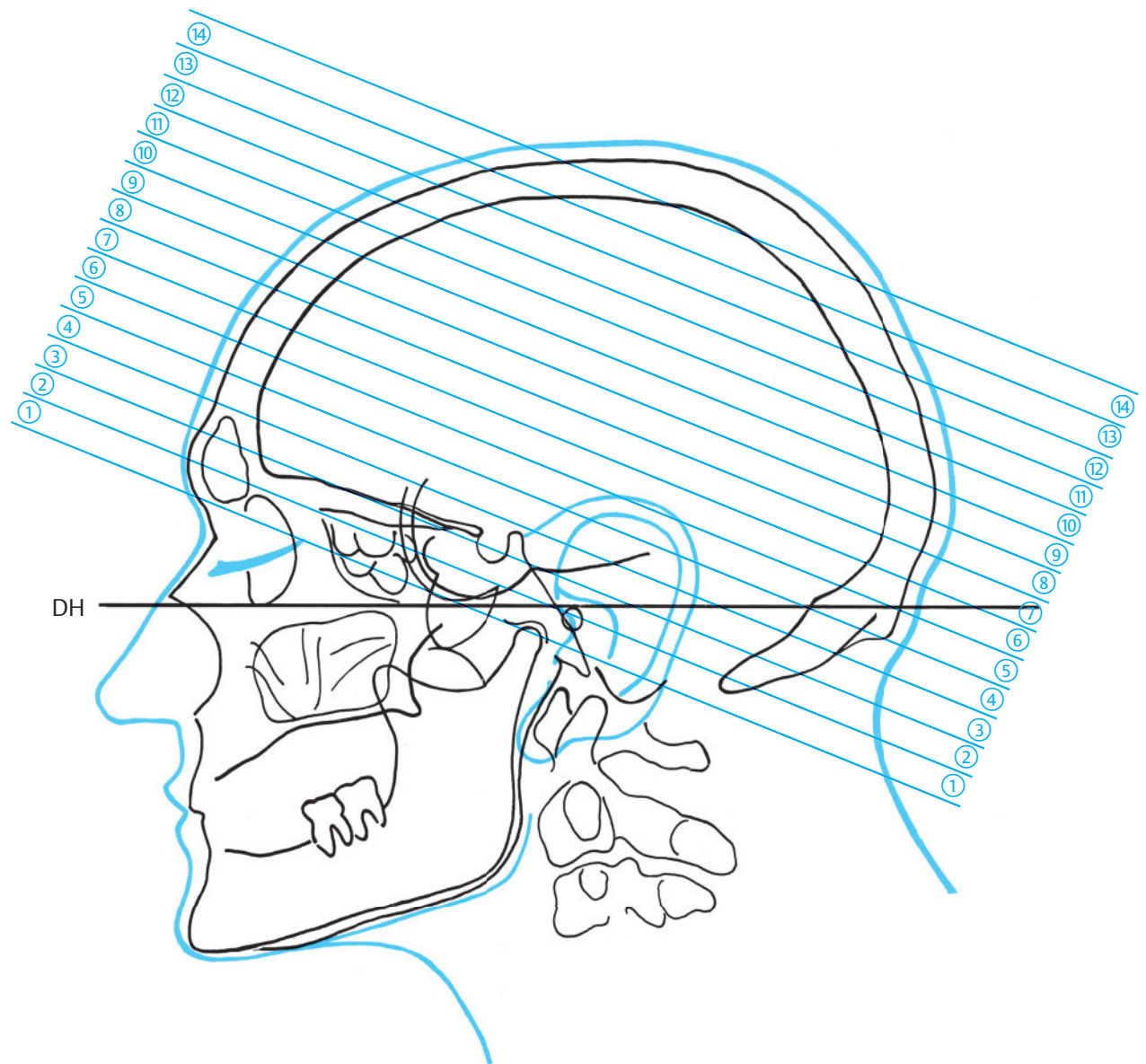


Fig. 5.16 Supraorbito-suboccipital sections. For specimen details see Chapter 12.

DH = German horizontal

Fig. 5.16a Illustration based on an X-ray image of the same head as in ► Fig. 5.1. The 14 slices of the supraorbito-suboccipital series have been contiguously numbered with encircled digits from inferior to superior.

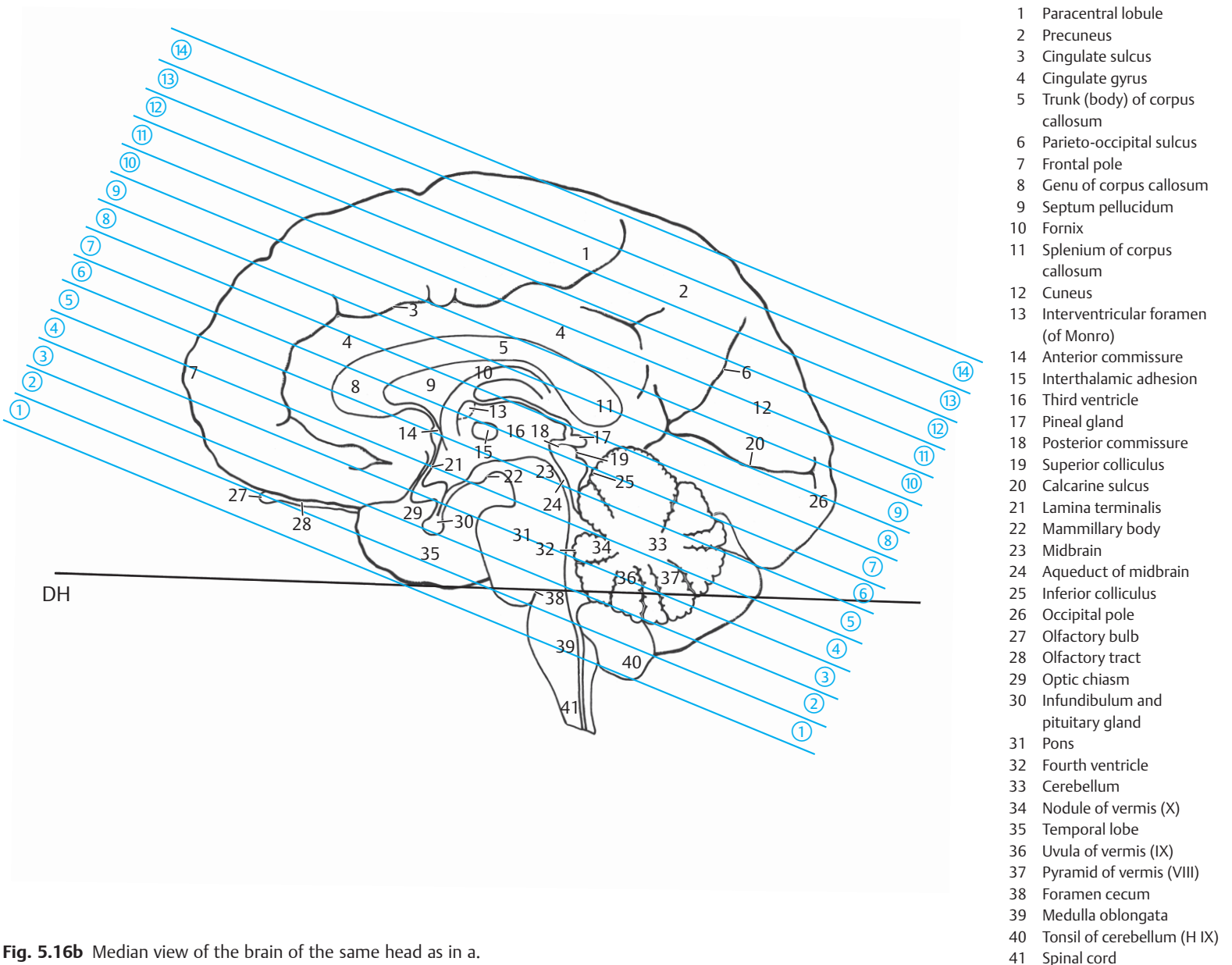
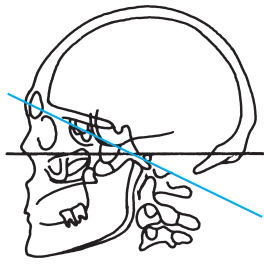


Fig. 5.16b Median view of the brain of the same head as in a. The sections of the su praorbito-suboccipital series have been numbered as in ► Fig. 5.1.



- 1 Frontal bone
- 2 Eyeball
- 3 Zygomatic bone
- 4 Orbit
- 5 Ethmoidal air cells
- 6 Pterygopalatine fossa
- 7 Sphenoid sinus
- 8 Zygomatic arch
- 9 Foramen spinosum with middle meningeal artery
- 10 Foramen ovale with mandibular nerve
- 11 Mandible
- 12 Internal carotid artery
- 13 Clivus
- 14 External acoustic canal
- 15 Vertebral artery
- 16 Internal jugular vein
- 17 Jugular foramen
- 18 External ear
- 19 Mastoid process
- 20 Mastoid cells
- 21 Medulla oblongata
- 22 Cerebellum
- 23 Foramen magnum
- 24 Occipital bone, basilar part

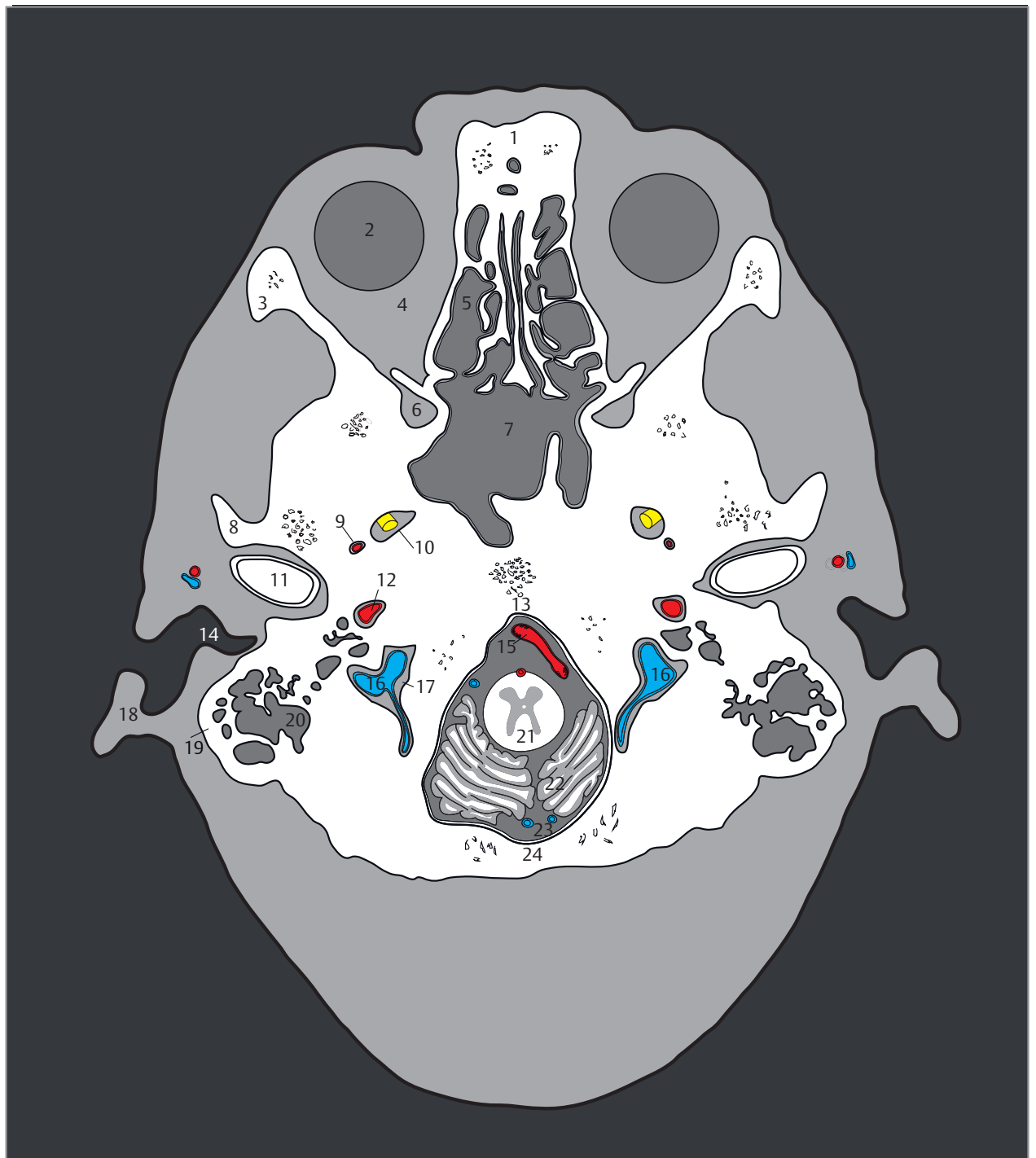
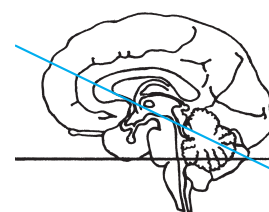
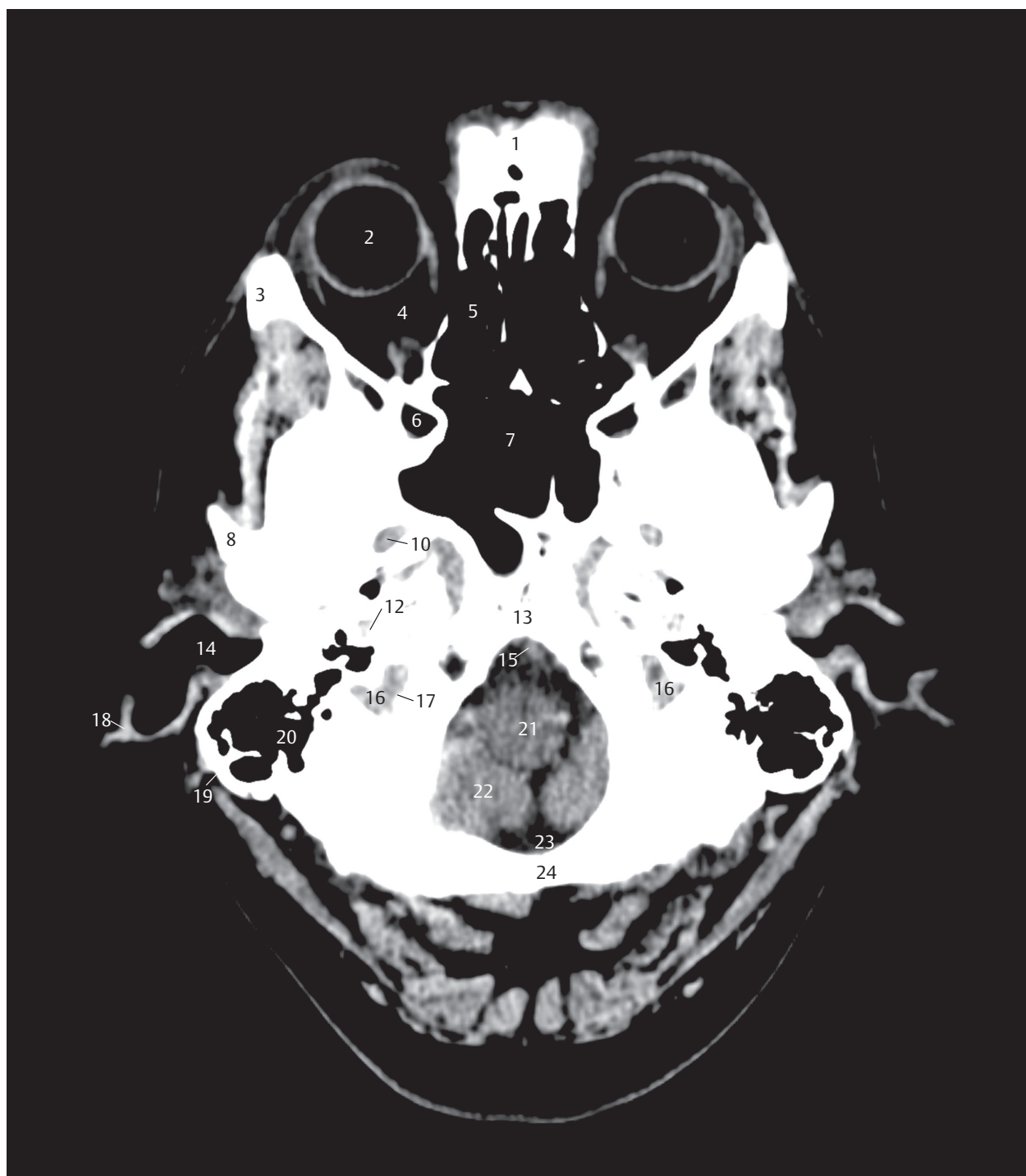


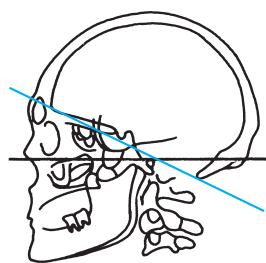
Fig. 5.17 1st supraorbito-suboccipital section.

Fig. 5.17a View of the 1st section of the supraorbito-suboccipital CT series. The sectional plane lies oblique to the foramen magnum just above the hypoglossal canal. The floor of the middle cranial fossa has been evenly sectioned. Brain structures, bone structures, and blood vessels.



- 1 Frontal bone
- 2 Eyeball
- 3 Zygomatic bone
- 4 Orbit
- 5 Ethmoidal air cells
- 6 Pterygopalatine fossa
- 7 Sphenoid sinus
- 8 Zygomatic arch
- 10 Foramen ovale with mandibular nerve
- 12 Internal carotid artery
- 13 Clivus
- 14 External acoustic canal
- 15 Vertebral artery
- 16 Internal jugular vein
- 17 Jugular foramen
- 18 External ear
- 19 Mastoid process
- 20 Mastoid cells
- 21 Medulla oblongata
- 22 Cerebellum
- 23 Foramen magnum
- 24 Occipital bone, basilar part

Fig. 5.17b Supraorbital-suboccipital oriented CT image of a 39-year-old woman from whom the other images of this series have also been obtained; for technical details see Chapter 12. The image corresponds exactly to the sectional plane in a (schematic representation based on respective CT images). Brain structures, bone structures, and blood vessels.



- 1 Frontal bone
- 2 Frontal sinus
- 3 Eyeball
- 4 Lacrimal gland
- 5 Orbit
- 6 Crista galli
- 7 Optic nerve
- 8 Ethmoidal air cells
- 9 Middle meningeal artery
- 10 Sphenoid bone
- 11 Superior orbital fissure
- 12 Temporal lobe
- 13 Sphenoid sinus
- 14 Cavernous sinus
- 15 Temporal artery
- 16 Trigeminal ganglion
- 17 Internal carotid artery
- 18 Temporal bone
- 19 Cochlea
- 20 Basilar artery
- 21 Tympanic cave with ossicles
- 22 Anterior median fissure
- 23 Mastoid cells
- 24 N. glossopharyngeus (N. IX)
- 25 Medulla oblongata
- 26 External ear
- 27 Sigmoid sinus
- 28 Mastoid process
- 29 Posterior inferior cerebellar artery
- 30 Cerebellar hemisphere
- 31 Posterior cerebellomedullary cistern (magna)
- 32 Occipital bone

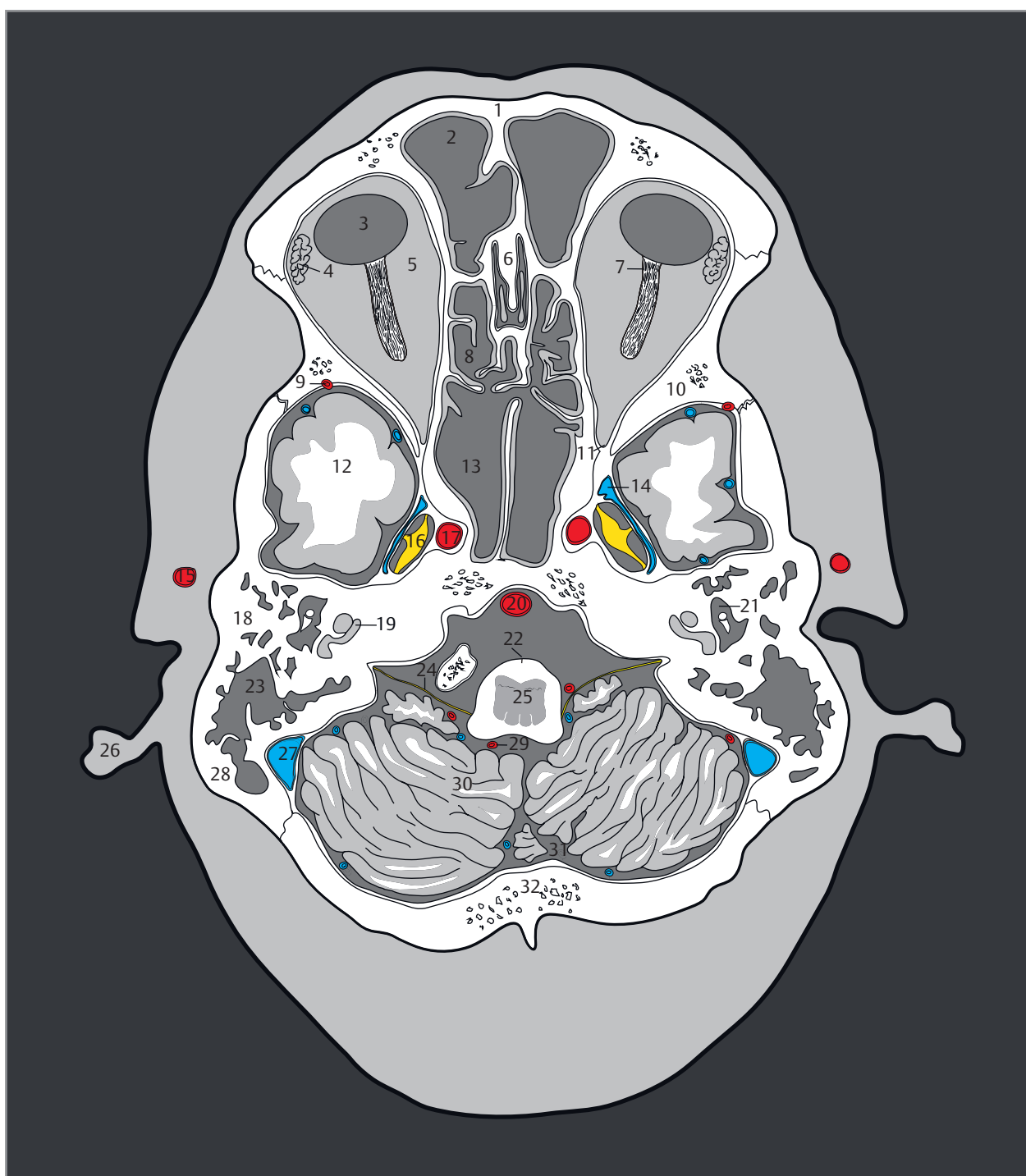
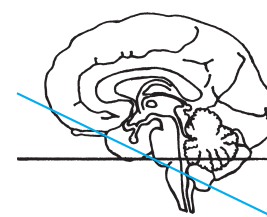


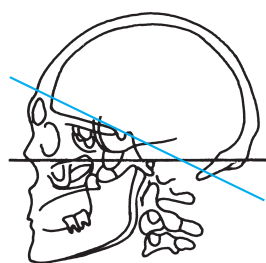
Fig. 5.18 2nd supraorbito-suboccipital section.

Fig. 5.18a View of the 2nd section of the supraorbito-suboccipital series. The sectional plane passes through the apical region of the orbit and through the medial aspects of the external auditory canals. The middle cranial fossa and the cerebellum have been sectioned. Brain structures, bone structures, and blood vessels.



- 1 Frontal bone
- 2 Frontal sinus
- 3 Eyeball
- 4 Lacrimal gland
- 5 Orbit
- 6 Crista galli
- 7 Optic nerve
- 8 Ethmoidal air cells
- 10 Sphenoid bone
- 11 Superior orbital fissure
- 12 Temporal lobe
- 13 Sphenoid sinus
- 14 Cavernous sinus
- 15 Temporal artery
- 16 Meckels cave with Trigeminal ganglion
- 17 Internal carotid artery
- 18 Temporal bone
- 20 Basilar artery
- 21 Tympanic cave with ossicles
- 22 Anterior median fissure
- 23 Mastoid cells
- 25 Medulla oblongata
- 26 External ear
- 27 Sigmoid sinus
- 28 Mastoid process
- 30 Cerebellar hemisphere
- 31 Posterior cerebellomedullary cistern (magna)
- 32 Occipital bone

Fig. 5.18b Supraorbital-suboccipital oriented CT image, corresponding exactly to the sectional plane in a.



- 1 Frontal bone
- 2 Frontal sinus
- 3 Crista galli
- 4 Orbit
- 5 Frontal lobe, base
- 6 Sphenoid bone
- 7 Optic nerve in the optic canal
- 8 Sphenoid sinus
- 9 Middle meningeal artery
- 10 Internal carotid artery
- 11 Sella with pituitary gland
- 12 Cavernous sinus
- 13 Temporal lobe
- 14 Sphenoid sinus
- 15 Temporal bone, flat part
- 16 Temporal artery
- 17 Clivus
- 18 Basilar artery
- 19 Semicircular canal
- 20 Pons
- 21 Temporal bone, petrous part
- 22 Mastoid cells
- 23 Middle cerebellar peduncle
- 24 External ear
- 25 Fourth ventricle
- 26 Sigmoid sinus
- 27 Posterior lobe of cerebellum, hemisphere
- 28 Vermis of cerebellum
- 29 Posterior cerebellomedullary cistern (magna)
- 30 Occipital bone

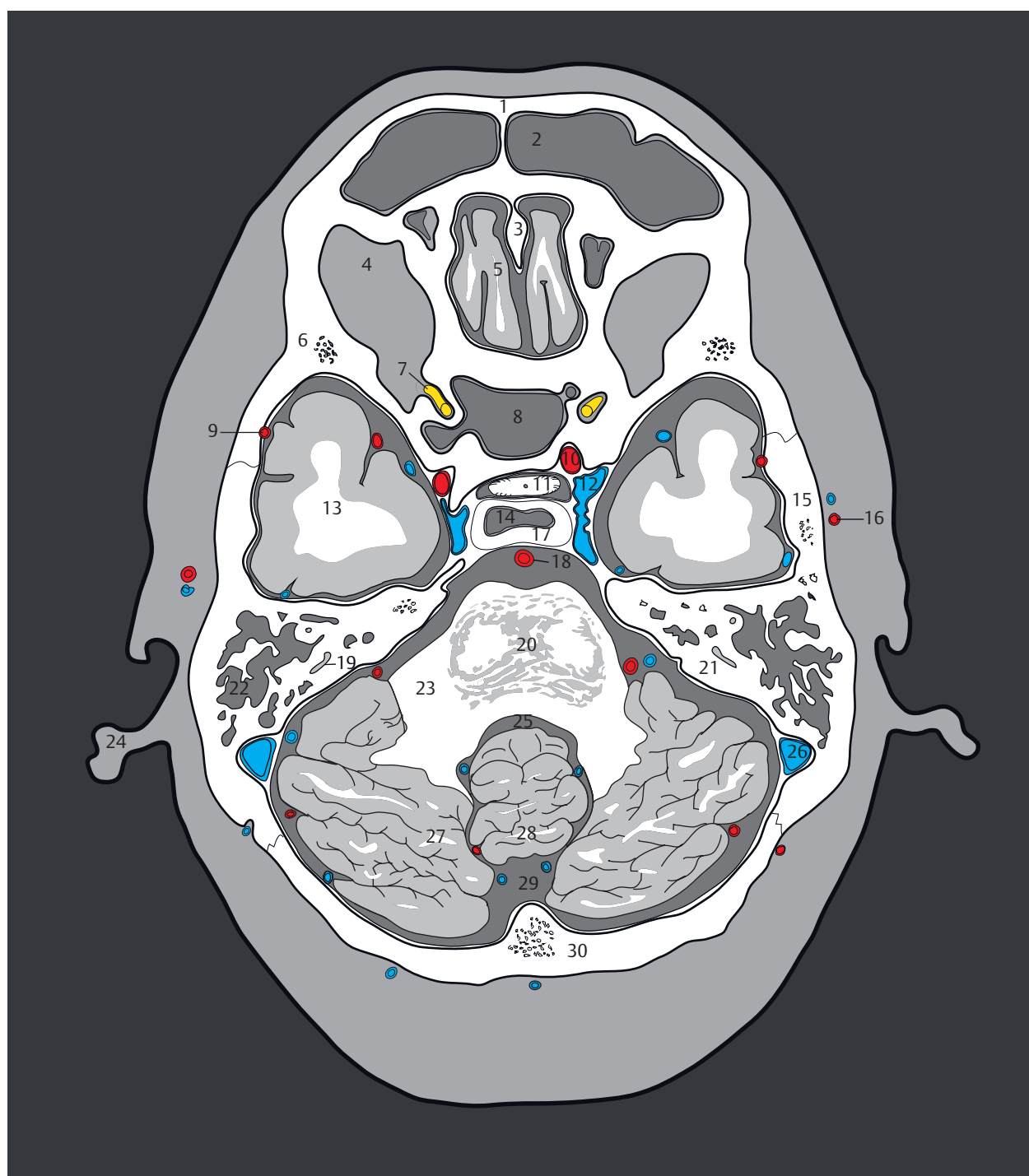
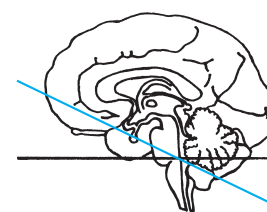
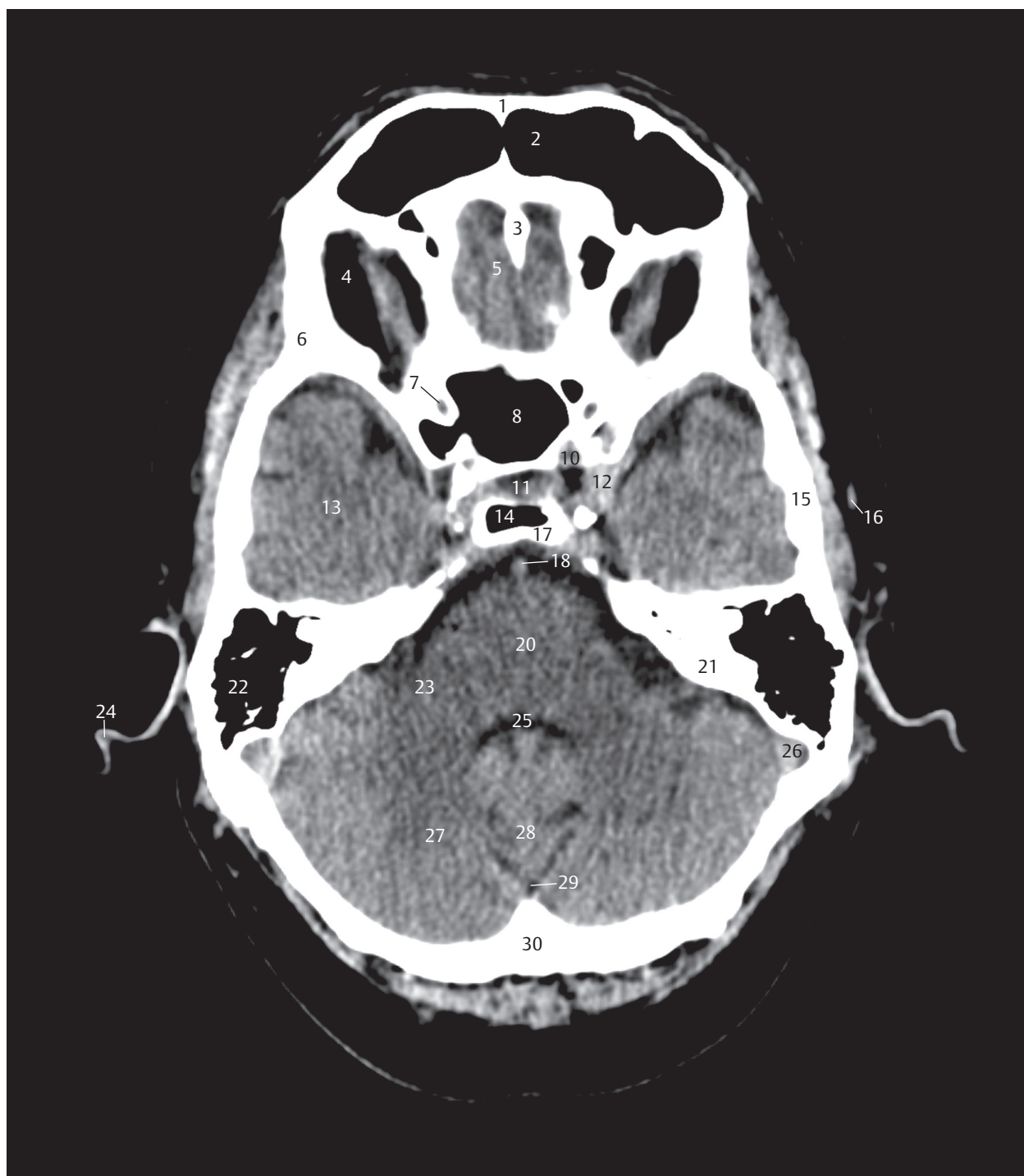


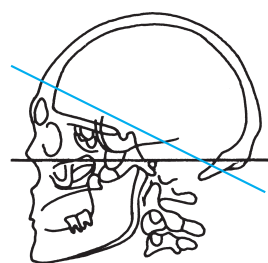
Fig. 5.19 3rd supraorbito-suboccipital section.

Fig. 5.19a View of the 3rd section of the supraorbito-suboccipital series. The sectional plane runs through the sella turcica and separates the dorsum sellae. The posterior cranial fossa is depicted with the left internal auditory canal. Brain structures, bony structures, and blood vessels.



- 1 Frontal bone
- 2 Frontal sinus
- 3 Crista galli
- 4 Orbit
- 5 Frontal lobe, base
- 6 Sphenoid bone
- 7 Optic nerve in the optic canal
- 8 Sphenoid sinus
- 10 Internal carotid artery
- 11 Sella with pituitary gland
- 12 Cavernous sinus
- 13 Temporal lobe
- 14 Sphenoid sinus
- 15 Temporal bone, flat part
- 16 Temporal artery
- 17 Clivus
- 18 Basilar artery
- 20 Pons
- 21 Temporal bone, petrous part
- 22 Mastoid cells
- 23 Middle cerebellar peduncle
- 24 External ear
- 25 Fourth ventricle
- 26 Sigmoid sinus
- 27 Posterior lobe of cerebellum, hemisphere
- 28 Vermis of cerebellum
- 29 Posterior cerebellomedullary cistern (magna)
- 30 Occipital bone

Fig. 5.19b Supraorbito-suboccipital oriented CT image, corresponding exactly to the sectional plane in a.



- 1 Frontal bone
- 2 Frontal sinus
- 3 Crista galli
- 4 Sphenoid bone
- 5 Frontal lobe
- 6 Middle meningeal artery
- 7 Optic canal
- 8 Sphenoid sinus
- 9 Optic nerve
- 10 Middle cerebral artery, branches
- 11 Internal carotid artery
- 12 Anterior clinoid process
- 13 Cavernous sinus
- 14 Pituitary gland
- 15 Amygdaloid body
- 16 Dorsum sellae, cut surface
- 17 Temporal lobe
- 18 Temporal bone, flat part
- 19 Basilar artery
- 20 Temporal artery
- 21 Temporal bone, petrous part
- 22 Trigeminal nerve
- 23 Pons
- 24 Pontocerebellar cistern
- 25 Fourth ventricle
- 26 Sigmoid sinus
- 27 Cerebellum, hemisphere
- 28 Vermis of cerebellum
- 29 Lambdoid suture
- 30 Occipital bone

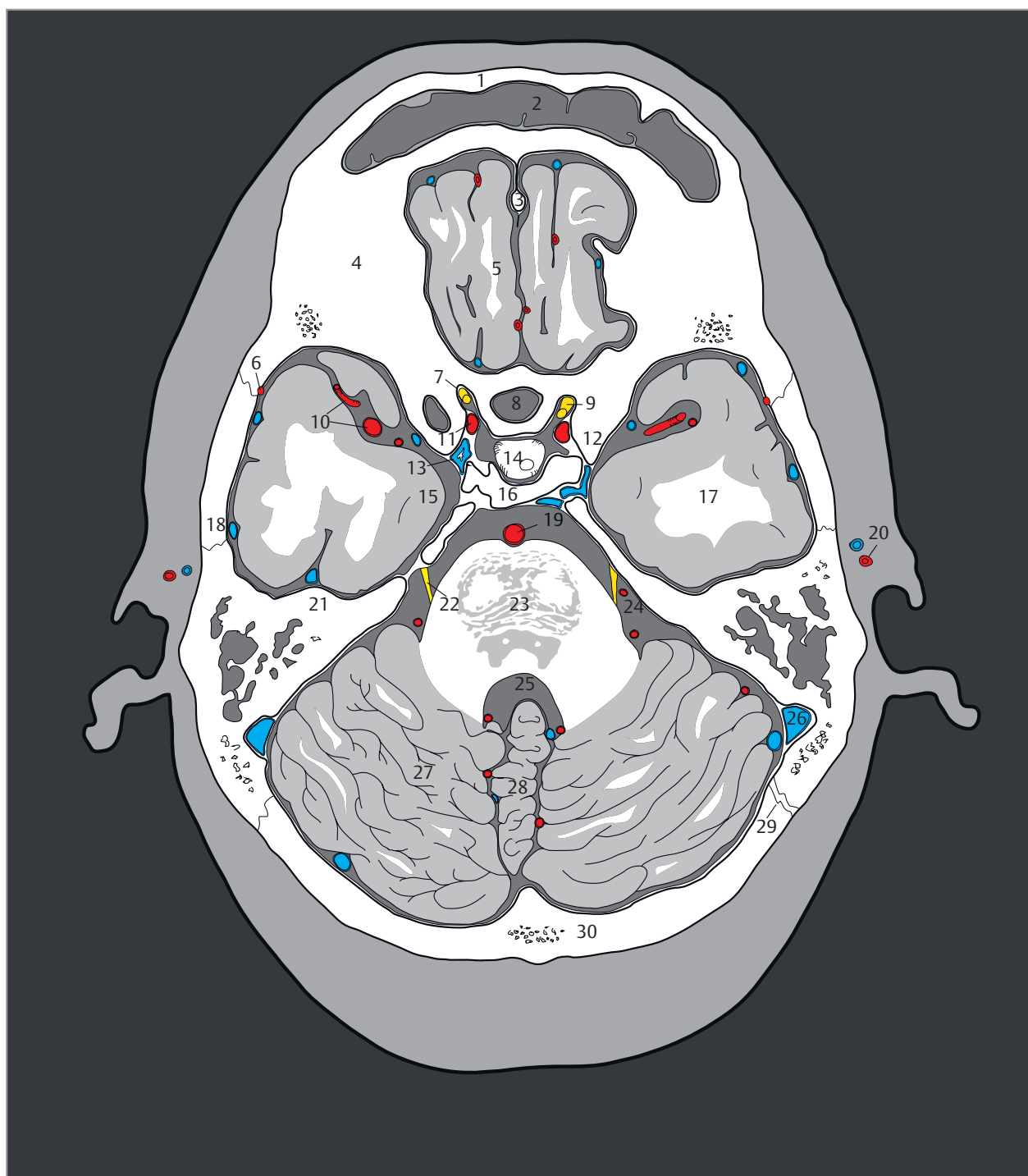
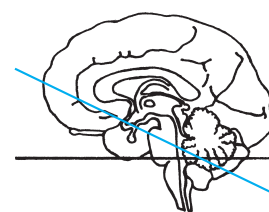
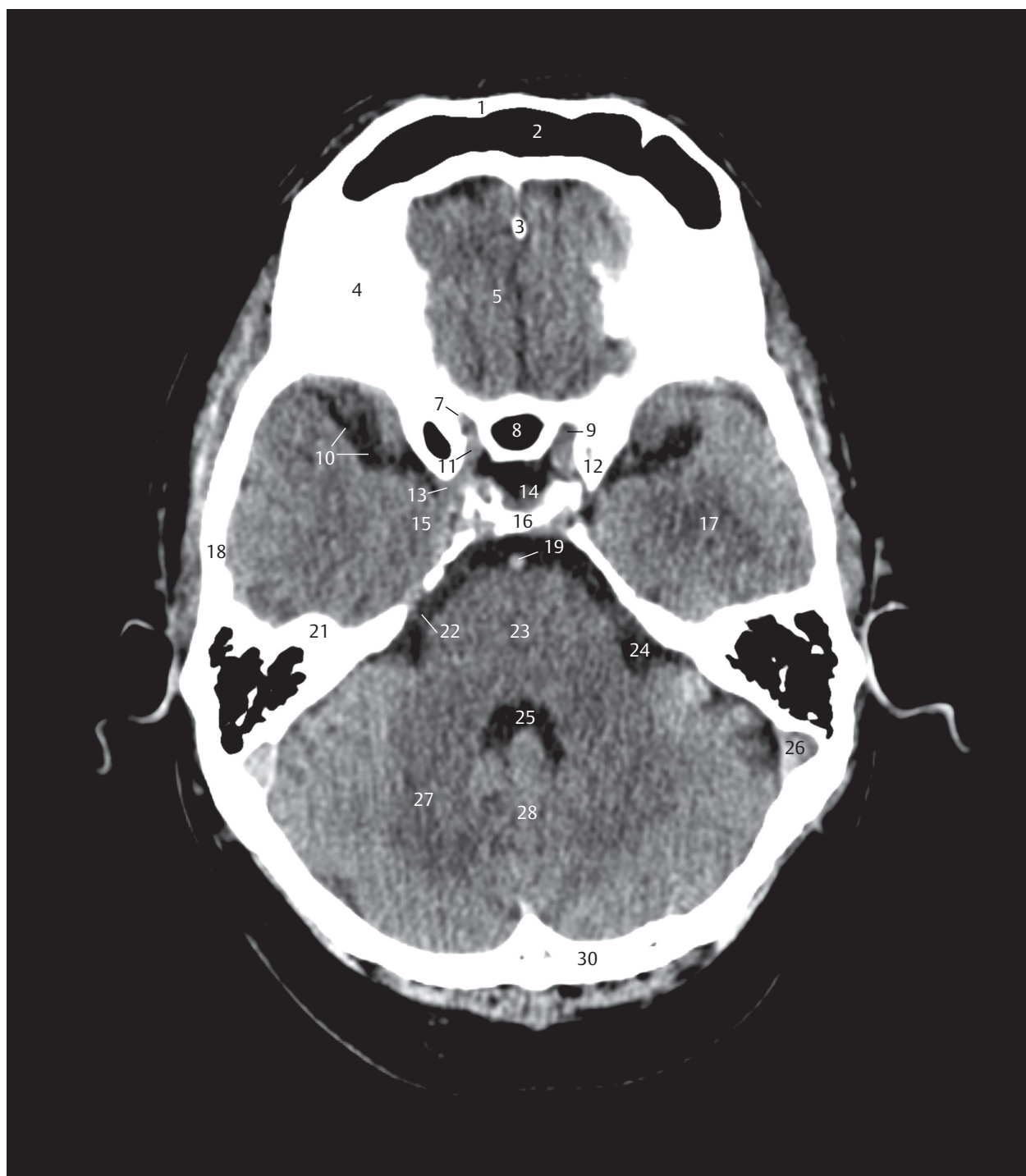


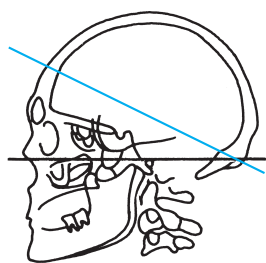
Fig. 5.20 4th supraorbito-suboccipital section.

Fig. 5.20a View of the 4th section of the supraorbito-suboccipital series. The optic chiasma and the internal auditory canal have been sectioned in the slice. The sectional plane passes through the frontal lobe, temporal horns, and the cerebellum. Brain structures, bony structures, and blood vessels.



- 1 Frontal bone
- 2 Frontal sinus
- 3 Crista galli
- 4 Sphenoid bone
- 5 Frontal lobe
- 7 Optic canal
- 8 Sphenoid sinus
- 9 Optic nerve
- 10 Middle cerebral artery, branches
- 11 Internal carotid artery
- 12 Anterior clinoid process
- 13 Cavernous sinus
- 14 Pituitary gland
- 15 Amygdaloid body
- 16 Dorsum sellae, cut surface
- 17 Temporal lobe
- 18 Temporal bone, flat part
- 19 Basilar artery
- 21 Temporal bone, petrous part
- 22 Trigeminal nerve
- 23 Pons
- 24 Pontocerebellar cistern
- 25 Fourth ventricle
- 26 Sigmoid sinus
- 27 Cerebellum, hemisphere
- 28 Vermis of cerebellum
- 30 Occipital bone

Fig. 5.20b Supraorbito-suboccipital oriented CT image, lying exactly in the selected sectional plane as in a.



- 1 Frontal bone
- 2 Frontal sinus
- 3 Anterior cranial fossa
- 4 Superior frontal gyrus
- 5 Middle frontal gyrus
- 6 Straight gyrus
- 7 Inferior frontal gyrus
- 8 Sphenoid bone
- 9 Cistern of lateral cerebral fossa
- 10 Optic chiasma
- 11 Infundibulum
- 12 Cistern of the vallicula of cerebrum
- 13 Internal carotid artery
- 14 Middle cerebral artery
- 15 Posterior communicating artery
- 16 Amygdaloid body
- 17 Temporal lobe
- 18 Lateral ventricle, temporal horn
- 19 Posterior cerebral artery
- 20 Basilar artery
- 21 Pons
- 22 Tentorium of cerebellum
- 23 Temporal bone
- 24 Fourth ventricle
- 25 Superior cerebellar peduncle
- 26 Sigmoid sinus
- 27 Vermis of cerebellum
- 28 Cerebellum, hemisphere
- 29 Lambdoid suture
- 30 Occipital bone

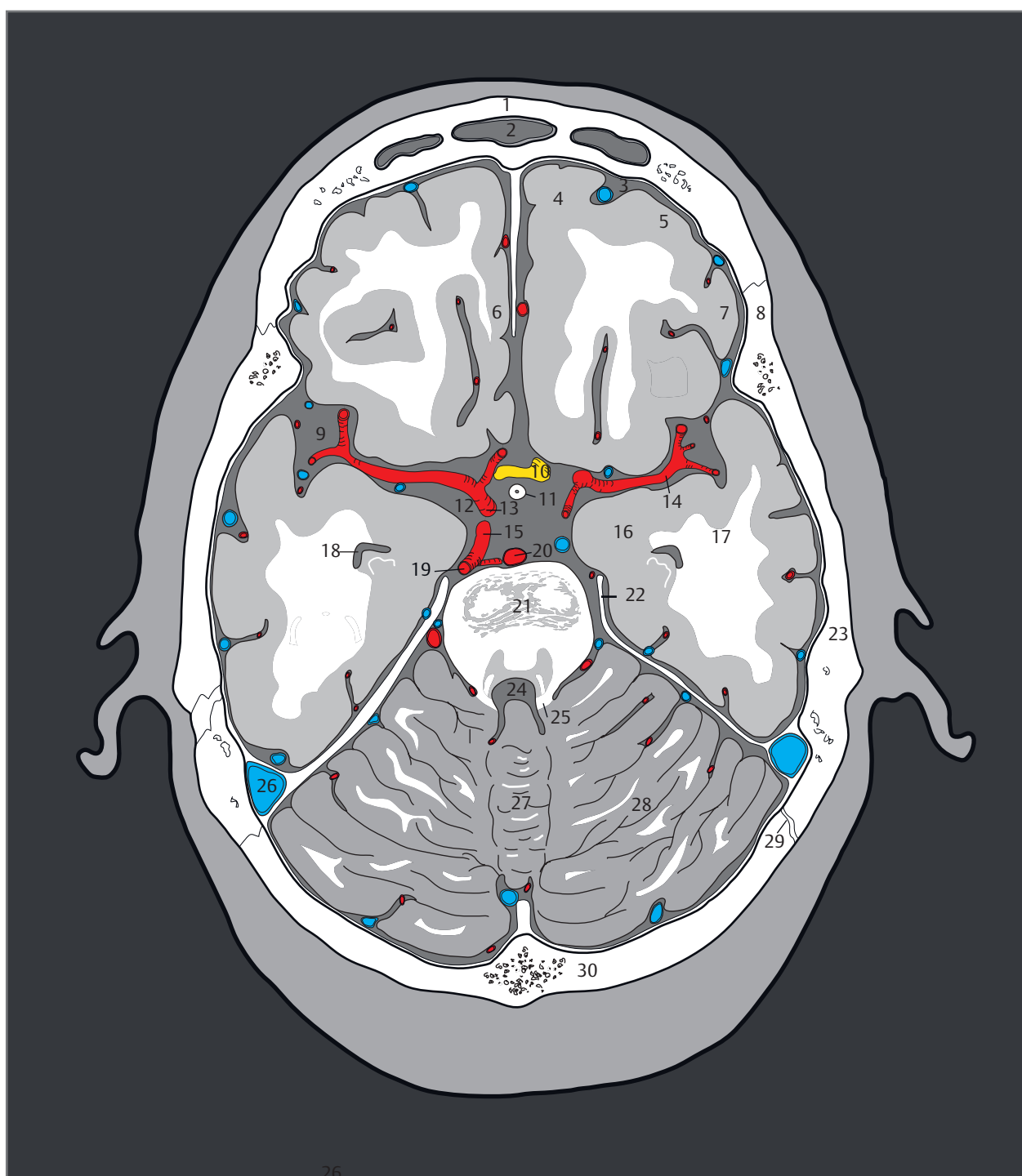
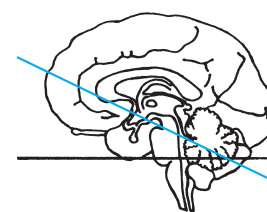
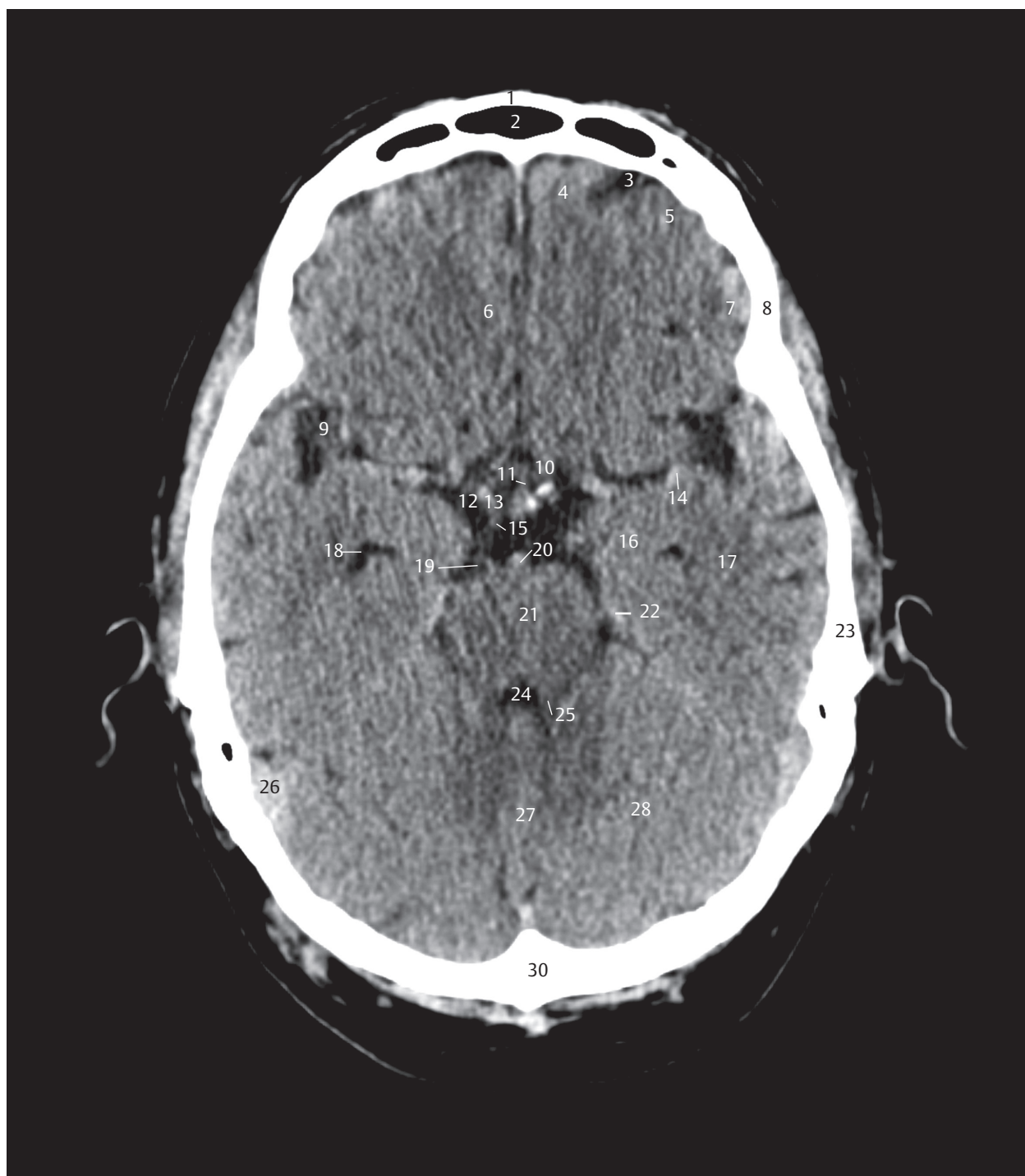


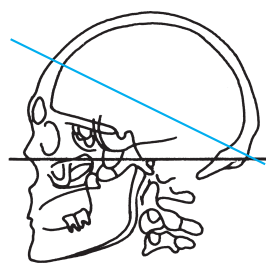
Fig. 5.21 5th supraorbito-suboccipital section.

Fig. 5.21a View of the 5th section of the supraorbito-suboccipital series. The image includes the circle of Willis, along with the anterior, middle, and posterior cranial fossae with their contents. The posterior cranial fossa is limited anteriorly by the sectioned tentorium of cerebellum. Brain structures, bony structures, and blood vessels.



- 1 Frontal bone
- 2 Frontal sinus
- 3 Anterior cranial fossa
- 4 Superior frontal gyrus
- 5 Middle frontal gyrus
- 6 Straight gyrus
- 7 Inferior frontal gyrus
- 8 Sphenoid bone
- 9 Cistern of lateral cerebral fossa
- 10 Optic chiasma
- 11 Infundibulum
- 12 Cistern of the vallecula of cerebrum
- 13 Internal carotid artery
- 14 Middle cerebral artery
- 15 Posterior communicating artery
- 16 Amygdaloid body
- 17 Temporal lobe
- 18 Lateral ventricle, temporal horn
- 19 Posterior cerebral artery
- 20 Basilar artery
- 21 Pons
- 22 Tentorium of cerebellum
- 23 Temporal bone
- 24 Fourth ventricle
- 25 Superior cerebellar peduncle
- 26 Sigmoid sinus
- 27 Vermis of cerebellum
- 28 Cerebellum, hemisphere
- 30 Occipital bone

Fig. 5.21b Supraorbito-suboccipital oriented CT image, lying exactly in the selected sectional plane as in a.

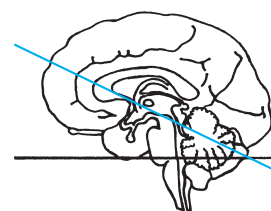
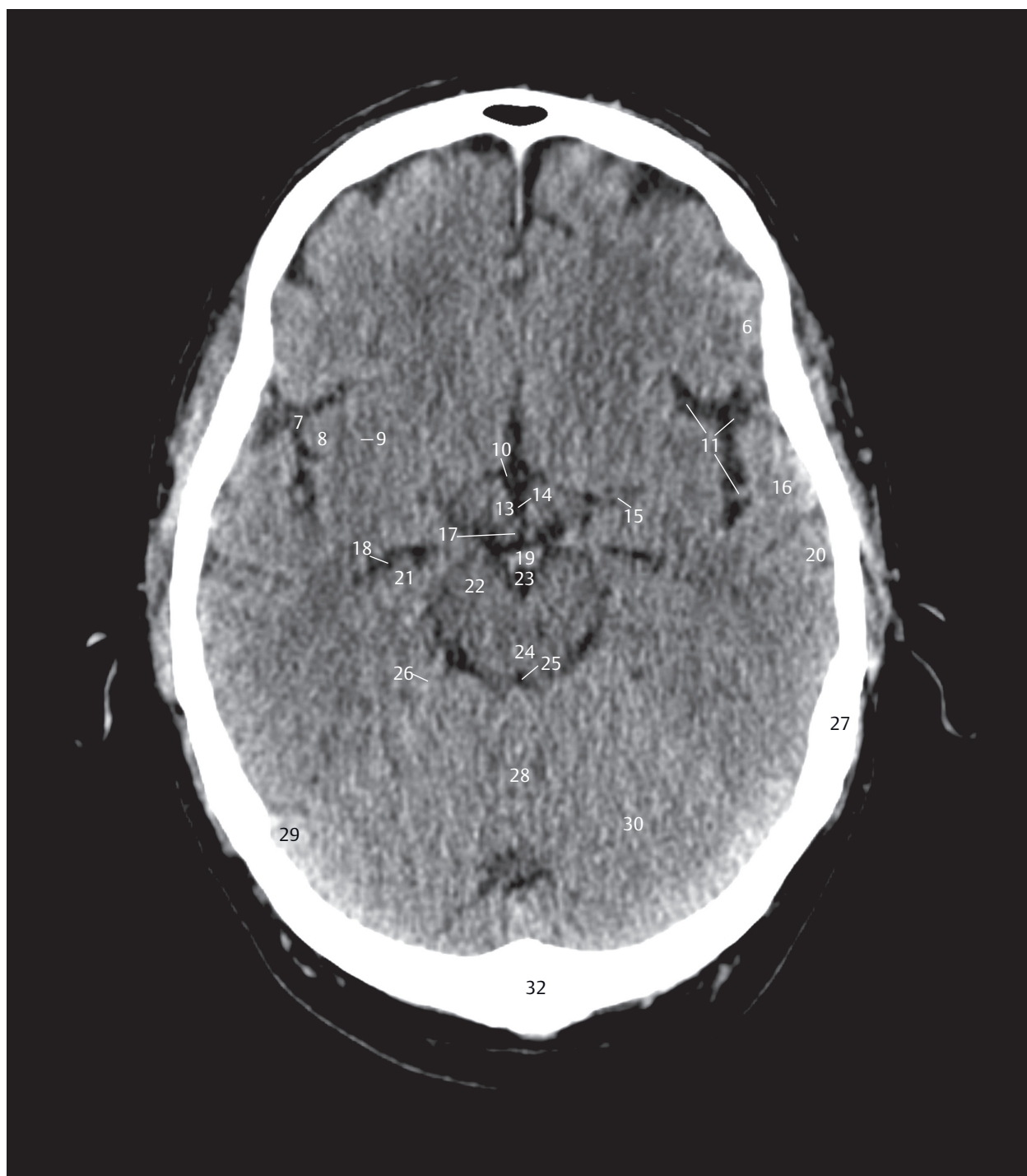


- 1 Frontal bone
- 2 Frontal sinus
- 3 Superior frontal gyrus
- 4 Middle frontal gyrus
- 5 Pericallosal artery
- 6 Frontal operculum, Inferior frontal gyrus
- 7 Cistern of lateral cerebral fossa
- 8 Insula
- 9 Claustrum
- 10 Anterior cerebral artery
- 11 Insular arteries
- 12 Lamina terminalis
- 13 Hypothalamus
- 14 Third ventricle
- 15 Middle cerebral artery
- 16 Superior temporal gyrus
- 17 Fornix
- 18 Lateral ventricle, temporal horn
- 19 Basilar artery
- 20 Middle temporal gyrus
- 21 Hippocampus
- 22 Cerebral crus
- 23 Interpeduncular cistern
- 24 Tegmentum of midbrain
- 25 Fourth ventricle
- 26 Tentorium of cerebellum
- 27 Temporal bone
- 28 Vermis of cerebellum
- 29 Sigmoid sinus
- 30 Cerebellum
- 31 Lambdoid suture
- 32 Occipital bone



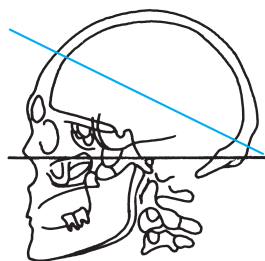
Fig. 5.22 6th supraorbito-suboccipital section.

Fig. 5.22a View of the 6th section of the supraorbito-suboccipital series. Parts of the anterior horns of the lateral ventricles lie in this plane. The third ventricle has been sectioned at its opening into the aqueduct of the midbrain. The inferior horns of the lateral ventricles have also been depicted. The anterior part of the tentorium of cerebellum has been sectioned. Brain structures, bony structures, and blood vessels.



- 1 Frontal bone
- 2 Frontal sinus
- 3 Superior frontal gyrus
- 4 Middle frontal gyrus
- 6 Frontal operculum, Inferior frontal gyrus
- 7 Cistern of lateral cerebral fossa
- 8 Insula
- 9 Claustrum
- 10 Anterior cerebral artery
- 11 Insular arteries
- 13 Hypothalamus
- 14 Third ventricle
- 15 Middle cerebral artery
- 16 Superior temporal gyrus
- 17 Fornix
- 18 Lateral ventricle, temporal horn
- 19 Basilar artery
- 20 Middle temporal gyrus
- 21 Hippocampus
- 22 Cerebral crus
- 23 Interpeduncular cistern
- 24 Tegmentum of midbrain
- 25 Fourth ventricle
- 26 Tentorium of cerebellum
- 27 Temporal bone
- 28 Vermis of cerebellum
- 29 Sigmoid sinus
- 30 Cerebellum
- 32 Occipital bone

Fig. 5.22b Supraorbital-suboccipital oriented CT image, lying exactly in the selected sectional plane as in a.



- 1 Frontal bone
- 2 Superior sagittal sinus
- 3 Superior frontal gyrus
- 4 Falx cerebri
- 5 Middle frontal gyrus
- 6 Cingulate gyrus
- 7 Anterior cerebral artery
- 8 Corpus callosum, genu
- 9 Lateral ventricle, frontal horn
- 10 Head of caudate nucleus
- 11 Lateral sulcus
- 12 Internal capsule, anterior limb
- 13 Insula
- 14 Superior temporal gyrus
- 15 Insular arteries
- 16 Fornix
- 17 Globus pallidus
- 18 Putamen
- 19 Claustrum
- 20 Third ventricle
- 21 Thalamus
- 22 Temporal bone
- 23 Cistern of lateral cerebral fossa
- 24 Middle temporal gyrus
- 25 Lateral ventricle, temporal horn
- 26 Hippocampus
- 27 Ambient cistern
- 28 Aqueduct of midbrain
- 29 Inferior colliculus
- 30 Quadrigeminal cistern
- 31 Vermis of cerebellum
- 32 Posterior lobe of cerebellum
- 33 Confluens of sinuses
- 34 Occipital bone

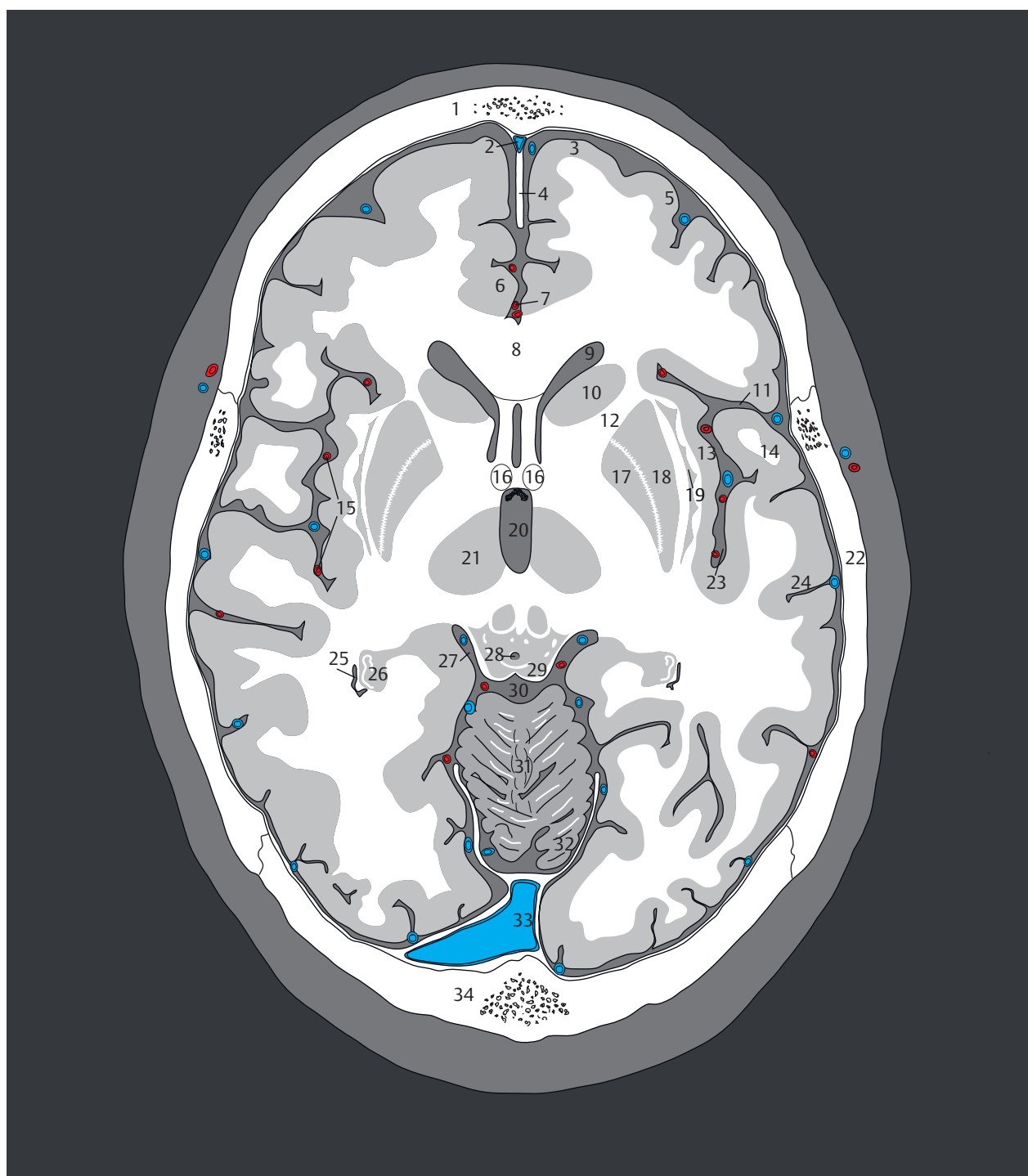
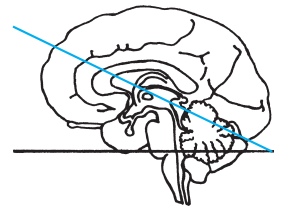
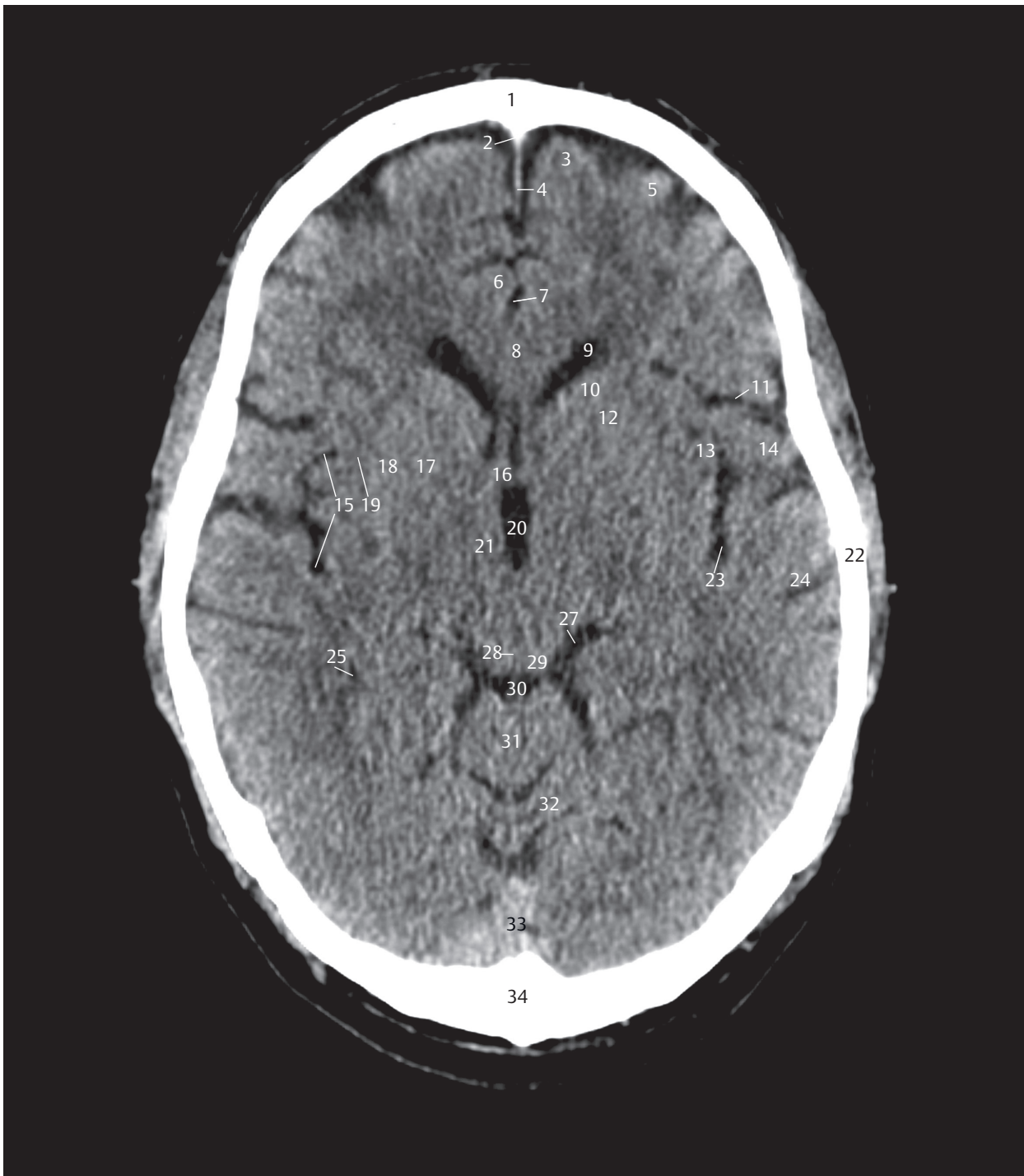


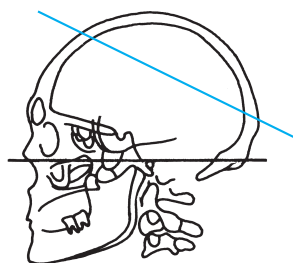
Fig. 5.23 7th supraorbito-suboccipital section.

Fig. 5.23a View of the 7th section of the supraorbito-suboccipital series. The sectional plane runs through the anterior horns of the lateral ventricles and the third ventricle. The quadrigeminal plate has been sectioned. Brain structures, bony structures, and blood vessels.



- 1 Frontal bone
- 2 Superior sagittal sinus
- 3 Superior frontal gyrus
- 4 Falx cerebri
- 5 Middle frontal gyrus
- 6 Cingulate gyrus
- 7 Anterior cerebral artery
- 8 Corpus callosum, genu
- 9 Lateral ventricle, frontal horn
- 10 Head of caudate nucleus
- 11 Lateral sulcus
- 12 Internal capsule, anterior limb
- 13 Insula
- 14 Superior temporal gyrus
- 15 Insular arteries
- 16 Fornix
- 17 Globus pallidus
- 18 Putamen
- 19 Claustrum
- 20 Third ventricle
- 21 Thalamus
- 22 Temporal bone
- 23 Cistern of lateral cerebral fossa
- 24 Middle temporal gyrus
- 25 Lateral ventricle, temporal horn
- 27 Ambient cistern
- 28 Aqueduct of midbrain
- 29 Inferior colliculus
- 30 Quadrigeminal cistern
- 31 Vermis of cerebellum
- 32 Cerebellum
- 33 Confluens of sinuses
- 34 Occipital bone

Fig. 5.23b Supraorbito-suboccipital oriented CT image, lying exactly in the selected sectional plane as in a.

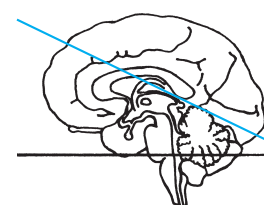
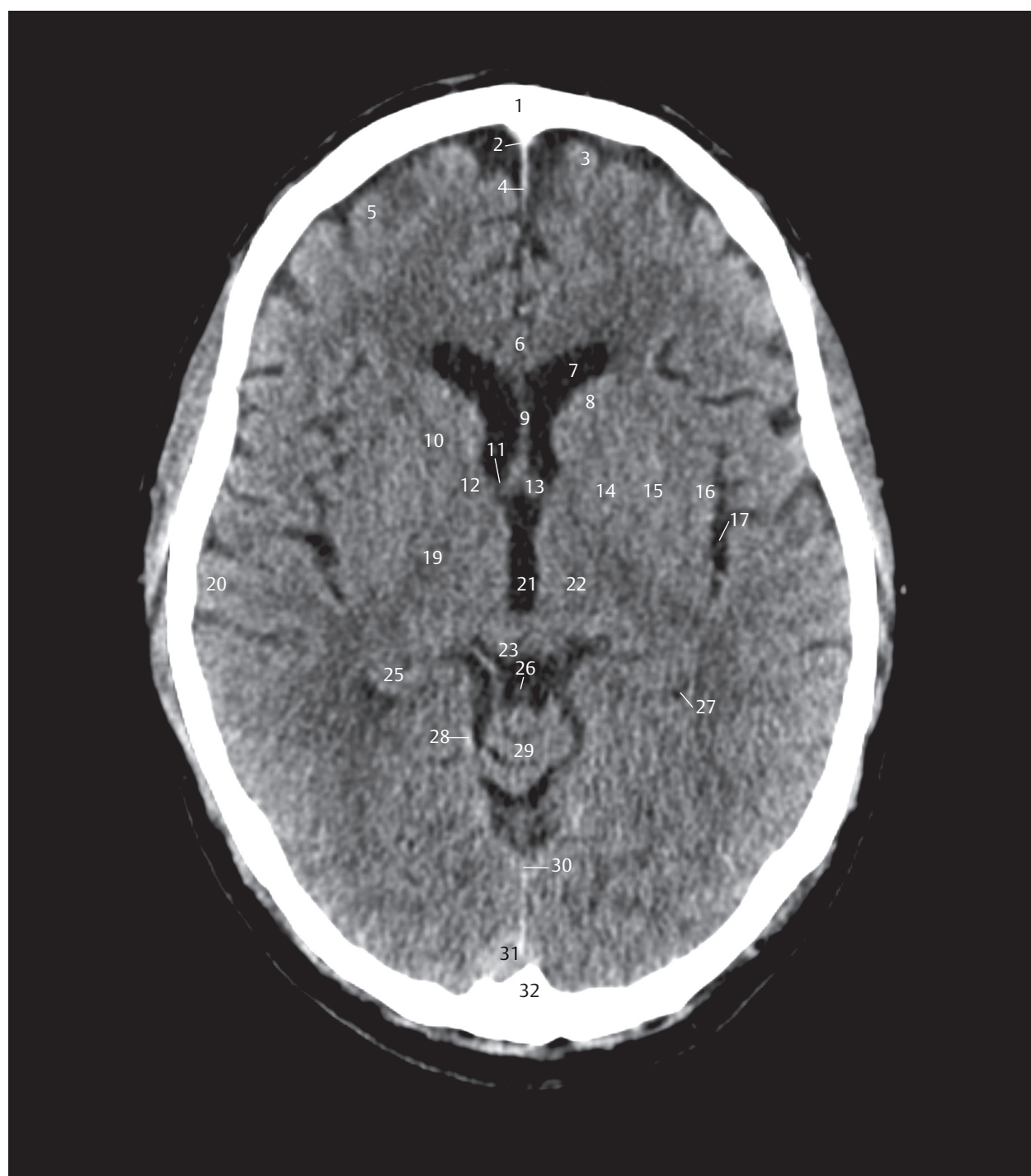


- 1 Frontal bone
- 2 Superior sagittal sinus
- 3 Superior frontal gyrus
- 4 Falx cerebri
- 5 Middle frontal gyrus
- 6 Corpus callosum, genu
- 7 Lateral ventricle, frontal horn
- 8 Head of caudate nucleus
- 9 Septum pellucidum
- 10 Internal capsule, anterior limb
- 11 Interventricular foramen (Monro)
- 12 Internal capsule, genu
- 13 Fornix
- 14 Globus pallidus
- 15 Putamen
- 16 Insula
- 17 Cistern of lateral cerebral fossa
- 18 Insular arteries
- 19 Internal capsule, posterior limb
- 20 Middle temporal gyrus
- 21 Third ventricle
- 22 Thalamus
- 23 Superior colliculus
- 24 Aqueduct of midbrain
- 25 Hippocampus
- 26 Vein of Galen
- 27 Choroid plexus of lateral ventricle
- 28 Cerebellar tentorium
- 29 Cerebellum, anterior lobe
- 30 Sinus rectus
- 31 Superior sagittal sinus
- 32 Occipital bone



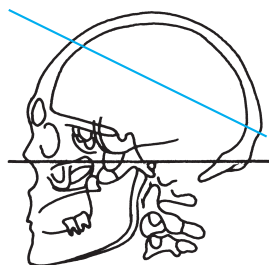
Fig. 5.24 8th supraorbito-suboccipital section.

Fig. 5.24a View of the 8th section of the supraorbito-suboccipital series. The sectional plane touches the lateral ventricles and slices the posterior horns just below the collateral trigone of the lateral ventricle. Brain structures, bony structures, and blood vessels.



- 1 Frontal bone
- 2 Superior sagittal sinus
- 3 Superior frontal gyrus
- 4 Falx cerebri
- 5 Middle frontal gyrus
- 6 Corpus callosum, genu
- 7 Lateral ventricle, frontal horn
- 8 Head of caudate nucleus
- 9 Septum pellucidum
- 10 Internal capsule, anterior limb
- 11 Interventricular foramen (Monro)
- 12 Internal capsule, genu
- 13 Fornix
- 14 Globus pallidus
- 15 Putamen
- 16 Insula
- 17 Cistern of lateral cerebral fossa
- 19 Internal capsule, posterior limb
- 20 Middle temporal gyrus
- 21 Third ventricle
- 22 Thalamus
- 23 Superior colliculus
- 25 Hippocampus
- 26 Vein of Galen
- 27 Choroid plexus of lateral ventricle
- 28 Cerebellar tentorium
- 29 Cerebellum, anterior lobe
- 30 Sinus rectus
- 31 Superior sagittal sinus
- 32 Occipital bone

Fig. 5.24b Supraorbito-suboccipital oriented CT image, lying exactly in the selected sectional plane as in a.



- 1 Frontal bone
- 2 Superior sagittal sinus
- 3 Superior frontal gyrus
- 4 Falx cerebri
- 5 Middle frontal gyrus
- 6 Cingulate gyrus
- 7 Corpus callosum
- 8 Lateral ventricle, frontal horn
- 9 Septum pellucidum
- 10 Head of caudate nucleus
- 11 Fornix
- 12 Interventricular foramen (Monro) with choroid plexus
- 13 Internal capsule, anterior limb
- 14 Putamen
- 15 Insula
- 16 Internal cerebral veins
- 17 Thalamus
- 18 Cistern of lateral cerebral fossa
- 19 Pineal gland
- 20 Collateral trigone and choroid plexus
- 21 Vermis of cerebellum
- 22 Cerebellar tentorium
- 23 Straight sinus
- 24 Superior sagittal sinus
- 25 Occipital gyri
- 26 Occipital bone

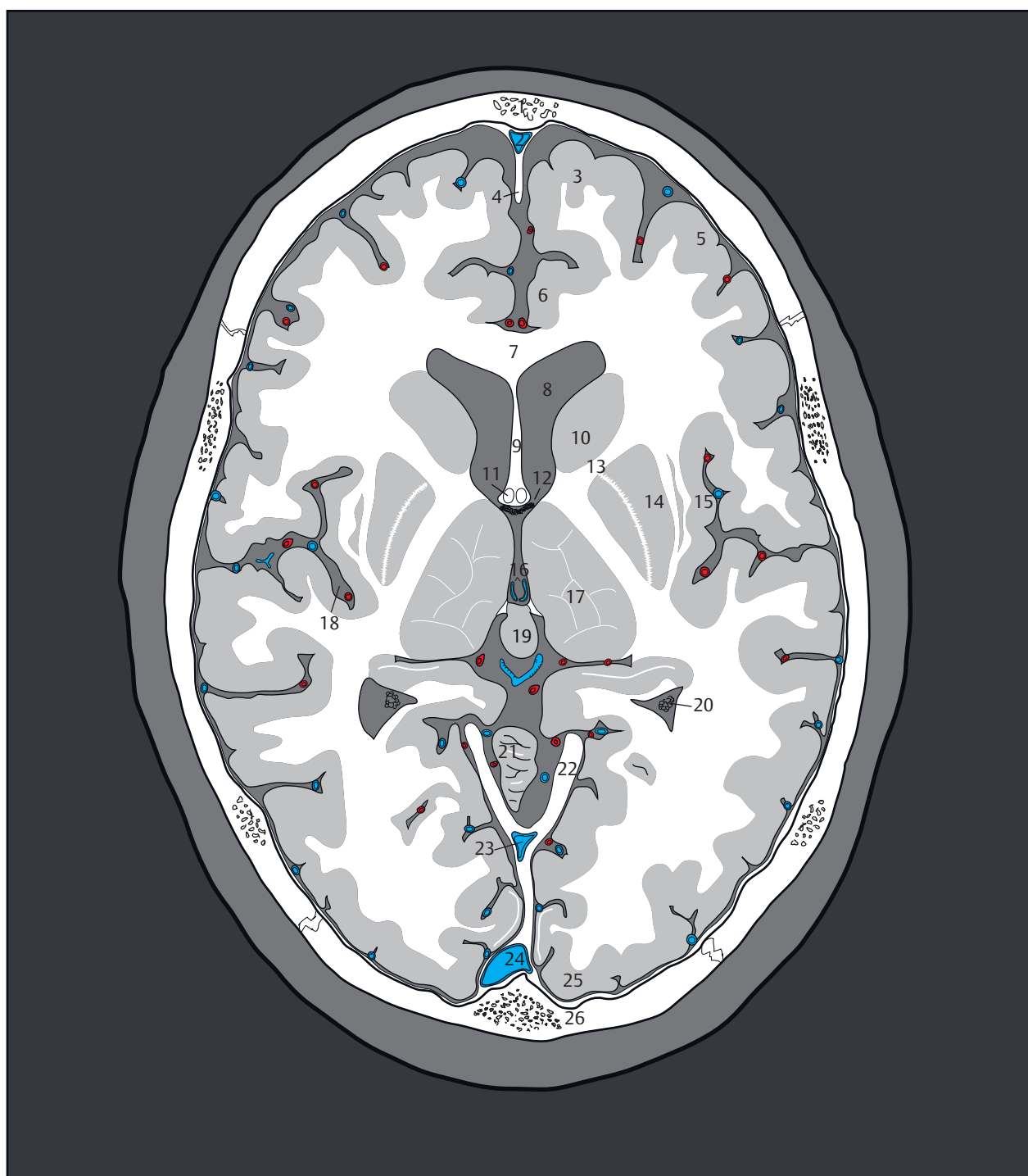
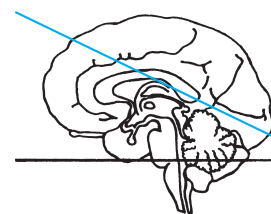
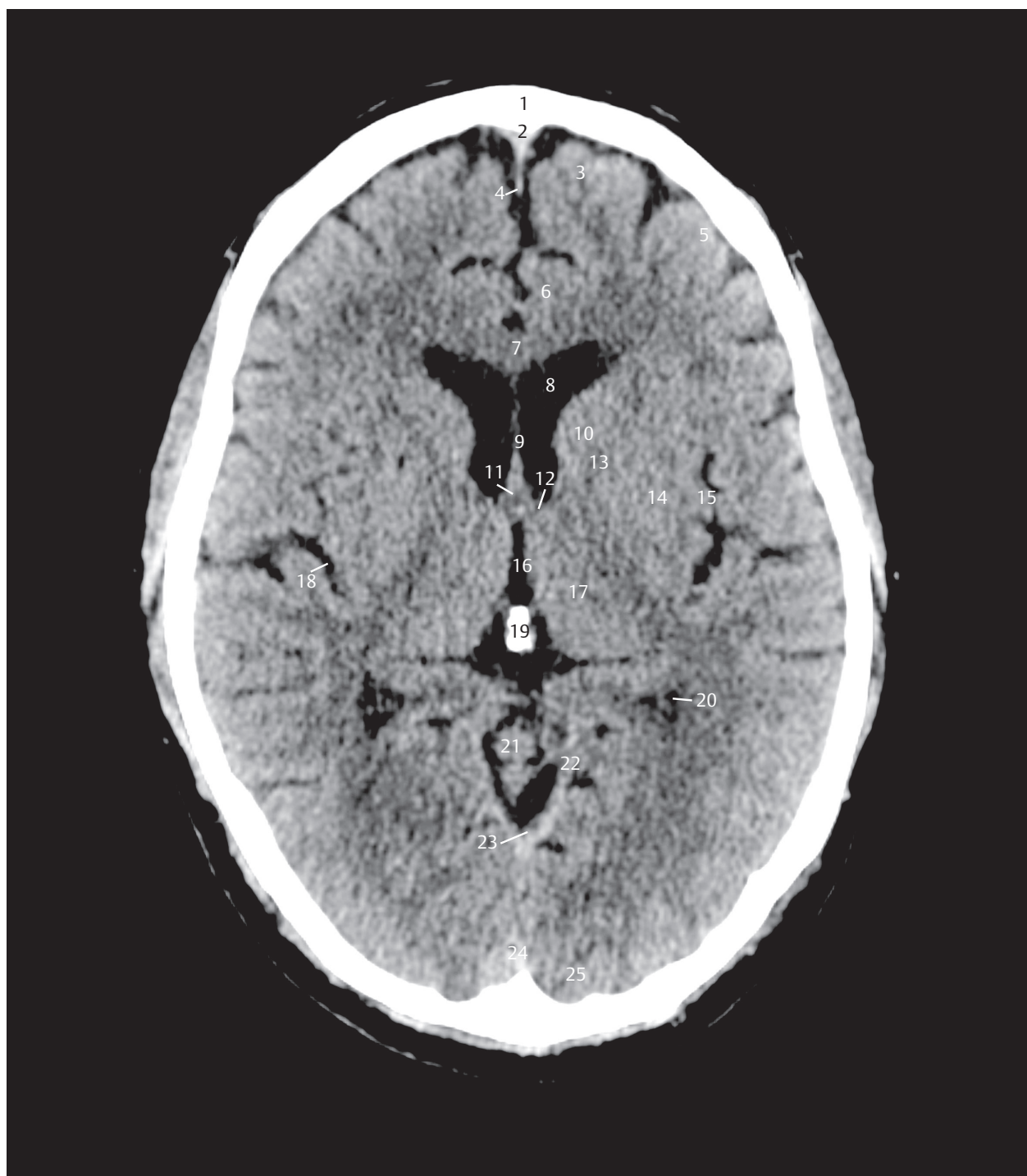


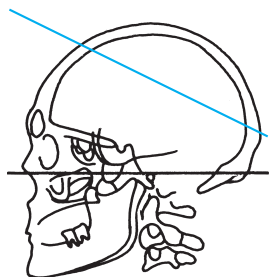
Fig. 5.25 9th supraorbito-suboccipital section.

Fig. 5.25a View of the 9th section of the supraorbito-suboccipital series. The thalamus and the collateral trigone of the lateral ventricle have been sectioned. Brain structures, bony structures, and blood vessels.



- 1 Frontal bone
- 2 Superior sagittal sinus
- 3 Superior frontal gyrus
- 4 Falx cerebri
- 5 Middle frontal gyrus
- 6 Cingulate gyrus
- 7 Corpus callosum
- 8 Lateral ventricle, frontal horn
- 9 Septum pellucidum
- 10 Head of caudate nucleus
- 11 Fornix
- 12 Interventricular foramen (Monro) with choroid plexus
- 13 Internal capsule, anterior limb
- 14 Putamen
- 15 Insula
- 17 Thalamus
- 18 Cistern of lateral cerebral fossa
- 19 Pineal gland
- 20 Collateral trigone and choroid plexus
- 21 Vermis of cerebellum
- 22 Cerebellar tentorium
- 23 Straight sinus
- 24 Superior sagittal sinus
- 25 Occipital gyri
- 26 Occipital bone

Fig. 5.25b Supraorbital-suboccipital oriented CT image, lying exactly in the selected sectional plane as in a.



- 1 Frontal bone
- 2 Superior sagittal sinus
- 3 Superior frontal gyrus
- 4 Falx cerebri
- 5 Middle frontal gyrus
- 6 Cingulate sulcus
- 7 Cingulate gyrus
- 8 Precentral sulcus
- 9 Precentral gyrus
- 10 Central sulcus
- 11 Postcentral gyrus
- 12 Head of caudate nucleus
- 13 Thalamostriate vein
- 14 Choroid plexus, lateral ventricle
- 15 Centrum semiovale
- 16 Thalamus
- 17 Parietal bone
- 18 Sylvian fissure
- 19 Corpus callosum, splenium
- 20 Straight venous sinus
- 21 Parieto-occipital sulcus
- 22 Superior sagittal sinus
- 23 Occipital gyri
- 24 Lambdoid suture
- 25 Occipital bone

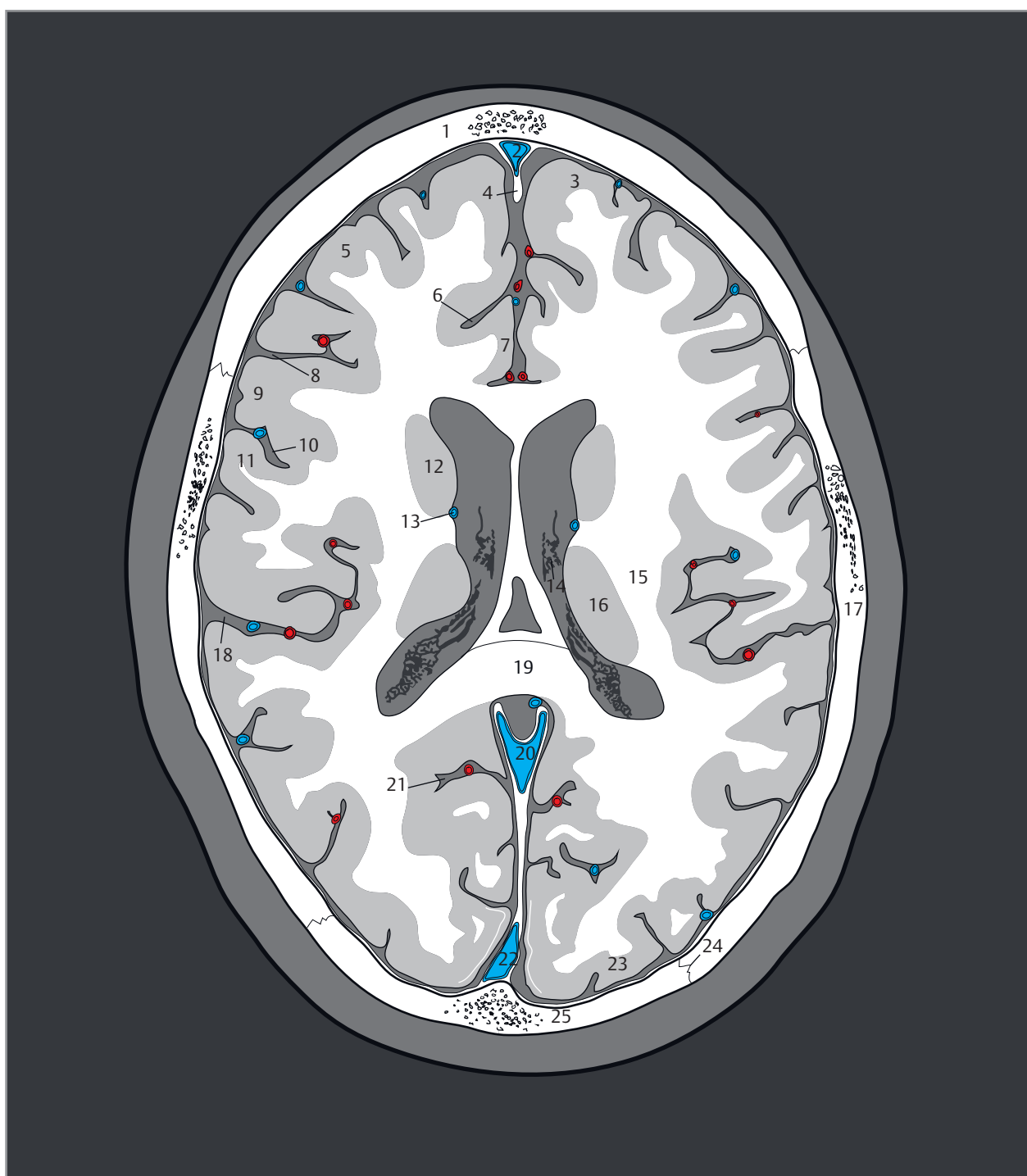
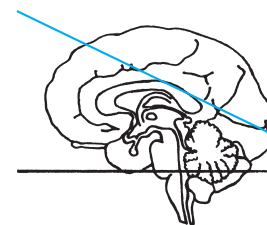
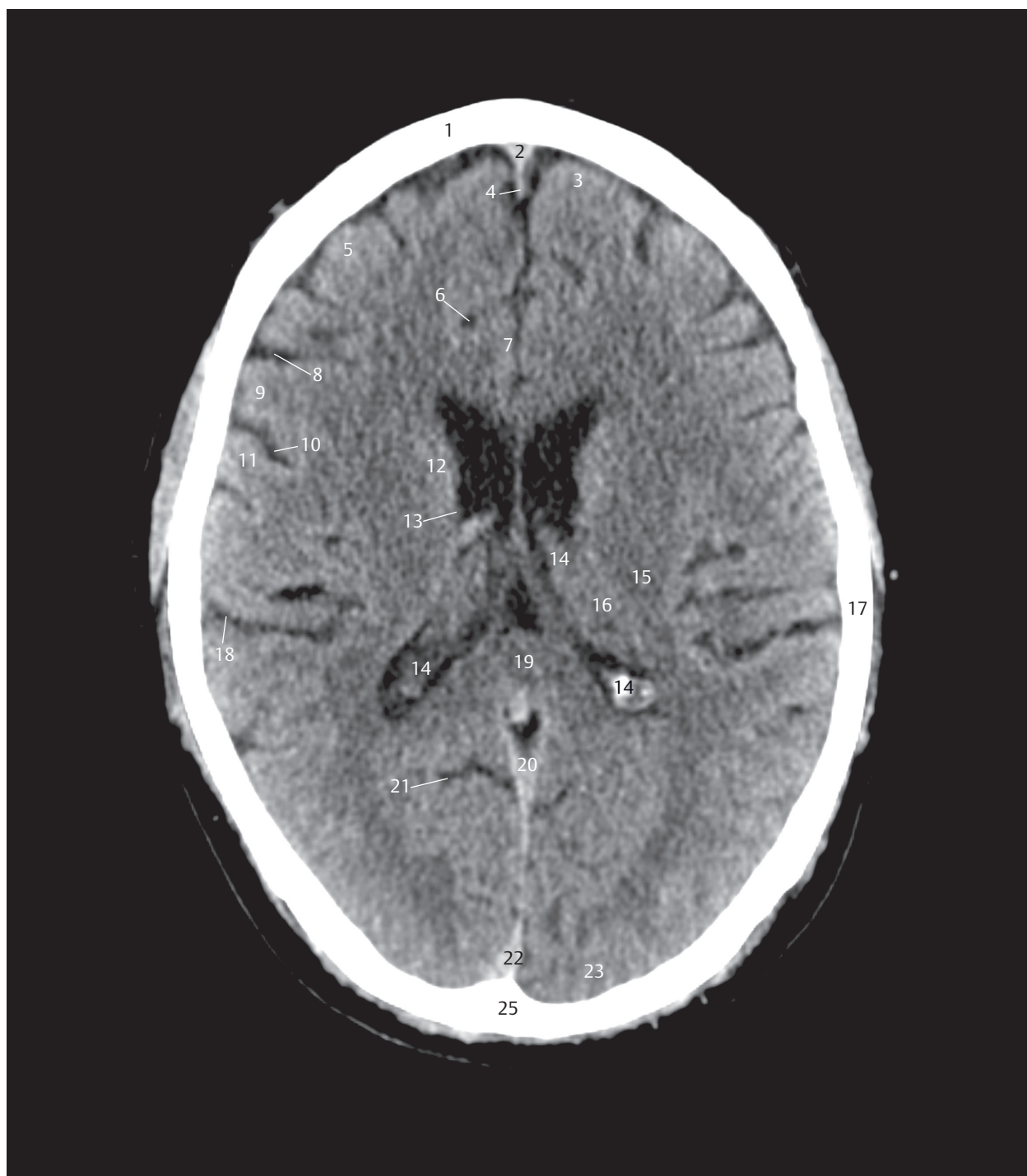


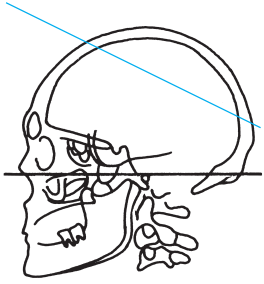
Fig. 5.26 10th supraorbital-suboccipital section.

Fig. 5.26a View of the 10th section of the supraorbital-suboccipital series. The corpus callosum builds the roof of the lateral ventricles which are still seen in the slice. Brain structures, bony structures, and blood vessels.



- 1 Frontal bone
- 2 Superior sagittal sinus
- 3 Superior frontal gyrus
- 4 Falx cerebri
- 5 Middle frontal gyrus
- 6 Cingulate sulcus
- 7 Cingulate gyrus
- 8 Precentral sulcus
- 9 Precentral gyrus
- 10 Central sulcus
- 11 Postcentral gyrus
- 12 Head of caudate nucleus
- 13 Thalamostriate vein
- 14 Choroid plexus, lateral ventricle
- 15 Centrum semiovale
- 16 Thalamus
- 17 Parietal bone
- 18 Sylvian fissure
- 19 Corpus callosum, splenium
- 20 Straight venous sinus
- 21 Parieto-occipital sulcus
- 22 Superior sagittal sinus
- 23 Occipital gyri
- 25 Occipital bone

Fig. 5.26b Supraorbito-suboccipital oriented CT image, lying exactly in the selected sectional plane as in a.



- 1 Frontal bone
- 2 Superior sagittal sinus
- 3 Superior frontal gyrus
- 4 Falx cerebri
- 5 Middle frontal gyrus
- 6 Precentral sulcus
- 7 Precentral gyrus
- 8 Central sulcus
- 9 Postcentral gyrus
- 10 Postcentral sulcus
- 11 Centrum semiovale
- 12 Inferior sagittal sinus
- 13 Parietal bone
- 14 Parieto-occipital sulcus
- 15 Superior sagittal sinus
- 16 Occipital bone

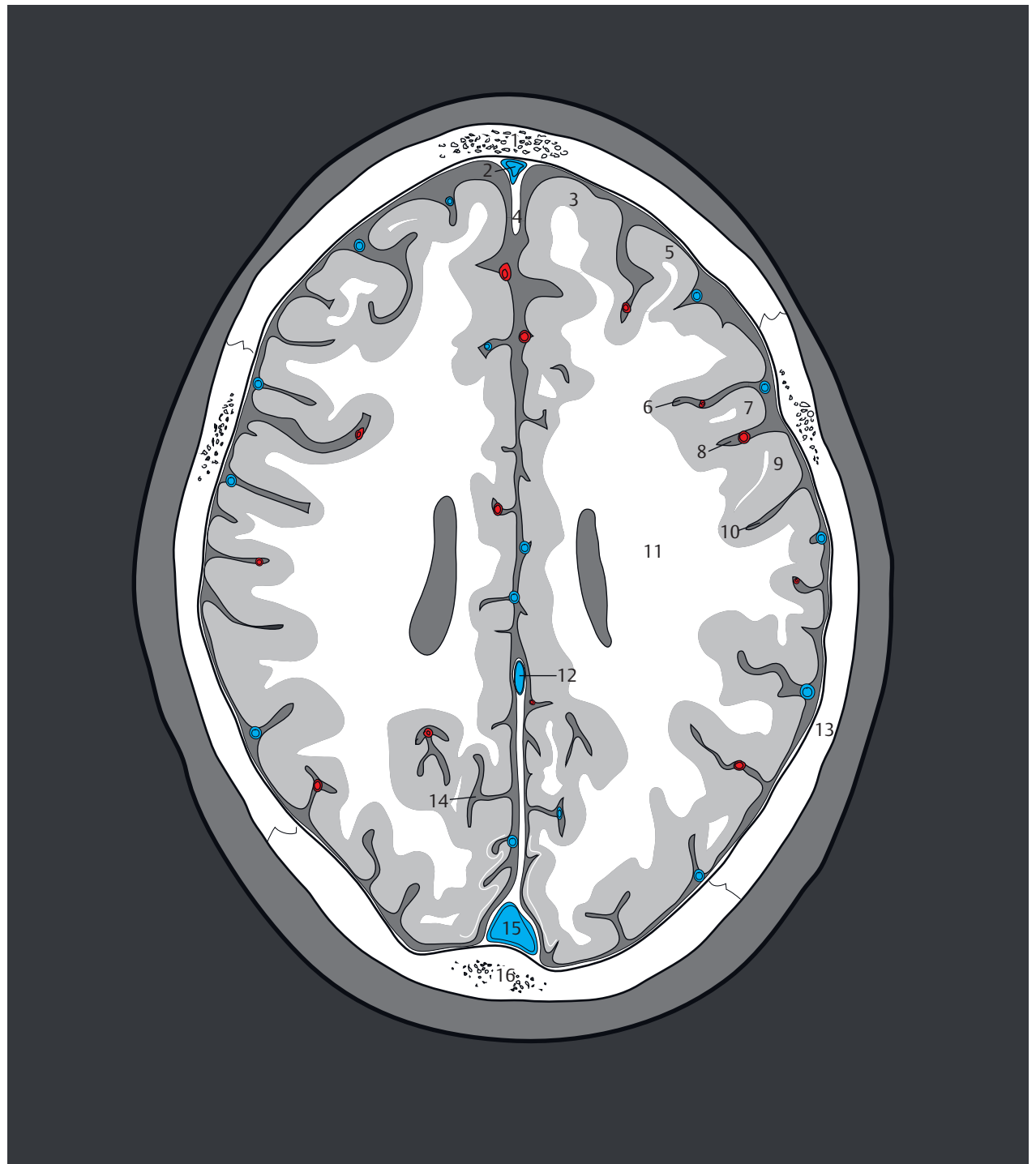
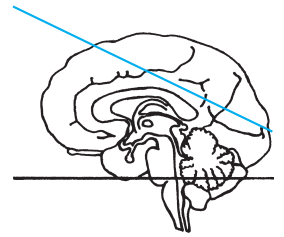
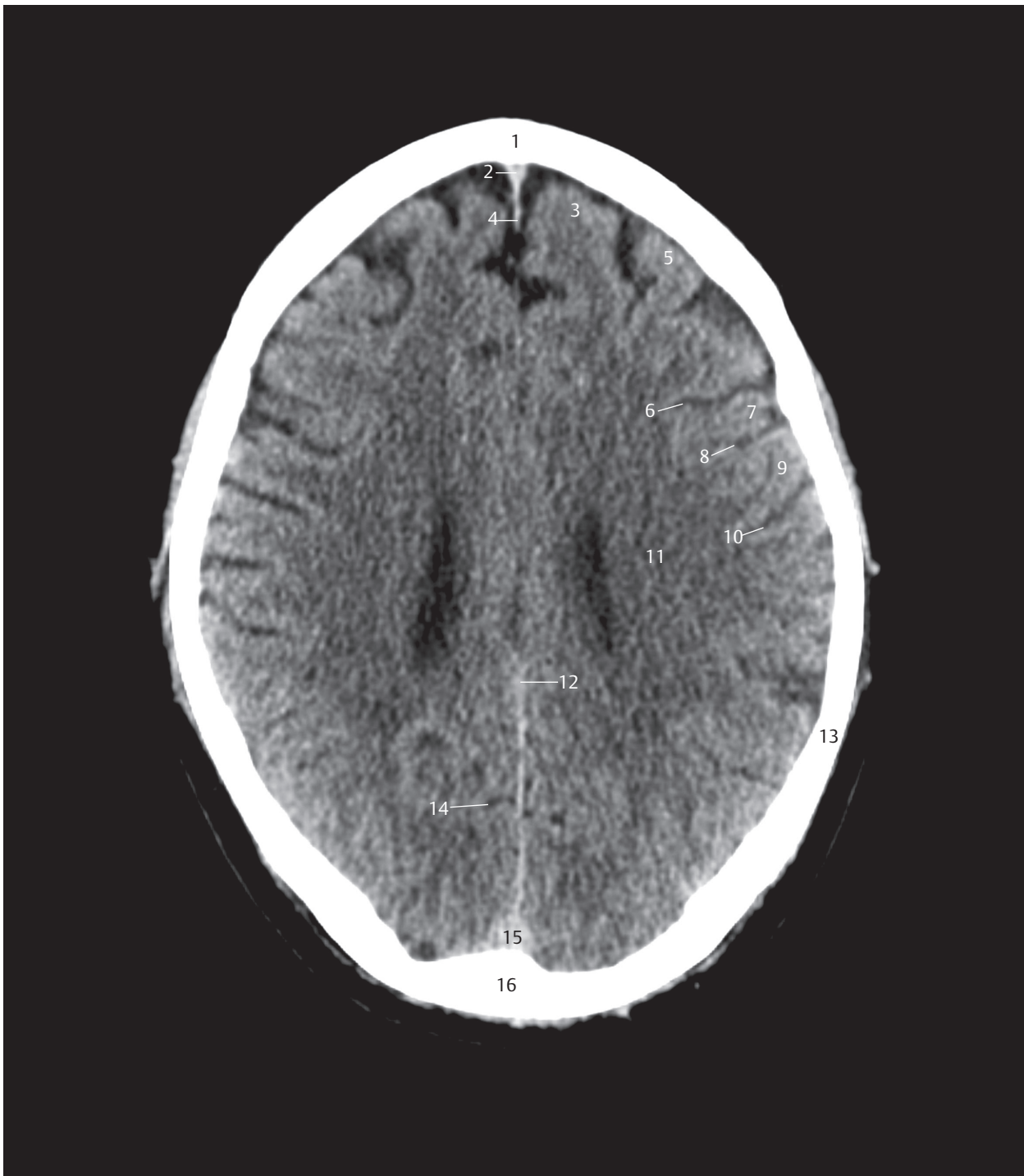


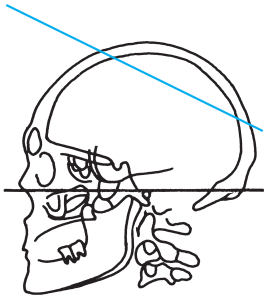
Fig. 5.27 11th supraorbito-suboccipital section.

Fig. 5.27a View of the 11th section of the supraorbito-suboccipital series. The sectional plane lies above the corpus callosum. Bony structures and blood vessels.



- 1 Frontal bone
- 2 Superior sagittal sinus
- 3 Superior frontal gyrus
- 4 Falx cerebri
- 5 Middle frontal gyrus
- 6 Precentral sulcus
- 7 Precentral gyrus
- 8 Central sulcus
- 9 Postcentral gyrus
- 10 Postcentral sulcus
- 11 Centrum semiovale
- 12 Inferior sagittal sinus
- 13 Parietal bone
- 14 Parieto-occipital sulcus
- 15 Superior sagittal sinus
- 16 Occipital bone

Fig. 5.27b Supraorbital-suboccipital oriented CT image, lying exactly in the selected sectional plane as in a.



- 1 Frontal bone
- 2 Superior sagittal sinus
- 3 Coronal suture
- 4 Falx cerebri
- 5 Superior frontal gyrus
- 6 Superior frontal sulcus
- 7 Middle frontal gyrus
- 8 Precentral sulcus
- 9 Precentral gyrus
- 10 Centrum semiovale
- 11 Central sulcus
- 12 Postcentral gyrus
- 13 Inferior parietal lobule
- 14 Parietal bone
- 15 Lambdoid suture

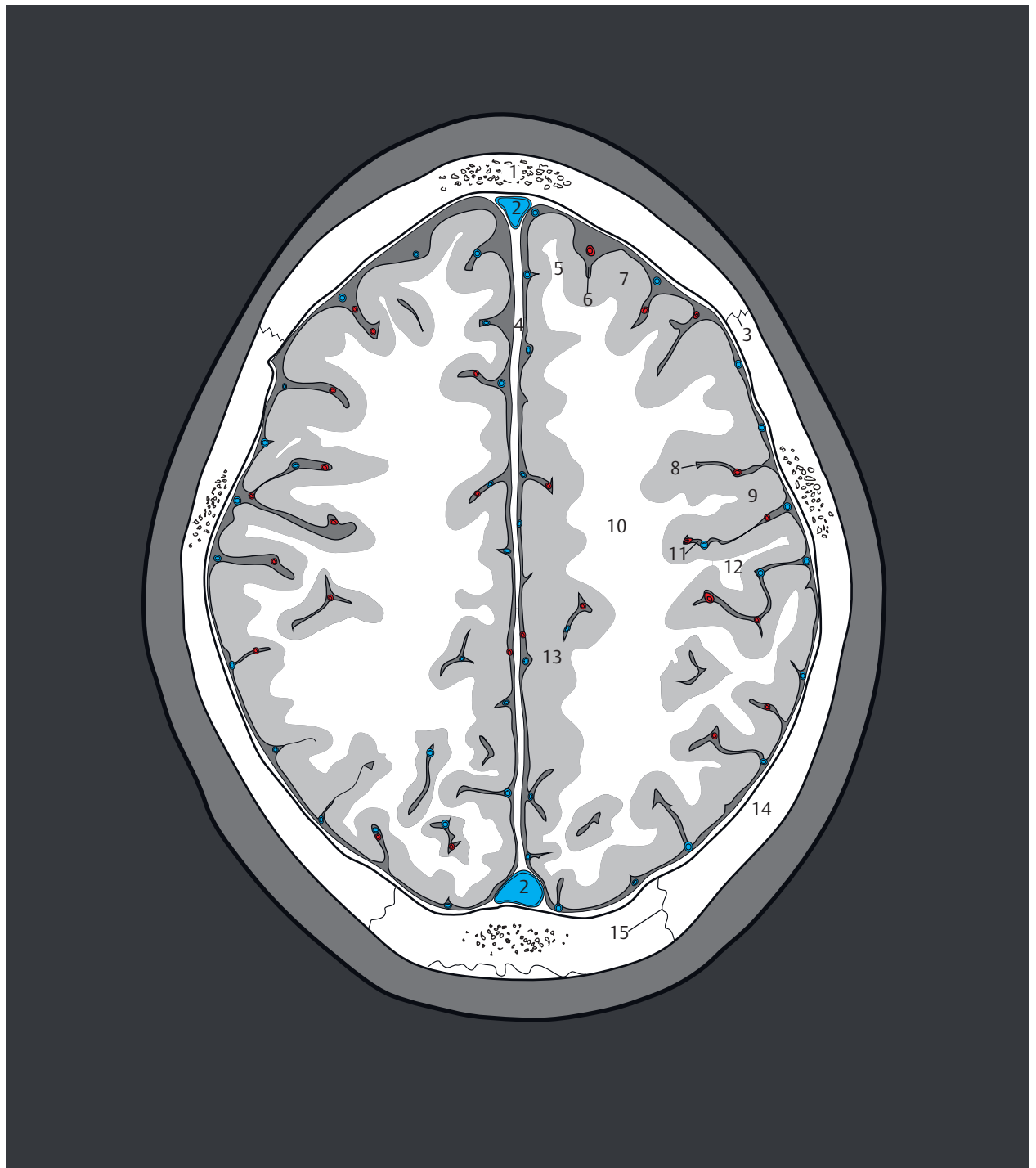
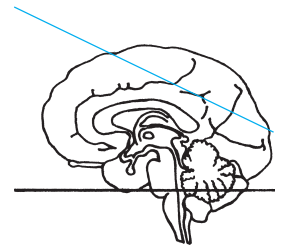
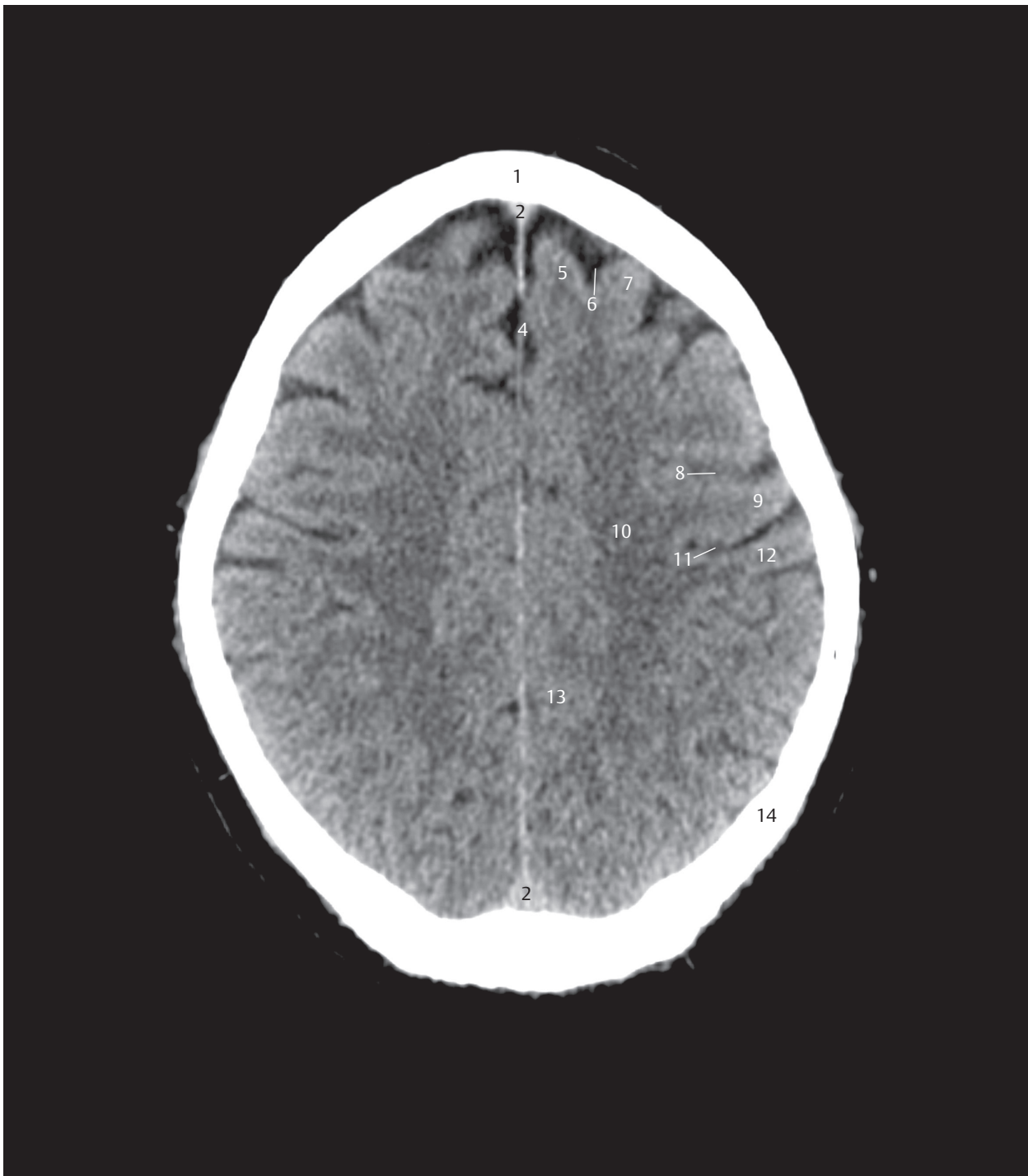


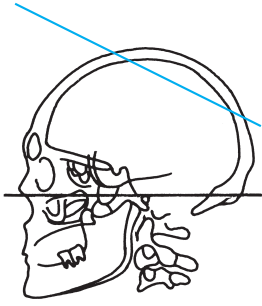
Fig. 5.28 12th supraorbito-suboccipital section.

Fig. 5.28a View of the 12th section of the supraorbito-suboccipital series. The sectional plane lies above the cingulate gyrus. Brain structures, bony structures, and blood vessels.



- 1 Frontal bone
- 2 Superior sagittal sinus
- 4 Falx cerebri
- 5 Superior frontal gyrus
- 6 Superior frontal sulcus
- 7 Middle frontal gyrus
- 8 Precentral sulcus
- 9 Precentral gyrus
- 10 Centrum semiovale
- 11 Central sulcus
- 12 Postcentral gyrus
- 13 Inferior parietal lobule
- 14 Parietal bone

Fig. 5.28b Supraorbital-suboccipital oriented CT image, lying exactly in the selected sectional plane as in a.



- 1 Frontal bone
- 2 Superior sagittal sinus
- 3 Superior frontal gyrus
- 4 Falx cerebri
- 5 Superior cerebral vein
- 6 Precentral sulcus
- 7 So-called knob on the precentral gyrus
- 8 Precentral gyrus
- 9 Central sulcus
- 10 Postcentral gyrus
- 11 Paracentral lobule
- 12 Postcentral sulcus
- 13 Cingulate sulcus, marginal branch
- 14 Paracentral artery
- 15 Superior parietal lobule
- 16 Parietal bone
- 17 Occipital bone

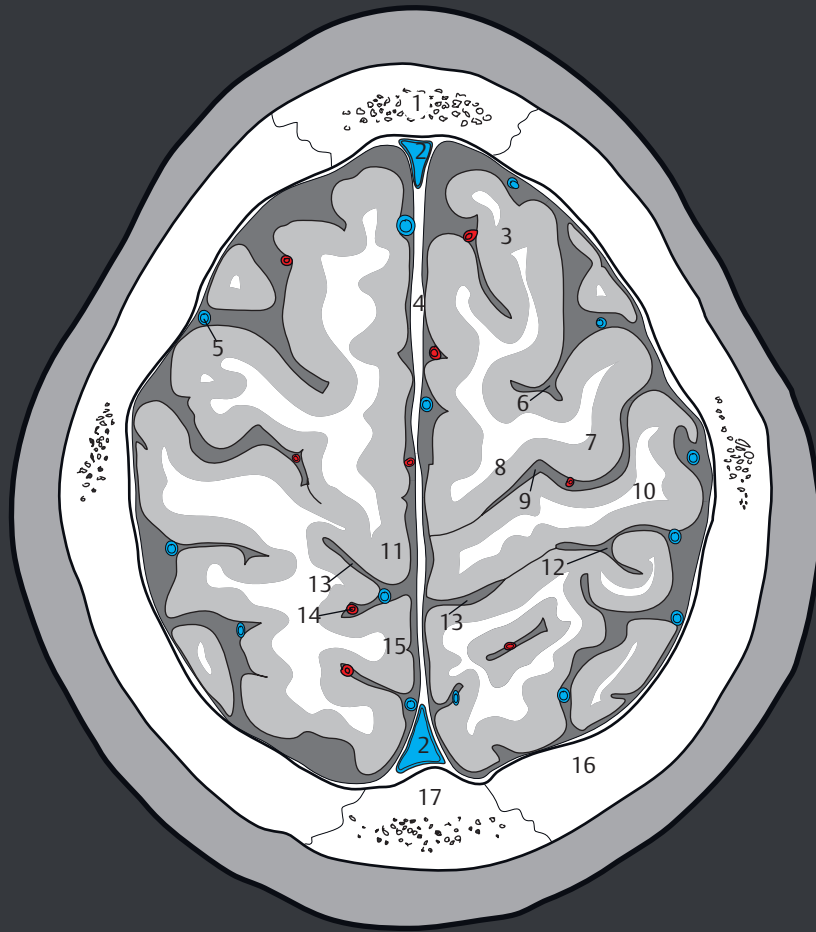
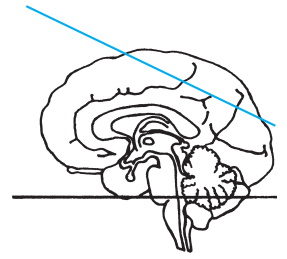
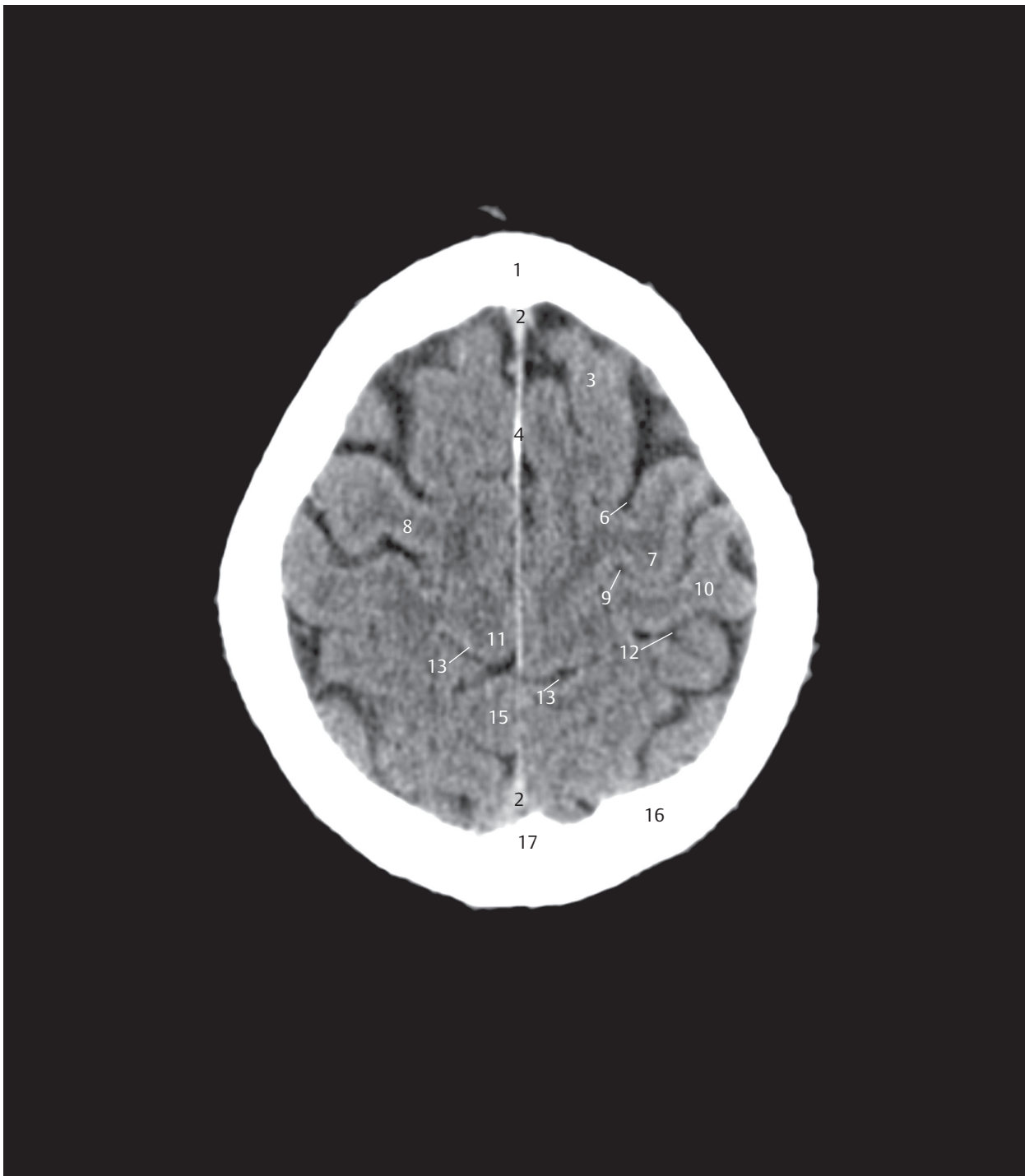


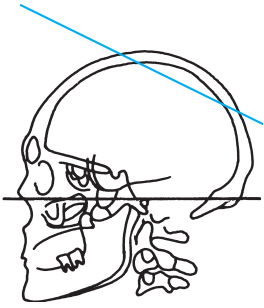
Fig. 5.29 13th supraorbito-suboccipital section.

Fig. 5.29a View of the 13th section of the supraorbito-suboccipital series. The sectional plane lies just beneath the cranial vault. Brain structures, bony structures, and blood vessels.



- 1 Frontal bone
- 2 Superior sagittal sinus
- 3 Superior frontal gyrus
- 4 Falx cerebri
- 6 Precentral sulcus
- 7 So-called knob on the precentral gyrus
- 8 Precentral gyrus
- 9 Central sulcus
- 10 Postcentral gyrus
- 11 Paracentral lobule
- 12 Postcentral sulcus
- 13 Cingulate sulcus, marginal branch
- 15 Superior parietal lobule
- 16 Parietal bone
- 17 Occipital bone

Fig. 5.29b Supraorbital-suboccipital oriented CT image, lying exactly in the selected sectional plane as in a.



- 1 Parietal bone
- 2 Sagittal suture
- 3 Superior sagittal sinus
- 4 Precentral gyrus
- 5 Central sulcus
- 6 Postcentral gyrus
- 7 Postcentral sulcus
- 8 Superior cerebral vein
- 9 Cingulate sulcus, marginal branch
- 10 Parietal lobule

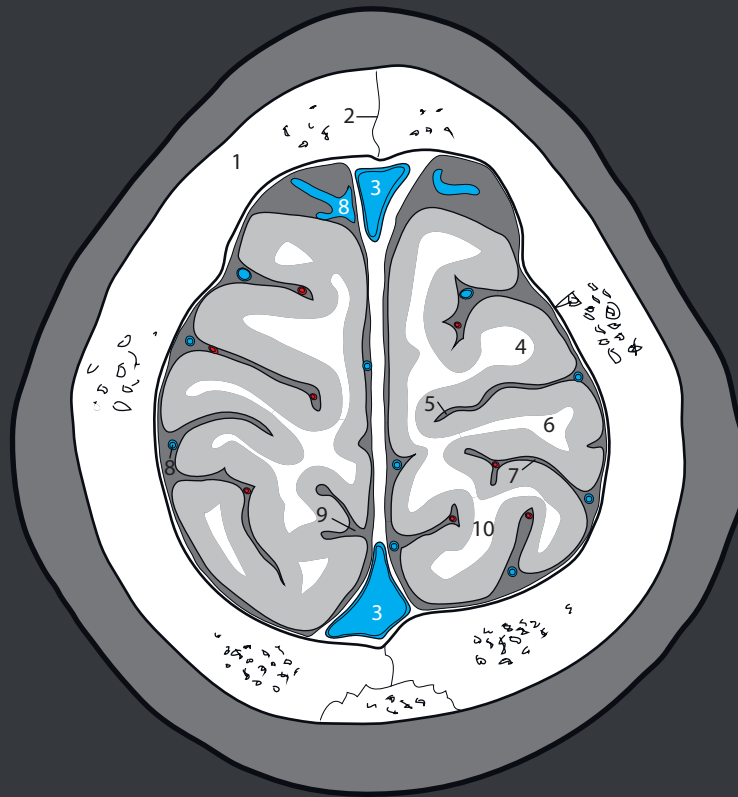
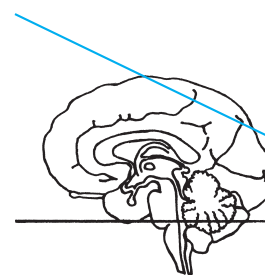
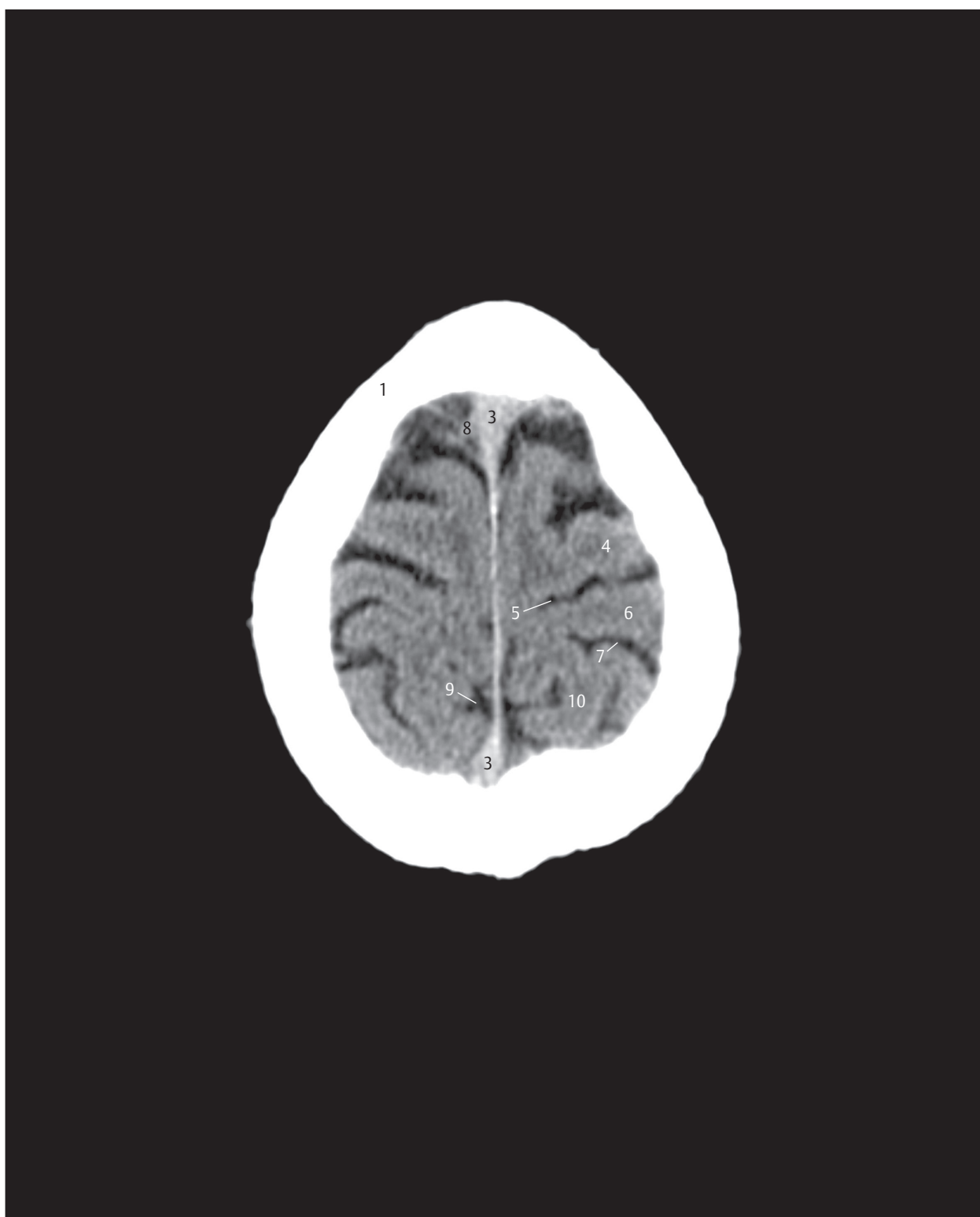


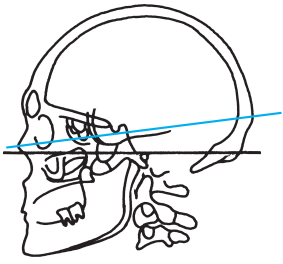
Fig. 5.30 14th supraorbital-suboccipital section.

Fig. 5.30a View of the 14th section of the supraorbital-suboccipital series. The sectional plane lies directly beneath the cranial vault. Brain structures, bony structures, and blood vessels.



- 1 Parietal bone
- 3 Superior sagittal sinus
- 4 Precentral gyrus
- 5 Central sulcus
- 6 Postcentral gyrus
- 7 Postcentral sulcus
- 8 Superior cerebral vein
- 9 Cingulate sulcus, marginal branch
- 10 Parietal lobule

Fig. 5.30b Supraorbito-suboccipital oriented CT image, lying exactly in the selected sectional plane as in a.



- 1 Nasal bone
- 2 Nasal septum
- 3 Zygomatic bone
- 4 Maxillary sinus
- 5 Coronoid process of mandible
- 6 Pterygoid process, lateral plate
- 7 Pterygoid fossa
- 8 Mandible
- 9 Styloid process
- 10 Clivus
- 11 Hypoglossal canal
- 12 Jugular foramen
- 13 External ear
- 14 Sigmoid sulcus
- 15 Mastoid cells
- 16 Emissary vein

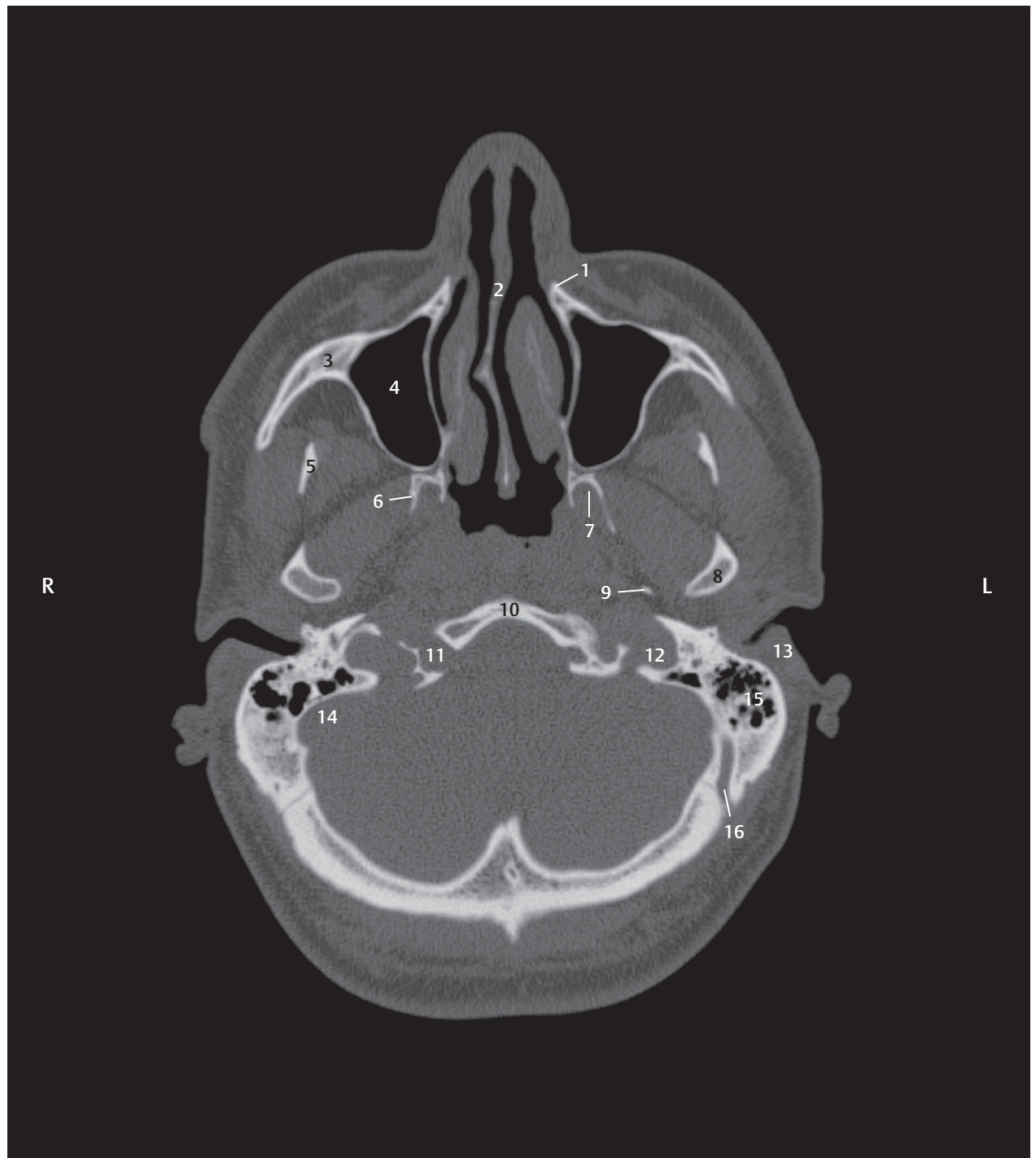
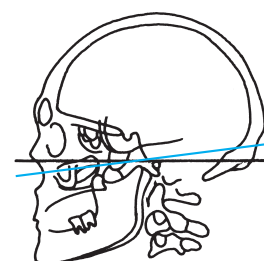
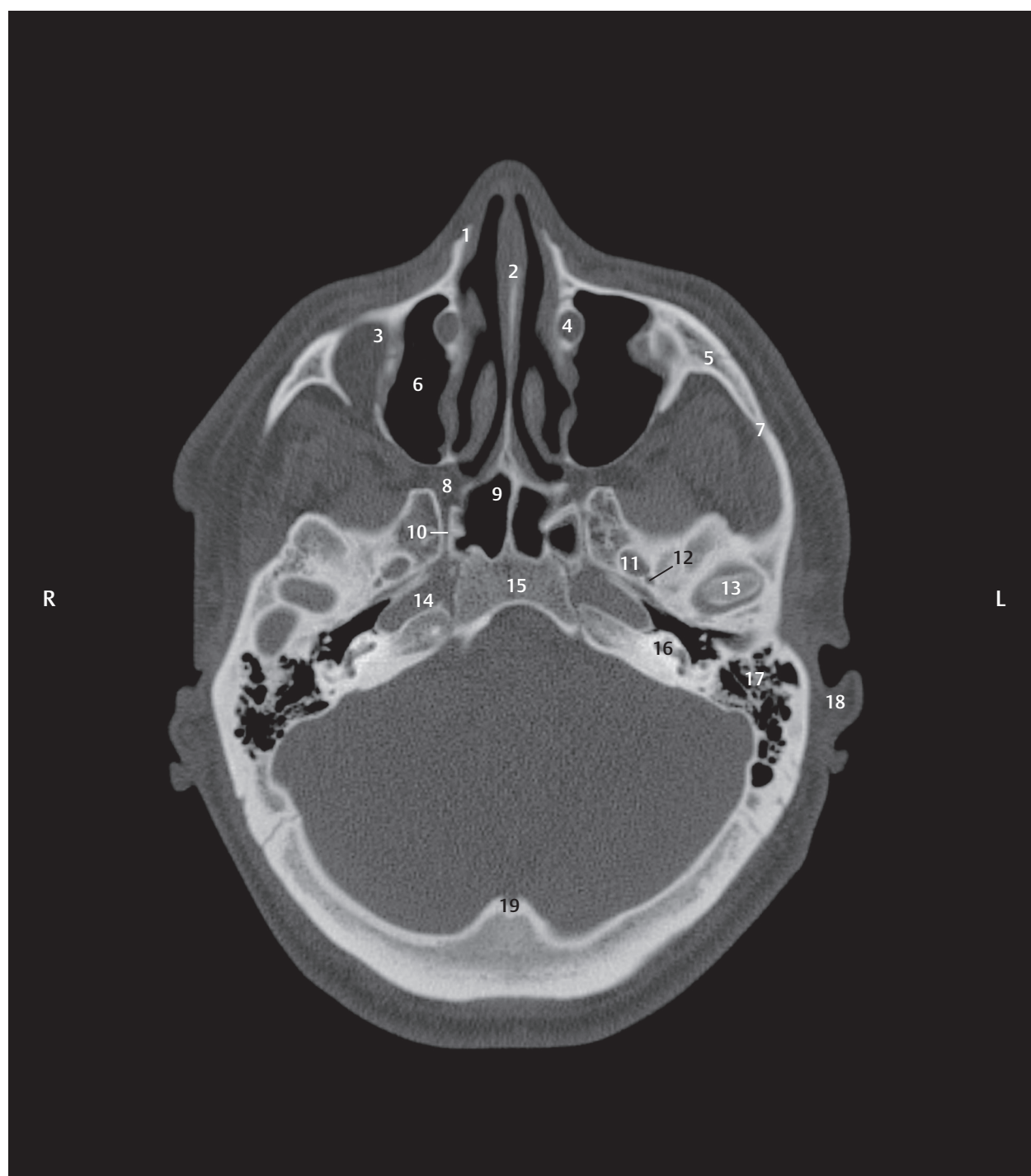
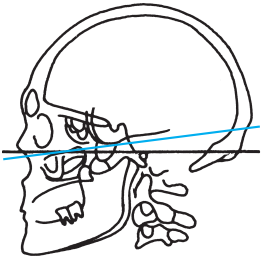


Fig. 5.31 Transverse image of the base of skull. CT image of the base of the skull, oriented perpendicular to the Meynert axis. This and the following images were reconstructed from a thin-section transverse data set of a diagnostic examination. Bony landmarks in this image are the turbinates, maxillary sinuses, the mastoid, and the occipital bone.



- 1 Nasal bone
- 2 Nasal septum
- 3 Orbit
- 4 Nasolacrimal duct
- 5 Zygomatic bone
- 6 Maxillary sinus
- 7 Zygomatic arch
- 8 Pterygopalatine fossa
- 9 Sphenoid sinus
- 10 Nerve of pterygoid canal (vidian)
- 11 Foramen ovale
- 12 Foramen spinosum
- 13 Mandible
- 14 Carotid canal
- 15 Clivus
- 16 Cochlea
- 17 Mastoid cells
- 18 External ear
- 19 Internal occipital protuberance

Fig. 5.32 Transverse image of the base of skull. CT image of the base of the skull, oriented perpendicular to the Meynert axis. Bony landmarks are the nasal bone, the nasal septum, and the petrous part of temporal bone. Exits of the V/3 cranial nerve and the middle meningeal artery have been depicted.



- 1 Nasolacrimal duct
- 2 Orbit
- 3 Zygomatic bone
- 4 Inferior orbital fissure
- 5 Pterygopalatine fossa
- 6 Sphenoid sinus
- 7 Sphenoid bone ,
floor of middle cranial fossa
- 8 Carotid canal
- 9 Temporal bone
- 10 Clivus
- 11 Internal acoustic meatus
- 12 Tympanum
- 13 Facial canal
(geniculate ganglion)
- 14 Occipital bone
- 15 Entrance to foramen ovale

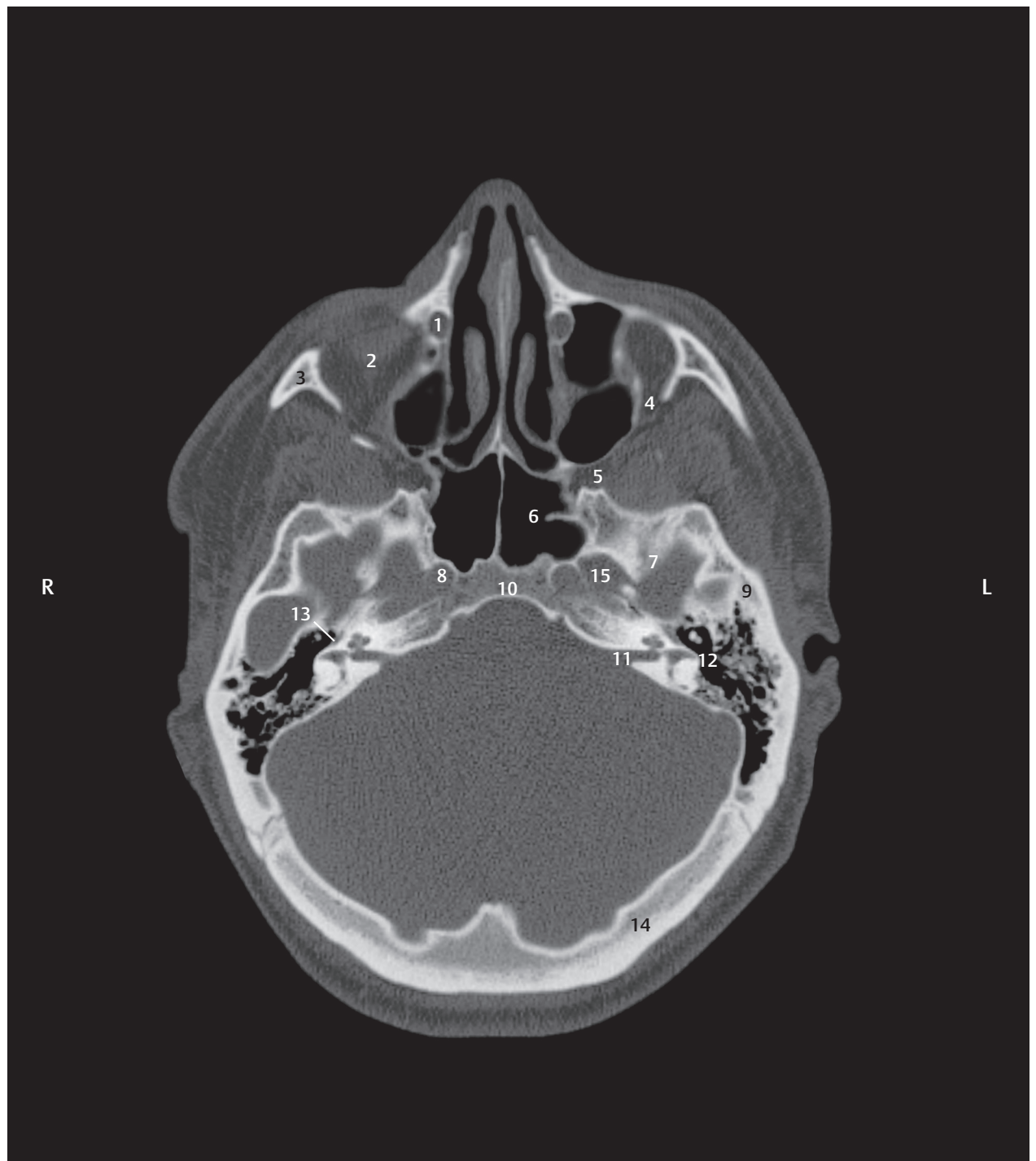
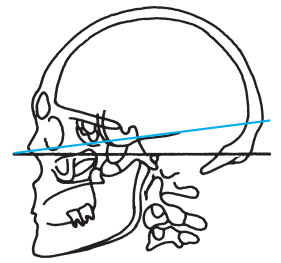
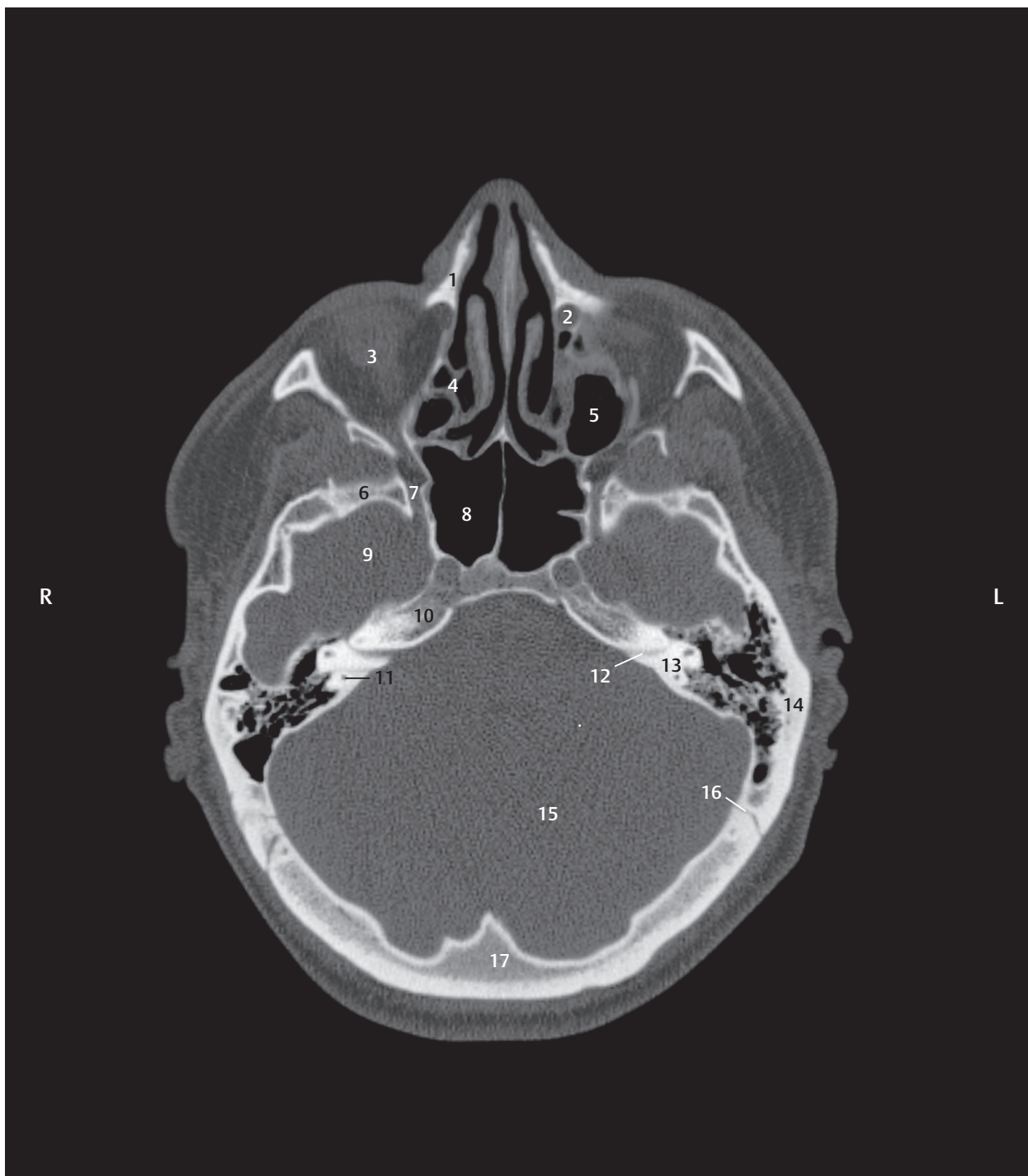
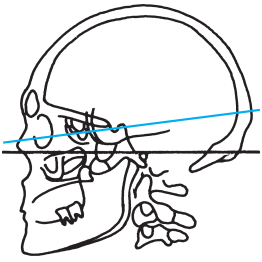


Fig. 5.33 Transverse image of the base of skull. CT image of the base of the skull, oriented perpendicular to the Meynert axis. The medial and lateral walls of the orbit have been sectioned. The sphenoid bone forms the floor of the middle cranial fossa. The occipital bone surrounds the posterior cranial fossa. Exits of the internal carotid artery and the V/3 and VIIth cranial nerves have been depicted.



- 1 Nasal bone
- 2 Nasolacrimal duct
- 3 Orbit
- 4 Ethmoidal air cells
- 5 Maxillary sinus
- 6 Sphenoid bone
- 7 Foramen rotundum
- 8 Sphenoid sinus
- 9 Middle cranial fossa
- 10 Petrous apex
- 11 Semicircular canal
- 12 Internal acoustic canal
- 13 Petrous part
- 14 Temporal bone
- 15 Posterior cranial fossa
- 16 Lambdoid suture
- 17 Occipital bone

Fig. 5.34 Transverse image of the base of skull. CT image of the base of the skull, oriented perpendicular to the Meynert axis. The inferior aspect of the orbit and the sphenoid sinus as well as the middle cranial fossa, exit of the V/2 cranial nerve, the petrous part of the temporal bone, and the posterior cranial fossa can be identified.



- 1 Ethmoidal air cells
- 2 Orbit
- 3 Lamina papyracea
- 4 Sphenoid
- 5 Superior orbital fissure
- 6 Anterior clinoid process
- 7 Middle cranial fossa
- 8 Hypophyseal fossa
- 9 Dorsum sellae
- 10 Posterior clinoid process
- 11 Posterior cranial fossa
- 12 Lambdoid suture
- 13 Internal occipital protuberance
- 14 Occipital bone

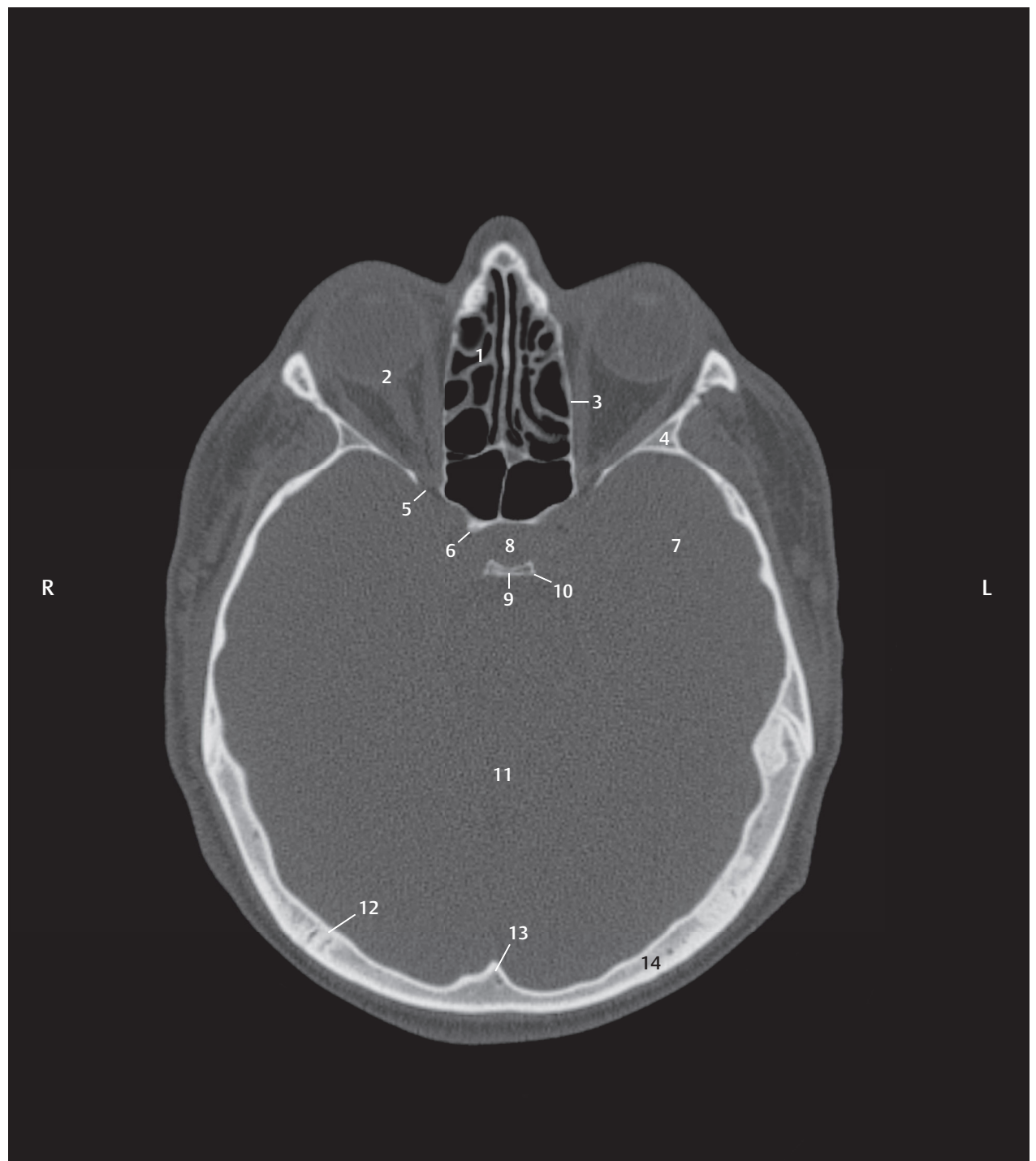
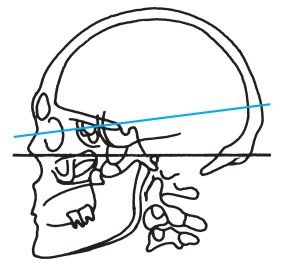


Fig. 5.35 Transverse image of the base of skull. CT image of the base of the skull, oriented perpendicular to the Meynert axis. The center of the orbit, ethmoid air cells, the dorsum sellae, and the superior orbital fissures have been sectioned.



- 1 Frontal bone
- 2 Frontal sinus
- 3 Ethmoidal air cells
- 4 Ethmoid fossa
- 5 Optic canal
- 6 Superior orbital fissure
- 7 Anterior clinoid process
- 8 Posterior clinoid process
- 9 Lambdoid suture
- 10 Occipital bone

Fig. 5.36 Transverse image of the base of skull. CT image of the base of the skull, oriented perpendicular to the Meynert axis. The cranial vault forms an oval bony ring. The anterior cranial fossa has been sectioned with the olfactory groove/ethmoid fossa.

- 1 **Foramen rotundum***
- 2 Maxillary nerve (V2)
- 3 **Optic canal**
- 4 Optic nerve
- 5 Ophthalmic artery
- 6 **Superior orbital fissure**
- 7 Superior ophthalmic vein
- 8 Ophthalmic nerve (II)
- 8a Lacrimal nerve
- 8b Frontal nerve
- 8c Nasociliary nerve
- 9 Abducens nerve (VI)
- 10 Oculomotor nerve (III)
- 11 Trochlear nerve (IV)
- 12 **Foramen ovale**
- 13 Pterygomenigeal artery
- 14 Mandibular nerve (V3)
- 15 Venous plexus of foramen ovale
- 16 **Foramen spinosum**
- 17 Middle meningeal artery
- 18 Meningeal branch of mandibular nerve
- 19 **Carotid canal**
- 20 Carotid artery
- 21 **Foramen lacerum**
(covered by the internal carotid artery) with the deep petrosal nerve and the greater petrosal nerve
- 24 **Hiatus for lesser petrosal nerve** with lesser petrosal nerve and superior tympanic artery
- 25 **Hiatus for greater petrosal nerve** with greater petrosal nerve and stylomastoid artery and vein
- 26 **Aperture and internal acoustic canal**
- 27 Facial nerve (with intermediate nerve)
- 28 Vestibulocochlear nerve
- 29 **Sphenopetrosal fissure** with lesser petrosal nerve
- 31 **Jugular foramen**
- 32 Glossopharyngeal nerve
- 33 Vagus nerve
- 34 Inferior petrosal sinus
- 35 Posterior meningeal artery
- 36 Internal jugular vein
- 37 Accessory nerve
- 38 **Hypoglossal canal**
- 39 Hypoglossal nerve with venous plexus of hypoglossal canal
- 40 **Foramen magnum**
- 41 Vertebral artery
- 43 Spinal cord
- 44 Spinal root of accessory nerve
- 45 Posterior spinal artery
- 50 **Condylar canal**
- 51 **Mastoid foramen** with mastoid emissary vein and mastoid branch of the occipital artery

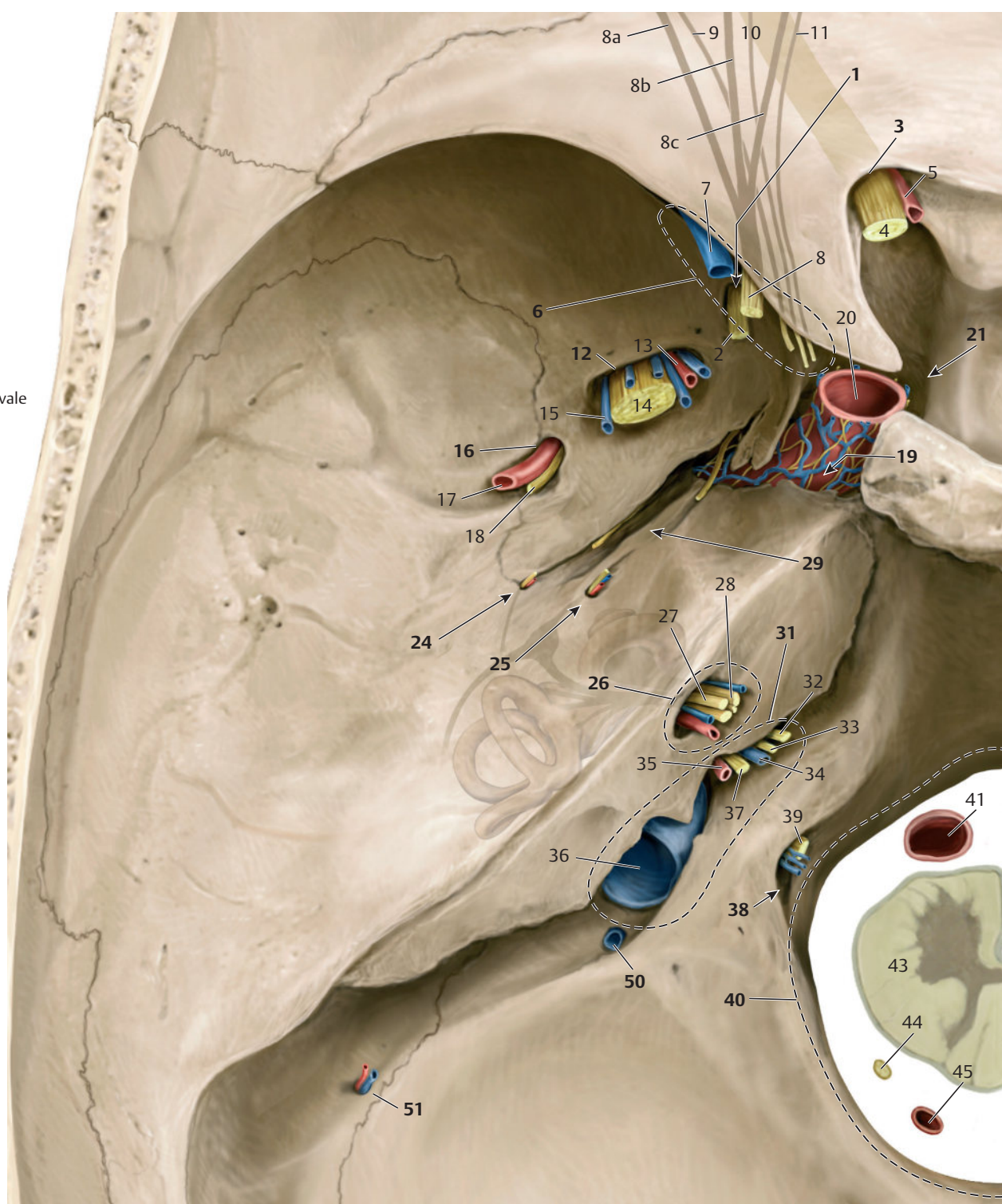
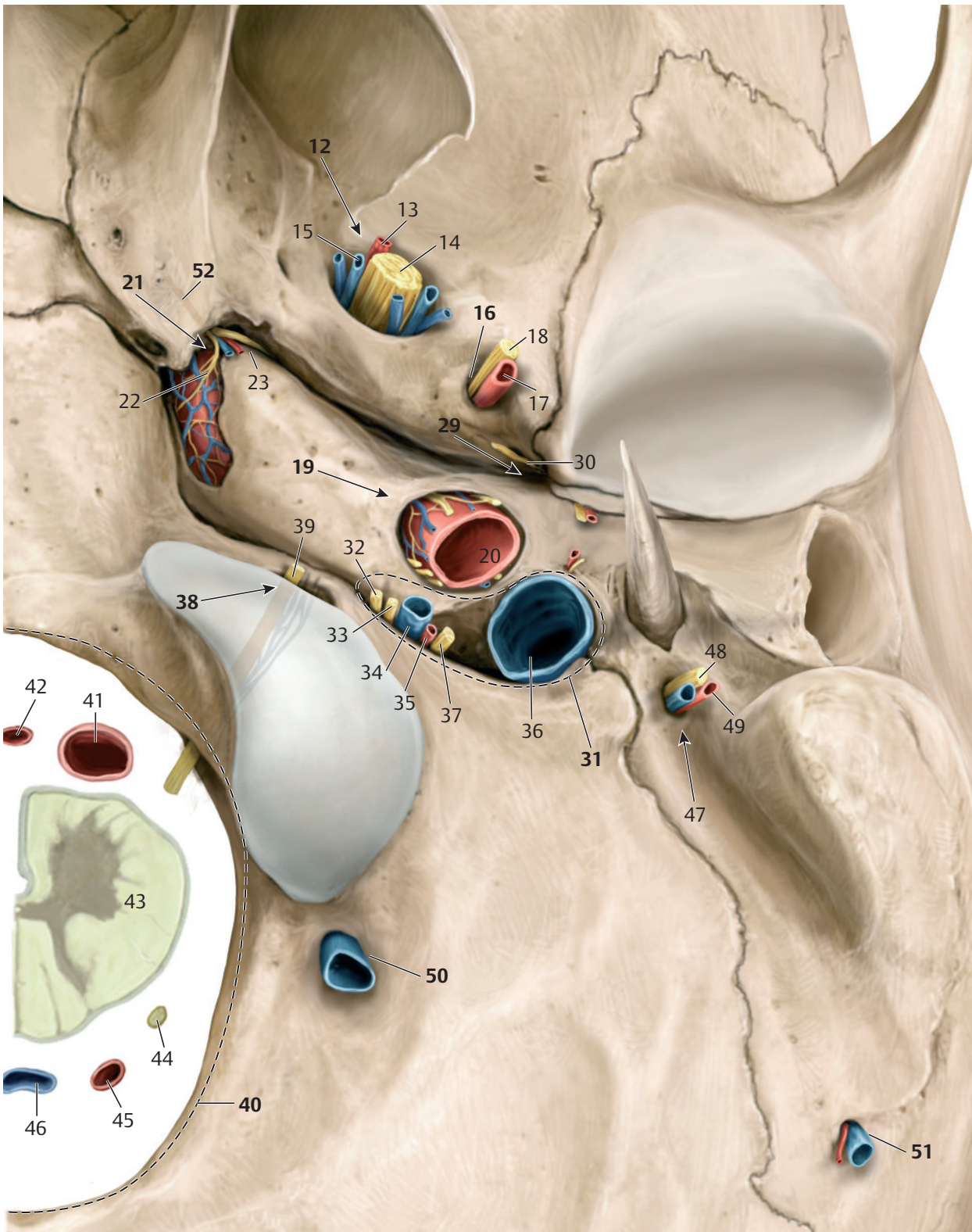


Fig. 5.37 Schematic 3D representation of the base of the skull. Bony exits for nerves and vessels of the central base of the skull are especially well seen. Exit points have been highlighted in bold in the captions, anatomic structures in following captions pass through them. An exit has been labelled as (a) or (b) if it is seen in one of two views. Exits to the pterygopalatine fossa have been indicated with an asterisk (*). (Reproduced from Schuenke, Schulte, and Schumacher, *Atlas of Anatomy*, 3rd edition, ©2012, Thieme Publishers, New York. Illustration by Karl Wesker/Markus Voll.)

Fig. 5.37a Intracranial 3D view of the base of the skull.



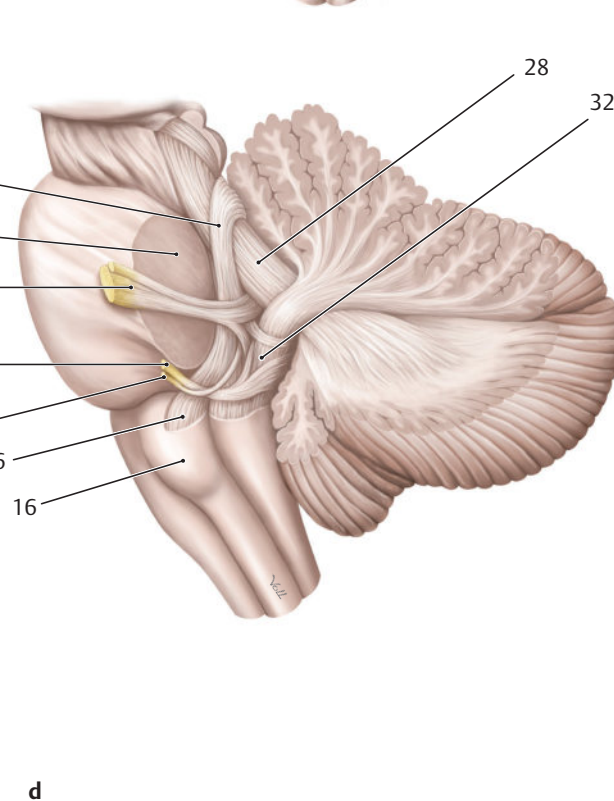
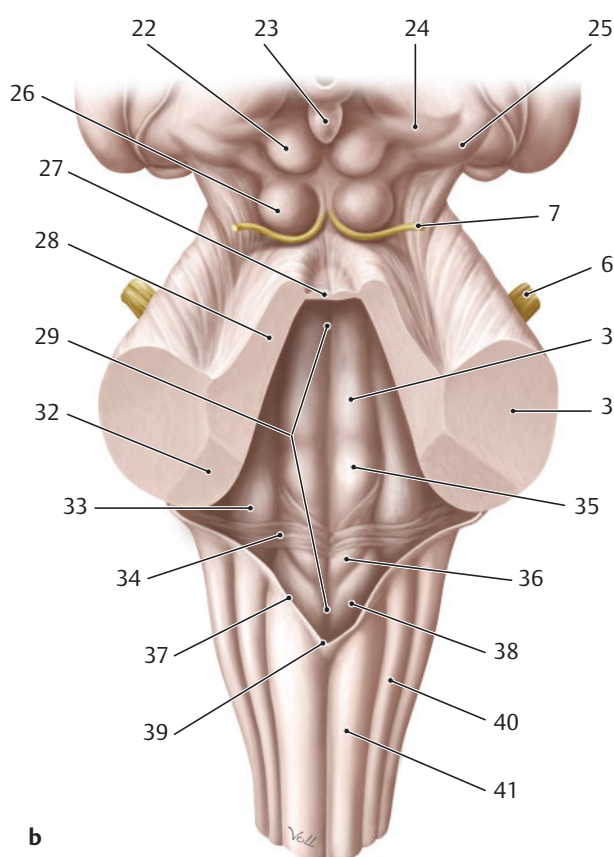
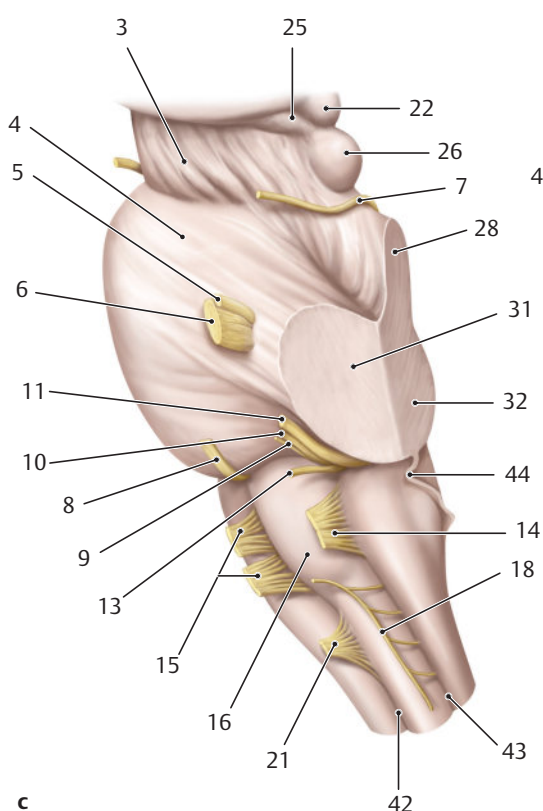
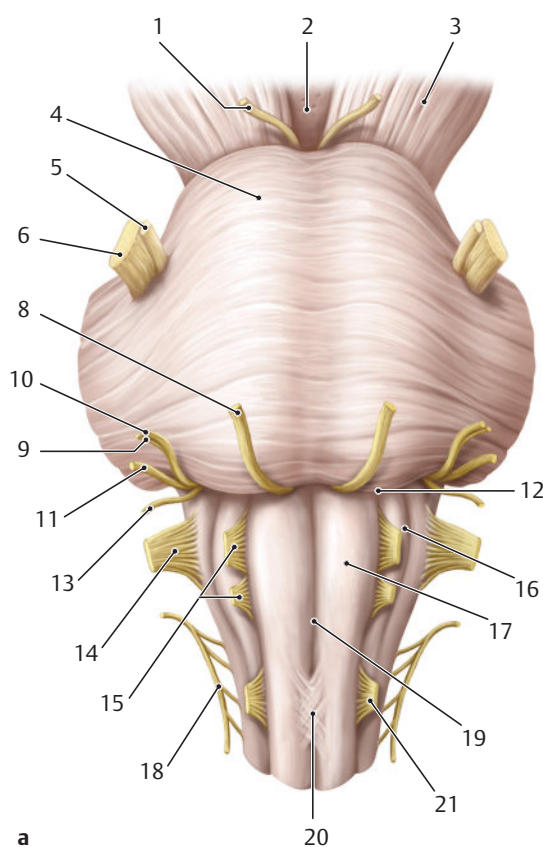
- 12 Foramen ovale**
- 13 Pterygomeningeal artery
- 14 Mandibular nerve (V3)
- 15 Venous plexus of foramen ovale
- 16 Foramen spinosum**
- 17 Middle meningeal artery
- 18 Meningeal branch of mandibular nerve
- 19 Carotid canal**
- 20 Carotid artery
- 21 Foramen lacerum
- 22 Deep petrosal nerve
- 23 Greater petrosal nerve
- 29 Sphenopetrosal fissure**
- 30 Lesser petrosal nerve
- 31 Jugular foramen**
- 32 Glossopharyngeal nerve
- 33 Vagus nerve
- 34 Inferior petrosal sinus
- 35 Posterior meningeal artery
- 36 Internal jugular vein
- 37 Accessory nerve
- 38 Hypoglossal canal**
- 39 Hypoglossal nerve with venous plexus of hypoglossal canal
- 40 Foramen magnum**
- 41 Vertebral arteries
- 42 Anterior spinal artery
- 43 Spinal cord
- 44 Spinal root of accessory nerve
- 45 Posterior spinal arteries
- 46 Spinal vein
- 47 Stylomastoid foramen**
- 48 Facial nerve
- 49 Stylomastoid artery/vein
- 50 Condylar canal with condylar emissary vein (inconstant)**
- 51 Mastoid foramen with mastoid emissary vein and mastoid branch of the occipital artery**
- 52 Pterygoid canal**
*with greater and deeper petrosal nerves and the artery and vein of the pterygoid canal

Fig. 5.37b External 3D view of the base of the skull.

6 Brainstem

3D views of the brainstem, its nuclei, and 10 brainstem sections, from inferior to superior, have been described in this section of the book. ► Fig. 6.1 illustrates the brainstem and cerebellar tracts and ► Fig. 6.2 shows the cranial nerve

nuclei, while ► Fig. 6.3 depicts the position of brainstem sections. Individual brainstem sections have been reproduced in ► Fig. 6.4, ► Fig. 6.5, ► Fig. 6.6, ► Fig. 6.7, ► Fig. 6.8, ► Fig. 6.9, ► Fig. 6.10, ► Fig. 6.11, ► Fig. 6.12, and ► Fig. 6.13.



- 1 Oculomotor nerve (III)
- 2 Interpeduncular fossa
- 3 Cerebral crus
- 4 Pons
- 5 Trigeminal nerve, motor root
- 6 Trigeminal nerve (V)
- 7 Trochlear nerve (IV)
- 8 Abducens nerve (VI)
- 9 Intermediate nerve
- 10 Facial nerve (VII)
- 11 Vestibulocochlear nerve (VIII)
- 12 Medullopontine sulcus
- 13 Glossopharyngeal nerve (IX)
- 14 Vagus nerve (X)
- 15 Hypoglossal nerve (XII)
- 16 Olive
- 17 Pyramid
- 18 Accessory nerve (XI)
- 19 Anterior median fissure
- 20 Decussation of pyramids
- 21 C1 spinal root
- 22 Superior colliculus
- 23 Pineal gland
- 24 Brachium of superior colliculus
- 25 Brachium of inferior colliculus
- 26 Inferior colliculus
- 27 Superior medullary velum
- 28 Superior cerebellar peduncle
- 29 Rhomboid fossa
- 30 Medial eminence
- 31 Middle cerebellar peduncle
- 32 Inferior cerebellar peduncle
- 33 Vestibular area
- 34 Medullary striae
- 35 Facial colliculus
- 36 Trigone of hypoglossal nerve
- 37 Taenia cinerea
- 38 Trigone of vagus nerve
- 39 Median aperture
- 40 Cuneate tubercle
- 41 Gracile tubercle
- 42 Lateral aperture
- 43 Anterolateral sulcus
- 44 Posterolateral sulcus
- 45 Anterior spinocerebellar tract
- 46 Central tegmental tract

Fig. 6.1 Brainstem views of external appearance and depiction of cerebellar tracts. (Reproduced from Schuenke, Schulte, and Schumacher, *Atlas of Anatomy*, 2nd and 3rd editions. ©2009, 2012, Thieme Publishers, Stuttgart. Illustration by Karl Wesker/Markus Voll.)

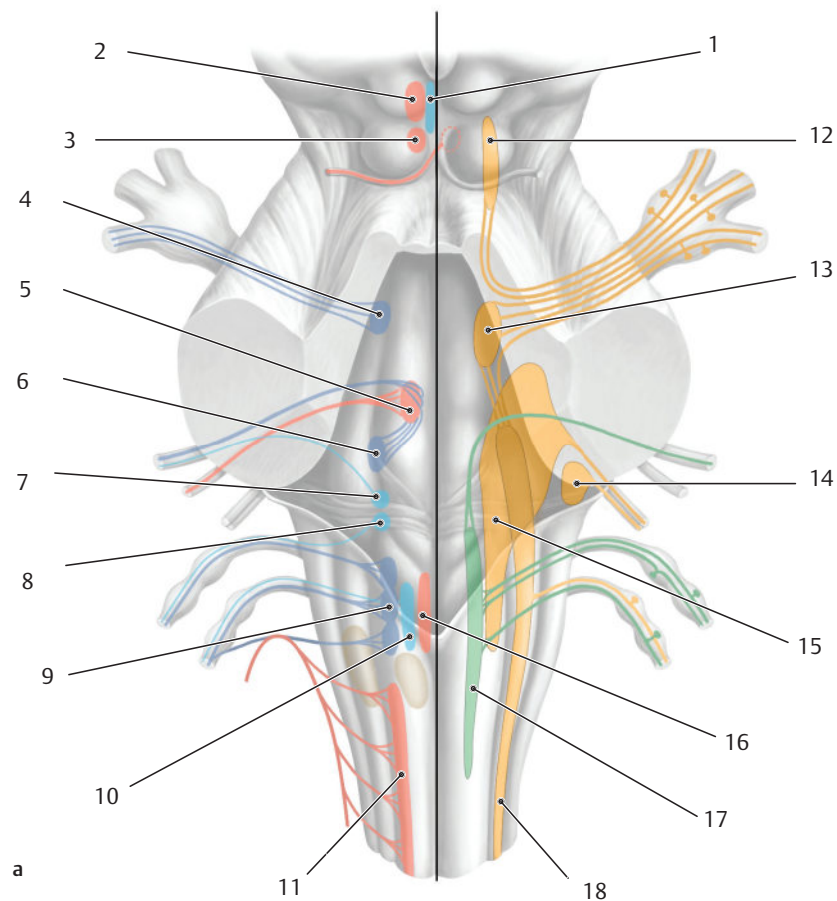
Fig. 6.1a Anterior view.

Fig. 6.1b Posterior view.

Fig. 6.1c View from the left.

Fig. 6.1d View from the left with cerebellum.

- 1 Accessory nucleus of oculomotor nerve
- 2 Nucleus of oculomotor nerve
- 3 Nucleus of trochlear nerve
- 4 Motor nucleus of trigeminal nerve
- 5 Nucleus of abducens nerve
- 6 Nucleus of facial nerve
- 7 Superior salivatory nucleus
- 8 Inferior salivatory nucleus
- 9 Nucleus ambiguus
- 10 Posterior nucleus of vagus nerve
- 11 Spinal nucleus of accessory nerve
- 12 Mesencephalic nucleus of trigeminal nerve
- 13 Principal sensory nucleus of trigeminal nerve
- 14 Cochlear nucleus
- 15 Vestibular nuclei
- 16 Nucleus of hypoglossal nerve
- 17 Nucleus of the solitary tract
- 18 Spinal nucleus of trigeminal nerve



- 1 Accessory nuclei of oculomotor nerve
- 2 Nucleus of oculomotor nerve
- 3 Nucleus of trochlear nerve
- 4 Motor nucleus of trigeminal nerve
- 5 Nucleus of abducens nerve
- 6 Nucleus of facial nerve
- 7 Superior salivatory nucleus
- 8 Inferior salivatory nucleus
- 9 Nucleus ambiguus
- 10 Posterior nucleus of vagus nerve
- 11 Spinal nucleus of accessory nerve
- 12 Mesencephalic nucleus of trigeminal nerve
- 13 Principal sensory nucleus of trigeminal nerve
- 16 Nucleus of hypoglossal nerve
- 17 Nucleus of the solitary tract
- 18 Spinal nucleus of trigeminal nerve
- 19 Internal genu of facial nerve

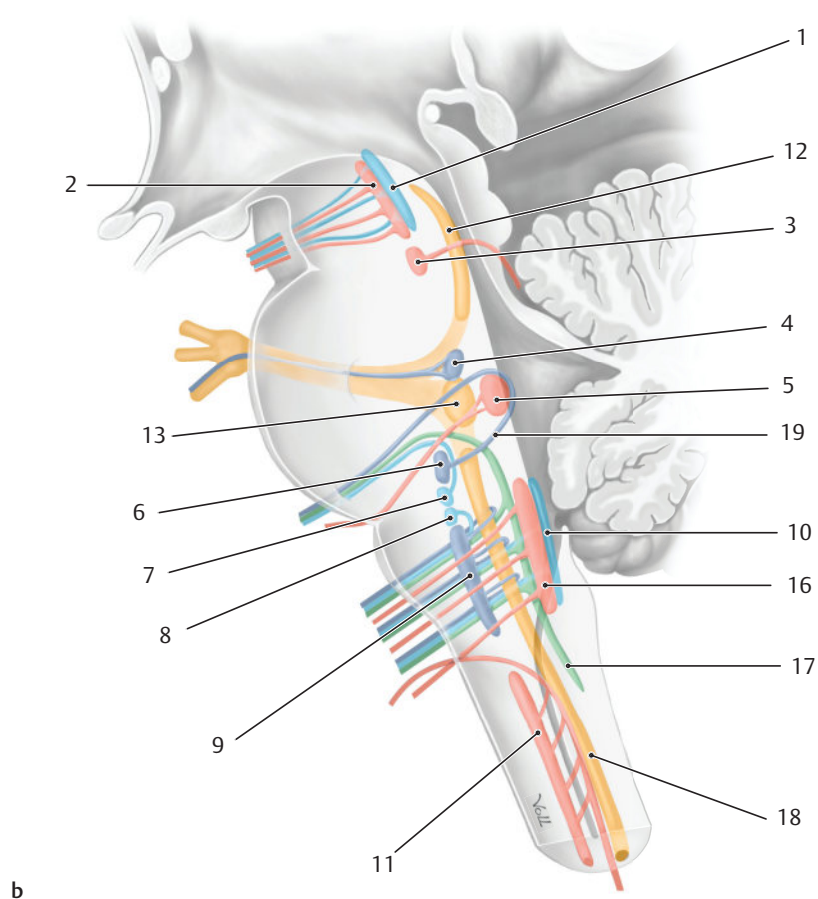


Fig. 6.2 Arrangement of cranial nerve nuclei in the brainstem. (Reproduced from Schuenke, Schulte, and Schumacher, *Atlas of Anatomy*, 3rd edition, ©2012, Thieme Publishers, Stuttgart. Illustration by Karl Wesker/Markus Voll.)

Fig. 6.2a Posterior view with cerebellum removed and view of the rhomboid fossa. Depiction of nuclei of origin to the left of midline with emerging efferent or motor fibers (red = somatic efferent or somatic motor nuclei; light blue = parasympathetic nuclei; dark blue = nuclei of branchial nerves). Nuclei of termination

are depicted to the right of the midline (dark green = general visceromotor fibers, light green = special visceromotor fibers, yellow = somato-afferent or somatosensory nuclei).

Fig. 6.2b Lateral view. Afferent and efferent tracts have been illustrated in addition to nuclei.

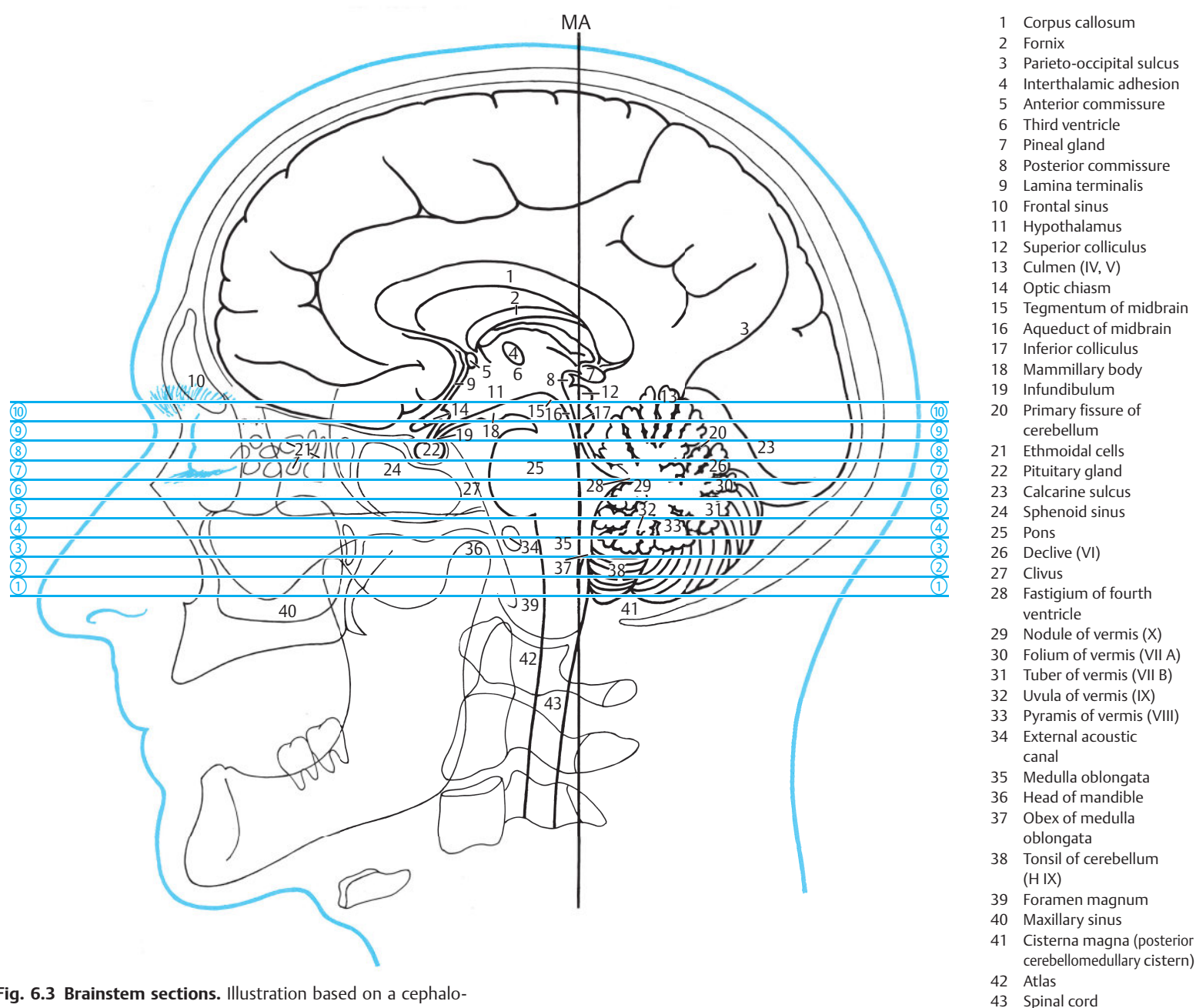
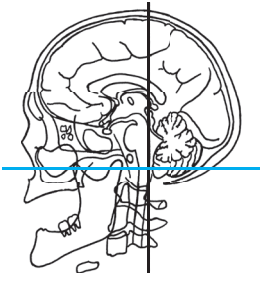


Fig. 6.3 Brainstem sections. Illustration based on a cephalogram and an MR image (see Chapter 12 for specimens). The 5-mm-thick slices of the brainstem series have been sectioned perpendicular to the Meynert axis, assembled and displayed. The Meynert axis runs tangentially through the floor of the rhomboid fossa and in the median plane. Sections have been contiguously numbered with encircled digits from inferior to superior (for details see Section 1.2). The illustrated section always corresponds to the line lying above the encircled number of the slice concerned. MA = Meynert axis.



- 1 Maxilla
- 2 Inferior nasal concha
- 3 Maxillary sinus
- 4 Zygomatic bone
- 5 Nasal cavity
- 6 Nasal septum
- 7 Coronoid process
- 8 Temporalis
- 9 Masseter
- 10 Nasopharynx
- 11 Lateral pterygoid
- 12 Pharyngotympanic tube
- 13 Head of mandible
- 14 Internal carotid artery
- 15 Facial nerve
- 16 Hypoglossal canal
- 17 Jugular foramen
- 18 Mastoid cells
- 19 Medulla oblongata
- 20 Mastoid process
- 21 Sigmoid sinus, left-right asymmetry (variant)
- 22 Tonsil of cerebellum (H IX)
- 23 Auricle (pinna)
- 24 Cisterna magna (posterior cerebellomedullary cistern)
- 25 Posterior lobe of cerebellum
- 26 Occipital bone

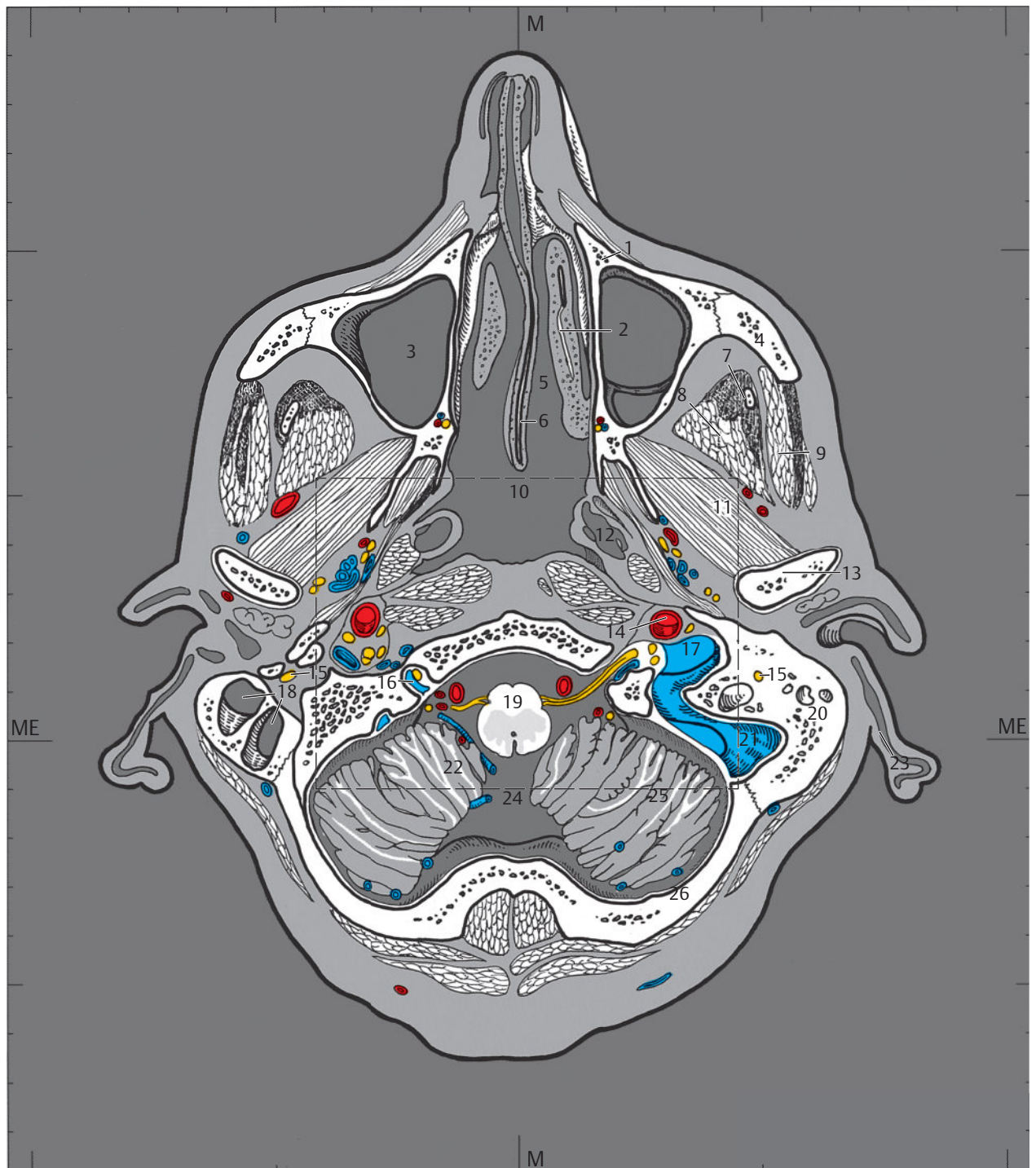
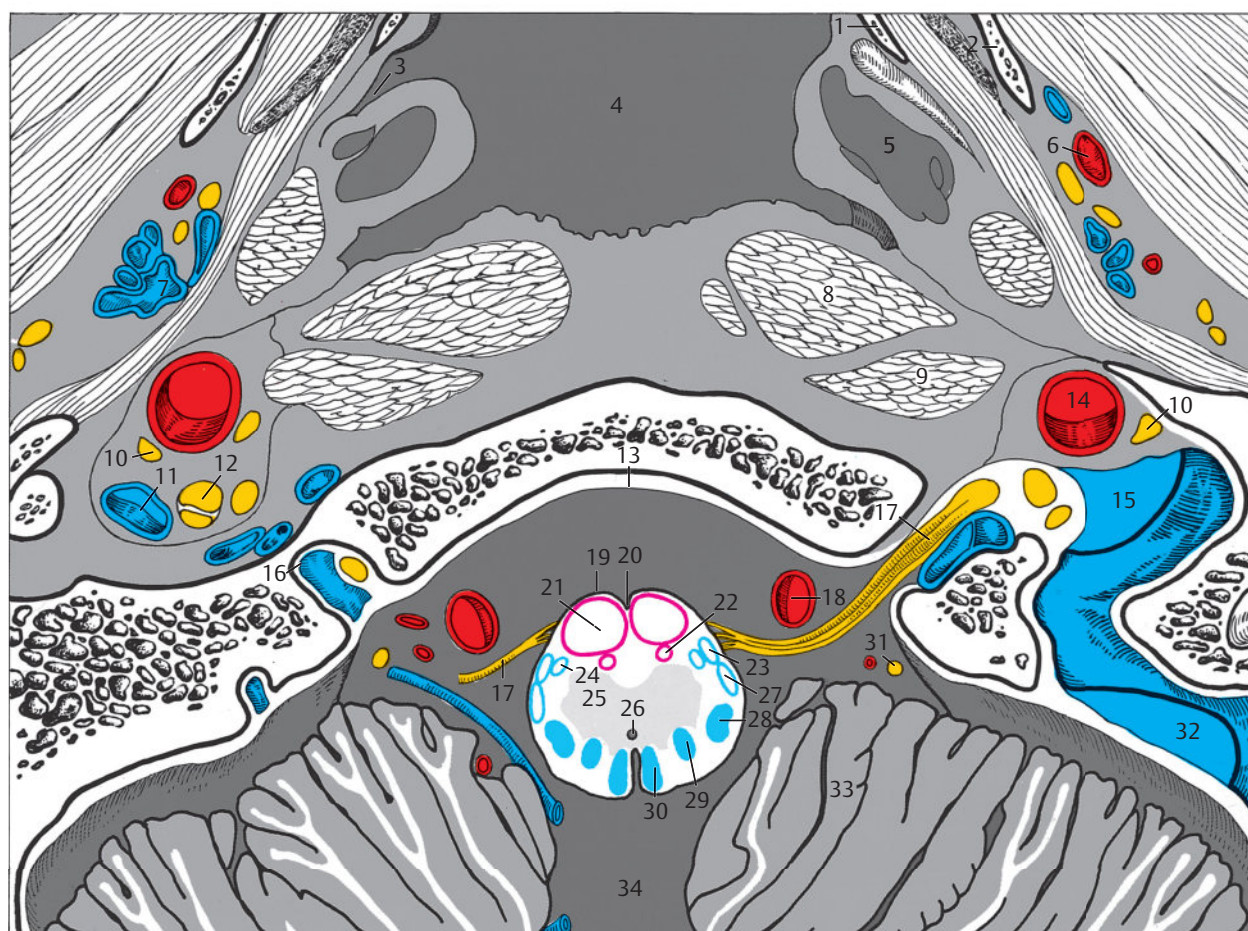


Fig. 6.4 Brainstem series.

M = median plane

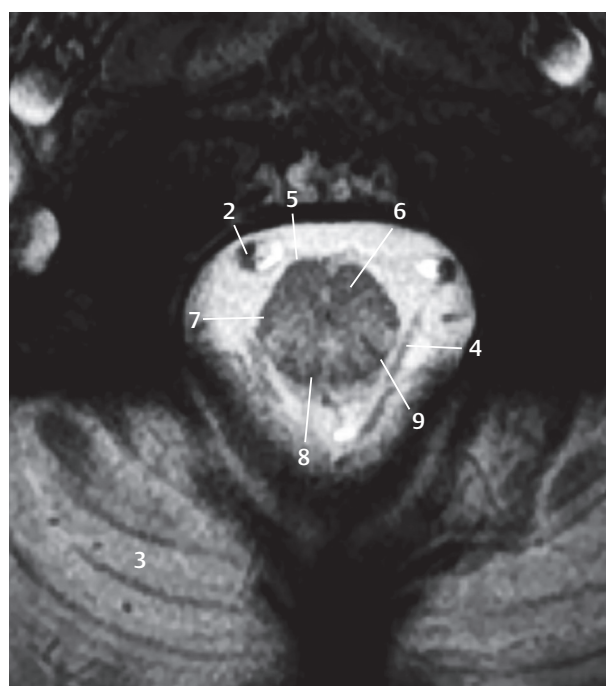
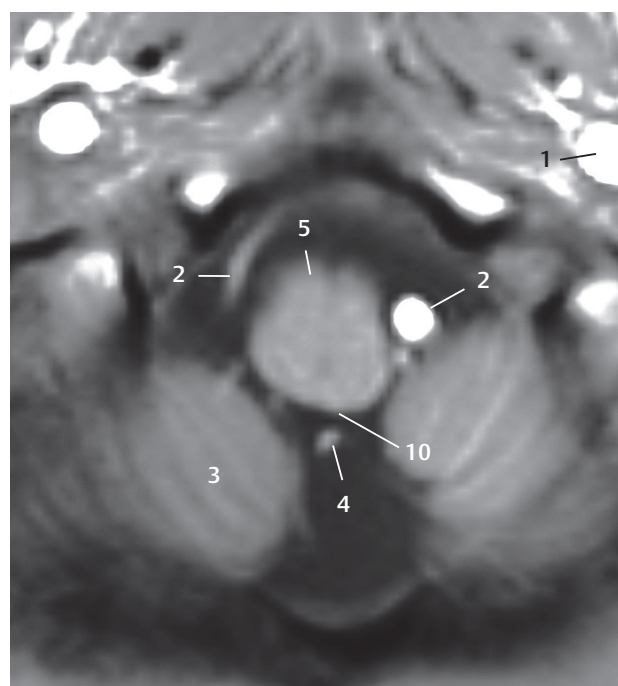
ME = Meynert plane

Fig. 6.4a View of the superior surface of the first anatomical section of the brainstem series, oriented perpendicular to the Meynert axis and to the median plane (see ► Fig. 6.3). The blue line at the top left signet indicates the position of the sectional plane at the level of the coronoid and condyloid processes of the mandible as well as the inferior part of the posterior cranial fossa. The maxillary sinus, the nasopharynx, and the posterior cranial fossa, the inferior aspect of the medulla oblongata and the cerebellar tonsils, about 1 cm above the foramen magnum, are visualized in this section (see ► Fig. 6.3).



- 1 Medial pterygoid plate
- 2 Lateral pterygoid plate
- 3 Pharyngeal opening of pharyngotympanic tube
- 4 Nasopharynx
- 5 Cartilage of pharyngotympanic tube
- 6 Maxillary artery
- 7 Pterygoid venous plexus
- 8 Longus capitis
- 9 Rectus capitis anterior
- 10 Glossopharyngeal nerve
- 11 Internal jugular vein, left-right asymmetry (variant)
- 12 Vagus nerve
- 13 Dura mater
- 14 Internal carotid artery
- 15 Bulb of internal jugular vein
- 16 Hypoglossal canal
- 17 Hypoglossal nerve
- 18 Vertebral artery
- 19 Pyramid of medulla oblongata
- 20 Anterior median fissure
- 21 Corticospinal tract
- 22 Medial longitudinal fasciculus
- 23 Anterior spinocerebellar tract
- 24 Spinothalamic tract
- 25 Reticular formation
- 26 Central canal
- 27 Posterior spinocerebellar tract
- 28 Caudal part of spinal nucleus of trigeminal nerve
- 29 Cuneate nucleus (of Burdach)
- 30 Gracile nucleus (of Goll)
- 31 Spinal root of accessory nerve
- 32 Sigmoid sinus, left-right asymmetry (variant)
- 33 Tonsil of cerebellum (H IX)
- 34 Cisterna magna (posterior cerebellomedullary cistern)

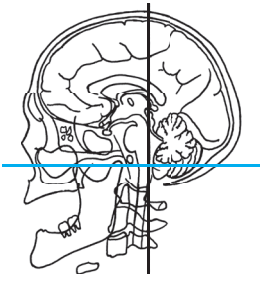
Fig. 6.4b Detail section enlarged from a, depicting the opening of the left auditory tube in the nasopharynx. The inferior part of the medulla oblongata, the roots of the hypoglossal nerve, and the hypoglossal canal have been sectioned.



- 1 Internal carotid artery
- 2 Vertebral artery
- 3 Cerebellum
- 4 Posterior inferior cerebellar artery
- 5 Medulla oblongata, pyramid (left)
- 6 Corticospinal tract (right)
- 7 Afferent anterolateral tract (right)
- 8 Gracile fasciculus (right)
- 9 Cuneate fasciculus (right)
- 10 Gracile tubercle (left)

Fig. 6.4c MR images oriented perpendicular to the Meynert axis, corresponding approximately to a and b. This MR series (see ► Fig. 6.4c, ► Fig. 6.5, ► Fig. 6.6, ► Fig. 6.7, ► Fig. 6.8, ► Fig. 6.9, ► Fig. 6.10, ► Fig. 6.11, ► Fig. 6.12, and ► Fig. 6.13c) has been obtained from 33- and 34-year-old men. T1w and T2w image pairs (see ► Fig. 6.4c, ► Fig. 6.5, ► Fig. 6.6, ► Fig. 6.7, ► Fig. 6.8, ► Fig. 6.9, ► Fig. 6.10, ► Fig. 6.11, ► Fig. 6.12, and ► Fig. 6.13c) have been described by a common legend. If a

structure is only seen in one of the MR image pairs, this has been indicated by “left” for “left image” or “right” for “right image” at the end. The T1w MR image (on the left) is a gradient echo FLASH sequence. Structures of the brain have been accentuated by the selected sequence. The T2w MR image (on the right) was obtained using a T2w MEDIC sequence. Fiber tracts appear hypointense against gray matter in the employed T2w sequence. For technical data see Chapter 12.



- 1 Maxilla
- 2 Inferior nasal concha
- 3 Nasal septum
- 4 Maxillary sinus
- 5 Zygomatic bone
- 6 Nasal cavity
- 7 Temporalis
- 8 Pterygoid process
- 9 Nasopharynx
- 10 Lateral pterygoid
- 11 Articular disc of temporomandibular joint
- 12 Head of mandible
- 13 Clivus
- 14 External acoustic canal
- 15 Jugular foramen
- 16 Internal jugular vein (variant)
- 17 Accessory nerve near opening of dura mater
- 18 Medulla oblongata
- 19 Bulb of internal jugular vein
- 20 Facial nerve
- 21 Sigmoid sinus
- 22 Temporal bone
- 23 Auricle (pinna)
- 24 Posterior lobe of cerebellum
- 25 Cisterna magna (posterior cerebellomedullary cistern)
- 26 Occipital bone

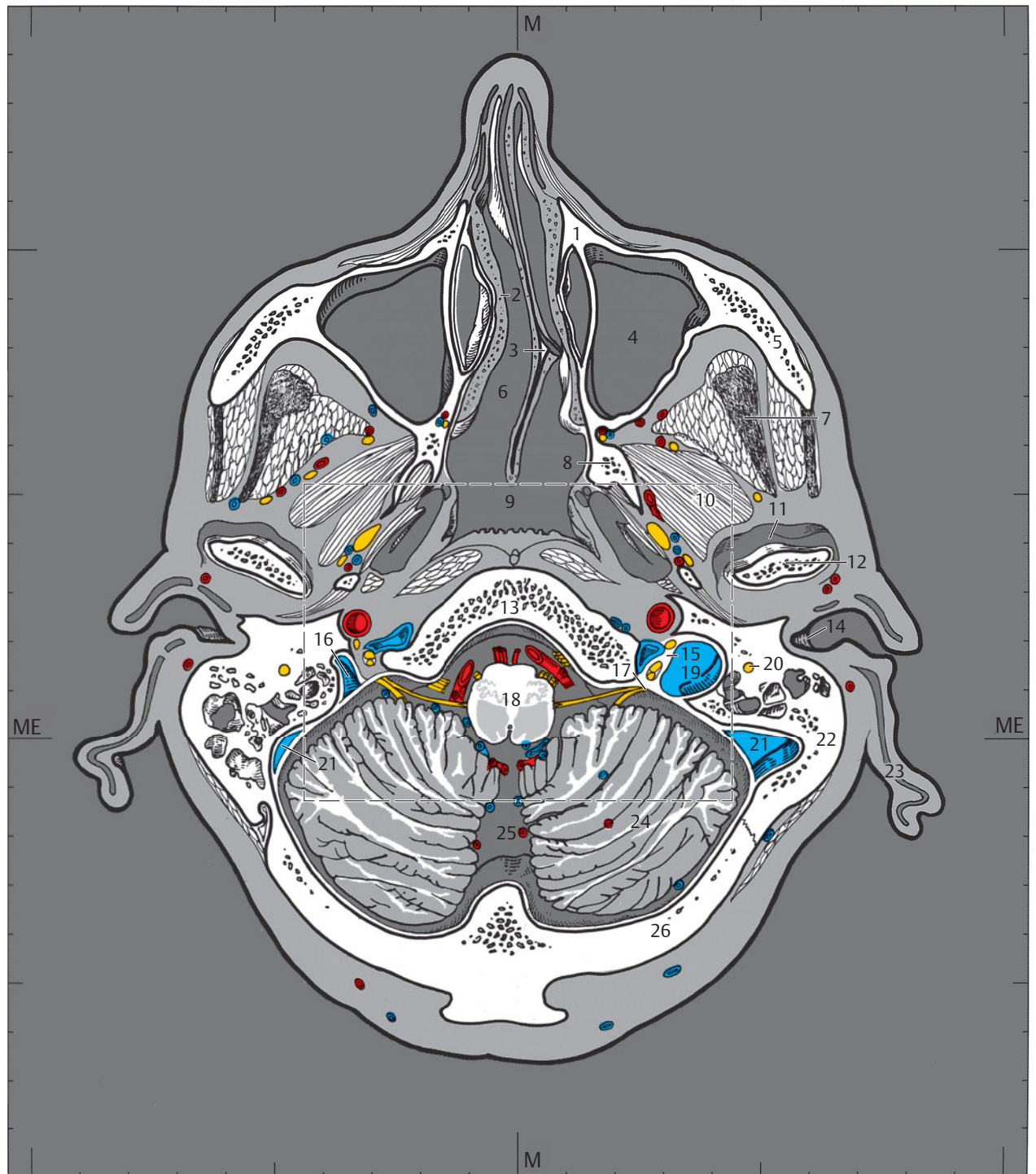


Fig. 6.5 Brainstem series.

M = median plane

ME = Meynert plane

Fig. 6.5a View of the superior surface of the second anatomical section of the brainstem series (see ►Fig. 6.3). The sectional plane passes through the inferior nasal turbinates, the temporomandibular joint, head of the mandible, and the jugular foramen. The medulla oblongata has been sectioned in the posterior cranial fossa at the level of the dural opening for the accessory nerve.

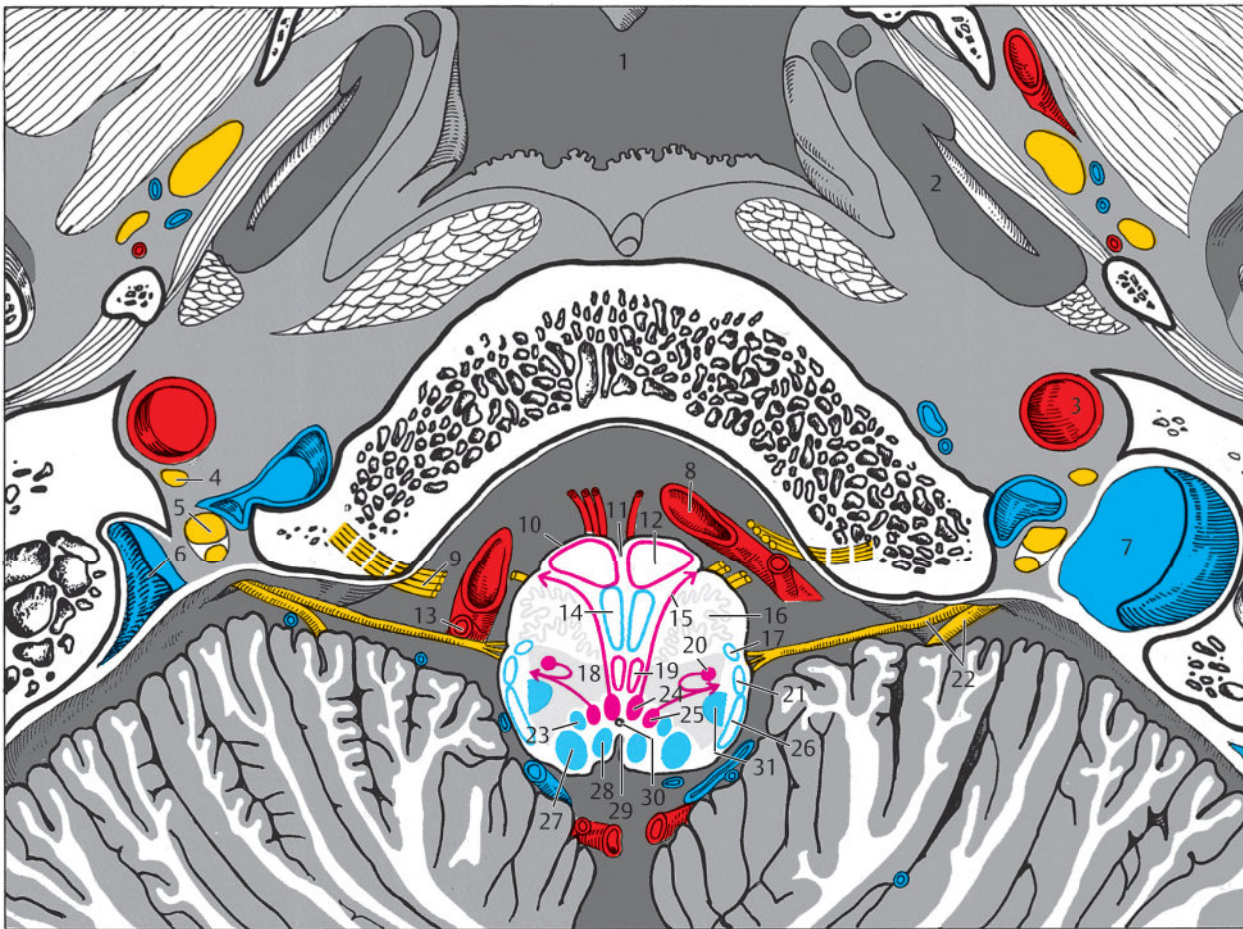
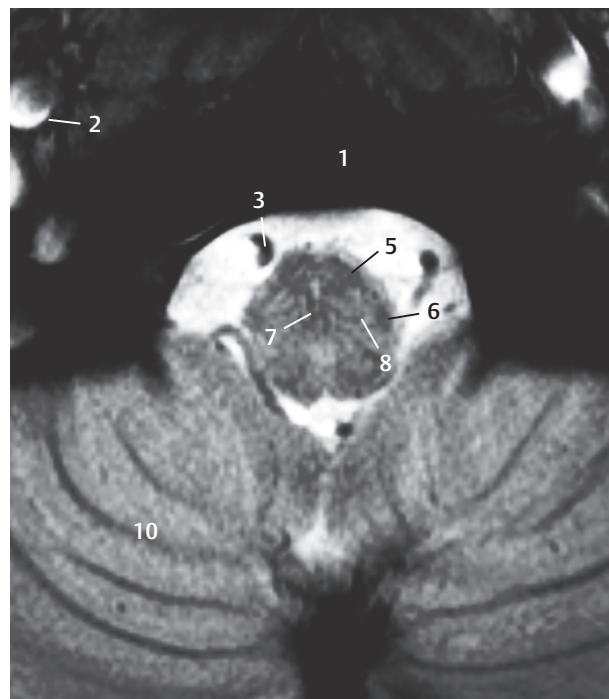
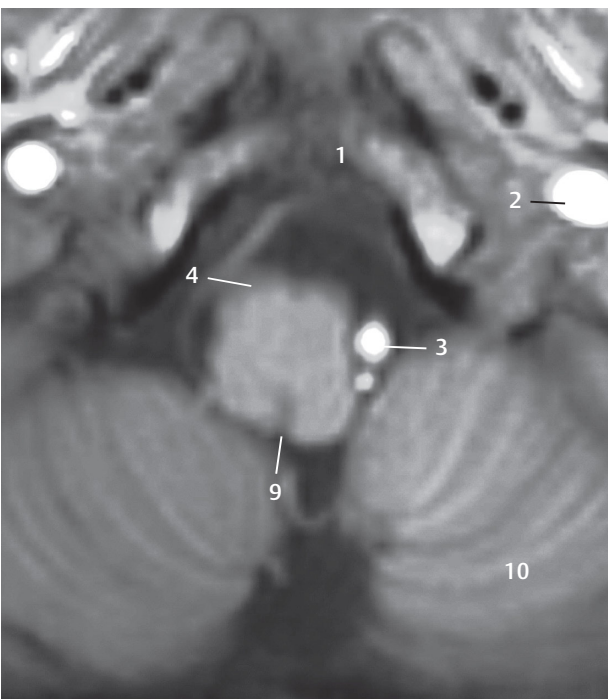


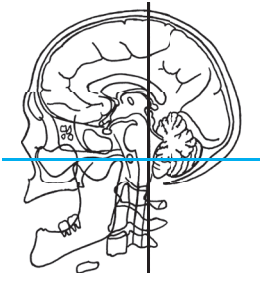
Fig. 6.5b Detail section enlarged from a. The cartilaginous part of the auditory tube, the inferior part of the inferior olivary nucleus, and the origin of the posterior inferior cerebellar artery from the vertebral artery have been sectioned. The two internal jugular veins are symmetrically visualized; the right jugular foramen is widened with an enlarged superior bulb of the internal jugular vein (variant).

- 1 Nasopharynx
- 2 Cartilage of pharyngotympanic tube
- 3 Internal carotid artery
- 4 Glossopharyngeal nerve
- 5 Vagus nerve
- 6 Internal jugular vein (variant)
- 7 Superior bulb of internal jugular vein
- 8 Vertebral artery
- 9 Hypoglossal nerve
- 10 Pyramid of medulla oblongata
- 11 Anterior median fissure
- 12 Corticospinal tract
- 13 Posterior inferior cerebellar artery (PICA)
- 14 Medial lemniscus
- 15 Hypoglossal nerve (within the slice)
- 16 Inferior olivary nucleus
- 17 Spinothalamic tract
- 18 Reticular formation
- 19 Medial longitudinal fasciculus
- 20 Nucleus ambiguus
- 21 Anterior spinocerebellar tract
- 22 Cranial and spinal roots of accessory nerve
- 23 Solitary nucleus
- 24 Hypoglossal nucleus
- 25 Posterior (dorsal) nucleus of vagus nerve
- 26 Posterior spinocerebellar tract
- 27 Cuneate nucleus (of Burdach)
- 28 Gracile nucleus (of Goll)
- 29 Obex of medulla oblongata
- 30 Central canal
- 31 Caudal part of spinal nucleus of trigeminal nerve



- 1 Clivus
- 2 Internal carotid artery
- 3 Vertebral artery
- 4 Medulla oblongata, pyramid (left)
- 5 Corticospinal tract (right)
- 6 Spinocerebellar and spinothalamic tracts (right)
- 7 Medial lemniscus (right)
- 8 Inferior olivary nucleus (right)
- 9 Obex (left)
- 10 Posterior lobe of cerebellum

Fig. 6.5c MR images oriented perpendicular to the Meynert axis corresponding approximately to a and b. T1w MR image on the left, with a T2w MEDIC MR image on the right. For technical data see Chapter 12.



- 1 Maxilla
- 2 Nasolacrimal duct
- 3 Maxillary sinus
- 4 Zygomatic bone
- 5 Nasal cavity
- 6 Nasal septum
- 7 Temporalis
- 8 Lateral pterygoid
- 9 Mandibular nerve
- 10 Temporomandibular joint
- 11 Articular disc of temporomandibular joint
- 12 External acoustic canal
- 13 Inferior petrosal sinus
- 14 Hypoglossal nerve
- 15 Facial nerve
- 16 Medulla oblongata
- 17 Inferior olive
- 18 Temporal bone
- 19 Floor of rhomboid fossa
- 20 Fourth ventricle
- 21 Sigmoid sinus
- 22 Auricle (pinna)
- 23 Uvula of vermis (IX)
- 24 Posterior lobe of cerebellum
- 25 Pyramis of vermis (VIII)
- 26 Occipital bone

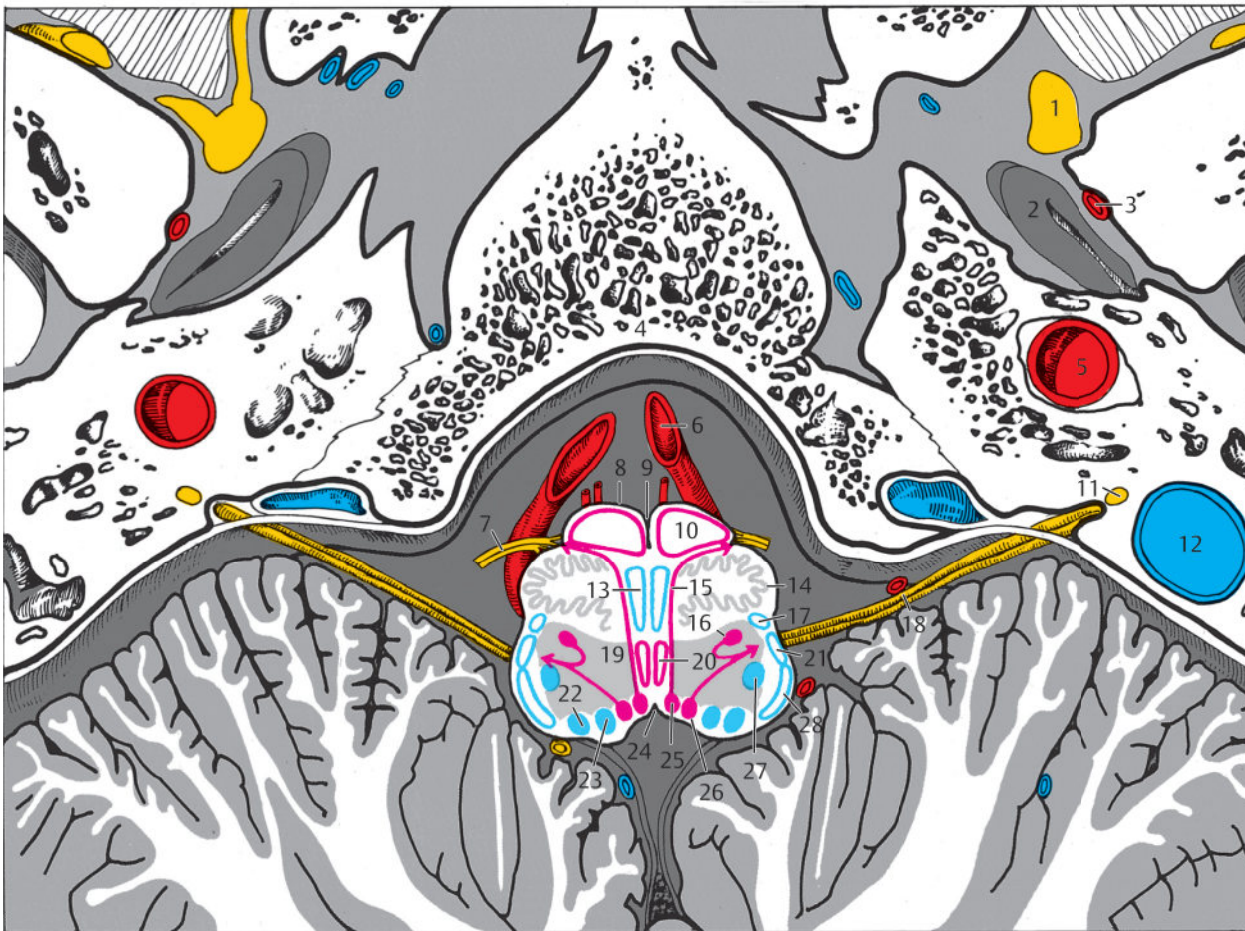


Fig. 6.6 Brainstem series.

M = median plane

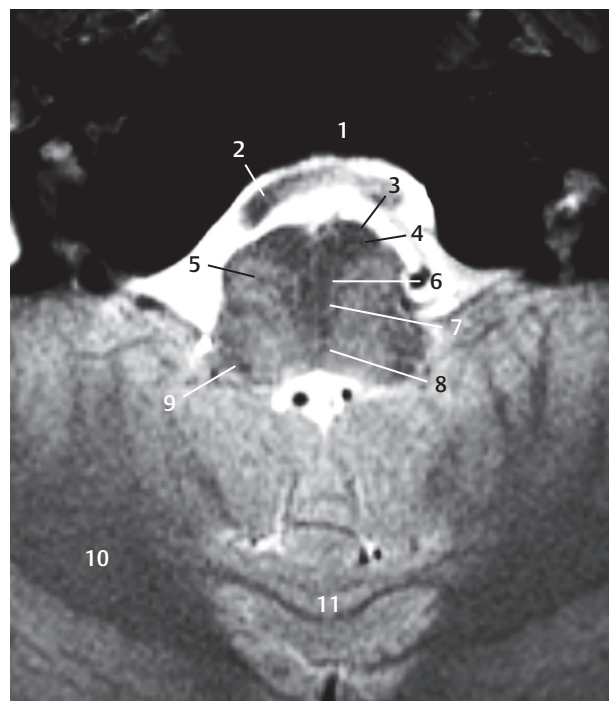
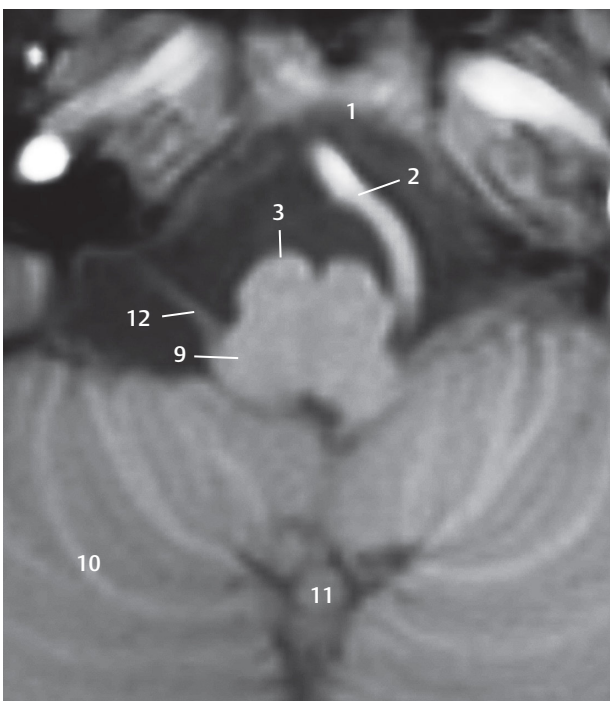
ME = Meynert plane

Fig. 6.6a View of the superior surface of the third anatomical section of the brainstem series. The sectional plane lies at the level of the external auditory canal and the attachment of the inferior nasal turbinate to the lateral wall of the nasal cavity. The medulla oblongata has been sectioned in the posterior cranial fossa at the inferior end of the rhomboid fossa.



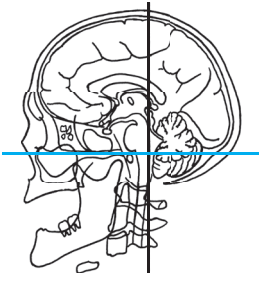
- 1 Mandibular nerve
- 2 Pharyngotympanic tube
- 3 Middle meningeal artery
- 4 Clivus
- 5 Internal carotid artery
- 6 Vertebral artery
- 7 Hypoglossal nerve
- 8 Pyramid of medulla oblongata
- 9 Anterior median fissure
- 10 Corticospinal tract
- 11 Glossopharyngeal nerve
- 12 Superior bulb of internal jugular vein
- 13 Medial lemniscus
- 14 Inferior olivary nucleus
- 15 Hypoglossal nerve (within the slice)
- 16 Nucleus ambiguus
- 17 Spinothalamic tract
- 18 Vagus nerve
- 19 Reticular formation
- 20 Medial longitudinal fasciculus
- 21 Anterior spinocerebellar tract
- 22 Cuneate nucleus (of Burdach)
- 23 Solitary nucleus
- 24 Median sulcus
- 25 Hypoglossal nucleus
- 26 Posterior (dorsal) nucleus of vagus nerve
- 27 Interpolated part of spinal nucleus of trigeminal nerve
- 28 Inferior cerebellar peduncle

Fig. 6.6b Detail section enlarged from a. The mandibular nerve lies just below the foramen ovale. The roots of the vagus nerve arise from the medulla oblongata.



- 1 Clivus
- 2 Vertebral artery
- 3 Medulla oblongata, pyramid
- 4 Corticospinal tract (right)
- 5 Inferior olivary nucleus (right)
- 6 Olivocerebellar tract (right)
- 7 Medial lemniscus (right)
- 8 Medial longitudinal fasciculus (right)
- 9 Inferior cerebellar peduncle
- 10 Cerebellar hemisphere
- 11 Pyramid of vermis (VIII)
- 12 Glossopharyngeal nerve/vagus nerve

Fig. 6.6c MR images oriented perpendicular to the Meynert axis, corresponding approximately to a and b. T1w MR image on the left, with a T2w MEDIC MR image on the right. For technical data see Chapter 12.



- 1 Nasal cavity
- 2 Nasolacrimal duct
- 3 Nasal septum
- 4 Maxillary sinus
- 5 Zygomatic bone
- 6 Middle nasal concha
- 7 Zygomatic arch
- 8 Temporalis
- 9 Floor of middle cranial fossa
- 10 Middle meningeal artery
- 11 Clivus
- 12 Temporal bone
- 13 Medulla oblongata
- 14 Flocculus (H X)
- 15 Lateral aperture (of Luschka) of fourth ventricle
- 16 Sigmoid sinus
- 17 Auricle (pinna)
- 18 Uvula of vermis (IX)
- 19 Pyramid of vermis (VIII)
- 20 Posterior lobe of cerebellum
- 21 Occipital bone

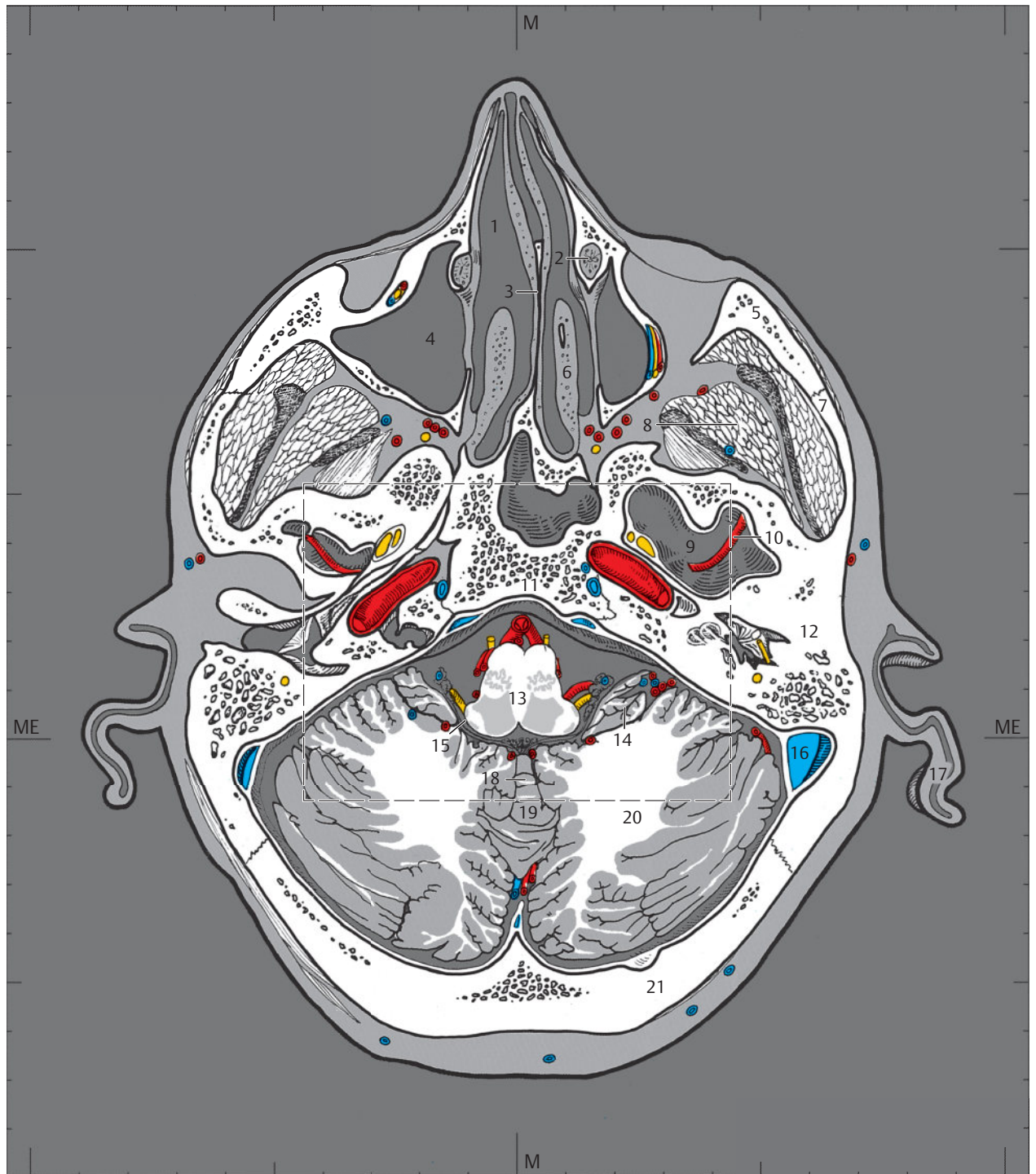


Fig. 6.7 Brainstem series.

M = median plane

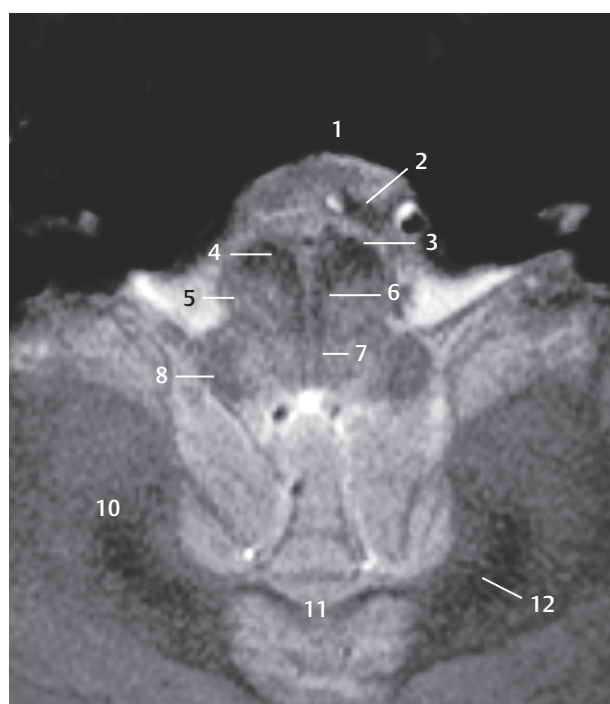
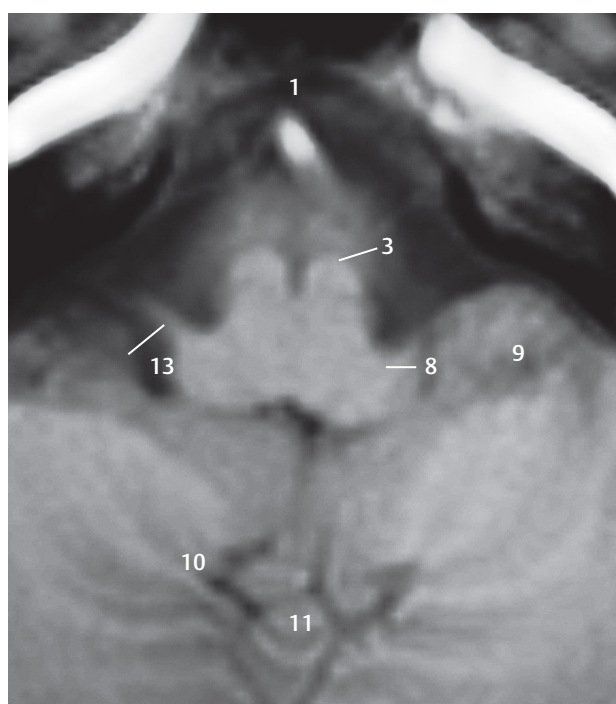
ME = Meynert plane

Fig. 6.7a View of the superior surface of the fourth anatomical section of the brainstem series. The middle turbinate has been sectioned in the nasal cavity. The sectional plane passes through the floor of the middle cranial fossa through the tympanic cavity of the temporal bone and the superior part of the medulla oblongata at the level of the lateral aperture of the fourth ventricle in the posterior cranial fossa.



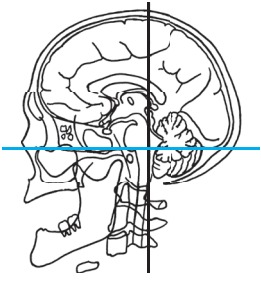
- 1 Sphenoid sinus
- 2 Mandibular nerve
- 3 Middle meningeal artery
- 4 Internal carotid artery
- 5 Basilar artery
- 6 Vertebral artery
- 7 Pyramid of medulla oblongata
- 8 Abducens nerve
- 9 Corticospinal tract
- 10 Abducens nerve (within the slice)
- 11 Medial lemniscus
- 12 Flocculus (H X)
- 13 Choroid plexus
- 14 Inferior olivary nucleus
- 15 Reticular formation
- 16 Medial longitudinal fasciculus
- 17 Nucleus ambiguus
- 18 Spinothalamic tract
- 19 Oral part of spinal nucleus of trigeminal nerve
- 20 Vestibulocochlear nerve
- 21 Lateral aperture (of Luschka) of fourth ventricle
- 22 Nucleus prepositus
- 23 Floor of rhomboid fossa and fourth ventricle
- 24 Vestibular nuclei
- 25 Inferior cerebellar peduncle
- 26 Posterior (dorsal) and anterior (ventral) cochlear nuclei
- 27 Uvula of vermis (IX)

Fig. 6.7b The detail section from a displays the confluence of the vertebral arteries with the basilar artery. The roots of the abducens nerve arise at the junction of the medulla oblongata and pons. The superior part of the inferior olivary nucleus lies in the medulla oblongata.



- 1 Clivus
- 2 Vertebral artery
- 3 Medulla oblongata, pyramid
- 4 Corticospinal tract (right)
- 5 Inferior olivary nucleus (right)
- 6 Medial lemniscus (right)
- 7 Medial longitudinal fasciculus (right)
- 8 Inferior cerebellar peduncle
- 9 Flocculus (left)
- 10 Cerebellar hemisphere
- 11 Pyramid of vermis (VIII)
- 12 Dentate nucleus (right)
- 13 Vestibulocochlear nerve (sectioned, left)

Fig. 6.7c MR images oriented perpendicular to the Meynert axis, corresponding approximately to a and b. T1w MR image on the left, with a T2w MEDIC MR image on the right. For technical data see Chapter 12.



- 1 Nasal cavity
- 2 Semilunar hiatus
- 3 Middle nasal concha
- 4 Inferior oblique
- 5 Zygomatic bone
- 6 Nasal septum
- 7 Inferior rectus
- 8 Sphenoid
- 9 Temporalis
- 10 Maxillary nerve
- 11 Sphenoid sinus
- 12 Middle meningeal artery
- 13 Base of temporal lobe
- 14 Malleus (hammer)
- 15 Internal acoustic canal
- 16 Pons
- 17 Posterior semicircular canal
- 18 Temporal bone
- 19 Auricle (pinna)
- 20 Sigmoid sinus
- 21 Dentate nucleus
- 22 Uvula of vermis (IX)
- 23 Pyramid of vermis (VIII)
- 24 Posterior lobe of cerebellum
- 25 Tentorium of cerebellum
- 26 Transverse sinus
- 27 Base of occipital lobe
- 28 Internal occipital protuberance
- 29 Occipital bone

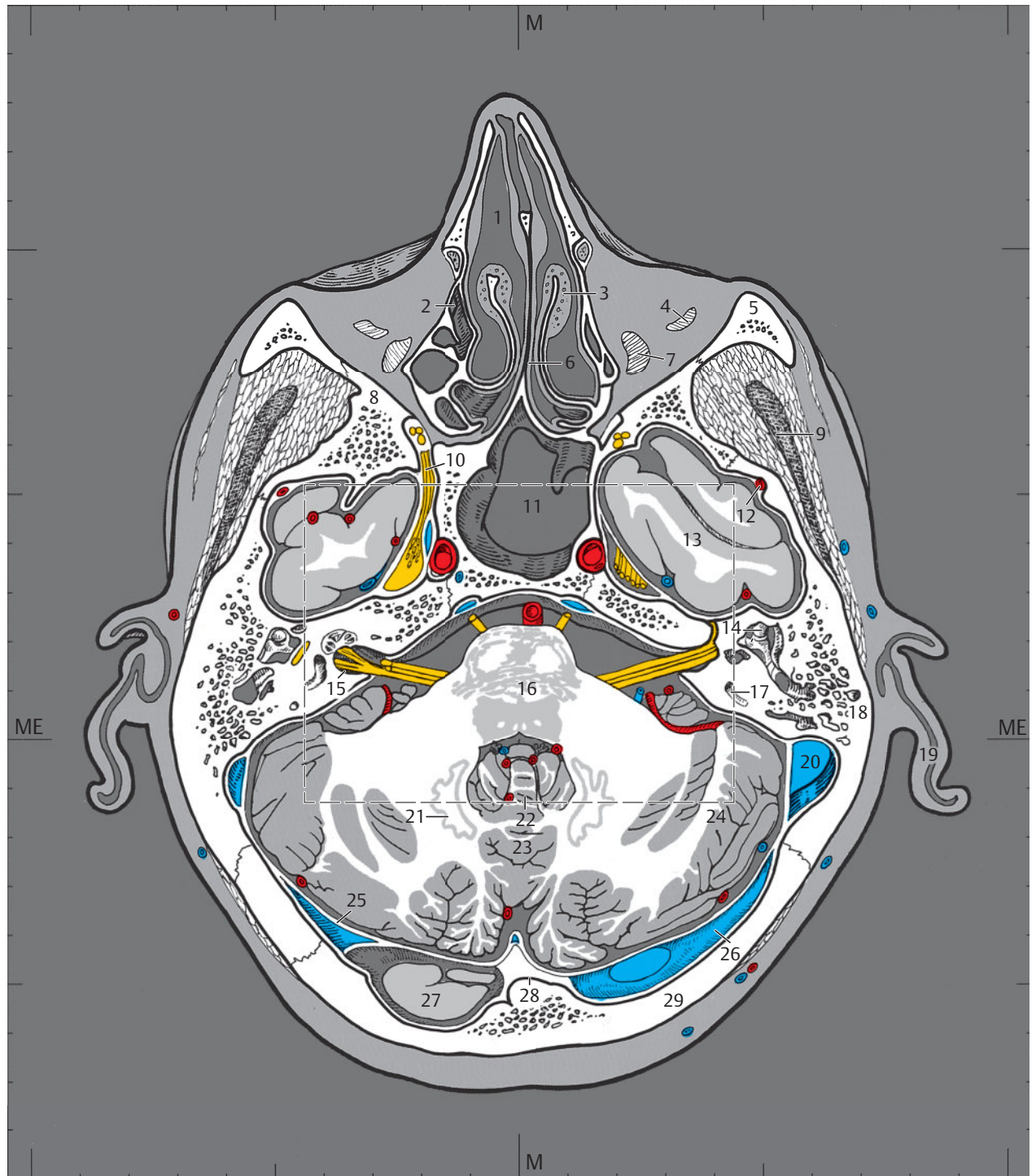


Fig. 6.8 Brainstem series.

M = median plane

ME = Meynert plane

Fig. 6.8a View of the superior surface of the fifth anatomical section of the brainstem series. The sectional plane runs just above the floor of the orbital cavity. The base of the temporal lobe lies in the middle cranial fossa. The hammer and the incus can be identified in the tympanic cavity. The posterior cranial fossa has been sectioned at the level of the inner auditory canal, pons, dentate nucleus, and the internal occipital protuberance. The pole of the left occipital lobe is seen on the left.

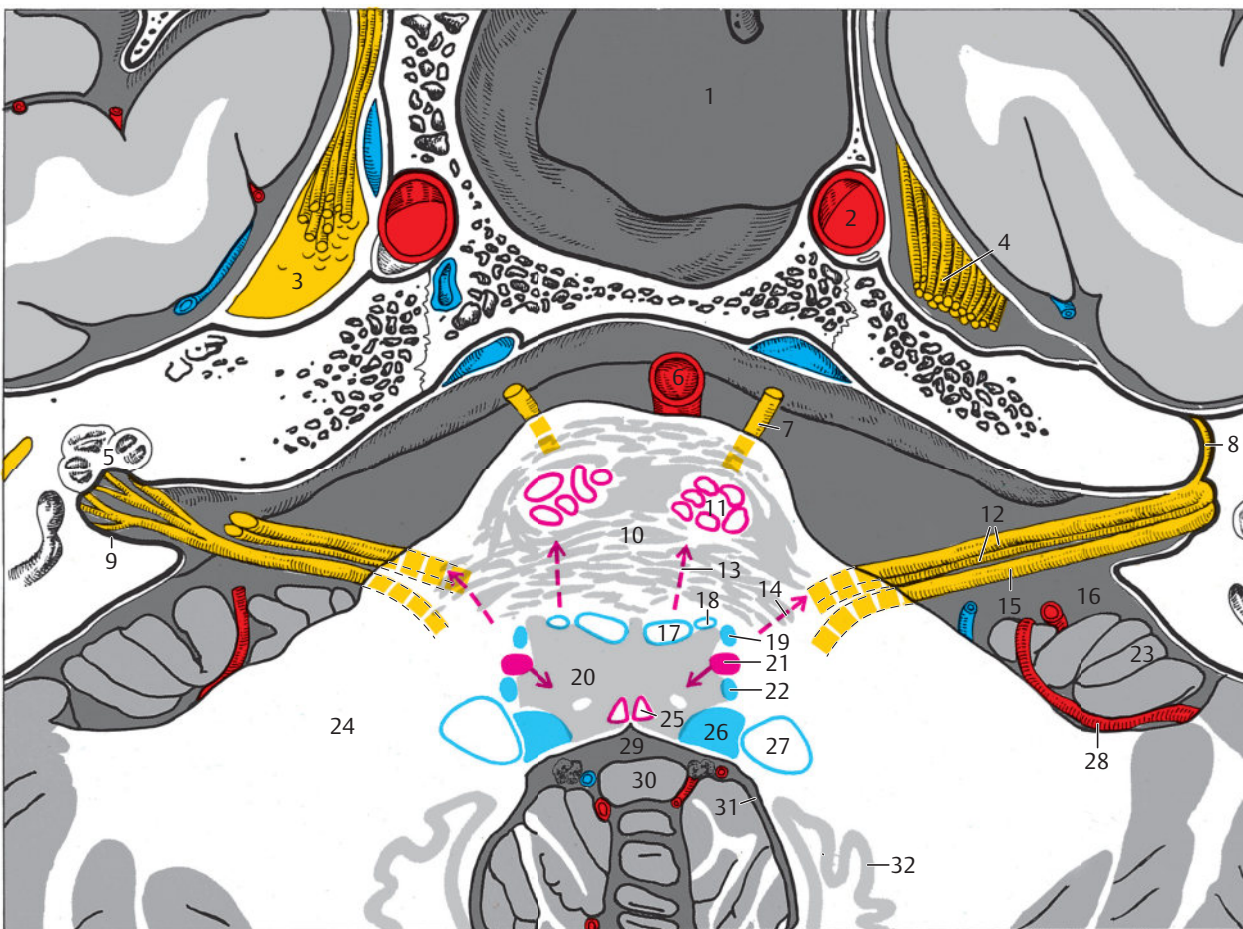
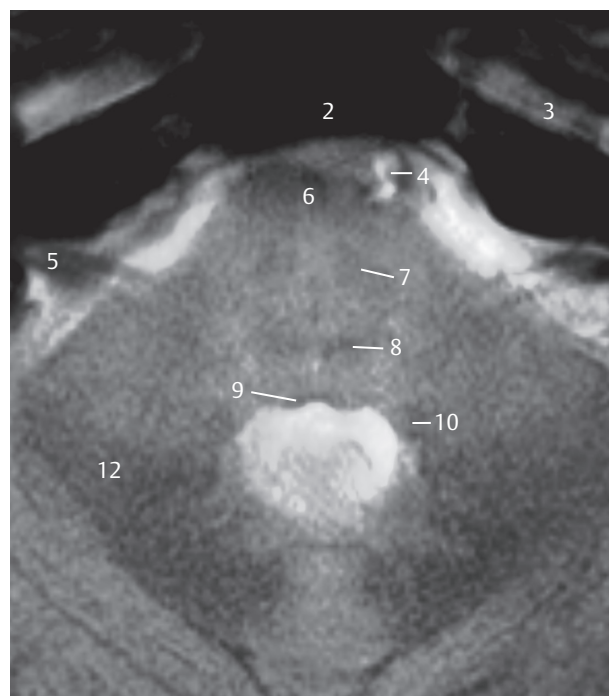
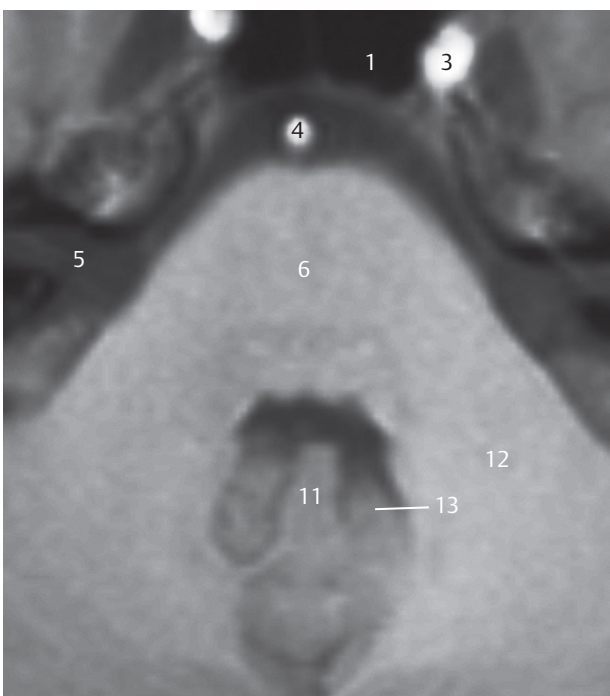


Fig. 6.8b The detail section from a shows the sphenoid sinus with the adjoining trigeminal ganglion (left) and the trigeminal nerve (right). The cross-section through the inferior part of the pons shows the middle cerebellar peduncle. The seventh and eighth cranial nerves enter the internal auditory canal.

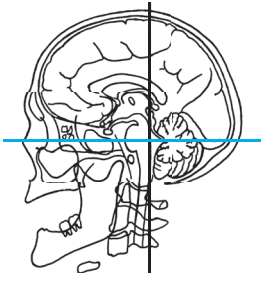
- 30 Nodule of vermis (X)
- 31 Posterior recess of fourth ventricle
- 32 Dentate nucleus

- 1 Sphenoid sinus
- 2 Internal carotid artery
- 3 Trigeminal (Gasserian) ganglion
- 4 Trigeminal nerve
- 5 Cochlea
- 6 Basilar artery
- 7 Abducens nerve
- 8 Greater petrosal nerve
- 9 Internal acoustic canal
- 10 Pontine nuclei
- 11 Corticospinal tract
- 12 Facial nerve and intermediate nerve
- 13 Abducens nerve (within the slice)
- 14 Facial nerve (within the slice)
- 15 Vestibulocochlear nerve
- 16 Cerebellopontine cistern
- 17 Medial lemniscus
- 18 Spinothalamic tract
- 19 Superior olivary nucleus
- 20 Reticular formation
- 21 Facial nucleus
- 22 Oral part of spinal nucleus of trigeminal nerve
- 23 Flocculus (H X)
- 24 Middle cerebellar peduncle
- 25 Medial longitudinal fasciculus
- 26 Vestibular nuclei
- 27 Inferior cerebellar peduncle
- 28 Anterior inferior cerebellar artery (AICA)
- 29 Fourth ventricle



- 1 Sphenoid sinus (left)
- 2 Clivus (right)
- 3 Internal carotid artery
- 4 Basilar artery
- 5 Internal acoustic canal
- 6 Pons, inferior part
- 7 Corticospinal tract (right)
- 8 Medial lemniscus (right)
- 9 Medial longitudinal fasciculus (right)
- 10 Inferior cerebellar peduncle (right)
- 11 Nodule of vermis (X) (left)
- 12 Middle cerebellar peduncle
- 13 Fourth ventricle, posterior recess (left)

Fig. 6.8c MR images oriented perpendicular to the Meynert axis, lying somewhat further superiorly than a and b. T1w MR image on the left, with a T2w MEDIC MR image on the right. For technical data see Chapter 12.



- 1 Nasal septum
- 2 Lower eyelid
- 3 Semilunar hiatus
- 4 Eyeball
- 5 Zygomatic bone
- 6 Ethmoidal bulla
- 7 Ethmoidal cells
- 8 Sphenoid
- 9 Inferior rectus
- 10 Sphenoid sinus
- 11 Middle meningeal artery
- 12 Temporal lobe
- 13 Temporalis
- 14 Anterior semicircular canal
- 15 Pons
- 16 Anterior lobe of cerebellum
- 17 Primary fissure of cerebellum
- 18 Arcuate eminence
- 19 Auricle (pinna)
- 20 Temporal bone
- 21 Dentate nucleus
- 22 Transverse sinus
- 23 Posterior lobe of cerebellum
- 24 Tentorium of cerebellum
- 25 Lambdoid suture
- 26 Confluence of sinuses (variant)
- 27 Base of occipital lobe
- 28 Occipital pole
- 29 Occipital bone

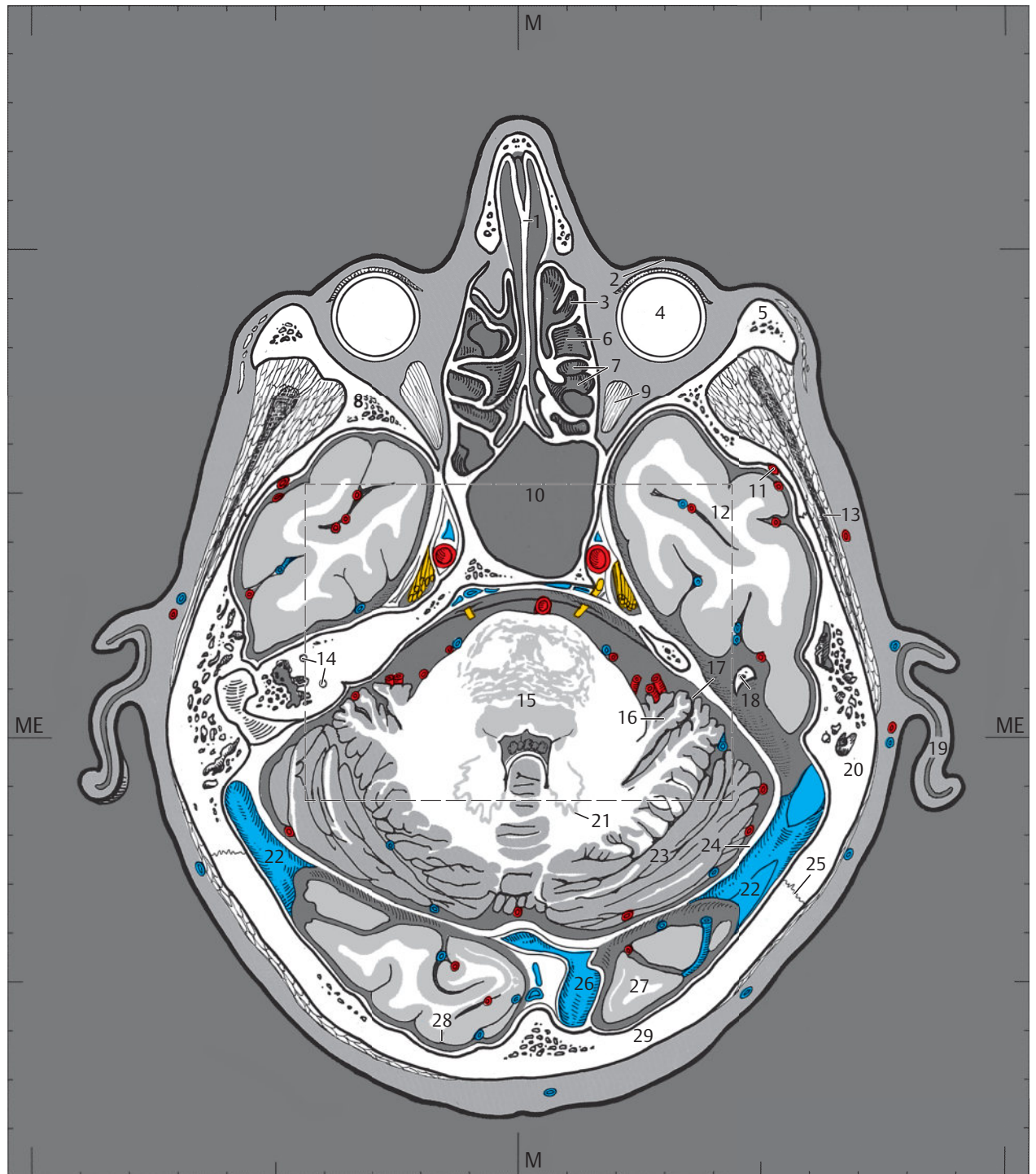


Fig. 6.9 Brainstem series.

M = median plane

ME = Meynert plane

Fig. 6.9a View of the superior surface of the sixth anatomical section of the brainstem series. The sectional plane lies at the level of the ethmoidal air cells, sphenoid sinus, and the upper part of the petrous bone. The pons and cerebellum lie in the infratentorial region of this section, while the bases of the occipital lobes lie in the supratentorial region. The two regions are separated by the cerebellar tentorium.

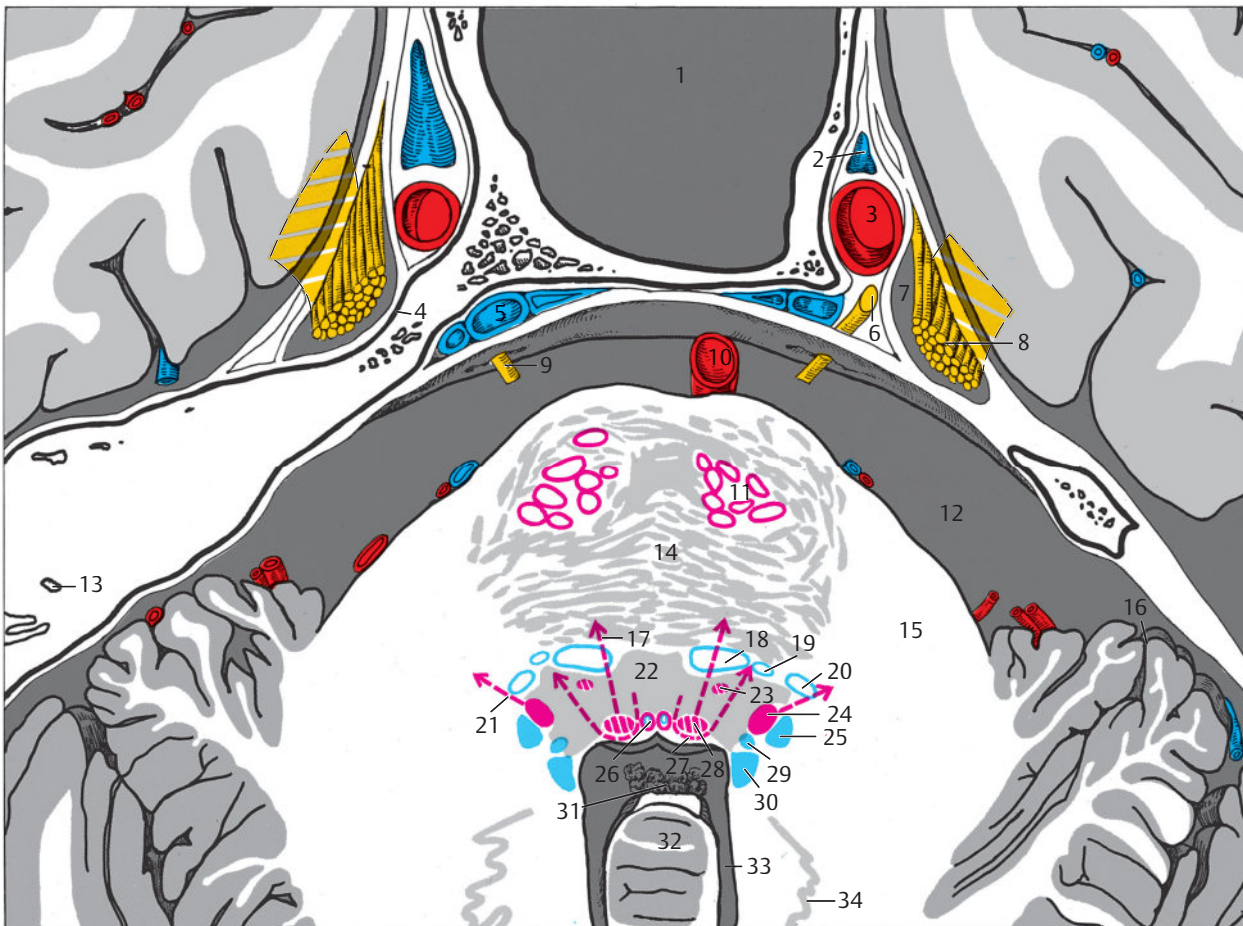
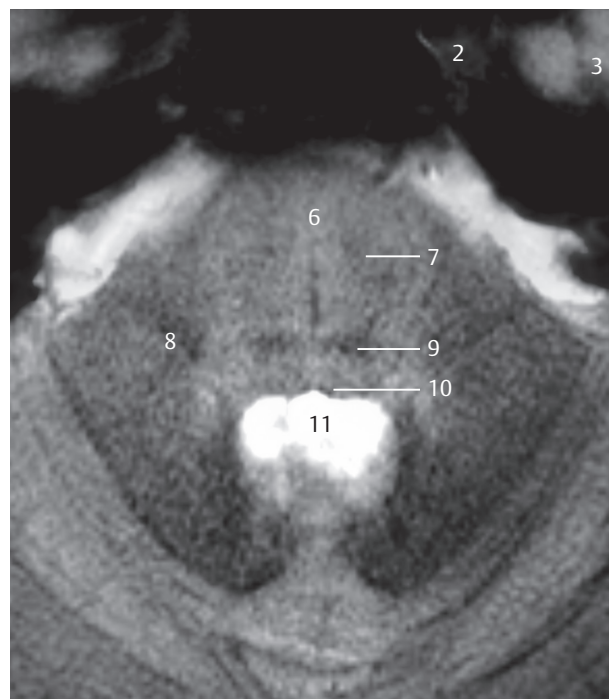
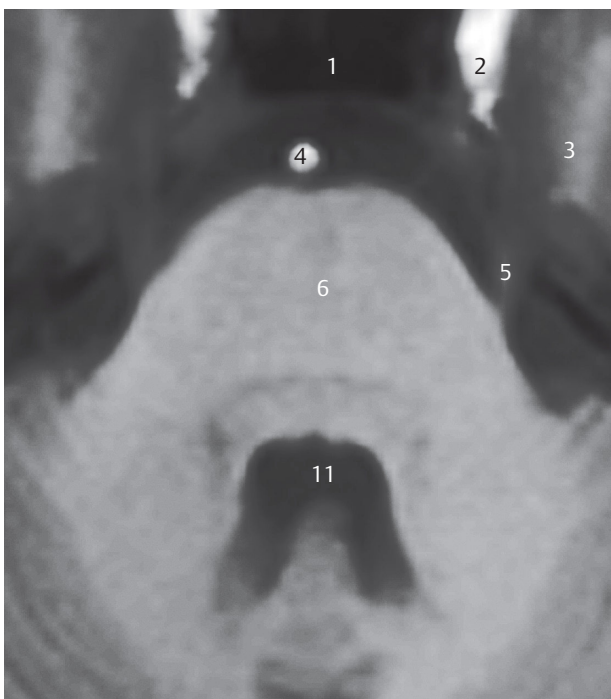


Fig. 6.9b The detail section from a shows the triangular part of the fifth cranial nerve with the sixth cranial nerve at the dural opening. The pons has been sectioned approximately in its center.

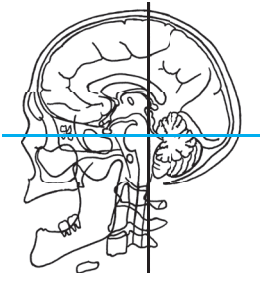
- | | |
|--|---|
| 29 Mesencephalic nucleus of trigeminal nerve | 32 Nodule of vermis (X) |
| 30 Superior vestibular nucleus | 33 Posterior recess of fourth ventricle |
| 31 Choroid plexus of fourth ventricle | 34 Dentate nucleus |

- 1 Sphenoid sinus
- 2 Cavernous sinus
- 3 Internal carotid artery
- 4 Trigeminal impression
- 5 Inferior petrosal sinus
- 6 Abducens nerve
- 7 Opening of trigeminal cistern
- 8 Triangular part of trigeminal nerve
- 9 Abducens nerve near opening of dura mater
- 10 Basilar artery
- 11 Corticospinal tract
- 12 Cerebellopontine cistern
- 13 Anterior semicircular canal
- 14 Pontine nuclei
- 15 Middle cerebellar peduncle
- 16 Primary fissure of cerebellum
- 17 Abducens nerve (within the slice)
- 18 Medial lemniscus
- 19 Spinothalamic tract
- 20 Lateral lemniscus
- 21 Motor root of trigeminal nerve (within the slice)
- 22 Reticular formation
- 23 Facial nucleus (in the inferior part of the slice)
- 24 Motor nucleus of trigeminal nerve
- 25 Principal sensory nucleus of trigeminal nerve
- 26 Medial longitudinal fasciculus
- 27 Genu of facial nerve
- 28 Abducens nucleus (within the slice)



- 1 Sphenoid sinus (left)
- 2 Internal carotid artery
- 3 Temporal lobe
- 4 Basilar artery (left)
- 5 Trigeminal nerve (left)
- 6 Pons
- 7 Corticospinal tract (right)
- 8 Middle cerebellar peduncle (right)
- 9 Medial lemniscus right)
- 10 Medial longitudinal fasciculus (right)
- 11 Fourth ventricle

Fig. 6.9c MR images oriented perpendicular to the Meynert axis, corresponding approximately to a and b. T1w MR image on the left, with a T2w MEDIC MR image on the right. For technical data see Chapter 12.



- 1 Upper eyelid
- 2 Lens
- 3 Orbital plate
- 4 Eyeball
- 5 Nasal septum
- 6 Ethmoidal cells
- 7 Sphenoid
- 8 Medial rectus
- 9 Optic nerve
- 10 Lateral rectus
- 11 Superior orbital fissure
- 12 Sphenoid sinus
- 13 Pituitary gland
- 14 Temporalis
- 15 Trigeminal nerve
- 16 Pons
- 17 Anterior lobe of cerebellum
- 18 Primary fissure of cerebellum
- 19 Temporal bone
- 20 Auricle (pinna)
- 21 Posterior lobe of cerebellum
- 22 Tentorium of cerebellum
- 23 Parietal bone
- 24 Straight sinus
- 25 Lambdoid suture
- 26 Superior sagittal sinus
- 27 Occipital bone



- 1 Meckel's cave
- 2 Internal carotid artery
- 3 Basilar artery
- 4 Trigeminal nerve
- 5 Pons
- 6 Fourth ventricle

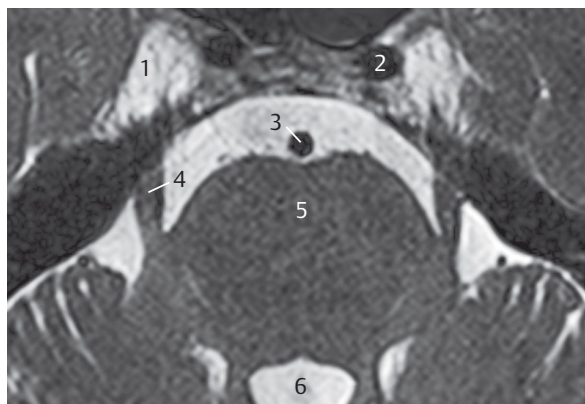


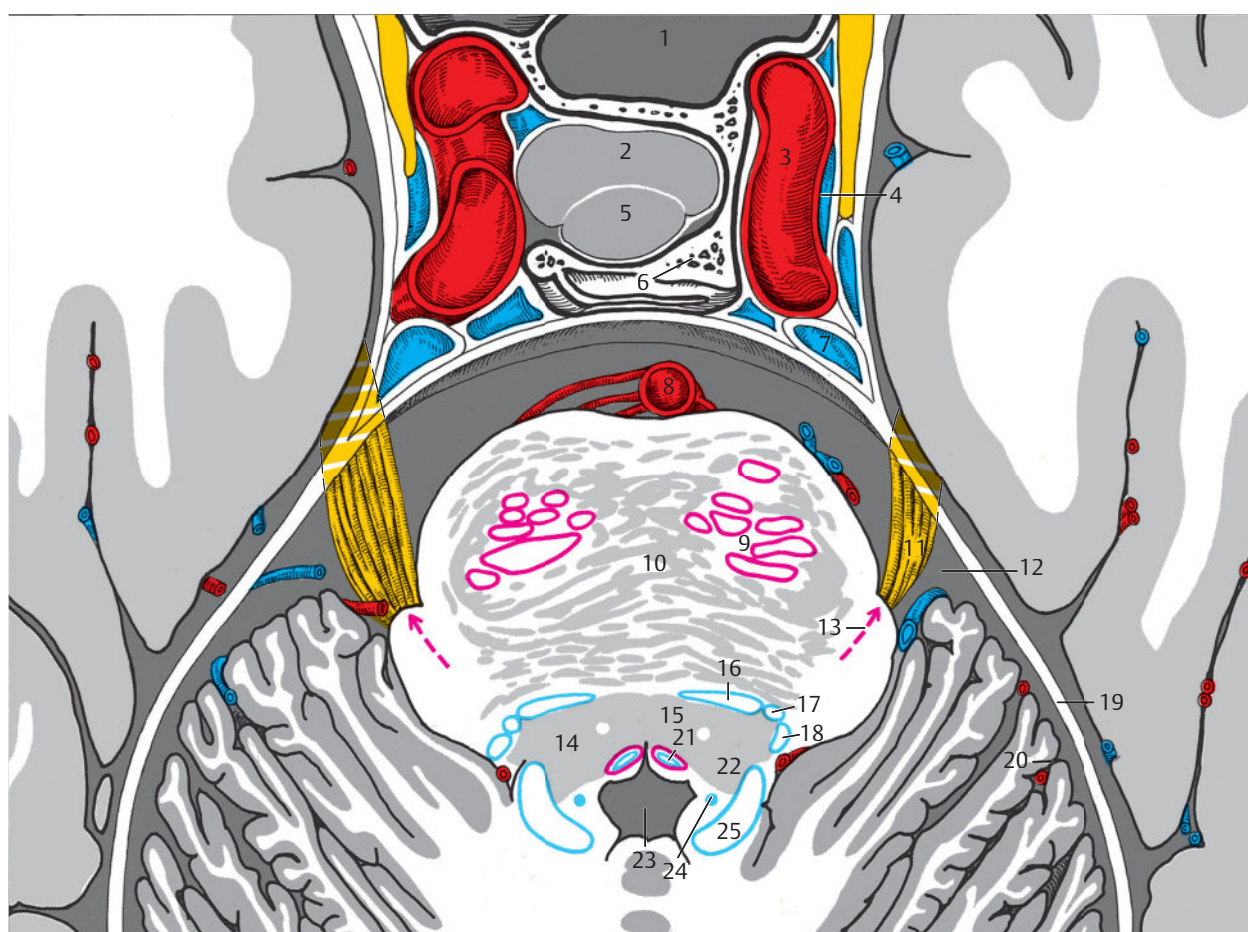
Fig. 6.10 Brainstem series.

M = median plane

ME = Meynert plane

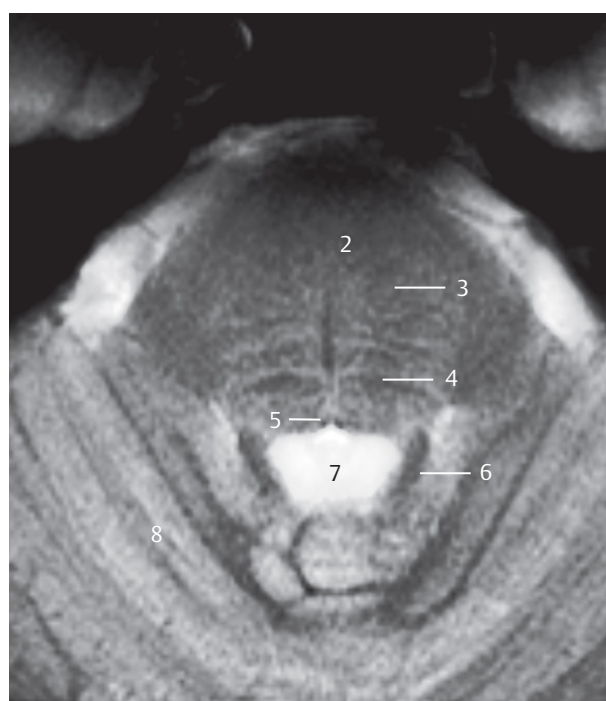
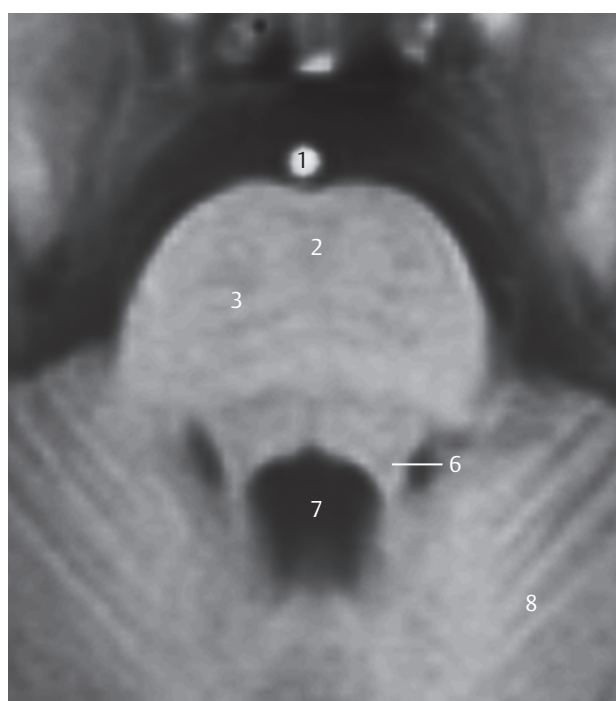
Fig. 6.10a View of the superior surface of the seventh anatomical section of the brainstem series. The sectional plane runs through the superior orbital fissure, the sella turcica with the pituitary gland as well as through the basal parts of the temporal and occipital lobes. The pons has been sectioned at the level of the exit of the trigeminal nerve.

Fig. 6.10d High-resolution T2w image of the trigeminal nerve and its entry into Meckel's cave.



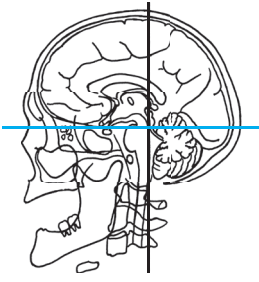
- 1 Sphenoid sinus
- 2 Adenohypophysis
- 3 Internal carotid artery
- 4 Cavernous sinus
- 5 Neurohypophysis
- 6 Dorsum sellae
- 7 Superior petrosal sinus
- 8 Basilar artery
- 9 Corticospinal tract
- 10 Pontine nuclei
- 11 Trigeminal nerve
- 12 Cerebellopontine cistern
- 13 Trigeminal nerve (within the slice)
- 14 Reticular formation
- 15 Paramedian pontine reticular formation (PPRF)
- 16 Medial lemniscus
- 17 Spinothalamic tract
- 18 Lateral lemniscus
- 19 Tentorium of cerebellum
- 20 Primary fissure of cerebellum
- 21 Medial longitudinal fasciculus
- 22 Cerebellar nucleus
- 23 Fourth ventricle
- 24 Mesencephalic nucleus of trigeminal nerve
- 25 Superior cerebellar peduncle

Fig. 6.10b The detail section from a shows the adeno- and the neurohypophysis with the laterally situated segments of the internal carotid arteries. The superior cerebellar peduncle lies lateral to the fourth ventricle.



- 1 Basilar artery (left)
- 2 Pons
- 3 Corticospinal tract
- 4 Medial lemniscus (right)
- 5 Medial longitudinal fasciculus (right)
- 6 Superior cerebellar peduncle
- 7 Fourth ventricle
- 8 Anterior lobe of cerebellum

Fig. 6.10c MR images oriented perpendicular to the Meynert axis, corresponding approximately to a and b. T1w MR image on the left, with a T2w MEDIC MR image on the right. For technical data see Chapter 12.



- 1 Upper eyelid
- 2 Lens
- 3 Eyeball
- 4 Lacrimal gland
- 5 Superior oblique
- 6 Olfactory bulb
- 7 Medial rectus
- 8 Ophthalmic artery
- 9 Lateral rectus
- 10 Superior rectus
- 11 Levator palpebrae superioris
- 12 Olfactory tract
- 13 Optic canal (within the slice)
- 14 Optic nerve
- 15 Middle meningeal artery
- 16 Temporalis
- 17 Temporal bone
- 18 Pons
- 19 Anterior lobe of cerebellum
- 20 Primary fissure of cerebellum
- 21 Posterior lobe of cerebellum
- 22 Tentorium of cerebellum
- 23 Straight sinus
- 24 Parietal bone
- 25 Falx cerebri
- 26 Lambdoid suture
- 27 Superior sagittal sinus
- 28 Occipital bone



Fig. 6.11 Brainstem series.

M = median plane

ME = Meynert plane

Fig. 6.11a View of the superior surface of the eighth anatomical section of the brainstem series. The olfactory bulb and tract have been sectioned in the depths of the anterior cranial fossa. The optic nerve enters the optic canal. The supratentorial region with the temporal and occipital lobes is significantly larger in this section than the infratentorial region with the pons and cerebellum.

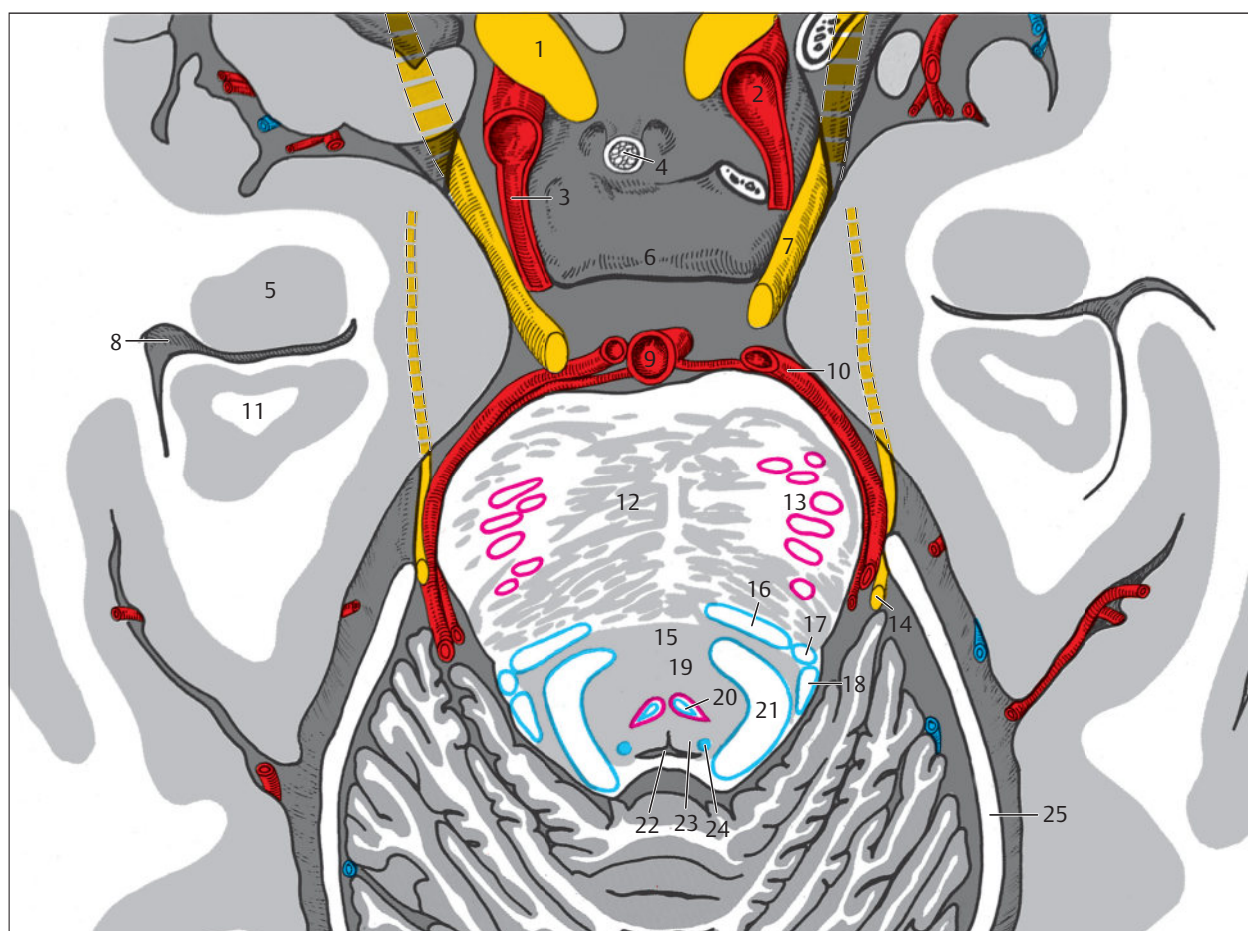


Fig. 6.11b The detail section from a displays a nearly horizontal stretch of the third and fourth cranial nerves. The infundibulum pierces the roof of the sella turcica. The fourth ventricle tapers in the upper part of the pons in the direction of the aqueduct of the midbrain.

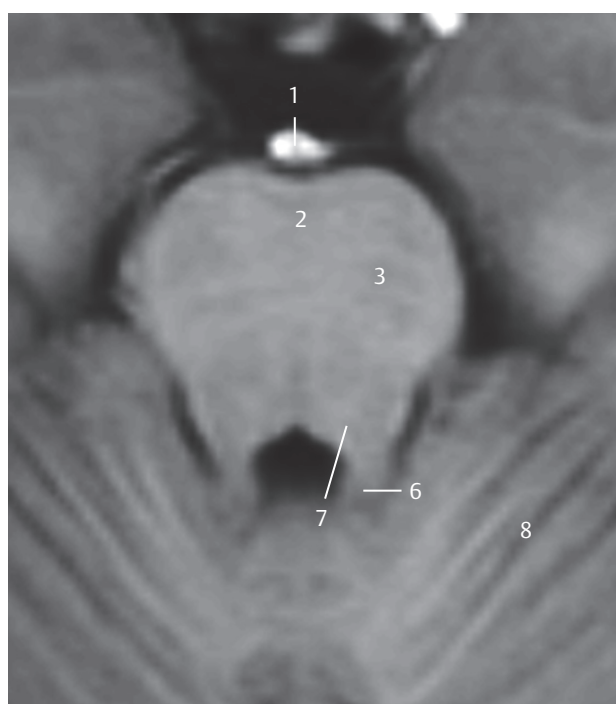
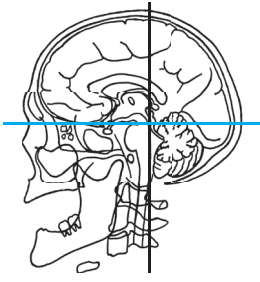


Fig. 6.11c MR images oriented perpendicular to the Meynert axis, lying somewhat further inferiorly than a and b. T1w MR image on the left, with a T2w MEDIC MR image on the right. For technical data see Chapter 12.



- 1 Frontal bone
- 2 Frontal sinus
- 3 Trochlea
- 4 Crista galli
- 5 Superior oblique
- 6 Superior rectus
- 7 Levator palpebrae superioris
- 8 Sphenoid
- 9 Straight gyrus
- 10 Temporalis
- 11 Temporal bone
- 12 Mammillary body
- 13 Interpeduncular cistern
- 14 Cerebral crus
- 15 Tegmentum of midbrain
- 16 Ambient cistern
- 17 Aqueduct of midbrain
- 18 Anterior lobe of cerebellum
- 19 Tentorium of cerebellum
- 20 Straight sinus
- 21 Parietal bone
- 22 Longitudinal cerebral (interhemispheric) fissure
- 23 Primary visual cortex
- 24 Falx cerebri
- 25 Calcarine sulcus
- 26 Lambdoid suture
- 27 Superior sagittal sinus
- 28 Occipital bone

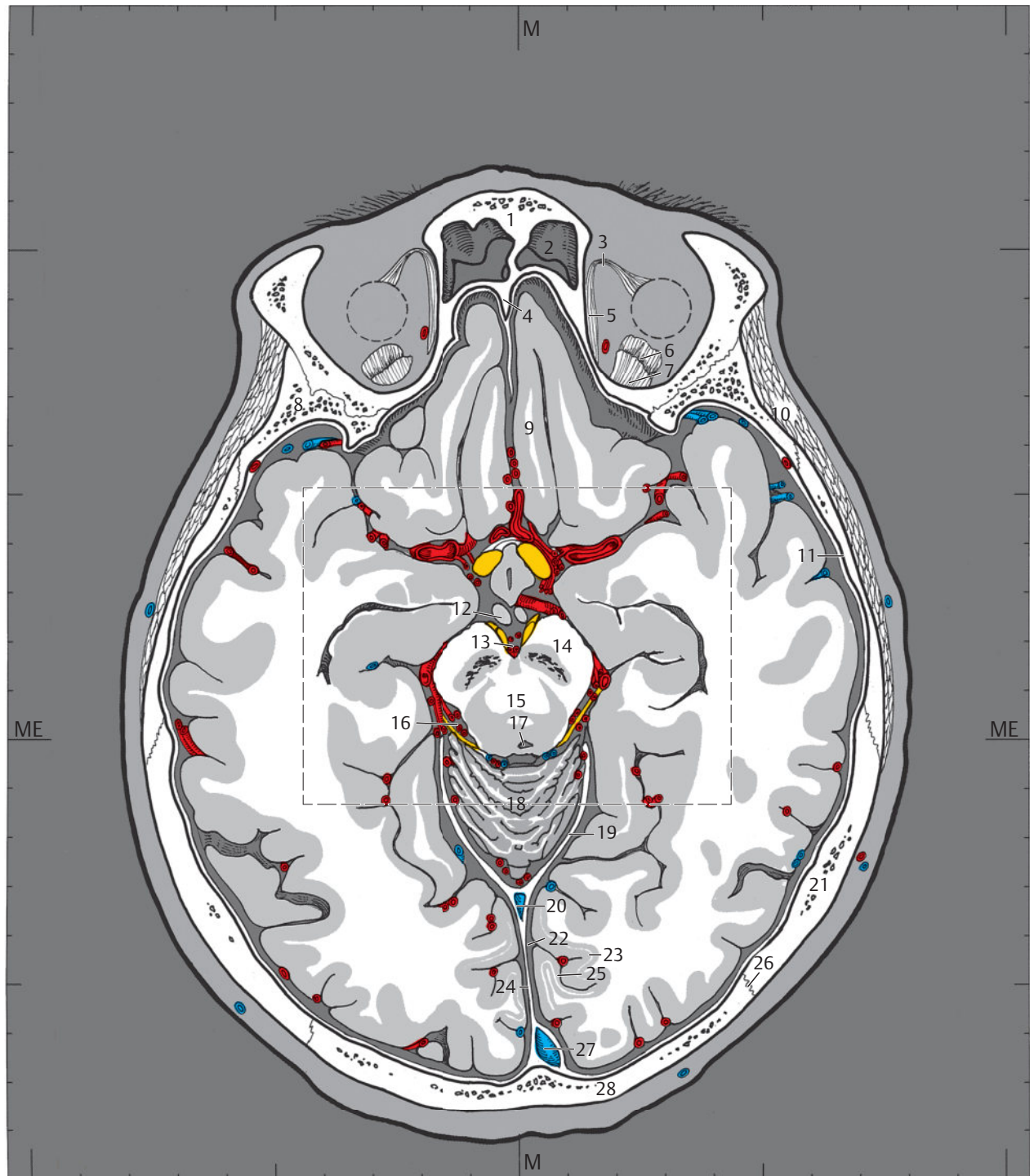
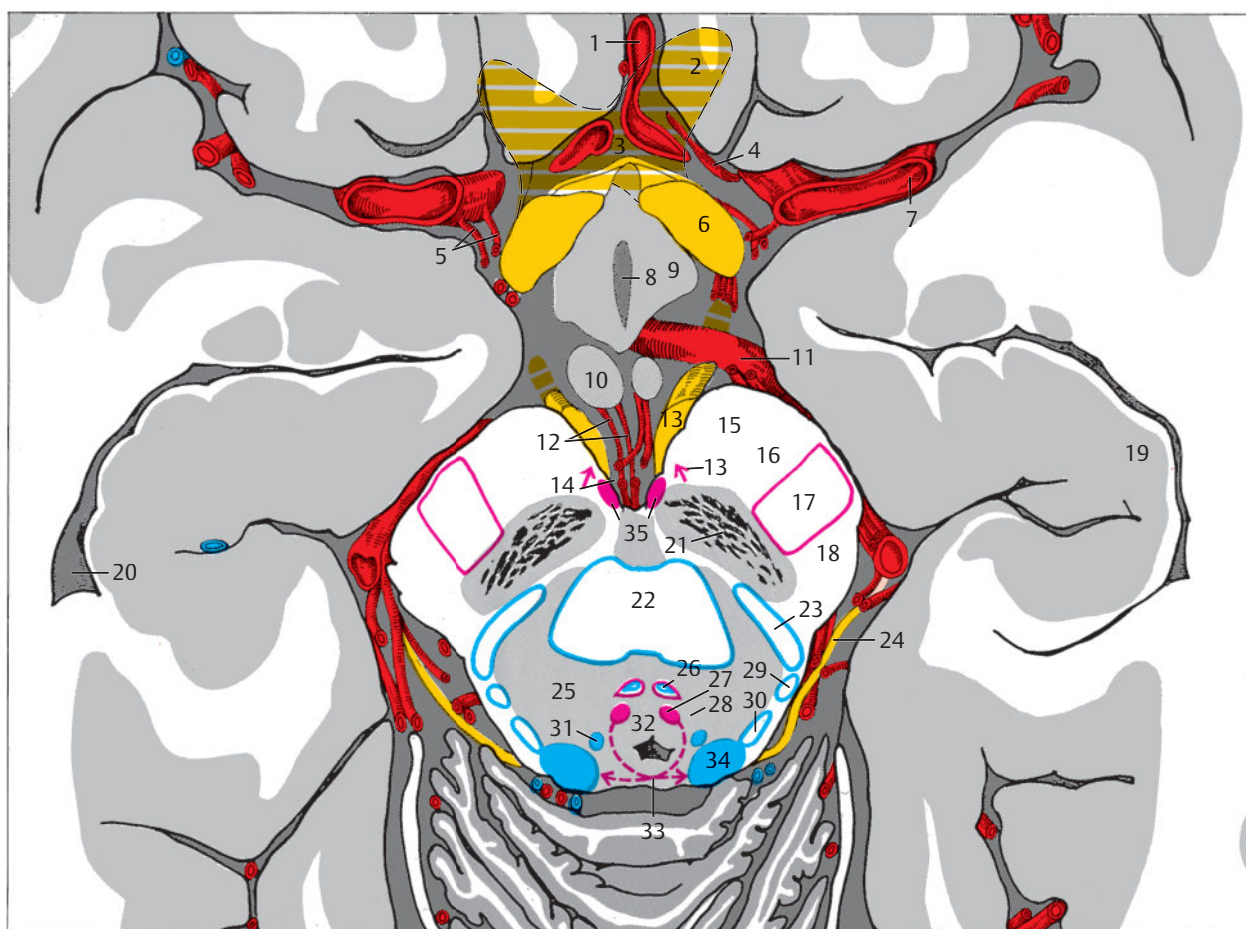


Fig. 6.12 Brainstem series.

M = median plane

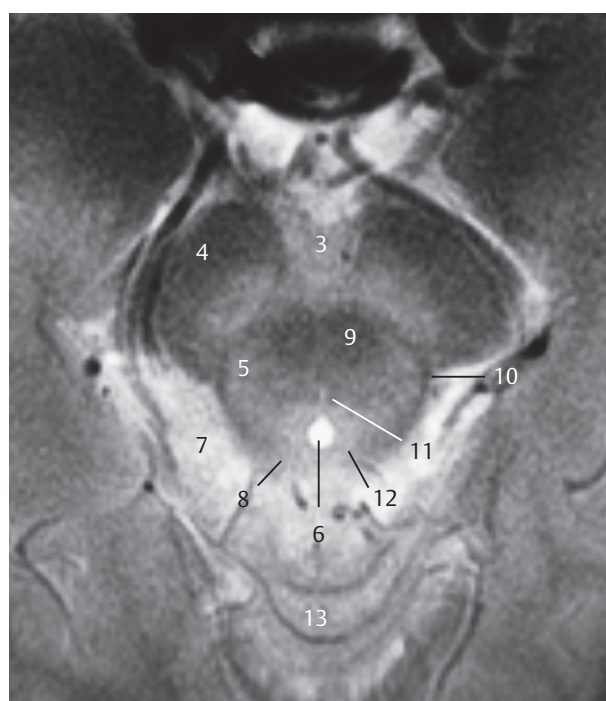
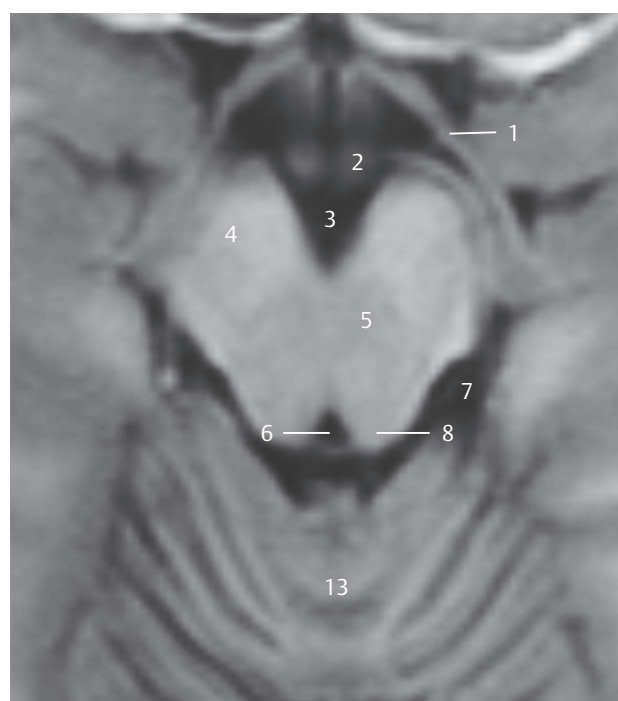
ME = Meynert plane

Fig. 6.12a View of the superior surface of the ninth anatomical section of the brainstem series. The sectional plane lies anteriorly just below the roof of orbit and medially behind it in the region of the straight gyrus above the anterior cranial fossa. The mammillary bodies and the midbrain at the level of the inferior colliculi are seen in this section.



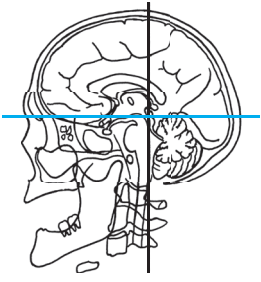
- 1 Anterior cerebral artery
- 2 Optic nerve (within the slice)
- 3 Optic chiasm (within the slice)
- 4 Anteromedial central artery
- 5 Anterolateral central arteries
- 6 Optic tract
- 7 Middle cerebral artery
- 8 Infundibular recess
- 9 Hypothalamus
- 10 Mammillary body
- 11 Posterior cerebral artery
- 12 Posteromedial central arteries
- 13 Oculomotor nerve and its roots (arrow)
- 14 Interpeduncular fossa
- 15 Frontopontine tract
- 16 Corticonuclear tract
- 17 Corticospinal tract
- 18 Occipitopontine and temporopontine tracts
- 19 Hippocampus
- 20 Temporal (inferior) horn of lateral ventricle
- 21 Substantia nigra
- 22 Decussation of superior cerebellar peduncles
- 23 Medial lemniscus
- 24 Trochlear nerve
- 25 Reticular formation
- 26 Medial longitudinal fasciculus
- 27 Trochlear nucleus
- 28 Cerulean nucleus
- 29 Spinothalamic tract
- 30 Lateral lemniscus
- 31 Mesencephalic nucleus of trigeminal nerve
- 32 Aqueduct of midbrain
- 33 Decussation of trochlear nerves (within the slice)
- 34 Inferior colliculus
- 35 Ventral tegmental area (VTA)

Fig. 6.12b The detail section from a shows the optic tract. The optic chiasm lies within this ninth section (interrupted yellow), posterior to which lies the hypothalamus with the mammillary bodies. The trochlear nerve is seen exiting the midbrain in this section behind the inferior colliculus.



- 1 Optic tract (left)
- 2 Mammillary body (left)
- 3 Interpeduncular cistern
- 4 Cerebral crus
- 5 Tegmentum of midbrain
- 6 Aqueduct of midbrain
- 7 Ambient cistern
- 8 Inferior colliculus
- 9 Superior cerebellar peduncle, intersection (right)
- 10 Medial lemniscus (right)
- 11 Medial longitudinal fasciculus (right)
- 12 Periaqueductal gray (right)
- 13 Anterior lobe of cerebellum, vermis

Fig. 6.12c MR images oriented perpendicular to the Meynert axis, corresponding approximately to a and b. T1w MR image on the left, with a T2w MEDIC MR image on the right. For technical data see Chapter 12.



- 1 Frontal sinus
- 2 Crista galli
- 3 Frontal bone
- 4 Longitudinal cerebral (interhemispheric) fissure
- 5 Temporalis
- 6 Insular arteries
- 7 Hypothalamus
- 8 Temporal bone
- 9 Tegmentum of midbrain
- 10 Aqueduct of midbrain
- 11 Anterior lobe of cerebellum
- 12 Occipital (posterior) horn of lateral ventricle
- 13 Tentorium of cerebellum
- 14 Straight sinus
- 15 Primary visual cortex
- 16 Parietal bone
- 17 Falx cerebri
- 18 Calcarine sulcus
- 19 Lambdoid suture
- 20 Superior sagittal sinus
- 21 Occipital bone

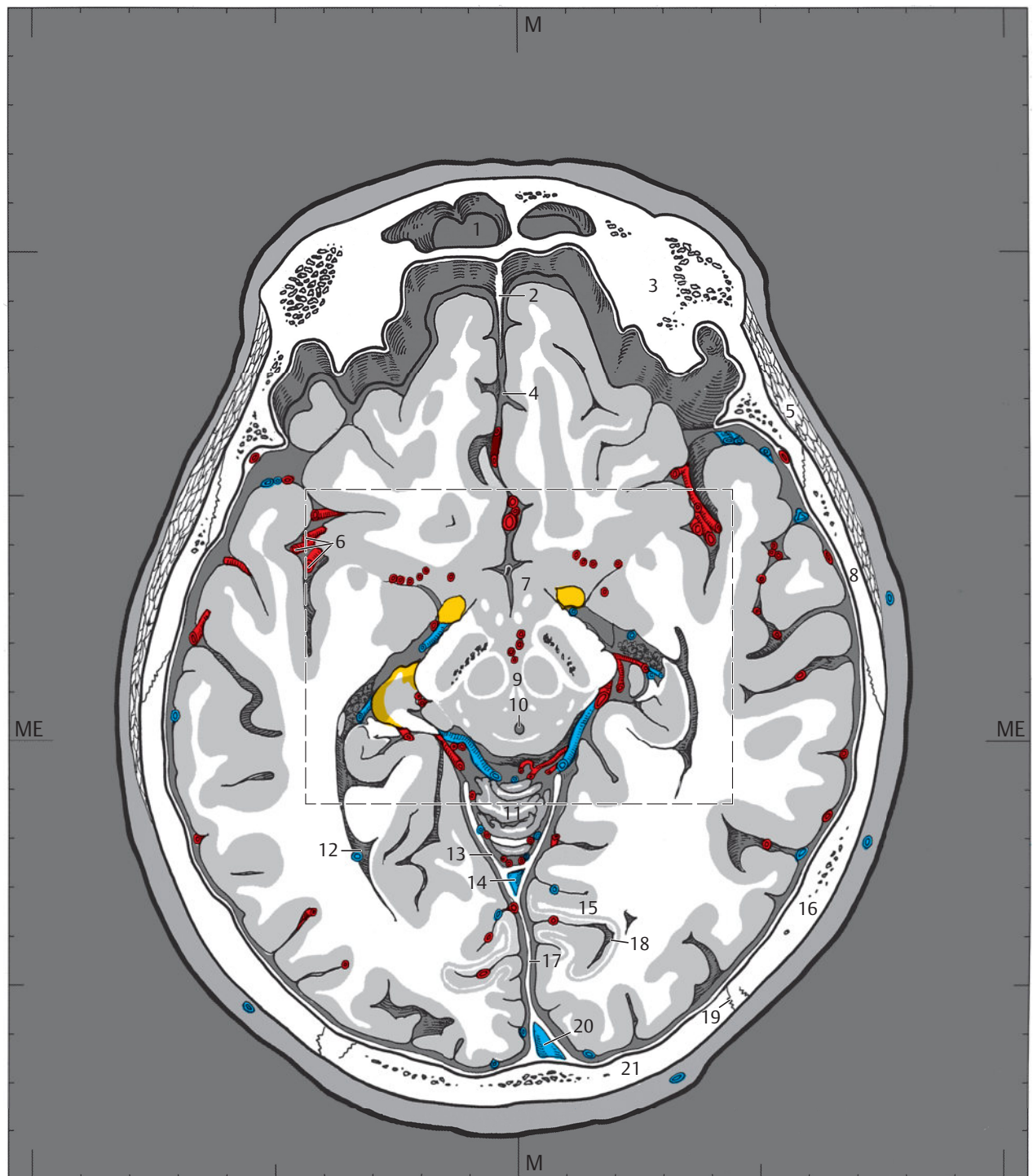
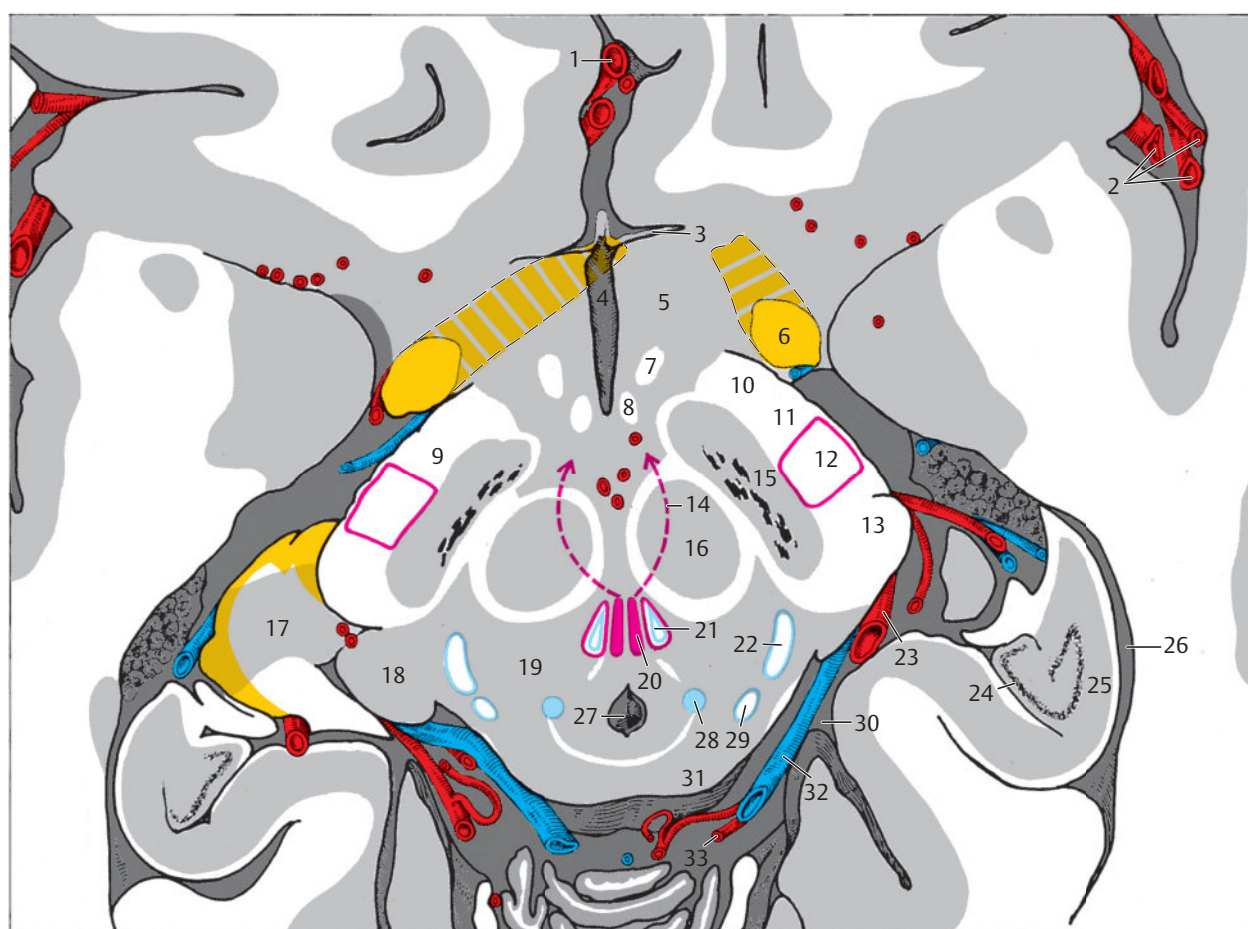


Fig. 6.13 Brainstem series.

M = median plane

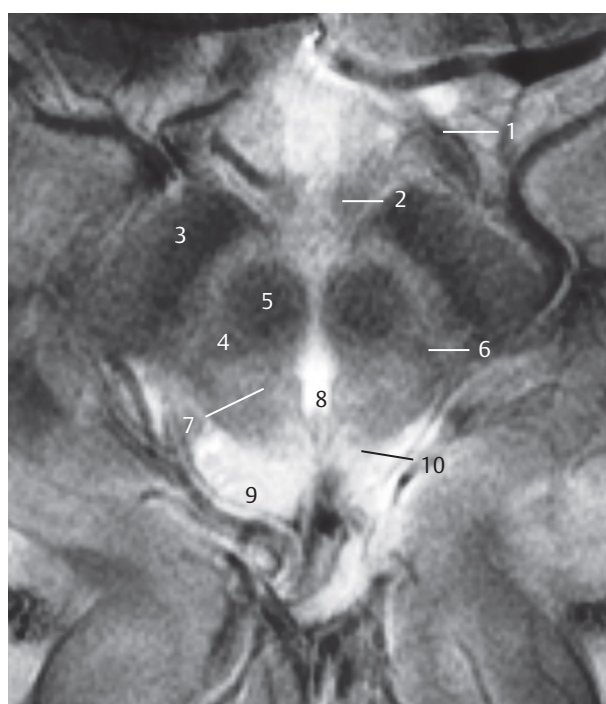
ME = Meynert plane

Fig. 6.13a View of the superior surface of the tenth anatomical section of the brainstem series. Sections of the frontal and temporal lobes, hypothalamus, and midbrain have been sectioned in this plane at the level of the superior colliculi.



- 1 Anterior cerebral artery
- 2 Insular arteries
- 3 Lamina terminalis
- 4 Third ventricle
- 5 Hypothalamus
- 6 Optic tract
- 7 Fornix
- 8 Mammillothalamic fasciculus (of Vicq d'Azyr)
- 9 Cerebral crus
- 10 Frontopontine tract
- 11 Corticonuclear tract
- 12 Corticospinal tract
- 13 Occipitopontine and temporopontine tracts
- 14 Oculomotor nerve (within the slice)
- 15 Substantia nigra
- 16 Red nucleus
- 17 Lateral geniculate body
- 18 Medial geniculate body
- 19 Reticular formation
- 20 Oculomotor nucleus
- 21 Medial longitudinal fasciculus
- 22 Medial lemniscus
- 23 Posterior cerebral artery
- 24 Dentate gyrus
- 25 Hippocampus
- 26 Temporal (inferior) horn of lateral ventricle
- 27 Aqueduct of midbrain
- 28 Mesencephalic nucleus of trigeminal nerve
- 29 Spinothalamic tract
- 30 Ambient cistern
- 31 Superior colliculus
- 32 Basal vein (of Rosenthal)
- 33 Posterior lateral choroidal artery

Fig. 6.13b The detail section from a portrays structures adjoining the optic tract-hypothalamus, midbrain at the level of the superior colliculi, and the hippocampus.



- 1 Optic tract
- 2 Mammillary body
- 3 Cerebral crus
- 4 Tegmentum of midbrain
- 5 Red nucleus (right)
- 6 Medial lemniscus (right)
- 7 Medial longitudinal fasciculus (right)
- 8 Aqueduct of midbrain
- 9 Ambient cistern
- 10 Superior colliculus

Fig. 6.13c MR images oriented perpendicular to the Meynert axis, lying somewhat further inferiorly than a and b. T1w MR image on the left, with a T2w MEDIC MR image on the right. For technical data see Chapter 12.

Part III
**Topography of the Head
and Neck**

7	Topography of the Cranium, Intracranial Spaces, and Contained Structures	224
8	Facial Topography	357
9	Topography of the Head–Neck Region	369



7 Topography of the Cranium, Intracranial Spaces, and Contained Structures

7.1 Cranial Vault

Five bones form the cranial vault, the neurocranium:

- Occipital bone
- Sphenoid
- Paired temporal bones
- Frontal bone
- Paired parietal bones

The cranial vault and the nasal skeleton are closely related, with the lamina cribrosa of the ethmoid bone forming part of the cranial cavity together with the aforementioned bones.

7.1.1 Occipital Bone

The **occipital bone** forms the boundary of most of the posterior cranial fossa and is divided into four different parts:

- Basal Part
- Two lateral parts
- Squamous part

All parts surround the foramen magnum (see ►Fig. 3.24, ►Fig. 3.25, ►Fig. 4.8, and ►Fig. 5.17).

The **basal part** forms the anterior edge of the foramen magnum and fuses in the 16th to 18th years of life with the sphenoid to form the clivus, a landmark for neuroimaging (see ►Fig. 4.2c). The pons and medulla oblongata lie posterior to the clivus (see ►Fig. 4.2a and ►Fig. 4.2b). The two **lateral parts** are related to the temporal bones. The articular processes, the occipital condyles, protrude from their inferior surface and correspond to the atlas. The hypoglossal canal, through which the XIIth cranial nerve exits, lies superior to the occipital condyles (see ►Fig. 4.3a, ►Fig. 4.9, ►Fig. 5.3a, and ►Fig. 5.31).

The **squamous part** is roughly triangular and appears bent in the median plane and seems to be composed of an upper and lower part. An external occipital prominence, the external occipital protuberance, is seen protruding roughly from the center of the outer aspect of the squamous part, right at the border of the upper and lower part (see ►Fig. 4.2c, 4.2d, ►Fig. 4.8, ►Fig. 5.1b, and ►Fig. 5.6a). An internal occipital prominence, the internal occipital protuberance, lies on the inner aspect of the squamous part, opposite to its external counterpart

(see ►Fig. 4.2 and ►Fig. 4.8). The confluence of sinuses is situated here, with the superior sagittal sinus draining into the transverse sinus. The dura of the transverse sinus also serves as the attachment for the tentorium of cerebellum, thereby forming an important topographic and neurosurgical boundary between the infra- and supratentorial regions.

7.1.2 Sphenoid

The **sphenoid** is located anteriorly and connected with the occipital bone and forms the central part of the base of the skull. Comparison with a wasp helps illustrate parts of the sphenoid:

- **Unpaired median portion of the sphenoid:** “Body” of the wasp from which two “pairs of wings” protrude upward.
- **Lesser wings:** First “pair of wings” of the wasp.
- **Greater wings:** Second “pair of wings” of the wasp, below the lesser wings.
- **Superior orbital fissure:** Cleft between both “pairs of wings” (see ►Fig. 3.5d, ►Fig. 3.18, ►Fig. 4.1b, ►Fig. 4.4c, ►Fig. 4.4d, ►Fig. 5.17, and ►Fig. 5.35).
- **Pterygoid processes:** Each with a medial and lateral plate (see ►Fig. 3.5c, ►Fig. 3.19, and ►Fig. 5.3), paired “legs” suspended inferiorly from the body of the wasp.

The **body of the sphenoid** is shaped like a cube and contains the sphenoid sinus, which has been described in Section 8.2. The cerebral surface of the body of the sphenoid is related to the cribriform plate of the ethmoid through the spheno-ethmoidal suture. Behind this lies the “Turkish saddle”, the sella turcica, that forms the hypophyseal fossa, a deep depression that accommodates the pituitary gland. The hypophyseal fossa is bounded by the tuberculum sellae anteriorly and posteriorly by the dorsum sellae (see ►Fig. 4.8 and ►Fig. 5.35). The posterior clinoid process protrudes laterally from the dorsum sellae on either side (see ►Fig. 5.35).

The paired **lesser wings** arise from the body of the sphenoid, each with two roots, encompassing the optic canal (see ►Fig. 3.18 and ►Fig. 5.36). The lesser wings form the boundary between the anterior and middle cranial fossae. The posteromedial edge of the lesser wing protrudes medially as the anterior clinoid process (see ►Fig. 3.1b, ►Fig. 3.6c, ►Fig. 5.1b, ►Fig. 5.19, and ►Fig. 5.36).

Clinical Notes

Onodi cells are pneumatized cells of the posterior ethmoid, lying superolateral to the sphenoid sinus and extending into the anterior clinoid processes. This anatomical variant is of clinical relevance due to immediate proximity to the optic nerve and internal carotid artery, ignorance of which may result in iatrogenic injury. Pneumatization of the sphenoid sinus may also extend into the anterior clinoid processes, which is then called “spheno-optic recess”. Axial and coronal CT images should therefore be obtained while planning surgery on the paranasal sinuses.^{85,369,437,652}

The **greater wings of the sphenoid** are paired structures arising from the posterior aspect of the sphenoid body. Two openings for nerves (second and third divisions of the Vth cranial nerve) perforate their roots, the foramen rotundum anteriorly and foramen ovale posteriorly. The foramen spinosum for the middle meningeal artery lies posterolateral to the foramen ovale. The greater wing of the sphenoid is related anteriorly to the maxilla at the pterygopalatine fossa, and to the orbit, forming part of the orbital wall. The temporal part of the greater wing of the sphenoid is directed laterally and forms a small part of the lateral cranial vault in the region of the temporal fossa.

The **pterygoid process** (see ► Fig. 3.19) originates with two roots from the body of the sphenoid which follow a downward course along the lateral wall of the choana. The pterygoid canal runs between the two roots of the **pterygoid process** and ends finally in the pterygopalatine fossa. The pterygoid process splits into medial and lateral laminae or plates, enclosing a longitudinal groove, the **pterygoid fossa** (see ► Fig. 3.19). The medial plate forms a hook-like projection, the pterygoid hamulus (see ► Fig. 3.5c, ► Fig. 3.5d, and ► Fig. 4.4c) around which the tendon of the tensor veli palatine is wrapped; the lateral plate exhibits a rounded inferior border.

7.1.3 Temporal Bone

Anja Gieseemann

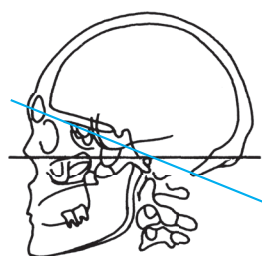
The paired **temporal bones** each form part of the base of skull and the lateral cranial vault. Each consists of four parts (five in the Anglo-American literature):

- **Petrous part:** This part encloses the inner ear and forms the boundary between the middle and posterior cranial fossae in the region of the base of skull.
- **Tympanic part:** The tympanic part forms the floor, anterior and lateral walls of the bony external auditory canal.
- **Squamous part:** This part continues between the occipital bone, parietal bone, and sphenoid, and articulates at its inferior surface with the head of the mandible.
- **Styloid process.**
- **Mastoid part:** In the Anglo-American literature the mastoid is considered to be a part of its own, while based on the terminology by the FCAT (Federative Committee on Anatomical Terminology) there are the petrous, the tympanic and the squamous part plus the styloid process.

Petrous Part of Temporal Bone

► Fig. 7.1, ► Fig. 7.2, ► Fig. 7.3, ► Fig. 7.4, ► Fig. 7.5, ► Fig. 7.6, ► Fig. 7.7a illustrate the structure of the petrous bone and the internal auditory canal. The **middle ear** is a sound conducting system, primarily consisting of the tympanic cavity with contained auditory ossicles and the tympanic membrane, and is bounded on all sides by parts of the temporal bone. The **inner ear** is a sound processing system and balancing organ and lies entirely within the petrous bone.

The pyramid-like part of the temporal bone extending into the interior of the skull is called its **petrous part** and is the hardest bone in the body. The lateral aspect of the petrous bone together with the squamous part of the temporal bone forms the **mastoid process**, which is pneumatized by the tympanic cavity and contains mastoid air cells. The apex of the petrous bone is directed anteromedially while its base is directed posterolaterally. As noted earlier, the superior border of the petrous bone forms an acute angle of 55° with the median plane and represents the boundary between the middle and posterior cranial fossae. The **apex of the petrous bone** lies anteromedial to the cochlea (see ► Fig. 7.1b). The lateral part of the petrous bone together with parts of the squamous form the roof of the tympanic cavity, the tegmen tympani. A prominent bony lamella forming the border between the petrous and squamous parts is the **Koerner's septum** (see ► Fig. 7.1d) and it is frequently well seen, traversing in the upper part of the tympanic cavity from posterolateral to anteromedial. A persistent petrosquamosus sinus is rarely visualized (1% of CT examinations) coursing along the border between the petrous and squamous parts.³⁰⁵ The inferior surface of the pyramid forms part of the outer base of the skull, floor of the tympanic cavity, and the bony part of the musculotubal canal. The **petro-occipital synchondrosis** (see ► Fig. 7.1a, ► Fig. 7.2a, and ► Fig. 7.2c) lies medially and fuses after the 16th year of life.³⁷⁶ The **foramen lacerum** lies anterior to this synchondrosis and medial to the carotid canal (see ► Fig. 7.1a), through which the greater and deeper petrosal nerves pass. The carotid canal begins in the center of the inferior surface of the pyramid and traverses anteromedially below the cochlea. The average distance between the carotid canal and the cochlea is a mere 1.2 m.⁶³⁶ The **jugular foramen** lies posterior to the carotid canal (see ► Fig. 3.24, ► Fig. 5.31, and ► Fig. 7.1a). Its posterior part transmits the sigmoid sinus, while its intermediate part transmits the IXth, Xth, and XIth cranial nerves and the posterior meningeal artery and its anterior part the inferior petrosal sinus. The sigmoid sinus continues as the jugular vein below the jugular foramen. The distinction between the carotid artery and the jugular vein is more difficult on coronal CT sections due to suboptimal delineation of largely soft tissue boundaries but is distinctly seen on the axial image by the small bony lamella in the apical section. The tympanic opening of the **auditory tube** lies anterior and lateral to the carotid canal (see ► Fig. 7.1a), while the tensor tympani lies immediately above it (see ► Fig. 7.1b). The auditory tube and the tensor tympani run together in the musculotubal canal (see ► Fig. 7.5).



- 1 Temporomandibular joint
- 2 Sphenosquamosal suture
- 3 Foramen ovale
- 4 Foramen spinosum
- 5 Temporal bone, tympanic part
- 6 Jugular foramen
- 7 Mastoid process
- 8 Carotid canal
- 9 Foramen lacerum
- 10 Petro-occipital synchondrosis
- 11 Hypotympanum
- 12 External acoustic meatus
- 13 Auditory tube, opening
- 14 Cochlea, basal turn
- 15 Facial nerve, mastoid part
- 16 Petro fissure (Glaserian fissure)
- 17 Tensor tympani
- 18 Mesotympanum
- 19 Handle of malleus
- 20 Promontory
- 21 Cochlea, apical turns
- 22 Apex of petrous part
- 23 Cochlear aqueduct
- 24 Malleus
- 25 Incus
- 26 Tendon of tensor tympani
- 27 Round window, fossa of round window
- 28 Temporal bone, petrous part
- 29 Stapes
- 30 Modiolus
- 31 Cochlear opening
- 32 Tympanic sinus
- 33 Pyramidal eminence with stapedius

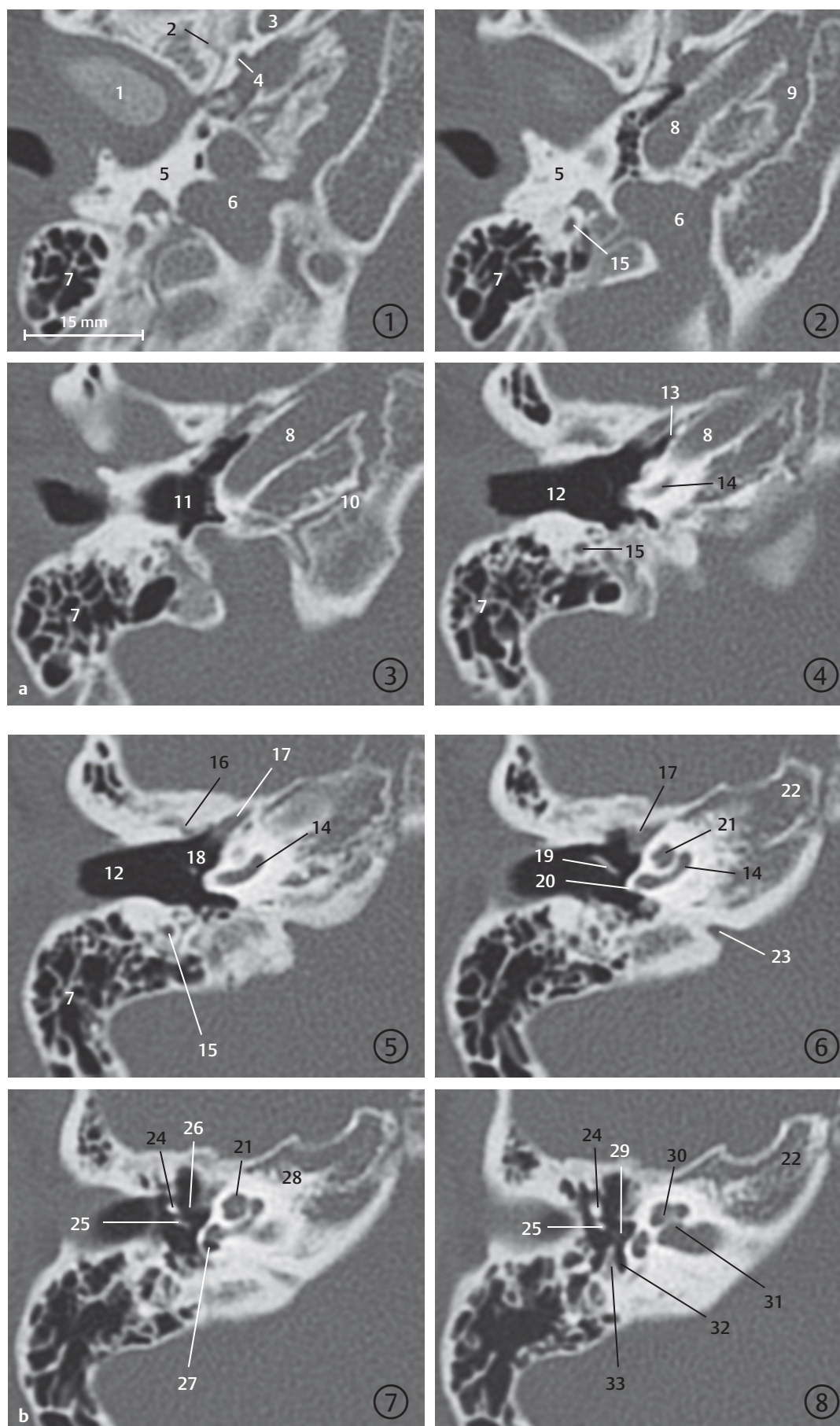
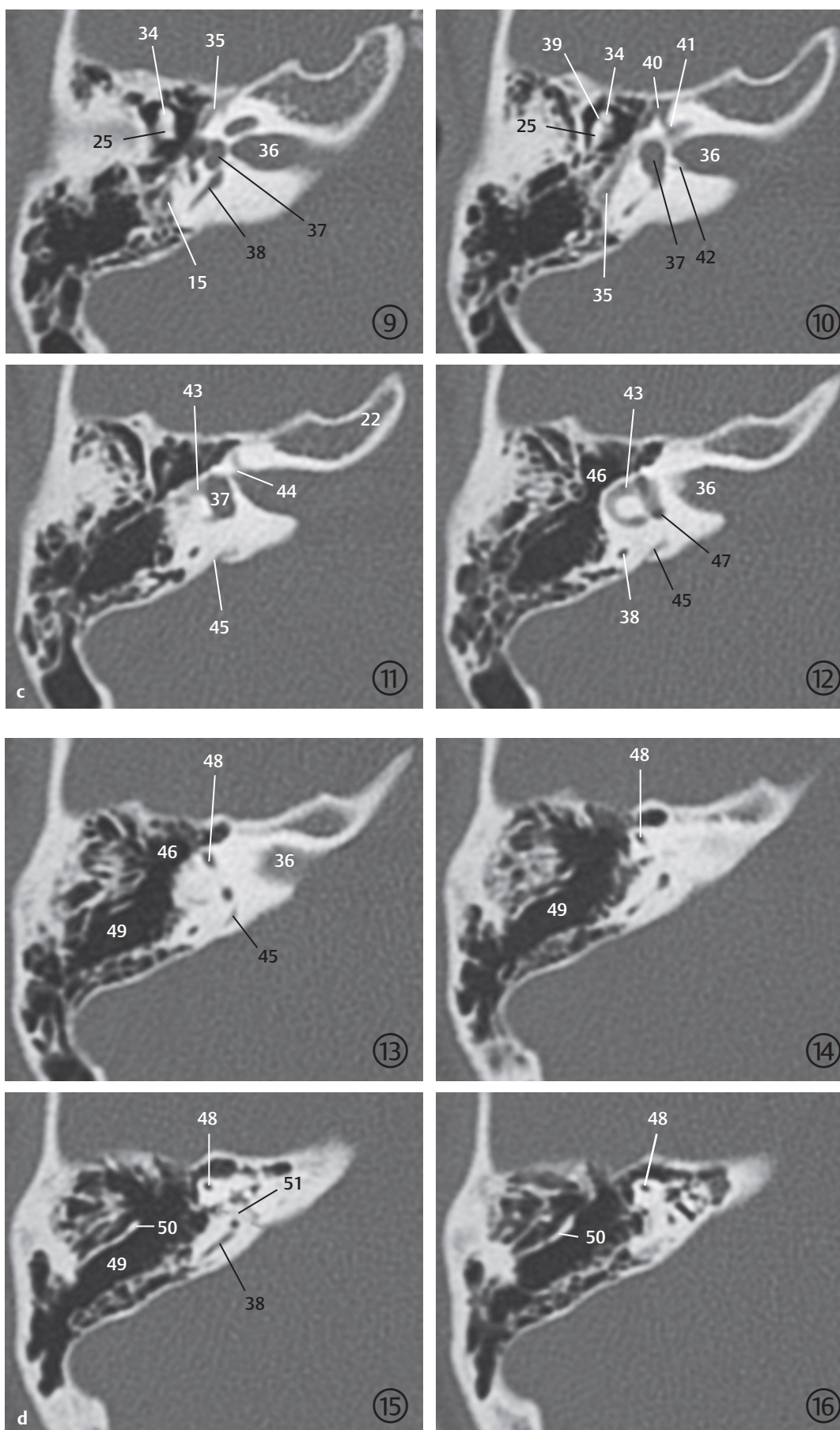


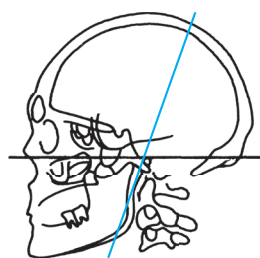
Fig. 7.1 Petrous part of the temporal bone in axial view. Transverse high-resolution CT images of relevant sections of the petrous part of the right temporal bone from inferior to superior (Viewed from below, slice thickness 0.625 mm). The encircled digit indicates the number of the slice in a series.

Fig. 7.1a 1st to 4th section.

Fig. 7.1b 5th to 8th section.



- 15 Facial nerve, mastoid part
- 22 Apex of petrous part
- 25 Incus
- 34 Head of malleus
- 35 Facial nerve, tympanic part
- 36 Internal acoustic meatus
- 37 Vestibule
- 38 Posterior semicircular canal
- 39 Incudomalleal joint
- 40 Geniculate ganglion
- 41 Facial nerve, labyrinthine part
- 42 Singular canal
- 43 Lateral semicircular canal
- 44 Vertical crest
- 45 Vestibular aqueduct
- 46 Epitympanum
- 47 Common bony limb (common limb of anterior and posterior semicircular canals)
- 48 Anterior semicircular canal
- 49 Mastoid antrum
- 50 Koerner's septum
- 51 Subarcuate canal



- 1 Temporomandibular joint
- 2 Geniculate ganglion
- 3 Tensor tympani
- 4 Carotid canal
- 5 Occipital bone
- 6 Head of malleus
- 7 Facial nerve, labyrinthine part
- 8 Facial nerve, tympanic part
- 9 Incudomalleal joint
- 10 Cochlea, basal turn
- 11 Cochlea, apical turns
- 12 Petro-occipital synchondrosis
- 13 Tendon of tensor tympani
- 14 Scutum
- 15 Epitympanum
- 16 External acoustic meatus
- 17 Incus
- 18 Anterior semicircular canal
- 19 Cochlear opening
- 20 Internal acoustic meatus
- 21 Hypotympanum
- 22 Tympanic annulus
- 23 Lateral semicircular canal
- 24 Vestibule
- 25 Promontory
- 26 Stapes
- 27 Mesotympanum
- 28 Temporal bone, tympanic part
- 29 Oval window with footplate of the stapes
- 30 Vestibulocochlear duct

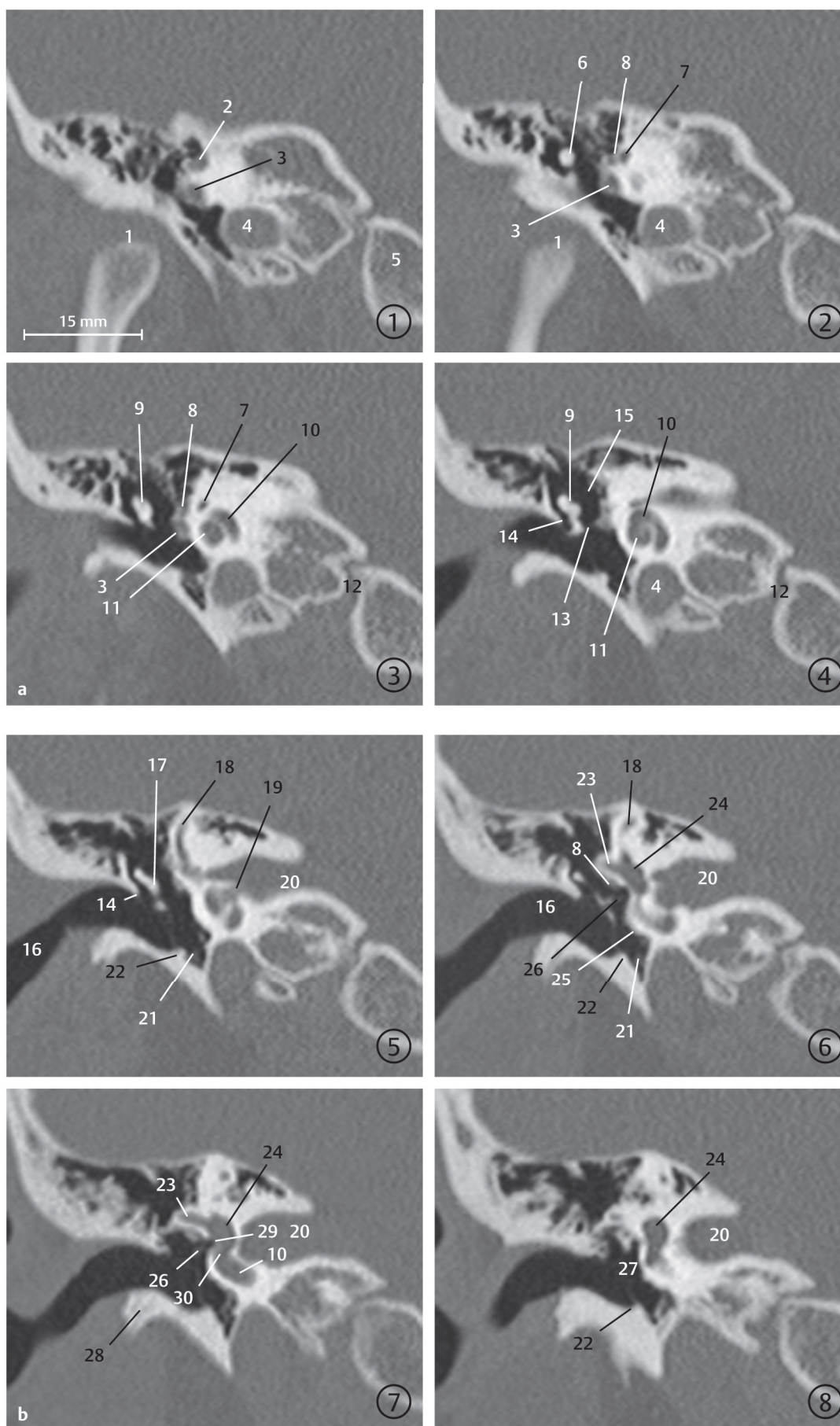


Fig. 7.2 Petrous part of the temporal bone in coronal view. Coronal high-resolution CT images of relevant sections of the petrous part of the right temporal bone from anterior to posterior (slice thickness 0.625 mm). The encircled digit indicates the number of the slice in a series.

Fig. 7.2a 1st to 4th section.

Fig. 7.2b 5th to 8th section.

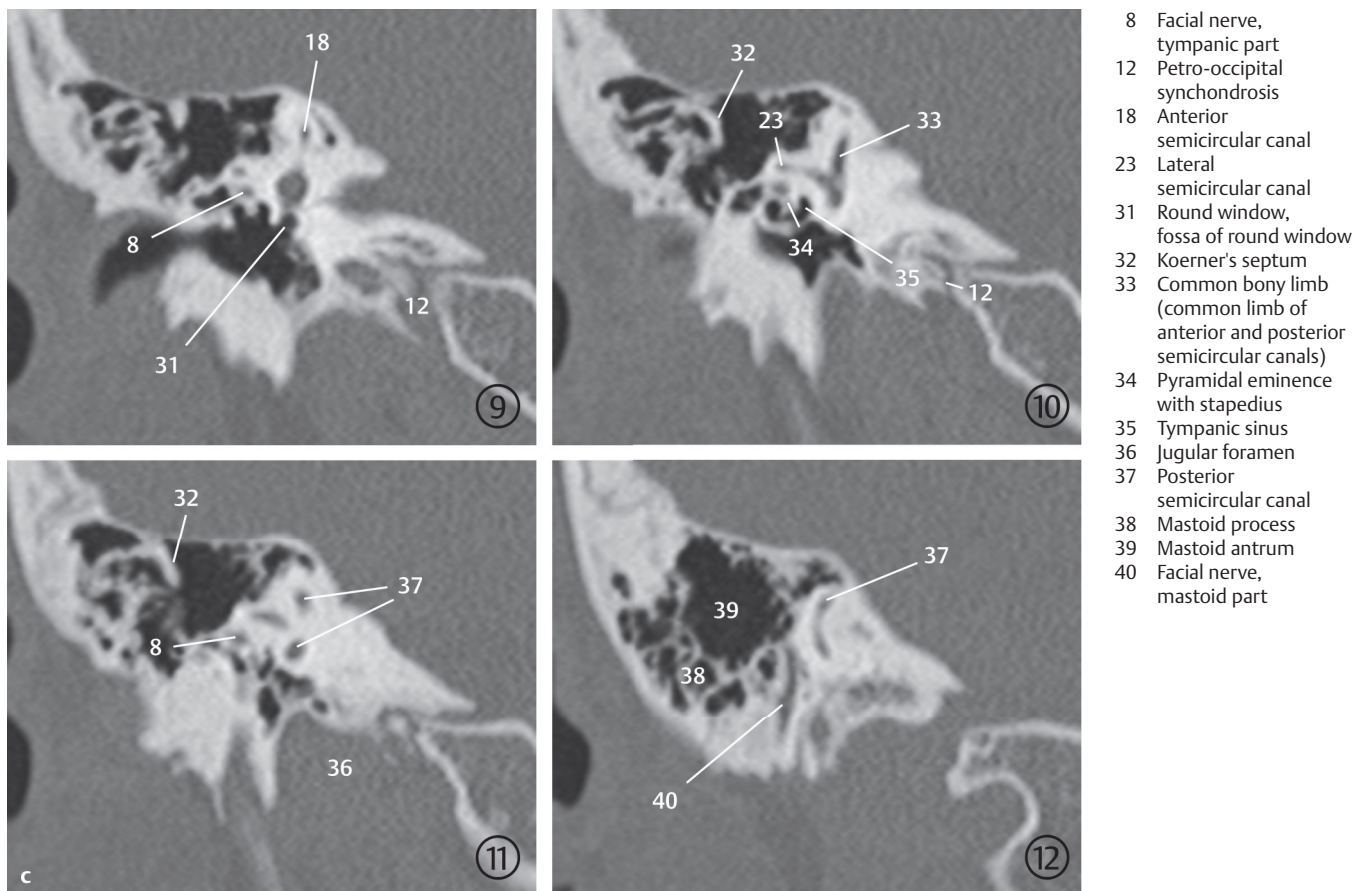
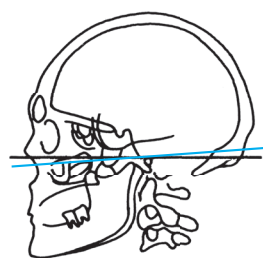


Fig. 7.2c 9th to 12th section.

The **squamous part** of the temporal bone forms part of the lateral wall of the skull, providing insertion for the temporalis. The zygomatic process arises anterolaterally with the masseter inserting on its inner surface. The squamous part is related anteromedially to the sphenoid, both of which form the floor of the middle cranial fossa. The sphenosquamous suture forms the boundary between the two bones (see ►Fig. 7.1a). Corresponding inferior slices with sections through the middle cranial fossa also depict the **foramen ovale** (see ►Fig. 7.1a and ►Fig. 5.37), which transmits the mandibular branch of the trigeminal nerve and the venous plexus of the foramen ovale. The foramen the spinosum lies somewhat posterior and lateral to the above (see ►Fig. 5.37 and ►Fig. 7.1a), often remaining partially ossified, and contains the middle meningeal artery and the meningeal branch of the mandibular nerve (third division of the Vth cranial nerve). Anteroinferiorly the squamous part forms the roof of the temporomandibular joint and thereby the socket for the mandibular condyle (see ►Fig. 4.13 and ►Fig. 7.1a), posterior to which the tympanic part (see ►Fig. 4.12 and ►Fig. 7.1a) forms the posterior wall of the temporomandibular joint. The petrotympanic fissure (**Glaserian fissure**) lies at the posteromedial

boundary of the temporomandibular joint and enters the mandibular fossa (see ►Fig. 7.1b) with the chorda tympani and the anterior tympanic artery coursing through it. Merging with the tympanic part, the squamous part forms the roof of the external auditory canal together with the lateral aspect of the tegmen tympani. The squamous and petrous parts form the mastoid posteriorly, which first develops in childhood.

The incomplete ring-like structure formed by the tympanic part of the temporal bone, which encloses the floor, anterior and lateral aspects of the **external auditory canal**, closes inferiorly at about the age of 7 months. The external auditory canal is thus the sole component of the hearing and vestibular apparatus which completes its bony development only after birth. The bony part of the external auditory canal is about 16 mm long and continues laterally as its cartilaginous part. The external acoustic canal is separated from the tympanum at its medial end by the **tympanic membrane**. The caudal insertion of the tympanic membrane is identified on the coronal image by the tympanic annulus (see ►Fig. 7.2b). The uppermost part of the membrane is the pars flaccida which lies directly below the scutum (see ►Fig. 7.2a and ►Fig. 7.2b), a spur which marks the medial boundary of the external auditory canal.



- 1 Osseous spiral lamina
- 2 Cochlea, basal turn
- 3 Scala vestibuli
- 4 Scala tympani
- 5 Round window, fossa of round window
- 6 Posterior semicircular canal
- 7 Cerebellum
- 8 Cochlea, apical turns
- 9 Vestibule
- 10 Lateral semicircular canal
- 11 Internal acoustic canal
- 12 Singular canal
- 13 Modiolus
- 14 Cochlear opening
- 15 Cochlear nerve
- 16 Vestibular nerve
- 17 Vestibulocochlear nerve
- 18 Vestibular aqueduct

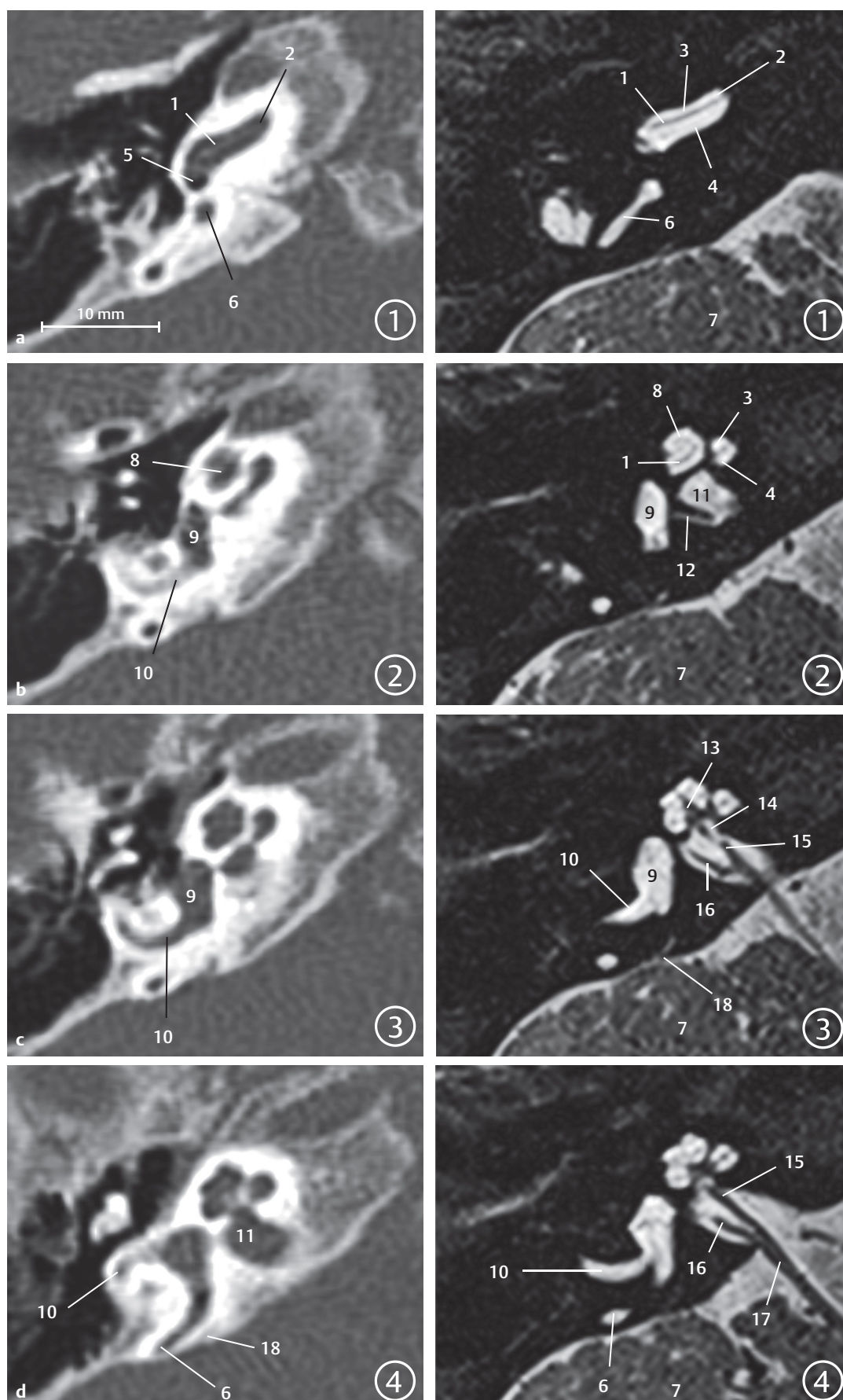


Fig. 7.3 Petrous part of temporal bone in CT and MRI. A comparative view of axial CT and MRI images of the right petrous bone from inferior to superior. The encircled digit indicates the number of the slice in a series. The images were obtained from a diagnostic examination of a 1-year-old child (slice thickness CT 0.625 mm, MR 0.4 mm).

Fig. 7.3a 1st CT (left) and MRI section (right).

Fig. 7.3b 2nd CT (left) and MR section (right).

Fig. 7.3c 3rd CT (left) and MR section (right).

Fig. 7.3d 4th CT (left) and MR section (right).

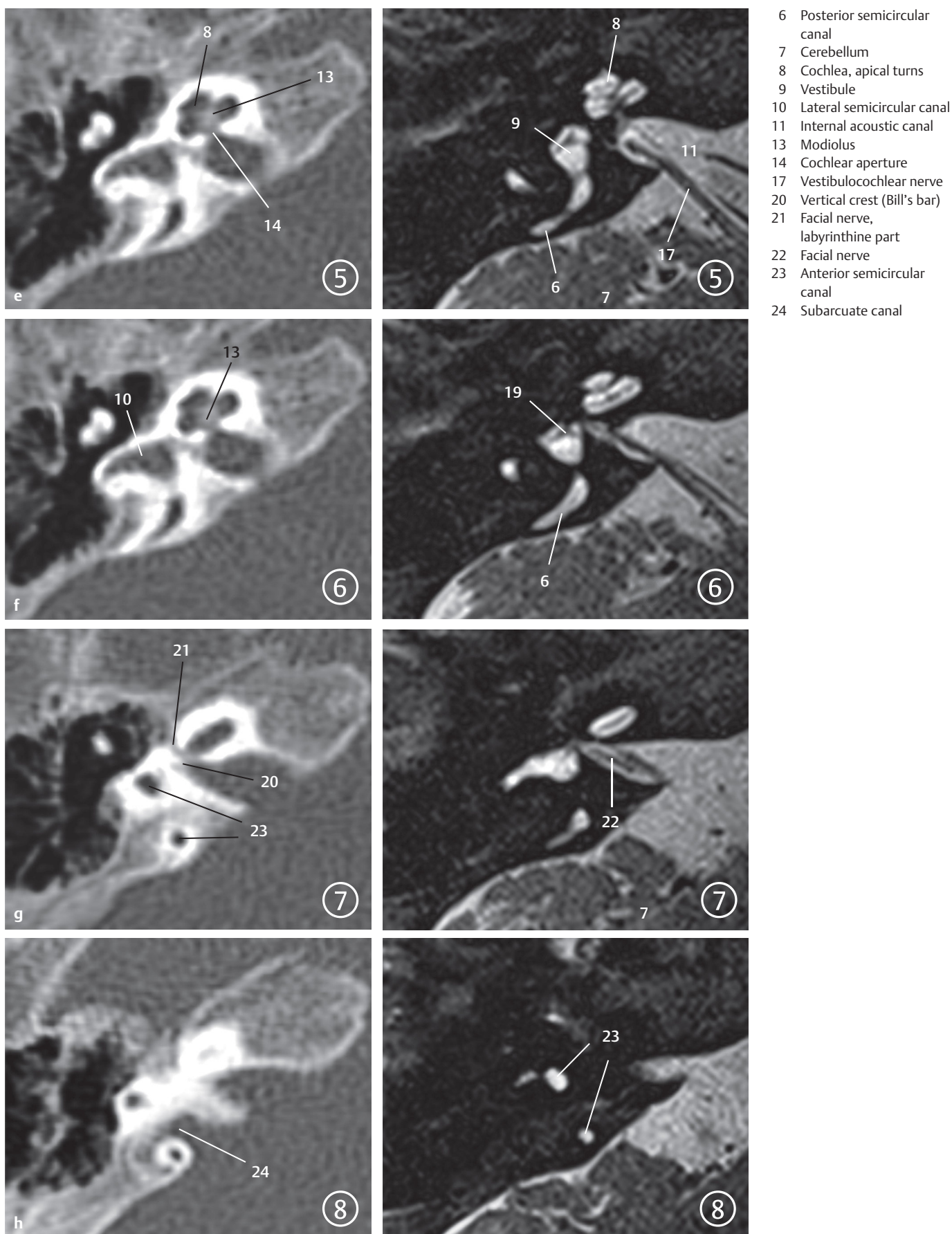


Fig. 7.3e 5th CT (left) and MR section (right).

Fig. 7.3f 6th CT (left) and MR section (right).

Fig. 7.3g 7th CT (left) and MR section (right).

Fig. 7.3h 8th CT (left) and MR section (right).

- 1 Facial nerve
- 2 Vestibular nerve, superior part
- 3 Cochlear nerve
- 4 Vestibular nerve, inferior part
- 5 Posterior ampullary nerve from the inferior vestibular nerve
- 6 Cochlea, basal turn
- 7 Transverse crest

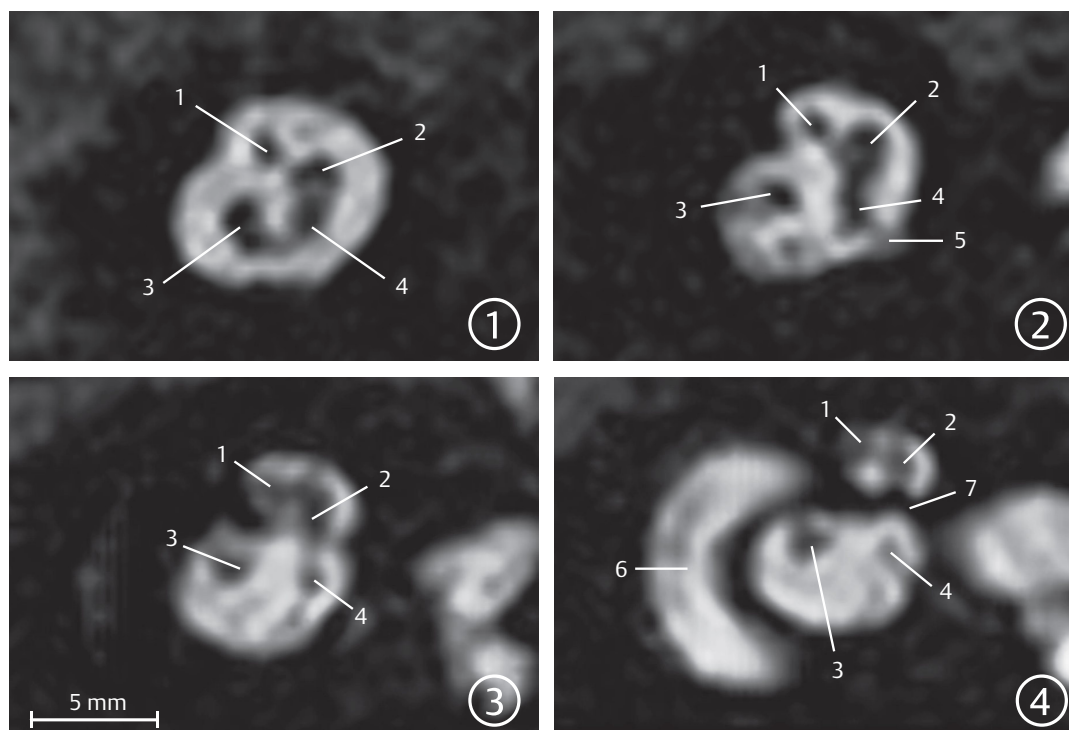


Fig. 7.4 Internal auditory canal. View of parasagittal reconstructions of the inner auditory canal from medial to lateral (perpendicular to the auditory canal), based on high-resolution MRI (T2w 3D sequence with variable flip angle and isotropic 0.4 mm voxels). The encircled digit indicates the number of the slice in a series.

Middle Ear

The middle ear is a space enclosed on all sides by the temporal bone and contains the auditory ossicular chain, which transmits sound waves to the fluid-filled space of the inner ear. The **tympanic cavity** is divided into the following compartments: epitympanum (see ►Fig. 7.1d and ►Fig. 7.2a), mesotympanum (see ►Fig. 7.2b), and hypotympanum (see ►Fig. 7.2b); the mastoid antrum (see ►Fig. 7.1d) characterizes the so-called atrium of mastoid cells. The mesotympanum represents a space lying medial to the tympanic membrane, with the epitympanum lying above it and the hypotympanum lying below. The lateral border of the tympanum is formed by the tympanic membrane and the tympanic and squamous parts of the temporal bone surrounding it. The **auditory ossicular chain** lies within the tympanic cavity and is composed of the **malleus, incus, and stapes** from lateral to medial (see ►Fig. 7.5). The handle of the malleus (see ►Fig. 7.1b) is inserted into the tympanic membrane and extends supero-anteriorly from somewhat below its center. Two thin folds, also called anterior and posterior malleolar folds of the tympanic membrane on either side of the malleolar handle, create a lax zone referred to as “pars flaccida”. It ends immediately below the scutum which is well seen on coronal CT. The rest of the ear drum is tightly stretched and is called the “pars tensa”. The so-called Prussak space lies between the pars flaccida and the neck of the malleus. The incudomalleolar joint is identified in the axial image typically as an “ice cream cone”, its anterior aspect

being formed by the head of the malleus and its posterior part by the body of the incus. The long process of the incus extends to the stapes in inferior sections (see ►Fig. 7.1b), articulating with head of the stapes to form the incudostapedial joint. The crura of the stapes are usually hardly defined, while the footplate of the stapes covers the oval window (see ►Fig. 7.2b). The tensor tympani (see ►Fig. 7.1b and ►Fig. 7.2a) lies anteromedially above the auditory tube and extends posteriorly over a bony protrusion, the processus cochleariformis. The tendon of the tensor tympani (see ►Fig. 7.1b, ►Fig. 7.2a, and ►Fig. 7.5) extends laterally to the head of malleus as a thin structure just anterior to the oval window. The stapedius arises within the pyramidal eminence (see ►Fig. 7.1b and ►Fig. 7.5). Its tendon extends anteriorly to the head of the stapes but is only inconsistently seen. The constant indentation of the sinus tympani (see ►Fig. 7.1b) is seen medial to the **pyramidal eminence**.

Clinical Notes

Cholesteatomas of the ear are distinguished by their site of localization in the pars flaccida and the pars tensa. Early stage cholesteatomas of the pars flaccida are seen in Prussak's space between the scutum and the ossicles, while those of the pars tensa are found initially in the region of the tympanic sinus, facial recess, and mastoid.

►Fig. 7.6 illustrates the arterial supply of the tympanum and mastoid.

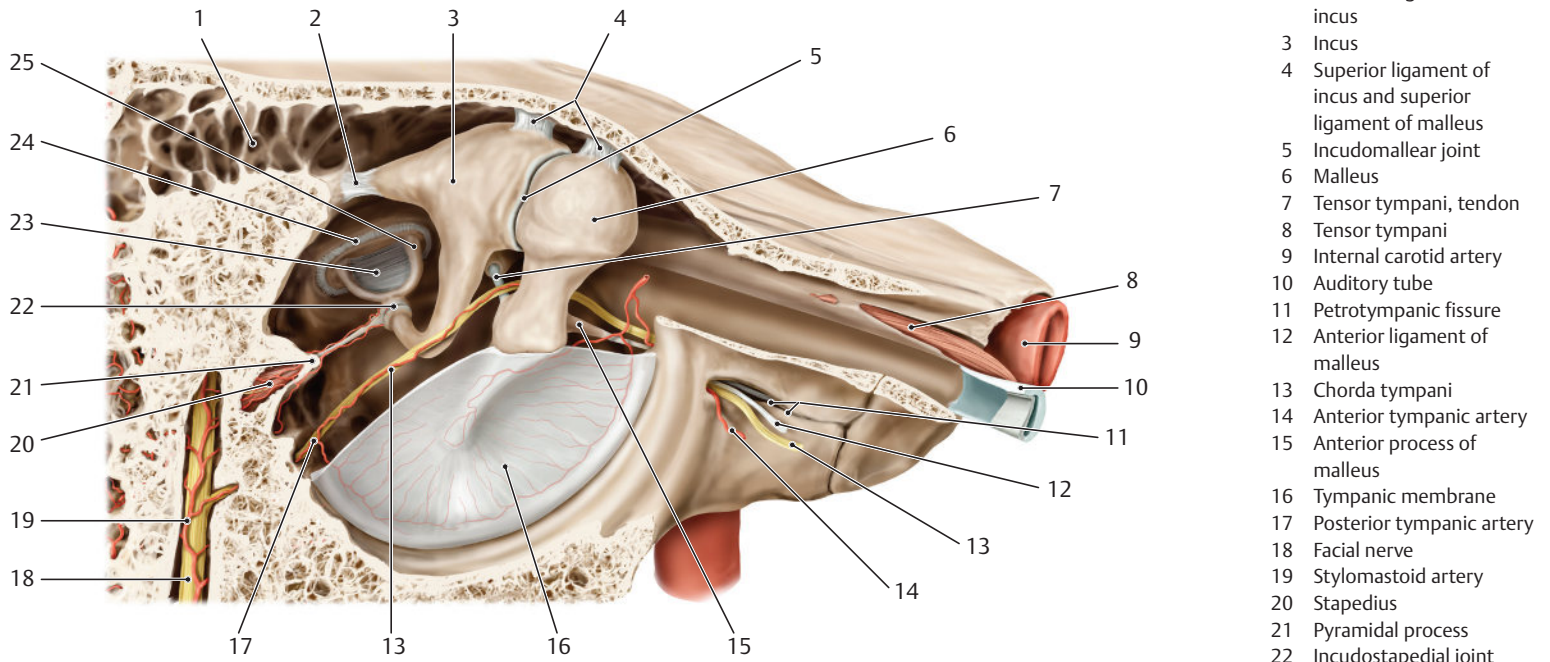


Fig. 7.5 Auditory ossicles. Spatial representation of the joints, ligaments and muscles of the auditory ossicles and adjacent nerves. Lateral view of the ear. (Reproduced from Schuenke, Schulte, and Schumacher, *Atlas of Anatomy*, 2nd edition, ©2009, Thieme Publishers, Stuttgart. Illustration by Karl Wesker/Markus Voll.⁵³⁵)

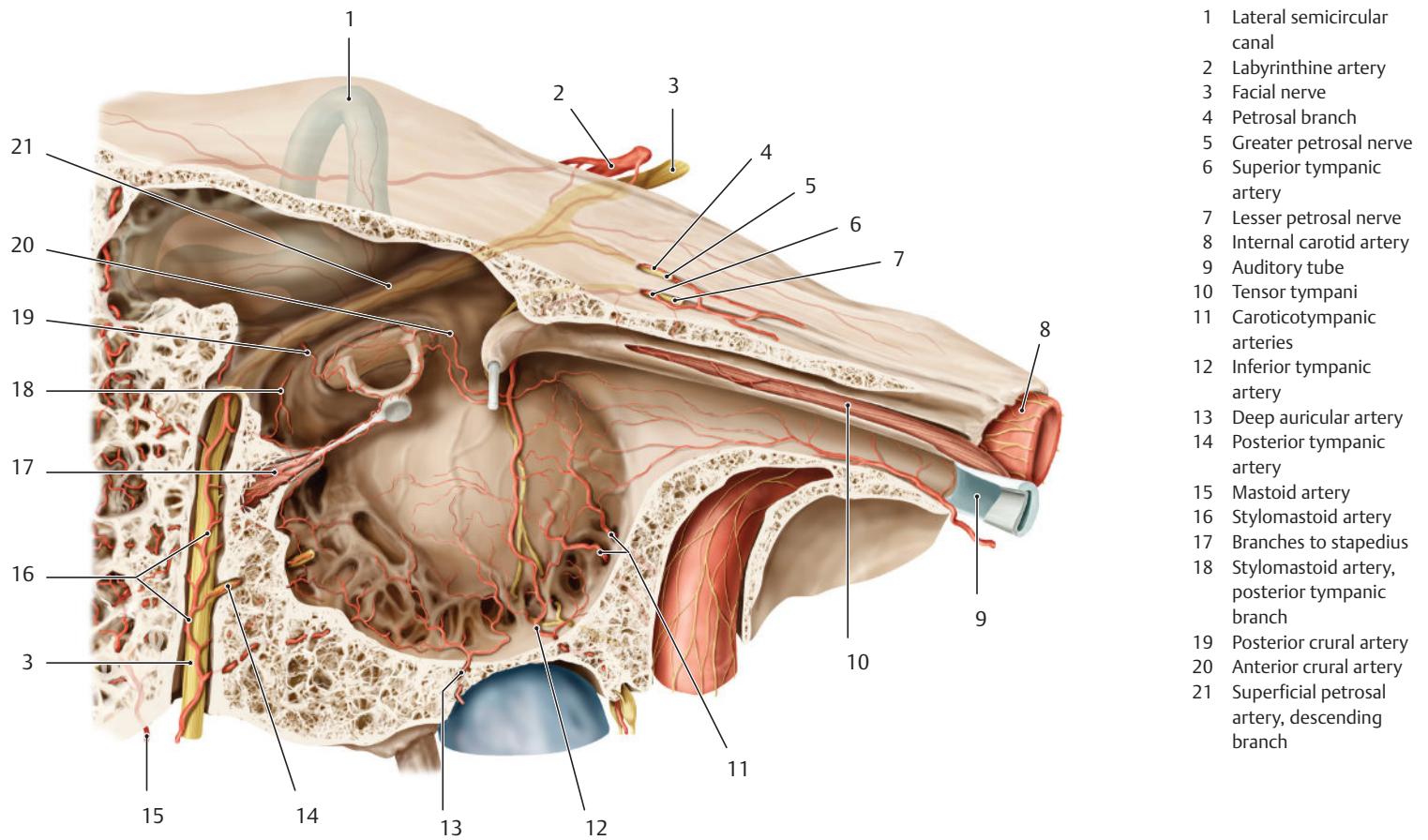


Fig. 7.6 Tympanic cavity and mastoid. Illustration of vascular supply. View from lateral. The malleus, incus and parts of the chorda tympani are not visualized. (Reproduced from Schuenke, Schulte, and Schumacher, *Atlas of Anatomy*, 2nd edition, ©2009, Thieme Publishers, Stuttgart. Illustration by Karl Wesker/Markus Voll.⁵³⁵)

The facial nerve is an important landmark and runs through the petrous part of the temporal bone and the tympanum. It exits the brainstem laterally at the level of the pontomedullary junction and passes through the cerebellopontine angle into the internal auditory canal, which it exits at its lateral end, coursing superiorly over the cochlea in an anterior direction. Its course within the bony canal is called its “labyrinthine segment” (see ►Fig. 7.1c). The nerve then enters the geniculate ganglion in an anterior direction (see ►Fig. 7.1c), where it gives rise to the greater petrosal nerve, with a concurrent change in direction posteriorly thereby forming a bend called the **geniculum of the facial nerve**. The adjoining tympanic segment (see ►Fig. 7.1c and ►Fig. 7.2) runs along the medial wall of the tympanum above the oval window and below the lateral semicircular canal. A second change in direction occurs at the level of the sinus tympani at the **second genu**, beyond which the nerve courses inferiorly into the mastoid (see ►Fig. 7.1a, ►Fig. 7.1b, and ►Fig. 7.1c). It exits the base of the skull through the **stylomastoid foramen** (see ►Fig. 5.37b). The facial nerve gives off the chorda tympani within the mastoid, which runs backward superiorly and anteriorly through the tympanum, exiting it at the anterior wall through the petrotympanic fissure (see ►Fig. 7.1b and ►Fig. 7.5).

Inner Ear

Functional components of the inner ear include the organs of balance and hearing. The cochlea is the organ of hearing while the organs of balance consist of the utricle, saccule, and the semicircular canals. The three semicircular canals determine directional balance in space, while horizontal and vertical acceleration are perceived by the utricle and the saccule, respectively. The utricle and saccule lie together in the central vestibule, from which both the semicircular canals as well as the vestibulocochlear duct arise (see ►Fig. 7.2b). All parts of the inner ear are enclosed in the bony labyrinth. The membranous labyrinth, filled with endolymph, is contained within. The space between membranous and bony labyrinths contains perilymph. Phylogenetically, the semicircular canals and the utricle are older than the cochlea and the saccule.

Clinical Notes

A serious malformation may involve the entire phylogenetically older part of the inner ear. An example is the CHARGE syndrome, a genetic defect that is associated with choanal atresia, cardiac malformations, colobomas of the eye, malformations of the genitourinary system, and ear deformities.

The bony labyrinth can generally be well evaluated on CT with optimal visualization of dense bony structures as well as identification of finer structures like the modiolus. Fluid-filled spaces such as peri- and endolymph are better seen on MRI. This diagnostic modality is also well suited for imaging the vestibulocochlear and facial nerves which appear as dark lines in the fluid-filled internal acoustic canal (see ►Fig. 7.4).

From inferior to superior, the basal turn of the **cochlea** is the first structure of the inner ear to be visualized on temporal bone CT (see ►Fig. 7.1a, also see ►Fig. 7.7a), below which the internal carotid artery and the carotid canal are identified (see ►Fig. 7.1a). The **osseous spiral lamina** is delineated as a line within the basal turn on MRI and CT (see ►Fig. 7.3a and ►Fig. 7.3b), dividing the cochlea into a superior scala vestibuli (see ►Fig. 7.3a and ►Fig. 7.3b) and an inferior scala tympani (see ►Fig. 7.3a and ►Fig. 7.3b). The scala media with the organ of Corti can usually not be identified using the current standard resolution. The bony prominence produced by the basal turn on the medial wall of the tympanum is called the **promontory** (see ►Fig. 7.1b). The fossa of the round window (see ►Fig. 7.1b and ►Fig. 7.7a) appears as a black, air-filled space at the posterolateral end of the basal turn, immediately proximal to its transition to the vestibule. The oval window may be seen in transverse sections in the same or adjoining slices as the stapes (see ►Fig. 7.1b and ►Fig. 7.7a), but is often better visualized in the coronal image (see ►Fig. 7.2b). Centered within the cochlea is a delicate, crown-shaped structure, the **modiolus** (see ►Fig. 7.1b and ►Fig. 7.7a), which is also well seen on MRI (see ►Fig. 7.3c). The boundary of the modiolus to the internal auditory canal forms the cochlear area, which transmits fibers of the cochlear nerve (see ►Fig. 7.3c and ►Fig. 7.3d). The opening of the **internal auditory canal** into the cochlea which leads the nerves into the cochlea is termed the **cochlear aperture** (see ►Fig. 7.1b and ►Fig. 7.2b). The facial and vestibulocochlear nerves pass into the internal auditory canal from the brainstem through the cerebellopontine angle (see ►Fig. 7.1c and ►Fig. 7.3e). The vestibulocochlear nerve (see ►Fig. 7.3e), lying somewhat postero-inferior to the facial nerve, divides within the acoustic canal into its superior and inferior divisions and the cochlear nerve. The facial nerve is the one running most superiorly above the cochlea and anteriorly to the vertical crest (Bill's bar) in its bony canal (see ►Fig. 7.1c) toward the geniculate ganglion (see ►Fig. 7.1c). Another narrow canal, the singular canal (see ►Fig. 7.1c and ►Fig. 7.3b), extends from the postero-inferior aspect of the internal auditory canal to the vestibule, and transmits the posterior ampullary nerve (see ►Fig. 7.4) which arises from the inferior division. The rest of the branches from the superior and inferior divisions enter the vestibule somewhat further distally through the superior or inferior vestibular areas.

The **vestibule** (see ►Fig. 7.1c) is seen as an oval structure in axial sections from which semicircular canals arise at different levels. The lateral semicircular canal is thus nearly completely visualized in ►Fig. 7.1c and ►Fig. 7.7a. The anterior and posterior semicircular canals have a common origin from the posteromedial region of the vestibule, the common bony limb (see ►Fig. 7.1c and ►Fig. 7.7a). A vascular channel, the subarcuate canal, is seen coursing through the two limbs in the uppermost sections proximal to the union of the anterior semicircular canal. Relatively wide in young children (see ►Fig. 7.3h), it is seen as a thinner canal in later life (see ►Fig. 7.1d). The vestibular aqueduct arises

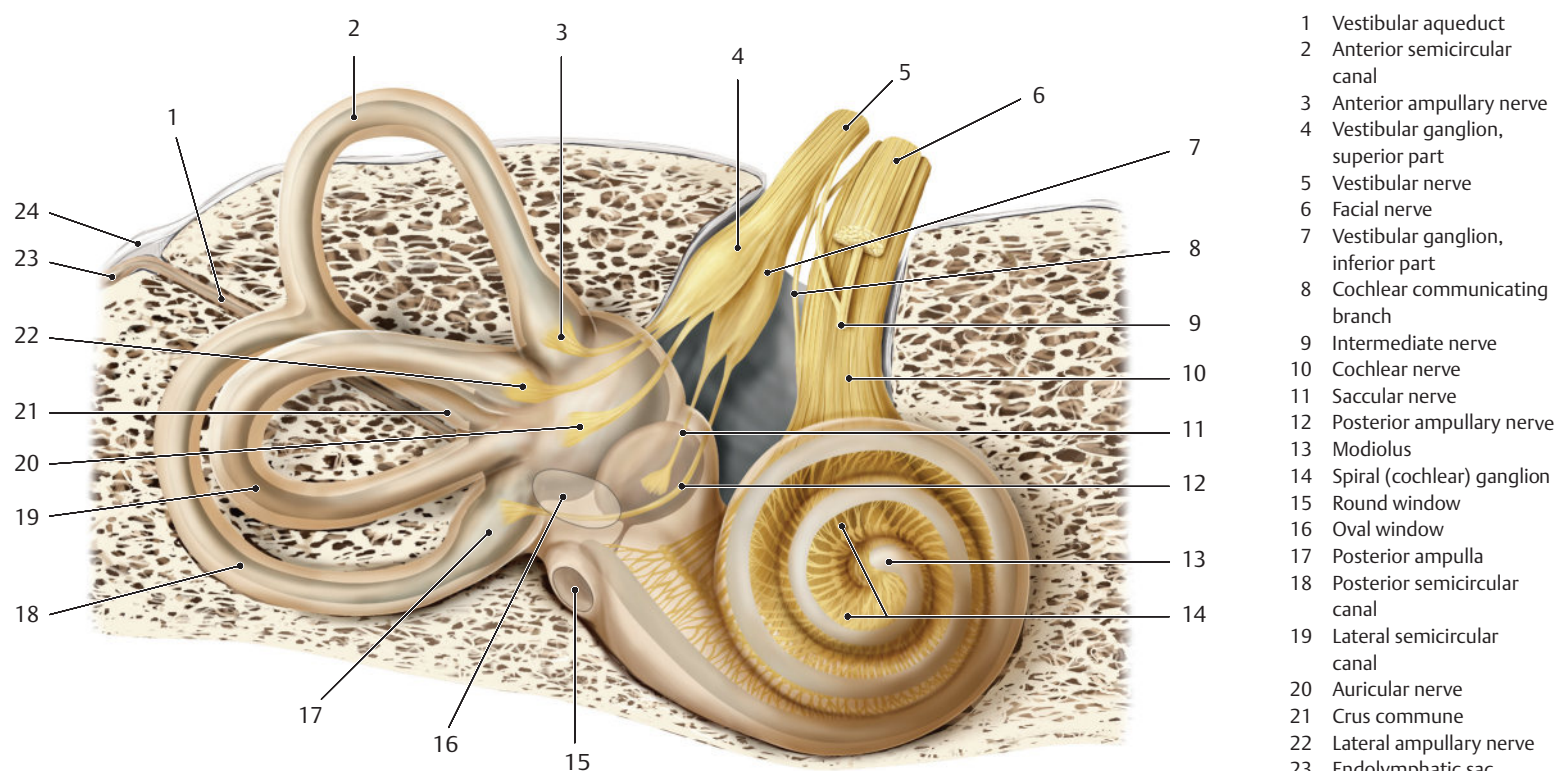


Fig. 7.7a Cochlea. Structure and innervation. (Reproduced from Schuenke, Schulte, and Schumacher, *Atlas of Anatomy*, 2nd edition, ©2009, Thieme Publishers, Stuttgart. Illustration by Karl Wesker/Markus Voll.⁵³⁵)

from the medial margin of the vestibule and opens at the posteromedial edge of the petrous part of the temporal bone. Its normal width at the aperture should be no more than the diameter of the posterior semicircular canal or 2 mm. It is often only just visible (see ► Fig. 7.1c, ► Fig. 7.1d, and ► Fig. 7.7a).

Clinical Notes

The promontory test involves placing a needle on the promontory by piercing the ear drum. The subsequent application of electrical current stimulates neural structures within the cochlea, especially in its basal turn which lies directly below the promontory. This may induce the perception of hearing in deaf patients if central auditory pathways are intact. A soft tissue lesion in the middle ear in the region of the promontory exhibiting contrast enhancement on MRI may represent a tumor of the glomerula placed in the tympanon, most commonly a tympanic paraganglioma/glomus tumor.

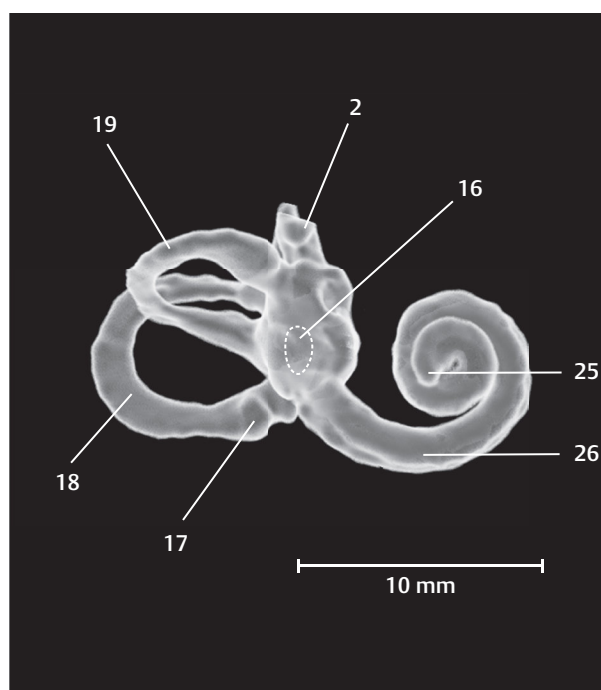


Fig. 7.7b Cochlear 3D representation. VRT using data from a high-resolution T2w 3D data set.

7.1.4 Frontal Bone

The **frontal bone** encloses the cranial cavity anteriorly, forms the greater part of the roof of orbit and abuts the upper aspect of the nasal cavity. It is divided into three parts:

- Squamous part
- Two orbital parts
- Nasal part

The squamous part is connected with the parietal bone at the coronal suture, and with the greater wing of the sphenoid at the sphenofrontal suture. The roofs of orbit, which bulge into the cranial cavity, are formed by the orbital parts, the medial margins of which abut the cribriform plate of the ethmoid bone. The unpaired nasal part connects the two orbital parts of the frontal bone.

7.1.5 Parietal Bone

The paired **parietal bones** are interposed between the occipital and frontal bones and form a large part of the roof and the side walls of the cranial vault (see ►Fig. 3.1b, ►Fig. 3.8c, ►Fig. 3.22, ►Fig. 4.2c, ►Fig. 4.8, and ►Fig. 5.1b). Each parietal bone has four borders:

- **Superior border:** forms the sagittal suture in the median plane together with the contralateral parietal bone (see ►Fig. 5.30a).
- **Anterior border:** articulates with the frontal bone at the coronal suture (see ►Fig. 4.2c, ►Fig. 4.5c, ►Fig. 4.7c, ►Fig. 5.9a, and ►Fig. 5.28a).
- **Posterior border:** articulates with the occipital bone at the lambdoid suture (see ►Fig. 4.2c, ►Fig. 4.3c, ►Fig. 4.8, ►Fig. 4.9, and ►Fig. 5.26a).
- **Inferior border:** forms the squamous suture with the squamous part of the temporal bone and the sphenoparietal suture with the greater wing of the sphenoid.

7.2 Cranial Cavity

The cranial cavity (see ►Fig. 3.2, ►Fig. 3.3, ►Fig. 3.4, ►Fig. 3.5, ►Fig. 3.6, ►Fig. 3.7, ►Fig. 3.8, ►Fig. 3.9, ►Fig. 3.10, ►Fig. 3.11, ►Fig. 3.12, ►Fig. 3.13, ►Fig. 3.14, and ►Fig. 3.15, ►Fig. 4.2, ►Fig. 4.3, ►Fig. 4.4, ►Fig. 4.5, 6, and ►Fig. 4.7, ►Fig. 5.2, ►Fig. 5.3, ►Fig. 5.4, ►Fig. 5.5, ►Fig. 5.6, ►Fig. 5.7, ►Fig. 5.8, ►Fig. 5.9, ►Fig. 5.10, ►Fig. 5.11, ►Fig. 5.12, ►Fig. 5.13, ►Fig. 5.14, and ►Fig. 5.15, ►Fig. 5.17, ►Fig. 5.18, ►Fig. 5.19, ►Fig. 5.20, ►Fig. 5.21, ►Fig. 5.22, ►Fig. 5.23, ►Fig. 5.24, ►Fig. 5.25, ►Fig. 5.26, ►Fig. 5.27, ►Fig. 5.28, ►Fig. 5.29, and ►Fig. 5.30) measures on an average 1,550 mL in volume in men and 1,425 mL in women, and is enclosed by a rigid capsule, within which the brain with its nerves and vessels is suspended in cerebrospinal fluid. Rigid dural septae divide the cranial cavity into compartments.

7.2.1 Infratentorial Region

The **tentorium of cerebellum** (see ►Fig. 3.11a, ►Fig. 3.13a, ►Fig. 4.2a, ►Fig. 5.6a, ►Fig. 5.7a, and ►Fig. 5.22b), a flat tent like structure, divides the cranial cavity into supra-

and infratentorial regions. The ambient cistern lies in the vicinity of the **tentorial incisure**, a notch in the tentorium of cerebellum through which the brainstem passes at the level of the midbrain. The second large opening of the infratentorial region is the **foramen magnum** (see ►Fig. 3.1b, ►Fig. 3.12c, ►Fig. 3.25, ►Fig. 4.8, and ►Fig. 5.17a). Varying in shape from oval to almost circular, it usually appears to be composed of variably sized crescents, its area averaging 8 cm² and ranging from 5 to 10 cm². Severe cerebral edema displaces the brainstem and cerebellum caudally, possibly causing the development of a pressure cone at the inferior aspect of the cerebellum.

7.2.2 Supratentorial Region

The **falx cerebri** partitions the supratentorial region partially (see ►Fig. 3.2a, ►Fig. 3.8a, ►Fig. 3.15a, ►Fig. 5.8a, ►Fig. 5.9a, and ►Fig. 5.13a). The adjoining structures of the cerebrum are cushioned by CSF within interhemispheric and pericallosal cisterns. The subdivision of the cranial cavity into separate compartments by sheets of dura determines the possibility and direction of mass displacement of cerebral structures due to intracranial space-occupying lesions. Increasing supratentorial volume may give rise to the midbrain syndrome by **compression of the midbrain** against the tentorial notch. Furthermore, the falx may be deflected to the contralateral side by a space-occupying lesion in one cerebral hemisphere. Precise knowledge of these changes is essential for diagnosis and surgery. The anatomy of cerebral venous sinuses coursing through the falx and tentorium must be kept in mind while planning surgical procedures. For further information see Section 7.4 and Section 7.5.

The topography of the cranial cavity is well demonstrated on coronal sections which clearly depict the overlying calvarium and the base of the skull (see ►Fig. 3.2, ►Fig. 3.3, ►Fig. 3.4, ►Fig. 3.5, ►Fig. 3.6, ►Fig. 3.7, ►Fig. 3.8, ►Fig. 3.9, ►Fig. 3.10, ►Fig. 3.11, ►Fig. 3.12, ►Fig. 3.13, ►Fig. 3.14, and ►Fig. 3.15). The structures of the supra- and infratentorial regions are especially well separated from each other on sagittal sections (see ►Fig. 4.2, ►Fig. 4.3, ►Fig. 4.4, ►Fig. 4.5, ►Fig. 4.6, and ►Fig. 4.7).

Osseous cross-sectional anatomy appears complicated in the region of the craniocervical junction and base of skull in parallel supraorbito-suboccipital sections, less so in the region of the cranial vault. The **calvarium** appears like a more or less oval bony ring in cross-section depending on the shape of the head (see ►Fig. 5.22, ►Fig. 5.23, ►Fig. 5.24, ►Fig. 5.25, ►Fig. 5.26, ►Fig. 5.27, ►Fig. 5.28, ►Fig. 5.29, and ►Fig. 5.30).

Slices through the craniocervical junction exhibit great variability in sections of the **upper cervical vertebrae** or their intervertebral spaces (see ►Fig. 5.2). The atlas is identified by its anterior and posterior arches, an absent vertebral body, and laterally positioned transverse foramina for the vertebral arteries, as seen on coronal CT reformations of the craniocervical junction (see ►Fig. 3.22). The axis is identified by a tooth-like structure, the dens.

The supraorbito-suboccipital plane sections the foramen magnum obliquely in ►Fig. 5.17a, such that the slice passes through the basal part of the occipital bone anteriorly while the posterior aspect of the slice lies immediately inferior to the foramen magnum.

7.2.3 Cranial Fossae

The topography of the posterior, middle, and anterior cranial fossae is best illustrated on the skull itself as spatial relationships are easily understood through a “hands-on” examination. Illustrations of the inner aspect of the base of skull in anatomic atlases may give the impression that the cranial fossae lie in the same horizontal plane. In reality, however, the three **cranial fossae** are arranged as **three terraces**, each set about 2.5 cm above or below the other.³³³ The floor of the middle cranial fossa lies approximately along Reid’s base line (see ►Fig. 5.16a).¹⁷⁹ The floor of the posterior cranial fossa lies about 2.5 cm lower and that of the anterior cranial fossa 2.5 cm higher than **Reid’s base line**. The sagittal series oriented in the coordinate system shows the topographic relationship of the cranial fossae to Reid’s base line most clearly in the slice where the middle cranial fossa is at its deepest (see ►Fig. 4.11). Knowledge of these simple spatial relationships is invaluable while evaluating cross-sectional images obtained parallel to the supraorbito-suboccipital plane. The CT image of the first supraorbito-suboccipital section (see ►Fig. 5.17a) depicts the jugular foramen in the posterior cranial fossa with the foramen spinosum, foramen ovale and the superior orbital fissure (see ►Fig. 5.18a) being seen in the middle cranial fossa. The **cribriform plate** is seen within the following section (see ►Fig. 5.18a), forming part of the anterior cranial fossa. Resting on the cribriform plate is the olfactory bulb. In this slice (see ►Fig. 5.18b), the middle and posterior cranial fossae are enclosed by the calvarium in the form of two forceps. The internal acoustic aperture opens into the posterior cranial fossa (see ►Fig. 5.5a and ►Fig. 5.33). The **superior orbital fissure** (see ►Fig. 4.4c and ►Fig. 6.10a) connects the middle cranial fossa with the orbit. The dorsum sellae is not yet visualized in the center of the image (see ►Fig. 5.18). The tentorium of cerebellum has been sectioned in the fifth slice (see ►Fig. 5.21). The infratentorial compartment decreases gradually in size in subsequent cranial slices up to the tentorium of cerebellum. The optic canal (see ►Fig. 5.20) is seen extending between the orbit and the middle cranial fossa (see ►Fig. 5.36) in the fourth axial CT image. The roof of orbit is visualized in the anterior cranial fossa (see ►Fig. 3.17 and ►Fig. 4.11). The bony contours of the skull appear to represent an oval ring (see ►Fig. 5.21b) from the sixth CT section onward. The infratentorial compartment is small compared to the supratentorial counterpart in the eighth CT section,

with the tentorium of cerebellum forming the boundary between the two (see ►Fig. 5.24).

7.3 Intracerebral CSF Spaces

Individual cerebrospinal fluid spaces have been described on coronal, sagittal, and bicommissural sections. ►Fig. 7.8 indicates the position of coronal sections while ►Fig. 7.9 illustrates the individual slices of this series. Cerebrospinal spaces are visualized on sagittal sections in ►Fig. 7.10 (position of sagittal sections, see ►Fig. 4.1). ►Fig. 7.11 indicates the position of bicommissural sections, while ►Fig. 7.12 illustrates CSF spaces in these slices.

7.3.1 Subarachnoid Space

The brain floats in a cushion of CSF due to the nearly identical specific gravity of brain substance and the cerebrospinal fluid. CSF is present within the ventricular system and the subarachnoid space. The subarachnoid space is enclosed between pia mater internally and the arachnoid mater externally and contains 25 to 50 mL of CSF.³³³ The arachnoid mater is closely applied to the dura, a tough fibrous membrane. Subarachnoid spaces of our anatomic preparations appear artificially enlarged due to alcohol-formalin fixation.

7.3.2 Cisterns

Widened CSF containing spaces are known as “cisterns” (see ►Fig. 7.8a, ►Fig. 7.9, ►Fig. 7.10, ►Fig. 7.11a, and ►Fig. 7.12). The cannula enters the **posterior cerebellomedullary cistern (cisterna magna)** in suboccipital punctures which occupies the space between the medulla oblongata, the roof of the IVth ventricle, and the inferior surface of the cerebellum. Approximately 3 cm wide and up to 2 cm deep in the sagittal plane, the cistern is indented in the median plane by the very variable falx cerebelli.

The **posterior** and **anterior basal cisterns** are enlargements of the subarachnoid space lying between the inferior surface of the brain and the base of the skull and extend from the foramen magnum to the crista galli at the anterior edge of the anterior cranial fossa. The posterior and anterior basal cisterns are separated by the dorsum sellae.³³³ The **pontine cistern** lies between the clivus and the pons in the posterior cranial fossa, while the paired **cerebellopontine cisterns** lie in the region of the cerebellopontine angle. The flocculus (HX) of the cerebellum protrudes into the cerebellopontine cistern at its lateral aspect. The lateral recess of the IVth ventricle opens into this cistern through its lateral aperture, identifiable on the inferior surface of the cerebellum as the so-called “Bochdalek’s bouquet”, a protrusion of the choroid plexus of the IVth ventricle through this aperture. The **superior cerebellar cistern** lies between the tentorium of cerebellum and the superior surface of the cerebellum.

- 1 Pericallosal cistern
- 2 Cistern of transverse fissure
- 3 Cistern of lamina terminalis
- 4 Pineal gland
- 5 Interpeduncular cistern
- 6 Ambient cistern
- 7 Quadrigeminal cistern (Great cerebral vein)
- 8 Superior cerebellar cistern
- 9 Anterior basal cistern (dotted line)
- 10 Chiasmatic cistern
- 11 Pontine cistern
- 12 Posterior basal cistern (interrupted line)
- 13 Posterior cerebellomedullary cistern (magna)
- 14 Spinal subarachnoid space

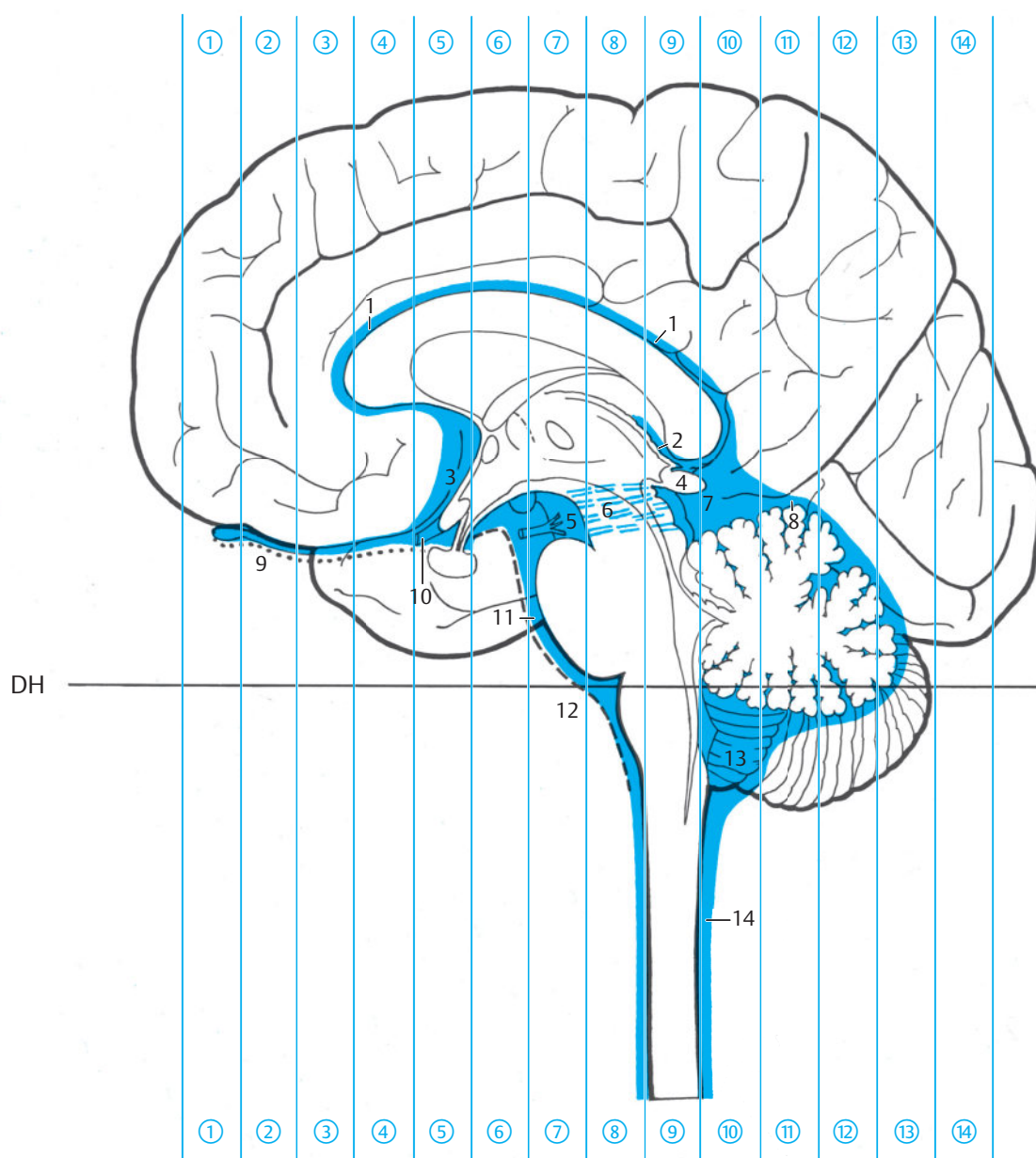


Fig. 7.8 Intracranial CSF spaces. Encircled digits indicate the number of 1 cm thick sections as viewed from anteriorly. DH = German horizontal

Fig. 7.8a Extracerebral CSF spaces in the cranial cavity and the vertebral canal in a median view of the coronally sectioned brain. The ambient cistern surrounds the cerebral peduncle and has therefore been indicated by interrupted blue lines.

The **interpeduncular cistern** (previously: intercrural cistern) forms the anterior part of the posterior basal cistern. Coming off from the interpeduncular fossa, it contains the IIIrd cranial nerve, terminal bifurcation of the basilar artery and the origins of the superior cerebellar and the posterior cerebral arteries (see ► Fig. 4.2d).

The **ambient cistern** (see Fig. 5.7) lies at the junction of the posterior and middle cranial fossae and communicates with the interpeduncular cistern. It encloses the lateral surfaces of the cerebral peduncles and forms a CSF cushion around the tentorial notch for the sharp edge of the tentorium of cerebellum. The ambient

cistern passes into the **quadrigeminal cistern** posteriorly (great cerebral vein; see ► Fig. 5.7 and ► Fig. 5.23) and continues in an anterior direction to the cistern of vallicula cerebri. The quadrigeminal cistern and the cistern of the great cerebral vein were considered as synonyms by the Federative Committee on Anatomical Terminology because both describe nearly the same region between the quadrigeminal lamina and the great cerebral vein. Furthermore, the ambient cistern is connected with the unpaired pericallosal cistern and the paired interhemispheric cisterns (see ► Fig. 3.2d and ► Fig. 3.14d). The ambient cistern contains three

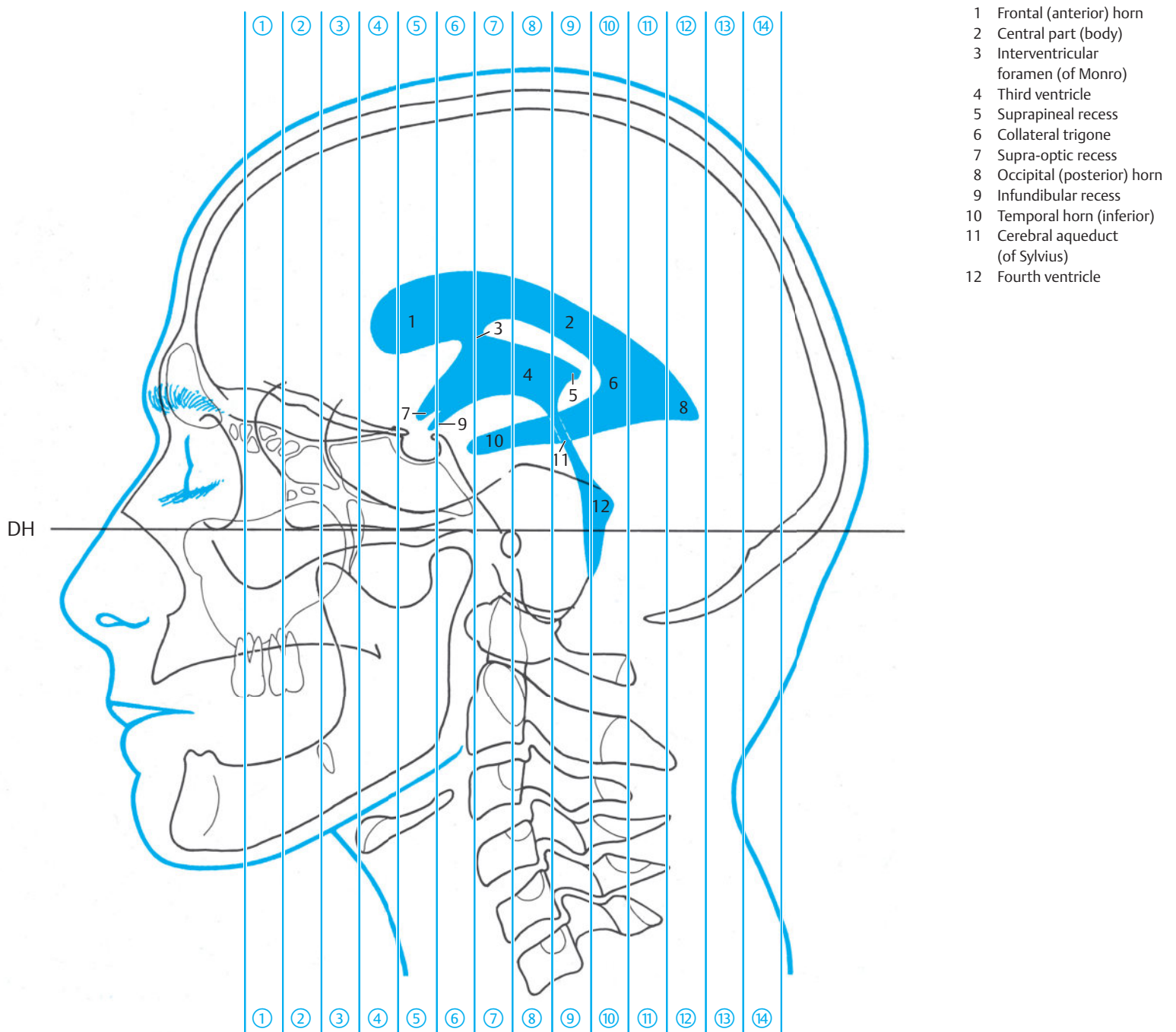


Fig. 7.8b Lateral view of the ventricular system of the coronally sectioned brain (see ► Fig. 3.1).

blood vessels, namely the posterior cerebral artery, the superior cerebellar artery, and the basal vein (of Rosenthal) all of which direct blood posteriorly. The trochlear nerve coursing through this cistern sends its efferent signals anteriorly.

The **trigeminal cistern** opens into the cerebellopontine cistern (see ► Fig. 5.20, ► Fig. 6.8b, and ► Fig. 6.9b) in the posterior cranial fossa. The flat, blind sac of the trigeminal cistern (see ► Fig. 6.9b, ► Fig. 7.9a, and ► Fig. 7.9b) abuts on the petrous part of the temporal bone and on the sphenoid in the middle cranial fossa and houses the

root of the Vth cranial nerve together with the trigeminal ganglion.

The anterior basal cistern extends from the dorsum sellae to the anterior edge of the anterior cranial fossa. It is bounded by the mammillary bodies, infundibulum, optic chiasm, optic tracts, olfactory bulbs and tracts, and the adjoining frontal lobes. A part of this cistern is the **chiasmatic cistern** which encloses the optic chiasm. Posteriorly, the anterior basal cistern continues into the interpeduncular cistern (see ► Fig. 3.9a, ► Fig. 3.9b, ► Fig. 3.9d, ► Fig. 5.7, and ► Fig. 5.22). The medial part of

- 1 Interhemispheric cistern
- 2 Anterior basal cistern
- 3 Pericallosal cistern
- 4 Frontal (anterior) horn of lateral ventricle
- 5 Cistern of lateral cerebral fossa (cistern of Sylvian fissure)
- 6 Cistern of lamina terminalis
- 7 Chiasmatic cistern
- 8 Third ventricle
- 9 Infundibular recess
- 10 Cistern of vallecule cerebri
- 11 Trigeminal cistern

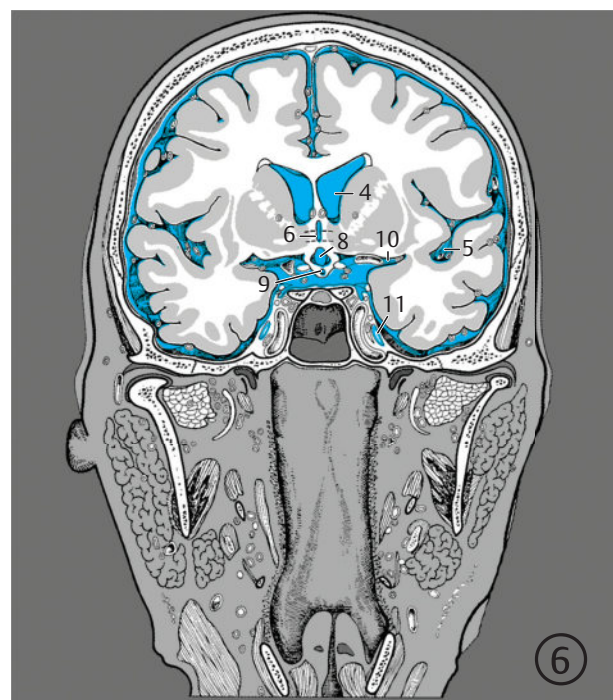
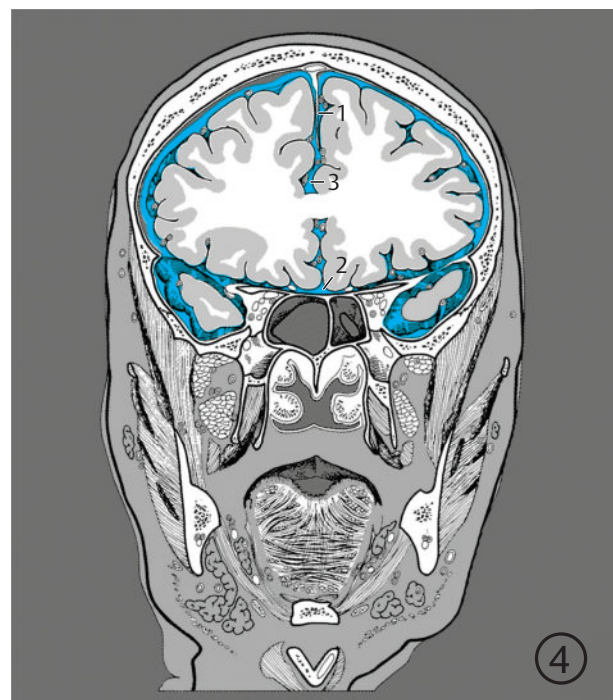
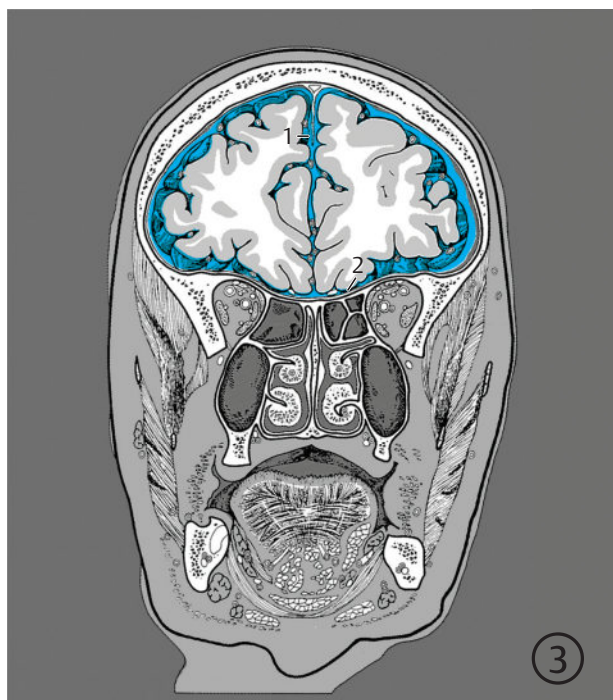


Fig. 7.9 Intracranial CSF spaces. Coronal images of CSF spaces in the cranial cavity and vertebral canal. Encircled digits indicate the number of the respective slice (see ► Fig. 3.1 and ► Fig. 7.8).

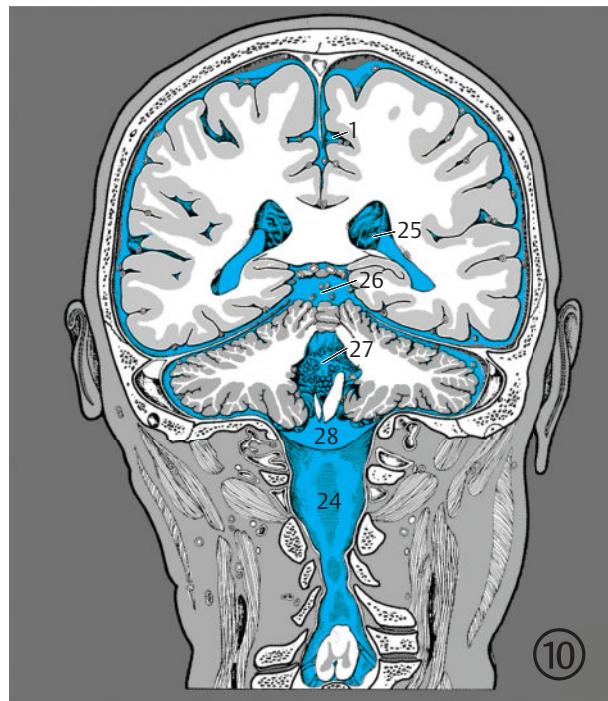
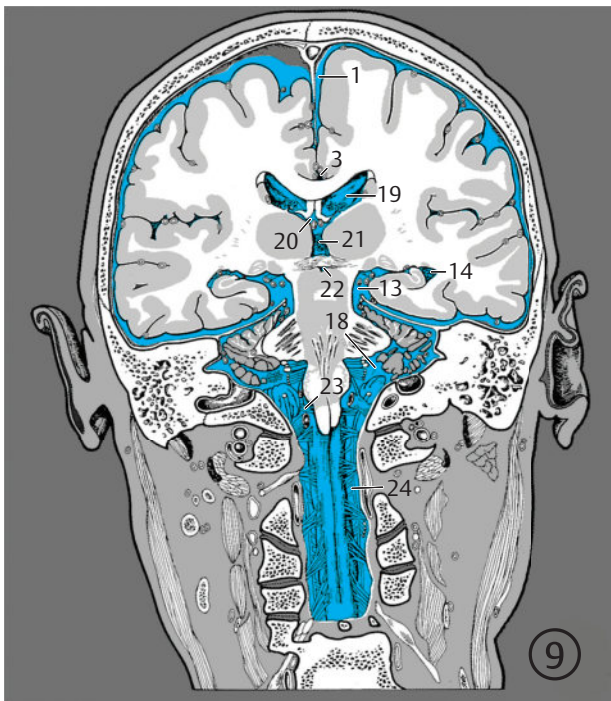
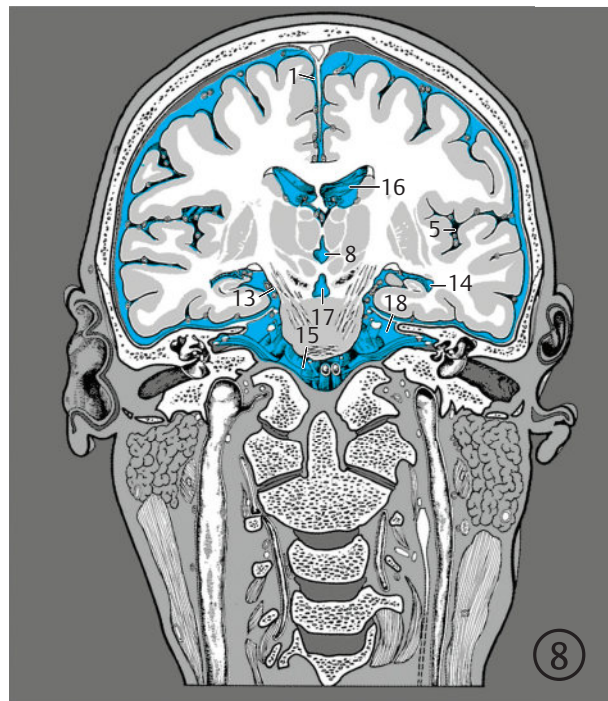
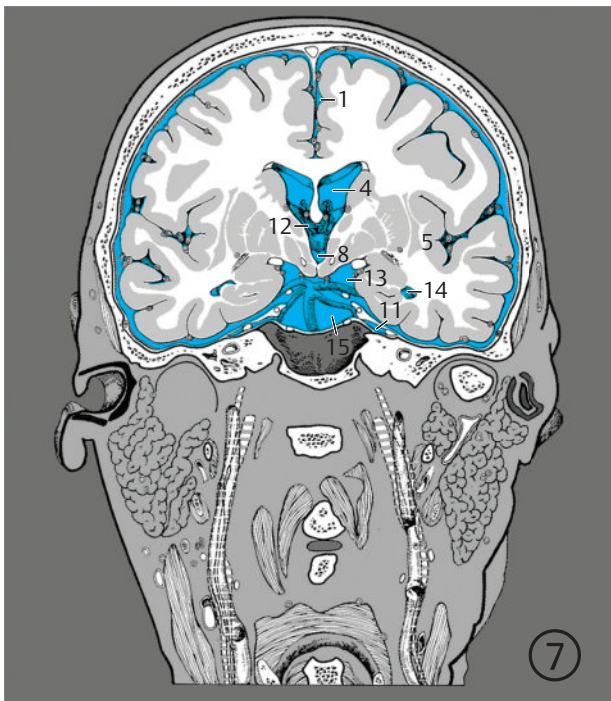
Fig. 7.9a 3rd to 6th sections.

the anterior basal cistern and the interpeduncular cistern are together called the “pentagon” (see ► Fig. 7.12a). The circle of Willis and its central branches lie in the region of the pentagon.

The anterior basal cistern communicates laterally with the cistern of lateral cerebral fossa via the **cistern of the vallecule cerebri** (see ► Fig. 5.21 and ► Fig. 7.9a). The cistern of vallecule cerebri is a CSF-filled space between the posterior edge of the lesser wing of the sphenoid and the anterior perforated substance containing the trunk of the middle cerebral artery.

The **cistern of lateral cerebral fossa (sylvian fissure;** see ► Fig. 4.6b, ► Fig. 5.7, ► Fig. 5.21, ► Fig. 7.9a, ► Fig. 7.9b, ► Fig. 7.10b, and ► Fig. 7.12b) forms the space between the insula and the opercular parts of the frontal, parietal, and temporal lobes.⁵⁶ It is therefore also known as the insular cistern, and contains branches of the middle cerebral artery, the insular arteries.

The **cistern of transverse fissure** (see ► Fig. 7.9b, ► Fig. 7.10a, and ► Fig. 7.11a) is a CSF cushion located in the fissure between the corpus callosum and the roof of the IIIrd ventricle including the thalamus that



- 1 Interhemispheric cistern
- 3 Pericallosal cistern
- 4 Frontal (anterior) horn of lateral ventricle
- 5 Cistern of lateral cerebral fossa (cistern of Sylvian fissure)
- 8 Third ventricle
- 11 Trigeminal cistern
- 12 Interventricular foramen (of Monro)
- 13 Ambient cistern
- 14 Temporal (inferior) horn of lateral ventricle
- 15 Pontine cistern
- 16 Lateral ventricle
- 17 Interpeduncular cistern
- 18 Cerebellopontine cistern
- 19 Central part (body) of lateral ventricle
- 20 Cistern of transverse cerebral fissure
- 21 Suprapineal recess
- 22 Aqueduct of midbrain
- 23 Posterior basal cistern
- 24 Spinal subarachnoid space
- 25 Atrium of lateral ventricle
- 26 Quadrigeminal cistern (cistern of great cerebral vein)
- 27 Roof of fourth ventricle
- 28 Cisterna magna (posterior cerebellomedullary cistern)

Fig. 7.9b 7th to 10th sections.

is between the telencephalon and diencephalon and was therefore earlier known as the “fissura telodien-cephalica”. This cistern extends anteriorly toward the interventricular foramen (of Monro; see ►Fig. 7.8a), measuring 2.5 cm in length sagittally with a transverse diameter of 4 cm. It contains the internal cerebral veins (see ►Fig. 5.9a) and segments of the posterior medial and posterior lateral choroidal arteries (see ►Fig. 5.8).

The cistern of transverse fissure is in turn continuous with the quadrigeminal, pericallosal, and interhemi-

spheric cisterns. The pericallosal cistern (see ►Fig. 7.8a and ►Fig. 7.10a) is the unpaired CSF-filled space between the corpus callosum and the inferior edge of the falx cerebri. The **interhemispheric cisterns** (see ►Fig. 3.2d and ►Fig. 7.9) are paired CSF spaces between the falx cerebri and the medial surface of the cerebral hemisphere on each side. The cistern of lamina terminalis (see ►Fig. 7.9a, ►Fig. 7.11a, and ►Fig. 7.12b) connects the chiasmatic cistern (see ►Fig. 7.8a, ►Fig. 7.9a, and ►Fig. 7.10a) with the pericallosal cistern enclosing the corpus callosum.

- 1 Interhemispheric cistern
- 28 Cisterna magna (posterior cerebellomedullary cistern)
- 29 Occipital (posterior) horn of lateral ventricle
- 30 Superior cerebellar cistern

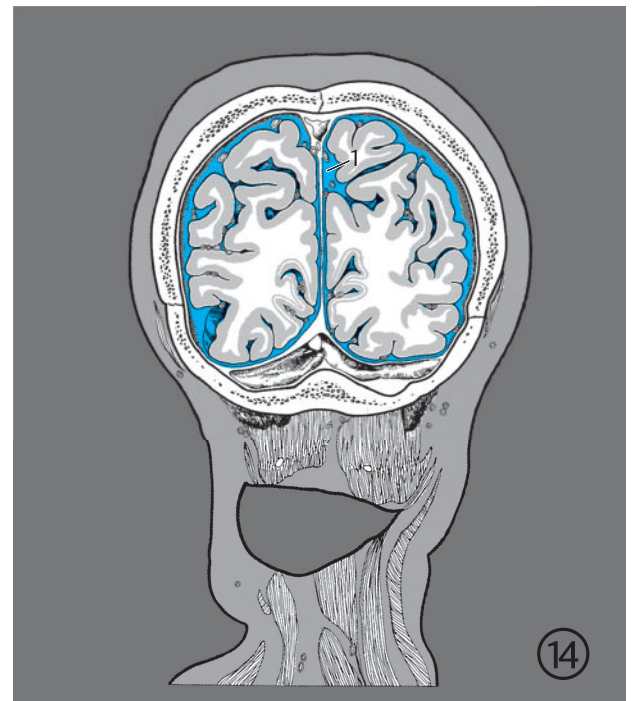
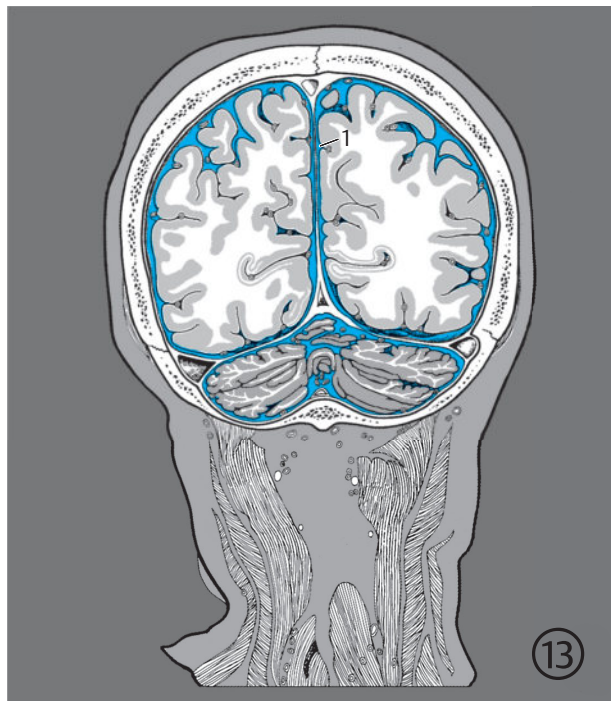
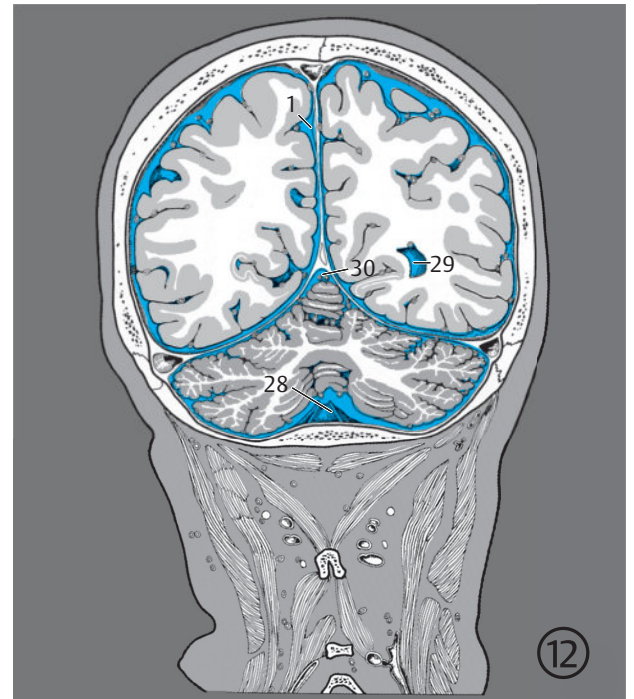
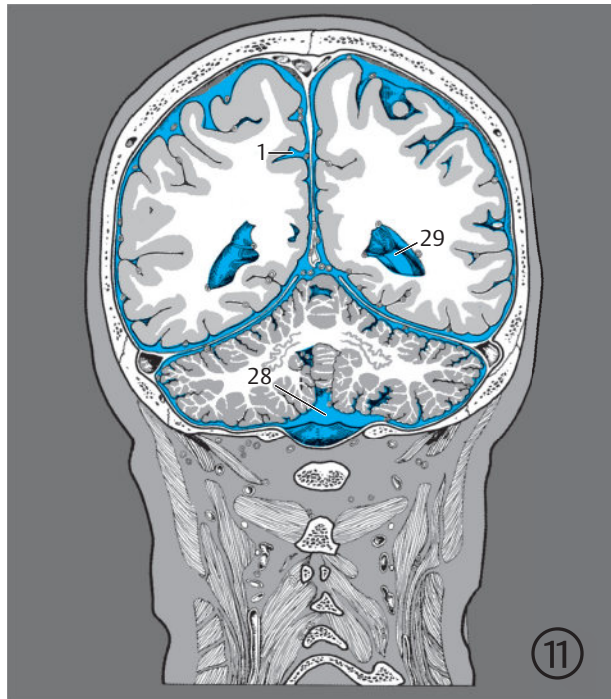


Fig. 7.9c 11th to 14th sections.

7.3.3 Ventricular System

The ventricular system (see ►Fig. 7.8b, ►Fig. 7.9, ►Fig. 7.10, ►Fig. 7.11, and ►Fig. 7.12) is composed of four interconnected CSF containing spaces within the brain which exhibit great variability in shape and volume in healthy people. The mean adult ventricular volume of extracranially fixed brains is about 20 mL (between 7 and 57 mL)^{299,343} and 31 mL (between 15 and 46 mL) as evaluated on CT examinations of healthy brains.⁷²

Fourth Ventricle

The IVth ventricle (see Fig. 3.1c, ►Fig. 3.11b, ►Fig. 3.11d, ►Fig. 4.2a, ►Fig. 4.2b, ►Fig. 6.6a, ►Fig. 6.8b, and ►Fig. 7.8b) communicates with extracerebral CSF spaces through three openings:

- At the obex (see ►Fig. 4.2a, ►Fig. 6.3, ►Fig. 6.5b, and ►Fig. 6.5c) through the unpaired foramen of Magendie (median aperture of the IVth ventricle).
- Laterally at the medulla oblongata near the VIIIth cranial nerve through the paired foramina of Luschka (lateral apertures of the IVth ventricle; see ►Fig. 6.7a and ►Fig. 6.7b).

The IVth ventricle is shaped like a small tent, with the rhomboid fossa forming its floor and the superior and inferior medullary vela, cerebellar peduncles, and the cerebellum forming its roof. The inferior medullary velum is continuous caudally with the choroid plexus of the IVth ventricle suspended from a plate of connective tissue, which closes the IVth ventricle posteriorly.

Aqueduct of Midbrain

The aqueduct of the midbrain (cerebral aqueduct; see ►Fig. 3.1c, ►Fig. 3.10a, ►Fig. 4.2b, ►Fig. 5.8, ►Fig. 5.24, ►Fig. 7.10a, and ►Fig. 7.12b) lies, as its name suggests, in the midbrain. Measuring approximately 15 mm in length, it is slightly curved in appearance and connects the IIIrd and IVth ventricles.

Third Ventricle

The IIIrd ventricle is an unpaired, slit-shaped space in the median plane, the walls of which are formed by the epithalamus, thalamus, and the hypothalamus from posterior to inferior. An **interthalamic adhesion** is present between the right and left thalami in 75% of cases. The anterior wall of the IIIrd ventricle is formed by the lamina terminalis (see ►Fig. 3.1c, ►Fig. 4.2a, ►Fig. 4.2b, and ►Fig. 5.7). A groove formed by the anterior commissure is seen at the level of the hypothalamic sulcus. Two diverticulae are seen in the region of the hypothalamus: the supra-optic recess (see ►Fig. 7.8b) extending in the direction of the optic chiasm and the infundibular recess (see ►Fig. 3.7a, ►Fig. 7.10a, and ►Fig. 7.11b) extending toward the pituitary stalk.

The choroid plexus forms the roof of the IIIrd ventricle above the **interventricular foramen (of Monro)**. The choroid plexus is attached to the tela choroidea, connective tissue which is stretched between the medullary striae of the thalamus, and forms a diverticulum above the pineal gland, the suprapineal recess (see ►Fig. 7.8b). A few millimeters below lies a small evagination, the pineal recess. The indentation of the habenular commissure lies above the pineal recess while the posterior commissure lies below it. The IIIrd ventricle transitions into the aqueduct of the midbrain further inferiorly.³³⁷

Lateral Ventricles

The lateral ventricles are two ram-horn shaped cavities in the telencephalon, connected to each other and with the IIIrd ventricle through the interventricular foramina. Each ventricle has four parts corresponding with four lobes of the telencephalon:

- Anterior or **frontal horn** in the frontal lobe (see ►Fig. 3.7a, ►Fig. 3.7b, ►Fig. 5.23, ►Fig. 5.24, and ►Fig. 7.10a).
- **Central part** in the parietal lobe (see ►Fig. 3.9a, ►Fig. 3.9b, ►Fig. 3.10a, ►Fig. 5.11a, ►Fig. 5.11b, and ►Fig. 7.10a).
- Posterior or **occipital horn** in the occipital lobe (see ►Fig. 3.12 and ►Fig. 7.10a).
- Inferior or **temporal horn** in the temporal lobe (see ►Fig. 3.9a, ►Fig. 3.9b, ►Fig. 4.5b, ►Fig. 4.5d, and ►Fig. 5.7b).

The **frontal horn** forms the anterior pole of the lateral ventricle up to the interventricular foramen (see ►Fig. 3.1c, ►Fig. 3.8a, ►Fig. 5.1c, ►Fig. 5.9a, ►Fig. 5.24, ►Fig. 7.10a, and ►Fig. 7.11b). The frontal horn is bounded medially by the septum pellucidum and laterally by the head of the caudate nucleus, while its roof is formed by the corpus callosum.

The **central part** is narrow, especially due to the protruding thalamus. The floor is formed medially by the lamina affixa and laterally by the body of the caudate nucleus while the corpus callosum forms the roof. Extending through the interventricular foramen, the choroid plexus protrudes into the lateral ventricle from its medial aspect. The central part or body of the lateral ventricle extends to the splenium where it bifurcates into the temporal and occipital horns. The junction of the body, temporal horns, and occipital horns is known as the “trigone” in clinical parlance. Anatomically, the collateral trigone (see ►Fig. 5.9a, ►Fig. 5.9b, and ►Fig. 5.25) is a triangular area at the beginning of the occipital horn, and is closely related topographically to the deep collateral sulcus. The roof of the **occipital horn** is formed by fibers of the corpus callosum, the major (occipital) forceps. A longitudinal eminence produced by the deep calcarine sulcus, the **calcarine spur**, is present on its medial wall.

- 1 Interhemispheric cistern
- 2 Pericallosal cistern
- 3 Interventricular foramen (of Monro)
- 4 Choroid plexus of third ventricle
- 5 Cistern of transverse cerebral fissure
- 6 Suprapineal recess
- 7 Pineal gland
- 8 Quadrigeminal cistern (cistern of great cerebral vein)
- 9 Cistern of lamina terminalis
- 10 Supraoptic recess
- 11 Infundibular recess
- 12 Third ventricle
- 13 Chiasmatic cistern
- 14 Interpeduncular cistern
- 15 Aqueduct of midbrain
- 16 Superior cerebellar cistern
- 17 Pontine cistern
- 18 Fourth ventricle
- 19 Choroid plexus of IVth ventricle
- 20 Posterior basal cistern
- 21 Central canal
- 22 Cisterna magna (posterior cerebellomedullary cistern)
- 23 Spinal subarachnoid space
- 24 Central part (body) of lateral ventricle
- 25 Frontal (anterior) horn of lateral ventricle
- 26 Anterior basal cistern
- 27 Ambient cistern
- 28 Lateral ventricle
- 29 Choroid plexus of lateral ventricle
- 30 Cistern of vallecule cerebri
- 31 Occipital (posterior) horn of lateral ventricle
- 32 Trigeminal cistern
- 33 Cerebellopontine cistern
- 34 Ventricular trigone
- 35 Temporal (inferior) horn of lateral ventricle

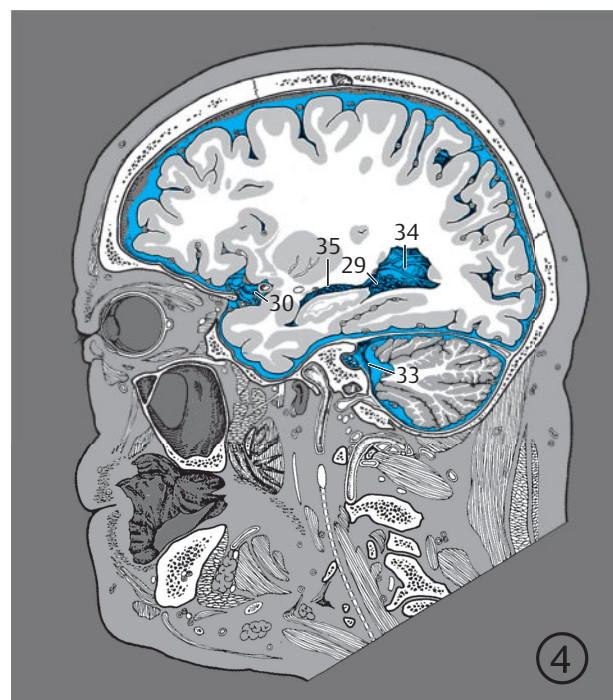
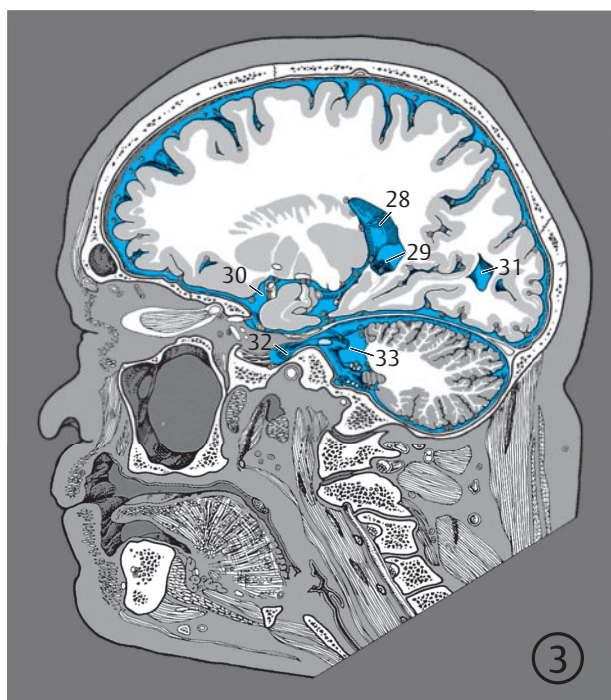
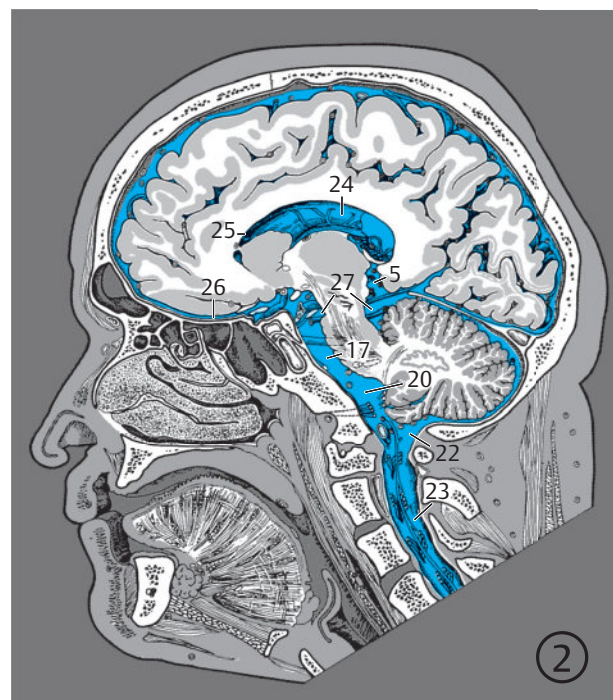
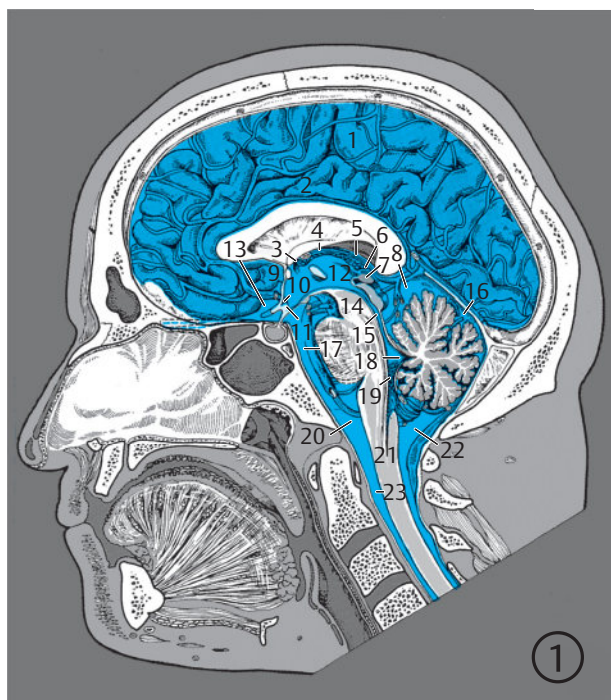
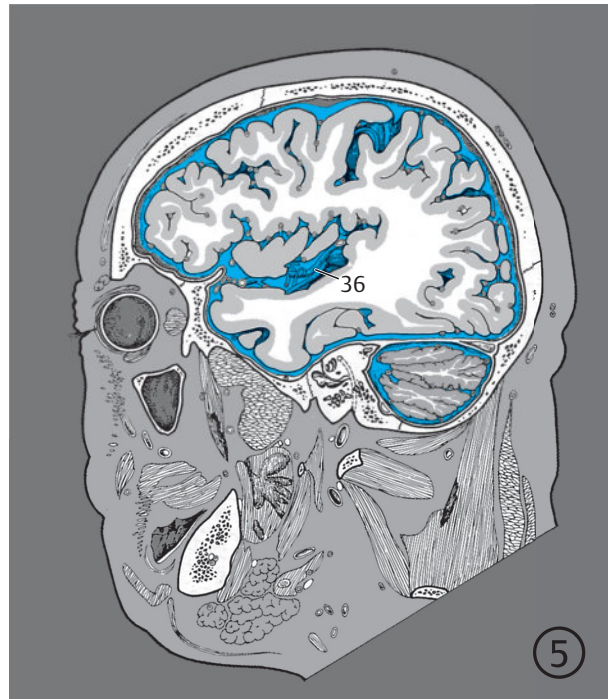


Fig. 7.10 Intracranial CSF spaces. Serial sagittal images of CSF spaces in the cranial cavity and vertebral canal. Encircled digits indicate the number of the respective slice (see ► Fig. 4.1).

Fig. 7.10a 1st to 4th sections.



36 Cistern of lateral cerebral fossa (cistern of Sylvian fissure)

Fig. 7.10b 5th section.

The temporal horn curves slightly backward and laterally, with the tail of the caudate nucleus forming its roof. The amygdaloid body lies at the tip of the temporal horn (see ►Fig. 3.8a, ►Fig. 3.8b, ►Fig. 4.5a, ►Fig. 4.5b, ►Fig. 5.6, ►Fig. 5.7, and ►Fig. 5.21). The choroid plexus joins the fimbria of hippocampus at the medial aspect of the temporal horn. The hippocampus lies at the mediobasal aspect of the temporal horn (see ►Fig. 3.8a, ►Fig. 3.8b, ►Fig. 3.9e, ►Fig. 4.5a, ►Fig. 4.5b, and ►Fig. 5.7), with its alveus bulging into this part of the ventricle (see ►Fig. 3.9e, ►Fig. 3.9f, ►Fig. 5.7, and ►Fig. 5.8).

Clinical Notes

The ventricular system and extracranial CSF spaces are important for the identification and evaluation of pathological intracranial processes despite the large interindividual and wide, age-dependent variation in their width and configuration. Lateral ventricular asymmetry, deformation of a ventricular wall or several ventricles, variable width of intra- and extracerebral cerebrospinal spaces, or a disparity in the width of the supratentorial ventricular system to that of the IVth ventricle draw the examiner's attention to certain disease processes or aid with topical and functional diagnostic orientation: obstructive, mal-resorptive, hypersecretory, internal and external hydrocephalus, and hydrocephalus e vacuo.^{245,272,323,519}

- 1 Pericallosal cistern
- 2 Cistern of transverse cerebral fissure
- 3 Pineal gland
- 4 Cistern of lamina terminalis
- 5 Quadrigeminal cistern (cistern of great cerebral vein)
- 6 Superior cerebellar cistern
- 7 Interpeduncular cistern
- 8 Ambient cistern
- 9 Anterior basal cistern (dotted line)
- 10 Chiasmatic cistern
- 11 Pontine cistern
- 12 Posterior basal cistern (black dashed line)
- 13 Cisterna magna (posterior cerebellomedullary cistern)

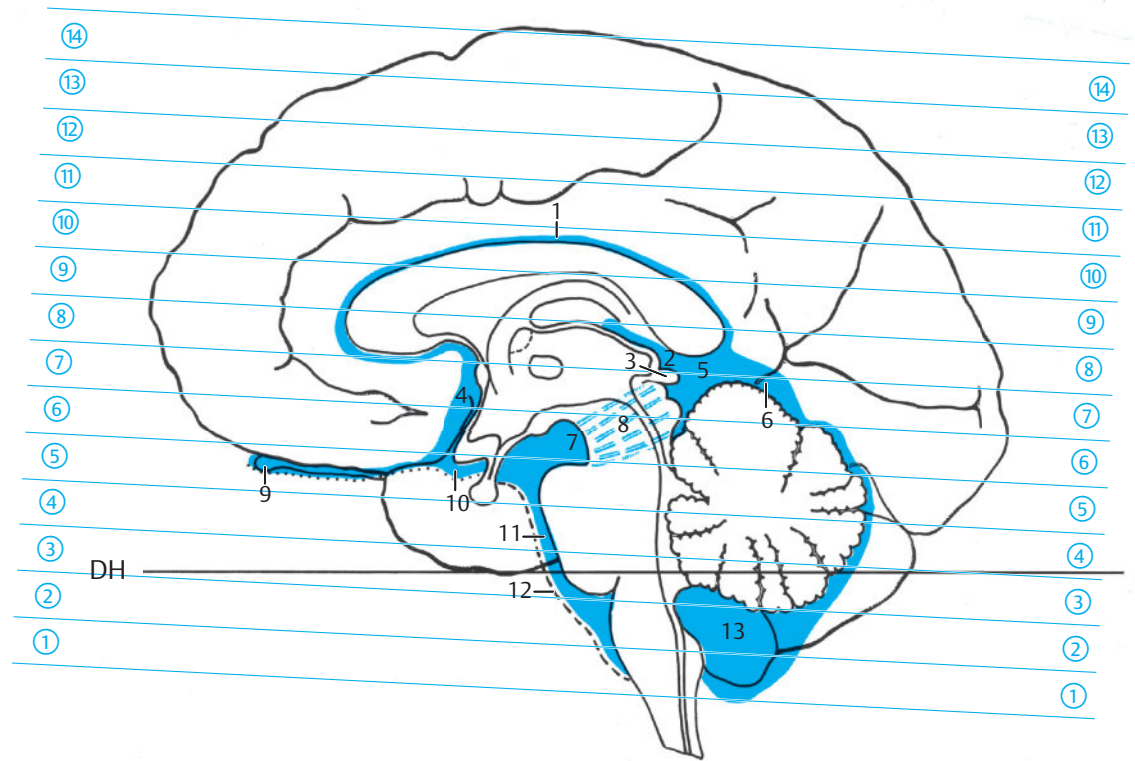


Fig. 7.11 Intracranial CSF spaces. Slices have been contiguously numbered with encircled digits from inferior to superior. DH = German horizontal

Fig. 7.11a Extracerebral CSF spaces in a median view of the brain in the bicommissural series. The ambient cistern surrounds the cerebral peduncle and the cistern has therefore been indicated by interrupted blue lines.

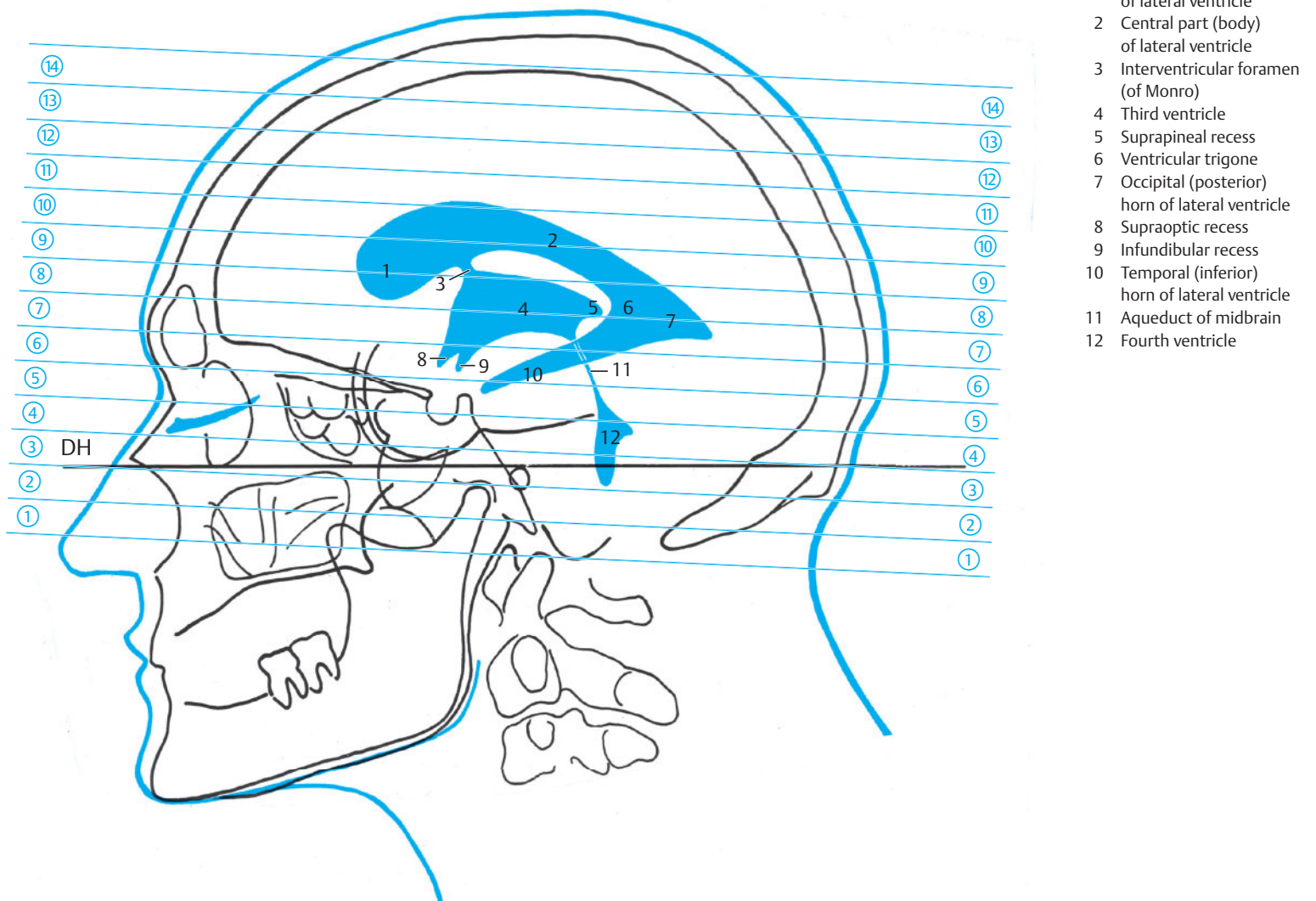


Fig. 7.11b Lateral view of the ventricular system based on an x-ray image of the head (see ► Fig. 5.1).

- 1 Posterior basal cistern
- 2 Cisterna magna (posterior cerebellomedullary cistern)
- 3 Anterior basal cistern
- 4 Pontine cistern
- 5 Trigeminal cistern
- 6 Cerebellopontine cistern
- 7 Fourth ventricle
- 8 Cistern of vallicula cerebri
- 9 Suprasellar cistern

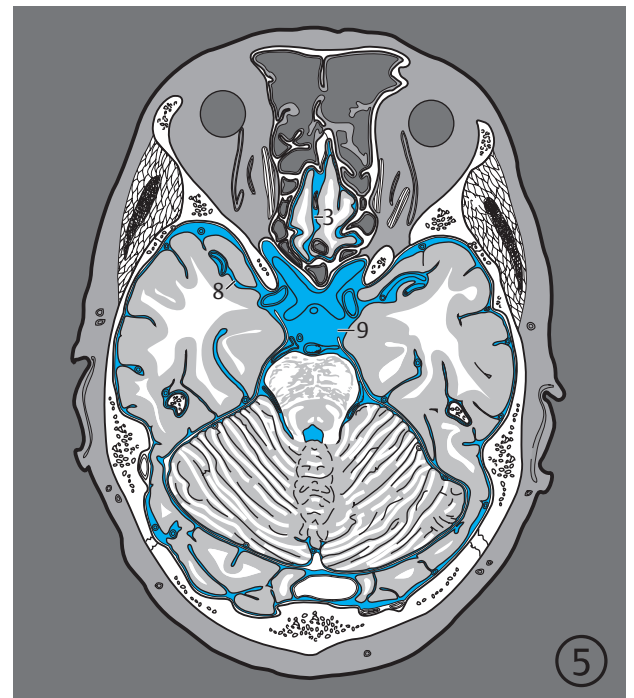
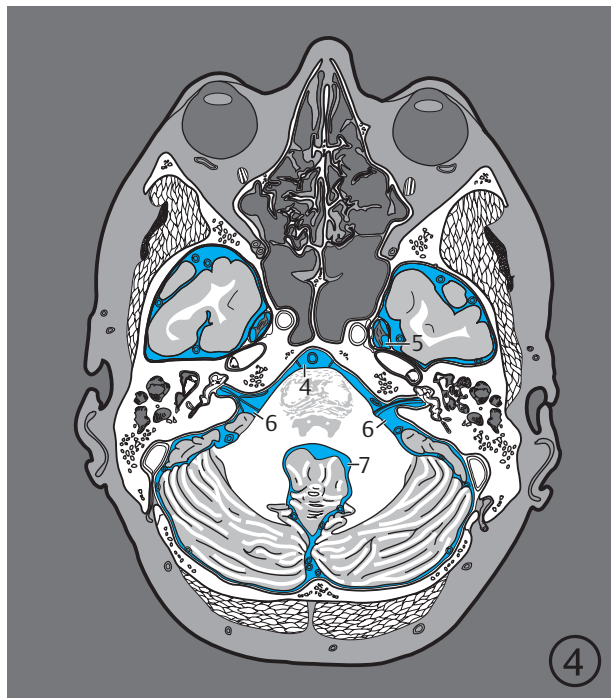
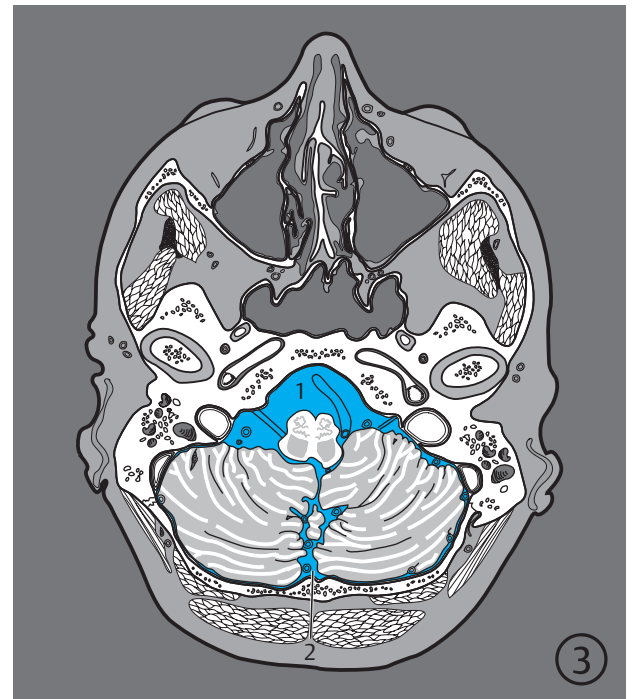
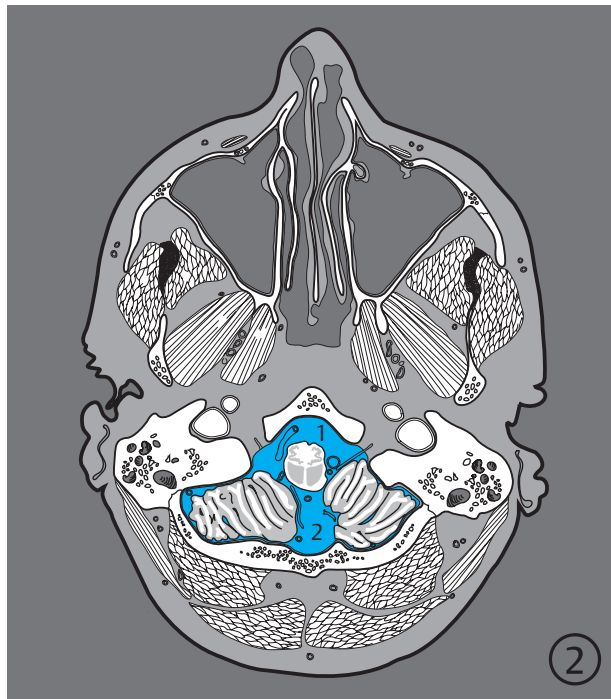
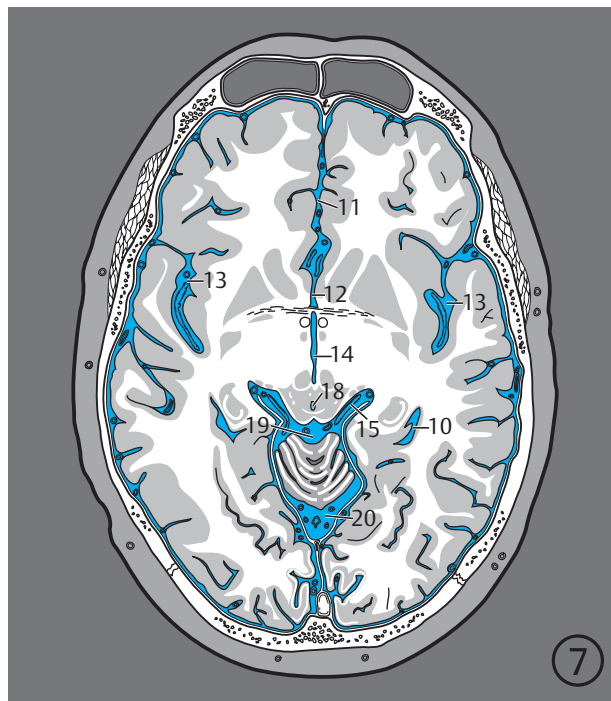
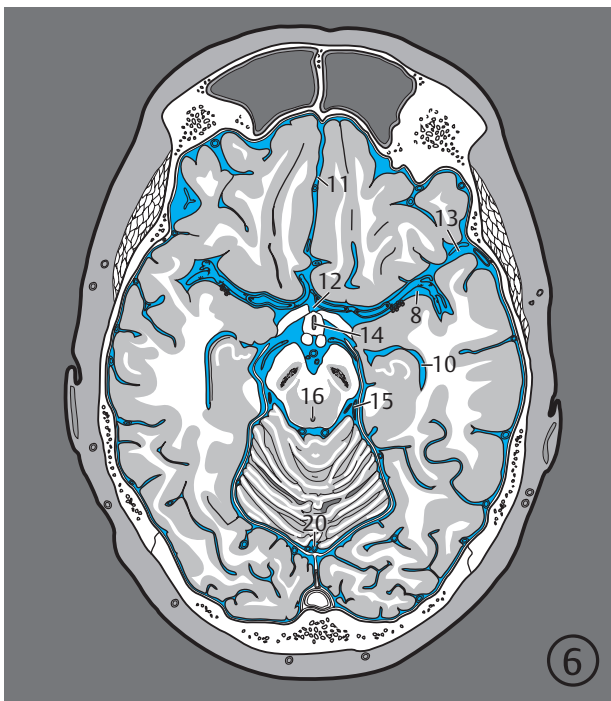


Fig. 7.12 Intracranial CSF spaces. Serial images of intracranial CSF spaces oriented along the bicommissural plane. Encircled digits indicate the number of the respective slice (see ► Fig. 5.1 and ► Fig. 7.11).

Fig. 7.12a 2nd to 5th sections.



- 8 Cistern of vallicula cerebri
- 10 Lateral ventricle
- 11 Interhemispheric cistern
- 12 Cistern of lamina terminalis
- 13 Cistern of lateral cerebral fossa (cistern of Sylvian fissure)
- 14 Third ventricle
- 15 Ambient cistern
- 16 Transition of aqueduct into the IVth ventricle
- 17 Pericallosal cistern
- 18 Aqueduct of midbrain
- 19 Quadrigeminal cistern (cistern of great cerebral vein)
- 20 Superior cerebellar cistern

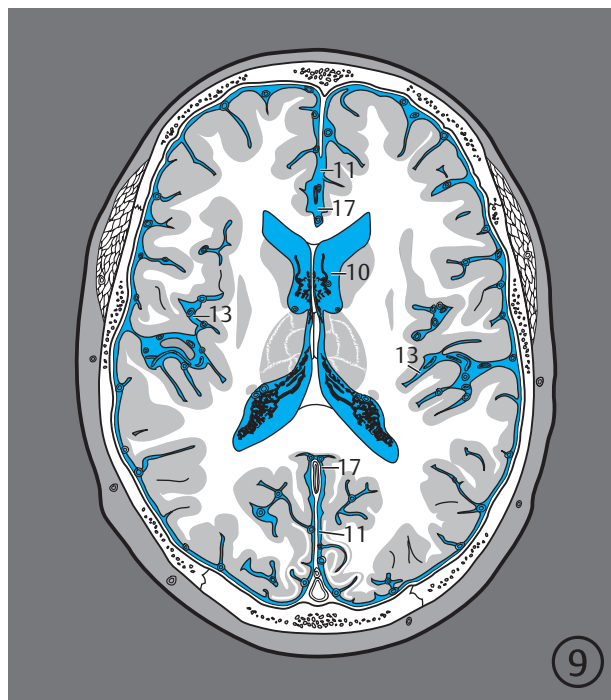
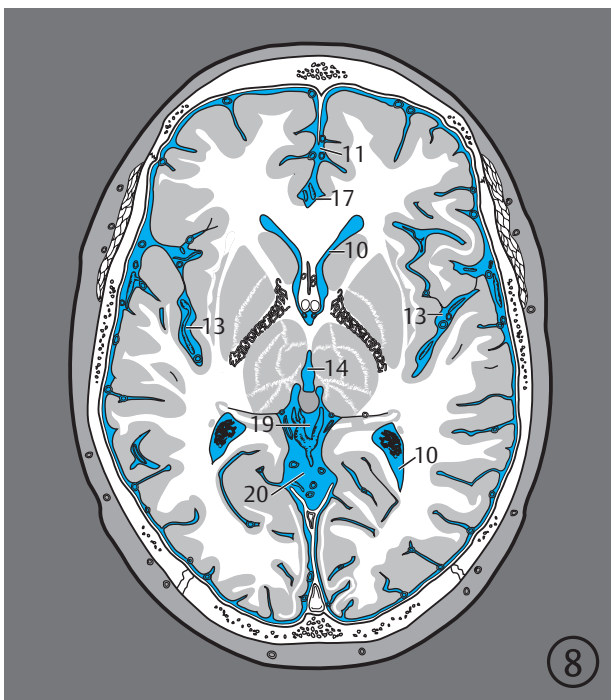


Fig. 7.12b 6th to 9th sections.

- 10 Lateral ventricle
- 11 Interhemispheric cistern
- 17 Pericallosal cistern

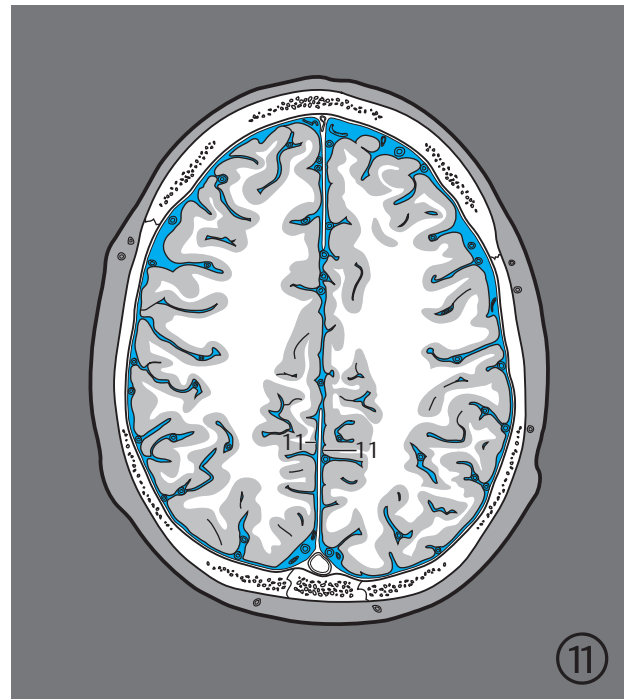
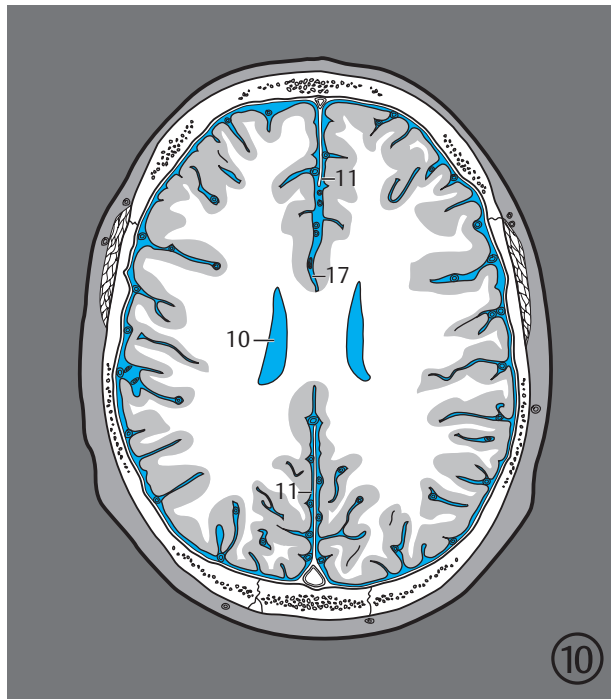


Fig. 7.12c 10th and 11th sections.

7.4 Cerebral Arteries and their Vascular Territories

Cerebral arteries (see ► Fig. 7.13, ► Fig. 7.14, ► Fig. 7.15, ► Fig. 7.16, ► Fig. 7.17, ► Fig. 7.18, ► Fig. 7.19, ► Fig. 7.20, ► Fig. 7.21, ► Fig. 7.22, ► Fig. 7.23, ► Fig. 7.24, ► Fig. 7.25, ► Fig. 7.26, ► Fig. 7.27, ► Fig. 7.28, ► Fig. 7.29, ► Fig. 7.30, ► Fig. 7.31, and ► Fig. 7.32) are only unsatisfactorily visualized on routine CT and MR examinations, such that supplementary **CTA** or **MRA** (see ► Fig. 7.15 and ► Fig. 7.27) are necessary in certain situations, as in vascular diseases, differential diagnosis of tumors, and operative planning. **Cerebral catheter angiography** is essential in some special cases. Consequences of vascular diseases and resulting insults such as edema, infarction, bleeding, or hydrocephalus are visualized on CT and MR. Topographical anatomy of the cerebral arteries, usually derived from angiographic coronal and lateral projections, should therefore be seen in conjunction with CT and MRI findings in 3D. Thus, angiograms of the commonest arterial variations have been compared with sectional images of arteries in brain specimens.

Occlusion of large cerebral arteries (middle cerebral and basilar arteries) may be identified on CT by hyperdense segments of the arteries and by absence of flow on MRI. Territorial infarctions induced thereby may be detected on CT within 30 minutes as discreet hypodense areas and by loss of corticomedullary differentiation in the involved arterial territory. Intracranial hemorrhage is immediately detectable on CT, on MRI it can be detected in the first few hours using T2*w and FLAIR examination sequences. MRI has a higher sensitivity than CT in cerebral infarction; this is largely attributable to improved detection of infarcts in the brainstem and cerebellum. The magnitude and extent of hypodensity in CT as well as abnormal signal in MRI representing edema and infarction are determined by the size of the occluded vessel, as also by the possible **collateral blood supply**. Aneurysms as small as 2 to 3 mm in diameter may be detected on both CTA and MRA. Small angiomas are however not reliably identified using these methods, for the diagnosis of which DSA still remains the examination method of choice.

Exhaustive studies have been carried out in recent decades on the **variability of cerebral arteries**.^{152,190,307,332,333,601} The internationally accepted nomenclature has been accepted by clinicians only to some extent. Synonyms are therefore often used in literature, and it thus appears necessary to include these in brackets after internationally accepted anatomical names. Several anatomical **names of cerebral arteries** are more than 100 years old. A single conspicuous topographical feature was often decisive for the naming of anatomical structures.⁴⁷ For instance, cerebellar arteries branch out into the cerebellum, but also give

off important circumferential branches to parts of the medulla oblongata, pons, and the midbrain. Proximal occlusion of a cerebellar artery can lead to disordered functioning of the medulla oblongata, pons, or the midbrain. The name of an artery usually indicates only a part of the territory it supplies.

7.4.1 Vertebral Artery

Emerging through the transverse foramen of the atlas, the vertebral artery (see ► Fig. 7.13 and ► Fig. 7.20) first courses posteriorly and then bends into its sulcus situated on the atlas (see ► Fig. 4.4c), thus forming a “reserve loop”, which allows for movements of the head. This is visualized as the **V3 segment** on a lateral view of the angiogram.

The artery then runs obliquely from its sulcus through the atlanto-occipital membrane, dura, and arachnoid. The atlanto-occipital sinus is located here together with the ampulloglomerular organ, which possibly represents a receptor for vascular reflexes. The vertebral artery initially follows an arcuate course, coming to lie anteriorly to the medulla oblongata (see ► Fig. 3.9c, ► Fig. 3.10c, ► Fig. 4.2c, and ► Fig. 5.3). Its intracranial course is termed the **V4 segment** (see ► Fig. 7.13b). The left and right vertebral arteries fuse to form the basilar artery usually at the inferior margin of the pons (in 66% of cases), rarely at the level of the anterior part of the medulla oblongata. The right or left vertebral artery may exhibit a larger lumen or may form a loop in its V4 segment.

The anterior spinal artery and the posterior inferior cerebellar artery (PICA) are angiographically demonstrable **branches of the vertebral artery**. The **anterior spinal artery** arises from the vertebral artery immediately proximal to its union with the contralateral artery and then runs in an inferomedial direction. In 77% of cases, the right and left arteries form an unpaired median anterior spinal artery approximately 2 to 3 cm from their origin.³³³ The anterior spinal artery is unilaterally absent in 20% of cases, while it does not unite with its counterpart in another 13%. Paramedian branches from the anterior spinal artery supply the medulla oblongata.

The **PICA** (see ► Fig. 3.10c, ► Fig. 4.2c, ► Fig. 4.3c, ► Fig. 4.3d, ► Fig. 5.3a, ► Fig. 7.13, and ► Fig. 7.14a) usually arises intracranially from the vertebral artery, originating caudal to the foramen magnum in 18% of individuals, while in another 10% it arises from the basilar artery. The PICA is unilaterally absent in 10% of cases, while bilateral absence has been noted in 2%. This cerebellar artery follows a very variable course along the lateral edge of the medulla oblongata.^{307,333} Fine branches pass from this vessel to the anterolateral, lateral, and parts of the posterior territories of the medulla oblongata, where the nucleus ambiguus and

- 1 Vertebral artery
- 2 Variation of posterior inferior cerebellar artery (PICA)
- 3 Posterior inferior cerebellar artery (PICA)
- 4 Basilar artery
- 5 Anterior inferior cerebellar artery (AICA)
- 6 Superior cerebellar artery
- 7 Origin of posterior cerebral artery
- 8 Posterior communicating artery
- 9 Internal carotid artery

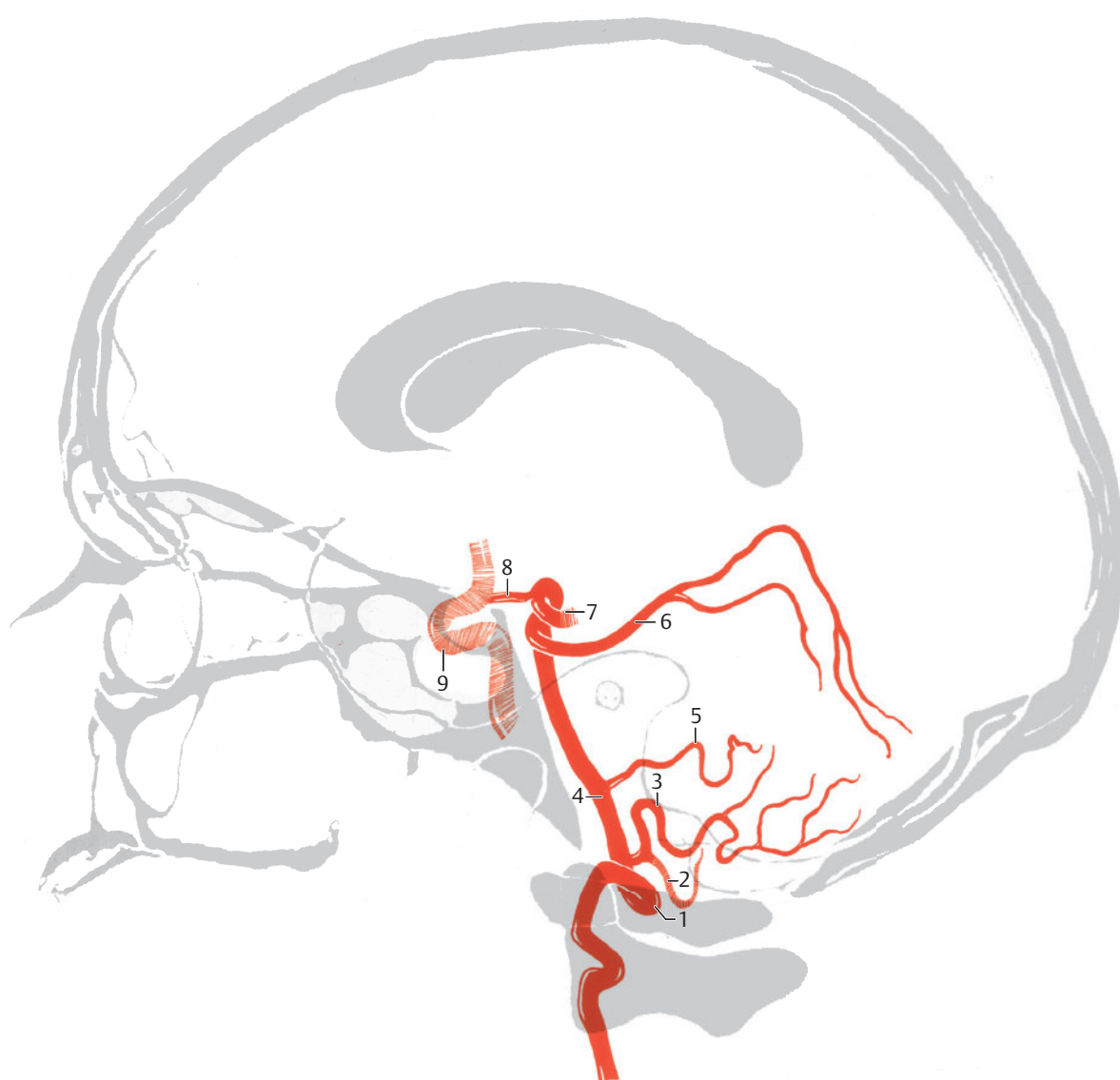


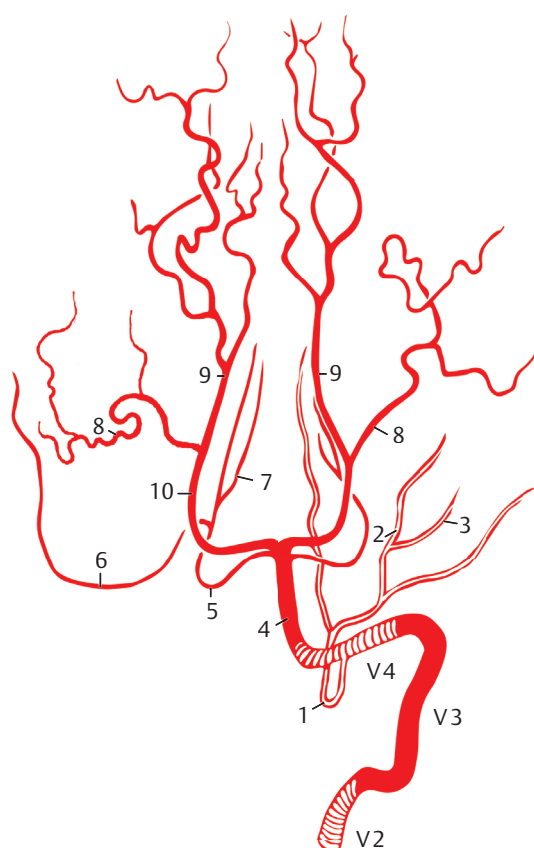
Fig. 7.13 Infratentorial arterial tree with its connection to the internal carotid artery.

Fig. 7.13a Lateral view.

other structures, including the central sympathetic pathway, spinal nucleus of the trigeminal nerve, and the spinothalamic tract are located (see ►Fig. 6.4b, ►Fig. 6.5b, and ►Fig. 6.6b). Thereafter, the artery may form a vascular loop on or around the tonsils of cerebellum. This vascular sling lies caudal to the foramen magnum in 18% of individuals, so an inference of brain edema with caudal displacement of the tonsils of cerebellum cannot be made with certainty in such cases. A branch of this cerebellar artery extends into the choroid plexus of the IVth ventricle. The terminal segment of the PICA courses over the inferior surface of the cerebellum and branches into two: a medial branch that supplies the inferior surface of the vermis and a lateral branch that supplies the inferior surface of the cerebellar hemisphere, including a small part of the dentate nucleus.

7.4.2 Basilar Artery

The basilar artery is formed by the union of the vertebral arteries (see ►Fig. 3.8b, ►Fig. 3.8c, ►Fig. 4.2c, ►Fig. 4.2d, ►Fig. 5.5, ►Fig. 5.6, ►Fig. 5.20, and ►Fig. 7.14) and traverses the basilar sulcus of the pons within the pontine cistern, passing superiorly to the interpeduncular cistern. It measures 32 mm in length on an average (15–40 mm). In 51% of cases the superior end of the basilar artery is seen lying at the level of the dorsum sellae, in 30% above it, and in 19% below it.³⁰⁷ The artery forms a right or left concave arch in 10% of cases, usually together with a wider contralateral vertebral artery, assumed to be the result of hemodynamic factors.²³⁴ This curved course is not to be confused with pathologic displacement due to a space-occupying lesion.



- V2 Vertebral artery in its second segment
- V3 Vertebral artery in its third segment (between axis and atlas)
- V4 Intracranial vertebral artery
- 1 Posterior inferior cerebellar artery
- 2 Inferior vermian branch
- 3 Tonsillohemispheric branch
- 4 Basilar artery
- 5 Superior cerebellar artery
- 6 Marginal artery (marginal branch)
- 7 Superior vermian branch
- 8 Temporo-occipital artery
- 9 Medial occipital artery
- 10 Posterior cerebral artery

Fig. 7.13b Infratentorial arterial tree in Towne's view as per Krayenbühl et al.³⁰⁷

Branches of the Basilar Artery (see ►Fig. 7.14 and ►Fig. 7.15):

- Pontine arteries (fine branches, not sectioned)
- Anterior inferior cerebellar artery (AICA) (see ►Fig. 4.2c, ►Fig. 4.4c, ►Fig. 5.5, and ►Fig. 7.14a)
- Superior cerebellar artery (see ►Fig. 3.8c, ►Fig. 4.2c, ►Fig. 4.2d, ►Fig. 5.6, ►Fig. 6.11b, ►Fig. 7.13a, and ►Fig. 7.14a)
- Posterior cerebral artery (see ►Fig. 3.8c, ►Fig. 4.2c, ►Fig. 4.2d, ►Fig. 5.6, ►Fig. 6.13b, ►Fig. 7.13a, and ►Fig. 7.14a)

The **pontine arteries**, usually about eight in number, arise almost at right angles from the basilar artery. Their medial branches supply the anteromedial, their lateral branches the anterolateral and lateral territories of the pons. Pontine arteries are generally not seen on angiograms.

The **AICA** originates in 52% of cases from the inferior third of the basilar artery, while in 46% it arises from the middle third and in 2% from the upper third of the basilar artery. In exceptional cases the AICA may arise from the vertebral artery. A unilateral duplication of the AICA is present in 10% of cases; unilateral absence is noted in 1% while bilateral absence is present only rarely. The first part of the AICA usually extends inferolaterally over the pons (see ►Fig. 7.14a) where it gives off a few fine branches, and then forms a sling from which the labyrinthine artery arises in approximately 70% of individuals. In the remaining instances, the labyrinthine artery arises directly from the basilar artery. The AICA either

crosses the flocculus (H X) or encircles it, supplying it with fine branches. Additional fine branches extend from this floccular part of the artery into the middle cerebellar peduncle of the pons and to the medulla oblongata. The hemispheric branches of the AICA supply the inferior surface of the cerebellum as well as the choroid plexus of the IVth ventricle.

The **superior cerebellar artery** is the most constant cerebellar artery, arising from the basilar artery immediately proximal its terminal bifurcation (see ►Fig. 7.14a and ►Fig. 7.15).

In about 4% of cases, this cerebellar artery arises from the posterior cerebral artery³³² and is bilaterally duplicated in about 10%. The superior cerebellar artery gives off fine branches to the posterior territory of the pons and partly to the posterior territory of the midbrain, as well as wider branches which supply the superior surface of the cerebellum (see ►Fig. 7.13b).

Cerebellar arteries anastomose with each other. The remaining cerebellar arteries may partially or completely compensate for the absence of anlage of one cerebellar artery. With an absent PICA, for instance, the AICA and the superior cerebellar artery take over the blood supply of the inferior surface of the cerebellum. A single PICA independently supplies the inferior surface of the cerebellum in 60% of cases and is supplemented by the AICA in 26% and by the superior cerebellar artery in 3% of cases. The superior surface of the cerebellum, on the other hand, is supplied in 67% of cases by the superior cerebellar artery, supplemented chiefly by the AICA and the PICA.³³³

- 1 Interpeduncular perforating arteries
- 2 Optic tract
- 3 Basilar artery
- 4 Short and long pontine arteries
- 5 Labyrinthine artery
- 6 Anterior inferior cerebellar artery (separate origin of branches)
- 7 Superior cerebellar artery, branches
- 8 Flocculus
- 9 Artery of the anterior median fissure
- 10 Anterior spinal artery
- 11 Posterior inferior cerebellar artery (descending type)
- 12 Vertebral artery
- 13 Posterior spinal artery
- 14 Artery of the olive
- 15 Posterior inferior cerebellar artery (ascending type)
- 16 Artery of posterolateral sulcus
- 17 Medial medullary branches
- 18 Anterior inferior cerebellar artery
- 19 Superior cerebellar artery
- 20 Short circumferential artery
- 21 Quadrigeminal artery
- 22 Thalamogeniculate artery
- 23 Posterior cerebral artery
- 24 Posterior communicating artery

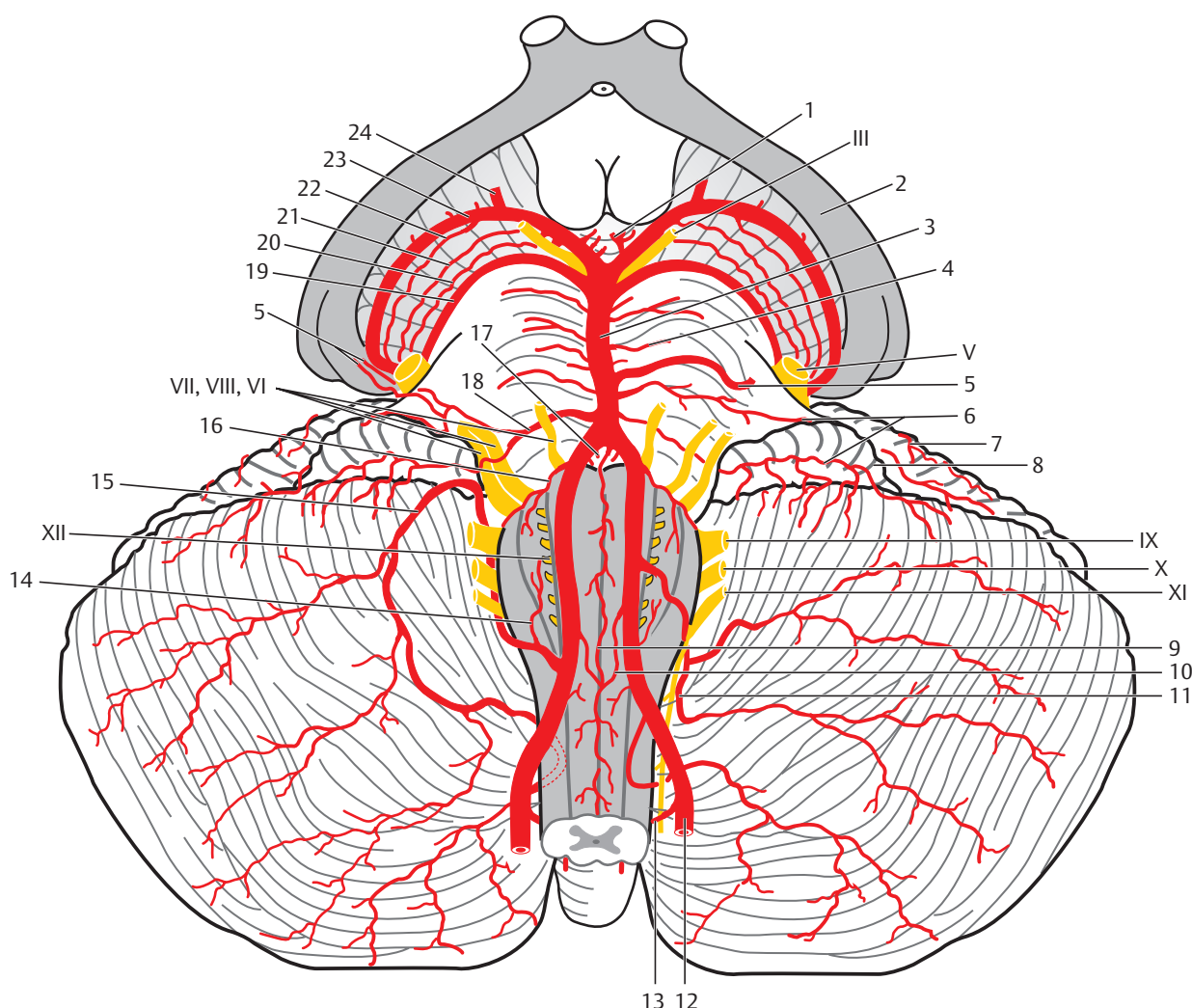


Fig. 7.14 Basilar artery and its branches. Schematic representation. Roman numerals indicate the corresponding cranial nerves. (Reproduced from Rauber et al.⁴⁸⁰)

Fig. 7.14a Branches of the basilar artery and the intracranial part of the vertebral artery.

- 1 Posterior cerebral artery
- 2 Basilar artery ("head")
- 3 Superior cerebellar artery
- 4 Basilar artery
- 5 Anterior inferior cerebellar artery
- 6 Vertebral artery
- 7 Posterior inferior cerebellar artery

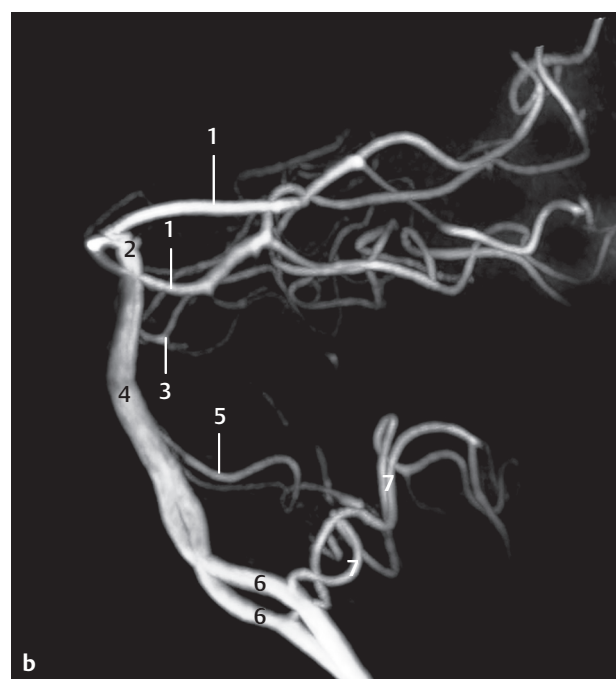
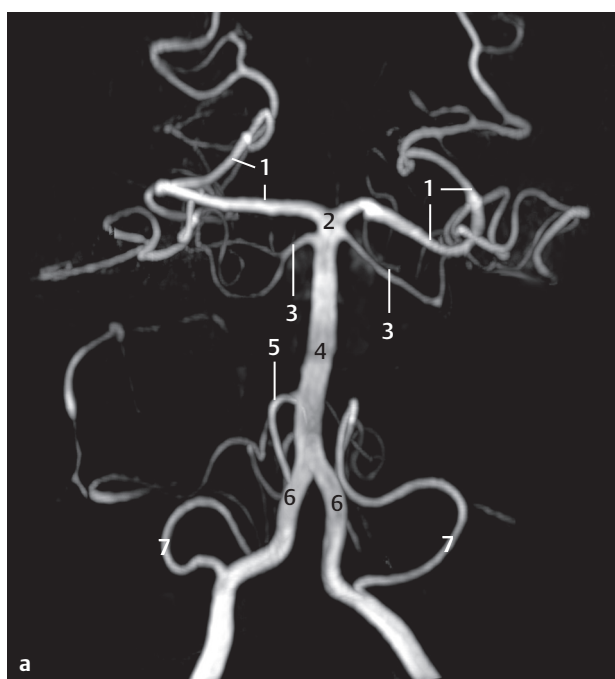


Fig. 7.15 Basilar artery and its branches. Branches of the basilar artery and the intracranial part of the vertebral artery. 3T MRA using Time of Flight technique (MIP image).

Fig. 7.15a Coronal view.

Fig. 7.15b Sagittal view.

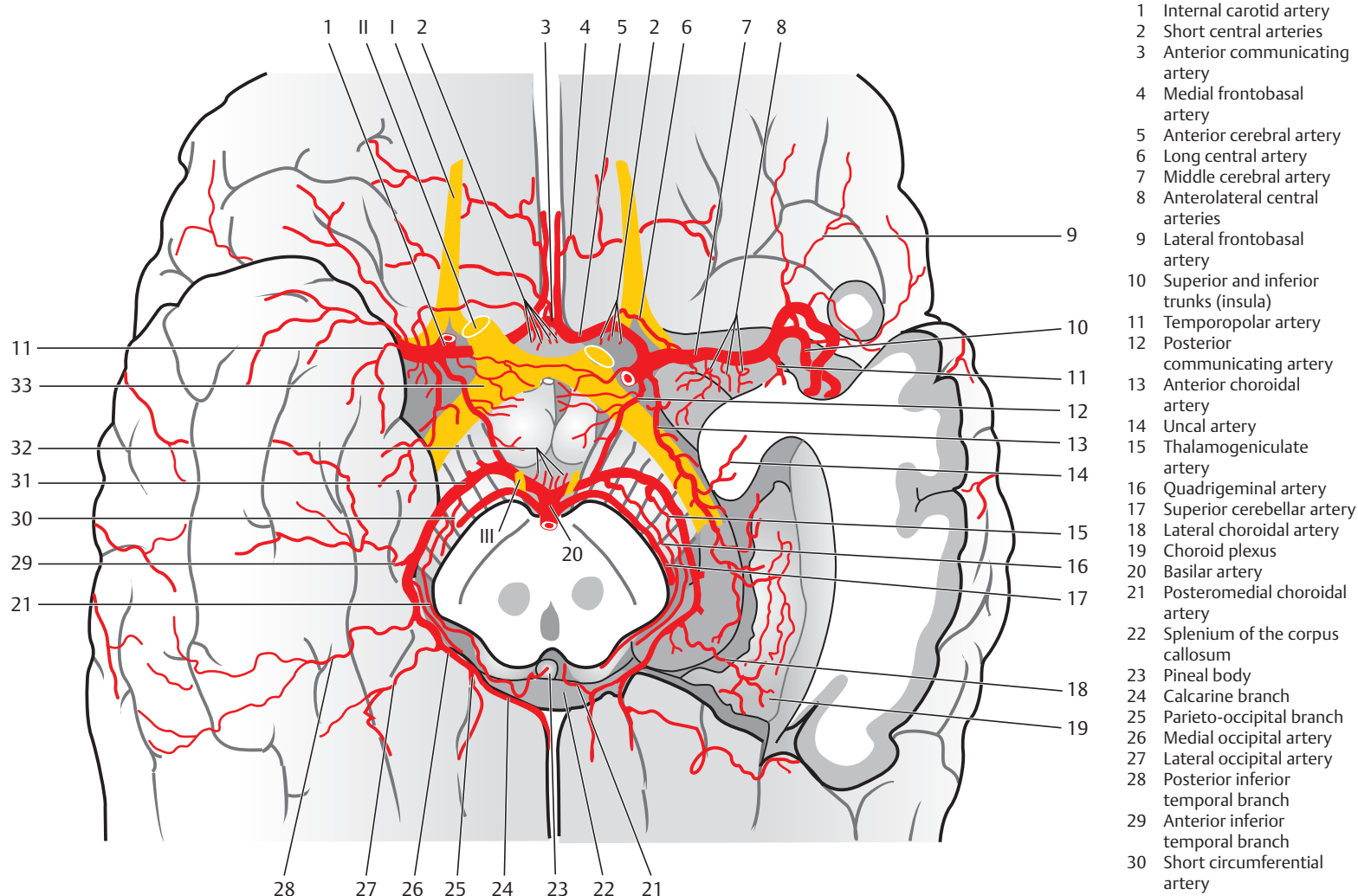


Fig. 7.15b Branches of the internal carotid arteries (cerebral part) and the terminal branches of the basilar artery and its anastomosis with the internal carotid artery. Circle of Willis.

7.4.3 Posterior Cerebral Artery

The posterior cerebral artery (see ►Fig. 7.16; see also ►Fig. 3.8c, ►Fig. 4.2c, ►Fig. 4.3c, ►Fig. 5.6a, ►Fig. 5.6b, ►Fig. 7.14a, ►Fig. 7.15, and ►Fig. 7.22a) arises as the terminal bifurcation of the basilar artery in about 90% of cases and extends into the interpeduncular cistern between the cerebral peduncles and the clivus (see ►Fig. 5.7a). A **fetal type** is present in the remaining 10%, whereby the posterior cerebral artery continues as an extension of the posterior communicating artery and is thus a branch of the internal carotid artery.

The segment of the posterior cerebral artery between the basilar and the posterior communicating arteries is referred to as the **precommunicating part** or “P1 segment” and measures 6 mm in length on an average (3–9 mm). Small penetrating branches of the precommunicating part (posteromedial and posterolateral central arteries; see ►Fig. 6.12b and ►Fig. 7.16) penetrate the anterior perforating substance to partially supply the midbrain and diencephalon. These fine arterial branches are seldom visualized on angiograms.³³²

The **postcommunicating part** of the posterior cerebral artery arches around the midbrain and lies in the

ambient cistern. Small penetrating arteries (posterolateral central arteries [see ►Fig. 7.16] and the collicular artery) arising from this postcommunicating segment supply posterior parts of the thalamus (see ►Fig. 7.17), tectum of the midbrain and the pineal gland.

The posterior cerebral artery divides into its two main branches inferior to the pulvinar and superior to the tentorium of cerebellum:

- **Medial occipital artery** (previously: internal occipital artery; see ►Fig. 3.10c, ►Fig. 4.3c, ►Fig. 5.7, ►Fig. 5.8, ►Fig. 7.14b, and ►Fig. 7.22a)
- **Lateral occipital artery** (previously: temporo-occipital or occipitotemporal artery; ►Fig. 3.10c, ►Fig. 3.10d, ►Fig. 4.4c, ►Fig. 5.8a, and ►Fig. 7.14b)

The **posterior medial and posterior lateral choroidal arteries** arise from the proximal aspect of the postcommunicating part of the posterior cerebral artery (see ►Fig. 7.17; see also ►Fig. 5.8 and ►Fig. 7.16). Running between the quadrigeminal plate and the parahippocampal gyrus, they supply the choroid plexus of the IIIrd and lateral ventricles. In addition, fine branches run to the pineal gland, quadrigeminal plate and to other parts of the diencephalon. Several branches

- 1 Vertebral artery
- 2 Origin of posterior inferior cerebellar artery (PICA)
- 3 Basilar artery
- 4 Origin of anterior inferior cerebellar artery (AICA)
- 5 Origin of superior cerebellar artery
- 6 Posterior cerebral artery
- 7 Posteromedial and posterolateral central arteries
- 8 Posterior medial and posterior lateral choroidal arteries
- 9 Medial occipital artery
- 10 Parieto-occipital artery
- 11 Calcarine artery
- 12 Lateral occipital artery
- 13 Temporal arteries
- 14 Posterior communicating artery
- 15 Internal carotid artery

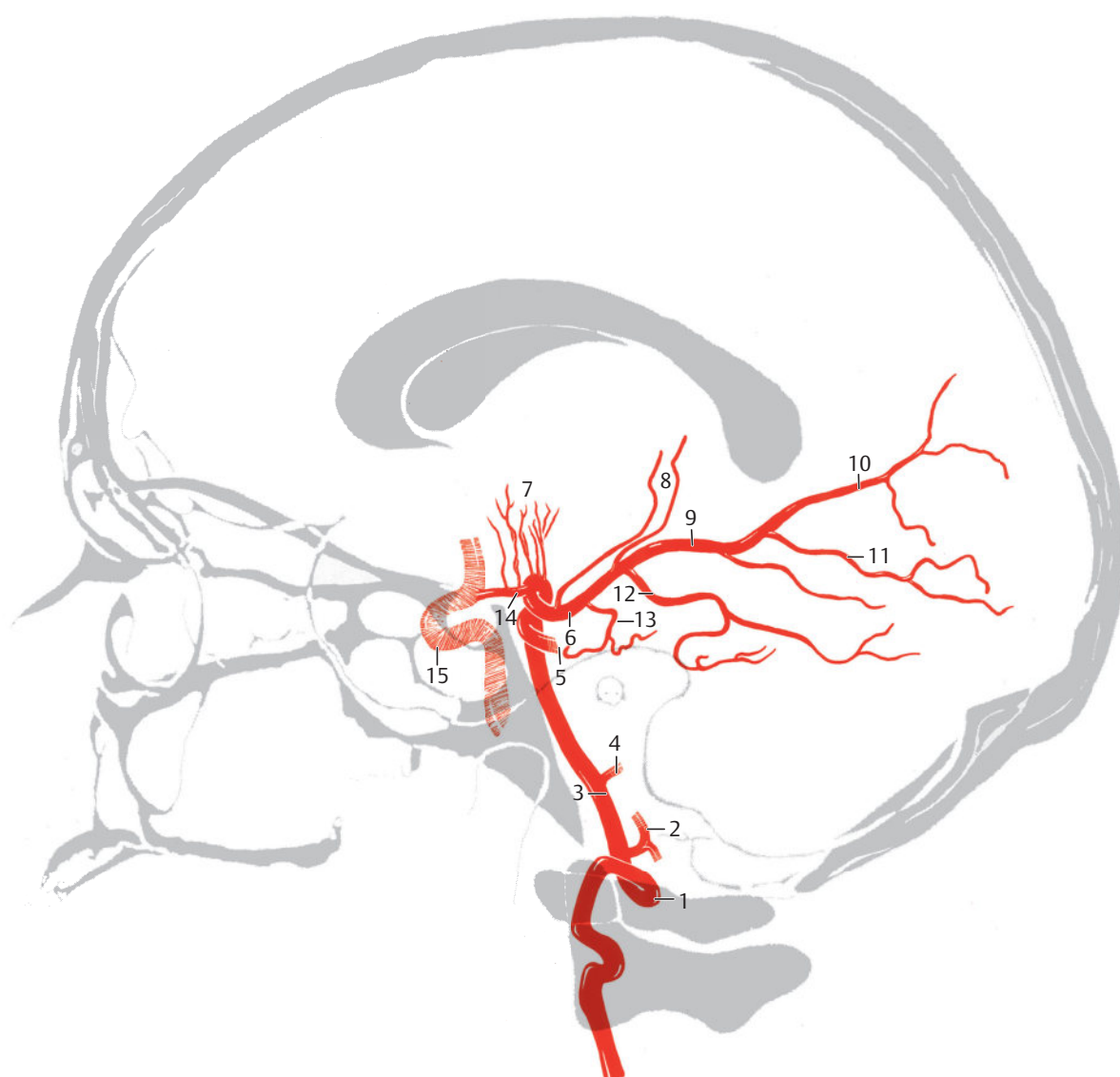


Fig. 7.16 Posterior cerebral artery. Lateral view. (For alternate terms listed in brackets, see Krayenbühl et al.³⁰⁷)

supply the lateral and medial geniculate bodies, the posterior aspect of the thalamus, and the parahippocampal gyrus. Between one and four branches of the parahippocampal arteries supply the parahippocampal gyrus, the hippocampal formation, and parts of the splenium of the corpus callosum. Branches of parahippocampal arteries may be strangulated by the tentorium of cerebellum in patients with cerebral edema, usually resulting in degeneration of Sommer's sector corresponding approximately to the H1 field³⁶⁰ of the hippocampal formation. Additional cortical branches supply the inferior aspect of the temporal lobe.

The division of the posterior cerebral artery into two approximately equal main branches usually occurs at the lateral aspect of the cerebral peduncle (see ►Fig. 7.13b and ►Fig. 7.16). This division is usually a bifurcation, sometimes a trifurcation, and very rarely a quadrifurcation.³³² Coursing over the posterior aspect of the parahippocampal gyrus, the **lateral occipital artery** supplies the inferior surface

of the occipital lobe. The **medial occipital artery** runs beneath the splenium of the corpus callosum and crosses the isthmus of the cingulate gyrus, dividing into its terminal branches, the parieto-occipital and calcarine arteries. The **parieto-occipital artery** (see ►Fig. 3.13c, ►Fig. 4.2c, ►Fig. 4.4c, ►Fig. 5.10a, and ►Fig. 7.16) runs, for the most part, in the sulcus of the same name, supplying the cuneus and precuneus. The **calcarine artery** (see Fig. 3.13c, ►Fig. 4.2c, ►Fig. 4.4c, ►Fig. 4.4d, ►Fig. 5.10a, ►Fig. 5.10b, and ►Fig. 7.16) lies on or in the calcarine sulcus and seldom arises from the lateral occipital artery. The calcarine artery supplies entirely the area striata or the primary visual cortex only in about one-fourth of cases,⁵⁴⁶ while in the remainder, the visual cortex is partially supplied by neighboring arteries. Vascular occlusions of the calcarine artery can give rise to a homonymous hemianopia with macular sparing when a neighboring artery adequately supplies that part of the area striata near the superior cerebral margin which has a one-on-one connection with the macula lutea.

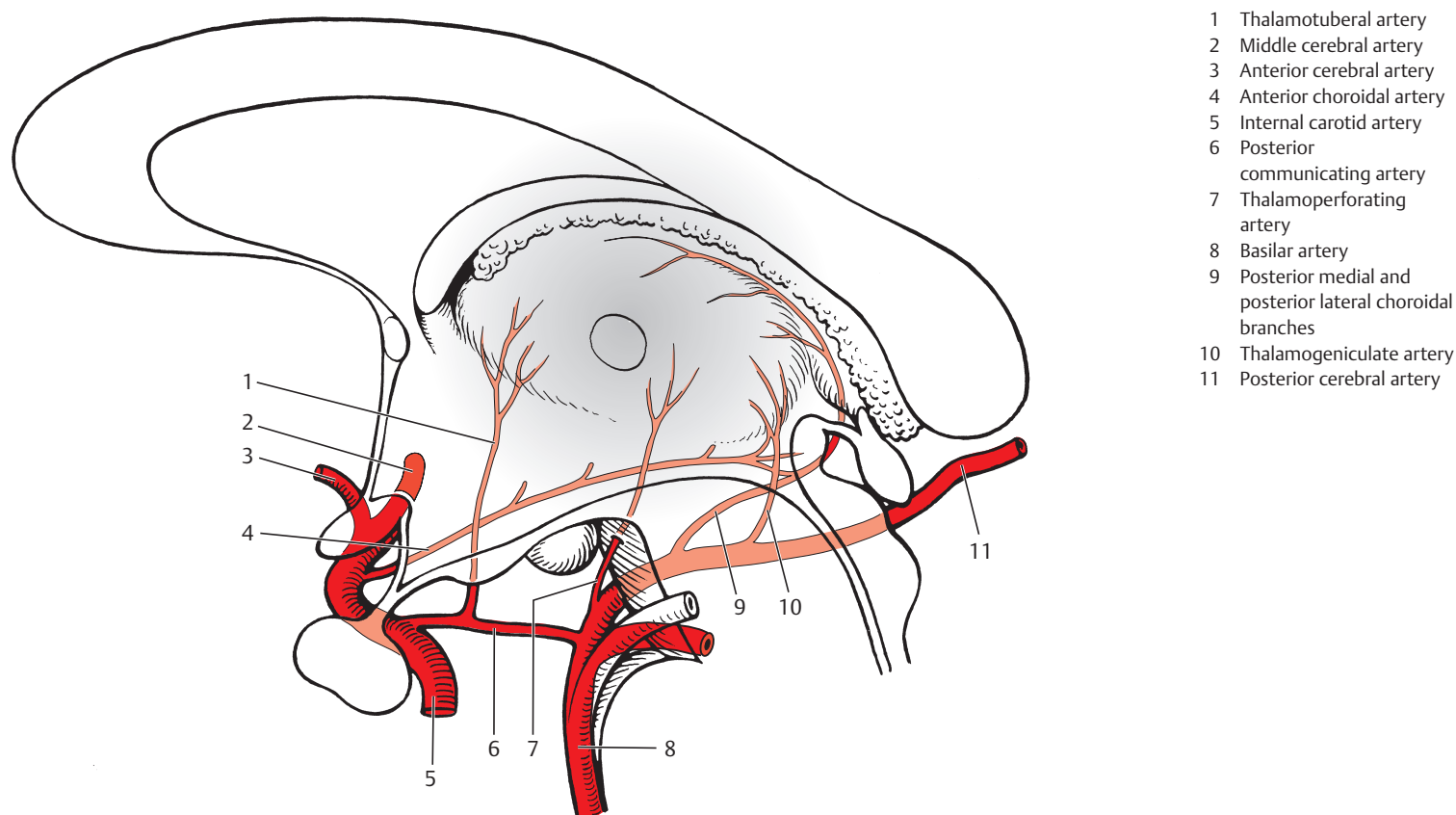


Fig. 7.17 Arterial blood supply of the thalamus. Schematic representation. (Reproduced from Duus.¹⁴⁹)

7.4.4 Arterial Territories of the Brainstem and Cerebellum

► Fig. 7.18 provides an overview of the arterial territories of the medulla oblongata, pons, cerebellum and midbrain. Despite the many **anastomoses** between arteries of the brain,³⁰⁷ sudden interruption of arterial blood supply leads to ischemic brain infarction, since arterial supply through neighboring collaterals usually does not suffice. Distinct arterial territories can be demarcated. The clinical symptoms of an infarct depend on the affected neurofunctional systems. Topographical knowledge of arterial territories and neurofunctional systems is therefore essential for the evaluation of neurovascular disorders.

Arterial Supply of the Brainstem

The arteries supplying the brainstem consist mainly of thin branches which arise directly from the larger arteries and penetrate the surface of the brainstem in three or four zones.^{152,576}

The arteries of the brainstem vascularize the following regions:

- Anteromedial territory
- Anterolateral territory
- Lateral territory
- Posterior territory (mostly)

The posterior territory is absent in the upper third of the medulla oblongata and in the lower two-thirds of the pons. The boundaries of these territories are variable and not identical to those of neurofunctional systems. Long nuclei and wide fiber tracts often lie in the region of two neighboring arterial territories. The medial lemniscus system for instance (see ►Fig. 6.4b [cuneate and gracile nuclei], ►Fig. 6.8b, ►Fig. 6.8c, ►Fig. 6.12b, ►Fig. 6.12c, and ►Fig. 10.5) runs from the medulla oblongata to the midbrain first largely through the posterior, then lateral, anterolateral, and anteromedial territories and, finally, through two territories (anteromedial and lateral; anterolateral and lateral). Injection of dye into the arteries of the brainstem reveals a **marked difference** in these territories as also between the left and right halves of the brainstem of the same brain.¹⁵²

Arterial territories of the medulla oblongata:

penetrating branches of the

- Anteromedial:
Anterior spinal artery
- Anterolateral:
Anterior spinal artery,
Vertebral artery,
Posterior inferior cerebellar artery
- Lateral:
Posterior inferior cerebellar artery
- Posterior:
Posterior spinal artery

Arterial territories of the cerebellum:

- Lateral branch of the posterior inferior cerebellar artery
- Medial branch of the posterior inferior cerebellar artery

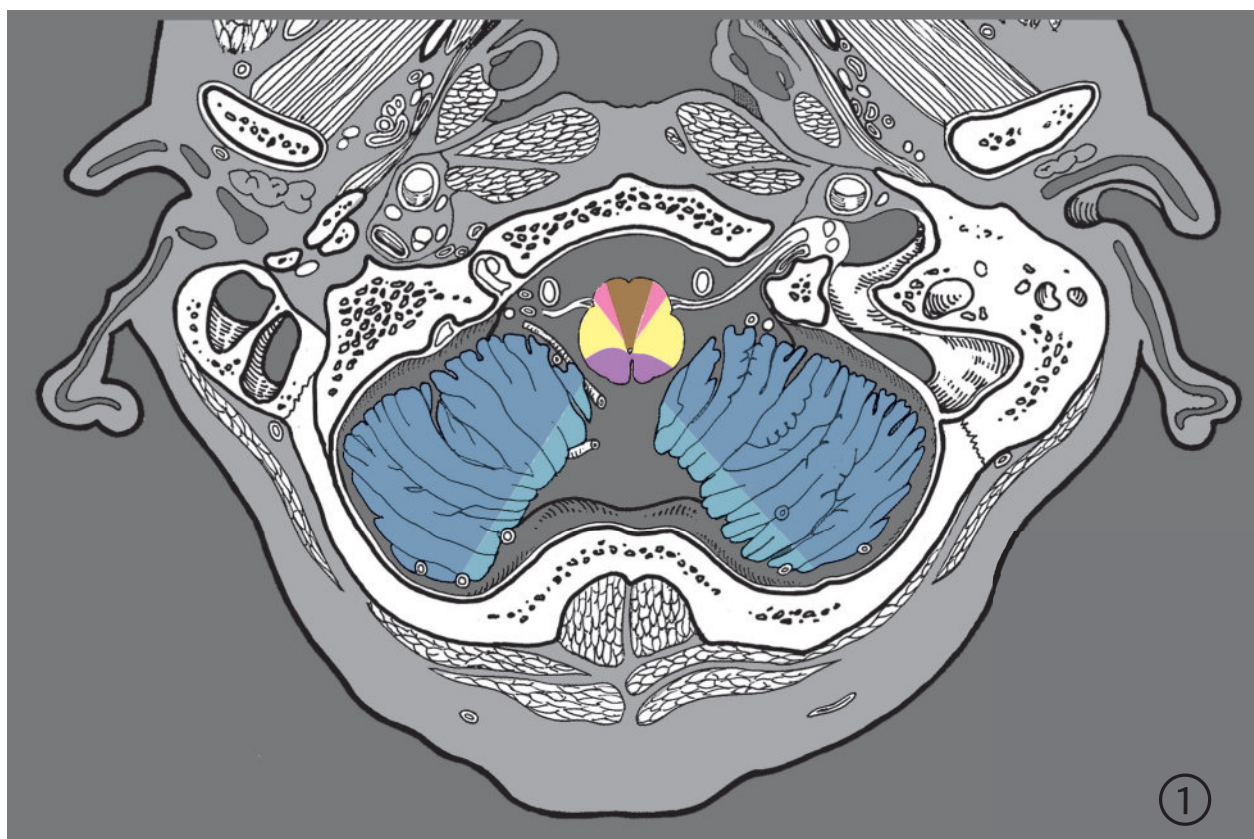


Fig. 7.18 Medulla oblongata, cerebellum, pons, and mid-brain with their arterial territories. (Reproduced from Duvernoy¹⁵² and Tatu et al.⁵⁷⁶) Serial images of the medulla oblongata, cerebellum, pons and the midbrain with their arterial territories oriented perpendicular to the median plane and Meynert's axis. Encircled digits indicate the number of the respective brainstem slice (see ►Fig. 6.4 and ►Fig. 6.13). These images are extracts from ►Fig. 6.4, ►Fig. 6.5, ►Fig. 6.6, ►Fig. 6.7, ►Fig. 6.8, ►Fig. 6.9, ►Fig. 6.10, ►Fig. 6.11, ►Fig. 6.12, and ►Fig. 6.13.

Fig. 7.18a Section 1.

Arterial territories of the medulla oblongata:

Penetrating branches of the

- Anteromedial:
Anterior spinal artery
- Anterolateral:
Anterior spinal artery,
Vertebral artery,
Posterior inferior cerebellar artery
- Lateral:
Posterior inferior cerebellar artery
- Posterior:
Posterior spinal artery

Arterial territories of the cerebellum:

- Lateral branch of the posterior inferior cerebellar artery
- Medial branch of the posterior inferior cerebellar artery

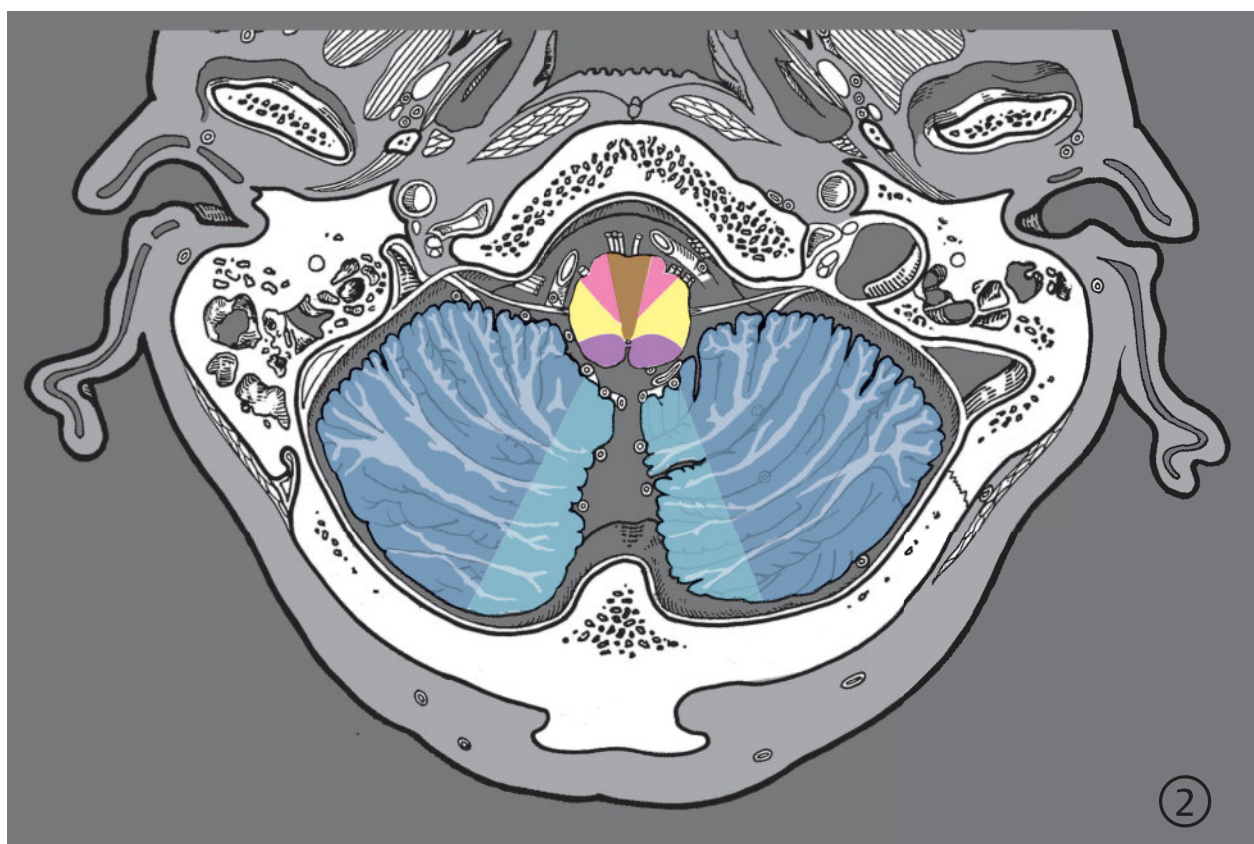


Fig. 7.18b Section 2.

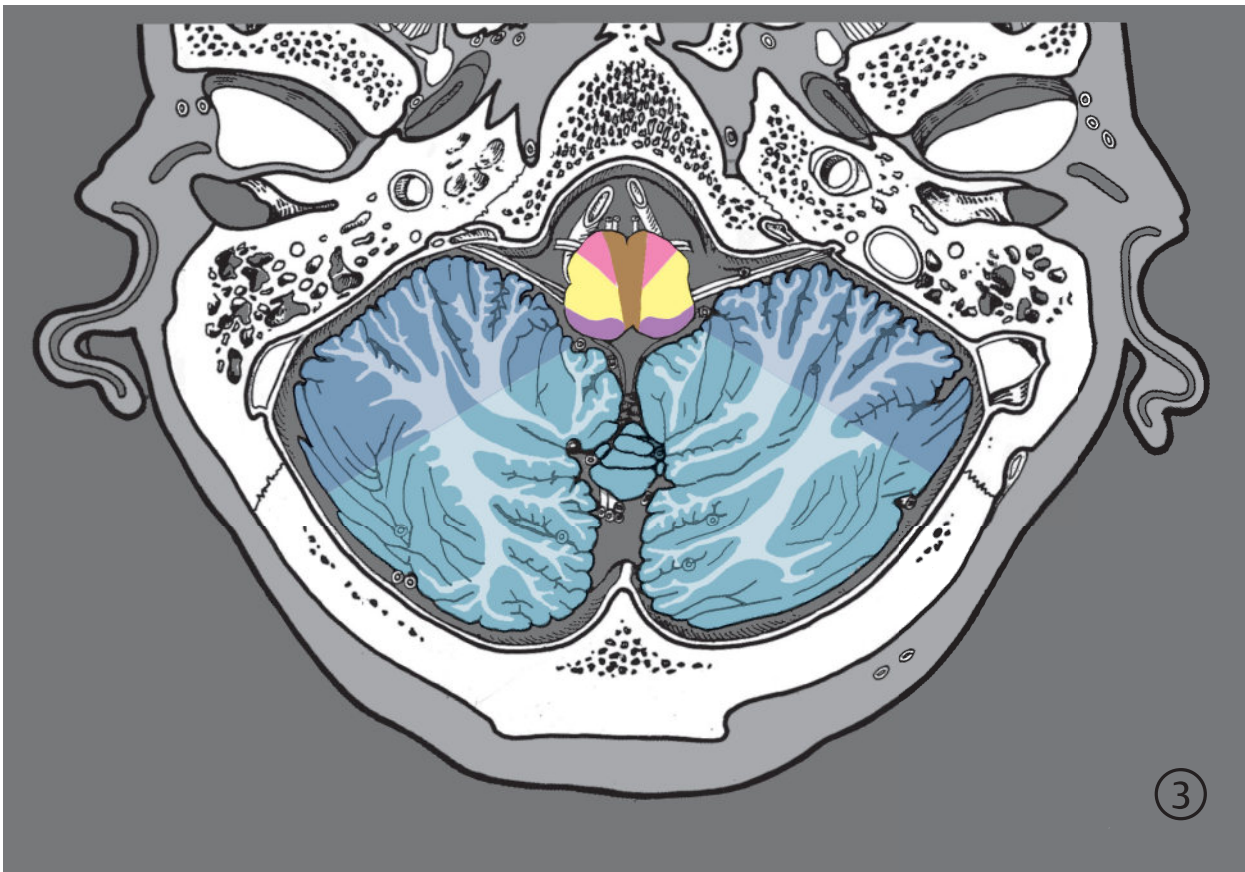


Fig. 7.18c Section 3.

Arterial territories of the medulla oblongata:
Penetrating branches of the

- Anteromedial: Anterior spinal artery
- Anterolateral: Anterior spinal artery, Vertebral artery, Posterior inferior cerebellar artery
- Lateral: Posterior inferior cerebellar artery
- Posterior: Posterior inferior cerebellar artery

Arterial territories of the cerebellum:

- Lateral branch of the posterior inferior cerebellar artery
- Medial branch of the posterior inferior cerebellar artery

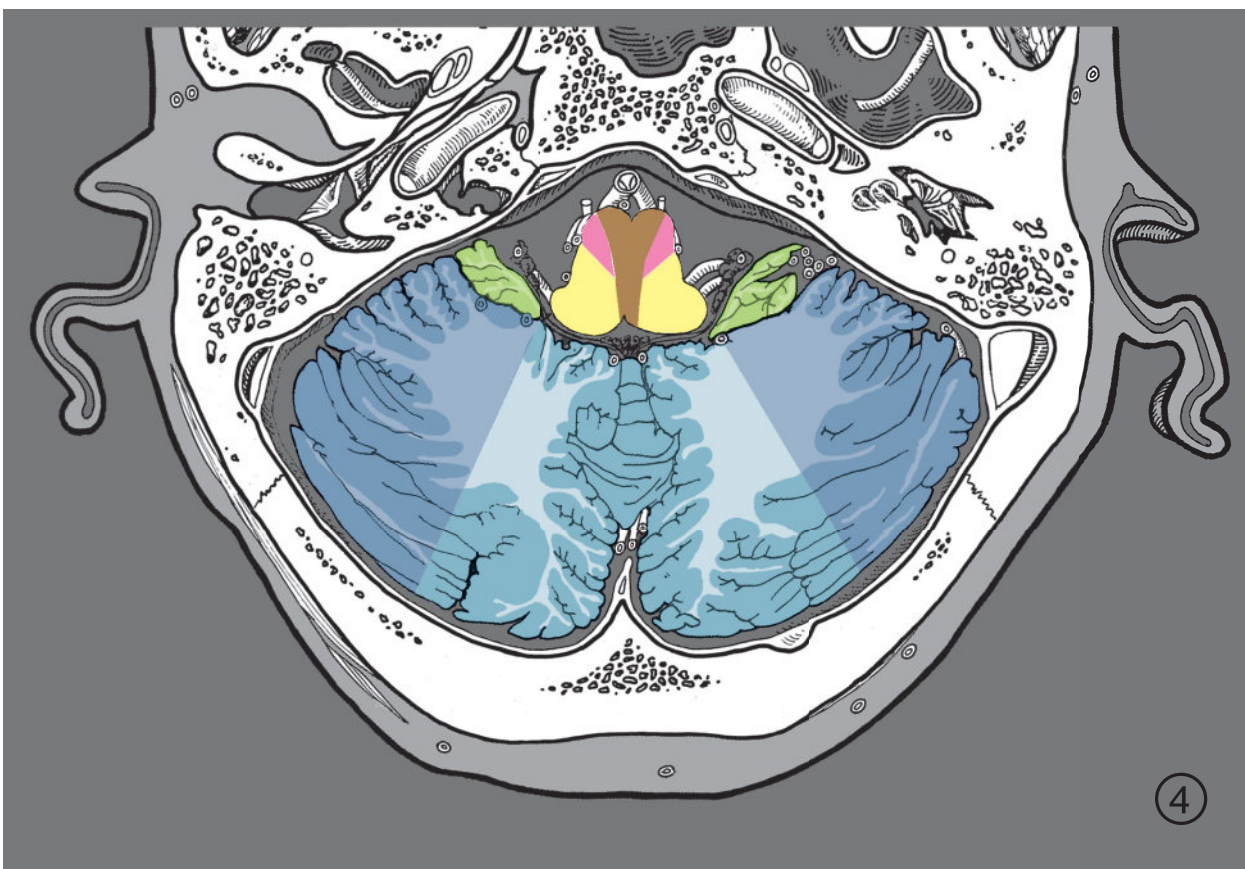


Fig. 7.18d Section 4.

Arterial territories of the medulla oblongata:
Penetrating branches of the

- Anteromedial: Anterior spinal artery
- Anterolateral: Anterior spinal artery, Vertebral artery, Posterior inferior cerebellar artery
- Lateral: Vertebral artery

Arterial territories of the cerebellum:

- Anterior inferior cerebellar artery
- Lateral branch of the posterior inferior cerebellar artery
- Medial branch of the posterior inferior cerebellar artery

Arterial territories of the pons:

Penetrating branches of the

- Anteromedial:
Medial pontine
arteries of the
basilar artery
- Anterolateral:
Lateral pontine
arteries of the basilar
artery
- Lateral:
Lateral pontine
arteries of the basilar
artery, Anterior
inferior cerebellar
artery

Arterial territories of the cerebellum:

- Anterior inferior
cerebellar artery
- Lateral branch of
the superior
cerebellar artery
- Medial branch of the
superior cerebellar
artery
- Medial branch of the
posterior inferior
cerebellar artery

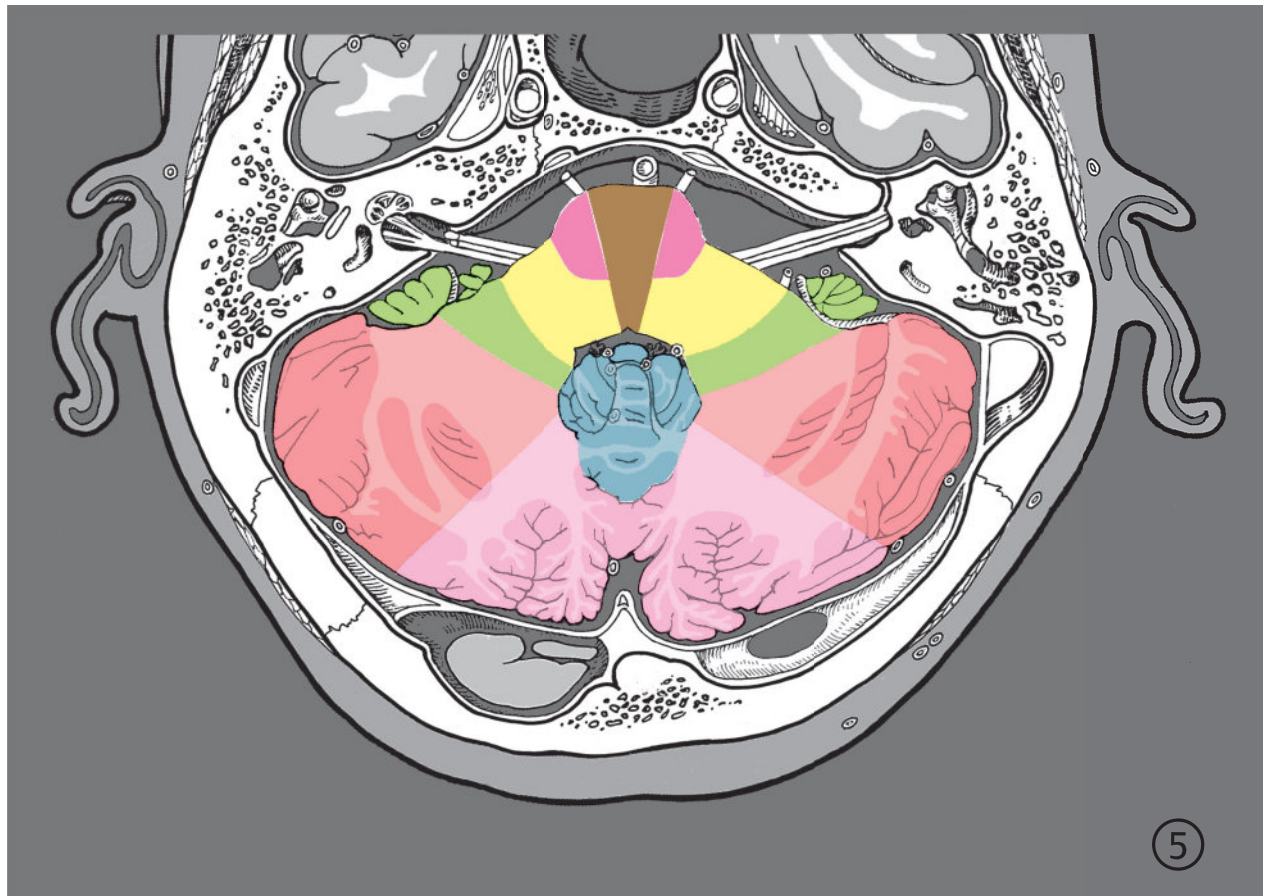


Fig. 7.18e Section 5.

Arterial territories of the pons:

penetrating branches of the

- Anteromedial:
Medial pontine
arteries of the basilar
artery
- Anterolateral:
Lateral pontine
arteries of the basilar
artery
- Lateral:
Lateral pontine
arteries of the basilar
artery, anterior
inferior cerebellar
artery

Arterial territories of the cerebellum:

- Anterior inferior
cerebellar artery
- Lateral branch of the
superior cerebellar
artery
- Medial branch of the
superior cerebellar
artery
- Medial branch of the
posterior inferior
cerebellar artery

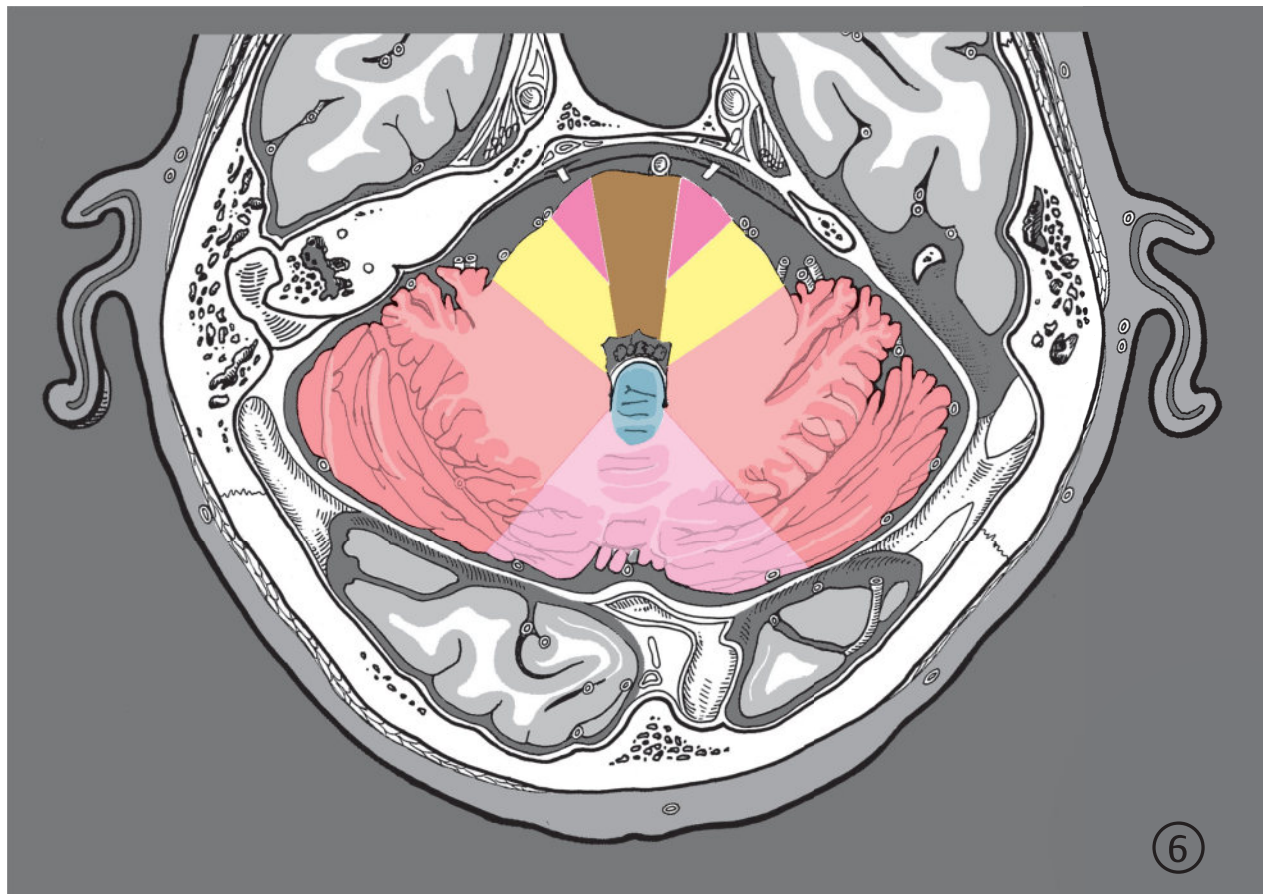
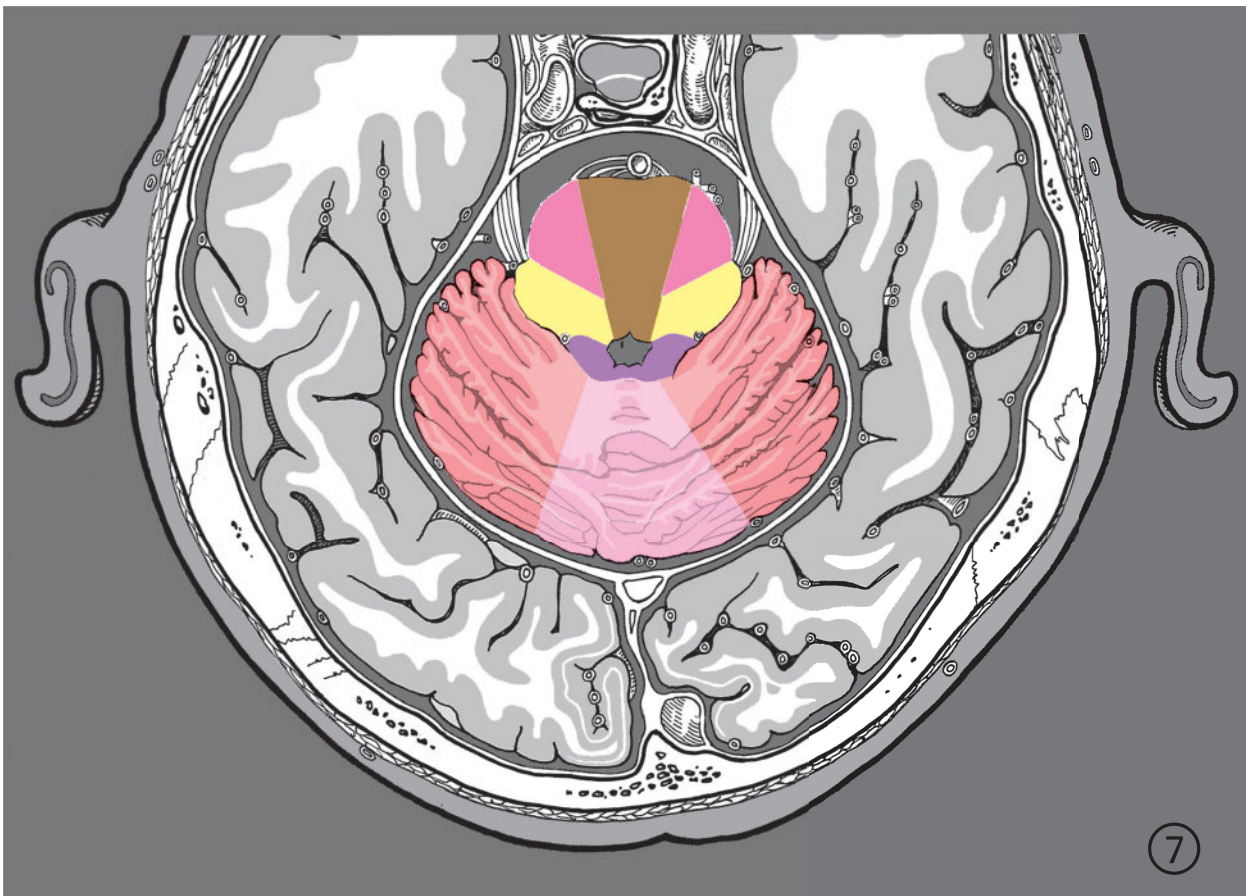


Fig. 7.18f Section 6.



Arterial territories of the pons:

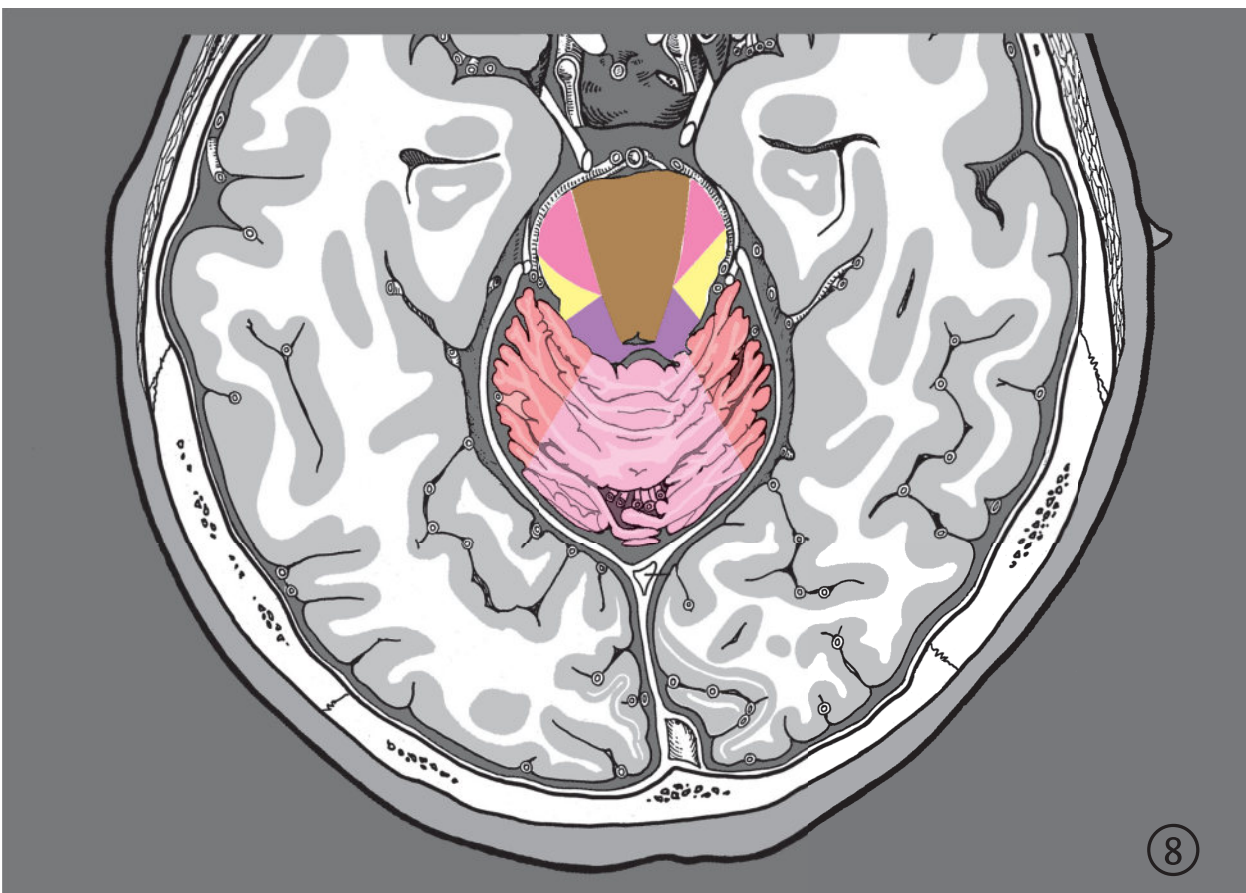
Penetrating branches of the

- Anteromedial: Medial pontine arteries of the basilar artery, Descending branches of the posteromedial central arteries of the posterior cerebral artery from the interpeduncular fossa
- Anterolateral: Lateral pontine arteries from the basilar artery
- Lateral: Pontine branches of the basilar artery
- Posterior: Superior cerebellar artery

Arterial territories of the cerebellum:

- Lateral branch of the superior cerebellar artery
- Medial branch of the superior cerebellar artery

Fig. 7.18g Section 7.



Arterial territories of the pons:

- Anteromedial: Medial pontine arteries of the basilar artery, Descending branches of the posteromedial central arteries of the posterior cerebral artery from the interpeduncular fossa
- Anterolateral: Lateral pontine arteries of the basilar artery
- Lateral: Superior cerebellar artery
- Posterior: Superior cerebellar artery

Arterial territories of the cerebellum:

- Lateral branch of the superior cerebellar artery
- Medial branch of the superior cerebellar artery

Fig. 7.18h Section 8.

Arterial territories of the midbrain:
penetrating branches of the—

- Anteromedial:
Posteromedial
central arteries of
the posterior
cerebral artery
- Anterolateral:
Collicular artery and
medial posterior
choroidal arteries
of the posterior
cerebral artery
- Lateral:
Collicular artery of
the posterior
cerebral artery
- Posterior:
Collicular artery of
the posterior
cerebral artery,
superior cerebellar
artery

Arterial territories
of the cerebellum:

- Lateral branch of
the superior
cerebellar artery
- Medial branch of
the superior
cerebellar artery

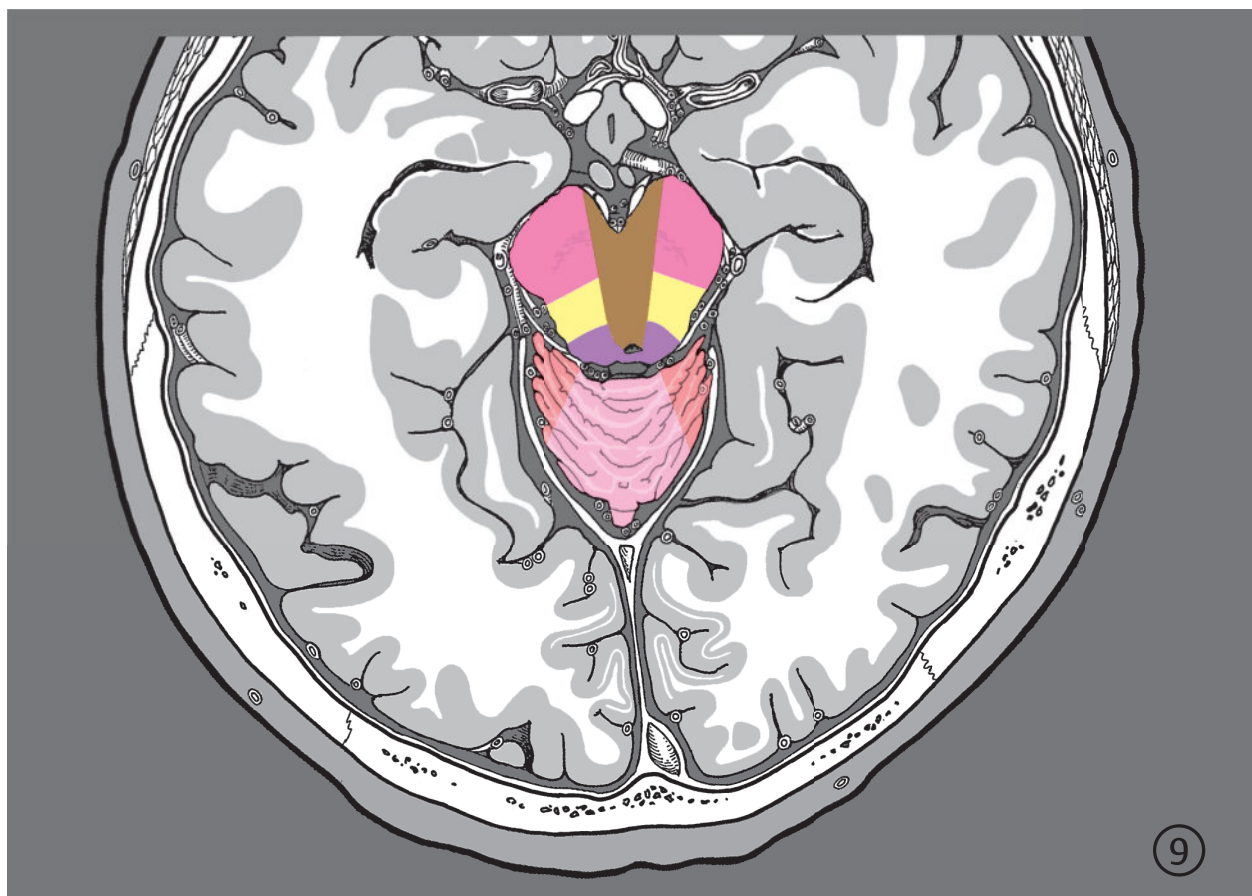


Fig. 7.18i Section 9.

Arterial territories of the
Midbrain:
Penetrating branches of the—

- Anteromedial:
Posteromedial
central arteries of
the Posterior
cerebral artery
- Anterolateral:
Collicular artery
and medial
posterior choroidal
arteries of the
posterior cerebral
artery
- Lateral:
Collicular artery
of the posterior
cerebral artery
- Posterior:
Collicular artery of
the posterior
cerebral artery,
superior cerebellar
artery

Arterial territories of the
cerebellum:

- Medial branch of
the superior
cerebellar artery

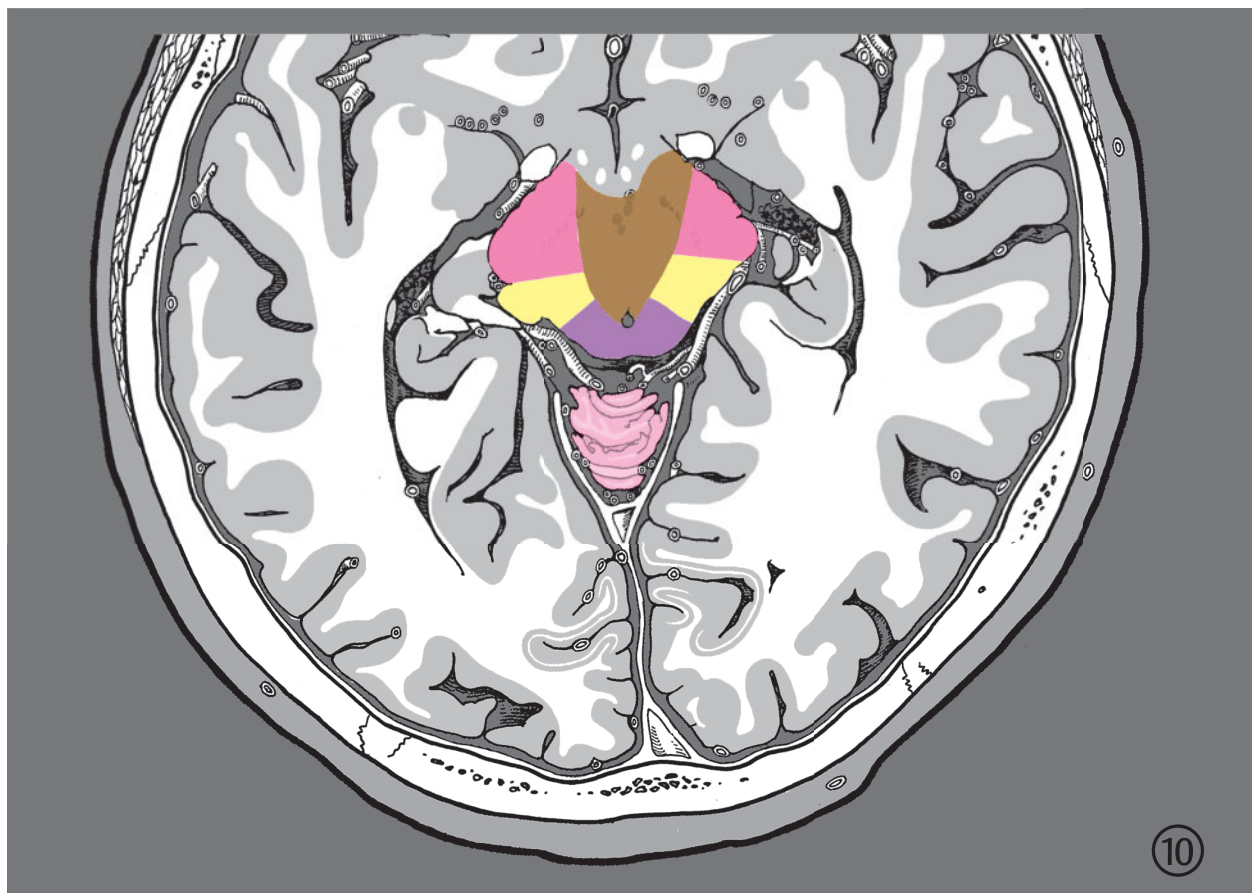


Fig. 7.18j Section 10.

Arterial Supply of the Medulla Oblongata

The medulla oblongata is mainly supplied by the branches from the anterior spinal, vertebral, posterior inferior cerebellar, and posterior spinal arteries. Thin branches of the basilar artery and the AICA vascularize a small lateral part of the medulla oblongata close to the pontomedullary junction.

Thin branches of the anterior spinal artery penetrate the surface of the medulla oblongata immediately adjacent to the anterior median fissure and then ramify in the **anteromedial territory**. Branches of the vertebral artery also supply the anteromedial territory in the upper fourth of the medulla oblongata. It contains the medial part of corticospinal fibers (see ►Fig. 6.4b, ►Fig. 6.5b, ►Fig. 6.6b, and ►Fig. 6.7b), the largest part of the medial lemniscus (see ►Fig. 6.5b, ►Fig. 6.6b, and ►Fig. 6.7b), the medial longitudinal fasciculus (see ►Fig. 6.4b, ►Fig. 6.5b, ►Fig. 6.6b, and ►Fig. 6.7b), as well as the largest part of the hypoglossal nucleus (see ►Fig. 6.5b and ►Fig. 6.6b) and the prepositus nucleus (see ►Fig. 6.7b). The **anterolateral territory** is vascularized by branches of the anterior spinal, vertebral, and PICAs. This territory includes the lateral part of corticospinal fibers (see Fig. 6.4b, ►Fig. 6.5b, ►Fig. 6.6b, and ►Fig. 6.7b), a small part of the medial lemniscus, medial parts of the inferior olivary nucleus (see Fig. 6.5b, ►Fig. 6.6b, and ►Fig. 6.7b) and the reticular formation. The **lateral territory** is supplied by the penetrating branches of the posterior inferior cerebellar and vertebral arteries. The spinothalamic (see ►Fig. 6.5b and ►Fig. 6.6b) and anterior spinocerebellar tracts (see ►Fig. 6.5b and ►Fig. 6.6b), small parts of the hypoglossal and vagal nuclei, a part of the nucleus of the solitary tract, the lateral part of the inferior olive, as well as roots of the glossopharyngeal nerve and vagus nerve belong to this territory. The anterior and posterior cochlear nuclei (see ►Fig. 6.7b) as well as the medial and inferior vestibular nuclei (see ►Fig. 6.7b) lie in the lateral territory of the upper part of the medulla oblongata.

The **posterior territory** is mainly vascularized by the posterior spinal artery. The gracile and cuneate nuclei, nucleus of the solitary tract, and the vagal nucleus lie in the lower part of the medulla oblongata (closed part with central canal). The area postrema, vagal nucleus and the nucleus of the solitary tract lie in the center of the medulla oblongata. The upper part of the medulla oblongata lacks a posterior territory bilaterally.

Arterial Supply of the Pons

The pons is mainly vascularized by branches of the basilar artery, the AICA, and the superior cerebellar artery. Three arterial territories are identifiable on each side in the middle and inferior parts of the pons, where the

rhomboid fossa is very wide: anteromedian, anterolateral, and lateral. A posterior territory is additionally present in the superior part of the pons.

The **anteromedial territory** is supplied by the medial pontine arteries of the basilar artery, which chiefly penetrate the surface of the basilar sulcus. On a pontine cross-section, the anteromedial territory appears as a paramedian strip extending from the basilar sulcus to the floor of the IVth ventricle, containing medial parts of the corticospinal tracts (see ►Fig. 6.8b, ►Fig. 6.9b, and ►Fig. 6.10b) as well as the medial lemniscus (see ►Fig. 6.8b, ►Fig. 6.9b, and ►Fig. 6.10b), extending into the inferior aspect of the pons to the abducens nucleus.

Periventricular areas of this territory in the inferior aspect of the pons are supplied by fine arteries which penetrate the foramen cecum before ascending further. Fine arteries descend through the interpeduncular fossa in the superior part of the pons to reach the periventricular zone of the anteromedial territory. Should these ascending and descending arteries remain patent in the presence of an anteromedial infarct, the floor of the IVth ventricle will remain unaffected by the ischemic process.¹⁵²

The **anterolateral territory** is related to the anteromedial territory at its lateral aspect and is confined to the basal part of the pons, away from the pontine tegmentum. This territory contains the lateral part of the corticospinal tract.

The **lateral territory** varies considerably in size and form, being larger in the inferior and central parts of the pons and smaller or absent in its superior part. It contains lateral parts of the anterior aspect of the pons and the tegmentum of pons. Present here are the roots of the trigeminal nerve (see ►Fig. 6.10b), parts of the motor and sensory nuclei of the trigeminal nerve (see ►Fig. 6.9b) as well as the lateral lemniscus, the superior olivary nucleus (see ►Fig. 6.8b), and the facial nucleus (see ►Fig. 6.8b).

The **posterior territory** in the superior portion of the pons is composed of parts of the superior cerebellar peduncle, the mesencephalic nucleus of the trigeminal nerve (see ►Fig. 6.10b), and the locus caeruleus (see ►Fig. 5.7 and ►Fig. 6.11b).

Arterial Supply of the Midbrain

Branches from the proximal (precommunicating) part of the posterior cerebral artery supply mainly the midbrain, together with the anterior choroidal artery and fine branches of the superior cerebellar artery.¹⁵² The short precommissural branches of the posterior cerebral artery, the posteromedial central arteries, penetrate the interpeduncular fossa to supply the **anteromedial territory**, where the oculomotor nucleus (see ►Fig. 6.13b), trochlear nucleus (see ►Fig. 6.12b), red nucleus (see ►Fig. 6.13b), and medial parts of the substantia nigra (see ►Fig. 6.12b and ►Fig. 6.13b) are located.

The **anterolateral territory** is supplied by the longer branches of the posterior cerebral artery, namely, the collicular artery and the posterior medial choroidal arteries. The cerebral crus with the corticospinal tract (see ►Fig. 6.12b and ►Fig. 6.13b), large parts of the substantia nigra (see ►Fig. 6.12b and ►Fig. 6.13b), and parts of the medial lemniscus (see ►Fig. 6.12b) lie in this region.

The **lateral territory**, which contains parts of the medial lemniscus, is supplied by the collicular artery and in the superior part of the midbrain by the anterior choroidal artery (see ►Fig. 6.12b and ►Fig. 6.13b).

The **posterior territory** is supplied mainly by the collicular and superior cerebellar arteries. This area corresponds roughly to the tectal plate with the inferior and superior colliculi (see ►Fig. 6.12 and ►Fig. 6.13b).

Arterial Supply of the Cerebellum

The cerebellum is supplied by three long arteries:

- Posterior inferior cerebellar artery (see ►Fig. 7.13a)
- Anterior inferior cerebellar artery (see ►Fig. 7.13a)
- Superior cerebellar artery (see ►Fig. 7.13a)

Cerebellar arterial supply is highly variable, as described in the introduction to Section 7.4 and in Section 7.4.1, in Section 7.4.2, and in Section 7.4.3; right-left asymmetry is not uncommon. Color-coded territories (see ►Fig. 7.18) may therefore only serve as a rough guide.

The **posterior inferior cerebellar artery** divides into a medial and a lateral branch, supplying the inferior aspect of the vermis and the inferior and posterior surfaces of the cerebellar hemispheres (see ►Fig. 7.14a).

The **anterior inferior cerebellar artery** supplies the middle cerebellar peduncle, the flocculus, the posterior quadrangular lobule [H VI] and the superior and inferior semilunar lobules (H VIIA) (see ►Fig. 7.14a).

The marked reciprocal variability of the posterior and AICAs has already been referred to above. If an artery supplies a smaller territory, the rest of the vascular supply is taken over by the other artery.

The **superior cerebellar artery** is the most constant of the three cerebellar arteries.

This artery consists of a medial and a lateral branch and vascularizes the upper half of the cerebellar hemisphere, the superior cerebellar vermis, and primarily the dentate nucleus.

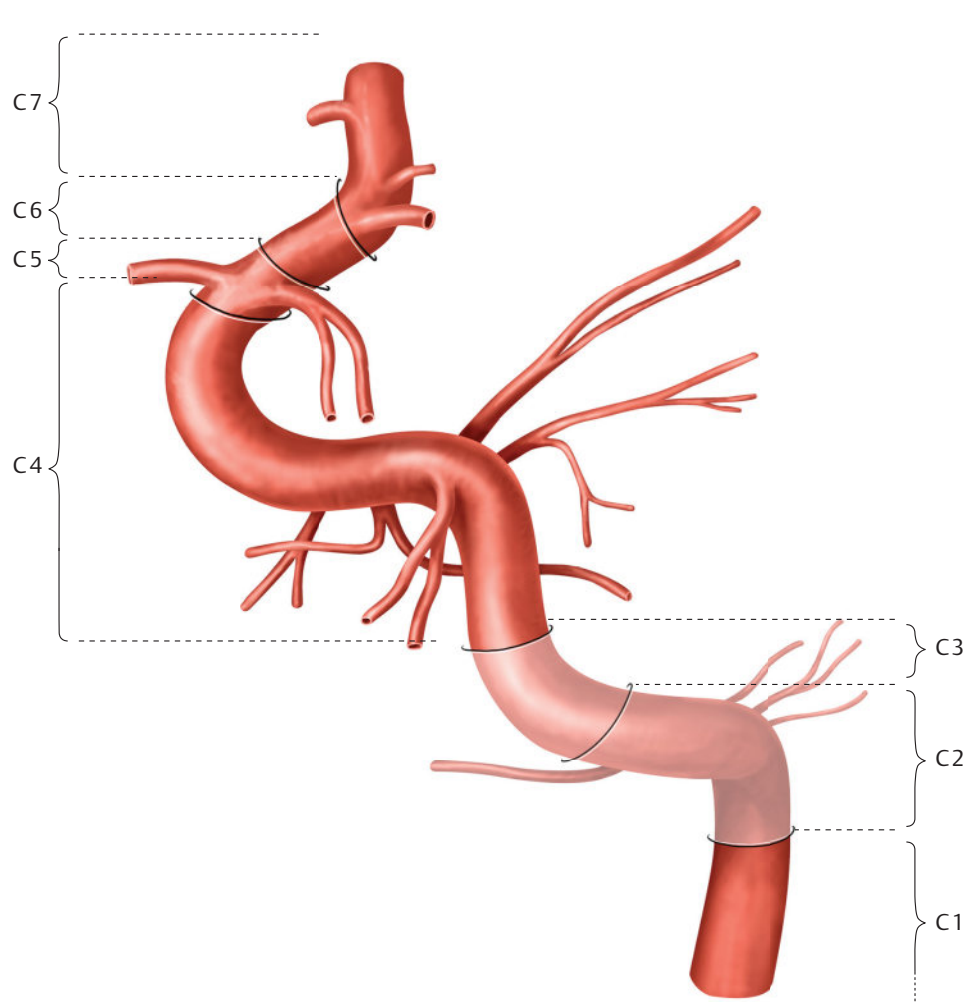
All three cerebellar arteries are involved in supplying the brainstem.

Clinical Notes

A unilateral lesion of the anteromedial and anterolateral territories of the medulla oblongata results in crossed paralyses. The motor neurons of the cranial nerves on the side of the lesion are affected, resulting in ipsilateral motor paralysis. The pyramidal tract is furthermore interrupted proximal to its decussation resulting in a contralateral hemiparesis. A unilateral lesion of the lateral medulla oblongata causes Wallenberg's syndrome with "crossed" disorders of pain and temperature sensation. Pain and temperature sensations from the ipsilateral side of the face are lost due to involvement of the spinal nucleus of the trigeminal nerve. An interruption of the spinothalamic tract (above the decussation) results in impaired pain and temperature transmission in the contralateral arm, trunk, and leg regions. A disorder of the vestibular system and the spinocerebellar tract causes vertigo, vomiting, nausea, nystagmus, and ipsilateral ataxia. A lesion of the IXth and Xth cranial nerves may result in dysphagia and hoarseness. An ipsilateral Horner's syndrome is usually present. Cerebellar infarcts are not as uniformly distributed as are cerebral infarcts due to the variable nature of the arterial supply of the cerebellum.²⁷²

7.4.5 Internal Carotid Artery

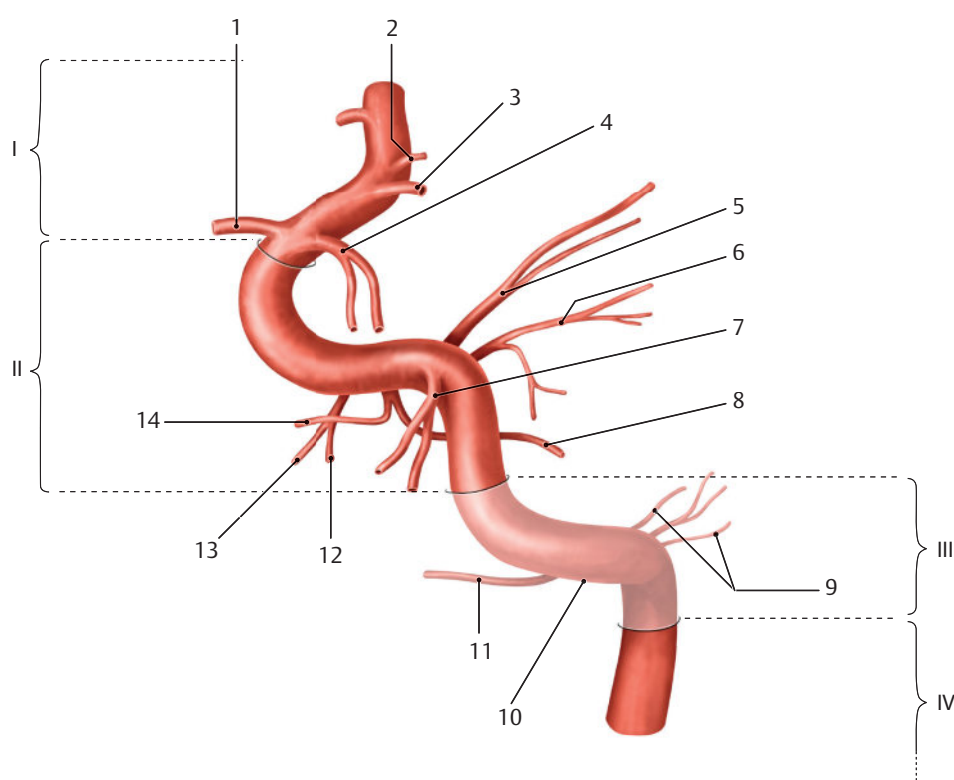
The internal carotid artery (see ►Fig. 7.19, see also ►Fig. 3.8c, ►Fig. 4.3c, ►Fig. 4.4c, ►Fig. 5.4, ►Fig. 5.18, ►Fig. 7.24, and ►Fig. 9.1) enters the base of the skull through the carotid canal in the petrous part of the temporal bone (C2 segment).⁶⁴ Running vertically at first, the artery then bends sharply in an anteromedial direction (C3 segment), penetrating the cavernous sinus in an anterior and vertical direction (C4 segment) (see ►Fig. 3.7c, ►Fig. 4.3c, ►Fig. 4.3d, ►Fig. 5.5, and ►Fig. 7.19). It then turns anteriorly, ascending under the anterior clinoid process where it turns posteriorly and forms an anteriorly directed convex arch, the carotid genu, which gives rise at its distal aspect to the ophthalmic artery (C5 segment). The intracavernous section of the internal carotid artery is mostly referred to as the juxtaseellar segment.³⁰⁷ Passing posteriorly through the dura and the arachnoid, the internal carotid artery enters the subarachnoid space (C6 segment). This subarachnoid part of the artery averages 13 mm in length, ranging from 8 to 18 mm,³³² ascending thereafter (C7 segment) up to its division into its terminal branches (see ►Fig. 7.21 and ►Fig. 7.26), the anterior cerebral artery see ►Fig. 3.6c, ►Fig. 3.6d, ►Fig. 4.2c, and ►Fig. 5.7) and the middle



- C1 cervical segment
- C2 petrous segment
- C3 foramen lacerum segment
- C4 cavernous segment
- C5 clinoid segment
- C6 ophthalmic segment
- C7 terminal segment

Fig. 7.19 Internal carotid artery. (Reproduced from Schuenke, Schulte, and Schumacher, Atlas of Anatomy, 2nd edition, ©2009, Thieme Publishers, Stuttgart. Illustration by Karl Wesker/Markus Voll.⁵³⁵)

Fig. 7.19a Classification into segments after Bouthillier et al.⁶⁴



- 1 Ophthalmic artery
- 2 Anterior choroidal artery
- 3 Posterior communicating artery
- 4 Superior hypophyseal artery
- 5 Basal tentorial branch
- 6 Marginal tentorial branch
- 7 Inferior hypophyseal artery
- 8 Trigeminal ganglion branch
- 9 Caroticotympanic arteries
- 10 Carotid canal
- 11 Artery of pterygoid canal
- 12 Cavernous sinus branch
- 13 Meningeal branch
- 14 Branches to nerves
- I Cerebral part
- II Cavernous part
- III Petrous part
- IV Cervical part

Fig. 7.19b Classification of branches.

- 1 Posterior communicating artery
- 2 Primitive trigeminal artery
- 3 Otic artery
- 4 Hypoglossal artery
- 5 Proatlantal intersegmental artery
- 6 First cervical vertebra
- 7 Second cervical vertebra
- 8 Third cervical vertebra
- 9 Clivus
- 10 Internal carotid artery
- 11 Vertebral artery

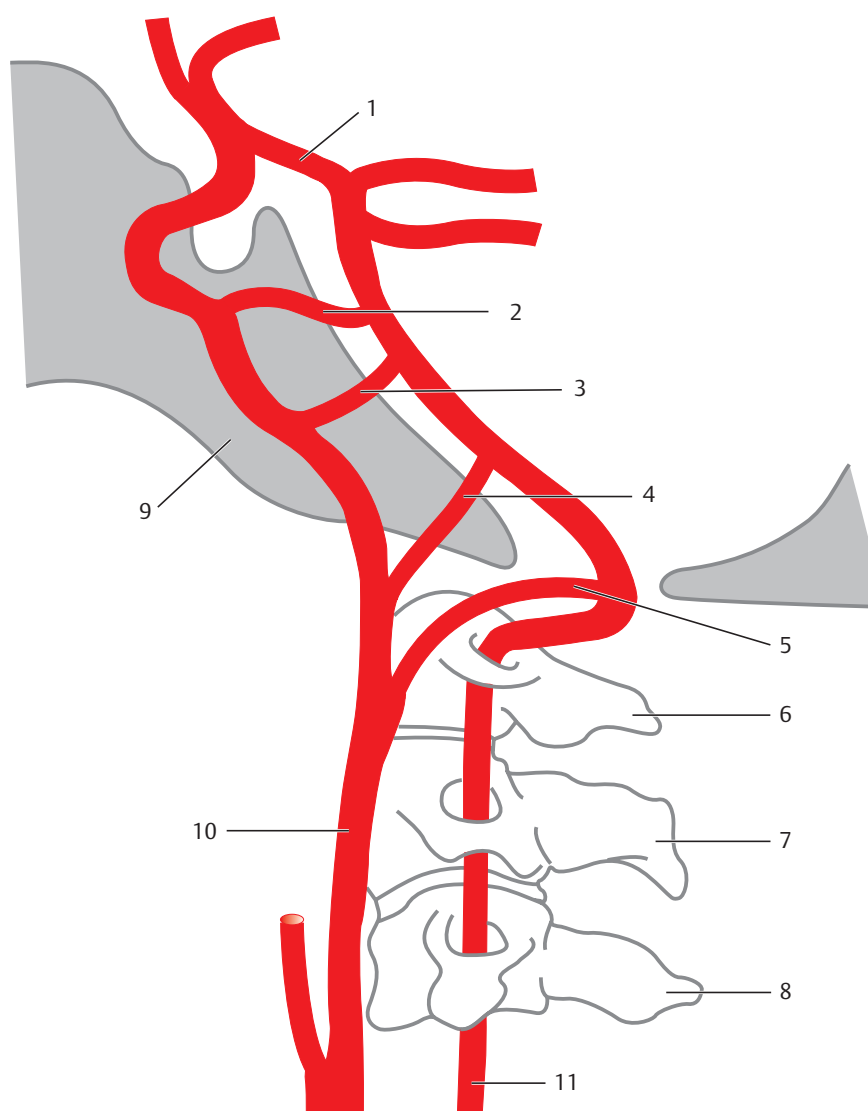


Fig. 7.20 Possible carotid-basilar anastomoses. Schematic representation. (Reproduced from Schild.⁵¹⁸)

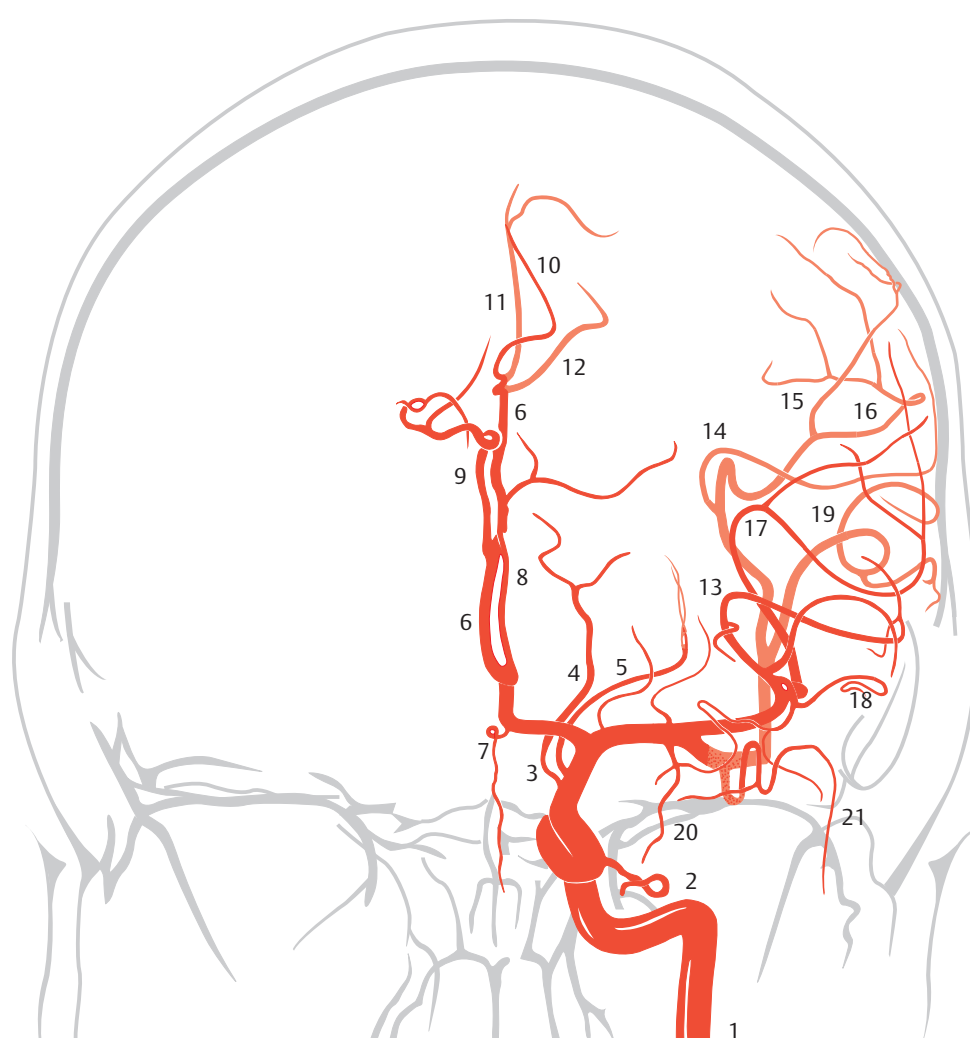
cerebral artery (see ►Fig. 3.6b, ►Fig. 3.6c, ►Fig. 3.7c, ►Fig. 4.4c, ►Fig. 5.6a, and ►Fig. 5.6b). Direct branches of the internal carotid artery supply the optic chiasm, the pituitary stalk, the anterior lobe of the pituitary gland, as well as small areas of the hypothalamus, the genu of the internal capsule, occasionally the globus pallidus and anterior parts of the thalamus (see ►Fig. 7.17 and ►Fig. 7.19b).³³³ During human embryological development, several connections develop between the internal carotid artery and the vertebrobasilar region. Some of these embryological connections may persist as variants (see ►Fig. 7.20), the knowledge of which is important in avoiding complications during interventional neuroradiological procedures, e.g., during embolization.

The **posterior communicating artery** (see ►Fig. 7.20, see also ►Fig. 5.6b and ►Fig. 7.19b) arises from the internal carotid artery in the region between the sella turcica and the tuber cinereum (see ►Fig. 4.2d) of the diencephalon, and runs in an occipital direction along the superior edge of the tentorium. The artery is absent in about 1% of cases.

A **fetal type** is present in 10% of cases, whereby the posterior communicating artery has such a large lumen that the posterior cerebral artery receives its blood flow

predominantly from the internal carotid artery through the posterior communicating artery.³³² Branches of the posterior communicating artery supply the optic chiasm, parts of the optic tract, hypothalamus, mammillary body, tuber cinereum, parts of the thalamus between the interthalamic adhesion and the interventricular foramen, cerebral peduncles, and the tail of the caudate nucleus.

The **anterior choroidal artery** almost always arises from the internal carotid artery distal to the origin of the posterior communicating artery and about 3 mm proximal to the bifurcation of the internal carotid artery.³³² Rarely, the anterior choroidal artery arises from the posterior communicating artery. Approximately 25 mm long, the anterior choroidal artery runs between the optic tract and the parahippocampal gyrus, enters the interpeduncular cistern, and passes through the ambient cistern to the tip of the temporal horn of the lateral ventricle into the choroid plexus. It also supplies parts of the telencephalon, diencephalon, and midbrain. Fine branches of the anterior choroidal artery reach the uncus of the parahippocampal gyrus, the amygdaloid body, the internal aspect of the globus pallidus, as well as the posterior limb of the internal capsule through which the corticonuclear and corticospinal tracts run.



- 1 Internal carotid artery
- 2 Ophthalmic artery
- 3 Posterior communicating artery
- 4 Posterior cerebral artery
- 5 Anterior choroidal artery
- 6 Pericallosal artery
- 7 Fronto-orbital artery
- 8 Frontopolar artery
- 9 Anterior internal frontal artery
- 10 Middle internal frontal artery
- 11 Posterior internal frontal artery
- 12 Superior internal parietal artery
- 13 Prefrontal arteries
- 14 Prerolandic artery
- 15 Anterior parietal artery
- 16 Posterior parietal artery
- 17 Artery of angular gyrus
- 18 Middle temporal artery
- 19 Posterior temporal artery
- 20 Temporopolar artery
- 21 Anterior temporal artery

Fig. 7.21 Course of anterior cerebral circulation arteries. Schematic representation of Towne's projection. (Reproduced from Krayenbühl et al.³⁰⁷)

7.4.6 Anterior Cerebral Artery

The anterior cerebral artery (see ►Fig. 3.5c, ►Fig. 3.5d, ►Fig. 4.2b, ►Fig. 4.2c, ►Fig. 4.2d, ►Fig. 5.7, ►Fig. 5.23, and ►Fig. 7.24) arises with the middle cerebral artery from the terminal bifurcation of the internal carotid artery. This bifurcation lies in the cleft between the optic chiasm and the temporal pole of the temporal lobe at approximately the level of the anterior clinoid process.

Aplasia of the anterior cerebral artery occurs rarely (less than 1% of cases).³³²

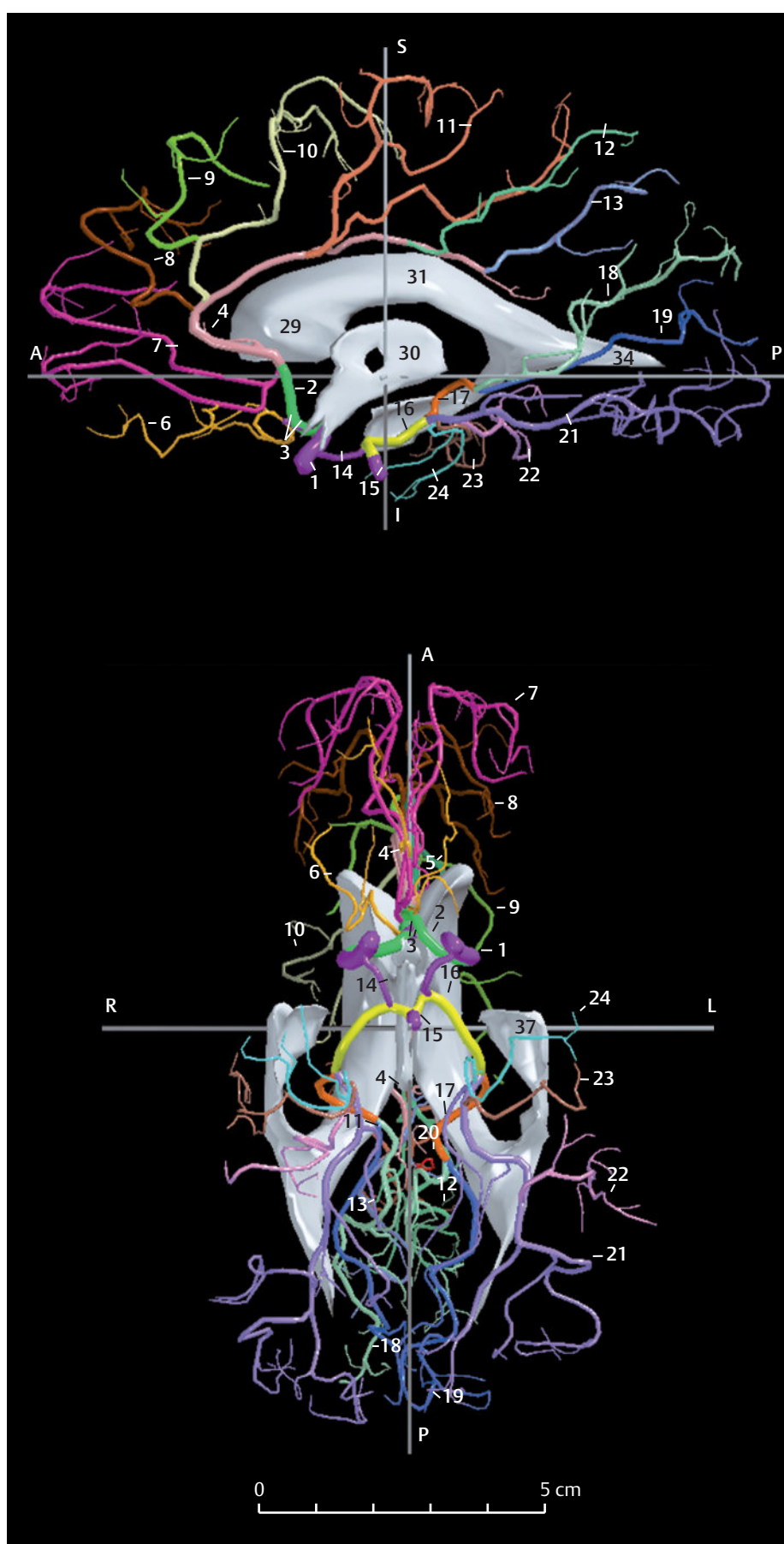
The anterior cerebral artery curves anteromedially after its origin and then lies above the optic nerve. Its initial precommunicating part or A1 segment averages 14 mm in length³³² and extends up to the anterior communicating artery. The second postcommunicating part or A2 segment begins distal to the anterior communicating artery (see ►Fig. 4.2c).

Several short central arteries arise from the **precommunicating part** of the anterior cerebral artery and penetrate the anterior perforated substance (see ►Fig. 7.23). The long central artery (**recurrent artery of Heubner**)

generally arises from the postcommunicating part and in only 10% from the precommunicating part.³³³ This penetrating artery and the anteromedial (central medial lenticulostriate) arteries supply the lamina terminalis, anterior commissure, anterior parts of the hypothalamus, occasionally the anterior tubercle of thalamus, anterior limb and genu of the internal capsule, anterior part of the globus pallidus, and the anteroinferior aspect of the head of the caudate nucleus.

Branches from the **postcommunicating part** of the anterior cerebral artery pass into the cerebral cortex. The medial frontobasal artery (see ►Fig. 3.4c, ►Fig. 4.2c, ►Fig. 4.2d, ►Fig. 5.6a, ►Fig. 7.22, and ►Fig. 7.24) arises in the region of the subcallosal area and supplies the medial aspect of the orbital part of the frontal lobe. The polar frontal artery (see ►Fig. 5.7) passes obliquely in an anterior direction toward the frontal pole and is used as a reference point in the interpretation of angiograms. The horizontal terminal part of the anterior cerebral artery is known as the pericallosal artery (see ►Fig. 3.5c, ►Fig. 3.5d, ►Fig. 3.7c, ►Fig. 3.7d, ►Fig. 4.2c, ►Fig. 4.2d, ►Fig. 5.9a, ►Fig. 5.9b, and ►Fig. 7.24).⁴⁸⁶

- 1 Terminal part of internal carotid artery (dark violet)
- 2 Anterior cerebral artery (green)
- 3 Anterior communicating artery (dark violet)
- 4 Pericallosal artery (pink)
- 5 Callosomarginal artery (dark green), only present in left hemisphere
- 6 Medial frontobasal artery (ocher)
- 7 Polar frontal artery (red-violet)
- 8 Anteromedial frontal artery (brown)
- 9 Intermediomedial frontal artery (light green)
- 10 Posteromedial frontal artery (yellow-green)
- 11 Paracentral artery (light orange)
- 12 Superior precuneal artery (blue-green)
- 13 Inferior precuneal artery (light blue)
- 14 Posterior communicating artery (dark violet)
- 15 Terminal part of basilar artery (dark violet)
- 16 Posterior cerebral artery (yellow)
- 17 Medial occipital artery (orange)
- 18 Parieto-occipital artery (light turquoise)
- 19 Calcarine artery (blue)
- 20 Posterior pericallosal artery (red), only present in left hemisphere
- 21 Lateral occipital artery (mauve)
- 22 Posterior inferior temporal artery (light violet)
- 23 Middle inferior temporal artery (light brown)
- 24 Anterior inferior temporal artery (turquoise)
- 29 Frontal (anterior) horn of lateral ventricle
- 30 Third ventricle
- 31 Central part (body) of lateral ventricle



- 34 Occipital (posterior) horn of lateral ventricle
- 37 Temporal (inferior) horn of lateral ventricle

Fig. 7.22 Anterior cerebral artery with the Circle of Willis and posterior cerebral artery. Circle of Willis, anterior cerebral artery and the posterior cerebral artery with their terminal branches within the bicommissural coordinate system. CT images

A = anterior R = right S = superior
P = posterior L = left I = inferior

Fig. 7.22a Median view of right-sided arteries with the right lateral and third ventricles (above). Inferior view of bilateral arteries with lateral and third ventricles (below).

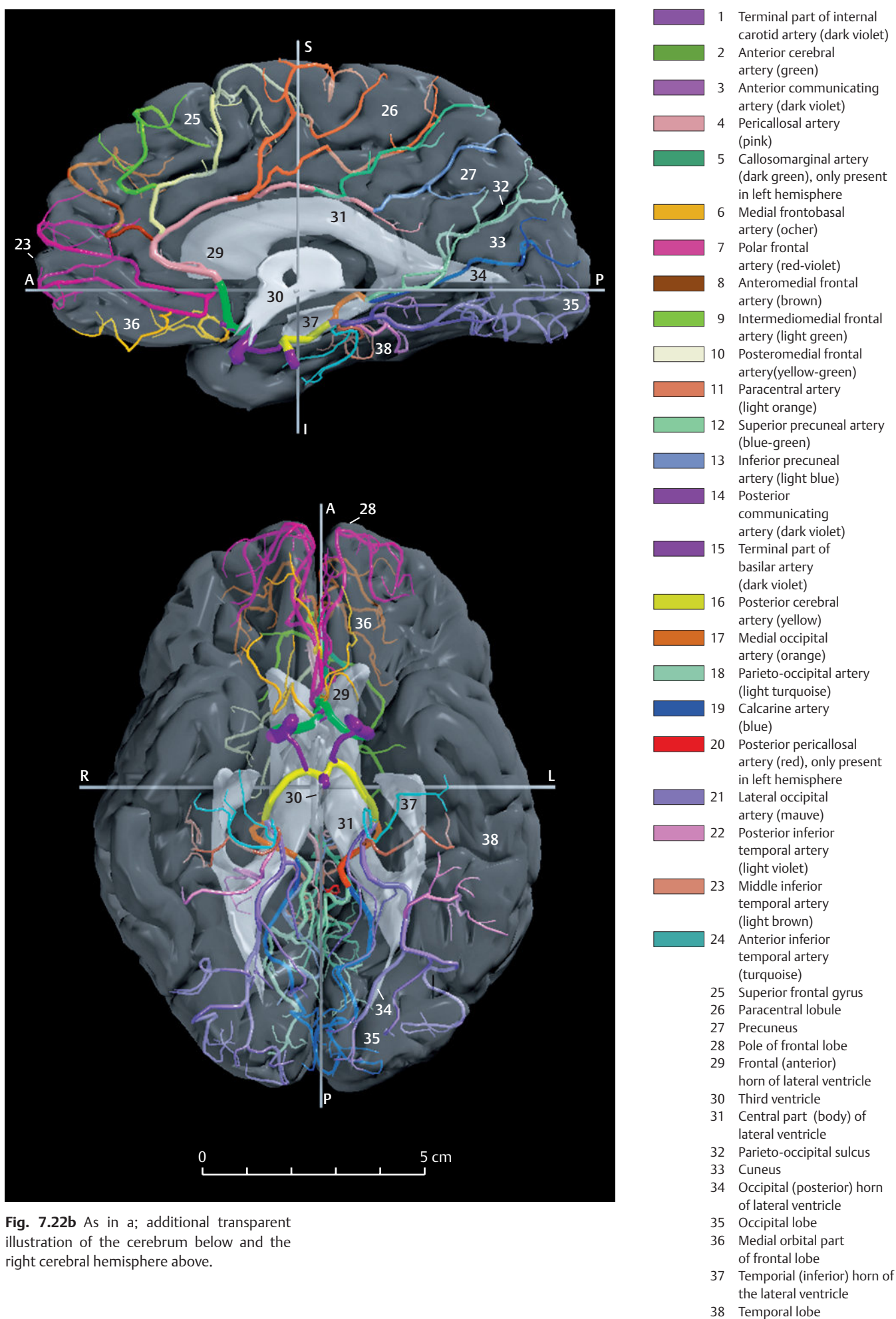


Fig. 7.22b As in a; additional transparent illustration of the cerebrum below and the right cerebral hemisphere above.

- 1 Medial lenticulostriate artery
- 2 Lateral lenticulostriate artery
- 3 Middle cerebral artery
- 4 Internal capsule
- 5 Lentiform nucleus
- 6 Pericallosal artery
- 7 Caudate nucleus
- 8 Thalamus
- 9 Short central arteries
- 10 Long central artery (Heubner)

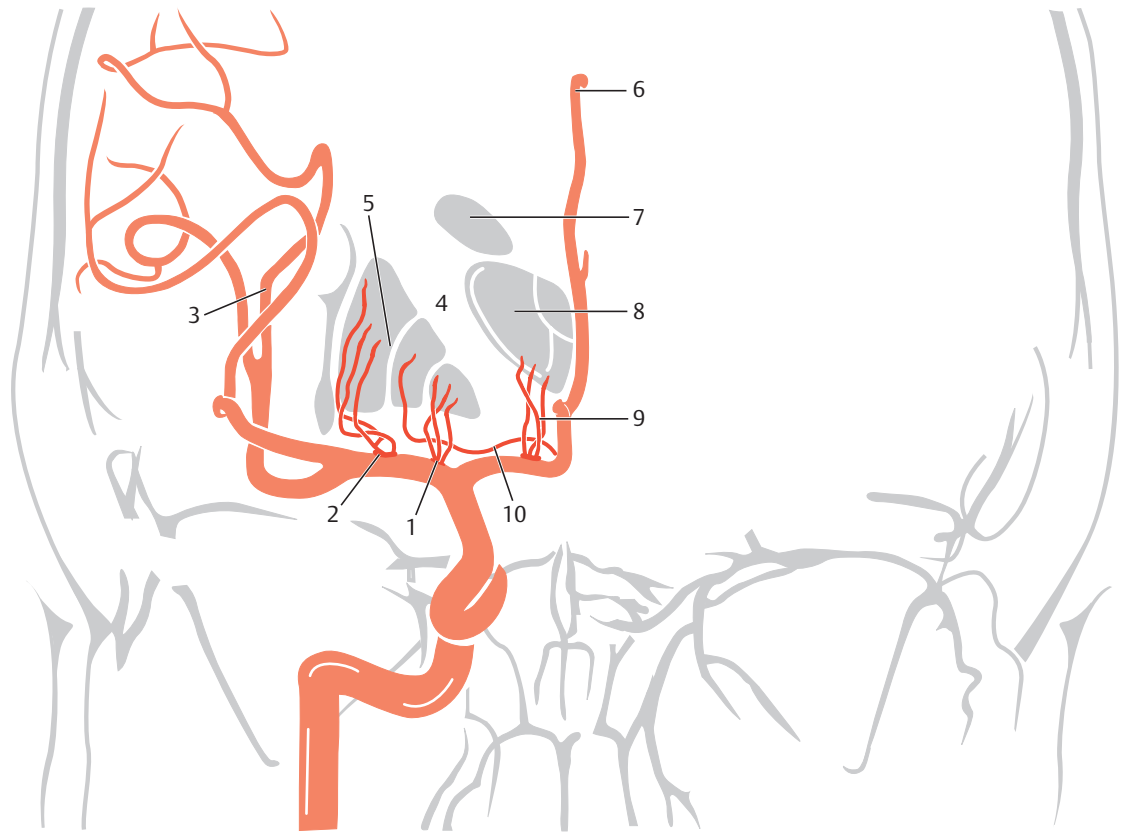


Fig. 7.23 Perforating arteries from the proximal anterior cerebral and middle cerebral arteries (lenticulostriate arteries). Schematic representation. (Reproduced from Krayenbühl et al.³⁰⁷)

- 1 Internal carotid artery
- 2 Branches of middle cerebral artery
- 3 Anterior cerebral artery
- 4 Medial frontobasal artery
- 5 Callosomarginal artery
- 6 Polar frontal artery
- 7 Anteromedial frontal artery (Anterior internal frontal artery)
- 8 Intermediomedial frontal artery
- 9 Pericallosal artery
- 10 Posteromedial frontal artery (Posterior internal frontal artery)
- 11 Paracentral artery
- 12 Superior precuneal artery (Superior internal parietal artery)
- 13 Inferior precuneal artery (Inferior internal parietal artery)

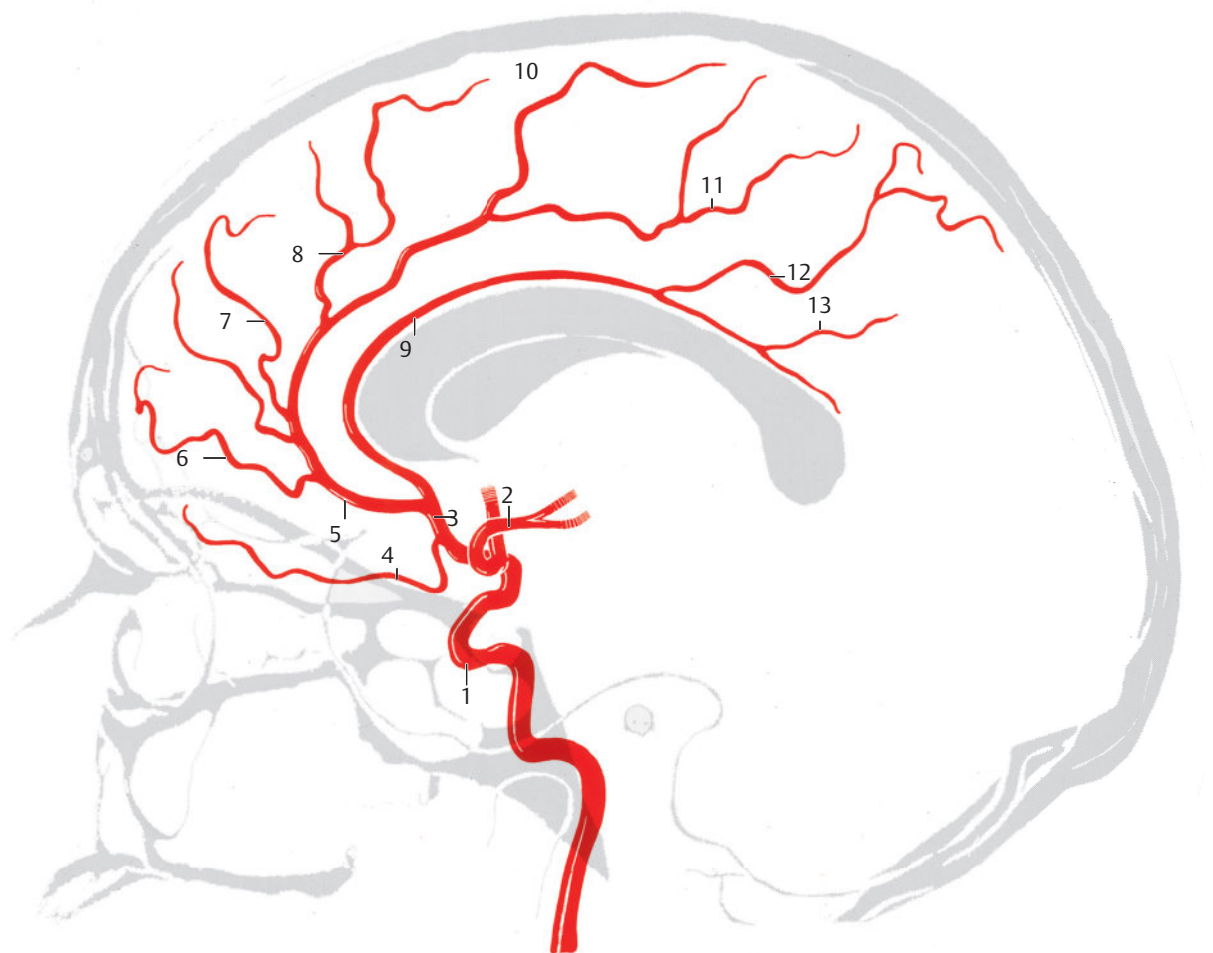


Fig. 7.24 Two main variants of the anterior cerebral artery. Lateral view. (For alternate terms listed in brackets, see Krayenbühl et al.³⁰⁷)

Fig. 7.24a The callosomarginal artery is a main branch of the anterior cerebral artery with side branches.

Further branching of the anterior cerebral artery generally takes one of two forms see ►Fig. 7.24):³⁰⁷

- A principal branch of the anterior cerebral artery, the callosomarginal artery (see ►Fig. 5.9a, ►Fig. 5.9b, ►Fig. 5.10a, ►Fig. 5.10b, ►Fig. 5.12, and ►Fig. 7.22a), lies in the cingulate sulcus and gives off lateral branches (see ►Fig. 7.24a)
- Lateral branches may arise directly from the anterior cerebral artery or from the pericallosal artery (see ►Fig. 7.24)

Terminal (previously: cortical) **branches** of the anterior cerebral artery supply the medial surface of the frontal and parietal lobes almost as far as the parieto-occipital sulcus.

The anterior cerebral artery supplies a 2 to 3 cm wide territory over the convexity of the cerebral hemisphere, including the superior frontal gyrus, the anterior part of the middle frontal gyrus, parts of the precentral and postcentral gyri near the superior margin, and a part of the superior parietal lobule. It also supplies the corpus callosum, except for the splenium.

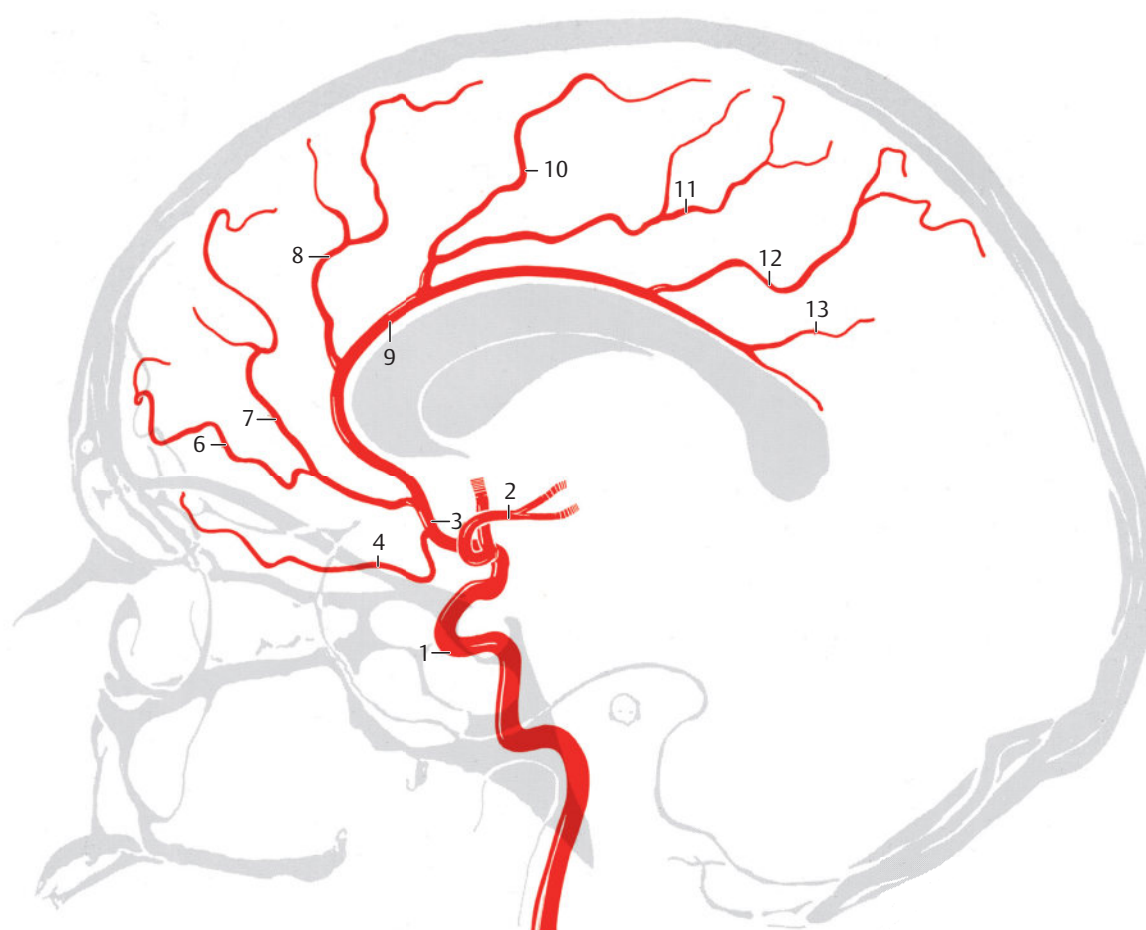
The **anterior communicating artery** (see ►Fig. 4.2c, ►Fig. 4.2d, ►Fig. 7.14b, and ►Fig. 7.22a) measures 3 mm in length and connects the right and left anterior cerebral arteries.

It lies above the optic chiasm at the level of the anterior clinoid process. Fine branches supply the optic chiasm, the infundibulum, and the preoptic area of the hypothalamus.

7.4.7 Middle Cerebral Artery

The middle cerebral artery (see Fig. 3.6b, ►Fig. 3.6d, ►Fig. 3.7c, ►Fig. 4.3d, ►Fig. 4.4c, and ►Fig. 7.25a) is a continuation of the internal carotid artery running medially from its origin into the depths of the cistern of the lateral cerebral fossa (Sylvius). The initial or sphenoid part (M1 segment) of the middle cerebral artery lies immediately inferior to the anterior perforated substance. Here three to thirteen thin, penetrating arteries, the anterolateral central (previously: lateral lenticulostriate) arteries, branch off to supply mainly the basal ganglia, including the genu of the internal capsule, predominantly the putamen and part of the globus pallidus.

The middle cerebral artery averages 16 mm (5–24 mm) in length before it divides into two or more branches. Aplasia of the middle cerebral artery is very rare and has been seen only in about 0.3% of cases.³³² The artery divides into its hemispheric branches as a **bifurcation** (see ►Fig. 7.25a) in 20% of cases in the region between the anterior perforated substance and the insula, as a **trifurcation** in about 50% (see ►Fig. 7.25b), and only rarely as a quadfurcation or quinfurcation.³³² These terminal (previously: cortical) arteries run obliquely upwards and posteriorly and lie on the insula; they are therefore termed **insular arteries** (M2 segment; see ►Fig. 3.6c, ►Fig. 3.9c, ►Fig. 3.9d, ►Fig. 4.6b, ►Fig. 4.6c, ►Fig. 4.6d, ►Fig. 5.8, ►Fig. 5.24,



- 1 Internal carotid artery
- 2 Branches of middle cerebral artery
- 3 Anterior cerebral artery
- 4 Medial frontobasal artery
- 6 Polar frontal artery
- 7 Anteromedial frontal artery
- 8 Intermediomedial frontal artery
- 9 Pericallosal artery
- 10 Posteromedial frontal artery
- 11 Paracentral artery
- 12 Superior precuneal artery
- 13 Inferior precuneal artery

Fig. 7.24b Side branches arise directly from the anterior cerebral artery.

- 1 Internal carotid artery
- 2 Middle cerebral artery
- 3 Origin of anterior cerebral artery
- 4 Lateral frontobasal artery
- 5 Insular arteries
- 6 Prefrontal arteries
- 7 Artery of precentral sulcus (prerolandic artery)
- 8 Artery of central sulcus (Rolandic artery)
- 9 Anterior parietal artery
- 10 Posterior parietal artery
- 11 Angular artery
- 12 Temporo-occipital artery
- 13 Posterior temporal artery
- 14 Middle temporal artery
- 15 Anterior temporal artery
- 16 Polar temporal artery

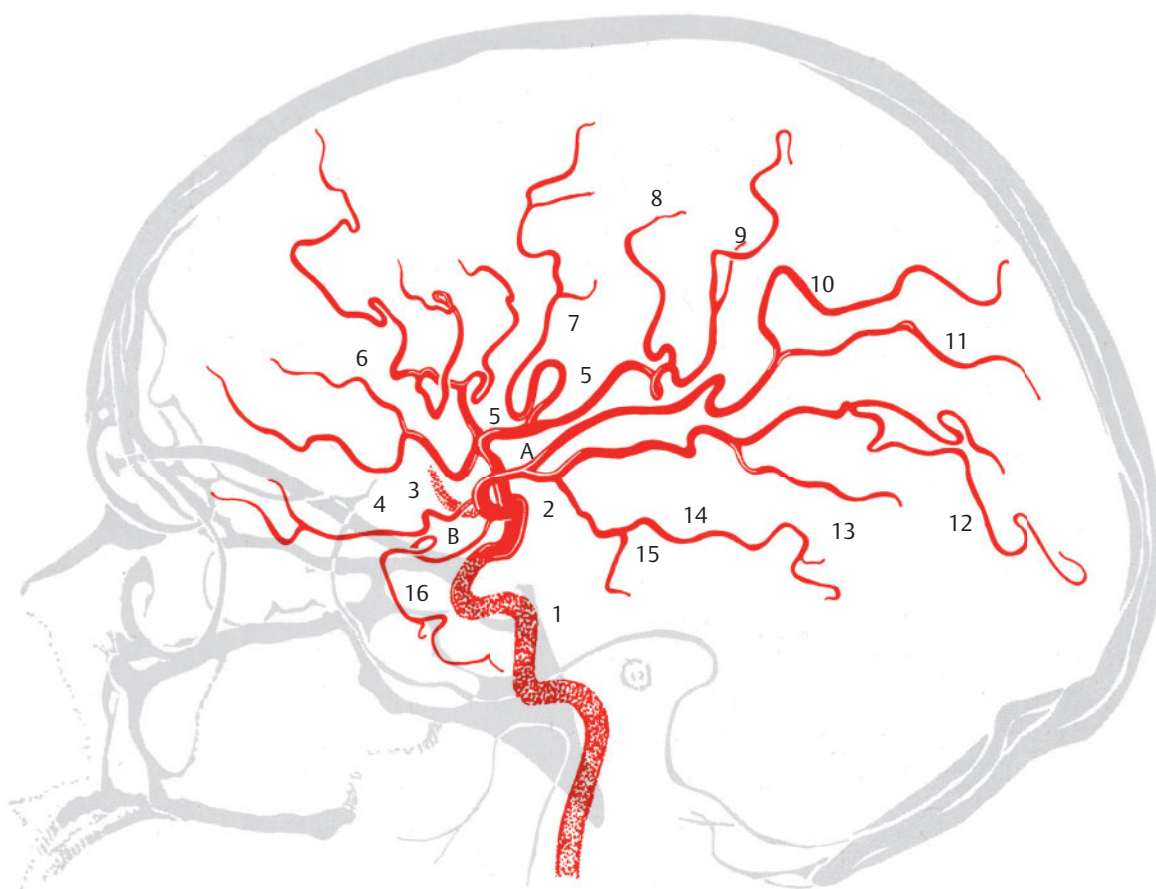


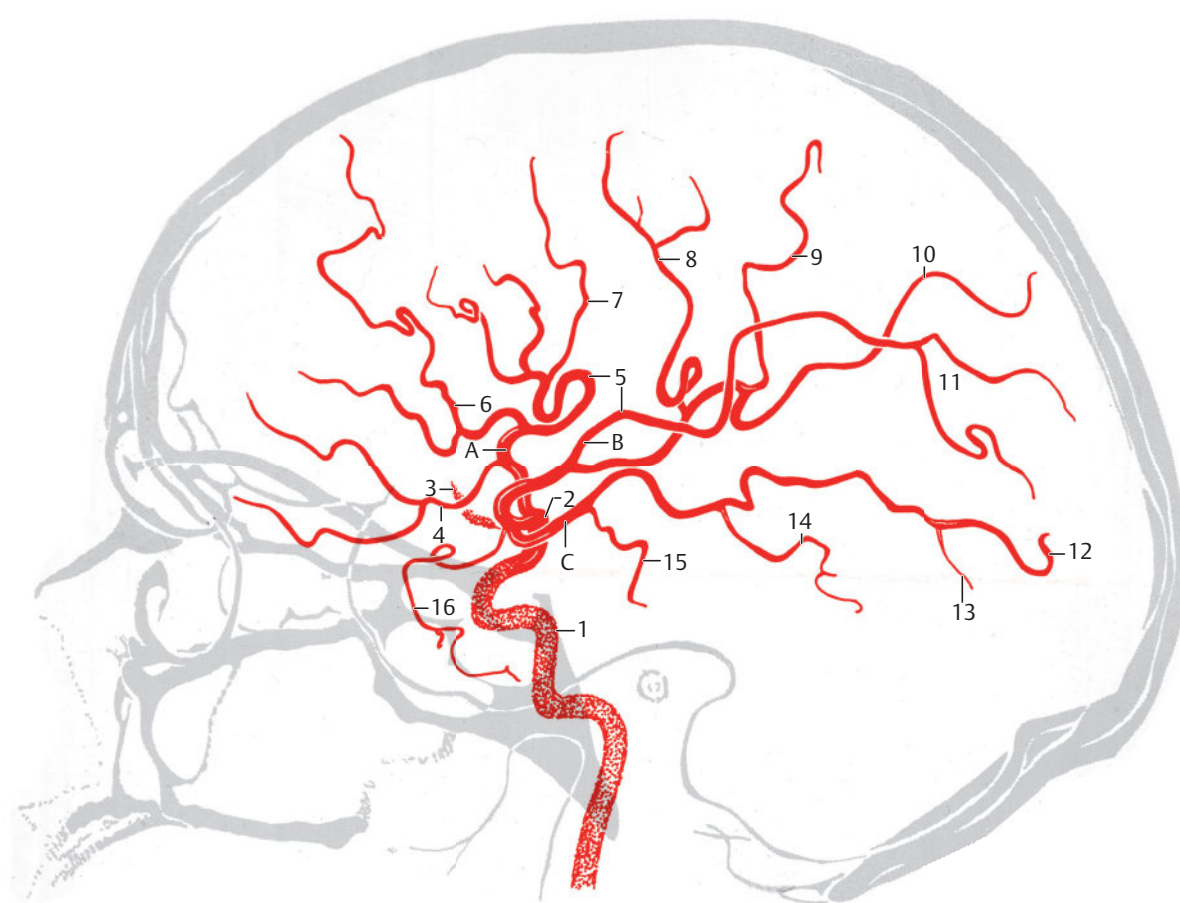
Fig. 7.25 Two variants of the middle cerebral artery. Lateral view. (For alternate terms listed in brackets, see Krayenbühl et al.³⁰⁷)

Fig. 7.25a With bifurcation (A and B).

and ►Fig. 6.13a). These arteries then course around the neocortex, which was pushed over the insula in a lid-like manner due to its enlargement during the evolutionary process.^{555,556} The arteries which encircle the opercula of the insula (M3 segment) assume the shape of a candelabra. The concavity of the ascending arteries is directed upwards, while it is directed downwards in the arteries descending to the temporal lobe. The terminal segments of the arteries connect over the surface of the cerebrum (M4 and M5 segments) and are named according to the peripheral territory that they supply.

The lateral frontobasal artery (see ►Fig. 3.4c, ►Fig. 4.5c, and ►Fig. 7.25a) supplies the inferior frontal gyrus and part of the orbital gyri. The prefrontal artery (see ►Fig. 3.4c, ►Fig. 3.5c, ►Fig. 4.5c, ►Fig. 5.11, and ►Fig. 5.12) lies on the triangular part of the operculum and

branches over the surface of the frontal lobe. The prerolandic artery (see ►Fig. 3.7c, ►Fig. 4.5c, and ►Fig. 5.11a) lies partly within the precentral sulcus and supplies the basal part of the precentral gyrus and the middle frontal gyrus. The artery of central sulcus (previously: rolandic artery; see ►Fig. 3.8c, ►Fig. 4.5c, ►Fig. 4.6c, ►Fig. 4.6d, ►Fig. 5.10a, and ►Fig. 7.26a) participates in supplying the precentral and postcentral gyri and adjoining areas. The anterior and posterior parietal arteries supply the anterior and posterior parts of the parietal lobe. The angular artery (see Fig. 3.10c, ►Fig. 4.5c, ►Fig. 5.11a, and ►Fig. 7.21) runs in the superior temporal sulcus to the angular gyrus and can be visualized as the terminal branch of the middle cerebral artery. The temporo-occipital artery runs over the superior temporal gyrus to the occipital lobe. Four other temporal arteries descend inferiorly (see ►Fig. 7.25).



- 1 Internal carotid artery
- 2 Middle cerebral artery
- 3 Origin of anterior cerebral artery
- 4 Lateral frontobasal artery
- 5 Insular arteries
- 6 Prefrontal arteries
- 7 Artery of precentral sulcus
- 8 Artery of central sulcus
- 9 Anterior parietal artery
- 10 Posterior parietal artery
- 11 Angular artery
- 12 Temporo-occipital artery
- 13 Posterior temporal artery
- 14 Middle temporal artery
- 15 Anterior temporal artery
- 16 Polar temporal artery

Fig. 7.25b With trifurcation (A, B, and C).

7.4.8 Circle of Willis

The circle of Willis forms a complete vascular ring in approximately 96% of cases connecting vascular territories of the basilar and internal carotid arteries (see ► Fig. 7.22 and ► Fig. 7.27), and facilitates distribution of blood during variation in blood supply through one of its arteries. The left or right posterior communicating artery is absent in about 2% of cases.³³³ Hemodynamically adequate connections between the large cerebral arteries are lacking in about 50%

of cases.¹² Arteriosclerosis preferentially involves this arterial circle and may further impair its ability to compensate. In adults, a complete ligation of one internal carotid artery generally results in neurologic deficits. The compensatory function of the Circle of Willis in the distribution of blood flow is further validated by the fact that brain infarcts are significantly more frequent in patients with a congenitally incomplete circle than in those with a complete arterial circle.

- 1 Terminal part of internal carotid artery
- 2 Middle cerebral artery, trunk
- 3 Lateral frontobasal artery
- 4 Prefrontal artery
- 5 Artery of precentral sulcus
- 6 Artery of central sulcus
- 7 Anterior parietal artery
- 8 Posterior parietal artery
- 9 Artery of angular gyrus
- 10 Temporo-occipital artery
- 11 Posterior temporal artery
- 12 Middle temporal artery
- 13 Anterior temporal artery
- 14 Temporopolar artery

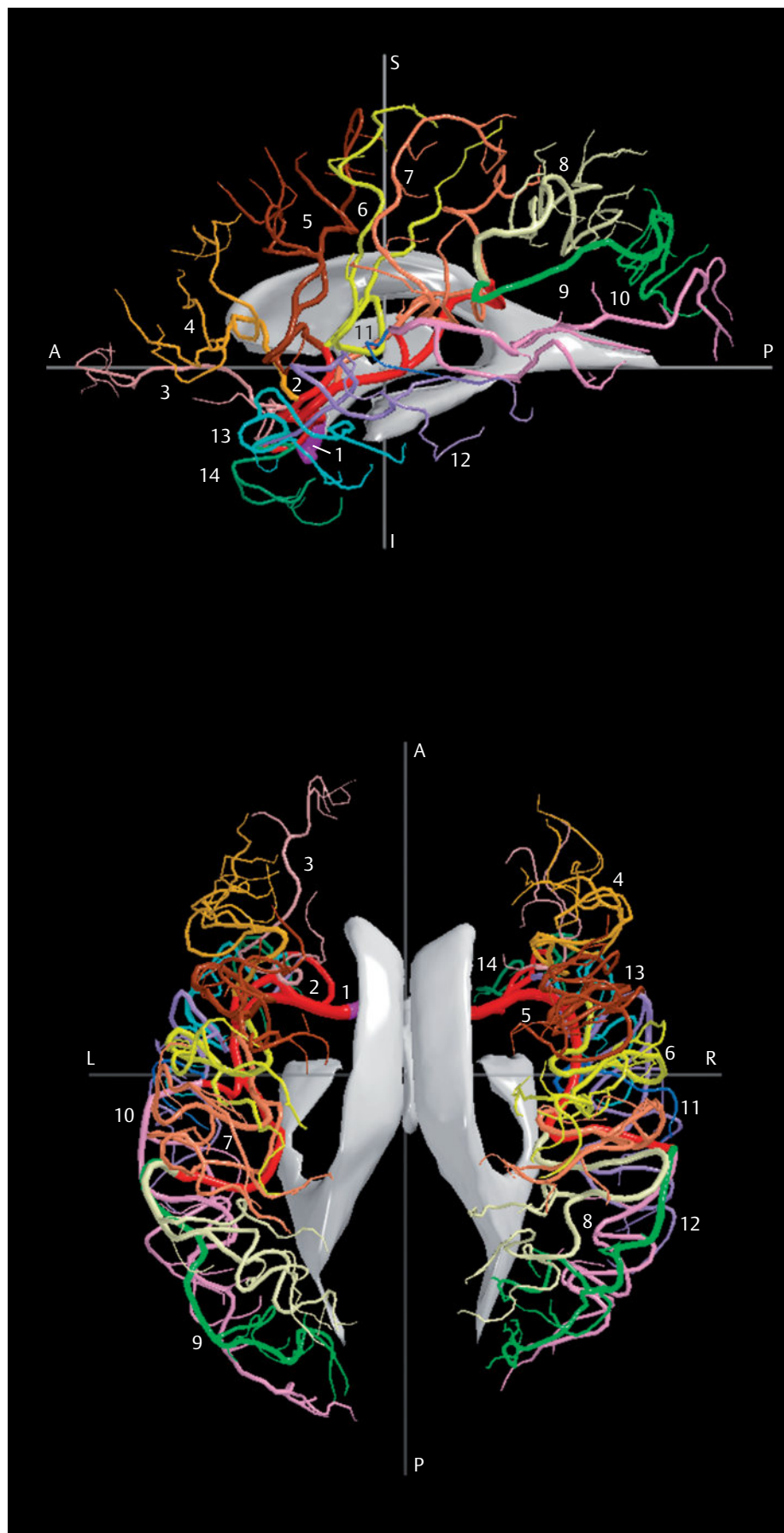


Fig. 7.26 Middle cerebral artery with its terminal branches and terminal part of the internal carotid artery. Bicommissural coordinate system. CT images and reconstructions. (Reproduced from Kretschmann et al.³¹⁴)

A = anterior R = right S = superior

P = posterior L = left I = inferior

Fig. 7.26a Lateral view of left-sided arteries with the left lateral and IIIrd ventricles (above). Superior view of bilateral arteries with lateral and IIIrd ventricles (below).

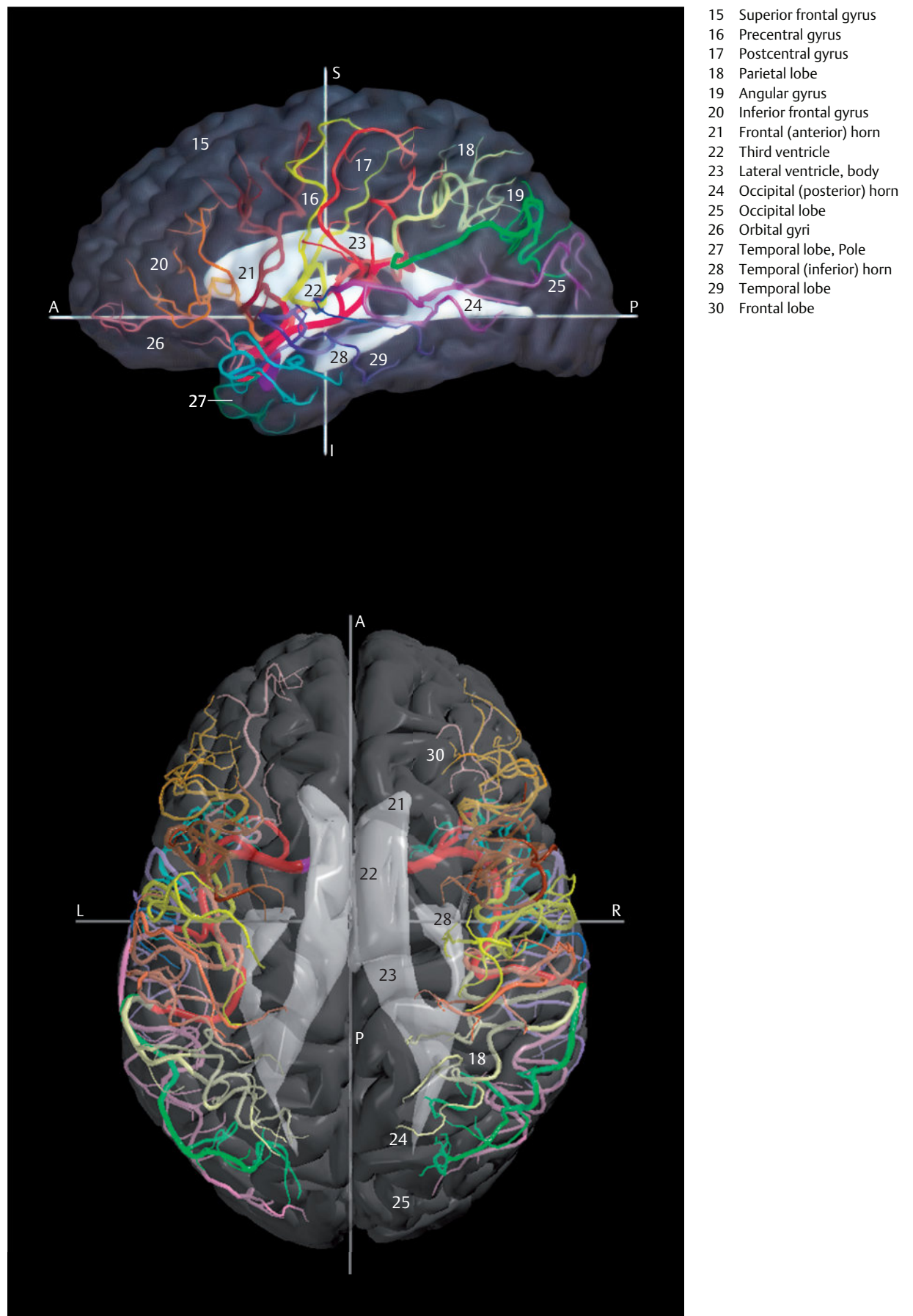


Fig. 7.26b As in a; additional transparent illustration of the cerebrum below and the left cerebral hemisphere above.

- 1 Internal carotid artery
- 2 Middle cerebral artery
- 3 Anterior cerebral artery
- 4 Posterior cerebral artery

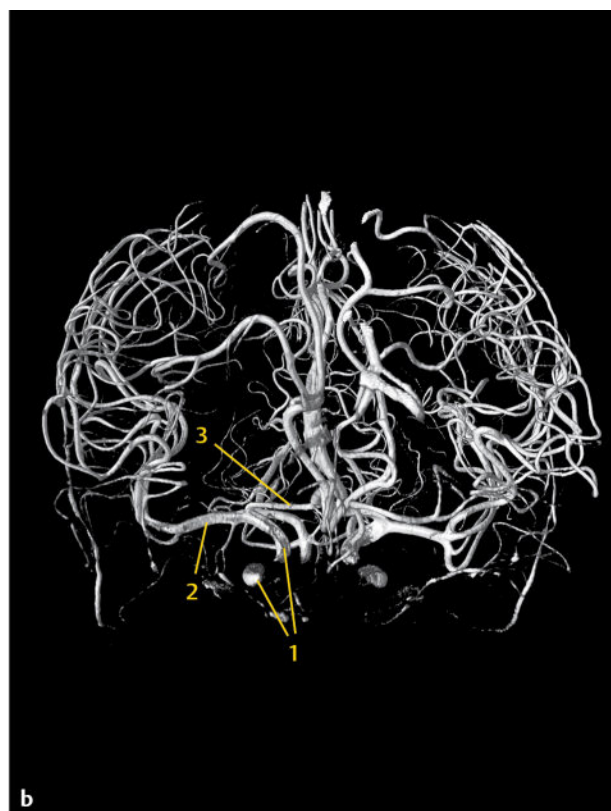


Fig. 7.27 Anterior, middle, and posterior cerebral arteries. Example of an MRA examination with a field strength of 7T. See Chapter 12 for technical details. (Source: With kind permission of Dr. Karsten Wrede, University Hospital, Essen.)

Fig. 7.27a Superior view.

Fig. 7.27b Anterior view.

7.4.9 Cerebral Arterial Anastomoses

Insufficient blood supply to the brain through the internal carotid and vertebral arteries may be compensated for to a certain extent by anastomoses from the facial (see ►Fig. 9.1) and superficial temporal arteries with the ophthalmic artery and a **reversal of the direction of flow** of the ophthalmic artery into the internal carotid artery. Furthermore, leptomeningeal anastomoses exist between the three main cerebral arteries as well as the three cerebellar arteries. Blood may be supplied to the contralateral hemisphere through the pericallosal artery and the callosomarginal artery. Several arterial anastomoses are generally present between the anterior choroidal and the posterior choroidal arteries.

7.4.10 Arterial Territories of the Forebrain

Two main arterial territories are identifiable (see ►Fig. 7.28, ►Fig. 7.29, ►Fig. 7.30, ►Fig. 7.31, and ►Fig. 7.32):

- **Central territories:** These lie in the diencephalon, caudate nucleus, putamen, and the internal capsule.
- **Terminal territories:** These lie in the cerebral cortex as also in the white matter situated directly beneath it. The commonly used synonym “cortical territory” (or “cortical artery”) describes this territory inadequately.

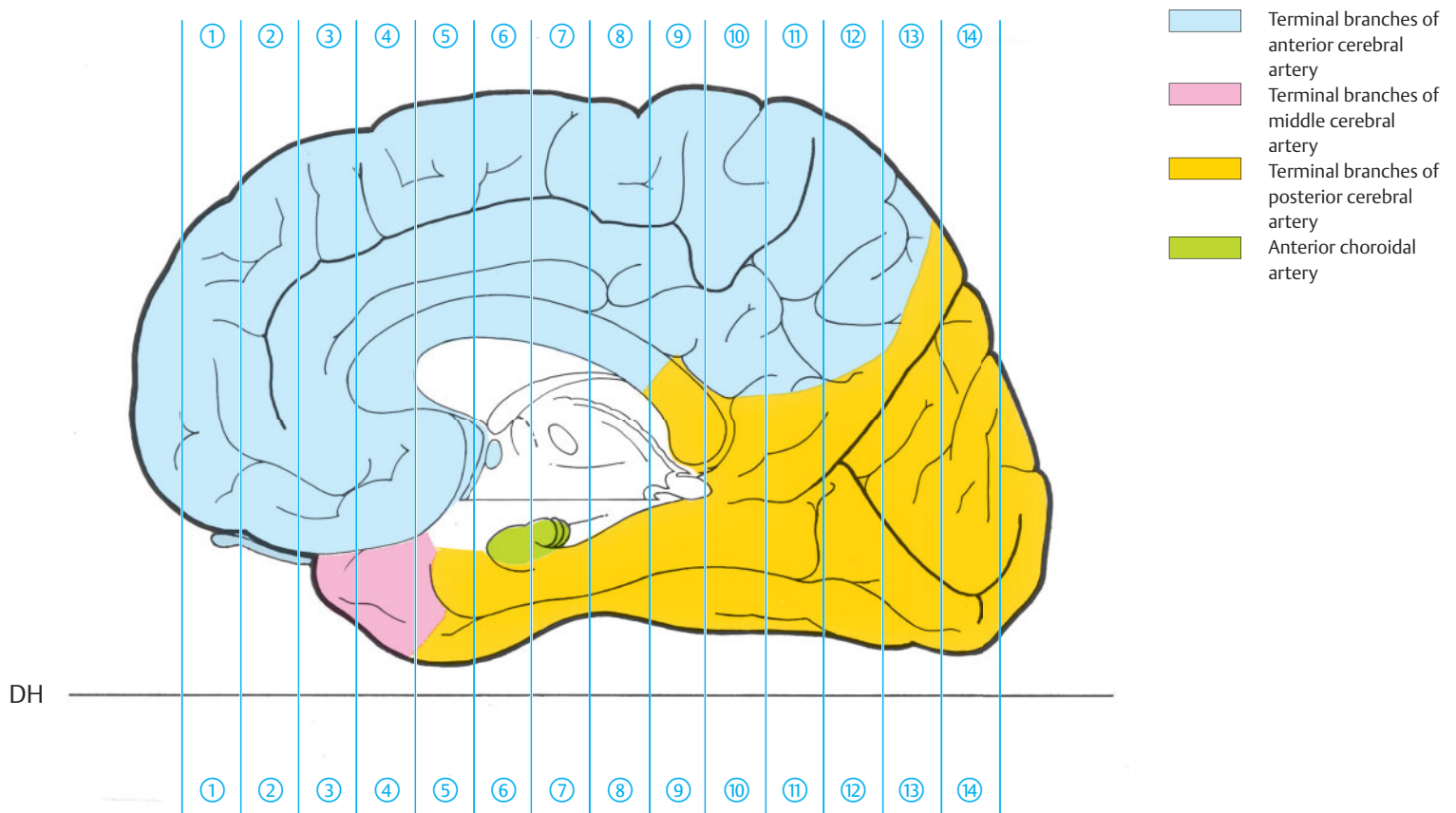


Fig. 7.28 Terminal arterial territories of the forebrain.

Encircled digits indicate the number of the respective slice (see ► Fig. 3.1).

DH = German horizontal

Fig. 7.28a Median view of the cerebrum sectioned in the coronal plane with the territories of the terminal (cortical) branches of the anterior, middle, and posterior cerebral arteries as well as the anterior choroidal artery.

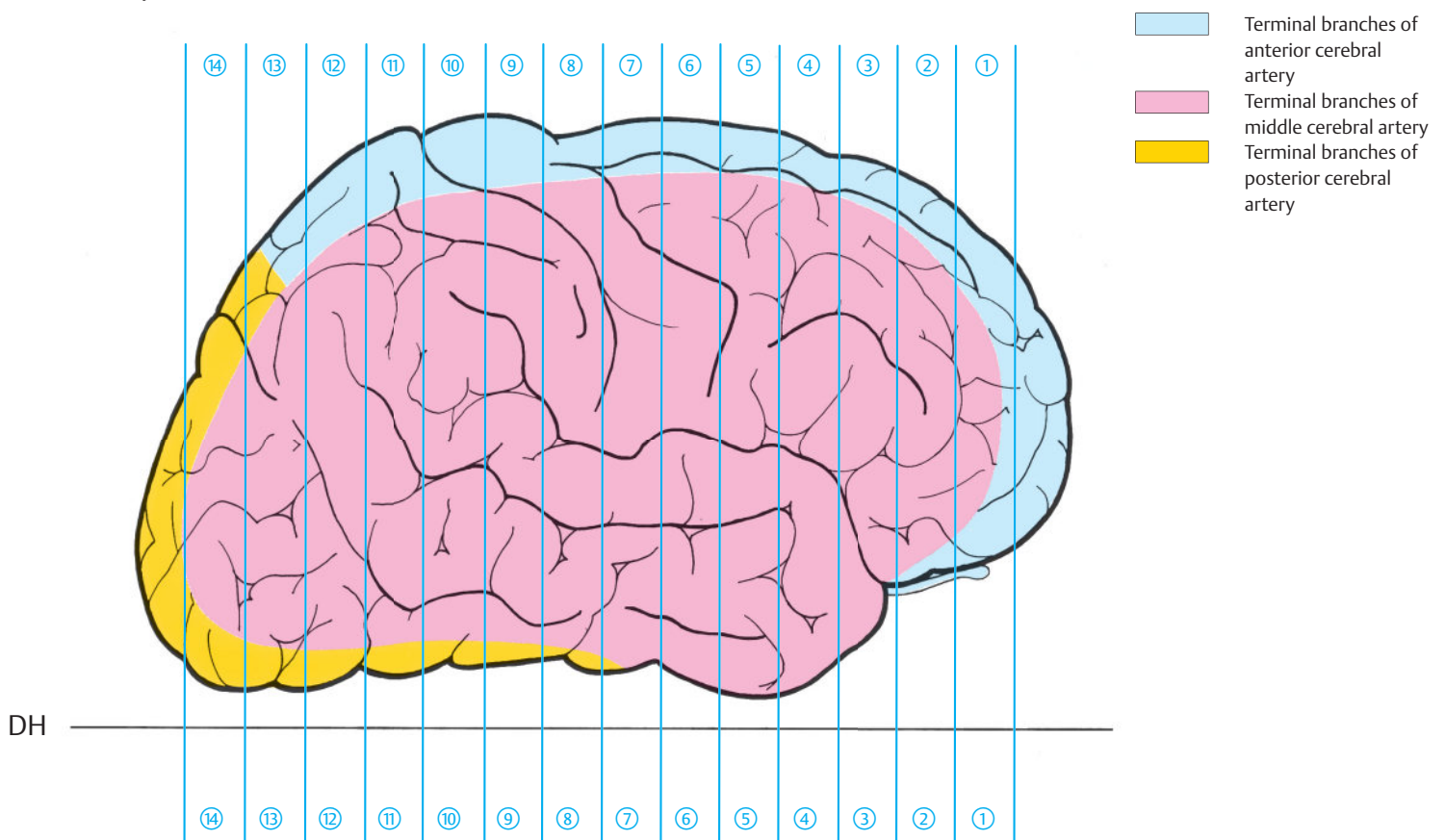


Fig. 7.28b Lateral view of the cerebrum sectioned in the coronal plane with the territories of the terminal (cortical) branches of the anterior, middle, and posterior cerebral arteries.

- Terminal branches of anterior cerebral artery
- Terminal branches of middle cerebral artery

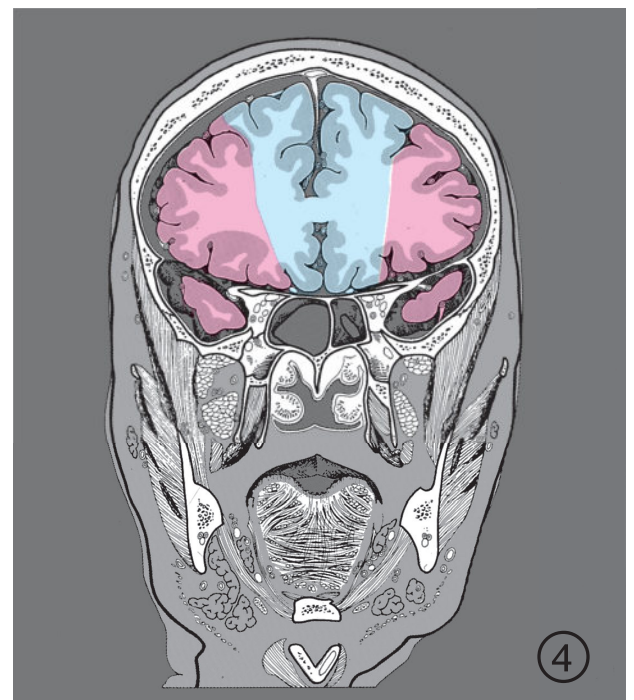
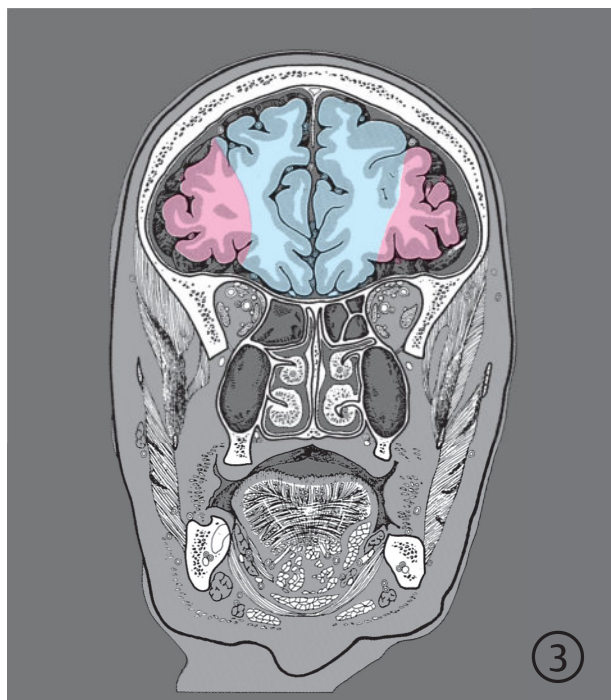
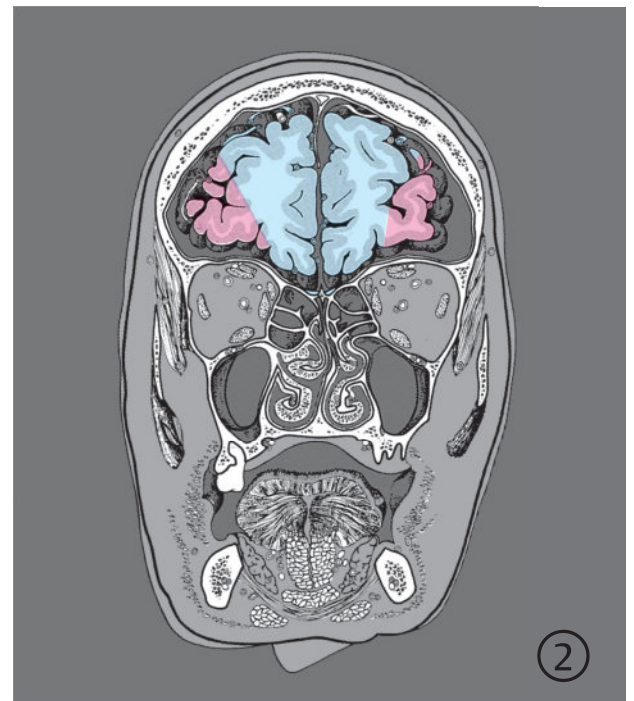
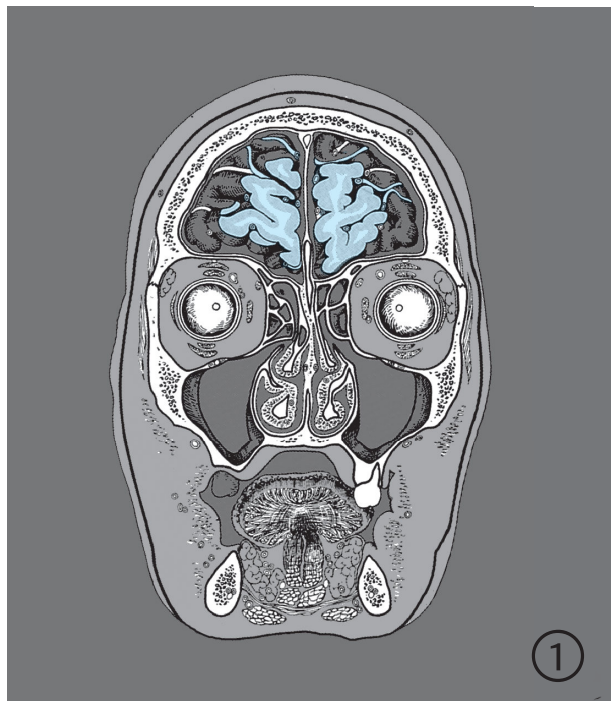


Fig. 7.29 Terminal and central arterial territories of the forebrain. Serial coronal images of the territories of the terminal (cortical) and central (penetrating) branches of the anterior, middle, and posterior cerebral arteries as well as the anterior choroidal artery. Encircled digits indicate the number of the respective slice (see ► Fig. 3.1 and ► Fig. 7.28).

Fig. 7.29a 1st to 4th sections.

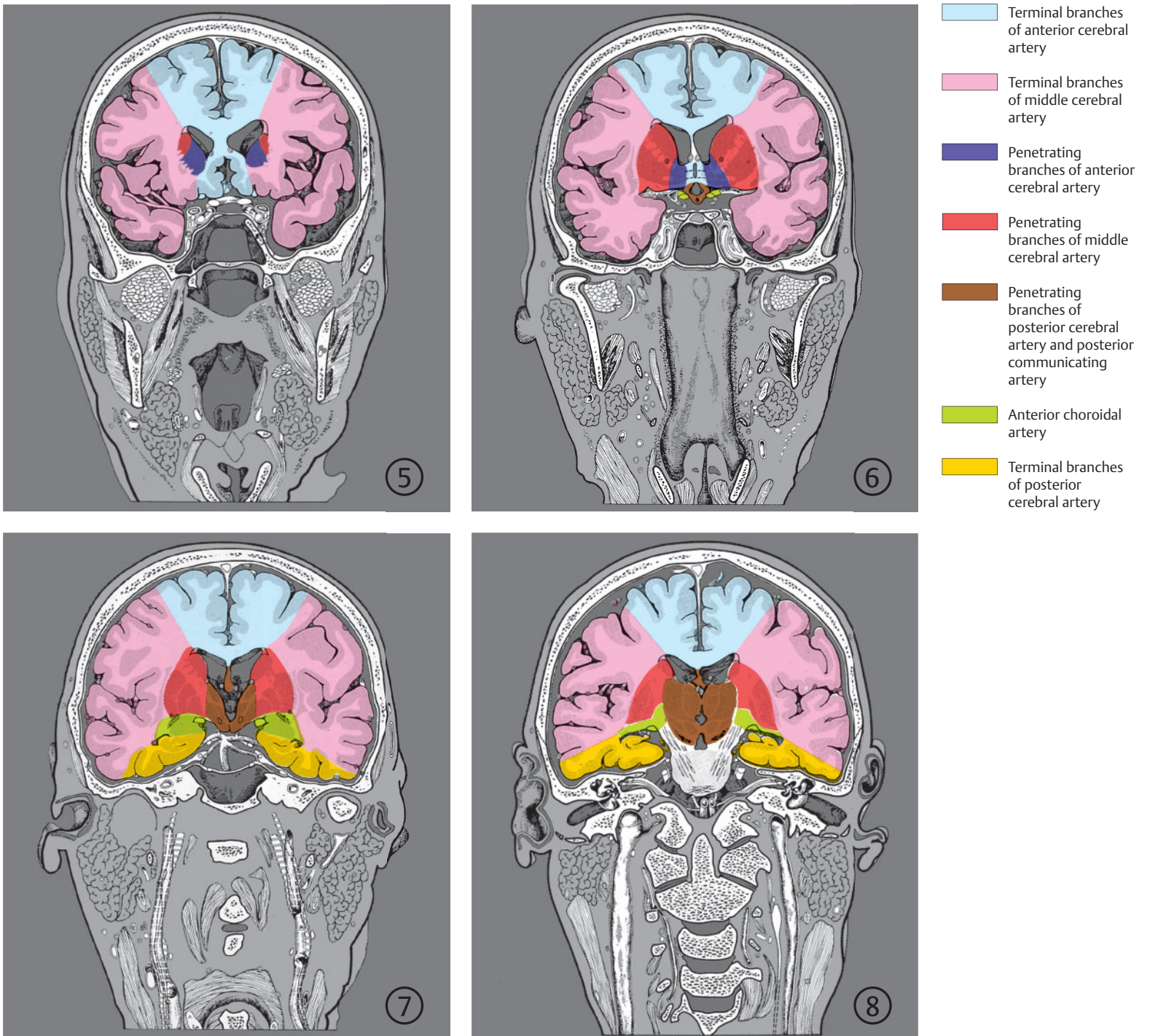


Fig. 7.29b 5th to 8th sections.

- Terminal branches of anterior cerebral artery
- Terminal branches of middle cerebral artery
- Terminal branches of posterior cerebral artery
- Penetrating branches of middle cerebral artery
- Penetrating branches of posterior cerebral artery

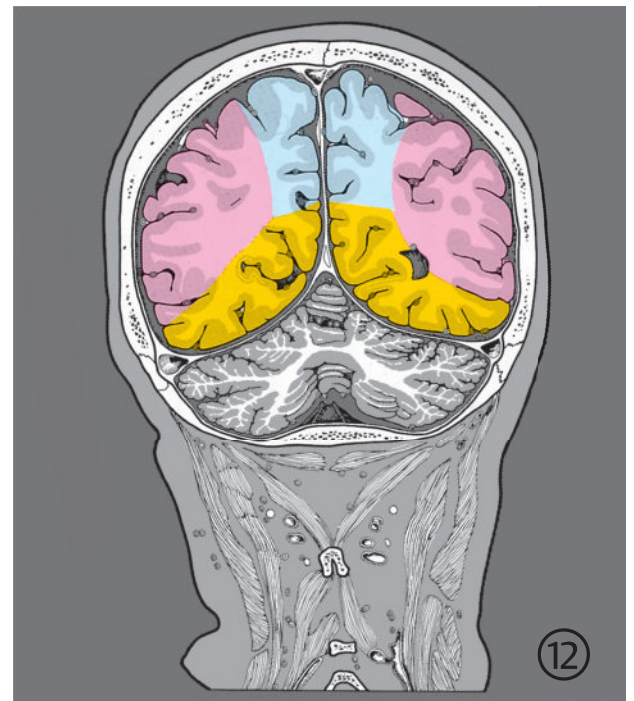
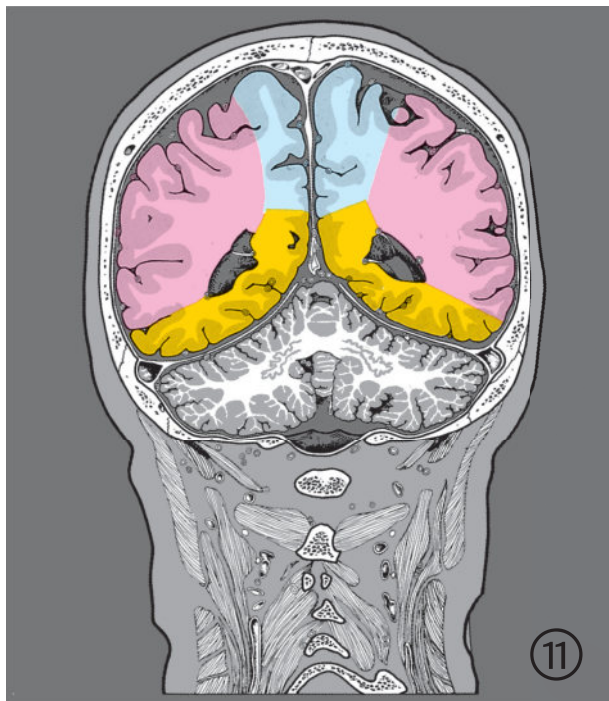
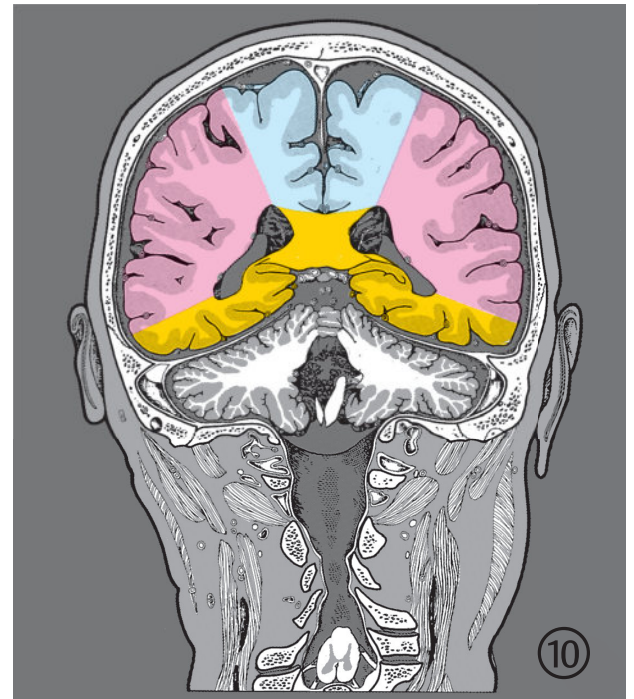
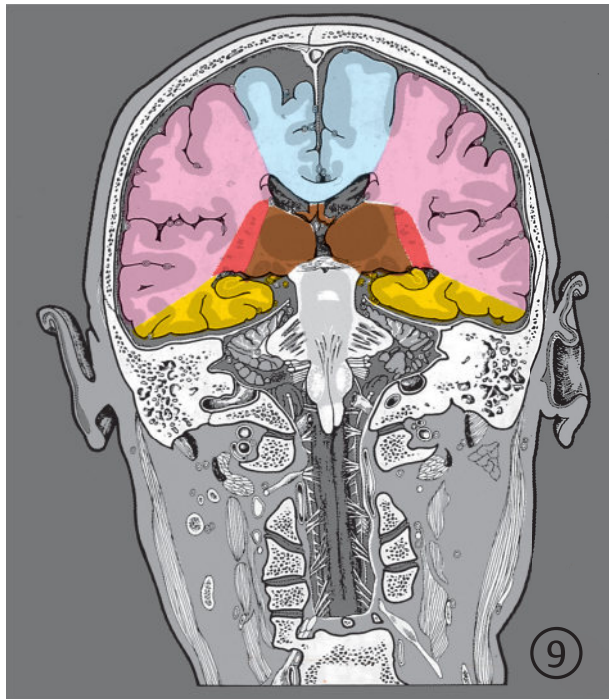


Fig. 7.29c 9th to 12th sections.

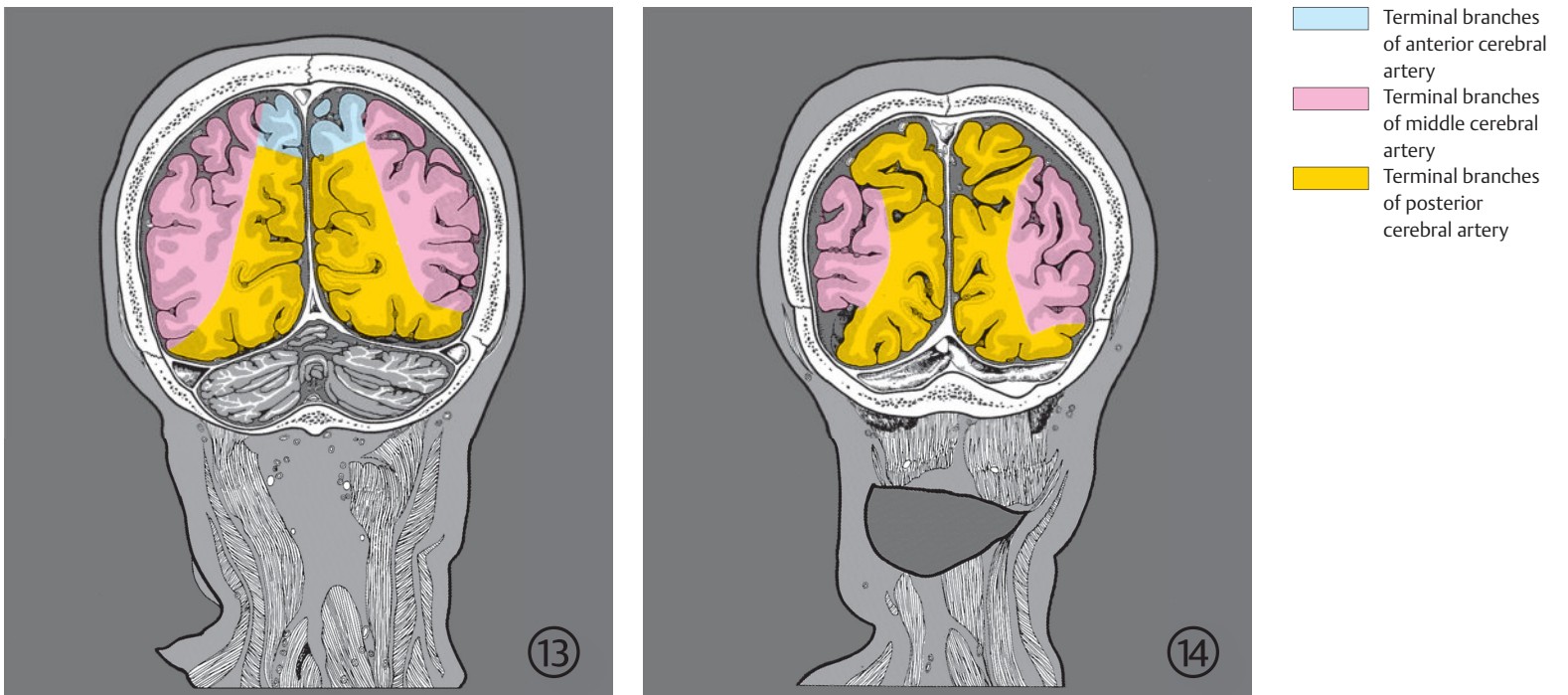


Fig. 7.29d 13th and 14th sections.

- Terminal branches of anterior cerebral artery
- Terminal branches of middle cerebral artery
- Terminal branches of posterior cerebral artery
- Penetrating branches of anterior cerebral artery
- Penetrating branches of middle cerebral artery
- Penetrating branches of posterior cerebral artery and posterior communicating artery
- Anterior choroidal artery

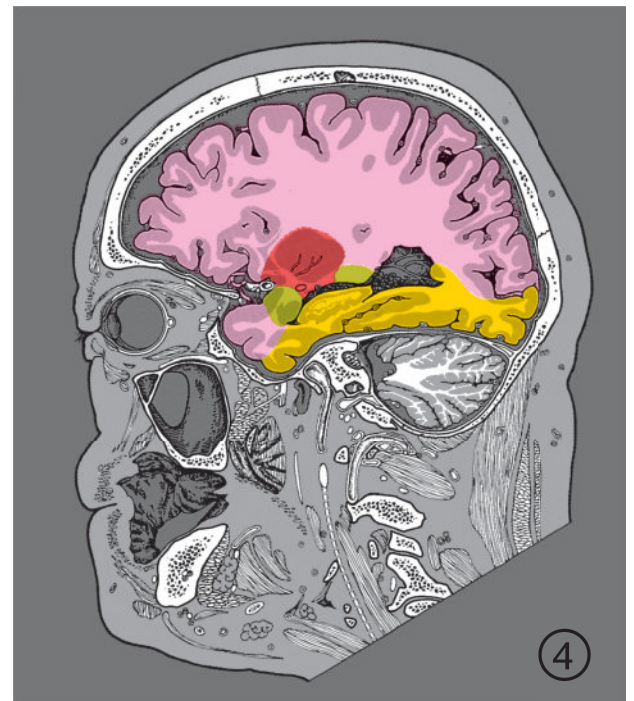
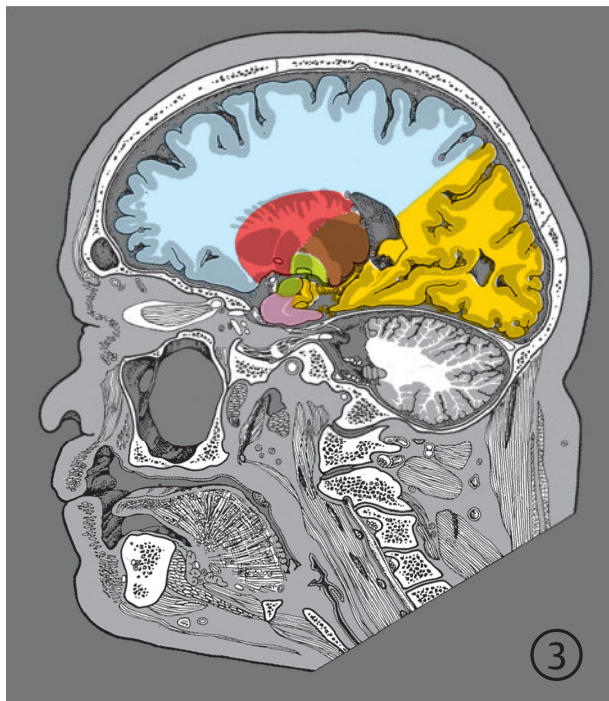
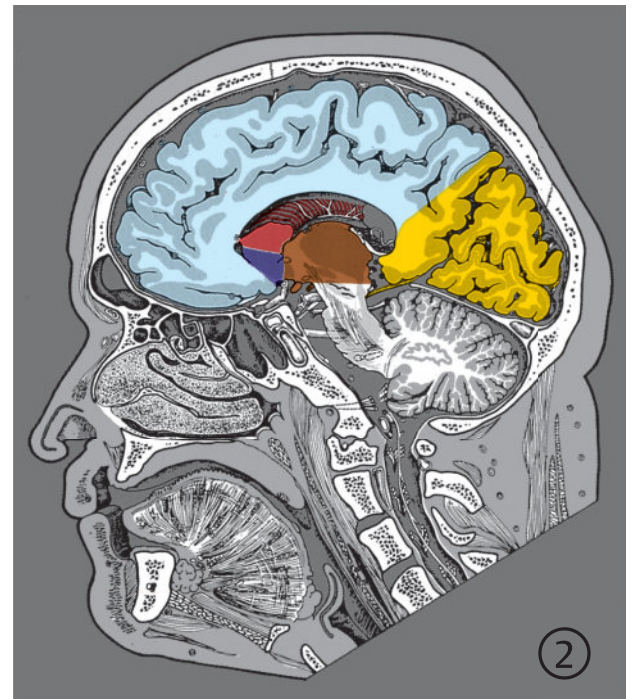
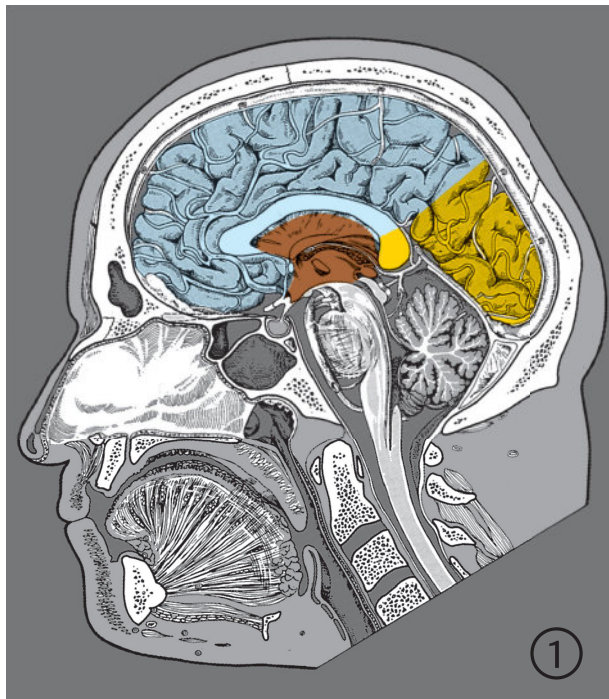


Fig. 7.30 Terminal and central arterial territories of the forebrain. Serial sagittal images of the territories of the terminal (cortical) and central (penetrating) branches of the anterior, middle, and posterior cerebral arteries as well as the anterior choroidal artery. Encircled digits indicate the number of the respective slice (see ► Fig. 4.1).

Fig. 7.30a 1st to 4th sections.



Fig. 7.30b 5th and 6th sections.

- Terminal branches of anterior cerebral artery
- Terminal branches of middle cerebral artery
- Terminal branches of posterior cerebral artery
- Anterior choroidal artery

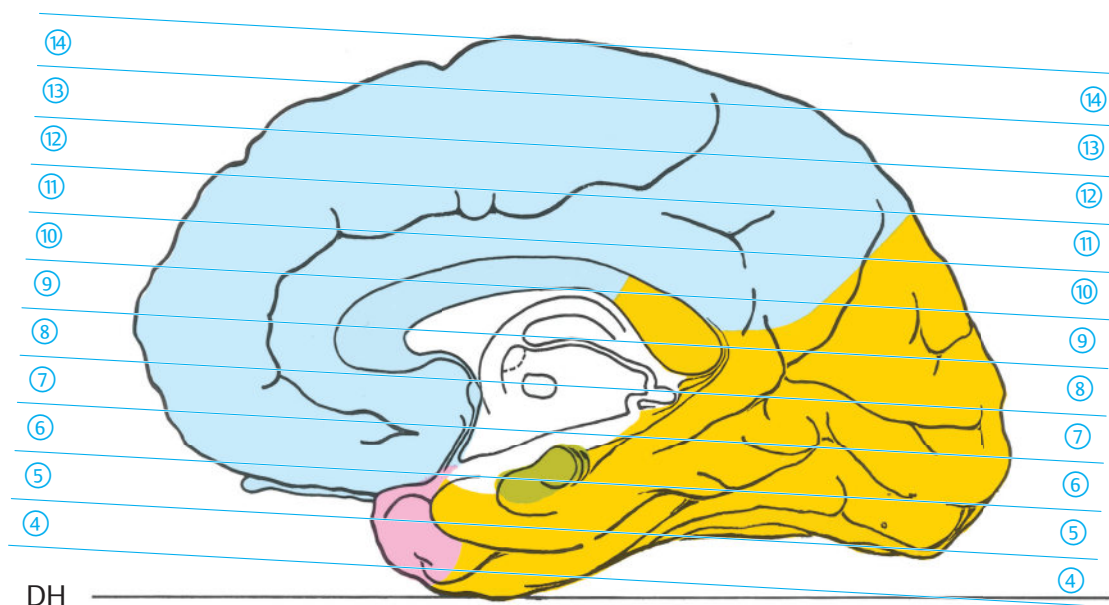


Fig. 7.31 Terminal arterial territories of the forebrain. Encircled digits indicate the number of the respective slice. DH = German horizontal

Fig. 7.31a Median view of the cerebrum sectioned in the bi-commissural plane with the territories of the terminal (cortical) branches of the anterior, middle, and posterior cerebral arteries.

Central Territories

The central territories of the forebrain are supplied by **penetrating arteries** (see ► Fig. 7.23).

They are so-called end arteries, that is, hypoperfusion results when a lesion is present. These are:

- The penetrating branches of the anterior cerebral artery include the **long central artery** (previously: recurrent artery of Heubner) and **anteromedial central arteries** (previously: medial lenticulostriate arteries; see ► Fig. 6.12b).⁵³ Reaching the forebrain through the anterior perforated substance, they supply the anteroinferior part of the caudate nucleus and putamen, and the anteroinferior part of the internal capsule.⁵³
- The **anterolateral central arteries** (previously: lateral lenticulostriate arteries; see ► Fig. 6.12b and ► Fig. 7.14b) are branches of the middle cerebral artery which penetrate basal parts of the forebrain to supply the innominate substance, the lateral part of the anterior commissure, most of the putamen, the lateral part of the globus pallidus, the superior half of the internal capsule and adjacent corona radiata, as well as the head and body except the anteroinferior part of the caudate nucleus.⁵⁴
- The **posteromedial and posterolateral central arteries** arise from the posterior cerebral artery with direct branches arising from the circle of Willis; these vessels penetrate the basal and posterior diencephalic areas, supplying the thalamus, metathalamus, hypothalamus, and subthalamic nucleus.

Clinical Notes

Occlusion of a penetrating artery produces a small, well-circumscribed infarct. Contralateral paresis occurs without sensory loss when solely the pyramidal tracts are involved. Infarcts in the ventral posterior nucleus of the thalamus produce pure hemisensory loss.

Occlusion of the so-called Percheron artery causes symmetrical, bilateral-paramedian thalamic infarcts, not infrequently with involvement of the midbrain. A variant of the normal bilateral thalamoperforating arteries is an unpaired artery from the P1 segment (Percheron artery), which supplies the central thalamic regions on both sides. Depending on the simultaneous involvement of the midbrain, the clinical picture of this ischemic lesion may include severe impairment of consciousness, impairment of memory and vertical visual paresis^{345,455} along with other symptoms.

Terminal Arterial Territories

The terminal arterial territories of a cerebral hemisphere are composed of three territories of the terminal branches of the anterior, medial, and posterior cerebral arteries, the boundaries of which (see ► Fig. 7.28 and ► Fig. 7.31) do not conform to boundaries of various lobes of the telencephalon.

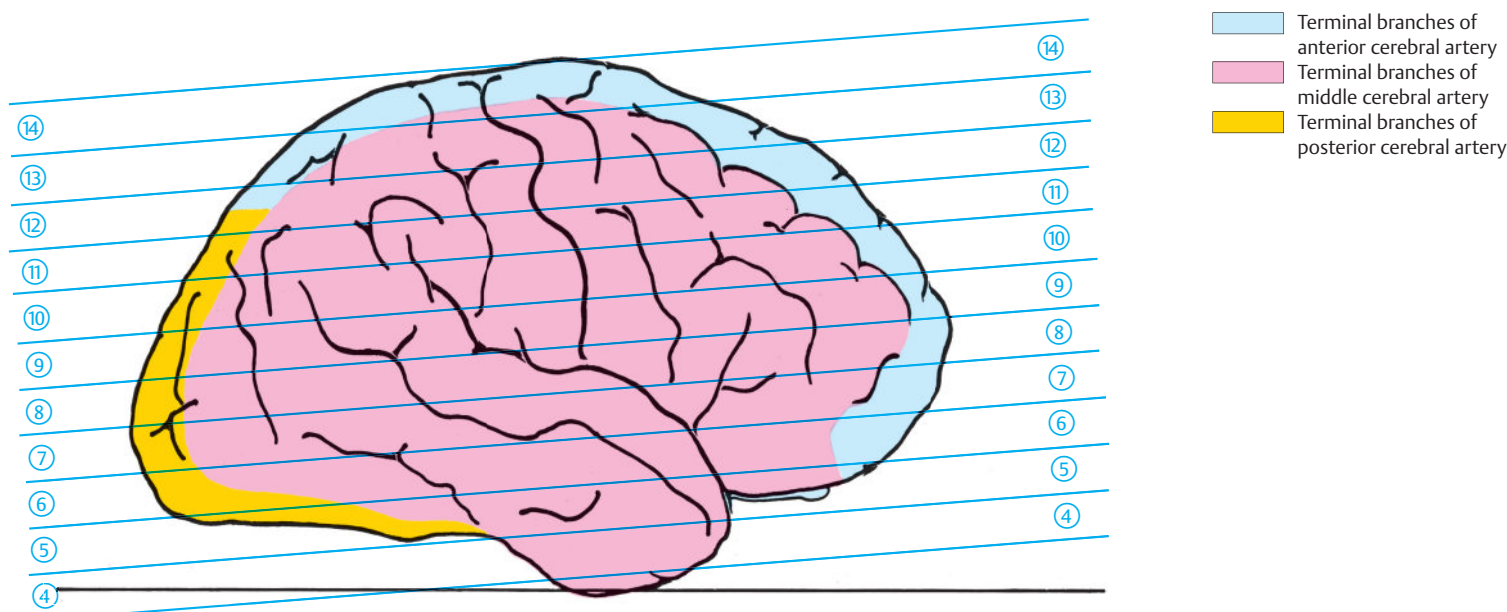


Fig. 7.31b Lateral view of the cerebrum sectioned in the bicommissural plane with the territories of the terminal (cortical) branches of the anterior, middle, and posterior cerebral arteries.

Terminal Branches of the Anterior Cerebral Artery

The anterior cerebral artery supplies most of the medial surface of the cerebral hemisphere, its vascular territory extends from frontal to parietal at the level of the parieto-occipital sulcus. Furthermore, it supplies four-fifths of the corpus callosum with exception of the splenium. Small branches in addition supply a 2–3 cm wide strip along the convexity of the hemisphere along the superior margin. This area includes the superior frontal gyrus, the parts of the pre and postcentral gyri close to the superior margin, as well as the superior parietal gyri. Located within these vascular territories are the primary motor and sensory areas for the contralateral leg.

Clinical Notes

Occlusions of the terminal branches of the anterior cerebral artery result in central motor weakness and sensory loss in the contralateral leg.

Terminal Branches of the Middle Cerebral Artery

The terminal branches of the middle cerebral artery supply the insula, frontal, parietal, and temporal opercula and an oval cortical area around the lateral

sulcus (see ►Fig. 7.29, ►Fig. 7.30, and ►Fig. 7.32). This territory includes the parts of the precentral and postcentral gyri in the vicinity of the central sulcus and thereby primary motor and sensory areas of the trunk, arm, and head. The middle cerebral artery also supplies the white matter beneath the parietal and temporal cortical areas. The upper part of the optic radiation lies in the parietal region while the lower part lies in the temporal region. The motor speech (Broca's) area lies within the frontal operculum of the dominant hemisphere while the sensory speech (Wernicke's) area is situated in the region of the superior temporal gyrus of the temporal operculum.

Clinical Notes

Terminal infarcts in the territory of the middle cerebral artery result in motor weakness and sensory disorders of the contralateral trunk, arm, and head. Furthermore, interruption of the upper half of the optic radiation gives rise to contralateral inferior quadrantanopia while lesions of the lower half of the optic radiation produce a contralateral superior quadrantanopia. Involvement of motor or sensory speech areas results in Broca's aphasia or Wernicke's aphasia respectively. Widespread opercular damage in the dominant hemisphere results in global aphasia with severe speech disorders.⁷⁹

- Terminal branches of anterior cerebral artery
- Terminal branches of middle cerebral artery
- Terminal branches of posterior cerebral artery
- Penetrating branches of anterior cerebral artery
- Penetrating branches of middle cerebral artery
- Penetrating branches of posterior cerebral artery and posterior communicating artery
- Anterior choroidal artery

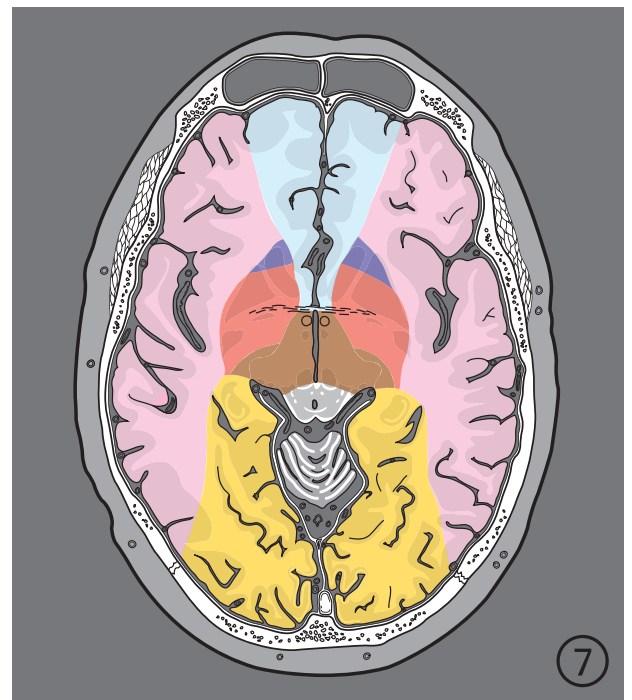
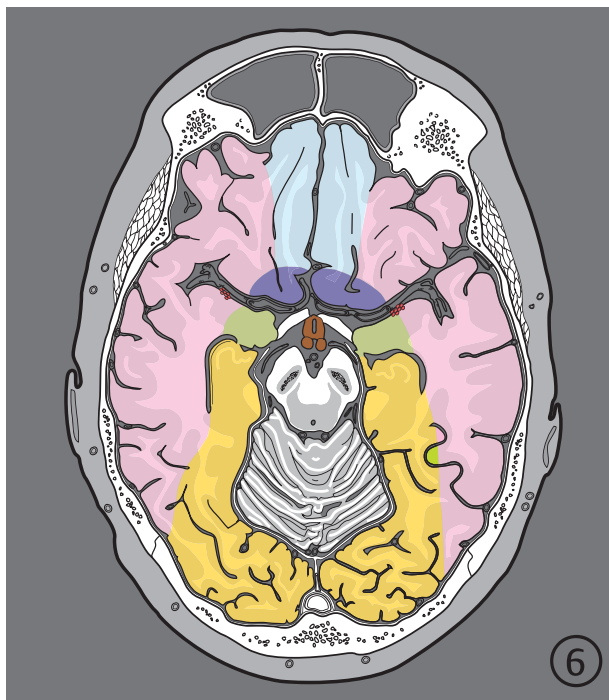
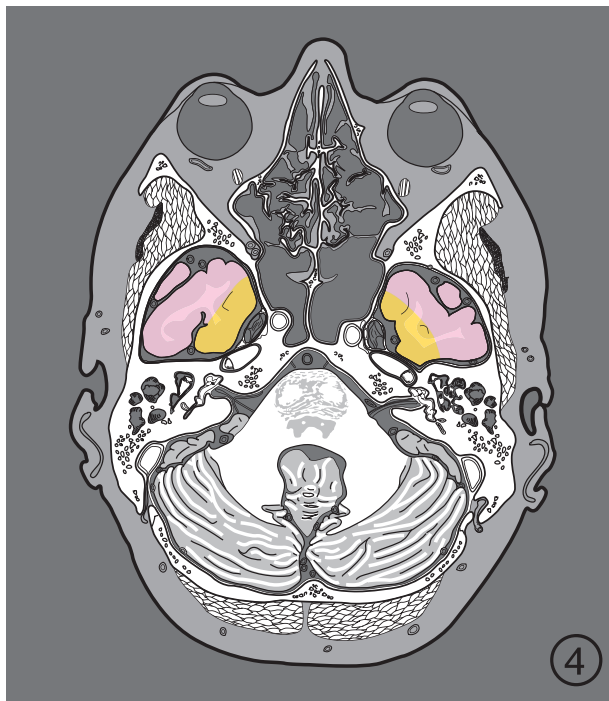


Fig. 7.32 Terminal and central arterial territories of the forebrain. Serial images of the territories of the terminal (cortical) and central (penetrating) branches of the anterior, middle, and posterior cerebral arteries as well as the anterior choroidal artery oriented in the bicommissural plane. Encircled digits indicate the number of the respective slice (see ► Fig. 5.1).

Fig. 7.32a 4th to 7th sections.

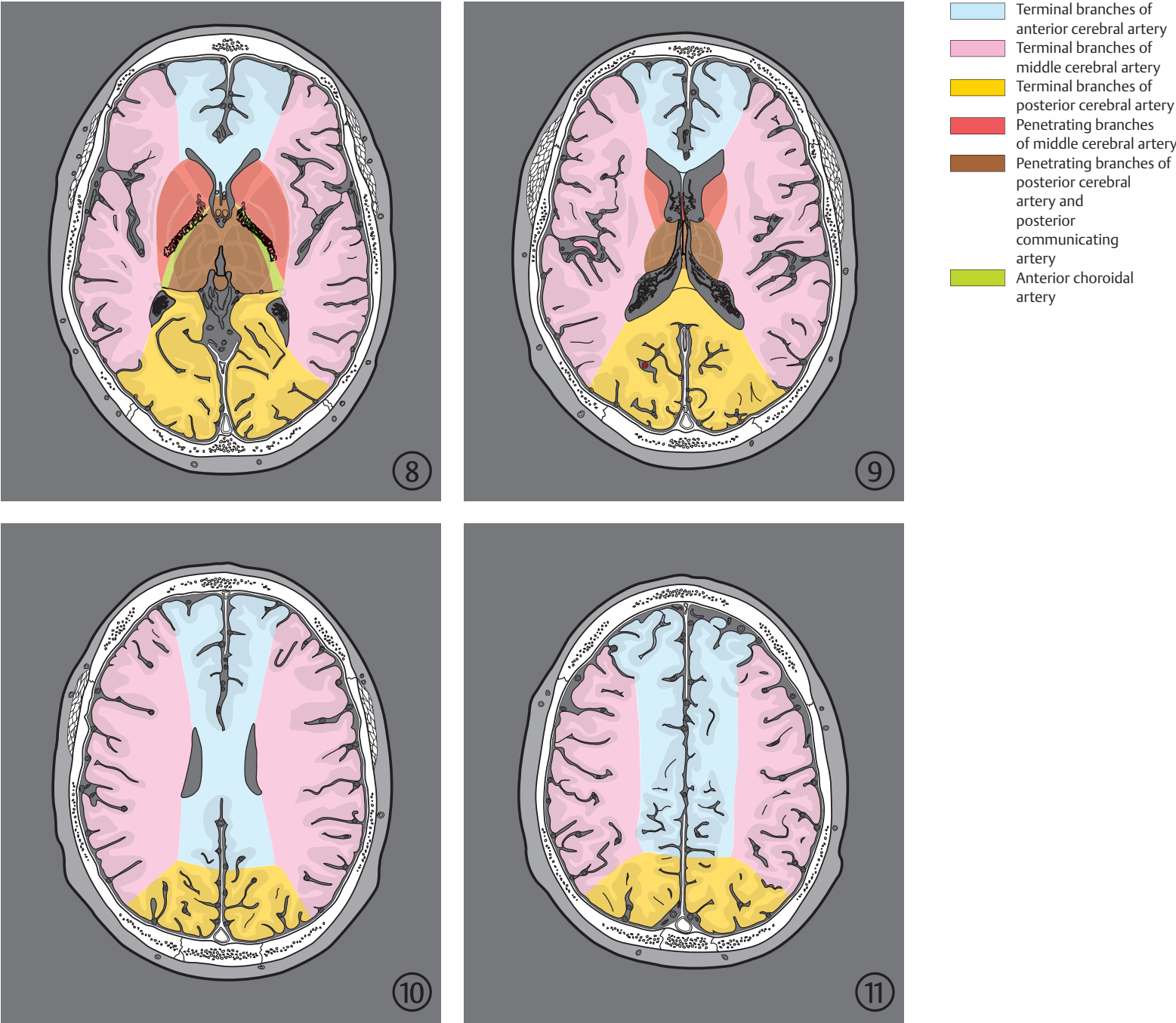


Fig. 7.32b 8th to 11th sections.

- Terminal branches of the anterior cerebral artery
- Terminal branches of the middle cerebral artery
- Terminal branches of the posterior cerebral artery

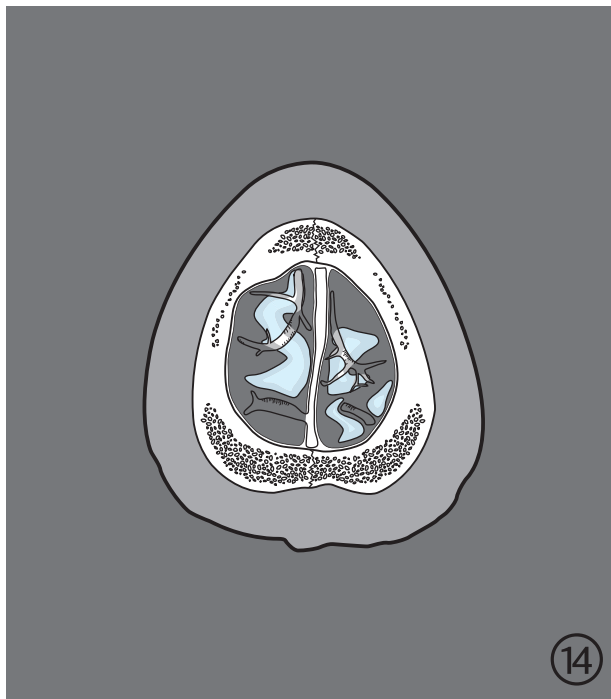
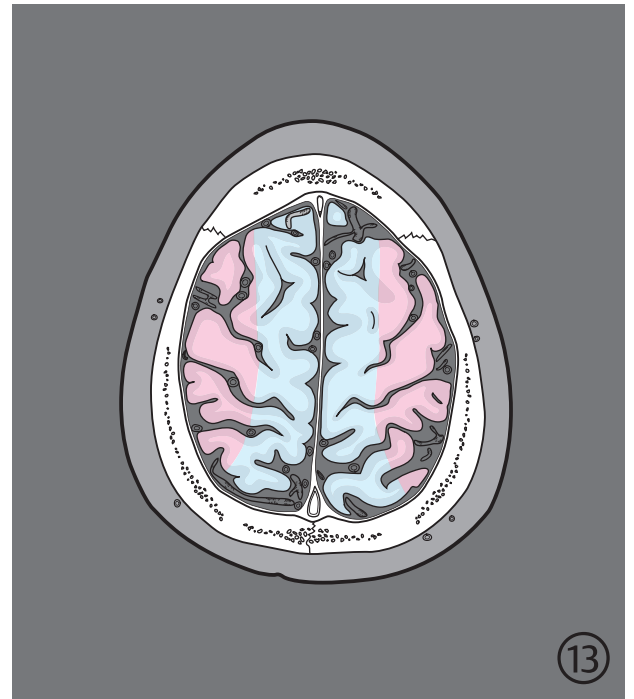
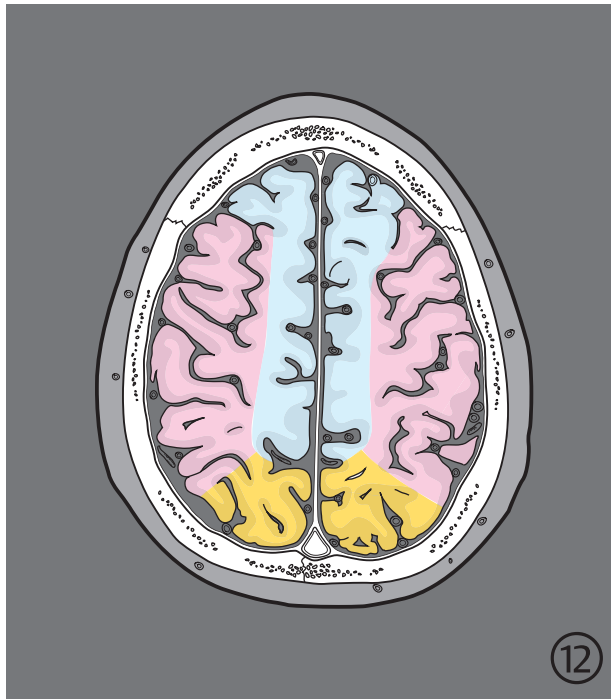


Fig. 7.32c 12th to 14th sections.

Terminal Branches of the Posterior Cerebral Artery

The terminal branches of the posterior cerebral artery supply large parts of the occipital lobe, especially the primary visual cortex with the area striata on the medial surface of the hemisphere (see ▶Fig. 7.28a and ▶Fig. 7.31a). A narrow strip of the occipital and temporal lobes is also supplied over the cerebral convexities (see ▶Fig. 7.28b and ▶Fig. 7.31b). The posterior cerebral artery also supplies the splenium of the corpus callosum.

Clinical Notes

An occlusion of the posterior cerebral artery causes a contralateral homonymous hemianopia. A lesion of the splenium leads to the disconnection of the primary visual cortex from areas of speech, resulting in reading difficulties (alexia or word blindness).

Arterial territories have been depicted in frontal, sagittal, and transversal sections in ▶Fig. 7.28, ▶Fig. 7.29, ▶Fig. 7.30, ▶Fig. 7.31, and ▶Fig. 7.32 in accordance with bibliographical references.^{53,54,79,122,236,307,333,601} A mean arterial territorial size was selected and inter-individual variability kept in mind since the extent of an infarction depends on collateral blood supply. Watershed or border zone infarcts constitute a special type of circulatory impairment. These occur in the border zones between the anterior, middle, and posterior cerebral territories when two (less commonly three) of these arteries are inadequately perfused.

Perfusion CT and MRI are suitable procedures for the assessment of regional vascular supply. Intracranial arteries may be imaged noninvasively with MRA and CTA, which help identify vascular anomalies, alteration in position, and intraluminal changes as well as abnormal blood flow patterns.

7.5 Cerebral Veins

Several veins of the body run together with corresponding arteries in vascular bundles.

Cerebral veins (see ▶Fig. 3.2c, ▶Fig. 3.3c, ▶Fig. 3.4c, ▶Fig. 3.5c, ▶Fig. 3.6c, ▶Fig. 3.7c, ▶Fig. 3.8c, ▶Fig. 3.9c, ▶Fig. 3.10c, ▶Fig. 3.11c, ▶Fig. 3.12c, ▶Fig. 3.13c, ▶Fig. 3.14c, and ▶Fig. 3.15c, ▶Fig. 4.2c, ▶Fig. 4.3c, ▶Fig. 4.4c, ▶Fig. 4.5c, ▶Fig. 4.6c, and ▶Fig. 4.7c, ▶Fig. 5.2, ▶Fig. 5.3, ▶Fig. 5.4, ▶Fig. 5.5, ▶Fig. 5.6, ▶Fig. 5.7, ▶Fig. 5.8, ▶Fig. 5.9, ▶Fig. 5.10, ▶Fig. 5.11, ▶Fig. 5.12, ▶Fig. 5.13, ▶Fig. 5.14, and ▶Fig. 5.15, ▶Fig. 5.17, ▶Fig. 5.18,

▶Fig. 5.19, ▶Fig. 5.20, ▶Fig. 5.21, ▶Fig. 5.22, ▶Fig. 5.23, ▶Fig. 5.24, ▶Fig. 5.25, ▶Fig. 5.26, ▶Fig. 5.27, ▶Fig. 5.28, ▶Fig. 5.29, and ▶Fig. 5.30 ▶Fig. 7.33, ▶Fig. 7.33b, and ▶Fig. 7.34b) however run **independent of cerebral arteries** (see ▶Fig. 7.33 and ▶Fig. 7.34) displaying larger variability than cerebral arteries, and following a well-structured pattern. The topography of deep intracerebral veins is of diagnostic significance while interpreting angiograms: while a space-occupying lesion may be identified by displacement of the deep cerebral veins on the venous phase of an angiogram, cerebral arteries lying superficially may be completely normal.

Cerebral veins and sinuses may serve as landmarks (see Section 2.3.5) in CT and MRI. Pathological changes or displacements are often discrete or unrecognizable. Shift of midline structures results in more pronounced changes in the ventricular system as compared to displacement of deep cerebral veins.

Veins of the brain contain no valves and form a tubular network with several anastomoses. Venous drainage occurs mainly via the venous sinuses through the **internal jugular vein** (see ▶Fig. 3.9c, ▶Fig. 3.9d, ▶Fig. 5.2, ▶Fig. 5.17, ▶Fig. 6.4b, and ▶Fig. 9.2), which leaves the cranial cavity through the jugular foramen (see ▶Fig. 3.23, ▶Fig. 4.5c, ▶Fig. 5.17, ▶Fig. 5.15, and ▶Fig. 5.31). Several veins may compensate for the drainage of the internal jugular vein.

- The **internal vertebral venous plexus** can drain blood from a basilar venous plexus situated on the clivus.
- The **cavernous sinus** may drain via ophthalmic veins into the facial vein (see ▶Fig. 7.35, ▶Fig. 7.35b, and ▶Fig. 9.2).
- Venous drainage of the brain may also take place via **veins passing through the foramen ovale** (see ▶Fig. 7.35a) into the pterygoid venous plexus, through **veins in the carotid canal** (not shown in ▶Fig. 7.33b), and via **emissary veins**.

Two sets of veins drain the telencephalon and diencephalon:

- **Superficial veins** drain blood predominantly from cortical regions.
- **Deep veins** receive most of their blood from white matter and its nuclear regions, also draining cortical areas in some instances. Blood from the tributaries of the deep veins flows cascade-like into the great cerebral vein (Galen; see ▶Fig. 4.2b, ▶Fig. 4.2c, ▶Fig. 4.2d, ▶Fig. 5.9a, and ▶Fig. 5.9b) which usually joins the confluence of the inferior sagittal sinus (see ▶Fig. 7.33b) and the straight sinus (see ▶Fig. 3.12c, ▶Fig. 4.2c, and ▶Fig. 7.33b).³³³

- 1 Rolandic vein
- 2 Superior sagittal sinus
- 3 Superior anastomotic vein (Trolard vein)
- 4 Parietal and occipital ascending veins
- 5 Inferior sagittal sinus
- 6 Thalamostriate vein
- 7 Frontal ascending veins
- 8 Venous angle
- 9 Internal cerebral vein
- 10 Straight sinus
- 11 Basal vein (of Rosenthal)
- 12 Confluence of sinuses (torcular herophili)
- 13 Transverse sinus
- 14 Veins of sylvian fossa
- 15 Vein of septum pellucidum
- 16 Sigmoid sinus

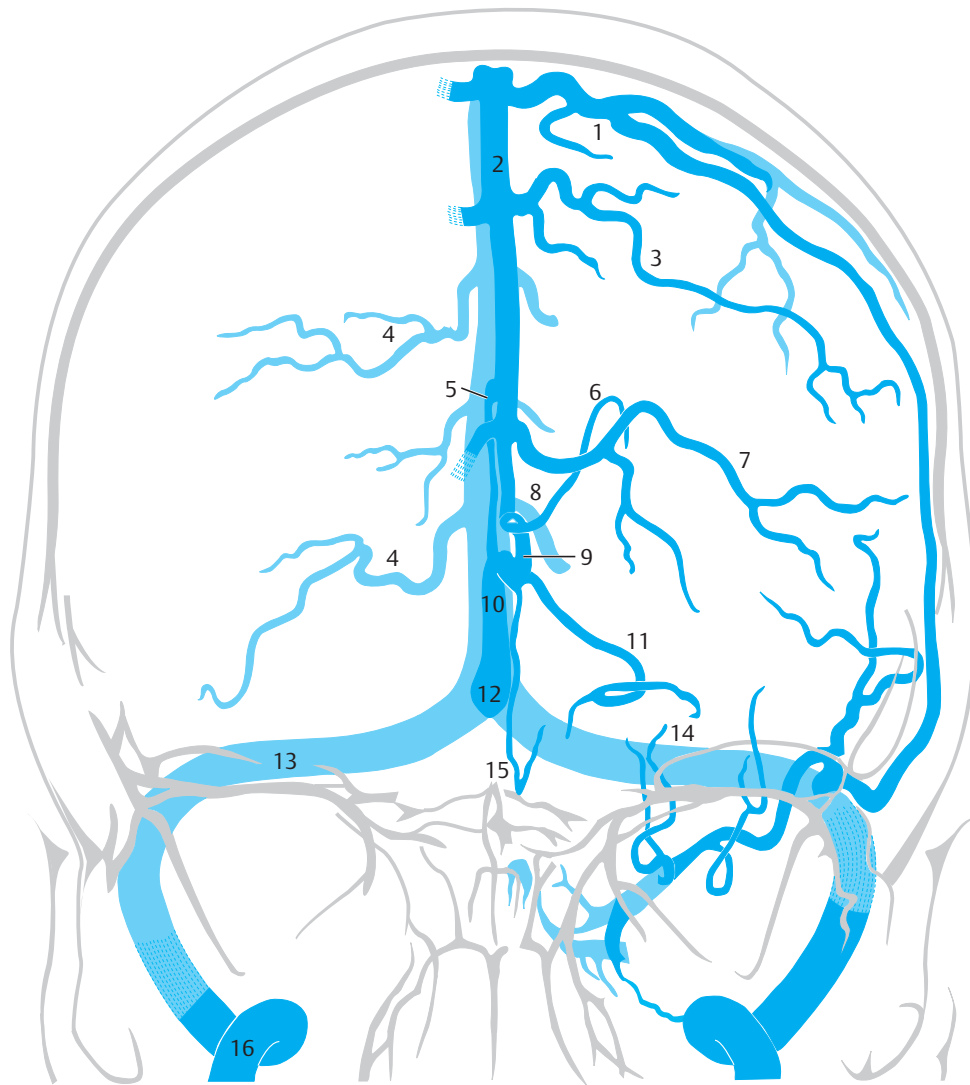
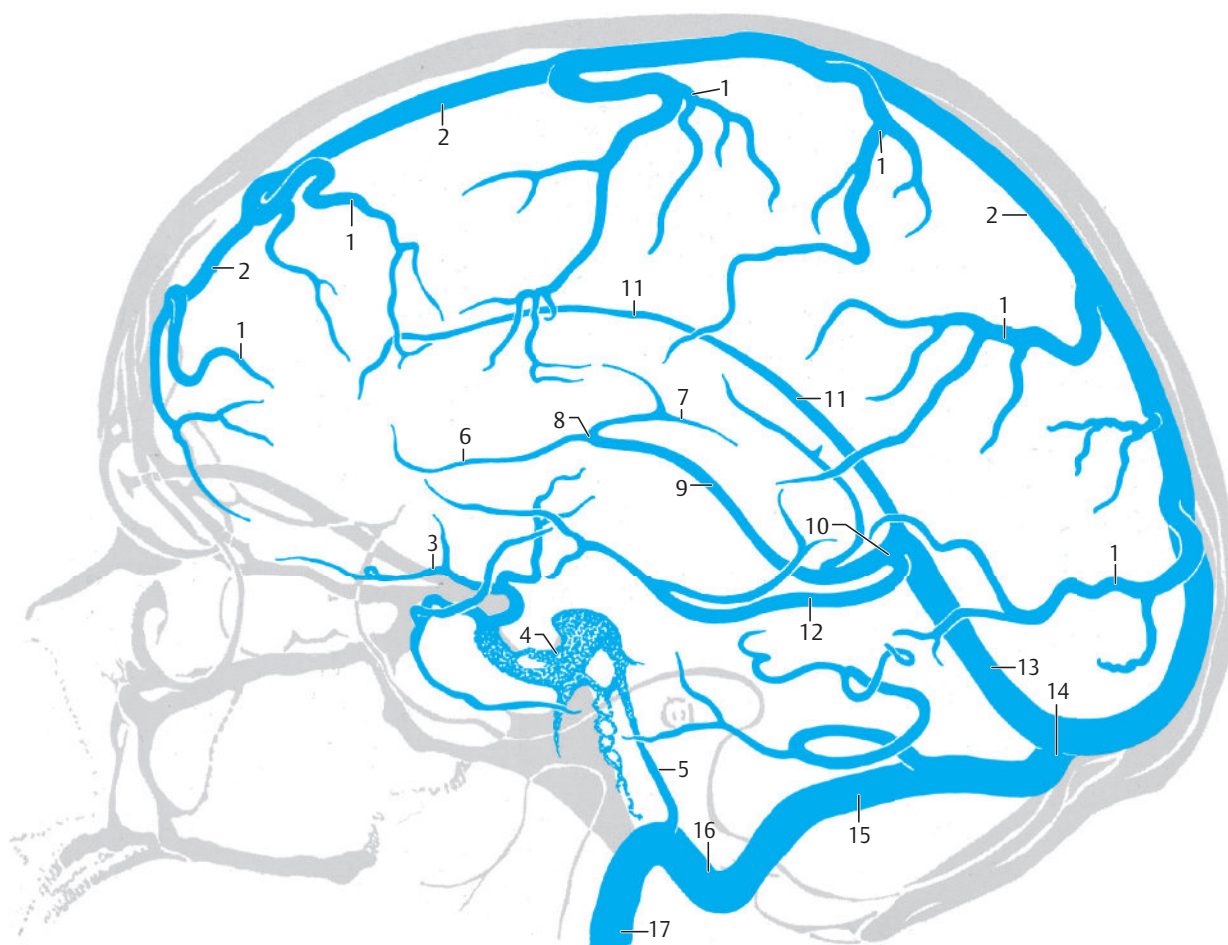


Fig. 7.33 Cerebral veins. Schematic representation.

Fig. 7.33a Image as per Towne's view. (Reproduced from Krayenbühl et al.³⁰⁷)



Superficial veins of cortical regions and their sinuses:

- 1 Superior cerebral veins
- 2 Superior sagittal sinus
- 3 Superficial middle cerebral vein
- 4 Cavernous sinus
- 5 Inferior petrosal sinus

Deep veins of central and nuclear regions and their sinuses:

- 6 Anterior vein of septum pellucidum
- 7 Superior thalamostriate (terminal) vein
- 8 Venous angle
- 9 Internal cerebral vein
- 10 Great cerebral vein (of Galen)
- 11 Inferior sagittal sinus
- 12 Basal vein (of Rosenthal)
- 13 Straight sinus
- 14 Confluence of sinuses
- 15 Transverse sinus
- 16 Sigmoid sinus
- 17 Internal jugular vein

Fig. 7.33b Lateral view. (The numbering sequence takes into account vascular territories and the direction of flow according to Krayenbühl et al.³⁰⁷)

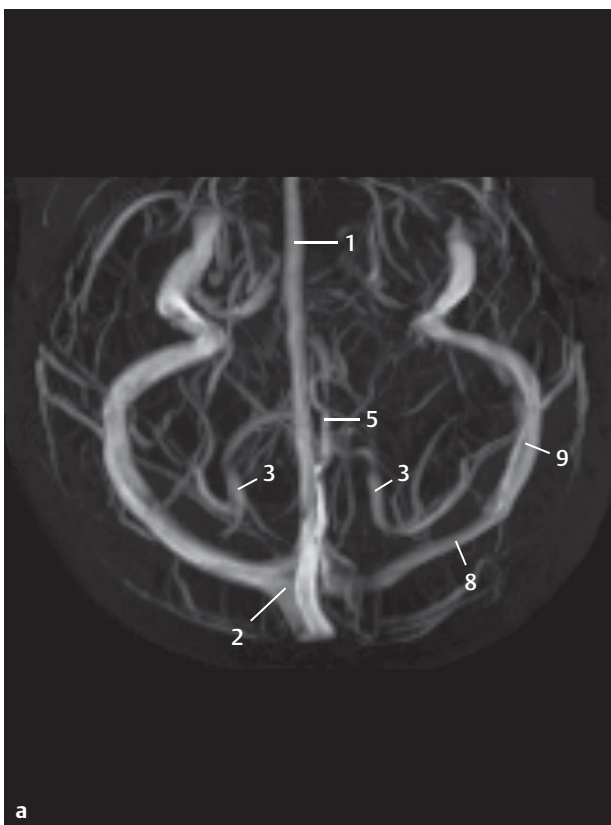


Fig. 7.34 Cerebral veins. Venous MRA of a healthy volunteer (35-year-old woman). For technical data, see Chapter 12.

Fig. 7.34a Axial MIP image.

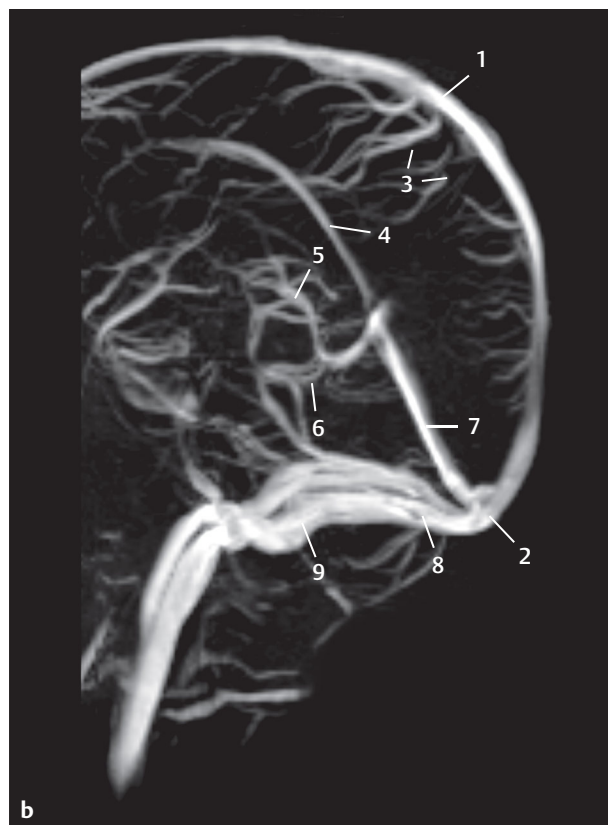


Fig. 7.34b Lateral view of MIP image.

- 1 Superior sagittal sinus
- 2 Confluence of sinuses
- 3 Superior cerebral veins
- 4 Inferior sagittal sinus
- 5 Internal cerebral veins
- 6 Basal vein (of Rosenthal)
- 7 Straight sinus
- 8 Transverse sinus
- 9 Sigmoid sinus

- 1 Sphenoparietal sinus
- 2 Anterior intercavernous sinus
- 3 Cavernous sinus
- 4 Posterior intercavernous sinus
- 5 Basilar plexus
- 6 Venous plexus of foramen ovale
- 7 Superior petrosal sinus
- 8 Inferior petrosal sinus
- 9 Internal jugular vein (running inferiorly)
- 10 Sigmoid sinus
- 11 Transverse sinus
- 12 Occipital sinus
- 13 Superior sagittal sinus
- 14 Confluence of sinuses

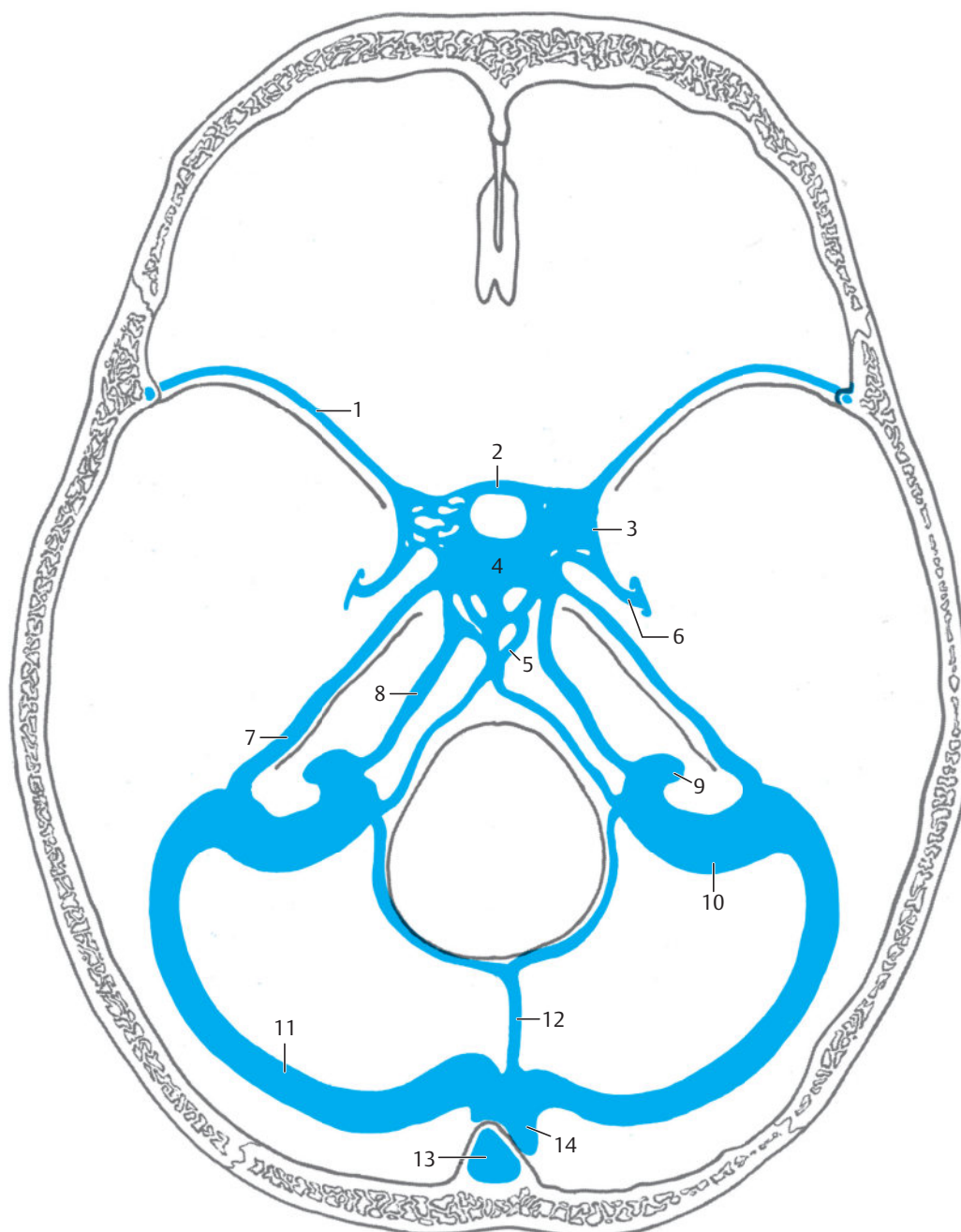


Fig. 7.35 Basal sinus. Schematic representation. (Reproduced from Krayenbühl et al.³⁰⁷)

Fig. 7.35a Horizontal section.

7.5.1 Superficial Cerebral Veins

These include the superior cerebral veins (see ► Fig. 5.9a, ► Fig. 5.9b, ► Fig. 5.12, ► Fig. 5.29, and ► Fig. 7.33b), inferior cerebral veins, and superficial middle cerebral veins (see ► Fig. 7.33a).

The superior cerebral veins ascend in an arc along the curvature of the cerebral hemisphere and drain into the superior sagittal sinus (see ► Fig. 3.2b, ► Fig. 3.2c, ► Fig. 3.2d, ► Fig. 3.7c, ► Fig. 3.7d, ► Fig. 3.15c, ► Fig. 3.15d, ► Fig. 4.2c, ► Fig. 4.2d, ► Fig. 5.11, and ► Fig. 5.29). Veins around the sinus pierce the arachnoid mater and their adventitia fuses with the tough connective tissue of the dura. These veins, referred to as **bridging veins**

(see ► Fig. 3.8e), are vulnerable to mechanical injury which may give rise to a subdural hematoma.²¹⁶

The superficial cerebral veins are subdivided into prefrontal, frontal, parietal, and occipital branches. The inferior cerebral veins descend from the external surfaces of the frontal, temporal, and occipital lobes. The frontal veins generally drain into the superficial middle cerebral vein, while the temporal and occipital veins flow either directly into the transverse sinus (see ► Fig. 3.12c, ► Fig. 3.14b, ► Fig. 3.14c, ► Fig. 3.14d, ► Fig. 3.15c, ► Fig. 3.15d, ► Fig. 4.3b, ► Fig. 4.3c, ► Fig. 4.3d, ► Fig. 4.7b, ► Fig. 4.7c, ► Fig. 4.7d, and ► Fig. 7.35) or indirectly into it via the posterior anastomotic vein. The superficial middle cerebral vein (previously: vein of the sylvian fossa) arises

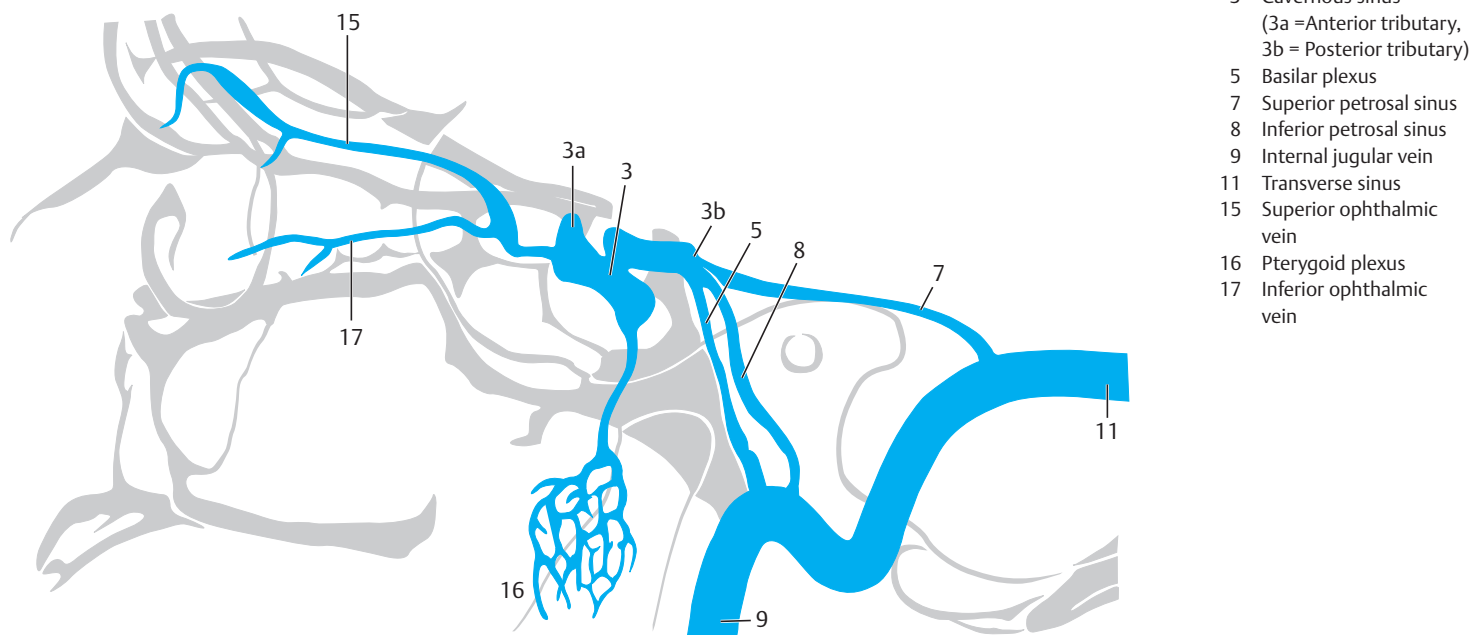


Fig. 7.35b Lateral view.

on the lateral wall of the cerebral hemisphere above the lateral sulcus, and drains either into the cavernous sinus (see ► Fig. 3.6c, ► Fig. 3.6d, ► Fig. 3.7c, ► Fig. 3.7d, ► Fig. 4.3c, ► Fig. 4.3d, ► Fig. 5.20, and ► Fig. 6.9b), sphenoparietal sinus, as the paracavernous sinus into the veins of foramen ovale, superior petrosal sinus (see ► Fig. 6.10b, ► Fig. 7.35, ► Fig. 7.36, ► Fig. 7.36b, and ► Fig. 7.36c) or into the sigmoid sinus (see ► Fig. 3.10c, ► Fig. 3.11c, ► Fig. 3.11d, ► Fig. 4.6c, ► Fig. 4.6d, ► Fig. 5.6a, ► Fig. 5.6b, ► Fig. 5.19, ► Fig. 5.21, ► Fig. 6.5a, and ► Fig. 6.8a).

7.5.2 Deep Cerebral Veins

► Fig. 7.35 and ► Fig. 7.36 provide an overview about basal sinuses and veins.

The deep cerebral veins drain into the roughly 1 cm long **great cerebral vein (of Galen)**.

Formed by the union of both internal cerebral veins (see ► Fig. 3.10c, ► Fig. 3.11c, ► Fig. 3.11d, ► Fig. 4.2c, ► Fig. 4.2d, ► Fig. 5.9a, ► Fig. 5.9b, and ► Fig. 5.25), it curves around the posterior surface of the splenium of the corpus callosum and usually drains into the confluence of the inferior sagittal sinus and the straight sinus. The cerebral falx joins the tentorium of cerebellum at this point.

The **internal cerebral vein** is formed by the confluence of the anterior vein of the septum pellucidum (see ► Fig. 7.33 and ► Fig. 7.36e), superior thalamostriate vein (terminal vein; ► Fig. 3.8c, ► Fig. 3.10c, ► Fig. 7.33, and ► Fig. 7.36), and the superior choroid vein (see ► Fig. 5.10). The anterior vein of the septum pellucidum may be seen opening into the superior thalamostriate vein on the lateral view. This junction is referred to as the venous angle and usually lies at the level of the interventricular foramen. Displacement of the venous angle is an important indicator of an intracranial space-occupying lesion, especially in the median plane.

The superior thalamostriate vein lies in about 50% of cases between the caudate nucleus and the thalamus. It may alter its course to run in an occipital direction before it reaches the interventricular foramen, in which case the venous angle lies a few millimeters occipital to the interventricular foramen.³³³

The internal cerebral vein follows an undulating course posteriorly within the cistern of the transverse fissure. The right and left internal cerebral veins join to form the great cerebral vein (of Galen) approximately 3.5 cm posterior to the interventricular foramen. An angiographically demonstrable displacement of the internal cerebral vein may indicate the presence of an ipsilateral supratentorial space-occupying lesion.

The **basal vein (of Rosenthal)** (see ► Fig. 3.6c, ► Fig. 3.10c, ► Fig. 3.10d, ► Fig. 3.11c, ► Fig. 3.11d, ► Fig. 5.7, ► Fig. 6.13b, and ► Fig. 7.34) arises variably by the confluence of the anterior cerebral vein, inferior central veins, and the deep cerebral vein of the anterior perforated substance.

These veins receive blood from the basal and medial parts of the frontal lobe, the basal ganglia, and the insula (see ► Fig. 7.36). The basal vein runs along the optic tract in an occipital direction between the cerebral peduncle and the diencephalon, and then courses in a posterosuperior direction around the cerebral peduncle. Its first basal segment receives blood from the temporal pole of the temporal lobes, the hippocampus as well as from parts of the midbrain and diencephalon, besides draining the frontal and insular parts of the brain.

The second posterolateral segment of the basal vein lies between the cerebral peduncle and its confluence either with the internal cerebral vein, the great cerebral vein, or the straight sinus.

- 1 Pericallosal vein
- 2 Olfactory vein
- 3 Anterior cerebral vein
- 4 Fronto-orbital vein
- 5 Inferior ventricular vein
- 6 Peduncular vein
- 7 Inferior choroid vein
- 8 Basal vein (of Rosenthal)
- 9 Internal cerebral vein
- 10 Inferior temporo-occipital vein
- 11 Calcarine vein
- 12 Anterior thalamic vein
- 13 Superior thalamic vein
- 14 Inferior thalamic veins
- 15 Superior veins of vermis
- 16 Anterior pontomesencephalic vein (mesencephalic segment)
- 17 Precentral cerebellar vein
- 18 Anterior pontomesencephalic vein (pontine segment)
- 19 Petrosal vein
- 20 Superior petrosal sinus
- 21 Inferior petrosal sinus
- 22 Inferior vein of vermis
- 23 Vein of lateral recess of IVth ventricle
- 24 Superior retrotentorial vein
- 25 Inferior retrotentorial vein
- 27 Posterior thalamic veins
- 28 Superior cerebellar vein
- 29 Straight sinus
- 30 Lateral mesencephalic vein
- 31 Pons
- 32 Cavernous sinus
- 33 Transverse pontine vein
- 34 Confluence of sinuses
- 35 Inferior hemispheric veins
- 36 Superior hemispheric vein
- 37 Tonsils of cerebellum
- 38 Copular point

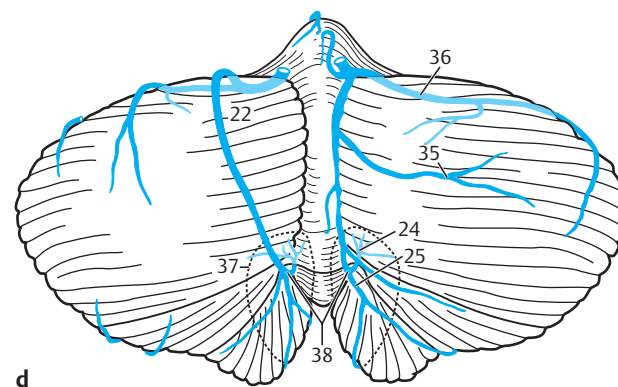
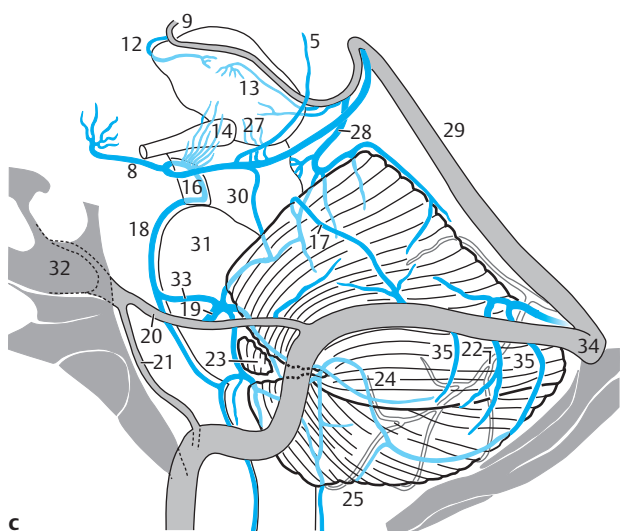
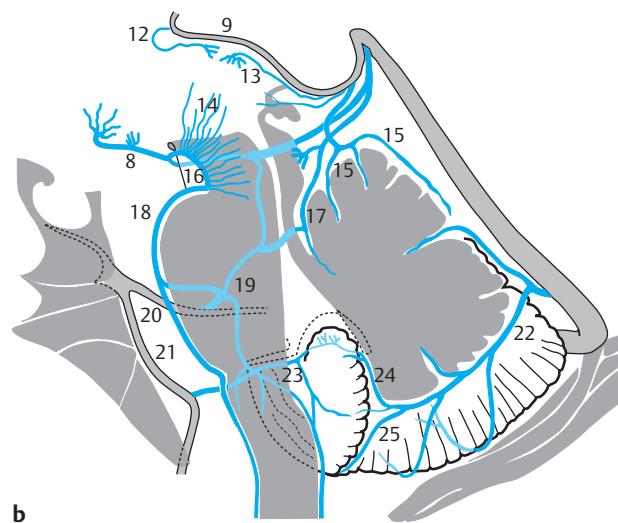
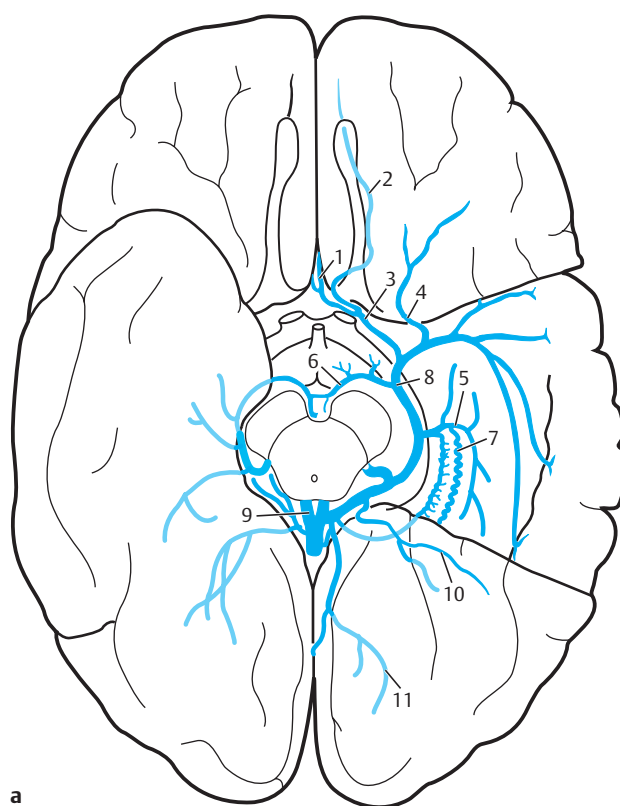


Fig. 7.36 Basal veins. Schematic representation of basal veins on the inferior aspect of the cerebrum, adjacent to the mid-brain (axial view) and the cerebellum (a–d). (Reproduced from Krayenbühl et al.³⁰⁷) Transverse 7T-SWI depiction (e) of deep and basal veins using MIP reconstruction (thickness 2 cm, for technical data, see Chapter 12). (Courtesy of Dr. A. Deistung, Jena.)

Fig. 7.36a Axial section.

Fig. 7.36b Profile view midline.

Fig. 7.36c Profile view lateral.

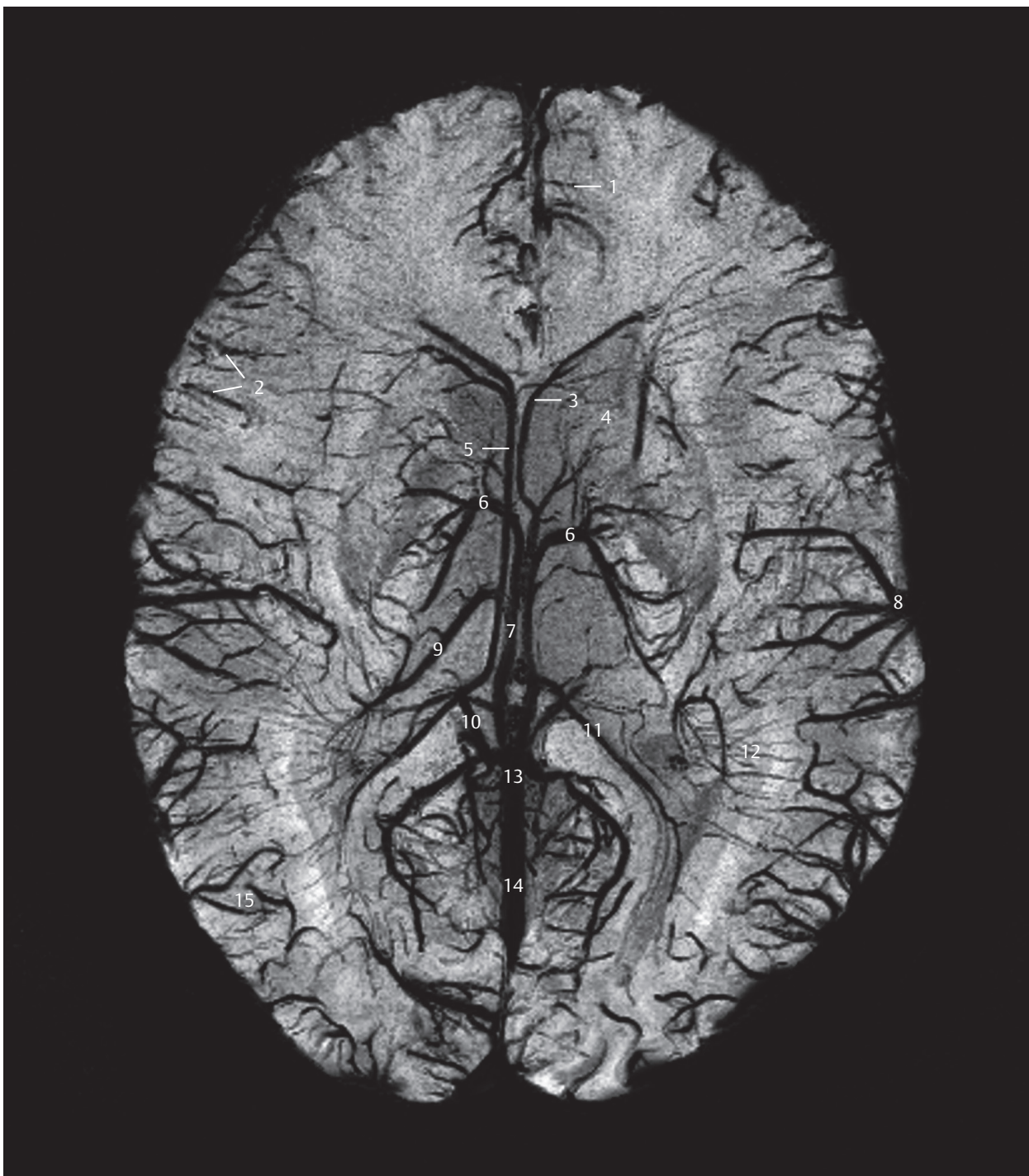
Fig. 7.36d Postero-inferior view.

The second segment receives venous blood from the cerebral peduncle, the tectum, the geniculate bodies, the body and splenium of the corpus callosum, the medial surface of the occipital lobe, and parts of the cerebellum (see ►Fig. 7.36).

The paired internal cerebral veins and the basal veins drain into the unpaired great cerebral vein and the straight sinus. These veins drain the large regions of the white matter of the telencephalon, diencephalon, stria-

tum, midbrain, pons, cerebellum, and medial and basal regions of the frontal, temporal, and occipital surfaces of the telencephalon.

The **straight sinus** drains together with the **superior sagittal sinus** (see ►Fig. 3.15c, ►Fig. 3.15d, ►Fig. 4.2b, ►Fig. 4.2c, ►Fig. 4.2d, ►Fig. 5.7, ►Fig. 6.10a, ►Fig. 7.33) into the transverse sinus through the confluence of sinuses. Venous blood then flows through the sigmoid sinus into the internal jugular vein.



- 1 Prefrontal veins
- 2 Frontal veins
- 3 Anterior vein of septum pellucidum
- 4 Veins of caudate nucleus
- 5 Anterior vein of septum pellucidum (variant)
- 6 Superior thalamostriate vein
- 7 Internal cerebral vein
- 8 Inferior cerebral veins
- 9 Direct vein of lateral ventricle
- 10 Basal vein (of Rosenthal)
- 11 Medial vein of lateral ventricle (medial atrial vein)
- 12 Deep medullary veins
- 13 Great cerebral vein (of Galen)
- 14 Straight sinus
- 15 Occipital veins

Fig. 7.36e SWI MIP image.

Venous drainage of the midbrain is principally provided by the great cerebral vein.

Furthermore, small veins draining the supero-anterior aspect of the cerebellum flow into the great cerebral vein. The large veins of the cerebellum run through the subarachnoid space independent of the arteries and drain into various venous sinuses in the posterior cranial fossa. The petrosal vein drains the antero-inferior part of

the cerebellum and the pons and flows into the superior petrosal sinus. The rest of the cerebellar veins drain into the straight sinus and into the confluence of sinuses and seldom into the transverse sinus. Venous drainage of the pons and the medulla oblongata is highly variable, being provided by tributaries of the basal vein, the transverse sinus, the inferior and superior petrosal sinuses, the occipital sinus, or the internal vertebral venous plexus.

Clinical Notes

Cerebral venous and sinus thromboses are clinically divided into bland and septic and functionally as well as anatomically into deep and superficial thrombotic lesions. A variety of uncharacteristic symptoms complicate the diagnosis. The initial mode of investigation is often CT,²⁵⁸ especially when cerebral venous and sinus thromboses have not been considered in the differential diagnosis. Suspicious findings on cross-sectional imaging include very narrow ventricles and/or extracerebral CSF spaces, as well as bilaterally symmetrical hypodensities or hemorrhage in atypical locations. Thrombosis of the cerebral veins and dural sinuses constitute the most frequent cerebral misdiagnosis.²⁵⁸ Imaging using specific blood-sensitive MR sequences and time-resolved MRA together with CT and CTA constitute diagnostic methods with a high degree of accuracy.^{272,590} T2-weighted images or contrast-enhanced T1-weighted sequences obtained perpendicular to the course of the sinus are useful in the detection of common anatomic asymmetries especially of the transverse sinus which may give rise to diagnostic difficulties.¹¹ A DSA is necessary in the event of a diagnostic dilemma on cross sectional imaging.

7.6 Cranial Nerves

The cranial nerves (see ► Fig. 7.37 and ► Fig. 7.38; see also ► Fig. 6.1, ► Fig. 6.2, ► Fig. 10.6, ► Fig. 10.11, ► Fig. 10.14, and ► Fig. 10.18) emerge from the base of the brain and pass through the basal extracerebral subarachnoid space before they penetrate the dura and exit through the foramina at the base of the skull. Only the IInd cranial nerve retains its dural sheath outside the confines of the cranial cavity. The seventh through XIIth cranial nerves exit via foramina in the posterior cranial fossa while the second through sixth nerves exit via foramina in the middle cranial fossa. The Ist cranial nerve emerges from the anterior cranial fossa through the cribriform plate.

Clinical Notes

High resolution, heavily T2-weighted 3D MR images are best suited for identification of cranial nerves (see ► Fig. 6.10d, ► Fig. 7.3d, and ► Fig. 7.4).

7.6.1 XIIth Cranial Nerve

The XIIth cranial nerve, the **hypoglossal nerve** (see ► Fig. 3.1d, ► Fig. 3.5a, ► Fig. 3.9a, ► Fig. 3.10a, ► Fig. 4.1c, ► Fig. 4.3a, and ► Fig. 5.3) arises as twelve to sixteen rootlets from the medulla oblongata between the pyramid and olive, which join to form several bundles usually lying posterior to the vertebral artery, and reach into the hypoglossal canal of the occipital bone. The hypoglossal nerve innervates muscles of the tongue.

7.6.2 XIth Cranial Nerve

The XIth cranial nerve, the **accessory nerve** (see ► Fig. 3.1d, ► Fig. 3.10a, ► Fig. 4.1c, ► Fig. 5.1d, ► Fig. 6.1, and ► Fig. 6.5b), arises as two roots:

- The **spinal root** (see ► Fig. 3.1d, ► Fig. 4.3a, ► Fig. 5.1d, and ► Fig. 6.5b) arises from spinal segments C1 to C6 (maximum C7, minimum C3). It courses in a cranial direction from the vertebral canal through the foramen magnum into the posterior cranial fossa.
- The **cranial root** arises from the lateral aspect of the medulla oblongata as three to six root fibers.

The two roots unite with the IXth and Xth cranial nerves close to the dural aperture in the region of the jugular foramen, with these three branchial nerves coursing together through the medial part of this foramen. The spinal root of the accessory nerve supplies the sternocleidomastoid and the trapezius together with direct branches from the cervical plexus.

The cranial root of the accessory nerve provides motor innervation of the pharynx, and to a lesser extent, motor supply of the laryngeal musculature (see ► Fig. 7.37).

7.6.3 Xth Cranial Nerve

The Xth cranial nerve, the **vagus**, (see ► Fig. 3.1d, ► Fig. 3.9a, ► Fig. 3.10a, ► Fig. 4.1c, ► Fig. 4.3a, ► Fig. 4.7a, ► Fig. 6.4b, and ► Fig. 6.6b), emerges along the lateral margin of the medulla oblongata as 10 to 18 fine nerve fibers. Its intracranial length up to the dural aperture above the jugular foramen is approximately 1.5 cm.³³³ The vagus carries sensory information from a small area in the external auditory canal and sensory taste buds of the pharynx while carrying visceromotor fibers from mucous membranes of chest viscera and upper abdominal organs. It is also responsible for motor innervation predominantly of laryngeal muscles and partially of pharyngeal musculature (see ► Fig. 7.37). As the main parasympathetic nerve, the vagus supplies thoracic and upper abdominal viscera and the intestinal tract up to the Cannon–Böhm point.

7.6.4 IXth Cranial Nerve

The IXth cranial or **glossopharyngeal nerve** (see ► Fig. 3.1d, ► Fig. 3.9a, ► Fig. 3.10a, ► Fig. 4.1c, ► Fig. 4.3a, and ► Fig. 6.5b) being a branchial nerve shares some morphologic similarities with the vagus: a lateral exit from the medulla oblongata and its passage through the jugular foramen at the base of the skull. The glossopharyngeal nerve also supplies primary branchial regions including palatal and pharyngeal mucosa and taste buds on the posterior third of the tongue while providing parasympathetic innervation of the parotid gland and some of the pharyngeal muscles.

7.6.5 VIIIth Cranial Nerve

The VIIIth cranial or **vestibulocochlear nerve** (see ► Fig. 3.1d, ► Fig. 3.9a, ► Fig. 3.10a, ► Fig. 4.1c, ► Fig. 4.4a, ► Fig. 5.5, ► Fig. 5.37, ► Fig. 7.3d, and ► Fig. 7.4) consists

of two distinct parts: one distributed to the vestibular system, the other to the auditory system. Afferent fibers of the nerve pass through the internal acoustic aperture and enter the medulla oblongata at its lateral margin close to the pons. The intracisternal length of the vestibulocochlear nerve is approximately 1.4 cm.³³³

7.6.6 VIIth Cranial Nerve

The VIIth cranial or **facial nerve** emerges from the brainstem between the pons and medulla together with the intermediate nerve (see ►Fig. 3.1d, ►Fig. 3.9a, ►Fig. 3.10a, ►Fig. 4.1c, ►Fig. 4.4a, and ►Fig. 7.3g). The intermediate nerve is a very thin bundle running inferiorly parallel to the main VIIth cranial nerve. The seventh nerve lies superior and anterior to the vestibulocochlear nerve in the internal acoustic canal (see ►Fig. 7.4) and measures approximately 1.6 cm in length from its origin to the internal acoustic aperture.³³³

The intermediate nerve carries sensory nerve fibers from the taste buds on the anterior two-thirds of the tongue, and parasympathetic fibers to the lacrimal glands, glands in the nasopharyngeal region as well as to sublingual and submandibular glands. Principally a motor nerve, the facial nerve innervates the muscles of facial expression, the stapedius, and part of the suprahyoid muscles (see ►Fig. 7.37).

Clinical Notes

The anterior inferior cerebellar artery forms a vascular loop in the immediate vicinity of the facial nerve in one third of individuals, which may compress the facial nerve and induce a hemifacial spasm.^{270,473,506}

7.6.7 VIth, IVth, and IIIrd Cranial Nerves

The abducens (VI), trochlear (IV), and oculomotor (III) nerves innervate the extraocular muscles:

The **abducens nerve** (see ►Fig. 3.1d, ►Fig. 3.8a, ►Fig. 3.9a, ►Fig. 4.1c, ►Fig. 4.2a, ►Fig. 4.3a, ►Fig. 5.5, and ►Fig. 6.7b) exits the basal surface of the brainstem through a groove between the pons and medulla oblongata in 94% cases, while in 6% it emerges marginally above this groove from the inferior aspect of the pons.⁶⁴² Coursing through the prepontine cistern it pierces the dura (see ►Fig. 5.5 and ►Fig. 6.9b) at the clivus, mediobasal to the apex of the petrous part of the temporal bone. The nerve measures 1.5 cm in length in its intracisternal course.³³³

Continuing through the basilar venous plexus while running through Dorello's canal it enters the cavernous sinus through its lateral wall. It then leaves the middle cranial fossa through the superior orbital fissure and innervates the lateral rectus. Paresis of the abducens results in convergent strabismus.

The **trochlear nerve** (see ►Fig. 3.10a, ►Fig. 4.4a, ►Fig. 6.11b, and ►Fig. 6.12b) is the only cranial nerve that emerges from the posterior aspect of the brainstem, exiting the midbrain immediately inferior to the inferior

colliculus of the tectum. Traversing the ambient cistern around the midbrain, it passes through the dura at the point of attachment of the tentorial notch to the posterior clinoid process. The nerve usually enters the dura about 1 cm inferior to the posterior clinoid process. Running along the roof of the cavernous sinus, the trochlear nerve passes through the superior orbital fissure into the orbit. It innervates the superior oblique, which rotates the eyeball downwards and laterally. In the event of trochlear nerve paresis, the antagonist muscles rotate the eyeball upwards and medially.

The **oculomotor nerve** (see ►Fig. 3.1c, ►Fig. 3.7a, ►Fig. 3.8a, ►Fig. 4.1c, ►Fig. 4.2a, ►Fig. 4.3a, ►Fig. 6.11b, and ►Fig. 6.12b) is the thickest nerve supplying the extra-ocular muscles, innervating the remaining four extra-ocular muscles and the levator palpebrae superioris. It also carries parasympathetic fibers to the sphincter pupillae and the ciliary muscles. The oculomotor nerve emerges from the interpeduncular fossa, traverses through the interpeduncular cistern, and courses between the superior cerebellar and the posterior cerebral arteries toward the cavernous sinus. Running in the lateral wall of this sinus, the nerve exits the middle cranial fossa through the superior orbital fissure.

7.6.8 Vth Cranial Nerve

The **trigeminal** or Vth cranial nerve (see ►Fig. 3.8a, ►Fig. 3.8b, ►Fig. 3.9a, ►Fig. 3.9b, ►Fig. 4.1c, ►Fig. 4.3a, ►Fig. 4.4a, ►Fig. 4.4d, ►Fig. 5.5, ►Fig. 6.8b, ►Fig. 6.9b, ►Fig. 6.10b, and ►Fig. 6.10d) exits the brainstem at the lateral aspect of the pons.¹⁰¹ It emerges from the posterior cranial fossa through its dural pore and enters the trigeminal (Meckel's) cave in the middle cranial fossa, a flat dural pouch lined by arachnoid mater. The trigeminal ganglion (see ►Fig. 3.7a, ►Fig. 4.4a, and ►Fig. 6.8b) lies within Meckel's cave and contains pseudo-unipolar neurons for the sensory root of the trigeminal nerve. Distal to the ganglion, the trigeminal nerve divides into its three large branches, namely the ophthalmic, maxillary, and mandibular nerves, which exit the middle cranial fossa through the superior orbital fissure (see ►Fig. 3.5c, ►Fig. 3.5d, ►Fig. 4.1b, and ►Fig. 5.35), foramen rotundum (see ►Fig. 3.18, ►Fig. 4.10, and ►Fig. 5.34), and foramen ovale (see ►Fig. 4.11, ►Fig. 5.17a, and ►Fig. 5.32), respectively. For the most part, the trigeminal nerve transmits afferent signals from the skin of the face, the conjunctiva and cornea, nasal and oral mucosa and the teeth. Afferent fibers from the muscle spindles in muscles of mastication relay in an unusual manner in the trigeminal system (see Section 10.1.3). The motor fibers of the trigeminal nerve lie medially within it and course toward the mandibular nerve without entering the trigeminal ganglion. These fibers innervate the muscles of mastication, the tensor tympani, and most of the muscles of the floor of the mouth (see ►Fig. 7.37).

Clinical Notes

Observations by neurosurgeons have shown that the trigeminal nerve may be compressed by the superior cerebellar artery, with resultant trigeminal neuralgia.^{269,271,506}

- Oculomotor nerve
- Trochlear nerve
- Abducens nerve
- Trigeminal nerve, motor root
- Facial nerve
- Hypoglossal nerve
- Cervical spinal nerves

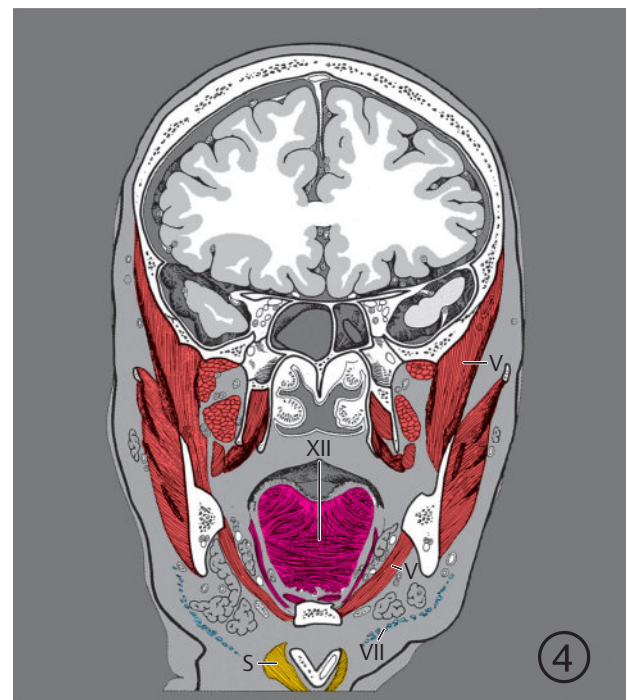
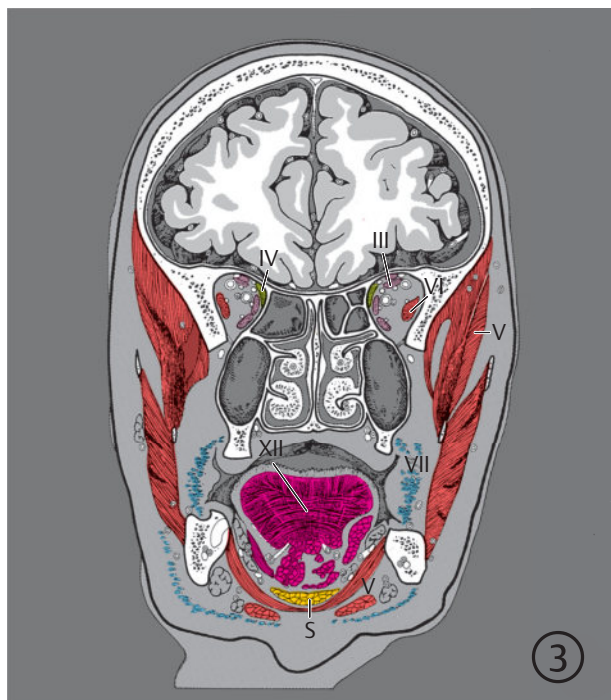
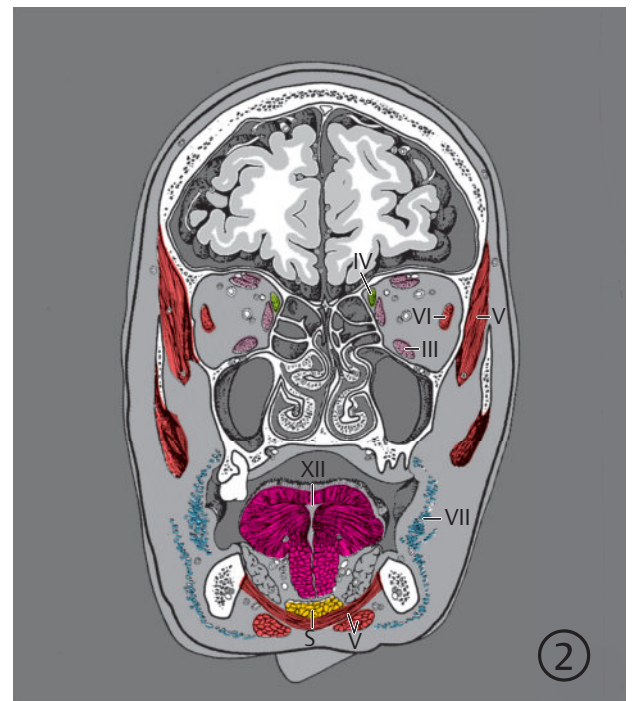
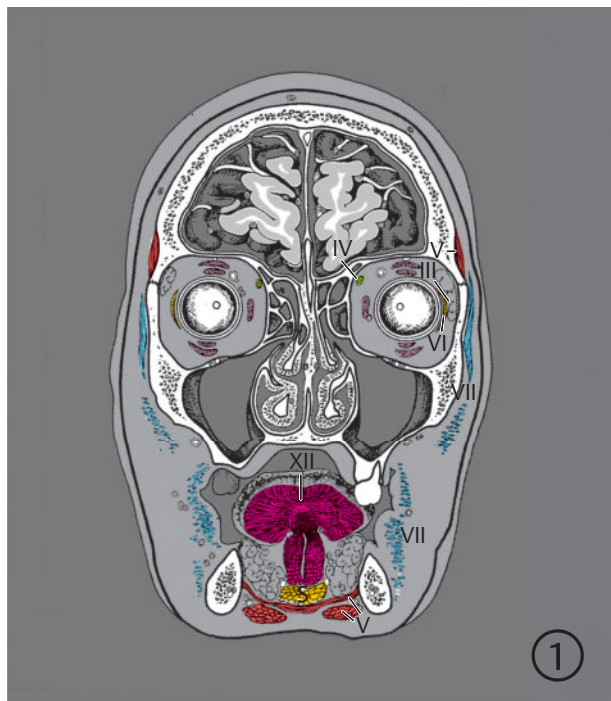
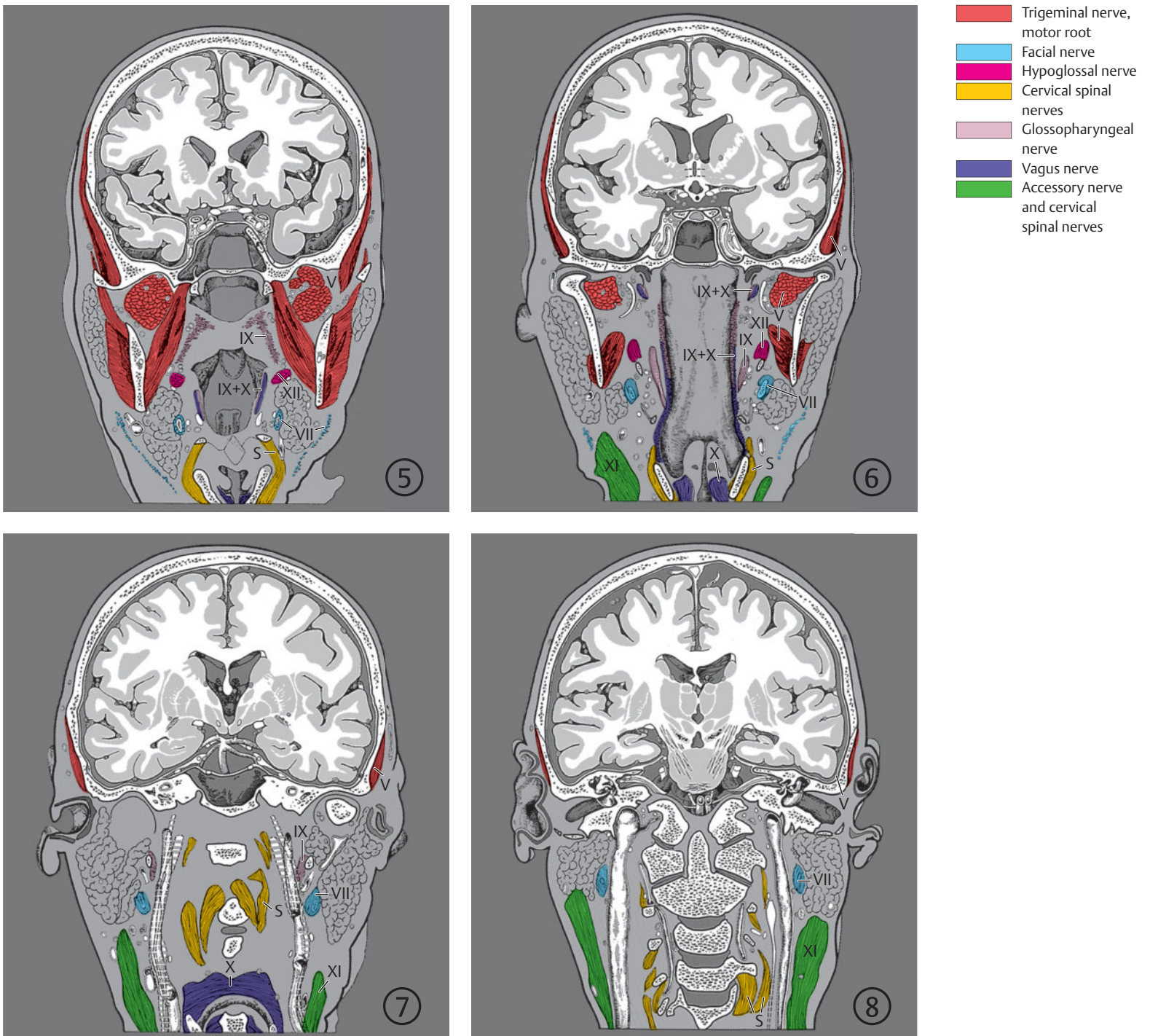


Fig. 7.37 Innervation of muscle groups in the head and neck region. Coronal image series of muscle groups supplied by cranial nerves (III, IV, V, VI, VII, IX, X, XI, XII) and/or by cervical spinal nerves (S). Encircled digits indicate the number of the respective slice (see ► Fig. 3.1).

Fig. 7.37a 1st to 4th sections.



- Trigeminal nerve, motor root
- Facial nerve
- Cervical spinal nerve
- Accessory nerve and cervical spinal nerves

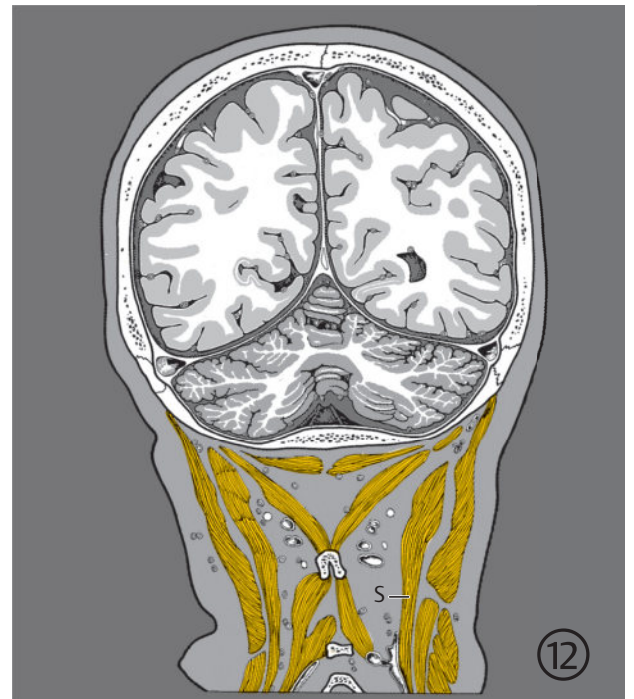
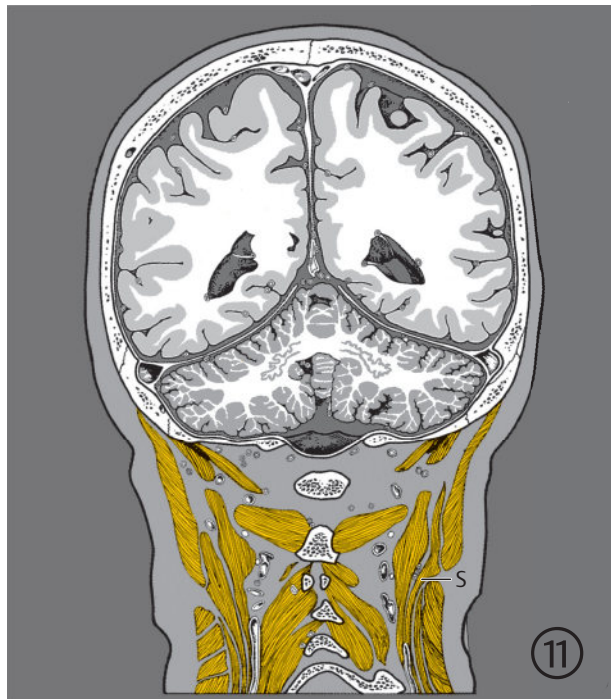
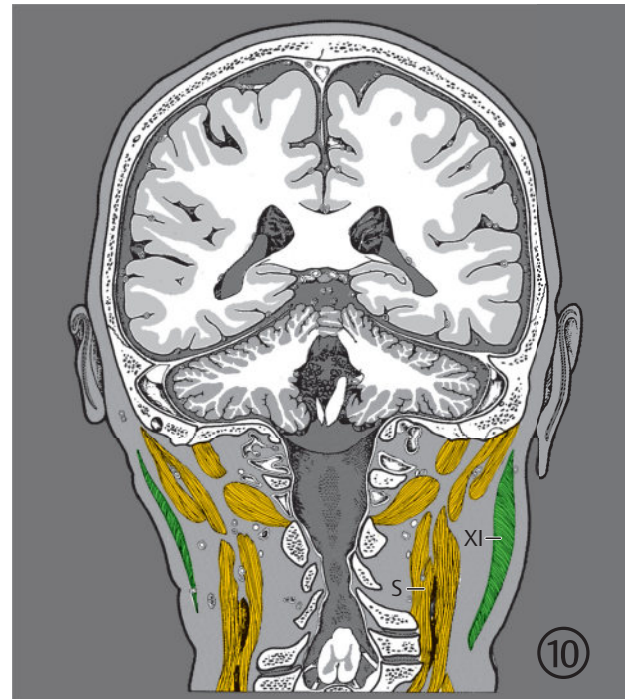
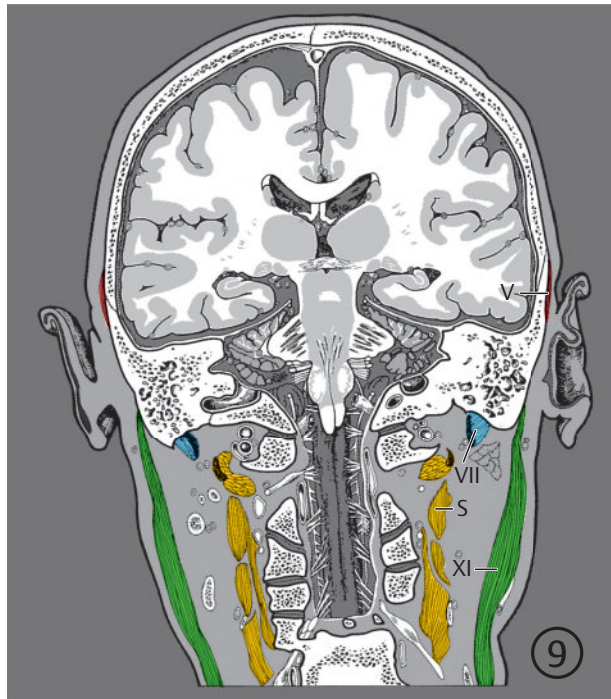
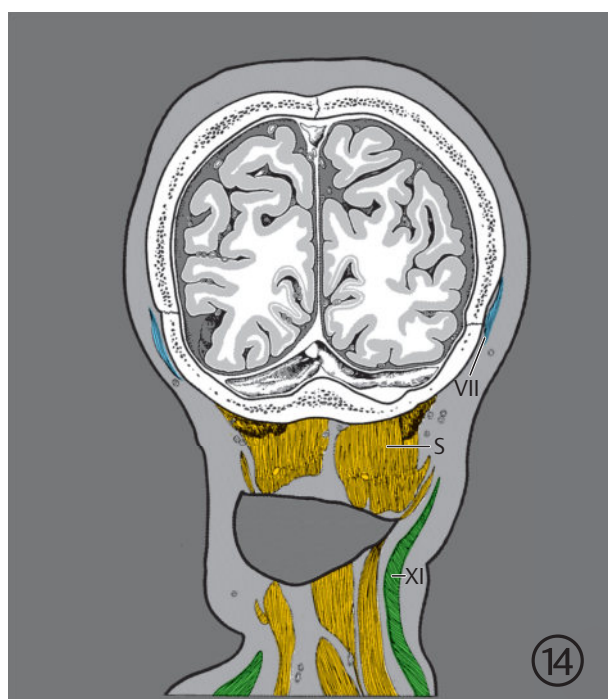
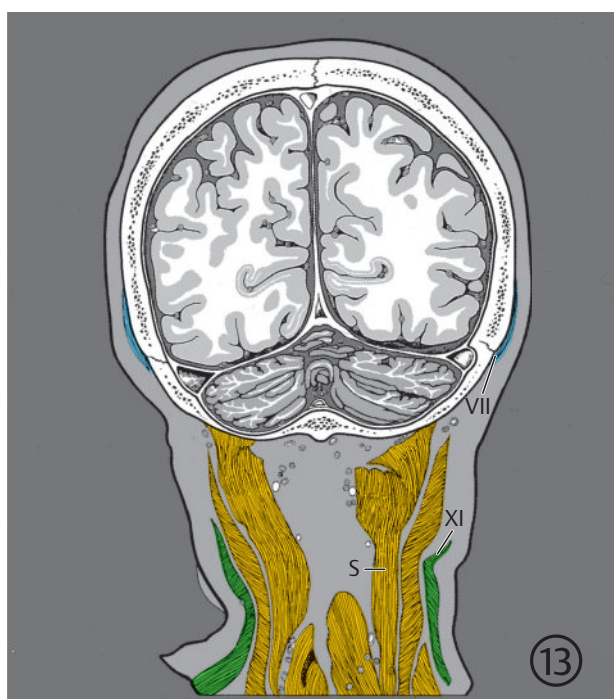
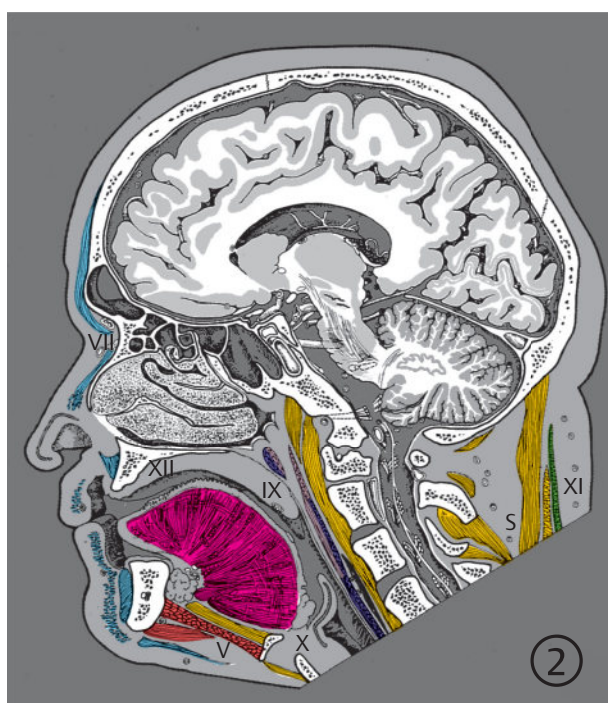
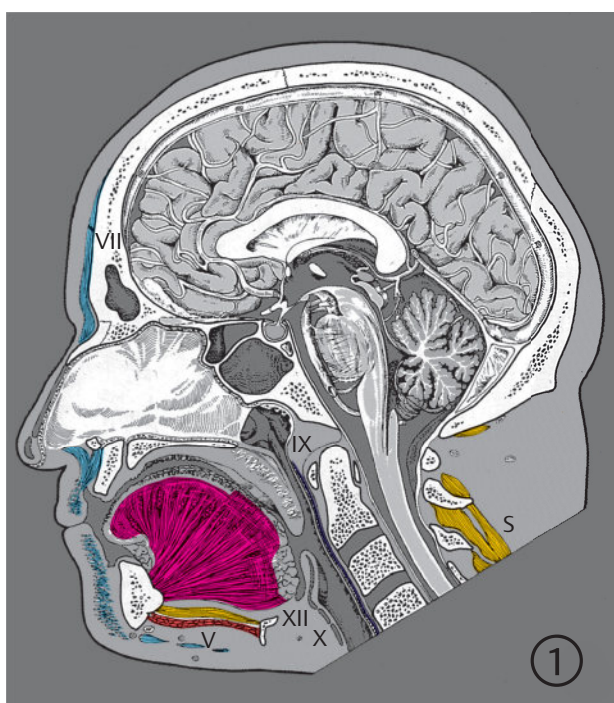


Fig. 7.37c 9th to 12th sections.



- Facial nerve
- Cervical spinal nerves
- Accessory nerve and cervical spinal nerves

Fig. 7.37d 13th to 14th sections.



- Trigeminal nerve, motor root
- Facial nerve
- Hypoglossal nerve
- Cervical spinal nerve
- Glossopharyngeal nerve
- Vagus nerve
- Accessory nerve and cervical spinal nerves

Fig. 7.38 Innervation of muscle groups in the head-neck region. Sagittal image series of muscle groups supplied by cranial nerves (III, IV, V, VI, VII, IX, X, XI, XII) and/or by cervical spinal nerves (S). Encircled digits indicate the number of the respective slice (see ► Fig. 4.1).

Fig. 7.38a 1st and 2nd sections.

- Oculomotor nerve
- Abducens nerve
- Trigeminal nerve, motor root
- Facial nerve
- Hypoglossal nerve
- Cervical spinal nerves
- Glossopharyngeal nerve
- Vagus nerve
- Accessory nerve and cervical spinal nerves

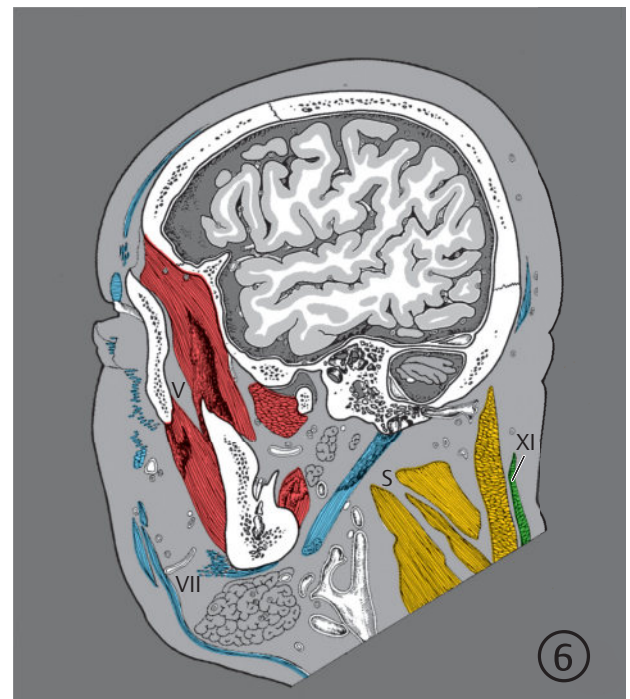
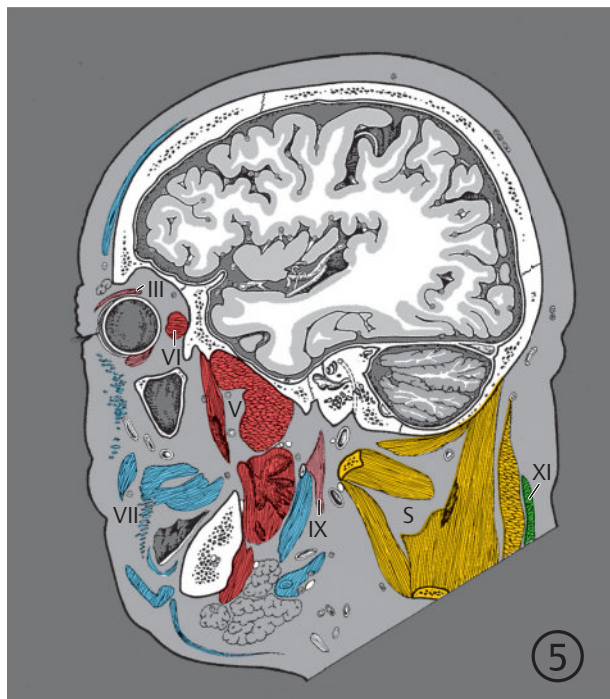
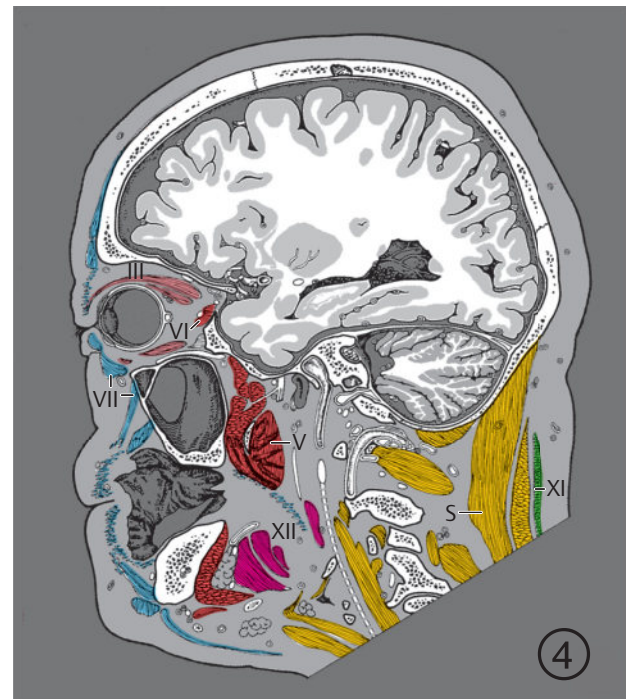
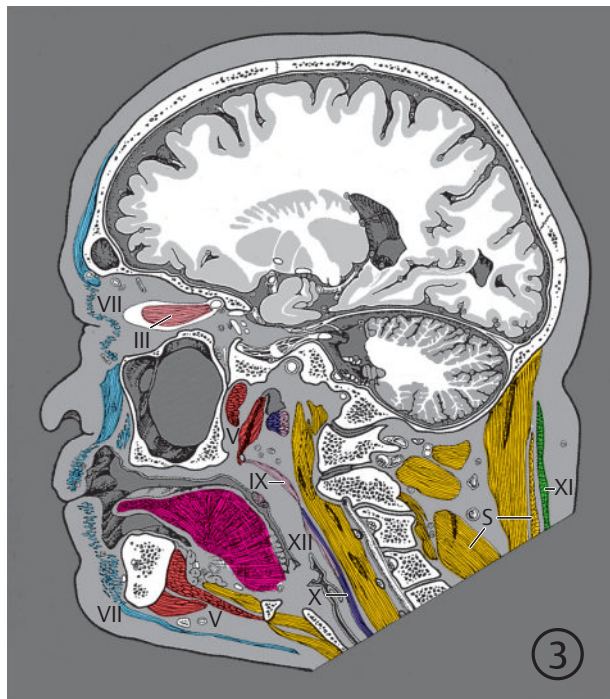


Fig. 7.38b 3rd to 6th sections.

7.6.9 IInd Cranial Nerve

The IInd cranial or the **optic nerve** (see ►Fig. 3.1c, ►Fig. 3.5a, ►Fig. 3.5b, ►Fig. 3.6a, ►Fig. 3.6b, ►Fig. 3.6d, ►Fig. 4.2a, ►Fig. 4.3a, ►Fig. 4.3b, ►Fig. 5.17, ►Fig. 5.19, ►Fig. 6.11b, and ►Fig. 6.1b) enters the middle cranial fossa through the optic canal.¹⁰¹ Its topography has been described with the visual system (see Section 10.6).

7.6.10 1st Cranial Nerve

The 1st cranial or the **olfactory nerve** passes through the cribriform plate into the anterior cranial fossa and has been described in depth with the olfactory system (see Section 10.7).

Clinical Notes

Cranial nerve syndromes:

Of clinical relevance is the topography of the cranial nerves, their relationships to each other and to structures of the skull base, to blood vessels and to different parts of the human brain. The simultaneous occurrence of lesions of several cranial nerves can indicate the location of the lesion, be it inflammation or a tumor involving the base of the skull or the brain itself. “Garcin’s syndrome” is characterized by symptoms arising from ipsilateral involvement of cranial nerves at the skull base, sometimes with unilateral involvement of only the fifth and seventh to twelfth nerves.

The jugular foramen syndrome includes disorders of the glossopharyngeal nerve with sensory impairment, frequently with pain suggestive of glossopharyngeal neuralgia, paresis of the soft palate, a lesion of the vagus nerve with vocal cord palsy and unilateral paresis of the accessory and hypoglossal nerves.

Contralateral hemiparesis due to medullary compression together with lower cranial nerves palsies as described above is known as “Vernet syndrome”.

The cerebellopontine angle syndrome results from disease processes of the Vth, VIth, and VIIth cranial nerves. Unilateral acoustic and vestibular disturbances, peripheral facial paresis, sensory impairment and/or facial pain may occur. Advanced disease may induce homolateral ataxia and nystagmus subsequent to cerebellar involvement, with paresis of the abducens nerve occurring occasionally.

“Gradenigo’s syndrome” or syndrome of the apex of the petrous part of the temporal bone is characterized by unilateral paresis of the abducens nerve and by involvement of the trigeminal nerve causing sensory impairment or facial pain, especially in the forehead. Extensive disease may cause peripheral facial paresis.

The cavernous sinus syndrome involves a disorder of the three ocular nerves, namely the IIIrd, IVth, and Vth cranial nerves, as well as the trigeminal nerve.

A syndrome of the superior orbital fissure results from involvement of the first trigeminal division in addition to the three ocular cranial nerves.

Associated unilateral headache, especially in the temporal region, and a nonpulsatile exophthalmos may indicate a “syndrome of the sphenoid wing”, most often due to meningiomas present in this region.

The orbital apex syndrome results from involvement of the optic nerve together with the third, fourth, sixth, and first division of the Vth cranial nerves. The primary

symptom is visual impairment resulting from progressive optic atrophy.

The olfactory groove syndrome presents first with unilateral and eventually with bilateral anosmia. The lesion may also affect the optic nerve thereby leading to visual field defects or blindness. Large and advanced space-occupying lesions, such as meningiomas, are often characterized by a frontal lobe syndrome with corresponding psychopathologic findings.

Lesions of the base of the skull causing these cranial nerve syndromes are not always demonstrable on CT in the initial stages. Additional thin CT sections, reformation, special bone windows (high resolution technique), and intravenous or intrathecal contrast medium administration, when needed, are necessary for optimal delineation. Pathological processes are often identified earlier on MRI than on CT and may also require thin sections, intravenous contrast medium administration and fat suppression methods. MRI is preferable to CT for early detection of lesions involving the skull base. Both diagnostic modalities employed together may improve diagnostic accuracy, as outlined in Section 2.4.

7.7 Subdivisions of the Brain

The brain may be divided into two parts (see ► Fig. 7.39, ► Fig. 7.40, ► Fig. 7.41, ► Fig. 7.42, ► Fig. 7.43, ► Fig. 7.44):

- Brainstem together with the cerebellum
- Forebrain or prosencephalon

The medulla oblongata, pons, and midbrain are collectively called the brainstem as per Terminologia Anatomica (contrary to clinical parlance). Three paired cerebellar peduncles connect the cerebellum to the brainstem. The forebrain is further divided into the diencephalon and telencephalon. The longitudinal axis of the brainstem (**Meynert’s axis**) and that of the forebrain (**Forel’s axis**) form an obtuse angle of 110 to 120° to one another as described briefly in the introduction of the book. Meynert’s axis runs tangentially across the floor of the IVth ventricle, while Forel’s axis extends from the frontal to the occipital pole of the telencephalon. The angle between the two axes as measured in brains fixed extracranially (see Section 1.3) usually differs from the angle measured in vivo.

► Fig. 7.39 demonstrates the position of coronal sections; ► Fig. 7.40 the individual sections of the coronal series. The position of sagittal sections has been shown in ► Fig. 7.41 while ► Fig. 7.42 gives an overview of parts of the brain in sagittal sections. ► Fig. 7.43 illustrates the position of bicommissural sections and ► Fig. 7.44 views parts of the brain in these slices.

- Cortex of telencephalon
- Diencephalon
- Midbrain
- Pons
- Cerebellum
- Medulla oblongata

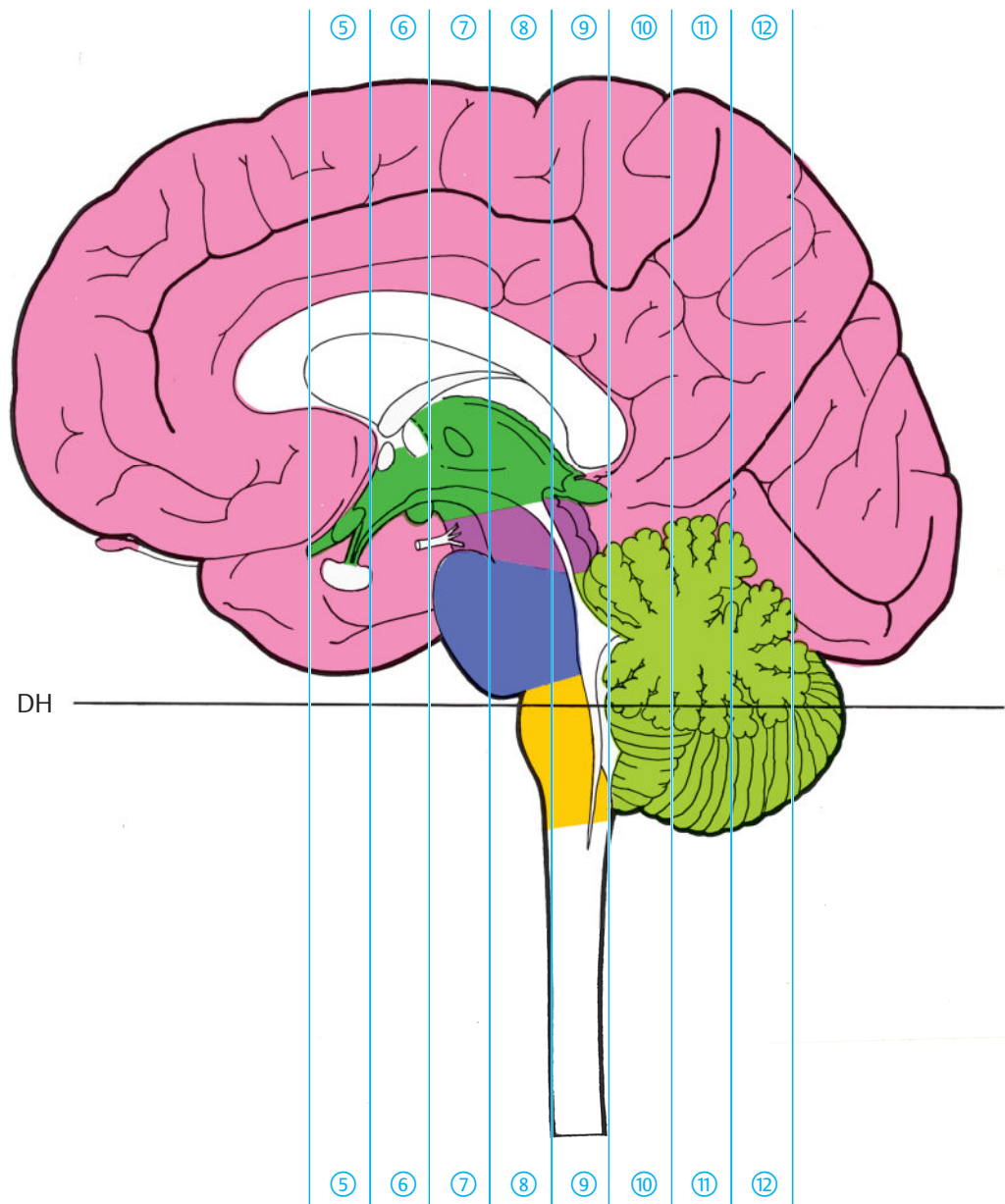


Fig. 7.39 Brain sections. Median view of the brain sectioned in the coronal plane (see ►Fig. 3.1c). The corpus callosum, anterior commissure, fornix, olfactory tract, pituitary and the oculomotor nerve remain white. For details, see Chapter 12.

DH = German horizontal

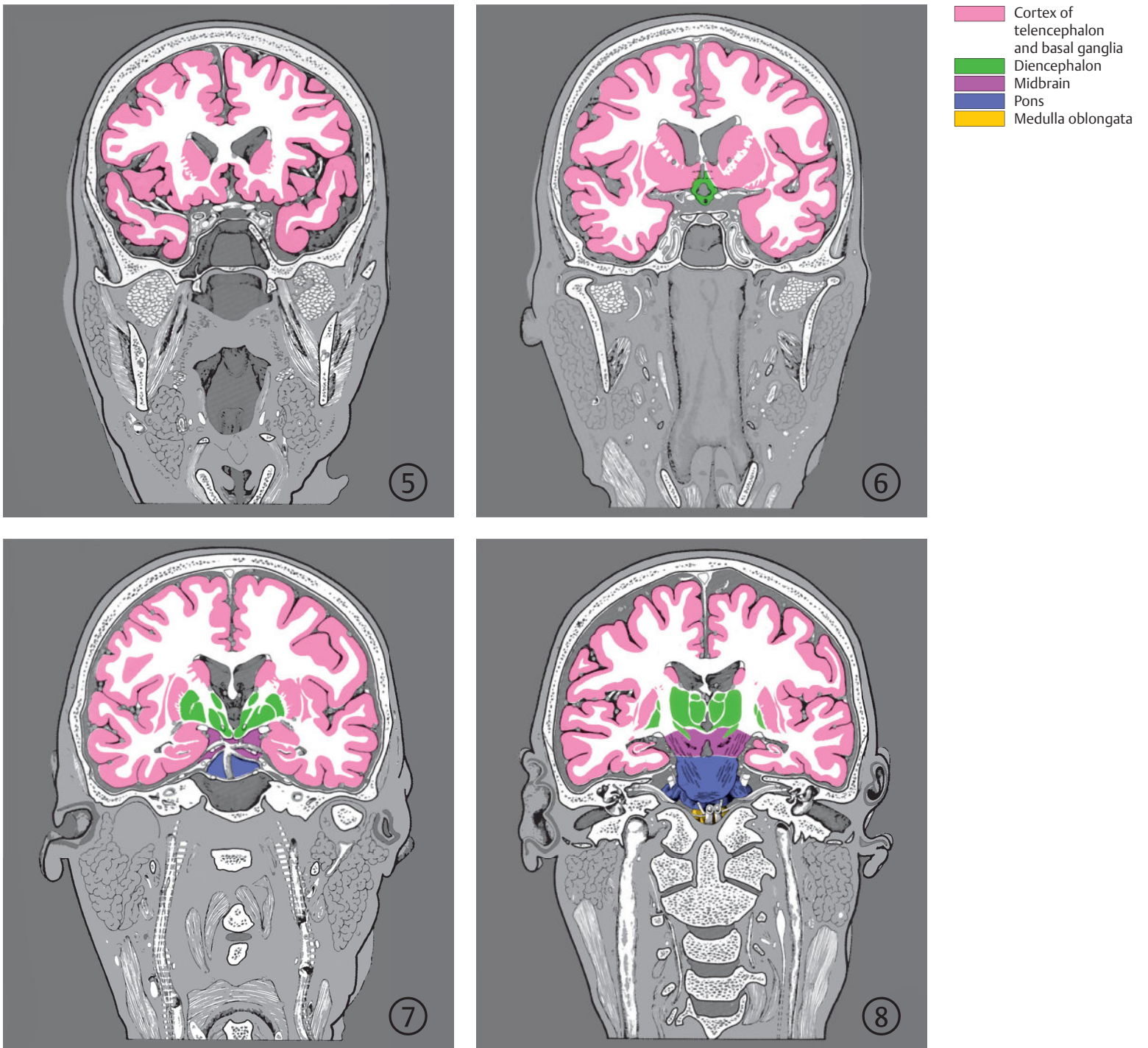


Fig. 7.40 Brain sections. Serial coronal images of sections of the brain. Encircled digits indicate the number of the respective slice (see ► Fig. 3.1).

Fig. 7.40a 5th to 8th sections.

- Cortex of telencephalon and basal ganglia
- Diencephalon
- Midbrain
- Cerebellum
- Pons
- Medulla oblongata

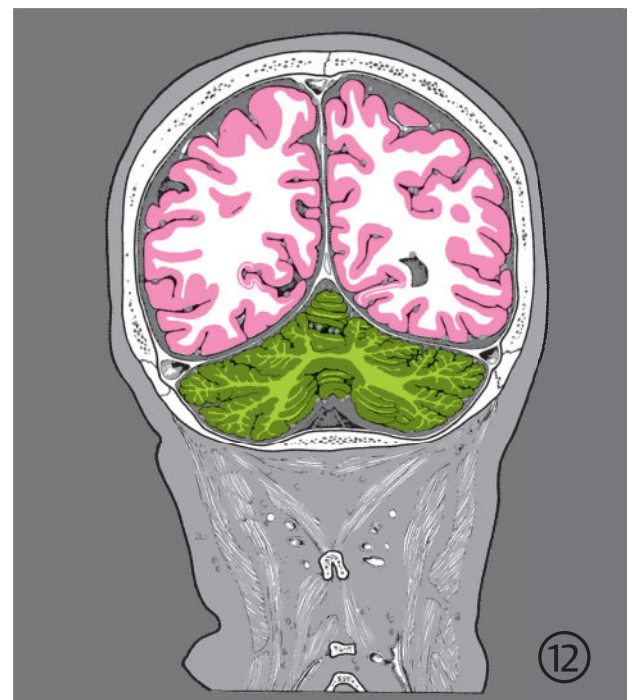
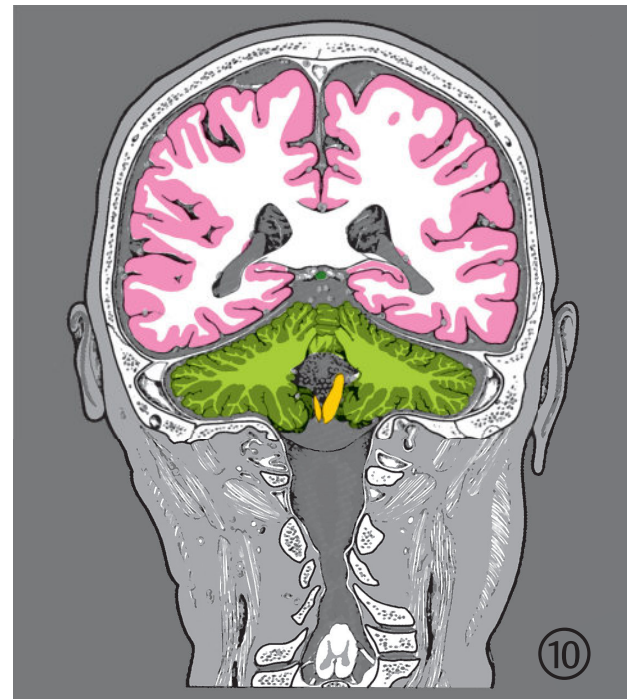


Fig. 7.40b 9th to 12th sections.

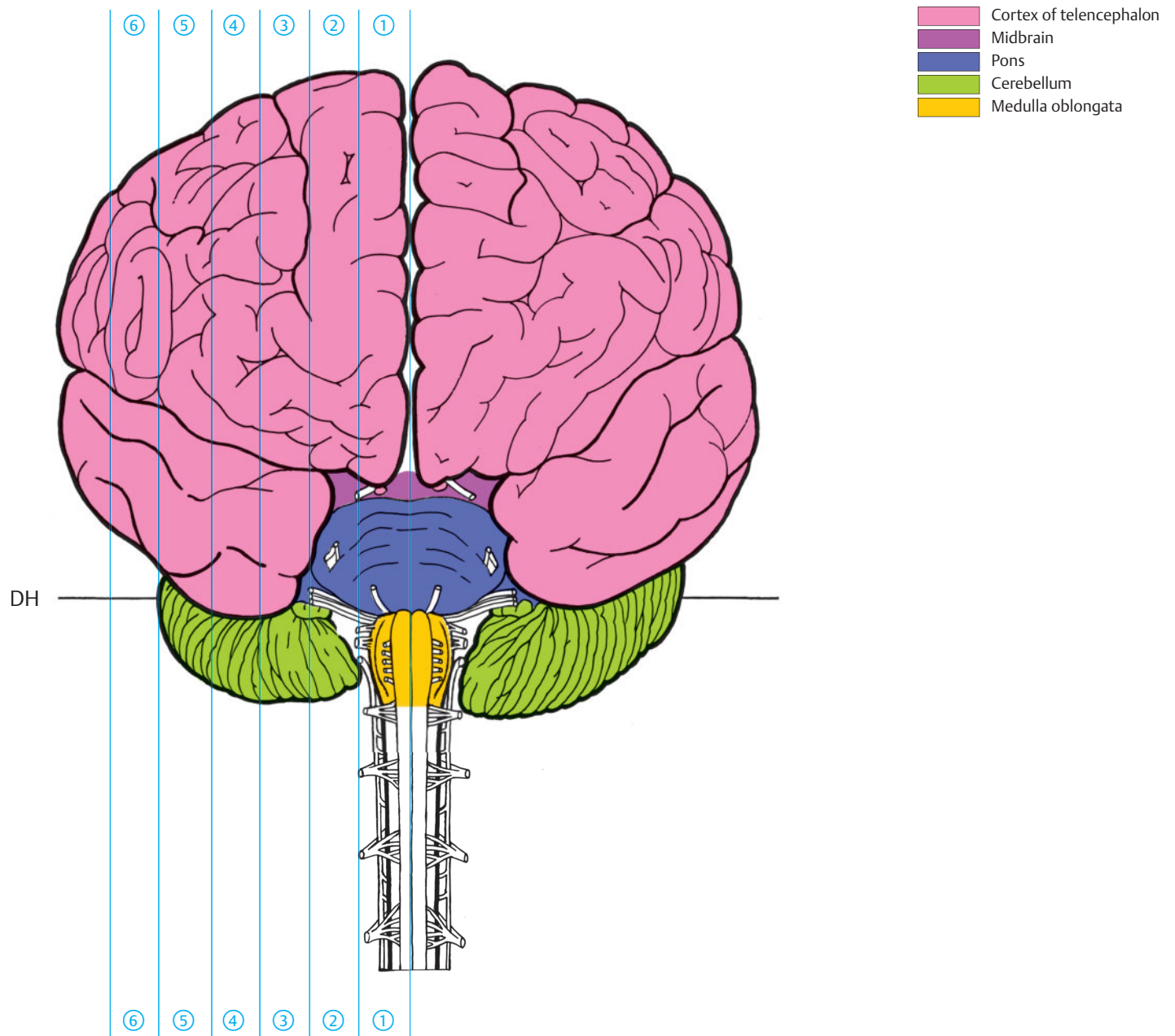


Fig. 7.41 Brain sections. Coronal view of the brain and spinal cord sectioned in the sagittal plane. Sagittal sections were put together and numbered as in ►Fig. 4.1c. For details see ►Chapter 12.

DH = German horizontal

- Cortex of telencephalon and basal ganglia
- Diencephalon
- Midbrain
- Pons
- Cerebellum
- Medulla oblongata

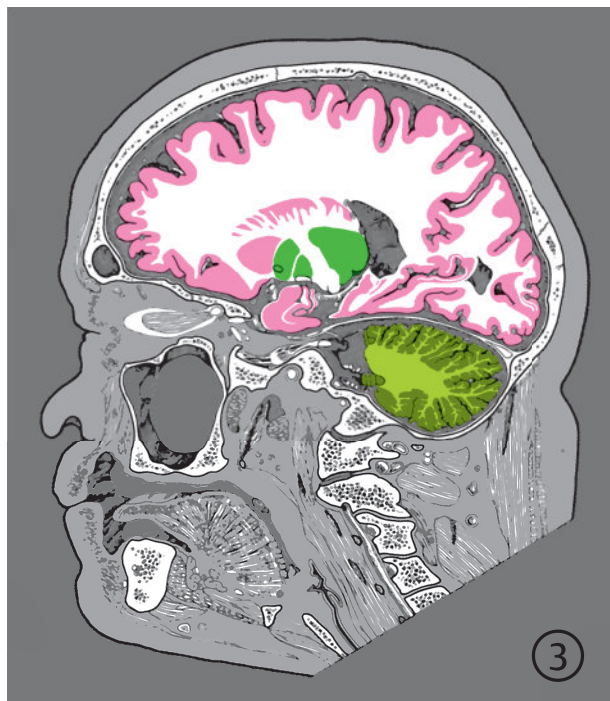
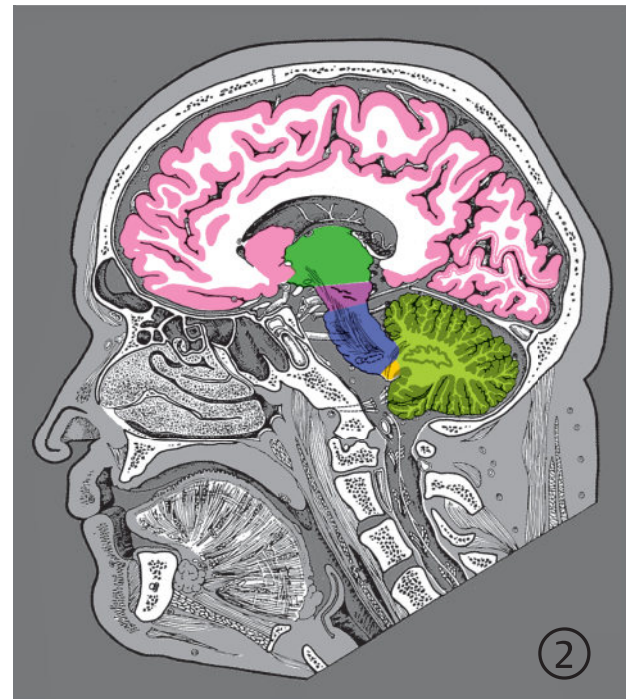
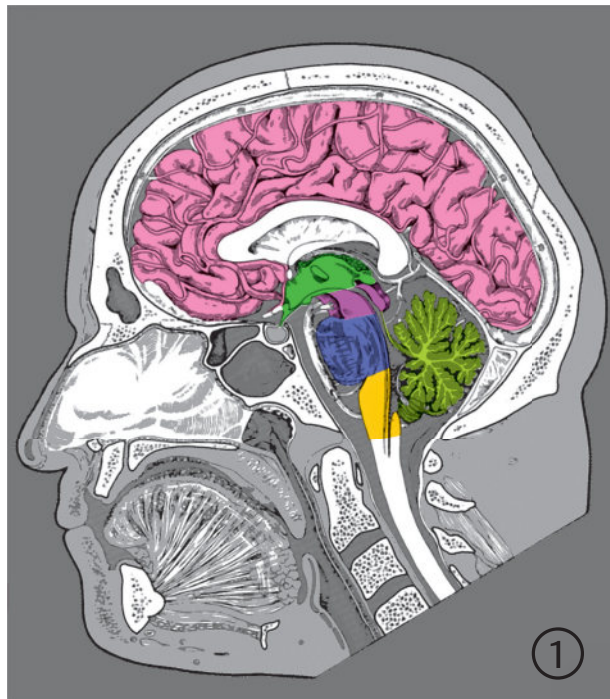


Fig. 7.42 Brain sections. Serial sagittal images of sections of the brain. The corpus callosum, anterior commissure, and the fornix remain white. Encircled digits indicate the number of the respective slice (see ► Fig. 4.1).

Fig. 7.42a 1st to 4th sections.

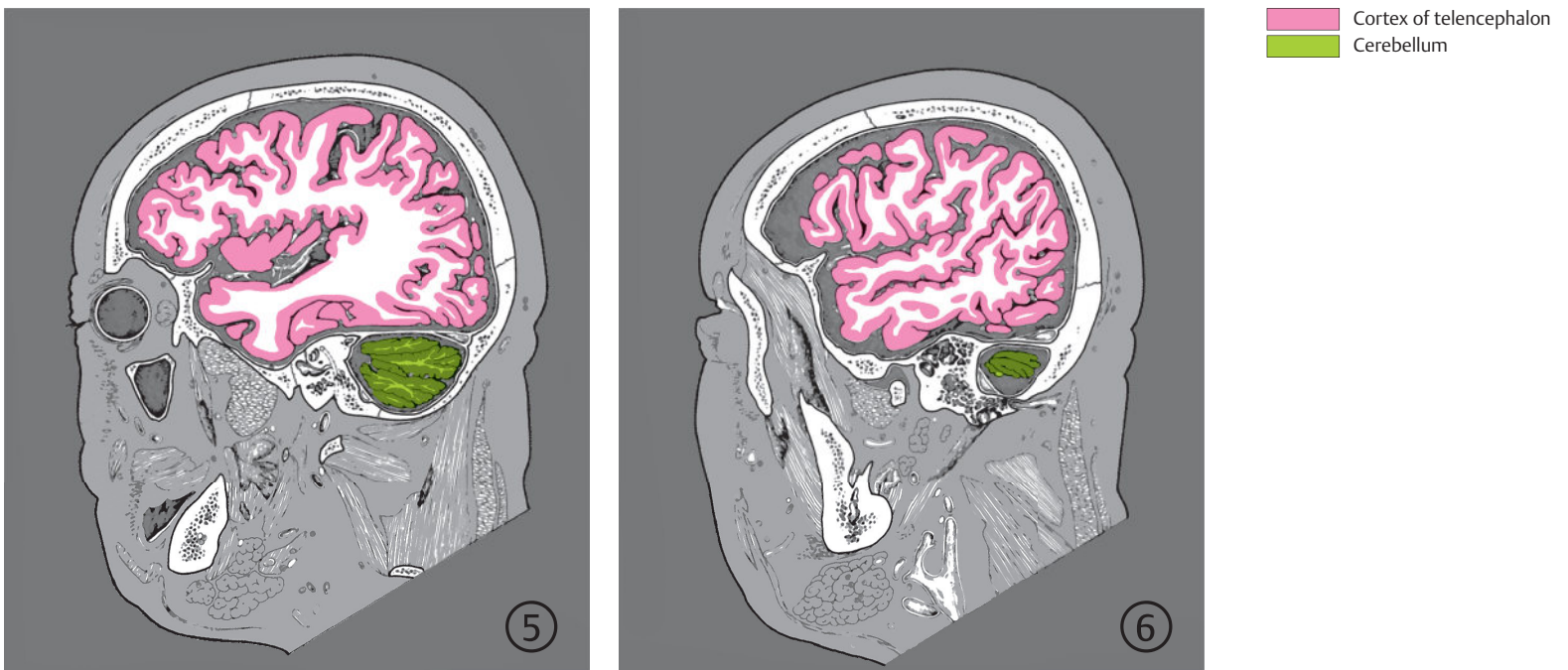


Fig. 7.42b 5th and 6th sections.

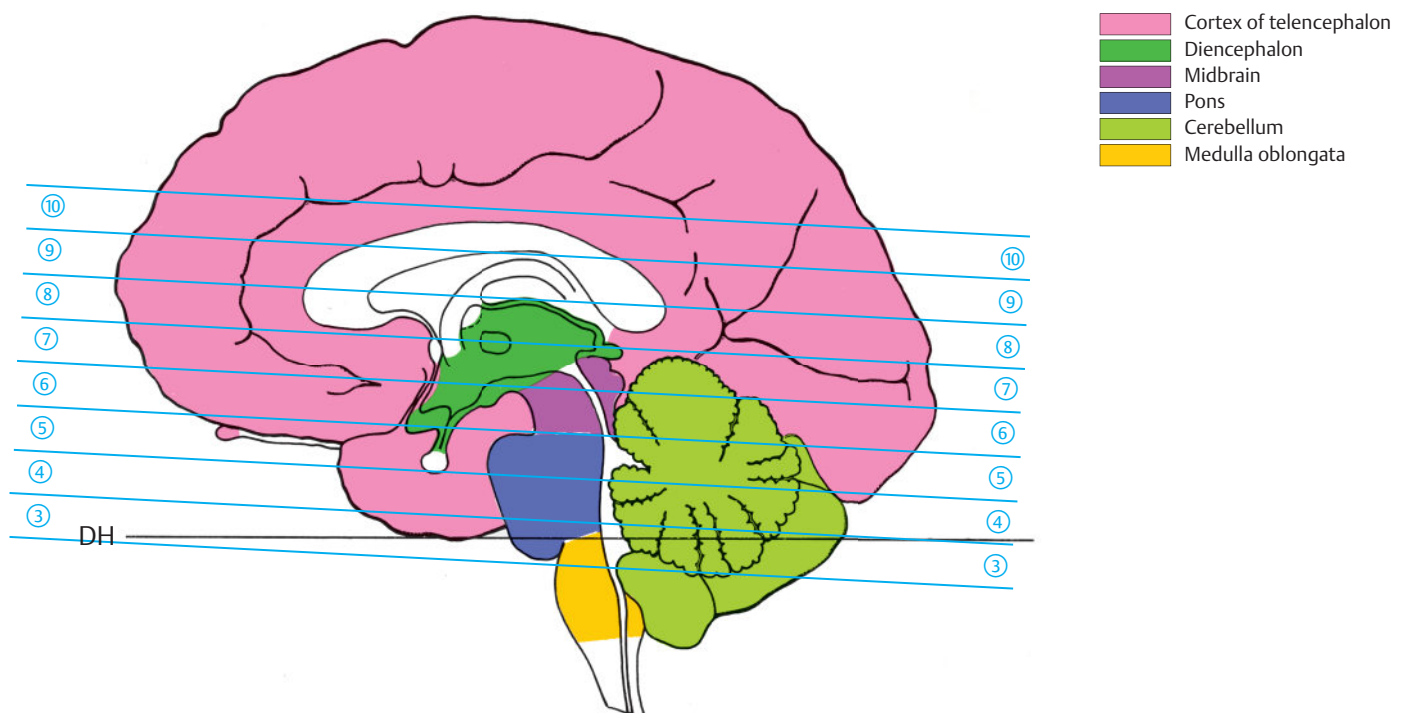


Fig. 7.43 Brain sections. Median view of brain sectioned in the bicommissural plane (see ► Fig. 5.1c). The corpus callosum, anterior commissure, fornix, olfactory tract, and the pituitary remain white. For details see Chapter 12.

DH = German horizontal

- Cortex of telencephalon and basal ganglia
- Diencephalon
- Mesencephalon
- Pons
- Cerebellum
- Medulla oblongata

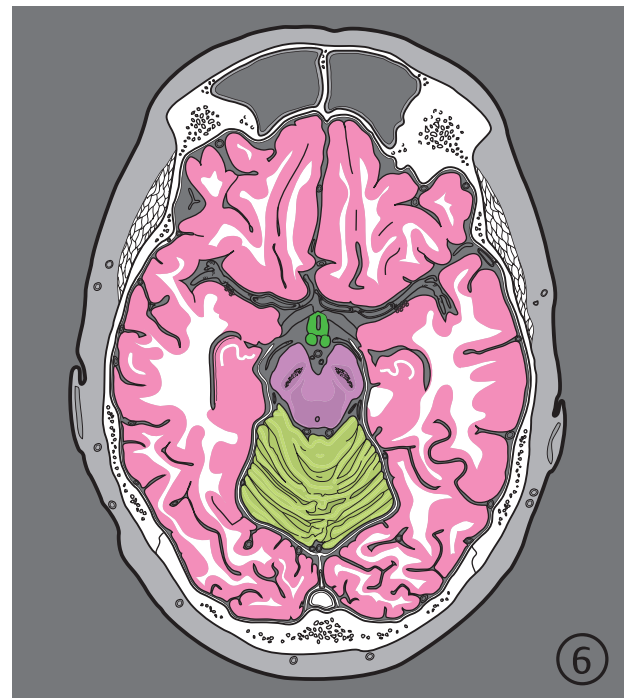


Fig. 7.44 Brain sections. Serial sections of the brain oriented along the bicommissural plane. Encircled digits indicate the number of the slice (see ► Fig. 5.1).

Fig. 7.44a 3rd to 6th sections.

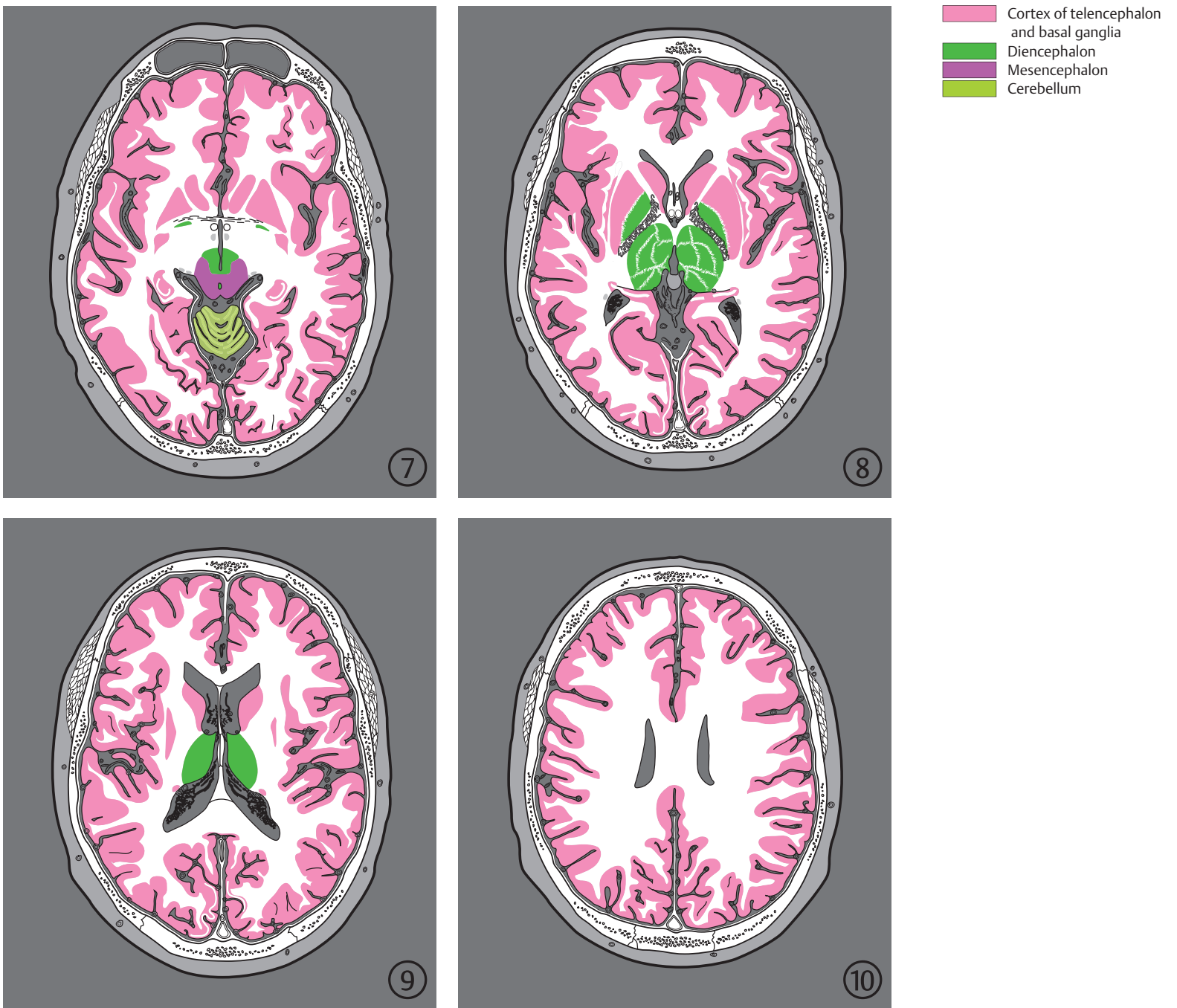


Fig. 7.44b 7th to 10th sections.

7.7.1 Medulla Oblongata and Pons

Appearance

Medulla oblongata

The medulla oblongata (see ►Fig. 7.39, ►Fig. 7.40, ►Fig. 7.41, ►Fig. 7.42, ►Fig. 7.43, and ►Fig. 7.44) is a small subdivision of the brain with a volume of about 7 ml; its basal surface between the spinal cord and pons is approximately 2 to 2.5 cm in length, while its inferior cross-sectional area is 1 cm².

The anterior median fissure continues into the spinal cord at the anterior aspect of the medulla oblongata. Raised areas on either side of the fissure represent the pyramidal tracts (see ►Fig. 4.1c, ►Fig. 6.4b, ►Fig. 6.4c, and ►Fig. 6.7b), with the pyramidal pathway and its decussation (see Section 10.8.1) lying deep within the fissure. The olive lies lateral to the pyramid and contains the inferior olivary nucleus. The dorsal column nuclei form small elevations on the posterior aspect of the medulla oblongata, the gracile and cuneate tubercles.

Other posterior parts of the medulla are visible when the cerebellum is separated along the peduncles (see ►Fig. 6.1b and ►Fig. 6.2a) and the IVth ventricle opened. The floor of the IVth ventricle is formed by the rhomboid fossa. The IVth ventricle continues into the central canal of the spinal cord at its inferior tip (see ►Fig. 4.2a and ►Fig. 6.4b). A small transverse fold, the obex (see ►Fig. 4.2a, ►Fig. 4.2b, ►Fig. 6.3, ►Fig. 6.5b, and ►Fig. 6.5c), forms the inferior boundary of the rhomboid fossa, at which point the medulla may be divided into superior (open) and inferior (closed) parts³³⁸:

- **Closed part:** This part of the medulla appears pear-shaped in cross-section (see ►Fig. 6.4b). The pyramids lie paramedian to the anterior median fissure (see ►Fig. 6.4b). The gracile and cuneate nuclei bulge outward (see ►Fig. 6.4b) posterior to the central canal (see ►Fig. 6.4b).
- **Open part:** The floor of the rhomboid fossa is visualized posteriorly in the open part of the medulla oblongata (see ►Fig. 6.6a and ►Fig. 6.7b), the walls of which are biconvex due to the outward bulge of the inferior olivary nuclei (see ►Fig. 6.6b).

A transitional zone between the closed and open parts of the medulla oblongata lies at the level of the obex (see ►Fig. 6.5b).

The XIIth cranial nerve exits the medulla oblongata as 12 to 16 rootlets between the pyramid and olive (see ►Fig. 6.1, ►Fig. 6.4b, ►Fig. 6.5b, and ►Fig. 6.6b) while the IXth, Xth, and XIth branchial nerves exit the medulla along its lateral wall posterior to the olives (see ►Fig. 6.5b and ►Fig. 6.6b). The VIIth and VIIIth cranial nerves exit laterally at the junction of the medulla oblongata and pons (see ►Fig. 6.1, ►Fig. 6.7b, and ►Fig. 6.8b,

represented by a dotted line). The VIth cranial nerve exits the brainstem anteriorly between the medulla and pons in 94% of cases (see ►Fig. 3.1d, ►Fig. 3.9a, ►Fig. 5.5, ►Fig. 6.1, and ►Fig. 6.7b).

Pons

The pons is almost twice as wide anteriorly as the superior part of the medulla oblongata and its superior boundary is formed by the cerebral crus of the midbrain. Both middle cerebellar peduncles arise from the lateral aspect of the pons (see ►Fig. 6.1b and ►Fig. 10.36a). The medulla oblongata continues into the pons without a sharp boundary in the floor of the rhomboid fossa. The median furrow along the floor of the rhomboid fossa, the posterior median sulcus (see ►Fig. 6.6b), can also be continuously traced from the medulla oblongata to the pons.

Cross-sections through the pons may be divided into three sections: lower, middle, and upper sections³⁸⁸:

- The **inferior part** of the pons extends from the boundary of the medulla oblongata to a level below the entry of the trigeminal nerve. The floor of the rhomboid fossa forms its posterior wall, becoming narrower toward the aqueduct of the midbrain. The IVth ventricle exhibits paired posterior recesses in the lower part of the pons (see ►Fig. 6.8b), which surround the nodule of the vermis laterally (X; see ►Fig. 3.1c, ►Fig. 4.2a, ►Fig. 4.2b, ►Fig. 6.8b, ►Fig. 6.8c, and ►Fig. 6.9b). The flocculus (HX; see ►Fig. 3.1d, ►Fig. 3.10a, ►Fig. 6.7a, ►Fig. 6.7b, and ►Fig. 6.8b) lies in the cerebellopontine cistern lateral to the middle cerebellar peduncle (see ►Fig. 6.8b). The flocculus (HX) may be mistaken for a tumor due to its elliptical shape and resultant partial volume effect.³⁸⁸
- The **central part** of the pons is identified on CT and MR by the exiting trigeminal nerve (see Fig. 6.10d). The Vth cranial nerve runs from the cerebellopontine cistern (see ►Fig. 5.20, ►Fig. 6.8, and ►Fig. 6.10b) into the trigeminal cistern in the middle cranial fossa.
- The **superior part** of the pons is characterized by the paired superior cerebellar peduncles (see ►Fig. 6.11b and ►Fig. 7.55), lying posteriorly and interrupting the continuity of the adjoining perimesencephalic cisterns. The narrow superior part of the IVth ventricle lies in between the superior cerebellar peduncles.

Anterior and posterior parts may be identified in all three vertical subdivisions of the pons on axial sections:

- Its **anterior part** contains relay nuclei, the pontine nuclei (see ►Fig. 6.8b, ►Fig. 6.9b, ►Fig. 6.10b, and ►Fig. 6.11b), in which the corticopontine fibers terminate. Pontocerebellar fibers run from the pontine nuclei into the cerebellum.
- The **posterior part** of the pons is the **tegmentum**, which merges inferiorly with the tegmentum of the medulla oblongata.

Internal Structure

A topographical and **functional arrangement of nuclei of the Vth to XIIth cranial nerves** is present in the tegmentum of the medulla oblongata and the pons (see ► Fig. 6.2).

Afferent cranial nerve nuclei lie laterally while efferent nuclei are located medially in the floor of the rhomboid fossa. Terminal afferent nuclei are separated from the efferent nuclei of origin by a poorly developed groove. Terminal nuclei are seen on the right in ► Fig. 6.2a while motor nuclei with efferent nerves have been depicted on the left.

The **terminal afferent nuclei** belong to the trigeminal (see Section 10.1.3), vestibular (see Section 10.4), auditory (see Section 10.5), and gustatory (see Section 10.2) systems.

The **afferent nucleus** for pain and temperature pathways from the ipsilateral side of the face is the caudal part of the spinal nucleus of trigeminal nerve (see ► Fig. 6.4b and ► Fig. 6.5b), which extends from the obex of the medulla oblongata (see ► Fig. 4.2a) to the third cervical segment of the spinal cord.

The mechanoreceptor signals of the trigeminal nerve are conveyed mainly to the principal sensory nucleus of trigeminal nerve in the central part of the pons (see ► Fig. 6.2 and ► Fig. 6.9b).

Signals predominantly from muscle spindles of masticatory muscles reach the mesencephalic nucleus of trigeminal nerve (see ► Fig. 6.2, ► Fig. 6.9b, ► Fig. 6.10b, ► Fig. 6.11b, ► Fig. 6.12b, and ► Fig. 6.13b), which extends from the central part of the pons upward as far as the midbrain.

The vestibular nuclei extend from the superior part of the medulla oblongata almost to the center of the pons (see ► Fig. 6.2a, ► Fig. 6.7b, ► Fig. 6.8b, and ► Fig. 6.9b).

The sensory nuclei for the auditory nerve, the cochlear nuclei (see ► Fig. 6.2a and ► Fig. 6.7b), lie in the superior part of the medulla oblongata close to the lateral apertures of the IVth ventricle. The sensory nucleus for the taste fibers, the solitary nucleus (see ► Fig. 6.2, ► Fig. 6.5b, and ► Fig. 6.6b) extends from the transitional area between the closed and open parts of the medulla oblongata almost up to the superior edge of the medulla.

The motor neurons of the XIIth, XIth, Xth, IXth, VIIth, VIth, and Vth cranial nerves and the visceroefferent nerve cells of the Xth, IXth, and VIIth cranial nerves lie within the **efferent nuclei**:

- **Hypoglossal nucleus** (see ► Fig. 6.2, ► Fig. 6.5b, and ► Fig. 6.6b): Consists of a cell column 10 mm long, which extends from the inferior aspect of the rhomboid fossa to the closed part of the medulla oblongata. Its axons exit as root fibers of the medulla oblongata anterior to the inferior olivary nucleus, and bundled as the XIIth cranial nerve, innervate the muscles of the tongue
- **Nucleus ambiguus** (see ► Fig. 6.2, ► Fig. 6.5b, ► Fig. 6.6b, and ► Fig. 6.7b): 16 mm long, this nucleus lies immediately posterior to the inferior

olivary nucleus predominantly in the upper part of the medulla oblongata. Its motor fibers run in the IXth, Xth, and XIth cranial nerves and innervate the muscles of the pharynx (in part), the larynx, and the esophagus, as well as parts of the sternocleidomastoid and the trapezius

- **Facial nucleus** (see ► Fig. 6.2, ► Fig. 6.8b, and ► Fig. 6.9b): 4 mm long (along Meynert's axis), the facial nucleus lies in the inferior part of the pons, anterior to the abducens nucleus. Its fibers loop around the abducens nucleus and form the inner genu of the facial nerve (see ► Fig. 6.2b and ► Fig. 6.9b)

The axons of the facial nucleus innervate the muscles of facial expression, the stapedius, and partially the suprahyoid muscles.

- **Motor nucleus of trigeminal nerve** see Fig. 6.2 and ► Fig. 6.9b): Measuring about 4 mm in length, this nucleus lies in the central part of the pons, and together with its axons forms the motor root of the trigeminal nerve which innervates the muscles of mastication, muscles of the floor of the mouth and the tensor tympani.

The following nuclei belong to the **visceroefferent nuclei**:

- **Posterior (dorsal) nucleus of vagus nerve** (see ► Fig. 6.2, ► Fig. 6.5b, and ► Fig. 6.6b): The nucleus lies primarily in the inferior part of the rhomboid fossa, its fibers form the parasympathetic component of the vagus nerve which innervates thoracic and abdominal viscera. The posterior nucleus of the vagus nerve is also the terminal nucleus for afferent fibers from the IXth and Xth cranial nerves.
- **Inferior salivatory nucleus** (see ► Fig. 6.2 and ► Fig. 10.43a): This small nucleus lies in the superior part of the medulla oblongata and its neurons supply parasympathetic fibers to the parotid gland.
- **Superior salivatory nucleus** (see ► Fig. 6.2 and ► Fig. 10.43a): This nucleus lies in the inferior part of the pons and its parasympathetic secretory fibers innervate the lacrimal, submandibular, and sublingual glands, as well as the glands of the nasal and oral mucosa.

Reticular Formation

The reticular formation is a loose network of large and small nerve cells situated in the medulla oblongata and the pons and may be divided into three poorly demarcated longitudinal zones:²⁴⁸

- The **median zone** contains the raphe nuclei (numbered B1–B8 from inferior to superior), in which serotonin and other neurotransmitters have been identified. Roughly simplified, these nuclei belong to the serotonergic nerve cells (see Section 11.2). The pontine visual center, the paramedian pontine reticular formation, lies in the center of the pons (see ► Fig. 6.10b and ► Fig. 6.11b).

- The **medial zone** contains many large nerve cells, the axons of which mostly contain a long ascending and a long descending branch with several synaptic connections.
- The **lateral zone** is predominantly composed of small nerve cells with presumed associative functions.

The reticular formation consists of polysynaptic connections joining it to afferent and efferent pathways and to the autonomic systems, lying in the vicinity of all afferent systems. Stimulation of the reticular formation in animals brings about arousal from sleep. Regulatory centers for circulation and respiration are also located in the reticular formation.

Inferior Olivary System

The inferior olivary nuclei (see ►Fig. 3.10a, ►Fig. 6.5b, ►Fig. 6.6b, and ►Fig. 6.7b) with their two accessory olivary nuclei are the most striking group of nuclei lying in the open part of the medulla oblongata. The inferior olivary nuclei measure 15 mm in length and extend into the superior aspect of the closed part of the medulla oblongata. These nuclei may be compared to a sack with a markedly folded wall, its opening pointing medially, and are relay centers for connections with the cerebellum. They receive signals from the spinal cord, midbrain, and from the motor cortex and basal ganglia of the telencephalon. The olivary system is by and large a relay station for the cerebellum.

Clinical Notes

Lesions in the Guillain Mollaret triangle result in hypertrophic degeneration of the olivary nucleus which has a striking appearance on MRI. The Guillain Mollaret triangle consists of the ipsilateral red nucleus and the inferior olivary nucleus, connected by the central tegmental tract (rubro-olivary fibers), as well as the contralateral dentate nucleus, connected with the inferior olivary nucleus through the inferior cerebellar peduncle (dento-olivary tract) and with the red nucleus through the superior cerebellar peduncle (dento-rubral tract). Damage to the dentate nucleus and / or the superior cerebellar peduncle injures the contralateral central tegmental tract and causes ipsilateral hypertrophic olivary degeneration. Not infrequently, degeneration occurs bilaterally.^{210,213,448}

Chemically Identifiable Neurons

Using histochemical techniques for identification of transmitters, the following monoaminergic group of nuclei and other neurons may be demonstrated predominantly in the reticular formation and partly within the medulla oblongata and pons:

- Noradrenergic cell groups (A1–A7; the locus caeruleus is the most conspicuous group due to the presence of melanin pigment [see ►Fig. 6.10b and ►Fig. 6.11b])
- Adrenergic cell groups lying in the superior part of the medulla oblongata

- Serotonergic cell groups (B1–B8; see above)
- Cholinergic cell groups
- Neuropeptide-containing cell groups

Pathways

Ascending pathways from the anterolateral (see Section 10.1.1), medial lemniscus (see Section 10.1.2), trigeminal (see Section 10.1.3), gustatory (see Section 10.2), vestibular (see Section 10.4), and auditory systems (see Section 10.5), as well as descending pathways from the motor (see Section 10.8) and cerebellar (see Section 10.9) systems, pass through the medulla oblongata and pons.

The medulla oblongata and the pons have been obliquely sectioned in the markedly angulated parallel supraorbital-suboccipital planes (CT) as compared to MRI, such that the resulting sectioning planes lie anteriorly in a more superior position and posteriorly in a more inferior position than transverse sections in conventional textbooks of neuroanatomy.^{75,115,147,281,315,363,424,446,472,484,517,535,623}

Clinical Notes

Lesions of the medulla oblongata and pons frequently involve cranial nerve nuclei and their connections with one another as well as their connections with the spinal cord, cerebellum, and cerebrum. Afferent and efferent pathways are usually simultaneously affected between the cerebrum or the basal ganglia and spinal cord. Small lesions lead to disorders of ipsilateral inferior cranial nerves and to paresis of contralateral extremities and/or sensory impairment. Clinical symptoms usually help in localizing damage and in classifying the type of brainstem syndrome. A uniform description of various syndromes is not available in literature and these are rarely seen clinically in their purest forms. Wallenberg syndrome is one of the commonest, with acute onset of rotatory vertigo, vomiting and hoarseness. Examination reveals nystagmus, ipsilateral Horner's syndrome, trigeminal disorder, palatal and pharyngeal paresis and hemiataxia of the extremities. Dissociated sensory loss (for pain and temperature) of the extremities and trunk is present on the contralateral side. Extensive lesions of the medulla oblongata and pons cause bulbar palsy with tetraplegia. Bony artifacts in CT preclude the visualization of most small lesions of the inferior brainstem. MRI is the method of choice for the demonstration of infarcts, lesions of multiple sclerosis and small brainstem tumors. Fresh hemorrhages may get overlooked or misinterpreted if specific sequences are not employed.

7.7.2 Cerebellum Appearance

The cerebellum (see ►Fig. 7.39, ►Fig. 7.44, ►Fig. 10.34, and ►Fig. 10.35) is composed of the vermis and two hemispheres. The anterior lobe of cerebellum is separated from the posterior lobe by the primary fissure (see

► Fig. 3.1c, ► Fig. 4.2a, ► Fig. 4.2b, ► Fig. 5.7, ► Fig. 6.3, ► Fig. 6.9a, ► Fig. 6.10a, and ► Fig. 6.11a). The lobes and lobules of the cerebellum are best identified in the median plane because the curved surface of the primary fissure only runs roughly vertically in the median plane and obliquely in the paramedian planes.

The vermis (not the hemispheres) exhibits the typical pattern of the arbor vitae with the deep cleft of the primary fissure between the culmen (IV and V) and the declive (VI) (see ► Fig. 10.34a). The anterior lobe lies in the upper axial plane corresponding to its description as anterior, in front of the posterior lobe (see ► Fig. 10.35). The sagittal series illustrates that large parts of the posterior lobe lie below the anterior lobe (see ► Fig. 10.34).

The flocculus (HX) (see ► Fig. 3.10a, ► Fig. 5.1d, ► Fig. 6.7a, ► Fig. 6.7c, ► Fig. 6.8b, and ► Fig. 10.34b) and the nodules of vermis (X; see ► Fig. 6.3, ► Fig. 6.8b, ► Fig. 6.9b, and ► Fig. 10.34a) form the flocculonodular lobe, which is separated by the posterolateral fissure from the posterior lobe (see ► Table 7.1).

Three paired cerebellar peduncles connect the cerebellum to the brainstem:

- Inferior cerebellar peduncle (see ► Fig. 10.36a) with the medulla oblongata
- Middle cerebellar peduncle (see ► Fig. 10.36a) with the pons
- Superior cerebellar peduncle (see ► Fig. 10.36a) with the midbrain

The functions and somatotopy of the lobules of the cerebellum have been examined using PET and fMRI and individual functions have been assigned to them. The lobules carry historical names which give no indication of their functions or development. Larseil suggested a clear alphanumerical nomenclature for the cerebellum (see ► Table 7.1),³⁴⁰ which was accepted as an alternative in 1998 by the Federative Committee on Anatomical Terminology.

The parts of the vermis have been numbered in topographic sequence using Roman numerals. In the

median section of the right half of the cerebellum (see ► Fig. 4.2a), most components of the vermis have been indicated by these numbers in brackets and are depicted in a clockwise direction. The letter H has been placed in front of the corresponding parts of the hemisphere, for example “wing of central lobule (H II, H III)” or “flocculus (H X)”. Names with alphanumerical abbreviations have been listed in ► Table 7.1 and are used in PET and fMRI examinations.⁵²²

Internal Structure

The cerebellum has a thin cortex of gray matter measuring approximately 1 mm in thickness. The following paired cerebellar nuclei lie in the white matter, from lateral to medial:

- Dentate nucleus
- Anterior interposed nucleus (emboliform)
- Posterior interposed nucleus (globose)
- Fastigial nucleus

Afferent and efferent cerebellar pathways have been described under cerebellar systems (see Section 10.9).

Topography

The larger part of the infratentorial region is occupied by the cerebellum, which measures on an average 150 mL in volume in males and 135 mL in females.^{498,611} The dominance of the cerebellum in the infratentorial region as compared to the medulla oblongata and pons is clearly evident in ► Fig. 7.40, ► Fig. 7.42, and ► Fig. 7.44. The tonsils of cerebellum (H IX) extend furthest inferiorly into the posterior cranial fossa (see ► Fig. 3.1c, ► Fig. 4.1c, ► Fig. 4.2a, ► Fig. 4.2b, ► Fig. 5.3, and ► Fig. 6.4b). The posterior lobe lies superior to the tonsils. The flocculus (H X; see ► Fig. 5.1d, ► Fig. 6.7c, and ► Fig. 6.8b) lies in the cerebellopontine cistern (see ► Fig. 6.8b, ► Fig. 6.10b, ► Fig. 7.9b, and ► Fig. 7.12a). The anterior lobe is seen lying superior most in axial sections (see ► Fig. 5.8, ► Fig. 5.25, ► Fig. 10.34, and ► Fig. 10.35).

Table 7.1 Description of parts of the vermis, lobules, and lobes of the cerebellum using numerical and alphanumerical abbreviations after Larseil

Lobes	Vermis	Hemisphere
Anterior lobe of cerebellum	<ul style="list-style-type: none"> • Lingula (I) • Central lobule (II, III) • Culmen (IV, V) 	<ul style="list-style-type: none"> • Wing of central lobule (H II, H III) • Anterior quadrangular lobule (H IV, H V)
Primary fissure		
Posterior lobe of cerebellum	<ul style="list-style-type: none"> • Declive (VI) • Folium of vermis (VII A) • Tuber vermis (VII B) • Pyramid of vermis (VIII) • Uvula of vermis (IX) 	<ul style="list-style-type: none"> • Posterior quadrangular lobule (H VI) • Superior and inferior semilunar lobule (H VII A) • Gracile lobule (H VII B) • Biventral lobule [H VIII] • Tonsils of cerebellum (H IX)
Posterolateral fissure		
Flocculonodular lobe	<ul style="list-style-type: none"> • Nodule of vermis (X) 	<ul style="list-style-type: none"> • Flocculus (H X)

Clinical Notes

Cerebellar lesions are characterized by dyssynergia (disturbances of muscular coordination with ataxia), postural anomalies, decreased muscle tone and disturbances of equilibrium and speech. Lesions of the vermis and flocculus result in disorders of equilibrium as well as truncal and gait ataxia due to impaired transmission of vestibular signals. Lesions of the lateral zone of the cerebellar hemisphere cause disordered movement in the ipsilateral extremities with ataxia, intention tremor, and dysdiadochokinesia. Nystagmus is also frequently present as a cerebellar symptom. Bony artifacts in CT may compromise image quality. MRI is therefore far superior in evaluating this region and its diagnostic accuracy is further improved by imaging in sagittal and coronal planes. Arnold-Chiari syndrome is characterized by elongated, tongue-like tonsils of cerebellum with caudal descent in the direction of the spinal canal.

7.7.3 Midbrain**Appearance**

The midbrain (see ►Fig. 7.39, ►Fig. 7.40, ►Fig. 7.41, ►Fig. 7.42, ►Fig. 7.43, and ►Fig. 7.44) is a small subdivision of the brain, measuring approximately 2 cm posteriorly and about 1.5 cm in length anteriorly, with a volume of about 10 mL.

The **posterior surface of the midbrain** is formed by the tectal (quadrigeminal) plate. The superior colliculi (see ►Fig. 3.1c, ►Fig. 4.2a, ►Fig. 4.2b, ►Fig. 6.13b, and ►Fig. 6.13c) are broader and higher than the inferior colliculi (see ►Fig. 3.1c, ►Fig. 4.2a, ►Fig. 4.2b, ►Fig. 5.23, ►Fig. 6.12b, and ►Fig. 6.12c). The IVth cranial nerve emerges as the only cranial nerve from the posterior surface of the brainstem immediately below the inferior colliculi (see ►Fig. 6.1b) and turning anteriorly, it runs through the orbit to the superior oblique.

On the **anterior surface** the paired cerebral peduncles, the cerebral crura (see ►Fig. 6.12a, ►Fig. 6.12c, and ►Fig. 6.13b) bulge forward surrounding the interpeduncular fossa (see ►Fig. 6.12b) and the interpeduncular cistern (see ►Fig. 6.12c). The IIIrd cranial nerve (see Fig. 4.2a, ►Fig. 4.2b, ►Fig. 6.1a, and ►Fig. 6.12b) emerges from this fossa and supplies extraocular and intrinsic ocular muscles.

Internal Structure

The midbrain is composed of three levels oriented around the aqueduct in the axial plane:

- Posteriorly lies the roof or the tectal (quadrigeminal) plate
- The tegmentum of the midbrain lies in the center
- The cerebral crura lie inferiorly

The aqueduct runs between the IIIrd and IVth ventricles in a superiorly convex arc.

Axial sections through the midbrain, which should run perpendicular to the aqueduct, cannot, therefore, be parallel to each other. Serial histological sections through a block of midbrain tissue may be oriented either along the superior or inferior axial plane of the aqueduct. Thus, axial images through the midbrain exhibit great variation.^{75,115,147,281,315,363,424,446,472,517,623} CT sections through the midbrain should ideally be obtained in the infraorbitomeatal plane in accordance with anatomic and CT studies. These images identify better with anatomical depictions of the midbrain than those obtained along the supraorbito-suboccipital plane. Furthermore, the interpeduncular cistern, ambient cistern, and quadrigeminal cistern (great cerebral vein), along with their vessels and nerves are seen more clearly on images oriented along the infraorbitomeatal plane. MRI is particularly advantageous for the intravital assessment of the midbrain since brain structures and cisterns may be imaged free of artifacts. Supplementary sagittal MR sections in addition to axial views improve topical orientation.

The **tectum of midbrain** (see ►Fig. 4.2d) is a thin plate with four elevations. The inferior colliculi are relay centers for the auditory system while the superior colliculi serve as a visual reflex center. The short tectobulbar and long tectospinal tracts descend to motor neurons in the brainstem and spinal cord from this region.

The **tegmentum of midbrain** contains motor nuclei of the IIIrd and IVth cranial nerves (see ►Fig. 6.2, ►Fig. 6.12b, and ►Fig. 6.13b). The medial and most superiorly located parasympathetic accessory nuclei of oculomotor nerve, the Edinger-Westphal nuclei (see ►Fig. 10.43a) innervate the sphincter pupillae and the ciliary muscle. The roots of the IIIrd cranial nerve course inferiorly through the red nucleus and emerge at the interpeduncular fossa. The motor nucleus of the IVth cranial nerve lies inferior to that of the IIIrd cranial nerve.

Coursing posteriorly, the roots of the trochlear nerve cross over and exit the midbrain inferior to the inferior colliculi (see ►Fig. 6.2 and ►Fig. 6.12b). Posterolateral to these motor nuclei lies the mesencephalic nucleus of the trigeminal nerve which has been described with the trigeminal system (see Section 10.1.3). The reticular formation forms the framework of the tegmentum, the structure and function of which have been described with the medulla oblongata and pons. The red nucleus and the substantia nigra lie within the tegmentum of the midbrain and are considered part of the basal ganglia (see Section 10.8.2). The iron content in both these nuclei results in the typical susceptibility effects on MRI images. The red nucleus (see ►Fig. 7.45) is shaped like a short ellipsoid surrounded by a capsule of longitudinally running fibers (see ►Fig. 6.13b).

The red nucleus abuts the superior cerebellar peduncle inferiorly, while it is separated anteriorly from the subthalamic nucleus by an almost 2 mm wide layer of fibers (see ► Fig. 7.45). The main part of the red nucleus is composed of small cells (parvocellular); only an inferior cap of about 1 mm contains large nerve cells (magnocellular). This last part contains fewer than 300 cells. The substantia nigra, a plate of nerve cells located in the basal part of the midbrain (see ► Fig. 5.7, ► Fig. 6.12b, ► Fig. 6.13b, and ► Fig. 7.45) is composed of melanin-containing pigment cells which cause its typical black color. Dopaminergic neurons (A9) are present in the substantia nigra, the axons of which extend to the striatum. These nigrostriatal neurons have been described with dopaminergic neurons (see Section 11.1.1).

The paired **cerebral crura** lie on the basal aspect of the midbrain and contain only descending pathways from the neocortex. From medial to lateral these are:

- Frontopontine tract (see Fig. 6.12b and ► Fig. 6.13b)
- Corticonuclear tract (see ► Fig. 6.12b and ► Fig. 6.13b)
- Pyramidal pathway or corticospinal tract (see ► Fig. 6.12b, ► Fig. 6.13b, and ► Fig. 7.55)
- Occipitotemporopontine tract (see ► Fig. 6.12b and ► Fig. 6.13b)

The pontine tracts belong to the cerebellar system (see Section 10.9) while the corticonuclear and corticospinal tracts are part of the pyramidal system (see Section 10.8.1). Ascending pathways course through the tegmentum of the midbrain. The medial lemniscus (see ► Fig. 6.9 and ► Fig. 6.13b) lies posterolateral to the red nucleus (see ► Fig. 6.13b and ► Fig. 7.45).

The medial lemniscus forms a system that goes by the same name (see Section 10.1.2) and lies in the immediate vicinity of the fibers of the anterolateral and the trigeminal systems. The lateral lemniscus (see ► Fig. 6.12b), a part of the auditory system (see Section 10.5), terminates at the inferior colliculus (see ► Fig. 6.12b).

Clinical Notes

Midbrain dysfunction is characterized by gaze paresis, disorders of eye muscles innervated by the IIIrd or IVth cranial nerves, ataxia, and occasionally tremor. Damage to the reticular formation and upper midbrain structures as well as of those located in the junctional zone between the midbrain and diencephalon cause akinetic mutism. These disorders often have a traumatic origin.

7.7.4 Diencephalon and Pituitary Diencephalon

Appearance

The diencephalon (see ► Fig. 7.39, ► Fig. 7.40, ► Fig. 7.41, ► Fig. 7.42, ► Fig. 7.43, and ► Fig. 7.44) surrounds the IIIrd ventricle and is bounded by the midbrain and telencephalon. It consists of nuclear regions traversed by fiber tracts.

Nuclear regions of the human diencephalon assumed new topographic positions due to the aforementioned shift of Forel's axis during evolution of the neocortex. Many of these diencephalic nuclear regions were first described in lower mammals in which the neocortex is not as highly developed, but retained their nomenclature in comparative human neuroanatomy. Thus, terms describing positions of the subnuclei of the human diencephalon like "ventral" and "dorsal" relate to Forel's axis and deviate from the directional information used elsewhere in anatomy. This inconsistency in the nomenclature is especially obvious in the illustrations of the forebrain made in the supraorbito-suboccipital parallel planes, as the anatomic position "ventral or dorsal" can be easily identified by the frontal (anterior) and occipital (posterior) part of the skull.

Arranged from inferior to superior, the illustrations of the diencephalon in the bicommissural plane first depict only the hypothalamus and its infundibulum (see Fig. 4.2a, ► Fig. 4.2b, ► Fig. 5.1c, ► Fig. 5.6a, ► Fig. 5.6b, ► Fig. 5.21, and ► Fig. 6.11b), with the hypothalamus (see ► Fig. 5.7) and the telencephalic lamina terminalis in the next image (see ► Fig. 5.7). Subsequent illustrations depict the hypothalamus (see ► Fig. 5.8), parts of the thalamus, the metathalamus (see ► Fig. 5.8) and the globus pallidus (see ► Fig. 5.8, ► Fig. 5.9a, and ► Fig. 5.9b). The thalamic subnuclei with the habenular nuclei (see ► Fig. 5.9a and ► Fig. 5.9b) and the globus pallidus (see ► Fig. 5.9a and ► Fig. 5.9b) are depicted in the next slice. The last and most superior section of the series shows only the thalamus (see ► Fig. 5.10a and ► Fig. 5.10b).

Internal Structure

The diencephalon is divided into the following parts from inferior to superior with some exceptions:

- Hypothalamus
- Subthalamus
- Metathalamus
- Thalamus
- Epithalamus

Hypothalamus

The hypothalamus forms the base of the diencephalon (see ►Fig. 5.7, ►Fig. 5.8, ►Fig. 6.3, ►Fig. 6.12b, and ►Fig. 6.13b) and surrounds the funnel-shaped inferior part of the **IIIrd ventricle**, which continues inferiorly into the infundibular recess. The infundibulum connects the hypothalamus with the pituitary gland. Anteriorly the hypothalamus abuts the lamina terminalis (see ►Fig. 3.1c, ►Fig. 4.2a, ►Fig. 5.7, and ►Fig. 6.13b) and the **anterior commissure** (see ►Fig. 3.1c, ►Fig. 4.2a, ►Fig. 4.2b, and ►Fig. 5.8). The optic chiasm lies below the hypothalamus (see ►Fig. 3.1c, ►Fig. 3.6a, ►Fig. 4.2a, ►Fig. 4.2b, ►Fig. 4.2d, ►Fig. 5.1c, ►Fig. 5.6a, ►Fig. 5.6b, ►Fig. 6.3, and ►Fig. 6.12b). The tuber cinereum and mammillary bodies are situated posterior to the infundibulum (see Fig. 3.1c, ►Fig. 3.8a, ►Fig. 4.2a, ►Fig. 4.2b, ►Fig. 5.1c, ►Fig. 6.3, and ►Fig. 6.12b). The hypothalamic sulcus, a groove in the lateral wall of IIIrd ventricle, marks the boundary between the thalamus and hypothalamus. Laterally the hypothalamus extends up to the subthalamic nucleus (see ►Fig. 7.45).

The hypothalamus is **closely related to the pituitary gland** both morphologically and functionally. Axonal fibers from neurosecretory cells pass from the hypothalamus through the infundibulum into the neurohypophysis or posterior lobe of the pituitary gland.

The neurohypophysial hormones oxytocin and vasopressin are produced by these neurosecretory cells; damage to this hypothalamic-neurohypophysial axis results in diabetes insipidus. The adenohypophysis or anterior lobe of pituitary is connected to the hypothalamus through the hypophyseal portal system. The hypothalamic-infundibular system produces substances that either trigger the release of hormones in the anterior lobe of the pituitary gland (releasing factors or liberins), or inhibit the secretion of hypophyseal hormones (inhibiting factors or statins). This system is controlled by the tubero-infundibular dopaminergic system (see Section 11.1.1).

The hypothalamus may be divided into the following regions based on its content of myelinated nerve fibers:

- **Weakly myelinated hypothalamus:** Nerve cells of the hypothalamic-neurohypophysial system, the hypothalamic-infundibular system and non-hypophyseal nerve cells constitute the weakly myelinated hypothalamus. The non-hypophyseal nerve cells predominantly lie in the lateral regions of the hypothalamus and control autonomic activities such as regulation of body temperature, food and water intake, sleep, and emotional behavior.
- **Heavily myelinated hypothalamus:** Nuclear groups of the mammillary body belong to the heavily myelinated hypothalamus and are closely related to the limbic system both morphologically and functionally (see Section 10.11).

Subthalamus

The subthalamus lies laterally in the diencephalon but does not abut the wall of the IIIrd ventricle. The subthalamic nucleus, the globus pallidus, and the zona incerta constitute the subthalamus. The subthalamus lies pos-

terior to the mammillary body and posteromedial to the posterior limb of the internal capsule deep within the seventh slice of the bicommissural series (see ►Fig. 10.30). The **subthalamic nucleus** is lenticular in shape and is well seen macroscopically (see ►Fig. 3.9a, ►Fig. 3.9b, ►Fig. 4.3a, and ►Fig. 7.45). The globus pallidus lies adjacent to the subthalamic nucleus and lateral to the internal capsule (see ►Fig. 3.8a, ►Fig. 3.8b, ►Fig. 3.9a, ►Fig. 3.9b, ►Fig. 4.4a, ►Fig. 5.8, ►Fig. 5.9a, ►Fig. 5.9b, and ►Fig. 7.45).

Laterally the globus pallidus is separated from the putamen by a thin layer of fibers, the lateral medullary lamina, and abuts the innominate substance and olfactory areas inferiorly. The globus pallidus is considered part of the basal ganglia (see Section 10.8.2) and is involved in motor activity. The **zona incerta** is a continuation of the reticular formation of the midbrain and consists of a thin layer of cells lying above the subthalamic nucleus, lying adjacent to two myelin-rich areas (Forel's fields H1 and H2).

Metathalamus

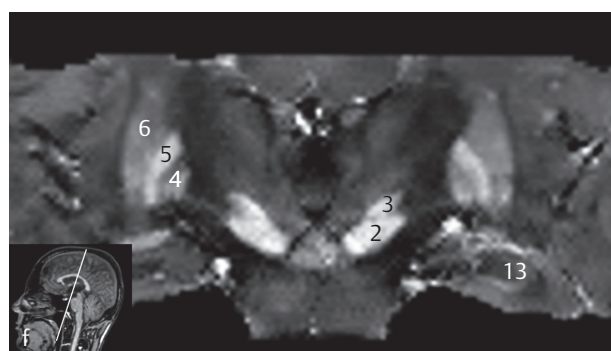
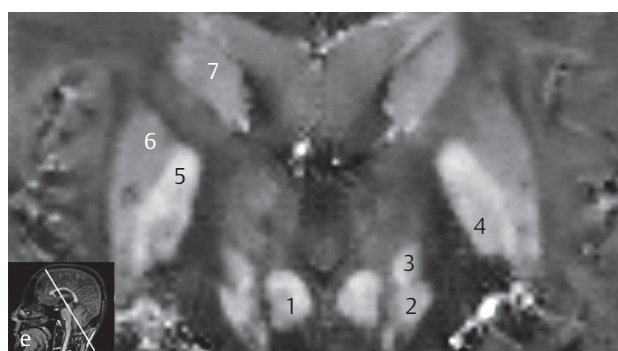
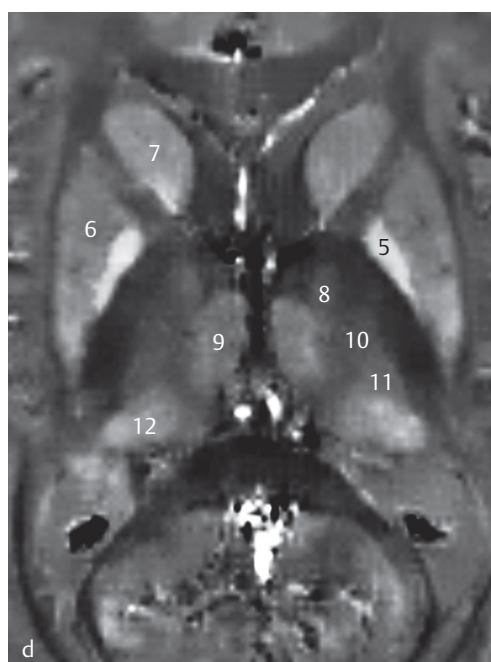
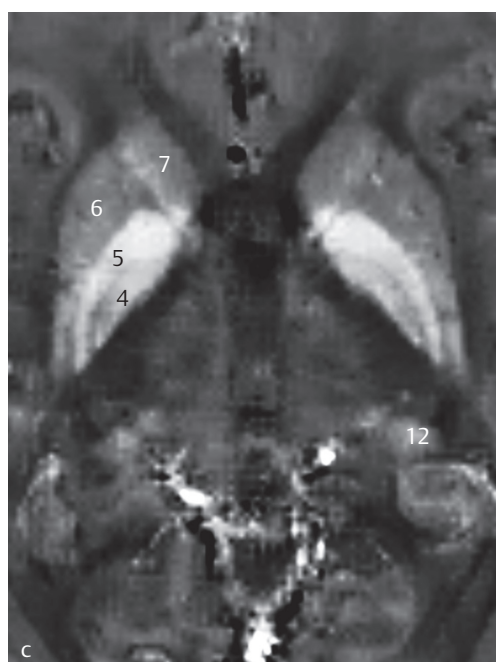
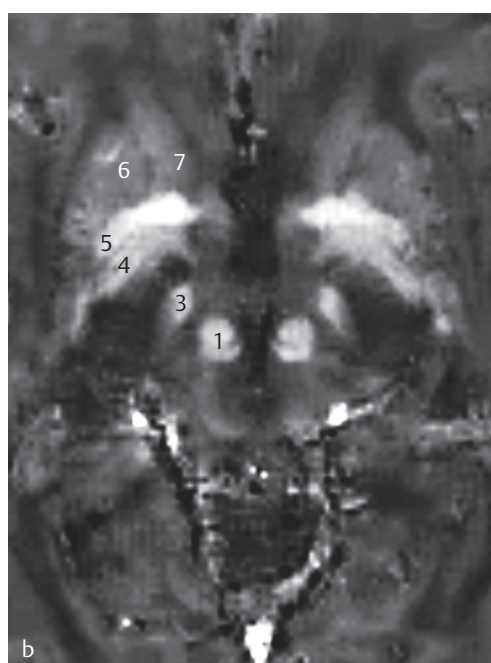
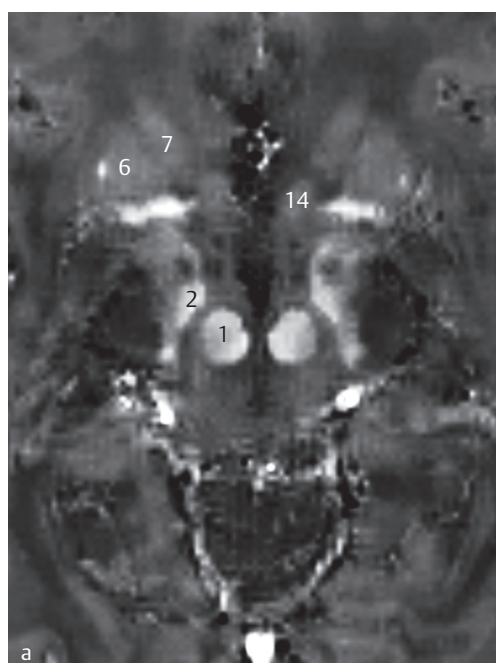
The metathalamus consists of the **medial** (see ►Fig. 3.10a, ►Fig. 4.4a, and ►Fig. 5.8) and **lateral geniculate bodies** (see ►Fig. 3.10a and ►Fig. 5.8), both of which lie posterior to the thalamus.

The medial geniculate body is a relay nucleus for the auditory system (see Section 10.5), while the lateral geniculate body is a relay center for the visual system (see Section 10.6).

Thalamus

The thalamus is a somewhat egg-shaped aggregate of numerous nuclear regions, the tip of which is directed toward the interventricular foramen (Monro; see ►Fig. 3.1c, ►Fig. 3.8a, ►Fig. 3.8b, ►Fig. 5.1c, ►Fig. 5.9a, ►Fig. 5.9b, ►Fig. 7.8b, and ►Fig. 7.10a). Its medial surface abuts the IIIrd ventricle while its lateral surface lies in contact with the posterior limb of the internal capsule (see ►Fig. 3.9a, ►Fig. 3.9b, ►Fig. 4.4a, ►Fig. 4.4b, ►Fig. 5.9a, ►Fig. 5.9b, and ►Fig. 5.24). The posterior region of the thalamus (see ►Fig. 3.10a, ►Fig. 3.10b, ►Fig. 4.3a, ►Fig. 4.3b, ►Fig. 5.9a, ►Fig. 5.9b, and ►Fig. 7.45) is known as the pulvinar. The two thalami on either side are usually bridged by the narrow interthalamic adhesion (see ►Fig. 3.1c, ►Fig. 4.2a, ►Fig. 4.2b, ►Fig. 5.1c, and ►Fig. 6.3), composed of glial cells. A narrow strip at the superior aspect of the thalamus termed the "lamina affixa" is incorporated into the floor of the body of lateral ventricle during embryonal life. It lies immediately above the sectioned thalamus in ►Fig. 5.10a and ►Fig. 5.10b (not otherwise specified). The caudate nucleus lies lateral and superior to the thalamus (see ►Fig. 3.8d, ►Fig. 3.9a, ►Fig. 3.9b, ►Fig. 3.10a, ►Fig. 3.10b, ►Fig. 4.4a, ►Fig. 4.4b, ►Fig. 4.4d, ►Fig. 5.8, and ►Fig. 5.23). The superior thalamostriate vein and the stria terminalis run in the groove between these two nuclear regions (see ►Fig. 3.7c, ►Fig. 3.7d, ►Fig. 3.9c, ►Fig. 3.10 c, ►Fig. 3.10d, ►Fig. 5.10a, and ►Fig. 5.10b).

The nuclear complex of the thalamus is divided by **lamellae of myelinated fibers** into several groups. Anteriorly, two lamellae separate the **anterior nuclei**



- 1 Red nucleus
- 2 Substantia nigra
- 3 Subthalamic nucleus
- 4 Globus pallidus medial segment
- 5 Globus pallidus lateral segment
- 6 Putamen
- 7 Head of caudate nucleus
- 8 Anterior nuclei of thalamus
- 9 Medial nuclei of thalamus
- 10 Ventral lateral nuclei of thalamus
- 11 Lateral posterior nuclei of thalamus
- 12 Pulvinar nuclei of thalamus
- 13 Hippocampus
- 14 Nucleus accumbens

Fig. 7.45 Midbrain and superiorly adjacent deep nuclei. QSM-MRI. The axial sections are aligned along the bicommissural plane and are visualized sequentially from inferior to superior (a–d). For technical data see ► Chapter 12.

Fig. 7.45a Inferior axial section.

Fig. 7.45b Section adjacent to a, located further superiorly.

Fig. 7.45c Section adjacent to b, located further superiorly.

Fig. 7.45d Section adjacent to c, located further superiorly.

Fig. 7.45e Section aligned along the red nucleus/dentate nucleus. This orientation enables the depiction of the subthalamic nucleus and the subdivision of the red nucleus.

Fig. 7.45f Slice reconstruction was angulated perpendicular to the line between anterior and posterior commissures.

of **thalamus** (see ►Fig. 3.8a, ►Fig. 5.9a, 5.9b, and ►Fig. 7.45). These nuclei are, for the most part, relay stations of the limbic system (see Section 10.11). A medial lamella marks the boundary of the **medial thalamic nuclei** (see Fig. 3.9a, ►Fig. 3.9b, ►Fig. 4.3a, ►Fig. 4.3b, ►Fig. 5.9a, ►Fig. 5.9b, and ►Fig. 7.45) which possess corticopetal and corticofugal connections with the frontal lobe of the telencephalon. Of the several lateral nuclei of the thalamus, only those which are of special importance to the neurofunctional systems will be described in this chapter. In general, thalamic nuclei possess both thalamocortical and corticothalamic fibers, although often only one projectional system may be mentioned. Stereotactic surgical procedures may be performed on some relay nuclei. Synonyms used clinically⁵¹⁴ have therefore been added to international names in brackets. The ventral lateral nuclei previously: ventro-oral nuclei; see ►Fig. 3.9a, ►Fig. 3.9b, ►Fig. 5.9a, ►Fig. 5.9b, and ►Fig. 7.45) are connected to area 4 lying anterior to the central sulcus in the frontal lobe. The anterior part of the ventral lateral nuclei receives afferent fibers from the globus pallidus, while the posterior part receives afferent fibers from the cerebellum.

The **ventral posterolateral nucleus** previously: external ventrocaudal nucleus; see ►Fig. 4.4a, ►Fig. 4.4b, ►Fig. 10.1, and ►Fig. 10.3) is a relay nucleus for the anterolateral system and the medial lemniscus. The **ventral posteromedial nucleus** (previously: internal ventrocaudal nucleus; see Fig. 10.6, ►Fig. 10.7b, and ►Fig. 10.8b) lies in its immediate vicinity. This nucleus provides a similar relay center for the trigeminal system (see Section 10.1.3) as its neighboring nucleus with a somatotopic projection into the postcentral gyrus. The ventral posterolateral and posteromedial nuclei belong to the specific nuclei of the thalamus with point-to-point connections with the periphery of the body and specific areas of the cerebral cortex.

This relay system thus differs from that of nonspecific nuclei, which project diffusely into large areas of the telencephalon. The intralaminar nuclei belong to these nonspecific thalamic nuclei; for more information, see the ascending reticular system (see Section 10.3). The **pulvinar** (see ►Fig. 7.45) transmits both auditory and optic signals and projects into secondary cortical areas of the telencephalon.

Epithalamus

The epithalamus is composed of structures located in the region of the roof of the IIIrd ventricle. These include:

- Choroid plexus of the IIIrd ventricle
- Stria medullaris of thalamus
- Habenular nuclei (see ►Fig. 5.9a, ►Fig. 5.9b, and ►Fig. 10.39)
- **Pineal gland** (pineal body; see ►Fig. 3.1c, ►Fig. 3.11a, ►Fig. 4.2a, ►Fig. 4.2b, ►Fig. 5.9a, ►Fig. 5.9b, ►Fig. 5.25, and ►Fig. 6.3)

Immediately anterior to the superior colliculi lies the **posterior commissure** (see ►Fig. 3.1c, ►Fig. 3.10a, ►Fig. 3.10b, ►Fig. 4.2a, ►Fig. 4.2b, ►Fig. 5.1c, and ►Fig. 6.3) which connects nuclear groups of the mid-brain. The pineal gland is almost 1 cm in length, lies on the tectum and is attached to the roof of the diencephalon. Acervulus (brain sand) has been seen within this structure in about 10% of school children. Pineal gland calcification is seen on CT in more than 50% of examined individuals above age 25,⁶²⁸ and serves as an imaging landmark for the pineal gland.

Clinical Significance

Diencephalic lesions result in characteristic functional disturbances which enable topical correlation on clinical examination in certain cases.

Clinical Notes

“Central” dysregulation of body temperature and / or the water balance points to hypothalamic or hypothalamic-neurohypophyseal dysfunction. Serious impairment of sympathetic or parasympathetic autonomic function is also symptomatic of disordered hypothalamic function. The subthalamus is closely related to the basal ganglia through the globus pallidus and a lesion of this region causes contralateral hemiballism, a vascular cause being the commonest etiological insult. A variety of functional disturbances of the thalamus are known to occur, and depend on its anatomy and function. Not only does it receive exteroceptive and proprioceptive impulses,¹⁴⁹ but also functions as a relay station for visual and auditory pathways, and serves as an important organ for the integration and coordination of afferent pathways. Lesions cause contralateral disturbances of both superficial (especially temperature), as well as deep sensations. Hemiataxia and involuntary movements may occur with the development of agitated choreatic-athetotic movements. Spontaneous pain and hyperpathia may also occur contralaterally. Thalamic disorders often have a vascular origin; tumors rarely cause a complete thalamic syndrome. A unilateral lesion of the medial geniculate body goes mostly unnoticed due to bilateral interconnections of auditory pathways, whereas a unilateral lesion of the lateral geniculate body leads to contralateral visual field defects including homonymous hemianopsia.

Pituitary Gland

The pituitary gland or hypophysis is an endocrine organ, related anatomically and functionally to the hypothalamus. It is bean-shaped, weighs 0.7 g on an average, and is situated within the hypophysial fossa of the body of the sphenoid. The gland is separated superiorly from the cranial cavity by a dural reflection, the diaphragma sellae, which exhibits a small opening for the passage of the infundibulum. The pituitary gland is divided into two parts:

- Adenohypophysis, anterior lobe (see ► Fig. 6.10b)
- Neurohypophysis, posterior lobe (see ► Fig. 6.10b)

The **adenohypophysis** or anterior lobe is further subdivided into distal, tuberal, and intermediate parts, of which the distal part is the largest. The tuberal part surrounds the pituitary stalk, while the intermediate part abuts the neurohypophysis. The adenohypophysis controls the activity of the other endocrine glands through glandotropic hormones. The following cells have been identified by electron microscopy and by immunohistochemical methods in the adenohypophysis for the hormones listed in parentheses:

- Somatotropic cells (growth hormone (GH) = STH)
- Thyrotropic cells (thyrotropic hormone = TSH)
- Mammatropic cells (prolactin = PRL)
- Corticotropic cells (adrenocorticotrophic hormone = ACTH)
- Gonadotropic cells (follicular stimulating hormone = FSH, luteinizing hormone = LH)

Melanotropin and lipotropin are produced by endocrine cells in the intermediate lobe.

The **neurohypophysis** is divided into:

- Infundibulum, infundibular stalk
- Posterior lobe of the pituitary gland

No hormones are produced in the neurohypophysis; instead, it stores and releases hormones that are transported to it via axons from nerve cells of the hypothalamus.

The following arteries supply the **pituitary gland**:

- Superior hypophyseal arteries from the internal carotid artery
- Inferior hypophyseal arteries from the circle of Willis

Both vessels supply the pituitary directly as well as through capillary plexuses formed around the stalk. Blood then enters one or two veins (portal veins) which run to the adenohypophysis, branching (once again) to form capillaries (**portal circulation of the pituitary gland**). The regulatory hypothalamic neurohormones are transported by these infundibular vessels to the adenohypophysis, their effector site.

7.7.5 Telencephalon

Appearance

The telencephalon (see ► Fig. 7.39, ► Fig. 7.40, ► Fig. 7.41, ► Fig. 7.42, ► Fig. 7.43, and ► Fig. 7.44) is the largest subdivision of the brain (more than 80% of total brain weight, average volume more than 1000 mL) and overlaps large parts of the diencephalon and the brainstem. The telencephalon is separated from the cerebellum by a deep transverse furrow, the transverse cerebral fissure, which accommodates the tentorium of cerebellum. The longitudinal cerebral fissure extends up to the corpus callosum and divides the telencephalon into two hemispheres which are separated by a continuous dural septum, the falx cerebri (see ► Fig. 3.2a, ► Fig. 3.2b, ► Fig. 3.4a, ► Fig. 3.4b, ► Fig. 3.8a, ► Fig. 3.8b, ► Fig. 3.15a, ► Fig. 3.15b, ► Fig. 5.8, and ► Fig. 5.29). The surface of the two hemispheres facing the median plane is called “medial cerebral surface” and merges into the lateral surface at the superior margin of the hemisphere. This lateral surface of cerebral hemispheres in humans is entirely composed of neocortex, the surface area of which increased during evolution due to the development of gyri and sulci. Each hemisphere is divided into four lobes and the insula; the olfactory bulb and tract lie beneath the frontal lobe and belong to the olfactory system (see Section 10.7).

Internal Structure

The telencephalon is composed of gray and white matter. **Gray matter, which contains nerve cells**, is composed of telencephalic nuclei and the cerebral cortex. **White matter** contains nerve fibers which transmit afferent and efferent signals and facilitate processing of information between the different regions of the telencephalon. Each hemisphere has a lateral ventricle which communicates with the third ventricle through the interventricular foramen.

Telencephalic Nuclei

The nuclei of the telencephalon (or cerebrum) flank the lateral ventricles. Ascending and descending fiber tracts of the neocortex divide these nuclei into the following groups:

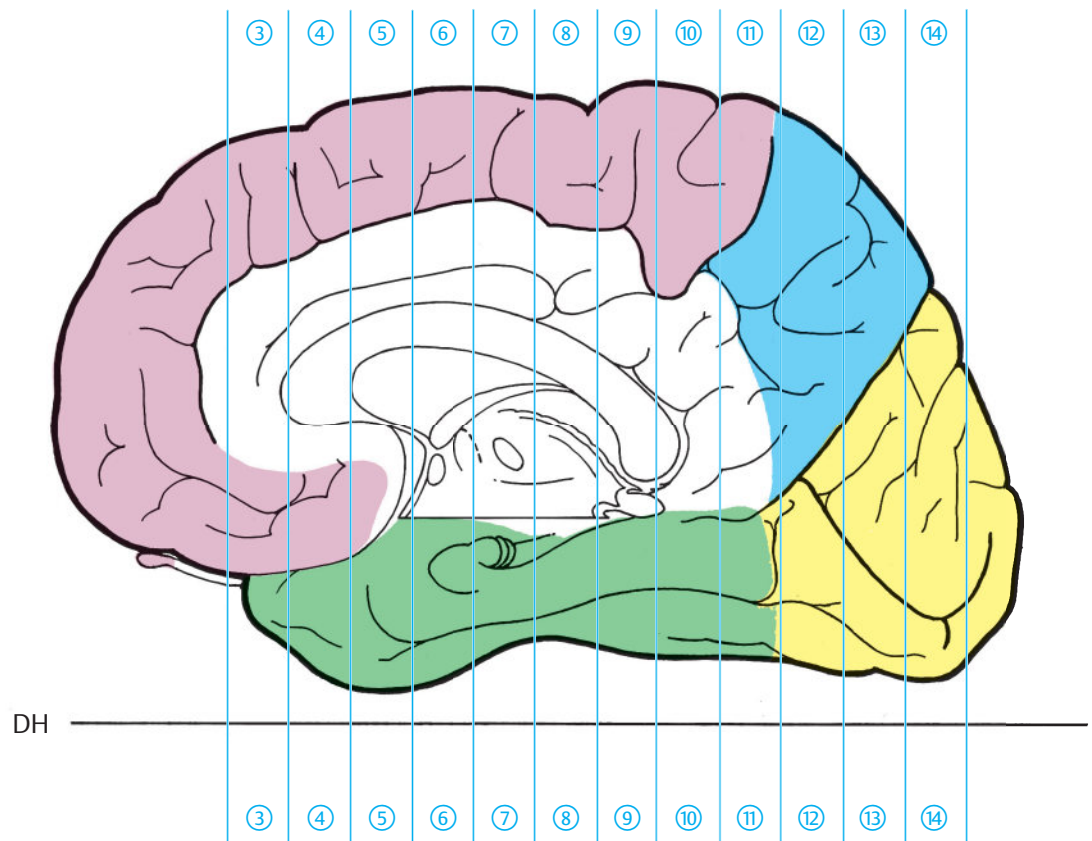
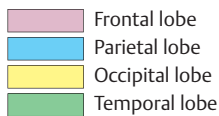


Fig. 7.46 Cerebral lobes. For specimen details see Chapter 12.
DH = German horizontal

Fig. 7.46a Median view of boundaries of the frontal, parietal, occipital, and temporal lobes of the cerebrum sectioned in the coronal plane. The cingulate and paraterminal gyri and the subcallosal area have not been included in any cerebral lobe.

- Caudate nucleus (see ► Fig. 3.6a, ► Fig. 3.6b, ► Fig. 3.8a, ► Fig. 3.8b, ► Fig. 3.10a, ► Fig. 3.10b, ► Fig. 4.3a, ► Fig. 4.3b, ► Fig. 4.4a, ► Fig. 4.4b, ► Fig. 4.5a, ► Fig. 4.5b, ► Fig. 5.8, ► Fig. 5.9a, ► Fig. 5.9b, ► Fig. 5.22, and ► Fig. 7.45)
- Putamen (see ► Fig. 3.7a, ► Fig. 3.9a, ► Fig. 3.9b, ► Fig. 4.4a, ► Fig. 4.4b, ► Fig. 4.5a, ► Fig. 4.5b, ► Fig. 5.8, ► Fig. 5.22, and ► Fig. 7.45)
- Claustrum (see ► Fig. 3.6b, ► Fig. 3.7a, ► Fig. 3.7b, ► Fig. 3.8a, ► Fig. 3.8b, ► Fig. 4.5a, ► Fig. 5.9a, ► Fig. 5.9b, ► Fig. 5.9, and ► Fig. 5.23)
- Amygdaloid body (see Fig. 3.8a, ► Fig. 3.8b, ► Fig. 4.5a, ► Fig. 4.5b, ► Fig. 5.6a, ► Fig. 5.6b, and ► Fig. 5.21)
- Septal nuclei (previously: septum verum; see ► Fig. 10.39)

During evolution of the neocortex, the **caudate nucleus** assumed a comma-like shape. The head is a relatively large bulging protuberance along the lateral wall of the frontal horn of the lateral ventricle. The body of the caudate nucleus extends in an occipital direction as the tail, which turns anteriorly in the roof of the occipital horn. Fiber

tracts of the neocortex separate the caudate nucleus from the putamen, except for areas located in the anterobasal region (floor of the striatum, see ► Fig. 3.6d). Nerve cells of both the caudate nucleus and putamen are similar in shape and function and these two structures are therefore collectively known as the **striatum**, which possesses an important motor function (see Section 10.8.2). The **putamen** is a shell-shaped structure and lies medial to the external capsule, with the globus pallidus of the diencephalon lying within the concavity of the putamen. Topographically, the putamen and globus pallidus form the lentiform nucleus; the nerve cells of these two nuclear regions however differ significantly. The **claustrum** lies as a small disc-like structure lateral to the putamen and is bounded by the external and extreme capsules. The **amygdaloid body** lies medially at the tip of the temporal horn of the lateral ventricle, a part of which belongs to the olfactory system (see Section 10.7), the rest to the limbic system (see Section 10.11). Septal nuclei (previously: septum verum) constitute a nuclear region lying anterior to the anterior commissure and to the column of the fornix and belong to the limbic system (see Section 10.11).

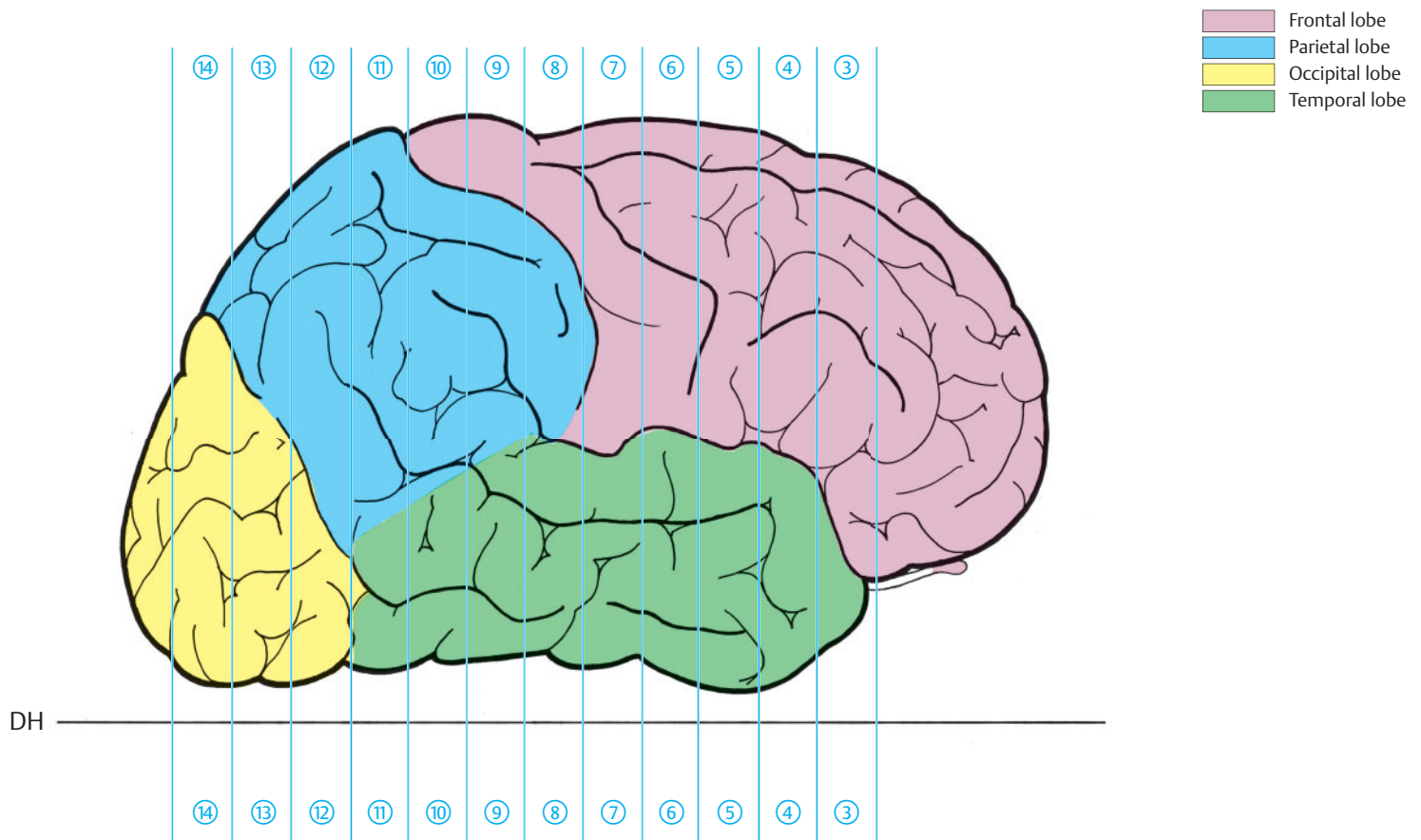


Fig. 7.46b Lateral view of boundaries of the frontal, parietal, occipital, and temporal lobes of the cerebrum sectioned in the coronal plane.

Cerebral cortex

The cerebral cortex surrounds the telencephalon or cerebrum and is a 2 to 5 mm in thickness layer of grey matter measuring 600 mL in volume in men and 540 mL in women. The difference between the two sexes is therefore significant. The cerebral cortex is divided into four lobes and the deeply situated insula (see ►Fig. 7.46, ►Fig. 7.47, ►Fig. 7.48, ►Fig. 7.49, and ►Fig. 7.50):

- Frontal lobe
- Parietal lobe
- Occipital lobe
- Temporal lobe
- Insula

The individual lobes are only partially separated by sulci (see ►Fig. 7.51).⁴³⁶

Located on the lateral surface of each hemisphere, the **central sulcus** (see ►Fig. 3.1d, ►Fig. 3.9a, ►Fig. 3.9b, ►Fig. 3.10a, ►Fig. 3.10b, ►Fig. 4.1d, ►Fig. 4.6a, ►Fig. 4.6b, ►Fig. 5.10a, ►Fig. 5.10b, ►Fig. 5.12, ►Fig. 5.14, ►Fig. 5.27, ►Fig. 5.29, ►Fig. 7.51, and ►Fig. 7.56) forms the boundary between the frontal and parietal lobes. The central sulcus extends as two curvilinear structures from the superior margin in the direction of the lateral sulcus. The superior curve borders the so-called “knob” (see ►Fig. 5.14, ►Fig. 5.29, ►Fig. 7.52, and ►Fig. 7.52a), which exhibits a protrusion posteriorly and a concavity anteriorly.^{231,578,641} The central sulcus is clearly identifiable in 3D illustrations (see ►Fig. 7.51). The different angles of inclination of the central sulcus to the median and bicommissural planes may be visualized with help of a PC, red–blue glasses, and a CD-ROM.³¹³

Cortex of frontal lobe
 Cortex of temporal lobe

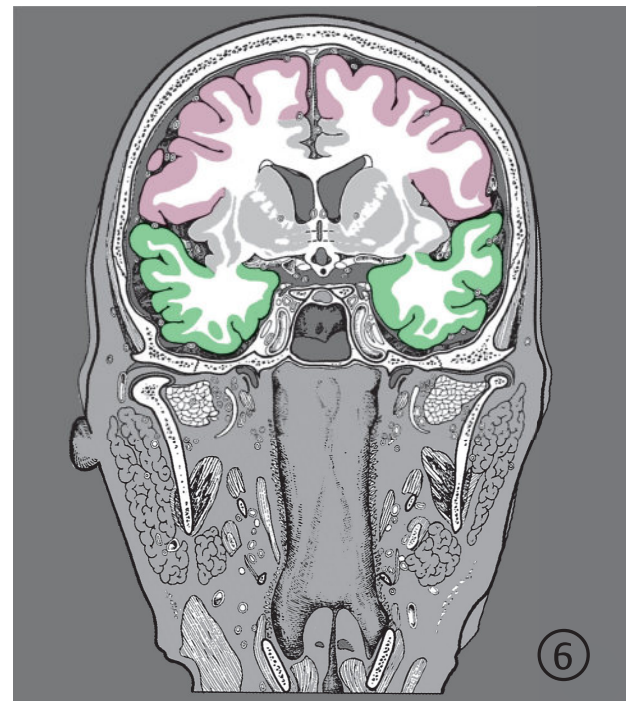
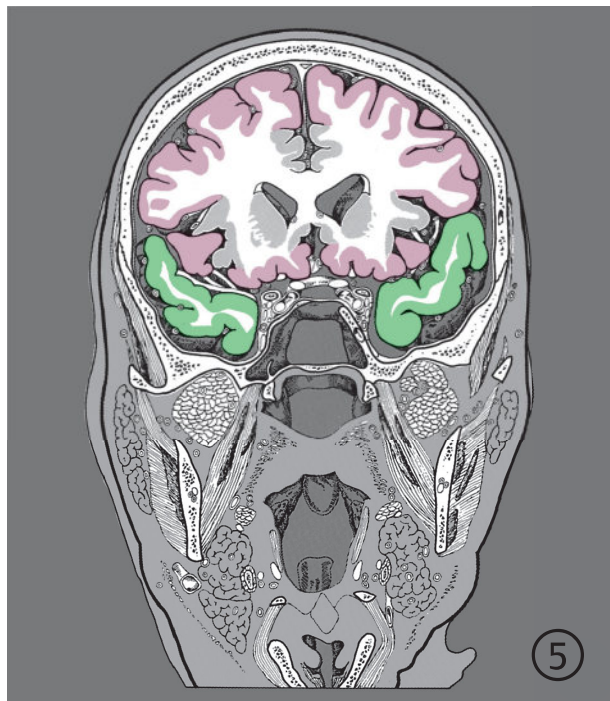
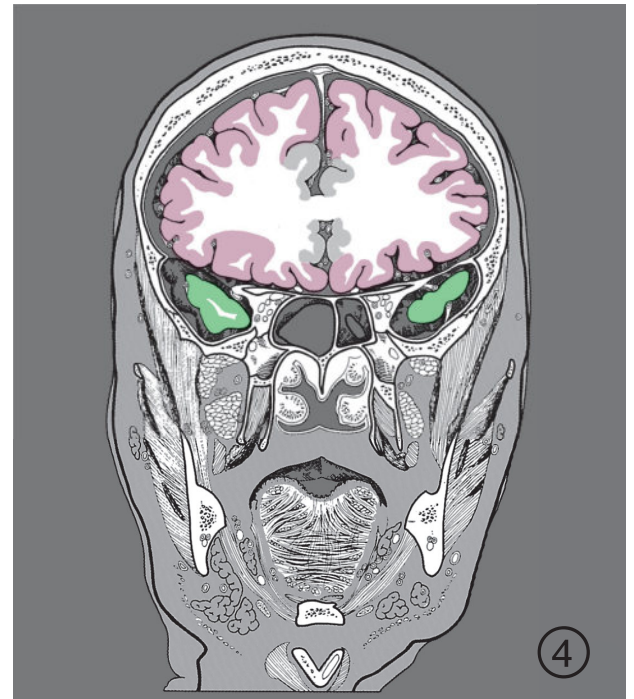
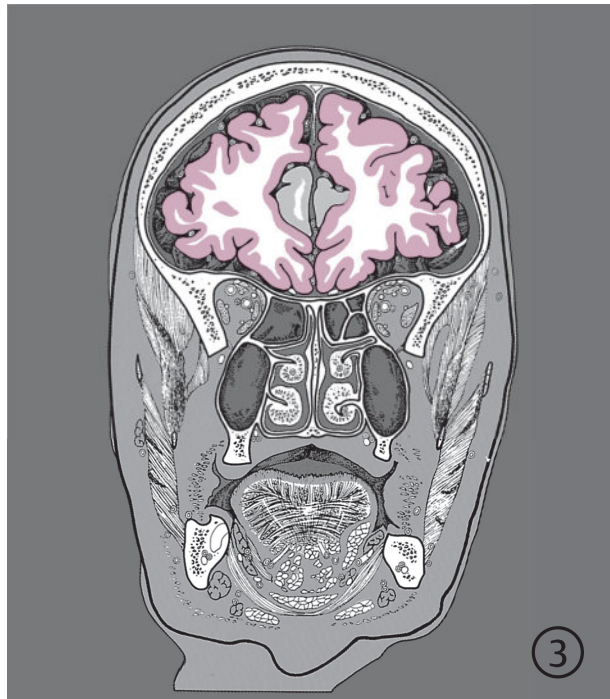


Fig. 7.47 Frontal, parietal, occipital, and temporal cortex. Serial coronal images. The insular cortex, cingulate gyrus, subcallosal area and the paraterminal gyrus have not been included in any cerebral lobe. Encircled digits indicate the number of the respective slice.

Fig. 7.47a 3rd to 6th sections.

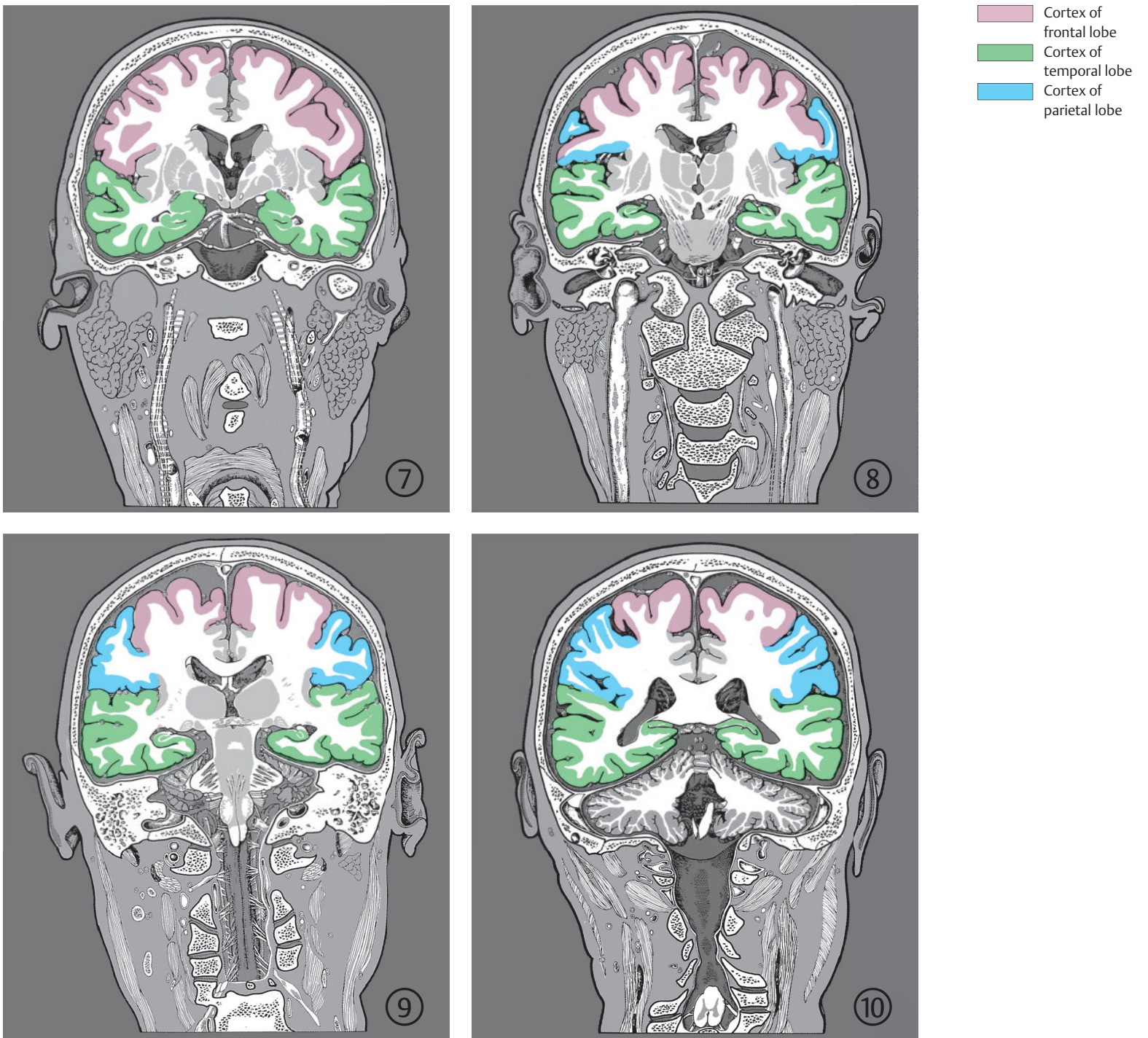


Fig. 7.47b 7th to 10th sections.

- Cortex of frontal lobe
- Cortex of temporal lobe
- Cortex of parietal lobe
- Cortex of occipital lobe

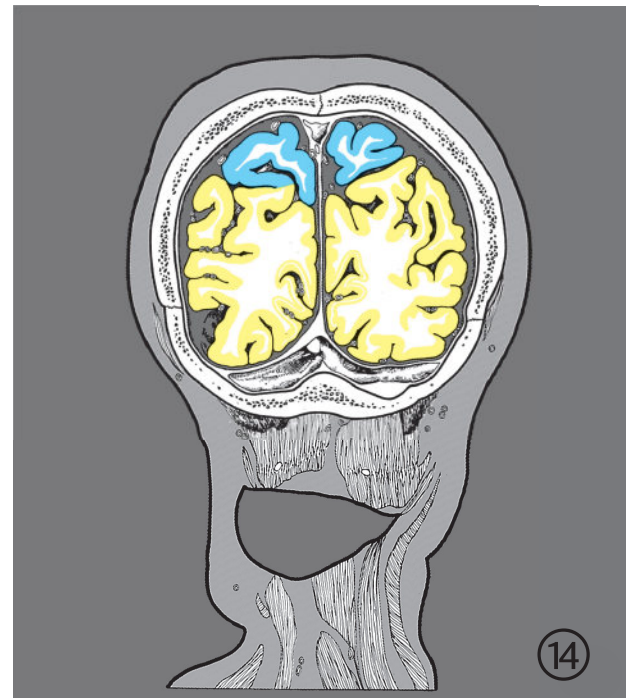
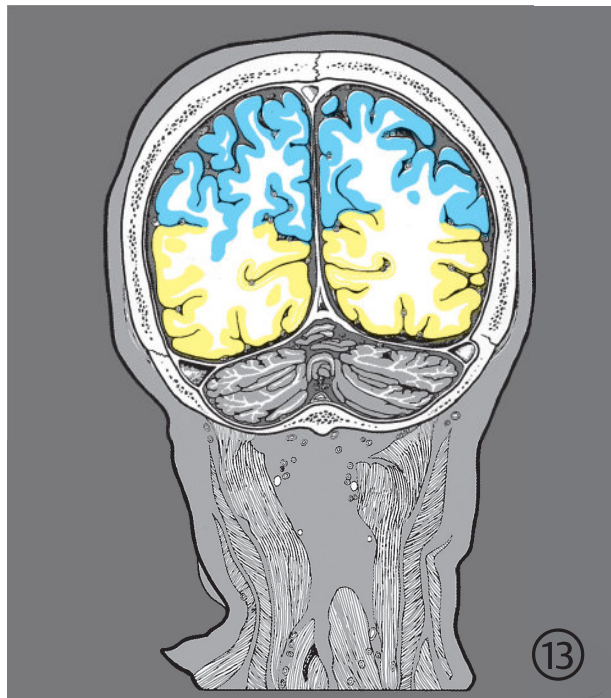
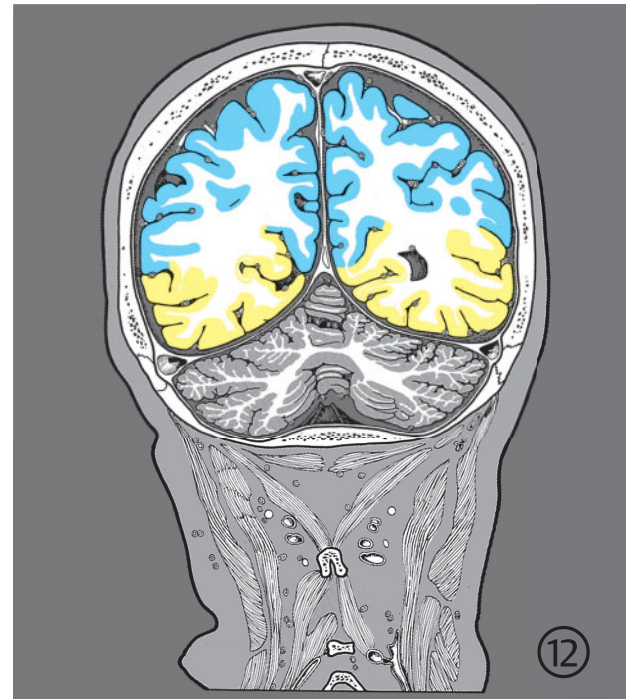
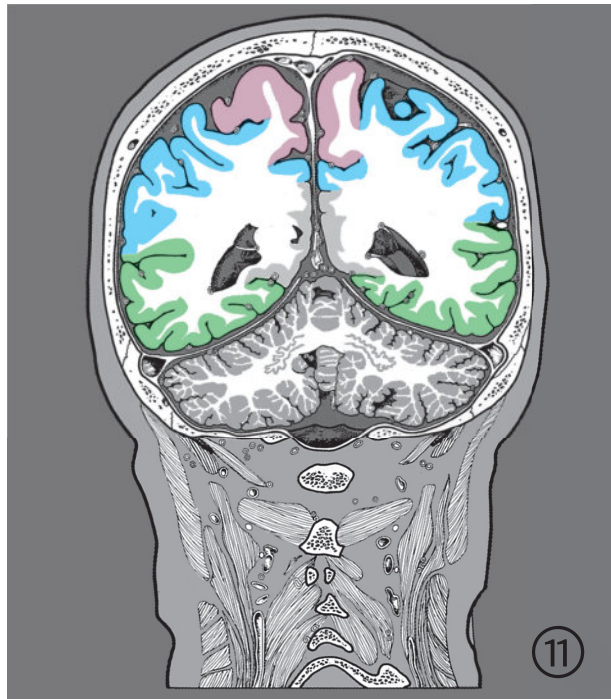


Fig. 7.47c 11th to 14th sections.

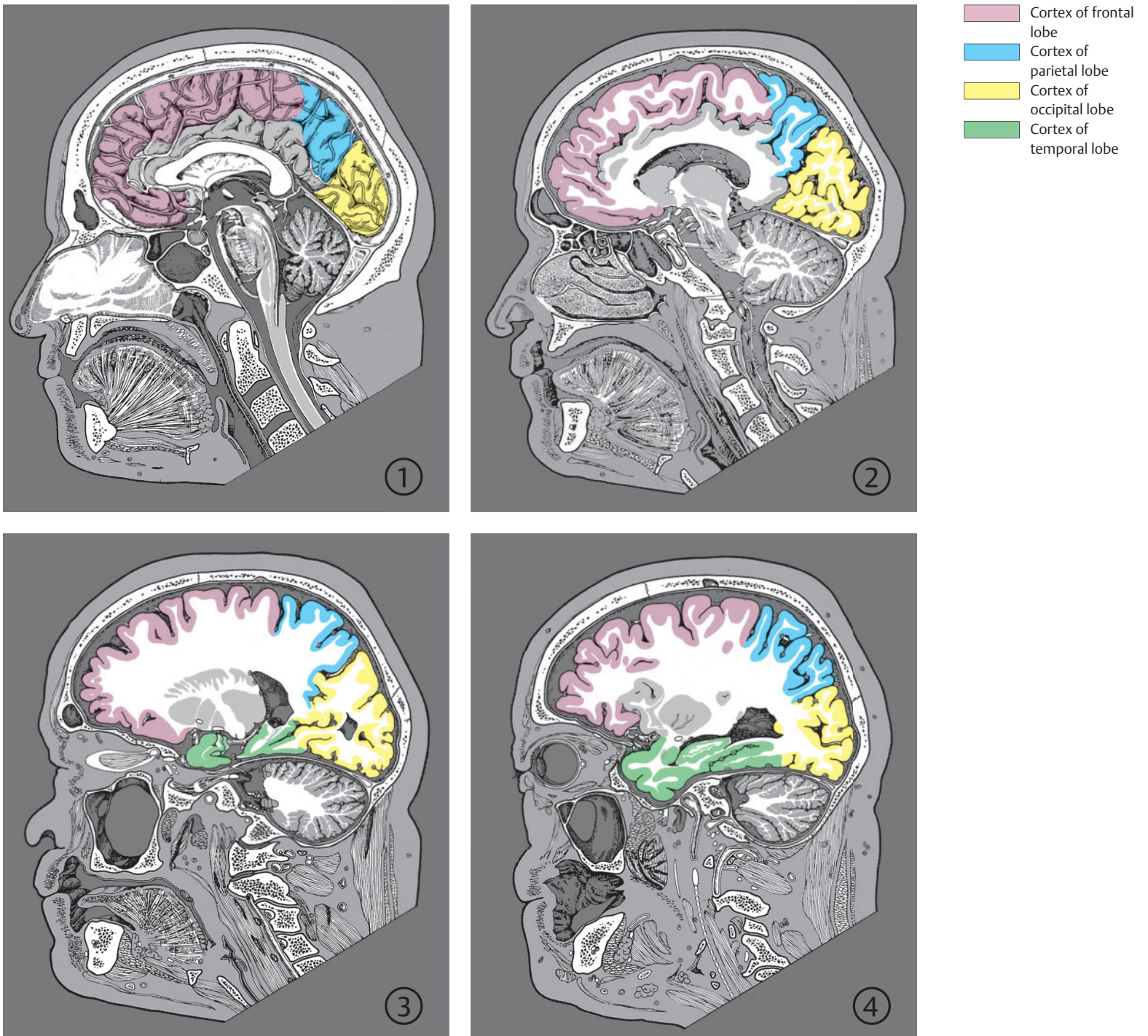


Fig. 7.48 Frontal, parietal, occipital, and temporal cortex. Serial sagittal images. The insular cortex, cingulate gyrus, subcallosal area, and the paraterminal gyrus have not been included in any cerebral lobe. Encircled digits indicate the number of the respective slice (see ► Fig. 4.1).

Fig. 7.48a 1st to 4th sections.

- Cortex of frontal lobe
- Cortex of parietal lobe
- Cortex of occipital lobe
- Cortex of temporal lobe

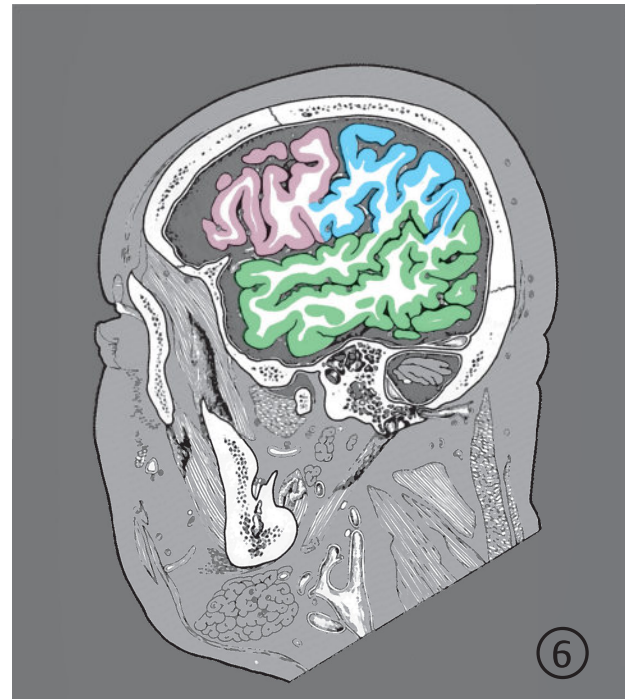
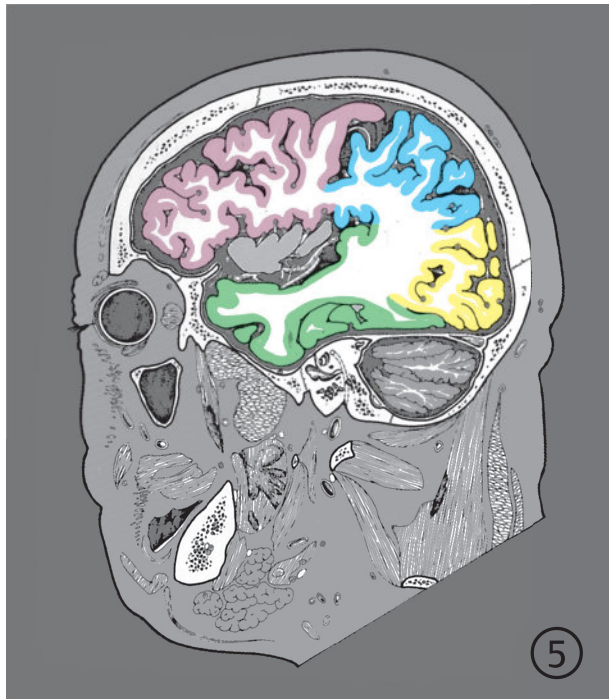


Fig. 7.48b 5th and 6th sections.

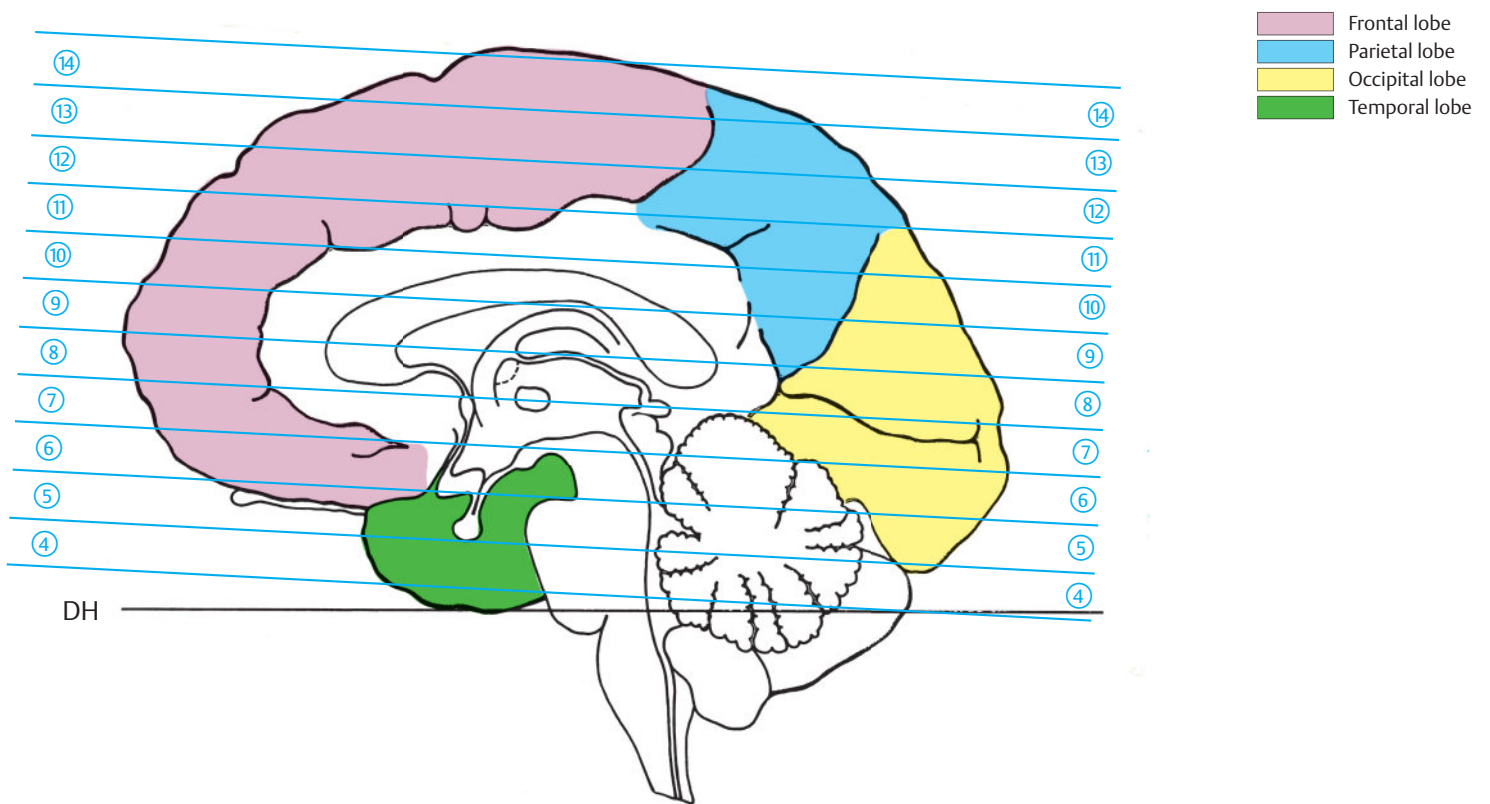


Fig. 7.49 Boundaries of the frontal, parietal, occipital, and temporal lobes. For specimen details see ► Chapter 12.
DH = German horizontal

Fig. 7.49a Median view of the brain sectioned in the bicommissural plane. The cingulate and paraterminal gyri and the subcallosal area have not been included in any cerebral lobe.

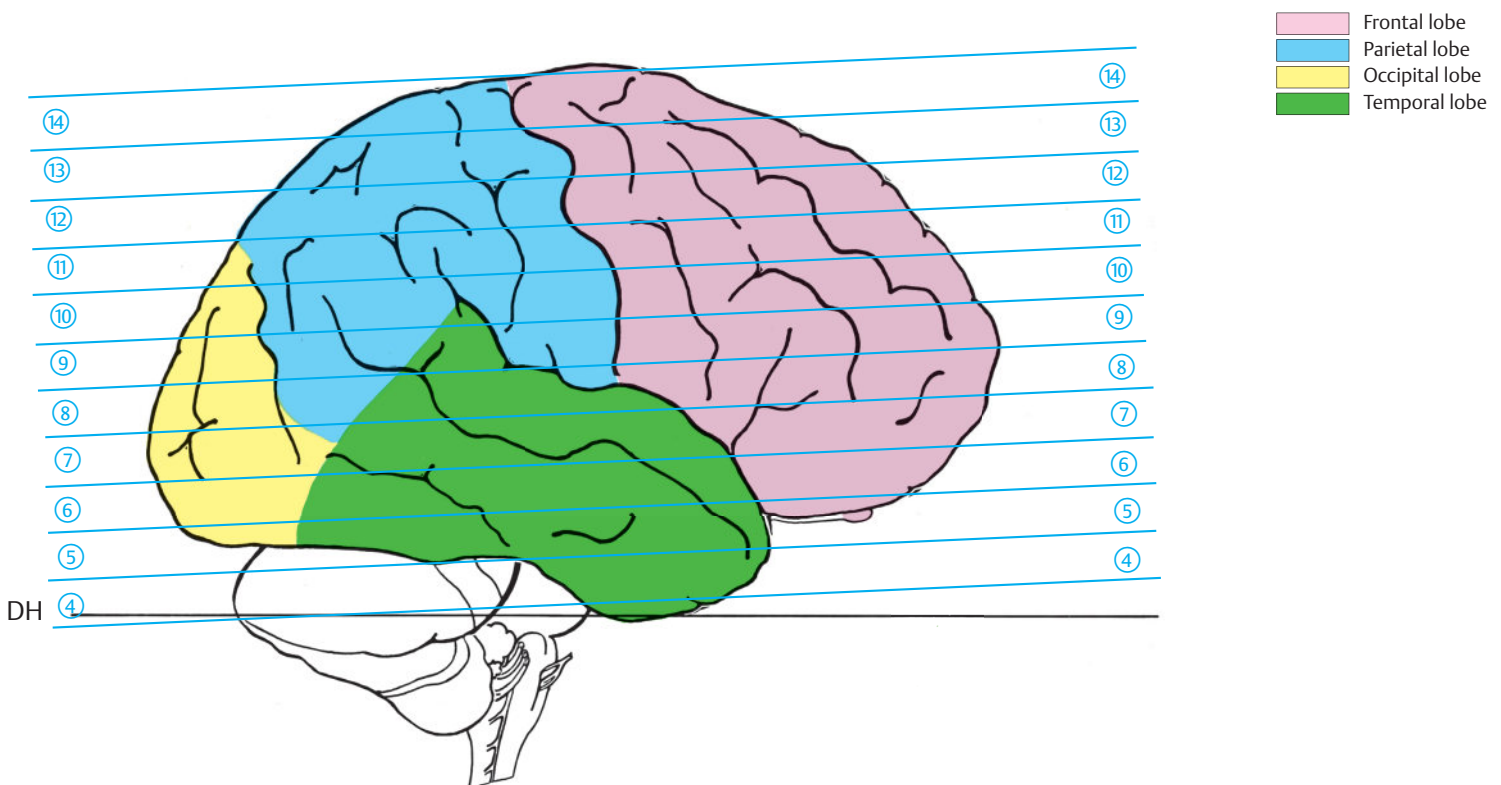


Fig. 7.49b Lateral view of the brain sectioned in the bicommissural plane.

- Cortex of frontal lobe
- Cortex of occipital lobe
- Cortex of temporal lobe

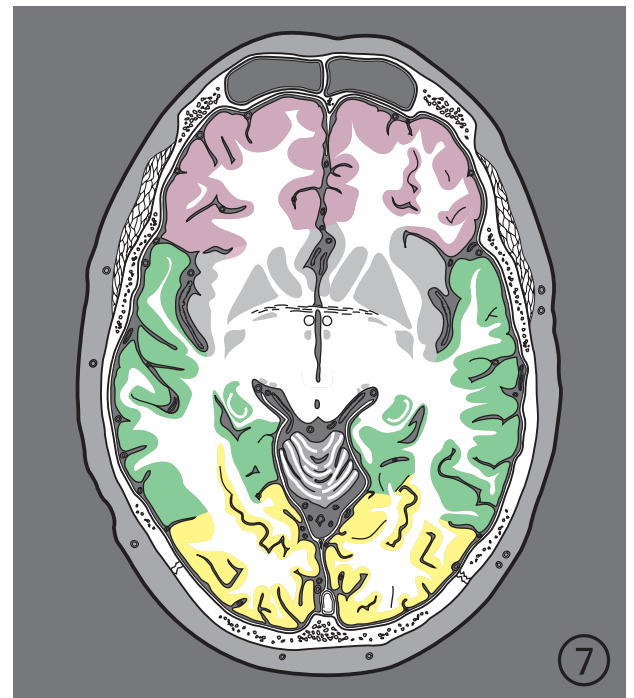
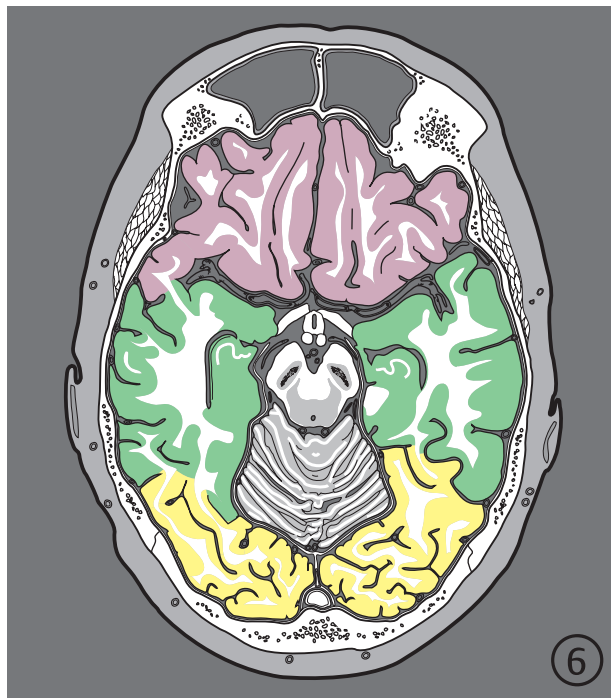
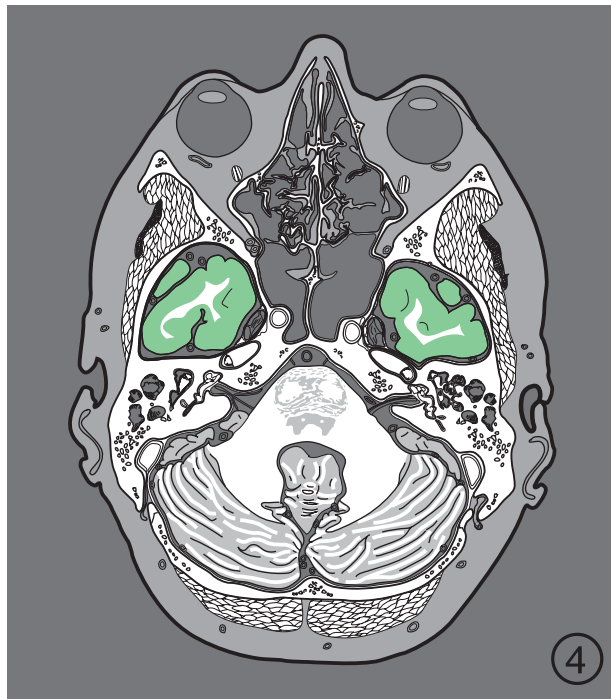


Fig. 7.50 Frontal, parietal, occipital, and temporal cortex. Serial images oriented along the bicommissural plane. The insular cortex, cingulate gyrus, subcallosal area, and the paraterminal gyrus have not been included in any cerebral lobe. Encircled digits indicate the number of the respective slice (see ► Fig. 5.1).

Fig. 7.50a 4th to 7th sections.

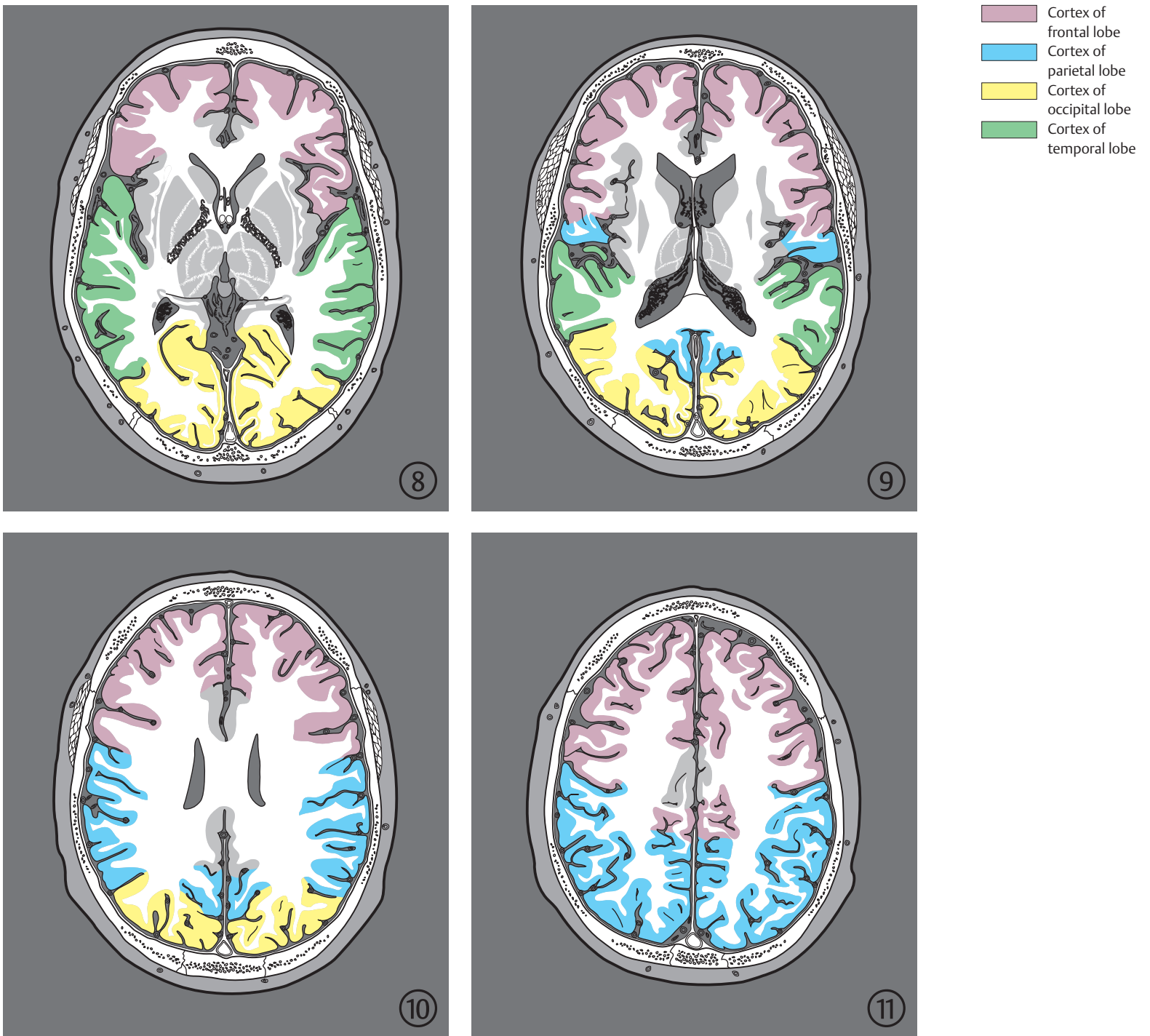


Fig. 7.50b 8th to 11th sections.

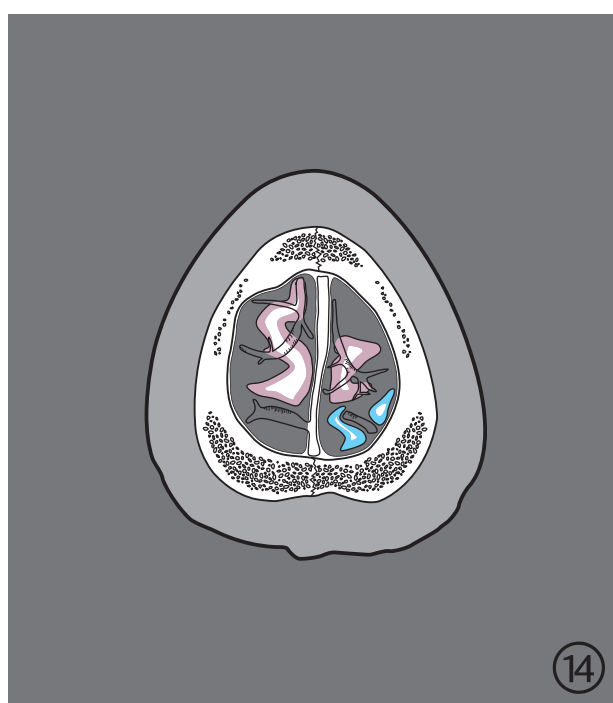
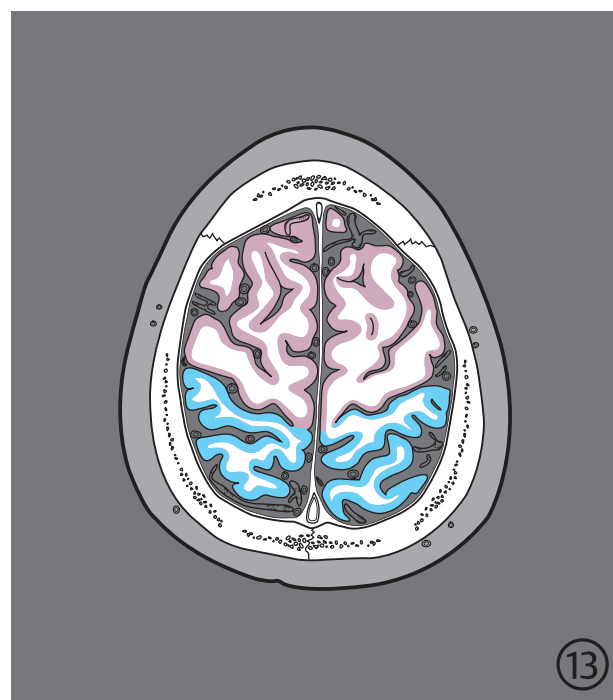
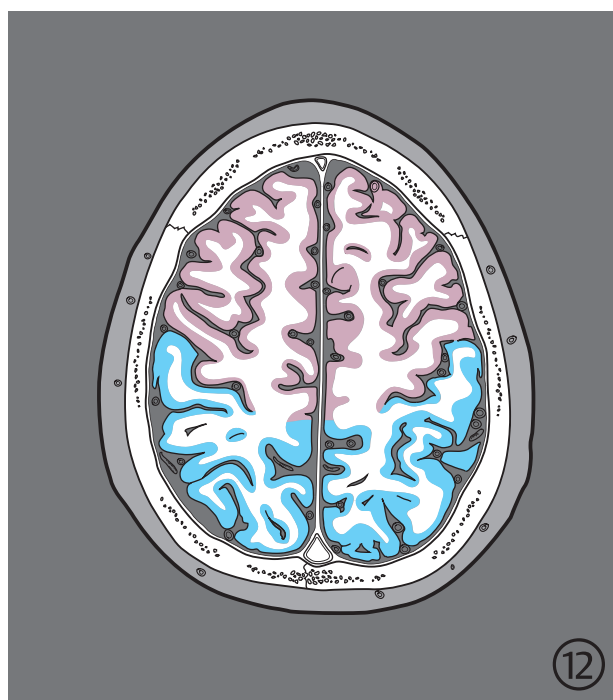
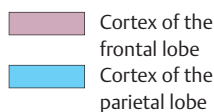


Fig. 7.50c 12th to 14th sections.

The **lateral sulcus** (see ► Fig. 3.6a, ► Fig. 3.6b, ► Fig. 3.8a, ► Fig. 3.8b, ► Fig. 3.11a, ► Fig. 3.11b, ► Fig. 4.6a, ► Fig. 4.6b, ► Fig. 5.7, ► Fig. 5.23, and ► Fig. 7.51) forms the boundary between the temporal and frontal lobes and extends deep into the brain toward the insula, also separating the temporal and parietal lobes over a short distance. On the medial surface of each hemisphere, the **parietooccipital sulcus** (see ► Fig. 3.1c, ► Fig. 3.13a, ► Fig. 3.13b, ► Fig. 3.15a, ► Fig. 3.15b, ► Fig. 4.2a, ► Fig. 4.2b, ► Fig. 4.3a, ► Fig. 4.3b, ► Fig. 5.9a, ► Fig. 5.9b, ► Fig. 5.11, and ► Fig. 5.27) separates the parietal and the occipital lobes. The parietal, occipital, and temporal lobes merge into each other without distinct boundaries on the lateral surface of the hemisphere.

Frontal Lobe

The lateral surface of the frontal lobe shows three arched gyri separated by incomplete sulci:

- **Superior frontal gyrus** (see ► Fig. 3.1d, ► Fig. 3.2a, ► Fig. 3.2b, ► Fig. 3.3a, ► Fig. 3.3b, ► Fig. 3.6a, ► Fig. 3.6b, ► Fig. 3.9a, ► Fig. 3.9b, ► Fig. 4.1c, ► Fig. 4.3a, ► Fig. 4.3b, ► Fig. 5.8, ► Fig. 5.11, ► Fig. 5.21, ► Fig. 5.24, and ► Fig. 5.28)
- **Middle frontal gyrus** (see ► Fig. 3.1d, ► Fig. 3.2a, ► Fig. 3.2b, ► Fig. 3.6a, ► Fig. 3.6b, ► Fig. 3.8a, ► Fig. 3.8b, ► Fig. 4.1c, ► Fig. 4.5a, ► Fig. 4.5b, ► Fig. 5.8, ► Fig. 5.12, ► Fig. 5.23, ► Fig. 5.26, ► Fig. 5.28, and ► Fig. 10.25a)
- **Inferior frontal gyrus** (see ► Fig. 3.1d, ► Fig. 3.3a, ► Fig. 3.3b, ► Fig. 3.6a, ► Fig. 3.6b, ► Fig. 3.7a, ► Fig. 4.1c, ► Fig. 4.1d, ► Fig. 4.6a, ► Fig. 4.6b, ► Fig. 4.6d, ► Fig. 5.7, ► Fig. 5.10a, and ► Fig. 5.10b)

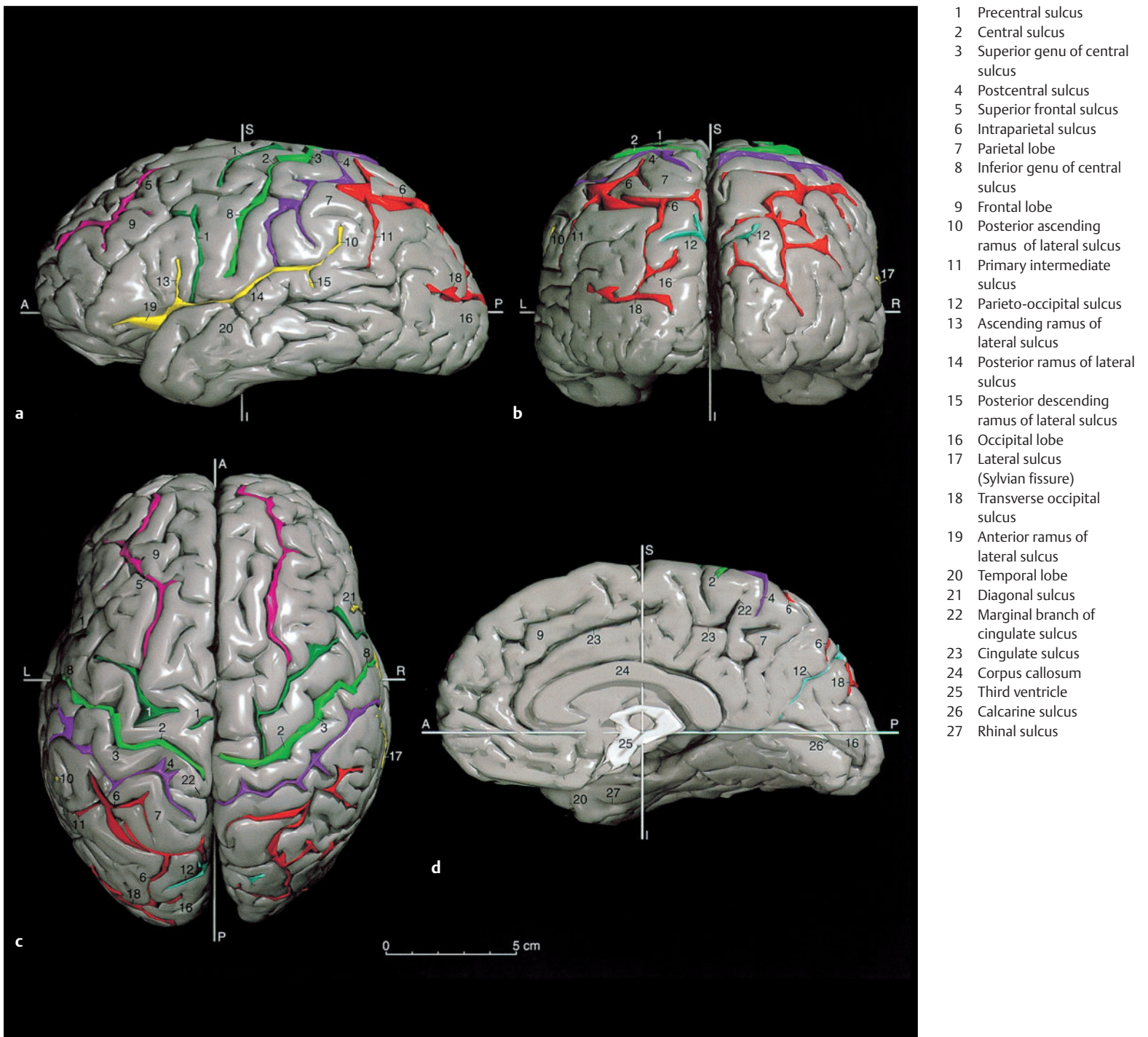


Fig. 7.51 Sulci of the brain. True-to-scale 3D model of cerebral sulci. (Reproduced from Kretschmann et al.³¹²)

A = anterior
 P = posterior
 R = right
 L = left
 S = superior
 I = inferior

Fig. 7.51a Lateral view of the left cerebral hemisphere.

Fig. 7.51b Posterior view.

Fig. 7.51c Superior view.

Fig. 7.51d Median view of the right cerebral hemisphere.

The inferior frontal gyrus is further divided by two branches of the lateral sulcus.

A somewhat skewed M-shaped cortical ribbon may often be identified in the region of the lateral sulcus on sagittal MR and CT images sectioned close to the surface of the inferior frontal gyrus (see ► Fig. 7.52b). The vertically ascending ramus of the lateral sulcus abuts the opercular and triangular parts of the inferior frontal gyrus. The V-form of the letter M is taken up by the triangular part. The anterior ramus of the lateral sulcus separates the triangular and orbital parts of the inferior

frontal gyrus.⁶⁴² Broca's area (motor language area) lies in the **frontal operculum** of the left hemisphere in more than 95% of all individuals. All three frontal gyri terminate at the precentral sulcus (see ► Fig. 3.1d, ► Fig. 4.1d, ► Fig. 4.6a, ► Fig. 4.6b, ► Fig. 4.7a, ► Fig. 4.7b, ► Fig. 5.11, ► Fig. 5.13, ► Fig. 5.26, and ► Fig. 5.29). Located between the precentral and central sulci is a motor region, the precentral gyrus (see ► Fig. 3.1d, ► Fig. 3.8a, ► Fig. 3.8b, ► Fig. 3.9a, ► Fig. 3.9b, ► Fig. 3.12a, ► Fig. 3.12b, ► Fig. 4.1d, ► Fig. 4.3a, ► Fig. 4.3b, ► Fig. 4.4a, ► Fig. 4.4b, ► Fig. 5.9a, ► Fig. 5.9b, ► Fig. 5.12, ► Fig. 5.14, and ► Fig. 5.28).

- Prefrontal sulcus
- precentral sulcus sign (upper T or L sign)
- Wide precentral gyrus sign
- Omega sign of the hand knob
- Bracket sign

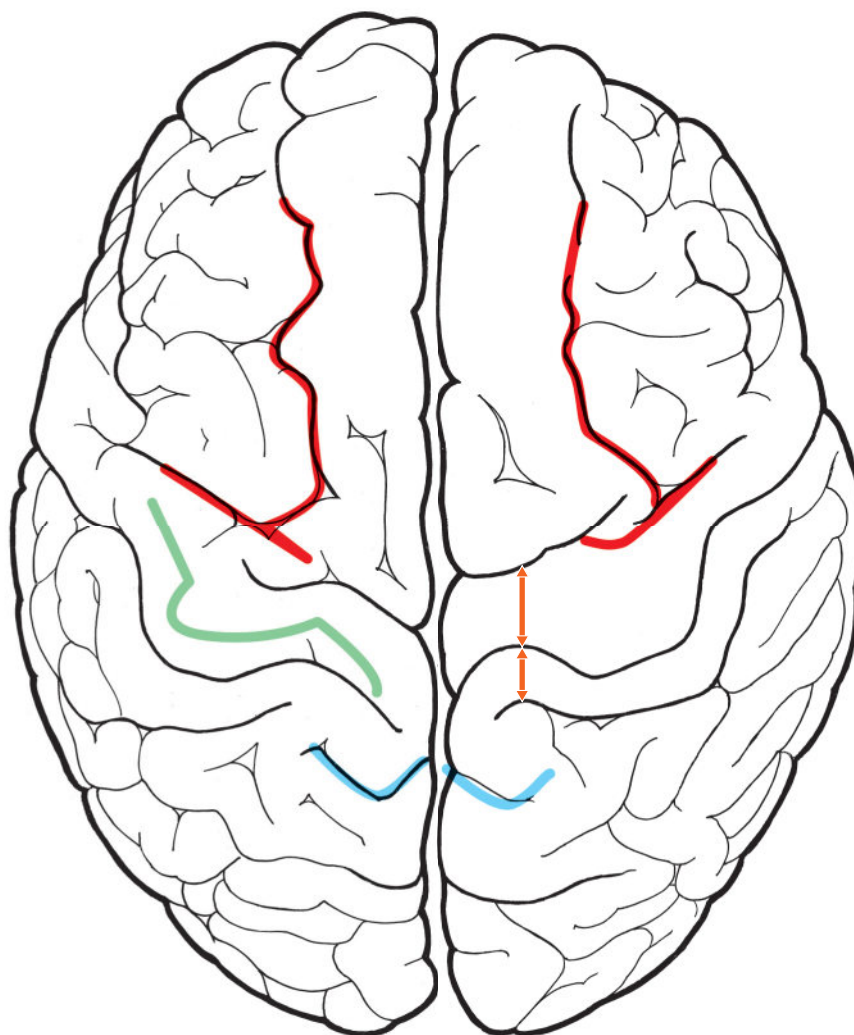


Fig. 7.52 Identification of the central sulcus using landmarks.

Fig. 7.52a Superior view of cerebral hemispheres.

On a lateral view of the cerebrum, the precentral gyrus is seen coursing obliquely from anteroinferior to posterosuperior toward the superior margin of the hemisphere.

It runs steeply to Reid's base line in cerebrums of the frontopetal type (see ►Fig. 5.1d) as compared to those of the occipital type (see ►Fig. 3.1d).^{179,336} On the coronal series, therefore, the precentral gyrus extends relatively far in an occipital direction at the superior margin of the hemisphere. The paracentral lobule, part of the motor region, is situated on the medial surface of each hemisphere and maybe considered to be part of the frontal lobe. The superior frontal gyrus lies also on the medial surface of each hemisphere (see ►Fig. 7.22b). Variable convolutions of the frontal lobe, the orbital gyri (see ►Fig. 3.3a, ►Fig. 3.3b, ►Fig. 3.4a, ►Fig. 3.4b, ►Fig. 5.1d, ►Fig. 5.7, and ►Fig. 7.26b), lie above the roof of orbit in the anterior cranial fossa. The straight gyrus abuts the olfactory sulcus at its lateral aspect (see ►Fig. 3.3a, ►Fig. 3.3b, ►Fig. 3.6a, ►Fig. 3.6b, ►Fig. 5.7, and ►Fig. 5.18).

Clinical Notes

On CT and, less frequently, MR images, this variable angle of inclination of the central sulcus to the median and bicommissural planes produces an irregular partial volume effect, resulting in indistinct depiction of the central sulcus, thereby making its identification difficult. The criteria for detection of the central sulcus are (see ►Fig. 7.51 and ►Fig. 7.52):

- Localization of the “knob” helps the localization of the central sulcus (see above).²⁹⁴
- Differences between cortical thickness and the entire width of the precentral and postcentral gyri indicate the position of the central sulcus. In regions where the central sulcus lies approximately vertical to the layers of the MR image, the cortex of the precentral gyrus is wider than that of the postcentral gyrus. A mean thickness of 2.7 mm was determined for the cortical thickness of the precentral gyrus and a mean value of 1.8 mm for the postcentral gyrus on the lateral walls of the central sulcus.^{231,642}

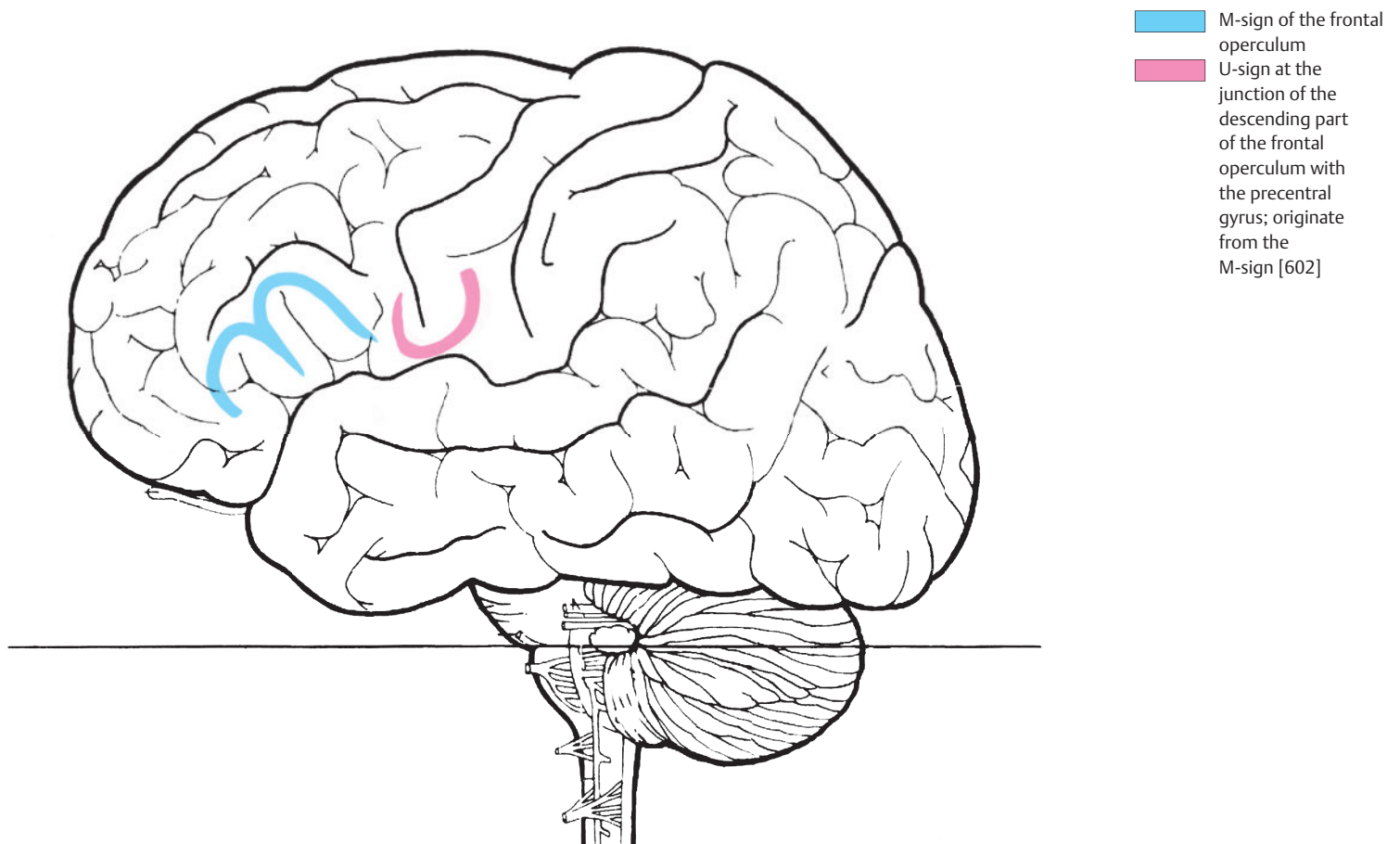


Fig. 7.52b Lateral view of left cerebral hemisphere.

- The superior frontal sulcus usually ends in the precentral sulcus, which runs immediately anterior to the central sulcus. This is best appreciated on axial sections.
- The bracket sign indicates the location of the central sulcus. Marginal branches of the two cingulate sulci appear to form an anteriorly open “bracket” toward the central sulcus close to the superior edge of the cerebrum, the ends of which point to the respective postcentral gyrus. The medial end of the central sulcus extends up to this “bracket region” in approximately 95% of cases, while the postcentral sulcus reaches it in about 3% of cases.^{231,642}

Parietal Lobe

The postcentral gyrus (see ►Fig. 3.1d, ►Fig. 3.9a, ►Fig. 3.9b, ►Fig. 3.11a, ►Fig. 3.11b, ►Fig. 4.1d, ►Fig. 4.3a, ►Fig. 4.3b, ►Fig. 4.4a, ►Fig. 4.4b, ►Fig. 4.7a, ►Fig. 4.7b, ►Fig. 5.10a, ►Fig. 5.10b, ►Fig. 5.13, ►Fig. 5.27, and

►Fig. 5.29) of the parietal lobe borders the central sulcus. A largely incomplete postcentral sulcus extends posteriorly from the postcentral gyrus and then separates the superior parietal lobule (see ►Fig. 3.1d, ►Fig. 3.13a, ►Fig. 3.13b, ►Fig. 4.1d, ►Fig. 5.13, ►Fig. 5.28, and ►Fig. 5.29). In addition, the supramarginal gyrus (see ►Fig. 3.1d, ►Fig. 3.10a, ►Fig. 3.10b, ►Fig. 3.11a, ►Fig. 3.11b, ►Fig. 4.1d, ►Fig. 4.6a, ►Fig. 4.6b, ►Fig. 4.7a, ►Fig. 4.7b, ►Fig. 5.1d, ►Fig. 5.11, and ►Fig. 5.12) and the angular gyrus (see ►Fig. 3.1 d, ►Fig. 3.13a, ►Fig. 3.13b, ►Fig. 3.14a, ►Fig. 3.14b, ►Fig. 4.1d, ►Fig. 4.5a, ►Fig. 4.5b, ►Fig. 4.6a, ►Fig. 4.6b, ►Fig. 5.1d, ►Fig. 5.11, and ►Fig. 7.26b) are considered parts of the parietal lobe. The supramarginal gyrus forms a concave turn around the posterior ramus of the lateral sulcus. The angular gyrus extends around the occipital end of the superior temporal sulcus. The **precuneus** on the medial surface of each hemisphere (see ►Fig. 3.1c, ►Fig. 3.13a, ►Fig. 3.13b, ►Fig. 3.15a, ►Fig. 3.15b, ►Fig. 4.3a, ►Fig. 4.3b, ►Fig. 5.1c, ►Fig. 5.11, ►Fig. 5.12, ►Fig. 5.14, and ►Fig. 7.22b) is also considered part of the parietal lobe.

Occipital Lobe

The **occipital gyri** are irregular convolutions on the lateral aspect of the occipital lobe (see ►Fig. 3.1d, ►Fig. 3.14a, ►Fig. 3.14b, ►Fig. 3.15a, ►Fig. 3.15b, ►Fig. 4.1d, ►Fig. 4.3a, ►Fig. 4.3b, ►Fig. 4.5a, ►Fig. 4.5b, ►Fig. 4.6a, ►Fig. 4.6b, ►Fig. 5.7, ►Fig. 5.9a, ►Fig. 5.9b, and ►Fig. 5.25).

The lateral occipitotemporal gyri (see ►Fig. 3.7a, ►Fig. 3.7b, ►Fig. 3.13a, ►Fig. 3.13b, ►Fig. 3.15a, ►Fig. 3.15b, ►Fig. 4.6a, ►Fig. 4.6b, ►Fig. 5.7, and ►Fig. 5.8b) as well as the medial occipitotemporal gyri (see ►Fig. 3.13a, ►Fig. 3.13b, ►Fig. 3.15a, ►Fig. 3.15b, ►Fig. 4.4, ►Fig. 4.5, and ►Fig. 5.8) lie on the inferior surface of the occipital lobe facing the tentorium of cerebellum. Half of these gyri belong to the occipital lobe and the other half to the temporal lobe. The **cuneus** lies on the medial aspect of the occipital lobe (see ►Fig. 3.1c, ►Fig. 3.14a, ►Fig. 3.14b, ►Fig. 3.15a, ►Fig. 3.15b, ►Fig. 5.1c, ►Fig. 5.11, and ►Fig. 5.12) between the parieto-occipital (see ►Fig. 4.3a and ►Fig. 4.3b) and calcarine sulci (see ►Fig. 4.3a and ►Fig. 4.3b). The areas on either side of the **calcarine sulcus** (see ►Fig. 3.1c, ►Fig. 3.13a, ►Fig. 3.13b, ►Fig. 3.15a, ►Fig. 3.15b, ►Fig. 3.15d, ►Fig. 4.2b, ►Fig. 4.3a, ►Fig. 4.3b, ►Fig. 5.1c, ►Fig. 6.3, and ►Fig. 10.18) belong to the primary visual cortex.

Temporal Lobe

The temporal lobe has three temporal gyri running obliquely to Reid's base line (see ►Fig. 5.7)

- **Superior temporal gyrus** (see ►Fig. 3.1d, ►Fig. 3.6a, ►Fig. 3.6b, ►Fig. 3.9a, ►Fig. 3.9b, ►Fig. 3.12a, ►Fig. 3.12b, ►Fig. 4.1c, ►Fig. 4.7a, ►Fig. 4.7b, ►Fig. 5.1d, ►Fig. 5.7, ►Fig. 5.9a, ►Fig. 5.9b, ►Fig. 5.22, and ►Fig. 5.23)
- **Middle temporal gyrus** (see ►Fig. 3.1d, ►Fig. 3.6a, ►Fig. 3.6b, ►Fig. 3.9a, ►Fig. 3.9b, ►Fig. 3.12a, ►Fig. 3.12b, ►Fig. 4.1c, ►Fig. 4.7a, ►Fig. 4.7b, ►Fig. 5.1d, ►Fig. 5.6a, ►Fig. 5.6b, ►Fig. 5.8, ►Fig. 5.22, and ►Fig. 5.24)
- **Inferior temporal gyrus** (see ►Fig. 3.1d, ►Fig. 3.7a, ►Fig. 3.7b, ►Fig. 3.12a, ►Fig. 3.12b, ►Fig. 4.6a, ►Fig. 4.6b, ►Fig. 4.7a, ►Fig. 4.7b, ►Fig. 5.5, and ►Fig. 5.7)

These temporal gyri are separated by superior and inferior temporal sulci. Lying within the depths of the lateral sulcus between the superior temporal gyrus and the inferior edge of the insula are the **transverse temporal gyri** (of Heschl). There are normally two transverse gyri on the right and only one on the left.^{183,184} They course from an anterolateral to posteromedial direction, running obliquely to the median plane, and are better seen on coronal (see ►Fig. 3.10a and ►Fig. 3.10b) and sagittal sections (see ►Fig. 4.6a, ►Fig. 4.6b, ►Fig. 4.7a, and ►Fig. 4.7b) than in sections oriented along the bicommissural plane (see ►Fig. 5.9). The transverse temporal gyrus forms a protrusion bulging superiorly in coronal MR images, while on sagittal MR images, this gyrus may be recognized by its omega (or mushroom) form (Ω).

The tomographic image may occasionally appear heart shaped. The transverse temporal gyrus typically courses obliquely from the median plane in an anterolateral direction on axial images.⁶⁴² The primary auditory cortex is largely located in the transverse temporal gyrus (of Heschl) or in the anterior transverse temporal gyrus when two transverse temporal gyri are present. Posteriorly the transverse temporal gyrus joins the planum temporale (see ►Fig. 4.7a and ►Fig. 4.7b), which is often larger on the left than on the right.^{182,184} This finding is thought to be related to the lateralization of language.¹⁸⁴

The lateral and medial occipitotemporal gyri about the inferior temporal gyrus on the inferior aspect of the temporal lobe. The **parahippocampal gyrus** (see ►Fig. 3.7, ►Fig. 3.8a, ►Fig. 3.8b, ►Fig. 3.10a, ►Fig. 3.10b, ►Fig. 4.4a, ►Fig. 4.4b, ►Fig. 5.6a, ►Fig. 5.6b, and ►Fig. 5.8) with its uncus (see ►Fig. 4.4a, ►Fig. 4.4b, and ►Fig. 5.7) lie further medially. These parts of the temporal lobe belong to the phylogenetically older divisions of the brain. The **hippocampus** lies deep in the temporal lobe and abuts the temporal horn of the lateral ventricle (see ►Fig. 3.8a, ►Fig. 3.8b, ►Fig. 3.9a, ►Fig. 3.9b, ►Fig. 3.9f, ►Fig. 3.11a, ►Fig. 3.11b, ►Fig. 4.5a, ►Fig. 4.5b, ►Fig. 4.5d, ►Fig. 5.8, ►Fig. 5.22, and ►Fig. 5.24)¹⁵¹ and, together with rudimentary cortical structures of the corpus callosum and a small gyrus anterior to the corpus callosum, it forms the inner boundary of the **limbic system** (see Section 10.11). The parahippocampal gyrus, part of the cingulate gyrus in the vicinity of the corpus callosum and the subcallosal area, forms the external gyral ring of the limbic system around the corpus callosum (see ►Fig. 3.1c, ►Fig. 3.4a, ►Fig. 3.4b, ►Fig. 3.7a, ►Fig. 3.7b, ►Fig. 3.11a, ►Fig. 3.11b, ►Fig. 4.3a, ►Fig. 4.3b, ►Fig. 5.1c, ►Fig. 5.8, ►Fig. 5.10a, ►Fig. 5.10b, ►Fig. 5.23, ►Fig. 5.26, and ►Fig. 10.39), which runs at the medial aspect of the cerebral hemisphere and blends in with the four lobes of the brain (see ►Fig. 7.46).

Insula

The insula lies within the depths of the lateral sulcus (see ►Fig. 3.6a, ►Fig. 3.6b, ►Fig. 3.8a, ►Fig. 3.8b, ►Fig. 4.6a, ►Fig. 4.6b, ►Fig. 5.8, ►Fig. 5.10a, ►Fig. 5.10b, ►Fig. 5.23, and ►Fig. 5.25) and is covered by the frontal, parietal, and temporal parts of the neocortex. The corresponding gyri are therefore referred to as the "frontal, parietal, and temporal opercula". Visceral areas are present within the insula.

Moving sequentially from inferior to superior in the bicommissural plane, the inferior surface of the temporal lobe is the first to be visualized (see ►Fig. 7.50, fourth section). The anterior cranial fossa with the lamina cribrosa containing the olfactory bulb and tract and basal parts of the frontal lobe have been sectioned 1 cm higher in the fifth slice. Larger sections of the frontal and temporal lobes are visualized in the sixth and seventh slices, with sections of the parietal lobe also being seen at the level of the body of the lateral ventricles. The temporal lobes are no longer seen in supraventricular sections, with the two uppermost sections containing only frontal and parietal lobes (see ►Fig. 7.50c).

Organization of the Cerebral Cortex

Based on phylogenetic and ontogenetic studies of the development of the telencephalon, the cerebral cortex may be divided into the following regions:

- **Paleocortex:** The paleocortex is a phylogenetically older part of the cerebral cortex, the olfactory cortex. Marked development of the neocortex resulted in its displacement to the mediobasal aspect of the temporal lobe. The paleocortex may be traced by following the lateral bundle of the olfactory tract (lateral olfactory stria) to the medial surface of the temporal lobe. The ambient and semilunar gyri present here are represented by two flat elevations roughly the size of a millet seed. These are covered by the prepiriform and periamygdaloid cortex, which belong to the paleocortex and to the olfactory system (see Section 10.7).
- **Archicortex:** The archicortex also consists of phylogenetically old cerebral cortex which was originally situated on the medial aspect of the hemisphere. The greater part of the archicortex, such as the dentate gyrus, hippocampus, and subiculum, was forced into the interior of the temporal lobe due to marked development of the neocortex.
- **Neocortex:** More than 90% of the human cerebral cortex is neocortex. During the process of phylogenesis it extended almost completely over the surface of the telencephalon and hence covered phylogenetically older neocortical areas such as the insula.

Based on cytoarchitectonic, myeloarchitectonic, glioarchitectonic, angioarchitectonic, chemoarchitectonic, and pigmentoarchitectonic examinations, the cerebral cortex may be divided into the following:

- **Isocortex:** This area of the cerebral cortex is organized principally similar in six layers of cells. The isocortex corresponds largely to the neocortex.⁵⁵⁶
- **Allocortex:** The allocortex consists mostly of three or four layers and includes the paleocortex and archicortex.
- **Mesocortex:** The mesocortex is transitional cortex which developed between the isocortex and the allocortex during the process of evolution. The structure of the mesocortex is intermediate between the typical six-layered isocortex and the three- or four-layered allocortex. The mesocortex is composed of the peripaleocortex and periarchicortex (together known as periallocortex) as well as the proisocortex. The peripaleocortex is very small in humans and surrounds the paleocortex. The periarchicortex surrounds the corpus callosum like an arc and consists of the paraterminal gyrus, part of the cingulate gyrus in the vicinity of the corpus callosum, fasciolar gyrus, and the entorhinal cortex. These regions belong to the limbic system (see Section 10.11). The proisocortex lies at the edge of the isocortex and developed during the process of evolution at the junction between the isocortex and periallocortex.

The **isocortex** may be differentiated into the following areas based on information obtained from morphologic, physiologic, and clinical studies:

- **Primary cortical areas:** The primary cortical areas have afferent and efferent topical connections with the periphery, characterized by point-to-point connections between the periphery and cortex or vice versa. The anterolateral, medial lemniscus, and trigeminal systems project into the postcentral gyrus (see Fig. 3.1d, ▶ Fig. 3.9a, ▶ Fig. 3.9b, ▶ Fig. 3.11, ▶ Fig. 4.1d, ▶ Fig. 4.3a, ▶ Fig. 4.3b, ▶ Fig. 4.3d, ▶ Fig. 4.4, ▶ Fig. 4.7, ▶ Fig. 5.11, ▶ Fig. 5.14, ▶ Fig. 5.27, and ▶ Fig. 5.29) in Brodmann's fields 3, 1, and 2 (see ▶ Fig. 7.53). These cytoarchitectonic fields form three stripes in the postcentral gyrus arranged in the 3, 1, 2 sequence. Their somatotopic organization has been described with the sensory systems (see Section 10.1). The primary cortical area of the gustatory system (see Section 10.2) lies in the parietal operculum and in an area at the edge of the insula. Connections between the vestibular system and parietal cortical areas are present around the intraparietal sulcus. The primary cortical area of the auditory system is about 2 cm in diameter. This lies deep within the lateral sulcus in the anterior transverse temporal gyrus (of Heschl) in the temporal lobe (see ▶ Fig. 3.10a, ▶ Fig. 3.10b, ▶ Fig. 4.6a, ▶ Fig. 4.6b, ▶ Fig. 4.7a, and ▶ Fig. 4.7b), corresponding cytoarchitectonically to Brodmann's area 41. The primary visual cortical areas of both hemispheres measure 12 ml in volume and may be identified macroscopically by the bundle of Vicq d'Azyr (stria of Gennari, ▶ Fig. 5.10c) located in the upper and lower lips of the calcarine sulcus (see ▶ Fig. 4.2d, ▶ Fig. 4.3a, ▶ Fig. 4.3b, ▶ Fig. 10.18, ▶ Fig. 10.19d, and ▶ Fig. 10.20a) in the occipital lobe. This area striata exhibits strictly a topical relationship with individual retinal regions, which has been explained in detail with the visual system (see Section 10.6). The primary efferent motor cortex lies for the most part in the precentral gyrus of the frontal lobe (see ▶ Fig. 3.1d, ▶ Fig. 3.8a, ▶ Fig. 3.8b, ▶ Fig. 3.12a, ▶ Fig. 3.12b, ▶ Fig. 4.1d, ▶ Fig. 4.3a, ▶ Fig. 4.3b, ▶ Fig. 4.3d, ▶ Fig. 4.4a, ▶ Fig. 4.4b, ▶ Fig. 5.9a, ▶ Fig. 5.9b, ▶ Fig. 5.12, ▶ Fig. 5.26, and ▶ Fig. 5.29) and its immediate surroundings, corresponding cytoarchitectonically to Brodmann's areas 4 and 6 (see ▶ Fig. 7.53b). Motor neurons also lie in Brodmann's somatosensory areas 3, 1, 2, and their neighboring parietal areas.^{135,342} The somatotopic pattern of the motor cortex has been described with the pyramidal system (see Section 10.8.1).
- **Secondary cortical areas:** These areas developed in a mosaic pattern especially in primates during evolution of the neocortex and are not topically connected by neurons either to the periphery or to the sense organs, but have primarily gnostic functions as "association" fields. Included among the secondary cortical

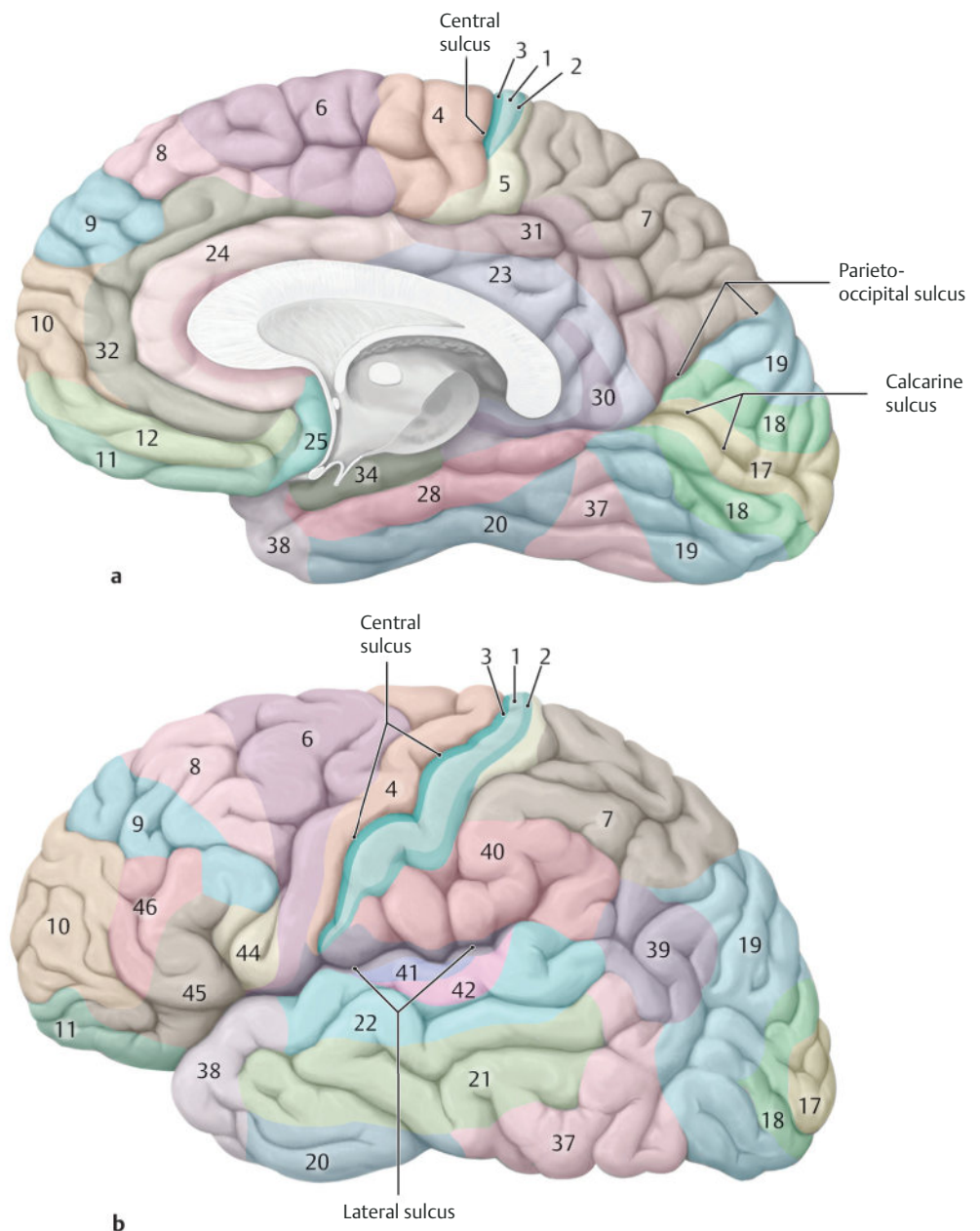


Fig. 7.53 Brodmann's areas in the neocortex. (Reproduced from Schuenke, Schulte, and Schumacher, *Atlas of Anatomy*, 2nd edition, ©2009, Thieme Publishers, Stuttgart. Illustration by Karl Wesker/Markus Voll.⁵³⁵)

Area 1/2/3 = primary somatosensory cortex

Area 4 = primary somatomotor cortex

Area 17 = visual cortex

Area 41/42 = primary auditory cortex

Fig. 7.53a Median sagittal section with a view of the right cerebral hemisphere.

Fig. 7.53b Lateral view of the left cerebral hemisphere.

areas are the following speech regions (see Section 10.10): motor speech region in the frontal operculum and the sensory speech region between the primary auditory cortex and the angular cortex.

- Supplementary fields: These supplementary areas lie at the boundary between the primary cortex and phylogenetically older regions of the brain:
 - The supplementary sensory area lies between the primary sensory cortex and insula on the lateral aspect of the hemisphere.⁵⁰⁷

- The supplementary auditory area is also located on the lateral aspect of the hemisphere, between the primary auditory cortex and insula.
- The supplementary visual area lies on the medial surface of the hemisphere between the area striata and periauricular cortex.⁵⁰⁷
- The supplementary motor area is a part of Brodmann's area 6 and lies on the medial surface of each hemisphere.^{69,454}

The topical relationship of the supplementary areas with the periphery is less well developed than that of primary areas but a supplementary area may nonetheless partially compensate the loss of function of the corresponding primary area.

White Matter

White matter lies beneath the cerebral cortex and is composed of several fiber tracts, which connect cortical areas with each other or with other regions of the central nervous system (see ►Fig. 7.54 and ►Fig. 7.55):

- Association fibers
- Commissural fibers
- Projection fibers

Association fibers interconnect cortical areas of a cerebral hemisphere with each other via short or long tracts. The short arcuate fibers follow an arc-like course between adjacent gyri and lie directly beneath the cerebral cortex. Long association fibers interconnect gyri of the individual cerebral lobes with each other. The cingulum (see ►Fig. 5.11, ►Fig. 7.54, ►Fig. 7.55, and ►Fig. 10.39) is a fiber bundle located in the white matter of the cingulate gyrus. Arching around the corpus callosum from the frontal to the temporal lobes, it is a part of the Papez circuit.

Commissural fibers interconnect corresponding cortical areas of the two hemispheres. The **anterior commissure** is visualized within the seventh section of the bicommissural series on the median view of the brain (see ►Fig. 5.1c). It connects the paleocortex (olfactory cortex) of each hemisphere with each other (see Section 10.7). In addition, the anterior commissure contains fibers which connect small neocortical areas of both frontal and temporal lobes with each other. The **corpus callosum** is a large transverse fiber tract connecting both sides of the neocortex. Parts of the corpus callosum as identified from frontal to occipital in the median view of the brain are the genu, body, and splenium (see Fig. 4.2a, ►Fig. 4.2b, and ►Fig. 5.1c). The genu of the corpus callosum (see ►Fig. 5.9a, ►Fig. 5.9b, ►Fig. 5.10a, and ►Fig. 5.10b), a part of the trunk (see ►Fig. 5.1c and ►Fig. 5.11), and the splenium see ►Fig. 5.10a and ►Fig. 5.10b) have been sectioned in slices parallel to the bicommissural plane. Two pincer-shaped fiber tracts emerge from the corpus callosum; the minor (frontal) forceps (see Fig. 5.10 and ►Fig. 7.55a) passes into the frontal lobes while the major (occipital) forceps (see ►Fig. 5.10 and ►Fig. 7.55a) extends into the occipital and temporal lobes.

The **posterior commissure** (see ►Fig. 3.1c, ►Fig. 3.10a, ►Fig. 3.10b, ►Fig. 4.2a, ►Fig. 4.2b, ►Fig. 5.1c, and ►Fig. 6.3) connects nuclear areas in

the tegmentum of the midbrain and is not a fiber tract of the telencephalon. Projection fiber tracts provide afferent and efferent connections between the cerebral cortex and deeper centers of the brain or spinal cord.

Projection fibers of the telencephalon include the terminal fibers of the sensory (see Section 10.1), gustatory (see Section 10.2), vestibular (see Section 10.4), auditory (see Section 10.5), visual (see Section 10.6), and olfactory (see Section 10.7) systems. They also include the initial parts of pyramidal (see Section 10.8.1) and oculomotor pathways (see Section 10.8.3). The limbic system (see Section 10.11) forms synaptic contacts predominantly with the diencephalon via projection fibers. During the process of evolution, **projection fibers of the neocortex** were bundled into fan-shaped fibers, called the corona radiata (see ►Fig. 7.54).

These projection fibers form the internal capsule which appears as two limbs forming a medially directed obtuse angle in the region of the diencephalon–telencephalon in sections parallel to bicommissural planes. At its lateral aspect, the **internal capsule** abuts the lentiform nucleus, composed of the globus pallidus and putamen. The anterior limb of the internal capsule lies between the head of the caudate nucleus and the lentiform nucleus, while the genu lies at the level of the interventricular foramen and the posterior limb between the thalamus and the lentiform nucleus (see ►Fig. 5.9, ►Fig. 5.23, ►Fig. 5.24, and ►Fig. 7.54). Efferent projection fibers run in the posterior limb of the internal capsule.

The acoustic and visual radiations run from the metathalamus behind the internal capsule to the auditory (see Section 10.5) and visual cortex (see Section 10.6). The projection fibers from the thalamus branch off in fan-shaped bundles and run in the anterior and posterior limbs. A small number of projection fibers form the **external capsule** (see ►Fig. 3.7a, ►Fig. 3.7b, ►Fig. 5.9, and ►Fig. 5.22), lying between the putamen and claustrum. Capsular fibers converge in the cerebral crus of the midbrain (see ►Fig. 5.7, ►Fig. 5.22, ►Fig. 6.12a, ►Fig. 6.13b, and ►Fig. 6.13c).

Projection fibers of the allocortex run from the hippocampal formation via the fimbria of the hippocampus and the fornix primarily to the hypothalamus (see ►Fig. 3.8, ►Fig. 3.9a, ►Fig. 3.9b, ►Fig. 3.9d, ►Fig. 3.10, ►Fig. 3.11a, ►Fig. 3.11b, ►Fig. 4.2a, ►Fig. 4.2b, ►Fig. 4.4a, ►Fig. 4.4b, ►Fig. 5.10a, ►Fig. 5.10b, ►Fig. 5.23, ►Fig. 5.25, ►Fig. 6.13b, and ►Fig. 10.39).

The term **centrum semiovale** refers to the white matter of the telencephalon above the corpus callosum (see ►Fig. 5.11, ►Fig. 5.12, ►Fig. 5.27, and ►Fig. 5.28). It exhibits a semioval shape in each hemisphere on axial sections and is composed of association, commissural, and projection fibers.

- 1 Corona radiata
- 2 Optic radiation
- 3 Internal capsule
- 4 Cerebral peduncle
- 5 Corpus callosum

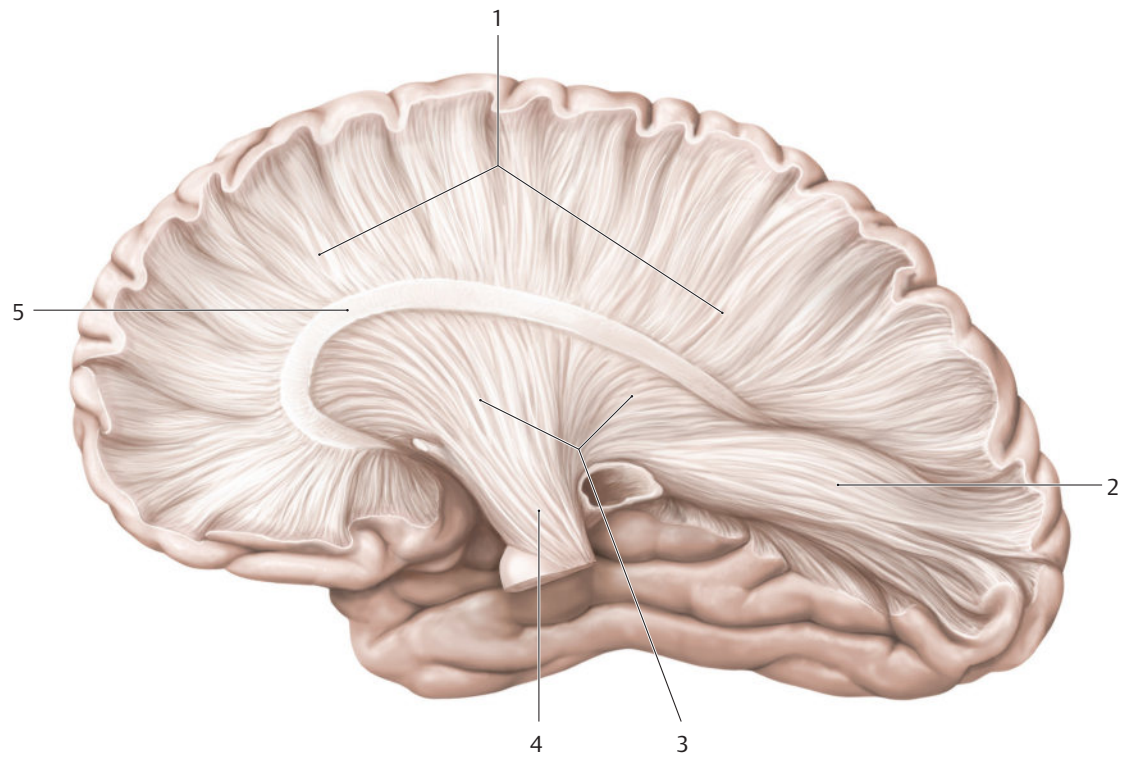


Fig. 7.54 White matter fiber tracts. Projections, commissural, and association tracts. (► Fig. 7.54a–c: Reproduced from Schuenke, Schulte, and Schumacher, *Atlas of Anatomy*, 2nd edition, ©2009, Thieme Publishers, Stuttgart. Illustration by Karl Wesker/Markus Voll⁵³⁵ and Larsell.³⁴⁰)

Fig. 7.54a Defibered specimen of the brain with depiction of projection fibers.

- 6 Arcuate fibers (U-fibers)
- 7 Superior longitudinal fasciculus
- 8 Fronto-temporal fasciculus

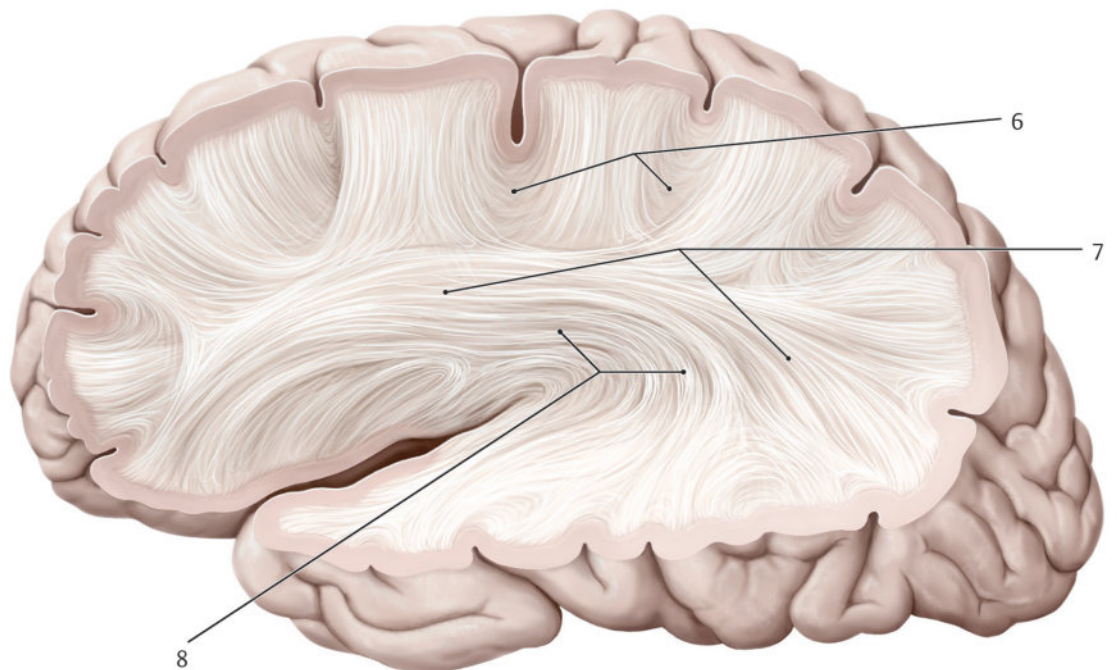
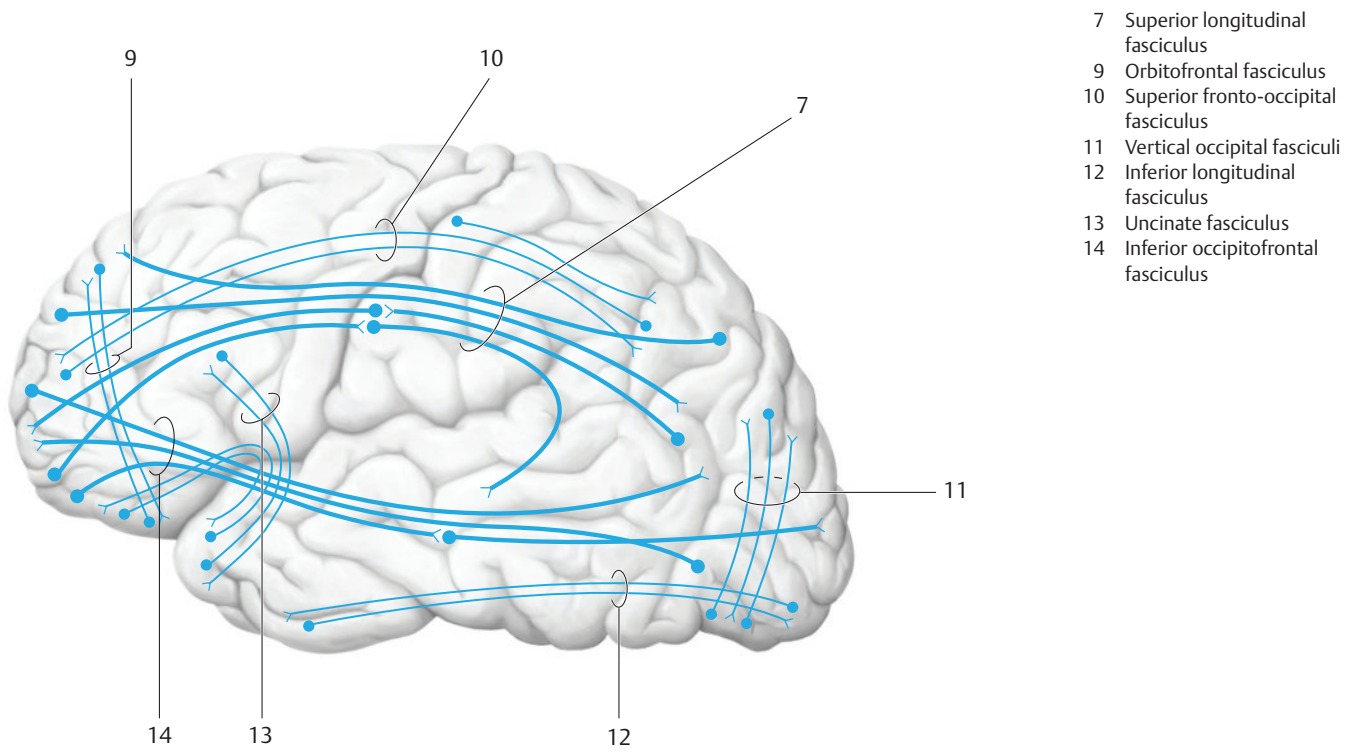
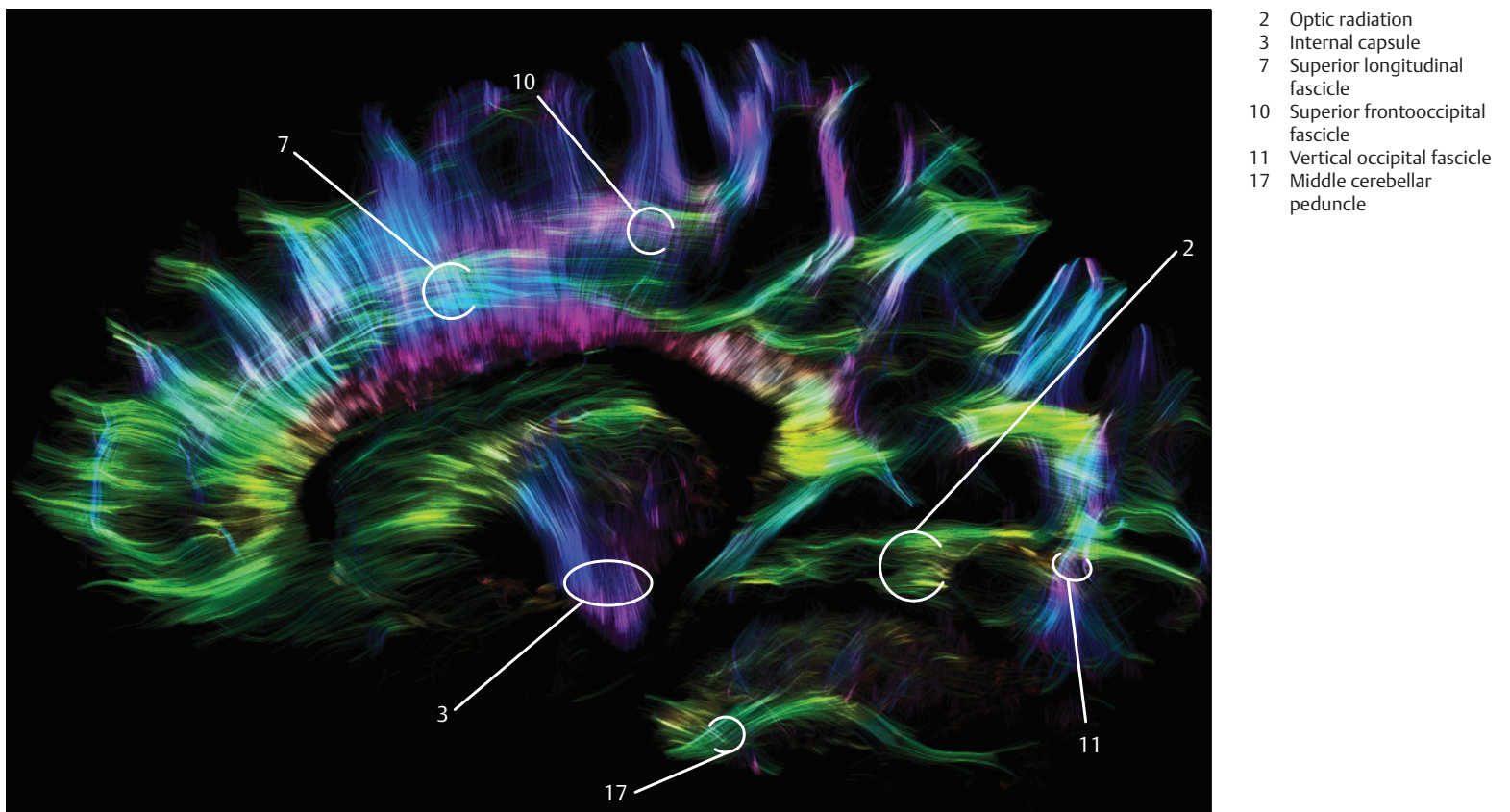


Fig. 7.54b Defibered specimen of the brain with depiction of association fibers.



c

Fig. 7.54c Association fibers.**Fig. 7.54d 3D MR-tractography.** Color-coded representation of white matter tracts based on a 7T-DTI examination. Sagittal paramedian view. See ► Chapter 12 for technical details. (With kind permission of Dr. A. Anwender, MPI for Human Cognitive and Brain Sciences, Leipzig, Germany.)

- 3 Internal capsule (projection fibers)
- 5 Corpus callosum
- 7 Superior longitudinal fasciculus
- 10 Superior fronto-occipital fasciculus
- 12 Inferior longitudinal fasciculus
- 13 Uncinate fasciculus
- 14 Cingulum
- 15 Anterior commissure
- 16 Inferior occipitofrontal fasciculus

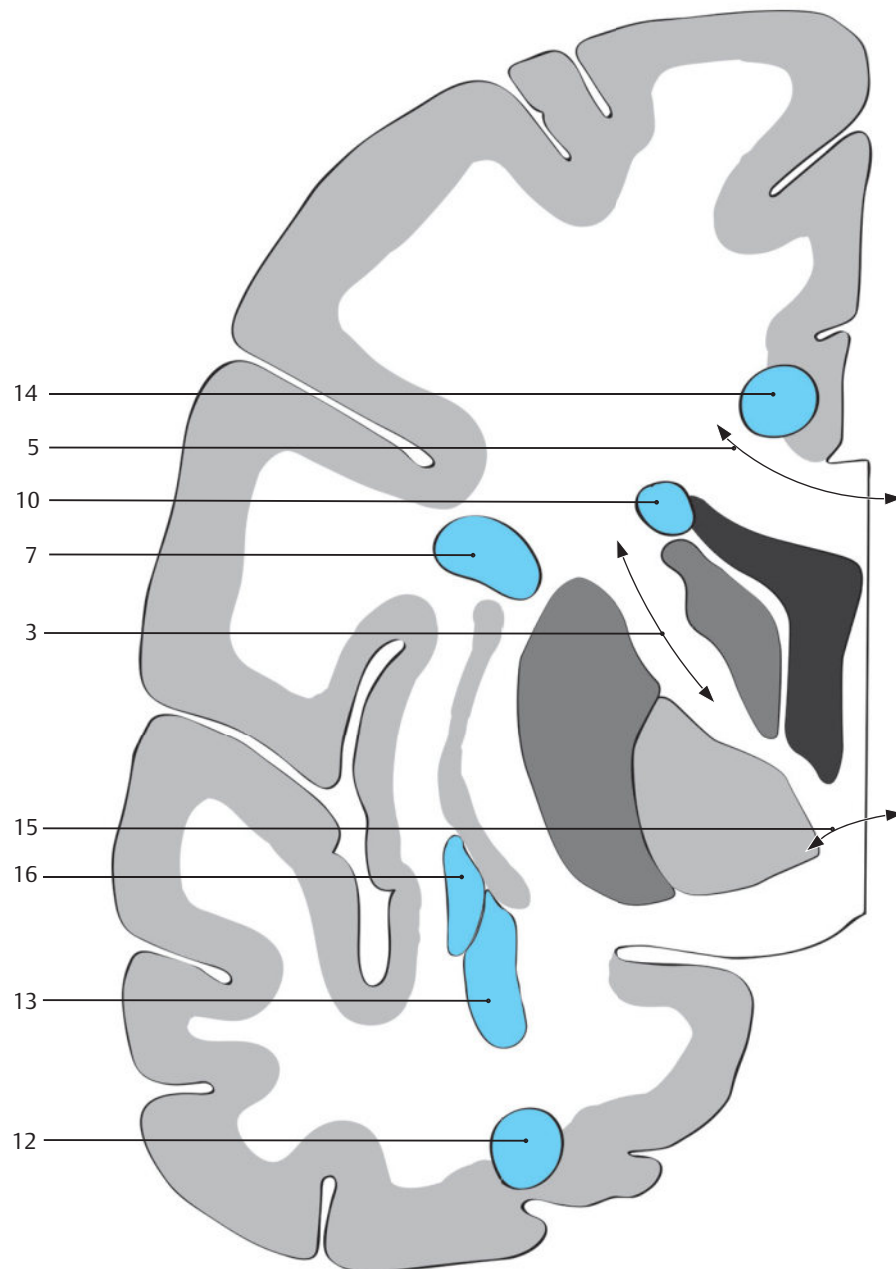


Fig. 7.54e Commissural and association tracts in a coronal section through the telencephalon. (Reproduced from Larsell.³⁴⁰)

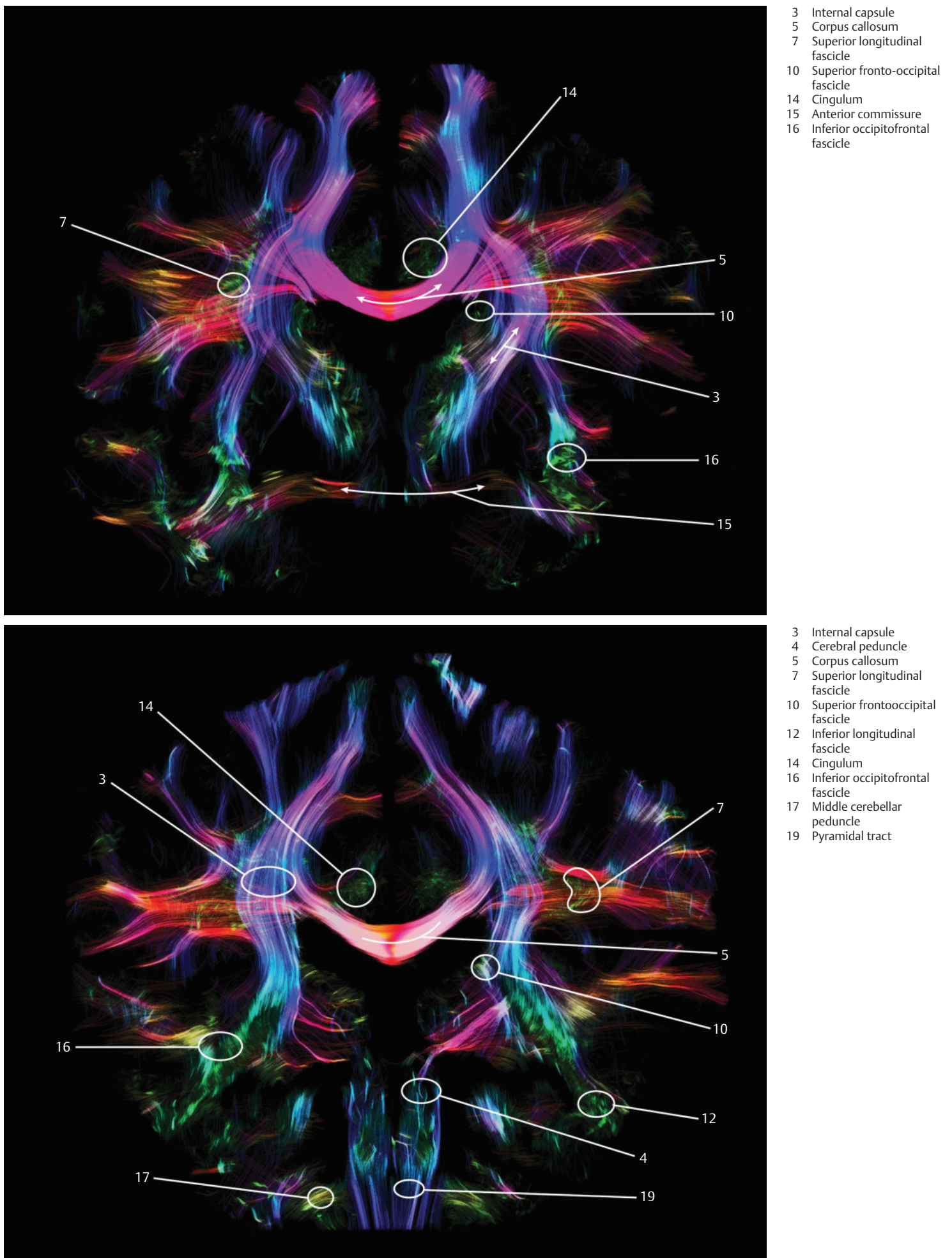


Fig. 7.54f and g 3D MR-tractography. Color-coded representation of white matter tracts based on a 7T-DTI examination. Two coronal views at the level of the anterior commissure and at the level of the pons, respectively. See ► Chapter 12 for technical details. (With kind permission of Dr. A. Anwander, MPI for Human Cognitive and Brain Sciences, Leipzig, Germany.)

- 1 Cingulum
- 2 Corpus callosum, minor forceps
- 3 Caudate nucleus, head
- 4 Corticospinal tract
- 5 Corpus callosum
- 6 Superior occipitofrontal fasciculus
- 7 Corona radiata
- 8 Corpus callosum, major forceps
- 9 External capsule
- 10 Internal capsule
- 11 Fornix
- 12 Optic radiation
- 13 Anterior commissure
- 14 Subcallosal area
- 15 Posterior commissure
- 16 Uncinate fasciculus
- 17 Optic tract
- 18 Dentatothalamic tract
- 19 Medial lemniscus
- 20 Spinothalamic tract
- 21 Optic nerve
- 22 Transverse pontine fibers
- 23 Superior cerebellar peduncle
- 24 Middle cerebellar peduncle
- 25 Inferior cerebellar peduncle
- 26 Cerebellorubral tract

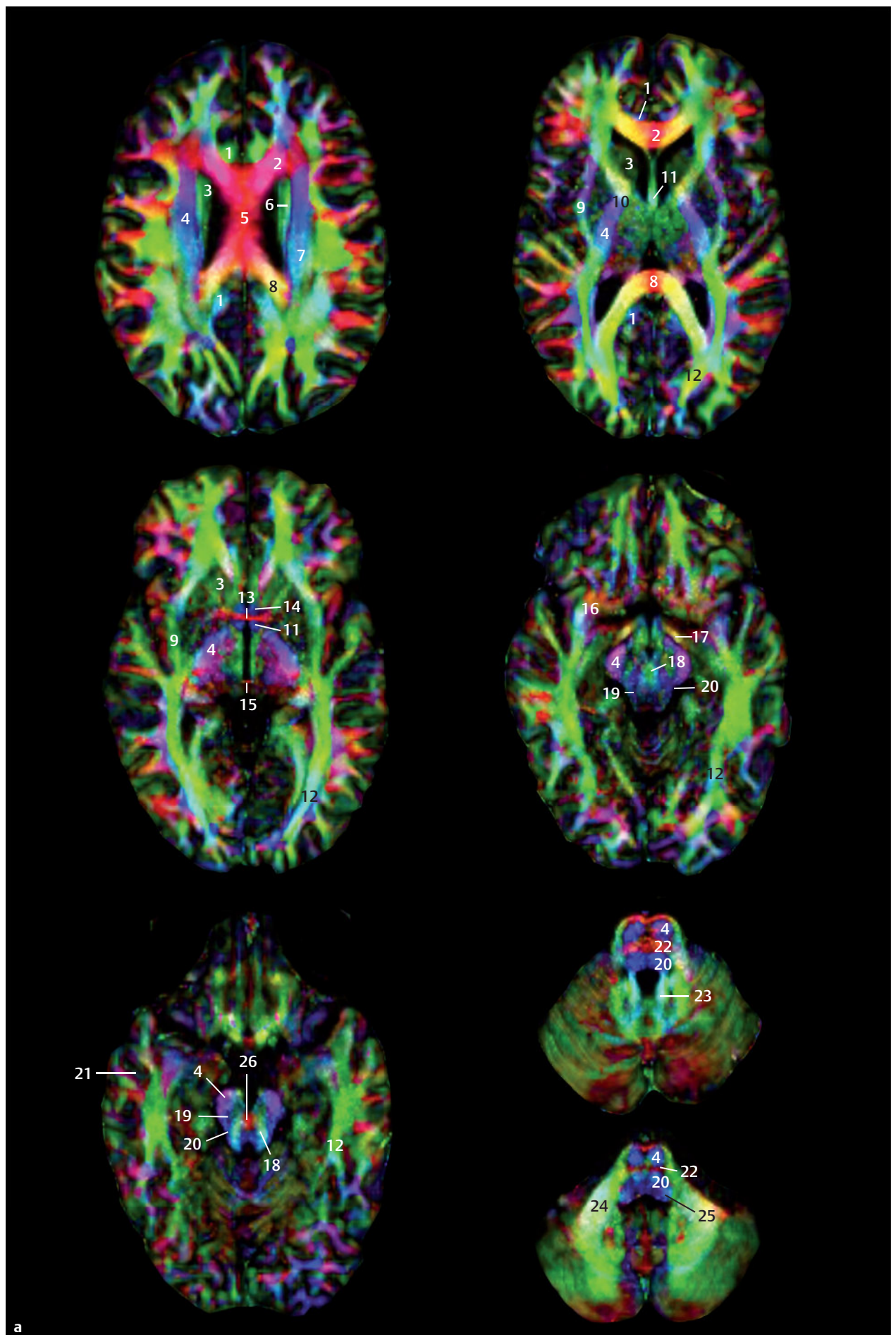


Fig. 7.55 White matter fiber tracts. Depiction of white matter fiber tracts by means of MR diffusion tensor imaging; for measurement parameters see Chapter 12. The primary direction of diffusion in tissue relative to the z axis of the MR equipment is calculated and color coded for each image pixel.

red = right/left

green = anterior/posterior

blue = cranial/caudal

Fig. 7.55a Sections oriented in the bicommissural plane.

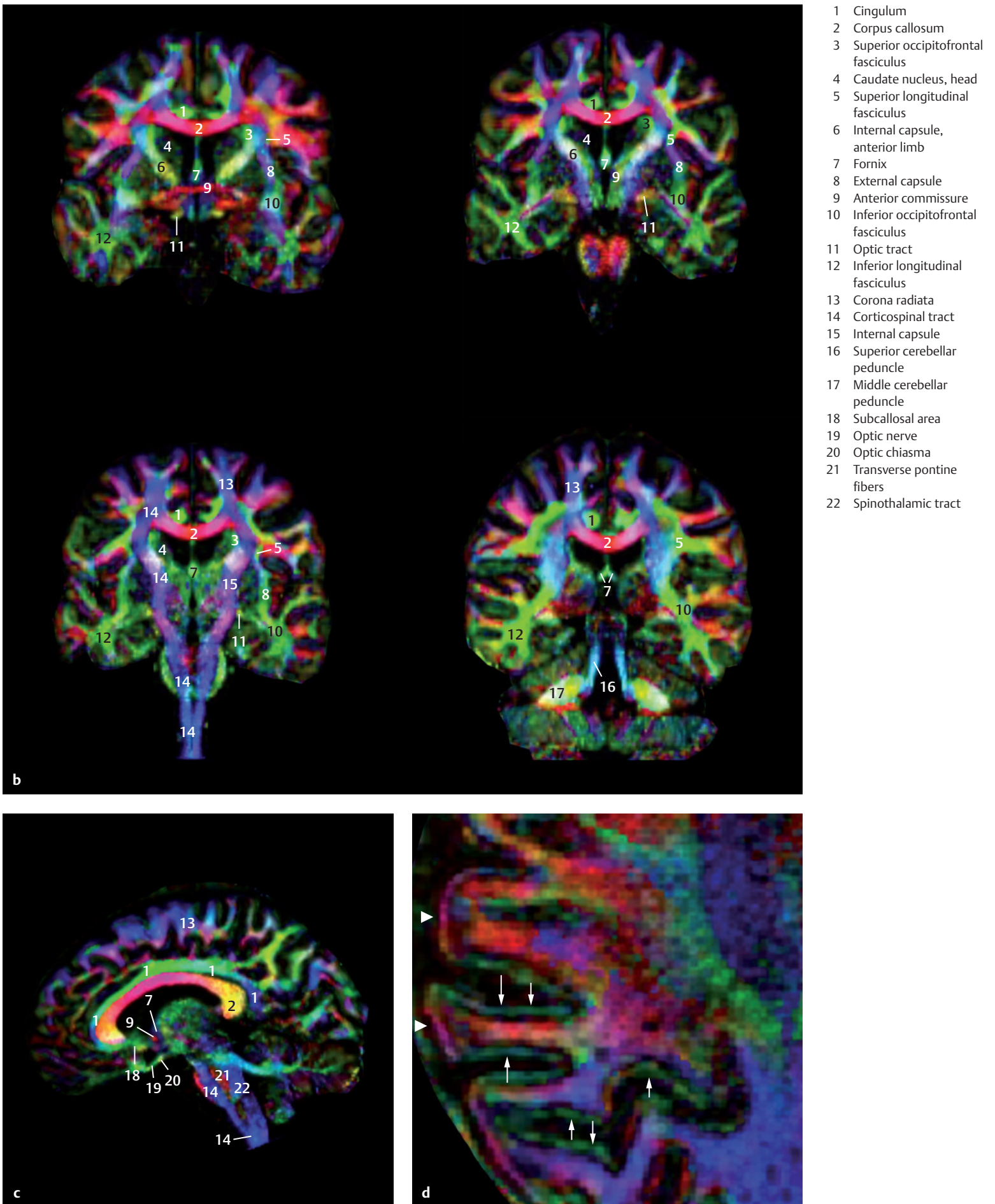


Fig. 7.55b Sections oriented in the coronal plane.

Fig. 7.55c Section oriented in the sagittal plane.

Fig. 7.55d Section obtained from the computation of a high-resolution measurement with a 1.0 mm isotropic matrix followed by 0.5 mm isotropic interpolation. Section obtained from the right parietal cortex depicts the columnar organization of the cortex based on change in color of the gyrus in its course through the cortex (*green* at the anterior and posterior edges [*arrows*], *red* at the lateral edge [*arrowheads*]).

Clinical Significance

Depending on their proximity to neurofunctional systems in various lobes, telencephalic lesions result in characteristic clinical symptoms, frequently enabling a topical clinical diagnosis to be made.

Clinical Notes

Lesions in the motor cortex of the frontal lobe may result in Jacksonian seizures which may initially present with focal motor symptoms. An acute lesion of the posterior part of the frontal lobe gives rise to a contralateral flaccid hemiplegia with a positive Babinski sign without spasticity. Only later may the reflexes be accentuated. Fine motor movements of the distal extremities remain permanently impaired. Lesions of the premotor cortex lead to a slowing of movements. Widespread injuries result in apraxia. Defects in the frontal operculum of the language-dominant hemisphere lead to dysarthria and motor aphasia. Injuries involving the base of the middle frontal gyrus may result in a gaze toward the side of the lesion. Extensive lesions of the frontal lobe cause an organic psychosyndrome with lack of initiative, psychomotoric inhibition and emotional impairment. A dysbasia is frequently present. The topographic relationship of the frontal lobe to the olfactory bulb and tract explains the development of anosmia with pathological changes in the anterior cranial fossa.

Lesions in the postcentral gyrus of the parietal lobe result in contralateral diminution of peripheral sensitivity and spatial orientation, while perception of vibration and pain are little affected. Lesions of the parietal lobe may trigger a sensory Jacksonian seizure. Characteristic symptoms of a parietal lobe syndrome are altered spatial and body orientation usually affecting the contralateral half of the body; this may rarely occur bilaterally. In such cases, patients often forget activities such as wearing a sock on the contralateral foot. Extensive lesions may cause severe apraxia and disordered position sense; adolescents may develop muscle atrophy and hemiatrophy. An injury of the lower part of the parietal cortex in the speech-dominant hemisphere causes amnesic or even sensory aphasia.

Lesions of the occipital lobe involving the optic radiation and/or the visual cortex are characterized by disturbances of contralateral visual fields. Lesions involving the optic tract may cause photopsia. Visual hallucinations arise with transient ischemia of the occipital pole and are frequently occurring together with migraine.⁴⁴⁹ Complete bilateral loss of the area striata leads to cortical blindness.

Pathological changes in the temporal lobe can cause a wide variety of symptoms. Bilateral lesions of the transverse temporal gyri (of Heschl) cause cortical deafness, while unilateral lesions may go clinically unnoticed. Lesions in the region of the superior temporal gyrus of the dominant hemisphere lead to Wernicke's aphasia. Bilateral lesions of the hippocampal formation result in

impaired memory and learning or even lead to a severe amnesic syndrome. Injuries of the posterior region of the temporal lobe may be associated with homonymous hemianopia or superior quadrantanopia. Pathological processes or scarring are frequently resulting in epileptic attacks (psychomotor epilepsy).

The commissural fibers of the corpus callosum transmit information from one hemisphere to the other. Interruption of the corpus callosum leads to a so-called interhemispheric disconnection effect. Lesions of the anterior corpus callosum produce a unilateral ataxia. Furthermore, tumors in this region may cause the patient to become apathetic with marked loss of drive resulting in mutism. Interruption of the posterior corpus callosum causes impairment of the patient's verbalization of knowledge acquired through the nonspeech dominant hemisphere.

7.8 Brain Maturation

Eva Bültmann

Knowledge of brain development and its classification into development stages are of decisive importance in the assessment of the pediatric brain. The surface of the neonatal brain is well developed at term with its sulci and gyri, but the maturation of white matter, so-called myelination, is by no means complete. Rather, this begins in the fifth month of pregnancy with the myelination of cranial nerves³⁰ and progresses relatively slowly, such that only a few areas of the brain are myelinated at birth. Myelination progresses in a continuous and fixed pattern from caudal to cranial and from posterior to anterior³⁰ in the postpartum period. In addition, posterior parts of each region of the brain are myelinated first and the process of myelination proceeds more rapidly in functional systems, which are used early in life, as compared to those that are deployed later.³⁰ Myelination proceeds rapidly within the first two years of life, after which it slows down significantly.²¹¹

MRI is an excellent imaging tool for the assessment of the surface of the brain. It enables a detailed depiction of white matter maturation with increasing myelination.^{30,31,296}

Signal alterations associated with rapid myelination during the first two years of life have been frequently depicted on conventional T1- and T2-weighted MR images^{30,31,224,296,558} should be largely completed at the age of 2 years. With further development of MR technology and the introduction of new sequences and deployment of higher field strengths, it is now possible to examine the process of myelination even more closely. For instance, an analysis of relaxation times reveals that T1 shortening of white and gray matter continues into adolescence, possibly due to increasing myelination and consecutive decrease of water content.⁵⁵⁸ The myelination of fibers between association regions

of the brain occasionally continues up to the third and fourth decades of life.³⁰ Conventional MRI imaging continues to be the most important modality for the delineation of myelination, since classification into a stage of myelination is of great significance in particular at age up to 24 months. The main steps of maturation have been depicted below using conventional T1- and T2-weighted images.^{30,211,224} Prerequisite for this is a term birth after 40 weeks of gestation.

In general, changes in the myelination during the first 6 to 8 months of life are best seen on T1-weighted images, while T2-weighted images are more sensitive to depict the progress of myelination at the age of 6 to 24 months.

At **term birth**, only a few parts of the brain are myelinated with white matter being T1 hypointense as compared to the gray matter (see ► Fig. 7.56). The image thus resembles a T2-weighted image of the adult brain. Only posterior ascending brainstem structures exhibit a hyperintense T1-weighted signal at birth, morphologically signifying myelination. Lateral parts of the thalamus, posterior parts of the posterior limb of the internal capsule, and the central part of the corona radiata, as also pre- and postcentral gyri are supratentorial structures which are T1-weighted hyperintense at birth. On T2-weighted images, posterior brainstem structures and the cerebellar vermis are hypointense at birth, while in the supratentorial region, anterolateral parts of the thalamus, a small segment of the posterior limb of the internal capsule and the lateral margin of the putamen exhibit a hypointense signal. The cortical band of the pre- and postcentral gyri is also mildly hypointense as compared to the rest of the cortex.

As myelination progresses, the T1-weighted signal of deep and later subcortical white cerebellar matter increases such that the appearance of the cerebellum at age **3 months** is similar to that of the adult (see ► Fig. 7.57). The anterior brainstem, on the other hand, is still minimally hypointense as compared to the posterior brainstem indicating incomplete myelination in this anterior region. In the supratentorial region, the posterior limb of the internal capsule exhibits a clearly hyperintense T1-weighted signal, the anterior limb, as well as the deep, occipital white matter display a faint increase in signal. In the perirolandic corona radiata, the maturation process of the white matter slightly progresses from posterior to anterior. White matter is otherwise largely unmyelinated and thus T1-weighted hypointense. On T2-weighted images, signs of myelination in these regions are still much more discrete at this point; the anterior limb of the internal capsule and the deep occipital white matter still show no reduction in T2-weighted signal.

At age 6 months, infratentorial structures are myelinated on T1-weighted images; the pattern does not differ from that of an adult brain (see ► Fig. 7.58). In the supratentorial region, the internal capsule is completely hyperintense, as is the genu and splenium of the corpus callosum. As part of the ongoing myelination process, the

T1-weighted signal has also risen, particularly that of the deep white matter, especially in the parietal and occipital regions, while it is still hypointense in the frontal and temporal subcortical regions. On T2-weighted images, the brainstem is homogeneously hypointense, and the middle cerebellar peduncle is now heavily myelinated. In the supratentorial region, myelination of the internal capsule and of the corpus callosum have progressed from posterior to anterior, such that the posterior limb and the splenium are distinctly hypointense, while the anterior limb and the genu are less hypointense. White matter of the perirolandic corona radiata shows a lowering of signal, while the rest of the supratentorial white matter is still unmyelinated and hyperintense.

At age of **9 months** the supratentorial pattern on T1-weighted images approximates that of an adult (see ► Fig. 7.59), barring subcortical temporal white matter which is still unmyelinated and thus T1-weighted hypointense. In comparison to the parieto-occipital white matter, myelination is still incomplete in the frontal, subcortical white matter; thus it appears less hypointense.

On T2-weighted images, signs of myelination in the cerebellar hemispheres are also advanced with a decrease in signal of cerebellar white matter. In the supratentorial region, the anterior limb of the internal capsule and the genu are now also markedly hypointense. Myelination of the deep white matter has increased markedly, especially in the paracentral and occipital regions. The subcortical white matter, on the other hand, is still largely immature and hyperintense on T2-weighted images.

T1-weighted images almost approximate those of the adult brain at age **12 months** (see ► Fig. 7.60).

Temporal white matter remains incompletely myelinated however, and is also incomplete in subcortical areas of the supratentorial region. Myelination of cerebellar white matter has further increased on T2-weighted images. In the supratentorial region, temporal white matter remains unmyelinated and T2-weighted hyperintense; a distinct signal reduction especially of the deep white matter is otherwise noted, progressing from the parieto-occipital to frontal regions.

At age of **18 months**, the T1-weighted image shows a mature pattern that corresponds to that of the adult (see ► Fig. 7.61).

On T2-weighted images, myelination is complete in the infratentorial region and is also far advanced in the supratentorial region with only temporal white matter remaining hyperintense.

With progressive maturation of the white matter of the corona radiata, some areas posterosuperior to the trigone and lateral to the lateral ventricles often retain an increased signal (see ► Fig. 7.63), the so-called terminal zones of the myelination. These are mostly visible during the first decade, sometimes even up to the second decade of life. Myelination of temporal and frontal subcortical white matter occurs last, so that T2-weighted signal reduction is not yet complete.

At age **24 months**, the process of myelination is terminated on T1-weighted images with T1-weighted hyperintense white matter in both supra and infratentorial regions (see ►Fig. 7.62). On T2-weighted images, myelination is almost complete, but signal reduction may progress mildly in the subcortical region up to the

30th month of life, especially in the temporal regions. The terminal zones lateral to the lateral ventricles as well as posterosuperior to the trigone may exhibit high T2-weighted signal until the second decade of life (see ►Fig. 7.63). ►Table 7.2 summarizes the age-related process of myelination.

Table 7.2 Age-dependent myelination (based on Barcovic)³⁰

Anatomical structure	T1w	T2w
Posterior brainstem	25–27 weeks of gestation	27–30 weeks of gestation
Middle cerebellar peduncle	Birth	0–2 months
Cerebellar white matter	0–4 months	3–5 months
Internal capsule, posterior limb:		
anterior part	1 month	4–7 months
posterior part	36 weeks of gestation	40 weeks of gestation
Internal capsule, anterior limb	2–3 months	7–11 months
Corpus callosum:		
Genu	4–6 months	5–8 months
Splenum	3–4 months	4–6 months
Centrum semiovale	2–4 months	7–11 months
Occipital white matter:		
deep	3–5 months	9–14 months
subcortical	4–7 months	11–15 months
Frontal white matter:		
deep	3–8 months	11–18 months
subcortical	7–15 months	14–30 months

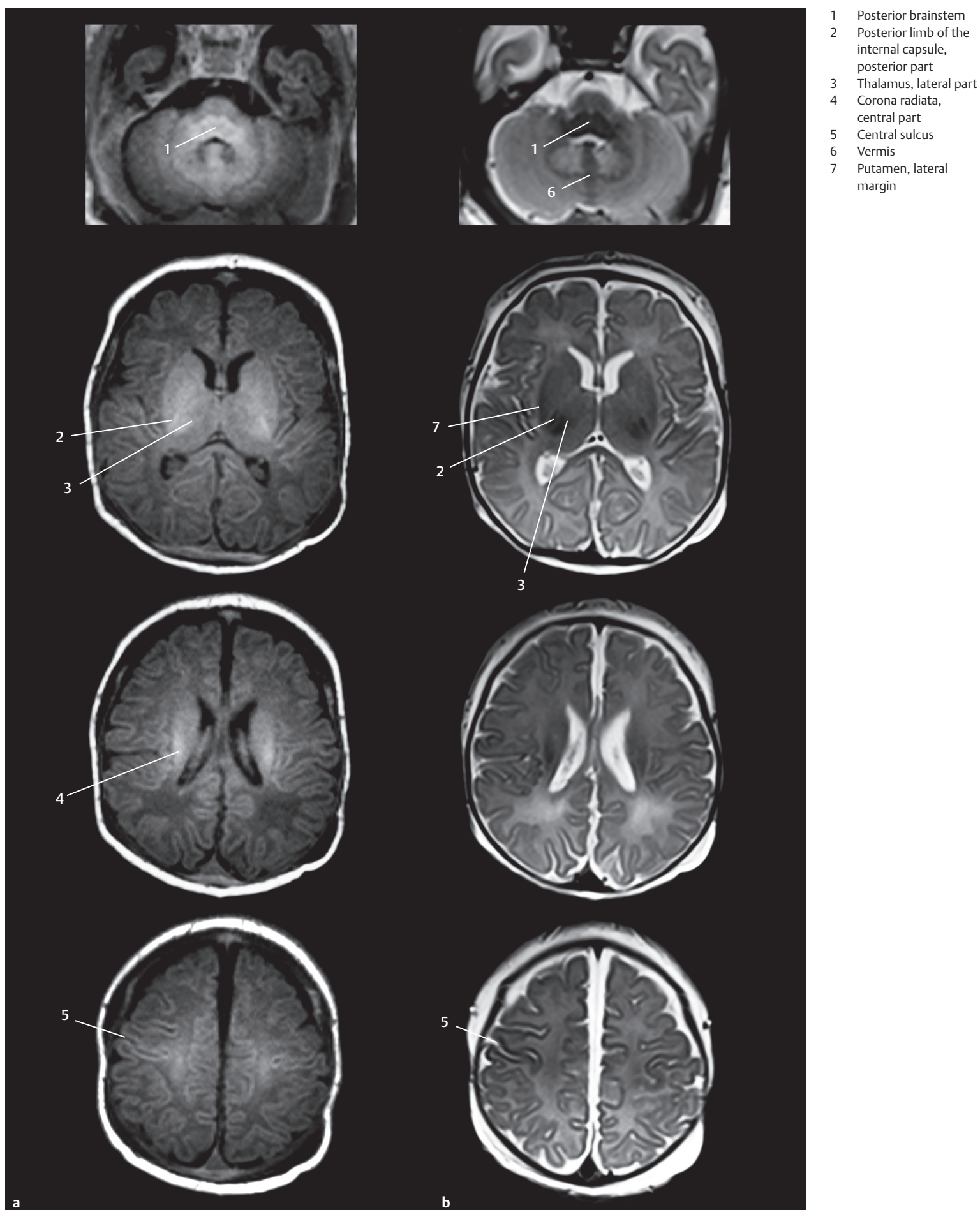


Fig. 7.56 Neonatal brain at term.

Fig. 7.56a T1w images.

Fig. 7.56b T2w images.

- 1 Anterior brainstem
- 2 Deep cerebellar white matter
- 3 Internal capsule, anterior limb
- 4 Internal capsule, posterior limb
- 5 Deep occipital white matter
- 6 Frontal unmyelinated white matter
- 7 Perirolandic corona radiata
- 8 Parietal unmyelinated white matter

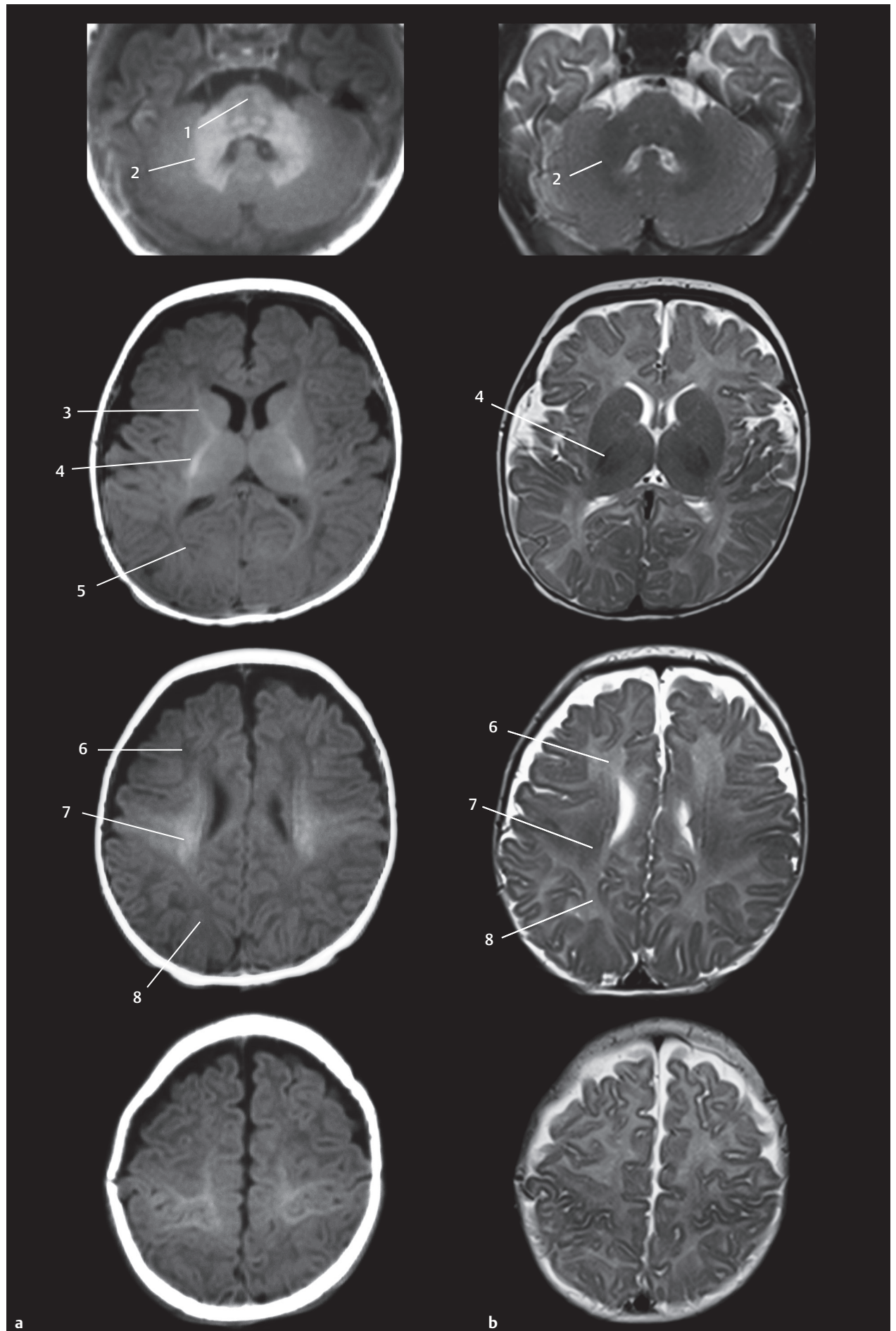


Fig. 7.57 Brain at age 3 months.

Fig. 7.57a T1w images.

Fig. 7.57b T2w images.

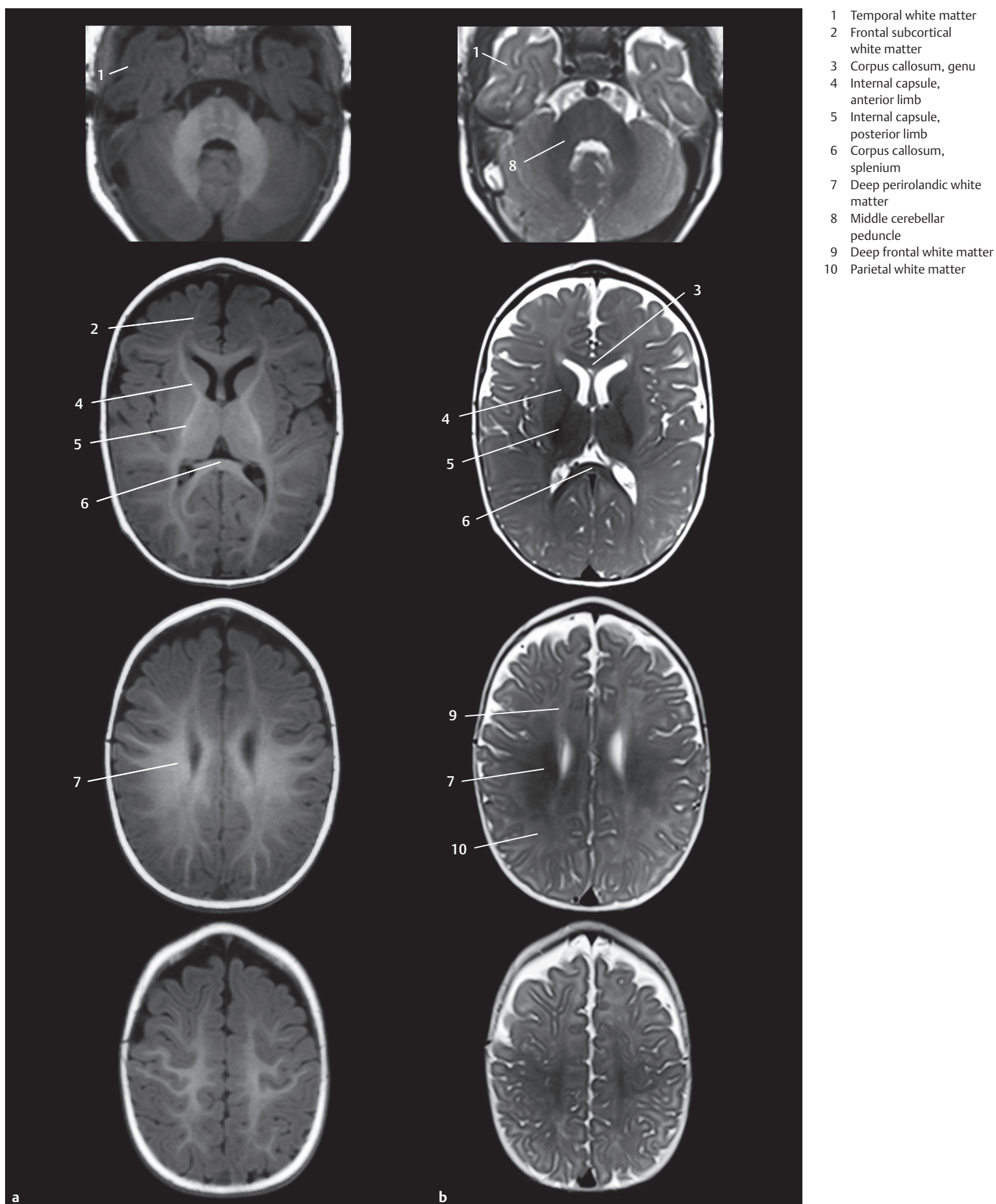


Fig. 7.58 Brain at age 6 months.

Fig. 7.58a T1w images.

Fig. 7.58b T2w images.

- 1 Subcortical temporal white matter
- 2 Subcortical frontal white matter
- 3 Parieto-occipital white matter
- 4 Peripheral cerebellar white matter
- 5 Corpus callosum, genu
- 6 Internal capsule, anterior limb
- 7 Deep perirolandic white matter

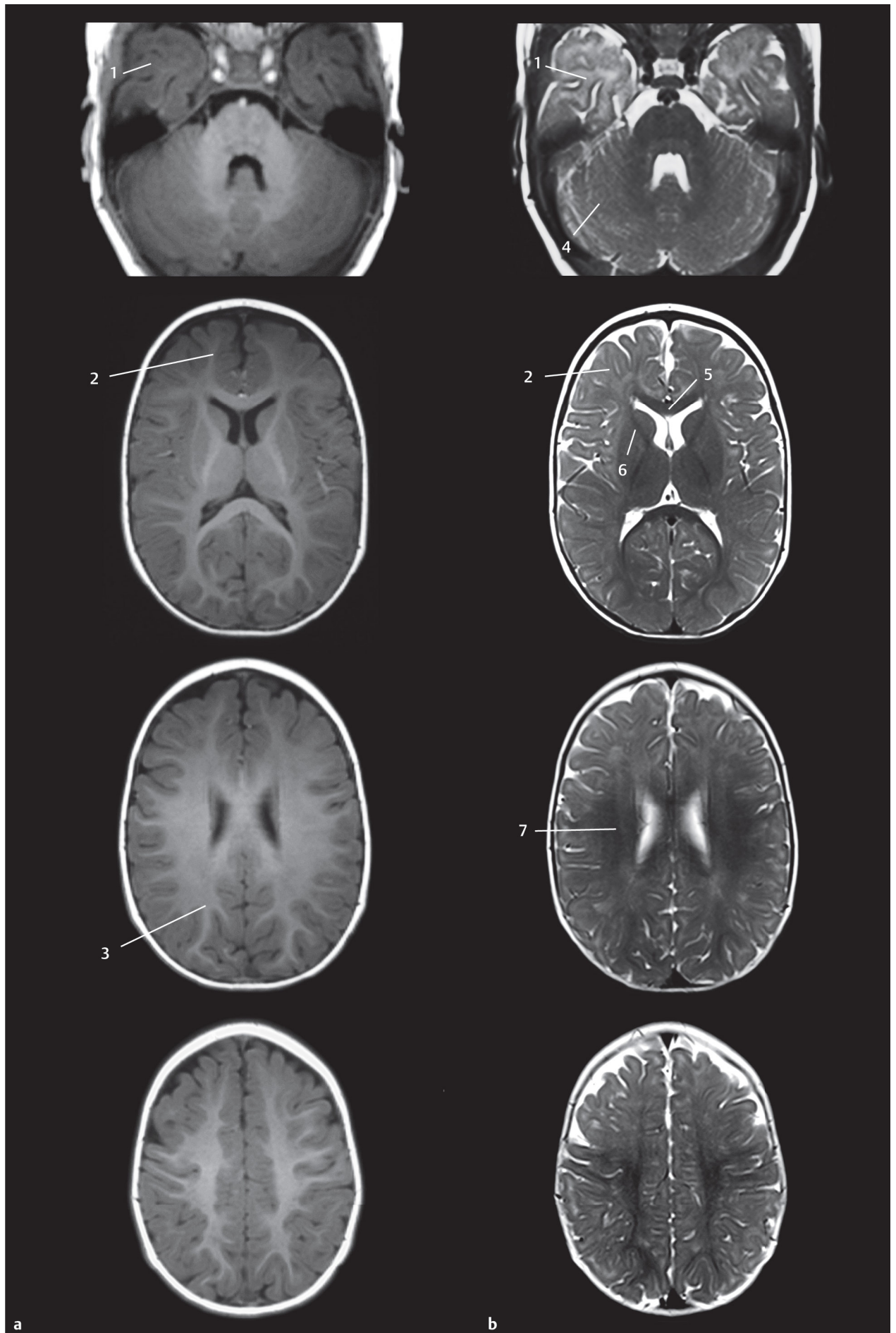


Fig. 7.59 Brain at age 9 months.

Fig. 7.58a T1w images.

Fig. 7.58b T2w images.

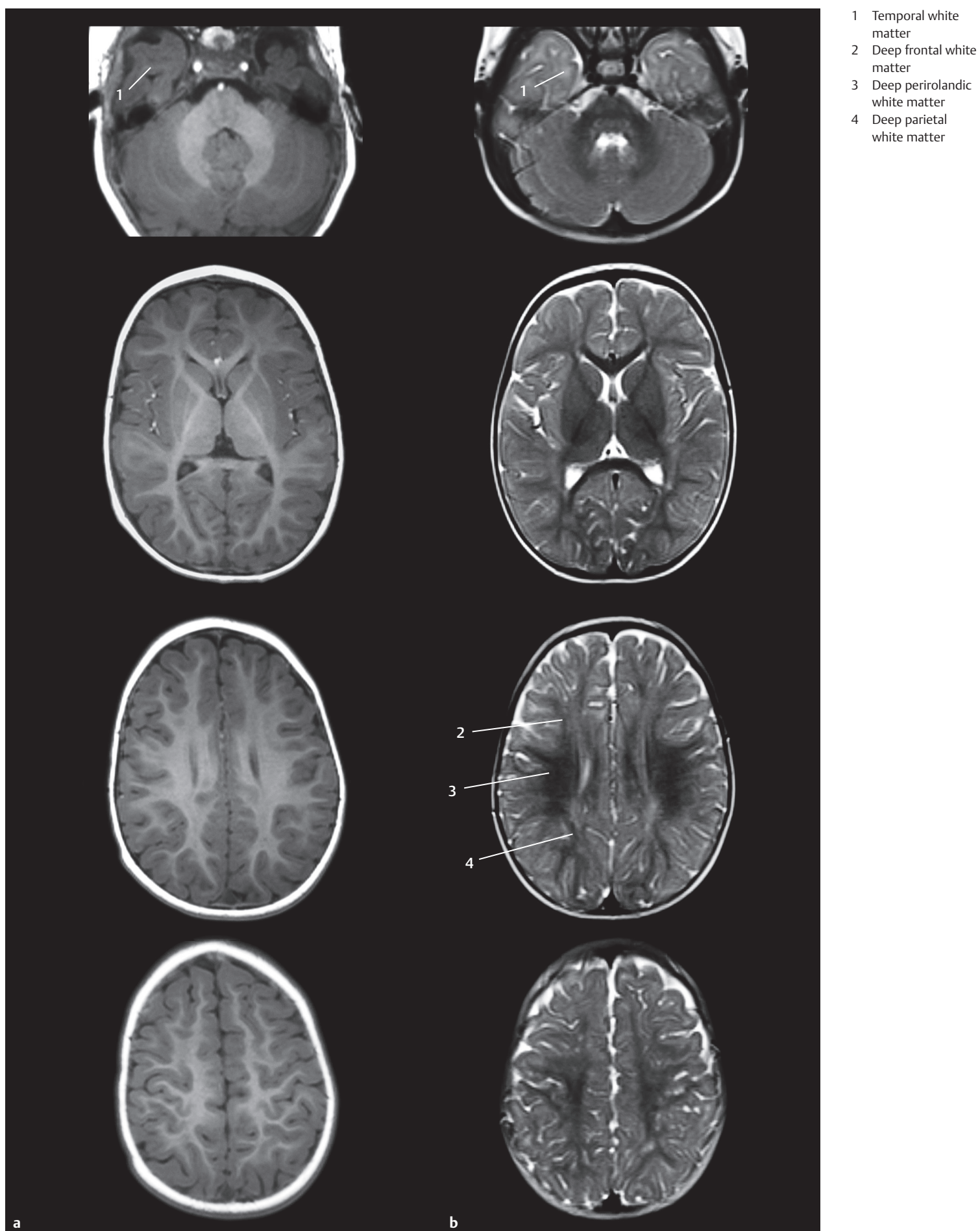


Fig. 7.60 Brain at age 12 months.

Fig. 7.60a T1w images.

Fig. 7.60b T2w images.

- 1 Temporal white matter
- 2 Terminal zones

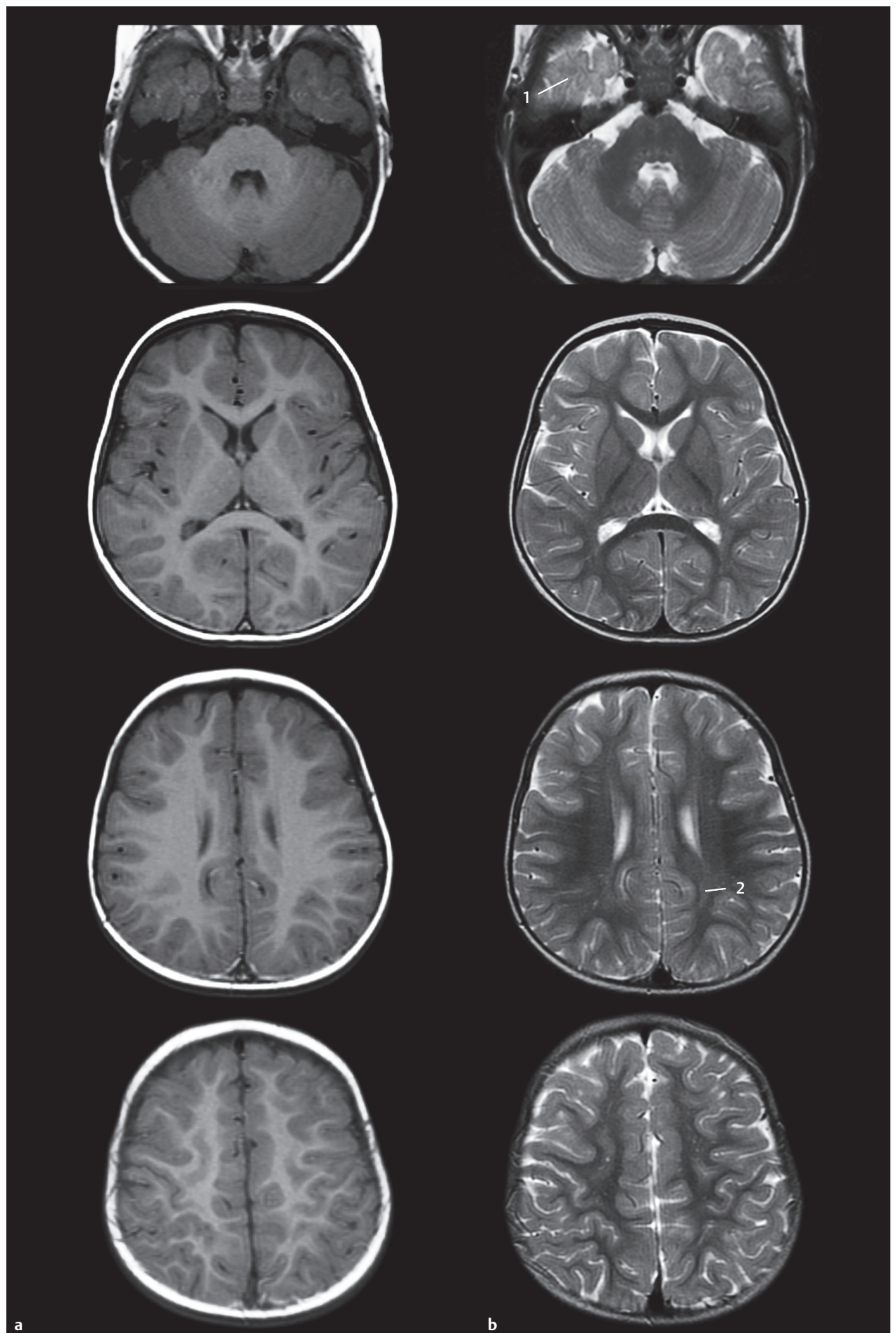
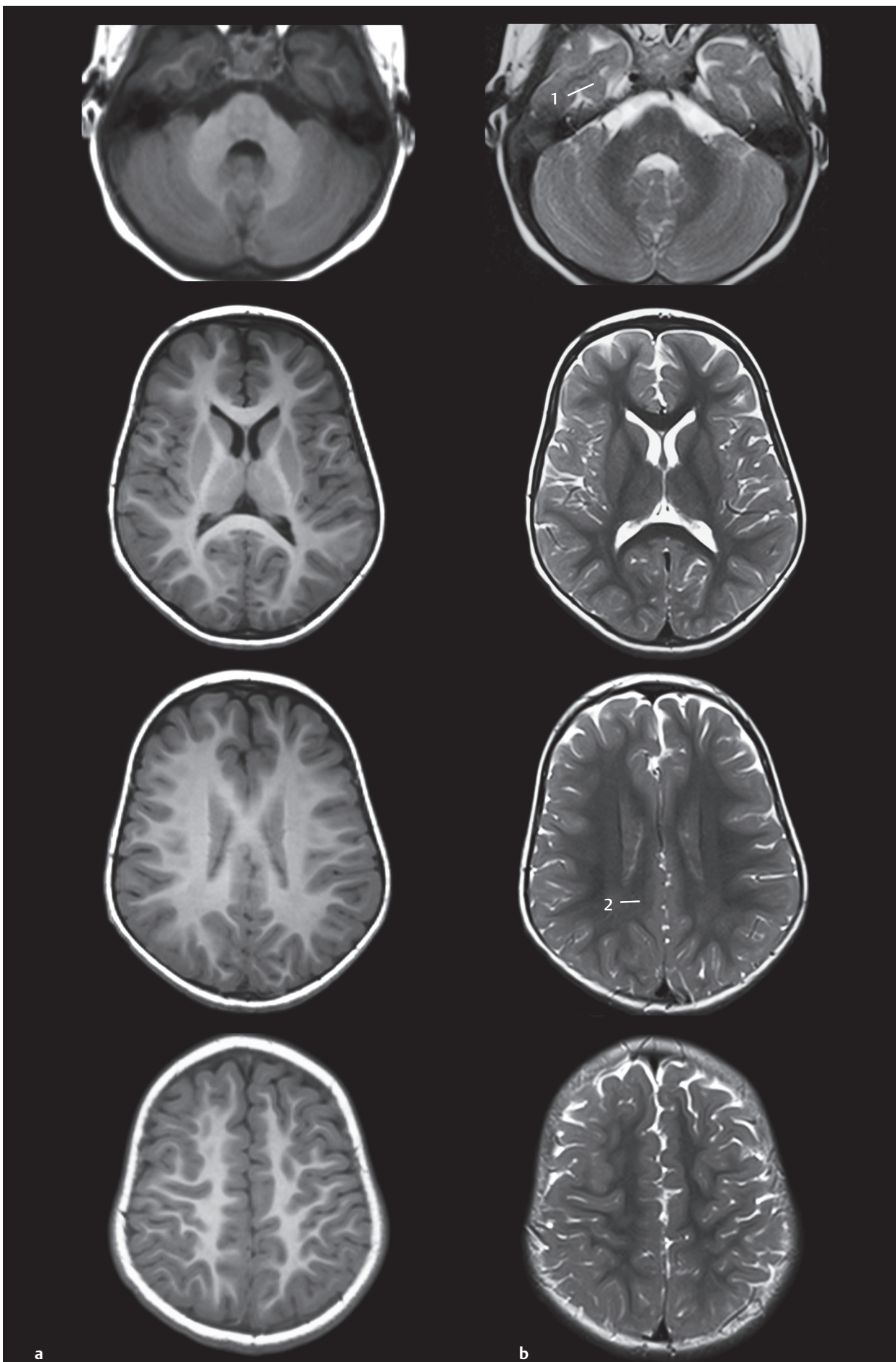


Fig. 7.61 Brain at age 18 months.

Fig. 7.61a T1w images.

Fig. 7.61b T2w images.



- 1 Temporal white matter
- 2 Terminal zones

Fig. 7.62 Brain at age 24 months.

Fig. 7.62a T1w images.

Fig. 7.62b T2w images.

1 Terminal zones

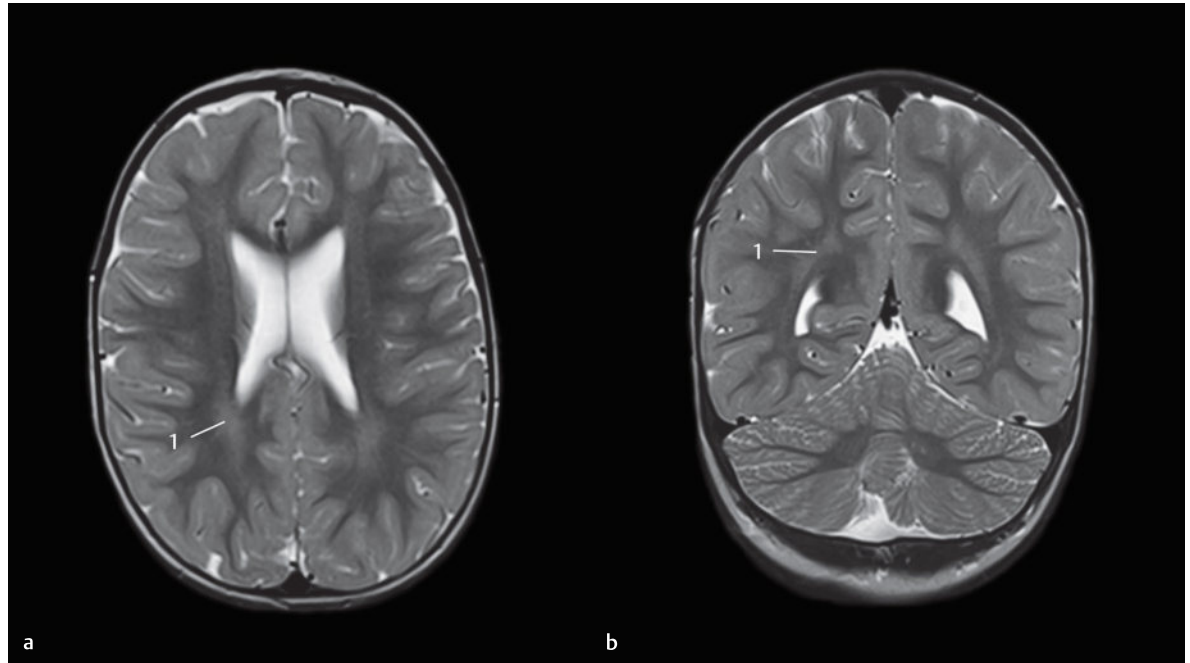


Fig. 7.63 Late myelination. Shown using the example of the supratrigonal terminal zone, which exhibits persistently increased T2w signal in a 12-year-old child.

Fig. 7.63a Axial section.

Fig. 7.63b Coronal section.

8 Facial Topography

Topography describes the positional relationship of anatomical structures. Standard textbooks of cranial topography prior to the era of cross-sectional imaging favored the depiction of anatomic structures as conceived from dissected specimens, thereby drawing on the vast experience of surgical specialties.

Progress made in cross-sectional imaging methods requires a special **3D knowledge of anatomic structures** for interpretation of parallel sections. Equidistant serial CT and MR images of the head may be likened to an architect's rendition of an entire building and its different floors. While right-angled objects predominate in architecture, anatomical structures have more complicated shapes and result in variable patterns.

The **position of the individual slice** is of special importance in anatomy. This may be seen in ►Fig. 3.1 for the coronal series in lateral view, ►Fig. 4.1a and ►Fig. 4.1b for the sagittal series in frontal view, and ►Fig. 5.1, ►Fig. 5.16, and ►Fig. 6.3 for the bicommissural, supraorbito-suboccipital, and the brainstem series in lateral view, respectively. The coronal series (see ►Fig. 3.2 up to ►Fig. 3.25) corresponds to an anterior view. Therefore, the anterior line of a slice determines sectioned structures within the slice (see ►Fig. 3.1). Anatomical structures lie in the intervals between adjacent lines; MR images were selected according to the schematic representation. The sagittal series has been depicted from the medial aspect (see ►Fig. 4.2 to ►Fig. 4.13). The bicommissural and supraorbito-suboccipital series (see ►Fig. 5.2 to ►Fig. 5.30) as well as the brainstem series (see ►Fig. 6.4 to ►Fig. 6.13) have been viewed from below. Therefore, the line below each encircled digit determines sectioned structures within the slice (see ►Fig. 5.1, ►Fig. 5.16, and ►Fig. 6.3).

8.1 Facial Bones

The facial skeleton or the **viscerocranium** forms the bony confines for the proximal ends of the respiratory and digestive systems and encloses the orbital cavity. The nasal skeleton is composed of five bones, while the jaw is composed of four. Individual bones may form part of two or more regions due to their proximity to each other. The hard palate thus forms the floor of the nasal cavity as well as the roof of the oral cavity.

8.1.1 Bones of the Nasal Skeleton

The **ethmoid** develops as an unpaired bone in the cartilaginous nasal capsule, and is composed of a central T-piece and paired lateral parts as seen on coronal sections:

- **Cribriform plate** (lamina cribrosa; see ►Fig. 3.3c, ►Fig. 3.17, and ►Fig. 4.8): forms the horizontal limb of the “T.”
- **Perpendicular plate**: corresponds to the vertical limb of the “T.”

- **Ethmoid cells** (see ►Fig. 3.1b, ►Fig. 3.2a, ►Fig. 3.2b, ►Fig. 3.16, ►Fig. 4.1b, ►Fig. 4.3a, ►Fig. 4.3b, ►Fig. 4.9, ►Fig. 5.1b, ►Fig. 5.4, ►Fig. 5.17, ►Fig. 5.35, and ►Fig. 6.9a): these lie between the nasal and orbital cavities and inferior to the anterior cranial fossa.

The cribriform plate inserts into the frontal bone as a median and paramedian structure. This thin bony plate exhibits several perforations traversed by olfactory nerves, which pass from the olfactory mucosa to the olfactory bulb in the olfactory fossa.

Clinical Notes

The depth of the olfactory fossa from the roof of the ethmoid is relevant to the planning of a surgical procedure on the ethmoid cells.

This is divided into three types in accordance with Keros classification:

1. **Keros Type I:** 1–3 mm
2. **Keros Type II:** 4–7 mm
3. **Keros Type III:** 8–16 mm (also termed the “dangerous ethmoid”)^{189,289}

The **crista galli** protrudes into the cranial cavity from the ethmoidal plate in the median plane (see ►Fig. 3.2c, ►Fig. 3.2d, ►Fig. 3.16, ►Fig. 4.1b, ►Fig. 4.2c, ►Fig. 4.2d, ►Fig. 4.8, ►Fig. 5.6a, ►Fig. 5.6b, ►Fig. 5.18, ►Fig. 6.12a, and ►Fig. 6.13a). The falx cerebri is attached to this bony process.

The perpendicular plate is a continuation of the crista galli below the cribriform plate and forms the upper part of the bony nasal septum. The orbital plate (previously: papyracea, see ►Fig. 3.2c, ►Fig. 3.2d, ►Fig. 3.3c, ►Fig. 3.3d, ►Fig. 3.16, ►Fig. 3.17, and ►Fig. 6.10a) forms the lateral boundary of ethmoid cells, separating them from the orbital cavity. The **ethmoid cells** are air-containing spaces which communicate with the nasal cavity. The anterior and middle ethmoidal cells open below the middle nasal concha while the posterior ethmoidal cells open above it. The entire ethmoidal labyrinth measures approximately 10 mL in volume.³³⁶ The **superior and medial nasal conchae** protrude into the nasal cavity from the medial aspect of the ethmoid labyrinth. The middle canal lies below the middle concha (see ►Fig. 3.2a, ►Fig. 3.2b, ►Fig. 3.3a, ►Fig. 3.3b, ►Fig. 3.4a, and ►Fig. 3.4b). The anterior and middle ethmoid cells as well as the maxillary and frontal sinuses drain into a crescent shaped opening in the middle canal, the hiatus semilunaris (see ►Fig. 3.2a, ►Fig. 3.3a, ►Fig. 4.3a, ►Fig. 6.8a, and ►Fig. 6.9a). This drainage area together with the middle canal is also known as the “ostiomeatal complex”.

The independent **inferior nasal concha** with a length of about 4 cm is larger than the other conchae. This hook shaped structure seen above the palate on coronal sections forms a landmark for imaging (see ►Fig. 3.2a,

►Fig. 3.2b, ►Fig. 3.3a, ►Fig. 3.3b, ►Fig. 3.4a, ►Fig. 3.4b, ►Fig. 3.16, ►Fig. 3.17, ►Fig. 4.3a, ►Fig. 4.3b, ►Fig. 5.3, ►Fig. 6.4a, and ►Fig. 6.5a).

The lower part of the bony nasal septum is formed by the **vomer**, an unpaired bone. The **nasal septum** is composed of a cartilaginous component in addition to its two bony parts.

The paired **nasal bones** are small oblong bones forming the upper part of the nasal bridge.

The small, four-sided, and paired lacrimal bones lie within the medial wall of the orbit, forming part of the lateral nasal wall.

8.1.2 Skeletal Anatomy of the Jaw

The **maxilla** is the central bone of the face, abutting the orbital, nasal, and oral cavities and forming most of the hard palate. It comprises of a central piece or body and three processes:

- The **maxillary sinus** occupies the large body of the maxilla and is visualized as the largest pneumatized paranasal sinus in coronal (see ►Fig. 3.1b, ►Fig. 3.2a, ►Fig. 3.2b, ►Fig. 3.3a, ►Fig. 3.3b, ►Fig. 3.4a, ►Fig. 3.4b, and ►Fig. 3.17), sagittal (see ►Fig. 4.1b, ►Fig. 4.4a, ►Fig. 4.4b, ►Fig. 4.6a, ►Fig. 4.6b, and ►Fig. 4.10), and axial sections (see ►Fig. 5.1b, ►Fig. 5.31, and ►Fig. 6.3).
- The frontal process of maxilla extends between the nasal and lacrimal bones up to the frontal bone.
- The zygomatic process abuts the zygomatic bone.
- The palatal process is a horizontal bony plate which abuts the palatine bone at its posterior aspect, both of these forming the **hard palate** (see ►Fig. 3.1b, ►Fig. 3.2c, ►Fig. 3.2d, ►Fig. 3.3c, ►Fig. 3.3d, ►Fig. 3.4c, ►Fig. 3.4d, ►Fig. 3.16, ►Fig. 3.17, ►Fig. 4.3c, ►Fig. 4.3d, and ►Fig. 4.8).
- The alveolar process contains alveoli that hold the teeth of the upper jaw, which is resorbed following tooth loss, as is well seen in the maxilla on the sagittal series. The maxilla is narrow at the site where the upper teeth were located and lacks the rugged alveolar process which extends into the oral cavity (see ►Fig. 3.3c, ►Fig. 3.3d, ►Fig. 4.8, ►Fig. 4.9, and ►Fig. 5.2).

The **palatine bone** is composed of the horizontal plate forming part of the hard palate and an approximately vertical plate which forms the medial boundary of the pterygopalatine fossa.

The **zygomatic bone** inserts between the maxilla, temporal bone, and frontal bones (see ►Fig. 3.1b, ►Fig. 3.2c, ►Fig. 3.2d, ►Fig. 3.5b, ►Fig. 3.17, ►Fig. 4.1b, ►Fig. 4.7c, ►Fig. 4.7d, ►Fig. 5.3, ►Fig. 5.5, ►Fig. 5.17, ►Fig. 5.31, and ►Fig. 6.5a).

The lower jaw or **mandible** is the only mobile facial bone which articulates with the base of the skull. The anterior part or body resembles a bent horseshoe (see ►Fig. 3.1b, ►Fig. 3.2c, ►Fig. 3.2d, ►Fig. 3.3c, ►Fig. 3.3d, ►Fig. 3.16, ►Fig. 4.1b, ►Fig. 4.2c, ►Fig. 4.2d, ►Fig. 4.4c, ►Fig. 4.4d, and ►Fig. 4.8), while the ramus of the mandible projects

upwards from the body (see ►Fig. 3.1b, ►Fig. 3.5c, ►Fig. 3.5d, ►Fig. 3.6c, ►Fig. 3.6d, ►Fig. 3.20, ►Fig. 4.1b, ►Fig. 4.7c, and ►Fig. 4.12). The teeth of the lower jaw are contained within the alveoli of the body of mandible. The alveolar part undergoes resorption following loss of teeth, such that the mandibular canal comes to lie closer to the toothless alveolar margin (see ►Fig. 3.16 and ►Fig. 3.18). Running upward from the body at the angle of the mandible, the ramus of the mandible then divides into two processes, the pointed coronoid process (anterior, see ►Fig. 3.1b and ►Fig. 4.13) and the condylar process (posterior, see ►Fig. 4.13). The coronoid process may be considered to represent an ossified tendon as it lies buried within the tendinous fibers of the temporalis (see ►Fig. 4.7c). The condylar process first tapers to the neck of the mandible (see ►Fig. 3.1b and ►Fig. 3.21), extending superiorly to the transversely positioned head of mandible (see ►Fig. 3.1b, Fig. 3.7c, ►Fig. 3.7d, and ►Fig. 3.21). The mandibular foramen lies on the inner aspect of the ramus, through which the inferior alveolar nerve and vessels enter the mandibular canal (see ►Fig. 4.7a, ►Fig. 4.7c, and ►Fig. 4.12). Complex spatial relationships of pathological changes involving the facial skeleton (fractures, destructions) are well illustrated with high-resolution spiral CT techniques or modern volume tomographs (e.g., dental volume tomography) using thin slices.³⁶⁵ Axial and reformatted coronal and sagittal sections are employed during **CT examinations**. Axial images are preferably obtained by sectioning parallel to the infraorbitomeatal plane,^{254,365} with a wide window being used to image bony structures and a narrow window for soft tissues.

8.2 Nasal Cavity and Paranasal Sinuses

8.2.1 Topography

The paired nasal cavities extend from the nostrils and continue via the vestibule into the nasal cavity proper, which in turn opens into the nasopharynx at the posterior nasal openings or choanae. The nasal cavity is divided by the nasal septum into right and left halves.

All paranasal sinuses are connected to the nasal cavity and are composed of the following:

- Ethmoid air cells
- Maxillary sinus
- Sphenoid sinus
- Frontal sinus

The centrally positioned nasal cavity and paranasal sinuses, extending above and below Reid's baseline, are well seen on coronal and sagittal sections (see ►Fig. 3.2 to ►Fig. 3.25 and ►Fig. 4.2 to ►Fig. 4.13). The sphenoid sinus may extend almost up to the meatoververtical line posteriorly. The nasal cavities and paranasal sinuses lie inferior to the anterior cranial fossa, inferomedial to the orbits and the middle cranial fossa, and superior to the oral cavity. Posteriorly, the nasal cavity continues into the pharynx through the choanae between the

fourth and fifth coronal sections. The sphenoid sinus (see ►Fig. 3.6a and ►Fig. 3.6b) is seen lying above the pharynx (see ►Fig. 3.6a and ►Fig. 3.6b) in the fifth coronal section. These regions exhibit great interindividual variability. The paranasal sinuses are of clinical importance since they may be involved by infectious processes, tumors, and trauma. Ultrasound, CT, MRI, and endoscopy are all useful diagnostic methods in the evaluation of such lesions.

The medial wall of the nasal cavity is formed by the nasal septum (see ►Fig. 3.2a, ►Fig. 3.2b, ►Fig. 3.3a, ►Fig. 3.3b, ►Fig. 3.16, ►Fig. 4.1b, ►Fig. 4.2b, ►Fig. 4.8, ►Fig. 5.3, ►Fig. 5.31, and ►Fig. 6.6a), which lies nearly in the midline, and may be laterally deviated in its anterior or posterior parts. This is termed “septal deviation” (see ►Fig. 3.3a, ►Fig. 3.3b, and ►Fig. 3.17).

The lateral wall of the nasal cavity is enlarged by medially projecting conchae, each roofing a canal:

- The **superior nasal canal** is short, averaging less than 2 cm in length,³³² into which the posterior ethmoidal cells drain.
- The **middle nasal canal** is connected to the frontal sinus, anterior, and middle ethmoidal cells, and to the maxillary sinus via the **hiatus semilunaris** (see ►Fig. 3.2a, ►Fig. 3.2b, ►Fig. 3.3a, ►Fig. 4.3a, and ►Fig. 6.9a). The middle nasal concha has been partly sectioned tangentially in ►Fig. 4.3a such that the anterior and superior parts of the semilunar hiatus (see ►Fig. 4.3a) are visible. The postero-inferior part, which is obscured by the middle concha, has been indicated by a broken line. The nasolacrimal duct (see ►Fig. 6.6a and ►Fig. 8.1) drains into the **inferior canal** and carries tears into the nasal cavity.

Ethmoidal cells and the maxillary sinus have already been described along with their corresponding bones. The sphenoid and frontal sinuses are paired, with the paired **sphenoid sinus** usually lying within the body of the sphenoid. In 12% of cases the sphenoid sinus extends only as far as a perpendicular drawn through the tuberculum sellae (presellar type); it surrounds the pituitary fossa in 84% (sellar type); and is located outside the body of the sphenoid in 4%.³³² A sphenoid sinus of the sellar type is seen in the coronal series (see ►Fig. 3.1b, ►Fig. 3.5a, ►Fig. 3.5b, ►Fig. 3.6a, ►Fig. 3.6b, ►Fig. 3.7a, ►Fig. 3.7b, and ►Fig. 3.8a). The sphenoid sinus drains into the sphenoethmoidal recess above the superior concha. The septum separating both sphenoid sinuses is frequently asymmetrical (see ►Fig. 3.5a). The roof of the sphenoid sinus is closely related to the optic nerve (see ►Fig. 3.5a and ►Fig. 3.5b). Familiarity with the sphenoid sinus is of special importance in the trans-sphenoid approach for surgeries on the pituitary gland (Onodi cells, spheno-optic recess). Parts of the optic canal are formed only by the sheath of the optic nerve and the mucous membrane of the sinus in four percent of cases. The optic nerve is therefore vulnerable to injury in the trans-sphenoid approach to the pituitary.³³²

The **frontal sinus** is highly variable and often asymmetrical (see ►Fig. 4.1b). The left frontal sinus has been

sectioned in the anterior part of the frontal bone on the right of the head (see ►Fig. 4.2a and ►Fig. 4.2b). Its anterior wall forms the bony supraciliary arch, which exhibits individual variations. The floor of the frontal sinus is separated from the orbit by a thin plate of bone.

8.2.2 Blood Supply of Paranasal Sinuses

The walls of the nasal cavity are supplied by branches of the **maxillary and ophthalmic arteries**. The maxillary artery (see ►Fig. 9.1) gives off the sphenopalatine artery, which exits the pterygopalatine fossa through the sphenopalatine foramen under the nasal mucus membrane, supplying the posterior aspect of the lateral and medial walls of the nasal cavity. The anterior ethmoidal artery arises from the **ophthalmic artery** that enters the nasal cavity following a circuitous course through the cranium. This complicated course was probably an outcome of late phylogenetic development of an entirely bony orbital cavity, together with the marked enlargement of the neocortex in mammals. The anterior ethmoidal artery exits the orbital cavity through the anterior ethmoidal foramen and first enters the anterior cranial fossa; passing through the cribriform plate into the anterior part of the nasal cavity, it divides to supply its medial and lateral walls.

Veins arising in the nasal mucosa drain into the orbital veins, the pterygoid venous plexus and facial veins. Lymph nodes at the angle of the jaw and posterior to the pharynx receive lymphatic drainage from the nasal mucosa.

8.2.3 Nerve Supply of the Nasal Cavity

The region of the **olfactory epithelium** in the nasal mucus membrane may be differentiated from the ciliated **respiratory epithelium** as it is thicker and has a slightly brown tinge. The olfactory region is composed of four Cent-like sized fields in the center of the superior nasal concha and the corresponding area of the nasal septum opposing it. Histologically, the olfactory epithelium contains olfactory cells, the basal axons of which give rise to **olfactory fibers**. These fibers of the first (olfactory) cranial nerve then run through the cribriform plate of the ethmoid into the cranial cavity and terminate in the olfactory bulb.

Sensory supply of the nasal cavity is provided by the ophthalmic and maxillary nerves, the terminal branches of which carry viscerosecretory fibers to the mucous glands in the nasal mucosa.

The **ophthalmic nerve** gives off the nasociliary nerve, which in turn gives rise to the anterior ethmoidal nerve. This then accompanies the anterior ethmoidal artery in its circuitous course through the anterior cranial fossa to supply the anterior nasal mucosa.

Branches of the **maxillary nerve** supply the posterior aspect of the nasal mucosa on its medial and lateral aspects.

The greater petrosal nerve contains parasympathetic preganglionic nerve fibers to nasal mucosal glands. Postganglionic fibers from the pterygopalatine ganglion (see ► Fig. 10.43b) join sensory fibers in the pterygopalatine fossa.

Sympathetic postganglionic nerve fibers also run alongside arterial branches to the pterygopalatine fossa and continue with sensory fibers to nasal mucosal glands.

8.3 Orbit

8.3.1 Topography

The orbit contains the globe of the eye and is the receptor organ of the visual system (see ► Section 10.6). The eyeball is protected by the following structures ⁷⁷:

- Bony walls of the orbit
- Eyelids
- Conjunctiva
- Lacrimal apparatus

A fascial sheath or Tenon's capsule surrounds the eyeball as a joint capsule might surround a sphere.

The extraocular muscles enable extremely precise movements of the eyeball.

The optic nerve courses posteriorly from the globe to the optic chiasma.

The shape of the orbital cavity resembles a hollow four-sided pyramid. Its base is directed outward with the optic canal forming its apex, at which point the optic nerve exits the orbit. The apex of the pyramid is directed posteromedially.

The **four walls of the orbit** are best seen in coronal sections (roof of orbit, see ► Fig. 3.2c and ► Fig. 3.2d; floor of orbit, see ► Fig. 3.2c and ► Fig. 3.2d) and appear markedly rounded posteriorly, where they merge into each other (see ► Fig. 3.4 and ► Fig. 3.17). The ophthalmic artery and optic nerves are closely opposed to one another within the optic canal (see ► Fig. 3.5a, ► Fig. 3.5b, and ► Fig. 3.5c).

The anterior pole of the eyeball lies approximately in a plane tangential to the superior and inferior margins of the orbit. The globe is displaced in a sagittal direction by space-occupying retrobulbar processes within the orbit. Edema, hematomas, inflammatory lesions, and tumors can all push the eyeball forward if the bony walls of the orbit do not give way. Blunt compression injury, such as a blow with a fist, can result in a blow-out fracture of the thin orbital floor whereby orbital contents are forced into the maxillary sinus (see ► Fig. 3.2a, ► Fig. 3.2b, ► Fig. 3.3a, and ► Fig. 3.3b).

The orbit is connected to the following structures via several openings:

- The middle cranial fossa, through the **optic canal** (see ► Fig. 3.18 and ► Fig. 5.37) for the optic nerve and the ophthalmic artery, and through the **superior orbital fissure** (see ► Fig. 3.18) for the third, fourth, the first

division of the Vth and the VIth cranial nerves and the superior ophthalmic vein.

- The infratemporal and pterygopalatine fossae, through the **inferior orbital fissure** for the zygomatic nerve and inferior ophthalmic vein.
- The nasal cavity, through the **nasolacrimal canal** for the nasolacrimal duct.
- The face, through the **infraorbital canal** (see ► Fig. 3.2b, ► Fig. 3.16, and ► Fig. 3.17) for infraorbital vessels and nerves (see ► Fig. 3.2b, ► Fig. 3.2d, ► Fig. 3.3a, ► Fig. 3.3b, ► Fig. 3.3c, and ► Fig. 3.3d).
- The anterior cranial fossa, through the anterior ethmoidal foramen for the anterior ethmoidal vessels and nerves.
- Posterior ethmoidal cells and the sphenoid sinus, through the posterior ethmoidal foramen for posterior ethmoidal vessels and nerves.

The invention of the ophthalmoscope by Hermann von Helmholtz in 1850 refined ophthalmoscopic examination of the globe which is of significance even today. High-resolution retinal examinations are furthermore possible using optic coherence tomography.⁶⁵⁹ Advances in new imaging techniques (MRI) are most evident in the diagnosis of retrobulbar pathology of the orbit; the retrobulbar space will therefore be described in greater topographic detail.

8.3.2 Eyelids and Lacrimal Apparatus

The eyelids and the lacrimal apparatus protect the cornea from drying, clouding, and/or ulceration. The lacrimal and palpebral parts of the **orbicularis oculi** lie within the larger upper lid (see ► Fig. 4.5a and ► Fig. 4.5b) and the smaller lower lid. The lacrimal portion of this muscle arises from parts of the lacrimal ducts, while its orbital part extends partly over the orbital margin (see ► Fig. 3.2c). The three parts of the orbicularis oculi surround the palpebral fissure like a ring. It facilitates closure of the eyelids and its lacrimal part directs tears into the nasal cavity. The muscle is innervated by the facial nerve.

The **levator palpebrae superioris** (see ► Fig. 3.2c, ► Fig. 3.3c, ► Fig. 3.3d, ► Fig. 3.4c, ► Fig. 4.5c, and ► Fig. 4.6c) arises from the common tendinous ring of the extraocular muscles and inserts into the connective tissue of the upper eyelid. It elevates the superior eyelid and derives its nerve supply from the oculomotor nerve.

The **superior and inferior tarsal muscles** form a ring consisting of a thin layer of smooth muscle between striated muscles and the eyelids. The superior tarsal muscle arises from the levator palpebrae superioris and spreads out toward the tarsus (tough connective tissue) of the upper eyelid, while the weaker inferior tarsal muscle originates from the inferior rectus and is inserted into the tarsus of the lower lid. Increase in tone of smooth tarsal muscles innervated by cervical sympathetic fibers may cause

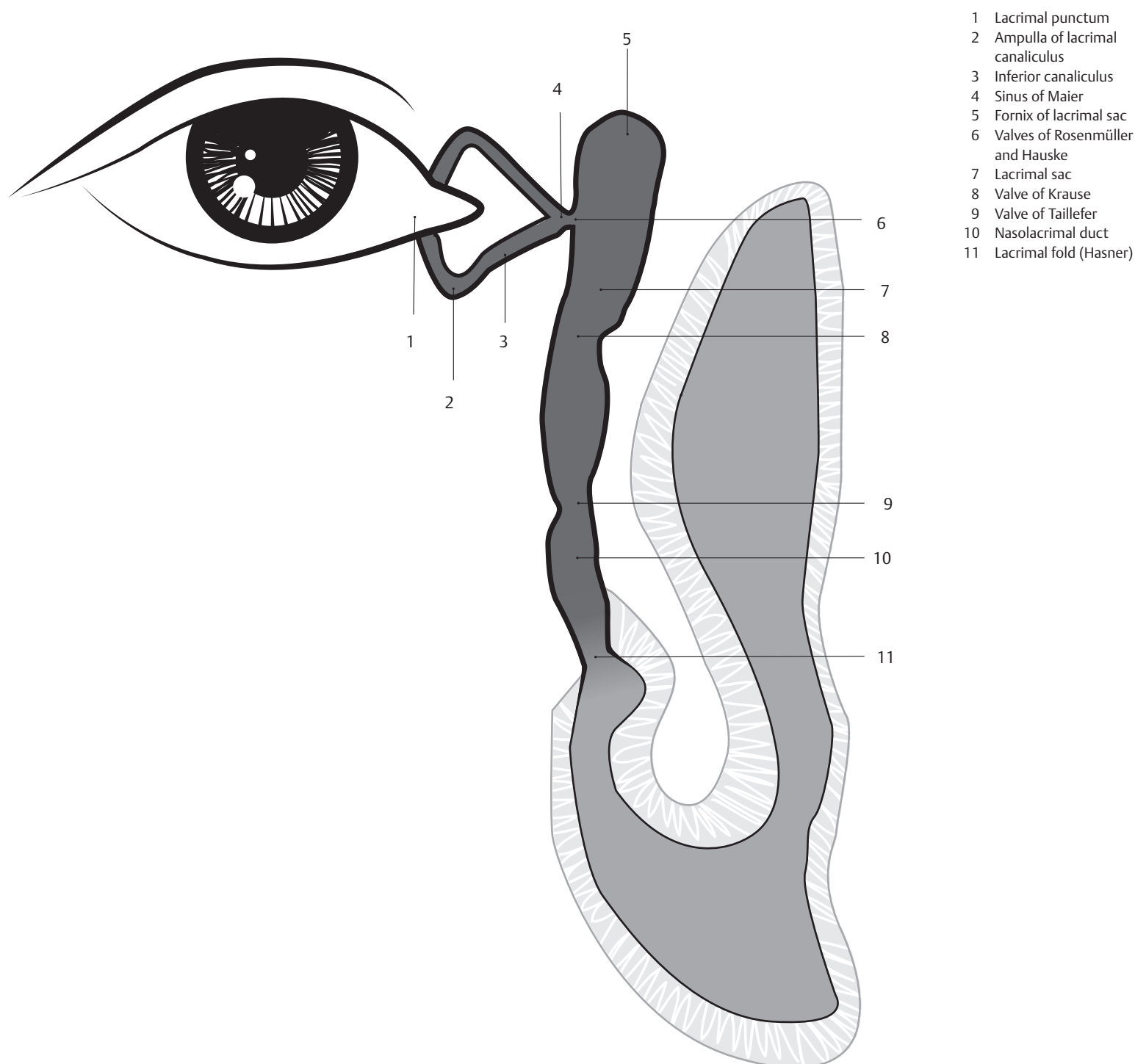


Fig. 8.1 Anatomy of the normal lacrimal system. Schematic representation of the right eye, anterior view.

widening of the palpebral fissure while reduced sympathetic tone (as in fatigue) may result in its narrowing.

Branches of the first division of the trigeminal nerve provide sensory innervation of the upper eyelid while the lower eyelid receives sensory fibers from its second division.

The **conjunctiva** lines the posterior surface of the upper and lower eyelids as well as the sclera of the eyeball, continuing up to the margins of the cornea and thereby forming a small conjunctival sac which is filled with tears.

Located in the upper, outer corner of the eye lies the **lacrimal gland** which is closely related to the frontal

bone (see ►Fig. 3.2c, ►Fig. 3.2d, ►Fig. 4.6c, ►Fig. 5.18, and ►Fig. 8.2). It is innervated by parasympathetic fibers from the facial nerve via the greater petrosal nerve, pterygopalatine ganglion, zygomatic and lacrimal nerves, and receives sympathetic fibers from the cervical sympathetic trunk through the periarterial vascular plexus. Tears secreted by the lacrimal gland into the conjunctival sac are then transported by lid movements to the medial angle of the eye. These are then drained by the lacrimal ducts together with the lacrimal portion of the orbicularis oculi and carried through the lacrimal sac and the nasolacrimal duct into the inferior nasal canal (see ►Fig. 8.1).

8.3.3 Fascial Sheath of the Eyeball

The fascial sheath or **Tenon's capsule** forms a sort of joint cavity in which the eyeball, as in a ball-and-socket joint, can freely rotate in three main axes. The visual axis of the eyeball may be rotated medially (adduction) or laterally (abduction) around an imaginary vertical axis which runs through its center. The visual axis may be elevated or depressed around the frontal axis while it may be rotated medially or laterally around the sagittal axis. The function(s) of the extraocular muscles are decided by their positions and directions of pull relative to the individual main axes. Tenon's capsule consists of a firm connective tissue sheath which is attached to the sclera only at the point of entry of the optic nerve and at the corneoscleral junction (corneal limbus). The tendons of extraocular muscles run through slits in this fascial sheath before they attach to the eyeball.

8.3.4 Extraocular Muscles

The six extraocular muscles lie within the orbital fat and enable movements of the eyeball. Five of these muscles as well as the levator palpebrae superioris arise from the common tendinous ring, a ring of fibrous tissue surrounding the optic canal at its entrance to the orbit and spanning across the central part of the superior orbital fissure. It forms the apex of a muscular pyramid through which the optic nerve and the ophthalmic artery pass from the optic canal together with the oculomotor, nasociliary, and abducens nerves from the superior orbital fissure. The extraocular muscles are easily identified in coronal sections since their positional relationships, namely superior-inferior and medial-lateral, are distinctly seen.

The **superior rectus** (see ► Fig. 3.2c, ► Fig. 3.2d, ► Fig. 3.3c, ► Fig. 3.3d, ► Fig. 3.4c, ► Fig. 3.4d, ► Fig. 4.5c, ► Fig. 4.5d, ► Fig. 5.6, and ► Fig. 6.12a) runs obliquely, forming an angle of 25° with the sagittal visual axis. Its effective terminal segment lies medial to the vertical axis when the visual axis is directed straight and forwards. The superior rectus mainly acts as an elevator with ancillary functions of adduction and internal rotation. The effective terminal segment of the muscle shifts to the vertical axis with abduction of the eye to 25°, such that it functions as a pure elevator in this position. The superior rectus is innervated by the oculomotor nerve.

The **inferior rectus** (see ► Fig. 3.2c, ► Fig. 3.2d, ► Fig. 3.3b, ► Fig. 3.3c, ► Fig. 3.3d, ► Fig. 3.4c, ► Fig. 3.4d, ► Fig. 4.5c, ► Fig. 4.5d, ► Fig. 5.5, and ► Fig. 6.9a) runs forward obliquely beneath the eyeball forming an angle of 25° to the visual axis. Its effective terminal segment is similar to that of the rectus superior above, lying medial to the vertical axis when the visual axis is directed straight and forward. It is principally an ocular depressor with ancillary functions of adduction and external rotation and is innervated by the oculomotor nerve.

The **medial rectus** (see ► Fig. 3.2c, ► Fig. 3.2d, ► Fig. 3.3b, ► Fig. 3.3c, ► Fig. 3.3d, ► Fig. 3.4c, ► Fig. 3.4d, ► Fig. 4.4c, ► Fig. 4.4d, ► Fig. 5.6a, ► Fig. 5.6b, ► Fig. 6.10a, and ► Fig. 6.11a) runs medial to the eyeball. Its effective terminal segment lies medial to the vertical axis, runs through the main frontal axis of ocular elevation and depression, and in the same direction as the axis of rotation. The muscle is, therefore, a pure adductor and is innervated by the oculomotor nerve.

The **lateral rectus** (see ► Fig. 3.2c, ► Fig. 3.2d, ► Fig. 3.3c, ► Fig. 3.3d, ► Fig. 3.4c, ► Fig. 3.4d, ► Fig. 4.5c, ► Fig. 4.6c, ► Fig. 4.6d, ► Fig. 6.10a, and ► Fig. 6.11a) lies lateral to the eyeball. Its effective terminal segment lies lateral to the vertical axis in all positions of the globe. The muscle moves the eye laterally (pure abductor) and is supplied by the abducens nerve.

The **superior oblique** (see ► Fig. 3.2c, ► Fig. 3.2d, ► Fig. 3.3c, ► Fig. 3.3d, ► Fig. 3.4b, ► Fig. 3.4c, ► Fig. 3.4d, and ► Fig. 6.12a) first runs forward to the superior aspect of the medial orbital wall. Its tendon then runs through a cartilaginous half-ring, the trochlea, and turning back at an angle of 55°, it then runs medially to the vertical axis to the postero-lateral quadrant of the eyeball. It is mainly an ocular depressor, as its effective terminal segment pulls anteriorly, while also abducting and internally rotating the eye. Internal rotation increases in direct proportion to the degree of abduction. The muscle is innervated by the trochlear nerve.

The **inferior oblique** (see ► Fig. 3.2c, ► Fig. 4.5c, ► Fig. 4.5d, ► Fig. 4.6c, and ► Fig. 6.8a) originates anteriorly from the floor of the orbit close to the entrance of the nasolacrimal duct, and running obliquely backward, it forms an angle of about 50° with the visual axis. Its tendon inserts into the posterior and lateral quadrants and its effective terminal segment lies medial to the vertical axis. The muscle elevates the eye and causes abduction and outward rotation. It is innervated by the oculomotor nerve.

See ► Section 10.8.3 for clinical notes pertaining to functional disturbances of ocular muscles.

8.3.5 Vessels of the Orbit

The **ophthalmic artery**, a branch of the internal carotid, is the main artery of the orbit and exits the middle cranial fossa through the optic canal, lying below the optic nerve. It enters the orbit through the common tendinous ring. It usually crosses the optic nerve and lies laterally (see ► Fig. 3.4c, ► Fig. 3.5c, ► Fig. 3.5d, ► Fig. 5.6a, ► Fig. 5.6b, and ► Fig. 7.19b) running forward above the superior oblique (see ► Fig. 3.3c). Branches of the ophthalmic artery supply the contents of the orbit and contribute to the blood supply of the eyelids, mucous membranes of the ethmoid and sphenoid sinuses, and the face and scalp regions. In the orbit, it usually **anastomoses** with branches of the middle meningeal artery. The artery receives most of its vascular supply from the middle meningeal artery in four percent of cases. Larger anastomoses with terminal branches of the ophthalmic artery with the facial artery

are seen at the medial canthus of the eye and in the temporal region with the superficial temporal branch of the external carotid artery. These arterial anastomoses between the branches of the internal and external carotid arteries are of clinical significance. Blood supply can often be maintained by these anastomoses in the presence of stenoses or occlusions of the internal carotid artery. The direction of flow in the ophthalmic artery may be determined by Doppler sonography.^{20,421,618}

Branches of the Ophthalmic Artery:

- The central artery of the retina, measuring 0.2 mm in width, supplies the optic nerve and its occlusion leads to blindness.
- Other branches from the ophthalmic artery supply the choroid of the eyeball, the lacrimal gland, ethmoidal cells and sphenoid sinus, the medial canthus, and the forehead.
- The anterior ethmoidal artery has already been mentioned in the description of the nasal cavity. This artery courses through the anterior ethmoidal foramen and reaches the anterior cranial fossa where it gives off the anterior meningeal artery. It then passes through the lamina cribrosa into the anterior part of the nasal cavity.

The **veins of the orbit** almost always run independent of the arteries and are generally wider in caliber. The superior ophthalmic vein (see ► Fig. 3.3c, ► Fig. 3.4c, ► Fig. 3.4d, ► Fig. 3.5c, ► Fig. 5.6a, ► Fig. 5.6b, and ► Fig. 7.35b) drains blood from the eyeball, upper part of the orbit, eyelid, and ethmoidal cells. It anastomoses with the facial vein and, via the superior orbital fissure, with the cavernous sinus. Blood from the orbital cavity drains not only for-

ward to the face but also posteriorly to the cavernous sinus due to the absence of valves in both the superior ophthalmic and the facial veins. Furuncles or purulent infections of the face may result in meningitis due to venous drainage into the cavernous sinus. The inferior ophthalmic vein runs along the floor of the orbit and drains into the superior ophthalmic vein, or through the inferior orbital fissure into the pterygoid venous plexus.

8.3.6 Nerves of the Orbit

Branches of the **ophthalmic nerve** arising from the trigeminal nerve provide sensory innervation to the eyeball, mainly to the cornea and the conjunctiva, but also to the lacrimal gland, upper lid, the skin of the forehead and medial canthus, the mucous membrane of ethmoidal cells and sphenoid sinus, as well as to the anterior part of the nasal mucosa and the skin of the bridge of the nose (see ► Fig. 8.2).

The ophthalmic nerve divides as a rule into its **four main branches** before it enters the superior orbital fissure:

- A branch which courses backward toward the tentorium cerebelli.
- Lacrimal nerve, which runs over the lateralis rectus to the lacrimal gland.
- Frontal nerve (see ► Fig. 3.4a, ► Fig. 8.2, and ► Fig. 10.7a), which lies on the levator palpebrae superioris and then divides into branches for the forehead (including the supraorbital nerve (see ► Fig. 3.2a, ► Fig. 3.3a, ► Fig. 8.2, and ► Fig. 10.7a), a pressure point for the first division of the Vth cranial nerve above the orbit).

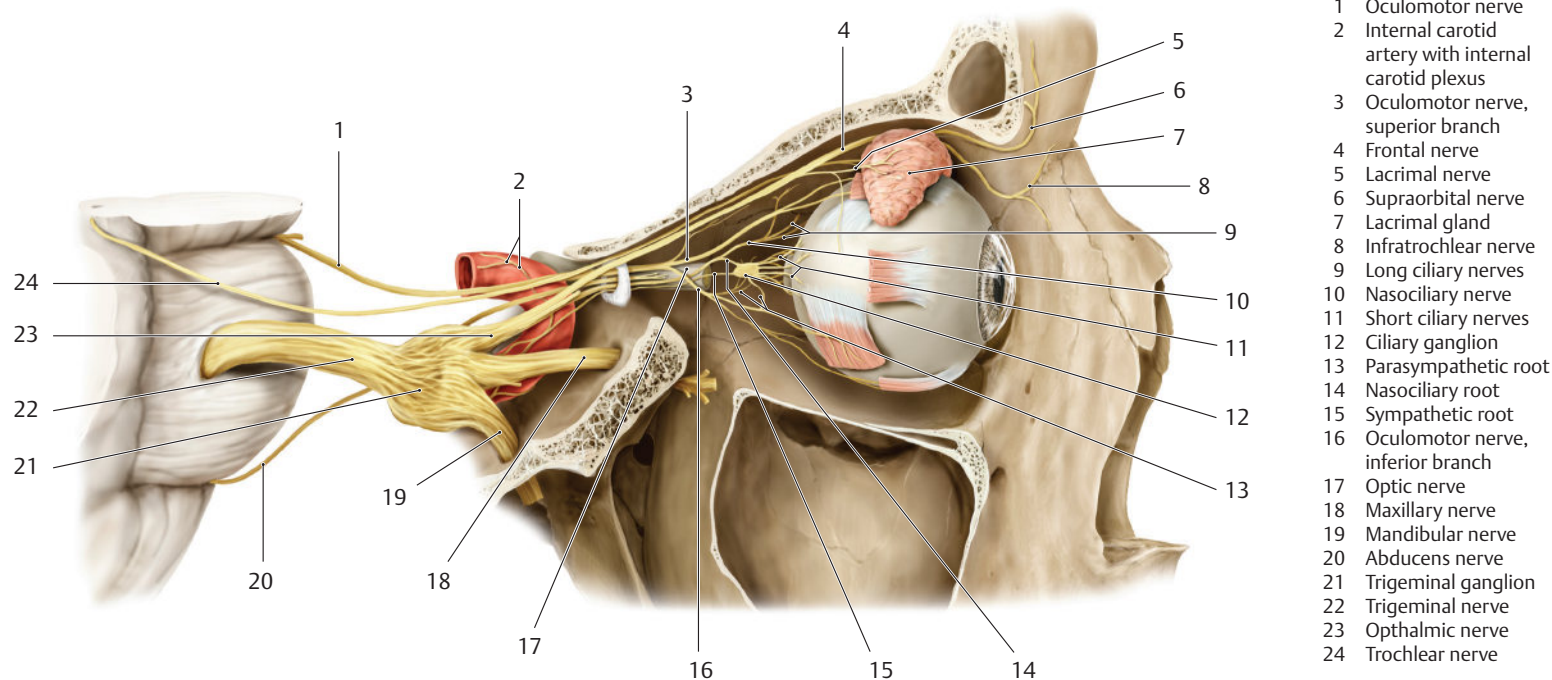


Fig. 8.2 Innervation of the orbit. Schematic representation of the right orbit after removal of the temporal wall. (Reproduced from Schuenke, Schulte, and Schumacher, *Atlas of Anatomy*, 2nd edition, ©2009, Thieme Publishers, Stuttgart. Illustration by Karl Wesker/Markus Voll.⁵³⁵)

- Nasociliary nerve (see ►Fig. 3.3a, ►Fig. 3.4a, ►Fig. 8.2, and ►Fig. 10.7a), which lies within the muscular cone and gives branches to the eyeball, the mucus membrane lining ethmoidal cells and sphenoid sinus as well as to the anterior nasal cavity, and finally branches to the skin of the medial canthus and the bridge of the nose.

The motor nerve supply to the six extraocular muscles and the levator palpebrae superioris is derived from the IIIrd, IVth, and VIth cranial nerves. In addition, the IIIrd cranial nerve transmits parasympathetic impulses to the ciliary ganglion, which are then relayed to postganglionic fibers innervating intrinsic muscles of the eye, namely the sphincter pupillae and the ciliary muscle.

The **oculomotor nerve** (see ►Fig. 3.1c, ►Fig. 3.5a, and ►Fig. 8.2) enters the orbit through the superior orbital fissure and the common tendinous ring. It then divides into a superior division for the superior rectus and the levator palpebrae superioris, and a larger inferior division (see ►Fig. 3.4a) which supplies the medial rectus, inferior rectus, and the inferior oblique. In addition, this inferior division gives off a branch to the ciliary ganglion (see ►Fig. 8.2 and ►Fig. 10.43b). This parasympathetic ganglion is, on average, 3 mm long and is situated 18 mm behind the eyeball.³³²

The **trochlear nerve** (see ►Fig. 3.4a and ►Fig. 3.5a) runs through the superior orbital fissure and above the common tendinous ring. This nerve thus lies above the muscle cone and supplies the superior oblique.

The **abducens nerve** (see ►Fig. 3.4a and ►Fig. 3.5a) runs through the superior orbital fissure and the common tendinous ring to supply the lateral rectus.

The infraorbital nerve runs on or within the floor of the orbit (see ►Fig. 3.2a, ►Fig. 3.2b, ►Fig. 3.3a, ►Fig. 3.3b, ►Fig. 3.4a, ►Fig. 3.4b, ►Fig. 4.5a, ►Fig. 5.3, and ►Fig. 10.7a) without supplying any of its contents.

8.3.7 Eyeball

The eyeball (see ►Fig. 3.2a, ►Fig. 3.2b, ►Fig. 4.5a, ►Fig. 4.5b, ►Fig. 4.6a, ►Fig. 4.6b, ►Fig. 5.5, ►Fig. 5.17, ►Fig. 6.10a, and ►Fig. 10.18) is approximately spherical in shape with a diameter of 24 mm. Anteriorly the eyeball is covered by the translucent cornea. The axis of the globe runs through its anterior and posterior poles. The optic nerve leaves the eyeball immediately medial to the posterior pole in the region of the optic disc (see ►Fig. 3.2a), where retinal nerve fibers converge. The fovea centralis of the retina (see ►Fig. 3.2a), the center of the eye's sharpest vision, is located lateral to the optic disc. The optic axis runs through the fovea centralis and through the point of maximal curvature of the lens and the cornea. The equator of the globe is the maximum diameter of the eyeball in the coronal plane.

The **wall of the eyeball** is composed of three layers:

- The external layer is comprised of two parts: the sclera and the cornea.

- The middle layer (uvea) consists of the choroid, the ciliary body, and the iris. The sphincter and dilator pupillae lie within the iris.
- The inner layer is the retina, comprising an optic part containing the rods and/or cones (visual receptor cells) and a nonvisual retina (devoid of receptor cells).

The anterior segment of the eyeball has two chambers, anterior and posterior, separated by the iris. The posterior chamber abuts the vitreous body.

The **lens** (see ►Fig. 4.5a and ►Fig. 6.10a) is suspended by zonular fibers in the posterior chamber. Ocular structures involved in accommodation for near and far vision include the lens, zonular fibers, ciliary body, and iris. Contraction and dilatation of the pupils are coordinated by the sphincter and dilator pupillae during accommodation. Further details about the eyeball maybe found in the literature.^{263,332}

8.3.8 Optic Nerve

The **optic nerve** (see ►Fig. 3.3a, ►Fig. 3.3b, ►Fig. 3.4a, ►Fig. 3.4b, ►Fig. 3.5a, ►Fig. 3.5b, ►Fig. 4.4a, ►Fig. 4.5a, ►Fig. 4.5b, ►Fig. 5.17, and ►Fig. 6.10a) begins at the lamina cribrosa of the sclera. Its average intraorbital length is 3 cm³³² and it is surrounded by a firm dural layer as well as by pia and arachnoid. The slightly sinuous course of the optic nerve in the orbit facilitates the free movement of the eyeball. The sheath of the optic nerve is closely attached to the bony walls of the optic canal. MRI is an important diagnostic tool in the assessment of various lesions involving the optic nerve.

8.4 Oral Cavity

The **oral cavity** (see ►Fig. 3.2a, ►Fig. 3.2b, ►Fig. 3.3a, ►Fig. 3.4a, ►Fig. 3.4b, ►Fig. 3.5a, ►Fig. 4.2a, ►Fig. 4.2b, ►Fig. 4.3a, ►Fig. 4.4a, and ►Fig. 4.5a) begins at the lips and extends up to the isthmus of the fauces (see ►Fig. 3.6a and ►Fig. 3.6b). The mouth is divided into two regions by the two rows of teeth and the alveolar margins of the maxilla and mandible covered by the gums: the oral vestibule, a slit-like space between the lips or cheeks and the teeth, and the oral cavity proper.

Inspection and palpation of oral lesions, and tumor biopsy if necessary, often suffice for clinical diagnosis. Modern imaging methods may be required for therapy planning and follow-up to enable accurate assessment of the extent and nature of a neoplastic growth as well as its malignant behavior. Such information is essential for a surgeon, for instance, who must decide whether a given patient requires a partial or total glossectomy. Topographic relationships of the oral cavity, particularly with its neighboring areas such as the infratemporal fossa (deep lateral facial region) and the oropharynx, will therefore be emphasized on in this chapter and in the following sections. The reader should refer to special literature for systematic description of the oral cavity.^{176,517,623}

8.4.1 Roof of the Mouth

The roof of the mouth is formed in its anterior two-thirds by the hard palate and in its posterior one-third by the soft palate.

The **hard palate** (see ► Fig. 3.1b, ► Fig. 3.2c, ► Fig. 3.2d, ► Fig. 3.3c, ► Fig. 3.3d, ► Fig. 3.4c, ► Fig. 3.4d, ► Fig. 3.16, ► Fig. 3.17, ► Fig. 4.3c, ► Fig. 4.3d, and ► Fig. 4.8) also forms the floor of the nasal cavity. A branch of the sphenopalatine artery and a branch of the nasopalatine nerve run from the nasal cavity into the mouth through the **incisive canal** (see ► Fig. 4.2c and ► Fig. 4.8).

The **soft palate** (see ► Fig. 3.5c, ► Fig. 3.5d, ► Fig. 3.6c, and ► Fig. 3.18) is mobile and extends posteriorly up to the median unpaired uvula (see ► Fig. 3.6a, ► Fig. 3.6c, ► Fig. 4.2a, and ► Fig. 4.2b). The muscles of the soft palate, namely the tensor veli palatini (see ► Fig. 3.5c, ► Fig. 3.5d, and ► Fig. 4.4c) and the levator veli palatini, function as its tensor and elevator, respectively.

8.4.2 Floor of the Mouth

The floor of the mouth is muscular, being comprised of the mylohyoid, geniohyoid, and digastric muscles which are connected either directly or indirectly with the hyoid bone.

- The **mylohyoid** (see ► Fig. 3.2c, ► Fig. 3.2d, ► Fig. 3.3c, ► Fig. 3.3d, ► Fig. 3.4c, ► Fig. 3.4d, ► Fig. 3.5c, ► Fig. 4.2c, ► Fig. 4.3c, ► Fig. 4.4c, and ► Fig. 4.5c) is a paired muscle forming the muscular floor of the oral cavity. Each muscle arises from the respective mylohyoid line of the mandible and is innervated by the mylohyoid nerve from the third division of the trigeminal nerve and the mandibular nerve.
- The **geniohyoid** (see ► Fig. 3.2c, ► Fig. 3.2d, ► Fig. 3.3c, ► Fig. 3.3d, ► Fig. 3.4c, ► Fig. 3.4d, ► Fig. 4.2c, ► Fig. 4.3c, and ► Fig. 4.4c) lies along the medial aspect of the mylohyoid and is innervated by the second spinal nerve.
- The anterior belly of the **digastric** arises from the inner surface of the mandible and lies below the mylohyoid (see ► Fig. 3.2c, ► Fig. 3.2d, ► Fig. 3.3c, ► Fig. 3.3d, ► Fig. 3.4c, ► Fig. 3.4d, ► Fig. 4.3c, and ► Fig. 4.4c). The digastric possesses an intermediate tendon that passes into the posterior belly (see ► Fig. 3.5c, ► Fig. 3.6c, and ► Fig. 4.5c). The muscle is innervated by the mylohyoid nerve from the third division of the trigeminal nerve and the mandibular nerve. The posterior belly of the digastric finds attachment at the inner aspect of the mastoid process (see ► Fig. 3.7c, ► Fig. 3.7d, ► Fig. 3.8c, ► Fig. 3.8d, ► Fig. 3.9c, ► Fig. 3.9d, ► Fig. 3.10c, ► Fig. 3.10d, ► Fig. 4.6c, ► Fig. 4.6d, and ► Fig. 4.7c) and is innervated by the facial nerve.

8.4.3 Tongue

The tongue lies on the floor of the mouth. Bounded by the mandible it appears mushroom or block shaped in coronal sections (see ► Fig. 3.2a, ► Fig. 3.2b, ► Fig. 3.3a, ► Fig. 3.3b, ► Fig. 3.4a, ► Fig. 3.4b, ► Fig. 3.5a, and ► Fig. 3.5b) while its tip, body and base may be identified in sagittal sections (see ► Fig. 4.2a, ► Fig. 4.2b, ► Fig. 4.3a,

► Fig. 4.3b, and ► Fig. 4.4a). The tongue is a muscular organ lined by mucous membrane. On the dorsum of the tongue a shallow furrow, the terminal sulcus, divides the tongue into the posterior base and the anterior body. Vallate papillae lie immediately anterior to the sulcus.

The tongue is very mobile. Its extrinsic muscles arise from the inner aspect of the mandible, hyoid, and styloid process and allow the tongue to move in their direction of pull:

- Genioglossus
- Hyoglossus
- Styloglossus

The intrinsic muscles of the tongue permit a change in shape and consist of vertical, longitudinal, and transverse muscle fibers which interweave perpendicularly in the three spatial planes. The tongue is innervated by the hypoglossal nerve which reaches the tongue from the floor of the mouth (see ► Fig. 3.2a, ► Fig. 3.3a, ► Fig. 3.4a, ► Fig. 3.5a, ► Fig. 3.10a, ► Fig. 4.3a, and ► Fig. 4.4a).

Clinical Notes

A peripheral paresis of the hypoglossal nerve results in a puckering of the surface of the tongue and a reduction of its muscle mass. With unilateral peripheral hypoglossal paresis, the tongue deviates to the paretic side when extended.

8.4.4 Isthmus of Fauces

The isthmus of fauces (see ► Fig. 3.6a and ► Fig. 3.6b) connects the oral cavity with the oropharynx. Two mobile palatal folds are identified, the palatoglossal and the palatopharyngeal arches which can close off the oropharynx. Similarly named muscles are present within the palatoglossal and palatopharyngeal arches, spreading out into the soft palate. During nasal breathing these muscles, together with the muscles of the uvula, close off the oral cavity.

The **palatoglossus** and **palatopharyngeus** surround the palatine tonsil, which is seen as a small structure on the coronal (see ► Fig. 3.6a and ► Fig. 3.6b) and sagittal images (see ► Fig. 4.3a and 4.3b).

8.4.5 Vessels of the Oral Cavity

The walls of the oral cavity receive a rich blood supply from branches of the external carotid artery which have several anastomoses. The lingual artery runs above the hyoid bone (see ► Fig. 3.6c, ► Fig. 3.7c, and ► Fig. 9.1) and supplies the tongue. The floor of the mouth is supplied by the submental artery (see ► Fig. 3.2c, ► Fig. 3.3c, ► Fig. 3.4c, and ► Fig. 3.5c), a branch of the facial artery, while the roof of the mouth receives its arterial supply through branches of the facial, maxillary, and ascending pharyngeal arteries (see ► Fig. 9.1).

Venous drainage of the oral cavity takes place through tributaries of the internal jugular vein (see ► Fig. 9.2).

Regional lymphatic pathways from the tongue and the palate drain to the submandibular and to the deep cervical lymph nodes.

8.4.6 Afferent Nerves of the Oral Cavity

The **lingual nerve**, a branch of the mandibular nerve (see ►Fig. 3.3a, ►Fig. 3.4a, ►Fig. 3.5a, ►Fig. 3.6a, ►Fig. 4.3a, ►Fig. 4.4a, and ►Fig. 4.5a), supplies sensory innervation to the mucous membrane of the tip of the tongue, while the **glossopharyngeal nerve** innervates the region of the terminal sulcus, and the vagus nerve innervates the base of the tongue. The **chorda tympani** (see ►Fig. 7.5 and ►Fig. 10.43b), a branch of the facial nerve, carries afferent taste sensations from the anterior two-thirds of the tongue. The taste buds of the vallate papillae are supplied by the glossopharyngeal nerve and taste receptors in the base of the tongue receive sensory fibers from the vagus. The roof of the mouth receives its sensory innervation from branches of the maxillary nerve (second division of the Vth cranial nerve).

8.5 Masticatory Apparatus

8.5.1 Temporomandibular Joint

The head of the mandible articulates with the articular surface of the mandibular fossa and the articular tubercle to form the temporomandibular joint (see ►Fig. 3.7c, ►Fig. 3.7d, ►Fig. 4.7c, ►Fig. 4.7d, and ►Fig. 4.13). An articular cartilage named the articular disc is interposed between the head of the mandible and the articular surface of the temporal bone (see ►Fig. 3.7c, ►Fig. 4.7c, ►Fig. 4.7d, ►Fig. 6.5a, and ►Fig. 6.6a). The articular surface of the mandibular fossa is much larger than that of the head of the mandible, which together with a slack joint capsule allows great mobility to the heads of the mandible. As the mouth opens, the heads of the mandible glide forward on their articular discs onto their articular tubercles, a combination of hinge and gliding movements. During mastication the mandible performs unilateral rotational movements around a vertical axis, alternating between the two sides.

8.5.2 Muscles of Mastication

These are a group of four muscles that arise from the lateral wall or the base of the skull and insert into the mandible and are supplied by motor branches of the third division of the mandibular nerve. Their topography is clearly seen in coronal sections (see ►Fig. 7.37).

- The **temporalis** (see ►Fig. 3.2c, ►Fig. 3.2d, ►Fig. 3.3c, ►Fig. 3.3d, ►Fig. 3.4b, ►Fig. 3.4c, ►Fig. 3.4d, ►Fig. 3.5c, ►Fig. 3.5d, ►Fig. 3.6c, ►Fig. 3.6d, ►Fig. 3.7c, ►Fig. 3.7d, ►Fig. 3.8c, ►Fig. 4.6c, ►Fig. 4.6d, ►Fig. 4.7c, ►Fig. 4.7d, ►Fig. 5.5, and ►Fig. 6.5a) is a fan-shaped muscle and arises from the temporal fossa. Its fibers converge to insert into the coronoid process of the mandible (see ►Fig. 3.1b, ►Fig. 3.4c, ►Fig. 3.4d, ►Fig. 3.5c, ►Fig. 3.5d, ►Fig. 4.7c, and ►Fig. 4.7d). Muscle fibers

of the temporalis are arranged in a bipennate fashion, exhibiting a complex cross-sectional appearance. It is a powerful muscle for biting.

- The **masseter** (see ►Fig. 3.3c, ►Fig. 3.3d, ►Fig. 3.4b, ►Fig. 3.4c, ►Fig. 3.4d, ►Fig. 3.5c, ►Fig. 3.5d, ►Fig. 3.6c, ►Fig. 3.6d, ►Fig. 3.7c, ►Fig. 4.7c, ►Fig. 4.7d, ►Fig. 5.2, ►Fig. 5.3, and ►Fig. 6.4a) arises from the zygomatic arch (see ►Fig. 3.1b, ►Fig. 3.4c, ►Fig. 3.4d, ►Fig. 3.5c, ►Fig. 3.5d, ►Fig. 3.6c, and ►Fig. 3.6d) and inserts into the lateral aspect of the ramus of the mandible (see ►Fig. 3.5c, ►Fig. 3.5d, ►Fig. 3.6c, ►Fig. 3.6d, ►Fig. 3.7c, ►Fig. 3.7d, and ►Fig. 4.12). It works in tandem with the temporal and medial pterygoid muscles.
- The **medial pterygoid** arises from the pterygoid fossa of the sphenoid (see ►Fig. 3.5c and ►Fig. 3.5d) and inserts into the medial surface of the ramus of the mandible (see ►Fig. 3.6c, ►Fig. 3.6d, ►Fig. 3.7c, and ►Fig. 3.7d) and forms a muscular sling with the masseter.
- The **lateral pterygoid** originates as two headed muscle (see ►Fig. 3.5c, ►Fig. 3.5d, and ►Fig. 5.2). The upper (superior) head arises from the under surface of the greater wing of the sphenoid, while the lower (inferior) head arises from the lateral pterygoid plate. Both parts run together nearly horizontally and are therefore sectioned transversely in coronal sections (see ►Fig. 3.6c, ►Fig. 3.6d, ►Fig. 3.7c, and ►Fig. 3.7d). The muscle runs obliquely from medial to lateral and is hence obliquely sectioned in the sagittal plane (see ►Fig. 4.5c, ►Fig. 4.5d, ►Fig. 4.6c, ►Fig. 4.6d, and ►Fig. 4.7c). The muscle is inserted into the condylar process of the mandible and pulls the corresponding ramus of the mandible obliquely forward and inward. Unilateral contraction enables grinding movements for chewing; bilateral contraction assists in opening the mouth by gliding movements.

The muscles of the lips, the cheeks, and the tongue also participate in the act of chewing along with the muscles of mastication.

8.6 Lateral Facial Region

The lateral facial region includes the space that extends from the zygomatic arch above (see ►Fig. 3.1b, ►Fig. 3.4c, ►Fig. 3.4d, ►Fig. 3.5c, ►Fig. 3.5d, ►Fig. 3.6c, and ►Fig. 3.6d) to the angle of the mandible below (see ►Fig. 3.1b). Anteriorly the lateral facial region continues into the cheeks without a sharp boundary, includes the auricle and the external acoustic canal posteriorly (see ►Fig. 3.9c and ►Fig. 3.9d), and is divided by the ramus of the mandible (see ►Fig. 3.5c, ►Fig. 3.5d, ►Fig. 3.6c, ►Fig. 3.6d, ►Fig. 3.7c, and ►Fig. 3.7d) into superficial and deep lateral facial regions.

8.6.1 Superficial Lateral Facial Region

The superficial lateral facial region contains the masseter (see ►Fig. 3.4c, ►Fig. 3.4d, ►Fig. 3.5c, ►Fig. 3.5d,

►Fig. 3.6c, and ►Fig. 3.6d), a powerful muscle of mastication (see ►Section 8.5.2). Anterior to this muscle lies the buccal pad of fat and posteriorly the **parotid gland** (see ►Fig. 3.6c, ►Fig. 3.6d, ►Fig. 3.7b, ►Fig. 3.7c, ►Fig. 3.7d, ►Fig. 3.8, and ►Fig. 5.2), with only a small part of this gland lying superficial to the masseter (see ►Fig. 3.6c and ►Fig. 3.6d). The parotid duct arises from the upper part of the gland and drains into the vestibule of the mouth (see ►Fig. 3.4c and ►Fig. 3.4d). The parotid is ensheathed by the parotid fascia which contains the gland, a plexus formed by the facial nerve, branches of the auriculotemporal nerve, a segment of the external carotid artery, the retromandibular vein (see ►Fig. 9.2), and lymph nodes.

The external ear consists of the **auricle or pinna** (see ►Fig. 3.9c and ►Fig. 3.9d) and the **external acoustic canal** (see ►Fig. 3.9c). In adults, the external acoustic canal is about 36 mm long. The medial two-thirds of the canal lie within the temporal bone while the lateral third is reinforced with cartilage and lies for the large part behind the head of the mandible (see ►Fig. 3.8c, ►Fig. 3.8d, and ►Fig. 4.13). The tympanic membrane or eardrum (see ►Fig. 3.9c) is a thin membrane separating the external acoustic canal from the tympanic cavity (see ►Fig. 3.9c and ►Fig. 7.5).

8.6.2 Deep Lateral Facial Region

The deep lateral facial region is largely occupied by the infratemporal fossa. The lateral wall of the infratemporal fossa, the ramus of the mandible has already been mentioned. Its medial wall is formed by the lateral pterygoid plate of the sphenoid bone (see ►Fig. 3.5c, ►Fig. 3.5d, and ►Fig. 3.18). The infratemporal fossa continues backward and medially into the parapharyngeal space, the border between these two spaces being formed by the medial surfaces of the lateral and medial pterygoid (see ►Fig. 3.7c and ►Fig. 3.7d). Anteriorly the infratemporal fossa extends up to the posterior wall of the maxillary sinus (see ►Fig. 3.4 and ►Fig. 4.10). This interface lies within the third coronal slice (see ►Fig. 3.4c). The infratemporal fossa continues into the superficial lateral facial region further posteriorly beyond the ramus of the mandible. The roof of the infratemporal fossa is formed by the infratemporal surface of the greater wing of the sphenoid containing the foramen ovale (see ►Fig. 4.11 and ►Fig. 5.37b). The infratemporal fossa also continues superolaterally into the temporal fossa, with the inferior part of the temporalis being located in this region (see ►Fig. 4.7c and ►Fig. 4.7d).

8.6.3 Vessels of the Lateral Facial Region

The **external carotid artery** runs vertically through the parotid gland. In the coronal series this section of the artery is located within the sixth slice (see ►Fig. 3.7c) and is, therefore, not visible on the surface of the section. The external carotid artery bifurcates into its two

terminal branches, the superficial temporal and the maxillary arteries at the level of the temporomandibular joint (see ►Fig. 9.1). The maxillary artery runs medially from the neck of the mandible to the infratemporal fossa usually lying lateral to the lateral pterygoid (see ►Fig. 4.6c and ►Fig. 4.6d). The artery is seen on the medial aspect of the lateral pterygoid in ►Fig. 3.7c, ►Fig. 3.7d, ►Fig. 3.6c, and ►Fig. 3.6d of the coronal series. Running into the pterygopalatine fossa (see ►Fig. 4.4c and ►Fig. 4.4d) it then divides into its terminal branches. The maxillary artery supplies the muscles of mastication and most of the nasal and oral mucosa, the teeth, the palate, the greater part of the dura, and bones of the skull.

Veins form the pterygoid venous plexus in the infratemporal fossa (see ►Fig. 3.7c and ►Fig. 7.35b), an extensive network that drains through the maxillary veins into the retromandibular vein (see ►Fig. 9.2).

The lymphatic vessels drain into deep cervical and retropharyngeal lymph nodes.

8.6.4 Nerve Supply of the Lateral Facial Region

The facial nerve (see ►Fig. 3.9a) emerges from the stylomastoid foramen (see ►Fig. 3.9c and ►Fig. 5.37b), giving off a small branch to the posterior belly of the digastric. The nerve then runs through the parotid gland where it divides into separate branches that supply the muscles of facial expression.

The **mandibular nerve** (see ►Fig. 4.5a and ►Fig. 4.5b) runs through the foramen ovale to the infratemporal fossa, the main trunk of the nerve being closely related to the otic ganglion immediately below the base of the skull (see ►Fig. 4.5a, ►Fig. 4.5b, and ►Fig. 10.43b). The mandibular nerve provides motor innervation to the muscles of mastication and of the floor of the mouth. It is the sensory nerve to the floor of the mouth, to the lingual mucosa in its anterior two-thirds, as well as to the skin over the lower jaw. The mandibular nerve (see ►Fig. 3.7a, ►Fig. 4.5a, and ►Fig. 4.5b) divides in the upper part of the infratemporal fossa:

- Some branches innervate muscles of mastication.
- The buccal nerve innervates the mucous membrane and skin over the lower jaw.
- The inferior alveolar nerve supplies teeth of the lower jaw. It enters the mandibular foramen (see ►Fig. 4.7a and ►Fig. 4.7c) and runs in the mandibular canal (see ►Fig. 3.2a, ►Fig. 3.3a, ►Fig. 3.4a, ►Fig. 3.5a, ►Fig. 3.6a, ►Fig. 4.3a, ►Fig. 4.4a, ►Fig. 4.5a, and ►Fig. 4.6a). Its terminal branch emerges through the mental foramen and supplies the skin of the chin and the lower lip.
- The **lingual nerve** (see ►Fig. 3.3a, ►Fig. 3.4a, ►Fig. 3.5a, and ►Fig. 3.6a) innervates the lingual mucous membrane. In the infratemporal fossa, it is joined posteriorly by the **chorda tympani** which carries the preganglionic parasympathetic fibers to the submandibular ganglion and contains taste fibers for the tongue.

9 Topography of the Head–Neck Region

The head–neck region may be described as the region between the head and neck. From a systematic view point, the pharynx is considered part of the neck. In clinical practice, lesions of the nasal cavity spread easily into the nasopharynx or vice versa. Anatomically and pathologically the oral cavity is closely related to the oropharynx. The topography of the pharynx will first be elaborated upon in this chapter, particularly in the clinical context of its relationships with the nasal and oral cavities. The region of the craniocervical junction extending from the postero-inferior surface of the base of the skull (level of the mastoid processes to the external occipital protuberance), down to the first two cervical vertebrae and the attached muscles³³² will be described thereafter.

9.1 Pharynx and Parapharyngeal Space

9.1.1 Topography of the Pharynx

The **pharynx** is a 12- to 15-cm-long fibromuscular tube extending from the base of the skull to the commencement of the esophagus at the level of the cricoid cartilage. It lies anterior to the cervical spine and extends up to the VIth cervical vertebra. Flexion and extension of the cervical spine can alter the cross-sectional appearance of the pharynx. In the coronal series, the posterior wall of the pharynx is imaged in a coronal plane (see ► Fig. 3.7c and 3.7d); while in the sagittal series, it runs obliquely to the coronal plane (see ► Fig. 4.2a and ► Fig. 4.2b).

Unlike the closed posterior wall, the anterior wall exhibits three openings for the passage of air and food. The pharynx is thus divided into:

- **Nasopharynx:** This proximal part (previously: epipharynx) communicates with the nasal cavities through the choanae.
- **Oropharynx:** This middle part (previously: mesopharynx) communicates with the oral cavity through the isthmus of fauces.
- **Laryngopharynx:** The distal part of the pharynx from where the aditus laryngis continues into the larynx.

Median and paramedian sections are best suited for evaluation of the nasopharynx and the oropharynx, which also enable optimal delineation of the retropharyngeal space.

The **nasopharynx** (see ► Fig. 3.6a, ► Fig. 3.6b, ► Fig. 3.7c, ► Fig. 3.7d, ► Fig. 4.2a, and ► Fig. 4.2b) is functionally similar to the nasal cavity with a similar mucus membrane and a multilayered ciliated epithelium. The roof of the nasopharynx forms the outer aspect of the base of the skull, between the pharyngeal tubercle of the occipital bone, the apex of the temporal bone, and a small part of the inferior surface of the sphenoid. The unpaired pharyngeal tonsil lies on the posterior wall of the nasopharynx. ► Fig. 4.2a demonstrates an atrophic pharyngeal tonsil of a 70-year-old man. The pharyngeal opening of

the **pharyngotympanic tube** (Eustachian tube) is present on the lateral wall of the nasopharynx along the posterior prolongation of the inferior nasal concha. The superior and posterior edges of this opening are elevated by the cartilaginous part of the tube. The levator veli palatini produces an elevation of the mucous membrane at the lower margin of the tubal opening. Lymphoreticular connective tissue, the tubal tonsil, is present within the mucosa of the tubal orifice. This forms part of pharyngeal lymphoid tissue, which if pathologically enlarged may interfere with ventilation of the tympanic cavity.

The **oropharynx** (see ► Fig. 3.7c, ► Fig. 4.2a, ► Fig. 4.2b, and ► Fig. 4.3a) is the space behind the root of the tongue, the paired palatopharyngeal arches, and the uvula. Radiologists⁵⁹⁴ define the oropharynx as the part of the pharynx extending from the level of the hard palate to the hyoid bone.

The most inferior part of the pharynx, the **laryngopharynx**, begins opposite the laryngeal opening and extends downward up to the entrance to the esophagus. The posterior wall of the larynx bulges into the lumen of the pharynx.

9.1.2 Muscles of the Pharyngeal Wall

The muscles of the pharyngeal wall comprise:

- Constrictors of the pharynx
- Slender elevators of the pharynx, namely the palatopharyngeus and the stylopharyngeus

The topography of these thin muscles of the pharyngeal wall can best be understood by comparison of coronal and sagittal series (see ► Fig. 7.37 and ► Fig. 7.38).

The superior, middle, and inferior **constrictors of the pharynx** arise from the skull, the hyoid bone, and the larynx and their fibers run posteriorly and upward to meet in the midline raphe on the posterior wall of the pharynx. Contraction of the pharyngeal constrictors pulls the hyoid bone and the larynx upwards simultaneously. The superior constrictor bulges into the pharyngeal lumen (Passavant's ridge), which provides resistance against the soft palate closing off the nasal cavity. The pharyngeal constrictor is innervated by the glossopharyngeal (N. IX) and vagus (N. X) nerves.

The **pharyngeal elevators** contract and elevate the walls of the pharynx and the larynx and insert into the larynx. They are supplied by the glossopharyngeal (N. IX) nerve.

9.1.3 Vessels of the Pharyngeal Wall

The **ascending pharyngeal artery** supplies the wall of the pharynx and forms numerous anastomoses with branches from the superior and inferior thyroid and lingual arteries.

Venous drainage takes place through the pharyngeal plexus, which lies posterior to the constrictors of the pharynx.

Lymphatics from the pharyngeal wall run via retro-pharyngeal lymph nodes to deep cervical lymph nodes.

9.1.4 Nerves of the Pharyngeal Wall

Afferent and efferent innervation of the pharyngeal wall is provided by the glossopharyngeal (N. IX) and vagus (N. X) nerves and the sympathetic trunk. They are pathways of vital reflexes such as the swallowing and the protective reflexes. Afferent and efferent pathways of the swallowing reflex are coordinated in the swallow-center of the medulla oblongata.

9.1.5 Parapharyngeal Space

The parapharyngeal (lateral pharyngeal) space lies in the transitional zone between head and neck, lateral and posterolateral to the pharynx. Laterally this space is bounded by the lateral and medial pterygoids and the fascial capsule of the parotid gland, while medially it extends up to the pharyngeal wall. Its cranial boundary is marked by the triangular area at the base of the skull, which contains the openings for the internal carotid arteries, the jugular foramen, and the hypoglossal canal. Caudally it extends into the connective tissue layer of the carotid triangle. The styloid process with the stylopharyngeus, styloglossus, and stylohyoid project cranially into the parapharyngeal space, dividing it into anterior and posterior compartments.

- The **anterior compartment** contains fat through which run small vessels including the ascending pharyngeal artery (see ► Fig. 9.1).
- All of the following course through the **posterior compartment**: the internal carotid artery (see ► Fig. 3.8c, ► Fig. 3.8d, ► Fig. 4.5c, and ► Fig. 4.5d), the internal jugular vein (see ► Fig. 3.9c, ► Fig. 3.9d, ► Fig. 4.6c, and ► Fig. 4.6d), the glossopharyngeal nerve (see ► Fig. 3.9a and ► Fig. 4.5a), the vagus nerve (see ► Fig. 3.8a and ► Fig. 4.5a), the accessory nerve (see ► Fig. 3.9a and ► Fig. 4.5a), and the hypoglossal nerve (see ► Fig. 3.9a and ► Fig. 4.5a).

Division into spaces is presently based on the layers of cervical fascia and the pathways through which disease processes may spread and the probability of their occurrence (see ► Fig. 5.2a). Abbreviations used conform to their generally acknowledged English names (e.g., BS = buccal space). The parapharyngeal space is easily identified on coronal sections and is usually bilaterally symmetrical, with any departure from this symmetry suggesting a space-occupying lesion. This space is identified on T1-weighted MR images by contained fatty tissue between the muscles of mastication and the constrictors of the pharynx.⁵⁹⁴ The retropharyngeal space is the cleft between the posterior wall of the pharynx and the deep cervical fascia, the prevertebral layer anterior to the cervical vertebrae.

9.2 Craniocervical Junction

The craniocervical junction includes the postero-inferior part of the base of the skull extending from the level of the external occipital protuberance (see ► Fig. 4.2c, ► Fig. 4.2d, ► Fig. 4.8, ► Fig. 5.1b, ► Fig. 5.6a, and ► Fig. 5.6b) to the pharyngeal tubercle (see ► Fig. 4.2c, ► Fig. 4.2d, and ► Fig. 4.8) of the occipital bone, the first two cervical vertebrae (see ► Fig. 3.1b) and the attached muscles. Laterally the region extends to the mastoid processes (see ► Fig. 3.1b, ► Fig. 3.10c, ► Fig. 3.10d, ► Fig. 3.24, ► Fig. 4.1b, ► Fig. 4.7c, ► Fig. 4.7d, ► Fig. 4.13, ► Fig. 5.1b, ► Fig. 5.3, and ► Fig. 5.18). The occipital bone, atlas, and axis form a functional articular unit enabling free movement in three directions. Muscles form a cone-like structure around the cranial end of the vertebral column, extending up to the skull. This muscular cone consists posteriorly and laterally of the superficial and deep neck muscles; two prevertebral muscles are present anteriorly. The individual state of contraction of the muscles in the three spatial axes can result in highly variable images of the craniocervical junction, thereby complicating the interpretation of CT and MR scans in this region. Median and paramedian slices facilitate anatomic orientation.

9.2.1 Bones of the Craniocervical Junction

Predominant bones of the craniocervical junction are:

- The occipital bone is bowl-shaped, with the foramen magnum placed eccentrically (see ► Fig. 3.1b, ► Fig. 3.12c, ► Fig. 3.12d, ► Fig. 3.24, ► Fig. 3.25, ► Fig. 4.8, ► Fig. 5.17, and ► Fig. 6.3). The lambdoid suture (see ► Fig. 4.8) extends beyond the superior boundary of the craniocervical junction, the external occipital protuberance (see ► Fig. 4.8). The paired occipital condyles (see ► Fig. 3.9c, ► Fig. 3.9d, ► Fig. 3.23, ► Fig. 4.1, ► Fig. 4.4d, ► Fig. 4.9, and ► Fig. 4.10) lie anterolateral to the foramen magnum (see ► Fig. 3.23) and form the convex articular surface for the atlanto-occipital joint.
- The nearly ring-like **atlas** (see ► Fig. 3.1b and ► Fig. 4.1b) possesses a delicate anterior arch (see ► Fig. 3.8c, ► Fig. 3.21, ► Fig. 4.2c, ► Fig. 4.2d, and ► Fig. 4.8) and a posterior arch (see ► Fig. 3.11c, ► Fig. 3.25, ► Fig. 4.2c, ► Fig. 4.2d, ► Fig. 4.8, and ► Fig. 5.2), as well as two sturdy lateral masses (see ► Fig. 3.9c, ► Fig. 3.9d, ► Fig. 3.10c, ► Fig. 3.22, ► Fig. 3.24, ► Fig. 4.4c, ► Fig. 4.4d, ► Fig. 4.10, and ► Fig. 5.2). Concave articular surfaces are present on the superior aspect of the lateral masses articulating with the condyles of the occipital bone (see ► Fig. 3.10c, ► Fig. 3.23, ► Fig. 4.4c, ► Fig. 4.4d, and ► Fig. 4.10). The nearly flat inferior surfaces of the lateral masses articulate with the lateral atlantoaxial joints (see ► Fig. 3.9c, ► Fig. 3.9d, ► Fig. 3.23, ► Fig. 4.4c, ► Fig. 4.4d, and ► Fig. 4.10). The posteriorly directed inner aspect of the anterior arch (see ► Fig. 4.8)

contains a smooth facet for the median atlantoaxial joint (see ► Fig. 4.8). The vertebral artery and its accompanying veins run in a groove on the posterior arch of the atlas (see ► Fig. 3.10c, ► Fig. 3.10d, and ► Fig. 3.11c). The atlas usually stands out on coronal images as it is broader than the adjoining cervical vertebrae (see ► Fig. 3.23).

- A characteristic feature of the second cervical vertebra, the **axis** (see ► Fig. 3.1b), is the peg-shaped dens (see ► Fig. 3.1b, ► Fig. 3.9c, ► Fig. 3.22, ► Fig. 4.2c, ► Fig. 4.2d, ► Fig. 4.8, and ► Fig. 5.2) which projects upward into the ring of the atlas forming the axis of a pivot joint. It articulates with the facet on the inner aspect of the anterior arch of the atlas as the median atlantoaxial joint (see ► Fig. 4.8).

9.2.2 Joints of the Head

The articulations between the occipital bone, the atlas, and axis constitute the following two joints:

- Atlanto-occipital joint
- Atlantoaxial joint

The **atlanto-occipital joint** (see ► Fig. 3.10, ► Fig. 4.4c, and ► Fig. 4.4d) constitutes a pair of ellipsoid joints between the occipital condyles and the articular surfaces on the upper aspect of the atlas. Flexion and extension (nodding movements) occur around a coronal axis while side-to-side movements take place around a sagittal axis. Strong ligaments between the occipital bone and the atlas reinforce these two joints.

The **median atlantoaxial joint** is an articulation between the odontoid process of the axis and the ring formed by the anterior arch and the transverse ligament of the atlas. The two joints between the anterior arch of atlas (see ► Fig. 4.2c and ► Fig. 4.2d) and the dens (see ► Fig. 4.2c and ► Fig. 4.2d) and between the dens and the transverse ligament of the atlas (see ► Fig. 4.2c and ► Fig. 4.2d) can be identified on a median section. The axis of this pivot joint runs longitudinally through the dens of axis. These two median joints are functionally paired with the two lateral atlantoaxial joints. The lateral atlantoaxial joints (see ► Fig. 3.9c, ► Fig. 3.9d, ► Fig. 3.23, ► Fig. 4.4c, ► Fig. 4.4d, and ► Fig. 4.10) are formed by the nearly flat, paired joint surfaces on the inferior aspect of the atlas and the corresponding paired facets on its superior surface. These two joints are enclosed in a loose capsule so that rotatory movements of about 25° are possible to either side.

9.2.3 Muscles of the Craniocervical Junction

Cervical muscle groups around the cervical vertebrae extend up to the base of the skull in a cone-like fashion. Several particularly robust muscles lying posterior and lateral to the cervical spine are termed “nuchal muscles” and have both superficial and deep nuchal components. These can pull the head backward, as well as turn it right and left around the long axis of the dens. The ante-

rior part of the muscle cone lies anterior to the cervical spine, especially its two flexors, the longus capitis and the rectus capitis anterior.

Muscles of the Neck

The descending part of the **trapezius** is the most superficial muscle at the back of the neck (see ► Fig. 3.14c, ► Fig. 3.14d, ► Fig. 3.15c, ► Fig. 3.15d, ► Fig. 4.3c, ► Fig. 4.3d, ► Fig. 4.4c, ► Fig. 4.4d, ► Fig. 4.5c, ► Fig. 4.5d, ► Fig. 4.6c, ► Fig. 4.6d, ► Fig. 4.7c, ► Fig. 4.7d, and ► Fig. 5.2). It arises primarily aside from the external occipital protuberance (see ► Fig. 4.2c and ► Fig. 4.2d) and from spinous processes of the cervical vertebrae and inserts into the clavicle and scapula. The trapezius receives motor innervation from the accessory nerve and anterior branches from the cervical spinal nerves. The erector spinae muscles lie deep to the trapezius and posterior to the vertebral column and are supplied by the posterior rami of spinal nerves. The following muscles are arranged in layers from superficial to deep:

- Splenius capitis
- Semispinalis capitis and longissimus capitis
- Deep or short nuchal muscles

The **splenius capitis** (see ► Fig. 3.12c, ► Fig. 3.12d, ► Fig. 3.13c, ► Fig. 3.13d, ► Fig. 3.14c, ► Fig. 4.3c, ► Fig. 4.3d, ► Fig. 4.4c, ► Fig. 4.4d, ► Fig. 4.5c, ► Fig. 4.5d, ► Fig. 4.6c, ► Fig. 4.6d, ► Fig. 4.7, and ► Fig. 5.2) appears flat and four-sided. Arising from the spinous processes of the third cervical to the third thoracic vertebrae, it inserts into the mastoid process. The splenius cervicis is related caudally to the splenius capitis.

The **semispinalis capitis** (see ► Fig. 3.14c, ► Fig. 3.15c, ► Fig. 4.3c, ► Fig. 4.4c, ► Fig. 4.4d, ► Fig. 4.5c, ► Fig. 4.6c, ► Fig. 4.6d, and ► Fig. 5.2) arises from the transverse processes of the third cervical to the sixth thoracic vertebrae and inserts into the posterior aspect of the occipital bone, lateral to the external occipital protuberance.

The **longissimus capitis** lies lateral to the semispinalis capitis. It arises from the transverse processes of the third cervical to the third thoracic vertebrae, and inserts into the mastoid process.

The **deep, short nuchal muscles** lie between the axis and occipital bone and are closely apposed to the bone, enabling finer movements of the head. Four pairs of deep nuchal muscles are present:

- The **rectus capitis posterior minor** (see ► Fig. 3.12c, ► Fig. 3.12d, ► Fig. 3.13c, ► Fig. 3.13d, and ► Fig. 5.2) arises from a small tubercle on the posterior arch of the atlas and extends up to the outer aspect of the occipital bone, about 1 cm further posterior to the posterior edge of the foramen magnum.
- The **rectus capitis posterior major** (see ► Fig. 3.13c, ► Fig. 3.13d, and ► Fig. 5.2) arises from the spinous process of the axis (see ► Fig. 3.1b and ► Fig. 3.13c) and inserts laterally alongside its smaller counterpart into the outer surface of the occipital bone.
- The **obliquus capitis superior** (see ► Fig. 3.11c, ► Fig. 3.11d, ► Fig. 3.12c, ► Fig. 3.12d, and ► Fig. 5.2)

arises from the transverse process of the atlas (see ► Fig. 3.23 and ► Fig. 4.1b) and is inserted laterally to the attachment of the rectus capitis posterior major on the outer surface of the occipital bone, about 2 cm lateral to the border of the foramen magnum.

- The **obliquus capitis inferior** (see ► Fig. 3.11c, ► Fig. 3.12c, ► Fig. 4.4c, ► Fig. 4.4d, ► Fig. 4.5c, ► Fig. 4.5d, ► Fig. 4.6c, and ► Fig. 4.6d) takes its origin from the spinous process of the axis (see ► Fig. 3.1b and ► Fig. 3.12c) and inserts into the transverse process of the atlas (see ► Fig. 3.23, ► Fig. 4.1b, and ► Fig. 4.6c).
- The **levator scapulae** lies nearly lateral to the cervical spine; it originates from the transverse processes of the upper cervical vertebrae and inserts into the scapula. It forms part of the muscles of the shoulder girdle and is innervated by anterior branches of the spinal nerves via the brachial plexus and by the posterior scapular nerve.

Anterior Part of the Muscle Cone

Two prevertebral muscles form the anterior part of the muscle cone. The **longus capitis** (see ► Fig. 4.3c) arises from the transverse processes of the third to the sixth cervical vertebrae and inserts into the base of the occipital bone. The short **rectus capitis anterior** arises from the transverse process of the atlas and follows a similar course as the longus capitis.

9.2.4 Vessels of the Craniocervical Junction

The posterior region of the craniocervical junction is supplied by three vessels which form multiple anastomoses:

The **occipital artery** is a branch of the external carotid artery and runs medially from the posterior belly of the digastric (see ► Fig. 3.8c, ► Fig. 3.8d, ► Fig. 3.9c, ► Fig. 3.9d, ► Fig. 3.10c, and ► Fig. 3.10d) and along the medial aspect of the mastoid process in the region of the neck (see ► Fig. 3.11c, ► Fig. 3.12c, ► Fig. 3.12d, ► Fig. 3.13c, ► Fig. 3.13d, ► Fig. 3.14c, ► Fig. 3.15c, and ► Fig. 9.1). The **vertebral artery** arises as the first branch of the subclavian artery (see ► Fig. 9.1), enters the transverse foramen of the sixth cervical vertebra and runs cranially through the transverse foramina of the rest of the cervical vertebrae. The artery emerges lateral to the lateral mass of the atlas and then turns to run in a medial direction (see ► Fig. 3.10c, ► Fig. 3.10d, ► Fig. 3.11c, and ► Fig. 9.1) where it gives off branches to the deep cervical muscles. The further course of the vertebral artery through the atlanto-occipital membrane into the cranial cavity will be described with the arteries of the brain (see Section 7.4).

The small **deep cervical artery** arises from the subclavian artery and runs between the last cervical vertebra and the transverse process of the first thoracic vertebra into the deep posterior neck where it supplies the cervical muscles.

Venous drainage of the neck takes place through superficial veins into the external jugular vein (see ► Fig. 9.2) and through two deep veins, the vertebral and the deep

cervical veins, into the **brachiocephalic vein**. The veins anastomose with the occipital vein and the suboccipital venous plexus (see ► Fig. 3.11c, ► Fig. 3.11d, ► Fig. 3.12c, ► Fig. 3.13c, and ► Fig. 9.2). This venous network joins the confluence of sinuses (see ► Fig. 3.15c, ► Fig. 3.15d, ► Fig. 4.2, ► Fig. 5.6, ► Fig. 7.33b, and ► Fig. 7.35a) and the sigmoid sinus through emissary veins (see ► Fig. 3.10c, ► Fig. 3.11c, ► Fig. 3.11d, ► Fig. 4.6c, ► Fig. 4.6d, ► Fig. 4.7c, ► Fig. 4.7d, ► Fig. 5.6a, ► Fig. 5.6b, ► Fig. 5.19, ► Fig. 7.33b, and ► Fig. 7.35a).

9.2.5 Nerves of the Craniocervical Junction

The muscles of the craniocervical junction are innervated by:

- Accessory nerve with anterior branches from cervical spinal nerves
- Posterior branches of cervical spinal nerves
- Anterior branches of cervical spinal nerves

The corresponding muscles and groups of muscles are topographically arranged, which can be clearly seen in the coronal series (see ► Fig. 7.37). The trapezius, innervated by the **accessory nerve** and the anterior branches of the upper spinal nerves, lies posteriorly and is the most superficial of these muscles. The posterior branches of the spinal nerves run to the various parts of the erector spinae. The posterior branch of the first cervical spinal nerve is the **suboccipital nerve**. Largely a motor nerve, it innervates the deep muscles of the neck, namely the longissimus capitis and the semispinalis capitis. The large posterior branch of the second cervical nerve, the **greater occipital nerve** (see ► Fig. 3.11a, ► Fig. 3.12a, ► Fig. 3.13a, ► Fig. 3.14a, and ► Fig. 3.15a) is mainly sensory. Its branches supply the skin over the posterior aspect of the head.

9.2.6 Clinical Significance of the Craniocervical Junction

The clinical importance of the craniocervical junction ranges from fractures and dislocations to congenital anomalies.

Clinical Notes

Fractures and dislocations are most frequently a result of traffic accidents with resultant whiplash injury or following a head-first dive into shallow water. The first two cervical vertebrae are thereby most commonly fractured. The posterior arch of the atlas is more frequently fractured than the anterior. A fracture of the dens of axis is the most frequent injury of the second cervical vertebra.³³² No neurologic deficits may occur in the absence of significant luxation between the first and second cervical vertebrae. The fracture may only be discovered later by the development of a pseudoarthrosis. Luxations may result from hyperextension of the cervical spine with tearing

of the transverse ligament of the atlas (see ►Fig. 4.2c and ►Fig. 4.2d). The dens of axis (see ►Fig. 4.2c and ►Fig. 4.2d) may be displaced backward, thereby compressing the spinal cord (see ►Fig. 3.10a, ►Fig. 3.10b, ►Fig. 3.11a, ►Fig. 4.1c, ►Fig. 4.2a, ►Fig. 4.2b, ►Fig. 4.2d, ►Fig. 5.2, and ►Fig. 6.3) and causing paraplegia. Subluxations are seen in severe rheumatoid arthritis and atlantoaxial dislocation with rupture of ligaments.^{4,7}

Congenital malformations of the craniocervical junction include atlas assimilations, basilar impressions, Arnold–Chiari syndrome or Dandy–Walker malformation.^{4,87,245}

- The atlas is fused with the occipital bone in atlas assimilation and the foramen magnum is reduced in size and often deformed. The axis is thus the first mobile vertebra. The dens may be displaced backward resulting in impaired vertebral artery flow as well as compromised circulation of cerebrospinal fluid. Ischemia of the medulla oblongata and hydrocephalus may occur as a result.
- Basilar impression may produce similar symptoms. It is characterized by changes in the foramen magnum and the upper cervical vertebrae.
- The tonsils of cerebellum are elongated and tongue-shaped in the Arnold–Chiari syndrome with displacement into the spinal canal; the medulla oblongata is deformed and caudally displaced. These changes are easily identified in median and paramedian MR images. Neurosurgical decompression of the medulla oblongata and restoration of CSF circulation may be indicated.^{255,323,468}
- Features of the Dandy–Walker malformation include hypoplasia of the vermis of the cerebellum and grotesque ballooning of the IVth ventricle. Furthermore, dysplasia of the corpus callosum, other cerebral and several extracerebral deformities may be present.

MRI may be used to depict anatomical relationships in the presence of clinical evidence of malformations or anomalies.

9.3 Vessels of the Head–Neck Region

The large vascular bundle between the trunk and the head runs through the neck and contains the following vessels:

- Common carotid artery
- Internal jugular vein
- A network of lymphatic vessels merging to form the jugular trunk that drains into the venous angle at the junction of the internal jugular and subclavian veins.

The vagus nerve also runs in this neurovascular bundle which courses closely behind the sternoclavicular joint. The bundle leaves the thoracic inlet, runs medially to the sternocleidomastoid, and then enters the carotid triangle. Above the thyroid cartilage the internal carotid

artery follows the course of the common carotid artery into the parapharyngeal space (see Section 9.1.5).

9.3.1 Arteries of the Head–Neck Region

The **common carotid artery** (see ►Fig. 3.8c, ►Fig. 4.5d, ►Fig. 4.7c, and ►Fig. 9.1) divides at the level of the fourth cervical vertebra into the external carotid artery (see ►Fig. 3.8c, ►Fig. 4.7c, and ►Fig. 9.1) and into the internal carotid artery (see ►Fig. 3.8c, ►Fig. 3.8d, and ►Fig. 4.7c) in two-thirds of cases. In the remainder the artery divides either at the level of the third or fifth, rarely at the level of the second or sixth cervical vertebrae.³³⁹

The **internal carotid artery** (see ►Fig. 4.5c, ►Fig. 4.5d, and ►Fig. 7.24) runs into the carotid canal at the base of the skull, without giving off branches in this part of its course. The rest of its course will be described with the cerebral arteries (see Section 7.4).

The **external carotid artery** divides in the carotid triangle into branches for organs in the neck, the face, and the scalp (see ►Fig. 9.1):

- Anteriorly:
 - Superior thyroid artery
 - Lingual artery
 - Facial artery
 - Maxillary artery
- Medially:
 - Ascending pharyngeal artery
- Posteriorly:
 - Occipital artery
- Superiorly:
 - Superficial temporal artery

The **superior thyroid artery** descends in the neck to the thyroid gland (see ►Fig. 9.1). The **lingual artery** (see ►Fig. 3.6c, ►Fig. 3.7c, ►Fig. 4.6c, and ►Fig. 9.1) arises in the carotid triangle in the neck and runs to the tip of the tongue. This vessel has been described in the section on the oral cavity. The **facial artery** (see ►Fig. 3.6c, ►Fig. 3.7c, ►Fig. 4.6c, ►Fig. 4.7c, and ►Fig. 9.1) also branches off the external carotid artery in the carotid triangle. It first runs along the mandible, crossing the lower border of the mandible at the anterior border of the masseter, and then runs into the face. The facial artery anastomoses at the medial canthus with terminal branches of the ophthalmic, supratrochlear, and supraorbital arteries. The **maxillary artery** (see ►Fig. 3.5c, ►Fig. 3.5d, ►Fig. 3.6c, ►Fig. 3.6d, ►Fig. 3.7c, ►Fig. 3.7d, ►Fig. 4.6c, ►Fig. 4.6d, ►Fig. 4.7c, ►Fig. 5.2, ►Fig. 6.4b, and ►Fig. 9.1) supplies the deeper regions of the face (see Section 8.6.2).

The small **ascending pharyngeal artery** runs in the parapharyngeal space toward the base of the skull (see ►Fig. 9.1).

The **occipital artery** runs posteriorly to the region of the craniocervical junction (see ►Fig. 9.1).

The **superficial temporal artery** (see ►Fig. 3.4c, ►Fig. 3.4d, ►Fig. 3.5c, ►Fig. 3.5d, and ►Fig. 9.1) runs over the zygomatic bone into the temporal region and, like the facial artery, anastomoses with the supratrochlear and the supraorbital arteries.

- 1 Common carotid artery
- 2 External carotid artery
- 3 Superior thyroid artery
- 4 Lingual artery
- 5 Facial artery
- 6 Inferior labial branch
- 7 Superior labial branch
- 8 Middle meningeal artery
- 9 Superficial temporal artery
- 10 Angular artery
- 11 Posterior auricular artery
- 12 Maxillary artery
- 13 Occipital artery
- 14 Ascending pharyngeal artery
- 15 Internal carotid artery
- 16 Carotid bifurcation with carotid body
- 17 Vertebral artery
- 18 Thyrocervical trunk
- 19 Subclavian artery

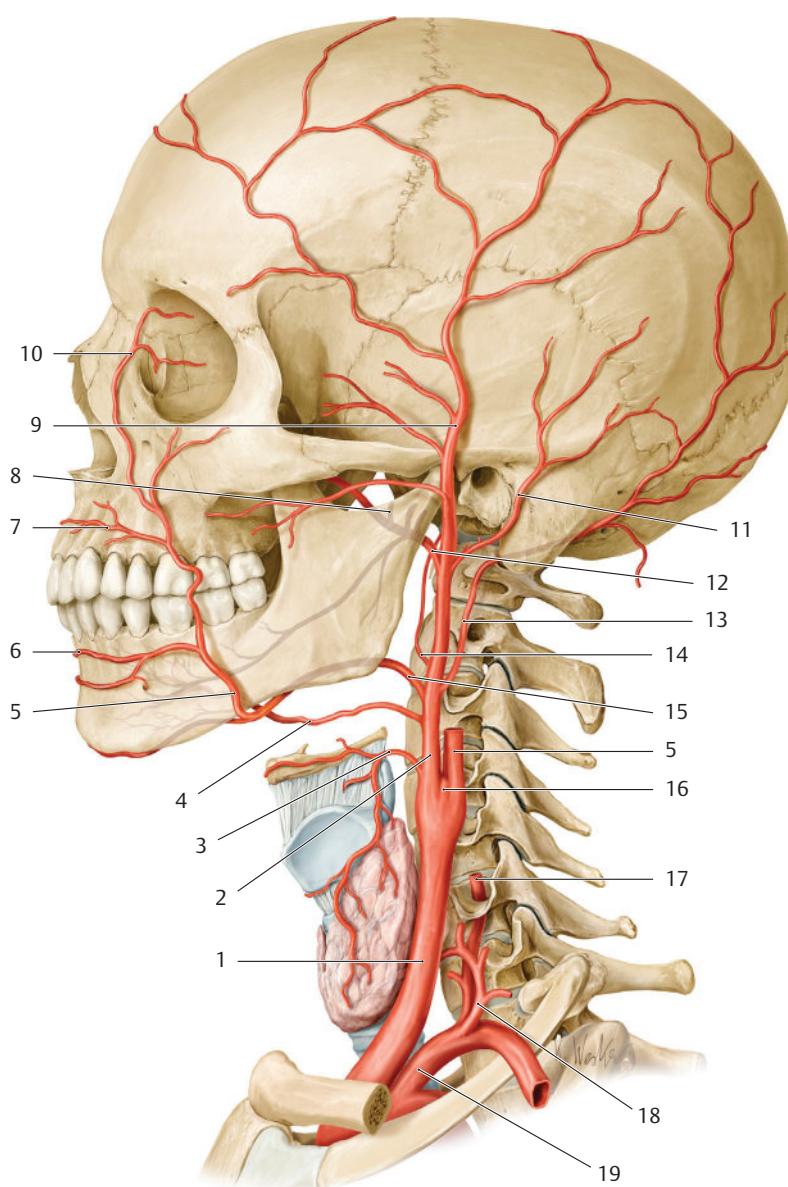


Fig. 9.1 Branches of the external carotid artery. Schematic representation of arterial supply of the head and neck in lateral view. (Reproduced from Schuenke, Schulte, and Schumacher, *Atlas of Anatomy*, 2nd edition, ©2009, Thieme Publishers, Stuttgart. Illustration by Karl Wesker/Markus Voll.⁵³⁵)

Clinical Notes

Important for interventional neuroradiologists is the knowledge of and a thorough search for so-called dangerous anastomoses during an interventional procedure. The most important and potential extra/intracranial anastomoses with branches of the external carotid artery are:³⁷⁵

- From the facial artery via the ophthalmic artery to the internal carotid artery
- From the maxillary/ethmoidal artery via the ophthalmic artery/artery of foramen rotundum to the internal carotid artery
- From the middle meningeal artery via the petrosal branch to the labyrinthine artery
- From the occipital artery via so-called C1/C2 anastomoses to the vertebral artery
- From the occipital artery via the stylomastoid artery to the anterior inferior cerebellar artery

- From the ascending pharyngeal artery (occipital part), via the vasa nervorum of basal cranial nerves to the anterior inferior and posterior inferior cerebellar arteries

In healthy individuals, the blood pressure of the branches of the internal carotid artery is higher than in those of the external carotid. As a result, blood flows from the cranial cavity through the ophthalmic artery and its terminal branches into the branches of the facial and superficial temporal arteries. This physiological direction of flow from an intracranial to an extracranial direction diminishes and may even be reversed in the presence of uncompensated stenosis or occlusion of the internal carotid artery. Velocity and direction of flow may be measured by means of noninvasive Doppler sonography.

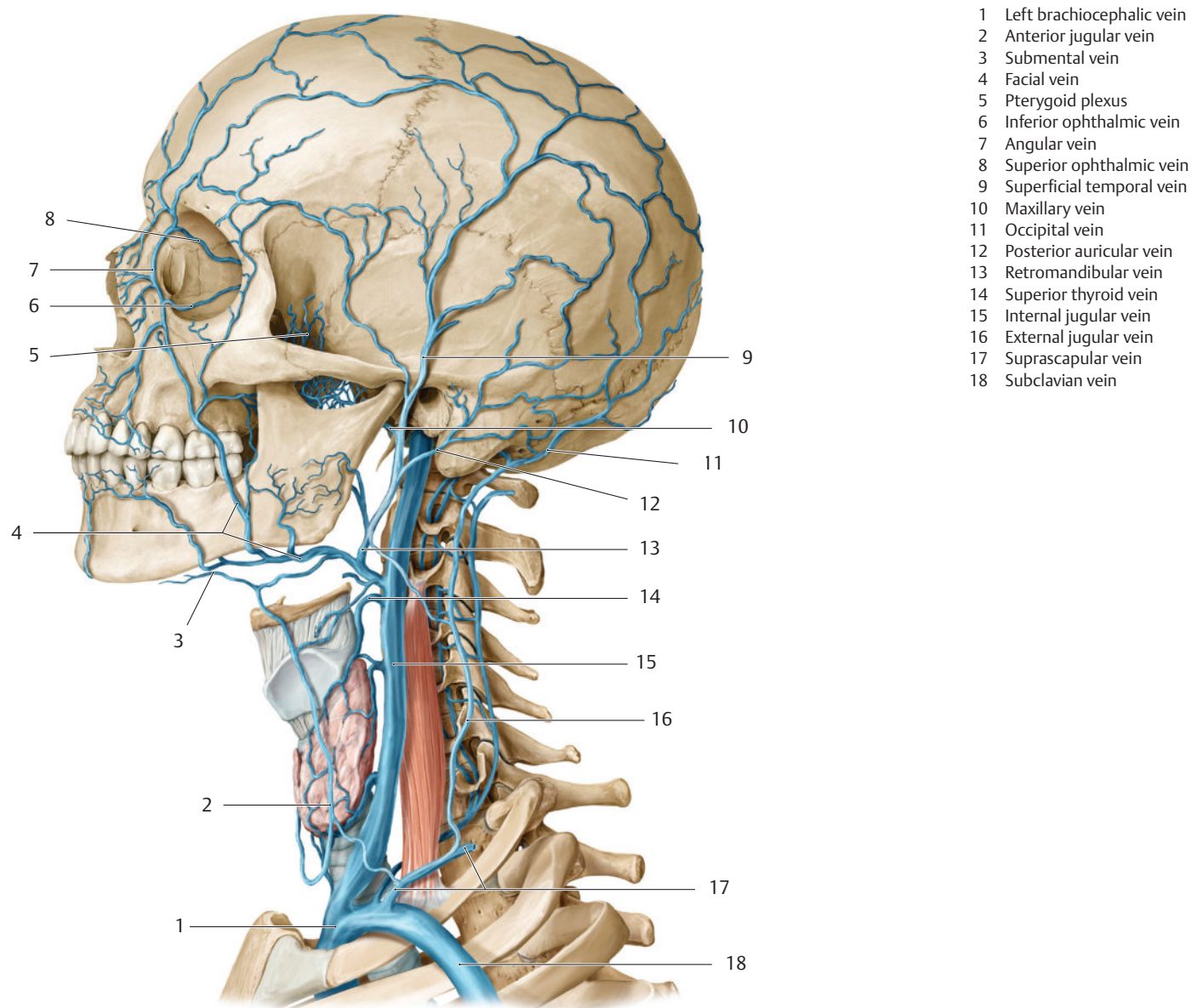


Fig. 9.2 Overview of the principal superficial head and neck veins. (Reproduced from Schuenke, Schulte, and Schumacher, *Atlas of Anatomy*, 2nd edition, ©2009, Thieme Publishers, Stuttgart. Illustration by Karl Wesker/Markus Voll.⁵³⁵)

9.3.2 Veins of the Head–Neck Region

The diploic veins are thin-walled veins within the spongiosa of the calvarium, communicating via emissary veins (see ► Fig. 3.8e, ► Fig. 4.7c, and ► Fig. 5.4) with the dural sinuses and with the veins of the scalp. Blood from the soft tissues of the head is collected in the following veins and plexus (see ► 9.2):

- The **facial vein** collects the blood from the superficial facial region. Beginning at the medial canthus, it runs obliquely across the cheek and the mandible.
- The **pterygoid venous plexus** (see ► Fig. 3.7c, ► Fig. 5.2, ► Fig. 7.35b, and ► 9-2) is a network of veins in the deep facial region, see ► Section 8.6.2, which drains into the facial and retromandibular veins and communicates with the cavernous sinus.
- The **retromandibular vein** collects blood from the temporal region, runs in front of the external

acoustic canal behind the mandible and through the parotid gland in the direction of the internal jugular vein.

- The **external jugular vein** receives blood mainly from the region of the neck and drains into the internal jugular or subclavian veins.

The **internal jugular vein** drains blood from the venous sinuses of the cranial cavity and is usually larger on the right than on the left. In the brainstem series this difference is very marked (see ► Fig. 6.5a). The internal jugular vein begins at the jugular foramen (see ► Fig. 3.23). It lies (see ► Fig. 3.9c, ► Fig. 3.9d, ► Fig. 4.5c, and ► 9.2) posterior to the internal carotid artery (see ► Fig. 3.8c, ► Fig. 3.8d, ► Fig. 4.5, and ► Fig. 5.2), and lies lateral to the common carotid artery in the neurovascular sheath. The internal jugular vein joins the subclavian vein to form the brachiocephalic vein behind the sternoclavicular joint.

Part IV

**Nervous
System—Neurofunctional
Systems and Neuroactive
Substances**

10 Neurofunctional Systems	379
11 Neurotransmitters and Neuromodulators	483

IV

10 Neurofunctional Systems

“Neurofunctional systems” are **orders of neuron populations** that process and transmit afferent or efferent signals while processing neural information and include, for instance, gustatory, auditory, visual, olfactory, or motor functions. Descriptions in this chapter have been restricted to those systems that may easily be tested clinically and are known to be of diagnostic significance. The science of neuronal pathways, **hodology**, collates findings from studies in neurohistology, neurophysiology, ontogenetics, neuropathology, animal experiments, neurology, neurosurgery, and neuroradiology. For example, the somatotopic order of the pyramidal tract in the precentral gyrus was first identified in 1870 by neurosurgical interventions performed by Fritsch and Hitzig¹⁷⁷ and has been corroborated several times thereafter.^{170,424,453} The boundary between the corticospinal and the corticonuclear cortex fields, that is, between the motor innervation of the trunk and that of the head, lies approximately at the boundary between the two-thirds of the precentral gyrus being close to the superior cerebral margin and the third of the precentral gyrus close to the lateral sulcus. There exists a regional overlap of areas perceiving a stimulus from the trunk-extremity region (corticospinal neurons) and from the head (corticonuclear neurons).

Contractions of different muscles were recorded^{170,453} during repeated stimulation of an identical site of the precentral gyrus. Only a gradual reduction in the size of the Betz giant cells may be seen on neurohistology from the superior cerebral margin to the lateral sulcus in area 4. Distinct labeling methods have been used in animal experiments to localize neuronal connections between individual cortical nerve cells and the motor periphery.

In recent years, PET, fMRI, and MEG have been successfully used as imaging techniques for localization of somatosensory and motor areas.^{137,294,398} The illustrations in this book therefore represent only current state of knowledge pertaining to probable topography of neurofunctional systems.

Neurofunctional systems are incompletely developed in prenatal life and nerve cells possess great **plasticity** in embryonal life. The younger the brain, the better it compensates for neuronal lesions. If the cerebellum fails to develop in the initial embryonic period due to genetic or external causes, other neuronal populations can take over its functions almost completely. Cases of congenital hypoplasia of the cerebellum have been described with complete absence of cerebellar symptoms during life. Similar observations have been noted with congenital aplasia of the corpus callosum.⁵⁹³ Even infant brains can compensate for neurofunctional deficiencies much

better than adult brains. However, perinatal lesions of certain neuronal structures may cause severe functional loss, such as blindness following bilateral occipital cortical defects. The ability to compensate for neurofunctional damage in childhood is probably due to synaptic connections between existing neurons. Studies on mammals have shown that a larger number of nerve cells are formed and developed perinatally than those that begin functioning later in the postnatal period. Recent findings suggest that the adult brain also has a great potency for cortical reorganization after brain damage.^{9,98,205,226,329} The field of stem-cell research examines the role of stem cells in the reorganization of both the infant and the adult brain.^{286,550,570}

The **localization theory**, which assigns specific functions to individual neuronal populations in the central nervous system, was based primarily on neurological findings of school children, adolescents, and adults. With increasing complexity of cognitive, as also emotional–motivational functions, localization in clearly defined neuronal populations becomes increasingly difficult. These complex functions have been described in Section 10.13.

Newer approaches for the depiction of complex neuronal networks may illustrate interactions between different regions of the brain and thus explain why lesions in multimodal areas may result in loss of completely different higher functions. Targeted examination of **resting activation** of the brain has expanded our understanding of its functions, so that activation in characteristic **networks** may be observed even in the absence of external stimuli.¹⁷¹

A new interdisciplinary subdivision within neurosciences, so-called connectomics, examines the importance of neuronal networks in intellectual functions under conditions of activation and rest. The term **connectome** refers to the totality of all connections in the nervous system of a living being. In 1986, the biologist John White and his colleagues succeeded in completely reconstructing the nervous system of the nematode *Caenorhabditis elegans* using electron microscopy.⁶¹⁴ Implementing a similar project in the human brain would be far more complicated because of the much larger number of neurons, but this has been addressed by the **Human Connectome Project** (National Institutes of Health) since 2010. At the heart of this project is the macroscopic depiction of individual connectomes of test subjects using imaging procedures. Anatomical or functional properties are, for instance, employed to depict connections between brain regions as nodes in network graphs. Influencing factors for the expression

of these connections, such as (epi)genetic factors, the influence of learning processes or pathological changes in the brain substance may also be included in the models of these network graphs.

It must be noted that active states do not indicate why a particular region is required for a specific function; the principle of the network elucidates why discrete lesions may result in diffuse damage.⁴⁹³ Currently available data reveals that, despite the presence of discrete neurofunctional systems, the number of anatomically clearly distinguishable subdomains responsible only for a specific function is comparatively low. The brain appears to represent a complex, manifold interconnected macrosystem in which individual brain regions are involved in a variety of physiological, cognitive, and emotional–motivational functions.

Positions of the neurofunctional systems have been depicted in series of slides and illustrated in the atlas in ►Fig. 3.2, ►Fig. 3.3, ►Fig. 3.4, ►Fig. 3.5, ►Fig. 3.6, ►Fig. 3.7, ►Fig. 3.8, ►Fig. 3.9, ►Fig. 3.10, ►Fig. 3.11, ►Fig. 3.12, ►Fig. 3.13, ►Fig. 3.14, and ►Fig. 3.15 (coronal series), ►Fig. 4.2, ►Fig. 4.3, ►Fig. 4.4, ►Fig. 4.5, ►Fig. 4.6, and ►Fig. 4.7 (sagittal series), ►Fig. 5.2, ►Fig. 5.3, ►Fig. 5.4, ►Fig. 5.5, ►Fig. 5.6, ►Fig. 5.7, ►Fig. 5.8, ►Fig. 5.9, ►Fig. 5.10, ►Fig. 5.11, ►Fig. 5.12, ►Fig. 5.13, ►Fig. 5.14, and ►Fig. 5.15 (bicommissural series), and ►Fig. 6.4, ►Fig. 6.5, ►Fig. 6.6, ►Fig. 6.7, ►Fig. 6.8, ►Fig. 6.9, ►Fig. 6.10, ►Fig. 6.11, ►Fig. 6.12, and ►Fig. 6.13 (brainstem series).

Neuronal networks presented in Section 10.13 have been illustrated in ►Fig. 10.44, ►Fig. 10.45, ►Fig. 10.46, ►Fig. 10.47, ►Fig. 10.48, ►Fig. 10.49, ►Fig. 10.50, ►Fig. 10.51, ►Fig. 10.52 in lateral and/or medial views, respectively, in a highly simplified manner based on conventionally depicted fMRI data. The difficulties inherent in transposing cadaveric neuroanatomical findings to in vivo studies have been critically reviewed in Section 1.3 and must be taken into consideration in the analysis of neurofunctional systems. Only a few studies about individual variability of neurofunctional systems have been published to date.^{84,191,319,527,608} Despite these limitations, hemianopia, ataxia, aphasia, and many other neurologic syndromes are diagnosed daily in clinical practice and are correlated with the probable site of the lesion. The principal neurofunctional pathways depicted in this book in parallel coronal, sagittal, and bicommissural planes should serve as an aid to diagnosis. Current hodological knowledge is being constantly upgraded by scientific correlation

of clinical findings with results of modern imaging and functional diagnostic procedures.

10.1 Sensory Systems

10.1.1 Anterolateral System

The anterolateral system (see ►Fig. 10.1 and ►Fig. 10.2) receives its signals from nociceptors (pain), thermoreceptors (heat, cold), and mechanoreceptors located in the legs, trunk, arms, and neck. The cell bodies of the **first-order neurons** together with their pseudounipolar nerve cells lie in the **spinal ganglia** and their central axons terminate in the sensory neurons of the posterior horns of the spinal cord. **Second-order neurons** arising here extend in a cranial direction as the anterior and lateral spinothalamic and the spinoreticular tracts. The spinothalamic tracts cross in the anterior white commissure of the spinal cord and then ascend contralaterally in the anterolateral tract. The spinoreticular tract extends as a polysynaptic pathway to the medial reticular formation of the hindbrain and further upward to the **intralaminar nuclei of the thalamus**. These **thalamic neurons** project widely throughout the cerebral cortex, notably into certain cortical areas of the cingulate gyrus and the prefrontal cortex. Psychological pain is probably perceived in the cingulate gyrus.⁶⁵¹

The united **spinothalamic tract** passes lateral to the reticular formation through the medulla oblongata and pons. It joins the medial lemniscus in the pons–midbrain region, where an isolated lesion involving only one pathway is unlikely. The spinothalamic tracts terminate in the **ventral posterolateral nuclei of the thalamus**; axons of the third-order neurons pass from here as thalamoparietal fibers through the posterior limb of the internal capsule to the postcentral gyrus. Located in the **postcentral gyrus** is the sensory projection field with cytoarchitectonic fields 3, 1, and 2 as described by Brodmann (see ►Fig. 7.53). These somatosensory areas are arranged in a somatotopic fashion in this small cortical region: projection fields for the contralateral leg are localized at the superior margin of the cerebral hemisphere. The areas for the trunk, arm, and neck of the opposite side lie in the upper two-thirds of the postcentral gyrus between the superior margin and the lateral sulcus (see ►Fig. 10.1). A secondary pain area is additionally present in the parietal operculum (see ►Fig. 10.1). Pain is consciously localized in both primary and secondary areas. Interruption of the spinothalamic tract results in disorders of pain and temperature perception.⁶²⁵

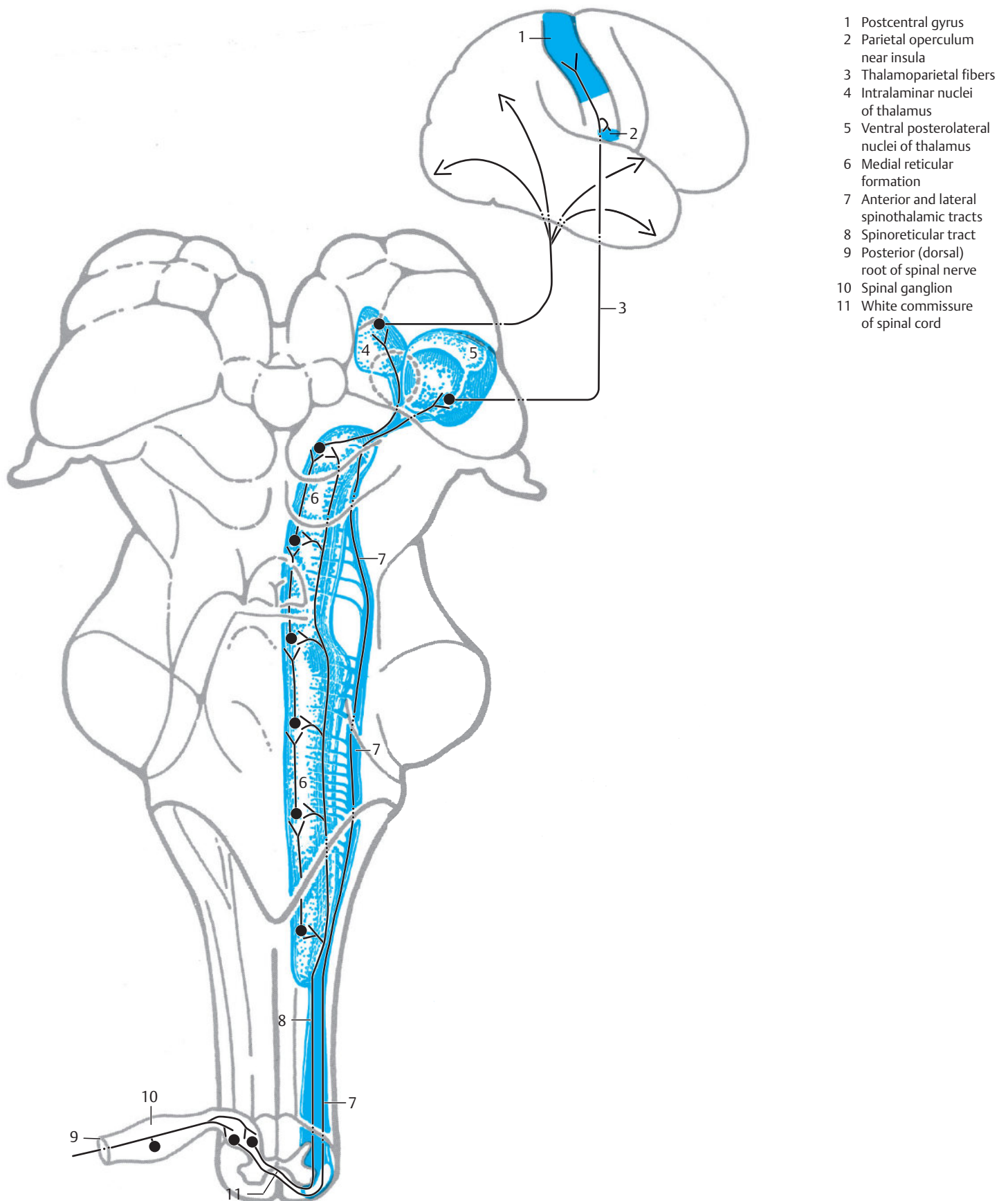


Fig. 10.1 Anterolateral and ascending reticular systems.

Viewed posteriorly in the spinal cord, medulla oblongata, pons, midbrain, and diencephalon and laterally in the cerebrum. Painful stimuli activate the prefrontal cortex of the cerebrum in the ascending reticular system, and in the cingulate gyrus on the medial aspect of the cerebrum. This has only been implied in the illustration. (Reproduced from Nieuwenhuys et al.⁴²⁴)

1 Anterior and lateral spinothalamic tracts

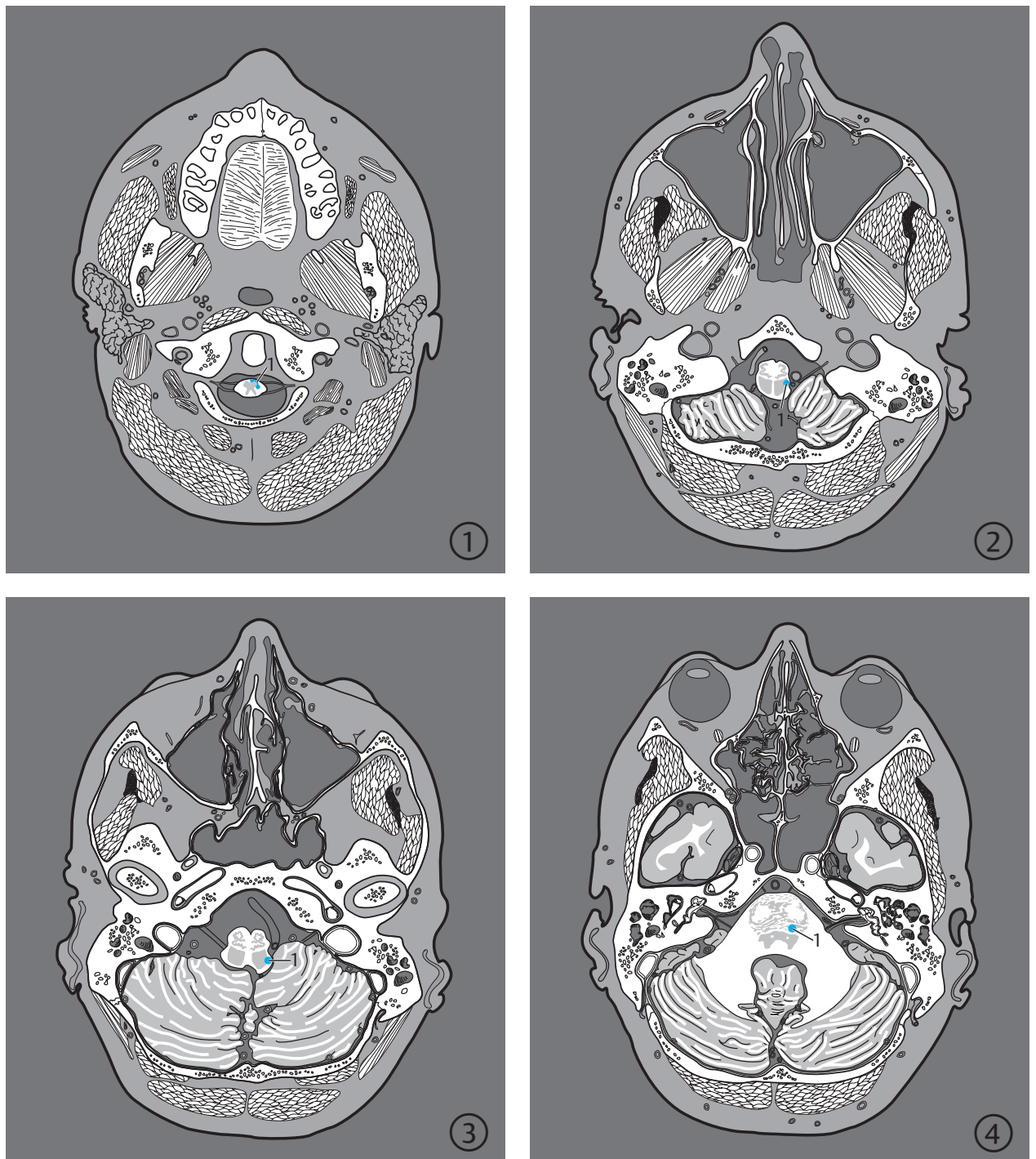
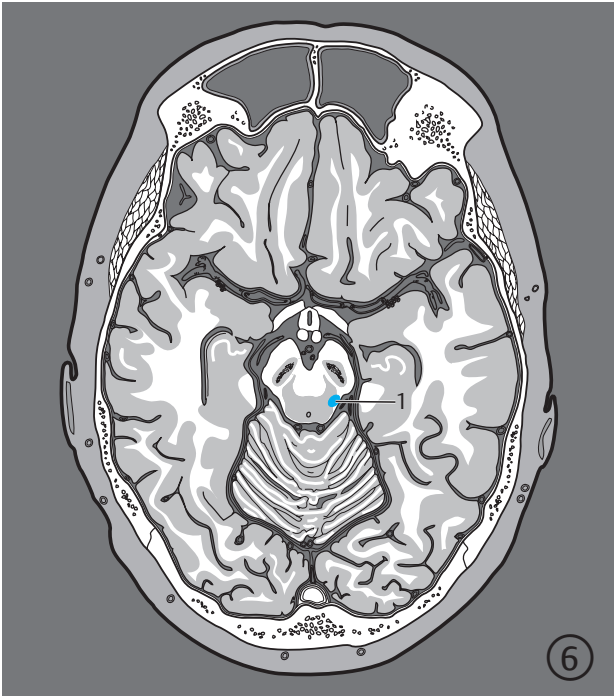
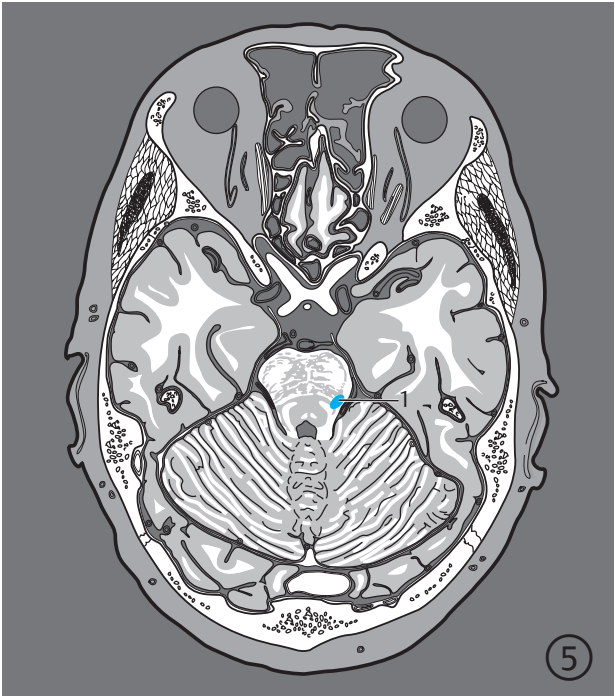


Fig. 10.2 Anterolateral system. Serial images oriented along the bicommissural plane. Encircled digits indicate the number of the respective slice (see ► Fig. 5.1).

Fig. 10.2a 1st to 4th sections.



- 1 Anterior and lateral spinothalamic tracts
- 2 Ventral posterolateral nucleus of thalamus (slightly above the slice position)
- 3 Thalamoparietal fibers

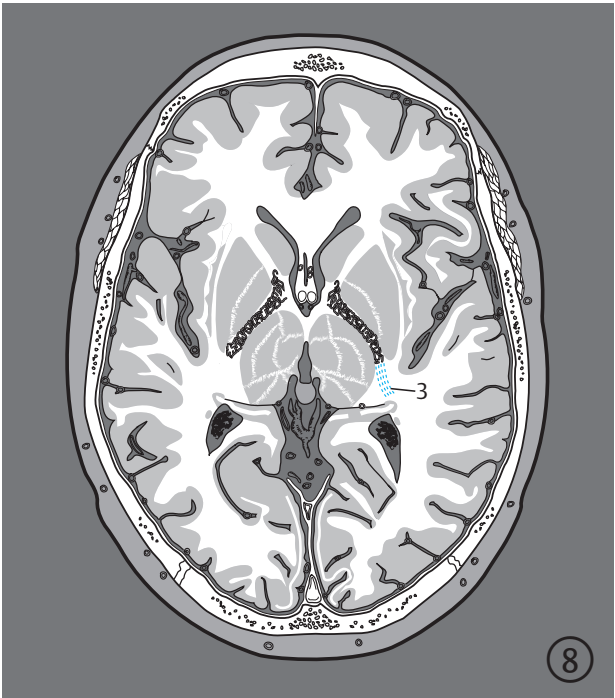
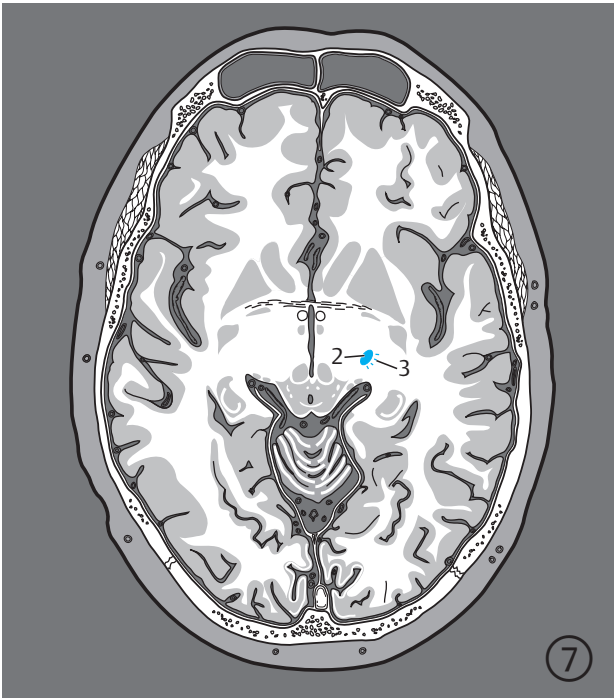


Fig. 10.2b 5th to 8th sections.

- 3 Thalamoparietal fibers
- 4 Postcentral gyrus

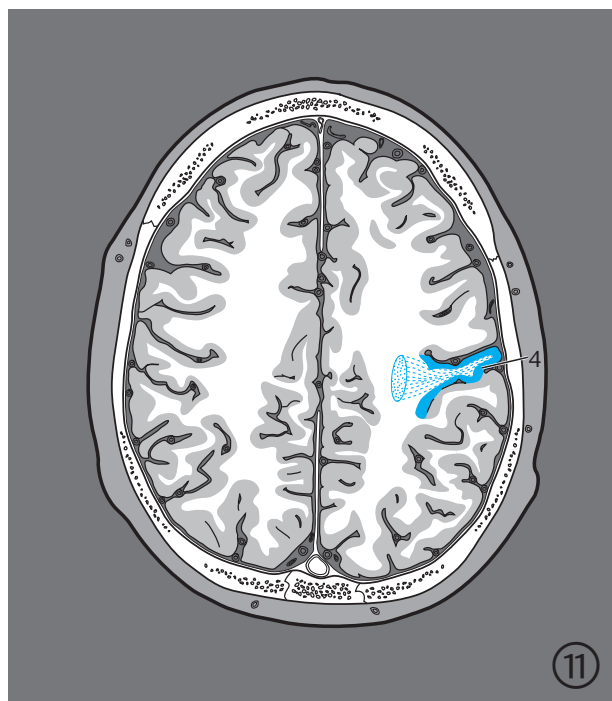
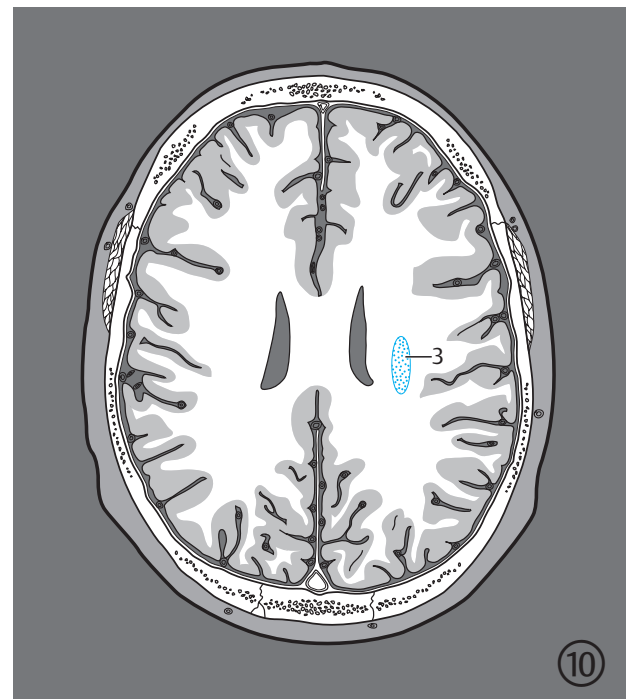
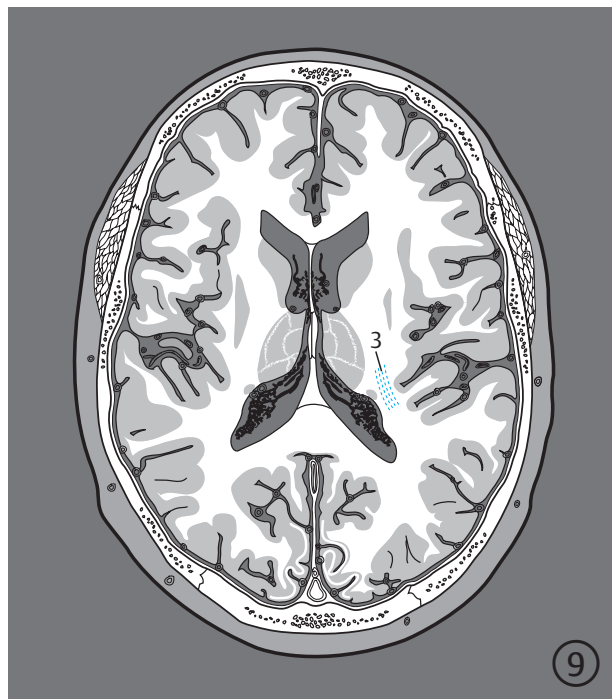
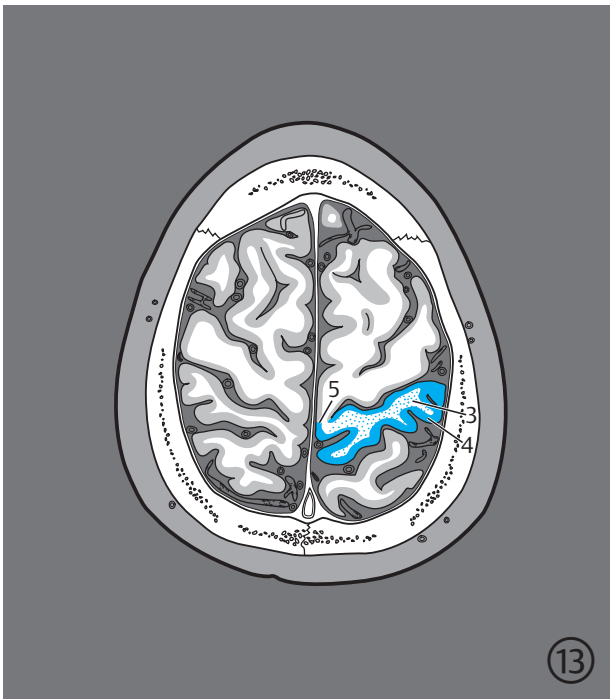


Fig. 10.2c 9th to 12th sections.



- 3 Thalamoparietal fibers
- 4 Postcentral gyrus
- 5 Primary somatic sensory cortex in paracentral lobule

Fig. 10.2d 13th and 14th sections.

10.1.2 Medial Lemniscus System

The sensory receptors of the medial lemniscus system (dorsal column pathway; see ► Fig. 10.3, ► Fig. 10.4, and ► Fig. 10.5) are mechanoreceptors in the skin, muscle spindles, tendon organs and other proprioceptive stimulus converters in the legs, trunk, arms, and neck. Cell bodies of **first-order neurons** lie in the **spinal ganglia**. The axons of these unipolar nerve cells are arranged in a somatotopic fashion in the dorsal column of the spinal cord, that is, the pathways from each dermatome are organized in layers. Axons from the caudal half of the body run in the gracile fasciculus (medial spinobulbar tract) while those from the cranial half form the cuneate fasciculus (lateral spinobulbar tract).

The gracile fasciculus terminates in the **gracile nucleus** in the medulla oblongata (Goll; see ► Fig. 6.4b and ► Fig. 6.4c) while the cuneate fasciculus ends in the **cuneate nucleus** (Burdach; see ► Fig. 6.4b and ► Fig. 6.4c). The gracile and cuneate nuclei are grouped together as “dorsal column nuclei” in accordance with their position at the upper end of the dorsal column of the spinal cord. They lie in the inferior region of the medulla oblongata at its junction with the spinal cord and their inferior ends lie at the level of the crossing-over of pyramidal tracts.

These nuclei form two macroscopically visible protrusions together with their fascicles on the posterior surface of the medulla oblongata, medially the gracile

tubercle (see ► Fig. 6.4c) and laterally, the cuneate tubercle (see ► Fig. 6.4c). Axons of these **second-order neurons** extend in an arcuate direction to the opposite side from nerve cells of the gracile and cuneate nuclei, and then run upward as the medial lemniscus close to the median plane of the medulla oblongata (see ► Fig. 6.5c). The medial lemnisci appear as two bands abutting each other in the median plane in a cross-section of the medulla oblongata. In the pons, the medial lemniscus lies close to the anterior margin of the tegmentum of the pons (see ► Fig. 6.9c) while it lies at the lateral aspect of the tegmentum in the midbrain (see ► Fig. 6.12c). The medial lemniscus moves from medial to lateral at the junction of the midbrain and diencephalon and terminates in the **ventral posterolateral nuclei of the thalamus**. It may be identified through its shape and its contrast to surrounding structures on axial T2-weighted MR images.^{70,130}

The posterior border of the **ventral posterolateral nucleus** where it lies adjacent to the pulvinar is demarcated by a nearly triangular, fiber-containing area (of Wernicke).^{229,514} It forms a groove inferiorly at the lateral aspect of the thalamus. The ventral posterolateral nucleus may be identified on axial MR images with the posterior limb of the internal capsule, the pulvinar, and to some extent the triangular area (of Wernicke)⁴⁰⁴ serving as landmarks.^{511,608} **Third-order neurons** project from the ventral posterolateral nucleus as the thalamoparietal tract to the postcentral gyrus and paracentral lobule.

- 1 Postcentral gyrus
- 2 Thalamoparietal fibers
- 3 Ventral posterolateral nuclei of thalamus
- 4 Medial lemniscus
- 5 Internal arcuate fibers
- 6 Cuneate nucleus (of Burdach)
- 7 Gracile nucleus (of Goll)
- 8 Cuneate fasciculus
- 9 Gracile fasciculus
- 10 Posterior (dorsal) root of spinal nerve
- 11 Spinal ganglion

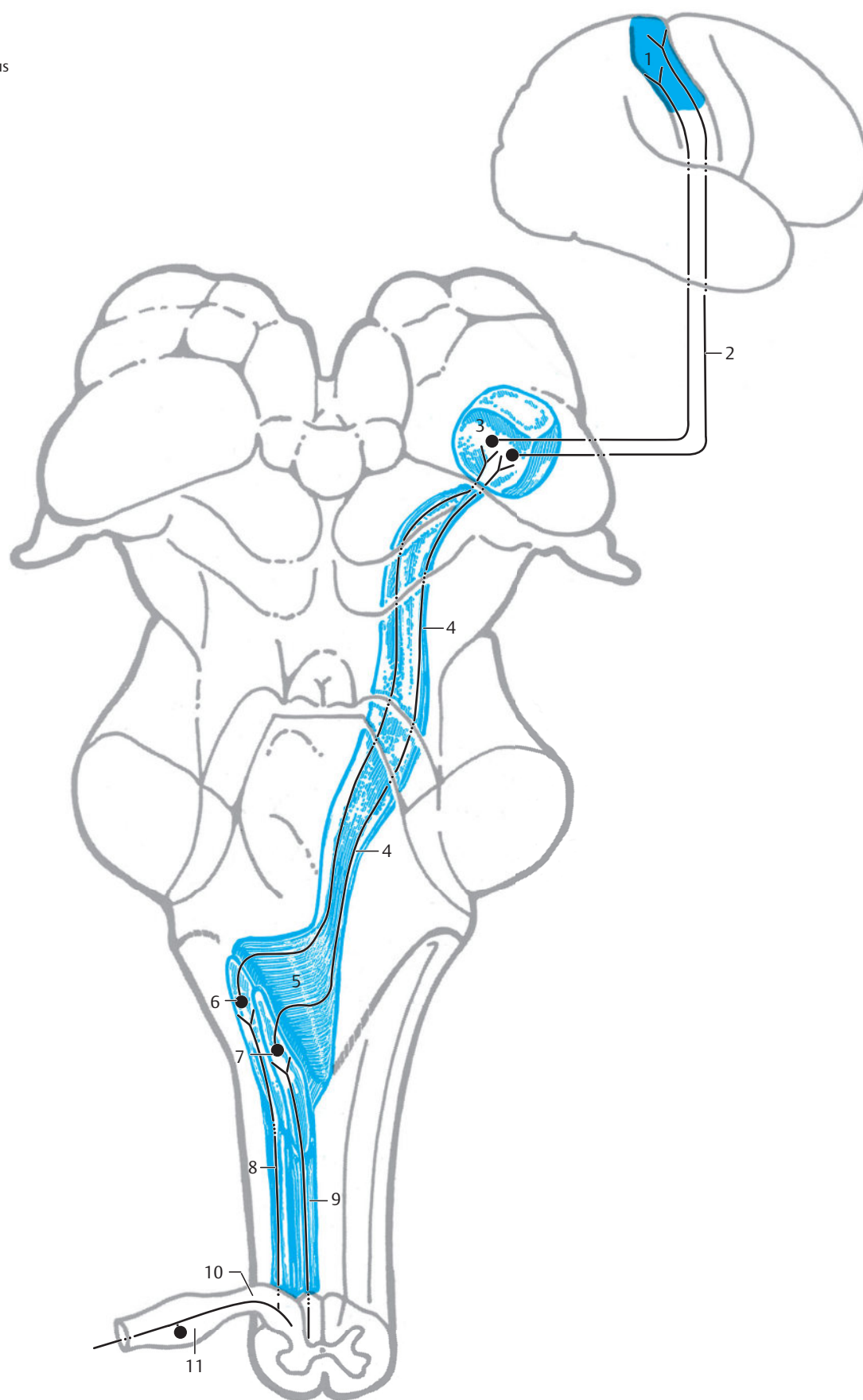


Fig. 10.3 Medial lemniscus system. Viewed posteriorly in the spinal cord, brainstem, and diencephalon and laterally in the cerebrum. (Reproduced from Nieuwenhuys et al.⁴²⁴)

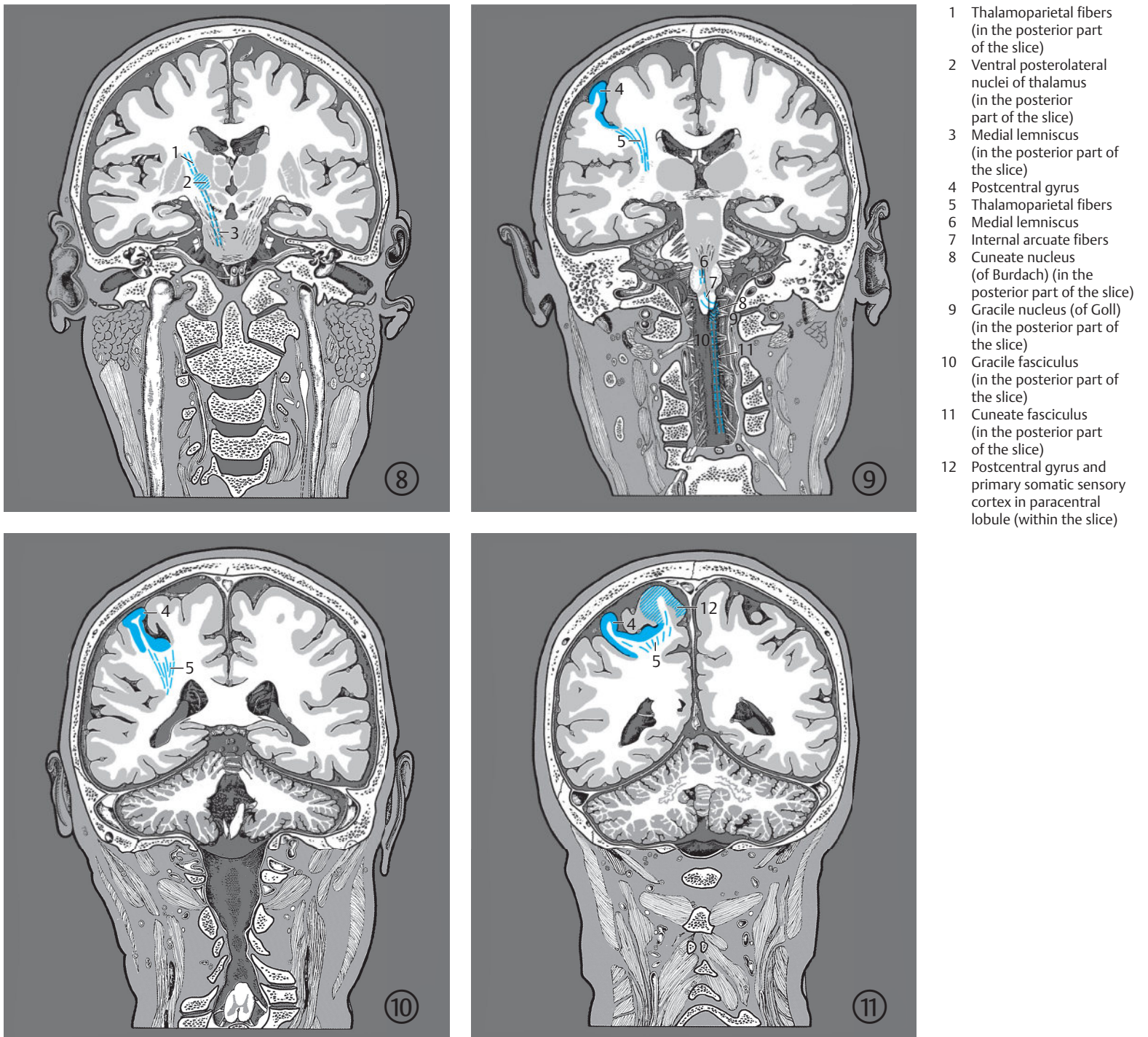


Fig. 10.4 Medial lemniscus system. Serial coronal images. Encircled digits indicate the number of the respective slice (see ►Fig. 3.1).

- 1 Cuneate fasciculus
- 2 Gracile fasciculus
- 3 Internal arcuate fibers
- 4 Cuneate nucleus (of Burdach)
- 5 Gracile nucleus (of Goll)
- 6 Medial lemniscus

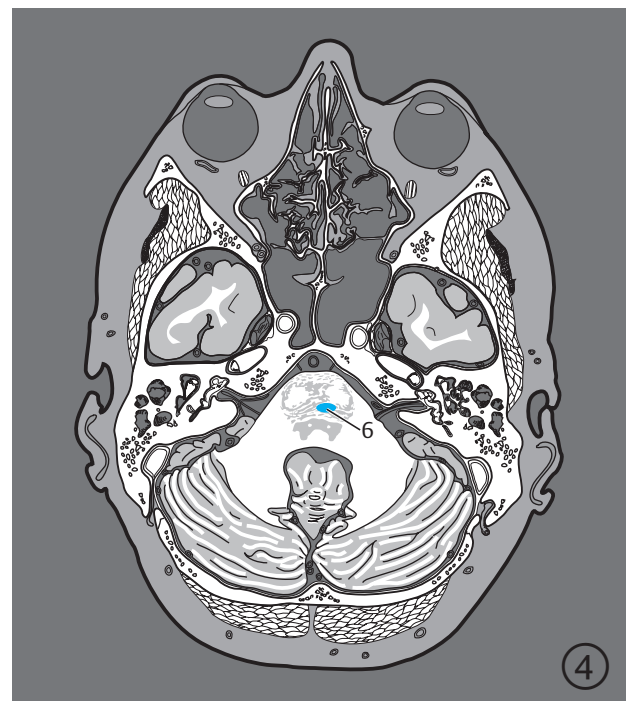
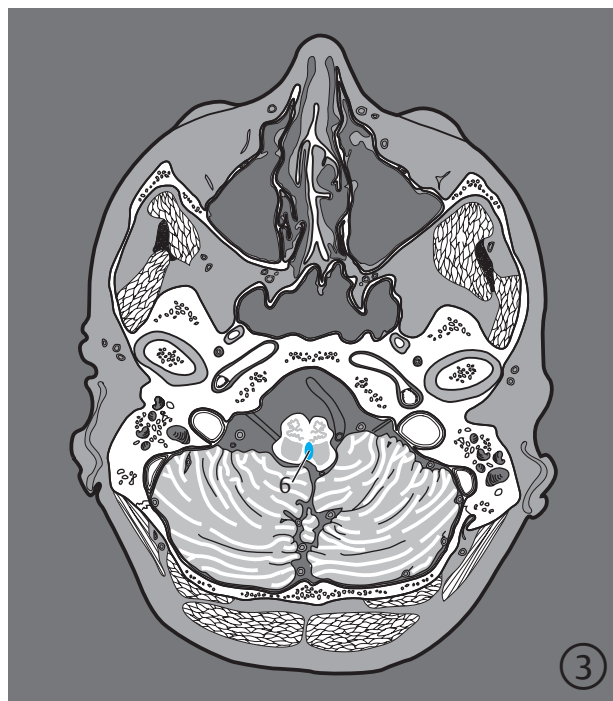
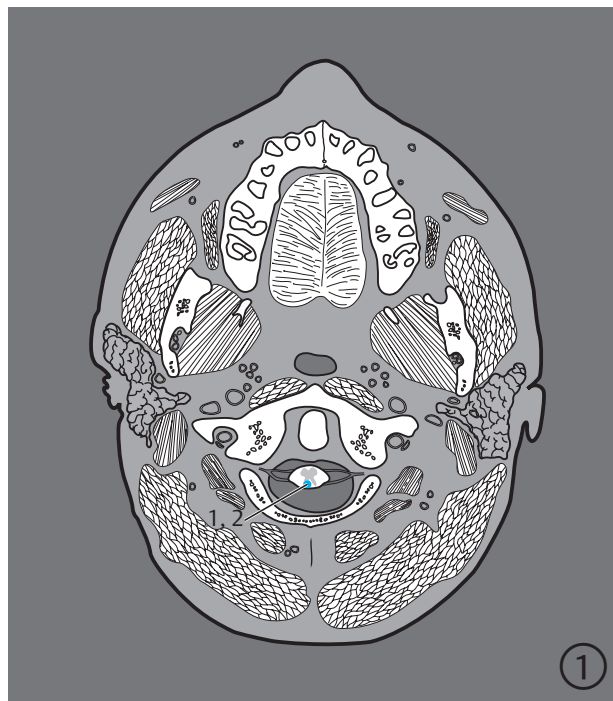


Fig. 10.5 Medial lemniscus system. Serial images oriented along the bicommissural plane. Encircled digits indicate the number of the respective slice (see ► Fig. 5.1).

Fig. 10.5a 1st to 4th sections.

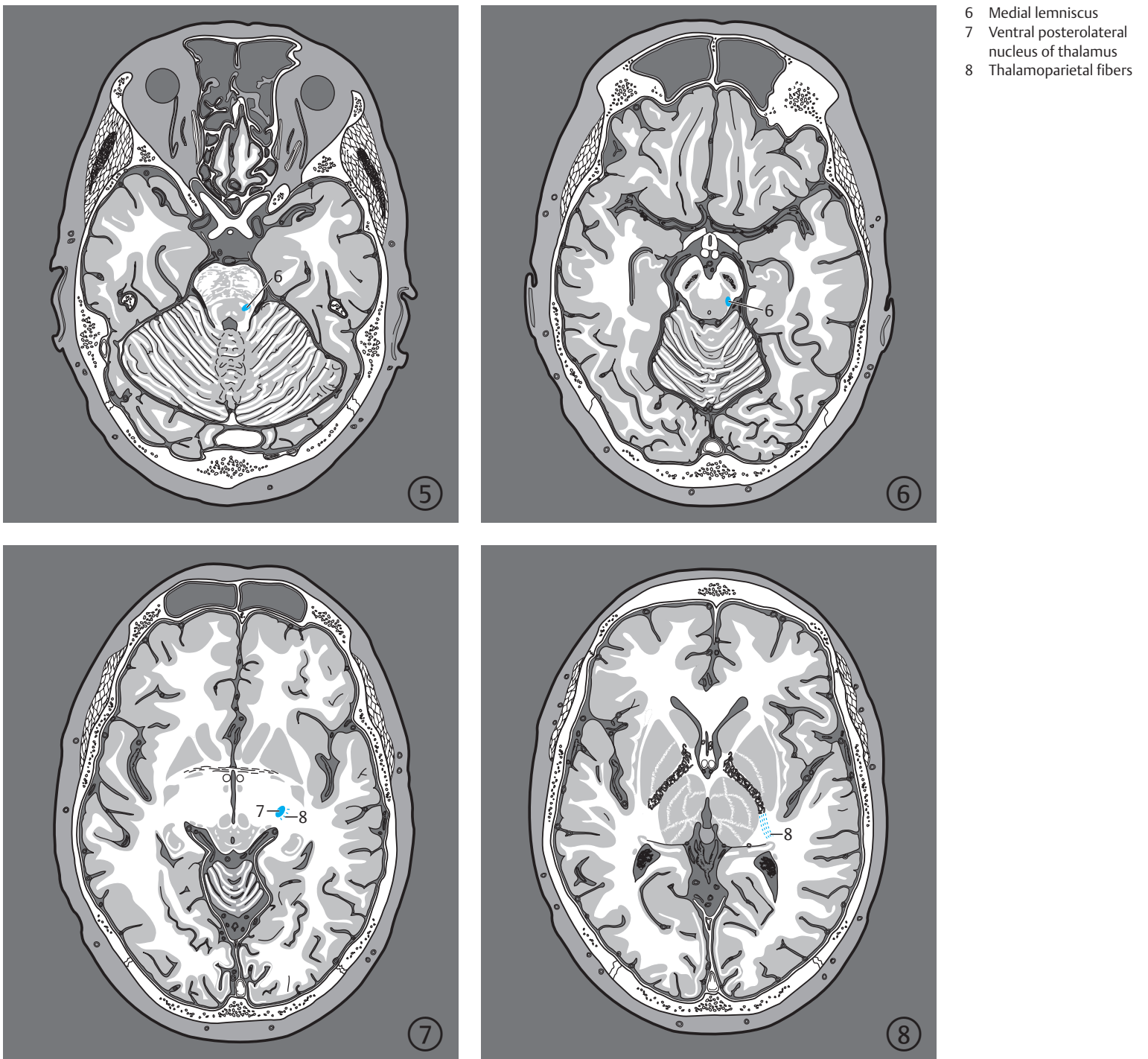


Fig. 10.5b 5th to 8th sections.

- 8 Thalamoparietal fibers
- 9 Postcentral gyrus

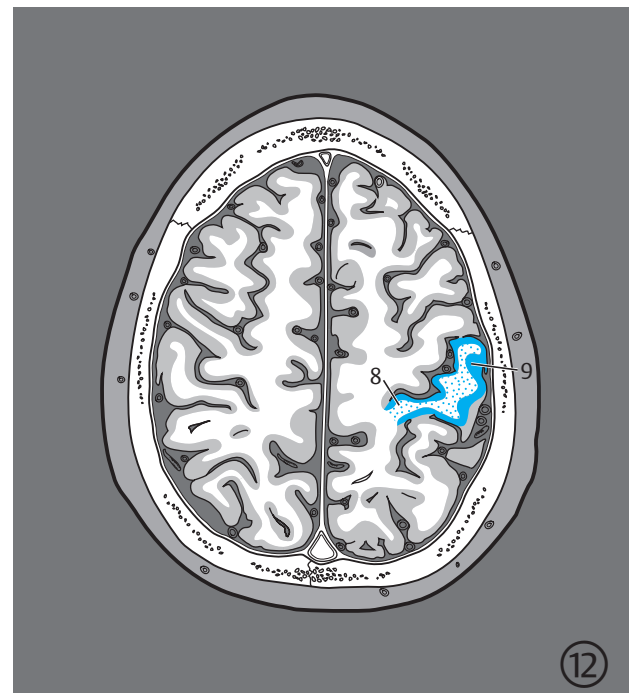
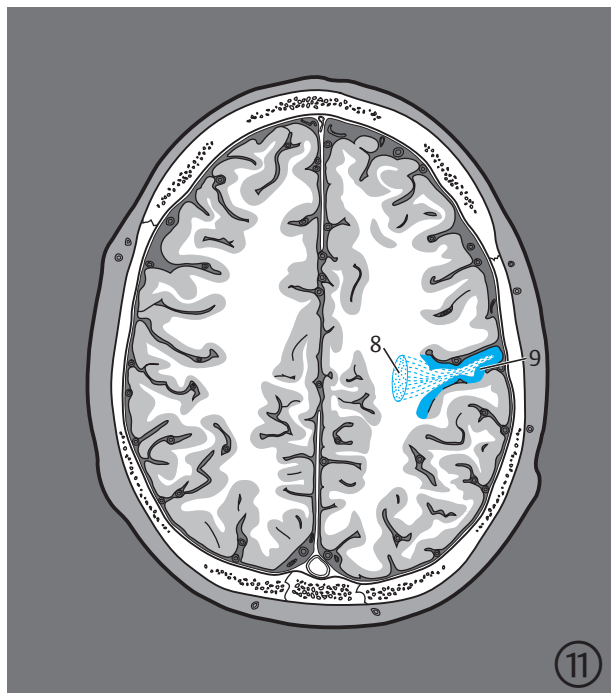
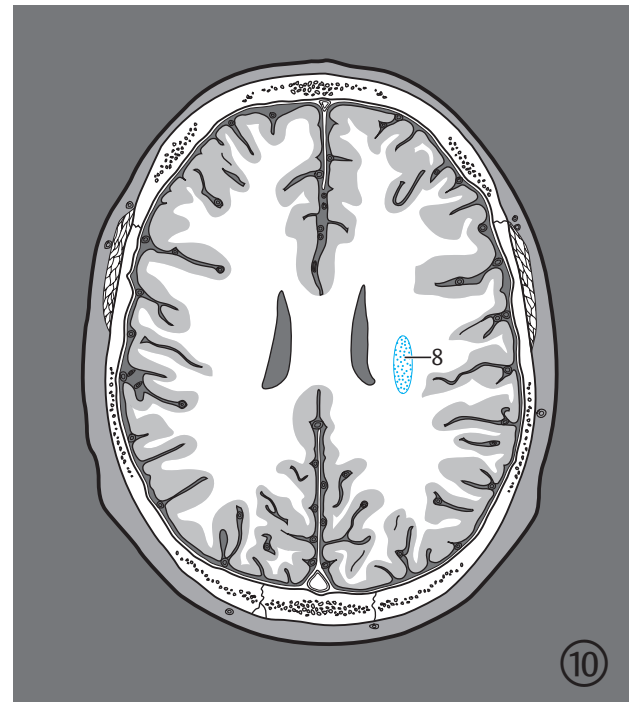
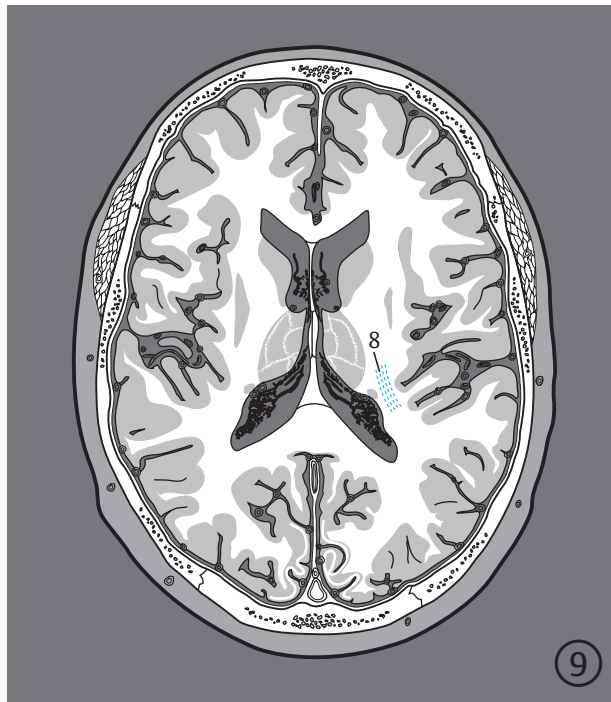
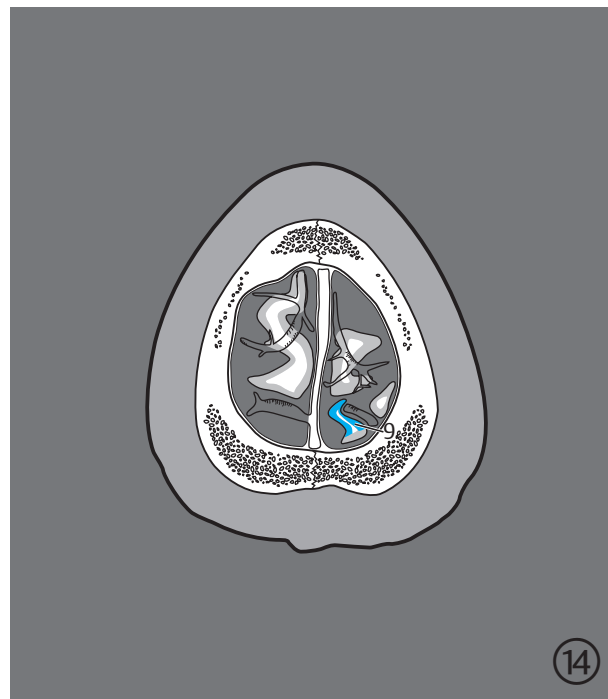
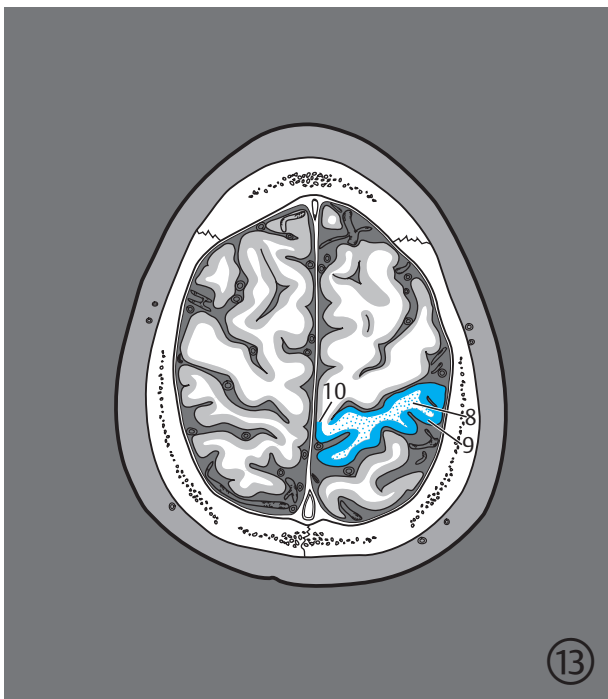


Fig. 10.5c 9th to 12th sections.



- 8 Thalamoparietal fiber
- 9 Postcentral gyrus
- 10 Primary somatic sensory cortex in paracentral lobule

Fig. 10.5d 13th and 14th sections.

Thalamoparietal fibers cannot be definitively identified either macro- or microscopically in specimens of adult human brains. They have therefore been demarcated in comparison with histological sections of infant brains.^{463,608} These fibers course diagonally upward in a lateral direction through the posterior limb of the internal capsule, posterior to the corticospinal tract. Superior to the optic radiation, they run at the lateral edge of the corona radiata to the postcentral gyrus and the paracentral lobule. The anterior border of the primary somatosensory cortex in the **postcentral gyrus** is formed by the floor of the central sulcus, even though the somatosensory and motor regions seldom meet exactly at the floor of the sulcus.⁴⁶³ The floor of the postcentral sulcus has therefore been defined as its posterior boundary. Inferiorly, in the region of the postcentral gyrus, the primary somatosensory cortex of the medial lemniscus system cannot be morphologically demarcated from the primary sensory cortex of the trigeminal system. This boundary has thus been demarcated based on physiological-experimental descriptions.⁶³⁰ The primary somatosensory cortex of neurosurgical patients was stimulated under local anesthesia by means of electrodes applied directly to the cerebral surface. Stimulation produced paresthesiae in specific parts of the body as described by the patients. In accordance with these investigations,⁶³⁰ the distance from the superior cerebral margin to the lateral sulcus in the region of the postcentral gyrus was calculated in a similar fashion to a measurement

using a tape measure.⁶⁰⁸ The boundary between representative areas of the medial lemniscus system and the trigeminal system was determined by selecting a section of the brain lying just below the upper 70% of the determined measurement. The central sulcus may be used as an orienting point to identify the postcentral gyrus on MR images since it is visualized on both sagittal as well as on axial planes (see ► Fig. 7.52a).^{231,511,602}

The primary somatosensory cortex on the medial side of the hemisphere in the **paracentral lobule** is a triangular structure, similar to that depicted in Brodmann's illustrations⁷⁶ (see ► Fig. 7.53). The terminal end of the central sulcus perpendicular to inferior sections in the direction of the cingulate sulcus is transposed as the anterior border; the inferior end of this triangular cortical area is assumed to be represented by the boundary between the upper two-thirds and the inferior thirds of this connecting line. The marginal branch of the cingulate sulcus helps identify the paracentral lobule in axial MR images, which is usually seen on the medial aspect as a furrow immediately posterior to the central sulcus.^{231,511}

Somatotopic organization of the medial lemniscus system corresponds to that of the spinothalamic system (see Section 10.1.1). An interruption of the medial lemniscus system leads to an impaired perception of deep sensations (vibration and position) as well as some superficial sensations (disordered two-point discrimination).

10.1.3 Trigeminal System

Pain, cold, and heat receptors of skin of the face, as well as those of the mucous membranes of the nose and paranasal sinuses, the oral cavity and the teeth transmit their signals via branches of the trigeminal nerve (see ► Fig. 10.6, ► Fig. 10.7, and ► Fig. 10.8) to the pseudounipolar nerve cells of the **trigeminal (Gasserian) ganglion**. The central axons of the trigeminal ganglion run to the pons, passing through it as the spinal tract of the trigeminal nerve to reach the **caudal part of the spinal nucleus of the trigeminal nerve**. This part of the nucleus lies at the lateral aspect of the medulla oblongata and extends from the obex down to the cervical segment of the spinal cord at C2. It corresponds to sensory neurons in the dorsal gray horn of the spinal cord, which also transmit pain and thermal signals. The **lateral trigeminothalamic tract** arises from second-order neurons at the caudal aspect of the spinal nucleus of the trigeminal nerve, and passing upward, it crosses in the medulla oblongata. It then passes together with the spinothalamic tract to the thalamus and thereafter to the postcentral gyrus. The primary somatosensory fields for these pathways lie at the base of the postcentral gyrus in the vicinity of the lateral sulcus. The suboral nucleus (approximate length 14 mm) of the spinal nucleus of the trigeminal nerve lies in the lower part of the pons while its interpolar part (approximate length 11 mm) lies in the medulla oblongata⁶ and transmits pain sensations from the teeth.^{199,613}

The mechanoreceptors of the skin of the face, eyes and the nasal and oral cavities transmit their signals via branches of the trigeminal nerve to pseudounipolar nerve cells of the **trigeminal ganglion**. The central axons of this ganglion extend as the sensory root (portio major) of the trigeminal nerve, mainly to the **principal sensory nucleus of the trigeminal nerve**. This nucleus was earlier known as the “pontine nucleus of the trigeminal nerve” and was renamed, since the oral part of the spinal nucleus of the trigeminal nucleus also lies in the pons. The principal sensory nucleus of the trigeminal nerve lies in the lateral

part of the tegmentum of the pons at the same level as the entrance of the trigeminal nerve. Axons of the **second-order neurons** from the principal sensory nucleus cross over to the opposite side and continue as trigeminothalamic fibers to the ventral posteromedial nuclei of the thalamus. **Third-order neurons** arise as thalamoparietal fibers from this nucleus and pass to the **lower third of the postcentral gyrus**. These pathways carry superficial and depth sensations, except for pain and temperature. Uncrossed fibers coursing from the principal sensory nucleus to the ventral posteromedial nucleus are known as the Wallenberg tract or the posterior trigeminothalamic tract,⁵²⁷ which courses further posteriorly in the tegmentum of the pons and the midbrain than the main pathway from the principal sensory nucleus. The ipsilateral and contralateral tracts lie directly next to one another just short of the **ventral posteromedial nucleus**.

► Fig. 10.6 depicts the lateral trigeminothalamic tract (pain and temperature signals), the anterior trigeminothalamic tract (pain and temperature signals), and the trigeminothalamic tract from the principal sensory nucleus (mechanosensibility) running close to each other at the level of the pontomesencephalic junction before they simultaneously reach the ventral posteromedial nucleus. This **trigeminal lemniscus** runs so close to the medial lemniscus in the upper part of the pons and the midbrain such that these two fiber pathways may only be differentiated histologically after experimental marking in mammalian brains. Histological findings reveal that the fibers of the trigeminal lemniscus lie posterior to those of the medial lemniscus within this common fiber bundle.

Muscle spindle afferents of masticatory muscles pass through pseudounipolar nerve cells that lie not in the trigeminal ganglion but in the **mesencephalic nucleus of the trigeminal nerve**, which extends from the lateral aspect of the floor of the rhomboid fossa of the pons to the central periaqueductal gray matter of the midbrain. Central axons of pseudounipolar nerve cells connect with the motor nucleus of the trigeminal nerve, thus providing a monosynaptic pathway for the masseter reflex.

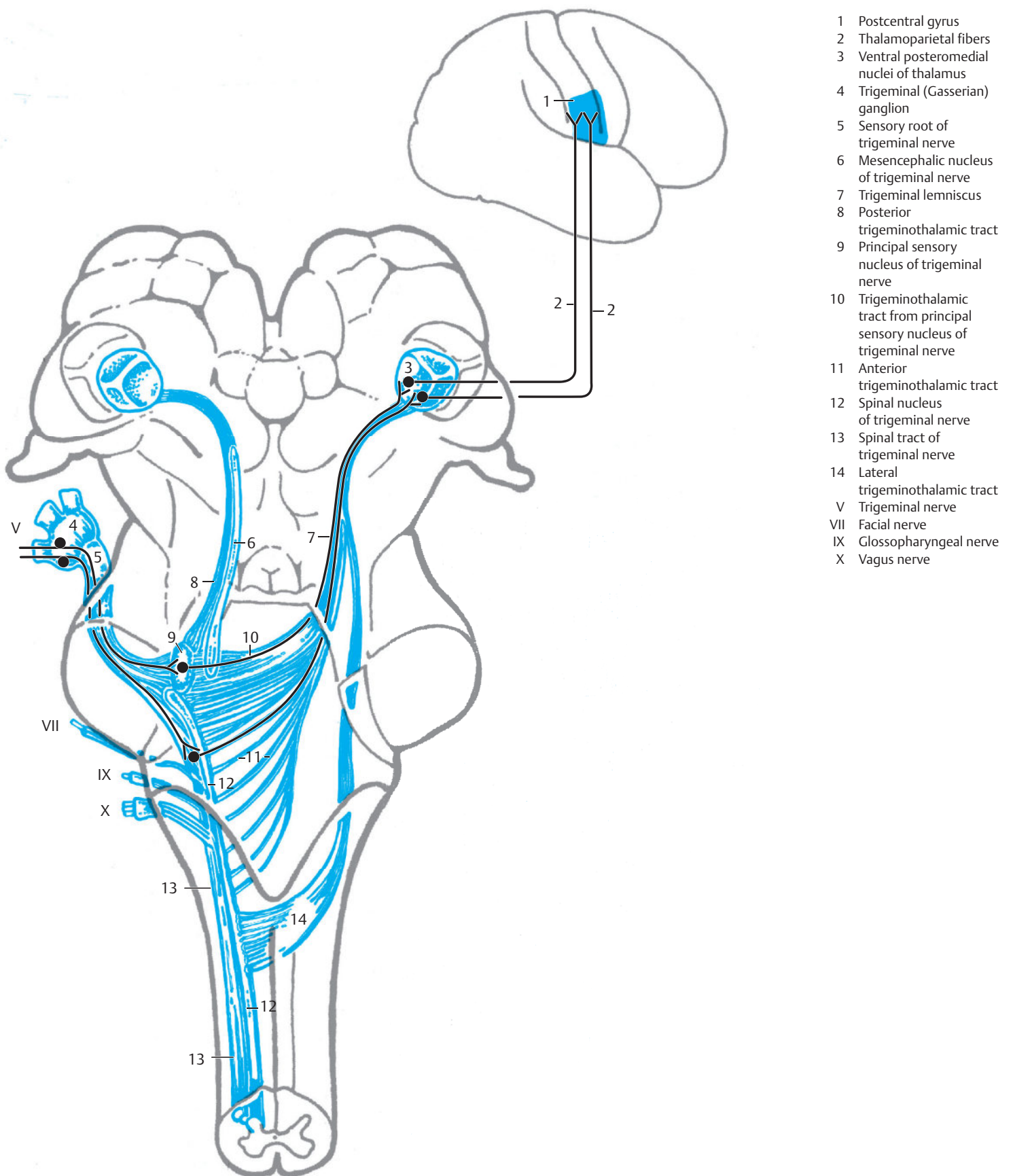


Fig. 10.6 Trigeminal system. Viewed posteriorly in the spinal cord, brainstem, and diencephalon and laterally in the cerebrum. (Reproduced from Nieuwenhuys et al.⁴²⁴ and Schmidt⁵²⁷). The Roman numerals indicate the number of the cranial nerve.

- 1 Supraorbital nerve
- 2 Infraorbital nerve
- 3 Inferior alveolar nerve
- 4 Nasociliary nerve
- 5 Greater palatine nerve
- 6 Lingual nerve
- 7 Frontal nerve
- 8 Palatine nerves
- 9 Ophthalmic nerve
- 10 Maxillary nerve

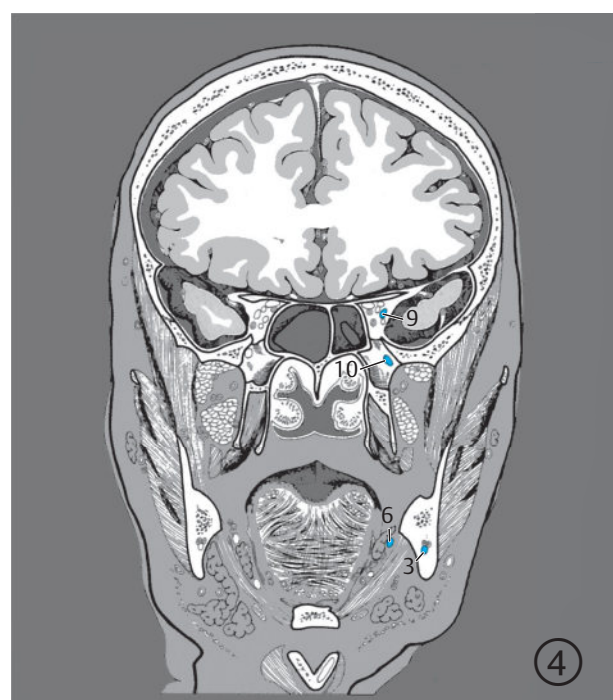
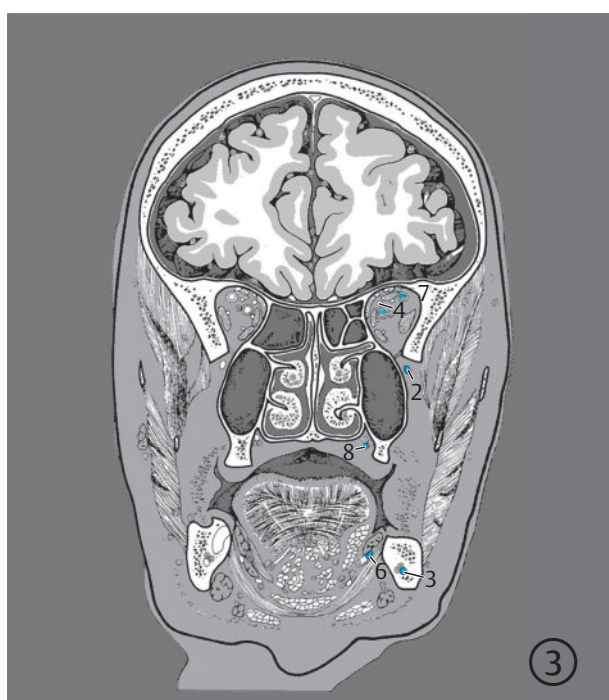
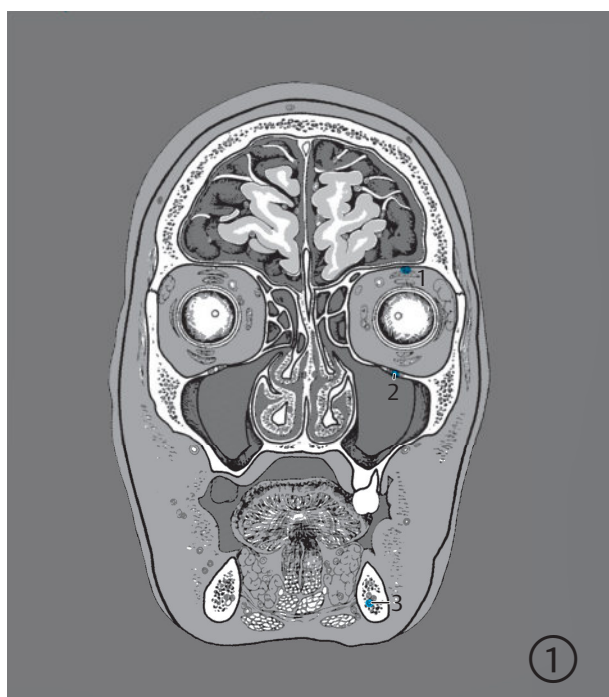
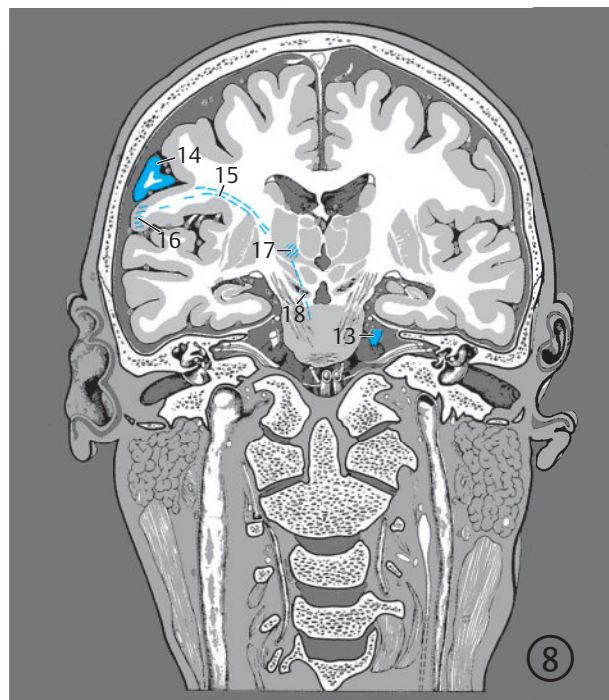
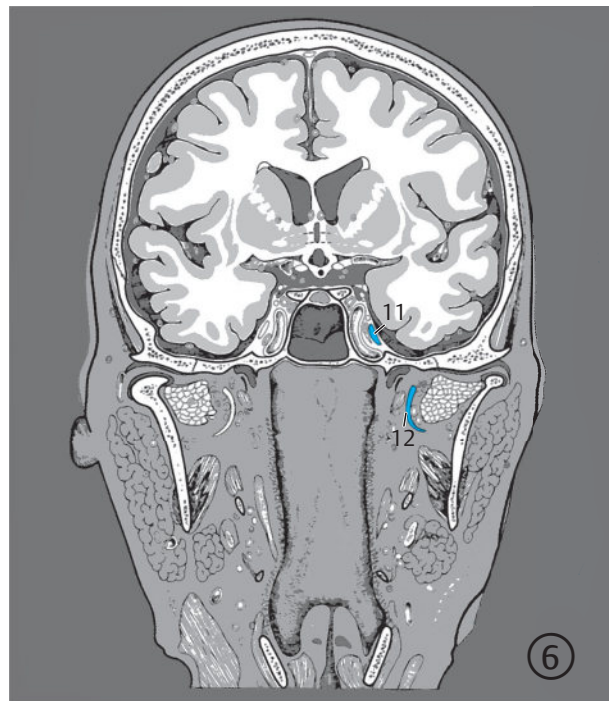


Fig. 10.7 Peripheral and central trigeminal system. Serial coronal images reproduced from Maiden-Tilsen³⁸⁰ and Schmidt.⁵²⁷ Encircled digits indicate the number of the respective slice (see ► Fig. 3.1).

Fig. 10.7a 1st to 4th sections.



- 3 Inferior alveolar nerve
- 6 Lingual nerve
- 9 Ophthalmic nerve
- 10 Maxillary nerve
- 11 Trigeminal (Gasserian) ganglion
- 12 Mandibular nerve
- 13 Trigeminal nerve
- 14 Postcentral gyrus
- 15 Thalamoparietal fibers
- 16 Postcentral gyrus (within the slice)
- 17 Ventral posteromedial nuclei of thalamus (in the posterior part of the slice)
- 18 Trigeminal lemniscus (within the slice)

Fig. 10.7b 5th to 8th sections.

- 14 Postcentral gyrus
- 15 Thalamoparietal fibers
- 18 Trigeminal lemniscus (within the slice)
- 19 Principal sensory nucleus of trigeminal nerve (in the posterior part of the slice)
- 20 Spinal nucleus of trigeminal nerve (within the slice)
- 21 Lateral trigeminothalamic tract (within the slice)

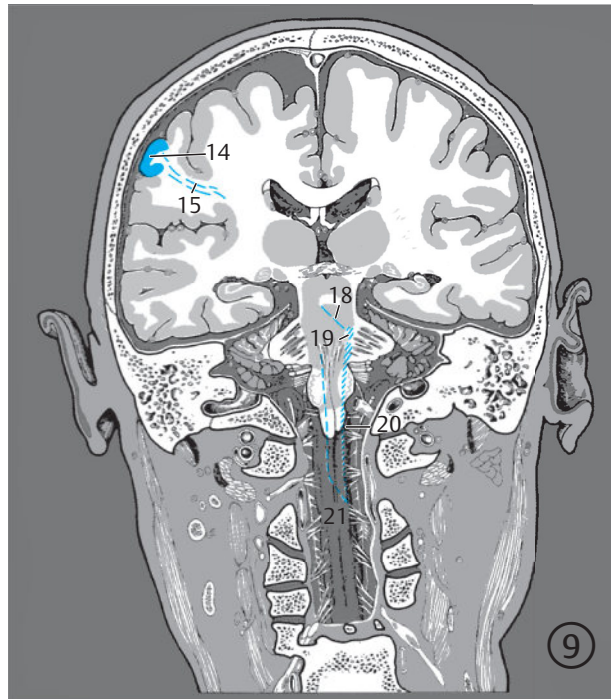
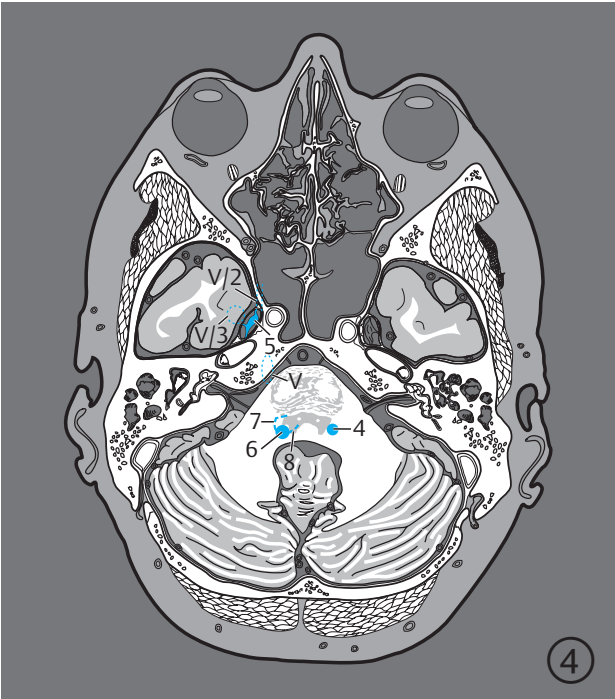
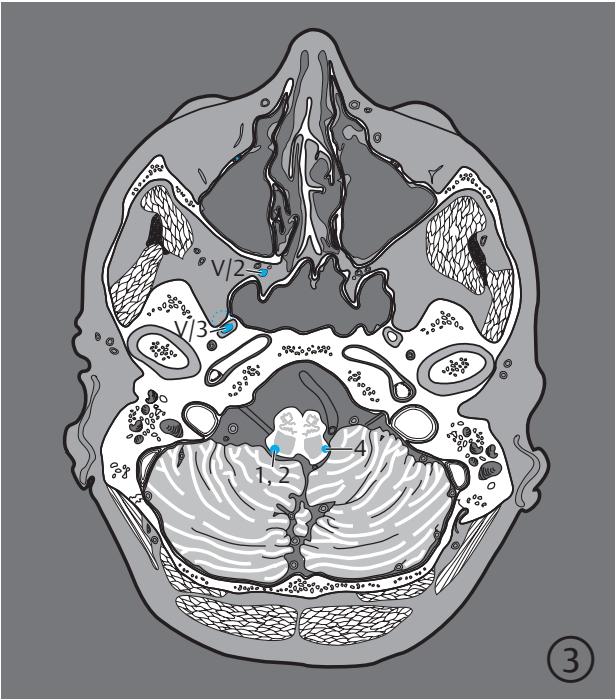


Fig. 10.7c 9th section.



- 1 Spinal tract of trigeminal nerve
- 2 Spinal nucleus of trigeminal nerve
- 3 Lateral trigeminothalamic tract (within the slice)
- 4 Lateral trigeminothalamic tract
- 5 Trigeminal (Gasserian) ganglion
- 6 Principal sensory nucleus of trigeminal nerve
- 7 Trigeminothalamic tract from principal sensory nucleus of trigeminal nerve
- 8 Posterior trigeminothalamic tract
- V Trigeminal nerve
- V/2 Maxillary nerve
- V/3 Mandibular nerve

Fig. 10.8 Trigeminal system. Serial images oriented in the bicommissural plane. (Based on Maiden-Tilsen³⁸⁰ and Schmidt⁵²⁷.) Encircled digits indicate the number of the respective slice (see ►Fig. 5.1).

Fig. 10.8a 1st to 4th sections.

- 4 Lateral trigeminothalamic tract
- 7 Trigeminothalamic tract from principal sensory nucleus of trigeminal nerve
- 8 Posterior trigeminothalamic tract
- 9 Trigeminal lemniscus
- 10 Mesencephalic nucleus of trigeminal nerve
- 11 Ventral posteromedial nuclei of thalamus
- 12 Thalamoparietal fibers

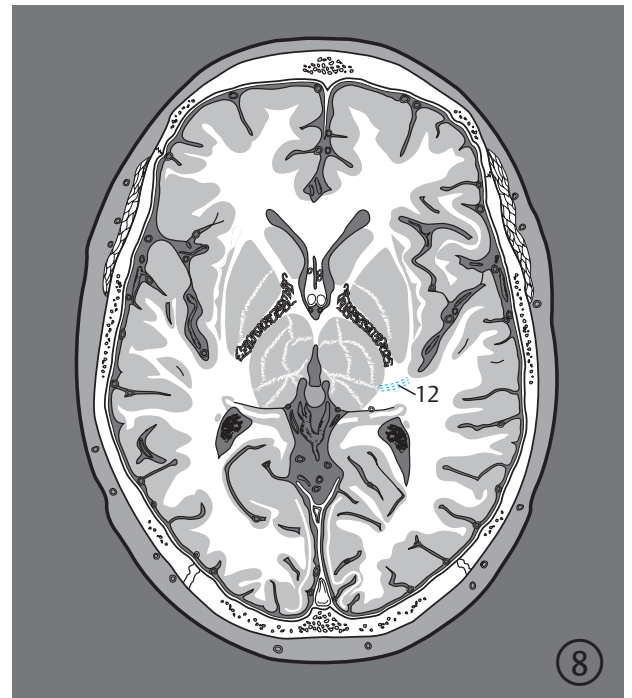
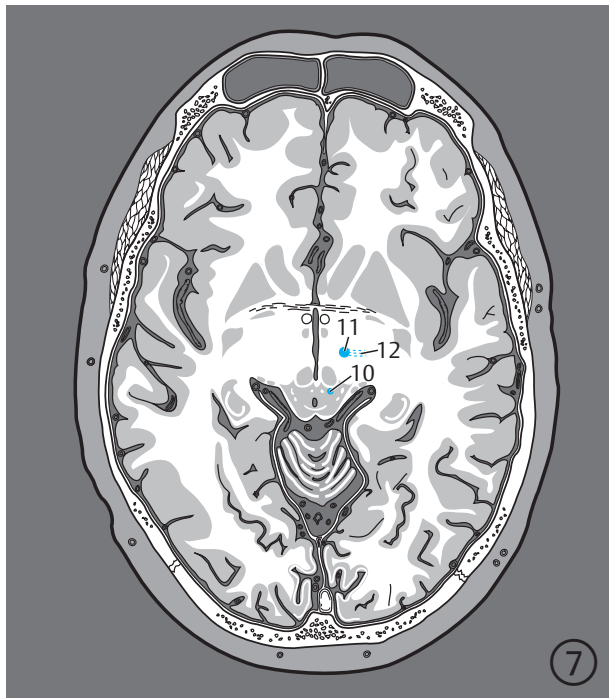
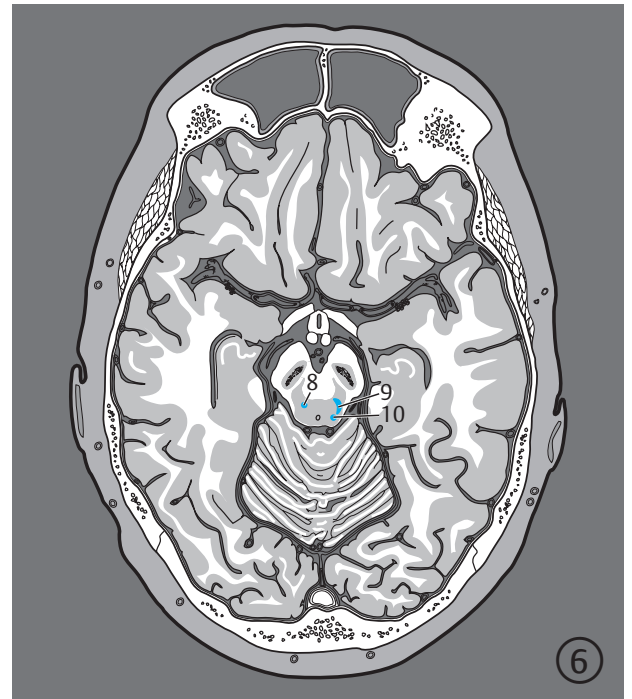
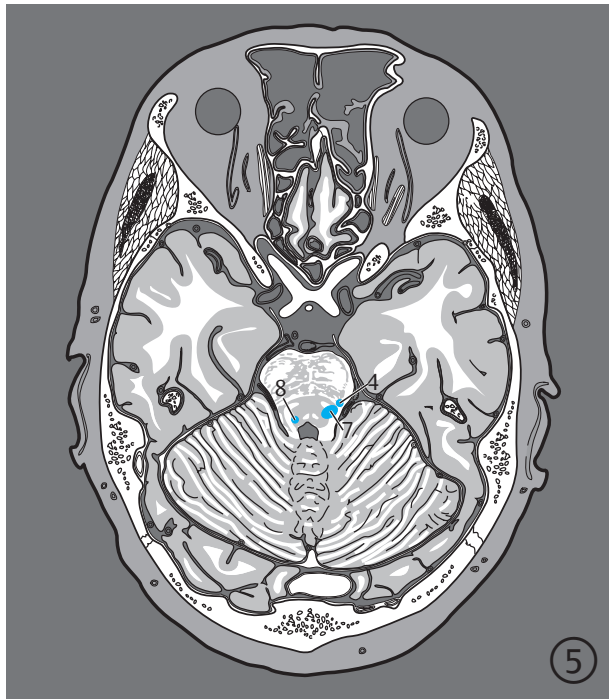
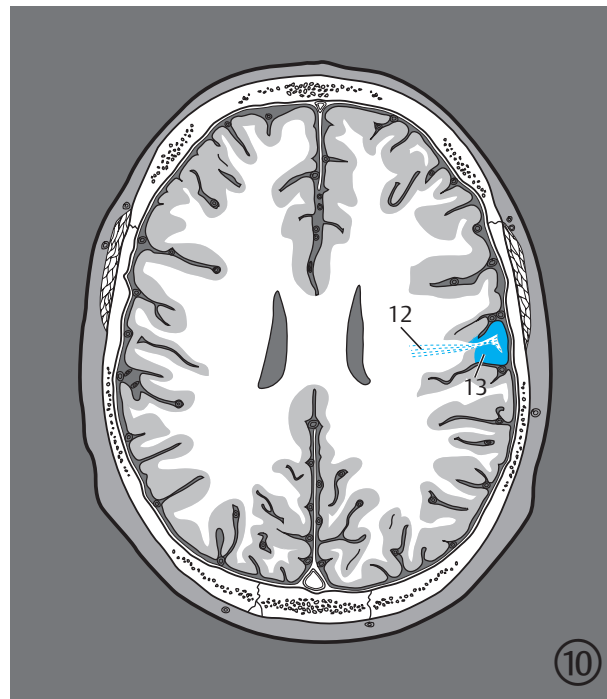
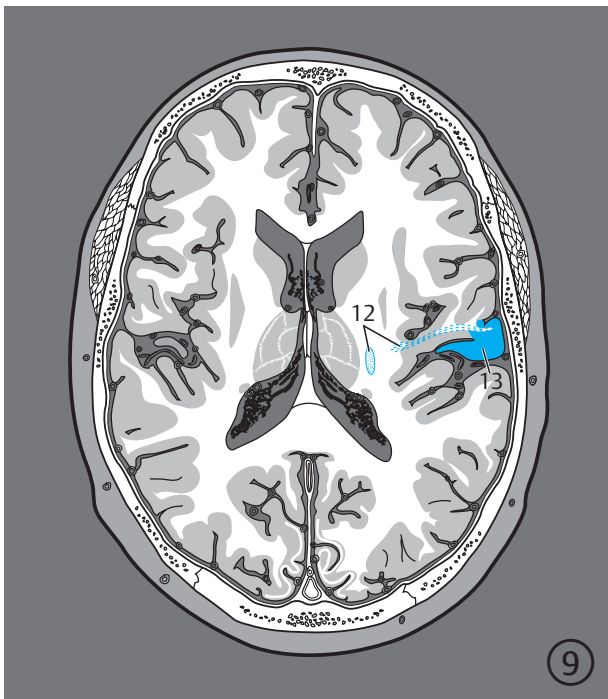


Fig. 10.8b 5th to 8th sections.



- 12 Thalamoparietal fibers
- 13 Postcentral gyrus

Fig. 10.8c 9th and 10th sections.

10.1.4 Clinical Significance

The effects of lesions on individual sensory systems have been summarized as follows:

Clinical Notes

The separate course of the anterolateral and medial lemniscus systems in the medulla oblongata explains the appearance of a dissociated sensory disorder due to an isolated lesion of the anterolateral system in the medulla oblongata. These are often an outcome of vascular insults, which cause a contralateral disturbance of pain and sensation. Additional lesions of first-order sensory neurons and/or of the initial part of second-order trigeminal neurons may cause ipsilateral sensory impairment involving the face. This gives rise to crossed sensory impairment, such as that of Wallenberg's syndrome, caused by lesions in the lateral medulla oblongata.

A lesion of the medial lemniscus impairs tactile discrimination, that is, sensations of touch, position, and vibration sense. Lesions close to the midline of the medulla oblongata may result in uni or bilateral

impairment of this sensory system. Dissociated sensory disorders above the pons are rare due to the proximity of both sensory systems. The same is true for the trigeminal system. Isolated sensory loss, such as those of pain and temperature sensations, appears only as an outcome of injuries of the upper cervical spinal cord and/or the medulla oblongata.

Lesions in the posterior region of the internal capsule usually cause sensory disorders involving the entire contralateral side of the body due to the compact bundling of all sensory systems in this region. Increasing somatotopic fanning out of thalamocortical pathways in the centrum semiovale up to the sensory cortex results in isolated sensory disorders of individual (contralateral) parts of the body, which then include the entire range of sensations. Records of somatosensory evoked potentials (SEP) enable objective measurements of functional disturbances of both peripheral and central sensory systems. Repeated electrical stimulation of a nerve allows topical localization if typical SEP patterns are obtained using surface electrodes over the spinal cord, brainstem, and the primary cortical somatosensory field.^{366,521,564}

10.2 Gustatory System

The **facial**, **glossopharyngeal**, and **vagus** nerves carry gustatory signals from taste buds and free nerve endings to the medulla oblongata (see ► Fig. 10.9 and ► Fig. 10.10). The perikarya or cell bodies of the first-order neurons lie within the **geniculate ganglion** and the **superior and inferior ganglia** of the IXth and Xth cranial nerves. Their central axons terminate in the gustatory part of the **solitary nucleus** and in its superior extension, the nucleus ovalis. The pathway then ascends, coursing in a similar fashion as the trigeminal system close to the medial lemniscus and reaches a **thalamic** subnucleus. Third-order neurons project from here to the **parietal operculum** and to an area at the edge of the insula.^{48,88}

Clinical Notes

Impaired taste sensations are predominantly accounted for by peripheral lesions of the taste buds or lesions of the VIIth, IXth, and/or Xth cranial nerves and not by lesions in the gustatory nuclei and cortical areas.

10.3 Ascending Reticular System

The **reticular formation** (see ► Fig. 6.12b and ► Fig. 10.1) consists of a network of organized nerve cells in the central zone of the tegmentum of the medulla oblongata, pons and midbrain and is surrounded by cranial nerve nuclei, several relay nuclei, and descending fiber tracts.

The medial lemniscus system passes through the reticular formation⁴⁶⁹; the latter receives **afferent signals** from the spinal cord and from all sensory cranial nerves which are then relayed through intralaminar nuclei of the thalamus via widely dispersed projections to the cerebral cortex. The reticular formation forms a nonspecific system of neurons between receptors and cortical nerve cells due to polysynaptic impulse propagation and a **well-developed network**. Specific processing systems, in contrast, exhibit a point-to-point relay between the signal-producing receptors and nerve cells in the primary regions of the cerebrum. Examples of such systems include the medial lemniscus system and the visual pathway. The ascending reticular system also projects into numerous subcortical centers, including the striatum, preoptic region, septal nuclei, and hypothalamic regions^{65,424} and is closely related to the descending reticular system.⁷⁵

Clinical Notes

The complicated interconnections of the reticular formation with its numerous connections with motor, limbic, and several other systems explains the difficulty of analyzing isolated functional disorders of this complex system. Ascending fibers emerging from the reticular formation have an activating effect on the forebrain. Damage to the reticular system may result in altered attentiveness, impaired consciousness as well as unconsciousness.^{255,651}

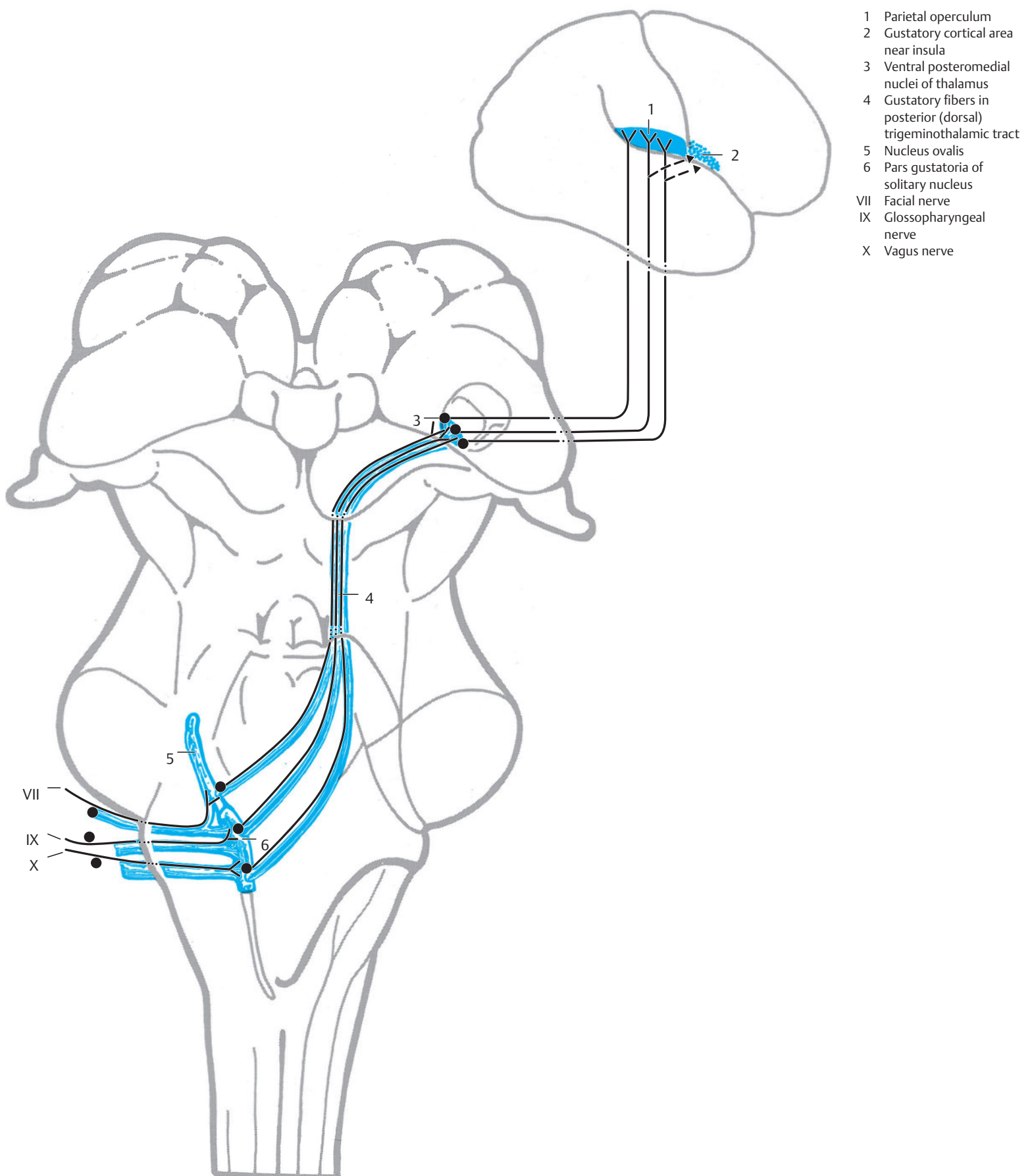


Fig. 10.9 Gustatory system. Viewed posteriorly in the brainstem and diencephalon and laterally in the cerebrum. (Reproduced from Nieuwenhuys et al.⁴²⁴) Roman numerals indicate the facial, glossopharyngeal, and vagus nerves.

- 1 Glossopharyngeal nerve, vagus nerve
- 2 Facial nerve with chorda tympani
- 3 Solitary nucleus (within the slice)
- 4 Gustatory fibers in posterior (dorsal) trigeminothalamic tract

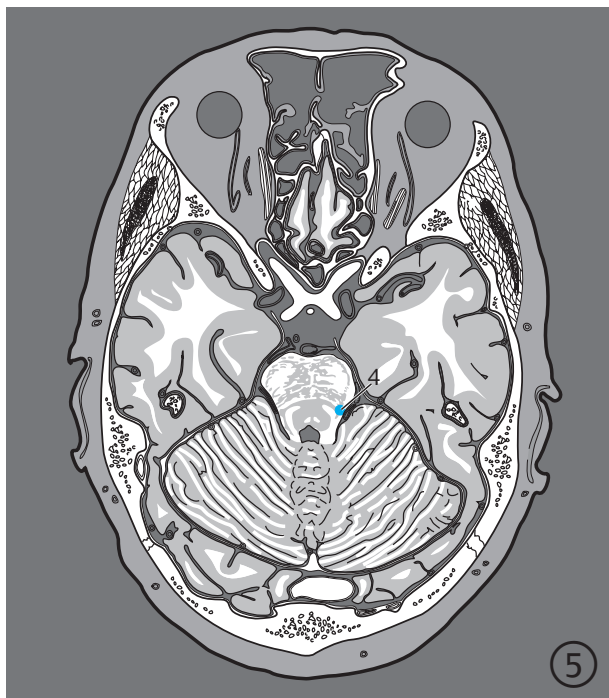
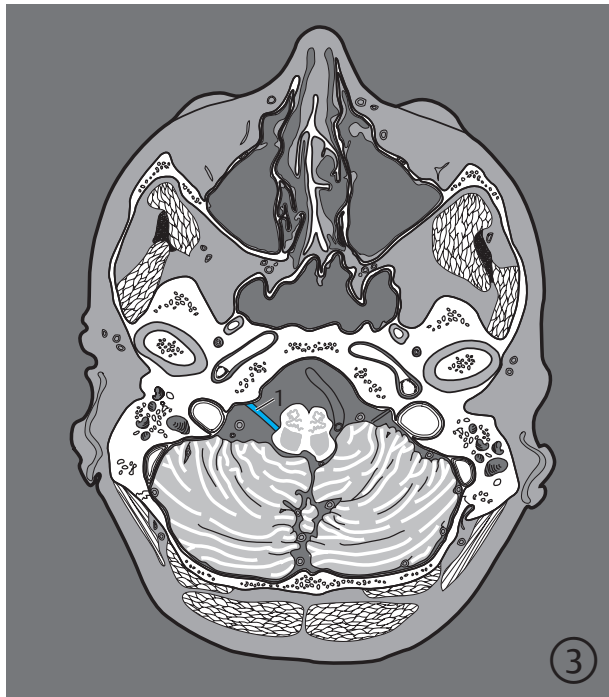
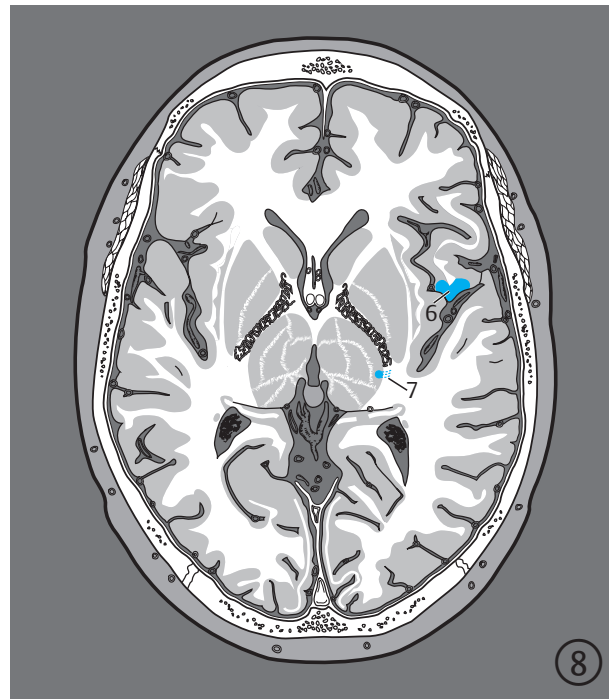
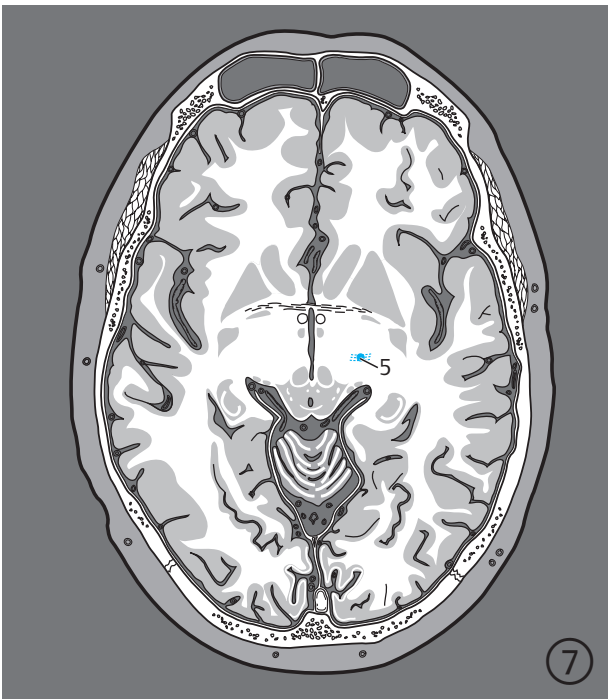


Fig. 10.10 Gustatory system. Serial images oriented along the bicommissural plane. Encircled digits indicate the number of the respective slice (see ► Fig. 5.1).

Fig. 10.10a 3rd to 6th sections.



- 5 Ventral posteromedial nuclei of thalamus
- 6 Parietal operculum
- 7 Hypothetical fibers from thalamus to parietal operculum

Fig. 10.10b 7th and 8th sections.

10.4 Vestibular System

Sensory receptors of the vestibular system (see ►Fig. 10.11, ►Fig. 10.12, and ►Fig. 10.13) lie in the **semicircular canals** as well as within the **saccul** and **utricle**. Sensory cells of the semicircular canals monitor angular acceleration of the head while sensory cells within the saccul and utricle monitor the effect of linear acceleration via small calcium carbonate crystals embedded in a gelatinous matrix. Information pertaining to linear acceleration in the gravitational field of the earth is thus relayed to the central nervous system.⁹³

The signals of angular and linear acceleration are transmitted by the neurons of the vestibular system. Cell bodies of the first-order vestibular neurons lie in the **vestibular ganglion** in the internal acoustic canal. The peripheral axons of these bipolar cells ramify in the sensory cells of the semicircular canals and those of the saccul and utricle. The central axons form the **vestibular component** of the VIIIth cranial nerve which enters the brainstem at the cerebellopontine angle. Fibers from sensory cells of the semicircular canals terminate

primarily in the superior and medial vestibular nuclei while some extend directly to the flocculonodular lobe of the cerebellum. These fibers, with synaptic connections with sensory cells in the saccul and the utricle then preferentially run to the inferior vestibular nucleus. Only a few of the primary vestibular afferent fibers terminate in the large-celled lateral vestibular nucleus (of Deiters).

Vestibular nuclei receive afferent signals from the spinal cord, reticular formation and cerebellum. Efferent connections from the lateral vestibular nucleus descend in the lateral vestibulospinal tract to the spinal cord. Fibers from the remaining vestibular nuclei run in the medial longitudinal fasciculus to motor neurons in the brainstem for the extraocular and neck muscles and via the vestibulospinal tract to the spinal cord. These pathways form a compensatory system which stabilizes the position of the eyes and posture of the head in the presence of disturbing influences. Each movement of the head is followed by reflex movement of the eyes such that the viewed object forms a constant image on the retina, thereby ensuring visual orientation in space.

- 1 Vestibular parietal cortical area
- 2 Ventral intermediate nucleus of thalamus
- 3 Oculomotor nucleus
- 4 Trochlear nucleus
- 5 Vestibulothalamic tract
- 6 Cerebellum
- 7 Medial longitudinal fasciculus
- 8 Superior vestibular nucleus
- 9 Abducens nucleus
- 10 Vestibular nerve
- 11 Inferior vestibular nucleus
- 12 Medial vestibular nucleus (of Deiters)
- 13 Lateral vestibular nucleus (of Deiters)
- 14 Lateral vestibulospinal tract
- 15 Medial vestibulospinal tract

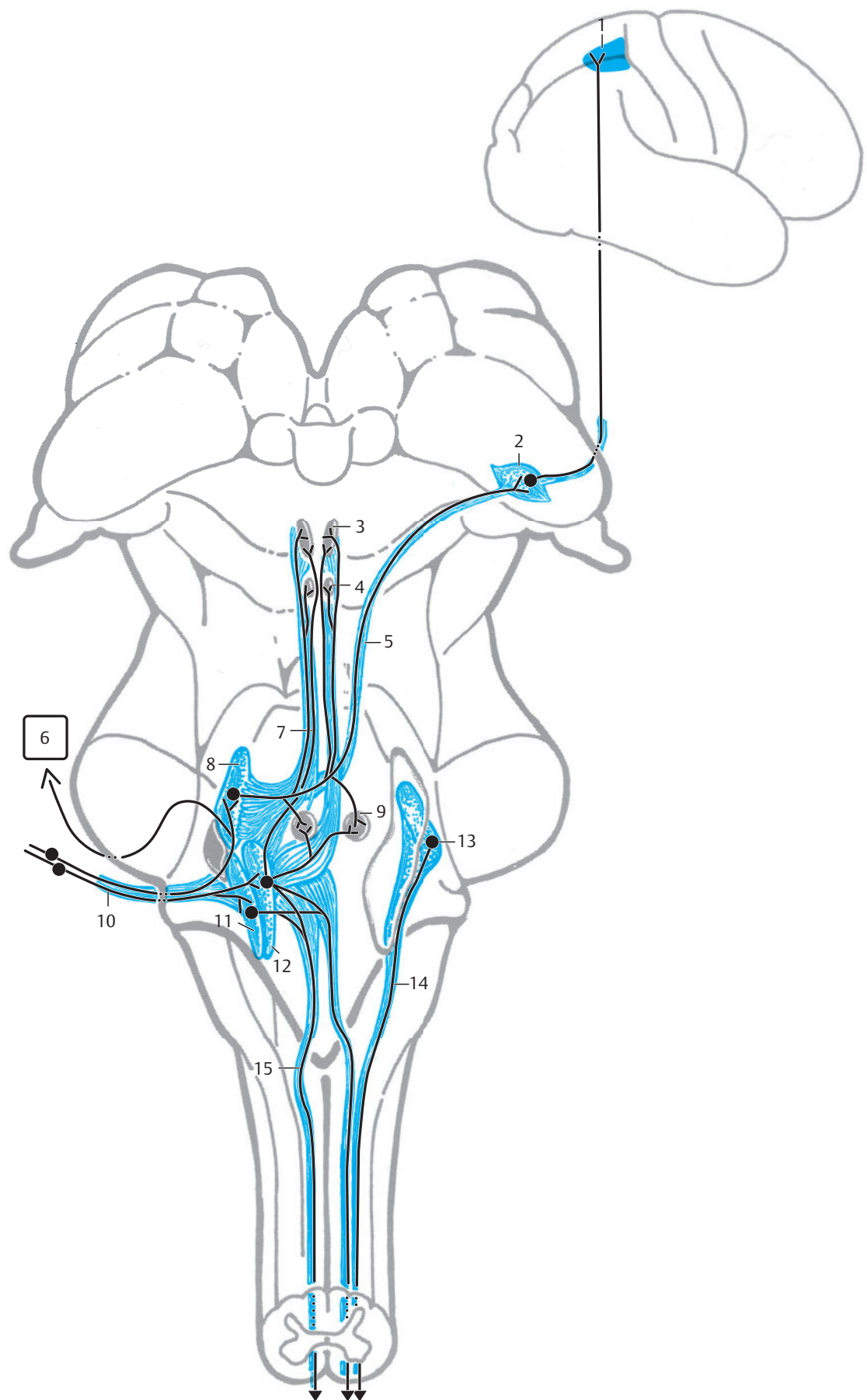
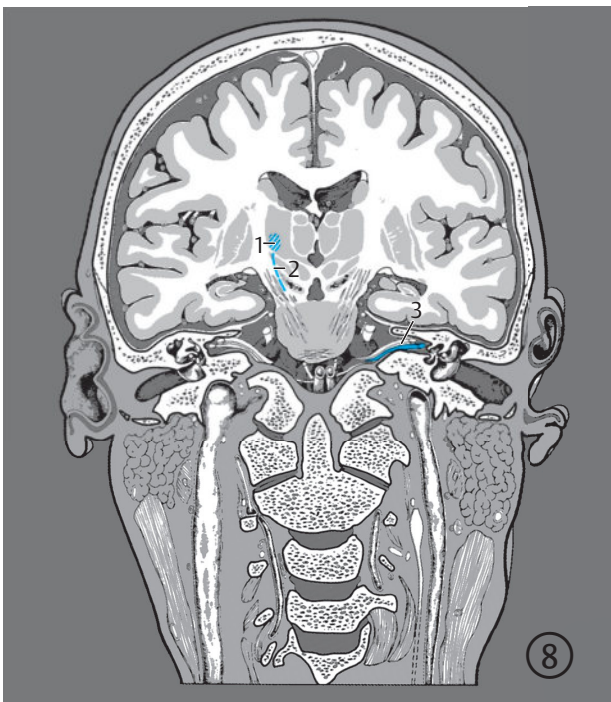


Fig. 10.11 Vestibular system. Viewed posteriorly in the spinal cord, brainstem, and diencephalon and laterally in the cerebellum. (Reproduced from Nieuwenhuys et al.⁴²⁴)



- 1 Ventral intermediate nuclei of thalamus (within the slice)
- 2 Vestibulothalamic tract (within the slice)
- 3 Vestibular nerve
- 4 Hypothetical fibers from thalamus to parietal cortical area
- 5 Vestibulothalamic tract (within the slice)
- 6 Lateral vestibular nucleus (of Deiters) (within the slice)
- 7 Vestibular nuclei (within the slice)
- 8 Lateral vestibulospinal tract (within the slice)
- 9 Medial vestibulospinal tract (within the slice)
- 10 Lateral and medial vestibulospinal tract (within the slice)
- 11 Vestibular parietal cortical area

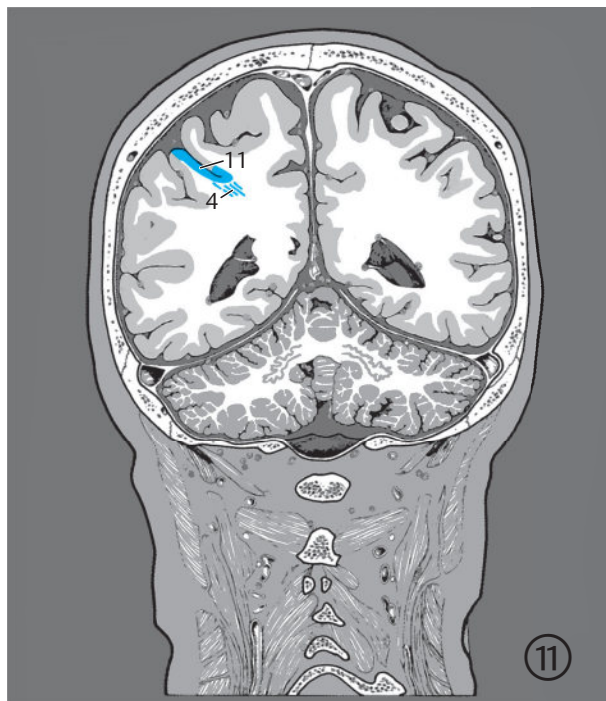
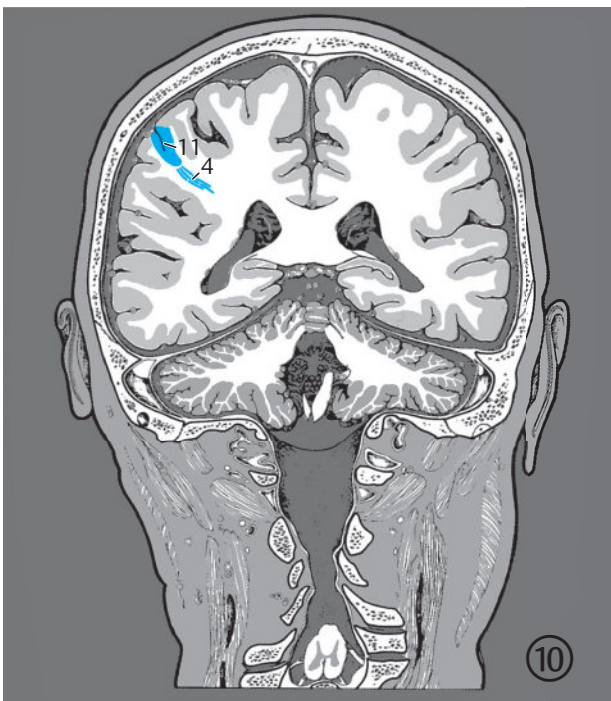


Fig. 10.12 Vestibular system. Serial coronal images. Encircled digits indicate the number of the respective slice (see ► Fig. 3.1).

- 1 Medial vestibulospinal tract
- 2 Lateral vestibulospinal tract
- 3 Vestibular nerve
- 4 Vestibular nuclei
- 5 Lateral vestibular nucleus (of Deiters)

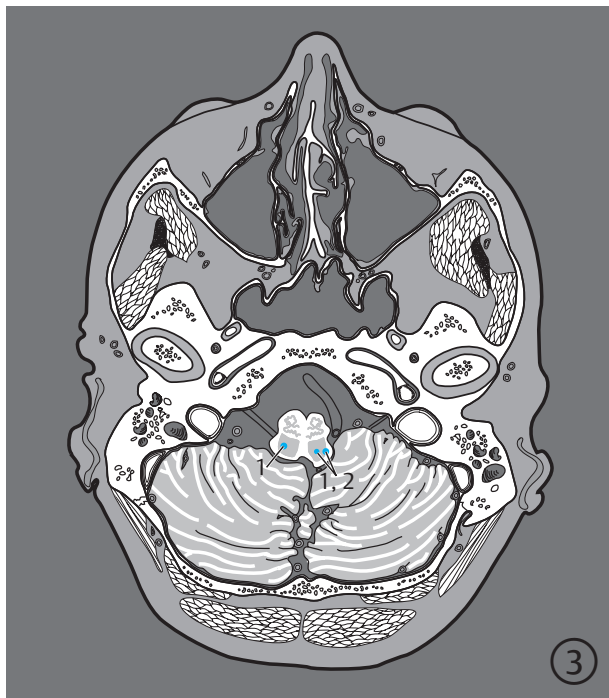
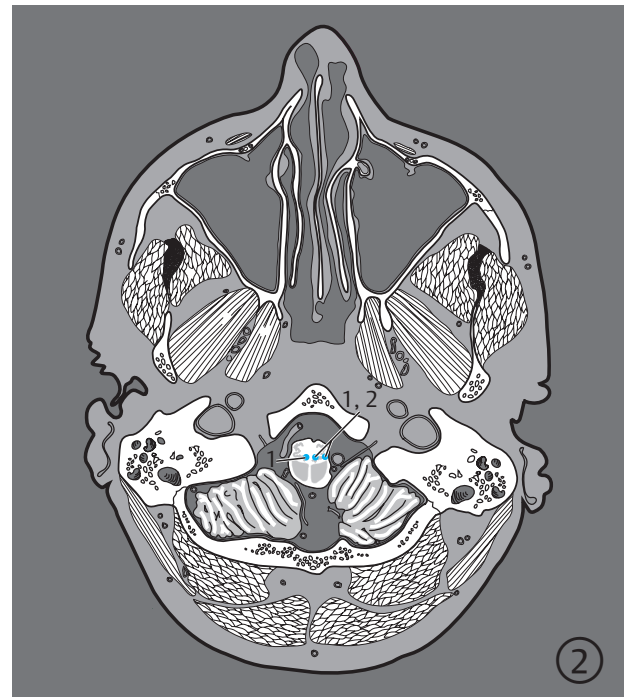
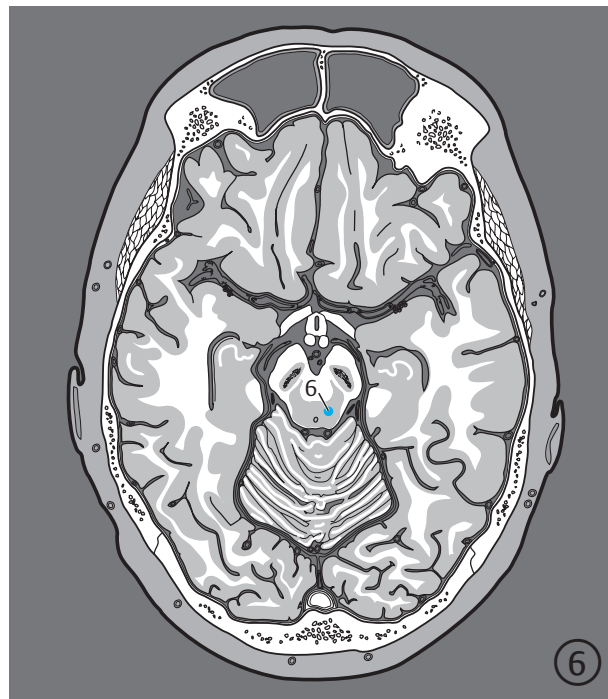
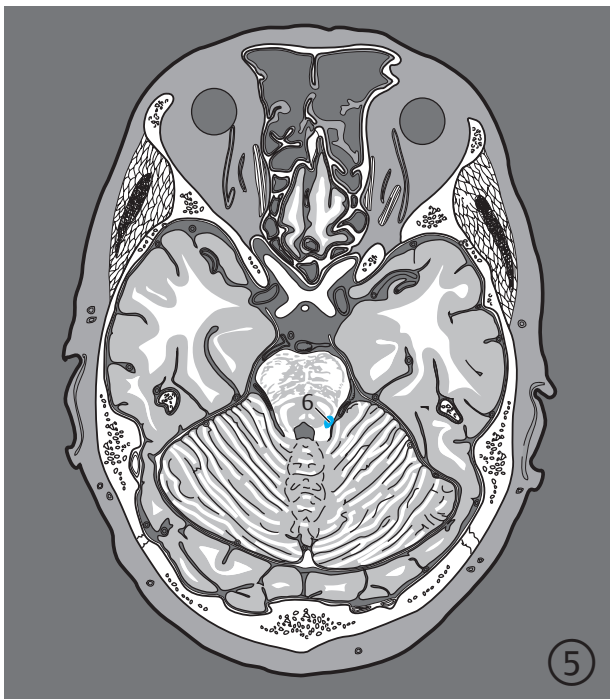


Fig. 10.13 Vestibular system. Serial images oriented along the bicommissural plane. Encircled digits indicate the number of the respective slice (see ► Fig. 5.1).

Fig. 10.13a 1st to 4th sections.

The vestibular system has numerous connections with the motor neurons of the eye, neck, trunk, arm, and leg muscles (vestibular reflexes). There are fewer pathways between the vestibular system and the cerebral cortex and these are probably relayed in the small contralateral ventral posterior nuclei of the thalamus⁴²⁴ and then in a parietal cortical area around

the intraparietal sulcus. Another pathway runs via the ventral posterolateral nuclei of the thalamus to area 3 in the postcentral gyrus but has not been demonstrated in ► Fig. 10.11, ► Fig. 10.12, and ► Fig. 10.13. Other small vestibular cortical areas (area 7, parieto-insular and insular cortical areas) have been demonstrated in monkeys.⁹⁴



- 6 Vestibulothalamic tract
- 7 Ventral intermediate nuclei of thalamus (within the slice)

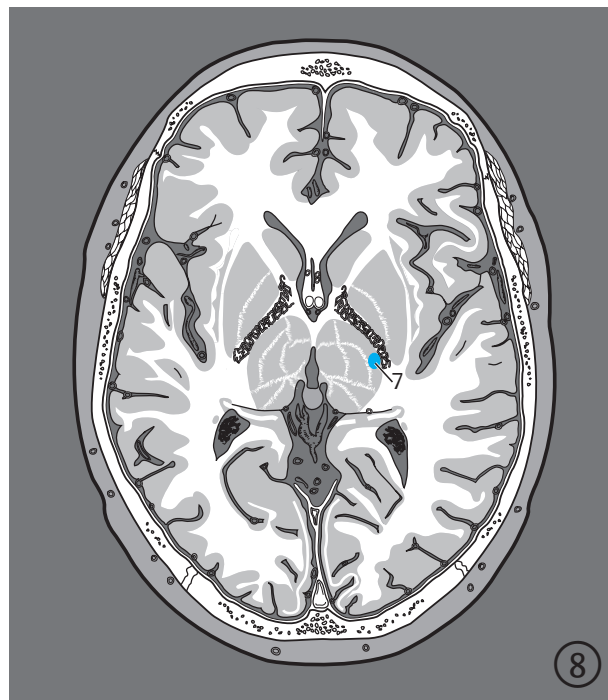
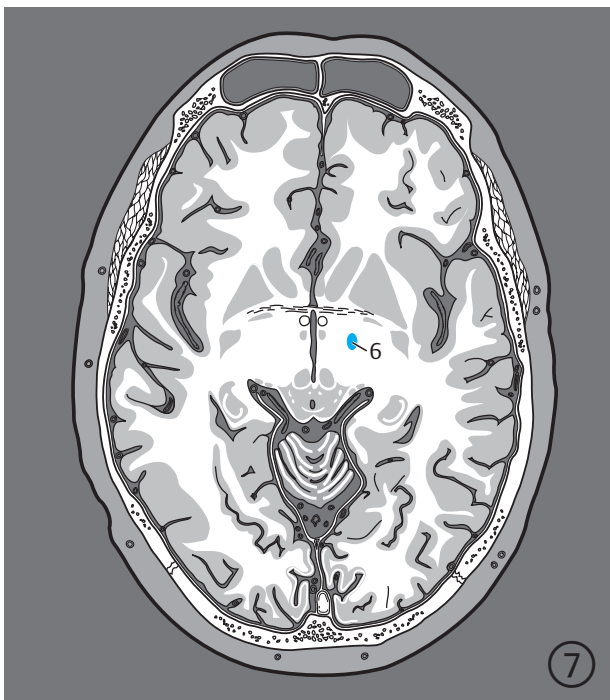


Fig. 10.13b 5th to 8th sections.

- 8 Hypothetical fibers from thalamus to parietal cortical area
- 9 Vestibular parietal cortical area

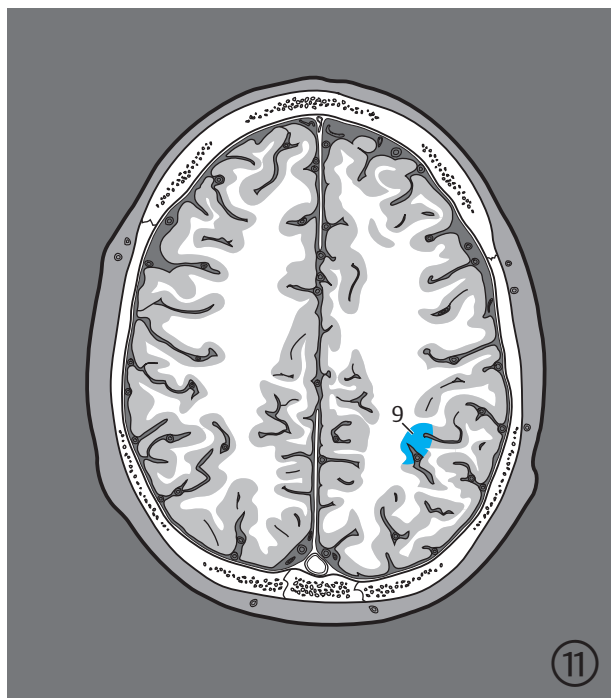
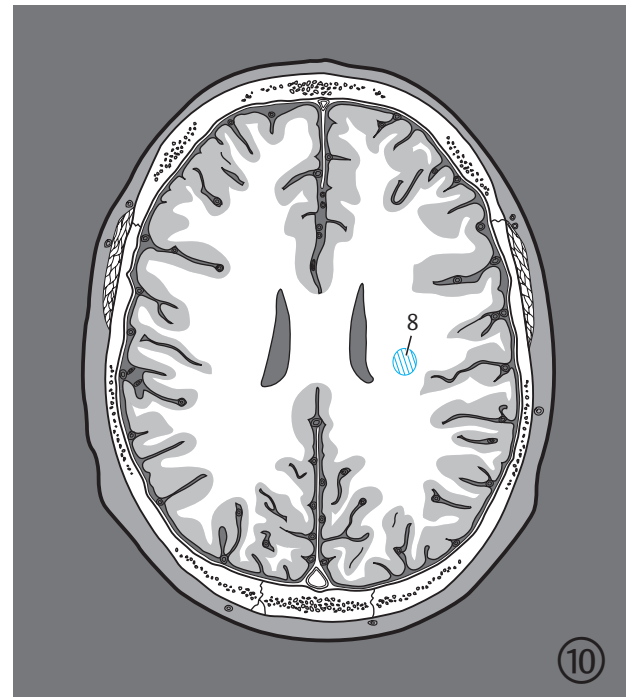
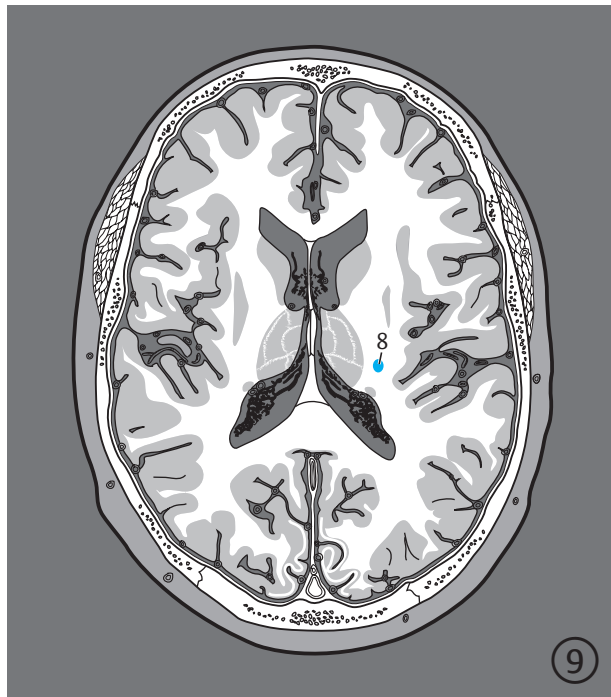


Fig. 10.13c 9th to 11th sections.

Clinical Notes

Vestibular system lesions result in a disturbance of equilibrium. Acute vestibular lesions initially cause vertigo. Unilateral lesions of the vestibular apparatus are compensated for after several weeks while unsteadiness of gait persists with bilateral lesions.^{149,387,407,408}

“Nystagmus” implies a sequence of involuntary or reflex triggering of movements of both eyeballs with slow and rapid components, triggered by saccadic generators via brainstem pathways. Spontaneous nystagmus is always pathological and is indicative of a peripheral or central lesion. Peripheral lesions affect receptors in the semicircular canals and/or the first vestibular neuron while central disturbances affect subsequent neurons of the vestibular system. Gaze-dependent nystagmus is seen with lesions of the cerebellum, medulla oblongata as well as mesencephalic and diencephalic structures serving visual motor function.^{351,387} Fixation nystagmus occurs as pendulous movements during fixation of the globe and is a central congenital disorder of the oculomotor system. Spontaneous nystagmus is observed after elimination of fixation by means of illuminated glasses and is seen both with peripheral and central vestibular disorders. Since different lesions may result in similar forms of nystagmus, the presence of nystagmus alone is inadequate for topical diagnosis. Dissociated nystagmus, whereby the abducting eye exhibits larger excursions of the globe, indicates a lesion near the midline in the region of nuclei of extraocular muscles in the brainstem. Rotatory and vertical nystagmus also indicates the presence of a central lesion.

10.5 Auditory System

Sound waves reach the tympanic membrane through the external acoustic canal; its vibration is mechanically amplified by auditory ossicles in the middle ear which are then transmitted to the oval window (see ► Fig. 7.5 and ► Fig. 7.6). The resulting movements of the endolymph are perceived by **hair cells of the organ of Corti** in the cochlea and are transmitted to the chain of neurons of the auditory system (see ► Fig. 10.14, ► Fig. 10.15, ► Fig. 10.16, and, ► Fig. 10.17). Anatomically speaking, retrocochlear hearing loss results from a lesion of this chain of neurons. The first-order neurons of this chain are formed in the cochlea by the bipolar nerve cells of the **cochlear (spiral) ganglion**. Their peripheral processes innervate the bases of the hair cells. The central axons of bipolar ganglion cells form the **cochlear nerve** (cochlear division of the VIIIth cranial nerve), which emerges from the petrous part of the temporal bone through the internal acoustic opening and enters the medulla oblongata

at the cerebellopontine angle. The central axons then divide into two branches: one extending toward the posterior cochlear nucleus and the other in the direction of the anterior cochlear nucleus. The second-order auditory neurons originate in these two nuclei:

- The axons of the **posterior cochlear nucleus** belong to the posterior part of the auditory pathway and pass along the floor of the rhomboid fossa immediately beneath the medullary striae of the IVth ventricle. Crossing over to the opposite side, they pass anteriorly and ascend in the **lateral lemniscus** to reach the inferior colliculus. Additional neurons may be connected along the way. Auditory signals are carried from the axons of nerve cells of the **inferior colliculus** via the brachium of the inferior colliculus to the **medial geniculate body**; the last neurons of this auditory chain pass from here through the auditory radiation to the primary auditory cortex (area 41, see ► Fig. 7.53). The latter is located approximately in the **anterior transverse temporal gyrus (of Heschl)** in the depths of the lateral sulcus.²²⁵ Heschl's gyrus is only visible on the cerebral convexity by splaying the lateral sulcus.
- The anterior auditory pathway runs in the trapezoid body from the **anterior cochlear nucleus** via the **superior olivary nucleus** and via the nuclei of the trapezoid body, crossing to the opposite side to join the **lateral lemniscus**. It then follows an identical course as the posterior part of the auditory pathway already described. Another part of the anterior auditory pathway remains on the same side, ascending ipsilaterally through the aforementioned subcortical centers to the **primary auditory cortex of the cerebrum** (area 41).

This ipsilateral and contralateral course of the auditory pathway allows highly specialized neurons to determine travel time between two **sources of sound** when one is more distant from one ear than from the other, thereby enabling directional localization of a source of sound by hearing alone. The second-order and higher auditory neurons are highly specialized in the interpretation of specific sound patterns, and may filter out useful sounds, for example, speech from background noise.

The **posterior and anterior cochlear nuclei** (see ► Fig. 6.7b) are situated in the medulla oblongata immediately anterior to the point of entry of the vestibulocochlear nerve at the pontomedullary junction.⁵⁷⁹ The cochlear nuclei lie on the lateral surface of the medulla oblongata at the level of the lateral recess of the IVth ventricle (see ► Fig. 6.7b and ► Fig. 10.15). The inferior cerebellar peduncle borders the cochlear nuclei at their anteromedial aspect, which helps in indirect localization of cochlear nuclei in MR images.¹⁹

- 1 Optic chiasm
- 2 Temporal lobe
- 3 Third ventricle
- 4 Primary auditory cortex in transverse temporal gyrus (of Heschl)
- 5 Thalamus
- 6 Pineal gland
- 7 Lateral ventricle
- 8 Splenium of corpus callosum
- 9 Acoustic radiation
- 10 Medial geniculate body
- 11 Brachium of inferior colliculus
- 12 Inferior colliculus
- 13 Commissure of inferior colliculus
- 14 Nucleus of lateral lemniscus
- 15 Lateral lemniscus
- 16 Pons
- 17 Superior olivary nucleus
- 18 Bipolar nerve cells in spiral ganglion
- 19 Cochlear nerve
- 20 Anterior (ventral) cochlear nucleus
- 21 Trapezoid body
- 22 Nuclei of trapezoid body
- 23 Posterior (dorsal) cochlear nucleus
- 24 Posterior acoustic stria
- 25 Medulla oblongata

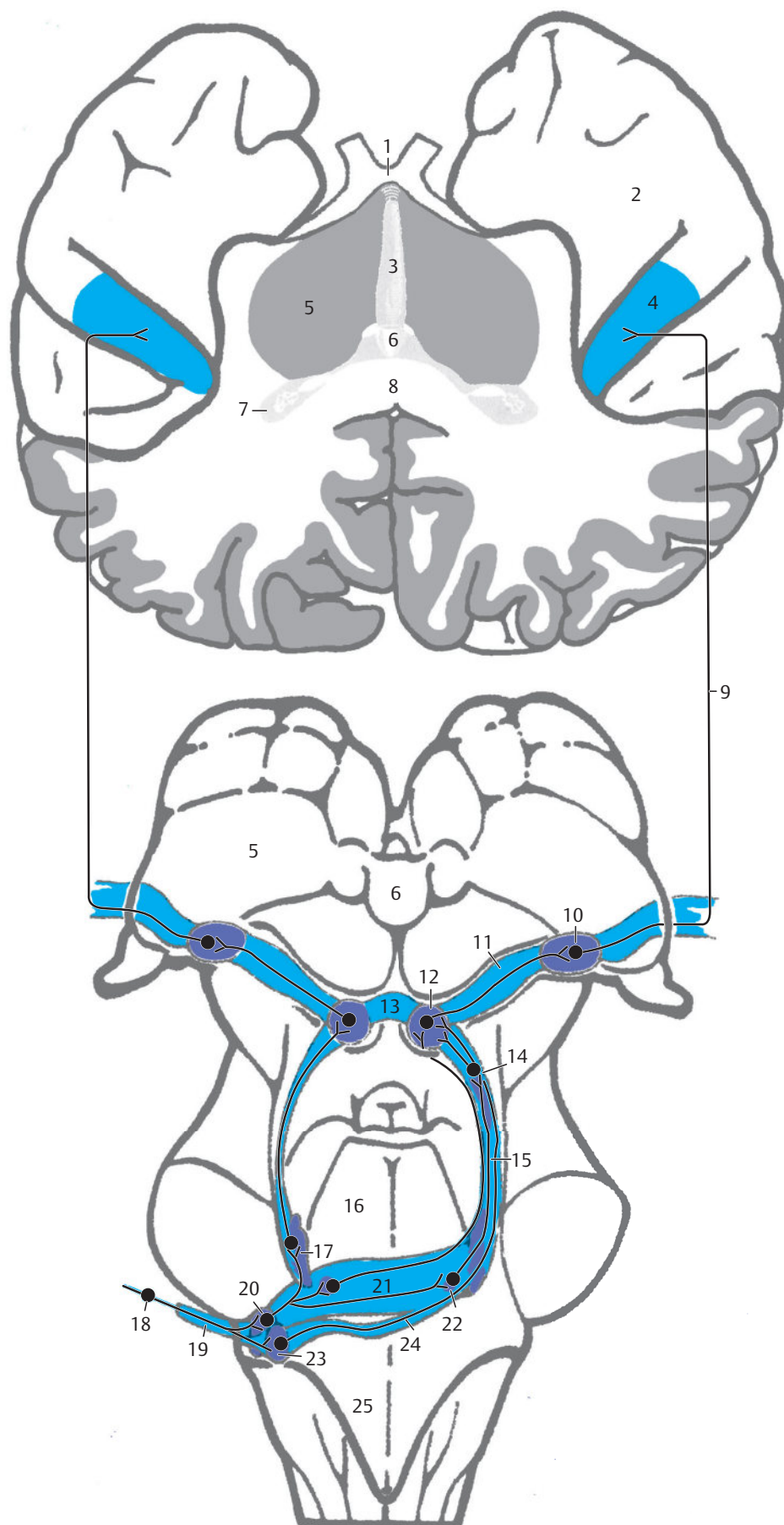
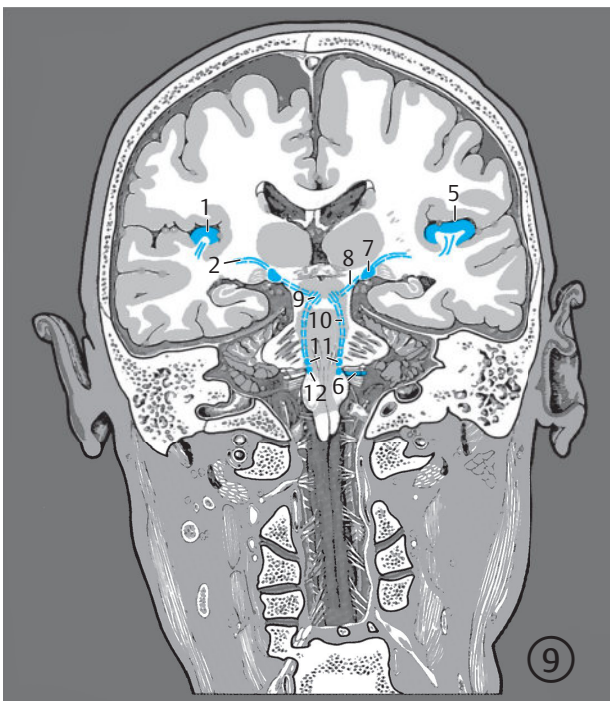


Fig. 10.14 Auditory system. Schematic representation of the neuronal circuit of the auditory system in the brainstem and the diencephalon in posterior and superior views of both temporal lobes, as well as on a cross section passing just above the optic chiasm and through the center of the splenium of the corpus callosum. (Reproduced from Nieuwenhuys et al.⁴²⁴) This sectional plane lies anteriorly about 20° below and posteriorly about 20° above the bicommissural plane.



- 1 Anterior transverse temporal gyrus (of Heschl)
- 2 Acoustic radiation
- 3 Transverse temporal gyrus (of Heschl) (in the posterior part of the slice)
- 4 Medial geniculate body (in the posterior part of the slice)
- 5 Transverse temporal gyrus (of Heschl)
- 6 Cochlear nerve
- 7 Medial geniculate body
- 8 Brachium of inferior colliculus
- 9 Inferior colliculus (in the posterior part of the slice)
- 10 Lateral lemniscus (within the slice)
- 11 Superior olivary nucleus
- 12 Anterior (ventral) and posterior (dorsal) cochlear nuclei (within the slice)

Fig. 10.15 Auditory system. Serial coronal images. Encircled digits indicate the number of the respective slice (see ► Fig. 3.1). Ipsilateral and contralateral parts of the anterior auditory tract seen emerging from the left cochlear nerve. Two transverse temporal gyri are present in the right hemisphere.

- 1 Inferior colliculus
- 2 Lateral lemniscus (in the lateral part of the slice)
- 3 Trapezoid body
- 4 Medullary striae of IVth ventricle
- 5 Brachium of inferior colliculus
- 6 Lateral lemniscus
- 7 Superior olivary nucleus
- 8 Cochlear nerve (within the slice)
- 9 Posterior (dorsal) and anterior (ventral) cochlear nuclei (within the slice)
- 10 Acoustic radiation (in the lateral part of the slice)
- 11 Medial geniculate body
- 12 Cochlear nerve
- 13 Acoustic radiation (partially within the slice)

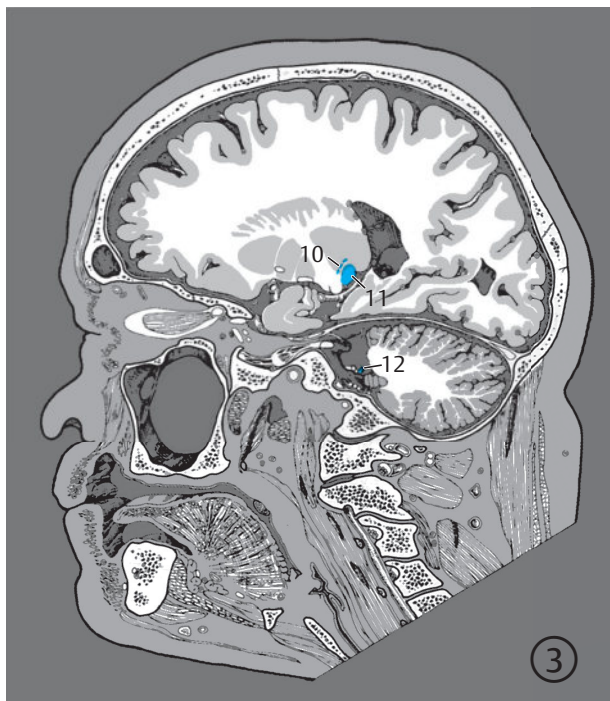
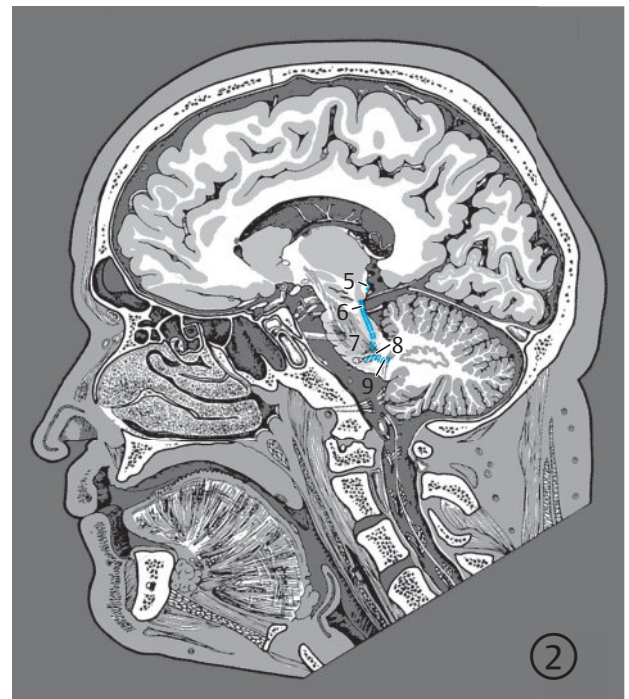
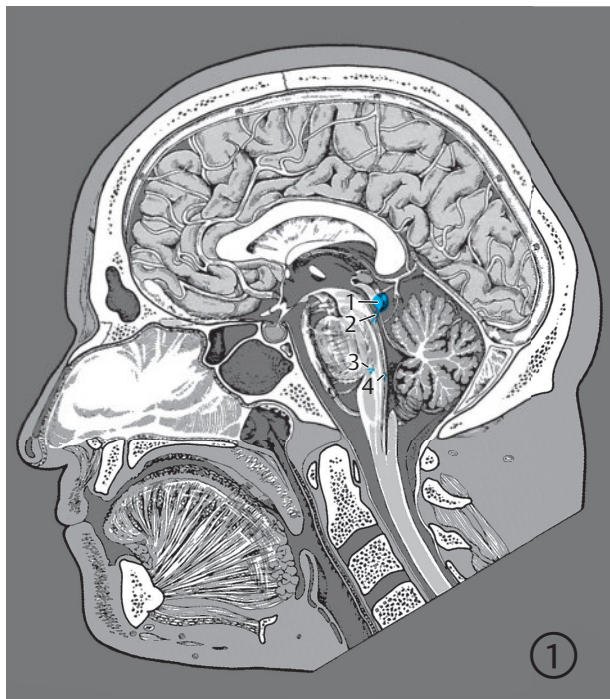
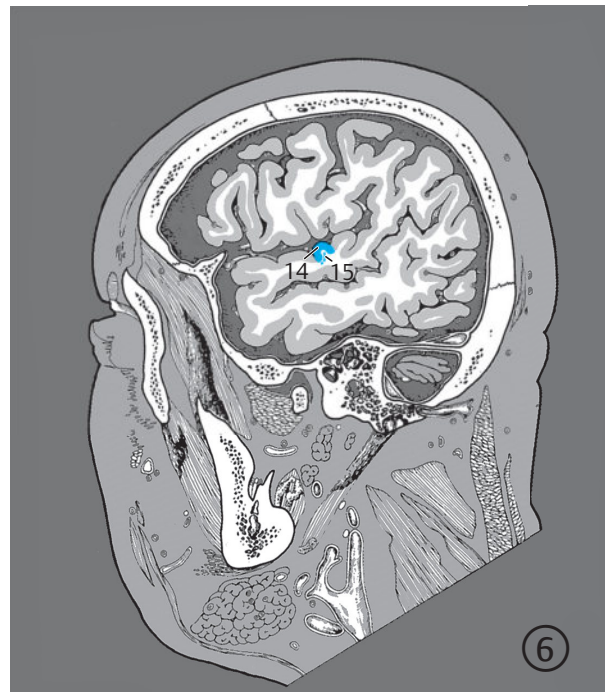
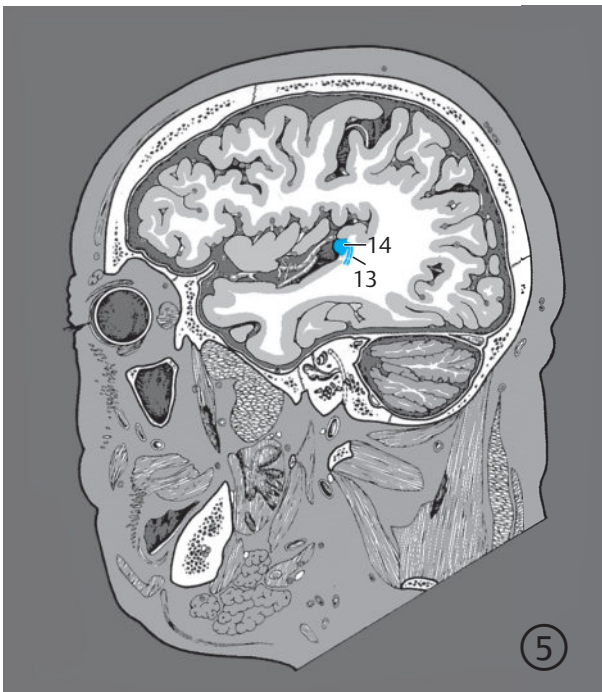


Fig. 10.16 Auditory system. Serial sagittal images. Encircled digits indicate the number of the respective slice (see ► Fig. 4.3, ► Fig. 4.4a, ► Fig. 4.4b, and ► Fig. 4.5).

Fig. 10.16 a 1st to 4th sections.



- 13 Acoustic radiation (partially within the slice)
- 14 Anterior transverse temporal gyrus (of Heschl)
- 15 Acoustic radiation

Fig. 10.16b 5th and 6th sections.

Only the larger, anterior part of the auditory pathway is represented in ► Fig. 10.15, ► Fig. 10.16, and ► Fig. 10.17 and courses through the **trapezoid body**. Fibers of the trapezoid body exit the cochlear nuclei at their anterior border and run in a gradual upward direction anterior to the inferior cerebellar peduncle and continue to the ipsilateral and contralateral auditory complex consisting of the superior olivary nucleus and the nuclei of the trapezoid body. The fibers traverse the anterior part of the medial lemniscus and are situated posterior to pontine nuclei in the inferior region of the pons. The trapezoid body may be identified directly on MR images as well as by virtue of its topographic relationship to the medial lemniscus.¹⁹

The **lateral lemniscus** (see ► Fig. 6.9b, ► Fig. 6.10b, ► Fig. 6.11b, and ► Fig. 10.14) originates in the nuclear complex of the superior olivary nucleus and in the nuclei of the trapezoid body and terminates in the inferior colliculus (see ► Fig. 6.12b). It measures approximately 25 mm in length. Auditory signals may be relayed through synapses in one or more nuclei of the lateral lemniscus. These have not been described in greater detail here and have not been depicted in ► Fig. 10.14, ► Fig. 10.15, ► Fig. 10.16, ► Fig. 10.17. The lateral lemniscus runs upward in the lateral part of the tegmentum of the pons and lies immediately beneath the posterolateral surface of the pontine tegmentum at the junction between midbrain and pons. It borders the **lateral surface** of the superior cerebellar peduncle near the inferior colliculus, radiating into the latter from its anterolateral aspect.

The **inferior colliculus** is visualized in the first sagittal section as an inferior bulge of the quadrigeminal plate

lying posterior to the aqueduct of the midbrain (see ► Fig. 4.2a and ► Fig. 4.2b). The lateral lemniscus may be identified on axial MR images by virtue of its contrast with neighboring structures.¹³⁰ The inferior colliculus is clearly visualized on sagittal, axial, and coronal MR images due to its exposed position.^{19,511}

Perikaryal axons of the inferior colliculus form the **brachium of inferior colliculus**, a narrow band of fibers on the lateral aspect of the tegmentum of the midbrain. At the junction of the midbrain and the diencephalon, the brachium of the inferior colliculus curves laterally over about 5 mm to enter the **medial geniculate body** at its posteromedial aspect. The medial geniculate body lies laterally to the midbrain inferiorly within the diencephalon. The anterior surface of the medial geniculate body (see ► Fig. 3.10a, ► Fig. 3.10b, ► Fig. 4.4a, ► Fig. 4.4b, and ► Fig. 5.8) borders the internal capsule. The medial geniculate body measures approximately 8 to 9 mm in its largest diameter and 5 to 6 mm in its vertical span. It is composed of three parts:

- **Secondary medial nucleus:** This small, secondary nucleus lies posteromedial to the principal nucleus and contains large cells.³⁹⁹ Electrophysiological examinations indicate that it obtains somatosensory, vestibular and auditory afferents and is thus multimodal.^{10,399}
- **Secondary dorsal nucleus:** This is a small triangular nuclear area which receives visual and auditory signals.
- **Secondary ventral nucleus:** This is the largest nuclear area, and contains small cells. Also termed the “principal division”, it receives purely auditory signals.²⁷⁹

- 1 Cochlear nerve
- 2 Cochlear nuclei (within the slice)
- 3 Trapezoid body (within the slice)
- 4 Lateral lemniscus
- 5 Medial geniculate body
- 6 Brachium of inferior colliculus
- 7 Inferior colliculus

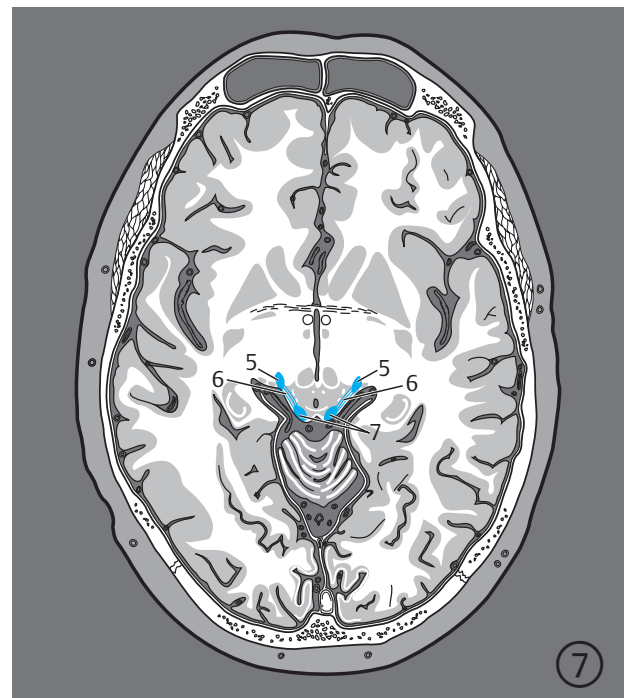
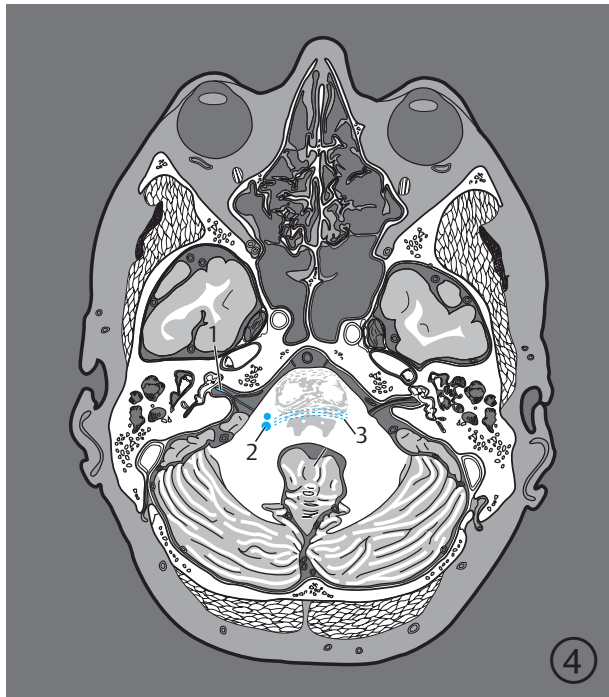
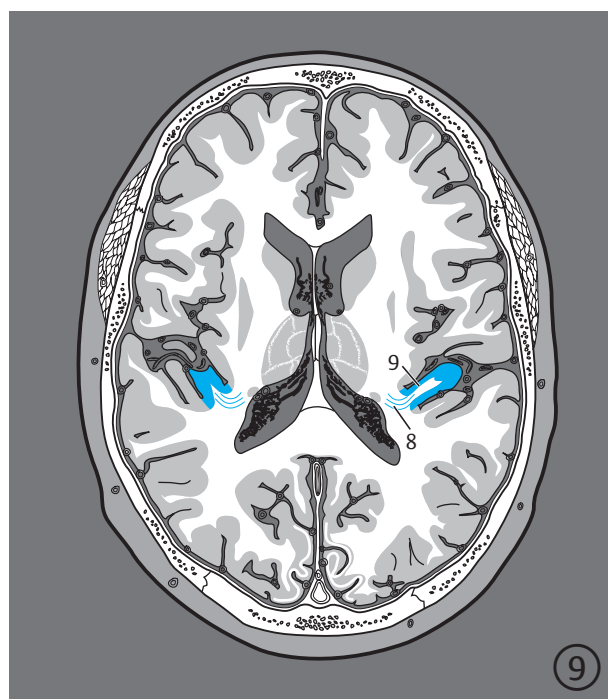
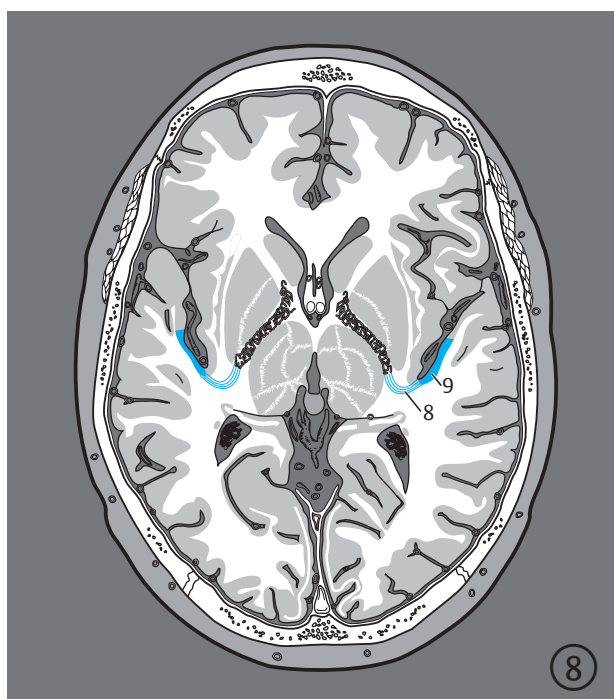


Fig. 10.17 Auditory system. Serial images oriented along the bicommissural plane. Encircled digits indicate the number of the slice (see ► Fig. 5.1).

Fig. 10.17a 4th to 7th sections.



- 8 Acoustic radiation
- 9 Transverse temporal gyrus (of Heschl)

Fig. 10.17b 8th and 9th sections.

The fibers of the brachium of the inferior colliculus reach the posteromedial aspect of the medial geniculate body; emerging fibers exit as the acoustic radiation anterolaterally.^{312,314}

The **acoustic radiation** interconnects the medial geniculate body with the primary auditory cortex. It was described for the first time in humans on myelogenetic microscopic specimens of infant brains⁴⁶¹ and further details were revealed by subsequent studies.^{73,315}

The acoustic radiation begins at the anterolateral border of the medial geniculate body and its initial fibers ascend while curving laterally, lying above the optic tract and below thalamoparietal fibers.

It is bordered by the lateral geniculate body posteroinferiorly, posterosuperiorly by the pulvinar and anterosuperiorly by the rest of the thalamus. Further laterally, the optic radiation borders the acoustic radiation at its posterior aspect. The acoustic radiation passes through the **posterior end of the posterior limb** of the internal capsule and then posterior to the lateral part of the globus pallidus and along the putamen and claustrum. It finally curves anteriorly around the **posterior border of the insular cortex** and ascends in the white matter of the transverse temporal gyrus to reach the primary auditory cortex.

The **primary auditory cortex** is known as “area 41” in cytoarchitectonic terms.⁶⁵⁰ Brodmann⁷⁶ localized area 41 roughly in the transverse temporal gyrus region (see ► Fig. 7.53). Area 41 continues in an anterior direction over the transverse temporal gyrus. Area 42 forms an arc encompassing field 41. The area corresponding to

field 41 is described as “area supratemporalis granulosa” on the **anterior transverse temporal gyrus (of Heschl)**.¹⁵⁵ The primary auditory cortex was localized in the medial aspect of the transverse temporal gyrus and the adjoining part of the planum temporale using pigmentarchitectonic methods.^{68,69} Auditory evoked potentials from cortical auditory fields were recorded intraoperatively in over 20 patients^{102,307} as part of electrophysiological studies. Potentials were relatively constant and had short latencies over the medial two-thirds of the anterior and posterior transverse temporal gyri while the area surrounding the planum temporale and the superior temporal gyrus showed potentials with smaller amplitudes and long latencies. As a rule, two transverse temporal (Heschl) gyri (anterior and posterior) are seen on the right while one is visualized on the left.^{182,183} The **transverse temporal gyrus** lies above the superior temporal gyrus in the depths of the lateral sulcus. It runs from the posterior edge of the insula separated from it by its circular sulcus, descends obliquely from posteromedial to anterolateral and is limited posteriorly by the transverse temporal sulcus. The entire transverse temporal gyrus and the primary auditory cortex are covered by the **parietal operculum** and are therefore not directly visible with an intact hemisphere. The transverse temporal gyrus may be easily identified on transversal, coronal and sagittal MR images.^{19,639,642}

The auditory system (see Section 10.5) is the shortest neurofunctional system as compared with the medial lemniscus, visual, and corticospinal systems. Its primary cortical area lies in the depth of the lateral sulcus.^{312,314}

Clinical Notes

Some of the mentioned brainstem nuclei are not merely relay nuclei but also reflex centers, connecting nuclei of the trapezoid body with motor nuclei of the VIIth cranial nerve, thereby forming a reflex arc from the spiral organ of Corti to the stapedius. This muscle contracts reflexively in response to high intensity sound and consequently dampens the transmission of sound waves from the tympanic membrane to the stapes (stapedius reflex). Loss of this reflex results in hyperacusis.

Additional reflex pathways extend from the inferior to the superior colliculi and modulate reflexes associated with eye and head movements in response to auditory stimuli. In addition, neurons of the reticular formation are interconnected in parallel with ascending sections of the auditory pathway.

A pathway from the auditory cortex and the inferior colliculi descends to the periolivary nuclei in the inferior part of the pons. An efferent pathway (olivocochlear tract of Rasmussen) originates in these periolivary nuclei and extends into the cochlea, terminating in the hair cells of the organ of Corti. This tract contains cholinergic (see Section 11.4) and enkephalinergic fibers (see Section 11.7.4). Experimentally, impulses arising in the auditory nerve can be suppressed by stimulation of this olivocochlear tract.

Clinical Notes

Clinically, middle ear, cochlear, and retrocochlear hearing loss may be differentiated. Identification of middle ear deafness involves a simple examination using a tuning fork. In addition to audiometry, neurophysiological tests such as AEP or BERA are employed to distinguish a cochlear or retrocochlear hearing defect. Early acoustic evoked brainstem potentials were thus named in inconsistent international nomenclature.^{387,564} Recording AEP using surface electrodes following repeated acoustic stimuli enables localization of lesions both at the periphery and centrally at various levels in the brainstem.³⁶⁶

MRI or alternatively thin-section CT with IV contrast are diagnostic modalities of choice in suspected cases of acoustic schwannoma (commonly known as “acoustic neurinoma”) or other space-occupying lesions of the cerebellopontine angle as well as in patients with central hearing loss.

10.6 Visual System

The photoreceptors of the visual system lie in the **retina** (see ► Fig. 10.18, ► Fig. 10.19, ► Fig. 10.20, ► Fig. 10.21). Optical signals emitted from the rods and cones are transmitted through bipolar nerve cells to large multipolar nerve cells. The neurites of these multipolar neurons extend along the inner layer of the retina and converge at the optic disc, they pass through the lamina cribrosa of the sclera to form the **optic nerve**. Within the orbit, the optic nerve measures approximately 3 cm in length and pursues a slightly curved course to allow for free movements of the globe. This nerve crosses the bicommissural plane at an acute angle. The optic nerve passes through the **optic canal**, a bony channel approximately 5 mm in length, to reach the **optic chiasm** (see ► Fig. 10.21a). The nerve is repositioned medially in the orbit with lateral movements of the eyeball.⁵⁰⁴ The optic nerve is ensheathed by the pia, arachnoid, and dura mater within the orbit with a narrow subarachnoid space; while these meningeal layers are firmly fused with the bony wall of the optic canal.

Inferiorly to the **optic chiasm** lie the sphenoid sinus and the sella turcica containing the pituitary gland (hypophysis). The hypothalamus is related posterosuperiorly while the internal carotid arteries lie laterally to the optic chiasm. Fibers from the nasal half of the retina (temporal visual field) cross in the optic chiasm, while fibers from the temporal half of the retina (nasal visual field) remain on the same side.

Both **crossed and uncrossed fibers** form the approximately 4 cm long optic tract. This tract arches along the border between the midbrain and the diencephalon to the lateral geniculate body where most of the fibers terminate (see ► Fig. 3.10a, ► Fig. 3.10b, ► Fig. 5.8, ► Fig. 10.19c, ► Fig. 10.20a, and ► Fig. 10.21b).

The **lateral geniculate body** lies inferiorly to the pulvinar nuclei of the thalamus and immediately laterally to the medial geniculate body. The largest axial cross section of the lateral geniculate body resembles the shape of a hat, with a maximum diameter of approximately 8 to 9 mm. Microscopically, the lateral geniculate body is composed of six cell layers separated by thin white zones (fibers of the optic tract). Most fibers of the optic tract terminate here in fourth-order neurons. Crossed optic nerve fibers terminate in layers 1, 4, and 6 and uncrossed fibers in layers 2, 3, and 5. Layers 1 and 2 are composed of magnocellular nerve cells while layers 3 to 6 consist of parvocellular nerve cells. A small section of optic tract fibers extends to the superior colliculi and pretectal areas which modulate reflexes of intrinsic and extraocular muscles. A third group of fibers forms the extrageniculate pathway leading to the cerebral cortex (see ► Fig 10.19d).

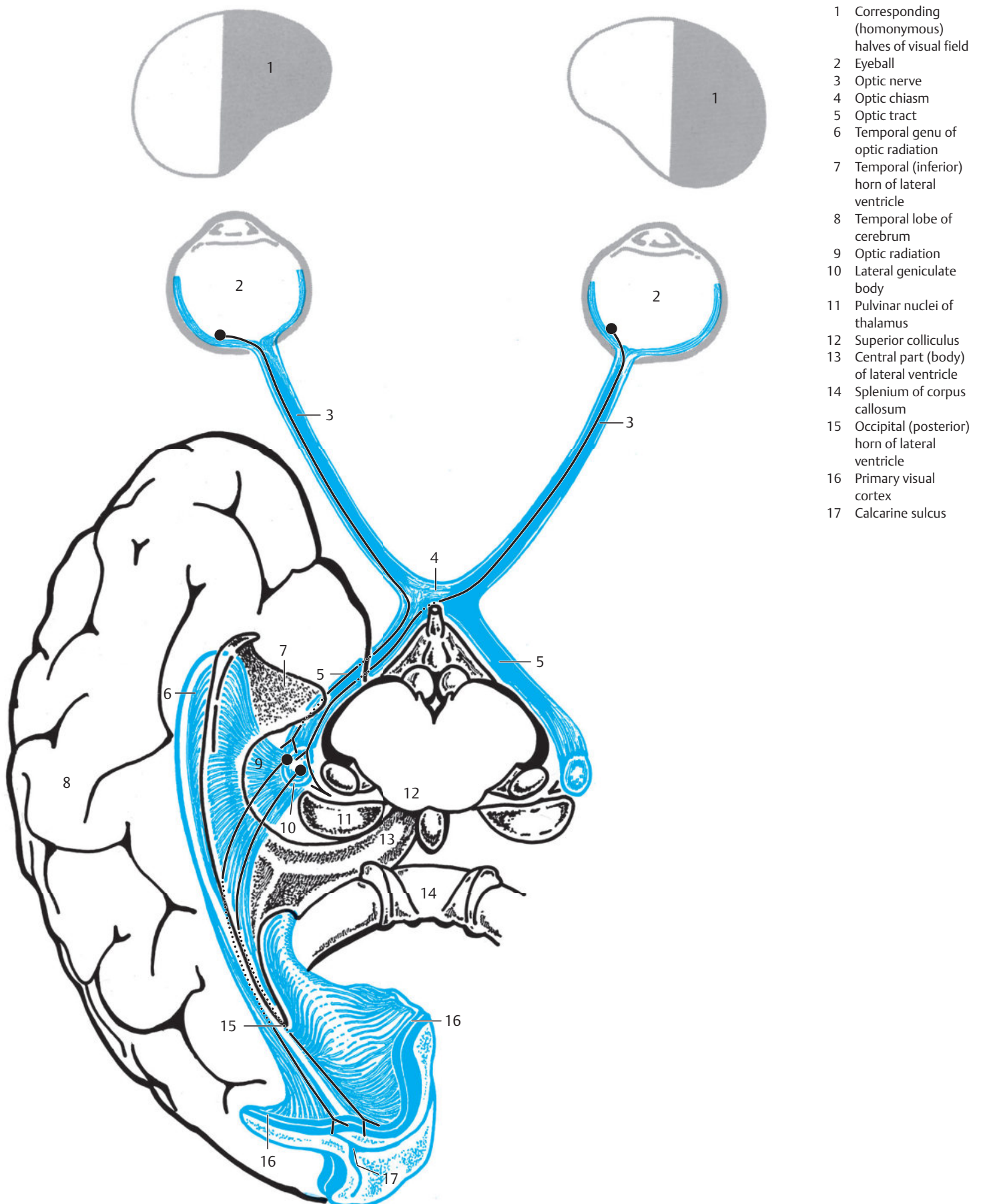


Fig. 10.18 Visual system. Inferior view. (Reproduced from Nieuwenhuys et al.⁴²⁴) Basal parts of the diencephalon and the midbrain lie between both optic tracts. Only the temporal and occipital lobes have been mapped from the right telencephalon. Two homonymous halves of visual fields have been shaded in grey. The schematic diagram delineates the pathway from each retina to the visual cortex.

- 1 Optic disc
- 2 Retina
- 3 Optic nerve

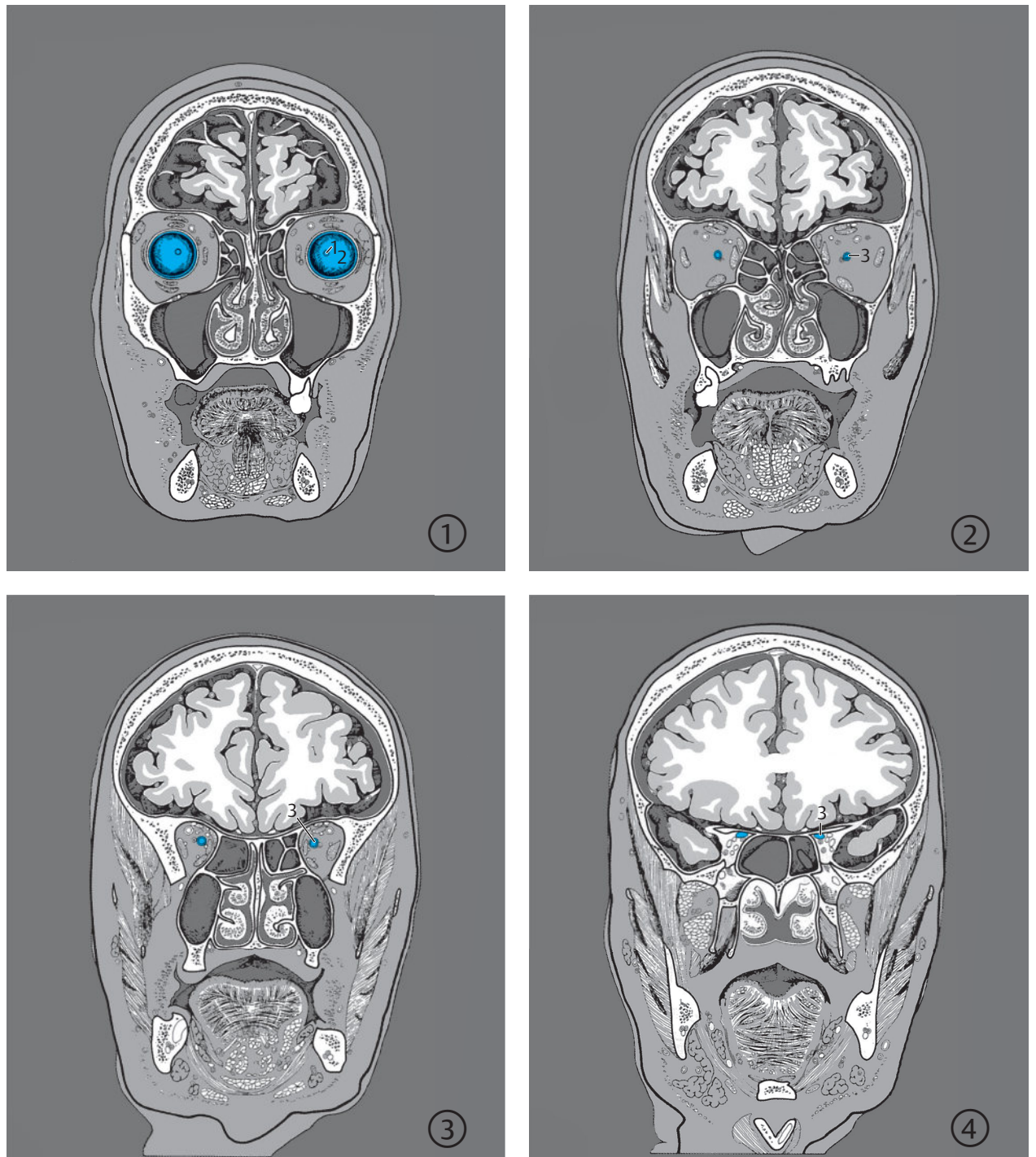
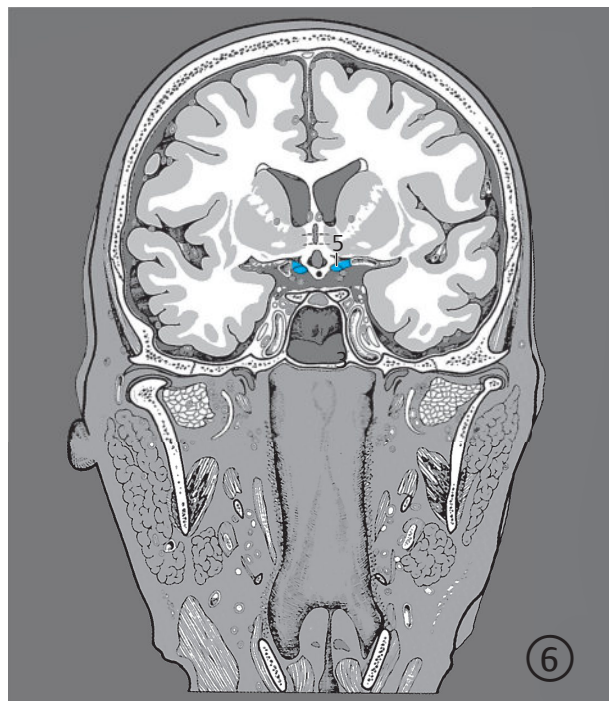
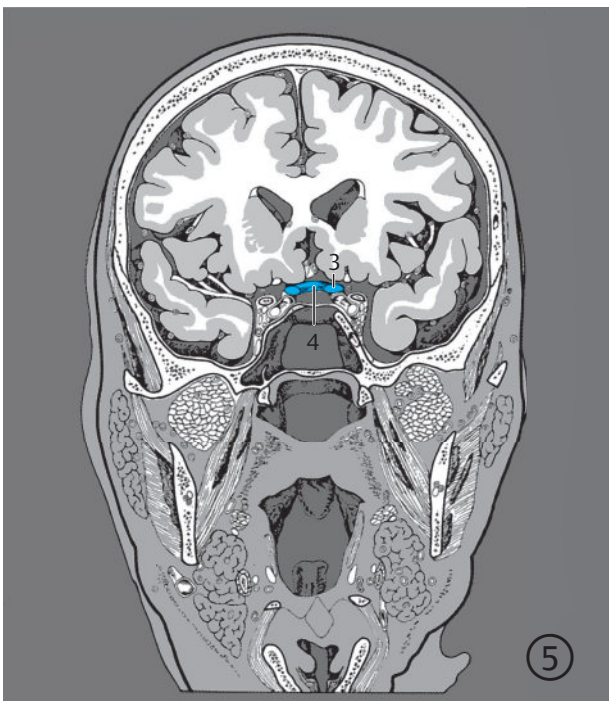


Fig. 10.19 Visual system. Serial coronal images. The optic radiation has been depicted in accordance with Talairach et al.⁵⁷³ Encircled digits indicate the number of the respective slice (see ►Fig. 3.1).

Fig. 10.19a 1st to 4th sections.



- 3 Optic nerve
- 4 Optic chiasm
- 5 Optic tract
- 6 Optic radiation, Meyer's loop

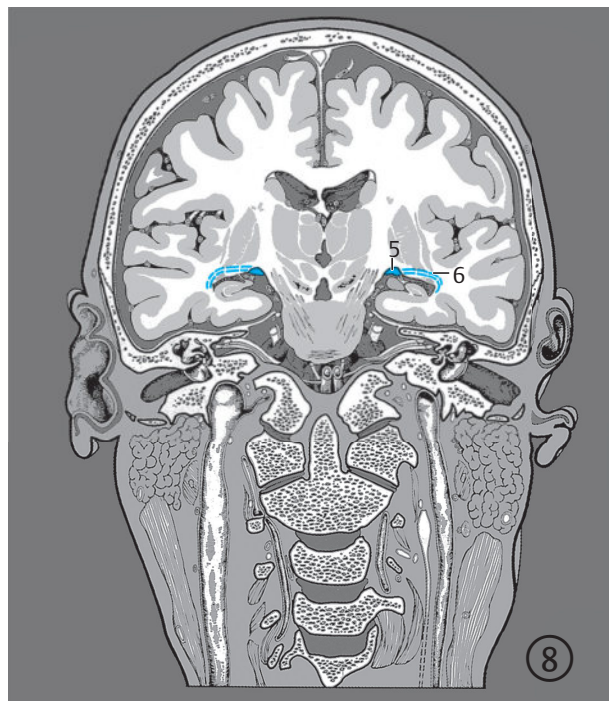


Fig. 10.19b 5th to 8th sections.

- 7 Lateral geniculate body
- 8 Optic radiation
- 9 Primary visual cortex, inferior lip

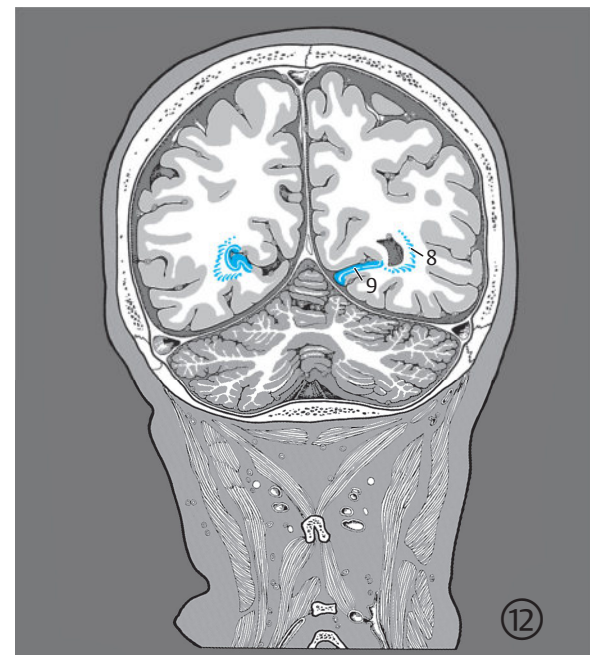
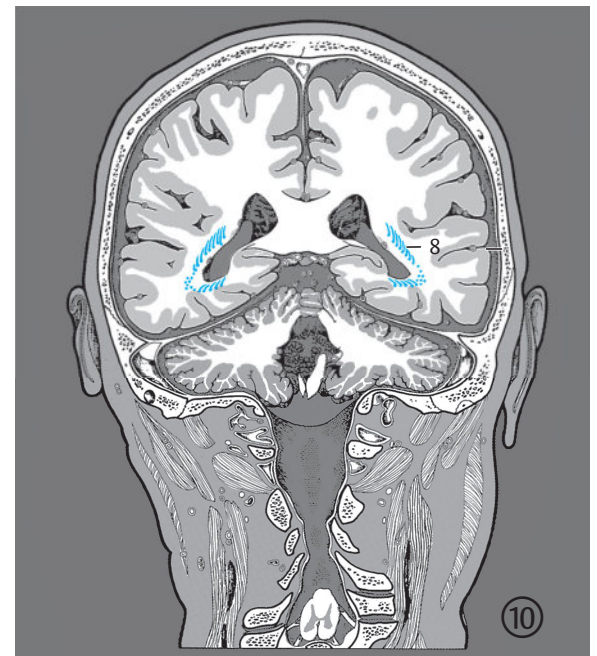
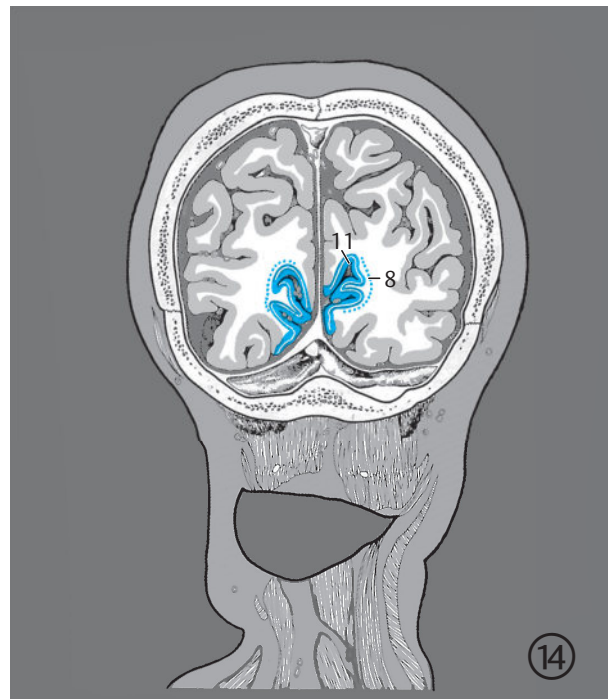
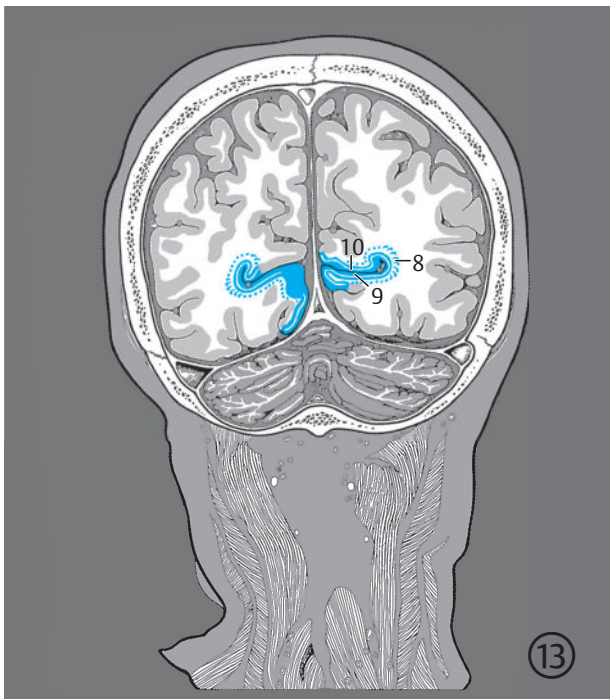


Fig. 10.19c 9th to 12th sections.



- 8 Optic radiation
- 9 Primary visual cortex, inferior lip
- 10 Primary visual cortex, superior lip
- 11 Primary visual cortex

Fig. 10.19d 13th and 14th sections.

The **optic radiation** arises from the lateral geniculate body arching at first over the temporal horn of the lateral ventricle before turning medially toward the visual cortex.^{106,107,263,603} Nerve cells from the medial half of the lateral geniculate body project mainly into the superior lip of the primary visual cortex and those from its lateral half to its inferior lip. The optic radiation may be identified on MR images and in histologic sections of infant brains aged 3 to 12 months.³⁸⁴ It lies lateral to the temporal and occipital horns of the lateral ventricle in an approximately sagittal plane (see ►Fig. 10.19c) and appears hook-shaped in coronal sections, with the open part of the hook directed medially. These fibers of the optic radiation arise in the posterior half of the lateral aspect of the **lateral geniculate body**. The upper layer of fibers in the optic radiation contains extramacular fibers which run to the anterior part of the upper lip of the primary visual cortex, while its middle part contains fibers which carry signals from the macula lutea of the retina to the occipital region of the primary visual cortex. The lower layer of fibers of the optic radiation runs through the loop at the anterior edge of the temporal horn of the

lateral ventricle, and passing underneath it, continues to the anterior part of the inferior lip of the primary visual cortex. Selective damage to this region impairs perception in the peripheral (extramacular) part of the upper quadrant of the visual field.²³⁶

The arc-like proximal part of the optic radiation, its **genu** or Meyer's loop, is not clearly demarcated in histological specimens of juvenile and adult brains since it is combined with other fibers and appears "matted" in histological sections. These may be stained in isolation and their course identified only in infant brains in whom large projection tracts, such as the optic radiation, develop first. It must be remembered that the volume of infant brains more than doubles as growth occurs while transposing these findings to adult brains.

Therefore, only an approximate reconstruction of the genu of the optic radiation is possible in adult life. The further course of the optic radiation in the stratum sagittale externum has been identified histologically and macroscopically with a magnifying glass and lies in the regions of the temporal and occipital horns of the lateral ventricle.

- 1 Optic nerve
- 2 Optic chiasm
- 3 Optic tract (within the slice)
- 4 Primary visual cortex, superior lip
- 5 Primary visual cortex, inferior lip
- 6 Optic nerve (within the slice)
- 7 Optic tract
- 8 Lateral geniculate body (within the slice)
- 9 Optic radiation
- 10 Primary visual cortex
- 11 Retina
- 12 Optic radiation (within the slice)

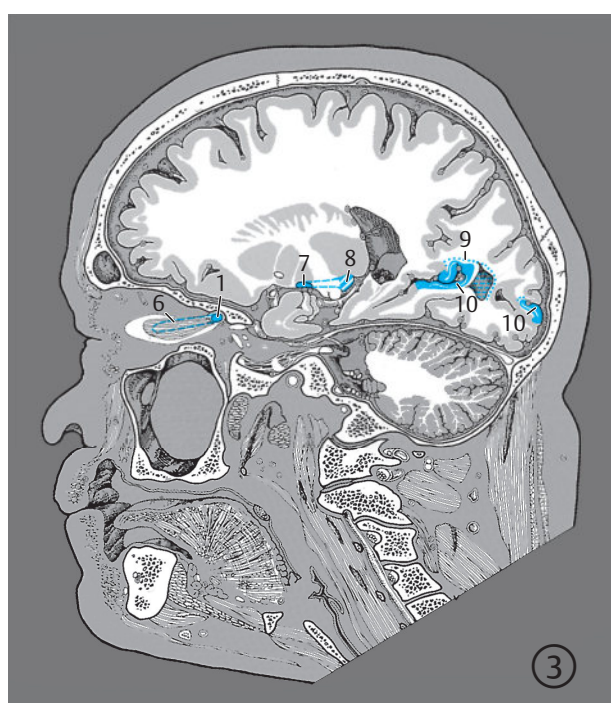
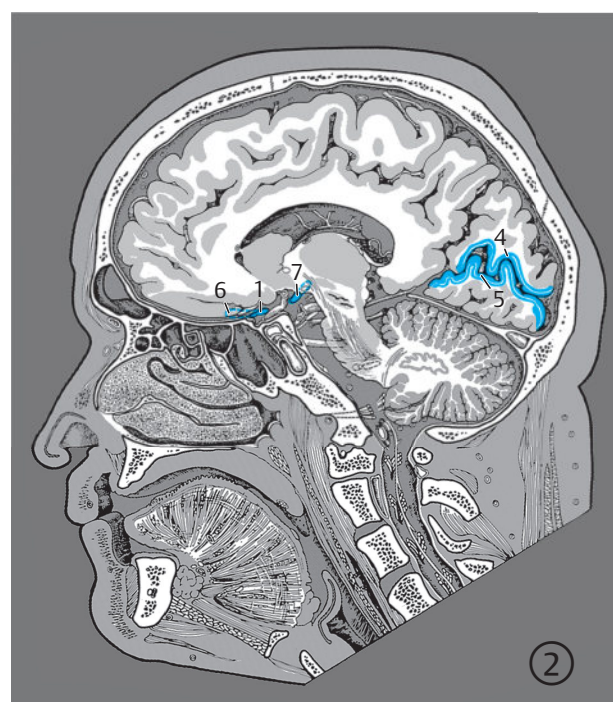
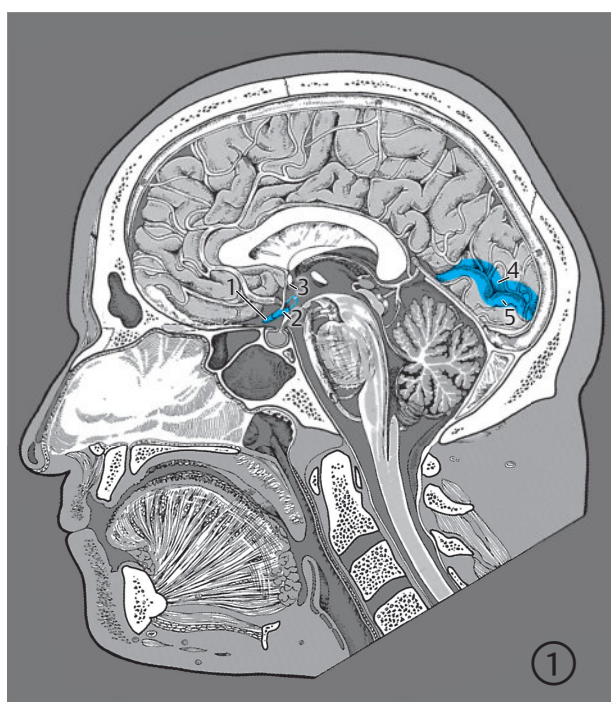
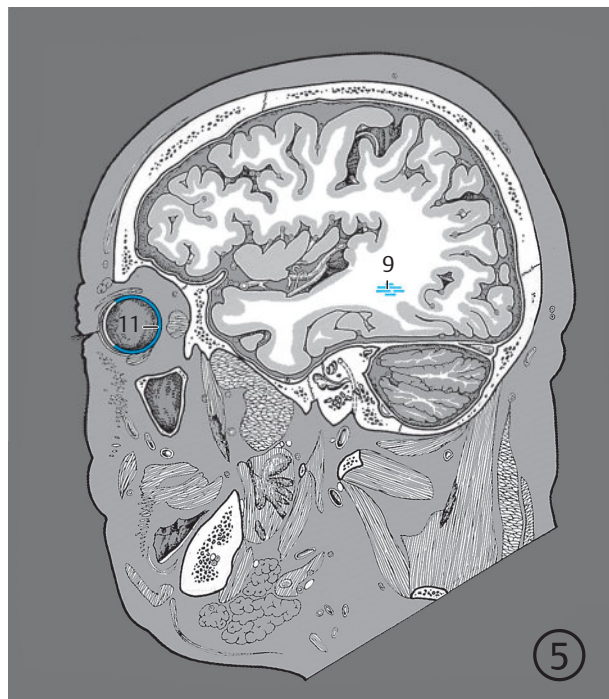


Fig. 10.20 Visual system. Serial sagittal images. The optic radiation has been depicted in accordance with Talairach et al.⁵⁷³ Encircled digits indicate the number of the respective slice (see ► Fig. 4.1).

Fig. 10.20a 1st to 4th sections.



- 9 Optic radiation
- 11 Retina

Fig. 10.20b 5th section.

- 1 Retina
- 2 Optic nerve
- 3 Optic chiasm
- 4 Optic tract

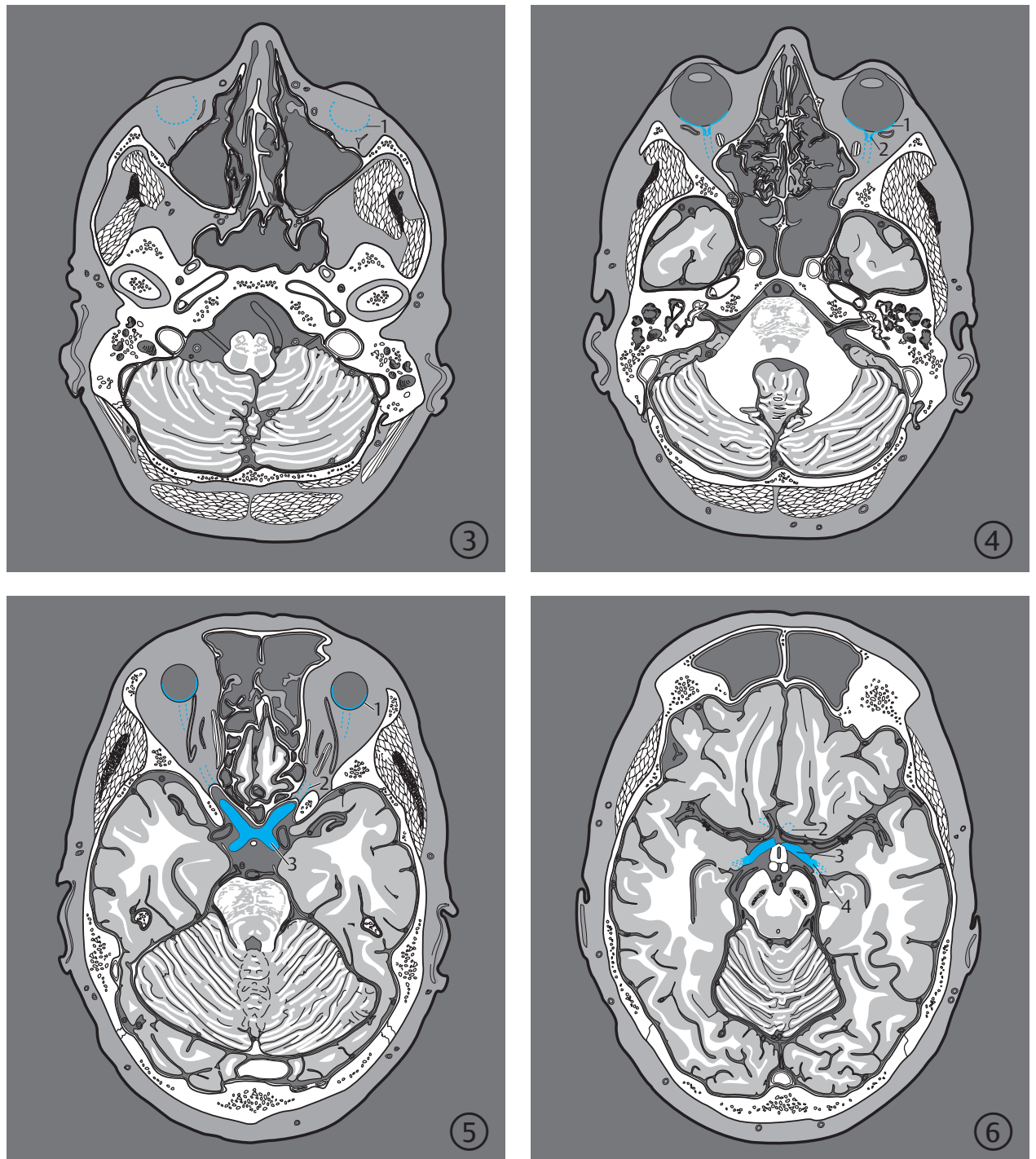
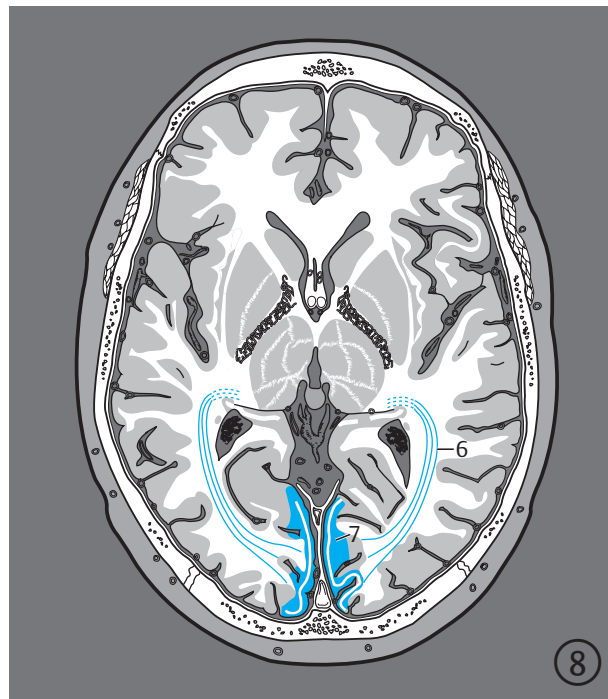
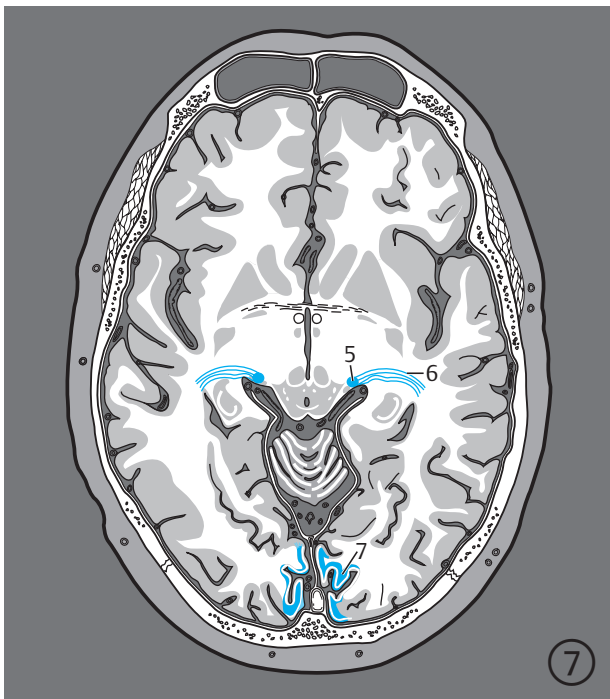


Fig. 10.21 Visual system. Serial images oriented along the bicommissural plane. Encircled digits indicate the number of the respective slice (see ► Fig. 5.1).

Fig. 10.21a 3rd to 6th sections.

The **primary visual cortex** [striate area or area 17 according to Brodmann (see Fig. 7.53)], lies mainly in the medial part of the occipital lobe surrounding the calcarine sulcus; see also neuronal networks for higher-order visual fields. More than half of the primary visual cortex lies on the inner surface of the **calcarine sulcus**, which extends deep into the occipital lobe up to the lateral ventricle. The white matter of the primary visual cortex borders the occipital horn of the lateral ventricle in the region of the calcarine spur. The visual cortex extends anteriorly inferior to the calcarine sulcus before it joins the parieto-occipital sulcus. The shape of the primary

visual cortex of the right and left hemispheres is asymmetrical, exhibits interindividual variability,⁵⁶⁰ and may extend up to the occipital pole of the cerebrum. It largely follows a course akin to that of the bicommissural plane.⁵⁷⁴ Variable arches and depressions of the cortex are present within the calcarine sulcus.⁵⁰⁸ The primary visual cortex is histologically classified as being of a granular, sensory type. A macroscopically and microscopically visible fiber layer, known as the **occipital stripe of Gennari** (see ► Fig. 5.10c), is present in the fourth layer and is composed of myelinated axons extending from the lateral geniculate body to the primary visual cortex.



- 5 Lateral geniculate body
- 6 Optic radiation
- 7 Primary visual cortex



Fig. 10.21b 7th to 9th sections.

Clinical Notes

Clinical experience with temporal corticectomies showed no impairment of the visual field if excisions lay more than 1 cm anterior to the verticofrontal plane of the posterior commissure.⁵⁷³ This plane runs through the posterior commissure and is perpendicular to the median plane and the bicommissural plane of Talairach. These findings suggest that the optic radiation lies at a variable distance from the frontal pole of the temporal horn of the lateral ventricle, and does not extend as far anteriorly as has been described under Meyer's loop.²⁶³ Furthermore, partial temporal lobectomy may result in small, large, or no visual field defects.²³ These results suggest a variability of Meyer's loop.

The **calcarine sulcus** is easily identified on median and paramedian sections of MR images (see ►Fig. 4.2b, ►Fig. 4.2d, ►Fig. 4.3a, ►Fig. 4.3b, and ►Fig. 4.3d). It joins the parieto-occipital sulcus anteriorly and both sulci enclose a wedge-shaped part of the occipital lobe, the **cuneus**.

The superior and inferior lips of the visual cortex cannot be definitively differentiated from each other in axial sections as the calcarine sulcus follows a wavy course, running nearly parallel to the axial plane. These are also discerned with difficulty on macroscopic axial sections, whereas they are well seen on coronal slices. The calcarine sulcus extends deep into the occipital lobe (see ►Fig. 3.13a, ►Fig. 3.14a, ►Fig. 3.14b, ►Fig. 3.14d, ►Fig. 3.15a, ►Fig. 3.15b, and ►Fig. 3.15d). The visual cortex with its white substance borders the

occipital horn of the lateral ventricle in the calcar avis. The ocular dominance columns of the primary visual cortex can be demonstrated by means of the echoplanar fMRI technique.¹²⁹

10.6.1 Retinotopic Maps

Reversed, inverted and smaller images of objects in one's field of vision are formed on retinal photoreceptors in both eyes. The **spatial configuration** of these photoreceptors remains constant from the retina to the primary visual cortex and is known as the "retinotopic map."

Retinotopic localization has been substantiated on fMRI studies.¹²⁹

The following spatial arrangement exists between the photoreceptors of the retina and the primary visual cortex:

- As a result of the **partial crossing** of optic nerve fibers in the optic chiasm, optic signals arising from the right halves of both retinae (and thereby left halves of visual fields) reach the right primary visual cortex (area striata).
- The lower homonymous quadrants of the retina (corresponding to the upper homonymous quadrants of the visual field) project into the part of the visual cortex situated below the calcarine sulcus ("lower lip of the primary visual cortex").
- The macula lutea of the retina, specialized for maximal visual acuity, has the largest field of projection onto the primary visual cortex which lies at the **occipital pole**. The visual cortex of the peripheral (extramacular) binocular visual field lies anterior to the occipital pole, while that of the peripheral monocular visual field is situated close to the parieto-occipital sulcus.

A small, secondary, **extrageniculate** pathway also exists in addition to the main optic pathway, which may partially compensate for deficits of the latter. This extrageniculate projection bypasses the lateral geniculate body and reaches the superior colliculi and the pulvinar nuclei of the thalamus. Optic signals are transmitted from thalamic nuclear areas to primary and secondary visual cortical areas.^{456,470,543}

Clinical Notes

Although the retina can be well evaluated with the ophthalmoscope and OCT, supplementary imaging procedures may be necessary, especially in the identification of lesions in the anterior parts of the retina that cannot be seen with the ophthalmoscope. Imaging may also aid in the identification of intraocular tumors, clouding of refractive media, as also for evaluation of the retrobulbar space of the orbit. Clinical signs of a retrobulbar disorder may include monocular visual disturbances, pain on movement of the eye, exophthalmos and edema of the eyelids. Sonography and MRI are indicated for the evaluation of pathological changes and functional disorders of the optic nerve as well as lesions in the retrobulbar space. The optic nerve, the recti, and the maximal circumference of the eyeball are clearly imaged and constantly reproducible with these diagnostic modalities. MR and CT images depict changes in the optic nerve and demonstrate pathological structures in the retrobulbar space. The diameter of the optic nerve may be determined by selecting coronal imaging planes.⁴⁷⁶ Elicitation of visual evoked potentials (VEP) is a sensitive diagnostic procedure in the evaluation of minimal functional disorders of the optic nerve, especially in cases of optic neuritis.³⁶⁶ MRI may also identify lesions of multiple sclerosis in the optic nerves. Disorders in the region of the optic chiasm may result in visual field defects in the form of bitemporal and, less frequently, binasal hemianopia. These symptoms, as well as hormonal disorders or an incidentally detected expansion of the sella turcica on X-rays of the skull require further evaluation by neuroimaging. Pathological disease processes in the region of the optic chiasm may be detected on CT; bony destruction of the sella turcica may occasionally be identified. MRI is of great diagnostic value in the evaluation of this region. Lesions of the optic tract and/or lateral geniculate body may result in a contralateral homonymous hemianopia. Higher sensitivity, multiplanar imaging technique and the absence of CT bony artifacts in the region of the skull base explain the preferential use of MRI over CT in the evaluation of suspected lesions of the optic nerve and the optic chiasm. Homonymous quadrantanopia and homonymous hemianopia together with symptoms of irritation such as photopsia and amaurosis fugax indicate a pathological process in the region of the optic radiation. Vascular or traumatic injuries affecting the visual cortex bilaterally may result in cortical blindness.

10.7 Olfactory System

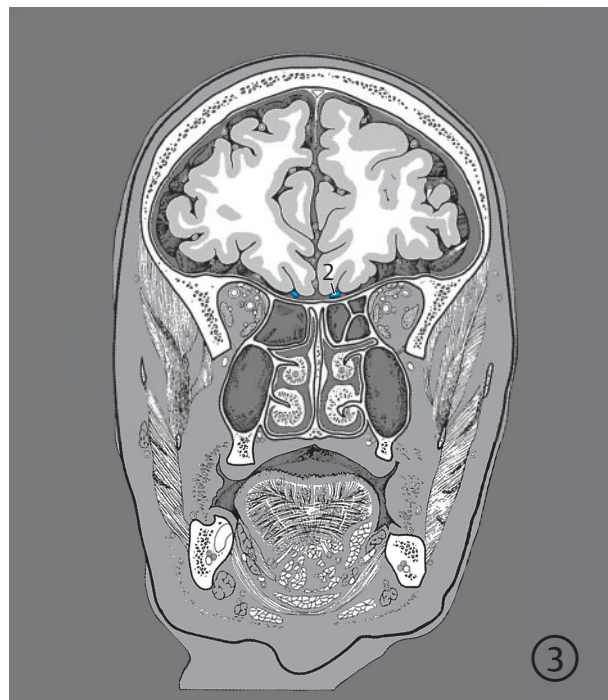
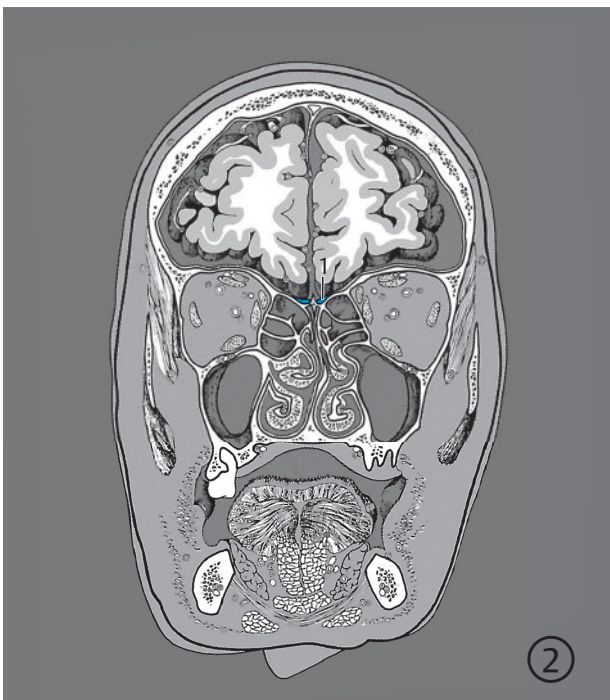
The **olfactory epithelium** lies in the roof of the nasal cavity just below the cribriform plate of the ethmoid and contains olfactory receptor cells over an area of 2 cm² (see ►Fig. 10.22 and ►Fig. 10.23; see also ►Fig. 10.39). Approximately 20 olfactory fila arise on each side with their central processes and extend through the cribriform plate as the **olfactory nerve**. The first-order neurons terminate in the olfactory bulb, forming several synaptic ball-like terminals, the olfactory glomeruli. They are the ones which establish the contact with mitral cells. The olfactory bulb is small and vertically flattened in humans as compared with monkeys and apes,⁵⁶¹ measuring, on an average, 10 mm in length and 4.5 mm in width.⁵²⁶

The axons of the mitral cells form the **olfactory tract**. This extends into small cortical areas at the base of the telencephalon belonging to the paleocortex, and is divided into medial and lateral olfactory striae. The medial olfactory stria extends toward the **olfactory trigone** below the genu of the corpus callosum, corresponding to the olfactory tubercle of macromammalian animals. Extending laterally, the lateral olfactory stria bends sharply around

the edge of the insula and projects into the **prepiriform cortex** and **periamygdaloid cortex** of the gyrus semilunaris (see ►Fig. 5.7).⁵⁶² These small cortical areas lie hidden in the angle between the temporal lobe, and the edge of the neighboring insula. The periamygdaloid cortex forms part of the amygdaloid body. The olfactory pathway runs directly to the ipsilateral olfactory cortex without crossing over. The left and right olfactory centers are connected by the anterior commissure.

Clinical Notes

Loss of the sense of smell is associated with subjective impairment of the sense of taste, probably accounted for by the common cortical processing of olfactory and gustatory signals. Diminution of the sense of smell results from injury to nasal mucosa or damage to the olfactory nerves and/or bulbs. These are frequently posttraumatic in origin but may also be caused by a meningioma of the olfactory groove. Unilateral impairment is seldom noticed spontaneously by the patient. Olfactory hallucinations may arise due to lesions in the region of the olfactory tract and as an associated symptom of temporal lobe epilepsy (so-called “uncinate crisis”).



- 1 Olfactory bulb
- 2 Olfactory tract

Fig. 10.22 Olfactory system. Serial coronal images. Encircled digits indicate the number of the respective slice (see ►Fig. 3.1).

Fig. 10.22a 2nd and 3rd sections.

- 2 Olfactory tract
- 3 Lateral olfactory stria
- 4 Prepiriform and periamygdaloid cortical areas
- 5 Periamygdaloid cortex

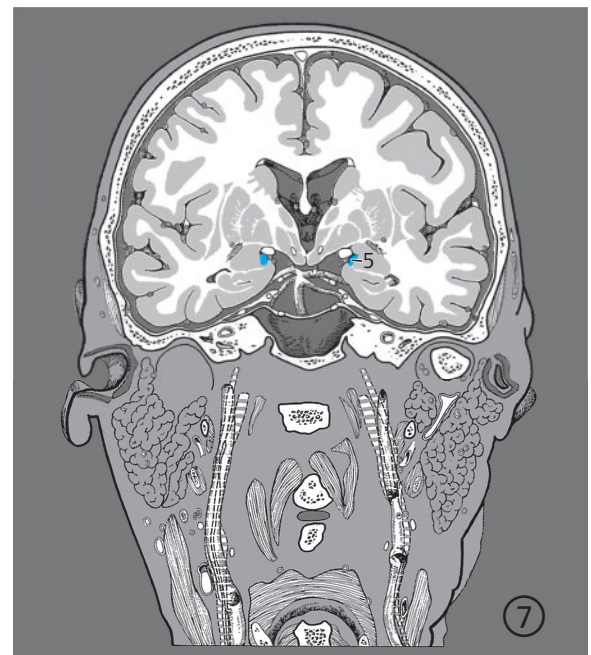
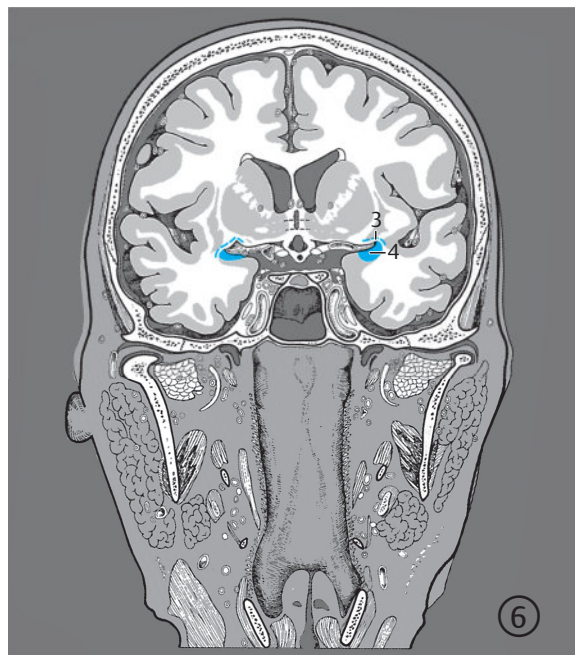
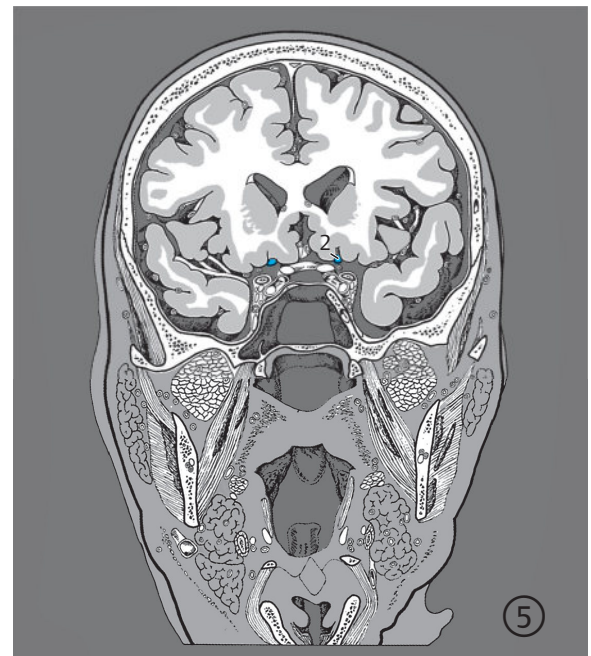
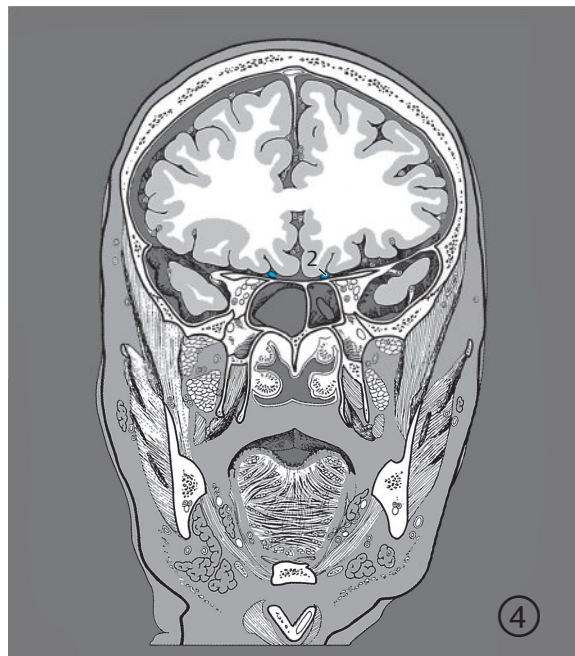
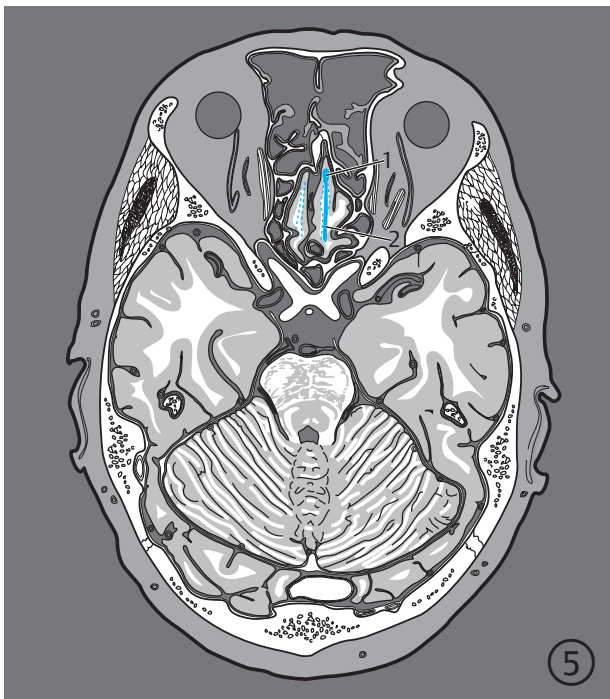


Fig. 10.22b 4th to 7th sections.



- 1 Olfactory bulb
- 2 Olfactory tract
- 3 Olfactory trigone (within the slice)
- 4 Prepiriform and periamygdaloid cortical areas (partially within the slice)

Fig. 10.23 Olfactory system. Serial images oriented along the bicommissural plane. Encircled digits indicate the number of the respective slice (see ► Fig. 5.1).

10.8 Motor Systems

Cortical and subcortical neurons are connected synaptically with motor neurons of the midbrain, pons, medulla oblongata, and spinal cord.^{326,327,328} Anatomic and physiological research over the past few decades has revealed that cortical and subcortical nerve cells are closely linked via feedback loops, a discovery which has led to a revision of the classical concept of two separate motor systems, namely the pyramidal (voluntary) and the extrapyramidal (involuntary) systems. Every day activities, such as swinging the arms while walking or running, illustrate the connection between these movements and automatisms. Voluntary movements, therefore, represent a combination of voluntary and involuntary actions. The pyramidal pathway is therefore also an important output route for individual basal ganglia as well as for main striatothalamic circuits.

Clinical Notes

Clinical examinations and neuropathological investigations help relate neurological symptoms to the pyramidal system or to specific basal ganglia. The Babinski reflex, for instance, may be a result of a disorder in the pyramidal pathway or hypokinesia due to a lesion in the substantia nigra. We would therefore like to retain use of the term “pyramidal system.” The individual motor systems of the basal ganglia, however, will be treated separately. Detection of disorders in the motor systems is of primary importance in clinical diagnosis. An optimal examination of motor function is often possible involving unconscious or only partially cooperative patients. Motor disturbances may be clinically obvious so that a simple neurological examination may suffice for approximate localization of the lesion. Therefore, more urgent diagnostic or therapeutic measures can be undertaken prior to a complete neurological examination of the patient.

Central damage to the so-called “first-order motor neurons” is characterized by paralysis, loss of polysynaptic reflexes (e.g., superficial abdominal reflex), and the appearance of pathologic reflexes of the Babinski group. In addition, spasticity of paralyzed extremities and hyperreflexia develop with variable rapidity depending on the localization of the lesion. A typical clinical picture finally emerges, usually with distally accentuated paralysis and development of a typical posture (e.g., Wernicke–Mann paralysis).

10.8.1 Pyramidal System

The pyramidal system (see ►Fig. 10.24, ►Fig. 10.25, ►Fig. 10.26, and ►Fig. 10.27) begins in the pyramidal cells of the **cerebral motor cortex**, anterior and posterior to the central sulcus and in and around pre- and postcentral gyri. In cytoarchitectonic terms, this primarily includes areas 4 and 6, as well as areas 3, 1, 2, and 5, in which two regions, the primary motor cortex and the supplementary motor area, lie. Sensorimotor areas lie posterior to the central sulcus (see Section 10.13.3).^{135,175,342}

The **primary motor cortex** (area 4) (see ►Fig. 7.53) exhibits fine somatotopic organization. Nerve cells supplying motor neurons for leg muscles lie on the medial surface of the hemisphere. Cortical regions responsible for innervation of the trunk, arm, and facial, masticatory, lingual, and laryngeal muscles extend from the superior margin toward the lateral sulcus. All motor neurons receive afferent signals contralaterally. Ipsilateral innervation is also received by motor neurons of the muscles of mastication, larynx, and some muscles of facial expression—the occipitofrontalis and orbicularis oculi.

Three cerebral regions participate in preparing for and initiating voluntary movements:

- The **supplementary motor area** (part of area 6, SMA)^{69,454} lies on the medial surface of the hemisphere in the superior frontal gyrus anterior to the paracentral lobule and exhibits basic somatotopic organization. Movements are planned in this area.^{137,172,491}
- The **premotor cortex** corresponds to a large part of area 6 which lies anterior to area 4 in the frontal lobe and is responsible for complex, mostly learned movements.^{174,447,626}
- The **upper parietal cortex** (area 5) lies posterior to the postcentral gyrus and provides spatial information for the motor system.

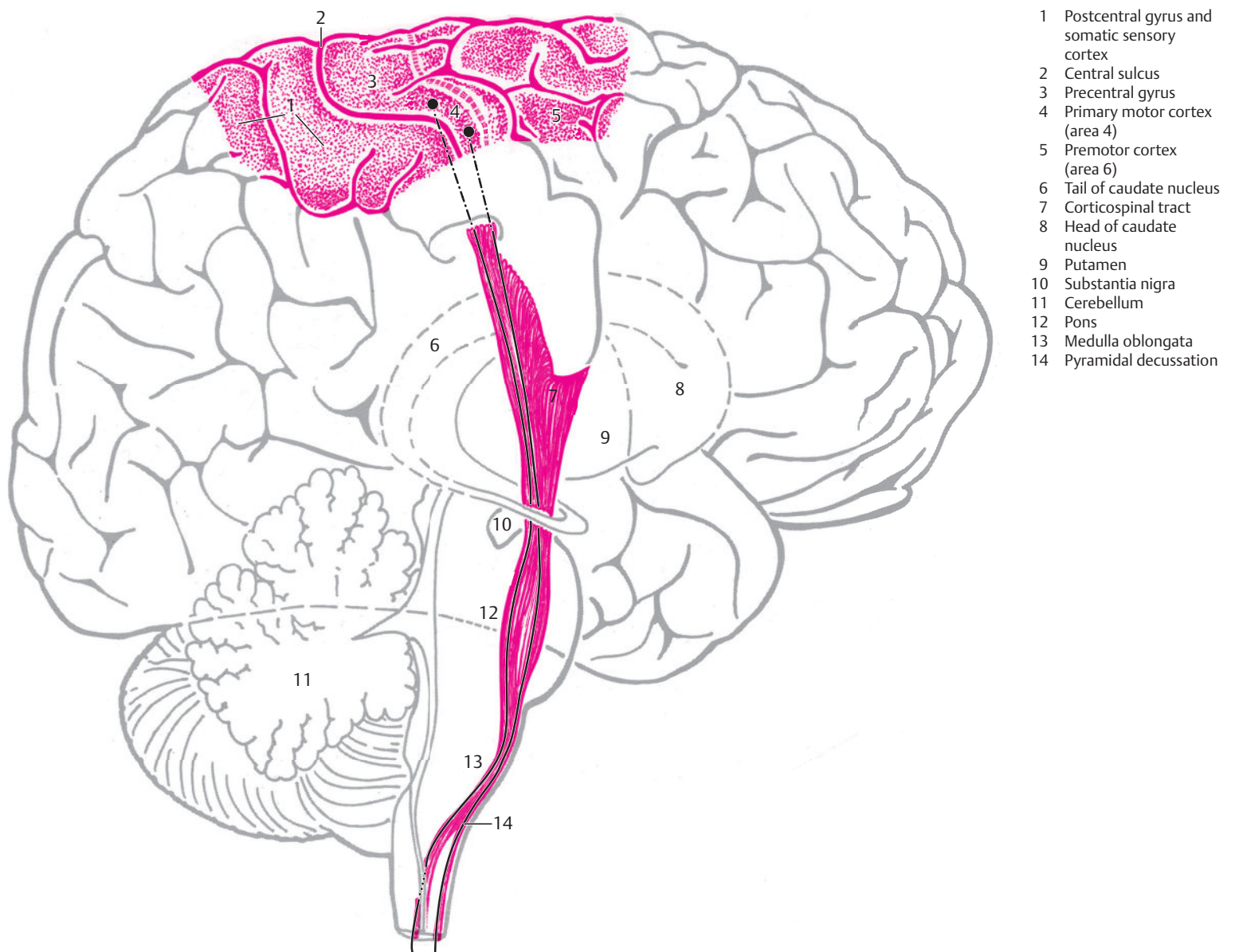


Fig. 10.24 Pyramidal system. Lateral view of the pyramidal tract. (Reproduced from Nieuwenhuys et al.⁴²⁴) The origin of the pyramidal tract in the cerebral cortex and the long corticofugal system have been drawn transparently. The brainstem and the cerebellum have been sectioned in the midline, and the respective right half removed except for the pyramidal tract and the substantia nigra.

- 1 Superior frontal gyrus
- 2 Middle frontal gyrus
- 3 Corticospinal tract
- 4 Corticospinal tract in cerebral crus (within the slice)
- 5 Supplementary motor area
- 6 Precentral gyrus
- 7 Corticospinal tract in posterior limb of internal capsule (within the slice)
- 8 Precentral gyrus
- 9 Postcentral gyrus
- 10 Corticospinal tract in pyramid
- 11 Pyramidal decussation
- 12 Anterior corticospinal tract in anterior funiculus (within the slice)
- 13 Lateral corticospinal tract in lateral funiculus (within the slice)

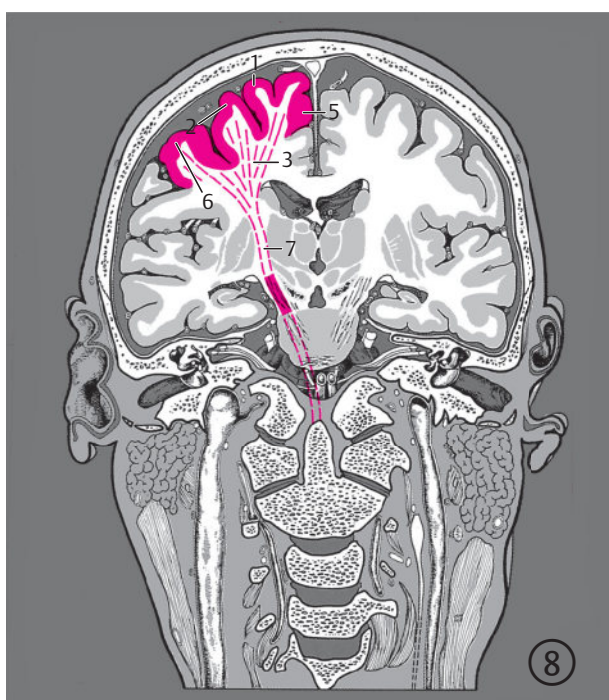


Fig. 10.25 Pyramidal system. Serial coronal images of the pyramidal tract and its areas of origin. Encircled digits indicate the number of the respective slice (see ► Fig. 3.1).

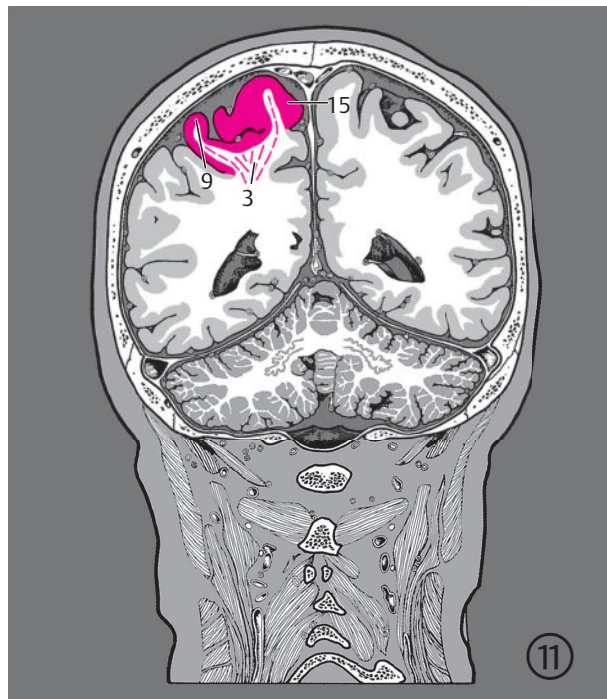
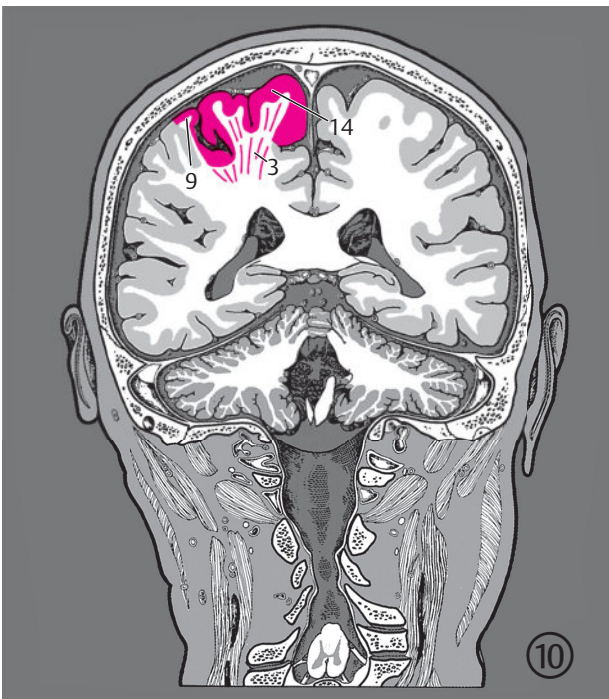
Fig. 10.25a 6th to 9th sections.

The primary motor cortex (area 4) receives and processes signals from the supplementary motor area, the premotor cortex, the upper parietal cortex and the cerebellum.

Pyramidal cells of the primary motor cortex, as well as the pyramidal cells of the supplementary motor field and the premotor cortex, issue motor commands to motor neurons of the spinal cord (via the corticospinal tract) and the brainstem (via corticonuclear fibers).

The **corticospinal system** principally originates from the motor cortex in the upper part of the lateral aspect of the precentral gyrus and in the neighboring central

part of the paracentral lobule on the medial aspect of the hemisphere. Roughly 60 to 80% of corticospinal fibers stem from the precentral gyrus¹⁶⁸; several fibers from somatosensory areas 3, 1, and 2 end synaptically at the afferent nerve cells of spinal posterior horns, thereby influencing afferent signals. Area 4 (of Brodmann)⁷⁶ or the primary motor cortex occupies both the precentral gyrus and the paracentral lobule, occupying the entire width of the precentral gyrus close to the superior margin of the hemisphere and remains confined to its posterior lip inferiorly.⁷⁶ This corresponds with recent pigmentarchitectonic studies which reveal that area 4



- 3 Corticospinal tract
- 9 Postcentral gyrus
- 14 Precentral gyrus (muscles of the lower extremity)
- 15 Precentral gyrus (muscles of the foot)

Fig. 10.25b 10th and 11th sections.

in the precentral gyrus lies close to the central sulcus, predominantly in its anterior wall and occupies approximately the middle third of the paracentral lobule.⁶⁹

Corticospinal fibers (pyramidal pathway) transmit motor impulses to contralateral spinal motor neurons.^{84,85,620} Originating in the somatotopically organized regions of the cerebral cortex, axons of the small and large pyramidal cells extend through the **internal capsule**, the cerebral crus, anterior part of the pons, and the medulla oblongata. On axial sections, the posterior limb of the internal capsule may be delineated between the thalamus and lentiform nucleus by means of an approximate rectangle.⁸⁵ This narrow rectangle is divided into three parts in an anterior–posterior direction and the position of the corticospinal tract is approximately localized by specifying its anterior, middle, and posterior thirds. This tract lies roughly in the middle third of this rectangle in the upper diencephalon and in its posterior third in the lower diencephalon, except for its posterior-most region. The corticospinal tract lies largely in the middle third of the **cerebral crus**. Pontine nuclei are seen lying between the fibers of the corticospinal tract in the anterior part of the pons, resulting in its larger external circumference as compared to its compact fiber bundle in the cerebral crus. The pyramidal pathways form bilateral, cordlike protrusions or pyramids (hence the name) on the anterior surface of the medulla oblongata. Up to 90% of fibers cross at the **pyramidal decussation** at the junction between the medulla oblongata and the spinal cord, forming the lateral corticospinal tract which descends in the lateral funiculus. The smaller, uncrossed part of the pyramidal pathway runs in the anterior funiculus as the anterior

corticospinal tract to the center of the thoracic spinal cord and crosses at the level of the corresponding spinal segment. Interneurons acting as relays between the pyramidal pathway and spinal motor neurons usually connect with numerous motor neurons or form parts of inhibitory feedback loops.

PET examinations demonstrated an increase in vascularity of the contra and ipsilateral motor cortex on movements of individual muscles. Unilateral magnetic stimulation of the motor cortex also resulted in effects on the axial trunk muscles bilaterally. An inference of **contra and ipsilateral innervation** of motor neurons for the proximal extremities and axial trunk muscles may therefore be drawn from these observations.

Corticonuclear fibers originate in the pyramidal cells of the inferior third of the precentral gyrus, the neighboring premotor cortex, adjacent somatosensory areas 3, 1, 2, and 5. These fibers then descend through the internal capsule, pass through the cerebral crus and reach the **motor nuclei of the Vth, VIIth, IXth, Xth, XIIth, and partially the XIth cranial nerves** in the tegmentum of the pons and the medulla oblongata. The motor nuclei of the Vth, IXth, and Xth cranial nerves receive additional input from the ipsilateral motor cortex and, therefore, are bilaterally innervated. The motor nuclei of the XIth and XIIth cranial nerves receive their input from the contralateral cerebral cortex alone. The motor nucleus of the facial nerve has two differently innervated regions: The motor neurons of the frontal belly of the occipitofrontalis and the orbicularis oculi receive inputs via both ipsilateral and contralateral connections while those for the rest of the facial muscles receive only contralateral signals.

- 1 Supplementary motor area
- 2 Paracentral lobule
- 3 Corticospinal tract in cerebral crus (within the slice)
- 4 Corticospinal tract in pons (within the slice)
- 5 Corticospinal tract in pyramid
- 6 Pyramidal decussation
- 7 Anterior corticospinal tract (contralateral origin)
- 8 Precentral gyrus (muscles of the lower extremity)
- 9 Postcentral gyrus
- 10 Corticospinal tract
- 11 Corticospinal tract (within the slice)
- 12 Corticospinal tract in pons

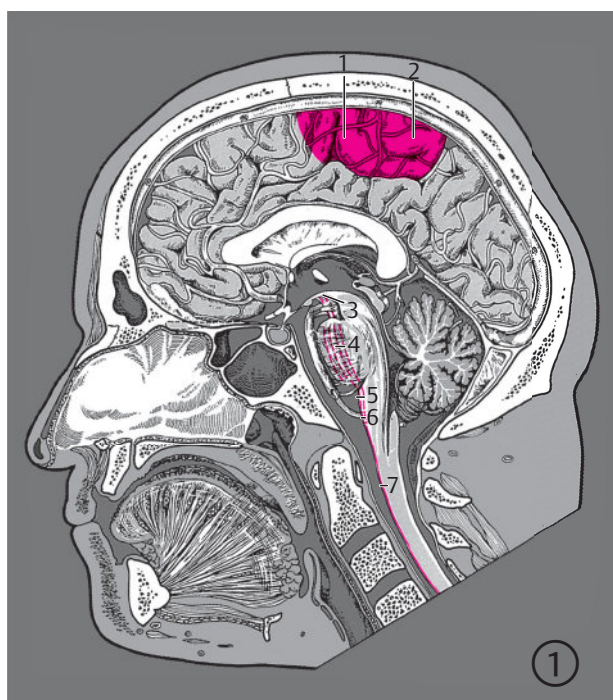


Fig. 10.26 Pyramidal system. Serial sagittal images of the pyramidal tract and its areas of origin. Encircled digits indicate the number of the respective slice (see ► Fig. 4.1).

Fig. 10.26a 1st and 2nd sections.

Clinical Notes

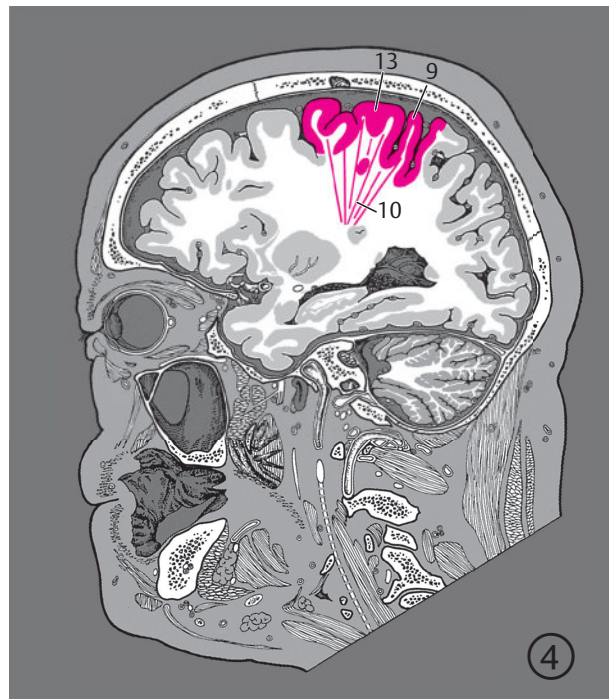
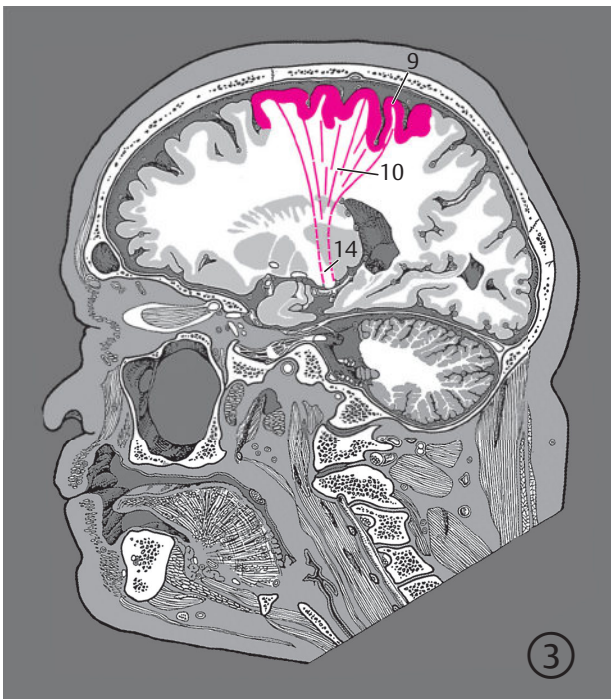
Knowledge of this variable innervation of the motor nucleus of the facial nerve is necessary to be able to distinguish between central and peripheral facial paralysis. A unilateral lesion of the internal capsule involving corticonuclear fibers due to a stroke, for instance, results in paralysis of all contralateral facial muscles except the anterior belly of the occipitofrontalis and the orbicularis oculi. The patient can wrinkle the forehead on the affected side, while facial muscles of the cheek and mouth are paretic (central paralysis). Transection of the facial nerve results in a paralysis of all ipsilateral facial muscles (peripheral paralysis).

The somatotopic organization of the motor cortex with its relatively wide divergence of the corticospinal and corticonuclear fibers explains the frequent occurrence of partial paralyses or monopareses in patients with lesions in and around the motor cortex. Irritative processes in the motor cortex may lead to focal epileptic seizures.

Severe contralateral hemiplegia results from a lesion in the internal capsule accounted for by the tight bundling of all motor fibers of one hemisphere in the internal

capsule. The topographic proximity of motor tracts to the terminal sensory pathway in the posterior limb of the internal capsule accounts for the simultaneous occurrence of hemisensory disorders together with hemiplegia. Lesions of the posterior part of the internal capsule may also damage the optic pathway resulting thereby in a homonymous hemianopia on the opposite side. Hemiparesis with central facial paralysis and ocular muscle disorders is indicative of a lesion of the midbrain and/or the pontine tegmentum. Damage to the pons and medulla oblongata cause homolateral cranial nerve disorders with swallowing and speech disturbances (IXth, Xth, and XIIth cranial nerves) and contralateral hemiparesis.

Transcranial magnetic stimulation allows functional assessment of motor pathways by determination of central conduction time. This noninvasive measurement is carried out by generating a strong magnetic field exhibiting temporal variability in an electric coil placed over the vertex, followed by measurement of the motor response of the contralateral extremity. A lesion of the corticospinal fibers results in the loss of response potential with complete disruption of the tract while partial disruption causes amplitude reduction.^{108,366,564}



- 9 Postcentral gyrus
- 10 Corticospinal tract
- 13 Precentral gyrus
- 14 Corticospinal tract in posterior limb of internal capsule

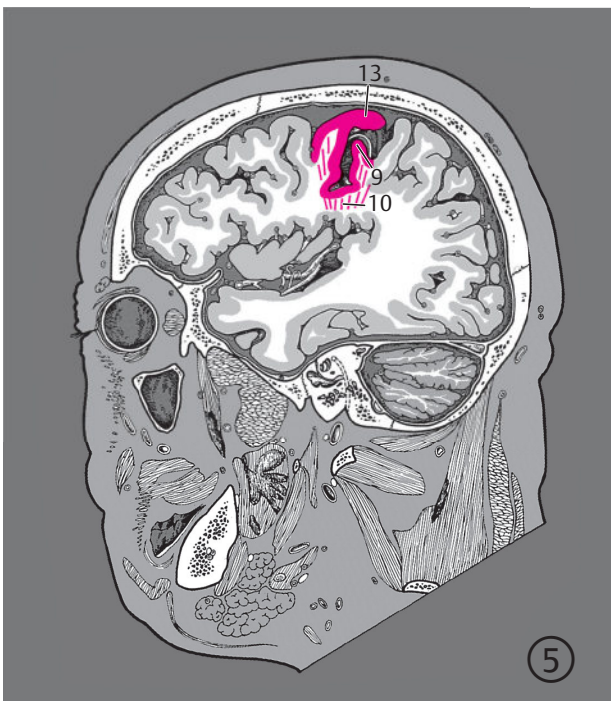


Fig. 10.26b 3rd to 5th sections.

- 1 Lateral corticospinal tract
- 2 Anterior corticospinal tract
- 3 Corticospinal tract

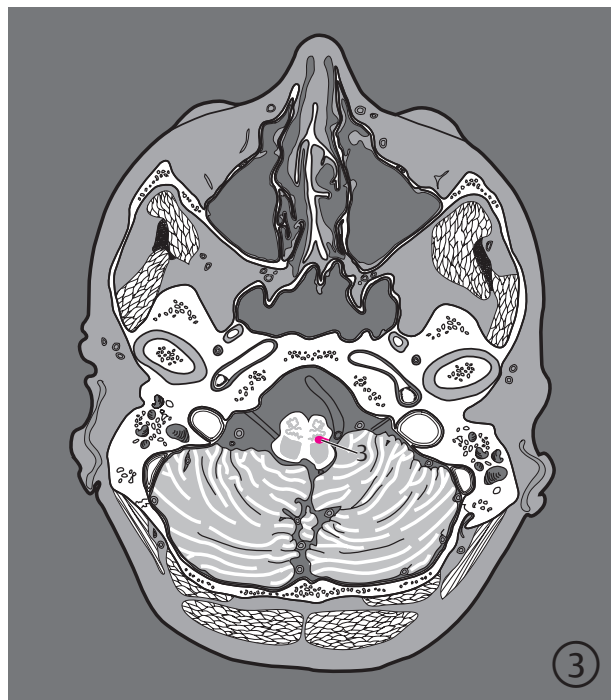
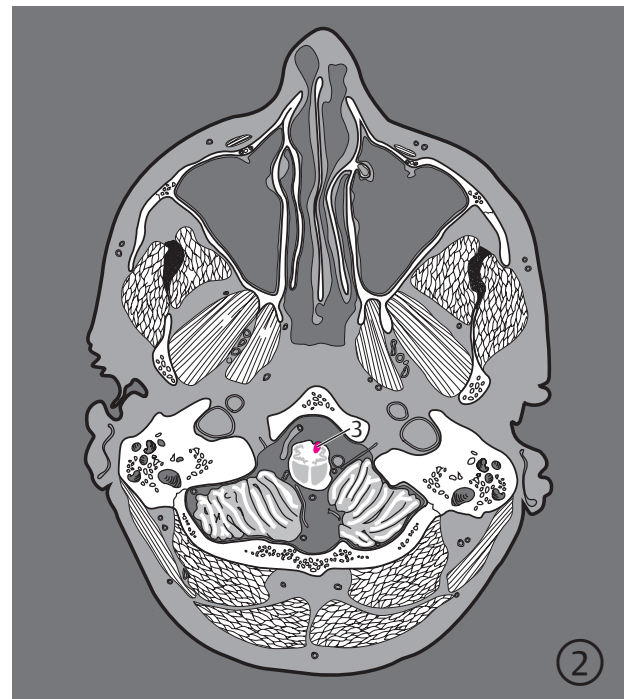


Fig. 10.27 Pyramidal system. Serial images of the pyramidal tract and its areas of origin oriented along the bicommissural plane. Encircled digits indicate the number of the respective slice (see ► Fig. 5.1).

Fig. 10.27a 1st to 4th sections.

3 Corticospinal tract

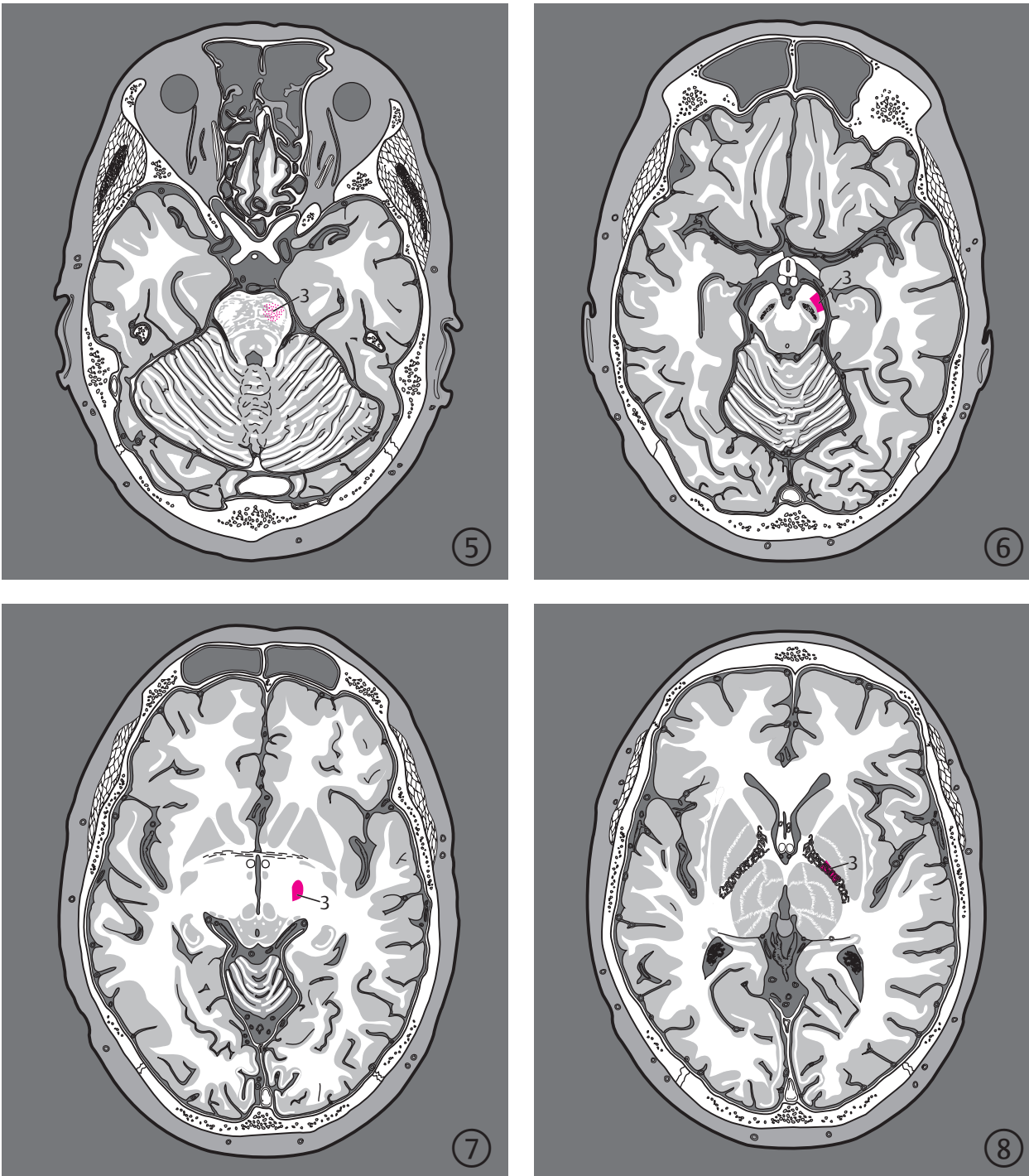


Fig. 10.27b 5th to 8th sections.

- 3 Corticospinal tract
- 4 Precentral gyrus
- 5 Premotor cortex
- 6 Somatic sensory cortex
- 7 Paracentral lobule

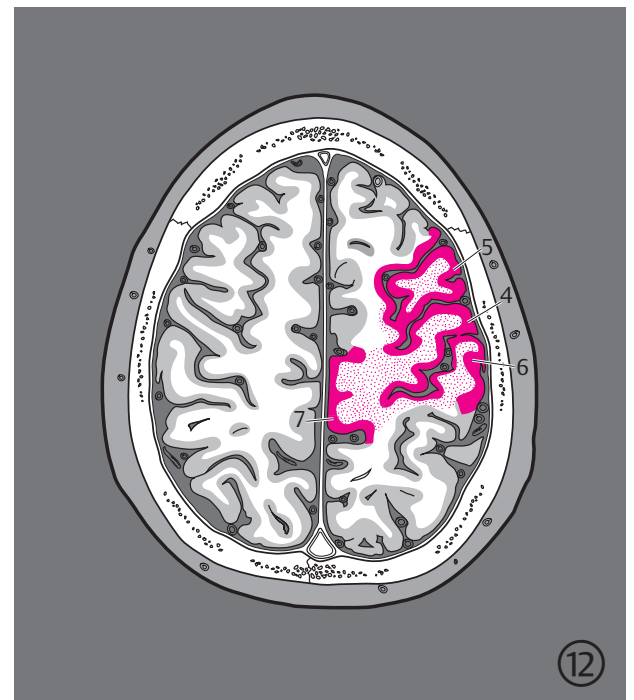
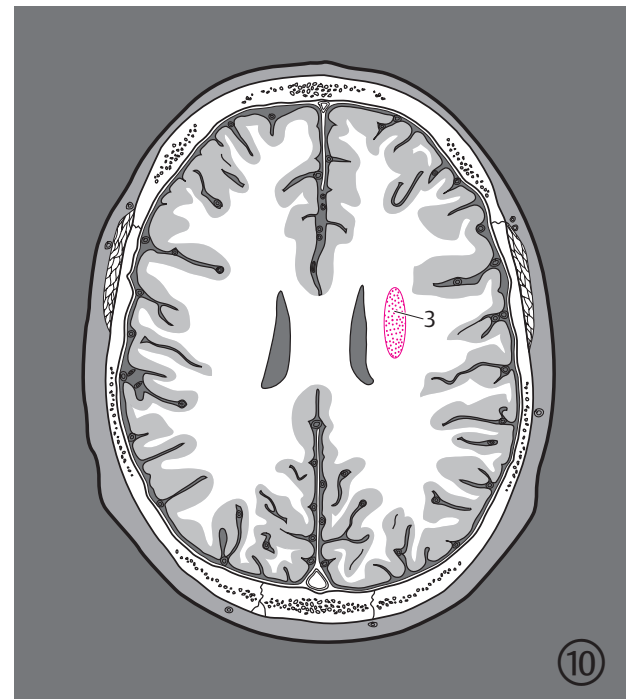
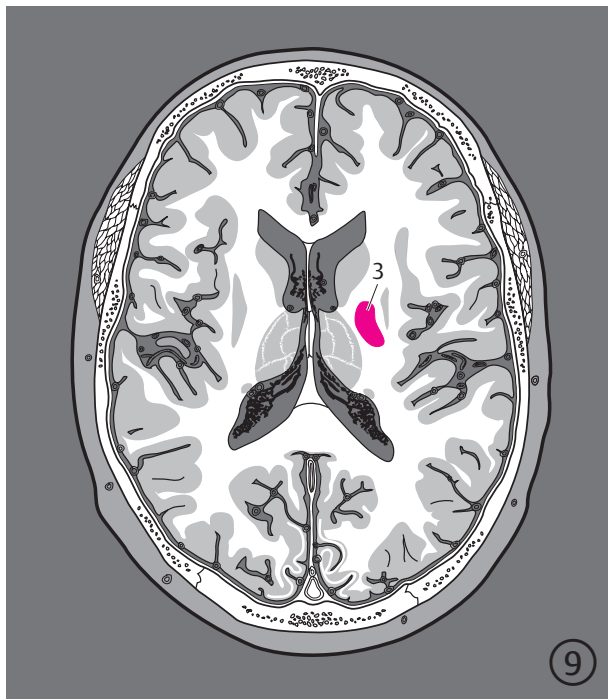
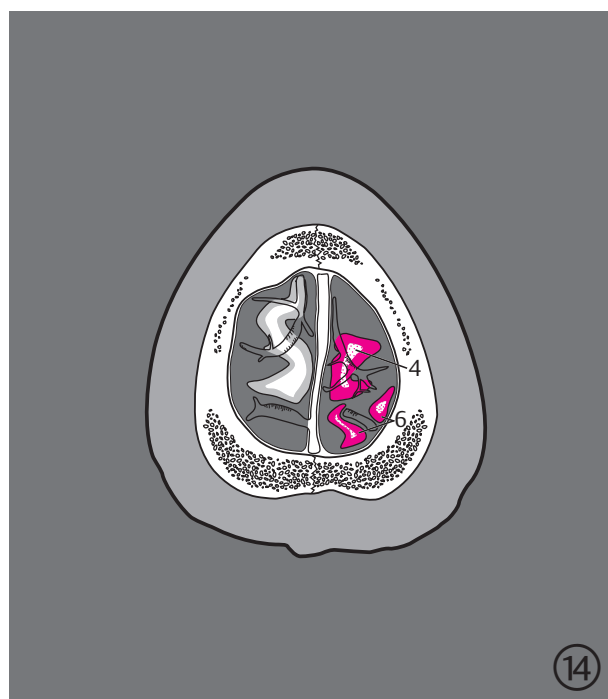
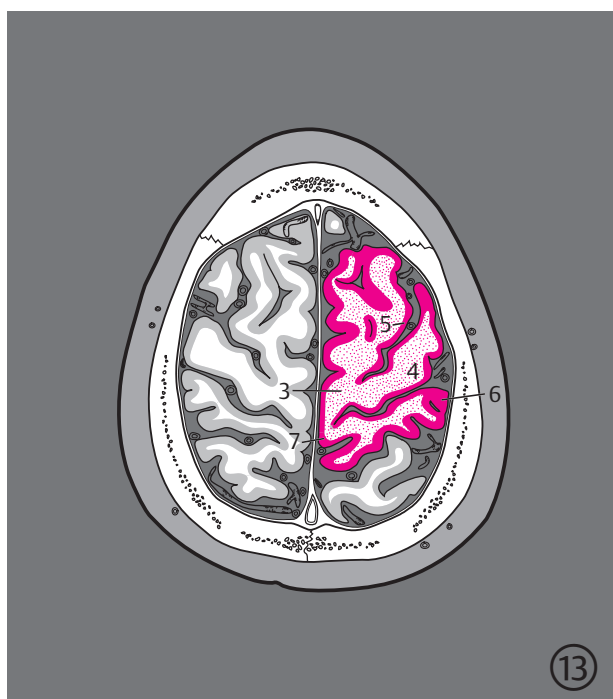


Fig. 10.27c 9th to 12th sections.



- 3 Corticospinal tract
- 4 Precentral gyrus
- 5 Premotor cortex
- 6 Somatic sensory cortex
- 7 Paracentral lobule

Fig. 10.27d 13th and 14th sections.

10.8.2 Motor Systems of the Basal Ganglia

Motor systems of the basal ganglia (see ►Fig. 10.28, ►Fig. 10.29, and ►Fig. 10.30) are composed of subcortical groups of nuclei which exhibit extensive connections with the motor cortex and form several loops or circuits among themselves. Basal ganglial neurons form several **regulatory circuits** corresponding to these neuronal loops. The neurons receive their incoming signals (input) from the reticular formation, vestibular system, cerebellum and cortical regions and send outgoing signals (output) primarily via pyramidal tracts as also via descending multisynaptic pathways including the reticulospinal and vestibulospinal tracts.

Structures comprising the **basal ganglia** include the striatum (putamen and caudate nucleus), globus pallidus, subthalamic nucleus, substantia nigra, red nucleus, and lateral vestibular nucleus. Stereotactic operations have demonstrated that small nuclei of the lateral thalamic nucleus, namely the ventral anterior and ventral lateral nuclei, can significantly influence rigidity and tremor. These smaller nuclei may therefore also be considered part of the basal ganglia.

Important **afferent signals** reaching the basal ganglia arrive in the striatum from the reticular formation via small thalamic nuclei, such as the intralaminar nuclei. Pathways project from the dentate nucleus in the cerebellum, via the ventral lateral nuclei of the thalamus, to the pallidum and the motor cortex. The mesostriatal serotonergic system, the cell bodies of which lie in the posterior raphe nucleus of the midbrain, terminates in the striatum.

The **main circuit** of the basal ganglia projects from the neocortex to the striatum, and is relayed via the globus

pallidus into the ventral anterior and ventral lateral nuclei of the thalamus which in turn project to the motor cortex (areas 4 and 6). This loop apparently “collects” information from the entire neocortex and processes it for the motor cortex. In addition, three accessory circuits connect the aforementioned nuclei of the basal ganglia with the striatum playing a central role:

- The **first accessory loop** extends from the striatum to the globus pallidus, continuing to the centromedian nuclei of the thalamus and finally back to the striatum.
- The **second accessory loop** connects the globus pallidus to the subthalamic nucleus and back to the globus pallidus.
- The **third accessory loop** (striatum → substantia nigra → striatum) contains two different neurotransmitters: GABA and dopamine. The striatonigral fibers use GABA while nigrostriatal fibers are dopaminergic.

Corticonuclear and corticospinal fibers are important efferent pathways of the basal ganglia which originate in the motor cortex and receive signals from the striatal circuit. Motor signals are transmitted along descending parallel pathways in addition to pyramidal tracts. Parallel projections originating in the basal ganglia extend via the substantia nigra to the tectum and the reticular formation and then descend as the tectospinal and reticulospinal tracts into the spinal cord. Some descending fibers of the lateral vestibular nucleus, such as the lateral vestibulospinal tract, also receive output from the basal ganglia.

Fiber bundles connect the basal ganglia with the **limbic system**. Pallidohabenular fibers connect the medial segment of the pallidum with the lateral habenular nucleus, a part of the limbic system.

- 1 Head of caudate nucleus (in the posterior part of the slice)
- 2 Head of caudate nucleus
- 3 Putamen
- 4 Claustrum
- 5 Body of caudate nucleus
- 6 Ventral lateral nuclei of thalamus (within the slice)
- 7 Globus pallidus

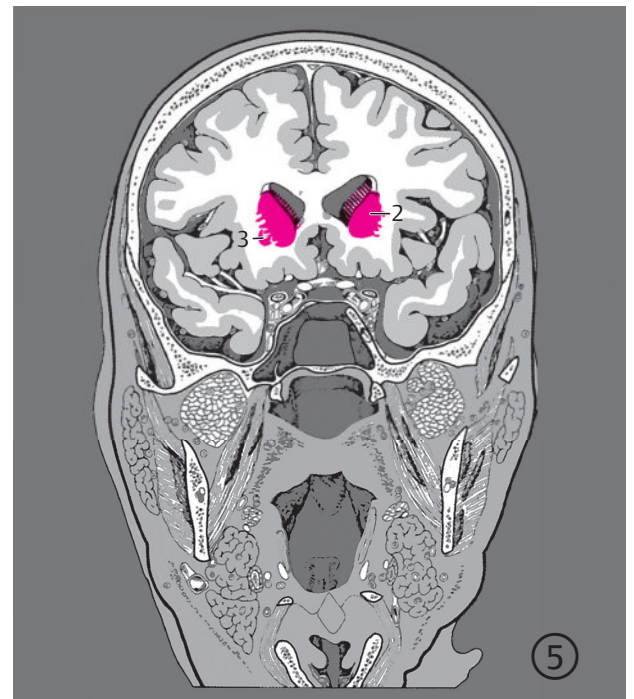
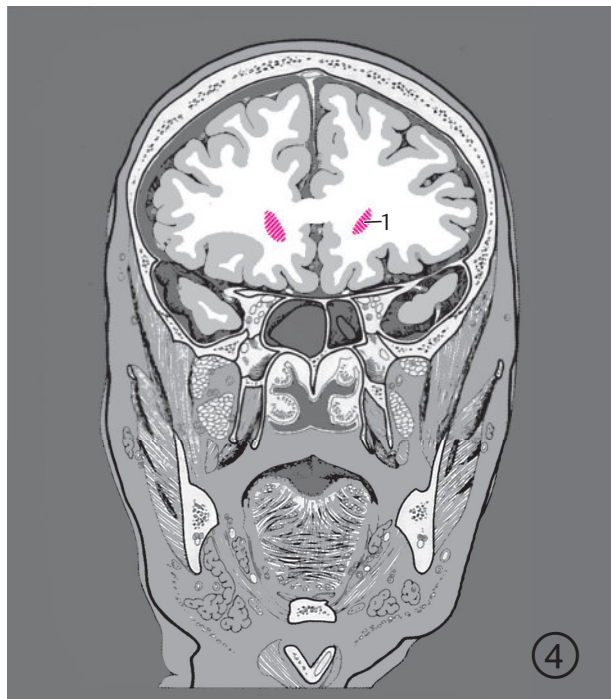
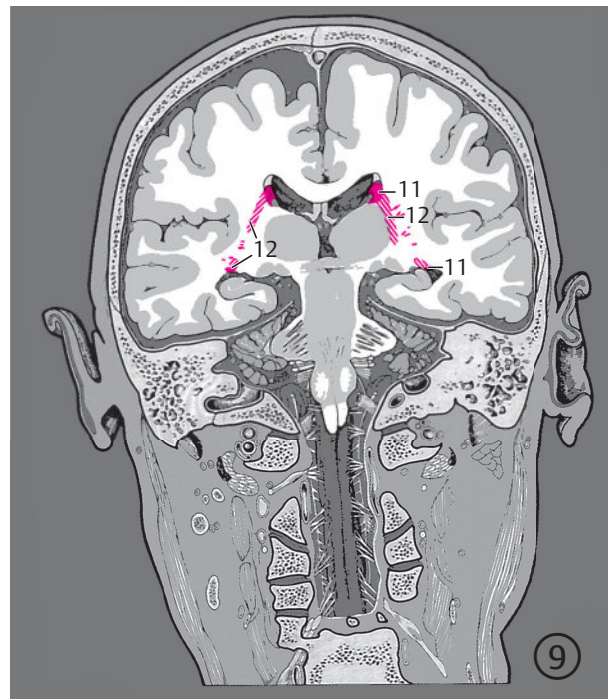


Fig. 10.28 Basal ganglial systems. Serial coronal images of basal ganglia. Encircled digits indicate the number of the respective slice (see ► Fig. 3.1).

Fig. 10.28a 4th to 7th sections.



- 3 Putamen
- 4 Caudate nucleus
- 5 Body of caudate nucleus
- 7 Globus pallidus
- 8 Red nucleus
- 9 Subthalamic nucleus
- 10 Substantia nigra
- 11 Tail of caudate nucleus
- 12 Tail of caudate nucleus (within the slice)

Fig. 10.28b 8th to 10th sections.

- 1 Subthalamic nucleus (within the slice)
- 2 Red nucleus (within the slice)
- 3 Substantia nigra (within the slice)
- 4 Body of caudate nucleus (within the slice)
- 5 Head of caudate nucleus
- 6 Ventral lateral nuclei of thalamus
- 7 Subthalamic nucleus
- 8 Substantia nigra
- 9 Body of caudate nucleus
- 10 Tail of caudate nucleus
- 11 Putamen
- 12 Lateral part of globus pallidus
- 13 Medial part of globus pallidus

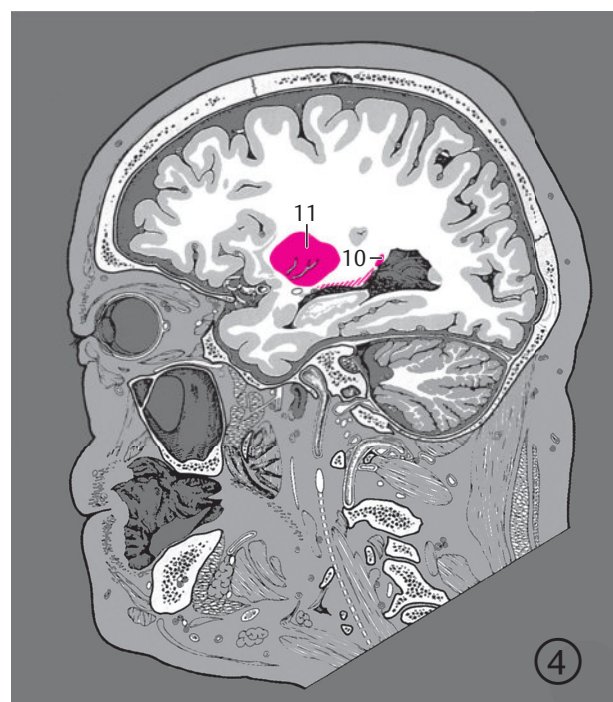
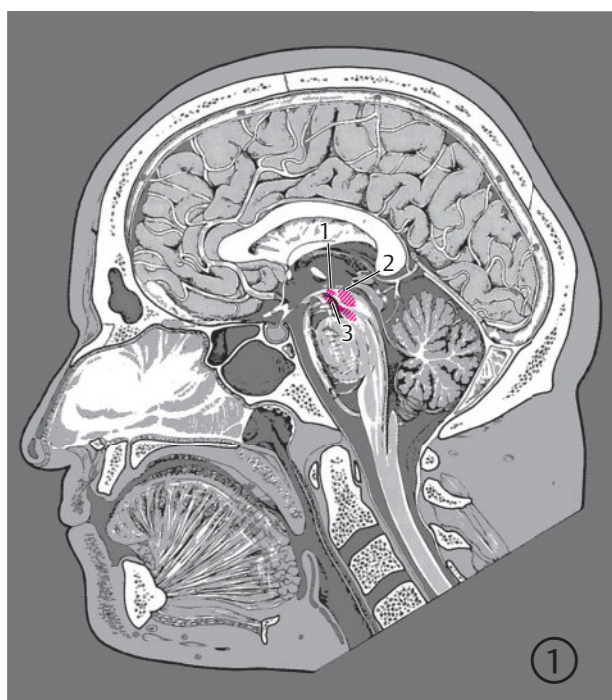


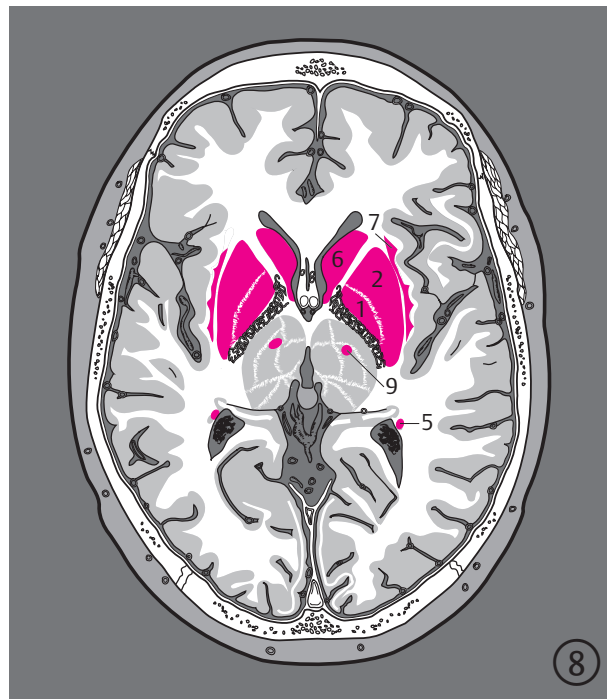
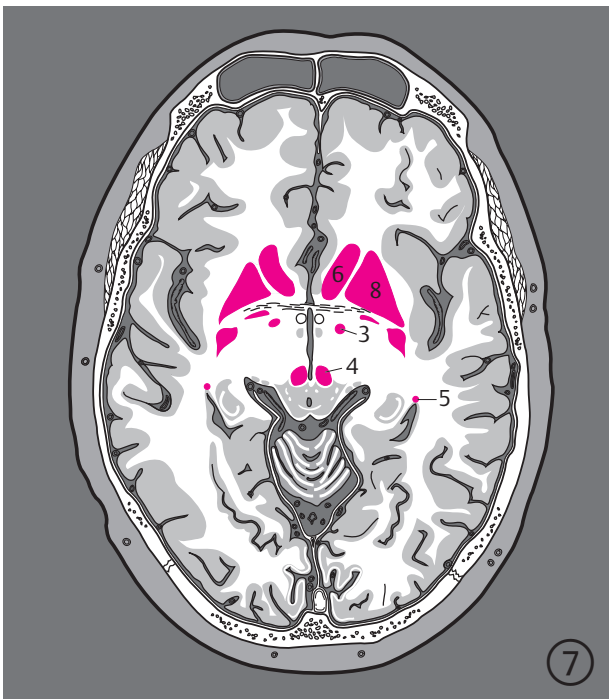
Fig. 10.29 Basal ganglia systems. Serial sagittal images of basal ganglia. Encircled digits indicate the number of the respective slice (see ► Fig. 4.1).

Clinical Notes

Disorders of the basal ganglia cause characteristic changes in motor functions and speech: spontaneous hyperkinesia, tonus changes (especially rigidity, but also hypokinesia), tremor, and characteristic postural disorders. In hereditary Huntington's chorea, the severity of the clinical symptoms (hyperkinesia and dementia) often correlates with ventricular enlargement demonstrable on CT and MR scans, consequent to diffuse, subcortical cerebral atrophy and preferential atrophy of the

caudate nucleus and putamen.⁵⁶⁵ A reduction of basal ganglia metabolism may be demonstrated even before the appearance of clinical symptoms, and prior to manifestations of brain atrophy.^{86,619}

Fewer consistent pathological findings are seen on CT in patients with Parkinson's syndrome. While normal findings are relatively rare, hydrocephalus and/or widening of subarachnoid spaces is seen relatively frequently. Parkinson's syndrome is generally recognized as being primarily a disorder of the nigrostriatal dopaminergic



- 1 Globus pallidus
- 2 Putamen
- 3 Subthalamic nucleus (within the slice)
- 4 Red nucleus (partially within the slice)
- 5 Tail of caudate nucleus
- 6 Head of caudate nucleus
- 7 Caudate nucleus
- 8 Striatum
- 9 Ventral lateral nuclei of thalamus



Fig. 10.30 Basal ganglial systems. Serial sections of the basal ganglia oriented along the bicommissural plane. Encircled digits indicate the number of the respective slice (see ► Fig. 5.1).

system (see Section 11.1.1). PET and SPECT may be employed to differentiate between Parkinson's disease and clinically similar motor disorders.⁸⁶

Anatomically inconsistent lesions may give rise to athetosis and give rise to variable CT and MR findings. Hemiballism is often associated with a cerebrovascular lesion involving the subthalamic nucleus or its connections.

10.8.3 Oculomotor Systems

The oculomotor systems (see ► Fig. 10.31, ► Fig. 10.32, and ► Fig. 10.33) control movements of extraocular muscles via the IIIrd, IVth, and VIth cranial nerves. Disturbances of ocular movements are of clinical significance: paralysis of gaze, impaired pupillary reactions, convergence paralysis, nystagmus, and paralysis of the IIIrd, IVth, and VIth

cranial nerves are obvious clinical symptoms. Neurological examination of eye movements alone often aids in the localization of lesions.^{263,264,351,582} Eye movements are of several types, such as saccades (rapid eye movements), slow pursuit eye movements, vestibulo-ocular reflexes, and convergence movements, all of which are controlled by relatively independent neuronal connections. These

- 1 Posterior parietal cortex
- 2 Supplementary eye field (on the medial side of the hemisphere)
- 3 Frontal eye field
- 4 Dorsolateral prefrontal cortex
- 5 Corticofugal fibers
- 6 Rostral interstitial nucleus of the medial longitudinal fasciculus
- 7 Superior colliculus
- 8 Oculomotor nucleus
- 9 Trochlear nucleus
- 10 Paramedian pontine reticular formation (PPRF)
- 11 Abducens nucleus

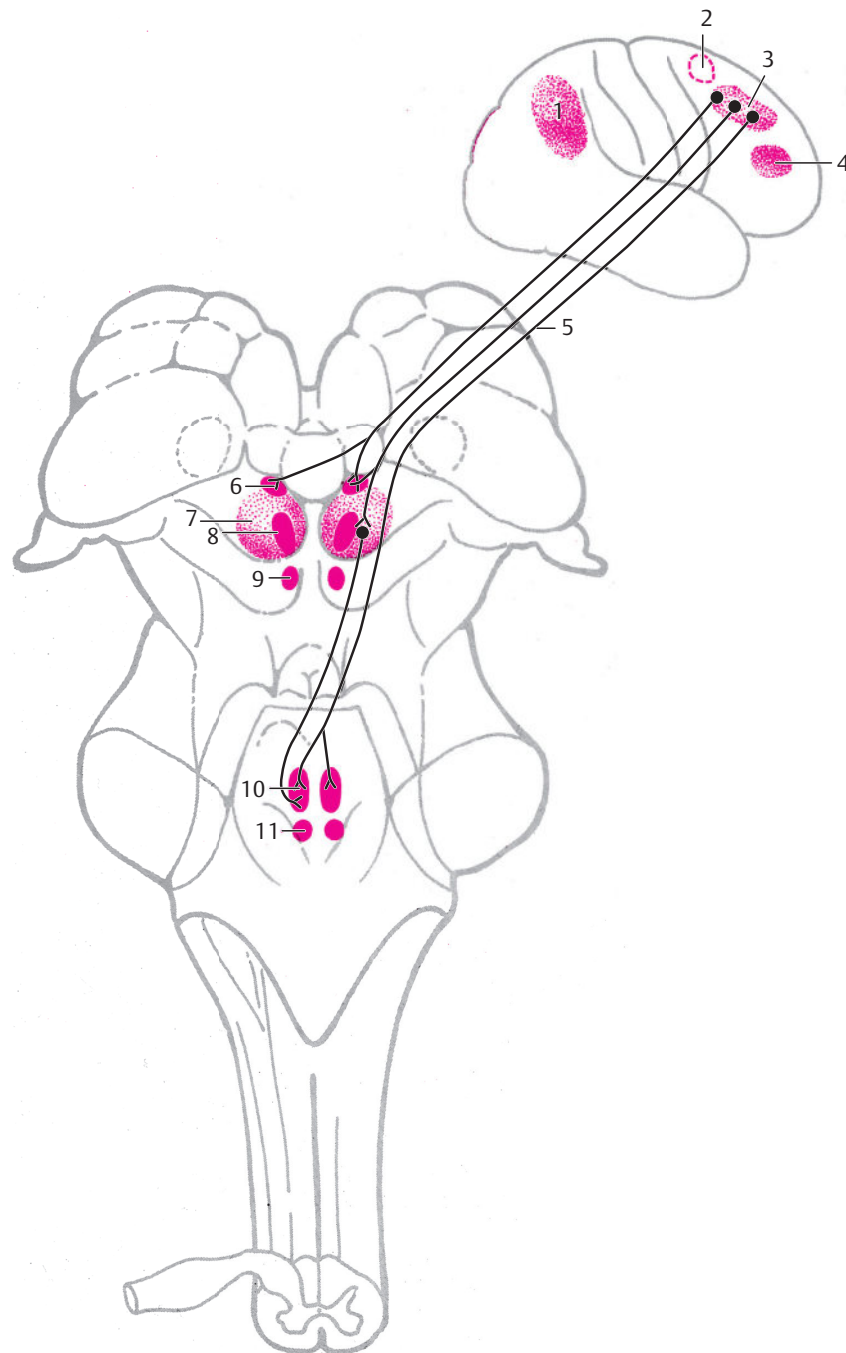


Fig. 10.31 System of rapid targeted eye movements (saccades) as part of oculomotor function. Viewed from lateral in the cerebrum and from posterior in the brainstem and diencephalon. (Reproduced from Büttner-Ennever⁹²; Horn et al.^{256,257}; Kömpf et al.³⁰²) The neural circuit of the saccadic eye movements has been depicted up to the superior colliculi and supranuclear visual centers. Supranuclear visual centers include the rostral interstitial nucleus of the medial longitudinal fasciculus and the paramedian pontine reticular formation.



- 1 Frontal eye field
- 2 Corticofugal fibers
- 3 Supplementary eye field
- 4 Rostral interstitial nucleus of the medial longitudinal fasciculus
- 5 Dorsolateral pontine nuclei (within the slice)
- 6 Superior colliculus (in the posterior part of the slice)
- 7 Oculomotor nucleus (within the slice)
- 8 Trochlear nucleus (within the slice)
- 9 Paramedian pontine reticular formation (PPRF) (within the slice)
- 10 Vestibular nuclei
- 11 Abducens nucleus (within the slice)
- 12 Prepositus nucleus (within the slice)
- 13 Flocculus (H X)

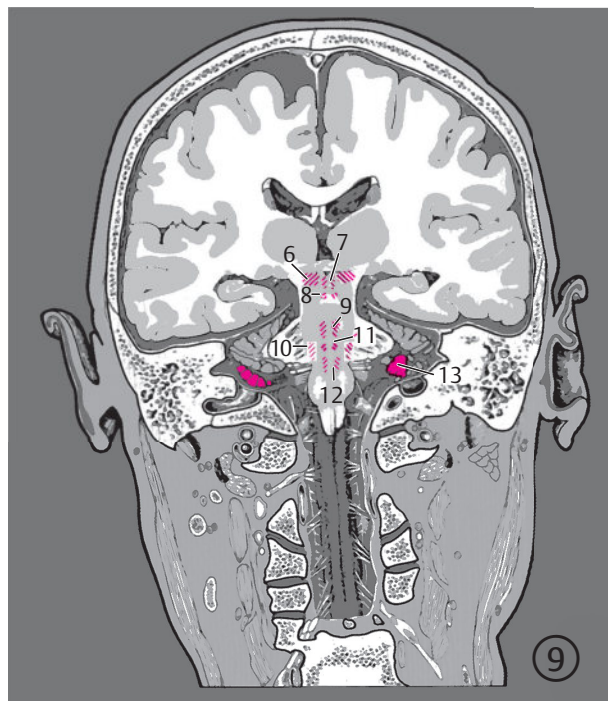
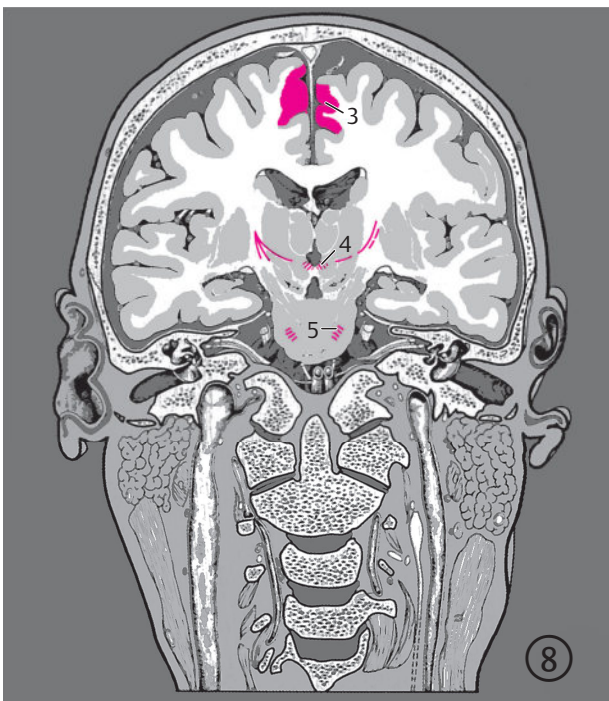


Fig. 10.32 System of rapid targeted eye movements (saccades) and slow pursuit movements as part of oculomotor function. Serial coronal images. Encircled digits indicate the number of the respective slice (see ► Fig. 3.1).

Fig. 10.32a 6th to 9th sections.

neuronal networks converge at the level of the motor neurons of the IIIrd, IVth, and VIth cranial nerves. The nuclei of the IIIrd and IVth cranial nerves lie in the floor of the aqueduct in the tegmentum of the midbrain (see ► Fig. 6.2, ► Fig. 6.12b, and ► Fig. 6.13b). The abducens nucleus (of the

VIth cranial nerve) lies in the pontine tegmentum under the floor of the IVth ventricle (see ► Fig. 6.2 and ► Fig. 6.9b). Valuable information about these oculomotor connections has been obtained from animal experiments in the last decades particularly on primates.^{92,256,257,263}

- 14 Posterior parietal cortex
- 15 Parieto-occipital cortex
- 16 Primary visual cortex
- 17 Declive (VI)
- 18 Folium of vermis (VII A)

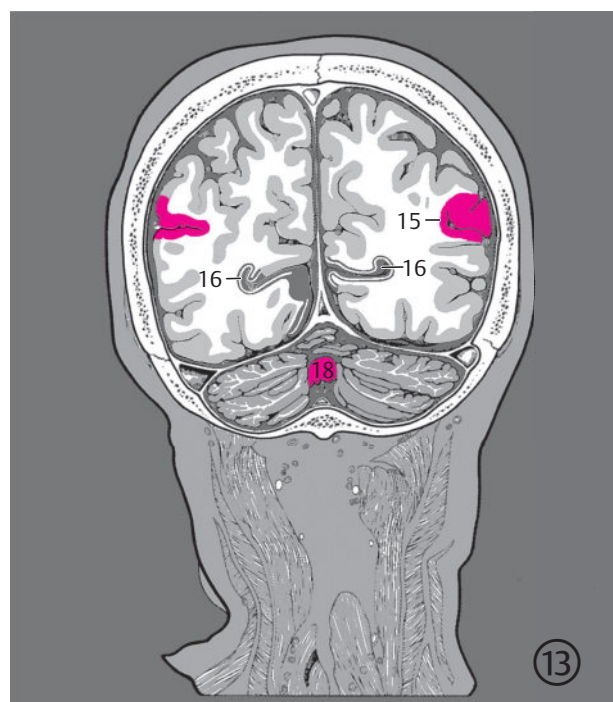
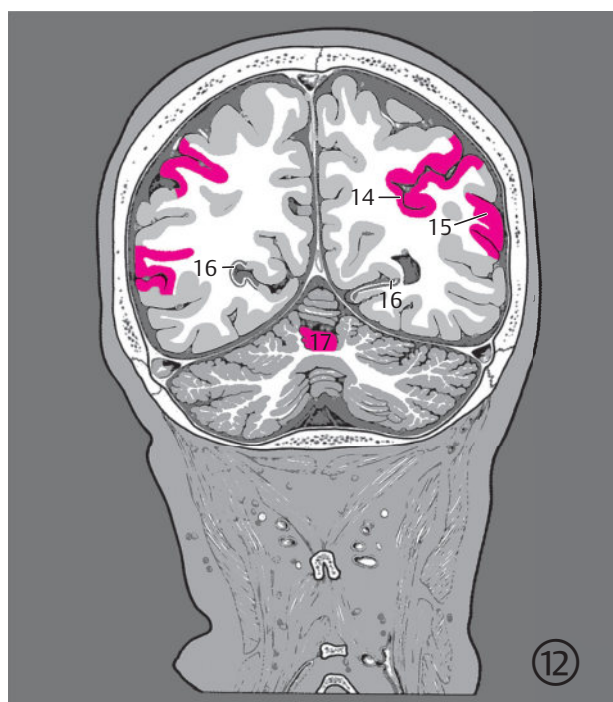


Fig. 10.32b 10th to 13th sections.

Saccades

Saccades are rapid movements of the eyes as they move from one fixation point to the other. The fovea centralis of the retina is thereby centered on a specific object of view. These saccadic movements may be controlled voluntarily by various areas of the cerebral cortex or may be triggered by the vestibular system (see Section 10.4). Both **frontal eye fields** and the **superior colliculus** are involved in saccadic movements and animal experiments have revealed that only combined lesions in these regions result in permanent impairment of saccadic eye movements.

These saccades are controlled by a neuronal **network of parietal and frontal cerebral areas** (see ► Fig. 10.31). The **posterior parietal cortex** receives visual signals from the primary visual cortex (see ► Fig. 10.31, ► Fig. 10.32b,

and ► Fig. 10.33b) and transmits these further to the **frontal eye field** (see ► Fig. 10.31, ► Fig. 10.32a, and ► Fig. 10.33b). The frontal eye field is further connected to a supplementary eye field and to the dorsolateral prefrontal cortex (see ► Fig. 10.31). PET studies have helped localize the frontal eye field to the center of the precentral sulcus and the adjacent precentral gyrus.^{302,460} The corticofugal fibers of the frontal eye field extend through the internal capsule to reach the superior colliculus, the supranuclear center of fixation in the mesodiencephalic junction, pons, as well as the basal ganglia and the thalamus. The rostral interstitial nucleus of the medial longitudinal fasciculus (see ► Fig. 10.31, ► Fig. 10.32a, and ► Fig. 10.33a) and the interstitial nucleus of Cajal lie at the mesodiencephalic junction. Vertical saccades

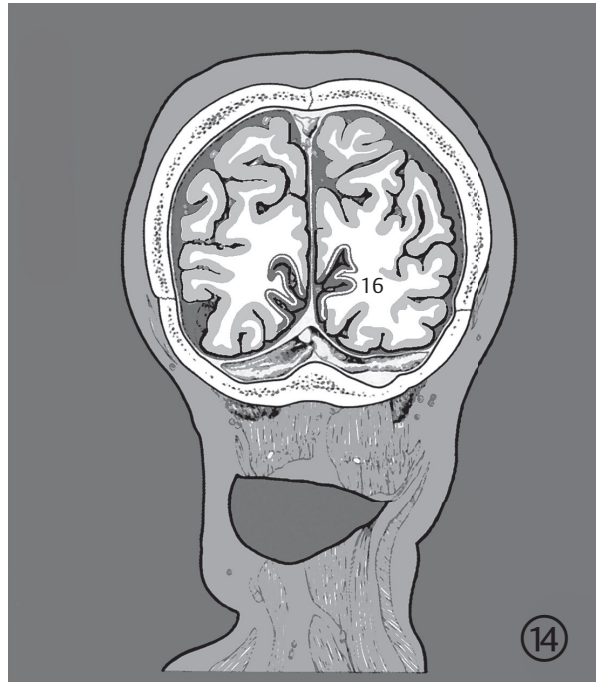


Fig. 10.32c 14th section.

are generated by nerve cells of the rostral interstitial nucleus of the medial longitudinal fasciculus. The neurons of the interstitial nucleus of Cajal stabilize vertical gaze.^{256,257} Horizontal saccades are triggered by the paramedian pontine reticular formation (see ► Fig. 10.31, ► Fig. 10.32a, and ► Fig. 10.33a) which projects to the ipsilateral abducens nucleus, containing both motor and interneurons. These interneurons exhibit strong synaptic connections with the motor neurons of the nucleus for the contralateral medial rectus via the medial longitudinal fasciculus. This circuit forms the basis for conjugate eye movements, because synergists of conjugate eye movements receive their commands from motor neurons and interneurons within the same nuclear area. A similar connection through interneurons has also been demonstrated for vertical conjugate eye movements.⁹²

Smooth Pursuit Eye Movements

Smooth pursuit eye movements allow the eyes to closely follow moving objects, such that they are continuously imaged on the fovea of the retina. This system controls the eye muscles in such a way that the rotation angle and velocity of eye movement correspond to the speed of the object. Pursuit eye movements require motivation and attention. Visual signals reach the visual cortex via the retina, the optic nerve and the lateral geniculate body. During experiments on rhesus monkeys, lesions were produced in the medial superior temporal (MST) area of the parieto-occipital cortex which resulted in impairment of smooth pursuit eye movements. The homologue of this parieto-occipital cortex in the human cerebrum lies approximately in areas 19 and 39 (see ► Fig. 7.53) according to Brodmann,⁵⁸⁰ with fiber tracts

- 1 Supplementary eye field
- 2 Primary visual cortex
- 3 Rostral interstitial nucleus of medial longitudinal fasciculus
- 4 Superior colliculus
- 5 Nucleus of oculomotor nerve
- 6 Nucleus of trochlear nerve
- 7 Paramedian pontine reticular formation
- 8 Nucleus of abducens nerve
- 9 Prepositus nucleus
- 10 Declive (VI)
- 11 Folium of vermis (VII A)
- 12 Tuber of vermis (VII B)
- 13 Dorsolateral pontine nuclei

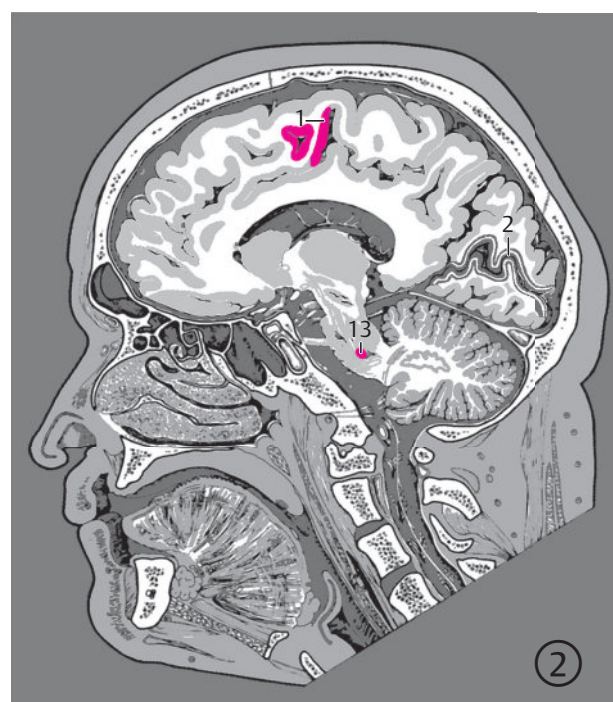
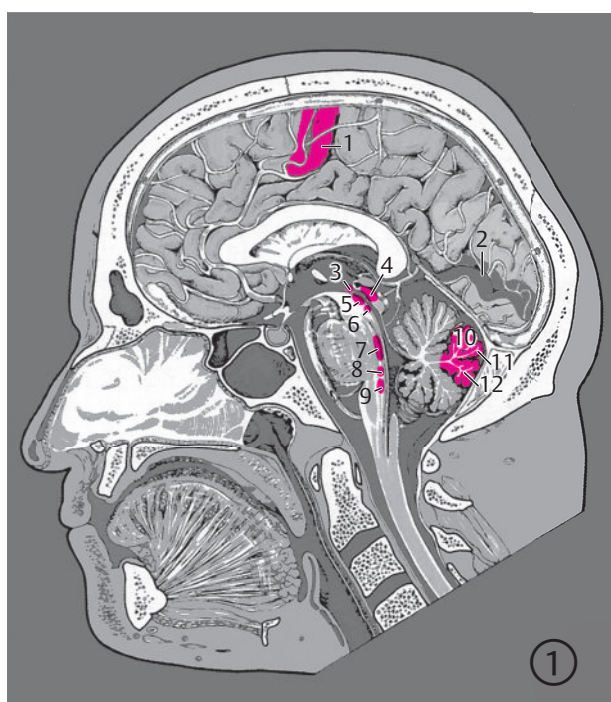


Fig. 10.33 System of rapid targeted eye movements (saccades) and slow pursuit movements as part of oculomotor function. Serial sagittal images. Encircled digits indicate the number of the respective slice (see ► Fig. 4.1).

Fig. 10.33a 1st and 2nd sections.

connecting these regions to the frontal eye fields. Both the **parieto-occipital cortex** and the **frontal eye fields** possess corticofugal pathways leading to posterolateral pontine nuclei. Neuronal pathways for smooth pursuit eye movements course further via the **cerebellum**, namely through the flocculus (H X), declive (VI), and the folium of vermis (VII A), finally reaching the nuclei for ocular muscles via the vestibular nuclei.^{302,351} Removal of the cerebellum in monkeys results in complete loss of smooth pursuit eye movements completely.⁶¹²

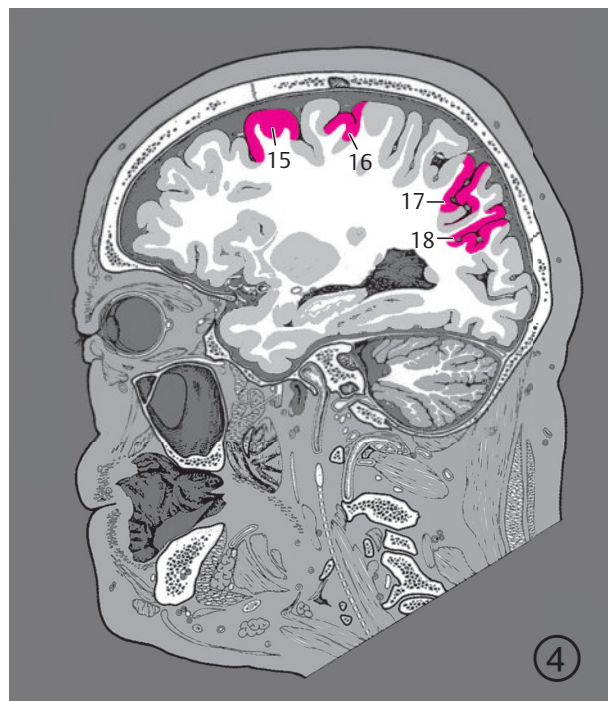
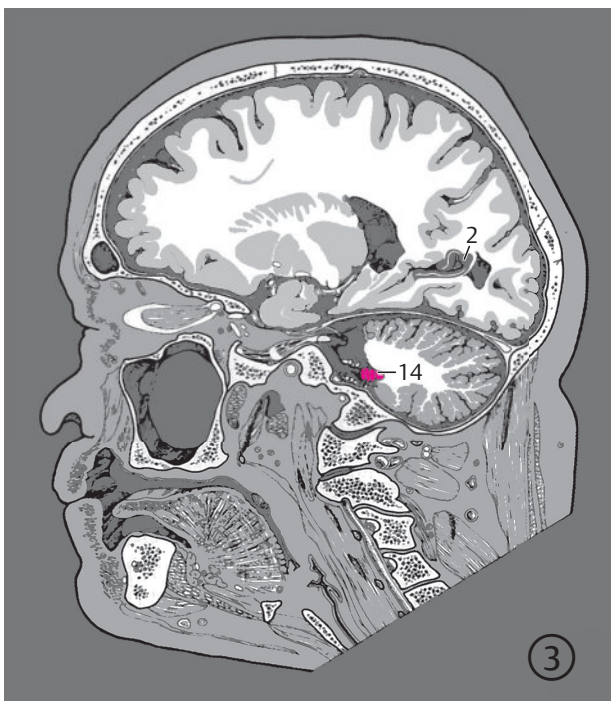
Vestibulo-ocular Reflexes

Vestibulo-ocular reflexes compensate for movements of the head through eye movements to stabilize the visual image on the retina. If, for example, the head is turned left, both eyes compensatorily turn right so that the fovea of the retina receives the same image of the outside world. The **vestibulo-ocular reflex** may be demonstrated even in unconscious patients. The **neuronal network** for this reflex consists fundamentally of three sets of neurons: the first-order neuron whose cell bodies lie in the vestibular ganglion; this

receives its signals during rotatory movements from the semicircular ducts and transmits them to the vestibular nuclei (second-order neuron). Signals generated during linear acceleration arrive via the otoliths of sensory cells of the utricle and saccule (see Section 10.4). Motor neurons of the ocular muscles form the third and effector set of neurons. These eye movements belong to the fastest eye movements only because three neuronal groups are involved. This reflex pathway has been depicted with the vestibular system (see ► Fig. 10.11).

Vergence Movements

The convergence of both eyes serves the binocular fixation of near objects. Their premotor neurons lie at the mesodiencephalic junction.²⁵⁶ The prepositus nucleus (formerly nucleus prepositus hypoglossi) shown in ► Fig. 10.33a has neuronal connections to and from most oculomotor areas, including the vestibular nuclei and parts of the cerebellum. It may thus be supposed that the prepositus nucleus receives oculomotor efference copies and thus stabilizes the direction of fixation.



- 2 Primary visual cortex
- 14 Flocculus (H X)
- 15 Dorsolateral prefrontal cortex
- 16 Frontal eye field
- 17 Posterior parietal cortex
- 18 Parieto-occipital cortex

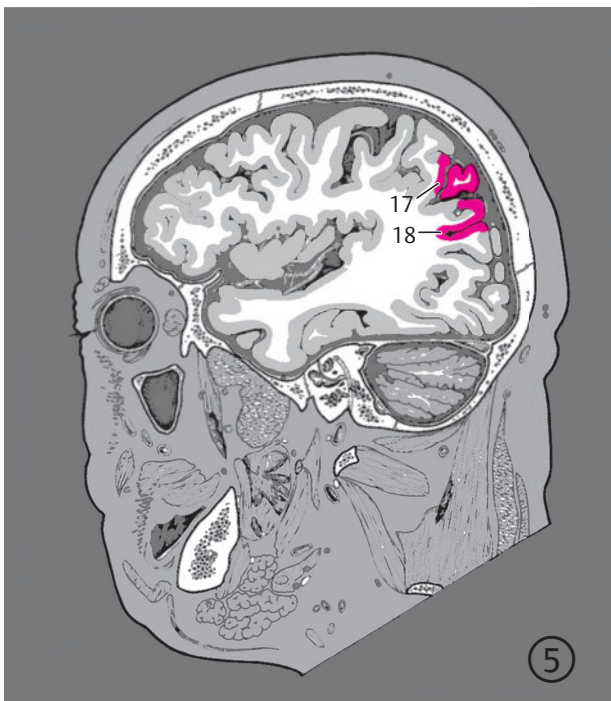


Fig. 10.33b 3rd to 5th sections.

Clinical Significance

Disorders of various oculomotor systems result in different symptoms.

Clinical Notes

Gaze palsies are characterized by restriction or absence of conjugate movements of the eyes in the horizontal or vertical directions. Gaze palsies are predominantly supranuclear in origin so that vestibulo-ocular reflexes and occasionally smooth pursuit eye movements remain intact. There is usually no diplopia. A lesion of the abducens nucleus results in loss of both motor and internuclear neurons, supplying the contralateral medial rectus, thereby causing gaze palsy to the ipsilateral side (internuclear ophthalmoplegia).⁹² An isolated lesion of the lateral rectus cannot therefore be due to a lesion of the abducens nucleus.

Horizontal gaze palsy to the contralateral side due to cerebral lesions causing ipsilateral interruption of corticopontine fibers is usually transient and is accompanied by a transient bilateral conjugate deviation (*Déviatio*n conjugée) which is masked by gaze paralysis, directed toward the lesion and especially marked in unconscious patients. Cerebral irritation as in epilepsy results in paroxysmal deviation of gaze to the side contralateral to the lesion. Pontine lesions can cause gaze palsy toward the side of the lesion with conjugate deviation to the opposite side.

Vertical gaze palsy occurs with lesions in the rostral interstitial nucleus of the medial longitudinal fasciculus, a paralysis of upward gaze being much more frequent. This together with convergence paralysis is

called “Parinaud’s syndrome.” A lesion of the medial longitudinal fasciculus with interruption of the connections between the abducens or oculomotor nuclei results in internuclear ophthalmoplegia with impaired abduction of one or both eyes and gaze-evoked nystagmus. No diplopia occurs when looking straight ahead. These disorders may be due to multiple sclerosis or vascular lesions.^{302,351}

Lesions of the oculomotor, trochlear, and abducens nerves cause diplopia as a cardinal symptom. The clinical distinction between myogenic and neurogenic paresis can be difficult in the absence of other neurological symptoms. Infranuclear and nuclear pathology should be considered with neurogenic lesions. History and associated symptoms are decisive in making a diagnosis. Infranuclear paralyzes of ocular muscles and involvement of the first division of the trigeminal nerve result in the “syndrome of the superior orbital fissure”. The orbital apex syndrome may be considered an advanced version thereof, with accompanying disorders of the optic nerve, ophthalmic artery and orbital veins.

Pupillary anomalies play an important role in clinical diagnosis. Midbrain lesions result in abnormal bilateral pupillary dilatation, while abnormally small pupils indicate lesions in the pons. Pupils of unequal size may be the result of a unilateral mydriasis as seen in oculomotor paresis—frequently with ptosis and impaired motility of the eyes—or of a unilateral miosis (Horner’s syndrome, a combination of miosis with ipsilateral ptosis and enophthalmos). Abnormal pupillary reactions may be caused by optic nerve lesions (amaurotic fixed pupil), an oculomotor nerve disorder, or, frequently, by functional intra-ocular lesions.

10.9 Cerebellar Systems

The cerebellum receives afferent connections from virtually all receptors in the human body including proprioceptive, exteroceptive, vestibular, auditory, visual, and other sensory receptors (see ►Fig. 10.34, ►Fig. 10.35, and ►Fig. 10.36).⁷⁵ Corticopontocerebellar tracts pass from the neocortex of the cerebrum via pontine nuclei to the cerebellum. These afferent cerebellar pathways pass through the massive middle cerebellar peduncle.

Most efferent pathways originate in cerebellar nuclei and exit the cerebellum mainly via the superior cerebellar peduncles. The ratio of afferent to efferent fibers in the cerebellum is 40:1.²³⁷ This input:output ratio underlies the **coordinative role** of the cerebellum for all motor functions from standing and walking to speaking.

The cerebellum receives information from the vestibular nuclei concerning the spatial position of the head. The vestibulocerebellar tract forwards signals from the **vestibular system** mainly to the nodule of vermis (X). The final destination of these signals was earlier believed to be the flocculonodular lobe. More recent animal experiments have shown that the flocculus predominantly receives visceromotor afferents.³³⁸ **Proprioceptive signals** from the musculoskeletal system of the extremities and the trunk are received by the cerebellum via the anterior and posterior spinocerebellar tracts (see ►Fig. 10.36) as well as the cuneocerebellar tract, terminating in the anterior lobe, the pyramids of vermis (VIII), and the gracile lobe of the cerebellum (H VII B). Other **afferent connections** to the cerebellum

are the auditory and visual pathways. The olivocerebellar tract of the inferior olivary nucleus projects to all areas of the cerebellum.⁴⁴⁶ The fibers of noradrenergic and serotonergic neurons of the brainstem also reach all areas of the cerebellar cortex. Under experimental conditions these seem to stimulate excitatory transmission to mossy and climbing fibers. The afferent systems end mostly in the cerebellar cortex with afferent collaterals also reaching cerebellar nuclei. The axons of the Purkinje cells link the cerebellar cortex with cerebellar nuclei.

Numerous connections exist between the cerebral neocortex and the cerebellar cortex in the lateral zone of the cerebellar hemisphere. The corticopontine tract extends from the cerebral cortex through the internal capsule to reach the pontine nuclei. Neuronal axons of the pontine nuclei in turn pass to the contralateral cerebellar cortex in the lateral zone of the cerebellar hemispheres after giving off collaterals to cerebellar nuclei. The cerebellar cortex receives information about intended motor activity from the neocortex via this **corticopontocerebellar connection**.

The cerebellar cortex is divided functionally into **longitudinal zones** according to its efferent pathways. These zones are oriented perpendicular to interlobular sulci. Three corticonuclear zones have been described for each half of the cerebellum from medial to lateral:

- Cerebellar vermis
- Narrow, intermediate zone at the junction of the vermis and hemisphere (intermediate part)
- Large, lateral zone of the cerebellar hemisphere (lateral part)

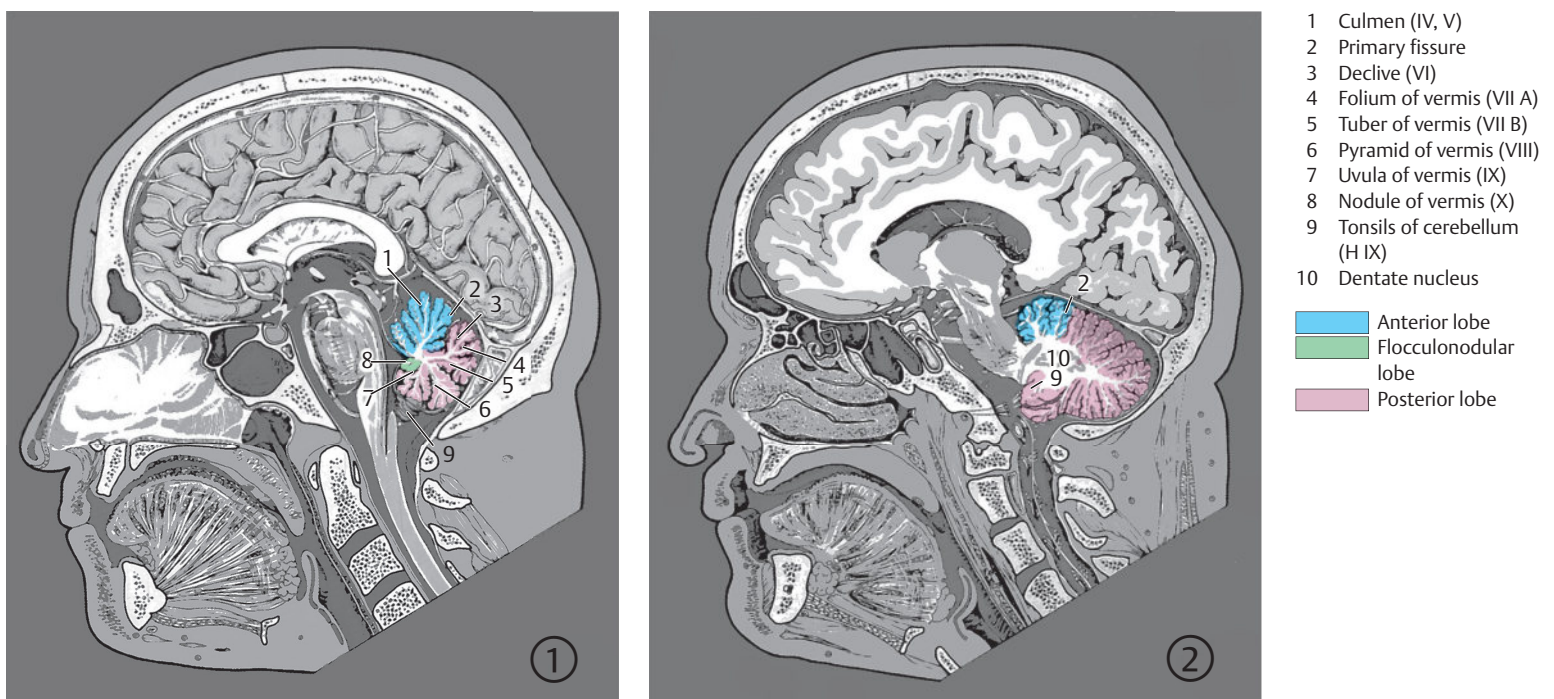


Fig. 10.34 Cerebellar systems. Serial sagittal images of cerebellar lobes. Encircled digits indicate the number of the respective slice (see ►Fig. 4.1).

Fig. 10.34a 1st and 2nd sections.

- 2 Primary fissure
- 11 Flocculus (H X)
- Anterior lobe
- Flocculonodular lobe
- Posterior lobe

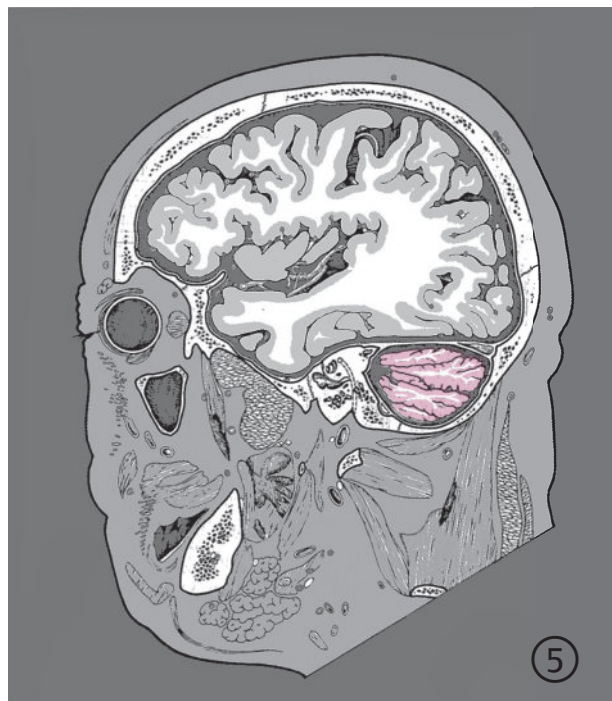
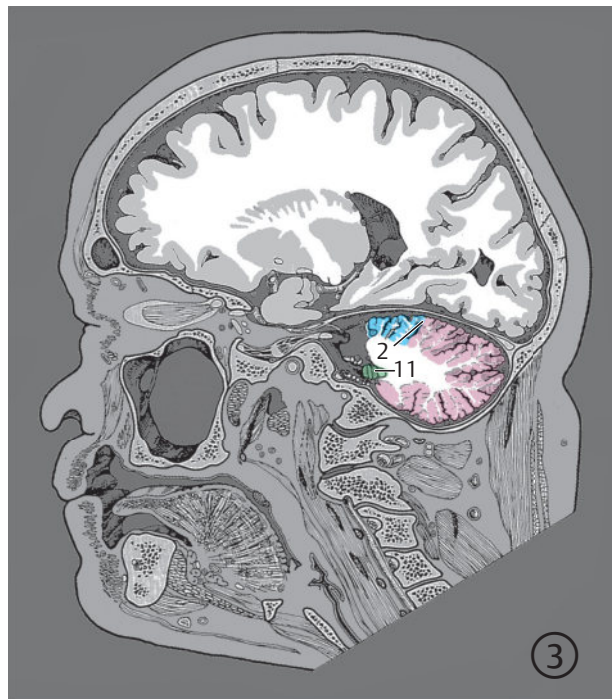


Fig. 10.34b 3rd to 6th sections.

The transitions between the three zones are continuous and not separated by a visible macroscopic border.

The Purkinje cells of these projection zones are connected with the ipsilateral nuclei. The Purkinje cells of the vermis project to the fastigial and vestibular nuclei while those of the intermediate zone project to the interpositus nuclei (globose and emboliform nuclei). The Purkinje cells of the lateral zone are connected with the dentate nucleus.

The axons of the interpositus and dentate nuclei extend through the superior cerebellar peduncle (see ►Fig. 10.36b), cross in the midbrain, and end in the red nucleus (see ►Fig. 10.36b) and in the ventral lateral nuclei of the thalamus (see ►Fig. 10.36b). The red nucleus receives signals from the motor cortex via collaterals of motor pathways. The **red nucleus** may thus be viewed as a relay station, which transfers the learning process of movement to the corticospinal pathway and automatic movements to the rubrospinal tract. The cerebellum can exert influence on the motor cortex in the frontal lobes via the ventral lateral nuclei.

The Purkinje cells of the cerebellar cortex receive time signals via afferent tracts signaling the position of the musculoskeletal system and information about intended movements via the corticopontocerebellar pathways. Comparison of these signals allows harmonious functioning of the motor system. Cerebellar lesions

therefore do not cause paralysis of the motor system, but rather a lack of timed coordination of movements.

Each cerebellar hemisphere is connected with the ipsilateral spinal cord due to the **decussation** of the efferent cerebellar pathways in the midbrain and to the **reddecussation** of the rubrospinal and of the pyramidal tracts. Unilateral cerebellar lesions therefore result in **ipsilateral functional deficits**.

Clinical Notes

Lesions of the cerebellar vermis cause disordered bilateral movement and balance with truncal ataxia without other cerebellar symptoms.^{38,446,468} These patients typically exhibit a staggering (“drunken”) gait.

Lesions of the lateral zone of the cerebellar hemisphere are characterized by impaired motor coordination, with loss of harmonious functioning of involved muscles in cerebellar ataxia, even in the presence of visual cues. An intention tremor is seen on the finger–nose test even with the eyes open. Rapid, repetitive movements can no longer be performed (adiadochokinesis). Targeted movements are incorrectly performed (dysmetria). Speech is often irregular and jerky and words are broken up into syllables (the typical disorder being scanning dysarthria). Muscle tone is reduced (hypotonic muscles). A nystagmus is often observed.

- 1 Tonsils of cerebellum (H IX)
 - 2 Uvula of vermis (IX)
 - 3 Pyramid of vermis (VIII)
 - 4 Nodule of vermis (X)
 - 5 Flocculus (H X)
- Anterior lobe
Flocculonodular lobe
Posterior lobe

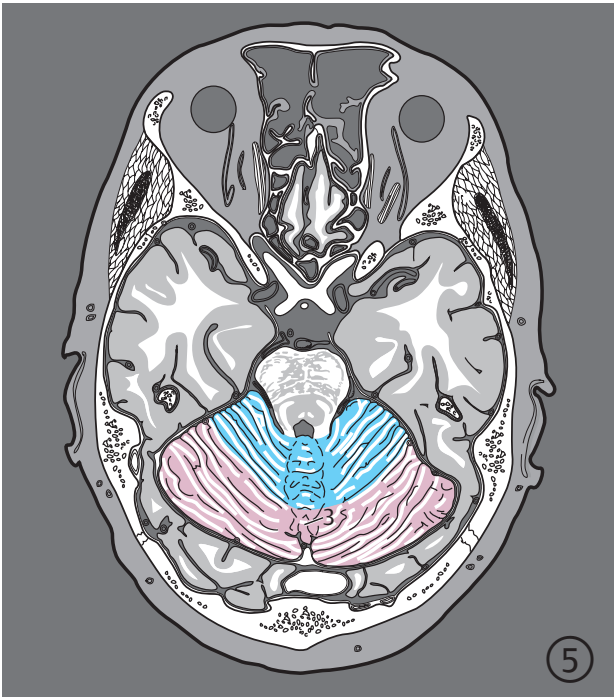
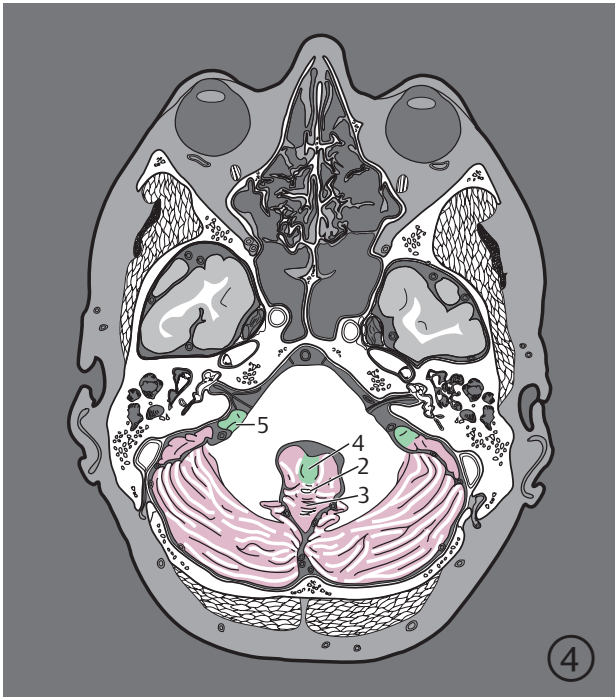
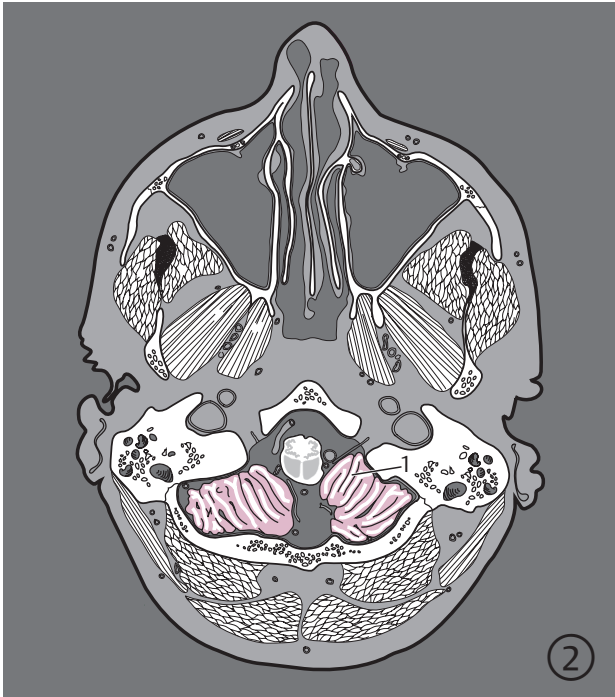


Fig. 10.35 Cerebellar systems. Serial sections of the cerebellar lobes oriented along the bicommissural plane. Encircled digits indicate the number of the respective slice (see ► Fig. 5.1).

Fig. 10.35a 2nd to 5th sections.

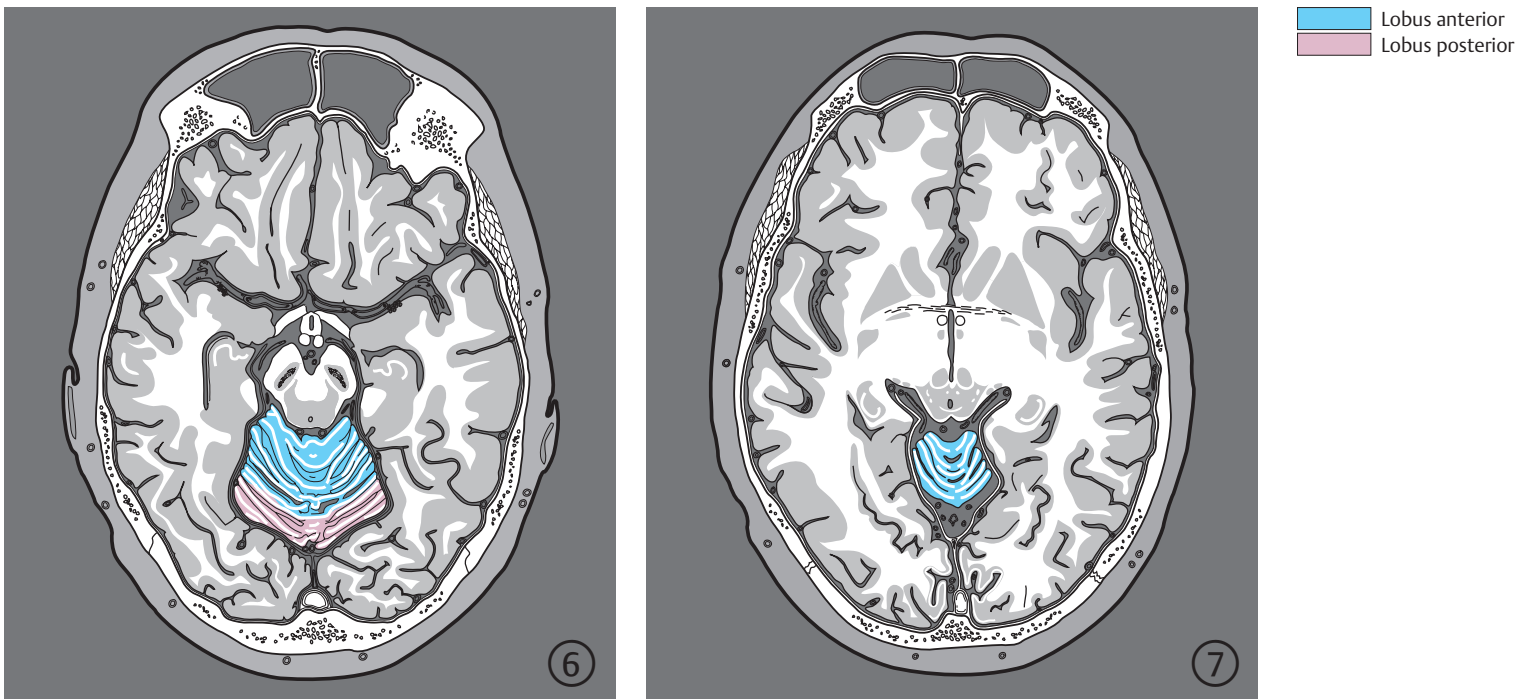


Fig. 10.35b 6th and 7th sections.

- 1 Thalamus
- 2 Corticopontine tract
- 3 Red nucleus
- 4 Tectum of midbrain
- 5 Decussation of superior cerebellar peduncles
- 6 Superior cerebellar peduncle
- 7 Vermis of anterior lobe of cerebellum
- 8 Anterior spinocerebellar tract
- 9 Primary fissure
- 10 Pons
- 11 Trigeminal nerve
- 12 Pontocerebellar tract
- 13 Inferior cerebellar peduncle
- 14 Middle cerebellar peduncle
- 15 Inferior olivary nucleus
- 16 Olivocerebellar tract
- 17 Hemisphere of posterior lobe
- 18 External arcuate fibers
- 19 Posterior spinocerebellar tract

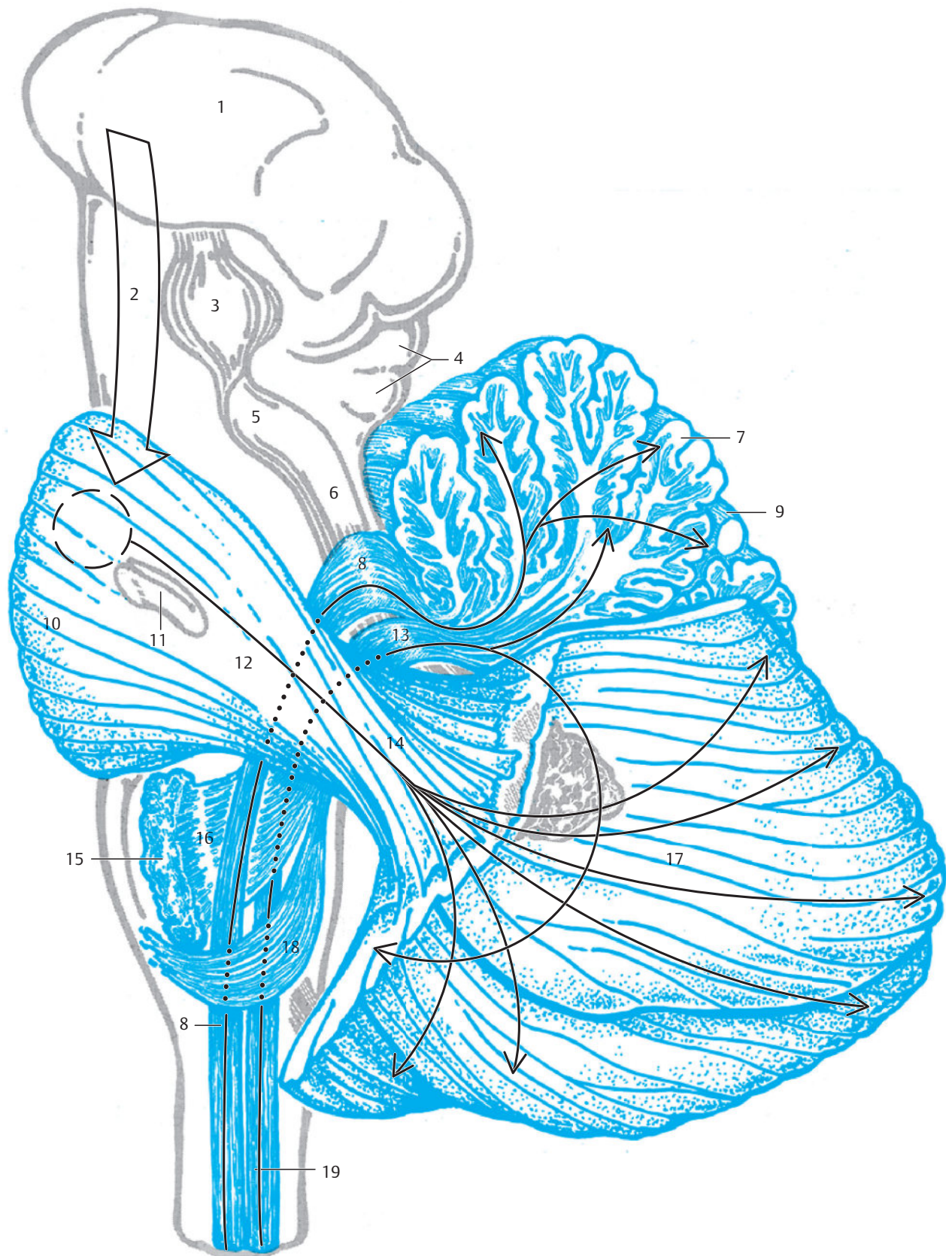


Fig. 10.36 Cerebellar systems.

Fig. 10.36a Lateral view of systems afferent to the cerebellar cortex. The left half of the anterior lobe of the cerebellum has been sectioned. The flocculonodular lobe and a part of the left posterior lobe have been laterally defibered from the middle cerebellar peduncle and removed. (Reproduced from Nieuwenhuys et al.⁴²⁴)

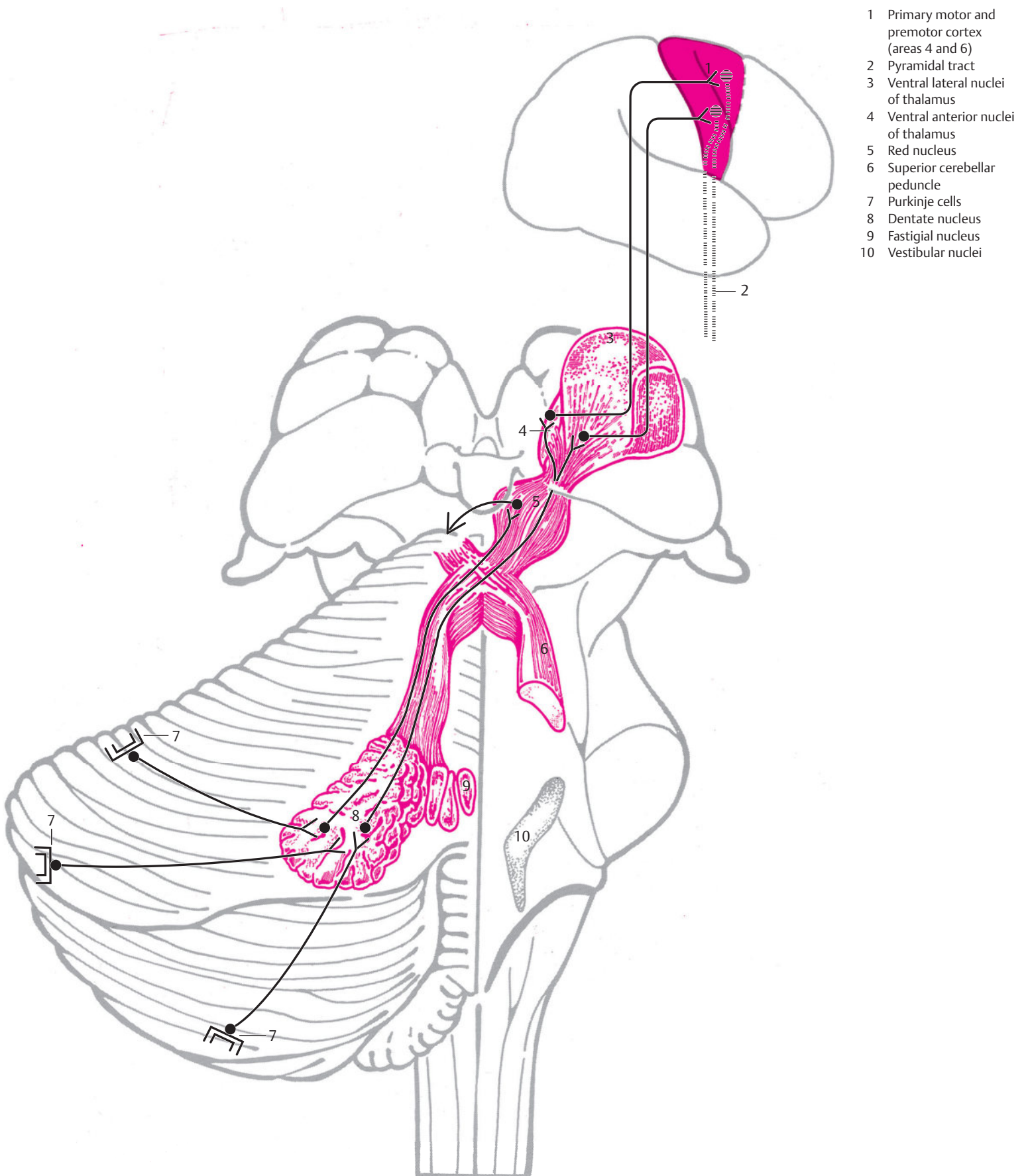


Fig. 10.36b Efferent cerebellar systems. Tracts and nuclei viewed from posterior. The cerebellum has been sectioned in the midline and the right half removed with exception of the superior cerebellar peduncle. (Reproduced from Nieuwenhuys et al.⁴²⁴)

10.10 Speech Areas

Credit has to be given to Broca (1861) and Wernicke (1874), clinicians who first localized speech and language areas. Research on the localization of aphasia was then mainly carried out by clinicians and in recent decades also by linguists, since the diagnosis of “aphasia” can only be made in the living.

The left hemisphere is involved in more than 95% of patients with aphasia,¹⁹² indicating that speech regions are lateralized. The left hemisphere is dominant in more than 99% of right-handed individuals. Approximately 60% of the left-handed individuals are left hemisphere dominant while the rest appear to use both hemispheres for language processing.⁴⁹ The topography of speech areas was derived from **clinical findings**.

Speech disorders are usually the result of vascular occlusion.^{192,227,352} The pathological lesion may then be larger than the actual speech region as the precise localization of this region cannot be narrowed down by morphological criteria. A variety of topical descriptions have therefore been published. The boundaries of the three speech regions have been shown in ►Fig. 10.37

and ►Fig. 10.38 such that their size corresponds to their minimal extent as described in literature.^{192,227,352} PET studies with estimation of glucose metabolism, local oxygen utilization, and regional cerebral circulation and fMRI provide further information.^{3,374,416} These however require follow-up studies on a large number of aphasic patients and extensive studies on healthy volunteers.

The **sensory speech region** or Wernicke's area lies in the superior temporal gyrus between the primary auditory cortex and the angular gyrus and is supplied by the posterior temporal artery, a branch of the middle cerebral artery.²²⁷ The visual speech area lies in the angular gyrus.¹⁹² Speech areas lie adjacent to their corresponding primary fields in the neocortex.

The **motor speech or Broca's area** lies in the frontal lobe anterior to the primary motor cortex and occupies the opercular part of the inferior frontal gyrus (see ►Fig. 7.53). Based on cytoarchitectonic criteria, this area corresponds to Brodmann's area 44 (see ►Fig. 7.53).¹⁴⁹ The sensory speech region lies between the auditory, visual and sensory primary fields, that is, between the transverse temporal gyri (of Heschl), the area striata and the postcentral gyrus.

- 1 Superior longitudinal (arcuate) fasciculus
- 2 Broca's area

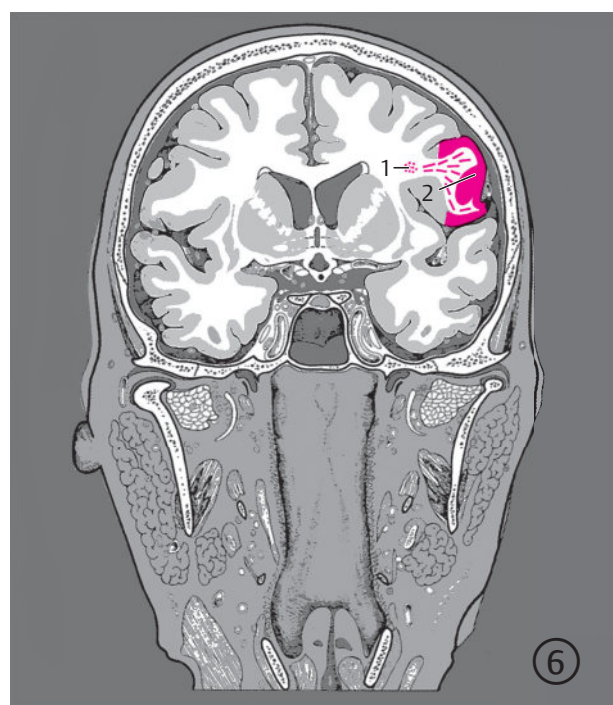


Fig. 10.37 Speech regions. Anterior view of serial coronal images. Encircled digits indicate the number of the respective slice (see ►Fig. 3.1).

Fig. 10.37a 5th and 6th sections.

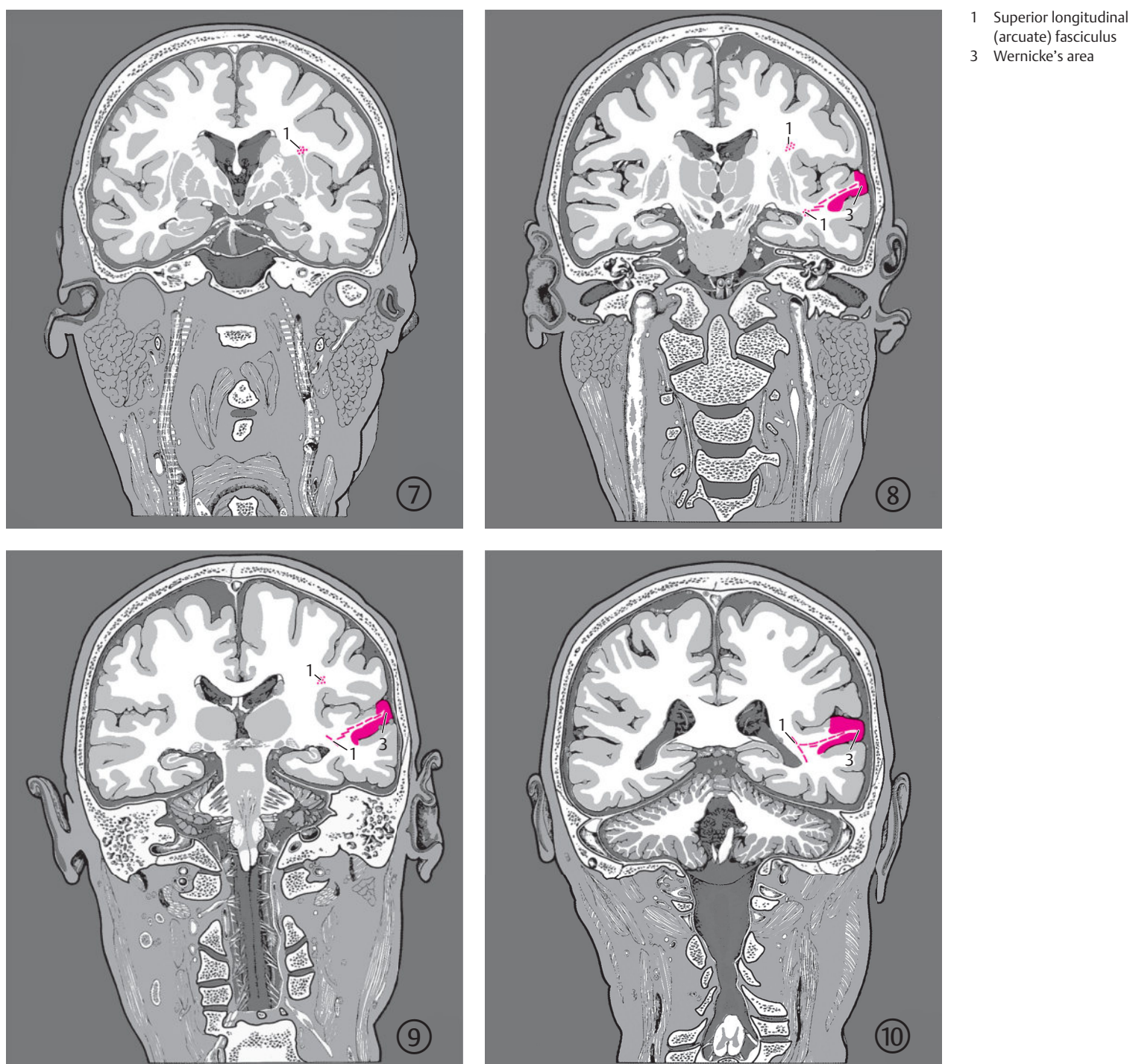


Fig. 10.37b 7th to 10th sections.

An occlusion of the artery of the precentral sulcus²²⁷ damages Broca's area and the neighboring insular region as seen on CT.⁵⁹

The **superior longitudinal fasciculus** (see ► Fig. 7.54, ► Fig. 7.55, and ► Fig. 10.37) lies at the posterolateral border of the putamen between the projection pathways of the external and internal capsules. These fibers of the

superior longitudinal fasciculus (**arcuate fasciculus**) run in an arc-like fashion between the temporal, parietal, and frontal lobes, thereby connecting Wernicke's, visual speech, and Broca's areas with one another.

Other speech regions have been identified in the supplementary motor area and in the head of the caudate nucleus.¹²³

- 1 Superior longitudinal (arcuate) fasciculus
- 4 Angular gyrus

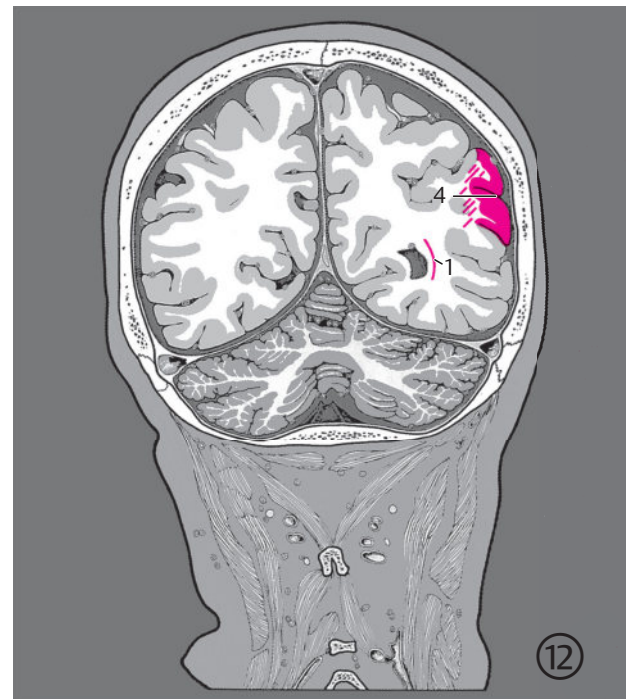
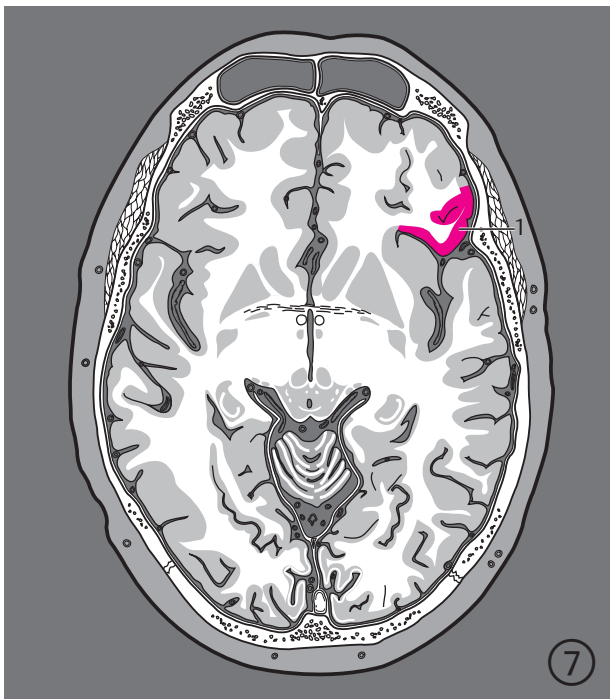


Fig. 10.37c 11th to 13th sections.



- 1 Broca's area
- 2 Wernicke's area
- 3 Angular gyrus

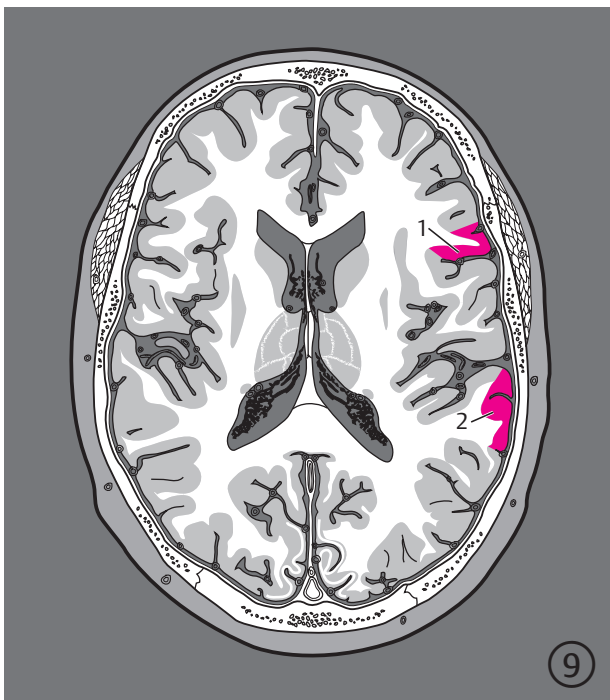


Fig. 10.38 Speech regions. Inferior view of serial images oriented along the bicommissural plane. Encircled digits indicate the number of the slice (see ► Fig. 5.1).

Clinical Notes

Global aphasia results in serious speech disorders with speech automatism being a cardinal symptom. The flow of speech is markedly impaired and is often dysarthric with communication being barely possible.

A dominant symptom of sensory aphasia (also known as Wernicke's, receptive, syntactic, acoustic, or pragmatic aphasia) on the other hand is the loss of ability to understand speech with associated phonetic and semantic paraphasia. The flow of speech is however preserved.

Motor aphasia (also known as Broca's, expressive, and verbal aphasia) usually arises from a lesion of Broca's area and is characterized by agrammatism, preserved but restricted speech comprehension and slowing down of speech. Articulation may also be impaired.

Word-retrieval failure characterizes amnesic aphasia. While verbal fluency is preserved, frequent sentence breaks and a searching behavior are the norm. Communication is only mildly disturbed.

Classifications into "fluent" and "non-fluent" aphasia are frequently used in literature. Fluent aphasia is caused by a lesion located behind the central sulcus, whereas nonfluent aphasia is caused by a lesion located in front of the central sulcus.⁴⁹ Both cortical lesions and subcortical brain lesions may cause aphasia, better known as "conduction aphasia." Special attention has been paid to aphasia due to lesions of the left thalamus,^{8,80,432,483} clinically distinguishable from conduction aphasia by unaffected repetitive speech. Infarctions of the supplementary motor area (see ►Fig. 10.25a and ►Fig. 10.26a) of the dominant hemisphere initially lead to severe speech disorders, occasionally with mutism, and later to a slowing down of speech. Most of these patients show a generalized akinesia. Lesions in the head of the caudate nucleus (see ►Fig. 3.7a, ►Fig. 3.7b, ►Fig. 4.3a, and ►Fig. 4.3b), anterior putamen and the anterior limb of the internal capsule of the dominant hemisphere cause atypical speech disorders with only a few symptoms characteristic of Broca's and Wernicke's aphasia. These lesions are typically caused by infarcts in the vascular territory of the central anterolateral arteries (lateral lenticulostriate arteries; see ►Fig. 7.29, ►Fig. 7.30, and ►Fig. 7.32).¹²³

Noninvasive fMRI may be employed as an alternative to the rarely used invasive Wada test to determine the language-dominant hemisphere.^{371,553}

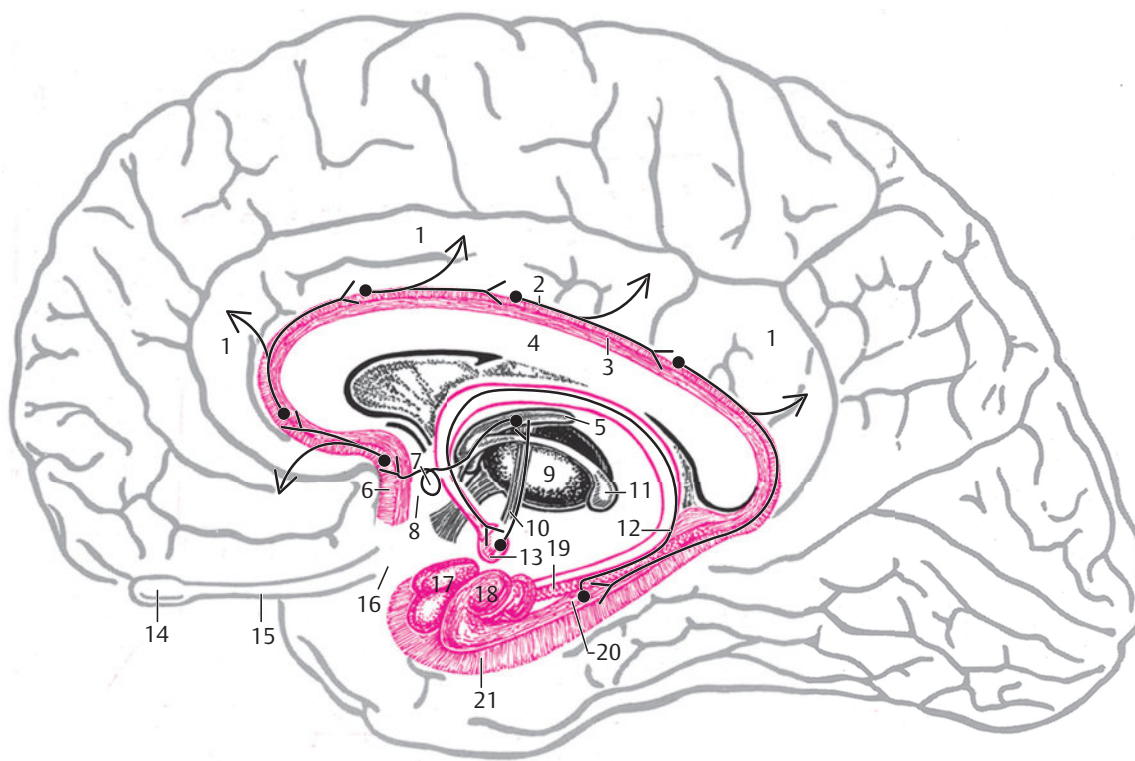
10.11 Limbic System

The limbic system (see ►Fig. 10.39, ►Fig. 10.40►, ►Fig. 10.41, ►Fig. 10.42►) comprises cortical and subcortical regions. The cortical areas develop from the phylogenetically old archicortex and periarthicortex, and were pushed during evolution against the medial and inferior aspects of both cerebral hemispheres due to the developing neocortex. These cortical regions form a margin around the corpus callosum and are therefore named "limbic" (rim). The archicortex and periarthicortex lie in front, above, and behind the corpus callosum and are thus divided into the pre-, supra-, and retro-commissural cortical areas. Archicortical parts form the inner edge of the rim, while the periarthicortical regions form its outer edge. The precommissural part of the archicortex includes the inner part of the subcallosal area; the supracommissural part includes the supracallosal indusium griseum and the retrocommissural region includes the hippocampal formation. The outer ring around the corpus callosum is formed by the outer part of the subcallosal area, the part of the cingulate gyrus close to the corpus callosum and the parahippocampal gyrus.⁵⁶¹ Electrophysiological stimulation of these regions leads to emotional reactions such as anger, fear, desire and sexual aggression, with corresponding effects on the autonomic nervous system. These observations led MacLean to name the limbic system the "visceral brain."

Cortical limbic regions possess afferent and efferent connections with certain subcortical structures. These subcortical structures - septal nuclei, preoptic area, mammillary body and other hypothalamic subnuclei, anterior nuclei of the thalamus, and limbic midbrain nuclei - are also considered part of the limbic system.

The subcallosal area and indusium griseum are relatively poorly developed in humans. However, the hippocampal formation is larger in man than in apes^{309,561} and lies in the medial part of the temporal lobe. During ontogenesis, the **hippocampal formation** was folded inward in the direction of the temporal horn of the lateral ventricle. It thereby encompasses the hippocampal sulcus as a C-shaped structure with two curved lips (see ►Fig. 3.9e and ►Fig. 3.9f). The **dentate gyrus** lies in the upper limb of this structure. The term dentate refers to the notched appearance of its surface. The curved part of the **hippocampus proper** (Ammon's horn) projects into the lateral ventricle. The inferior limb of the "C" is formed mainly by the subiculum.

The hippocampal formation has afferent connections with the parts of the hippocampal gyrus, septal nuclei,



- 1 Cingulate gyrus
- 2 Cingulum
- 3 Indusium griseum
- 4 Corpus callosum
- 5 Anterior nuclei of thalamus
- 6 Subcallosal area
- 7 Anterior commissure
- 8 Septal nuclei
- 9 Medial nuclei of thalamus
- 10 Mammillothalamic fasciculus (of Vicq d'Azyr)
- 11 Habenular nuclei
- 12 Fornix
- 13 Mammillary body
- 14 Olfactory bulb
- 15 Olfactory tract
- 16 Prepiriform cortex
- 17 Amygdaloid body
- 18 Hippocampus
- 19 Dentate gyrus
- 20 Subiculum
- 21 Parahippocampal gyrus

Fig. 10.39 Limbic and olfactory systems. Median view. (Reproduced from Nieuwenhuys et al.⁴²⁴; Stephan.⁵⁶¹) The wall of the IIIrd ventricle was omitted. The Papez circuit is thus visible, including the mammillothalamic tract and anterior thalamic nuclei.

hypothalamic subnuclei, and the dopaminergic (see Section 11.1.1) and serotonergic (see Section 11.2) centers of the brainstem. The principal tract is the **fornix**, a compact bundle of fibers which carries mainly efferent axons from the hippocampal formation. The initial fornical fibers form the alveus, a thin white layer lining the ventricular surface of the hippocampus proper. These fibers continue as the fimbria of hippocampus and arch beneath the corpus callosum as the posterior pillar (crus) of the fornix. Some fibers cross in the fornical commissure at the point where the right crus of the fornix meets the left. The body of the fornix continues under the anterior part of the corpus callosum descending toward the interventricular foramen (of Monro). The tracts then separate into the two pillars of fornix which form the medial boundary of the interventricular foramen, continuing inferiorly toward the hypothalamus, posterior to the anterior commissure. Precommissural fibers extend to the **septal nuclei**, straight gyrus, and frontal cortex directly above the anterior commissure, while branching fiber bundles reach the nuclei of the stria terminalis and the anterior nuclei of the thalamus below the anterior commissure. The main bundle of the fornix passes to the **hypothalamus**, where most fibers terminate in the mammillary body.

The mammillothalamic fasciculus (Vicq d'Azyr's bundle) arises from the **mammillary body** and passes to the **anterior nuclei of the thalamus**. Fiber tracts from these regions return via the cingulum to the hippocampal formation. This circuit (hippocampal formation, mammillary body, anterior nuclei of the thalamus, cingulum, hippocampal formation) is known as the **Papez circuit**. Connections radiate from here into the frontal cortex, cingulate gyrus, and parahippocampal gyrus. These neuronal connections are likely damaged when **bilateral lesions of the hippocampal formation**, the fornices, or the mammillary bodies cause dramatic **loss of recent memory**.^{267,495} The **amygdaloid body** is a complex of several nuclei and a cortical area and lies medially at the tip of the temporal horn of the lateral ventricle. It belongs partly to the olfactory region (see Section 10.7) and partly to the limbic system. The **amygdaloid body** has afferent connections with the olfactory bulb, specific hypothalamic nuclei, brainstem, and cortical regions of the telencephalon. The main efferent pathways are the stria terminalis and the ventral amygdalofugal fibers. The stria terminalis arches between the caudate nucleus and the thalamus and projects into the septal nuclei, hypothalamic nuclei, reticular formation, and into specific telencephalic regions.

- 1 Periarbarchicortex in cingulate gyrus (within the slice)
- 2 Periarbarchicortex in cingulate gyrus
- 3 Subcallosal area (partially within the slice)
- 4 Septal nuclei (within the slice)
- 5 Fornix (within the slice)

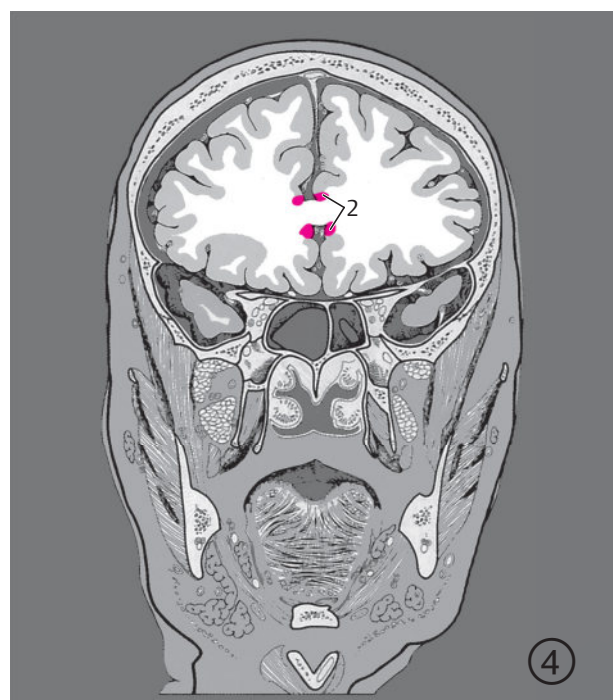
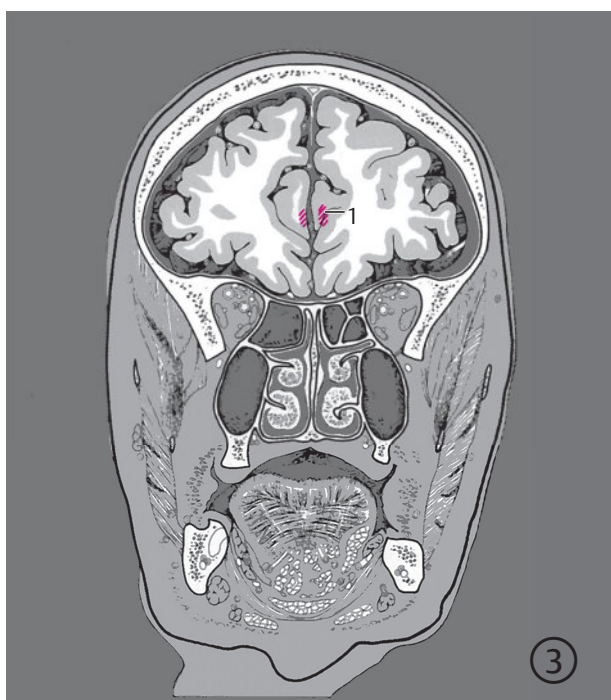


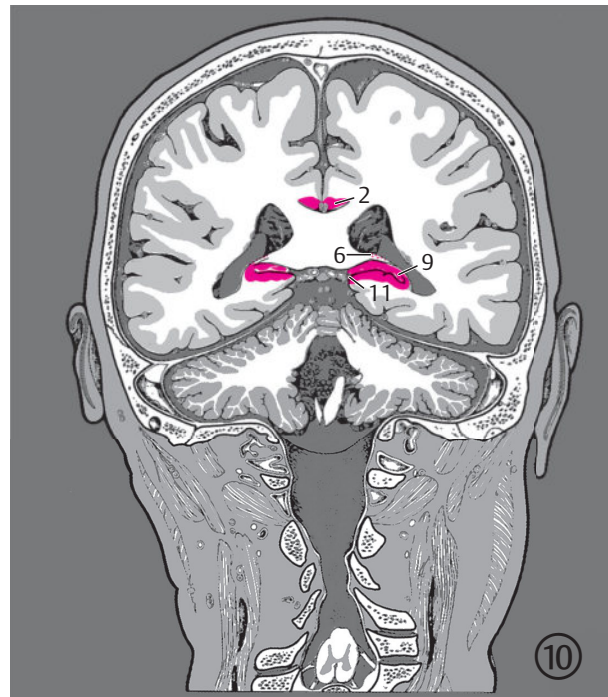
Fig. 10.40 Limbic system. Serial coronal images of cortical areas and important nuclear regions of the limbic system with fornix and mammillary body. Encircled digits indicate the number of the respective slice (see ► Fig. 3.1).

Fig. 10.40a 3rd to 6th sections.

The **septal nuclei** (formerly septum verum or pre-commissural septum) play a central role among the **subcortical nuclear areas of the limbic system**. The medial forebrain bundle connects these nuclei with important centers in the hypothalamus and midbrain.

This connection is twofold, namely septomesencephalic and mesencephaloseptal. These regions are the preoptic regions of the hypothalamus, lateral and medial hypothalamic nuclei, and limbic nuclear areas of the midbrain. The latter include an anterior region of the tegmentum of the midbrain, the interpedun-

cular nucleus, as well as the posterior raphe nucleus and the posterior tegmental nucleus (of Gudden). The mamillo- tegmental fasciculus connects the mammillary body with the tegmentum of the midbrain. A further connection exists between these nuclear regions and the medulla oblongata via the **posterior longitudinal fasciculus (of Schütz)**. The striae medullares of thalamus bypass the hypothalamus to run from limbic areas to the habenular nuclei; the habenulo-interpeduncular tract runs from these nuclei to the interpeduncular nucleus.



- 2 Periarhchicortex in cingulate gyrus
- 6 Fornix
- 7 Mammillary body
- 8 Amygdaloid body (partially limbic)
- 9 Hippocampal formation
- 10 Parahippocampal gyrus
- 11 Periarhchicortex

Fig. 10.40b 7th to 10th sections.

- 2 Periarthcortex in cingulate gyrus

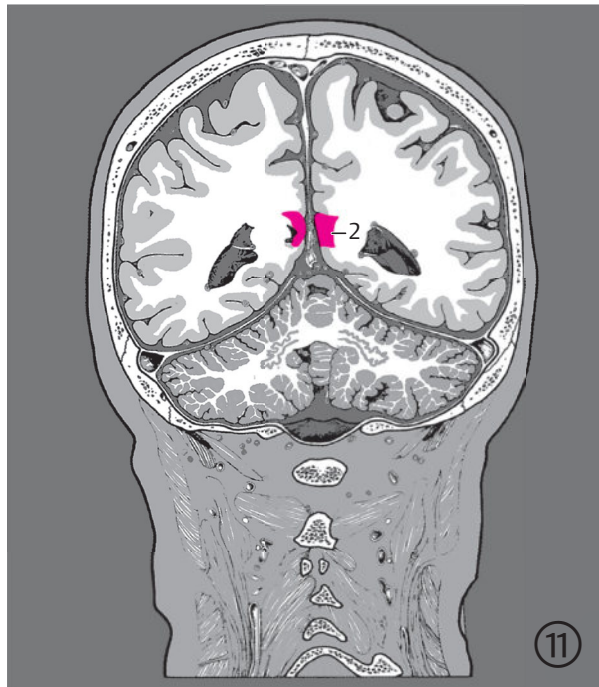


Fig. 10.40C 11th section.

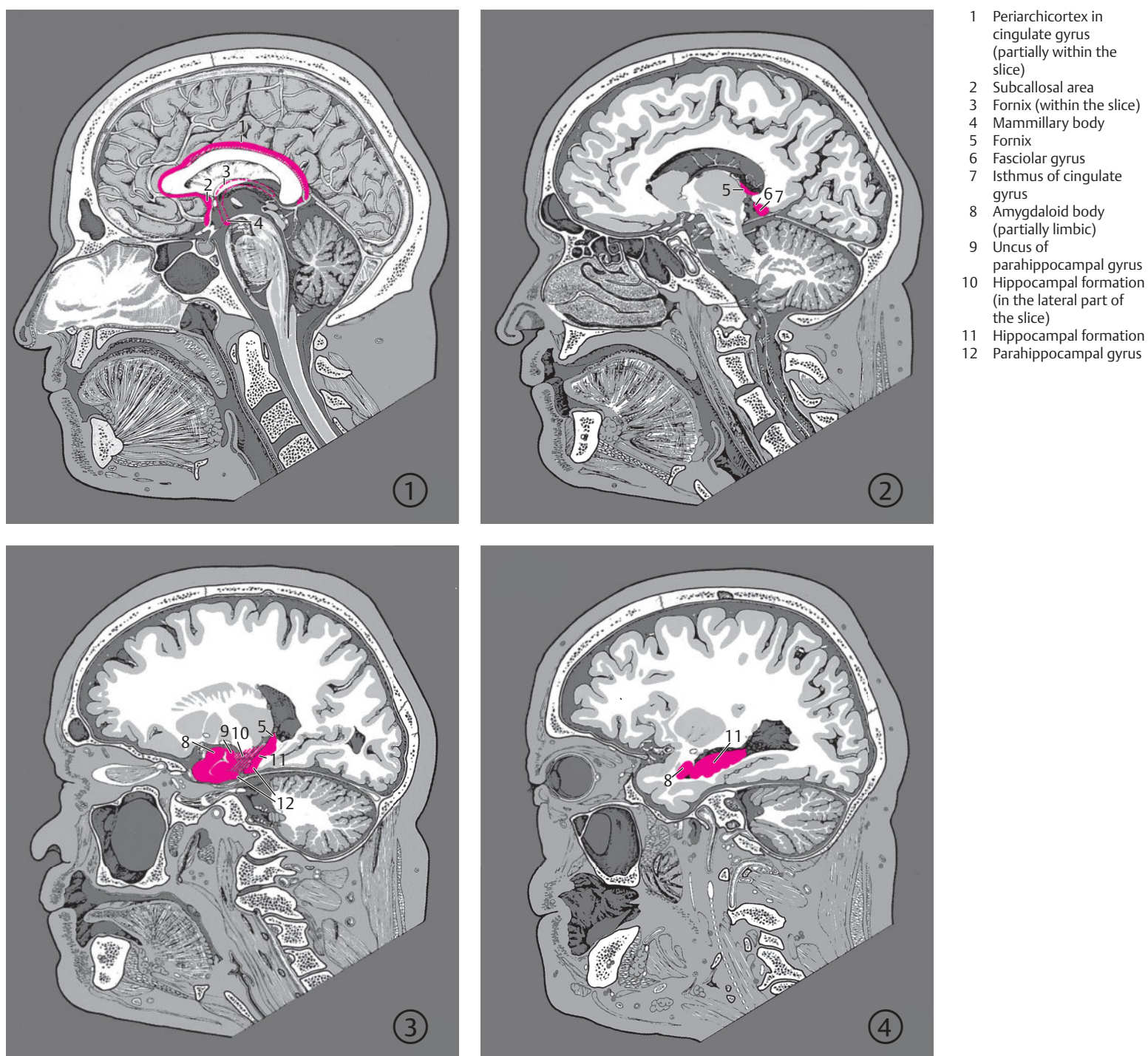


Fig. 10.41 Limbic system. Serial sagittal images of cortical areas and important nuclear regions of the limbic system with fornix and mammillary body. Encircled digits indicate the number of the respective slice (see ► Fig. 4.1).

- 1 Periarhchikortex, retrocommissural
- 2 Amygdaloid body (only partially limbic)
- 3 Hippocampal formation
- 4 Subcallosal area
- 5 Mammillary body (within the slice)
- 6 Parahippocampal cortex, uncus
- 7 Parahippocampal cortex
- 9 Fornix

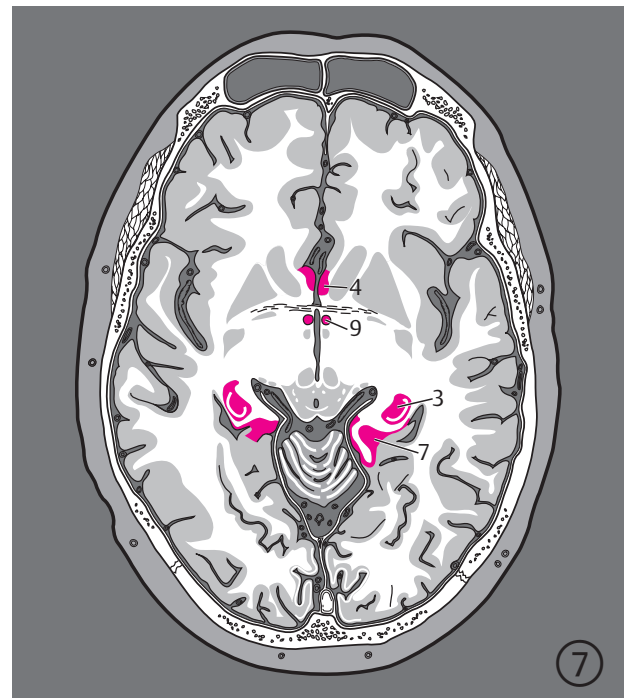
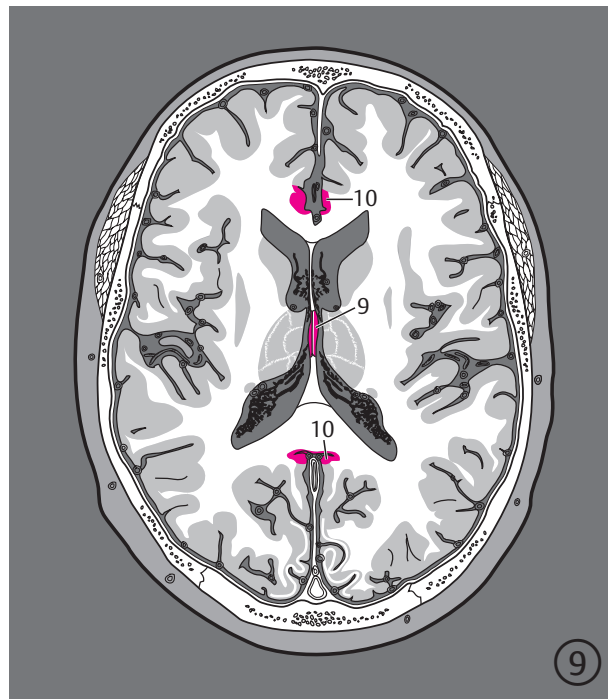
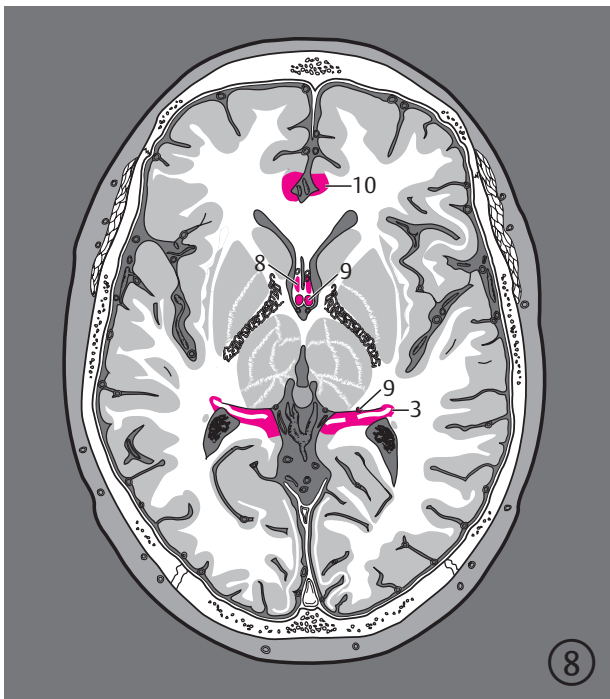


Fig. 10.42 Limbic system. Serial images of cortical areas and important nuclear regions of the limbic system with fornix and mammillary body oriented along the bicommissural plane. Encircled digits indicate the number of the respective slice (see ► Fig. 5.1).

Fig. 10.42a 4th to 7th sections.



- 3 Hippocampal formation
- 8 Septal nuclei
- 9 Fornix
- 10 Periarbocortex, cingulate cortex (part close to corpus callosum)

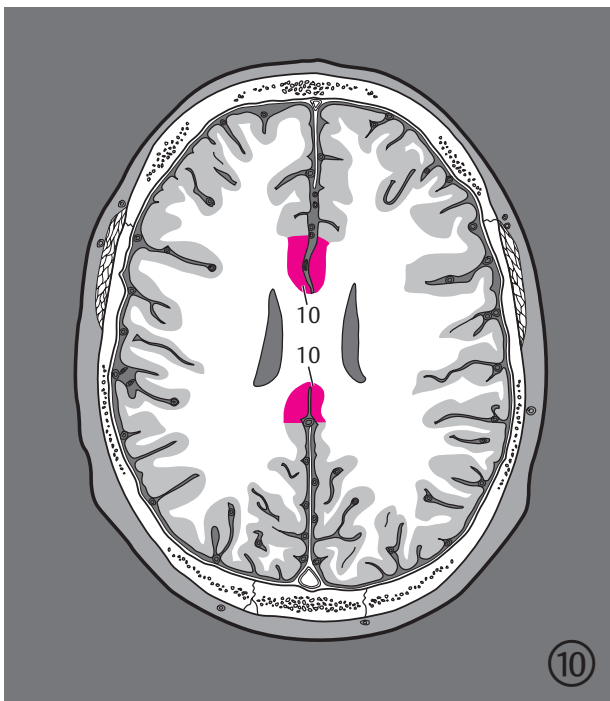


Fig. 10.42b 8th to 10th sections.

10.12 Autonomic Nervous System

The autonomic nervous system of the head (see ►Fig. 10.43) innervates the smooth muscles of the eye and the orbit, lacrimal and salivary glands, smooth muscle cells of blood vessels and the sweat glands of the scalp, and the erectile smooth muscle of hair on the scalp. This efferent innervation is binauronal as per classical theory. The cell bodies of the first-order neurons lie in the central nervous system while those of second-order neurons lie in the ganglia outside the CNS. The preganglionic fibers leave the CNS and are connected synaptically with second-order neurons. Postganglionic fibers run to target or end organs. As in other parts of the body these efferent autonomic fibers are divided into a **parasympathetic** part and a **sympathetic** part. The parasympathetic part assumes trophotropic functions of digestion and energy synthesis (anabolism); the sympathetic part assumes ergotropic functions of physical activity, the “fight or flight” reaction and the associated large output of energy thereby. The classical concept of the autonomic nervous system has been broadened through the discovery of the synaptic effects of certain **neuropeptides** (see Section 11.7).^{168,422} Neuropeptides modulate the effects of the transmitter substances of the parasympathetic and sympathetic nervous systems.

10.12.1 Parasympathetic Nervous System of the Head

The **cell bodies of the first-order parasympathetic neurons** of the head lie in the midbrain, pons, and in the medulla oblongata. The preganglionic fibers leave the brain with the IIIrd, VIIth, and IXth cranial nerves. The **parasympathetic** (ciliary, pterygopalatine, submandibular, and otic) **ganglia** lie close to their target organs and the postganglionic course of parasympathetic fibers is thus relatively short.

The parasympathetic **motor nucleus of oculomotor nerve (of Edinger–Westphal)** lies in the **tegmentum of the midbrain** immediately anterolateral to the aqueduct. The preganglionic fibers join the oculomotor nerve and run through the superior orbital fissure into the orbit to the ciliary ganglion (see ►Fig. 8.2 and ►Fig. 10.43b). This lies approximately 18 mm behind the eyeball, lateral to the optic nerve. The postganglionic fibers of the nerve cells in the ciliary ganglion reach the sphincter pupillae (pupillary constriction) and the ciliary muscle (accommodation of the eye). The binauronal pathway from the accessory nucleus of oculomotor nerve (of Edinger–Westphal) to the sphincter pupillae also represents the efferent pathway for the **pupillary reflex**.

The **cell bodies of the first-order parasympathetic neurons of the facial nerve** lie in the **superior salivatory**

- 1 Oculomotor nerve
- 2 Accessory nucleus of oculomotor nerve (of Edinger–Westphal)
- 3 Superior salivatory nucleus
- 4 Inferior salivatory nucleus
- 5 Sympathetic fibers in the wall of vertebral artery
- 6 Sympathetic fibers in the wall of internal carotid artery
- 7 Intermediate nerve
- 8 Glossopharyngeal nerve

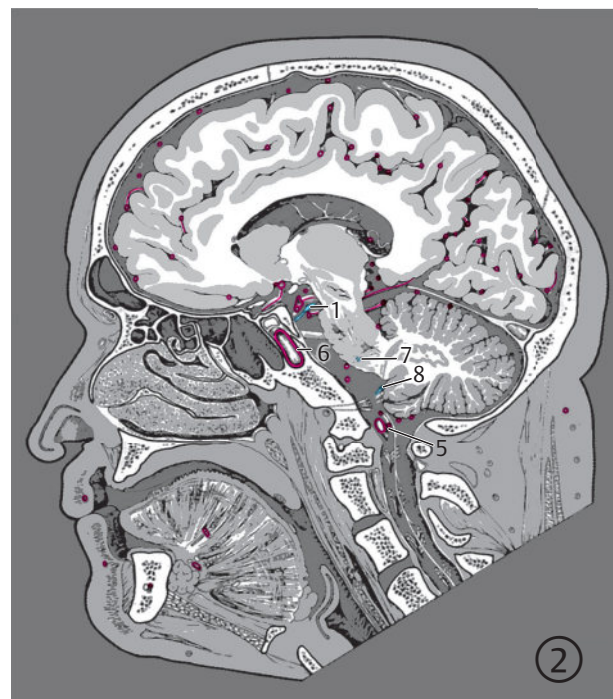
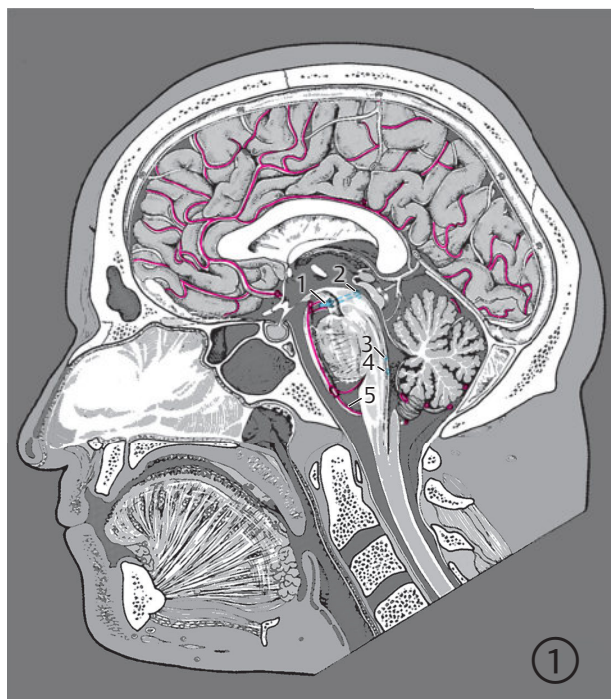
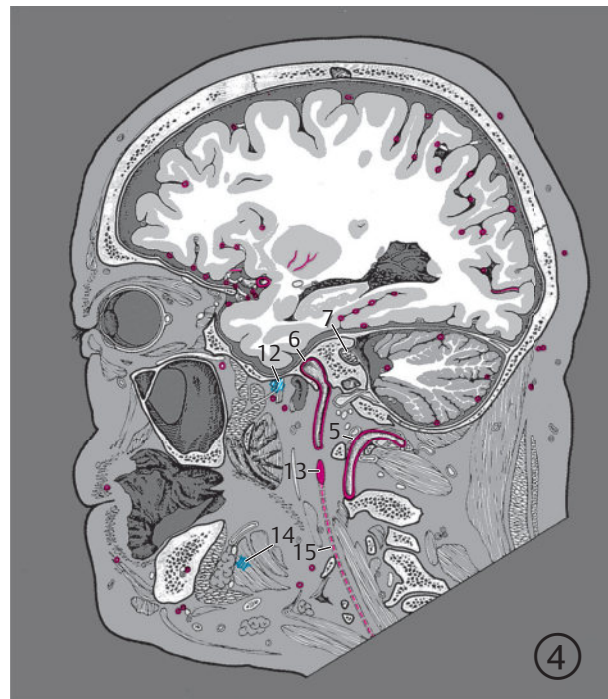
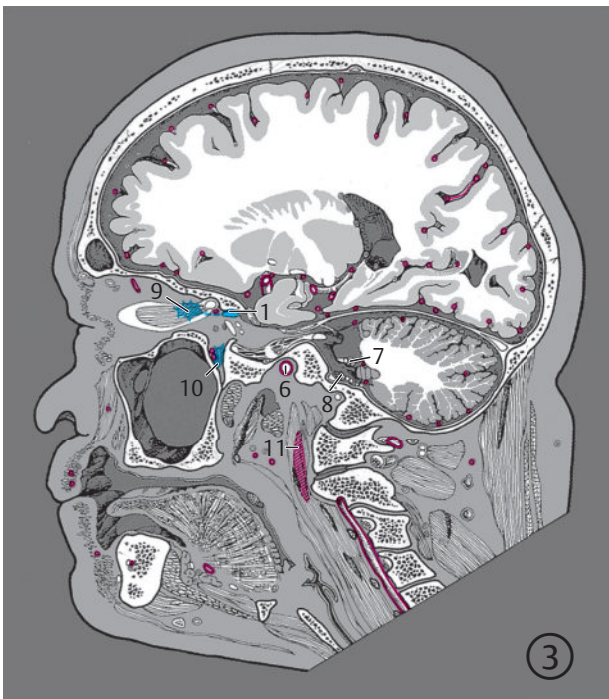


Fig. 10.43 Autonomic system. Serial sagittal images of the autonomic system of the head. The parasympathetic part is marked in blue and the sympathetic part in red. Encircled digits indicate the number of the respective slice (see ►Fig. 4.1).

Fig. 10.43a 1st and 2nd sections.



- 1 Oculomotor nerve
- 5 Sympathetic fibers in the wall of vertebral artery
- 6 Sympathetic fibers in the wall of internal carotid artery
- 7 Intermediate nerve
- 8 Glossopharyngeal nerve
- 9 Ciliary ganglion (in the lateral part of the slice)
- 10 Pterygopalatine ganglion (within the slice)
- 11 Superior cervical ganglion (in the lateral part of the slice)
- 12 Otic ganglion
- 13 Superior cervical ganglion
- 14 Submandibular ganglion (in the lateral part of the slice)
- 15 Sympathetic trunk
- 16 Greater petrosal nerve
- 17 Chorda tympani
- 18 Sympathetic fibers in the wall of external carotid artery



Fig. 10.43b 3rd to 6th sections.

nucleus immediately below the floor of the rhomboid fossa in the inferior part of the pons. The preganglionic fibers run in the intermediate nerve of the facial nerve to the internal acoustic canal in the petrous bone (see ►Fig. 7.4). The greater petrosal nerve branches off from the intermediate nerve at the entrance of the facial canal. This nerve leaves the petrous bone, runs underneath the dura of the middle cranial fossa, and passing through the small bony pterygoid canal (or Vidian canal), it reaches the **pterygopalatine ganglion** which lies in the pterygopalatine fossa (see ►Fig. 3.5c, ►Fig. 3.5d, and ►Fig. 5.4; ganglion: see ►Fig. 10.43b). Its postganglionic fibers run with the zygomatic nerve to the lacrimal gland and through nasal and palatine

nerves to the glands of the nasal cavity and the palate. The **chorda tympani** branches off the intermediate branch of the facial nerve at the end of the facial canal and just above the stylomastoid foramen. It runs underneath the mucous membrane of the tympanic cavity, passes through a fine bony canal and reaches the infratemporal fossa at the base of the skull, posteromedial to the temporomandibular joint. Here the chorda tympani joins the lingual nerve. The preganglionic fibers reach the submandibular ganglion (see ►Fig. 10.43b) in the submandibular triangle at the posterior border of the mylohyoid. The postganglionic fibers run to the submandibular and sublingual glands and the glands of the tongue.

Cell bodies of first-order parasympathetic neurons of the **glossopharyngeal nerve** lie in the **inferior salivatory nucleus** close to the floor of the rhomboid fossa in the superior part of the medulla oblongata. Its preganglionic fibers first run in the glossopharyngeal nerve through the jugular foramen and enter the petrous bone. The short lesser petrosal nerve arises from a nerve plexus. It leaves the petrous bone, runs underneath the dura mater in the middle cranial fossa and after passing through a fine bony canal reaches the **otic ganglion** (see ► Fig. 4.5 and ► Fig. 10.43b). This ganglion lies just beneath the foramen ovale on the medial aspect of the mandibular nerve. The postganglionic fibers join the auriculotemporal nerve and innervate the parotid gland.

The **vagus nerve** together with its parasympathetic fibers exits the medulla oblongata at its lateral aspect and runs through the jugular foramen (see ► Fig. 3.23, ► Fig. 5.31, and ► Fig. 6.5b). This nerve runs in the neurovascular bundle between the internal carotid artery and the internal jugular vein in the neck (see ► Fig. 3.9c and ► Fig. 3.9d). The **parasympathetic innervation of the vagus nerve** reaches the heart, lungs, and gastrointestinal tract. This nerve has therefore not been depicted in ► Fig. 10.43.

10.12.2 Sympathetic Nervous System of the Head

The cell bodies of the first-order sympathetic neurons of the head lie in the **lateral gray horns of the spinal cord** in the segments C8, T1 to T3.⁴²² The preganglionic fibers leave the spinal canal with the corresponding spinal nerves and ascend with the spinal sympathetic trunk reaching primarily the **superior cervical ganglion** where the second-order neurons lie. The superior cervical ganglion (see ► Fig. 3.8a, ► Fig. 4.4a, and ► Fig. 4.5a) is a spindle-shaped swelling, measuring on an average 28 mm in length.³³⁶ This ganglion lies behind the internal carotid artery at the level of the first and second cervical vertebrae and is enveloped by the deep cervical fascia. The postganglionic fibers form periarterial plexuses around the cranial arteries and innervate the smooth muscle fibers of the dilator pupillae (pupillary dilatation) and the tarsal muscles (widening of the palpebral fissure), smooth muscles of the arteries, sweat glands of the scalp (excitatory), and lacrimal and salivary glands (inhibitory).

Clinical Notes

An ipsilateral Horner's syndrome results from a unilateral lesion of the cervical sympathetic: the pupil is constricted due to the paralysis of the dilator pupillae (miosis). The upper lid droops due to loss of nerve supply of the tarsal muscle (ptosis). Enophthalmos results from paralysis of the orbitalis (see ► Fig. 3.4c, ► Fig. 3.4d, and ► Fig. 4.5c) or a reduction of blood flow through retrobulbar fat. Conjunctival hyperemia is present. Ipsilateral sweat production on the face, arm, and thorax is decreased or lost (autonomic upper quadrant syndrome), and the secretion of tears is also decreased ipsilaterally.

10.13 Neuronal Networks

Dina Wittfoth

10.13.1 Task Dependent Activation versus Activation at Rest

Simple activation paradigms were employed for the investigation of neuronal networks during early **fMRI** studies. The aim was to localize neuronal correlates of the desired function by **subtracting brain activity** under diverse conditions. Subtraction logic requires that conditions differ only with respect to the function to be examined, but are otherwise as identical as possible. In a landmark study on object recognition, Rafi Malach and coworkers examined the difference between activation during recognition of objects with that during the perception of abstract images. The results were verified using statistical tests for significance and revealed activation in the lateral occipital cortex.³⁸¹ It should be noted, however, that the two conditions vary in more than one respect which does not permit a distinct localization of the function "object recognition" in the lateral occipital cortex. For example, complexity, luminance, naming, awareness and the degree of attention given to the stimulus differ from one another. Moreover, it cannot be determined whether all test subjects understand and perform tasks in an identical manner, particularly with complex cognitive or affective group studies. Other thought processes also usually run in the background, especially if the task is not difficult. In addition, difficulties arise particularly when the participant cannot handle the intended task, due to cognitive or motor limitations, for instance. Newer developments however allow information on brain activity to be obtained even in such cases. The **measurement of resting activation** is a very useful approach which enables mapping of the functional organization of the brain independent of cognitive and/or motor skills, and even independent of the level of consciousness (e.g., in anesthetized or comatose patients). The study of **functional connectivity** using **resting-state fMRI**, that is, measurement of brain activity at rest (rs-fMRI) has already identified several so-called **intrinsic networks**, which were consistently replicated in healthy individuals as well as across varying states of consciousness and different species.^{58,109,494} Knowledge that "resting phases" within activation paradigms are also associated with characteristic activation patterns led to the development of rs-fMRI. Systematic study of these patterns then revealed a replicable pattern of resting activation networks similar to those seen during activation conditions but with additional components. **Regional interactions** are examined using established functional imaging sequences in rs-fMRI, while participants rest inside the MRI and do not perform an explicit task.⁵⁸ Activation at rest, similar to activation during an explicit task, results in changes in cerebral blood flow and oxygenation; changes in

blood oxygenation, in turn, may be mapped as so-called **BOLD contrast**. **Networks** identified by rs-fMRI, also known as “components,” consist of functionally inter-related regions with highly correlated BOLD activation profiles.^{349,403} These components are moreover very robust with respect to different measurement parameters, individual groups, measurement sites and sample sizes,^{403,549} and may also be validated using other methods such as EEG or MEG.

10.13.2 Neural Processing in Networks

Most resting activation components represent functional networks that underlie cognitive functions under conditions of activation.^{494,549} These networks may be further subdivided into **subnetworks** depending on the dimensionality of evaluation, which in turn may be associated with increasingly specific functions. Higher-dimensional approaches are however, less consistent, so that often no generalized inference may be derived therefrom. Characteristic of these correlates at rest is the fact that they partly correspond with, but are not limited to, anatomical connections.⁶⁴⁷ Neuronal networks thus represent a **substrate of “higher” functions**, which enable coupling of external stimuli and internal processes.

Based on the **cytoarchitectonic mapping** of 47 brain regions by Korbinian Brodmann (so-called **Brodmann areas**, see ► Fig. 7.53), M. Mesulam³⁹¹ assumed a **functional division of the cortex** into five different regions. Primary cortical fields, unimodal association fields, heteromodal association fields, paralimbic and limbic areas are thereby differentiated according to increasing complexity. An external to internal gradient may furthermore be identified: uni and heteromodal cortical fields are primarily concerned with the processing of external sensory input, while limbic areas are associated with the affective–motivational internal milieu.

Characteristics of **external sensory perceptions** primarily influence the mode of neuronal processing. Various information processing pathways may be identified, for instance, for different classes of external stimuli. In the **visual domain**, a **dorsal** pathway extending from the primary visual cortex to the parietal lobe mainly handles spatial information, while a **ventral** pathway leading from the visual cortex across the occipitotemporal junction is associated with the processing of object-related information.⁴⁵⁰ In addition, the central nervous system of highly developed species is specialized to rapidly recognize unknown events or objects and to prevent automated reactions, if needed, provided these are no longer appropriate. Large parts of the cerebral neocortex are therefore reserved for unimodal (modality-specific) processing to ensure accuracy of sensory encoding. Extensive **hetero and multimodal association areas** also enable subsequent integration of sensory perceptions.

The prefrontal cortex, posterior parietal cortex, as well as parts of the lateral temporal cortex and the parahippocampal gyrus belong to heteromodal association areas. These regions are characterized by the convergent afferents of unimodal areas of different modalities; lesions in these regions therefore always lead to deficits in various modalities. The **paralimbic regions** are divided into a temporopolar, insular, and orbitofrontal part and a hippocampal part. Cytoarchitectonically, these regions represent a transitional zone between the homotypic isocortex and the more primitive allocortex of limbic structures. These include the hippocampal complex, the amygdaloid complex, the prepiriform olfactory cortex, the septal region and the substantia innominata. They exhibit primitive allocortical architecture together with marked **reciprocal connectivity with the hypothalamus**. **Transmodal** refers to the entirety of heteromodal, paralimbic, and limbic areas, since they do not exhibit specificity for sensory input from a particular modality. They receive afferent signals from downstream unimodal areas as well as from other transmodal regions. These reciprocal compounds form so-called **multimodal convergence zones** and can, by means of top–down or feedback loops, exercise their influence on processing in unimodal areas.³⁹¹

The architecture of networks showing increased activation in response to internal or external stimuli, however, depends not only on the characteristics of the particular stimulus but to a great extent also on the **current state and objectives of an organism**. In general, neuronal networks may be ascribed to some basic, domain-independent psychological functions, such as core affects, conceptualization, executive attention functions, or exteroceptive sensory perception; these functions serve as elements of diverse mental states.

The study of superordinate intrinsic networks is particularly useful in the comprehensive understanding of mental states and operations and can integrate evidence of new neuroscientific research.^{361,391,438} This concept also correlates well with findings of lesion studies suggesting a distinct relationship between specific regions and particular functions, shown by the complex relationship between the site of a lesion and the clinical picture. For example, spastic paralysis is clearly associated with lesions of the motor cortex and its ascending pathways, while cognitive syndromes, such as attention deficits, may occur because of diverse lesions.⁴⁵⁰ Some principal neuronal networks and their associated mental functions have been described in greater detail below. We have only elaborated upon those higher cognitive and affective networks which have been most frequently examined and replicated by functional imaging, thereby enabling generalized assertions to be made.

To this end, findings of rs-fMRI examinations as well as those of activation studies on functional imaging have been used and integrated.

10.13.3 Sensory and Motor Functions

Basal sensory functions such as visual and auditory perception, as well as motor activity, are also associated with activation within a network of cortical areas.

Visual network

Initial cortical processing of visual stimuli occurs in the primary visual cortex (V1, also striate cortex, calcarine cortex or BA 17), which covers the calcarine sulcus (see ► Fig. 10.44; also see ► Fig. 3.14a, ► Fig. 3.14b, ► Fig. 4.2b, and ► Fig. 7.53) and exclusively processes projections from magnocellular and parvocellular layers of the lateral geniculate body.

This creates a precise retinotopic image of the visual field. The neurons of this region are sensitive to orientation, movement, binocular disparity, length, spatial frequency, wavelength, and luminance. The downstream, occipital **visual association areas** (V2 = BA18, V3, V4, and V5 [MT] = BA 19) are monosynaptically connected to V1; their localization exhibits interindividual differences, unlike V1. Unimodal visual association regions may be divided into an upstream peristriate component (BA 18/19) as well as a downstream temporal component (inferotemporal regions, such as BA 21–22, lateral occipitotemporal gyrus [also referred to as fusiform gyrus; see ► Fig. 3.7a, ► Fig. 3.7b, ► Fig. 4.6a, ► Fig. 4.6b, ► Fig. 5.8, and ► Fig. 7.53]). Upstream network nodes consist of neuronal networks specialized in the encoding of relatively elementary attributes of visual impressions. Downstream areas, on the other hand, are mainly specialized in the encoding of compound properties. Patterns and forms may be discriminated in the fusiform gyrus as well as adjacent parts of the lingual and the inferior occipital gyri. Reacting neuronal populations selectively assigned to specific visual categories, such as those of the face (fusiform face area [FFA], occipital face area [OFA], objects (lateral occipital complex [LO]) or words are identified in the **fusiform gyrus** during subsequent stages of processing. Certain neuronal populations in the parahippocampal gyrus are specialized in the perception of large-scale environmental features such as buildings (parahippocampal place area [PPA]). Intrinsic correlations between visual areas extending over primary and secondary, medial and lateral occipital and extrastriate regions are also seen at rest. At the behavioral level, these regions are primarily associated with cognitive dimensions, language, orthography and spatial orientation.^{361,391,549}

Auditory Network

An auditory component associated with functions such as auditory perception, as well as language comprehension and production, can also be replicated in the resting state and is specifically represented by activation in the superior temporal and **transverse temporal (Heschl's) gyri** as well as in primary and secondary auditory association cortices (see ► Fig. 10.45, see also Section 10.5).^{361,549} The primary auditory cortex (also designated A1) is located

on the underside of the cistern of the lateral cerebral fossa (of Sylvius) in the planum temporale.

The primary dimension of auditory perception is tonotopic mapping. A1 neurons are mainly specialized for perception of pitch and fundamental frequency. Unimodal **auditory association cortices** lie in the superior temporal gyrus (BA 22) as well as in parts of the medial temporal gyrus (BA 21) (see ► Fig. 7.53). The middle and anterior parts of the superior temporal gyrus are more specialized in the coding of specific phonetic parameters, important for comprehension of spoken language.^{391,645}

Sensorimotor Network

The interplay between the pre and postcentral gyri, supplementary motor (SMA) and somatosensory cortex as well as the posterior insula constitutes a sensorimotor network (see ► Fig. 10.46), which, alongside a cerebellar component of resting activation, is associated with the execution of actions as well as body and pain perception. Sensorimotor information is first processed in the primary somatosensory cortex (BA 3b on the anterior flank of the postcentral gyrus, also known as S1) and in the primary motor cortex (posterior edge of BA 6 in the precentral gyrus; also known as M1) (see ► Fig. 7.53). Unimodal somatosensory association areas lie downstream in parts of the superior parietal cortex in BA 5, BA 7, and BA 2.^{403,549}

10.13.4 Executive Functions and Attention

Executive Functions

Higher-order mental processes occurring within a complex neural network are summarized under the term “executive functions” but cannot so far be explained by a single comprehensive definition of all appertaining functions. Executive functions essentially comprise all mental processes related to anticipation, planning and initiation of actions, cognitive flexibility, as well as the coordination, sequencing and monitoring of information and processes. The purpose of executive functions is therefore the planning and tracking of actions or intentions over several stages, which takes place by focusing on information relevant to the action concerned as well as by inhibiting unwanted information. Above all, executive functions are a prerequisite in unfamiliar situations to enable adequate adaptation to a changing environment and optimizing behavior over the long term.^{42,113,121,588} Executive functions, as well as attention, are sometimes referred to as **frontal lobe functions**. According to Smith and Jonides,⁵⁴⁷ the following five components of memory and executive processes can be identified:

- Attention and inhibition
- Task management
- Planning
- Monitoring
- Coding (representation in working memory)

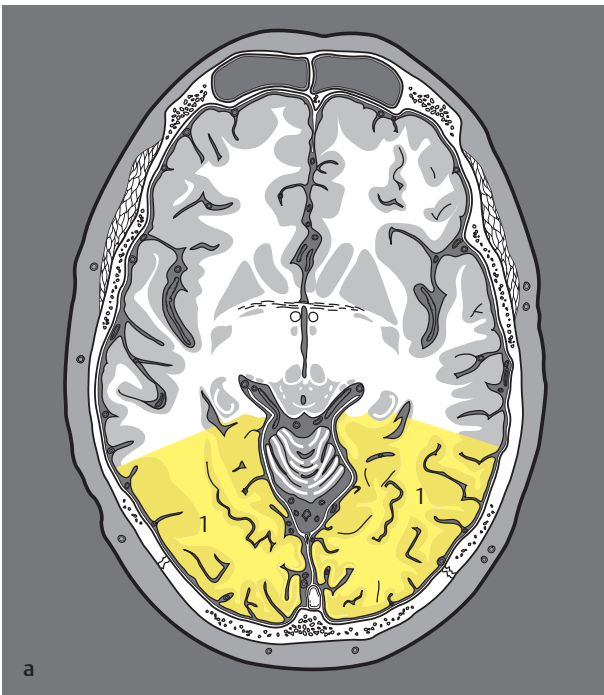
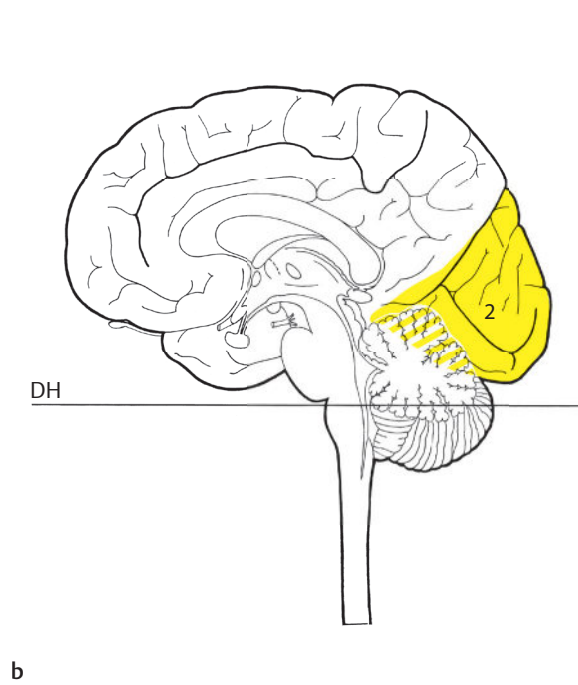


Fig. 10.44 Visual system.

DH = German horizontal.

Fig. 10.44a 7th bicommissural section.

Fig. 10.44b Median view of the brain and the upper spinal cord.



- 1 V1-V5 lateral, Fusiform gyrus Lingual gyrus Inferior occipital gyrus (IOG)
- 2 V1-V5 medial, IOG

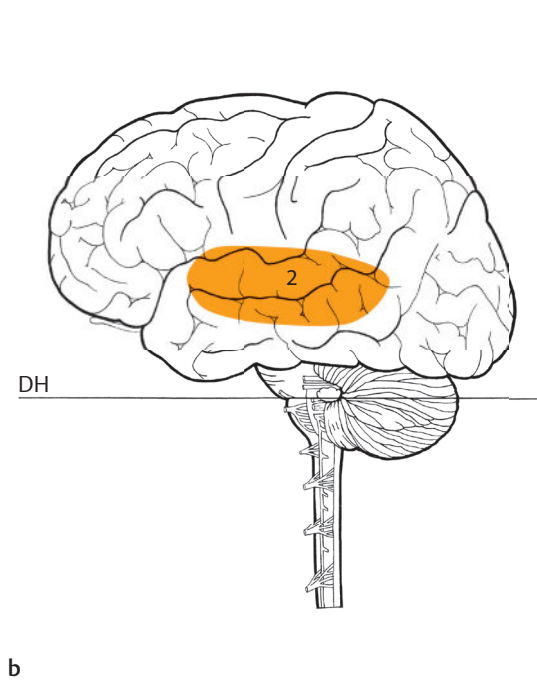


Fig. 10.45 Auditory system.

DH = German horizontal.

Fig. 10.45a 8th bicommissural section.

Fig. 10.45b Lateral view of the brain and the upper spinal cord.



- 1 Transverse temporal gyrus (Heschl) Superior temporal gyrus (STG) Middle temporal gyrus (MTG)
- 2 STG MTG

- 1 Supplementary motor area (SMA)
Primary motor cortex, medial parts
Somatosensory cortex, medial parts
- 2 Premotor cortex
Somatosensory cortex, lateral parts
- 3 Primary motor cortex, lateral parts
Premotor cortex, lateral parts
Somatosensory cortex, lateral parts
Parts of the superior parietal lobule (SPL)

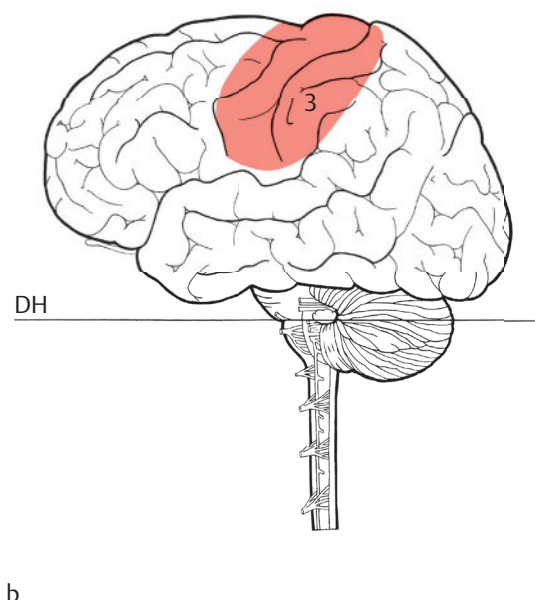


Fig. 10.46 Sensorimotor network.

DH = German horizontal.

Fig. 10.46a 12th bicommissural section.

Fig. 10.46b Lateral view of the brain and the upper spinal cord.

Functional imaging as well as lesion studies show that these functions are indeed strongly associated with the frontal lobe (see ► Fig. 10.47), although the frontal cortex should not be equated with the above. The frontal cortex is composed of Brodmann areas 8 to 12 and 44 to 47, areas 24 and 32 (see ► Fig. 7.53), as well as the frontal and cingulate regions.²⁰⁹

The posterior part of the frontal cortex consists of the motor, premotor, and supplementary motor regions; the anterior part of the frontal cortex is referred to as a prefrontal cortex and receives afferent signals mainly from the thalamus as well as from the brain stem.

Due to its rich reciprocal interconnections, the **prefrontal cortex** is a central relay station for higher cognitive functions.⁵⁸¹ Functionally the premotor cortex comprises of the dorsolateral and ventrolateral cortex (cognitive functions, DLPFC/VLPFC), orbitofrontal cortex (emotional, motivational and social behavior, OFC) as well as the dorsal and ventral frontomedial cortex (control and monitoring functions, DMPFC/VMPFC).

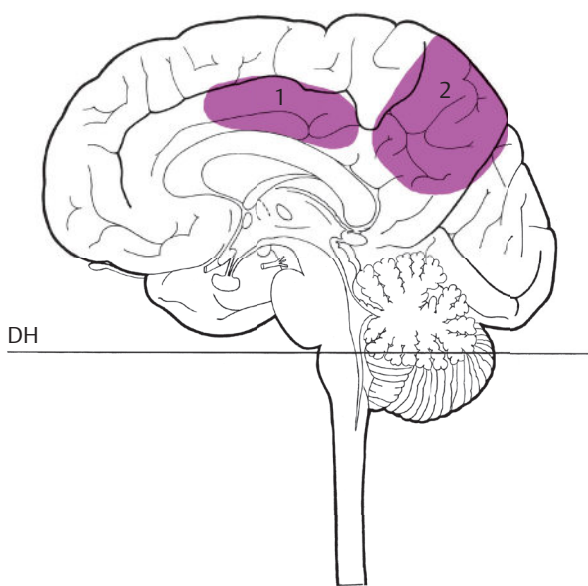
An intrinsic frontoparietal or **executive control network**, consisting of bilateral dorsolateral prefrontal cortex (DLPFC), inferoparietal cortex and intraparietal sulcus (IPC and IPS), praecuneus and middle cingulate cortex (MCC), modulates the activity of other networks

and participates in the building of a uniform level of consciousness by selection of important content while inhibiting what is unimportant.^{361,471,538,633}

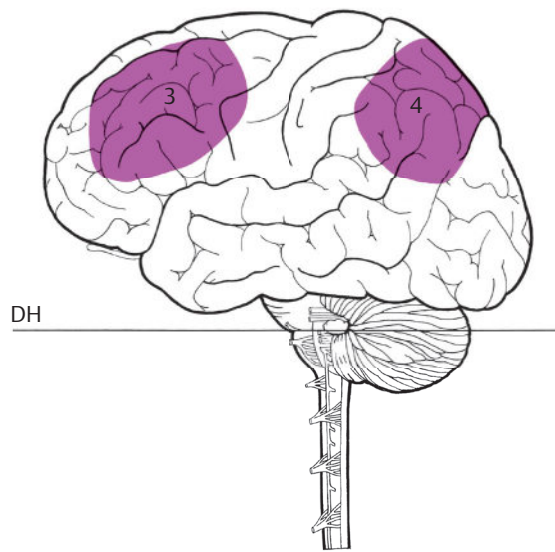
Attention

In addition to the frontoparietal network, the dorsal attention network can also be linked to the modulation of the activity of exteroceptive sensory regions within the framework of intrinsic network functions. This network includes the frontal eye fields (FEF), posterior parietal cortex, fusiform gyrus and area MT + (middle and superomedial temporal cortex) and is associated primarily with visual-spatial attention processes (see ► Fig. 10.48).^{361,538,633}

A network component known as the **ventral attention or salience network** (see ► Fig. 10.49; the term “salience” in psychology refers to any aspect of a stimulus that stands out due to its unusual properties, e.g., figure-ground contrast), arises because of continuous activation of medial frontal areas (anterior [ACC] and paracingulate cortex [pACC]), anterior insula and frontal operculum. These regions shape body-directed attention, which relies on representation of body status to direct attention and behavior.^{361,549}



a



b

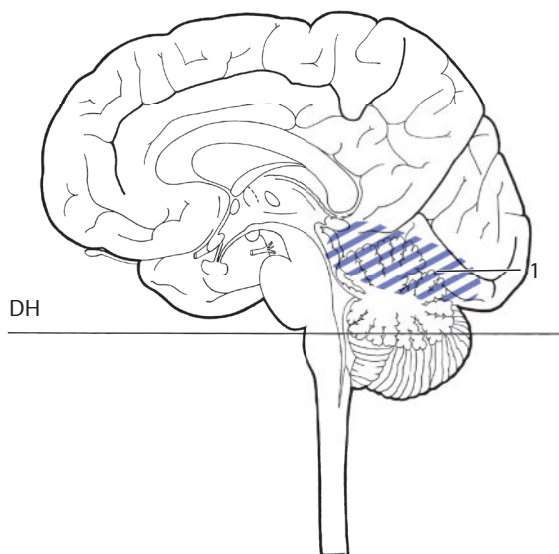
- 1 Cingulate cortex, midpart (MCC)
- 2 Precuneus
- 3 Dorsolateral prefrontal cortex (DLPFC)
- 4 Inferior parietal lobule/ intraparietal sulcus (IPL/IPS) and superior parietal lobule (SPL)

Fig. 10.47 Executive control network.

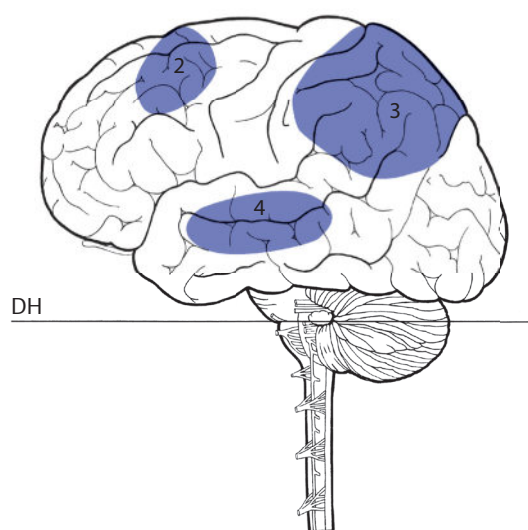
DH = German horizontal.

Fig. 10.47a Median view of the brain and the upper spinal cord.

Fig. 10.47b Lateral view of the brain and the upper spinal cord.



a



b

- 1 Area MT+, fusiform gyrus
- 2 Frontal eye field (FEF)
- 3 Posterior parietal cortex
- 4 Middle temporal gyrus (MTG), superior temporal gyrus (STG)

Fig. 10.48 Dorsal attention network.

DH = German horizontal.

Fig. 10.48a Median view of the brain and the upper spinal cord.

Fig. 10.48b Lateral view of the brain and the upper spinal cord.

- 1 Cingulate cortex, anterior part (= ACC)
Paracingulate cortex
- 2 Frontal operculum
- 3 Anterior insula

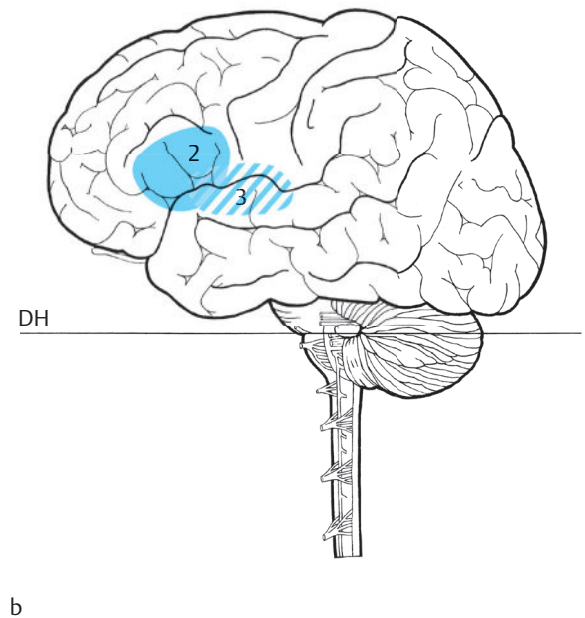
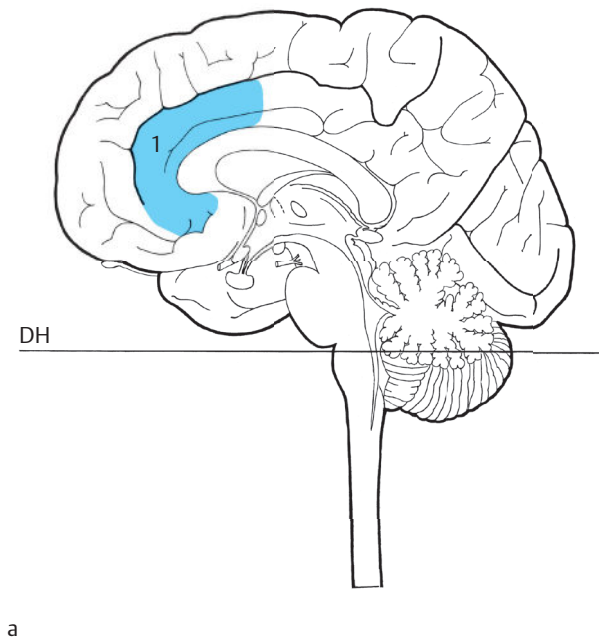


Fig. 10.49 Ventral attention network.

DH = German horizontal.

Fig. 10.49a Median view of the brain and the upper spinal cord.

Fig. 10.49b Lateral view of the brain and the upper spinal cord.

10.13.5 Mnestic, Affective, and Interoceptive Functions

Although the perception of basic attributes, such as space, color, movement, or form, is at first quite unaffected by personal experiences, mental activity is largely influenced by idiosyncratic/specific associations composed of exteroceptive, interoceptive and proprioceptive signals and renders these perceptions uniquely personal.

All components of unimodal and transmodal areas are involved in the learning of associations in their specific areas in the human brain. Perception of and adaptation to the environment are inseparably linked to a **personal evaluation** by the discerning individual due to spatial proximity and partial overlap of memory systems and affective networks. Attention processes play an important role thereby, providing an initial filter for behaviorally relevant information. Emotion, mood, and motivation also influence the way in which sensory impressions are processed. Neurofunctionally, these processes are closely associated with the function of the **hypothalamus, amygdaloid bodies, and paralimbic areas**.^{118,362} Behavioral contexts are quickly learned by the limbic system and stored as permanent memory content when of great significance. Using learned associations and their emotional–motivational content for behavioral adaptation in a changing environment requires reliable storage and contextually congruent retrieval. This occurs in a dynamic fashion by means of memory processes, which are intertwined and hierarchically organized. The more extensive and stable the

associations, the better they are consolidated over time and their retrieval is that much more efficient.^{24,391}

A well-known case which highlighted the relationship between ability to act, personality and affective function and proved paradigmatic for functional brain anatomy was that of Phineas Gage. This railway worker suffered severe lesions of the orbitofrontal and ventromedial prefrontal cortex, after an iron rod went through his skull following an explosion. He survived this serious injury for several years, but fell victim to extreme social decline due to a consequent **frontal lobe syndrome** resulting in dramatic alteration of his character.¹²⁰ The physician John D. Harlow examined P. Gage several times in the aftermath of the accident and found that basic functions, such as memory, intelligence, motor skills, perception and language ability remained unaffected, but P. Gage's behavior, contrary to his previous nature, was childish, impulsive and unreliable; a clearly circumscribed lesion was thus related to a **complex interplay of different functions** rather than a single mental function. Different functions influencing Gage's personality were thus affected, such as planning, self-awareness, affective (dys)regulation and social competence. This finding is not surprising, given the highly developed anatomical connections between the amygdaloid body and (orbito)frontal regions. Interruption of connections between these areas results in severe disorders during retrieval of emotional states, causing marked impairment of judgment, insight, and behavior.¹¹⁸

Similar deficits could also be observed in lesions in the ventromedial part of the prefrontal cortex. Bechara, Damasio, and coworkers⁴¹ allowed patients with lesions

in this area to play a card game where the best strategy ignored direct profits and favored later gains.

This rule was learned implicitly, that is, without conscious effort. Healthy control participants stated that their success strategy was mainly due to their “gut feeling.” Corresponding physiological responses (increased skin conductance) were demonstrable with anticipated poor card selection, but were lacking in patients. Patients were thus unable to achieve any success with learning over time as they lacked a critical brain area to integrate somatic information for behavioral control. This finding suggests that the neuronal processing of experiences or the encoding of the acquired **importance of sensory impressions** is processed in a network consisting of the ventromedial prefrontal cortex, the orbitofrontal cortex and the amygdaloid body. **Hierarchically structured memory functions** help retain newly learned content with its affective–motivational features.

10.13.6 Memory

In general, memory may be differentiated into **short-term** and **long-term memory**. The latter is further subdivided into explicit (or declarative) memory and implicit (or nondeclarative) memory:

- **Explicit memory** includes episodic memory, which represents our memory of experiences and specific events in time and space, and semantic memory, which is a more structured record of facts, meanings, concepts, and knowledge about the external world. Neuronal correlates of episodic memory are found in the hippocampus, medial temporal cortex, and in various neocortical areas such as the inferofrontal cortex. The anterior and lateral temporal cortex as well as the prefrontal cortex are associated with semantic memory (see ► Fig. 10.50).⁵⁵⁴
- **Implicit memory** includes procedural memory, priming and perceptual learning, classical conditioning, and non-associative learning. Procedural memory includes the learning of motor skills and habits and is accompanied by neuronal activation in the striatum, motor cortex and cerebellum. The amygdala and the cerebellum play a major role in classical conditioning, whereas priming (i.e., largely unconscious activation of special contents of implicit memory by appropriate stimuli) and perceptual learning occur in the neocortex. Non-associative learning is primarily concerned

with reflex pathways; higher cortical areas are not recruited thereby.³³

Due to the limited processing capacity of the brain, information must remain temporarily accessible to ensure sequential processing. This function is fulfilled by so-called **short-term memory**, in which contents can be retained for several seconds up to several minutes.^{25,391} The so-called **working memory** comprises of the phonological loop, the visual–spatial notepad and the central executive. Neuronal correlates of phonological working memory are predominantly left-hemispherical; more specifically in BA 40 and in Broca’s area (BA 6/44) (see ► Fig. 7.53). Visual–spatial working memory is associated primarily with right-hemispherical neuronal activation. The inferior parietal cortex (BA 40) also plays a role, as does the right premotor cortex (BA 6) and the inferior frontal cortex (BA 47). Numerous studies on visual–spatial working memory indicate the existence of a **dorsal pathway for object-related information** as well as a **ventral pathway for spatial information**.

Central executive memory, like other executive functions, is also strongly associated with (pre)frontal regions. Activation occurs in the dorsolateral prefrontal cortex bilaterally (BA 9/46), the inferofrontal cortex (BA 6/44), as also in the parietal cortex (BA 7/44). The intensity of activation correlates positively with task difficulty in these regions.^{24,471}

The amygdaloid body also plays a central role in the **consolidation of memory contents**.

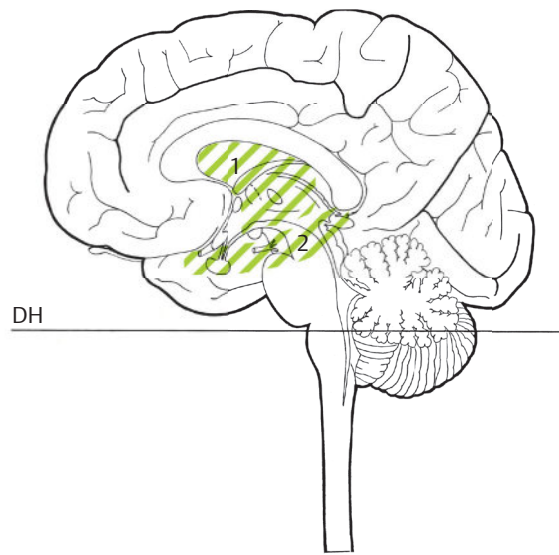
It has been shown that glucose metabolism of the amygdaloid bodies during the encoding of emotional stimuli in healthy brains could predict their retrieval up to a few weeks.^{97,218}

In a landmark study in 1995,⁹⁶ L. Cahill and coworkers showed that a patient with a selective lesion of the amygdala, in contrast to healthy individuals, did not show improved memory for emotional as against unemotional aspects of stories. In addition, the explicit retrieval of memories may be preserved while autonomous responses coupled with memory are erased with lesions of the amygdaloid body.⁴³ Comorbidities of emotional and memory disorders frequently seen in clinical practice (e.g., in the context of depression or dementia) may be explained by the close interplay and partial overlap between affective and memory systems.

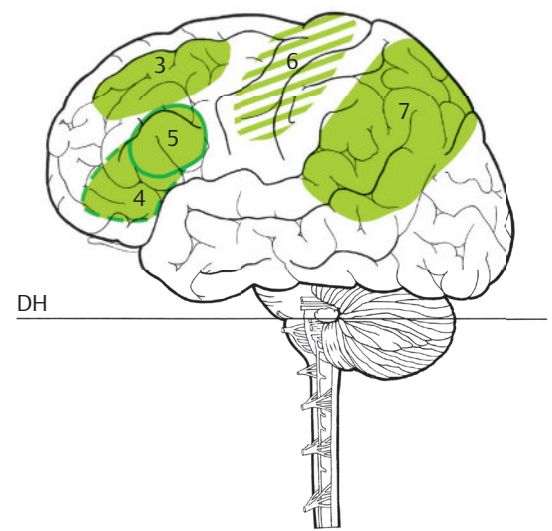
- 1 Striatum
- 2 Hippocampus
- 3 Parts of: dorsolateral prefrontal cortex (DLPFC)
- 4 Inferior frontal gyrus (IFG)
- 5 Broca's area (Part of IFG)

Parts of:

- 6 Premotor cortex
- Primary motor cortex
- Inferior parietal lobule (IPL) (only right)
- 7 Parietal cortex and temporoparietal junction (only left)



a



b

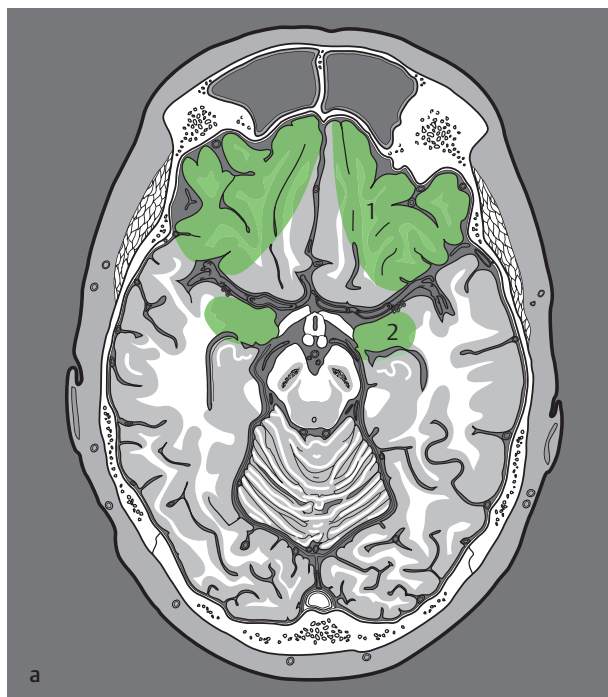
Fig. 10.50 Memory network.

DH = German horizontal.

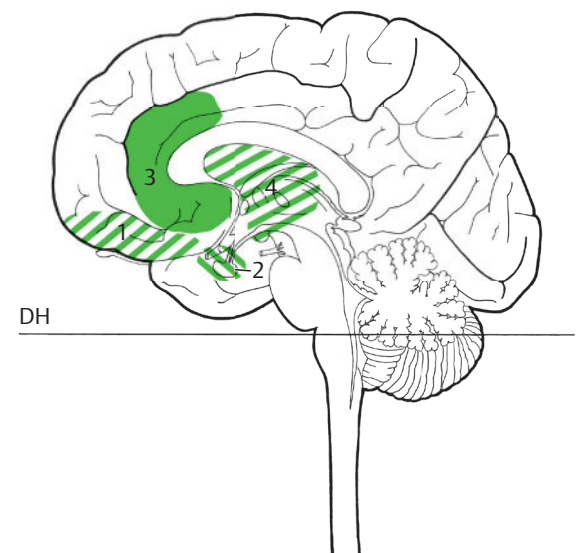
Fig. 10.50a Median view of the brain and the upper spinal cord.

Fig. 10.50b Lateral view of the brain and the upper spinal cord.

- 1 Medial: orbitofrontal cortex (OFC)
lateral: ventrolateral prefrontal cortex (VLPFC)
- 2 Amygdaloid bodies
- 3 Cingulate cortex, anterior part (ACC) with subgenual part (sACC), rostral part (rACC), perigenual part (pgACC)
- 4 Striatum



a



b

Fig. 10.51 Emotion network.

DH = German horizontal.

Fig. 10.51a 6th bicommissural section.

Fig. 10.51b Median view of the brain and the upper spinal cord.

10.13.7 Emotion

Limbic and neocortical regions are consistently involved in activation studies which examine emotional and/or motivational functions. Affective processing principally occurs in areas belonging to the limbic system (see Section 10.11), such as the amygdaloid body, insular cortex, prefrontal cortex (predominantly its dorsomedial and orbital–ventromedial parts), the anterior cingulate cortex (ACC), striatal regions, such as the globus pallidus, nucleus accumbens, and caudate nucleus, as well as the hypothalamus (see ► Fig. 10.51).^{118,348,362}

Some of these limbic structures predominantly responsible for generation of core affects (comfort or discomfort with different degrees of arousal [denotes the general degree of activation of the CNS, e.g., alertness, attention, responsiveness]) are also functionally connected under resting conditions. Motor components of the basal ganglia previously described in the context of motor systems (see Section 10.8) also belong to this network. For example, the activation of amygdaloid body, medial temporal lobe, temporal pole, subgenual anterior cingulum, striatum or lentiform nucleus, thalamus, and cerebellum was noted at rest.⁴⁰³

Reciprocal connections between the amygdaloid body and unimodal sensory association cortices in superior and inferior temporal areas allow selective modulation of sensory responses in accordance with the intrinsic salience of stimuli.⁴³⁴

The **amygdaloid body** thus appears to function as a neuronal junction providing a link between primary and secondary amplifiers and emotional and motivational valence.³⁹¹

However, the amygdaloid body also plays an important role in the processing of social emotional stimuli, especially the processing of facial expressions, which activates the amygdaloid bodies even outside of conscious perception.^{118,180,235,621} For example, selective amygdaloid body lesions lead to characteristic deficits in the processing of emotional, especially anxious facial expressions.^{5,635} The selective enhancement of processing capacity for stimuli with high emotional or hedonic salience (hedonism[Greek] = desire, joy) as well as the association between sensory impressions and emotional valence are the main pathways along which the amygdaloid bodies influence attention and memory processes.^{15,97,458,600} However, attention and control processes also influence the activation of the amygdaloid body: More attention can lead to greater,^{457,458} more cognitive control to reduced activation of the amygdaloid body.^{431,515,605}

Other regions that are primarily associated with the processing of primary and secondary enhancers are the ventral striatum (especially nucleus accumbens), the hypothalamus and the ventral pallidum.^{1,32,300,372} The processing of reward stimuli, especially their motivational significance, also leads to activation in the orbitofrontal cortex.^{317,492}

10.13.8 Interoception

Interoception is defined as the sensory perception of the physiological condition of the body.^{110,518} Interoceptive

processes are distinguished from exteroceptive, proprioceptive and nociceptive processes. In a physiological sense, interoception combines information from internal mechano and chemoreceptors as well as from afferent sensory signals of the vagus nerve. Some body signals that play a role in interoceptive processes are, for example, respiratory rate, salt, sugar, or hormone levels, temperature or vasodilatation. Afferent visceral and somatic information is transmitted to the hypothalamus and structures of the limbic system during interoceptive processes. Sensory information is relayed from the body to the cortex via a lamina-I spinothal-amocortical pathway. From the vagus nerve they are relayed via the spinal nucleus of the trigeminal nerve, the pontine nucleus of the trigeminal nerve and the solitary nucleus (see ► Fig. 6.2). Information carried by the vagus nerve is transmitted to cortical structures, especially to the insular cortex, to the (para)cingulate cortex (BA 24/32), to the posterior cingulum (BA 23/30/31), and to the basal medial precuneus (BA 7). These regions monitor visceral and autonomous homeostatic information as well as emotional and social stimuli, function as **interoceptive projection and association regions**, and integrate proprioceptive sensory perceptions with memory contents.¹¹¹

The close association of interoceptive and affective signals in neuronal stimulus processing is shown, for instance in the neuropsychobehavioral (based on the interplay of neuronal, psychological, and behavioral factors) effects of an experimental influence on physiological processes. The nasal administration of oxytocin, for example, influences the activation of limbic areas, such as the amygdaloid body^{39,144,145} and globus pallidus,⁶²⁷ depending on the valence (behaviorally relevant appraisal of a stimulus) and social salience, reduces stress and cortisol response in social situations,^{143,241,393} affects memory processes for emotional and attachment-related content^{34,242,485} and leads to higher investment in neuroeconomic trust games.^{39,304} As early as 1962, Schachter and Singer⁵¹³ postulated that similar patterns of physical excitement can not only be interpreted as rage, but also as joy, depending on the social and cognitive context. A **feeling of self** arises through the combination of the emotionally colored external sensory perceptions with internal body perceptions. In his theory of so-called **somatic markers**, Antonio Damasio expanded on Schachter and Singer's approach and described somatic markers as physiological responses (e.g., changes in the activity of the autonomic nervous system) that mark certain, previously emotionally significant events. Thus, somatic markers provide a signal for those current events or stimuli that have had emotional consequences in the past.^{120,121} Above all, Damasio regards the **ventromedial prefrontal cortex** as the region responsible for processing these somatic codes and enables the individual to make a decision even under uncertain conditions, based on emotional characteristics of stimuli. The processes that are subsumed under the concept of "somatic markers" thus specifically include the perception of one's bodily state.¹¹⁸

- 1 Medial prefrontal cortex (MPFC)
- 2 Cingulate cortex, posterior part (PCC)
Precuneus, retrosplenial cortex
- 3 Lateral prefrontal cortex
- 4 Lateral parietal cortex
- 5 Superior temporal sulcus (STS)
- 6 Hippocampus

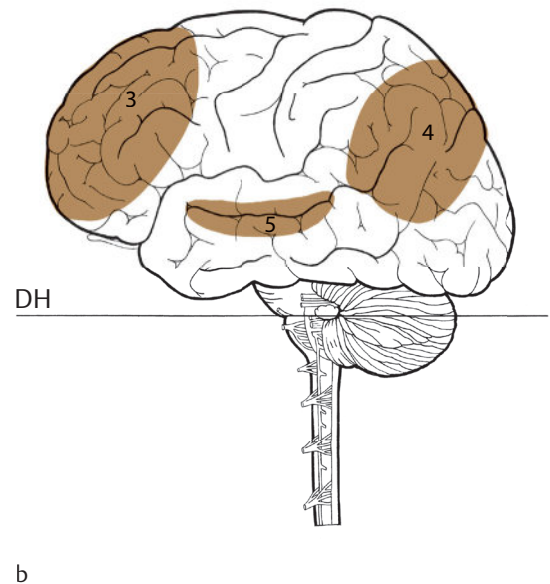
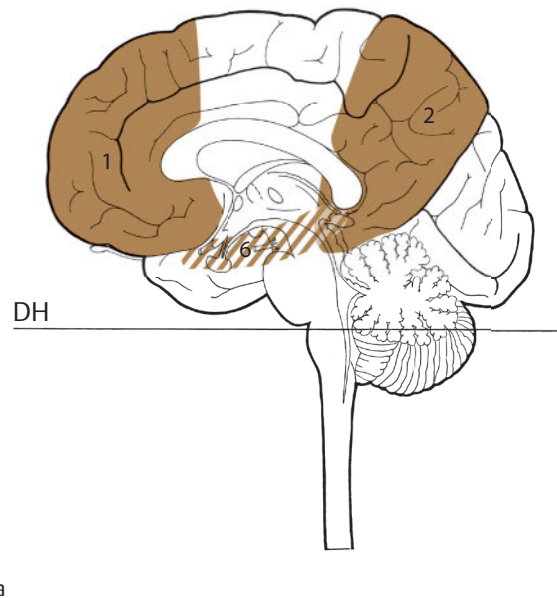


Fig. 10.52 Default mode network.

DH = German horizontal.

Fig. 10.52a Median view of the brain and the upper spinal cord.

Fig. 10.52b Lateral view of the brain and the upper spinal cord.

An overlap of emotional processing and interoceptive consciousness is notably observed in neuronal populations in the **insula**.^{114,643} Functions associated with the insular cortex, apart from interoceptive processes, include various other components involved in a contextually adapted “feeling of self,” such as awareness of body movements and emotions, recognition of one’s own image, vocalization and musical perception, perception of time or the monitoring of decisions and actions. This region is regarded as a convergence zone for the representation of body and emotion.¹¹² The **anterior cingulate cortex** is another convergence zone, which is associated with the integration of visceral, emotional, and attentional information due to the ascending projections of lamina-I neurons, and thus can regulate affects, decisions, and actions.^{118,591,592,596,597} Functionally, a **posterior “cognitive”** and an **anterior “emotional”** network of anterior insula and cingulate cortex as well as another network of posterior insula and primary and secondary motor (PMA, SMA) and somatosensory (S1, S2) cortices may be differentiated.^{89,131} The function of these networks is to monitor possible conflicts between the functional status of the organism and new information with potential emotional or motivational consequences. If conflicts are detected, they are forwarded to **prefrontal areas**, which in turn can adjust affective and behavioral responses through feedback projections.¹¹⁸

10.13.9 Default Mode Network

Intrinsic networks, which assume functions of core affect generation and body-directed attention, are, as

mentioned above, the limbic and the salience or ventral attention network, consisting of insular, opercular and medial parts of the frontal and temporal cortex.^{361,538,633} Although cortical midline structures have been associated with a variety of different tasks, they also represent a substantial part of those structures which, due to their higher activation at rest belong to the so-called default mode network.

The default mode network is the most frequently studied resting network and refers to those brain regions which exhibit activity while a person is awake and at rest.^{83,207} The medial prefrontal cortex (MPFC), retrosplenial cortex, posterior cingulate cortex (PCC) or precuneus, structures of the medial temporal lobe (e.g., the hippocampus) as well as bilateral superior temporal sulci (STS) and the angular gyrus (see ► Fig. 10.52) all belong to the default mode network. What is common to these brain regions is that they are involved in various conceptualization processes. These range from object perception and complex linguistic functions through autobiographical memories to the experience of emotions.³⁶¹ Interconnections exist within anatomically defined regions, which are primarily activated when strictly internal processes occur, for example, during day dreaming, during recall of memories or when a person empathizes with another. A key feature of the default mode network is that the participating regions correlate negatively with other areas that are responsible for processing external visual stimuli.²⁰⁷ The default mode network may also be depicted by contrasting resting and activation phases within an activation paradigm.⁴²⁸

11 Neurotransmitters and Neuromodulators

Neurotransmitters convey signals at the synapses between neurons or between neurons and effector organs (muscle cells, glandular cells). **Neuromodulators** **presynaptically** influence the amount of neurotransmitter being liberated or its reuptake into nerve cells. **Neuromodulators** also regulate the sensitivity of transmitter receptors **postsynaptically**. A transmitter receptor is a protein in the cell membrane of a nerve or glial cell; one end of the receptor lies in the extracellular space and the other in the intracellular space. Neuro-modulators thereby regulate the degree of excitability at the synapses and alter the effect of neurotransmitters. Neuronal information processing at the synapses is thus more complex due to different regulatory mechanisms than was previously assumed. Neurotransmitters and neuromodulators are grouped together as **neuroactive substances**.

Several neurons contain more than one neuroactive substance.^{252,370} Nerve cells containing more than one neurotransmitter release only one transmitter on stimulation. A single neurotransmitter, acetylcholine, for instance, may have either excitatory or inhibitory effects depending on transmitter receptors of postsynaptic neurons. Dopamine has been proven to function both as a neurotransmitter and a neuromodulator.⁴²² These diverse effects of transmitters indicate their manifold functions in the central nervous system. Several neuroactive substances are usually involved within a neurofunctional system; as a corollary, one neuroactive substance generally influences several neurofunctional systems. This may be illustrated, for example, by different sites of action of dopaminergic neuronal groups. Nigrostriatal neurons target the motor system of the basal ganglia (see ►Section 10.8.2), mesolimbic neurons target the limbic system (see ►Section 10.11), tubero-infundibular neurons target the hypothalamo-hypophysial system, and a small group of neurons (A15) target the olfactory system. These neuronal groups are only parts of different neurofunctional systems. This knowledge is important for interpretation of pharmacologic actions and side effects.

Nieuwenhuys⁴²² provided an interesting overview of the chemo-architecture of the brain. He suggested three new terms that describe the topical arrangement of some of the neuronal groups referred to in the following chapters:

- The so-called **core** is a periventricular area in the brainstem and forebrain, the nerve cells of which are rich in neuromodulators. Paracrine release of the active substance occurs from these nerve cells, delivering the active substance via the intercellular space to their neighboring cells (i.e., not via synapses).

A functional connection most likely exists with circumventricular organs which do not possess a blood–brain

barrier and, therefore, seem to be especially well-suited for neuroendocrinal regulation. The following areas belong to the core: posterior (dorsal) nucleus of the vagus nerve (see ►Fig. 6.5b), the superficial zone of the spinal nucleus of the trigeminal nerve (see ►Fig. 6.4b and ►Fig. 6.5b), parabrachial nuclei, central periaqueductal gray substance (see ►Fig. 3.10a and ►Fig. 6.12c), small periventricular nuclei of the hypothalamus, septal nuclei (see ►Fig. 10.39 and ►Fig. 10.42b), and parts of the limbic system (see ►Section 10.11).

- The **median paracore** lies adjacent to the core in the center of the tegmentum of the brainstem and consists of a series of raphe nuclei containing, among others, serotonergic nerve cells (see ►Section 11.2).
- The **lateral paracore** lies adjacent to the core in the anterolateral part of the tegmentum of the brainstem and contains catecholaminergic (see below) and some cholinergic neurons (see ►Section 11.4).

11.1 Catecholaminergic Neurons

Cell bodies and cell processes of catecholaminergic neurons contain transmitters dopamine, noradrenaline, and adrenaline. These molecules are derived from the amino acid tyrosine. Dihydroxybenzyl is produced during the biosynthesis of these transmitters, and is a central catechol moiety, forming catecholamines together with a side chain and an amino group. Dopamine, noradrenaline, and adrenaline are relatively small molecules and consequently diffuse out of nerve cells and their axons soon after death. Thus conventional histologic techniques cannot be reliably used to map sites of production and storage of these compounds.

Dopaminergic, noradrenergic, and adrenergic neurons were identified by freezing living nerve cells in vivo, drying them and visualizing them on fluorescence microscopy.

Green fluorescence of dopamine and noradrenaline¹⁶⁰ was demonstrated using histochemical methods in 1962. Today, highly sensitive immunofluorescent methods enable a more accurate detection of catecholaminergic neurons. **Noradrenergic and dopaminergic** neurons were labelled A1 to A15 and **adrenergic** nerve cells C1 to C3. An ascending numbering sequence was selected for the brainstem, that is, from inferior to superior.

The localization of catecholaminergic neurons is the subject of research even today. Data obtained thus far from rats and lower primate brains must be extrapolated to the human brain.

Dopaminergic, noradrenergic, and adrenergic nerve cell groups, however, correspond closely in the adult human brain with neuromelanin-containing neurons,^{61,509} which provide the first line of information

about catecholamine-containing cell populations in neuropathological specimens. The nigrostriatal dopaminergic system is of interest in Parkinson's disease and its therapy.

11.1.1 Dopaminergic Neurons

Dopamine-synthesizing nerve cells are found in the midbrain, diencephalon, and telencephalon. The largest and most striking group of dopaminergic nerve cells is the **pars compacta of the substantia nigra** (A9; see ►Fig. 3.9a, ►Fig. 4.3a, ►Fig. 5.7, ►Fig. 6.12b, ►Fig. 6.13b, ►Fig. 7.45, and ►Fig. 10.24). Their axons form an ascending pathway that runs through the lateral part of the hypothalamus and traverses the internal capsule. The nigrostriatal fibers then run to the striatum (caudate nucleus, see ►Fig. 3.6a, ►Fig. 3.6b, ►Fig. 3.8a, ►Fig. 3.8b, ►Fig. 3.10a, ►Fig. 3.10b, ►Fig. 4.3a, ►Fig. 4.3b, ►Fig. 4.4a, ►Fig. 4.4b, ►Fig. 4.5a, ►Fig. 4.5b, ►Fig. 5.9a, ►Fig. 5.9b, and ►Fig. 5.24 and Putamen, see ►Fig. 3.7a, ►Fig. 3.7b, ►Fig. 3.9a, ►Fig. 3.9b, ►Fig. 4.4a, ►Fig. 4.4b, ►Fig. 4.5a, ►Fig. 4.5b, ►Fig. 5.8, and ►Fig. 5.23). The A9 nerve cell group forms the nigrostriatal system together with a small group of A8 nerve cells from the reticular formation of the midbrain. The substantia nigra belongs to the basal ganglia in keeping with its synaptic connections (see ►Section 10.8.2).

A second dopaminergic nerve cell group runs from the A10 cell group in the midbrain to parts of the limbic system and is therefore termed "mesolimbic". Drugs affecting this system are believed to produce psychic effects.³⁷³ The A10 group lies in the form of an anterior "cap" over the interpeduncular nucleus in the tegmentum of the midbrain. The axons run in the medial forebrain bundle to the following structures of the limbic system (see ►Fig. 10.39):

- Inner nucleus of the stria terminalis
- Olfactory tubercle
- Nucleus accumbens,
- Septal nuclei
- Several parts of the frontal, cingulate, and entorhinal cortex

Certain substances such as opiates, cocaine, and alcohol are perceived as a reward by the mesolimbic system and may therefore trigger the "reward mechanism". This mechanism may therefore be regarded as the neurobiological basis for drug addiction.

A third dopaminergic system, termed **tuberoinfundibular**, lies in the diencephalon. The A12 cell group lies in the tuber cinereum (see ►Fig. 4.2d) and projects to the infundibulum (see ►Fig. 3.1c, ►Fig. 4.2a, ►Fig. 4.2b, ►Fig. 5.1c, ►Fig. 5.6a, ►Fig. 5.6b, ►Fig. 5.21, ►Fig. 6.3, and ►Fig. 6.11b). This system is believed to have a neuroendocrine function. The other diencephalic nerve cell groups A11, A13, and A14 and their target cells are also located in the hypothalamus.

A small group A15 lies scattered within the olfactory bulb (see ►Fig. 3.1c, ►Fig. 3.3a, ►Fig. 3.3b, ►Fig. 5.1c,

►Fig. 5.1d, ►Fig. 5.6a, and ►Fig. 6.11a) and is the only telencephalic dopaminergic group of neurons.

Clinical Notes

Dopamine deficiency, especially in the substantia nigra, is of clinical significance since therapeutic substitution is used in the treatment of Parkinson's syndrome (see ►Section 10.8.2).

Dopamine and its agonist bromocriptine function as adenylohypophysiotropic prolactin-inhibiting factors. This explains the clinical use of bromocriptine for the conservative treatment of prolactinomas, in addition to its use in the treatment of Parkinson's disease.

11.1.2 Noradrenergic Neurons

Noradrenergic nerve cells are found only in a narrow anterolateral zone of the tegmentum of the medulla oblongata and pons. Although the A1 to A7 cell groups were originally described in rats,^{116,117} a similar arrangement has been seen in primates.^{163,188,261,262,373,427} The fibers leaving these groups of nerve cells either ascend toward the midbrain or descend toward the spinal region. Noradrenergic cells are also connected with the cerebellum. Noradrenergic fibers branch more widely than dopaminergic ones. Notable is the proximity of noradrenergic fibers to cerebral arterioles and capillaries and these fibers are believed to play a role in the regulation of cerebral blood flow.^{228,477}

The largest noradrenergic cell group A6 lies in the **cerulean nucleus** and contains almost half of all noradrenergic cells.⁵⁶⁷ The cerulean nucleus in adults contains neuromelanin-containing nerve cells that form a dark-blue, 1-cm-long strip (see ►Fig. 5.6a, ►Fig. 5.6b, ►Fig. 5.7, ►Fig. 6.10b, ►Fig. 6.11b, and ►Fig. 6.12b) in the pontine region on the floor of the IVth ventricle, ending below the inferior colliculi (see ►Fig. 6.12b). The posterior noradrenergic bundle originates from the A6 nerve cell group. Running through the tegmentum of the midbrain anterolateral to the central periaqueductal gray substance, it enters the hypothalamus, passes to the septal nuclei and then runs in the cingulum. On this course noradrenergic fibers are connected with the following structures:

- In the **midbrain** to the posterior raphe nucleus and to the inferior and superior colliculi (see ►Fig. 3.1c, ►Fig. 4.2a, ►Fig. 4.2b, ►Fig. 6.12b, and ►Fig. 6.13b)
- To the anterior nuclei of thalamus and the medial and lateral geniculate bodies in the **diencephalon** (see ►Fig. 3.10, ►Fig. 3.10b, ►Fig. 4.4a, ►Fig. 4.4b, and ►Fig. 5.8)
- In the **telencephalon** with the amygdaloid body (see ►Fig. 3.8a, ►Fig. 3.8b, ►Fig. 4.5a, ►Fig. 4.5b, ►Fig. 5.6a, ►Fig. 5.6b, and ►Fig. 5.21), hippocampal formation (see ►Fig. 3.8a, ►Fig. 3.8b, ►Fig. 3.9a, ►Fig. 3.9b, ►Fig. 3.11a, ►Fig. 3.11b, ►Fig. 4.5a, ►Fig. 4.5b, ►Fig. 5.6a, ►Fig. 5.6b, and ►Fig. 5.24), the cingulate, retrosplenial, and entorhinal cortex, as well as the entire neocortex

Additional efferent fibers from the A6 cell group run to the cerebellum through the superior cerebellar peduncle (see ► Fig. 5.6a, ► Fig. 5.6b, ► Fig. 6.1, ► Fig. 6.10b, ► Fig. 6.10c, ► Fig. 6.11b, ► Fig. 7.55, ► Fig. 10.36a, and ► Fig. 10.36b). Descending fibers from the cerulean nucleus are joined by fibers from the neighboring A7 cell group, and supply the posterior (dorsal) nucleus of the vagus nerve (see ► Fig. 6.2, ► Fig. 6.5b, and ► Fig. 6.6b), the inferior olivary nucleus (see ► Fig. 3.10a, ► Fig. 3.10b, ► Fig. 6.5b, ► Fig. 6.6b, ► Fig. 6.7b, and ► Fig. 6.7c), and the spinal cord. The anterolateral ceruleospinal tract gives off noradrenergic fibers to the ventral and dorsal gray horn in the spinal cord.⁴³⁰ Taken together, the few noradrenergic cells of the cerulean nucleus project widely, reaching regions of the brainstem, forebrain, cerebellum, and the spinal cord.

A1 and A2 nerve cell groups lie in the medulla oblongata and form the anterior ascending noradrenergic neurons together with the pontine cell groups A5 and A7. In the midbrain they project into the periaqueductal gray substance (see ► Fig. 3.10a) and into the reticular formation, in the diencephalon into the entire hypothalamus (see ► Fig. 5.7, ► Fig. 5.8, ► Fig. 6.3, ► Fig. 6.12b, and ► Fig. 6.13b) and in the telencephalon into the olfactory bulb. Bulbosplinal fibers also run into the spinal cord from these cell groups (A1, A2, A5, and A7).

11.1.3 Adrenergic Neurons

Adrenaline-synthesizing nerve cells are found only in the medulla oblongata in a small anterolateral area (lateral paracore⁴²²). The largest cell group C1 lies posterior to the inferior olivary nucleus (see ► Fig. 3.10, ► Fig. 5.3, ► Fig. 6.5b, ► Fig. 6.6b, and ► Fig. 6.7b), while the middle cell group C2 lies near the solitary nucleus (see ► Fig. 6.2, ► Fig. 6.5b, and ► Fig. 6.6b) and the cell group C3 immediately beneath the periventricular gray. The C1 to C3 efferents run to the posterior (dorsal) nucleus of the vagus nerve, the solitary nucleus, cerulean nucleus, the periventricular gray of the pons, the periaqueductal gray substance of the midbrain, the hypothalamus and to the paraventricular nucleus. Physiological experiments^{124,200} have shown that the cell group C1 is a highly sensitive vasopressor center.

11.2 Serotonergic Neurons

The serotonergic nerve cells were discovered by fluorescence microscopy simultaneously with catecholaminergic nerve cells and exhibit **yellow fluorescence**.¹⁶⁰ Serotonin is derived from the amino acid tryptophan.

The serotonergic nerve cells B1 to B9 are found in the medulla oblongata, pons, and midbrain (in accordance with nomenclature^{116,117}). Most of these cell groups lie in the median zone of the brainstem (fusion zone = raphe) and, therefore, are called **raphe nuclei**. B1 raphe nuclei (nucleus raphes pallidus) and B2 (nucleus raphes obscurus) lie in the medulla oblongata, B3 (nucleus raphes magnus) in the border zone between

the medulla oblongata and pons, B5 (nucleus raphes pontis) in the pons, and B7 (nucleus raphes posterior) in the midbrain. Cell groups B6 and B8 (nucleus centralis superior of Bechterew) are found in the tegmentum of the pons and midbrain. Nerve cells containing other neurotransmitters such as dopamine, noradrenaline, GABA, enkephalin, and substance P are also present in the raphe nuclei; substance P has also been demonstrated in serotonergic nerve cells. Thus raphe nuclei are also called **multiple transmitter centers**.

The projections of the serotonergic nerve cells ascend and descend in a similar fashion as noradrenergic fibers and mainly project to the **limbic system** as well as to the reticular formation and the spinal cord; a close association exists with the cerulean nucleus, the largest center of noradrenergic nerve cells.

The large anterior ascending tract arises from the cell groups B6, B8, and B7. It runs anteriorly through the tegmentum of the midbrain and laterally through the hypothalamus, then dividing into the fiber tracts of the fornix and the cingulum. Along this route, cell groups B6, B8, and B7 are synaptically connected with the following:

- Interpeduncular nucleus and substantia nigra (see ► Fig. 3.9a, ► Fig. 4.3a, ► Fig. 5.7, ► Fig. 6.12b, and ► Fig. 6.13b) in the **midbrain**
- Habenular nuclei (see ► Fig. 5.9a, ► Fig. 5.9b, and ► Fig. 10.39), subnuclei of the thalamus, and nuclei of the hypothalamus in the **diencephalon**
- Septal nuclei (see ► Fig. 10.40a and ► Fig. 10.42b) and the olfactory bulb (see ► Fig. 3.1c, ► Fig. 3.3a, ► Fig. 3.3b, ► Fig. 4.2, ► Fig. 5.1, ► Fig. 5.6a, and ► Fig. 6.11a) in the **telencephalon**

Numerous projections also exist in other limbic areas, including the hippocampus (see ► Fig. 3.8a, ► Fig. 3.8b, ► Fig. 3.9a, ► Fig. 3.9b, ► Fig. 3.11a, ► Fig. 3.11b, ► Fig. 4.5a, ► Fig. 4.5b, ► Fig. 5.7, and ► Fig. 5.23), subiculum, cingulate, and entorhinal cortex, in addition to connections to the striatum and the frontal neocortex. The shorter posterior ascending tract connects the cell groups B3, B5, and B7 through the posterior longitudinal fasciculus (of Schütz) with the periaqueductal gray substance and the posterior hypothalamic area. Serotonergic projections also exist in the cerebellum (from B6 and B7) and in the spinal cord (from B1 to B3) as well as numerous fiber connections to the reticular formation.

Ascending serotonergic fibers are possibly involved in the regulation of sleep. An inhibitory effect of the descending serotonergic fibers on the first sympathetic neuron in the spinal cord has been demonstrated physiologically. Raphe neurons in the medulla oblongata are also believed to control the conduction of pain in the anterolateral system.⁴²²

11.3 Histaminergic Neurons

Histaminergic nerve cells lie in the inferior part of the hypothalamus close to the infundibulum and form histamine from the amino acid histidine by means of

histidine decarboxylase. Neurochemical, neurophysiological, and neuropharmacological findings have identified histamine as a neurotransmitter. Antibodies against histidine decarboxylase have been used in immunocytochemistry studies to localize histaminergic nerve cells.

Short and long branching fibers from the histaminergic nerve cells in the inferior part of the **hypothalamus** run to the:

- **Diencephalon**, to the posterior, lateral, and anterior parts of the hypothalamus. The mammillary body (see ► Fig. 3.1c, ► Fig. 3.8a, ► Fig. 3.8b, ► Fig. 4.2a, ► Fig. 4.2b, ► Fig. 5.1c, ► Fig. 6.3, ► Fig. 6.12b, and ► Fig. 6.12c) is rich in histaminergic fibers. Histaminergic fibers in the thalamus branch into the periventricular nuclei and the lateral geniculate body.
- **Telencephalon**, to the diagonal band of Broca, nucleus accumbens, amygdaloid body (see ► Fig. 3.8a, ► Fig. 3.8b, ► Fig. 4.5a, ► Fig. 4.5b, ► Fig. 5.6a, ► Fig. 5.6b, and ► Fig. 5.21), and the cerebral cortex.
- **Brainstem**, within its posterior and periventricular zone. Histaminergic fibers reach the periaqueductal gray substance, nucleus raphe posterior, medial vestibular nucleus, solitary nucleus (see ► Fig. 6.2, ► Fig. 6.5b, and ► Fig. 6.6b), posterior nucleus of vagus nerve (see ► Fig. 6.2, ► Fig. 6.5b, and ► Fig. 6.6b), facial nucleus (see ► Fig. 6.2, ► Fig. 6.8b, and ► Fig. 6.9b), anterior and posterior cochlear nuclei (see ► Fig. 6.2a, ► Fig. 6.7b, and ► Fig. 10.14), lateral lemniscus (see ► Fig. 6.9b, ► Fig. 6.10b, ► Fig. 6.11b, and ► Fig. 6.12b), and the inferior colliculus (see ► Fig. 3.1c, ► Fig. 4.2a, ► Fig. 4.2b, ► Fig. 5.23, and ► Fig. 6.12b). These results were obtained from rat brains.⁶⁰⁷

11.4 Cholinergic Neurons

Acetylcholine has been known as a neurotransmitter since 1914. The first evidence of cholinergic cell bodies was obtained with the help of acetylcholinesterase, but the results were unreliable. It is only during the last 20 years that it has been possible to accurately identify cholinergic nerve cells with immunohistochemistry by using antibodies against choline acetyltransferase. The **alpha (α) and gamma (γ)-motor neurons** of the IIIrd, IVth, Vth, VIth, VIIth, IXth, Xth, XIth, and XIIth cranial nerves (see ► Fig. 6.2) and of the spinal nerves are cholinergic. Their axons form the common terminal ends of the motor systems (see ► Section 10.8 and ► Section 10.13.3) and contained acetylcholine within them influences contraction of skeletal muscles.⁶⁵¹ The preganglionic neurons of the autonomic system are cholinergic and stimulate the postganglionic neurons of this system (see ► Section 10.12).⁶⁵¹ Other cholinergic nerve cells have been assigned alphanumerical identifiers from superior to inferior (in contrast to catecholaminergic and the serotonergic cell groups): The cholinergic neurons Ch1 form about 10% of the cells of the medial septal nucleus, while Ch2 neurons form 70% of the cells of the vertical limb of the diagonal band (of Broca), and Ch3 neurons 1% of the cells of the horizontal limb of the diagonal band

of Broca. All three groups of neurons project downward into the medial habenular nucleus and the interpeduncular nucleus. Ch1 neurons are connected through ascending fibers via the fornix with the hippocampus, as described in the limbic system (see ► Section 10.11). The cell group Ch3 synapses with nerve cells of the olfactory bulb (see ► Fig. 3.1c, ► Fig. 3.3a, ► Fig. 3.3b, ► Fig. 5.1c, ► Fig. 5.1d, ► Fig. 5.6a, and ► Fig. 6.11a).

The cell group Ch4 is relatively large in the human brain and corresponds to the **nucleus basalis of Meynert** (see ► Fig. 3.8a), lying in the innominate substance inferior to the globus pallidus (see ► Fig. 3.8a). About 90% of all cells of this nucleus are cholinergic. This nucleus receives afferent input from the subcortical diencephalic or telencephalic regions and from the limbic-paralimbic cerebral cortex. The anterior cells of the nucleus basalis project their efferent signals to the frontal and parietal neocortex, while posterior cells project to the occipital and temporal neocortex. This nucleus is, therefore, a relay station between the limbic-paralimbic regions and the neocortex. These findings are of interest since patients with senile **dementia as in Alzheimer's disease** show evidence of reduced choline acetyltransferase in basal nuclei with marked neuronal degeneration.^{615,626} It is yet however unclear whether this degeneration is primary or secondary following the loss of neocortical nerve cells.³⁹² In younger patients suffering from Alzheimer's disease an even greater loss of cells in the **cerulean nucleus** (A6) has been observed than in the basal nucleus.³⁸²

Two small cholinergic cell groups Ch5 and Ch6 lie in the pons and are regarded as part of the ascending reticular system.⁴²²

A small group of cells (**periolivary nucleus**) consisting partly of cholinergic cells lies at the edge of the trapezoid body in the lower part of the pons. Its efferent fibers run to the sensory receptors of the auditory system (see ► Section 10.5). This cholinergic subsystem influences the transfer of auditory signals.

11.5 GABAergic Neurons

GABAergic neurons contain the amino acid GABA, which functions as a neurotransmitter. It is derived biochemically from glutamic acid by the action of the enzyme glutamic acid decarboxylase and may be detected immunohistochemically with antibodies against this enzyme. GABA is the most important **inhibitory neurotransmitter** in the central nervous system.⁶⁵¹

It is found in the spinal cord in interneurons which inhibit afferent systems pre- and postsynaptically. Individual hypothalamo-cortical connections are GABAergic. Locally interconnected GABAergic nerve cells are found in the olfactory system and in the limbic system (basket cells of the hippocampus). The following efferents of the motor system of the basal ganglia contain GABA:

- Striatonigral tracts
- Pallidonigral tracts
- Subthalamopallidal tracts

Purkinje cells of the cerebellum contain GABA (see ► Fig. 10.36b); their efferents end in the cerebellar nuclei and in the lateral vestibular nucleus. Intracortical GABAergic nerve cells of the cerebellar cortex include Golgi, stellate, and basket cells.

11.6 Glutamatergic and Aspartatergic Neurons

Glutamate and aspartate, both similar amino acids, have been classified electrophysiologically as **excitatory neurotransmitters** and are usually identified together by immunohistochemical and autoradiographic means. They have thus been grouped together in this overview. Nerve cells with glutamate and/or aspartate transmitters have been identified in the auditory system. These neurons probably represent first-order neurons of the auditory system (see ► Fig. 10.14). Neurons with glutamate and aspartate transmitters in the olfactory system are nerve cells which connect the olfactory bulb with the prepiriform cortex. In the limbic system the axons of the glutamate- or aspartate-containing pyramidal cells of the hippocampus run to the septal nuclei. Pyramidal cells of the neocortex contain glutamate. Glutamate has also been detected in the following pathways which arise from pyramidal cells: corticostriatal, corticothalamic, corticotectal, corticopontine, and corticospinal tracts.⁴²²

11.7 Peptidergic Neurons

Peptidergic neurons include:

- Hypothalamo-neurohypophysial nerve cells with the peptides oxytocin and vasopressin (see Section 7.7.4)
- Nerve cells with hypophysiotropic peptides such as somatostatin, corticoliberin, thyroliberin, and luteinizing hormone-releasing hormone (see Section 7.7.4)
- Nerve cells with “gut-brain” peptides, such as substance P, vasoactive intestinal polypeptide (VIP), and cholecystokinin
- Nerve cells, the peptides of which are derived from pro-opiomelanocortin, such as corticotropin and β -endorphin
- Enkephalinergic nerve cells

The neurotransmitter and/or neuromodulator function of many peptides is still disputed.⁴²² Only a few substances have therefore been discussed as examples.

11.7.1 Substance P

The chemical structure of substance P, detected almost 45 years ago, was found to be a peptide composed of 11 amino acids. Soon after its discovery the slow in onset but long-lasting **excitatory effects** of substance P on neurons were demonstrated.

About one-fifth of nerve cells in the **spinal ganglia** and the **trigeminal (Gasserian) ganglion** (see ► Fig. 3.7a, ► Fig. 3.7b, ► Fig. 4.4a, ► Fig. 4.4b, ► Fig. 6.8b, and ► Fig. 10.6) are composed of nerve cells which contain

substance P; these cells are small with none or very thin myelin sheaths and probably conduct pain signals.

Brush cells in the **olfactory bulb** have been shown to contain substance P. Numerous nerve cells containing this neurotransmitter are present in the brainstem, especially in the periventricular gray substance. Efferent connections run into the spinal cord from three centers: nucleus raphe magnus, periaqueductal gray substance (see ► Fig. 3.10a), and accessory oculomotor nucleus (of Edinger-Westphal) (see ► Fig. 6.2 and ► Fig. 10.43a).

Substance P-containing neurons of the habenular nuclei run from the diencephalon to the interpeduncular nucleus. The striatum possesses substance P-containing nigrostriatal fibers which are assumed to be part of the motor system of the basal ganglia. Furthermore, substance P has been detected within small cells in certain parts of the baboon's neocortex, predominantly in layers V and VI.

11.7.2 Vasoactive Intestinal Polypeptide

Vasoactive intestinal polypeptide (VIP) is a peptide composed of 28 amino acids. It brings about marked dilatation of blood vessels in the gastrointestinal tract and stimulates the transformation of glycogen into glucose, while it is believed to be an **excitatory neurotransmitter** and/or a neuromodulator in the nervous system.⁴²² In the brainstem, VIP-containing nerve cells are present in the solitary nucleus (see ► Fig. 6.2, ► Fig. 6.5b, and ► Fig. 6.6b) and are locally interconnected in this nuclear area. The **periaqueductal gray substance** (see ► Fig. 3.10a) contains VIP-containing neurons which ascend to the hypothalamus, the interstitial nucleus of the stria terminalis, and the amygdaloid body (see ► Fig. 3.8a, ► Fig. 3.8b, ► Fig. 4.5a, ► Fig. 4.5b, ► Fig. 5.6a, ► Fig. 5.6b, and ► Fig. 5.21) and are thereby connected with the limbic system. Several VIP-containing nerve cells are present in the suprachiasmatic nucleus and are connected with hypothalamic nuclei; these are probably involved in regulating circadian rhythms. The highest concentration of VIP is found in the **neocortex**, mostly in bipolar cells which exhibit intracortical connections. VIP possibly regulates energy metabolism of the neocortex.

11.7.3 β -Endorphin

β -Endorphin is a peptide composed of 31 amino acids and functions as an **inhibitory** neuromodulator in the brain. Endorphinergic cell bodies are found in the mediobasal hypothalamus and in the inferior part of the solitary nucleus in the medulla oblongata (see ► Fig. 6.2 and ► Fig. 6.5b). Ascending efferents of hypothalamic endorphinergic nerve cells run to the paraventricular nucleus, preoptic area, septal nuclei (see ► Fig. 7.45), and parts of the amygdaloid body (see ► Fig. 3.8a, ► Fig. 3.8b, ► Fig. 4.5a, ► Fig. 4.5b, ► Fig. 5.6a, ► Fig. 5.6b, and ► Fig. 6.11b); descending efferents run to

the periaqueductal gray substance of the midbrain (see ►Fig. 3.10a and Fig. 6.12c), to the cerulean nucleus (see ►Fig. 5.6a, ►Fig. 5.6b, ►Fig. 5.7, ►Fig. 6.10b, and ►Fig. 6.11b), and to the reticular formation of the pons and the medulla oblongata. Intraventricular administration of β -endorphin or injection of this substance into the periaqueductal gray substance of the midbrain produces analgesia. Endorphinergic nerve cells are thus believed to play a role in the **central regulation of stress-induced analgesia**. It has furthermore been demonstrated that the endorphinergic nerve cells stimulate release of growth hormone, prolactin, and vasopressin.

11.7.4 Enkephalinergic Neurons

Enkephalin is a peptide composed of five amino acids and has been electrophysiologically identified as an **inhibitory neurotransmitter**. Enkephalin has been demonstrated in interneurons with short processes and in those with long projection fibers using immunohistochemical methods. Enkephalin functions as an endogenous **ligand** for **opiate receptors**. The superficial dorsal layer of the dorsal gray horn of the spinal cord and the spinal nucleus of trigeminal nerve contain

a dense plexus of enkephalinergic fibers and are rich in opiate receptors. Numerous small enkephalinergic neurons also present in this layer and these probably presynaptically inhibit the release of substance P from synaptic endings of the primary neurons in pain-conducting systems. Enkephalin-containing nerve cells are also found in the periolivary nucleus (auditory system) and in the olfactory bulb (see ►Fig. 3.1c, ►Fig. 3.3a, ►Fig. 3.3b, ►Fig. 5.1c, ►Fig. 5.1d, ►Fig. 5.6a, ►Fig. 6.11a, and Section 10.7). Furthermore, there are abundant enkephalin-containing nerve cells in the raphe nuclei, particularly in the nuclei raphes magnus und posterior. The periaqueductal gray substance (see ►Fig. 3.10a) has the highest concentration of opiate receptors. An electric stimulus or a microinjection of an opiate in this area produces analgesia. Enkephalinergic nerve cells act on the hypothalamo-hypophysial regulation of oxytocin and vasopressin, as well as on the regulation of several liberins and statins. The substantia innominata is the area of the brain which is most rich in enkephalin. The striatum possesses enkephalin-containing nerve cells which project to the pallidum. Enkephalin-containing nerve cells are also present in the neocortex and allocortex and possess intracortical connections.

Part V
Appendix

12 Specimens and Technique	491
13 Bibliography	495



12 Specimens and Technique

Using specimens from the neuroanatomical collection of the Hannover Medical School the authors have been able to gain valuable information about the sectional anatomy of the head and variability of neuroanatomical structures. This collection comprises 35 intracranially fixed brains of deceased individuals who bequeathed themselves for teaching and research at the Center for Anatomy of the Hannover Medical School. In addition, the collection contains serial neurohistological sections from 34 brains that were fixed after removal.

All illustrations in this atlas have been largely depicted with the aid of original sections; axial illustrations were based on corresponding MR and CT images except the brainstem series. The original specimens for the illustrations were obtained from three deceased individuals and those for the axial imaging from one subject; age, sex, length, head measurements, and possible cause of death of these four subjects have been listed in ►Table 12.1. The maximum width of the head was measured above the external acoustic canal, while its maximum length was measured between the glabella and opisthion. Facial height was measured between the nasion and gnathion and the width of the zygomatic arch was measured between the most lateral points of the zygomatic bones. Serial CT images of the skull base were obtained retrospectively from a diagnostic examination of a 32-year-old male patient with no available details about cranial parameters. CT images aligned along the supraorbito-suboccipital plane were also obtained retrospectively from a diagnostic examination of a 64-year-old female patient.

Cerebrospinal fluid of the corpse was drained by suboccipital and lumbar puncture, and the same amount of 37% formalin (Merck) was injected into the subarachnoid space. A fixation mixture of 86 parts 96% alcohol, 8 parts 37% formalin, 3 parts glycerin DAB 7, and 3 parts saturated phenol solution DAB 8 were perfused through the femoral artery.

MR images of the test subject were obtained conforming to coronal, sagittal, and brainstem series, which closely approximated atlas illustrations. **Sectional planes were specified in accordance with stereotactic principles.** These coordinate planes have been described earlier in ►Section 1.2 for coordinate systems oriented in the coronal, sagittal, and axial planes together with a description of the Meynert plane, which was employed in the coordinate system of the brainstem series.

The corresponding **coordinate planes** must be visible on individual cranial sections such that these sections may be spatially oriented in the coordinate system. Thus, corresponding coordinate planes, such as the median plane, Reid's baseline, the meatoververtical plane, and Meynert's plane, were marked on the head using deep, circular incisions which later served as orientation for individual cranial sections, thereby enabling correct alignment of these sections within the coordinate frame.

These heads were subsequently frozen at –26°C for 6 days and then cut through using a KS 400 band saw (Reich, Nürtingen). A special guide was then used to obtain sections at 10 mm intervals while brainstem sections were obtained at intervals of 5 mm. Sawing reduced the thickness of each section by 1 mm.

The **cut surfaces of these sections** were photographed and photo prints were obtained on a scale of 1:1. Illustrations were made with acetate overlays and permanent ink directly from photographs while comparing them throughout with original preparations. Individual structures were identified using a Zeiss stereomicroscope together with a Volpi cold light source Intralux 150 H. Gennari's band in the primary visual cortex, the corona radiata, and the alveus of the hippocampus were thus easily identifiable in the alcohol-formalin fixed brain slices. Small vessels were examined to histologically differentiate them into arteries or veins. Serial sections of neuroanatomical specimens at the Hannover Medical

Table 12.1 Examination specimens											
Image series	Protocol no.	Age (years)	Gender	Length (cm)	Width of head (cm)	Length of head (cm)	Width-length Index (%)	Facial height (cm)	Zygomatic arch width (cm)	Facial index (%)	Cause of death
Coronal series	S 63/86	65	♀	163	15.5	18.9	82	11.0	13.7	80	Gastric cancer
Sagittal Series	S 58/86	70	♂	175	17.0	20.2	84	12.6	16.6	76	Myocardial infarction
Brainstem series	S 66/87	62	♂	170	16.0	19.8	81	13.4	15.0	89	Gastric cancer
Bicommissural series		33	♂	196	13.5	15.5	74	11.5	12.0	95	None (test subject)

School were used for histological comparison. Furthermore, one of the authors (H.-J. K) studied the brains of the Yakovlev collection at the Walter Reed Hospital in Washington, D.C., for comparative purposes with a financial grant from the German Research Society (Kr 289/15). A digital drawing board was used to make schematic diagrams of axial sections oriented along the bicommissural plane based on the respective section.

Individual **gyri and sulci** of the cerebral hemispheres could only be identified with certainty after 1:1 brain models or plexiglass reconstructions were prepared and compared with a series of macroscopic sections from other brains and heads. Reconstructions of T1- and T2-weighted 3D data sets as well as venous and arterial MRA were used for **anatomical mapping of MRI images**.

Toward the final phase of investigation, the authors (H.-J. K., W.W) assembled cranial sections for the precise localization of sectional planes on radiographs.

To compensate for the 1 mm loss in thickness of the slices due to the width of the blade (approximately 14 mm for 14 sections), the radiographs were cut into strips corresponding to slices and remounted with a 1 mm space between each individual slice. ▶Fig. 3.1c, ▶Fig. 4.1b, and ▶Fig. 5.1b were obtained in this way. Medial and lateral views of the brain (see ▶Fig. 3.1c, ▶Fig. 3.1d, ▶Fig. 4.1c, ▶Fig. 4.1d, ▶Fig. 5.1c, and ▶Fig. 5.1d) were obtained after a midline incision through sections of the brain with the freed halves being assembled into a complete hemisphere or brain. These were photographed, and the missing 1 mm intervals were compensated for. A computerized graphic reconstruction of the lateral view of the ventricular system (see ▶Fig. 7.8b and ▶Fig. 7.11b) was obtained using these slices (program by Dr. B. Sauer), and topographically superimposed within the outlines of the radiographic image of the cranium (see ▶Fig. 3.1c and ▶Fig. 5.1b).

The small **cerebral arteries** running within sulci of the cerebrum are often very tortuous and have many branches. The course of these fine arteries could not be reconstructed with certainty on 1-cm-thick sections. Therefore, when referring to these branches of the anterior cerebral artery the precuneal artery is meant in general without attempting to differentiate between superior and inferior precuneal arteries. Similarly, temporal and parietal branches of the middle cerebral artery are not subdivided further. Small arteries running entirely within a slice parallel to the sectioning plane have not been sectioned and have therefore not been depicted in the illustrations.

Graphic illustrations in the atlas were reduced in size for printing; coronal series (see ▶Fig. 3.2 to ▶Fig. 5.15) to 82%, sagittal series (see ▶Fig. 4.2 to ▶Fig. 4.7) to 71%, and the overall view of the brainstem series (see ▶Fig. 6.4a to ▶Fig. 6.13a) to 79%. The scale, in centimeters, may be read from the corresponding coordinate frame in the atlas illustrations of the coronal, sagittal, and brainstem series.

Serial MR and CT images of the brainstem series were acquired in coronal and sagittal planes in close approximation to the illustrations in the anatomic atlas. Sectional planes used in digital imaging were aligned with utmost care with anatomical sections. The most representative of several MR and CT images was placed next to atlas illustrations. **MR images** were obtained from a 33-year-old man. The MR examinations were carried out over several days on a Magnetom Verio 3T, a magnetic resonance tomograph (Siemens, Erlangen), using a 32 channel head coil. Measurement parameters for MR images were selected for acquisition and description of brain anatomy. The spatial relationship of individual structures to anatomically adjacent structures in the same section as also to those in adjoining slices may help delineate their morphology.

The **best possible depiction of neuroanatomical structures** for the selected examination sequence and **window settings** with good differentiation of gray and white matter was the main idea behind this book. Bones, muscles, tendons, and fat must remain discreetly in the background.

All T1-weighted MR images in the atlas were obtained with a T1-weighted gradient echo-FLASH sequence. A T1-weighted SE sequence was employed for imaging stages of brain maturation (see ▶Table 12.2 for measurement parameters). T2-weighted images of brain parenchyma were obtained using a TSE sequence. Other special sequences for various regions (DTI, QSM, high resolution images of the petrous bone) have been listed in ▶Table 12.2.

The QSM method is an advancement of SWI technology, whereby phase-shift information of MR signals are calculated and included into the image; substances with paramagnetic properties appear bright, while substances with diamagnetic properties appear dark. The so-called MEDI method was used in the calculation of the QSM image^{660,661} for ▶Fig. 7.45, using SWI images with varying echo times. A 3D time-of-flight sequence was used for the 7-T-MRA (see ▶Fig. 7.27) of a 26-year-old, healthy volunteer provided by Dr. Wrede (Essen) (pixel size: $0.22 \times 0.22 \times 0.41$ mm²⁷⁶). For the 7-T image of the hippocampus of a 38-year-old healthy volunteer provided by PD Dr. Theysohn (see ▶Fig. 3.9f), a T2-weighted TSE sequence with a resolution of $0.25 \times 0.25 \times 3.0$ mm was obtained (echo time: 95 ms, repetition time: 5,000 ms, flip angle: 150°, and parallel-imaging factor: 2). The 7-T-SWI image of the deep and basal veins provided by Dr. Deistung (Jena) (see ▶Fig. 7.36e) is a 2-cm-wide minimum-intensity projection (MinIP) of an SWI measurement with 3D flux compensation (echo time: 10.5 ms, repetition time: 17 ms, flip angle: 8°, matrix: $576 \times 414 \times 256$, and voxel size: $0.4 \times 0.4 \times 0.4$ mm). Data were collected in three different head angle positions relative to the direction of the B₀ field, and information was combined into a single image. Image contrast in this technique is based on a pronounced sensitivity of this

Table 12.2 Measurement parameters of employed standard and special sequences

Imaging series	Sequence	Matrix	FOV	Slice thickness (mm)	Echo time (ms)	Repetition time (ms)
Brainstem	T1w Flash	320	240	3	2.48	293
Brainstem	T2w Medic	320	180	3	17	497
Axial-canthomeatal	T2w TSE	384	240	4	79	8,420
Coronal	T1w Flash	320	240	4	2.48	293
Coronal	T2w TSE	384	240	4	79	8,420
Sagittal	T2w TSE	448	240	4	84	8,900
Sagittal	T1w Flash	320	240	4	2.5	310
Inner ear	T2w Space	384	200	0.3	139	3,000
Fiber tracts	DTI (30 directions)	110	220	2	101	10,300
Nuclear regions	QSM with SWI as base sequence	256	214	1	8 TE; 3.6–45	55
MRA arterial	3D-TOF	384	200	0.4	4.16	24
MRA venous	2D-TOF	256	250	2	5	20

sequence for disturbances of the magnetic field; signal loss within veins results from paramagnetic effects of deoxyhemoglobin.

The 7T-tractography images (see ►Fig. 7.54d, ►Fig. 7.54f, and ►Fig. 7.54g) were derived from a healthy volunteer using a 7T Magnetom MR scanner (Siemens Helathineers, Erlangen, Germany) with a strong gradient system (Siemens SC72, gradient amplitude 70 mT/m, slew rate 200 T/m/s), a 24-channel headcoil (Nova Medical, Massachusetts, USA) and a single refocussed spin-echo EPI sequence (voxel size $1 \times 1 \times 1$ mm, $b = 1000$, 60 diffusion directions, TE = 67 ms, TR 11, 2s, parallel imaging factor 3, band with 1089 Hz/pixel; 4 measurements). The diffusion data were corrected for motion artifacts and noise, the images were calculated using a deterministic tractography algorithm.

The reader's attention is drawn to the fact that the **specimens for atlas images** for the frontal, sagittal, and brainstem series was derived from three different individuals (see ►Table 12.1). MR images aligned along coronal, sagittal, and bicommissural planes, as well as those of the brainstem series have all been derived from one individual. The other **MR and CT images** in this book were obtained from different individuals. These interindividual differences in anatomic structures correspond with variations seen in routine clinical practice. Considerable anatomic variants and intracranial mass displacements were disregarded since the authors' aim was to **depict "normal" neuroanatomy**, thus enabling identification of pathological changes.

13 Bibliography

- [1] Acevedo BP, Aron A, Fisher HE, Brown LL. Neural correlates of long-term intense romantic love. *Soc Cogn Affect Neurosci*. 2012; 7(2):145–159
- [2] Ackermann H, Mathiak K. Symptomatologie, pathologisch-anatomische Grundlagen und Pathomechanismus zentraler Hörstörungen (reine Worttaubheit, auditive Agnosie, Rindentaubheit). *Fortschr Neurol Psychiatr*. 1999; 67:509–523
- [3] Ackermann H, Wildgruber D, Grodd W. Neuroradiologische Aktivierungsstudien zur zerebralen Organisation sprachlicher Leistungen. Eine Literaturübersicht. *Fortschr Neurol Psychiatr*. 1997; 65(4):182–194
- [4] Adams RD, Victor M, Ropper AH. Principles of neurology. New York, NY: McGraw-Hill; 1997
- [5] Adolphs R, Tranel D, Damasio H, Damasio A. Impaired recognition of emotion in facial expressions following bilateral damage to the human amygdala. *Nature*. 1994; 372(6507):669–672
- [6] Afshar F, Watkins ES, Yap JC. Stereotaxic atlas of the human brainstem and cerebellar nuclei. A variability study. New York, NY: Raven Press; 1978
- [7] Alexander K, Daniel WG, Diener HC, et al. Thiemes Innere Medizin TIM. Stuttgart: Thieme; 1999
- [8] Alexander MP, LoVerme SR, Jr. Aphasia after left hemispheric intracerebral hemorrhage. *Neurology*. 1980; 30(11):1193–1202
- [9] Alkadhi H, Kollias SS, Crelier GR, Golay X, Hepp-Reymond MC, Valavanis A. Plasticity of the human motor cortex in patients with arteriovenous malformations: a functional MR imaging study. *AJNR Am J Neuroradiol*. 2000; 21(8):1423–1433
- [10] Allon N, Yeshurun Y, Wollberg Z. Responses of single cells in the medial geniculate body of awake squirrel monkeys. *Exp Brain Res*. 1981; 41(3–4):222–232
- [11] Alper F, Kantarci M, Dane S, Gumustekin K, Onbas O, Durur I. Importance of anatomical asymmetries of transverse sinuses: an MR venographic study. *Cerebrovasc Dis*. 2004; 18(3):236–239
- [12] Alpers BJ, Berry RG. Circle of Willis in cerebral vascular disorders. The anatomical structure. *Arch Neurol*. 1963; 8:398–402
- [13] Ambrose J. Computerized transverse axial scanning (tomography). 2. Clinical application. *Br J Radiol*. 1973; 46(552):1023–1047
- [14] Amunts K, Zilles K. Advances in cytoarchitectonic mapping of the human cerebral cortex. *Neuroimaging Clin N Am*. 2001; 11(2):151–169, vii
- [15] Anderson AK, Phelps EA. Lesions of the human amygdala impair enhanced perception of emotionally salient events. *Nature*. 2001; 411(6835):305–309
- [16] Andrew J, Watkins ES. A stereotaxic atlas of the human thalamus and adjacent structures. Baltimore, MD: Williams and Wilkins; 1969
- [17] Angevine JB Jr, Mancall EL, Yakovlev PI. The human cerebellum. An atlas of cross topography in serial sections. Boston, MA: Little Brown & Co; 1961
- [18] Arlart IP, Bongartz GM, Marchal G, eds. Magnetic resonance angiography. Berlin: Springer; 1996
- [19] Armington WG, Harnsberger HR, Smoker WRK, Osborn AG. Normal and diseased acoustic pathway: evaluation with MR imaging. *Radiology*. 1988; 167(2):509–515
- [20] Arning C. Farbkodierte Duplexsonographie der hirnversorgenden Arterien. Stuttgart: Thieme; 1999
- [21] Atlas SW. Pocket atlas of cranial magnetic resonance imaging. Philadelphia, PA: Lippincott, Williams & Wilkins; 2001
- [22] Atlas SW. Magnetic resonance imaging of the brain and spine. Vol. 1, 2. Philadelphia, PA: Lippincott Williams & Wilkins; 2008
- [23] Babb TL, Wilson CL, Crandall PH. Asymmetry and ventral course of the human geniculostriate pathway as determined by hippocampal visual evoked potentials and subsequent visual field defects after temporal lobectomy. *Exp Brain Res*. 1982; 47(3):317–328
- [24] Baddeley A. Working memory: looking back and looking forward. *Nat Rev Neurosci*. 2003; 4(10):829–839
- [25] Baddeley A. Working memory. *Science*. 1992; 255(5044):556–559
- [26] Baloh RW, Furman JM, Yee RD. Dorsal midbrain syndrome: clinical and oculographic findings. *Neurology*. 1985; 35(1):54–60
- [27] Bancaud J, Talairach J. Organisation fonctionnelle de l'aire motrice supplémentaire. Enseignements apportés par la stéréo-E.E.G. *Neurochirurgie*. 1967; 13(3):343–356
- [28] Barkovich AJ. Pediatric neuroimaging. New York, NY: Raven Press; 1997
- [29] Barkovich AJ. MR of the normal neonatal brain: assessment of deep structures. *AJNR Am J Neuroradiol*. 1998; 19(8):1397–1403
- [30] Barkovich AJ. Normal development of the neonatal and infant brain, skull, and spine In: Barkovich AJ. Pediatric neuroimaging. Philadelphia, PA: Lippincott Williams & Wilkins; 2012:20–80
- [31] Barkovich AJ, Kjos BO, Jackson DE, Jr, Norman D. Normal maturation of the neonatal and infant brain: MR imaging at 1.5 T. *Radiology*. 1988; 166(1 Pt 1):173–180
- [32] Bartels A, Zeki S. The neural correlates of maternal and romantic love. *Neuroimage*. 2004; 21(3):1155–1166
- [33] Bartsch T, Butler C. Transient amnesic syndromes. *Nat Rev Neurol*. 2013; 9(2):86–97
- [34] Bartz JA, Zaki J, Ochsner KN, et al. Effects of oxytocin on recollections of maternal care and closeness. *Proc Natl Acad Sci U S A*. 2010; 107(50):21371–21375
- [35] Bauer A, de Langen-Müller U, Glindemann R, et al. Qualitätskriterien und Standards für die Therapie von Patienten mit erworbenen neurogenen Störungen der Sprache (Aphasie) und des Sprechens (Dysarthrie). *Akt Neurol*. 2002; 29:63–75
- [36] Bauer BL, Hellwig D. Minimal invasive endoskopische Neurochirurgie (MIEN). *Dtsch Arztebl*. 1995; 92:A2816–A2835
- [37] Bauer R. v. de Fliedert E, Mörike K. MR Tomography of the central nervous system. Stuttgart: Urban und Fischer; 1993
- [38] Baumgartner G. Funktion und Symptomatik einzelner Hirnregionen. In: Hopf HC, Poeck K, Schliack H II., Hrsg. Neurologie in Praxis und Klinik. Bd. 1. Stuttgart: Thieme; 1983:1.77–1.112
- [39] Baumgartner T, Heinrichs M, Vonlanthen A, Fischbacher U, Fehr E. Oxytocin shapes the neural circuitry of trust and trust adaptation in humans. *Neuron*. 2008; 58(4):639–650
- [40] Bear MF, Connors BW, Paradiso MA. Neuroscience: exploring the brain. Baltimore, MD: Williams and Wilkins; 1996
- [41] Bechara A, Damasio AR, Damasio H, Anderson SW. Insensitivity to future consequences following damage to human prefrontal cortex. *Cognition*. 1994; 50(1–3):7–15
- [42] Bechara A, Damasio H, Tranel D, Damasio AR. Deciding advantageously before knowing the advantageous strategy. *Science*. 1997; 275(5304):1293–1295
- [43] Bechara A, Tranel D, Damasio H, Adolphs R, Rockland C, Damasio AR. Double dissociation of conditioning and declarative knowledge relative to the amygdala and hippocampus in humans. *Science*. 1995; 269(5227):1115–1118
- [44] Becker G, Berg D. Neuroimaging in basal ganglia disorders: perspectives for transcranial ultrasound. *Mov Disord*. 2001; 16(1):23–32
- [45] Becker G, Naumann M, Scheubeck M, et al. Comparison of transcranial sonography, magnetic resonance imaging, and single photon emission computed tomography findings in idiopathic spasmodic torticollis. *Mov Disord*. 1997; 12(1):79–88
- [46] Becker H, Vonofakos D. Diagnostische Bedeutung von Hirntumorerkrankungen im Computertomogramm. *Radiologe*. 1983; 23(10):459–462
- [47] Beevor CE. On the distribution of the different arteries supplying the human brain. *Phil Trans*. 1909; 200:1–55
- [48] Benjamin RM, Burton H. Projection of taste nerve afferents to anterior opercular-insular cortex in squirrel monkey (*Saimiri sciureus*). *Brain Res*. 1968; 7(2):221–231

- [49] Benson DF. Neurological correlates of aphasia and apraxia. In: Matthews WB, Glaser GH, eds. Recent advances in clinical neurology. Edinburgh: Churchill Livingstone; 1981:163–175
- [50] Bentivoglio M. The anatomical organization of corticospinal connections. In: Rossini PM, Marsden CD, eds. Non-invasive Stimulation of Brain and Spinal Cord: Fundamentals and Clinical Applications. New York, NY: A. R. Liss; 1988:1–22
- [51] Bergstrand G, Bergström M, Nordell B, et al. Cardiac gated MR imaging of cerebrospinal fluid flow. *J Comput Assist Tomogr.* 1985; 9(6):1003–1006
- [52] Berlitz P, ed. Klinische Neurologie. Berlin: Springer; 1999
- [53] Berman SA, Hayman LA, Hinck VC. Correlation of CT cerebral vascular territories with function: I. Anterior cerebral artery. *AJR Am J Roentgenol.* 1980; 135(2):253–257
- [54] Berman SA, Hayman LA, Hinck VC. Correlation of CT cerebral vascular territories with function: 3. Middle cerebral artery. *AJR Am J Roentgenol.* 1984; 142(5):1035–1040
- [55] Berns TF, Daniels DL, Williams AL, Houghton VM. Mesencephalic anatomy: demonstration by computed tomography. *AJNR Am J Neuroradiol.* 1981; 2(1):65–67
- [56] Bierny J-P, Komar NN. The sylvian cistern on computed tomography scanning. *J Comput Assist Tomogr.* 1977; 1(2):227–230
- [57] Binder JR, Frost JA, Hammeke TA, Cox RW, Rao SM, Prieto T. Human brain language areas identified by functional magnetic resonance imaging. *J Neurosci.* 1997; 17(1):353–362
- [58] Biswal BB. Resting state fMRI: a personal history. *Neuroimage.* 2012; 62(2):938–944
- [59] Blunk R, De Bleser R, Willmes K, Zeumer H. A refined method to relate morphological and functional aspects of aphasia. *Eur Neurol.* 1981; 20(2):69–79
- [60] Bo WJ, Wolfman N. Basic atlas of sectional anatomy with correlated imaging. Philadelphia, PA: Saunders; 1998
- [61] Bogerts B. A brainstem atlas of catecholaminergic neurons in man, using melanin as a natural marker. *J Comp Neurol.* 1981; 197(1):63–80
- [62] Bonneville J-F, Cattin F, Dietemann J-L. Computed tomography of the pituitary gland. Berlin: Springer; 1986
- [63] Bosch DA. Stereotactic techniques in clinical neurosurgery. Wien: Springer; 1986
- [64] Bouthillier A, van Loveren HR, Keller JT. Segments of the internal carotid artery: a new classification. *Neurosurgery.* 1996; 38(3):425–432, discussion 432–433
- [65] Bowsher D. Diencephalic projections from the midbrain reticular formation. *Brain Res.* 1975; 95(2–3):211–220
- [66] Braak H. Über die Kerngebiete des menschlichen Hirnstammes. I. Oliva inferior, Nucleus conterminalis und Nucleus vermis corporis restiformis. *Z Zellforsch Mikrosk Anat.* 1970; 105(3):442–456
- [67] Braak H. Über die Kerngebiete des menschlichen Hirnstammes. II. Die Raphekerne. *Z Zellforsch Mikrosk Anat.* 1970; 107(1):123–141
- [68] Braak H. The pigment architecture of the human temporal lobe. *Anat Embryol (Berl).* 1978; 154(2):213–240
- [69] Braak H. Architectonics of the human telencephalic cortex. Berlin: Springer; 1980
- [70] Bradley WG, Jr. MR of the brain stem: a practical approach. *Radiology.* 1991; 179(2):319–332
- [71] Brandt T, Dichgans J, Diener HC, eds. Therapie und Verlauf neurologischer Erkrankungen. Stuttgart: Kohlmeier; 2000
- [72] Brassow F, Baumann K. Volume of brain ventricles in man determined by computer tomography. *Neuroradiology.* 1978; 16:187–189
- [73] Bredberg G. Innervation of the auditory system. *Scand Audiol Suppl.* 1981; 13(Suppl.):1–10
- [74] Broca P. Anatomie comparée circonvolutions cerebrales. Le grande lobe limbique et la scissure limbique dans la serie des mammiferes. *Rev Antropol.* 1878; 1:384–498
- [75] Brodal A. Neurological anatomy in relation to clinical medicine. New York, NY: Oxford University Press; 1981
- [76] Brodmann K. Vergleichende Lokalisationslehre der Großhirnrinde – in ihren Prinzipien dargestellt auf Grund des Zellenbaues. Leipzig: Barth; 1909
- [77] Bron AJ, Tripathi RC, Tripathi BJ. Wolff's anatomy of the eye and orbit. London: Chapman & Hall; 1997
- [78] Bruhn H. Untersuchungen physiologischer und pathophysiologischer Stoffwechselzustände und Hirnfunktionen des Menschen mit Hilfe neuer methodischer Entwicklungen zur orts aufgelösten Magnetresonanztomographie und funktionellen Magnetresonanztomographie. Habilitationsschrift der Medizinischen Fakultät der Humboldt-Universität Berlin; 2001
- [79] Brust JCM. Stroke. Diagnostic, anatomical, and physiological considerations. In: Kandel ER, Schwartz JH, eds. Principles of neural science. New York, NY: Elsevier; 1985:853–861
- [80] Bruyn RPM. Thalamic aphasia. A conceptional critique. *J Neurol.* 1989; 236(1):21–25
- [81] Bucher O, Wartenberg H. Cytologie, Histologie und mikroskopische Anatomie des Menschen. Bern: Huber; 1997
- [82] Buchner H, Adams L, Müller A, et al. Somatotopy of human hand somatosensory cortex revealed by dipole source analysis of early somatosensory evoked potentials and 3D-NMR tomography. *Electroencephalogr Clin Neurophysiol.* 1995; 96(2):121–134
- [83] Buckner RL. The serendipitous discovery of the brain's default network. *Neuroimage.* 2012; 62(2):1137–1145
- [84] Buhmann C. Computergestützte 3D-Rekonstruktion des corticospinalen Systems als Referenz für die bildgebenden Verfahren CT, MRT und PET. Medizinische Dissertation der Medizinischen Hochschule Hannover; 1994
- [85] Buhmann C, Kretschmann H-J. Computer-assisted three-dimensional reconstruction of the corticospinal system as a reference for CT and MRI. *Neuroradiology.* 1998; 40(9):549–557
- [86] Büll U, Schicha H, Biersack H-J, et al, eds. Nuklearmedizin. Stuttgart: Thieme; 1999
- [87] Burgener FA, Meyers SP, Tan RK, et al. Differenzialdiagnostik in der MRT. Stuttgart: Thieme; 2003
- [88] Burton H, Benjamin RM. Central projections of the gustatory system. In: Autrum H, Jung R, Loewenstein WR et al., eds. Handbook of sensory physiology. Vol. 4: Chemical senses, part 2. Berlin: Springer; 1971:148–164
- [89] Bush G, Luu P, Posner MI. Cognitive and emotional influences in anterior cingulate cortex. *Trends Cogn Sci.* 2000; 4(6):215–222
- [90] Butler P, ed. Imaging of the nervous system. Berlin: Springer; 1990
- [91] Butler P, Mitchel AWM, Ellis H, eds. Applied radiological anatomy. Cambridge: Cambridge University Press; 1999
- [92] Büttner-Ennever JA, ed. Neuroanatomy of the oculomotor system. In: Robinson DA, Collewijn H, eds. Reviews of Oculomotor Research. Vol. 2. Amsterdam: Elsevier; 1988
- [93] Büttner-Ennever JA. A review of otolith pathways to brainstem and cerebellum. *Ann N Y Acad Sci.* 1999; 871:51–64
- [94] Büttner-Ennever JA. Overview of the vestibular system: Anatomy. In: Anderson JH, Beitz AJ, eds. Neurochemistry of the Vestibular System. Boca Raton, FL: CRC Press; 2000:3–24
- [95] Büttner-Ennever JA, Büttner U, Cohen B, Baumgartner G. Vertical glaze paralysis and the rostral interstitial nucleus of the medial longitudinal fasciculus. *Brain.* 1982; 105(Pt 1):125–149
- [96] Cahill L, Babinsky R, Markowitsch HJ, McGaugh JL. The amygdala and emotional memory. *Nature.* 1995; 377(6547):295–296
- [97] Cahill L, Haier RJ, Fallon J, et al. Amygdala activity at encoding correlated with long-term, free recall of emotional information. *Proc Natl Acad Sci U S A.* 1996; 93(15):8016–8021
- [98] Calautti C, Baron JC. Functional neuroimaging studies of motor recovery after stroke in adults: a review. *Stroke.* 2003; 34(6):1553–1566
- [99] Carpenter MB. Anatomy and physiology of the basal ganglia. In: Schaltenbrand G, Walker AE, eds. Stereotaxy of the Human Brain. 2nd ed. Stuttgart: Thieme; 1982:233–268

- [100] Carpenter MB. Core Text of Neuroanatomy. Baltimore, MD: Williams and Wilkins; 1991
- [101] Casselman JW, Francke J-P, Dehaene I. Imaging of the Upper Cranial Nerves. CD-ROM. München: Nycomed Amersham Buchler GmbH; 1999
- [102] Celesia GG. Organization of auditory cortical areas in man. *Brain*. 1976; 99(3):403–414
- [103] Chaheres DW, Schmalbrock P. Fundamentals of Magnetic Resonance Imaging. Baltimore, MD: Williams and Wilkins; 1992
- [104] Chee MWL, Tan EWL, Thiel T. Mandarin and English single word processing studied with functional magnetic resonance imaging. *J Neurosci*. 1999; 19(8):3050–3056
- [105] Chollet F. Pharmacologic modulation of human cerebral activity: contribution of functional neuroimaging. *Neuroimaging Clin N Am*. 2001; 11(2):375–380, x
- [106] Citrin CM, Alper MG. Computed tomography of the visual pathways. *Comput Tomogr*. 1979; 3(4):305–331
- [107] Citrin CM, Alper MG. Computed tomography of the visual pathways. *Int Ophthalmol Clin*. 1982; 22(4):155–180
- [108] Claus D. Die transkranielle motorische Stimulation. Stuttgart: Fischer; 1989
- [109] Cole DM, Smith SM, Beckmann CF. Advances and pitfalls in the analysis and interpretation of resting-state fMRI data. *Front Syst Neurosci*. 2010; 4:8
- [110] Craig AD. How do you feel? Interoception: the sense of the physiological condition of the body. *Nat Rev Neurosci*. 2002; 3(8):655–666
- [111] Craig AD. Interoception: the sense of the physiological condition of the body. *Curr Opin Neurobiol*. 2003; 13(4):500–505
- [112] Craig AD. How do you feel – now? The anterior insula and human awareness. *Nat Rev Neurosci*. 2009; 10(1):59–70
- [113] Crammond DJ, Kalaska JF. Prior information in motor and premotor cortex: activity during the delay period and effect on pre-movement activity. *J Neurophysiol*. 2000; 84(2):986–1005
- [114] Critchley HD, Wiens S, Rotshtein P, Ohman A, Dolan RJ. Neural systems supporting interoceptive awareness. *Nat Neurosci*. 2004; 7(2):189–195
- [115] Crosby EC, Humphrey T, Lauer EW. Correlative Anatomy of the Nervous System. New York, NY: Macmillan; 1962
- [116] Dahlström A, Fuxe K. Evidence for the existence of monoamine-containing neurons in the central nervous system. I. Demonstration of monoamines in the cell bodies of brainstem neurons. *Acta Physiol Scand*. 1964; 62(Suppl. 232):1–55
- [117] Dahlström A, Fuxe K. Evidence for the existence of monoamine neurons in the central nervous system. II. Experimentally induced changes in the intraneuronal amine levels of bulbospinal neuron systems. *Acta Physiol Scand*. 1965; 64(Suppl. 247):1–36
- [118] Dalgleish T. The emotional brain. *Nat Rev Neurosci*. 2004; 5(7):583–589
- [119] Dalle R, Raboisson P, Auroy P, Woda A. The rostral part of the trigeminal sensory complex is involved in orofacial nociception. *Brain Res*. 1988; 448(1):7–19
- [120] Damasio AR. Descartes' error and the future of human life. *Sci Am*. 1994; 271(4):144
- [121] Damasio AR. The somatic marker hypothesis and the possible functions of the prefrontal cortex. *Philos Trans R Soc Lond B Biol Sci*. 1996; 351(1346):1413–1420
- [122] Damasio H. A computed tomographic guide to the identification of cerebral vascular territories. *Arch Neurol*. 1983; 40(3):138–142
- [123] Damasio H. Neuroimaging contributions to the understanding of aphasia. In: Boller F, Grafman J, eds. *Handbook of Neuropsychology*. Vol. 2. Amsterdam: Elsevier; 1989
- [124] Dampney RAL, Moon EA. Role of ventrolateral medulla in vasomotor response to cerebral ischemia. *Am J Physiol*. 1980; 239(3):H349–H358
- [125] Dani SU, Hori A, Walter GF. Principles of Neural Aging. Amsterdam: Elsevier; 1997
- [126] Danielsen ER, Ross B. Magnetic Resonance Spectroscopy Diagnosis of Neurological Diseases. New York, NY: Marcel Dekker; 1999
- [127] Davidoff RA. The pyramidal tract. *Neurology*. 1990; 40(2):332–339
- [128] De Armond SJ, Fusco MM, Dewey MM. Structure of the Human Brain. A Photographic Atlas. New York, NY: Oxford University Press; 1989
- [129] Dechent P, Frahm J. Direct mapping of ocular dominance columns in human primary visual cortex. *Neuroreport*. 2000; 11(14):3247–3249
- [130] De Coene B, Hajnal JV, Pennock JM, Bydder GM. MRI of the brain stem using fluid attenuated inversion recovery pulse sequences. *Neuroradiology*. 1993; 35(5):327–331
- [131] Deen B, Pitskel NB, Pelphrey KA. Three systems of insular functional connectivity identified with cluster analysis. *Cereb Cortex*. 2011; 21(7):1498–1506
- [132] Dejerine J. Anatomie des centres nerveux. Tome 1, 2. Paris: Masson; 1980
- [133] Delank H-W, Gehlen W. Neurologie. Stuttgart: Enke; 1999
- [134] Demaerel P. Recent advances in diagnostic neuroradiology. Berlin: Springer; 2001
- [135] Denny-Brown D. Relations and functions of the pyramidal tract. In: Schaltenbrand G, Walker AE, eds. *Stereotaxy of the Human Brain*. 2nd ed. Stuttgart: Thieme; 1982:131–139
- [136] Deschauer M, Georgiadis D, Lindner A. Hörverlust als Leitsymptom von Arteria cerebelli inferior anterior-Infarkten. *Fortschr Neurol Psychiatr*. 1998; 66(3):109–112
- [137] Dettmers C, Fink G, Rijntjes M, et al. Kortikale Kontrolle der Willkürmotorik: funktionelle Bildgebung der motorischen Exekutive des ZNS. *Neurol Rehabil*. 1997; 1:15–27
- [138] Dhermain FG, Hau P, Lanfermann H, Jacobs AH, van den Bent MJ. Advanced MRI and PET imaging for assessment of treatment response in patients with gliomas. *Lancet Neurol*. 2010; 9(9):906–920
- [139] Diehl RR, Berlit P. Funktionelle Dopplersonographie in der Neurologie. Berlin: Springer; 1996
- [140] Dieterich M. Ocular motor system: anatomy and functional magnetic resonance imaging. *Neuroimaging Clin N Am*. 2001; 11(2):251–261, viii–ix
- [141] Dieterich M, Brandt T. Vestibular system: anatomy and functional magnetic resonance imaging. *Neuroimaging Clin N Am*. 2001; 11(2):263–273, ix
- [142] Ding XQ, Maudsley AA, Sabati M, et al. Reproducibility and reliability of short-TE whole-brain MR spectroscopic imaging of human brain at 3T. *Magn Reson Med*. 2014; •••[Epub ahead of print]
- [143] Ditzel B, Schaer M, Gabriel B, Bodenmann G, Ehlert U, Heinrichs M. Intranasal oxytocin increases positive communication and reduces cortisol levels during couple conflict. *Biol Psychiatry*. 2009; 65(9):728–731
- [144] Domes G, Heinrichs M, Gläscher J, Büchel C, Braus DF, Herpertz SC. Oxytocin attenuates amygdala responses to emotional faces regardless of valence. *Biol Psychiatry*. 2007; 62(10):1187–1190
- [145] Domes G, Lischke A, Berger C, et al. Effects of intranasal oxytocin on emotional face processing in women. *Psychoneuroendocrinology*. 2010; 35(1):83–93
- [146] Donaghy M, ed. *Brain's Diseases of the Nervous System*. Oxford: Oxford University Press; 2001
- [147] Drenckhahn D, Zenker W, eds. Benninghoff: Makroskopische Anatomie, Embryologie und Histologie des Menschen. Bd. 2: Niere, Reproduktionsorgane, Nervensystem, Sinnesorgane, Haut. München: Urban und Schwarzenberg; 1994
- [148] Dudel J, Menzel R, Schmidt RF. Neurowissenschaft. Vom Mokekül zur Kognition. Berlin: Springer; 2001
- [149] Duus P. Neurologisch-topische Diagnostik. Anatomie, Physiologie, Klinik. Stuttgart: Thieme; 1995
- [150] Duvernoy HM. The Human Brain Stem and Cerebellum. Wien: Springer; 1995
- [151] Duvernoy HM. The human hippocampus. Berlin: Springer; 1998
- [152] Duvernoy HM. Human Brain Stem Vessels. Berlin: Springer; 1999
- [153] Ebeling U, Reulen HJ. Subcortical topography and proportions of the pyramidal tract. *Acta Neurochir (Wien)*. 1992; 118(3–4):164–171

- [154] Ebeling U, Huber P, Reulen HJ. Localization of the precentral gyrus in the computed tomogram and its clinical application. *J Neurol*. 1986; 233(2):73–76
- [155] von Economo C, Koskinas GN. Die Cytoarchitektonik der Hirnrinde des erwachsenen Menschen. Textband und Atlas. Wien: Springer; 1925
- [156] Edelman RR, Hesselink JR, Zlatkin MB. Clinical Magnetic Resonance Imaging. Philadelphia, PA: Saunders; 2006
- [157] Engelke C. Ganzkörper-Computertomographie: Spiral- und Multislice-CT. Stuttgart: Thieme; 2007
- [158] Englander RN, Netsky MG, Adelman LS. Location of human pyramidal tract in the internal capsule: anatomic evidence. *Neurology*. 1975; 25(9):823–826
- [159] Faerber EN. Cranial computed tomography in infants and children. Clinics in development medicine no. 93. Spastics International Medical Publications (SIMP). Oxford: Blackwell Scientific; 1991
- [160] Falck B, Hillarp N-A, Thieme G, et al. Fluorescence of catecholamines and related compounds condensed with formaldehyde. *J Histochem Cytochem*. 1962; 10:348–354
- [161] Farruggia S, Babcock DS. The cavum septi pellucidi: its appearance and incidence with cranial ultrasonography in infancy. *Radiology*. 1981; 139(1):147–150
- [162] Federative Committee on Anatomical Terminology (FCAT). Terminologia anatomica. International anatomical terminology. Stuttgart: Thieme; 1998
- [163] Felten DL, Laties AM, Carpenter MB. Monoamine-containing cell bodies in the squirrel monkey brain. *Am J Anat*. 1974; 139(2):153–165
- [164] Feneis H. Anatomisches Bildwörterbuch der internationalen Nomenklatur. Stuttgart: Thieme; 1998
- [165] Feneis H, Dauber W, eds. Anatomisches Bildwörterbuch. 8. Aufl. Stuttgart: Thieme; 2005
- [166] Fishman EK, Jeffrey BR. Spiral-CT. Stuttgart: Thieme; 2000
- [167] Fitschen J, Helus F, Jordan K, et al. Emissions-Computertomographie mit kurzlebigen zyklotron-produzierten Radiopharmaka. In: Hundeshagen H, Hrsg. Handbuch der medizinischen Radiologie. Bd. 15, Teil 1 B. Berlin: Springer; 1988
- [168] FitzGerald MJT, Folan-Curan J. Clinical Neuroanatomy and Related Neuroscience. Edinburgh: Saunders; 2002
- [169] Flechsig P. Zur Anatomie und Entwicklungsgeschichte der Leitungsbahnen im Grosshirn des Menschen. *Arch Anat Entwicklungsgesch*. 1881; 12–75
- [170] Foerster O. Motorische Felder und Bahnen. Sensible corticale Felder. In: Bumke O, Foerster O, Hrsg. Handbuch der Neurologie. Bd. 6. Berlin: Springer; 1936:1–488
- [171] Fox MD, Raichle ME. Spontaneous fluctuations in brain activity observed with functional magnetic resonance imaging. *Nat Rev Neurosci*. 2007; 8(9):700–711
- [172] Fox PT, Fox JM, Raichle ME, Burde RM. The role of cerebral cortex in the generation of voluntary saccades: a positron emission tomographic study. *J Neurophysiol*. 1985; 54(2):348–369
- [173] Frackowiak R, Friston KJ, Frith CD, et al. Human Brain Function. San Diego, CA: Academic Press; 1997
- [174] Freund H-J. Premotor area and preparation of movement. *Rev Neurol (Paris)*. 1990; 146(10):543–547
- [175] Freund H-J. Motorische Störungen bei kortikalen Läsionen. *Klin Neurophysiol*. 1999; 30:113–119
- [176] Frick H, Leonhardt H, Starck D. Spezielle Anatomie. Bd. 2: Eingeweide, Nervensystem, Systematik der Muskeln und Leitungsbahnen. Stuttgart: Thieme; 1992
- [177] Fritsch R, Hitzig E. Über die elektrische Erregbarkeit des Großhirns. *Arch Anat Physiol Wissenschaftl Med*. 1870; 37:300–332
- [178] Fritz P, Lenarz T, Haels J, et al. Feinstrukturanalyse des Felsenbeines mittels hochauflösender Dünnschicht-Computertomographie. Teil 1: Sensitivität der Strukturdarstellung bei einer standardisierten Untersuchungstechnik. *Fortschr Röntgenstr*. 1987; 147:266–271
- [179] Froriep A. Die Lagebeziehungen zwischen Großhirn und Schädeldach. Leipzig: Veit; 1897
- [180] Fusar-Poli P, Placentino A, Carletti F, et al. Functional atlas of emotional faces processing: a voxel-based meta-analysis of 105 functional magnetic resonance imaging studies. *J Psychiatry Neurosci*. 2009; 34(6):418–432
- [181] Gaa J, Lehmann K-J, Georgi M, eds. MR-Angiographie und Elektronenstrahl-CT-Angiographie. Stuttgart: Thieme; 2000
- [182] Galaburda A, Sanides F. Cytoarchitectonic organization of the human auditory cortex. *J Comp Neurol*. 1980; 190(3):597–610
- [183] Galaburda AM, LeMay M, Kemper TL, Geschwind N. Right-left asymmetries in the brain. *Science*. 1978; 199(4331):852–856
- [184] Galaburda AM, Sanides F, Geschwind N. Human brain. Cytoarchitectonic left-right asymmetries in the temporal speech region. *Arch Neurol*. 1978; 35(12):812–817
- [185] Galanski M, Dickob M, Wittkowski W. CT-Zisternographie der basalen Zisternen. *Fortschr Röntgenstr*. 1986; 145:149–157
- [186] Gallen CC, Sobel DF, Waltz T, et al. Noninvasive presurgical neuromagnetic mapping of somatosensory cortex. *Neurosurgery*. 1993; 33(2):260–268, discussion 268
- [187] Garnett ES, Nahmias C, Firnau G. Central dopaminergic pathways in hemiparkinsonism examined by positron emission tomography. *Can J Neurol Sci*. 1984; 11((1, Suppl):174–179
- [188] Garver DL, Sladek JR, Jr. Monoamine distribution in primate brain. I. Catecholamine-containing perikarya in the brain stem of *Macaca speciosa*. *J Comp Neurol*. 1975; 159(3):289–304
- [189] Gauba V, Saleh GM, Dua G, Agarwal S, Ell S, Vize C. Radiological classification of anterior skull base anatomy prior to performing medial orbital wall decompression. *Orbit*. 2006; 25(2):93–96
- [190] George B, Laurian C. The Vertebral Artery. Wien: Springer; 1987
- [191] Gerke M. Computerunterstützte dreidimensionale Rekonstruktion des limbischen Systems als Referenz für die bildgebenden Verfahren (Computertomographie, Magnetische Resonanztomographie und Positronen-Emissionstomographie). Medizinische Dissertation der Medizinischen Hochschule Hannover; 1988
- [192] Geschwind N. Die Großhirnrinde. In: Gehirn und Nervensystem. Heidelberg: Spektrum der Wissenschaft; 1979:127–136
- [193] Giesemann AM, Raab P, Lyutenski S, et al. Improved imaging of cochlear nerve hypoplasia using a 3-Tesla variable flip-angle turbo spin-echo sequence and a 7-cm surface coil. *Laryngoscope*. 2014; 124(3):751–754
- [194] Gillilan LA. The correlations of the blood supply of the human brain stem with clinical brain stem lesions. *J Neuropathol Exp Neurol*. 1964; 23:78–108
- [195] Gloger A, Gloger S. Dreidimensionale Computerrekonstruktion der terminalen Äste der drei Großhirnarterien des Menschen als Referenz für die Magnetresonanztomographie (MRT), die Computertomographie (CT) und die Positronen-Emissionstomographie (PET). Medizinische Dissertation der Medizinischen Hochschule Hannover; 1993
- [196] Gloger S, Gloger A, Vogt H, Kretschmann HJ. Computer-assisted 3D reconstruction of the terminal branches of the cerebral arteries. I. Anterior cerebral artery. *Neuroradiology*. 1994; 36(3):173–180
- [197] Gloger S, Gloger A, Vogt H, Kretschmann HJ. Computer-assisted 3D reconstruction of the terminal branches of the cerebral arteries. II. Middle cerebral artery. *Neuroradiology*. 1994; 36(3):181–187
- [198] Gloger S, Gloger A, Vogt H, Kretschmann HJ. Computer-assisted 3D reconstruction of the terminal branches of the cerebral arteries. III. Posterior cerebral artery and circle of Willis. *Neuroradiology*. 1994; 36(4):251–257
- [199] Gobel S, Binck JM. Degenerative changes in primary trigeminal axons and in neurons in nucleus caudalis following tooth pulp extirpations in the cat. *Brain Res*. 1977; 132(2):347–354
- [200] Goodchild AK, Moon EA, Dampney RAL, Howe PR. Evidence that adrenaline neurons in the rostral ventrolateral medulla have a vasopressor function. *Neurosci Lett*. 1984; 45(3):267–272
- [201] Gouaze A, Salamon G, eds. Brain Anatomy and Magnetic Resonance Imaging. Berlin: Springer; 1988
- [202] Graham DI, Lantos PL, eds. Greenfield's Neuropathology. London: Arnold Publishers; 2002

- [203] Grand W, Hopkins LN. *Vasculature of the Brain and Cranial Base*. New York, NY: Thieme; 1999
- [204] Greenberg JO. *Neuroimaging*. New York, NY: McGraw-Hill; 1995
- [205] Grefkes C, Fink GR. Connectivity-based approaches in stroke and recovery of function. *Lancet Neurol*. 2014; 13(2):206–216
- [206] Grehl H, Reinhardt F. *Checkliste Neurologie*. Stuttgart: Thieme; 2000
- [207] Greicius MD, Krasnow B, Reiss AL, Menon V. Functional connectivity in the resting brain: a network analysis of the default mode hypothesis. *Proc Natl Acad Sci U S A*. 2003; 100(1):253–258
- [208] de Groot J. *Correlative Neuroanatomy of Computed Tomography and Magnetic Resonance Imaging*. Philadelphia, PA: Lea and Febiger; 1991
- [209] Gruber O, Arendt T, von Cramon DY. Neurobiologische Grundlagen. In: Förstl H, ed. *Frontalhirn: Funktionen und Erkrankungen*. Heidelberg: Springer; 2002:16–40
- [210] Guillaumin G, Mollaret P. Deux cas de myoclonies synchrones et rythmées vélo-pharyngo-laryngo-oculo-diaphragmatiques. *Rev Neurol*. 1931; 12:545–566
- [211] Guleria S, Kelly TG. Myelin, myelination, and corresponding magnetic resonance imaging changes. *Radiol Clin North Am*. 2014; 52(2):227–239
- [212] Haaga JR, Alfidi RJ, eds. *Computed Tomography and Magnetic Resonance Imaging of the Whole Body*. St. Louis, MO: Mosby; 1994
- [213] Habas C, Guillevin R, Abanou A. In vivo structural and functional imaging of the human rubral and inferior olivary nuclei: a mini-review. *Cerebellum*. 2010; 9(2):167–173
- [214] Habel U, Posse S, Schneider F. Funktionelle Kernspintomographie in der klinischen Psychologie und Psychiatrie. *Fortschr Neurol Psychiatr*. 2002; 70(2):61–70
- [215] Hacke W, Hennerici M, Gelmers HJ, et al. *Cerebral Ischemia*. Berlin: Springer; 1991
- [216] Hacker H, Kühner G. *Die Brückenvenen*. Radiologe. 1972; 12:45–48
- [217] von Hagens G, Whalley A, Machke R, et al. *Schnittanatomie des menschlichen Gehirns*. Darmstadt: Steinkopff; 1990
- [218] Hamann SB, Ely TD, Grafton ST, Kilts CD. Amygdala activity related to enhanced memory for pleasant and aversive stimuli. *Nat Neurosci*. 1999; 2(3):289–293
- [219] Hanaway J. *The Brain Atlas. A Visual Guide to the Human Central Nervous System*. Bethesda, MD: Fitzgerald; 1998
- [220] Hanaway J, Young RR. Localization of the pyramidal tract in the internal capsule of man. *J Neurol Sci*. 1977; 34(1):63–70
- [221] Hanaway J, Woolsey TA, Gado MH. *The Brain Atlas*. Bethesda, MD: Fitzgerald Science Press; 1998
- [222] Hanaway J, Young R, Netsky M, Adelman L. Localization of the pyramidal tract in the internal capsule. *Neurology*. 1981; 31(3):365–367
- [223] Hardy TL, Bertrand G, Thompson CJ. The position and organization of motor fibers in the internal capsule found during stereotactic surgery. *Appl Neurophysiol*. 1979; 42(3):160–170
- [224] Harnsberger HR, Osborn AG, Macdonald AJ, et al. Diagnostic and surgical imaging anatomy: brain, head and neck, spine. *Amirsys*. 2006; 1:49–62
- [225] Harrison JM, Howe ME. Anatomy of the afferent auditory nervous system of mammals. In: Autrum H, Jung R, Loewenstein WR et al., eds. *Handbook of Sensory Physiology*. Vol. 5: Auditory System, part 1. Berlin: Springer; 1974:283–336
- [226] van Hartevelt TJ, Cabral J, Deco G, et al. Neural plasticity in human brain connectivity: the effects of long term deep brain stimulation of the subthalamic nucleus in Parkinson's disease. *PLoS One*. 2014; 9(1):e86496
- [227] Hartje W, Poock K. *Klinische Neuropsychologie*. Stuttgart: Thieme; 2002
- [228] Hartman BK. The innervation of cerebral blood vessels by central noradrenergic neurons. In: Usdin E, Snyder SH, eds. *Frontiers in Catecholamine Research*. Oxford: Pergamon Press; 1973:91–96
- [229] Hassler R. Architectonic organization of the thalamic nuclei. In: Schaltenbrand G, Walker AE, eds. *Stereotaxy of the Human Brain*. 2nd ed. Stuttgart: Thieme; 1982:140–180
- [230] Hattingen E, Delic O, Franz K, et al. (1)H MRSI and progression-free survival in patients with WHO grades II and III gliomas. *Neurol Res*. 2010; 32(6):593–602
- [231] Hattingen E, Good C, Weidauer S, et al. Brain surface reformatted images for fast and easy localization of peritumoral lesions. *J Neurosurg*. 2005; 102(2):302–310
- [232] Hattingen E, Raab P, Franz K, et al. Prognostic value of choline and creatine in WHO grade II gliomas. *Neuroradiology*. 2008; 50(9):759–767
- [233] Haug H. The significance of quantitative stereologic experimental procedures in pathology. *Pathol Res Pract*. 1980; 166(2–3):144–164
- [234] Haverling M. The tortuous basilar artery. *Acta Radiol Diagn (Stockh)*. 1974; 15(3):241–249
- [235] Haxby JV, Hoffman EA, Gobbini MI. Human neural systems for face recognition and social communication. *Biol Psychiatry*. 2002; 51(1):59–67
- [236] Hayman LA, Berman SA, Hinck VC. Correlation of CT cerebral vascular territories with function: II. Posterior cerebral artery. *AJR Am J Roentgenol*. 1981; 137(1):13–19
- [237] Heidary H, Tomasch J. Neuron numbers and perikaryon areas in the human cerebellar nuclei. *Acta Anat (Basel)*. 1969; 74(2):290–296
- [238] Heimer L. *The Human Brain and Spinal cord. Functional Neuroanatomy and Dissection Guide*. New York, NY: Springer; 1995
- [239] Heimer L, Robards MJ, eds. *Neuroanatomical Tract-Tracing Methods*. New York, NY: Plenum; 1989
- [240] Heindel W, Kugel H, Lackner K, eds. *Rationelle MR-Untersuchungstechniken*. Stuttgart: Thieme; 1997
- [241] Heinrichs M, Baumgartner T, Kirschbaum C, Ehlert U. Social support and oxytocin interact to suppress cortisol and subjective responses to psychosocial stress. *Biol Psychiatry*. 2003; 54(12):1389–1398
- [242] Heinrichs M, Meinlschmidt G, Wippich W, Ehlert U, Hellhammer DH. Selective amnesic effects of oxytocin on human memory. *Physiol Behav*. 2004; 83(1):31–38
- [243] Heiss WD, Raab P, Lanfermann H. Multimodality assessment of brain tumors and tumor recurrence. *J Nucl Med*. 2011; 52(10):1585–1600
- [244] Henry JM. Anatomy of the brainstem. In: Schaltenbrand G, Walker AE, eds. *Stereotaxy of the Human Brain*. 2nd ed. Stuttgart: Thieme; 1982; 37–59
- [245] Hentschel F, Heuck F, Vogt K, et al. *Schädel-Gehirn Wirbelsäule-Rückenmark*. Stuttgart: Thieme; 1999
- [246] Heym C, ed. *Histochemistry and Cell Biology of Autonomic Neurons and Paraganglia*. Berlin: Springer; 1987
- [247] Hirayama K, Tsubaki T, Toyokura Y, et al. The representation of the pyramidal tract in the internal capsule and basis pedunculi. *Neurology*. 1962; 12:337–342
- [248] Hobson JA, Brazier MAB, eds. *The Reticular Formation Revisited. Specifying Function for a Nonspecific System*. New York, NY: Raven Press; 1980
- [249] Hofer M. *Sono-Grundkurs*. Stuttgart: Thieme; 2012
- [250] Hofer M, Antoch G. *CT-Kursbuch*. Düsseldorf: Hofer Verlag Didamed; 2014
- [251] Hökfelt T, Fuxe K, Goldstein M, et al. Immunohistochemical evidence for the existence of adrenaline neurons in the rat brain. *Brain Res*. 1974; 66:235–251
- [252] Hökfelt T, Johansson O, Ljungdahl A, Lundberg JM, Schultzberg M. Peptidergic neurones. *Nature*. 1980; 284(5756):515–521
- [253] Holman BL, Hill TC, Magistretti PL. Brain imaging with emission computed tomography and radiolabeled amines. *Invest Radiol*. 1982; 17(3):206–215
- [254] Honda H, Watanabe K, Kusumoto S, et al. Optimal positioning for CT examinations of the skull base. *Experimental and clinical studies*. *Eur J Radiol*. 1987; 7(4):225–228

- [255] Hopf HC, Deuschl G, Diener HC, et al, eds. *Neurologie in Praxis und Klinik*. Bd. 1 und 2. Stuttgart: Thieme; 1999
- [256] Horn A, Büttner-Ennever JA. Neuroanatomie der okulomotorischen Kerne, Hirnstammzentren und -bahnen. In: Huber A, Kömpf A, eds. *Klinische Neuroophthalmologie*. Stuttgart: Thieme; 1998:34–47
- [257] Horn AK, Büttner-Ennever JA. Premotor neurons for vertical eye movements in the rostral mesencephalon of monkey and human: histologic identification by parvalbumin immunostaining. *J Comp Neurol*. 1998; 392(4):413–427
- [258] Hosten N, Liebig T. Computertomographie von Kopf und Wirbelsäule. Stuttgart: Thieme; 2011
- [259] Hounsfield GN. Computerized transverse axial scanning (tomography). 1. Description of system. *Br J Radiol*. 1973; 46(552):1016–1022
- [260] Howe PRC, Costa M, Furness JB, Chalmers JP. Simultaneous demonstration of phenylethanolamine N-methyltransferase immunofluorescent and catecholamine fluorescent nerve cell bodies in the rat medulla oblongata. *Neuroscience*. 1980; 5(12):2229–2238
- [261] Hubbard JE, Di Carlo V. Fluorescence histochemistry of monoamine-containing cell bodies in the brain stem of the squirrel monkey (*Saimiri sciureus*). II. Catecholamine-containing groups. *J Comp Neurol*. 1974; 153(4):369–384
- [262] Hubbard JE, Di Carlo V. Fluorescence histochemistry of monoamine-containing cell bodies in the brain stem of the squirrel monkey (*Saimiri sciureus*). 3. Serotonin-containing groups. *J Comp Neurol*. 1974; 153(4):385–398
- [263] Huber A, Kömpf D. *Klinische Neuroophthalmologie*. Stuttgart: Thieme; 1998
- [264] Hufschmidt A, Lücking CH. *Neurologie Compact*. Stuttgart: Thieme; 1999
- [265] Huk WJ, Gademann G, Friedmann G. *Magnetic Resonance Imaging of Central Nervous System Diseases*. Berlin: Springer; 1990
- [266] Isaacson RL. *The Limbic System*. New York, NY: Plenum; 1982
- [267] Iversen SD. Do hippocampal lesions produce amnesia in animals? *Int Rev Neurobiol*. 1976; 19:1–49
- [268] Jamieson D, Alavi A, Jolles P, Chawluk J, Reivich M. Positron emission tomography in the investigation of central nervous system disorders. *Radiol Clin North Am*. 1988; 26(5):1075–1088
- [269] Jannetta PJ. Observations on the etiology of trigeminal neuralgia, hemifacial spasm, acoustic nerve dysfunction and glossopharyngeal neuralgia. Definitive microsurgical treatment and results in 117 patients. *Neurochirurgia (Stuttg)*. 1977; 20(5):145–154
- [270] Jannetta PJ. Hemifacial spasm. In: Samii M, Jannetta PJ, eds. *The Cranial Nerves*. Berlin: Springer; 1981:484–493
- [271] Jannetta PJ, Bennett MH. The pathophysiology of trigeminal neuralgia. In: Samii M, Jannetta PJ, eds. *The Cranial Nerves*. Berlin: Springer; 1981:312–315
- [272] Jansen O, Forsting M, Sartor K, eds. *Neuroradiologie*, 4th ed. Stuttgart: Thieme; 2008
- [273] Jansen O, Schellinger PD, Fiebach JB, et al. Magnetresonanztomographie beim akuten Schlaganfall. *Dtsch Arztebl*. 2002; 99:1065–1070
- [274] Jørgensen G. *Atlas Anatomicum Cerebri Humani*. Amsterdam: Scheltema and Holkema N.V.; 1931
- [275] Jinkins JR. Encephalopathic cerebrovascular steal: dynamic CT of arteriovenous malformations. *Neuroradiology*. 1988; 30(3):201–210
- [276] Johst S, Wrede KH, Ladd ME, Maderwald S. Time-of-flight magnetic resonance angiography at 7 T using venous saturation pulses with reduced flip angles. *Invest Radiol*. 2012; 47(8):445–450
- [277] Jolesz FA, Kikinis R. Intraoperative imaging revolutionizes therapy. *Diagn Imaging (San Franc)*. 1995; 17(9):62–68
- [278] Jones EG. *The Thalamus*. New York, NY: Plenum; 1985
- [279] Joseph J-P. Communications: le rôle fonctionnel du cortex auditif: comparaison homme-animal. *Rev Laryngol*. 1980; 101:327–334
- [280] Jueptner M, Krukenberg M. Motor system: cortex, basal ganglia, and cerebellum. *Neuroimaging Clin N Am*. 2001; 11(2):203–219, viii
- [281] Kahle W, Frotscher M. *Taschenatlas der Anatomie*. Bd. 3: Nervensystem und Sinnesorgane. Stuttgart: Thieme; 2001
- [282] Kalender WA, Wedding K, Polacin A, et al. Grundlagen der Gefäßdarstellung mit Spiral-CT. *Akt Radiol*. 1994; 4:287–297
- [283] Kandel ER, Schwartz JH, Jessel TM, eds. *Principles of Neural Science*. New York, NY: McGraw-Hill, Health Professions; 2000
- [284] Kanski JJ, Spitznas M. *Lehrbuch der klinischen Ophthalmologie*. Stuttgart: Thieme; 1996
- [285] Kantarci M, Karasen RM, Alper F, Onbas O, Okur A, Karaman A. Remarkable anatomic variations in paranasal sinus region and their clinical importance. *Eur J Radiol*. 2004; 50(3):296–302
- [286] Karus M, Blaess S, Brüstle O. Self-organization of neural tissue architectures from pluripotent stem cells. *J Comp Neurol*. 2014; 522(12):2831–2844
- [287] Bundesvereinigung K. Richtlinien über Kriterien zur Qualitätsbeurteilung der Kernspintomographie. *Dtsch Arztebl*. 2001; 98:634–643
- [288] Kelter S. Aphasien. Hirnorganisch bedingte Sprachstörungen und kognitive Wissenschaft. Psychiatrie, Neurologie, Klinische Psychologie. Grundlagen-Methoden-Ergebnisse. In: Baumgartner G, Cohen R, Grüsser O-J et al., Hrsg. Stuttgart: Kohlhammer; 1990
- [289] Keros P. Über die praktische Bedeutung der Niveauunterschiede der Lamina cribrosa des Ethmoides. *Laryngol Rhinol Otol (Stuttg)*. 1965; 41:808–813
- [290] von Keyserlingk DG, Niemann K, Wasel J. A quantitative approach to spatial variation of human cerebral sulci. *Acta Anat (Basel)*. 1988; 131(2):127–131
- [291] Kido DK, LeMay M, Levinson AW, Benson WE. Computed tomographic localization of the precentral gyrus. *Radiology*. 1980; 135(2):373–377
- [292] Kim JS, Lee JH, Choi CG. Patterns of lateral medullary infarction: vascular lesion-magnetic resonance imaging correlation of 34 cases. *Stroke*. 1998; 29(3):645–652
- [293] Kim KHS, Relkin NR, Lee KM, Hirsch J. Distinct cortical areas associated with native and second languages. *Nature*. 1997; 388(6638):171–174
- [294] Kleinschmidt A, Nitschke MF, Frahm J. Somatotopy in the human motor cortex hand area. A high-resolution functional MRI study. *Eur J Neurosci*. 1997; 9(10):2178–2186
- [295] Klingler J. *Die makroskopische Anatomie der Ammonsformation*. Denkschriften der Schweizerischen Naturforschenden Gesellschaft. Bd. 78, Teil 1. Zürich: Fretz; 1948
- [296] van der Knaap MS, Valk J. MR imaging of the various stages of normal myelination during the first year of life. *Neuroradiology*. 1990; 31(6):459–470
- [297] van der Knaap MS, Valk J. *Magnetic Resonance of Myelin, Myelination and Myelin Disorders*. Berlin: Springer; 2011
- [298] Knecht S, Ringelstein E-B. Neuronale Plastizität am Beispiel des somatosensorischen Systems. *Nervenarzt*. 1999; 70(10):889–898
- [299] Knudsen PA. Ventrikulernes størrelseforhold i anatomisk normale hjerner fra voksne mennesker. Odense: Andelsbogtrykkeriet; 1958
- [300] Knutson B, Taylor J, Kaufman M, Peterson R, Glover G. Distributed neural representation of expected value. *J Neurosci*. 2005; 25(19):4806–4812
- [301] Koenig M, Klotz E, Luka B, Venderink DJ, Spittler JF, Heuser L. Perfusion CT of the brain: diagnostic approach for early detection of ischemic stroke. *Radiology*. 1998; 209(1):85–93
- [302] Kömpf D, Heide W. Zentralnervöse Strukturen—two goals, two modes, six systems. In: Huber A, Kömpf D, eds. *Klinische Neuroophthalmologie*. Stuttgart: Thieme; 1998:48–57
- [303] Konitzer M. Pathologie und Klinik des posterioren Thalamus. Vier Eigenbeobachtungen und eine Übersicht zum Thalamussyndrom nach Dejerine und Roussy. *Nervenarzt*. 1987; 58(7):413–423

- [304] Kosfeld M, Heinrichs M, Zak PJ, Fischbacher U, Fehr E. Oxytocin increases trust in humans. *Nature*. 2005; 435(7042):673–676
- [305] Koesling S, Kunkel P, Schul T. Vascular anomalies, sutures and small canals of the temporal bone on axial CT. *Eur J Radiol*. 2005; 54(3):335–343
- [306] Köster O. Computertomographie des Felsenbeines. Stuttgart: Thieme; 2004
- [307] Krayenbühl H, Yasargil MG. Cerebral Angiography. Stuttgart: Thieme; 1982
- [308] Kretschmann H-J. Localisation of the corticospinal fibres in the internal capsule in man. *J Anat*. 1988; 160:219–225
- [309] Kretschmann H-J, Kammradt G, Krauthausen I, et al. Growth of the hippocampal formation in man. *Bibliotheca anatomica*. Basel Karger Band. 1986; 28:27–52
- [310] Kretschmann H-J, Schleicher A, Grottschreiber J-F, Kullmann W. The Yakovlev Collection. A pilot study of its suitability for the morphometric documentation of the human brain. *J Neurol Sci*. 1979; 43(1):111–126
- [311] Kretschmann H-J, Tafesse U, Herrmann A. Different volume changes of cerebral cortex and white matter during histological preparation. *Microsc Acta*. 1982; 86(1):13–24
- [312] Kretschmann H-J, Weinrich W, Fiekert W, et al. Dreidimensionale Computergraphik neurofunktioneller Systeme. Stuttgart: Thieme; 1996
- [313] Kretschmann H-J, Weinrich W, Gerke M, et al. Dreidimensionale Computergraphik neurofunktioneller Systeme. CD-ROM. Stuttgart: Thieme; 1998
- [314] Kretschmann H-J, Weinrich W, Gerke M, et al. Neurofunctional Systems. CD-ROM. Stuttgart: Thieme; 1999
- [315] Krieg WJS. Functional Neuroanatomy. Bloomington, IL: Pantagraph Printing; 1966
- [316] Krieg WJS. Architectonics of human Cerebral Fiber Systems. Evanston, IL: Brain Books; 1973
- [317] Kringelbach ML, Rolls ET. The functional neuroanatomy of the human orbitofrontal cortex: evidence from neuroimaging and neuropsychology. *Prog Neurobiol*. 2004; 72(5):341–372
- [318] Krings T, Coenen VA, Axer H, et al. Three-dimensional visualization of motor cortex and pyramidal tracts employing functional and diffusion weighted MRI. *Klin Neuroradiol*. 2001; 11:105–121
- [319] Krönauer A. Computerunterstützte dreidimensionale Rekonstruktion der Basalganglien als Referenz für die bildgebenden Verfahren (Computertomographie, Magnetische Resonanztomographie und Positronen-Emissionstomographie). Medizinische Dissertation der Medizinische Hochschule Hannover; 1987
- [320] Kuhn MJ. Atlas der Neuroradiologie. Weinheim: Chapman & Hall; 1994
- [321] von Kummer R, Bozzao L, Manelfe C. Early CT Diagnosis of Hemispheric Infarction. Berlin: Springer; 1995
- [322] Kuni CC, DuCret RP. Manual of Nuclear Medicine Imaging. Stuttgart: Thieme; 1997
- [323] Kunze K, ed. Praxis der Neurologie. Stuttgart: Thieme; 1999
- [324] Kunze K, Zangemeister WH, Arlt A, eds. Clinical Problems of Brainstem Disorders. Stuttgart: Thieme; 1986
- [325] Künzle H, Akert K. Efferent connections of cortical, area 8 (frontal eye field) in *Macaca fascicularis*. A reinvestigation using the autoradiographic technique. *J Comp Neurol*. 1977; 173(1):147–164
- [326] Kuypers HGJM. Corticobulbar connexions to the pons and lower brain-stem in man. *Brain*. 1958; 81:364–388
- [327] Kuypers HGJM. Central cortical projections to motor and somatosensory cell groups. *Brain*. 1960; 83:161–184
- [328] Kuypers HGJM. Anatomy of the descending pathways. In: Brooks VB, ed. Handbook of physiology. Sec. 1: The Nervous System. Vol. 2: Motor Control, part 2. (American physiological society. ser.) Baltimore, MD: Williams and Wilkins; 1981:597–666
- [329] Kwon HG, Kim OL, Kim SH, Lee DG, Byun WM, Jang SH. Cortical reorganization of hand motor function to face somatotopy in a patient with brain injury: a functional MRI study. *NeuroRehabilitation*. 2011; 29(3):271–274
- [330] Lanfermann H, Herminghaus S, Pilatus U, et al. Grundlagen der 1H-MR-Spektroskopie intrakranieller Tumoren. *Klin Neuroradiol*. 2002; 12:1–17
- [331] Lanfermann H, Herminghaus S, Pilatus U, et al. Bedeutung der 1H-MR-Spektroskopie bei der Differenzialdiagnose und Gradiierung intrakranieller Tumoren. *Dtsch Arztebl*. 2004; 101:64
- [332] Lang J. Kopf, Gehirn- und Augenschädel. In: von Lanz T, Wachsmuth W, Hrsg. Praktische Anatomie. Bd. 1, Teil 1B. Berlin: Springer; 1979
- [333] Lang J. Klinische Anatomie des Kopfes. Neurokranium, Orbita, kraniozervikaler Übergang. Berlin: Springer; 1981
- [334] Lang J. Klinische Anatomie der Nase, Nasenhöhle und Nebenhöhlen. Stuttgart: Thieme; 1988
- [335] Lang J, Reiter U. Über die intrazisternale Länge der Hirnnerven VII–XII. *Neurochirurgia (Stuttg)*. 1985; 28(4):153–157
- [336] Lang J, Jensen H-P, Schröder F. Praktische Anatomie. In: von Lanz T, Wachsmuth W, Hrsg. Bd. 1, Teil 1: Kopf, Teil A: Übergeordnete Systeme. Berlin: Springer; 1985
- [337] Lang J, Stefanec P, Breitenbach W. Über Form und Masse des Ventriculus tertius, von Sehbahnanteilen und des N. oculomotorius. *Neurochirurgia (Stuttg)*. 1983; 26(1):1–5
- [338] Langer T, Fuchs AF, Scudder CA, Chubb MC. Afferents to the flocculus of the cerebellum in the rhesus macaque as revealed by retrograde transport of horseradish peroxidase. *J Comp Neurol*. 1985; 235(1):1–25
- [339] von Lanz T, Wachsmuth W. Praktische Anatomie. Bd. 1, Teil 2: Hals. Berlin: Springer; 1955
- [340] Larsell O. The Comparative Anatomy and Histology of the Cerebellum. Minneapolis, MN: University of Minnesota Press; 1970
- [341] Lasjaunias P, Berenstein A, ter Brugge KG. Surgical Neuroangiography. Berlin: Springer; 2001
- [342] Lassek AM. The Pyramidal Tract. Springfield, IL: Thomas; 1954
- [343] Last RJ, Tompsett DH. Casts of the cerebral ventricles. *Br J Surg*. 1953; 40(164):525–543
- [344] Laubenberger T, Laubenberger J. Technik der medizinischen Radiologie. Köln: Deutscher Ärzteverlag; 1999
- [345] Lazzaro NA, Wright B, Castillo M, et al. Artery of percheron infarction: imaging patterns and clinical spectrum. *AJNR Am J Neuroradiol*. 2010; 31(7):1283–1289
- [346] Leblanc A. The Cranial Nerves. Anatomy, Imaging, Vascularisation. Berlin: Springer; 1995
- [347] Leblanc A. Encephalo-Peripheral Nervous System. Berlin: Springer; 2001
- [348] LeDoux JE. Emotion circuits in the brain. *Annu Rev Neurosci*. 2000; 23:155–184
- [349] Lee MH, Hacker CD, Snyder AZ, et al. Clustering of resting state networks. *PLoS One*. 2012; 7(7):e40370
- [350] Lee SH, Rao KCVG, Zimmerman RA. Cranial MRI and CT. 4th ed. New York, NY: McGraw-Hill; 1998
- [351] Leigh RJ, Zee DS. The Neurology of Eye Movements. Philadelphia, PA: Davis; 1999
- [352] Leischner A. Aphasien und Sprachentwicklungsstörungen. Klinik und Behandlung. Stuttgart: Thieme; 1987
- [353] LeMay M. Asymmetries of the skull and handedness. *Phrenology revisited*. *J Neurol Sci*. 1977; 32(2):243–253
- [354] Lemke B. Validierung eines Matching-Verfahrens zur Projektion anatomischer 3D-Modelle von zentralen Gehirnstrukturen auf MR-Bilder. Medizinische Dissertation der Medizinischen Hochschule Hannover; 1996
- [355] Leonard CM, Martinez P, Weintraub BD, Hauser P. Magnetic resonance imaging of cerebral anomalies in subjects with resistance to thyroid hormone. *Am J Med Genet*. 1995; 60(3):238–243
- [356] Leonhardt H. Ependym und circumventriculäre Organe. In: von Möllendorff W, Bargmann W, Oksche A et al., Hrsg. Handbuch der mikroskopischen Anatomie des Menschen. Bd. 4: Nervensystem, Teil 10. Berlin: Springer; 1980:177–666
- [357] Levin DN, Pelizzari CA, Chen GTY, Chen CT, Cooper MD. Retrospective geometric correlation of MR, CT, and PET images. *Radiology*. 1988; 169(3):817–823

- [358] Liegeois-Chauvel C, Musolino A, Chauvel P. Localization of the primary auditory area in man. *Brain*. 1991; 114 (Pt 1A):139–151
- [359] Liepert J, Bauder H, Miltner WHR, et al. Therapie-induzierte kortikale Reorganisation bei Schlaganfallpatienten. *Neurol Rehabil*. 2000; 6:177–183
- [360] Lindenberg R. Die Gefäßversorgung und ihre Bedeutung für Art und Ort von kreislaufbedingten Gewebsschäden und Gefäßprozessen. In: Lubarsch O, Henke F, Rössle R et al., Hrsg. *Handbuch der speziellen pathologischen Anatomie und Histologie*. Bd. 13: Nervensystem, Teil 1/B. Berlin: Springer; 1957:1071–1164
- [361] Lindquist KA, Barrett LF. A functional architecture of the human brain: emerging insights from the science of emotion. *Trends Cogn Sci*. 2012; 16(11):533–540
- [362] Lindquist KA, Wager TD, Kober H, Bliss-Moreau E, Barrett LF. The brain basis of emotion: a meta-analytic review. *Behav Brain Sci*. 2012; 35(3):121–143
- [363] Lippert H. *Lehrbuch Anatomie*. München: Urban und Schwarzenberg; 2000
- [364] Lissner J, Seiderer M, eds. *Klinische Kernspintomographie*. Stuttgart: Enke; 1990
- [365] Lloyd GAS. *Diagnostic Imaging of the Nose and Paranasal Sinuses*. London: Springer; 1988
- [366] Lowitzsch K, Hopf HC, Buchner H, et al. *Das EP-Buch*. Stuttgart: Thieme; 2000
- [367] Lübke WT. Computerunterstützte dreidimensionale Rekonstruktion des Kleinhirns als Referenz für die bildgebenden Verfahren (Computertomographie, Magnetische Resonanztomographie und Positronen-Emissionstomographie). Medizinische Dissertation der Medizinischen Hochschule Hannover; 1994
- [368] Ludwig E, Klingler J. *Atlas Cerebri Humani*. Basel: Karger; 1956
- [369] Lund VJ, Stammberger H, Fokkens WJ, et al. European position paper on the anatomical terminology of the internal nose and paranasal sinuses. *Rhinol Suppl*. 2014; 24 (Suppl. 24):1–34
- [370] Lundberg JM, Hökfelt T. Coexistence of peptides and classical neurotransmitters. *Trends Neurosci*. 1983; 6:325–333
- [371] Lurito JT, Dziedzic M. Determination of cerebral hemisphere language dominance with functional magnetic resonance imaging. *Neuroimaging Clin N Am*. 2001; 11(2):355–363, x
- [372] McClure SM, Berns GS, Montague PR. Temporal prediction errors in a passive learning task activate human striatum. *Neuron*. 2003; 38(2):339–346
- [373] McGeer PL, Eccles JC, McGeer EG. *Molecular Neurobiology of the Mammalian Brain*. New York, NY: Plenum; 1987
- [374] McGraw P, Mathews VP, Wang Y, Phillips MD. Approach to functional magnetic resonance imaging of language based on models of language organization. *Neuroimaging Clin N Am*. 2001; 11(2):343–353, x
- [375] Macht S, Turowski B. *Neuroradiologische Diagnostik und Interventionen bei Prozessen an der Schädelbasis*. HNO. 2011; 59(4):340–349
- [376] Madeline LA, Elster AD. Suture closure in the human chondrocranium: CT assessment. *Radiology*. 1995; 196(3):747–756
- [377] Mai JK, Assheuer JK, Paxinos G. *Atlas of the Human Brain*. San Diego, CA: Academic Press; 1997
- [378] Mai JK, Stephens PH, Hopf A, Cuello AC. Substance P in the human brain. *Neuroscience*. 1986; 17(3):709–739
- [379] Mai JK, Triepel J, Metz J. Neurotensin in the human brain. *Neuroscience*. 1987; 22(2):499–524
- [380] Maiden-Tilsen M. Computergestützte 3D-Rekonstruktion des 3. Neurons des intrakraniellen somatosensorischen Trigeminiussystems als Referenz für die bildgebenden Verfahren (unveröffentlicht)
- [381] Malach R, Reppas JB, Benson RR, et al. Object-related activity revealed by functional magnetic resonance imaging in human occipital cortex. *Proc Natl Acad Sci U S A*. 1995; 92(18):8135–8139
- [382] Mann DMA, Yates PO, Marcyniuk B. A comparison of changes in the nucleus basalis and locus caeruleus in Alzheimer's disease. *J Neurol Neurosurg Psychiatry*. 1984; 47(2):201–203
- [383] Marino R, Jr, Rasmussen T. Visual field changes after temporal lobectomy in man. *Neurology*. 1968; 18(9):825–835
- [384] Martin E, Kikinis R, Zuerrer M, et al. Developmental stages of human brain: an MR study. *J Comput Assist Tomogr*. 1988; 12(6):917–922
- [385] Martin JH. *Neuroanatomy. Text and Atlas*. New York, NY: Elsevier; 1996
- [386] Martin WRW, Beckman JH, Calne DB, et al. Cerebral glucose metabolism in Parkinson's disease. *Can J Neurol Sci*. 1984; 11((1, Suppl)):169–173
- [387] Maurer J. *Neurootologie*. Stuttgart: Thieme; 1999
- [388] Mawad ME, Silver AJ, Hilal SK, Ganti SR. Computed tomography of the brain stem with intrathecal metrizamide. Part I: the normal brain stem. *AJR Am J Roentgenol*. 1983; 140(3):553–563
- [389] Meese W, Kluge W, Grumme T, Hopfenmüller W. CT evaluation of the CSF spaces of healthy persons. *Neuroradiology*. 1980; 19(3):131–136
- [390] Meisenzahl EM, Schlösser R. Functional magnetic resonance imaging research in psychiatry. *Neuroimaging Clin N Am*. 2001; 11(2):365–374, x
- [391] Mesulam MM. From sensation to cognition. *Brain*. 1998; 121(Pt 6):1013–1052
- [392] Mesulam MM, Mufson EJ, Levey AI, Wainer BH. Cholinergic innervation of cortex by the basal forebrain: cytochemistry and cortical connections of the septal area, diagonal band nuclei, nucleus basalis (substantia innominata), and hypothalamus in the rhesus monkey. *J Comp Neurol*. 1983; 214(2):170–197
- [393] Meyer-Lindenberg A, Domes G, Kirsch P, Heinrichs M. Oxytocin and vasopressin in the human brain: social neuropeptides for translational medicine. *Nat Rev Neurosci*. 2011; 12(9):524–538
- [394] Miller DH, Kesselring J, McDonald WI, et al. *Magnetresonanz bei Multipler Sklerose*. Stuttgart: Kohlhammer; 1998
- [395] Möller TB, Reif E. *Taschenatlas der Schnittbildanatomie*. Bd. 1 Computertomographie, Kernspintomographie Kopf, Hals, Wirbelsäule, Gelenke. Stuttgart: Thieme; 2005
- [396] Möller TB, Reif E. *Taschenatlas Einstelltechnik Röntgendiagnostik, Angiographie, CT, MRT*. Stuttgart: Thieme; 2009
- [397] Möller-Hartmann W, Herminghaus S, Krings T, et al. Clinical application of proton magnetic resonance spectroscopy in the diagnosis of intracranial mass lesions. *Neuroradiology*. 2002; 44(5):371–381
- [398] Moonen CTW, Bandettini PA, eds. *Functional MRI*. Berlin: Springer; 2000
- [399] Moore JK, Karapas F, Moore RY. Projections of the inferior colliculus in insectivores and primates. *Brain Behav Evol*. 1977; 14(5):301–327
- [400] Moore RY, Bloom FE. Central catecholamine neuron systems: anatomy and physiology of the dopamine systems. *Annu Rev Neurosci*. 1978; 1:129–169
- [401] Moore RY, Bloom FE. Central catecholamine neuron systems: anatomy and physiology of the norepinephrine and epinephrine systems. *Annu Rev Neurosci*. 1979; 2:113–168
- [402] Mori K. Anomalies of the central nervous system. In: Nadjmi M, Harwood-Nash DE, eds. *Stuttgart: Thieme*; 1985
- [403] Moussa MN, Steen MR, Laurienti PJ, Hayasaka S. Consistency of network modules in resting-state fMRI connectome data. *PLoS One*. 2012; 7(8):e44428
- [404] Mugler JP III, Kiefer B, Brookeman JR. Three-dimensional T2-weighted imaging of the brain using very long spin-echo trains. *Proceedings of the International Society for Magnetic Resonance in medicine 2000 Eighth meeting, Denver Abstract 687*
- [405] Müller D. unveröffentlichtes manuskript; 1996
- [406]
- [407] Müller-Forell W. Bildgebende Diagnostik von Orbitaerkrankungen. *Klin Neuroradiol*. 2002; 12:101–126
- [408] Mumenthaler M. *Neurologische Differentialdiagnostik*. Stuttgart: Thieme; 1997
- [409] Mumenthaler M, Mattle H. *Neurologie*. Stuttgart: Thieme; 1997

- [410] Muramoto O, Kuru Y, Sugishita M, Toyokura Y. Pure memory loss with hippocampal lesions: a pneumoencephalographic study. *Arch Neurol*. 1979; 36(1):54–56
- [411] Nadimi M, Piepgras U, Vogelsang H. Kranielle Computertomographie. Stuttgart: Thieme; 1986
- [412] Naidich TP, Valavanis AG, Kubik S. Anatomic relationships along the low-middle convexity: part I—normal specimens and magnetic resonance imaging. *Neurosurgery*. 1995; 36(3):517–532
- [413] Naidich T, Brightbill TC. Systems for localizing frontoparietal gyri and sulci on axial CT and MRI. *Int J Neuroradiol*. 1996; 4:313–338
- [414] Naidich TP, Daniels DL, Haughton VM, Williams A, Pojunas K, Palacios E. Hippocampal formation and related structures of the limbic lobe: anatomic-MR correlation. Part I. Surface features and coronal sections. *Radiology*. 1987; 162(3):747–754
- [415] Naidich TP, Daniels DL, Haughton VM, et al. Hippocampal formation and related structures of the limbic lobe: anatomic-MR correlation. Part II. Sagittal sections. *Radiology*. 1987; 162(3):755–761
- [416] Naidich TP, Daniels DL, Pech P, Haughton VM, Williams A, Pojunas K. Anterior commissure: anatomic-MR correlation and use as a landmark in three orthogonal planes. *Radiology*. 1986; 158(2):421–429
- [417] Naidich TP, Hof PR, Gannon PJ, Yousry TA, Yousry I. Anatomic substrates of language: emphasizing speech. *Neuroimaging Clin N Am*. 2001; 11(2):305–341, ix
- [418] Naidich TP, Hof PR, Yousry TA, Yousry I. The motor cortex: anatomic substrates of function. *Neuroimaging Clin N Am*. 2001; 11(2):171–193, vii–viii
- [419] Naidich TP, Leeds NE, Kricheff II, Pudlowski RM, Naidich JB, Zimmerman RD. The tentorium in axial section. I. Normal CT appearance and non-neoplastic pathology. *Radiology*. 1977; 123(3):631–638
- [420] Nelson SJ. Multivoxel magnetic resonance spectroscopy of brain tumors. *Mol Cancer Ther*. 2003; 2(5):497–507
- [421] Nelson SJ, Vigneron DB, Dillon WP. Serial evaluation of patients with brain tumors using volume MRI and 3D 1H MRSI. *NMR Biomed*. 1999; 12(3):123–138
- [422] Neuerburg-Heusler D, Hennerici MG. Gefäßdiagnostik mit Ultraschall. Stuttgart: Thieme; 1999
- [423] Nieuwenhuys R. Chemoarchitecture of the Brain. Berlin: Springer; 1985
- [424] Nieuwenhuys R, Voogd J, van Huijzen C. Das Zentralnervensystem des Menschen. Ein Atlas mit Begleittext. Berlin: Springer; 1980
- [425] Nieuwenhuys R, Voogd J, van Huijzen C. Das Zentralnervensystem des Menschen. Berlin: Springer; 1991
- [426] Nitschke MF, Kleinschmidt A, Wessel K, Frahm J. Somatotopic motor representation in the human anterior cerebellum. A high-resolution functional MRI study. *Brain*. 1996; 119(Pt 3):1023–1029
- [427] Noback CR, Strominger NJ, Demarest RJ. The Nervous System. Baltimore, MD: Williams and Wilkins; 1996
- [428] Nobin A, Björklund A. Topography of the monoamine neuron systems in the human brain as revealed in fetuses. *Acta Physiol Scand Suppl*. 1973; 388(Suppl. 388):1–40
- [429] Northoff G, Qin P, Nakao T. Rest-stimulus interaction in the brain: a review. *Trends Neurosci*. 2010; 33(6):277–284
- [430] Novelline RA, Rhea JT, Rao PM, Stuk JL. Helical CT in emergency radiology. *Radiology*. 1999; 213(2):321–339
- [431] Nygrén L-G, Olson L. A new major projection from locus coeruleus: the main source of noradrenergic nerve terminals in the ventral and dorsal columns of the spinal cord. *Brain Res*. 1977; 132(1):85–93
- [432] Ochsner KN, Gross JJ. The cognitive control of emotion. *Trends Cogn Sci*. 2005; 9(5):242–249
- [433] Ojemann GA. The intrahemispheric organization of human language, derived with electrical stimulation techniques. *Trends Neurosci*. 1983; 6:184–189
- [434] Oldendorf WH. Isolated flying spot detection of radiodensity discontinuities—displaying the internal structural pattern of a complex object. *Ire Trans Biomed Electron*. 1961; BME-8:68–72
- [435] Olson IR, Plotzker A, Ezzyat Y. The Enigmatic temporal pole: a review of findings on social and emotional processing. *Brain*. 2007; 130(Pt 7):1718–1731
- [436] Olszewski J, Baxter D. Cytoarchitecture of the Human Brain Stem. Basel: Karger; 1982
- [437] Ono M, Kubik S, Abernathey CD. Atlas of the Cerebral Sulci. Stuttgart: Thieme; 1990
- [438] Onodi A. Des rapports entre le nerf optique et le sinus sphenoid. La cellule ethmoïdale postérieure en particulier. *Revue Hebd Laryng d'Otol Rhinol*. 1903; 25:72–140
- [439] Oosterwijk S, Lindquist KA, Anderson E, Dautoff R, Moriguchi Y, Barrett LF. States of mind: emotions, body feelings, and thoughts share distributed neural networks. *Neuroimage*. 2012; 62(3):2110–2128
- [440] Osborn AG. The medial tentorium and incisura: normal and pathological anatomy. *Neuroradiology*. 1977; 13(2):109–113
- [441] Osborn AG. Diagnostic Cerebral Angiography. Philadelphia, PA: Lippincott Williams & Wilkins; 1999
- [442] Osborn AG. Osborn's Brain: Imaging Pathology, and Anatomy. Salt Lake City, UT: Amirsys; 2012
- [443] Palacios E, Fine M, Haughton VM. Multiplanar Anatomy of the Head and Neck for Computed Tomography. New York, NY: Wiley; 1980
- [444] Palay L, Chan-Palay V. Cerebellar Cortex. Cytology and Organization. Berlin: Springer; 1974
- [445] Panofsky W, Staemmler M. Untersuchungen über Hirngewicht und Schädelkapazität nach der Reichardt'schen Methode. *Frankf Z Pathol*. 1922; 26:519–549
- [446] Papeschi R. Dopamine, extrapyramidal system, and psychomotor function. *Psychiatr Neurol Neurochir*. 1972; 75(1):13–48
- [447] Parent A. Carpenter's Human Neuroanatomy. Baltimore, MD: Williams and Wilkins; 1996
- [448] Passingham RE. Premotor cortex and preparation for movement. *Exp Brain Res*. 1988; 70(3):590–596
- [449] Patay Z, Enterkin J, Harreld JH, et al. MR imaging evaluation of inferior olivary nuclei: comparison of postoperative subjects with and without posterior fossa syndrome. *AJNR Am J Neuroradiol*. 2014; 35(4):797–802
- [450] Patten JP. Neurologische Differentialdiagnose. Berlin: Springer; 1998
- [451] Paulig M. Funktionelle Anatomie des Zentralnervensystems. In: Sturm W, Herrmann M, Münte TF, ed. Lehrbuch der Klinischen Neuropsychologie. Grundlagen-Methoden-Diagnostik-Therapie. Vol. 11. Heidelberg: Spektrum; 2009:58–67
- [452] Paxinos G, ed. The Human Nervous System. New York, NY: Academic Press; 1990
- [453] Paxinos G, Huang X-F. Atlas of the Human Brainstem. San Diego, CA: Academic Press; 1995
- [454] Penfield W, Rasmussen T. The Cerebral Cortex of Man. A Clinical Study of Localization of Function. New York, NY: Hafner; 1968
- [455] Penfield W, Welch K. The supplementary motor area of the cerebral cortex: a clinical and experimental study. *AMA Arch Neurol Psychiatry*. 1951; 66(3):289–317
- [456] Percheron G. The anatomy of the arterial supply of the human thalamus and its use for the interpretation of the thalamic vascular pathology. *Z Neurol*. 1973; 205(1):1–13
- [457] Perenin MT, Jeannerod M. Subcortical vision in man. *Trends Neurosci*. 1979; 2:204–207
- [458] Pessoa L, Kastner S, Ungerleider LG. Attentional control of the processing of neural and emotional stimuli. *Brain Res Cogn Brain Res*. 2002; 15(1):31–45
- [459] Pessoa L, Padmala S, Morland T. Fate of unattended fearful faces in the amygdala is determined by both attentional resources and cognitive modulation. *Neuroimage*. 2005; 28(1):249–255
- [460] Peters A, Palay SL, de Webster HF. The Fine Structure of the Nervous System: The Neurons and Supporting Cells. Philadelphia, PA: Saunders; 1991

- [461] Petit L, Clark VP, Ingeholm J, Haxby JV. Dissociation of saccade-related and pursuit-related activation in human frontal eye fields as revealed by fMRI. *J Neurophysiol.* 1997; 77(6):3386–3390
- [462] Pfeifer RA. Myelogenetisch-anatomische Untersuchungen über das kortikale Ende der Hörleitung. Leipzig: Teubner; 1920
- [463] Pfeifer RA. Myelogenetisch-anatomische Untersuchungen über den zentralen Abschnitt der Sehleitung. Berlin: Springer; 1925
- [464] Pfeifer RA. Myelogenetisch-anatomische Untersuchungen über den zentralen Abschnitt der Taststrahlung, der Pyramidenbahn, der Hirnnerven und zusätzlicher motorischer Bahnen. *Nova Acta Leopold.* 1934; 1:341–473– (Neue Folge)
- [465] Phillips DP. Introduction to anatomy and physiology of the central auditory nervous system. In: Jahn AF, Santos-Sacchi J, eds. *Physiology of the Ear.* New York, NY: Raven Press; 1988:407–427
- [466] Piepgras U. *Neuroradiologie.* Stuttgart: Thieme; 1977
- [467] Platzer W. *Atlas der topographischen Anatomie.* Stuttgart: Thieme; 1982
- [468] Platzer W. *Atlas der topographischen und angewandten Anatomie des Menschen.* Stuttgart: Thieme; 1994
- [469] Poeck K, Hacke W. *Neurologie.* Berlin: Springer; 2001
- [470] Pompeiano O. Reticular formation. In: Autrum H, Jung R, Loevenstein WR et al., eds. *Handbook of Sensory Physiology.* Vol. 2: Somatosensory System. Berlin: Springer; 1973:381–488
- [471] Pöppel E, Held R, Dowling JE. Neuronal mechanisms in visual perception. *Neurosci Res Program Bull.* 1977; 15(3):313–319, 323–553
- [472] Power JD, Cohen AL, Nelson SM, et al. Functional network organization of the human brain. *Neuron.* 2011; 72(4):665–678
- [473] Putz R, Pabst R. *Sobotta Atlas der Anatomie des Menschen.* Bd. 1: Kopf, Hals, obere Extremität. München: Urban und Fischer; 2000
- [474] Quaknine GE. Microsurgical anatomy of the arterial loops in the ponto-cerebellar angle and the internal acoustic meatus. In: Samii M, Jannetta PJ, eds. *The Cranial Nerves.* Berlin: Springer; 1981:378–390
- [475] Raab P, Hattungen E, Franz K, Zanella FE, Lanfermann H. Cerebral gliomas: diffusional kurtosis imaging analysis of microstructural differences. *Radiology.* 2010; 254(3):876–881
- [476] Raab P, Pilatus U, Lanfermann H, et al. Grundlagen und klinische Anwendung der MR-Spektroskopie des Gehirns. *Akt Neurol.* 2002; 29:53–62
- [477] Radü EW, Kendall BE, Moseley IF. *Computertomographie des Kopfes.* Stuttgart: Thieme; 1994
- [478] Raichle ME, Hartman BK, Eichling JO, Sharpe LG. Central noradrenergic regulation of cerebral blood flow and vascular permeability. *Proc Natl Acad Sci U S A.* 1975; 72(9):3726–3730
- [479] Ramsey R. *Neuroradiology.* Philadelphia, PA: Saunders; 1994
- [480] Ramsey R. *Teaching Atlas of Spine Imaging.* Stuttgart: Thieme; 1999
- [481] Rauber A, Kopsch F, Leonhardt H, et al. *Anatomie des Menschen Band III.* Stuttgart, New York, NY: Thieme; 1988
- [482] Reither M. *Magnetresonanztomographie in der Pädiatrie.* Berlin: Springer; 2000
- [483] Retzius G. *Das Menschenhirn. Studien in der makroskopischen Morphologie.* Bd. 1. Stockholm: Norstedt; 1896
- [484] Reynolds AF, Jr, Harris AB, Ojemann GA, Turner PT. Aphasia and left thalamic hemorrhage. *J Neurosurg.* 1978; 48(4):570–574
- [485] Riley HA. *An Atlas of the Basal Ganglia, Brain Stem, and Spinal Cord.* New York, NY: Hafner; 1960
- [486] Rimmele U, Hediger K, Heinrichs M, Klaver P. Oxytocin makes a face in memory familiar. *J Neurosci.* 2009; 29(1):38–42
- [487] Ring BA, Waddington MM. Roentgenographic anatomy of the pericallosal arteries. *Am J Roentgenol Radium Ther Nucl Med.* 1968; 104(1):109–118
- [488] Rohen JW, Yokochi C. *Anatomie des Menschen. Photographischer Atlas der systematischen und topographischen Anatomie.* Stuttgart: Schattauer; 1993
- [489] Rohkamm R. *Taschenatlas Neurologie.* Stuttgart: Thieme; 2000
- [490] Roland PE. Metabolic measurement of the working frontal cortex in man. *Trends Neurosci.* 1984; 7:430–435
- [491] Roland PE. Cortical organization of voluntary behavior in man. *Hum Neurobiol.* 1985; 4(3):155–167
- [492] Roland PE, Skinhøj E, Lassen NA, Larsen B. Different cortical areas in man in organization of voluntary movements in extra-personal space. *J Neurophysiol.* 1980; 43(1):137–150
- [493] Rolls ET, Grabenhorst F. The orbitofrontal cortex and beyond: from affect to decision-making. *Prog Neurobiol.* 2008; 86(3):216–244
- [494] Rorden C, Karnath H-O. Using human brain lesions to infer function: a relic from a past era in the fMRI age? *Nat Rev Neurosci.* 2004; 5(10):813–819
- [495] Rosazza C, Minati L. Resting-state brain networks: literature review and clinical applications. *Neurol Sci.* 2011; 32(5):773–785
- [496] Rosene DL, Van Hoesen GW. Hippocampal efferents reach widespread areas of cerebral cortex and amygdala in the rhesus monkey. *Science.* 1977; 198(4314):315–317
- [497] Ross ED. Localization of the pyramidal tract in the internal capsule by whole brain dissection. *Neurology.* 1980; 30(1):59–64
- [498] Röther J, Gass A, Busch E. Diffusions- und perfusionsgewichtete Magnetresonanztomographie bei der zerebralen Ischämie. *Akt Neurol.* 1999; 26:300–308
- [499] Röhlig W. Korrelationen zwischen Gesamthirn- und Kleinhirngewicht des Menschen im Laufe der Ontogenese. *J Hirnforsch.* 1974; 15(3):203–209
- [500] Rubin GD, Shiao MC, Schmidt AJ, et al. Computed tomographic angiography: historical perspective and new state-of-the-art using multi detector-row helical computed tomography. *J Comput Assist Tomogr.* 1999; 23(Suppl 1):S83–S90
- [501] Rumeau C, Tzourio N, Murayama N, et al. Location of hand function in the sensorimotor cortex: MR and functional correlation. *AJNR Am J Neuroradiol.* 1994; 15(3):567–572
- [502] Rutherford M, ed. *MRI of the Neonatal Brain.* London: Saunders; 2002
- [503] Sabattini L. Evaluation and measurement of the normal ventricular and subarachnoid spaces by CT. *Neuroradiology.* 1982; 23(1):1–5
- [504] Sadler TW. *Medizinische Embryologie.* Stuttgart: Thieme; 1998
- [505] Salvolini U, Cabanis EA, Rodallec A, Menichelli F, Pasquini U, Iba-Zizen MT. Computed tomography of the optic nerve: part I. Normal results. *J Comput Assist Tomogr.* 1978; 2(2):141–149
- [506] Samii M, Draf W. *Surgery of the Skull Base.* Berlin: Springer; 1989
- [507] Samii M, Jannetta PJ, eds. *The Cranial Nerves.* Berlin: Springer; 1981
- [508] Sanides F. Representation in the cerebral cortex and its areal lamination patterns. In: Bourne GH, ed. *The Structure and Function of Nervous Tissue.* New York, NY: Academic Press; 1972:329–453
- [509] Sanides F, Vitzthum H. Zur Architektonik der menschlichen Sehrinde und dem Prinzip ihrer Entwicklung. *Dtsch Z Nervenheilkd.* 1965; 187:680–707
- [510] Saper CB, Petit CK. Correspondence of melanin-pigmented neurons in human brain with A1-A14 catecholamine cell groups. *Brain.* 1982; 105(Pt 1):87–101
- [511] Sarkisoff SA, Filimonoff IN. *Atlas du cerveau de l'homme et des animaux.* Moscou: Institut du Cerveau de C.C.E. de-LURSS; 1937
- [512] Sartor KMR. *Imaging of the Skull and Brain.* Berlin: Springer; 1992
- [513] Savoiardo M, Bracchi M, Passerini A, Visciani A. The vascular territories in the cerebellum and brainstem: CT and MR study. *AJNR Am J Neuroradiol.* 1987; 8(2):199–209
- [514] Schachter S, Singer JE. Cognitive, social, and physiological determinants of emotional state. *Psychol Rev.* 1962; 69:379–399
- [515] Schaltenbrand G, Walker AE, eds. *Stereotaxy of the Human Brain. Anatomical, Physiological and Clinical Applications.* Stuttgart: Thieme; 1982
- [516] Schardt DM, Erk S, Nüsser C, et al. Volition diminishes genetically mediated amygdala hyperreactivity. *Neuroimage.* 2010; 53(3):943–951

- [517] Schering. Lexikon der Radiologie. Bearbeitet von der Lexikonredaktion des Verlages. Berlin: Blackwell Wissenschaftsverlag; 2005
- [518] Schiebeler TH, Schmidt W, Zilles K, eds. Anatomie. Berlin: Springer; 1999
- [519] Schild H. RRR Angiographie. 2. Aufl. Stuttgart: Thieme; 2003
- [520] Schirmer M. Neurochirurgie. München: Urban und Schwarzenberg; 1998
- [521] Schlegel U, Westphal M. Neuroonkologie. Stuttgart: Thieme; 1998
- [522] Schliack H, Hopf HC, eds. Diagnostik in der Neurologie. Stuttgart: Thieme; 1988
- [523] Schmähmann JD. Cerebellum and brainstem. In: Toga AW, Mazziotta JC. Brain Mapping. San Diego, CA: Academic Press; 2000:207–259
- [524] Schmähmann JD, Doyon J, McDonald D, et al. Three-dimensional MRI atlas of the human cerebellum in proportional stereotaxic space. Neuroimage. 1999; 10(3 Pt 1):233–260
- [525] Schmähmann JD, Loeber RT, Marjani J, et al. Topographic organization of cognitive functions in the human cerebellum. A meta-analysis of functional imaging studies. Neuroimage. 1998; 7:5721
- [526] Schmalstieg H, Becker H. 3D-CT der Schädelbasis. Klin Neuroradiol. 1995; 5:71–81
- [527] Schmid HM. Über Größe, Form und Lage von Bulbus und Tractus olfactorius des Menschen. Gegenbaurs Morph Jb (Lpzg.). 1973; 119:227–237
- [528] Schmidt AM. Computergestützte 3D-Rekonstruktion des trigeminalen Systems—vom Hirnstamm bis zum Eintritt in den Thalamus—als Referenz für die bildgebenden Verfahren CT, MRT und PET. Dissertation der Medizinischen Hochschule Hannover; 2002
- [529] Schmidt AM, Weber BP, Becker H. Functional magnetic resonance imaging of the auditory cortex as a diagnostic tool in cochlear implant candidates. Neuroimaging Clin N Am. 2001; 11(2):297–304, ix
- [530] Schmidt D, Malin J-P, eds. Erkrankungen der Hirnnerven. Stuttgart: Thieme; 1995
- [531] Schmidt RF, Schaible H-G, eds. Neuro- und Sinnesphysiologie. Berlin: Springer; 2001
- [532] Schneider JS, Lidsky TL, eds. Basal Ganglia and Behavior: Sensory Aspects of Motor Functioning. Toronto: Huber; 1987
- [533] Schnitzlein HN, Murtagh FR. Imaging Anatomy of the Head and Spine. Baltimore, MD: Urban und Schwarzenberg; 1990
- [534] Schnyder H, Reisine H, Hepp K, Henn V. Frontal eye field projection to the paramedian pontine reticular formation traced with wheat germ agglutinin in the monkey. Brain Res. 1985; 329(1–2):151–160
- [535] Schultze WH. Über Messungen und Untersuchungen des Liquor cerebrospinalis an der Leiche. In: Schmidt MB, Berblinger W, Hrsg. Centralblatt für allgemeine Pathologie und pathologische Anatomie. Ergänzungsheft zum Bd. 33. Jena: Fischer; 1923:291–296
- [536] Schünke M, Schulte E, Schumacher U. Prometheus: LernAtlas der Anatomie. Bd. Kopf, Hals und Neuroanatomie. Illustrationen von M. Voll/K. Wesker. 2. Aufl. Stuttgart: Thieme; 2009
- [537] Schünke M, Schulte E, Schumacher U. Prometheus: LernAtlas der Anatomie. Bd. Kopf, Hals und Neuroanatomie. Illustrationen von M. Voll/K. Wesker. 3. Aufl. Stuttgart: Thieme; 2012
- [538] Seeger W. Atlas of Topographical Anatomy of the Brain and Surrounding Structures for Neurosurgeons, Neuroradiologists, and Neuropathologists. Wien: Springer; 1985
- [539] Seeley WW, Menon V, Schatzberg AF, et al. Dissociable intrinsic connectivity networks for salience processing and executive control. J Neurosci. 2007; 27(9):2349–2356
- [540] Seifritz E, Di Salle F, Bilecen D, Radü EW, Scheffler K. Auditory system: functional magnetic resonance imaging. Neuroimaging Clin N Am. 2001; 11(2):275–296, ix
- [541] Senft C, Hattingen E, Pilatus U, et al. Diagnostic value of proton magnetic resonance spectroscopy in the noninvasive grading of solid gliomas: comparison of maximum and mean choline values. Neurosurgery. 2009; 65(5):908–913, discussion 913
- [542] Silverman SG, Collick BD, Figueira MR, et al. Interactive MR-guided biopsy in an open-configuration MR imaging system. Radiology. 1995; 197(1):175–181
- [543] Singer M, Yakovlev PI. The Human Brain in Sagittal Section. Springfield, IL: Thomas; 1964
- [544] Singer W. Control of thalamic transmission by corticofugal and ascending reticular pathways in the visual system. Physiol Rev. 1977; 57(3):386–420
- [545] Skalej M, Schiefer U, Nägele T, et al. Funktionelle Bildgebung des visuellen Kortex mit der MRT. Klin Neuroradiol. 1995; 5:176–183
- [546] de Slegte RGM, Valk J, Lohman AHM, et al. Cisternographic Anatomy of the Posterior Cranial Fossa. Assen/Maastricht: Van Gorcum; 1986
- [547] Smith CG, Richardson WFG. The course and distribution of the arteries supplying the visual (striate) cortex. Am J Ophthalmol. 1966; 61(6):1391–1396
- [548] Smith EE, Jonides J. Storage and executive processes in the frontal lobes. Science. 1999; 283(5408):1657–1661
- [549] Smith RL. Axonal projections and connections of the principal sensory trigeminal nucleus in the monkey. J Comp Neurol. 1975; 163(3):347–375
- [550] Smith SM, Fox PT, Miller KL, et al. Correspondence of the brain's functional architecture during activation and rest. Proc Natl Acad Sci U S A. 2009; 106(31):13040–13045
- [551] Snyder EY. Neural stem-like cells: developmental lessons with therapeutic potential. Neuroscientist. 1998; 4:408–425
- [552] Soininen HS, Partanen K, Pitkänen A, et al. Volumetric MRI analysis of the amygdala and the hippocampus in subjects with age-associated memory impairment: correlation to visual and verbal memory. Neurology. 1994; 44(9):1660–1668
- [553] Som P, Curtin H. Head and Neck Imaging. 2nd vol. set. 5th ed. Oxford: Elsevier; 2011
- [554] Spreer J, Ziyeh S, Wohlfahrt R, et al. Vergleich verschiedener Paradigmen für die fMRT zur Bestimmung der Hemisphären-dominanz für sprachliche Funktionen. Klin Neuroradiol. 1998; 8:173–181
- [555] Squire LR. Memory systems of the brain: a brief history and current perspective. Neurobiol Learn Mem. 2004; 82(3):171–177
- [556] Starck D. Die Evolution des Säugetier-Gehirns. Wiesbaden: Steiner; 1962
- [557] Starck D. Vergleichende Anatomie der Wirbeltiere. Bd. 3. Berlin: Springer; 1982
- [558] Stark D, Bradley WG. Magnetic Resonance Imaging. St. Louis, MO: Mosby; 1999
- [559] Steen RG, Ogg RJ, Reddick WE, Kingsley PB. Age-related changes in the pediatric brain: quantitative MR evidence of maturational changes during adolescence. AJNR Am J Neuroradiol. 1997; 18(5):819–828
- [560] Steinmetz H, Fürst G, Freund HJ. Cerebral cortical localization: application and validation of the proportional grid system in MR imaging. J Comput Assist Tomogr. 1989; 13(1):10–19
- [561] Stensaas SS, Eddington DK, Dobelle WH. The topography and variability of the primary visual cortex in man. J Neurosurg. 1974; 40(6):747–755
- [562] Stephan H. Allocortex. In: von Möllendorff W, Bargmann W, Oksche A et al., Hrsg. Handbuch der mikroskopischen Anatomie des Menschen. Bd. 4: Nervensystem, Teil 9. Berlin: Springer; 1975
- [563] Stephan H, Andy OJ. Anatomy of the limbic system. In: Schaltenbrand G, Walker AE, eds. Stereotaxy of the Human Brain. Stuttgart: Thieme; 1982:269–292
- [564] Stoeter P, Schumacher M, Huk W, et al. Magnetresonanztomographie in der Neuroradiologie. Leitlinien herausgegeben von der Deutschen Gesellschaft für Neuroradiologie. Klin Neuroradiol 2001; 11:1–5
- [565] Stöhr M, Dichgans J, Diener HC, et al. Evozierte Potentiale SEP–VEP–AEP–EKP–MEP. Berlin: Springer; 1996
- [566] Stoppe G, Hentschel F, Munz DL, eds. Bildgebende Verfahren in der Psychiatrie. Stuttgart: Thieme; 2000

- [567] Sunaert S, Yousry TA. Clinical applications of functional magnetic resonance imaging. *Neuroimaging Clin N Am*. 2001; 11(2):221–236, viii
- [568] Swanson LW. The locus coeruleus: a cytoarchitectonic, Golgi and immunohistochemical study in the albino rat. *Brain Res*. 1976; 110(1):39–56
- [569] Swartz JD, Harnsberger HR. *Imaging of the Temporal Bone*. Stuttgart: Thieme; 1998
- [570] Swobodnik W, Herrmann M, Altwein JE, eds. *Atlas der internistischen Ultraschallanatomie*. Stuttgart: Thieme; 1999
- [571] Tailor J, Andreska T, Kittappa R. From stem cells to dopamine neurons: developmental biology meets neurodegeneration. *CNS Neurol Disord Drug Targets*. 2012; 11(7):893–896
- [572] Tailor J, Kittappa R, Leto K, et al. Stem cells expanded from the human embryonic hindbrain stably retain regional specification and high neurogenic potency. *J Neurosci*. 2013; 33(30):12407–12422
- [573] Takahashi S, ed. *Illustrated Computer Tomography*. Berlin: Springer; 1983
- [574] Talairach J, Tournoux P. *Co-Planar Stereotaxic Atlas of the Human Brain*. Stuttgart: Thieme; 1988
- [575] Talairach J, Szikla G, Tournoux P, et al. *Atlas d'anatomie stéréotaxique du télencéphale*. Paris: Masson; 1967
- [576] Tamraz JC, Comair YG. *Atlas of Regional Anatomy of the Brain Using MRI*. Berlin: Springer; 2000
- [577] Tatu L, Moulin T, Bogousslavsky J, Duvernoy H. Arterial territories of human brain: brainstem and cerebellum. *Neurology*. 1996; 47(5):1125–1135
- [578] Taveras JM, ed. *Radiology*. Vol. 3. Philadelphia, PA: Lippincott/Raven Press; 1996
- [579] Tei H. Monoparesis of the right hand following a localised infarct in the left "precentral knob." *Neuroradiology*. 1999; 41(4):269–270
- [580] Terr LI, Edgerton BJ. Surface topography of the cochlear nuclei in humans: two- and three-dimensional analysis. *Hear Res*. 1985; 17(1):51–59
- [581] Thier P. Das System der langsamen Augenfolgebewegungen. In: Huber A, Kömpf D, eds. *Klinische Neuroophthalmologie*. Stuttgart: Thieme; 1998:65–74
- [582] Thier P. Die funktionelle Architektur des präfrontalen Kortex. In: Karnath H, Thier P, ed. *Neuropsychologie*. Heidelberg: Springer; 2003:495–504
- [583] Thömke F. *Augenbewegungsstörungen*. Stuttgart: Thieme; 2001
- [584] Thurn P, Bücheler E. *Einführung in die radiologische Diagnostik*. Stuttgart: Thieme; 1998
- [585] Tiedemann K. *Anatomy of the Head and Neck: A Multiplanar Atlas for Radiologists and Surgeons*. Weinheim: VCH; 1993
- [586] Timmann D, Kolb FP, Diener HC. Klinische Pathophysiologie der Ataxie. *Klin Neurophysiol*. 1999; 30:128–144
- [587] Toga AW, Mazziotta JC, eds. *Brain Mapping. The Systems*. San Diego, CA: Academic Press; 2000
- [588] Toole JF. *Cerebrovascular Disorders*. Philadelphia, PA: Lippincott, Williams & Wilkins; 1999
- [589] Tranel D, Damasio H, Damasio AR. A neural basis for the retrieval of conceptual knowledge. *Neuropsychologia*. 1997; 35(10):1319–1327
- [590] Truwit C. *High Resolution Atlas of Cranial Neuroanatomy*. Philadelphia, PA: Lippincott; 1994
- [591] Uhlenbrock D. *MRT und MRA des Kopfes*. Stuttgart: Thieme; 2007
- [592] Ullsperger M, von Cramon DY. Subprocesses of performance monitoring: a dissociation of error processing and response competition revealed by event-related fMRI and ERPs. *Neuroimage*. 2001; 14(6):1387–1401
- [593] Ullsperger M, von Cramon DY. The role of intact frontostriatal circuits in error processing. *J Cogn Neurosci*. 2006; 18(4):651–664
- [594] Unterharnscheidt F, Jachnik D, Gött H. *Der Balkenmangel*. Berlin: Springer; 1968
- [595] Valvassori GE, Mafee MF, Carter BL. *Imaging of the Head and Neck*. Stuttgart: Thieme; 1995
- [596] Vanier M, Lecours AR, Ethier R, et al. Proportional localization system for anatomical interpretation of cerebral computed tomograms. *J Comput Assist Tomogr*. 1985; 9(4):715–724
- [597] Vogt BA. Pain and emotion interactions in subregions of the cingulate gyrus. *Nat Rev Neurosci*. 2005; 6(7):533–544
- [598] Vogt BA, Vogt L, Laureys S. Cytology and functionally correlated circuits of human posterior cingulate areas. *Neuroimage*. 2006; 29(2):452–466
- [599] Vogt H. *Ein Algorithmus zur Oberflächenrekonstruktion von Großhirnarterien*. Dissertation der Medizinischen Hochschule Hannover; 1997
- [600] Voogd J. *The Cerebellum of the Cat*. Assen: Van Gorcum; 1964
- [601] Vuilleumier P. How brains beware: neural mechanisms of emotional attention. *Trends Cogn Sci*. 2005; 9(12):585–594
- [602] Waddington MM. *Atlas of cerebral angiography with Anatomic Correlations*. Boston, MA: Little Brown & Co; 1974
- [603] Wagner M, Jurcoane A, Hattingen E. The U sign: tenth landmark to the central region on brain surface reformatted MR imaging. *AJNR Am J Neuroradiol*. 2013; 34(2):323–326
- [604] Wahler-Lück M, Schütz T, Kretschmann H-J. A new anatomical representation of the human visual pathways. *Graefes Arch Clin Exp Ophthalmol*. 1991; 229(3):201–205
- [605] Walker AE. Normal and pathological physiology of the thalamus. In: Schaltenbrand G, Walker AE, eds. *Stereotaxy of the Human Brain*. 2nd ed. Stuttgart: Thieme; 1982:181–217
- [606] Walter H, von Kalckreuth A, Scharadt D, Stephan A, Goschke T, Erk S. The temporal dynamics of voluntary emotion regulation. *PLoS One*. 2009; 4(8):e6726
- [607] Warabi T, Miyasaka K, Inoue K, Nakamura N. Computed tomographic studies of the basis pedunculi in chronic hemiplegic patients: topographic correlation between cerebral lesion and midbrain shrinkage. *Neuroradiology*. 1987; 29(5):409–415
- [608] Watanabe T, Taguchi Y, Shiosaka S, et al. Distribution of the histaminergic neuron system in the central nervous system of rats: a fluorescent immunohistochemical analysis with histidine decarboxylase as a marker. *Brain Res*. 1984; 295(1):13–25
- [609] Weirich D. *Computergestützte 3D-Rekonstruktion des medialen Lemniscussystems als Referenz für die bildgebenden Verfahren CT, MRT und PET*. Medizinische Dissertation der Medizinischen Hochschule Hannover; 1994
- [610] Weismann M, Yousry I, Heuberger E, et al. Functional magnetic resonance imaging of human olfaction. *Neuroimaging Clin N Am*. 2001; 11(2):237–250, viii
- [611] Wellhöner H-H. *Allgemeine und systematische Pharmakologie und Toxikologie*. Berlin: Springer; 1997
- [612] Wessely W. Biometrische Analyse der Frischvolumina des Rhombencephalon, des Cerebellum und der Ventrikel von 31 adulten menschlichen Gehirnen. *J Hirnforsch*. 1970; 12(1):11–28
- [613] Westheimer G, Blair SM. Oculomotor defects in cerebellectomized monkeys. *Invest Ophthalmol*. 1973; 12(8):618–621
- [614] Westrum LE, Canfield RC, Black RG. Transganglionic degeneration in the spinal trigeminal nucleus following removal of tooth pulps in adult cats. *Brain Res*. 1976; 101(1):137–140
- [615] White JG, Southgate E, Thomson JN, Brenner S. The structure of the nervous system of the nematode *Caenorhabditis elegans*. *Philos Trans R Soc Lond B Biol Sci*. 1986; 314(1165):1–340
- [616] Whitehouse PJ, Price DL, Clark AW, Coyle JT, DeLong MR. Alzheimer disease: evidence for selective loss of cholinergic neurons in the nucleus basalis. *Ann Neurol*. 1981; 10(2):122–126
- [617] Whitehouse PJ, Price DL, Struble RG, Clark AW, Coyle JT, Delon MR. Alzheimer's disease and senile dementia: loss of neurons in the basal forebrain. *Science*. 1982; 215(4537):1237–1239
- [618] Wicke L. *Atlas der Röntgenanatomie*. München: Urban und Fischer; 2001
- [619] Widder B. *Doppler- und Duplexsonographie der hirnversorgenden Arterien*. Berlin: Springer; 2004
- [620] Wienhard K, Wagner R, Heiss W-D. *PET Grundlagen und Anwendungen der Positronen-Emissions-Tomographie*. Berlin: Springer; 1989

- [621] Wiesendanger M. The pyramidal tract: recent investigations on its morphology and function. *Ergeb Physiol.* 1969; 61:72–136
- [622] Wieser MJ, Brosch T. Faces in context: a review and systematization of contextual influences on affective face processing. *Front Psychol.* 2012; 3:471
- [623] Wilkins RH, Rengachary SS, eds. *Neurosurgery*. New York, NY: McGraw-Hill; 1995
- [624] Williams PL, Bannister LH. *Gray's Anatomy*. New York, NY: Churchill Livingstone; 1995
- [625] Williams TH, Gluhbegovic N, Jew JY. *The Human Brain*. Iowa City, IA: University of Iowa; 2000
- [626] Willis WD Jr. *The Pain System*. Basel: Karger; 1985
- [627] Wise SP. Frontal cortex activity and motor set. In: Ito M, ed. *Neural Programming*. Basel: Karger; 1989:25–38
- [628] Wittfoth-Schardt D, Gründing J, Wittfoth M, et al. Oxytocin modulates neural reactivity to children's faces as a function of social salience. *Neuropsychopharmacology.* 2012; 37(8):1799–1807
- [629] Wolf G. *Epiphysen und Plexusverkalkungen in der Computertomographie*. Medizinische Dissertation der Medizinischen Hochschule Hannover; 1980
- [630] Wolf KJ, Fobbe F. *Farbkodierte Duplexsonographie*. Stuttgart: Thieme; 2000
- [631] Woolsey CN, Erickson TC, Gilson WE. Localization in somatic sensory and motor areas of human cerebral cortex as determined by direct recording of evoked potentials and electrical stimulation. *J Neurosurg.* 1979; 51(4):476–506
- [632] Yagishita A, Nakano I, Oda M, Hirano A. Location of the corticospinal tract in the internal capsule at MR imaging. *Radiology.* 1994; 191(2):455–460
- [633] Yasargil MG, Smith RD, Young PH, et al. *Microneurosurgery*. Vol. 1. Stuttgart: Thieme-Stratton; 1984
- [634] Yeo BT, Krienen FM, Sepulcre J, et al. The organization of the human cerebral cortex estimated by intrinsic functional connectivity. *J Neurophysiol.* 2011; 106(3):1125–1165
- [635] Youmans JR. *Neurological Surgery: A Comprehensive Reference Guide to the Diagnosis and Management of Neurosurgical Problems*. Philadelphia, PA: Saunders; 1996
- [636] Young AW, Aggleton JP, Hellawell DJ, Johnson M, Brooks P, Hanley JR. Face processing impairments after amygdalotomy. *Brain.* 1995; 118(Pt 1):15–24
- [637] Young RJ, Shatzkes DR, Babb JS, Lalwani AK. The cochlear-carotid interval: anatomic variation and potential clinical implications. *AJNR Am J Neuroradiol.* 2006; 27(7):1486–1490
- [638] Yousry I, Naidich TP, Yousry TA. Functional magnetic resonance imaging: factors modulating the cortical activation pattern of the motor system. *Neuroimaging Clin N Am.* 2001; 11(2):195–202, viii
- [639] Yousry T, Schmidt D, Alkadhi H, et al. New anatomic landmark for the identification of the precentral gyrus: validation and characterization. *Radiology.* 1995; 197:373
- [640] Yousry TA, Fesl G, Büttner A, et al. Heschl's gyrus: anatomic description and methods of identification in MRI. *Int J Neurorad.* 1997; 3:2–12
- [641] Yousry TA, Schmid UD, Schmidt D, Hagen T, Jassoy A, Reiser MF. The central sulcal vein: a landmark for identification of the central sulcus using functional magnetic resonance imaging. *J Neurosurg.* 1996; 85(4):608–617
- [642] Yousry TA, Yousry I, Naidich TP. Progress in neuroanatomy. In: Demaerel P, ed. *Recent Advances in Diagnostic Neuroradiology*. Berlin: Springer; 2001
- [643] Zaki J, Davis JL, Ochsner KN. Overlapping activity in anterior insula during interoception and emotional experience. *Neuroimage.* 2012; 62(1):493–499
- [644] Zanella FE. *Bildgebung*. In: Schlegel U, Westphal M, Hrsg. *Neuroonkologie*. Stuttgart: Thieme; 1998
- [645] Zatorre RJ, Evans AC, Meyer E. Neural mechanisms underlying melodic perception and memory for pitch. *J Neurosci.* 1994; 14(4):1908–1919
- [646] Zeumer H, Hacke W, Hartwich P. A quantitative approach to measuring the cerebrospinal fluid space with CT. *Neuroradiology.* 1982; 22(4):193–197
- [647] Zhang D, Snyder AZ, Fox MD, Sansbury MW, Shimony JS, Raichle ME. Intrinsic functional relations between human cerebral cortex and thalamus. *J Neurophysiol.* 2008; 100(4):1740–1748
- [648] Zihl J. *Zerebrale Sehstörungen*. *Akt Neurol.* 2000; 27:13–21
- [649] Zihl J, von Cramon D. *Zerebrale Sehstörungen*. In: Baumgartner G, Cohen R, Grüsser O-J et al., Hrsg. *Psychiatrie, Neurologie, Klinische Psychologie. Grundlagen-Methoden-Ergebnisse*. Stuttgart: Kohlhammer; 1986
- [650] Zilles K. The cortex. In: Paxinos G, ed. *The Human Nervous System*. San Diego, CA: Academic Press; 1990:757–802
- [651] Zilles K, Rehkämper G. *Funktionelle Neuroanatomie*. Berlin: Thieme; 1998
- [652] Zimmermann K, Heider C, Kösling S. Anatomy and normal variations of paranasal sinuses in radiological imaging *Radiologe.* 2007; 47(7):584–590
- [653] Linn J, Wiesmann M, Brückmann H. *Atlas Klinische Neuroradiologie des Gehirns*. Heidelberg: Springer; 2011
- [654] Forsting M, Jansen O. *MRT des Zentralnervensystems*, 2. Aufl. Stuttgart: Thieme; 2014
- [655] Naidich TP, Castillo M, Cha S, et al. *Imaging of the Brain*. Philadelphia, PA: Elsevier; 2013
- [656] Duden-Wörterbuch medizinischer Fachbegriffe, 9. Aufl. Mannheim: Bibliografisches Institut; 2011
- [657] McRobbie DW, Moore EA, Graves MJ, Price MR. *MRI—From Picture to Proton*. Cambridge: Cambridge University Press; 2007
- [658] Hattingen E, Pilatus K. *Brain Tumor Imaging*. Heidelberg: Springer; 2015
- [659] Wolf S, Wolf-Schnurbusch U. Spectral-domain optical coherence tomography use in macular diseases: a review. *Ophthalmologica.* 2010; 224(6):333–340
- [660] Liu J, Liu T, de Rochefort L, et al. Morphology enabled dipole inversion for quantitative susceptibility mapping using structural consistency between the magnitude image and the susceptibility map. *Neuroimage.* 2012; 59(3):2560–2568
- [661] Liu T, Wisnieff C, Lou M, Chen W, Spincemaille P, Wang Y. Nonlinear formulation of the magnetic field to source relationship for robust quantitative susceptibility mapping. *Magn Reson Med.* 2013; 69(2):467–476

Index

Note: Page numbers set in **bold** or *italic* indicate headings or figures, respectively.

A

Abducens nerves 297, 364
Abducent nerves 36
Accessory nerve **296**
activation vs. activation at rest **472**
Adenohypophysis/anterior lobe 321
Adrenergic neurons 483, **485**
Afferent nerves of oral cavity **366**
Allocortex 337
Ambient cistern 238
Amygdaloid body 322
Anatomical structures
– importance of 3D knowledge of 357
– nomenclature terminology **9**
anatomy of 251
and sylvian fissures 14
Anterio cranial fossae 170
Anterior basal 237
Anterior cerebral arteries 266, **267**
– above optic chiasm 271
– anterior communicating artery 271
– aplasia of 267
– branches from postcommunicating part of 267
– callosomarginal artery 271
– central arteries arising from 267
– lateral branches from 271
– main variants of 270
– penetrating branches of 284
– side branches arising from 271
– terminal branches of 271, **285**
– with circle of Willis and posterior cerebral artery 268
Anterior cranial fossa 121, 140, 195, 216, 237
– terraces of 123
Anterior inferior cerebellar artery (AICA) 253, 264
Anterior part of upper cervical spine 86
Anterior spinal artery 251
– thin branches of 263
Anterolateral central arteries 284
Anterolateral reticular systems 381
Anterolateral system **380**, 382
Aphasia 458, 462
Aqueduct of midbrain **243**
Arachnoid mater 237
Archicortex 337
Area striata 149
Arterial supply
– of brainstem **257**
– of cerebellum **264**
– of medulla oblongata **263**
– of midbrain **263**
– of pons **263**
Arterial territories of brainstem and cerebellum **257**
– arterial supply of brainstem **257**
– arterial supply of cerebellum **264**
– arterial supply of midbrain **263**
– arterial supply of pons **263**
Arterial territories of forebrain **276**
– central territories **284**
– terminal arterial territories **284**
Arteriosclerosis 273
artery **255**
Articular cartilage 366
Ascending pharyngeal artery 369, 373
Ascending reticular system 381, **400**
Aspartatergic neurons **487**
Atlanto-occipital joint 371
Atlanto-occipital sinus 251
Auditory ossicles 233
Auditory ossicular chain 232
Auditory system **409**, 421
Autonomic nervous system **470**
– parasympathetic **470**
– sympathetic **472**
Autonomic system 470

B

Babinski reflex 430
Basal ganglia
– disorders of 442
– motor systems of **439**
Basal ganglial systems 440, 442–443
Basal sinus 292
Basal veins 293–294
Basilar artery **252**, 253–254
– and its branches 254
– anterior inferior cerebellar artery (AICA) 253
– branches of 253
– development 252
– pontine arteries 253
– posterior cerebral artery 253
– superior cerebellar artery 253
Basilar impression 373
Bicommissural line 4, 7, 13, 91
– definition 7

Bicommissural MRI series 129
– 11th section of 152
– 12th section of 154
– 13th section of 156
– 14th section of 158
– eighth section of 147
– fifth section of 140
– fourth section of 138
– inferior view of 132
– ninth section of 146, 148
– second section of 134
– seventh section of 144
– sixth section of 142
– T2w MR image 133, 137, 139, 141, 143, 145, 147, 149, 151, 153, 155, 157, 159, 205
– tenth section of 150
– third section of 136
Bicommissural planes 4, 6
– intracranial CSF spaces oriented along 248
– position of 128
Bicommissural sections 128
Blood vessels, cross-sectional imaging
– landmarks of **14**
– large arteries 14
– large blood vessels 14
– venous sinuses 14
Bochdalek's bouquet 237
Bony external auditory canal 54
Bony foramina 13
Bony labyrinths 234
Bony structures and air-filled regions 13
Brachiocephalic vein 372
Brain
– anterior view of 94
– development 3
– extracranial fixation of 9
– MR examinations of 7
– neuroanatomy 3
Brain anatomy
– depiction in atlas section 5
– reorientation of depiction of 3
Brain maturation **346**
– importance 346
– myelination 493
Brain, median view of
– bicommissural series 130–131
– supraorbital-suboccipital series sections 161
brain morphology **8**
Brain sections 304
– median view in bicommissural plane 309
– oriented along bicommissural plane 310
– serial coronal images of 305
– serial sagittal images of 308
Brain stem
– magnified rendition of 5
Brainstem 56, 104, 303
– landmarks for 96
– longitudinal axis of 303
– medulla oblongata 312
– pons **312**
Brainstem
– sections 201
– views of external appearance 199
Brainstem, 3D views of 199
brainstem and cerebellum **257**
Brainstem, arterial supply of **257**
– anterolateral and lateral territory 257
– posterior territory 257
– regions 257
Brainstem series
– perpendicular to Meynert axis 201
– superior surface of eighth anatomical section of 216
– superior surface of fifth anatomical section of 210
– superior surface of first anatomical section of 202
– superior surface of fourth anatomical section of 208
– superior surface of ninth anatomical section of 218
– superior surface of seventh anatomical section of 214–215
– superior surface of sixth anatomical section of 212
– superior surface of tenth anatomical section of 220
– superior surface of the second anatomical section of 204
– superior surface of third anatomical section of 206
Brain structure
– infratentorial region examination **8**
– supratentorial region examination 7
Brain structures, 3D coordinate systems for
– localization of **6**
– history 6
– sagittal planes 493
– transverse planes **6**
Brain, subdivisions of **303**
– brainstem 493
– cerebellum **314**
– forebrain 493
– midbrain **316**

Brain tissue
– volumes of 8–9
Bregma 158
Bridging veins 292
Brodmann's areas in neocortex 338

C

Calcarine arteries 256
Calcarine spur 243
Calvarium 80, 236
Carotid-basilar anastomoses 266
Catecholaminergic neurons **483**
– adrenergic neurons 483, **485**
– dihydroxybenzol 483
– dopaminergic neurons 483, **484**
– localization of 483
– noradrenergic neurons 483, **484**
Caudal opening
– at foramen magnum 89
Caudate nucleus 322
Cavernous sinus
– and foramen magnum 102
Cavernous sinus syndrome 303
Cella media and inferior horn 56
Central sulcus 156, 158, 323
– criteria for detection of 334
Central sulcus
– identification 334
Central territories 276, **284**
Cephalogram
– drawing based on 21
– in anteroposterior projection of head 93
cerebellar artery (PICA) 251
Cerebellar lesions 316
Cerebellar systems **451**, 452, 455–456
Cerebellar tracts
– depiction of 199
Cerebellopontine angle syndrome 303
Cerebellopontine cisterns 237
Cerebellum 60, 64, 72, 142, 168, 199, 258, **314**
– anterior lobe of 314
– appearance **314**
– cerebellar peduncles 315
– flocculus 315
– internal structure **315**
– lobules and lobes of 315
– pons and 138
– superior surface of 253
– tentorium of 68, 236
– tonsils of 373
– vermis 315
Cerebellum
– arterial supply of **264**
Cerebral aqueduct 493
Cerebral arteries **251**
– anastomoses 253, **276**
– anterior cerebral artery **267**
– basilar artery **252**, 254
– circle of Willis **273**
– CT and MR examinations 251
– infratentorial arterial tree 252–253
– internal carotid artery **264**
– large 493
– middle cerebral artery **271**
– variability of 251
– vertebral artery **251**
Cerebral catheter angiography 251
Cerebral cortex **323**, **337**
– allocortex 337
– anatomy 323
– archicortex 337
– central sulcus 323
– frontal lobe **332**
– insula **336**
– isocortex 337
– lateral sulcus 332
– mesocortex 337
– neocortex 337
– occipital lobe **336**
– paleocortex 337
– parietal lobe **335**
– parietooccipital sulcus 332
– temporal lobe **336**
Cerebral hemispheres
– posterior part of 76
Cerebral irritation 450
Cerebral sinus thromboses 296
Cerebral vascular malformations 14
Cerebral veins **289**
– and sinuses 289
– deep **293**
– superficial **292**
– variability 289
– venous drainage 289
Cerebral venous and sinus thromboses 296

- Cerebral venous thromboses 296
- Cerebrospinal fluid
 - volumes of 8–9
- Cerebrum 8, 269, 275, 285
 - in coronal plane 277
- Cervical fascia 132
- Cervical vertebrae 58, 70
 - contours of 122
- CHARGE syndrome 234
- Chiasmatic cistern 239
- Cholesteatomas 232
- Cholinergic neurons **486**
- Chorda tympani 366
- Choroid plexus 243
- Cingulate gyrus 184
- Cingulate sulcus 152
- Circle of Willis 170, **273**
- Cisterna magna 493
- Cisterns **237**
 - ambient 238
 - anterior basal 239–240
 - cerebellopontine 237
 - chiasmatic 239
 - definition 237
 - interpeduncular 238
 - of lateral cerebral fossa 240
 - of transverse fissure 240–241
 - of vallecule cerebri 240
 - pontine 237
 - posterior and anterior basal 237
 - posterior cerebellomedullary 237
 - quadrigeminal 238
 - trigeminal 239
- Cisterns, cross-sectional imaging landmarks of **13**
 - lateral cerebral fossa 14
 - pentagon 13
 - posterior cerebellomedullary 13
- Clastrum 322
- Cochlea 234–235
 - 3D representation 235
- Cochlea
 - and styloid process 86
- Cochlear aperture 234
- Collateral trigone of lateral ventricle 60
- Common carotid artery 373
- Confluence of sinuses 78
- Connectome 379
- Connectomics 379
- Contralateral hemiparesis 303
- Coordinate systems **8**
 - for bony structure localization 8
 - German horizontal and meatoververtical line 8
 - goals of 8
 - in stereotactic atlases 8
- Coronal planes **7**
- Coronal sections of head 19–20, 24
 - anterior view of 24, 26, 28, 30, 32, 34, 38, 40, 42, 44, 46, 48, 50, 52, 54, 56, 58, 60, 62, 64, 68, 70, 72, 74, 76, 78
 - cephalogram drawing 21
 - coronal CT image 80–89
 - coronal T1w MR image 25, 29, 33, 37, 41, 45, 49, 53, 57, 61, 65–66, 69, 73, 77
 - coronal T2w MR image 27, 31, 35, 39, 43, 47, 51, 55, 59, 63, 67, 71, 75, 79
 - position in lateral view 20
- Coronoid and condyloid processes 202
- Corpus callosum 36, 180, 182, 339
 - commissural fibers of 346
- Cranial cavity 52, 98
 - cranial fossae **237**
 - infratentorial region **236**
 - subdivision of 236
 - supratentorial region **236**
 - topography of 236
 - volume 236
- Cranial dura visualization 14
- Cranial fossae **237**
 - topography of 237
- Cranial nerves 52, 56, 112, 213, **296**
 - abducens (III) nerves 297
 - horizontal stretch of third and fourth 217
 - IInd cranial nerve **302**, 348
 - Ist cranial nerve 303
 - IXth cranial nerve **296**
 - nuclei arrangement in brainstem 200
 - oculomotor (III) nerves 297
 - trigeminal nerves 297
 - trochlear (IV) nerves 297
 - VIIIth cranial nerve **296**
 - VIth cranial nerve **297**
 - XIth cranial nerve **296**
 - XIIth cranial nerve **296**
 - Xth cranial nerve **296**
- Cranial nerves, nuclei of 313
 - afferent cranial nerve nuclei 313
 - efferent nuclei 313
 - facial nucleus 313
 - hypoglossal nucleus 313
 - inferior salivatory nucleus 313
 - mechanoreceptor signals 313
 - motor nucleus of trigeminal nerve 313
 - nucleus ambiguus 313
 - posterior (dorsal) nucleus of vagus nerve 313
 - sensory nuclei 313
 - superior salivatory nucleus 313
 - terminal afferent nuclei 313
 - vestibular nuclei 313
 - visceroefferent nuclei 313
- Cranial nerve syndromes 303
- Cranial vault 120, 186, 188, 195
 - and nasal skeleton 224
- Cranial vault, bones of 224
 - frontal bone **236**
 - occipital bone **224**
 - parietal bone **236**
 - sphenoid **224**
 - temporal bone **225**
- Cranial vault, cross-sectional imaging landmarks of **13**
- Craniocervical junction 91, 132, **370**
 - bones of **370**
 - clinical importance of **372**
 - joints of head **371**
 - muscles of **371**
 - nerves of **372**
 - slices through 236
 - vessels of **372**
- cribriform plate 357
- Cribriform plate 237, 357
- Crista galli 357
- Crossed and uncrossed fibers 416
- Cross-sectional imaging
 - Landmarks 12
- CSF spaces
 - as landmarks for CT 13
 - as landmarks for MRI 14
- CT 5, **11**
 - 2D gray-scale mapping of pixels in 12
 - bicommissural plane as reference plane for 4
 - image acquisition 11
 - image interpretation 12
 - iodinated contrast medium and 11
 - partial volume effects 11
 - spiral (helical) or volume technique 11
 - supraorbito-suboccipital line 4
 - transverse (axial) sections 3–4
- CT landmarks 12
 - blood vessels **14**
 - cranial vault **13**
 - dural structures **14**
 - facial bones **13**
 - Head–neck region **13**
- D**
- Dandy-Walker malformation 373
- Deep cerebral veins **293**
- Deep cervical artery 372
- Deep lateral facial region **367**
- Diencephalic lesions 320
- Diencephalon **317**
 - appearance **317**
 - epithalamus **320**
 - hypothalamus **318**
 - internal structure **317**
 - metathalamus **318**
 - subthalamus **318**
 - thalamus **318**
- Diencephalon
 - landmarks for 96
- Digital cross-sectional imaging methods
 - benefits of 5
 - reorientation of depiction of brain anatomy 3
 - tomographic images of human body 3
- Dihydroxybenzol 483
- Diploic veins 375
- Diplopia 450
- Dislocations 372
- Dissociated nystagmus 409
- Dopamine 483
- Dopamine deficiency 484
- Dopaminergic neurons 483, **484**
- Dorsum sellae 166
- Dural duplications 14
- Dural structures, cross-sectional imaging landmarks of **14**
- Dyssynergia 316
- E**
- Endbrain 52, 108, 116–119
 - gyri and sulci of 91
 - medial surface of 96
- Enkephalinergic neurons **488**
- Epithalamus **320**
- Ethmoidal cells 359
- Ethmoid bone 357
- Ethmoid cells 357
- examinations **7**
- External auditory canal 206, 229
- External auditory canals
 - medial aspects of 164–165
- External carotid artery 367, 373
 - branches of 374
- External ear 367
- External jugular vein 375
- Extracranial CSF spaces
 - importance of 245
- Extra/intracranial anastomoses 374
- Extraocular muscles **362**
- Eyeball 136, 360, **364**
 - anterior pole of 360
 - anterior segment of 364
 - fascia sheath of 493
 - lateral part of 114
 - lens 364
 - wall of 364
- Eyelids **360**
 - conjunctiva 361
 - functions 360
 - innervation of 361
 - levator palpebrae superioris 360
 - superior and inferior tarsal muscles 360
- Eye movements 444
- F**
- Facial bones **357**
 - jaw **358**
 - nasal skeleton **357**
- Facial bones, cross-sectional imaging landmarks of **13**
 - bony orientation 13
 - bony structures and air-filled regions 13
- Facial canal cells 87
- Facial nerve 234, **297**, 367
- Facial vein 375
- Falx cerebri 148, 150, 152, 154, 236
- Fascia sheath of eyeball **362**
- First-order parasympathetic neurons
 - cell bodies of 470, 472
- Fixation nystagmus 409
- Flocculus
 - lesions of 316
- fMRI 12
- Foramen lacerum 225
- Foramen magnum 70, 134
 - posterior part of 66
- Foramen magnum 162
- Foramen ovale 229
- Foramen rotundum 83
- Forebrain 303
 - central arterial territories 278
 - longitudinal axis of 303
 - terminal arterial territories 284
 - terminal arterial territories of 277
- formation 462
- Fourth ventricle **243**
- Fractures 372
- Frontal bone **236**
- Frontal cortex 324–327, 330–332
- Frontal horn 243
- Frontal lobe 36, 142, 156, 168, **332**, 334
 - boundaries of 323, 329
 - inferior frontal gyrus 332, 333
 - lesions in motor cortex of 346
 - middle frontal gyrus 332
 - M-shaped cortical ribbon 333
 - precentral gyrus 334
 - superior frontal gyrus 332
- Frontal sinus 359
- G**
- GABAergic neurons **486**
- Garcin's syndrome 303
- Gaze-dependent nystagmus 409
- Gaze palsies 450
- Geniohyoid 365
- Glossopharyngeal nerve **296**
- Glutamatergic neurons **487**
- Gradenigo's syndrome 303
- Greater petrosal nerve 360
- Greater wings 225
- Guillian Mollaret triangle, lesions in 314
- Gustatory system **400**, 401–403
- Gyri of endbrain 91
- H**
- Hard palate 365
- Head
 - joints of **371**
- Head–neck junction
 - soft tissues of 132
- Head–neck region
 - arteries of **373**
 - craniocervical junction **370**
 - definition 369
 - innervation of muscle groups in 298, 301–302, 309
 - parapharyngeal space **369**
 - pharynx **369**
 - veins 375

Head–neck region, cross-sectional imaging
 landmarks of
 – air-filled regions 13
 – bony vertebral canal 13
 – cross-sectional imaging landmarks of **13**
 – large neck vessels 13
 – skull base 13
 Head–neck region, vessels of **373**
 – ascending pharyngeal artery 373
 – common carotid artery 373
 – external carotid artery 373
 – internal carotid artery 373
 – occipital artery 373
 – superior thyroid artery 373
 Heavily myelinated hypothalamus 318
 Hippocampal formation
 – high resolution T2w MR image of 55
 Hippocampus 336
 – anatomical structure of 54
 Histaminergic neurons **485**
 Hodology 5
 Horizontal gaze palsy 450
 Human Connectome Project 380
 Human head
 – asymmetry of 6
 Hydrogen nuclei excitation sequences 11
 Hyoid bone 85
 – lateral parts of 84
 Hypoglossal canal 162, 203
 Hypoglossal nerves 36, 40, **296**
 – roots of 203
 Hypophysis 91
 Hypothalamic–infundibular system 318
 Hypothalamus 142, 144, **318**

I

β-Endorphin **487**
 Incisura of tentorium
 – topographical position of 14
 Inferior alveolar nerve 367
 Inferior horn and cella media 56
 Inferior nasal concha 357
 Inferior nasal turbinate 206
 Inferior oblique muscle 362
 Inferior olivary system **314**
 Inferior rectus muscle 362
 Inferior temporal gyrus 336
 Inferior thalamus 144
 Inferior frontal gyrus 332–333
 Infratentorial region 64, **236**
 Infratentorial region examination **8**
 Inner ear 225, **234**
 – cochlea 493
 – functional components of 234
 – vestibule 234
 Insula 112, 146, **336**
 Interbrain 52
 Internal auditory canal 54, 168, 232, 234
 Internal auditory canal cells 87
 Internal capsule 146
 Internal carotid arteries **264**, 373
 – anterior choroidal artery 266
 – branches of 255
 – direct branches of 264
 – embryological development 266
 – fetal type 266
 – juxtaseal segment 264
 – posterior communicating artery 266
 – subarachnoid part of 264
 – terminal part of 274
 Internal cerebral vein 293–294
 Internal jugular vein 375
 – drainage of 289
 – lateral view 293
 – venous MRA of 291
 Internal occipital protuberance 98
 International anatomical nomenclature 9
 Interpeduncular cistern 238
 Interthalamic adhesion 243
 Interventional neuroradiology
 – importance 3
 Interventricular foramina 48
 Intracerebral coordinates **7**
 Intracerebral coordinate systems
 – reference planes **7**
 Intracranial compartment
 – volumes of **8**
 Intracranial CSF spaces 238, 240, 246
 – aqueduct of midbrain **243**
 – bicommissural sections. 237
 – cisterns **237**
 – coronal sections 237
 – fourth ventricle **243**
 – lateral ventricles **243**
 – oriented along bicommissural plane 248
 – sagittal sections 237
 – subarachnoid space **237**
 – third ventricle **243**
 – ventricular system **243**
 Intracranially fixed brains 9
 Intraorbital retrobulbar fat 13

Intravital neuroanatomy **8**
 In vivo MRS 12
 Iodinated contrast medium
 – intravenous (IV) administration 11
 Ipsilateral functional deficits 453
 Ipsilateral Horner's syndrome 472
 Isocortex 337
 Isthmus of fauces **365**

J

Jaw
 – skeletal anatomy of **358**
 Jugular foramen
 – in posterior cranial fossa 237
 Jugular foramen syndrome 303

K

Koerner's septum 225

L

Lacrimal apparatus **360**
 – functions 360
 Lacrimal gland 361
 Lacrimal system
 – anatomy of 361
 Landmarks 12
 Large cerebral arteries
 – occlusion of 251
 Laryngopharynx 369
 Lateral entricles 172
 Lateral facial region **366**
 – deep **367**
 – nerve supply of **367**
 – superficial **366**
 – vessels of **367**
 Lateral frontobasal artery 272
 Lateral geniculate body 416
 Lateral pterygoid muscle 366
 Lateral rectus muscle 362
 Lateral sulcus 332
 Lateral ventricles 180, **243**
 – cella media of 108
 – central part 243
 – collateral trigone of 60, 178
 – frontal horn 40, 243
 – lobes of telencephalon 243
 – occipital horn 243
 – posterior horn of 64
 – temporal horn 243
 Left cerebral hemisphere
 – lateral view of 335
 Left hemisphere 458
 Leptomenigeal anastomoses 276
 Lesser wings 224
 Levator scapulae 372
 Limbic system 336, **462**–464, 467–468
 – components of 462
 – cortical regions 462
 – mammillothalamic fasciculus 463
 – Papez circuit 463
 – subcallosal area and indusium griseum 462
 Lingual nerves 40, 366–367
 Localization theory 379
 Longissimus capitis muscle 371
 Longus capitis 372
 Loss of sense of smell 427

M

Magnetic resonance imaging examinations
 – transverse planes **7**
 Mammillary bodies 48
 Mandible 81, 122
 Mandibular nerve 36, 367
 – below foramen ovale 207
 Masseter muscle 366
 Mastication
 – muscles of **366**
 Masticatory apparatus **366**
 – lateral facial region 493
 – muscles of mastication **366**
 – temporomandibular joint **366**
 Mastoid 233
 Mastoid air cells 87
 Mastoid process 58, 125, 225
 Maxilla bone 358
 Maxillary arteries 359
 Maxillary nerve 359
 Maxillary sinus 81, 122, 358
 Medial geniculate body 104
 Medial lemniscus system 383–389, 399
 – boundary between representative areas of 391
 – gracile and cuneate nuclei 385
 – lesion of 399
 – sensory receptors of 385
 – ventral posterolateral nucleus 385
 Medial pterygoid muscle 366

Medial rectus muscle 362
 Median atlantoaxial joint 371
 Median plane 6
 Medulla oblongata 134, 203, 258, 312
 – anterior aspect of 312
 – ascending pathways 314
 – closed part of 312
 – cranial nerves and 312
 – descending pathways 314
 – inferior olivary system **314**
 – lesions of 314
 – nuclei of cranial nerves 493
 – open part of 312
 – posterior parts of 312
 – reticular formation **313**
 – unilateral lesion of anteromedial and anterolateral territories of 264
 Medulla oblongata, arterial supply of **263**
 – lateral territory 263
 – posterior territory 263
 Melanotropin and lipotropin 321
 Mesocortex 337
 Metathalamus **318**
 Meynert axis
 – MR images oriented perpendicular to 207, 209, 211, 213, 215, 217, 219, 221
 – MR images oriented perpendicular to 203, 205
 Midbrain 52, 142, 220, **316**, 319
 – anterior surface 316
 – appearance **316**
 – cerebral crura 317
 – internal structure **316**
 – posterior surface 316
 – tectum of midbrain 316
 – tegmentum of midbrain 316
 – venous drainage of 295
 – with arterial territories 258
 Midbrain
 – and pons 100
 Midbrain, arterial supply of **263**
 – anterolateral territory 264
 – lateral territory 264
 – posterior territory 264
 Middle cerebral arteries
 – perforating arteries from 270
 – with terminal branches 274
 Middle cerebral artery **271**
 – aplasia of 271
 – bifurcation 271
 – branches 271
 – lateral frontobasal artery 272
 – sphenoid part 271
 – terminal branches of **285**
 – variants of 272
 Middle cranial fossa 84–85, 106, 138, 193, 208, 210, 237
 – anterior poles of 38
 Middle cranial fossae 170
 – terraces of 123
 Middle ear **232**
 – auditory ossicular chain 232
 – definition 232
 – mastoid antrum 232
 – pars flaccida 232
 – stapes 232
 – tympanic cavity 232–233
 – tympanum 232
 Middle frontal gyrus 332
 Middle nasal canal 359
 Middle temporal gyrus 336
 Middle turbinate 208
 Model brain 5
 Motor aphasia 462
 Motor disturbances 430
 Motor nerve 364
 Motor speech area 458
 Motor systems **430**
 – oculomotor systems **444**
 – of basal ganglia **439**
 – pyramidal system **430**
 Mouth
 – floor of **365**
 – roof of **365**
 MRI **5**, **11**
 – advantages 12
 – applications 12
 – clinical significance of **15**
 – contrast medium administration 12
 – fMRI 12
 – for treatment follow-up 3
 – gradient echo sequences 11
 – hydrogen nuclei excitation sequences 11
 – image interpretation 12
 – image processing and reconstruction 11
 – in vivo 12
 – measurement criteria selection for 11
 – MR signal 11
 – paramagnetic substances as contrast medium 11
 – parameters for for image acquisition 11
 – physical and chemical processes determining 12
 – potential error possibility 11
 – sectional plane 3

- transverse sections 4
- working principle 11
- MRI landmarks 12
- blood vessels **14**
- cranial vault **13**
- dural structures **14**
- facial bones **13**
- Head–neck region **13**
- Myelination
 - brain at age 3 months 347, 350
 - brain at age 6 months 347, 351
 - brain at age 9 months 347, 352
 - brain at age 12 months 347, 353
 - brain at age 18 months 347, 354
 - brain at age 24 months 348
 - cerebellar white matter 347
 - changes during first 6 to 8 months of life 347, 349, 351
 - fibers between association regions of brain 346
 - in postpartum period 346
 - MR technology advances and 346
 - neonatal brain at term 347, 349
 - signal alterations associated with 346
 - signs in cerebellar hemispheres 347
 - temporal white matter 347
 - terminal zones of 347
- Mylohyoid 365

N

- Nasal cavity **358**
 - blood supply of **359**
 - lateral wall of 359
 - medial wall of 359
 - nerve supply of **359**
 - topography **358**
- Nasal conchae 357
- Nasal skeleton
 - bones of **357**
- Nasal turbinates 13, 81
- Nasopharynx 369
 - opening of left auditory tube in 203
- Neocortex 337
 - Brodmann's areas in 338
- Nerves of orbit **363**
- Neural processing **473**
- Neuroactive substances 483
- Neuroanatomy 3, **8**
 - human brain 3
- Neurofunctional systems 5, **379**, 380, 483
 - ascending reticular system **400**
 - auditory system **409**
 - autonomic nervous system **470**
 - cerebellar systems **451**
 - definition 379
 - gustatory system **400**
 - in multiplanar parallel slices 5
 - limbic system **462**
 - localization theory 379
 - motor systems **430**
 - neuronal networks **472**
 - olfactory system **427**
 - positions of 380
 - sensory systems **380**
 - speech areas **458**
 - vestibular system **403**
 - visual system **416**
- Neurohypophysis 215, 321
- Neuroimaging
 - disadvantages 3
 - for objective follow-up 3
 - for treatment follow-up 3
 - knowledge acquisition in 3
- Neuromodulators
 - functions of 483
- Neuronal networks 380, **472**
 - neural processing in **473**
 - visual network **474**
- Neurons 493
 - chemically identifiable **314**
- Neuroradiological techniques
 - merits and limitations 3
- Neurosciences 3
- Neurotransmitters
 - acetylcholine 483
 - catecholaminergic neurons 493
 - functions of 483
- Noradrenergic neurons 483, **484**
- Nuchal muscles 371
- Nystagmus 409

O

- Obliquus capitis inferior 372
- Obliquus capitis superior 371
- oblongata **263**
- Occipital artery 372, 373
- Occipital bone **224**, 370
 - parietal and 74
- Occipital cortex 324–327, 330–332
- Occipital gyri 336

- Occipital horn 243
- Occipital lobe 76, **336**
 - boundaries of 323, 329
 - lesions of 346
- Occipitotemporal gyri
 - lateral and medial 336
- Occlusion of penetrating artery 284
- Ocular movements, disturbances of 444
- Oculomotor nerves 36, 297, 364
 - parasympathetic motor nucleus of 470
- Oculomotor systems **444**
 - disorders of 450
 - functions of 444
 - saccades 444–448
 - smooth pursuit eye movements **447**
 - vergence movements **448**
 - vestibulo-ocular reflexes **448**
- of **15**
- Olfactory bulb 216
- Olfactory bulb
 - and tract 140
- Olfactory groove syndrome 303
- Olfactory hallucinations 427
- Olfactory nerve 303
- Olfactory system 140, **427**, 433
- Onodi cells 225
- Ophthalmic arteries 359
- Ophthalmic artery 362–363
- Ophthalmic nerve 359, 363
- Ophthalmoscope 360
- Optic canal 38, 82
- Optic chiasm 219
- Optic chiasm 416
- Optic chiasma 40
- Optic chiasma 168
- Optic nerve 36, **302**, 348, 360, **364**
- Optic radiation 421
- Optic tract 219
- Optic tract–hypothalamus 221
- Oral cavity **364**
 - afferent nerves of **366**
 - floor of mouth **365**
 - isthmus of fauces **365**
 - roof of mouth **365**
 - tongue **365**
 - vessels of **365**
- Orbit **360**
 - apical region of 164–165
 - connected to structures 360
 - extraocular muscles **362**
 - eyeball 360, **364**
 - eyelids and the lacrimal apparatus **360**
 - fascia sheath of eyeball **362**
 - innervation of 363
 - nerves of **363**
 - optic nerve 360, **364**
 - roof and floor of 81, 122
 - topography **360**
 - veins of 363
 - vessels of **362**
 - walls of 360
- Orbit
 - inferior aspect of 193
- Orbital apex 106
- Orbital apex syndrome 303
- Orbital cavity 210
 - shape of 360
- Oropharynx 369
- Osseous spiral lamina 234
- Osseous cross-sectional anatomy 236

P

- Paleocortex 337
- Parahippocampal gyrus 336
- Paranasal sinuses **358**
 - blood supply of **359**
 - composition of 358
 - topography **358**
- Parapharyngeal space 106, **369**, **370**
- Parasympathetic nervous system of head **470**
- Parietal bone
 - occipital and 74
- Parietal bone **236**
 - borders 236
- Parietal cortex 324–327, 330–332
- Parietal lobe 156, **335**
 - boundaries of 323, 329
 - lesions in postcentral gyrus of 346
 - occipital and 72
- Parieto-occipital artery 256
- Parietooccipital sulcus 332
- Parinaud's syndrome 450
- Pars compacta of substantia nigra 484
- Peptidergic neurons **487**
 - enkephalinergic neurons **488**
 - β -Endorphin **487**
 - substance P **487**
 - vasoactive intestinal polypeptide **487**
- Percheron artery
 - occlusion of 284
- Perpendicular plate 357

- Petro-occipital synchondrosis 225
- Petrous part of temporal bone 62, 86, 225
 - apex of 225
 - definition 225
 - facial nerve 234
 - in axial view 226
 - in coronal view 228
 - in CT and MRI 230
 - lateral part of 225
- Pharyngeal elevators 369
- Pharyngeal wall
 - muscles of **369**
 - nerves of **370**
 - vessels of **369**
- Pharynx 46, **369**
 - constrictors of 369
 - topography of **369**
- Pineal gland 60, 320
- Pituitary fossa 46, 102
- Pituitary gland **320**
 - adenohypophysis/anterior lobe 321
 - arteries supply 321
 - definition 320
 - melanotropin and lipotropin 321
 - neurohypophysis 321
- Pons 52, 258, **312**
 - anterior part 312
 - ascending pathways 314
 - central part 312
 - descending pathways 314
 - inferior part 312
 - lesions of 314
 - posterior part 312
 - superior part 312
- Pons
 - and cerebellum 138
- Pons, arterial supply of **263**
 - anterolateral territory 263
 - anteromedial territory 263
 - lateral territory 263
 - periventricular zone 263
 - posterior territory 263
- Pontine arteries 253
- Pontine cistern 237
- Posterior basal 237
- Posterior cerebellomedullary cistern 237
- Posterior cerebral artery 253, **255**
 - anterior cerebral artery with circle of Willis and 268
 - division into branches 255–256
 - fetal type 255
 - postcommunicating part of 255
 - segment of 255
 - terminal branches of **289**
- Posterior clinoid processes 46, 84
- Posterior commissure 56, 339
- Posterior communicating artery 266
- Posterior cranial fossa 88, 121, 138, 166, 170, 202, 237
 - terraces of 123
- Posterior inferior cerebellar artery (PICA) 251–252, 264
- Posterior part of foramen magnum 66
- Posterolateral central arteries 284
- Postmortem neuroanatomy **8**
- Precentral gyrus 334
- Premotor cortex 430
- Primary cortical areas 337
- Primary motor cortex 430, 432
- Primary visual cortex 424
- Promontory test 235
- Proximal anterior cerebral arteries
 - perforating arteries from 270
- Pterygoid process 224–225
- Pterygoid process of sphenoid bone 83
- Pterygoid venous plexus 375
- Pterygopalatine fossa 82
- Pupillary anomalies 450
- Putamen 322
- Pyramidal system 430, 434, 436

Q

- Quadrigeminal cistern 238
- Quadrigeminal plate 174

R

- Ramus of mandible 84
- Rectus capitis anterior 372
- Rectus capitis posterior major 371
- Rectus capitis posterior minor 371
- Reid's base 237
- Reid's base line 4
- Reticular formation **313**, 400
- Retinotopic maps **426**
- Retrobulbar disorder 426
- Retrocochlear hearing loss 409
- Retromandibular vein 375
- Reward mechanism 484
- Rhomboid fossa
 - Floor of 60

- Right eye 361
- Right lateral ventricle
 - anterior and central parts of 100

S

- Saccades 444–448
- Sacculle and utricle 403
- Sagittal MR images 493
 - advantages 91
- Sagittal planes 6
- Sagittal sections of head 91, 92
 - bicommissural line 91
 - brain and upper spinal cord 22–23
 - cephalogram 93
 - craniocervical junction 91
 - gyri and sulci of endbrain 91
 - hypophysis 91
 - medial view of 96, 98, 100–104, 106, 108, 110, 112, 114, 116–119
 - right half of head 98
 - sagittal CT image 120–125
 - sagittal T1w MR image 97, 105–107, 109, 113, 117
 - sagittal T2w MR image 99, 107, 111, 115, 119
 - structures seen in 91
 - view of brain 94–95
- Secondary cortical areas 337
- Sella turcica 166
- Semicircular canals 234, 403
- Semispinalis capitis muscle 371
- Sensory aphasia 462
- Sensory speech region 458
- Sensory systems 380
 - anterolateral system 380, 382
 - clinical significance 399
 - trigeminal system 392
- Septal nuclei 322
- Serotonergic neurons 485
- Skull base 114, 124
 - external 3D view of 197
 - transverse image of 493
- Skull base lesions
 - causing cranial nerve syndromes 303
- Slice position, importance of 357
- Smooth pursuit eye movements 447
- Soft palate 365
- Specimens and technique 491
- Speech areas 458, 459, 461
 - aphasia 458, 462
 - left hemisphere and 458
 - motor speech 458
 - research history of 458
 - sensory 458
- Speech disorders 458
- Sphenoid 224
 - body 224
 - greater wings 225
 - lesser wings 224
 - location of 224
 - parts of 224
 - pterygoid process 224–225
- Sphenoid bone 82, 192
 - pterygoid process of 83
- Sphenoid sinus 84, 359
 - inferior aspect of 193
- Sphenoid sinus
 - with adjoining trigeminal ganglion and trigeminal nerve 211
- Spinal canal 58, 98
- Spinal canal
 - at foramen magnum 88
- Spinothalamic tract 380
- Spiral (helical) CT scanners
 - operating principle 3
 - scan times of 3
- Spiral lamina 234
- Splenium of corpus callosum 60, 148
- Splenius capitis muscle 371
- Spontaneous nystagmus 409
- Striatum (putamen and caudate nucleus) 146
- Subarachnoid space 237
- Substance P 487
- Subthalamus 318
- Sulci of brain 333
- Sulci of endbrain 91
- Superficial lateral facial region 366
- Superior cerebellar artery 253, 264
- Superior cerebral veins 292
- Superior frontal gyrus 332
- Superior longitudinal fasciculus 459
- Superior nasal canal 359
- Superior oblique muscle 362
- Superior orbital fissure 38, 224, 237
 - medial aspect of 106
- Superior orbital fissure, syndrome of 303
- Superior part of insula 148
- Superior rectus muscle 362
- Superior sagittal sinus
 - structure with arachnoid granulations 50

- Superior temporal gyrus 336
- Superior thalamostriate vein 293
- Superior thyroid artery 373
- Supplementary auditory area 338
- Supplementary motor area 430
- Supplementary sensory area 338
- Supracommissural part of cingulate gyrus 150
- Supraorbital-meatal plane 4
- Supraorbital-suboccipital CT series 161
 - 10th section of 180
 - 11th section of 182
 - 12th section of 184
 - 13th section of 186
 - 14th section of 188
 - eighth section of 176
 - fifth section of 170
 - first section of 162
 - fourth section of 168
 - ninth section of 178
 - second section of 164–165
 - seventh section of 174
 - sixth section of 172
 - third section of 166
- Supraorbital-suboccipital oriented CT image 163, 165, 167, 169, 171, 173, 175, 177, 179, 181, 183, 185, 187, 189
- Supraorbital-suboccipital plane 4, 237
- Supratentorial region 236
 - examination of 7
- Sympathetic nervous system of head 472
- Sympathetic postganglionic nerve fibers 360
- system 13, 385

T

- Task dependent activation vs. activation at rest 472
- Taste sensations, impaired 400
- Technique and specimens 491
- Telencephalic nuclei 321
 - groups 321–322
- Telencephalon 321
 - appearance 321
 - internal structure 493
- Telencephalon, internal structure of
 - cerebral cortex 323, 337
 - frontal lobe 332
 - insula 336
 - occipital lobe 336
 - parietal lobe 335
 - telencephalic nuclei 321
 - temporal lobe 336
 - white matter 339
- Temporal bone 225
 - parts 225
 - petrous part of 493
 - squamous part of 229
 - tympani part of 225, 229
- Temporal bone, tympanic cavity of 208
- Temporal cortex 324–327, 330–332
- Temporal corticectomies 425
- Temporal horn 243
- Temporal horns 168
- Temporalis muscle 366
- Temporal lobe 138, 142, 336
 - boundaries of 323, 329
 - pathological changes in 346
- Temporomandibular joints 46, 85, 125, 136, 366
- Tenon's capsule 362
- Tentorium of cerebellum 172, 174, 176
- Term birth
 - myelination at 347, 349
- Terminal arterial territories 276, 284
 - anterior cerebral artery 285
 - middle cerebral artery 285
 - posterior cerebral artery 289
- Terminal infarcts 285
- Terminologia Anatomica 9
- Thalamus 146, 318
- Thalamus 178
- Third ventricle 243
 - anterior wall of 243
 - roof of 243
- Tomographic image mapping 12
- Tomographic images of human body 3
- Tongue 38, 365
 - extrinsic muscles 365
 - intrinsic muscles 365
- Tonsils of cerebellum 134
- Topography 357
- Transcranial doppler sonography 14
- Transverse CT sections 127
- Transverse image of skull base
 - CT image 190–195
- Transverse MRI sections 127
- Transverse planes 6
 - angulated CT sections 6
 - as orbitomeatal plane 6
 - coronal planes 7
 - German horizontal 6

- intracerebral coordinates 7
 - widespread clinical use of 6
- Transverse temporal gyri 336
 - Trapezius muscles 371
 - Trigeminal cistern 239
 - Trigeminal ganglion 392
 - Trigeminal nerve
 - mechanoreceptor signals 313
 - Trigeminal nerves 297
 - Trigeminal system 392, 393
 - lateral trigeminothalamic tract and 392
 - mechanoreceptors 392
 - peripheral and central 394, 396
 - trigeminal ganglion and 392
 - Trochlear nerve 364
 - Trochlear nerves 36, 297
 - Tuberoinfundibular system 484
 - Tympanic cavity 232–233
 - Tympanic cavity 54
 - Tympanic membrane 229
 - Tympanum 232

U

- Upper cervical vertebrae 62
- Upper parietal cortex 430

V

- Vagus 296
- Vagus nerve 472
- Vasoactive intestinal polypeptide 487
- Ventral posterolateral nuclei of thalamus 380
- Ventral posterolateral nucleus 320
- Ventricular system 243
 - importance of 245
 - lateral view of 247
- Ventricular system, cross-sectional imaging landmarks of 13, 14
- Vergence movements 448
- Vermis
 - lesions of 316
- Vertebral arteries 251, 372
 - atlanto-occipital sinus 251
 - branches of 251
 - confluence with basilar artery 209
 - reserve loop 251
 - through atlanto-occipital membrane 251
- Vertical gaze palsy 450
- Vessels of orbit 362
- Vestibular system 403, 404–408
 - connections with motor neurons 406
 - lesions 409
 - sensory receptors of 403
 - signals transmitted by 403
 - vestibular nuclei 403
- Vestibulocochlear nerve 296
- Vestibulo-ocular reflexes 448
- Viscerocranium 493
- Visual network 474
- Visual system 416, 417–420, 428
 - calcarine sulcus 425
 - crossed and uncrossed fibers 416
 - lateral geniculate body 416
 - optic chiasm and 416
 - optic radiation 421
 - photoreceptors of 416
 - primary visual cortex 424
 - retinotopic maps 426
- Voluntary movements, cerebral regions involved in 430
- Voxels
 - definition 3

W

- Weakly myelinated hypothalamus 318
- White matter 339
 - association fibers 339, 341
 - association tracts 340, 342
 - centrum semiovale 339
 - commissural fibers 339
 - commissural tracts 340, 342
 - fiber tracts 340
 - location and composition 339
 - projection fibers 339
 - projection tracts 340, 342
- White matter maturation 346, 493
 - MRI for 346
- White matter tracts 344
 - 3-dimensional MR-tractography 341, 343
 - MR diffusion tensor imaging 344

